UTM
UNIVERSITI TEKNOLOGI MALAYSIA
Faculty of Electrical Engineering

Proceedings of 2017 Electrical Engineering Symposium (EES2017) - Vol. 4

PROCEEDINGS OF 2017 ELECTRICAL ENGINEERING SYMPOSIUM (EES2017)

VOLUME 4

UTM UNIVERSITI TEKNOLOGI MALAYSIA
Faculty of Electrical Engineering

First Edition 2017

Diterbitkan oleh: Fakulti Kejuruteraan Elektrik, Universiti Teknologi Malaysia, 81310 Johor Bahru Johor, Malaysia

PREFACE

This book introduces several research works from final year undergraduate project till the level of master project by taught course. The projects have been evaluated by industries as well as academician to ensure that its fulfill the standard of each level before it can be published. The text emphasizes the combination of the research material in different field of engineering generally in power, electronic, communication, control and mechatronic which hampered by three main program offered by Faculty of Electrical Engineering.

This book is generally suitable as an accompaniment to students and researchers that generally involved with different field of study including modeling and control design for various example of application. There are also research on hardware design implementation which integrate both for simulation and experimental study as well as laboratory sessions available at a particular institution.

Mohamad Kamal A. Rahim
Md. Pauzi Abdullah
Faculty of Electrical Engineering
Universiti Teknologi Malaysia

2017 ELECTRICAL ENGINEERING SYMPOSIUM COMMITTEE

GENERAL CHAIR

PROFESSOR DR. MOHAMAD KAMAL A. RAHIM

CO-CHAIR

IR. DR. MD. PAUZI ABDULLAH

2017 ELECTRICAL ENGINEERING SYMPOSIUM MEMBERS

DR. KAMALUDIN MOHD. YUSOF

DR. SHAHARIN FADZLI ABD. RAHMAN

DR. YUSMEERAZ YUSOF

DR. MOHD. HAFIZI AHMAD

DR. NURUL EZAILA ALIAS

DR. ZULKARNAIN AHMAD NOORDEN

DR. MOHD. AFZAN OTHMAN

DR. MOHD. AMRI MD. YUNUS

DR. MOHD. RASHIDI SALIM

2017 ELECTRICAL ENGINEERING SYMPOSIUM SECRETARIAT STAFF

SABRINA ZAINAL ABIDIN

AZLINA MOHD. LAZIM

Mitigation of Voltage Sag and Harmonics using Unified Power Quality Conditioner (UPQC)

Syukur Bin Sulaiman
Faculty of electrical engineering
Universiti Teknologi Malaysia
Johor Bahru, Malaysia
syukur.sulaiman11@gmail.com

Dr. Ahmad Safawi Bin Mokhtar
Department of power
Faculty of electrical engineering
Universiti Teknolgi Malaysia
Johor Bahru, Malaysia
safawi@utm.my

***Abstract*—Power quality has become a main concern among electrical industry. The demand from the electrical user is high quality power supply continuously. Therefore, it is very important to protect the system from any disturbance so that the quality and reliability of the power system can be maintained. Voltage sags and harmonics are among the power quality problem that commonly occurred in distribution power system. These disturbances are caused by the increasing use of sensitive electronic equipment and non-linear load in electrical system which leads to the negative impact on distribution power system. Unified Power Quality Conditioner (UPQC) is one of the device that can offer the system to retain its power quality. Unified Power Quality Conditioner (UPQC) has the ability to mitigate most of the issues on the power system immediately with high speed precise response. The main purpose of this report is to implement the UPQC device with a proper controller to mitigate voltage sags and harmonics. MATLAB Simulink are used to shows that UPQC device has the potential to deal mutually with both supply voltage and load current imperfection. By implementing UPQC device, there is a reduction of percentage in sagging and total harmonic distortion to the value within the range set by IEEE standards. This show that the UPQC are able to restore sags and improve the current harmonics.**

***Keywords*—harmonics, voltage sag, modelling of UPQC, simulation**

I. INTRODUCTION (*HEADING 1*)

Nowadays, power quality issue has drawn attention from both utility side and the end user itself. This is because the increasing of usage of sensitive electronic equipment which is the biggest factor in the power quality problems. It is inconvenience to experience the power outages which affecting domestic, commercial, and industrial customer. This problem also could bring great financial losses especially for the industrial customer and also utility companies. It would be an operation interruption and cause the product quality reduction which results a lot of losses. On the side of utility companies, they need to supply a high quality of power supply to the consumers so that they would not experience any losses. Therefore, the expectation regarding the reliability of electrical power supply is necessary at this point.

Voltage sag and harmonics are the most common power quality problem that occur in the power system. These disturbances may affect the functionality of the equipment which is in a worst case it also could damage the system equipment. Power quality disturbances are come from the quality of current drawn by the load and the quality of supply voltage. Voltage sags occurred due to the fault in the distribution of transmission system while harmonics are caused by non-linear load.

There are several ways to improve the power quality in power system. Passive power filters is one of the method that can reduce the unwanted disturbance. Passive power filter are more economical to implement and it is a convenient way to suppress harmonics in distribution system. Furthermore, they can introduce some resonance in power system. As the result, Active Power Filter (APF) was introduced to overcome these problems.

However, they have some flaws in their performance which is limited to a certain type of load as they were custom designed for application [4] [5].

The ability of APF able to mitigate the voltage sags or swells and also reactive power in the distribution system and also harmonic suppression. APF are related with Custom Power Device. The most well-known CPD are Dynamic Voltage Restorer (DVR), Distribution Static Compensator (DSTATCOM) and Unified Power Quality Conditioner (UPQC) [7].

The best and most advanced device in CPD is UPQC as it is a combination between DVR and DSTATCOM. It has two voltage source inverter (VSI). One of VSI is connected in series and the other one is connected in shunt. UPQC is probably the best proposed device to deal with the both low quality of supply voltage and load current.

II. LITERATURE REVIEW

A. *Voltage Sag*

The voltage sags is defined as the reducing of the root means square (rms) voltage in the range between 0.1 and 0.9 per unit at the power frequency for the period of

0.5 cycles to 1 min by according to the IEEE standard 1159-1995 [9]. Voltage sags also can be defined as a temporary reduction between 10% and 90% of rms voltage at the power frequency for duration of 0.5 cycles to 1 minute [7] [8] [9] [10] [11]. Voltage sags is one of the most regular disturbance that is experienced by consumer. It is normally caused by short circuit or fault which can caused equipment failure in a network system. The energizing of heavy machines also can be the cause of voltage sag [12]. The fault happened in the distribution system can caused consumers to experienced voltage sag even the location of fault is far away. Voltage sag waveform, can be shown clearly in Figure 1

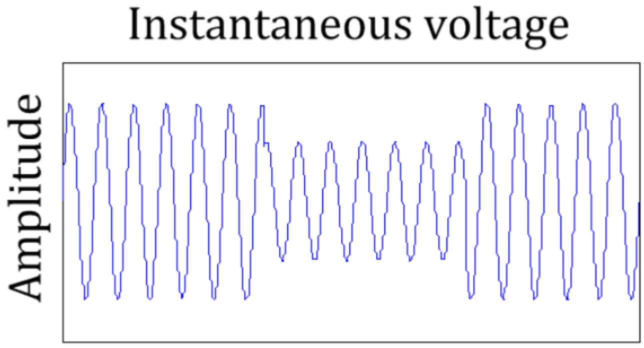

Figure 1: voltage sag waveform

B. Harmonics

Rapid used of non-linear load equipment can cause the electrical equipment to generate current harmonics [13]. WHEN non-linear load equipment connected with power system, the current waveform will transform to non-sinusoidal. This non-sinusoidal current waveform are the reasons for the voltage drop to the network system and produce voltage distortion [4] [16]. Basically, these harmonics produced from the combination of different frequency of various sine waves [5]. It causes the harmonics in the waveform and the waveform become distorted. Figure 2 show the harmonics distortion.

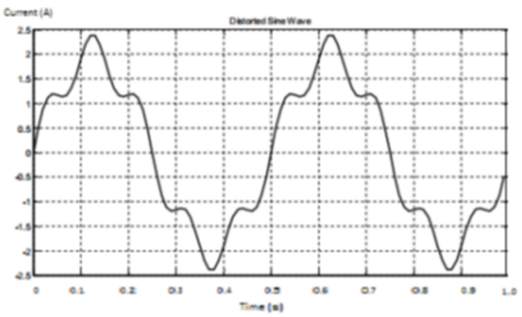

Figure 2: Harmonics Distortion

C. Unified power quality conditioner (UPQC)

Unified Power Quality Conditioner has excellent performance and widely used in the power system nowadays. It can deal with both voltage supply and load current imperfection mutually and it is the most advanced device in CPD. This is because UPQC is a combination between series and shunt Active Power Filter (APF). UPQC can solve various kinds of power quality issues such as harmonics, voltage sags, voltage swells, power factor correction, reactive power, power factor correction, and unbalanced current source [20]. Thus, this shows UPQC has the ability to overcome most of the problem related to power quality. UPQC has a precise identification of the disturbance signal and fast processing of reference signal and it show it reliability to improve power quality [3].

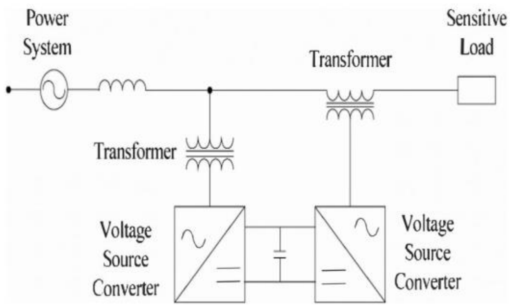

Figure 3: Basic Configuration of UPQC

Basic configuration of UPQC are shown in Figure 3. UPQC connected back-to-back with the DC capacitor and it consist of both series and shunt VSI. Other component in UPQC are high pass filter, low pass filter, and series and shunt transformer connected to power system.

VSI is connected in series in this system. It control voltage distortion by acting like DVR which is injecting voltage to the power system. In addition, it disable high frequency component produced by high frequency switching by using low pass filter and it used at series VSI.

On the other hand, shunt VSI is VSI shunt connected system. It has the ability to cancel harmonics currents at the load by acting like a current source and. It inject currents to the power system and also can correct the power factor and balance reactive current at load. High pass filter is apply with shunt VSI to absorb current switching ripple.

DC capacitor has two main purposes in this configuration which is to supply real power during the transient period by acting as energy storage elements and it is used to maintain DC voltage with a small ripple in steady state. Besides that, series and shunt transformer are being implemented in order to inject the compensation currents and voltage and make electrical isolation.

III. METHODOLOGY

A. Flow Chart of Project

Distribution system network can be design by using MATLAB Simulink. The network system is developed with the presence of fault and non-linear load and it will produce voltage sag and harmonics. Analysis can be done by using simulation. After that, the proposed device which is UPQC will be installed in the existing network. Lastly, UPQC and the controller will be execute with the existing network system to analyse the output. The project flow is shown in the flow chart in figure 4 below.

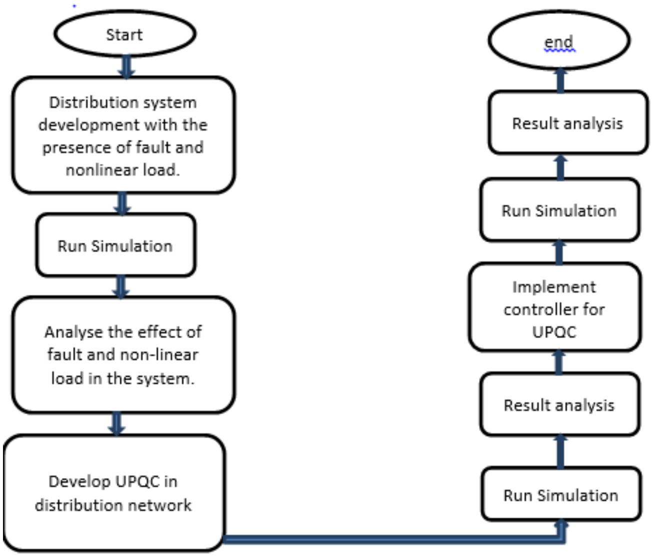

Figure 4: Research Flowchart

B. Simulation Model

Figure 5 below shows the single line diagram for network system with the addition of UPQC. This 3 bus system has been designed with Feeder A and Feeder B which are connected with different type of load. Feeder A connected to linear load while non-linear load is connected to the Feeder B. LG, LLG, and LLLG fault are introduced at Feeder. Hence, UPQC performance can be studied.

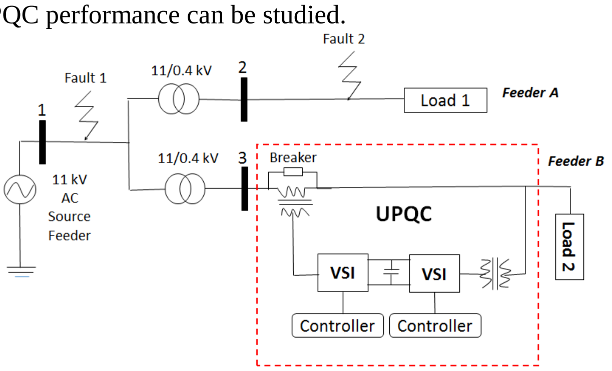

Figure 5: Single Line diagram for UPQC Model.

In this project, the system in single line diagram above is implemented into Simulink model in Matlab as shown in Figure 6. The simulation model is tested under 4 conditions which are normal condition (without fault and non-linear load), with fault condition (voltage sags), with non-linear load condition (harmonics) and lastly with UPQC condition. The voltage is measured at each feeder while load current is measured at Feeder B.

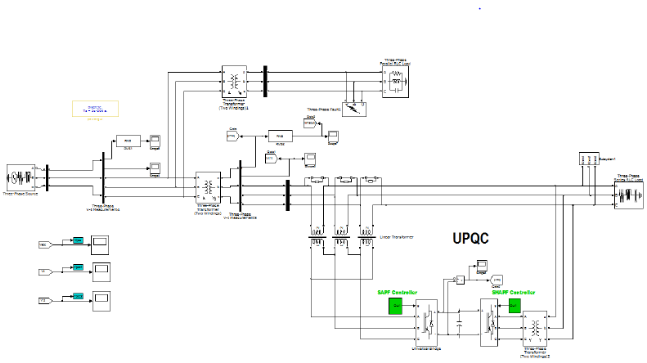

Figure 6: Simulink UPQC Model

C. Control Method for UPQC

Controlling method for UPQC for both shunt APF and series APF is same. The controlling method used is synchronous reference frame control or dq control. The controller configuration is shown as in the Figure 7. It uses abc to dq transformation to transform the current and voltage waveform at grid into a reference frame that rotates synchronously with grid voltage. The controlling would become easier as the control variables become dc values.

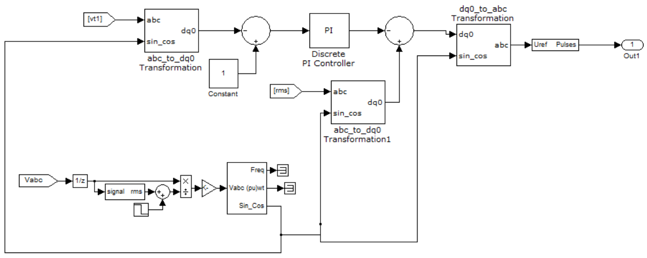

Figure 7: Series and Shunt APF Controller of UPQC

IV. SIMULATION RESULT

A. Effect of the three phase fault and non-linear load

Figure 8 shows the circuit of the system after three phase fault and non-linear load has been implemented.

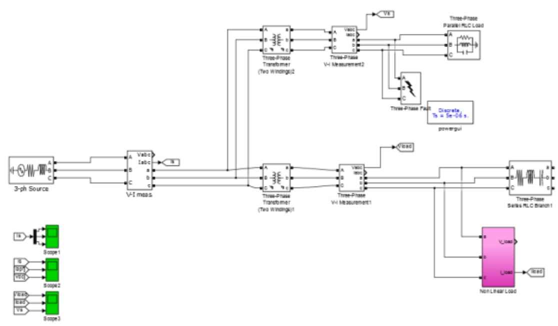

Figure 8: System with three phase fault and non-linear load.

Figure 9 and figure 10 below show the results of the waveform after implementation of three phase fault and non-linear load respectively.

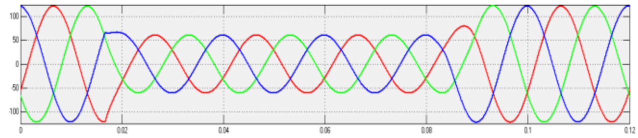

Figure 9: Voltage Sag Because Of the Fault

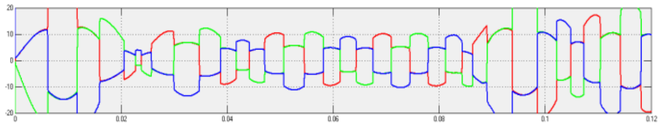

Figure 10: Harmonics Because Of Non-Linear Load

B. Voltage sag and harmonics mitigation after UPQC

Figure 11 shows the circuit of the UPQC with appropriate controller is being implemented in order to mitigate the voltage sag and harmonics

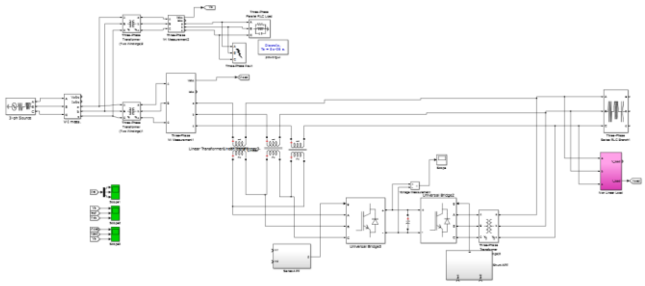

Figure 11: Circuit of UPQC Device

The figure 12 shows the result of the waveform of the system after UPQC device has been implemented into the system.

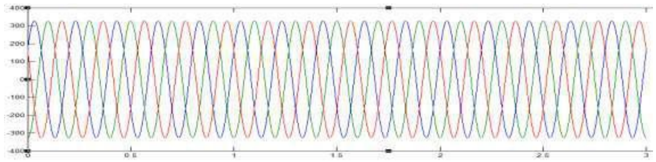

Figure 12: Voltage Waveform after UPQC

V. CONCLUSION

Furthermore, UPQC device has been successfully installed in the system in order to improve the power quality issues. The device has proved its ability to improve voltage sags and harmonics that are presented in the system. Results of the voltage and current waveform obtained by simulation show that UPQC can restore the sags of voltage and turned the non-sinusoidal current waveform back to the ideal waveform.

REFERENCE

[1] Dugan, R. C., McGranaghan, M. F and Beaty, H. W. Electrical Power System Quality. New York: McGraw-Hill, 1996. [2] IEC Std. 61000-2-1, Electromagnetic compatibility (EMC) - Part 2: Environment - Section 1: Description of the environment - Electromagnetic environment for low-frequency conducted disturbances and signalling in public power supply systems

[3] Faridullah Kakar. "Power Quality Improvement by Dynamic Voltage Restorer and Unified Power Quality Conditioner Using Fuzzy Logic", Degree of Master, Universiti Teknologi Malaysia; 2015

[4] M.Izhar, C.M.Hadzer, Sfrudin M, S.Taib, S.Idris, National Power & Energy Conference (PECon) 2004 Proceedings, Kuala Lumpur, Malaysia, "Performance for Passive and Active Power Filter in Reducing Harmonics in the Distribution System", 2004

[5] Anil Baitha, Dr Nitin Gupta, 2015 IEEE International Conference on Technological Advancements in Power & Energy, "A Comparative Analysis of Passive Filters for Power Quality Improvement", 2015

[6] Joaquin Cicedo, Felipe Nararro, Edwin Rivas, Francisco Santamaria, Electromagnetic Compatibility and Interference Group (GEM) Universidad Distrital Francisco Jose de Caldas Bogota, Columbia, "Voltage Sag Characterization with Matlab/Simulink", 2012

[7] Park Sang-Young, Park Jong-Keun, Power Engineering Society Winter Meeting, 2001, IEEE, "The Modelling and Analysis of Shunt Type Custom Power Device", 2001

[8] Rosli Omar, Nasrudin Abd Halim, ARPN Journal of Engineering and Applied, "Mitigation of Voltage Sags/Swells Using Dynamic Voltage Restorer (DVR), vol.4, No. 4, June 2009

[9] IEEE Recommended Practice for Monitoring Electric Power Quality, IEEE Std. 1159, 1995

[10] E.Babaei, M. Farhadi Kangarlu, IEEE Electrical Power and Energy Conference, "Three Phase Cross-Phase Voltage Sag Compensator to Compensate Balance/ Unbalanced Voltage Sags and Phase Outages in Distribution Systems", 2011

[11] IEEE Standards Coordinating Committee 22 on Power Quality. IEEE Std 1159. IEEE Recommended Practice for monitoring electric power quality. 1995

[12] Surya Hardi, I. Daut, The 4th International Power Engineering and Optimization Conf. (PEOCO2010), Shah Alam, Selangor, Malaysia, Sensitivity of Low Voltage Consumer

Equipment to Voltage Sags, 23-24 June 2010

[13] Ravi Kumar Jujjuvarapu, B.Basavaraja, International Journal of Power System Operation and Energy Management ISSN (PRINT): 2231 – 4407, Volume-1, Issue-4, "Modeling and Estimating Voltage and Current Harmonics of Variable

Speed Drive (VSD)", 2012

[14] Pinky Saxena, Rajan Chaudhary, Advance in Electronic and Electric Engineering.

ISSN 2231-1297, Volume 3, Number 4 (2013), pp. 503-508. Research India Publications, "Harmonics Modeling, Activity Analysis of Equipments with Switch Mode Power Supply and Reduction on Matlab/ Simulink", 2013

[15] K.R.Valluvan, A.Vetrivel, A.M.Natarajan, Jovitha Jerome, Proceedings of the 2008 International Conference on Computing, Communication and Networking (ICCCN 2008), "Minimisation of Harmonics Amplification Due to Resonance by Relocation of Capacitors Using ADALINE on a DSP", 2008

[16] K.R.Suja, Jacob Raglend, 2013 International Conference on Circuits, Power and Computing Technologies [ICCPCT-2013], "Fuzzy Based Unified Power Quality Conditioner for Power Quality Improvement", 2013

Power Flow Solution by Incorporating FACTS Device

Mariam Khalida Mohd Zakir
Faculty of Electrical Engineering
Universiti Teknologi Malaysia
Johor Bahru, Malaysia.
mariamzakir.29@gmail.com

Zaniah Muda
Department of Electrical Power Engineering
Faculty of Electrical Engineering
Universiti Teknologi Malaysia
Johor Bahru, Malaysia.
zaniah@fke.utm.my

***Abstract*— Large reactive flows are the result of high voltage difference between buses. This in return will lead to increased real power losses and possibly an increased possibility of voltage collapse. Land requirements, permit granting and cost considerations are some of the constraints why the constructions of new power grids and transmission lines is not the best choice. FACTS devices are capable of controlling the active and reactive power flows in a transmission line by controlling its series and shunt parameters. Thyristor Controlled Series Capacitor (TCSC) is used in AC transmission system to provide smooth control of series reactance to increase the capability of the reactive power compensation of the transmission line. The aim of this project is to reduce transmission losses and thus improve the power flow. The TCSC is modelled in series with the line of the corresponding buses. The optimal location and the optimal parameter setting of TCSC will be determined. The results of power flow on the IEEE 9-Bus & 30-Bus system after incorporating TCSC have been obtained with the help of MATPOWER.**

***Keywords*— Transmission lines; FACTS device; TCSC; transmission losses; load flow; Newton Raphson; MATPOWER**

I. INTRODUCTION

Among the most broadly studied themes in the power system community nowadays is the optimal power flow problems [1]. The aim of power flow is to choose the ideal operation condition of the power system by fulfilling the specific limitations. Optimal power flow is one of the problem under economic dispatch which considers a few parameters, for example, transformer tap change, generator voltage, static VAr compensator (SVC) and incorporates requirements such as transformer loading limits, transmission line, bus voltage limit, and stability margin limit [2]. The aim of the optimal power flow is to minimize total generation cost, improve bus voltage profile and reduce transmission lost while satisfying the given transmission and security constraints.

Large reactive flows will result when the voltage between buses different is high. This in return will lead to increased real power losses and possibly an increased possibility of voltage collapse. It is important for the system to be capable to work on the specified limits when a contingency occurs, without effecting the overall operation of the system [3]. Higher voltages are selected for transmission to keep the losses in an economically justifiable relationship to the real power. Reduction of reactive power becomes an essential factor for obtaining efficient operation. Hence, voltage and reactive power control (VAr) is vital. [4] In order to achieve efficient and reliable operation of power system, the voltage and reactive power should satisfy the following objectives [5]; voltages at all terminals of all equipment in the system are within limits; system stability is enhanced to maximize utilization of the transmission system; the reactive power flow is minimized so as to reduce real and reactive power losses. This ensures that the transmission system operates mainly for active power.

Incorporating FACTS devices into the power system is one of the best method in tackling these problems as FACTS devices can simultaneously control the active and reactive power control and is flexible to voltage-magnitude control. FACTS equipment is used to regulate key power system parameters, based on the incorporation of power electronic devices into the high-voltage side of the power network to make it electronically-controllable [6]. This is due to their fast control features and flexibility. With the aid of FACTS technology such as STATCOM, SVC, SSSC, TCSC and UPFC, the bus voltages, phase angle and line impedances in the power system can be controlled quickly [2]. TCSC is the FACTS device chosen for this paper.

II. LITERATURE REVIEW

A. *Flexible AC Transmission System (FACTS)*

FACTS is an acronym for Flexible AC Transmission System. The concept of FACTS was first discussed by Hingorani, N.G. in 1988. IEEE defines FACTS controller as a power electronic-based system and other static equipment that provide control of one or more AC transmission system parameters [10]. FACTS controllers are invented and implemented in power system to enhance the systems performance in terms of stability, voltage regulations, power transfer capability and much more. Flexible AC Transmission Systems (FACTS) has been proven to provide technical solution to the current system operating challenges. The use of FACTS devices is aimed to help the power system provide better operation. FACTS devices improve efficiency and transmission quality by supplying inductive and reactive power. [11]. It is a great idea to invest in FACTS devices as they can be controlled automatically. Plus, they provide reduction in implementation time than the need to construct new transmission lines [13]. In general, FACTS Controllers can be divided into four types which are series controllers, shunt controllers, combined series-series controllers and combined series-shunt controllers.

B. *Thyristor Controlled Series Compensator*

TCSC is an acronym for Thyristor Controlled Series Compensator. TCSC is a FACTS device whose main application is to maximize active power transfers by effectively modulating the electrical length of a transmission line [6]. TCSC is a capacitive reactance compensator which consists of a series capacitor bank shunted by thyristor controlled reactor in order to provide a smoothly variable series capacitive reactance [10]. TCSC is an economical and effective method of solving issues such as dynamic stability, transient stability, steady state stability and voltage stability in transmission lines. Through the introduction of a thyristor controlled capacitor in series with the transmission line, TCSC can control the line impedance. [13]. The main circuit of a TCSC is shown in Figure 1. The TCSC consists of three main components: capacitor bank C, bypass inductor L and bidirectional thyristors SCR1 and SCR2.

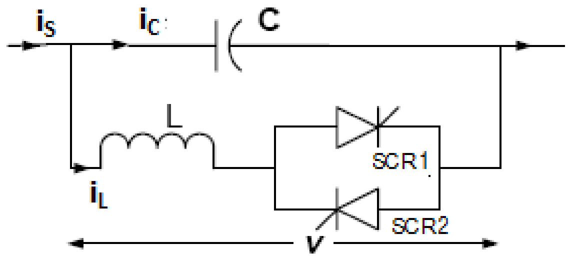

Fig. 1. TCSC Configuration

C. *Load Flow Solution*

When solving large power systems, load flow studies are increasingly used for purposes such as outage security assessment and for more complicated calculations such as optimization and stability [17]. Power flow analysis gives the voltage and phase angle at each bus which is further used to determine the power injection at all the busses along with power flow through interconnected nodes [8]. All these system parameters are needed for determining the optimal location as well as optimal capacity of proposed generation station, substation and new lines. In order to avoid the system unbalance condition, the voltage should be maintained within its tolerance limit with minimized line transmission losses.

Four quantities are associated with each bus. These are voltage magnitude |V|, phase angle δ, power P, and reactive power Q. [16] For this project, Newton-Raphson method was selected to be used in power flow analysis as it is mathematically superior to the Gauss- Seidel, less prone to divergence with ill- conditioned problems and it is more efficient and practical for large system [3].

D. *Power Flow Capabilities*

The power transfer between two ends of uncompensated transmission line is given by Equation 1:

$$P = \frac{V_S V_R}{X_L} sin\delta \qquad \textbf{(1)}$$

Where Vs and Vr are sending end and end voltages respectively, X_L is transmission line reactance (loss is neglected) and δ is the power angle. The power transfer through transmission line with series compensated by using TCSC is given by Equation (2): [14]

$$P = \frac{V_S V_R}{X_L + X_{TCSC}} sin\delta \qquad \textbf{(2)}$$

III. METHODOLOGY

The project starts by finding the suitable test system. For this project, an IEEE 9 bus system and an IEEE 30 bus system will be used as the test systems. Both test systems will be simulated using MATPOWER to obtain the power flow analysis. This first simulation will be done without incorporating any FACTS devices into the system. Several parameters of the power system such as the voltage magnitude at each bus, the active and reactive power flow, and total real and reactive power losses in the system are obtained by Newton Raphson method. The power flow result is recorded and tabulated.

Second step is to modify the original test system by increasing reactive load demand at one of the buses to create low voltage profile. Low voltage profile will then lead to increase in power losses. The reactive load is steadily increased until the bus voltage approach the bus voltage limit which is 0.9 p.u. Voltage control in an electrical power system is important to reduce transmission losses and to maintain the ability of the system to withstand and prevent voltage collapse. Besides that, we need to prevent voltage collapse for proper operation of the electrical power equipment to prevent damage such as overheating of generators and motors. This modified system will be called as the problematic system. The system will be simulated in MATPOWER and the power flow result is recorded and tabulated. The result of the problematic system should show higher transmission losses compared to the original system.

Next, the best location to install TCSC and the suitable value of ‘k’ will be determined. The aim of the project is to reduce transmission losses therefore, TCSC will be placed in the branch with the highest reactive loss based on the simulation result of the problematic system. The value of k will be varied between -0.7 to 0.2 of the transmission line.

After the best location and setting of the TCSC have been required, the problematic bus system will be simulated again with incorporating the TCSC. The result of the power system is recorded and tabulated. The only difference between this simulation and previous simulation is the installation of TCSC into the test system. The output of the simulation after installing TCSC will be observed and tabulated. The transmission losses should be reduced and the voltage profile is improved. Finally, the performance of the bus system with and without TCSC devices will be compared and analysed in terms of voltage profile and power losses. Figure 2 illustrates the overall workflow of the project.

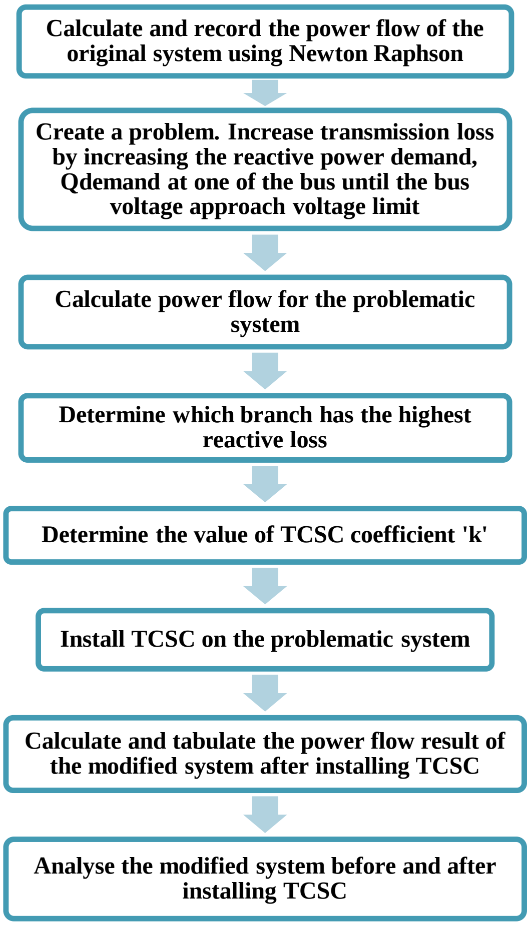

Fig. 2. Project Workflow

A. TCSC Modelling

The TCSC can serve as the capacitive or inductive compensation respectively by directly modifying the reactance of the transmission line. In this paper, the model of the TCSC is developed to be suitable for steady-state. It is modeled as variable reactance connected in series with transmission line. The model of transmission line with a TCSC connected between bus-i and bus-j is shown in Figure 3. [8]

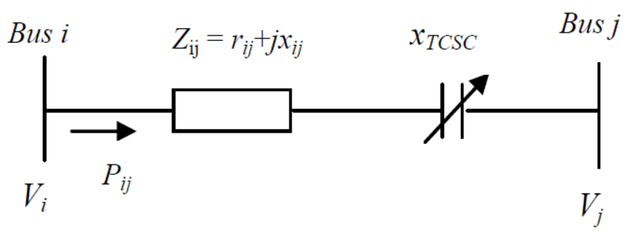

Fig. 3. Transmission line with TCSC

The rated value of TCSC is a function of the reactance of the transmission line where the TCSC is installed:

$$X_{line} = X_{ij} + X_{TCSC}$$

Where,

$$X_{TCSC} = k_{TCSC} + X_{line}$$

X_{line} is the overall line reactance between bus-i and bus-j. X_{TCSC} is the reactance of TCSC and k_{TCSC} is the coefficient which represents TCSC compensation level ($-0.7 \leq k_{TCSC} \leq 0.2$). The working range of reactance of TCSC will be fixed between $-0.7X_{line}$ and $0.2X_{line}$.

IV. RESULT & DISCUSSION

IEEE 9 bus system as shown in Figure 4 below is used for the preliminary test. The preliminary test system consists of 1 slack bus, 2 generator bus and 6 load buses. The configuration for the 9 bus power system is illustrated in Figure 4. The voltage and angle of load buses are set as V=1.0 p.u and δ=0° as the initial assumption. The angle of generator bus is also set to δ=0° as initial assumption. All the system data are in per unit system with 100 MVA base. Voltage limits, line thermal limits, generator power limits with other inequality constraints are considered in this test system. The voltage magnitude limit of each bus is within 0.9 pu and 1.1 pu.

A. Result for original test system

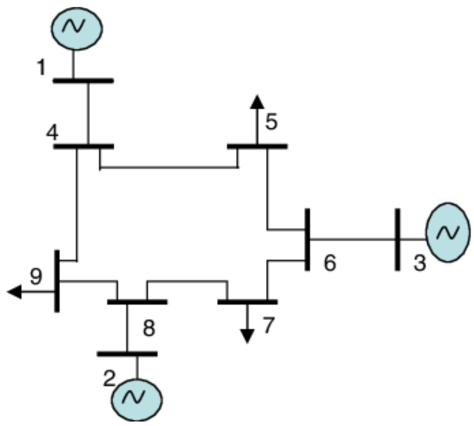

Fig. 2. IEEE 9 bus system

Table 1. Bus result for original system

Bus no	Voltage Mag (p.u)	Voltage Ang (deg)	Generation P (MW)	Generation Q (MVAr)	Load P (MW)	Load Q (MVAr)
1	1.100	0.000	89.80	12.94	-	-
2	1.097	4.893	134.32	0.05	-	-
3	1.087	3.249	94.19	-22.62	-	-
4	1.094	-2.463	-	-	-	-
5	1.084	-3.982	-	-	90.00	30.00
6	1.100	0.602	-	-	-	-
7	1.089	-1.197	-	-	100.00	35.00
8	1.100	0.905	-	-	-	-
9	1.072	-4.616	-	-	125.00	50.00
Total			**318.31**	**-9.63**	**315.00**	**115.00**

Table 2. Branch result for original system

Branch	From Bus	To Bus	From Bus Injection		To Bus Injection		Line loss	
			P (MW)	Q (MVAr)	P (MW)	Q (MVAr)	P (MW)	Q (MVAr)
1	1	4	89.80	12.94	-89.80	-9.02	0	3.92
2	4	5	35.22	-3.90	-35.04	-13.87	0.181	0.98
3	5	6	-54.96	-16.13	55.97	-22.18	1.01	4.40
4	3	6	94.19	-22.62	-94.19	27.28	0	4.66
5	6	7	38.22	-5.10	-38.07	-18.68	0.149	1.26
6	7	8	-61.93	-16.32	62.21	0.82	0.279	2.36
7	8	2	-134.32	9.32	134.32	0.05	0	9.36
8	8	9	72.11	-10.14	-70.72	-18.94	1.394	7.01
9	9	4	-54.28	-31.06	54.58	12.92	0.295	2.51
Total							**3.307**	**36.46**

Table 1 and Table 2 shows the power flow results for the bus and branch of the original test system. The system reactive load demand will be increased to create a system with high transmission losses so that TCSC can be implemented later on to prove the effectiveness of TCSC in improving the power flow of the system.

B. Result for modified system

Reactive load demand at bus 9 was increased from 50 MVAr to 220 MVAr. This will lead to increase in transmission losses.

Table 3. Bus result after increasing reactive power (before installing TCSC)

Bus no	Voltage		Generation		Load	
	Mag (p.u)	Ang (deg)	P (MW)	Q (MVAr)	P (MW)	Q (MVAr)
1	1.1	0	91.71	133.88	-	-
2	1.1	4.806	135.97	75.39	-	-
3	1.087	2.868	95.56	12.29	-	-
4	1.031	-2.670	-	-	-	-
5	1.035	-4.457	-	-	90.00	30.00
6	1.082	0.140	-	-	-	-
7	1.058	-1.669	-	-	100.00	35.00
8	1.060	0.627	-	-	-	-
9	0.903	-4.756	-	-	125.00	220.00
Total			**323.24**	**221.56**	**315.00**	**285.5**

Table 4. Branch result after increasing reactive power (before installing TCSC*)*

Branch	From Bus	To Bus	From Bus Injection		To Bus Injection		Line loss	
			P (MW)	Q (MVAr)	P (MW)	Q (MVAr)	P (MW)	Q (MVAr)
1	1	4	91.71	133.88	-91.71	-121.34	0	12.54
2	4	5	34.29	-18.58	-34.08	2.83	0.205	1.11
3	5	6	-55.92	-32.83	57.12	-2.04	1.206	5.26
4	3	6	95.56	12.29	-95.56	-7.69	0	4.60
5	6	7	38.44	9.73	-38.24	-31.97	0.199	1.69
6	7	8	-61.76	-3.03	62.06	-11.20	0.292	2.47
7	8	2	-135.97	-62.91	135.97	75.39	0	12.49
8	8	9	73.91	74.11	-69.98	-84.00	3.930	19.77
9	9	4	-55.02	-136.00	57.43	139.92	2.407	20.46
Total							**8.239**	**80.38**

From the result in Table 3 and Table 4, it can be observed that the total transmission losses for the modified system have increased after the reactive load demand at bus 9 was increased. The total real power loss has been escalated from 3.307 MW to 8.239 MW and reactive power has increased from 36.46 MVAr to 80.38 MVAr. The total loss of real power has shown a hike of 149.14% while the total loss of reactive power has shown an increase of 120.46%. The bus voltage also has been affected. From the original system, the bus voltage at bus 9 is 1.072 p.u but after the reactive load demand has been increased, the bus voltage at bus 9 has subsided to 0.903 p.u. From Table 4.4, line 9-4 shows the highest reactive power loss which is 20.46 MVAr.

C. System after incorporating TCSC

After the line with the highest transmission loss is identified, the TCSC is now ready to be incorporated into the problematic system. The value of the TCSC coefficient ‘k’ has been varied from -0.7 to 0.2. Value of k=-0.7 has shown the best result for reducing real power and reactive power loss. Table 5 and 6 shows the power flow result of the system after using TCSC.

Table 5. Bus result after incorporating TCSC

Bus no	Voltage		Generation		Load	
	Mag (p.u)	Ang (deg)	P (MW)	Q (MVAr)	P (MW)	Q (MVAr)
1	1.100	0	91.26	145.59	-	-
2	1.100	6.220	135.59	45.83	-	-
3	1.082	3.836	95.12	3.53	-	-
4	1.025	-2.672	-	-	-	-
5	1.030	-4.127	-	-	90.00	30.00
6	1.081	1.105	-	-	-	-
7	1.068	-0.360	-	-	100.00	35.00
8	1.077	2.117	-	-	-	-
9	0.979	-2.694	-	-	125.00	220.00
Total			**321.97**	**194.95**	**315.00**	**285.00**

Table 6: Branch result after incorporating TCSC

Branch	From Bus	To Bus	From Bus Injection		To Bus Injection		Line loss	
			P (MW)	Q (MVAr)	P (MW)	Q (MVAr)	P (MW)	Q (MVAr)
1	1	4	91.26	145.59	-91.26	-131.54	0	14.06
2	4	5	27.19	-18.81	-27.06	2.88	0.138	0.74
3	5	6	-62.94	-32.88	64.47	-0.39	1.527	6.66
4	3	6	95.12	3.53	-95.12	1.01	0	4.53
5	6	7	30.65	-0.61	-30.54	-22.59	0.109	0.93
6	7	8	-69.46	-12.41	69.82	-1.66	0.361	3.06
7	8	2	-135.59	-35.25	135.59	45.83	0	10.58
8	8	9	65.77	36.91	-63.75	-59.15	2.018	10.15
9	9	4	-61.25	-160.85	64.07	150.35	2.816	7.18
Total							**6.969**	**57.89**

After the installation of TCSC, it can be seen that the total real power loss of the system has been significantly reduced from 8.239 MW to 6.969 MW. Meanwhile, the total reactive power loss is reduced from 80.38 MVAr to 57.89 MVAr. The results display a 15.41% reduction in total real power loss while the total reactive power loss shows a 27.98% reduction. Figure 5 shows the total line losses before and after incorporating TCSC into the system. The voltage profile of respective bus has also shown improvement which is from 0.903 p.u to 0.979 p.u The aim of optimal power flow is to keep the voltage variation between buses to be minimal. This is to avoid large reactive power flow between buses. This is because large reactive power flow will lead to high real power loss. Therefore, the voltage variation between buses needs to be minimal. In this system, the ideal voltage value would be around 1.00 p.u.

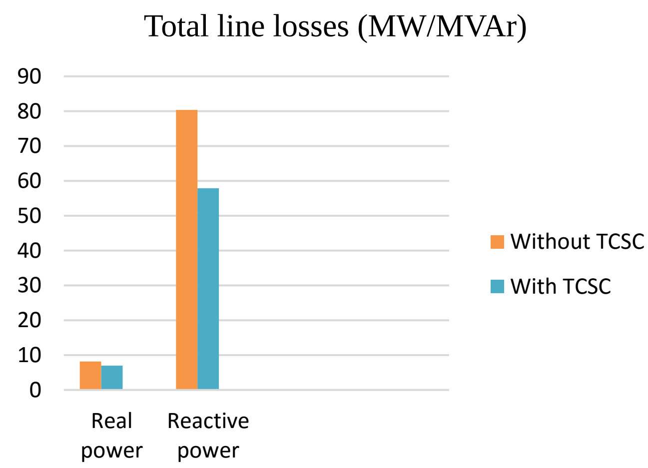

Fig. 3. Total line losses

V. CONCLUSION

As power flow continues to develop, the system will become more complex to operate. Hence, this will prompt the power system to become less secure for major outages. This would include excessive reactive power in different parts of the system, inadequate control of large power flows, large dynamic swings between various parts of the system and leads to higher transmission losses and also the incapability to utilize the maximum capacity of the transmission interconnections.

With the new technology and by using the latest power electronic equipment and methods, these problems can be solved by upgrading the existing transmission lines by installing FACTS devices in the system. Thyristor Controlled Series Compensator (TCSC) has been incorporated into an IEEE 9 bus system. TCSC was installed on the branch with the highest line loss with k_{TCSC}= -0.7. Based on the simulation results, the transmission losses have been successfully reduced.

REFERENCES

[1] R.-F. C. Zwe-Lee Gaing, "Security-Constrained Optimal Power Flow by Mixed-Integer," in 2006 IEEE Power Engineering Society General Meeting, 2006.

[2] C. R. B. P. Xiao-Ping Zhang, Flexible AC Transmission Systems: Modelling and Control, Berlin Heidelberg: Springer Heidelberg New York Dordrecht London, 2012.

[3] L. S. Tarek Bouktir, "Optimal Power Flow of the Algerian Electrical Network using an Ant Colony Optimization Method," Leonardo Journal of Sciences, no. 7, pp. 43-57, 2005.

[4] S. P. K. S. a. B. R. S. Jaganathan, "Application of Multi-Objective Technique to Incorporate UPFC in Optimal Power Flow using Modified Bacterial Foraging Technique," International Journal of Computer Applications, vol. 13, no. 2, pp. 18-24, 2011.

[5] K. R. a. M. Rajaram, "Optimal location of FACTS devices using Improved Particle Swarm Optimization," International Journal of Electrical Power & Energy Systems, vol. 49, pp. 333-338, 2013.

[6] C. E. M.-S. a. R. J. T. R. D. Zimmerman, "MATPOWER: Steady-State Operations, Planning, and Analysis Tools for Power Systems Research and Education," Power Systems, IEEE Transactions, vol. 26, no. 1, pp. 12-19, 2011.

[7] Y. R. S. Prashant Kumar Tiwari, "An Efficient Approach for Optimal Placement of TCSC in Double Auction Power Market," International Journal of Electronics and Electrical Engineering, vol. 6, no. 8, p. 322, 2012.

[8] T. Orfanogianni, "Flexible software environment for steady-state power flow optimization with series FACTS devices.," Zurich, 2000.

[9] I. M. W. Mustafa, Power System Analysis, Fifth Edition, Desktop Publisher.

[10] M. B. M. a. S. M. a. S. Maheswarapu, "Security Constraint Optimal Power Flow (SCOPF)-A Comprehensive Survey," International Journal of Computer Applications, vol. 11, pp. 42-52, 2010.

[11] M. B. M, "Security Constraint Optimal Power Flow (SCOPF) – A," International Journal of Computer Applications, vol. 11, no. 6, p. 11, 2010.

[12] Keerati Chayakulkheeree and Weerakorn Ongsakul, "Multi-Objective Optimal Power Flow Considering System," GMSARN International Journal, vol. 1, pp. 1-6, 2008.

[13] S. H. L. U. T. a. H. X. K. Mani Chandy, "A Simple Optimal Power Flow Model with Energy Storage," in 49th IEEE Conference on Decision and Control (CDC), Hilton Atlanta Hotel, Atlanta, GA, USA, 2010.

[14] D. M. Y. Hassan, Power System Control, Johor : Desktop Publisher, 2012.

[15] E. A. a. C. R. F.-E. H. Amhriz-PBrez, "Advanced SVC Models for Newton-Raphson Load," IEEE Transactions on Power Systems, vol. 15, no. 1, pp. 129-136, 2000.

[16] N. G. H. a. L. Gyugyi, Understanding FACTS concepts and technology of flexible AC transmission systems, New York: IEEE Press, 2000.

[17] C. T. a. B. Eua-Arporn, "Self-adaptive Differential Evolution Based Optimal Power Flow for Units with Non-smooth Fuel Cost Functions," Journal of Electrical Systems, vol. 3, no. 2, pp. 88-99, 2007.

[18] N. K. Easwaramoorthy, "Solution of Optimal Power Flow Problem Incorporating Various FACTS Devices," International Journal of Computer Applications, vol. 55, no. 4, p. 7, 2012.

[19] M. V. Deshpande, Electrical Power System Design, New Delhi: McGraw-Hill, 2000.

Transmission Line Fault Detection Using Wavelet

Najatul Shahira Bt Hanif
Faculty of Electrical Engineering
Universiti Teknologi Malaysia
Johor Bahru, Malaysia.
najatulshahira@gmail.com

Zaniah Bt Muda
Department of / Centre of
Faculty of Electrical Engineering
Universiti Teknologi Malaysia
Johor Bahru, Malaysia.
zaniah@fke.utm.my

***Abstract*— Fault diagnosis is a dominant area of scrutiny for transmission line system and always been very challenging task. Significant high frequency transient signal will appear in current and voltage waveform when there is any fault occurs in transmission line. This paper introduces wavelet transform as a method for fault detection and classification in transmission line. The discrete wavelet transform (DWT) is applied for decomposition of fault transient because its ability to extract information from transient signal, simultaneously both in time and frequency. Computing simulation using MATLAB software has been conducted as transmission line model is design and various faults is injected using fault toolbox. Simulation result indicates both classification and localization of fault. Four different type of fault which is single line to ground fault (SLG), line to line fault (L-L), double line to ground fault (DLG) and three phase fault (3P) can be recognized clearly by analysis the value of their standard deviation. It is found that the proposed method gives adequate result and will be very practical in development of protection in power system**

Keywords—wavelet transform; transmission line; MATLAB; transmission line fault ; three phase

I. INTRODUCTION

Transmission line is a vital segment in power system. Massive number of fault occurs in transmission line. In order to maintain the system stability and reliability it is essential that fault signal has to be analyzed meticulously. If fault is not properly recognized and detached , widespread damage or power system blackout may take place [1]. Basically, a fault occurs when two or more conductors come in contact with each other or to ground. The behavior of protective device may change with the various type of load such as linear and non-linear load connected with distribution system[1]. In three phase system , transmission line fault can be categorized as Single line-to ground faults, Line-to-line faults, Double line-to-ground faults, and three phase faults [2].

There are multiple technique used for fault detection and classification in transmission line including travelling wave approached , Kalman filtering , Neural network and Fourier analysis [3] . Fourier analysis are the most common method used for this purposes , however sometimes it is not precise enough [4] . In other way , neural-network show a great result in fault detection and classification but its drawback it required considerable amount of training effort for good performance , especially under wide variation of operating condition such as system loading level and fault resistance [3] . Wavelet transform is selected as the effective method because its ability to localize perfectly in time-frequency [5] .

II. LITERATURE REVIEW

A. Wavelet Analysis

Wavelet transform have been used widely in multi-scale representation and analyzing signal. The wavelet analysis procedure is adopt to wavelet prototype function known as 'mother wavelet'[6].Wavelet words is originate from the requirement that they should be integrated to zero, 'waving' above and below the x-axis [7] . Wavelet is a oscillation wave with amplitude that start with zero and increased that decreased back to zero. Basic wavelet can be expressed in mathematically as in equation (1) and (2)

$$\psi \in L^2(R) \tag{1}$$

$$\int_{-\infty}^{+\infty} \psi(t)dt = 0 \tag{2}$$

A wavelet transform decomposes transients into a series of wavelet component and localized in both frequency [7]. Analysis will decompose in to low and high frequency component. Low frequency component is a high-scaled decomposition while high frequency component is low-scaled decomposition [8].

Two important concept used in wavelet are scaling and shifting. Scaling is a stretching and shrinking signal in time, while shifting is a delaying or advancing the concept of wavelet along the signal. There are numerous type of wavelet such as Harr, Daubechies 4, Daubechies 8, Coifle 3, and Symmlet 8 [7] . Different wavelet have different purposes and different analysis.

B. Discrete Wavelet Transform

In a discrete wavelet transform (DWT), a time-scale representation of a digital signal is obtained using digital filtering techniques. In this case, filters of different cut-off frequencies are used to analyze the signal at different scales [8] .In wavelet analysis, approximations and details become the main concern

.The filtering process, at its most basic level, shows in Fig 1.

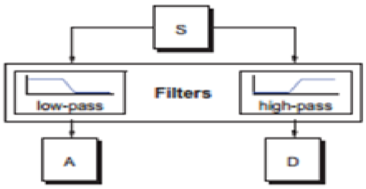

Fig. 1. Filtering process [9]

DWT is defined as:

$$C(j,k) = \sum_{n\in Z} s(n)gf,k(n) \qquad (j \in N, k \in Z) \tag{3}$$

where, s(n) is the signal to be analyzed and gj,k(n) is discrete wavelet function, which is defined by

$$g_{j,k}(n) = a_0^{-\frac{j}{2}} g(a_0^{-j} n - kb_0) \tag{4}$$

Select a_0 =2 , and b_0=1, the family of scaled and shifted mother wavelets constitute an orthonormal basis of I2(Z) (set of signals of finite energy). When simply choose a_0 =2 , and b_0=1, a dyadic-orthonormal wavelet transform is obtained [9].With this choice, there exists an elegant algorithm, the multi resolution signal decomposition (MSD) technique which can decompose a signal into levels with different time and frequency resolution [9].

C. Continous Wavelet Transform

Continuous wavelet transform is defined as:

$$C\big(a,b; f(t),\psi(t)\big) = \int_{-\infty}^{\infty} f(t)\frac{1}{\sqrt{a}}\psi * \left(\frac{t-b}{a}\right) dt \tag{5}$$

'a' is a scale parameter, b is the position (time) parameter while f(t) is the signal being transformed and ψ*(t) is the complex conjugate of ψ(t) [10]. Fundamentally, CWT compares the signal f(t) with wavelet function representing different scale and time position [10] .Wavelet is small wave that refers to the condition that this (window) function is of finite length.

The term mother suggests that the functions with different region of support that are used in the transformation process are derived from one main function, or the mother wavelet. [11] .The consequences of the transform are the Fourier coefficients, which when multiplied by a sinusoid of frequency yield the constituent sinusoidal components of the original signal [11] . Graphically, the process looks like Fig. 2.

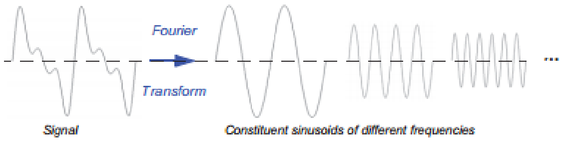

Fig. 2. Process when signal are multiplied by a sinusoid of frequency [11]

D. Mother Wavelet

The wavelet analysis procedure is to adopt a wavelet prototype function, called an analyzing wavelet or mother wavelet [12]. There are many families of wavelet that are available such as Haar [13], Daubechies [13], Biorthogonal [13], Coiflets [13], Symlets [13], Morlet [13], Mexican Hat [13], and Meyer [13]. This study applies Daubechies wavelet (db4). Daubechies wavelet is orthogonal and compactly supported wavelet thus it making discrete wavelet analysis practicable. The name of Daubechies family is written in dbN, where N is order and db are surname [13]. The figure below shows graphical of db at each level [13].

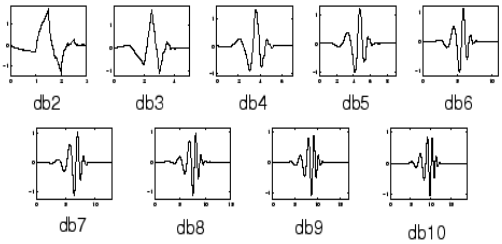

Fig. 3. Daubechies Wavelet [13]

III. PRORPOSED TEST SYSTEM

The single line diagram of the simulated power network is shown in figure below

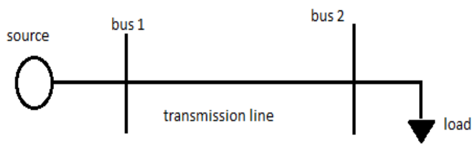

Fig. 4. Single line diagram of the power system.

Power system describe in this paper consist of three phase voltage source , transmission line and three phase load as shown in figure . Three phase resistive-inductive load is used in this study. The details of load are provided in table below.

TABLE I. MODEL PARAMETER

No.	Parameter	RL Load
1	Frequency	50 Hz
2	Voltage	500kV
3	Active Power	800kW
4	Reactive Power	600MVar

The transmission line for this system is measured for three different lengths which is 75km, 150km and 300km. It has been considered have three part having (25, 25, 25 km), (50, 50, 50 km) and (100 100 100 km) respectively. The fault is injected at the end of transmission line. The positive and zero sequence inductances of the transmission line are 0.97x10-3 and 0.99x10-3H/km respectively whereas the positive and zero sequence capacitances are 11.5x10-9 and 11.5x10-9 F/km respectively.

IV. PROPOSED METHODOLOGY

The wavelet transform (WT) are used to decompose signal into different level of resolution by dilating a signal prototype function. The features extracted by processing discrete wavelet transform are maximum coefficient , minimum coefficient and standard deviation at first 9 decomposition level (d1,d2,d3,d4,d5,d6,d7,d8,d9). The maximum coefficient , minimum coefficient and standard deviation of line current at level 8 is used for analyzing because it has highest value compared to others. The maximum coefficient, minimum coefficient and standard deviation of line current at level 8 are calculated for all different type of fault .The wavelet analysis of during single phase to ground fault at phase a, phase b and phase c are shown in fig fig fig respectively .The maximum coefficient, minimum coefficient and standard deviation of line current of normal condition at level 8 taken as references to compared to abnormal condition [14].The fault is occurring when the data of each phase of the d4 at level 8 are not in range with the normal condition.

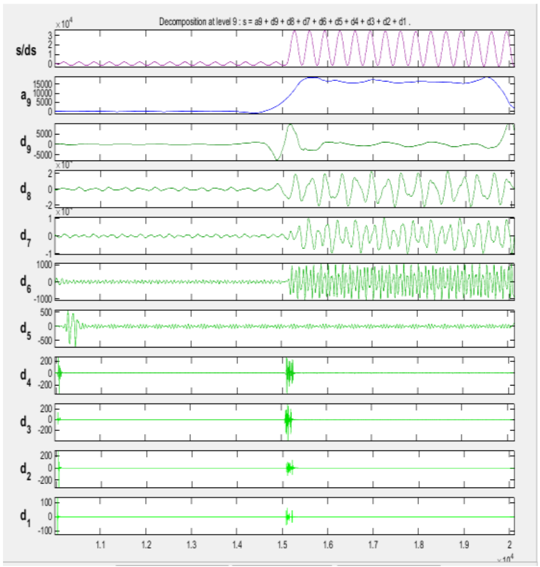

Fig. 5. DWT detailed coeffiecient level 1 to level 9 for single line to ground fault A-G , (Decomposition of phase A)

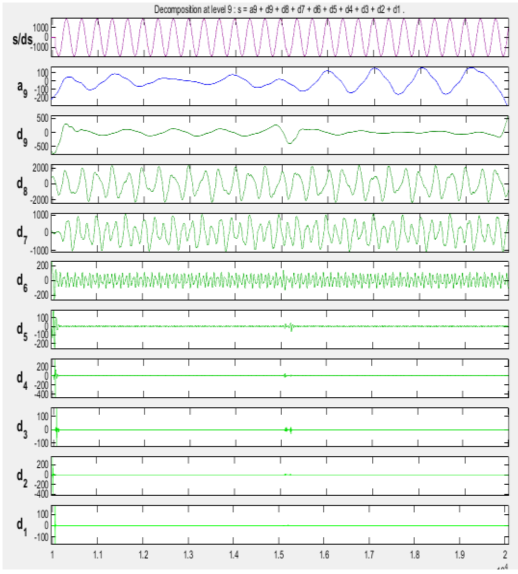

Fig. 6. DWT detailed coeffiecient level 1 to level 9 for single line to ground fault A-G , (Decomposition of phase B)

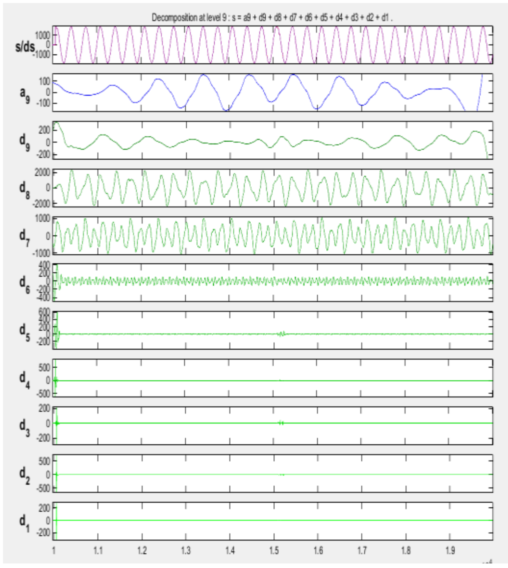

Fig. 7. DWT detailed coeffiecient level 1 to level 9 for single line to ground fault A-G , (Decomposition of phase C)

V. SIMULATION RESULT AND DISCUSSION

A. Normal Condition

Fig. 8 show three phase current signal (A blue, B purple, and C green color) . The Table II shows maximum coefficient, minimum coefficient and standard deviation of line current of normal condition at for db4 level 8. All the data for normal condition taken as references to compared to abnormal condition.

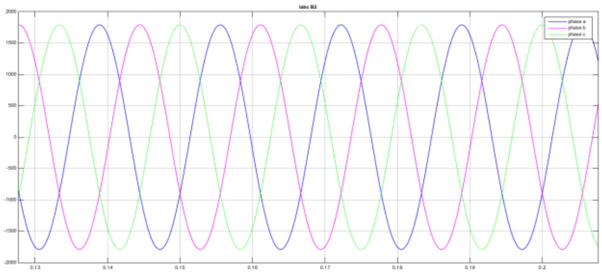

Fig. 8. Three phase current signal at normal condition

TABLE II. DETAILS OF EACH PHASE

Distance		Phase A	Phase B	Phase C
75km	***Max***	2324	2333	2325
	Min	-2329	-2317	-2474
	Std	856.1	861.3	866.1
150km	***Max***	2200	2202	2191
	Min	-2198	-2196	-2333
	Std	809.6	913.6	818.9
300km	***Max***	2007	2008	2154
	Min	-2005	-2003	-2008
	Std	737.7	744.3	745.3

B. *Single line to Ground Fault*

The phase to ground fault is created on phase A (A-G fault). Three phase current waveform during single phase to ground fault are shown in Fig. 9. The current of phase-A, phase-B and phase-C during A-G fault is decomposed using DWT up to level 9 with db4 as mother wavelet .From the wavelet analysis (db4 level 8) the maximum, minimum and standard deviation value is recorded and compared to data of normal condition. The fault is occurring when the data of each phase of the d4 at level 8 are not in range with the normal condition. However, when the data of the d4 at level 8 is in range with the normal condition, it can be state that there is no fault taken place in that phase. The process is repeated for B-G and C-G fault for 75km, 150km and 300km and the data is recorded in Table III , Table IV and Table V respectively .

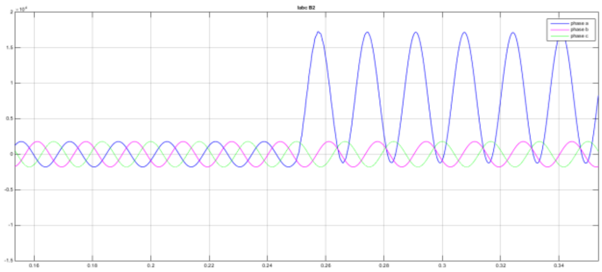

Fig. 9. Three phase current signal during single phase to ground fault , A-G

TABLE III. DETAILS OF EACH PHASE AT 75 KM

Fault type		Phase A	Phase B	Phase C
A-G	***Max***	2.25e+4	2329	2347
	Min	-2.21e+4	-2335	-2350
	Std	5858	858.9	861.1
B-G	***Max***	2434	2.25e+4	2359
	Min	-2335	-2.29e+4	-2347
	Std	861.6	5880	862.5
C-G	***Max***	2328	2338	2.25e+4
	Min	-2331	-2321	-2.25e+4
	Std	860.6	860.8	5894

TABLE IV. DETAILS OF EACH PHASE AT 150 KM

Fault type		Phase A	Phase B	Phase C
A-G	***Max***	1.13e+4	2211	2210
	Min	-1.13e+4	-2206	-2169
	Std	3019	814	819.8
B-G	***Max***	2299	1.13e+4	2231
	Min	-2202	1.16e+4	-2220
	Std	814.8	3000	814
C-G	***Max***	2218	2207	1.12e+4
	Min	-2201	-2210	-1.13e+4
	Std	814.2	814.4	3015

TABLE V. DETAILS OF EACH PHASE AT 300 KM

Fault type		Phase A	Phase B	Phase C
A-G	***Max***	5791	2007	2109
	Min	-6148	-1999	-2012
	Std	1595	746	748.3
B-G	***Max***	2026	5690	2002
	Min	-2006	5748	2017
	Std	736.1	1549	743.4
C-G	***Max***	2008	2046	5704
	Min	-2042	-2085	-5782
	Std	733.4	733.5	1614

C. *Line to Line Fault*

The line to line fault is simulated between phase A and phase B (A-B fault). Three phase current waveform during single phase to ground fault are shown in Fig. 10. The current of phase-A, phase-B and phase-C during A-B fault is decomposed using DWT up to level 9.From the wavelet analysis (db4 level 8) the maximum, minimum and standard deviation value is recorded and compared to data of normal condition. The fault is occurring when the data of each phase of the d4 at level 8 are not in range with the normal condition. However, when the data of the d4 at level 8 is in range with the normal condition, it can be state that there is no fault taken place in that phase. The process is repeated for A-C and B-C fault for 75km, 150km and 300km and the data is recorded in Table VI , Table VII and Table VII respectively.

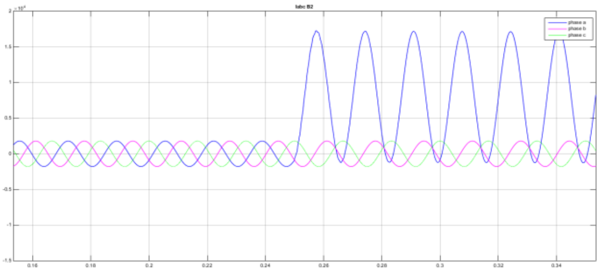

Fig. 10. Three phase current signal during line to line fault , A-B

TABLE VI. DETAILS OF EACH PHASE AT 75KM

Fault type		Phase A	Phase B	Phase C
A-B	***Max***	2.05e+4	1.86e+4	2347
	Min	-2.02e+4	-1.86e+4	-2376
	Std	5359	4907	860.1
A-C	***Max***	1.90e+4	2327	2.02e+4
	Min	1.87e+4	-2334	-2.09e+4
	Std	4892	856.8	5335
B-C	***Max***	2392	2.03e+4	1.89e+4
	Min	-2324	2.09e+4	1.87e+4
	Std	860	5362	4911

TABLE VII. DETAILS OF EACH PHASE AT 150KM

Fault type		Phase A	Phase B	Phase C
A-B	***Max***	1.06e+4	9068	2442
	Min	1.06e+4	-9380	2232
	Std	2834	2443	813.4
A-C	***Max***	8993	2155	1.05e+4
	Min	-9115	-2155	1.06e+4
	Std	2440	836.4	2851
B-C	***Max***	2740	1.07e+4	9116
	Min	-2738	-1.06e+4	-9058
	Std	791.4	2826	2443

TABLE VIII. DETAILS OF EACH PHASE AT 300KM

Fault type		Phase A	Phase B	Phase C
A-B	***Max***	5633	4586	2046
	Min	-5996	-4478	-2001
	Std	1575	1274	745.6
A-C	***Max***	4491	2006	5927
	Min	-4650	1999	-5687
	Std	1303	736.9	1595
B-C	***Max***	1998	5642	4389
	Min	-2007	-5631	-4487
	Std	739	1600	1301

D. Double Line to Ground Fault

Double line to ground is simulated by simultaneously grounding the phases band c .Three phase current waveform during double line to ground fault are shown in Fig. 11. The Table IX , Table X and Table X1 shows maximum coefficient, minimum coefficient and standard deviation of line current of A-B-G, A-B-C and B-C-G fault for 75km, 150km and 300km respectively.

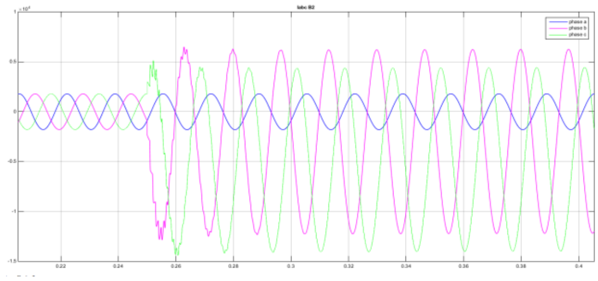

Fig. 11. Three phase current signal during double line to ground fault , B-C-G

TABLE IX. DETAILS OF EACH PHASE AT 75KM

Fault type		Phase A	Phase B	Phase C
A-B-G	***Max***	2.26e+4	2.25e+4	2347
	Min	-2.22e+4	2.36e+4	-2378
	Std	5884	5897	862.6
A-C-G	***Max***	2.24e+4	2333	2.26e+4
	Min	-2.24e+4	-2324	-2.24e+4
	Std	5837	861	5899
B-C-G	***Max***	2421	2.26e+4	2.26e+4
	Min	-2331	2.36e+4	-2.27e+4
	Std	862.8	5905	5899

TABLE X. DETAILS OF EACH PHASE AT 150KM

Fault type		Phase A	Phase B	Phase C
A-B-G	***Max***	1.13e+4	1.12e+4	2227
	Min	-1.14e+4	-1.15e+4	-2203
	Std	3034	3005	821.3
A-C-G	***Max***	1.12e+4	2214	1.14e+4
	Min	-1.13e+4	-2215	1.13e+4
	Std	3028	815.8	3031
B-C-G	***Max***	2222	1.14e+4	1.12e+4
	Min	-2198	1.12e4	-1.136e+4
	Std	814.8	3005	3019

TABLE XI. DETAILS OF EACH PHASE AT 300KM

Fault type		Phase A	Phase B	Phase C
A-B-G	***Max***	5876	5759	2015
	Min	-5782	-5681	-1997
	Std	1556	1565	752.1
A-C-G	***Max***	5720	2027	5770
	Min	-5739	-2008	-5886
	Std	1543	747.3	1596
B-C-G	***Max***	2128	5736	5782
	Min	2120	-5807	-5727
	Std	735.9	1632	1609

E. Three Phase Fault

Three phase fault involving ground has been simulated by grounding all three phases simultaneously. Three phase current waveform during three phase fault are shown in Fig. 12. The Table XII shows maximum coefficient, minimum coefficient and standard deviation of line current of fault for 75km, 150km and 300km respectively.

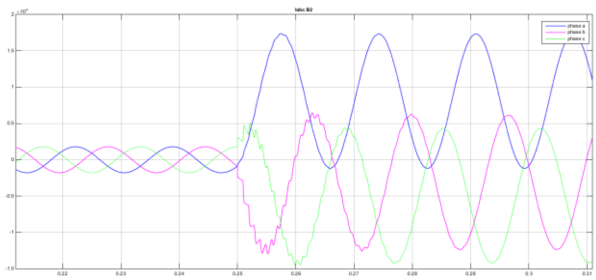

Fig. 12. Three phase current signal during three phase fault , A-B-C

TABLE XII. DETAILS OF EACH PHASE

Distance		Phase A	Phase B	Phase C
75km	***Max***	2.23e+a	2.26e+4	2.26e+4
	Min	-2.26e+4	- 2.31e+4	-2.26+4
	Std	5918	5915	5882
150km	***Max***	1.19e+4	1.12e+4	1.14e+4
	Min	-1.13e+4	- 1.14e+4	-1.12e+4
	Std	3037	3006	3034
300km	***Max***	5633	5859	5782
	Min	-5996	-5807	-5727
	Std	1575	1632	1609

VI. CONCLUSION

A discrete wavelet transform based methodology using db4 as mother wavelet has been presented in this paper. A case study has been conducted on transmission line model where ten different types of faults A-G, B-G, C-G, A-B-G, B-C-G, C-A-G, A-B, B-C, C-A and A-B-C. From the wavelet analysis (db4 level 8) the maximum, minimum and standard deviation value is recorded and compared to data of normal condition. The fault is occurring when the data of each phase of the d4 at level 8 are not in range with the normal condition. However, when the data of the d4 at level 8 is in range with the normal condition, it can be state that there is no fault taken place in that phase. Further, it has also been observed that the values of detail coefficients are different for different types of the faults. Therefore, the faults can be discriminated from each other. Therefore, it is concluded that DWT transform with dB4 mother wavelet and using a moving window can be effective in the detection of power system faults

REFERENCES

[1] V. S. Sruti and B. K. Mathew, "Classification of Transmission Line Faults Using Discrete Wavelet Transform," no. 10, pp. 21–24, 2013.

[2] P. Manivannan, "Fast and Accurate Fault Detection in Transmission Line using Wavelet Transform," vol. 2, no. 11, pp. 523–531, 2016.

[3] M. Singh, B. . Panigrahi, and R. P. Maheshwari, "Transmission line fault detection and classification," 2011 Int. Conf. Emerg. Trends Electr. Comput. Technol., pp. 15–22, 2011.

[4] T. Ladkrabang, "Fault Diagnosis In Transmission Lines Using Wavelet Transform Analyisis," pp. 2246–2250, 2002.

[5] K. Saravanababu, P. Balakrishnan, and D. K. Sathiyasekar, "Transmission Line Faults Detection , Classification , and Location Using Discrete Wavelet Transform," Int. Conf. Power, Energy Control, pp. 233–238, 2013.

[6] W. Zhao, Y. H. Song, and W. R. Chen, "Improved GPS travelling wave fault locator for power cables by using wavelet analysis," Int. J. Electr. Power Energy Syst., vol. 23, no. 5, pp. 403–411, 2001.

[7] K. Prakasam, B. R. Reddy, and M. S. Kalavathi, "2009 Annual Report Conference on Electrical Insulation and Dielectric Phenomena FAULT IDENTIFICATION AND CLASSIFICATION OF HIGH VOLTAGE UNDERGROUND CABLES BY WAVELET TRANSFORM," pp. 396–400, 2009.

[8] S. Barakat, M. B. Eteiba, and W. I. Wahba, "Fault location in underground cables using ANFIS nets and discrete wavelet transform," J. Electr. Syst. Inf. Technol., vol. 1, no. 3, pp. 198–211, 2014.

[9] W. Zhao, Y. H. Song, and Y. Min, "Wavelet analysis based scheme for fault detection and classification in underground power cable systems," Electr. Power Syst. Res., vol. 53, no. 1, pp. 23–30, 2000.

[10] Z. Long, N. H. Younan, T. O. Bialek, and A. C. Wavelets, "Underground Power Cable Fault Detection Using Complex Wavelet Analysis," pp. 59–62, 2012.

[11] M. Misiti, Y. Misiti, G. Oppenheim, and J.-M. Poggi, "Wavelet Toolbox TM 4 User ' s Guide," MathWorks Inc., …, pp. 11–47, 2009.

[12] A. Graps, "В Свижг Й И Гв Иг Я К А Из," vol. 2, pp. 1–18, 1995.

[13] M. Misiti and Y. Misiti, "Wavelet toolbox," MathWorks Inc., …, 1996.

[14] A. Eee, K. Academy, P. Balakrishnan, A. Ece, and K. S. R. C. Engineering, "Transmission Line Fault Detection and Classification Using Discrete Wavelet Transform and Artificial Neural Network," vol. 24, no. 4, pp. 1112–1121, 2016.

Analysis and Design of Buck Converter

Fatin Munirah binti Mohd Noh
Faculty of Electrical Engineering
Universiti Teknologi Malaysia
Johor Bahru, Malaysia.
fatin.munirahh@yahoo.com.my

Prof Madya Dr Awang bin Jusoh
Department of Power Electronic
Faculty of Electrical Engineering
Universiti Teknologi Malaysia
Johor Bahru, Malaysia.
awang@fke.utm.my

***Abstract*—This paper will discuss on the analysis and design of dc-dc buck converter with varied output voltage by changing the duty cycle of PWM. The design of the buck converter through a series of calculations and design consideration in determining the values of component such as capacitor, inductor and resistor. A step-down transformer is used to step down 240V from a power supply to 12V and be fed into a full bridge rectifier to produce a direct current (DC) for the buck converter to operate. The development of the buck converter involves in designing and simulating the circuit using MATLAB-Simulink before implementing on a PCB. A detailed analysis and design of the proposed circuit is presented**

***Keywords*—Buck converter; Pulse Width Modulation (PWM); Gate driver, Rectifier, Duty Cycle**

I. INTRODUCTION

The application of direct current is widely used in technology nowadays. For example, television, telephone, computer and other home appliances. Generally, a power supply provides 240V alternating current (AC) which will be converted into direct current (DC) and either step up or step down into desired DC voltage for the equipment to operate. There are two methods for a linear dc-dc converter which are linear regulator and switched-mode converter [1].

$$V_o = I_L R \tag{1}$$

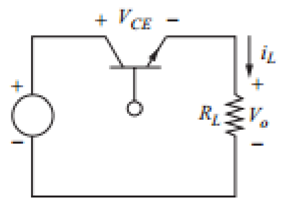

Fig. 1. Basic linear regulator circuit

From fig.1 transistor is used to control the load current. The base current could be adjusted to compensate the variation of supply voltage or load, resulted in regulating the output. An output voltage with range of 0 to Vs can also be obtain by adjusting the base current of transistor in a linear regulator. The problem with the linear regulator is the power are being absorbed to transistor and dissipate into heat energy. Although provision can be made by implementing heat sink for the cooling purpose, it also will make the linear regulator bulky and large [2]. Making it less efficient considering the power loss. Hence, linear regulator only suitable for low-power application [1]. In result of the increasing demand of the energy saving, a development in switching mode power supply (SMPS) technology had been rapidly increase throughout times. A switched-mode power supply (SMPS) can be define as an electronic circuit that converts power using switching devices that are turned on and off at high frequencies, and storage components such as inductors or capacitors to supply power when the switching device is in its non-conduction state [2]. Buck converter is one of the SMPS that will step down the dc voltage to a desired value and will be discuss on more further in this paper.

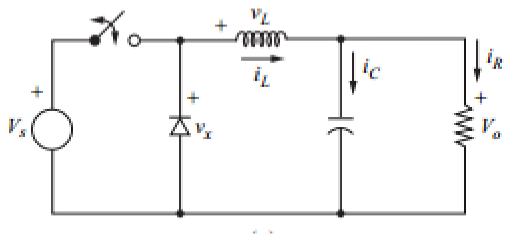

Fig. 2. Buck converter circuit

In order to obtain a pure DC voltage, a low pass filter which consists of inductor and capacitor have been added to the Fig. 1. The function of diode is to create a path for the inductor current during open switch and is reverse-biased during close switch. This circuit is a buck converter or a step-down converter circuit as shown in Fig. 2 because of the output voltage is less than the input voltage.

The main purpose of this project is to have more understanding on buck converter by involving designing, implementing and analysis of buck converter.

II. LITERATURE REVIEW

A. *Design Principle and Analysis*

The analysis of buck converter is based on its steady state. In a continuous-conduction current mode (CCM), there are continuous flow of current through an inductor [3]. The states of duty cycle consist of two, which are during open switch and during close switch. By controlling the duty cycle, a desired output voltage can be obtained. Before doing any analysis on buck converter, certain assumptions are made as following: circuit in a steady-state, inductor in a continuous current mode, constant output voltage, switching period of T with DT during close switch and (1-D) T during open switch and all the components are ideal.

$$V_L = V_{in} - V_{out} = L\frac{di_L}{dt} \quad (1)$$

$$\frac{di_L}{dt} = \frac{V_{in} - V_{out}}{L} \quad (2)$$

$$\frac{di_L}{dt} = \frac{-V_{out}}{L} \quad (3)$$

Inductor voltage, V_L can be expressed as in Eq. 1. When the switch is close, the derivatives of the inductor current is as shown in Eq. 2 [1]. It can be observed that the rate of change in inductor current is always positive during close switch mode. Thus, increasing the current linearly. While during the switch is open, input voltage is absent causing the derivatives of the inductor current always negatives as shown in Eq. 3 indicating the rate of change of inductor current is keep on decreasing.

$$V_{out} = V_{in}D \quad (4)$$

The sum of Eq.2 and Eq.3 is zero considering the net change of inductor current. Hence, forming an Eq. 4 that shows the output voltage produce from buck converter is less than or equal to input voltage [1].

$$I_{min} = V_{out}\left(\frac{1}{R} - \frac{1-D}{2Lf}\right) \quad (5)$$

$$L_{min} = \frac{(1-D)R}{2f} \quad (6)$$

For a dc-dc buck converter to work in a continuous current mode, a minimum inductor current must be positive. Eq. 5 is being equal to zero to determine the minimum value of inductor needed, thus, obtaining an Eq. 6.

There are two ways of controlling the output of the power supply which are current-mode control (CMC) and voltage-mode control (VMC). The voltage supply that run in VMC will keep constant voltage level while providing an adequate current to the load. Low output impedance of the supply usually use this type of control method. On the other hand, the power supply that run in CMC, work in the same way as the VMC voltage supply but limit and regulate the output of the supply current providing constant current to varied load voltage condition. High output impedance of the supply use this type of control method [4].

III. METHODOLOGY

In this project, an open loop buck converter was design and implement. There is no feedback from output voltage to ensure constant output voltage obtain. Only by varying the duty cycle to observe on the effect to the buck converter and analyzing the results.

A. *Component Selection for Buck Converter*

The components selection is determined by using calculation. The chosen input voltage for the buck converter is 15V and an output voltage of 4.6V. By using Eq. 4, a duty cycle of 0.3 was obtain. With a switching frequency of 40k Hz and resistor of 10Ω, a minimum inductor can be obtained by using Eq. 6. Practically, inductor needed is much bigger than calculated value, usually 25% bigger, thus, giving a value of 100μ H. The value of capacitor is obtained by using Eq. 7

$$C = \frac{1-D}{8L\left(\Delta V_{out}/V_{out}\right)f^2} \quad (7)$$

Practically, the value of capacitor should be bigger to limit the ripple voltage to 1%. Hence, a 400μF is chosen. With all the components, the circuit of buck converter signed being fed with output voltage from rectifier is being simulated in MATLAB-Simulink as in Fig. 3.

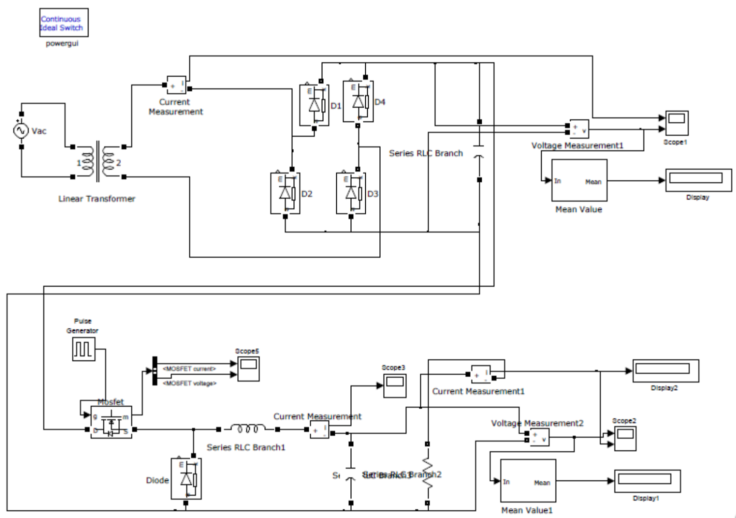

Fig. 3 Buck Converter with Rectifier Circuit

B. *Pulse Width Modulation*

The switching frequency of MOSFET is being controlled by the duty cycle of PWM. By using an integrated circuit (IC) of sg 3525, a PWM can be generated. An open loop PWM is designed to give desired PWM with switching frequency of 40k Hz and the connection with the parameter as shown in Fig. 4.

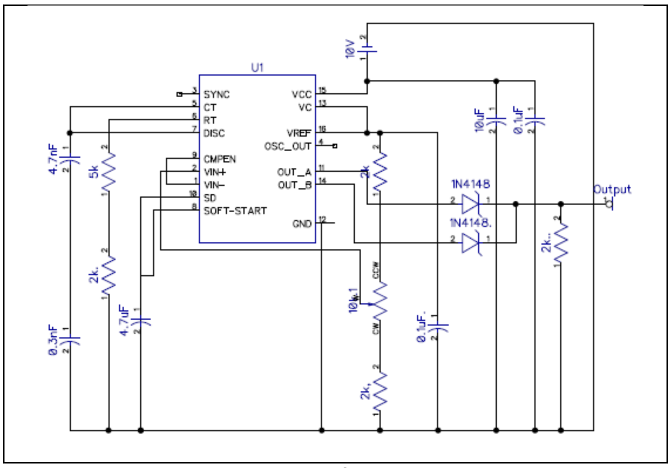

Fig. 4 Connection of Open Loop PWM

The chip is supplied by 10V at pin 15 and the on-board regulator regulate the voltage to produce 5V at pin 16. The 5V voltage produced is used as a voltage supply to the voltage divider circuit where potentiometer can be adjusted to have desired duty cycle and as to drive the internal circuit of chip. Value of timing resistor, R_T connected to pin 6 is determined by referring to the graph of oscillator charge time versus R_T time as in Fig, 4. The charge time can be calculated by dividing one to the switching frequency. The charge time used is 25µs and from the graph in Fig. 5, the values for timing resistor, R_T and timing capacitor, C_T are 7kΩ and 5nF respectively.

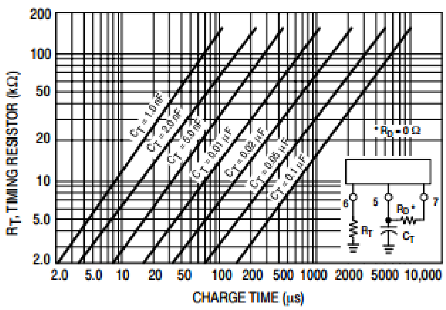

Fig. 5 Oscillator Charge Time versus RT

C. Gate Driver

Gate driver function as power amplifier that accepts a low-power input from a controller IC and produces a high-current drive input for the gate of a high-power transistor such as an IGBT or power MOSFET [6]. PWM which is the switching command from IC SG3525 is an input signal for a gate driver, HCPL3120. The connection of the gate driver is as in Fig. 6

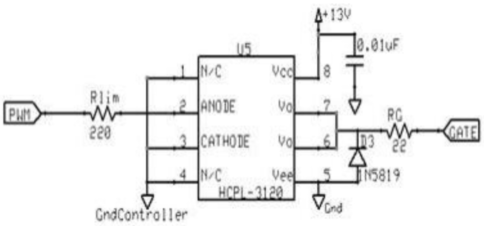

Fig. 6 Connection Circuit for IC HCP3120

IV. RESULT AND DISCUSSION

A. Full Bridge Rectifier

The objective of a rectifier is to produce a voltage or current that is purely dc or has specified dc component. In the AC to DC converter, rectifier is the fundamental component that will convert AC into DC. By using diodes and connection as in Fig. 3, a waveform as in Fig. 7 will be form. The waveform observe is only consist of positive part which is the most crucial property of direct current.

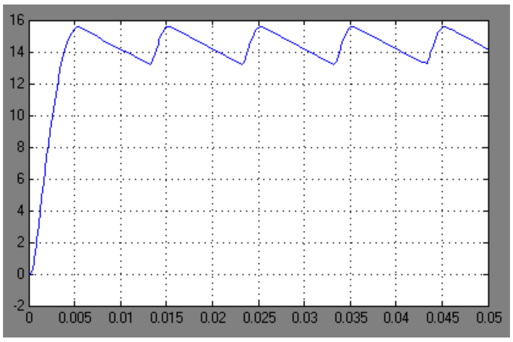

Fig. 7 The waveform of rectifier output voltage

After current flow into a rectifier, the waveform as in Fig. 8 is obtain. The voltage of the full bridge rectifier across a capacitor is 15.02V. It can be observed that the output voltage waveform is only at the positive part which is the basic characteristic of direct current. Before the voltage being supplied to a buck converter, a filter consists of a large capacitor is connected at the end of the rectifier to minimize the ripple and producing more linear dc voltage.

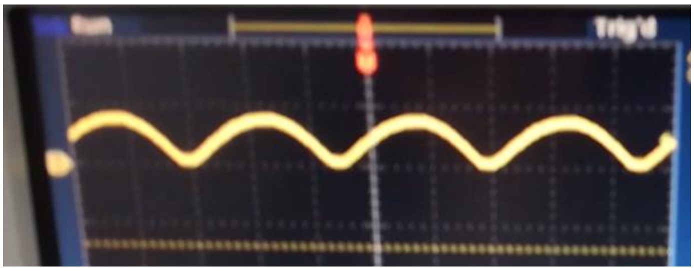

Fig. 8 The Output Voltage of Rectifier

B. Buck Converter

After simulating the model as in Fig. 3, with a duty cycle of 0.3 an output waveform of output voltage as in Fig.9 is obtain. With an average value of 3.96V

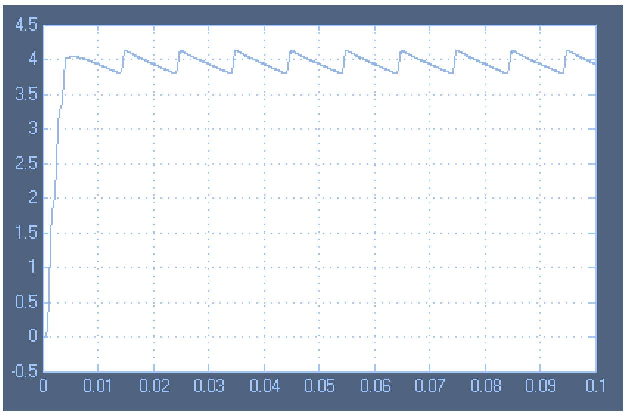

Fig.9 The waveform of output voltage with duty cycle of 0.3

By simulating the model as in Fig. 3, with a duty cycle of 0.4, an output waveform of output voltage as in Fig.10 is obtain with an average value of 5.31V. While, at duty cycle of 0.5, the average output voltage is 6.64V as in Fig.11.

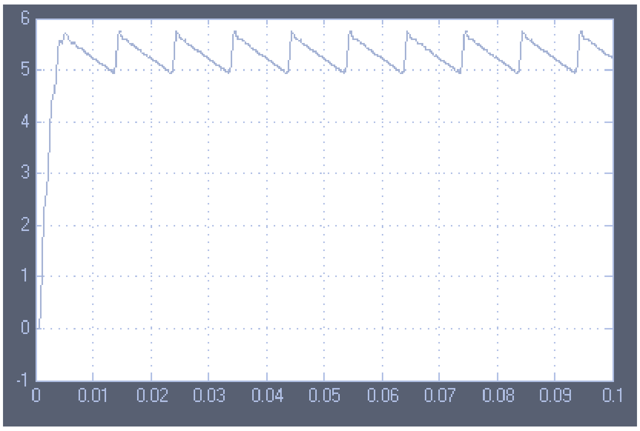

Fig.10 The waveform of output voltage with duty cycle of 0.4

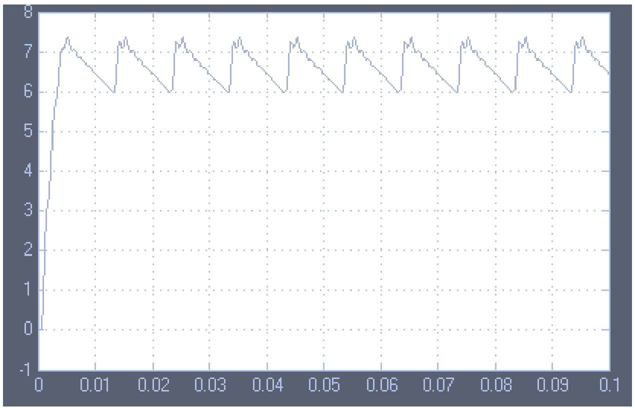

Fig.11 The waveform of output voltage with duty cycle of 0.5

It can be observed that by increasing duty cycle, the output voltage is also increasing which correlate with Eq. 4. The hardware design of the buck converter is in process of development as the desired output is not achieved yet. Troubleshooting and modifying is taken place.

V. CONCLUSION

In a conclusion, a design of buck converter had been successfully design through a MATLAB/Simulink. Understanding on a dc-dc converter through this project had been achieved. The problem regarding the hardware of the designed circuit had been explain in the discussion.

REFERENCES

[1] Hart, D. W. (2011). Power electronics. New York: McGraw-Hill

[2] Rahman, M. S. (2007). “Buck Converter Design Issues” (Published master's thesis). Linköping Institute of Technology.

[3] E. Cebeci and Y. Yaşa, "The development of DC-DC buck converter with practical design methods," *2016 National Conference on Electrical, Electronics and Biomedical Engineering (ELECO)*, Bursa, 2016, pp. 691-695..

[4] E. Guerrero, J. Linares, E. Guzman, H. Sira, G. Guerrero and A. Martinez, "DC Motor Speed Control through Parallel DC/DC Buck Converters," in *IEEE Latin America Transactions*, vol. 15, no. 5, pp. 819-826, May 2017.R. Nicole, “Title of paper with only first word capitalized,” J. Name Stand. Abbrev., in press.

[5] Hassan, N. N., & Daud, M. Z. (2012). Design of switched mode: DC-to-DC buck converter (Published thesis). Universiti Teknologi Malaysia

Smart Power Recovery for Consumer Application

Mohd Nur Aizat Bin Mohd Nazih
Faculty of Electrical Engineering
Universiti Teknologi Malaysia
Johor Bahru, Malaysia.
nazihaizat@gmail.com

Abdullah Asuhaimi Bin Mohd Zin
Faculty of Electrical Engineering
Universiti Teknologi Malaysia
Johor Bahru, Malaysia
asuhaimi@utm.my

***Abstract*— Discovery on earth leakage circuit breaker has brought significant contribution in power protection system especially for protection to the consumer. It is a safety device that equipped with high earth impedance to prevent shock and able to detect small stray voltages on the metal enclosures of electrical equipment. However it could affect the continuity of electrical supply to consumer. This event happen because of the internal and external disturbance occurred in the electrical system and this relate to the fault problem that might be occur in the system. Of course when fault occurred it will trigger the main protection system in distribution board of our house to trip or open. According to this statement, the tripping can bring many issues to the consumer especially for user that always leaving their house for others business. Thus in this research, a Smart Power Recovery System for Consumer Application is being developed to overcome an electricity trip problem and improve the system according to ours technology right know. The prototype of this project was built using the Espresso Lite V2 which already included with Wi-Fi module as the microcontroller for this system. While for the Wi-Fi module, it will be used to communicate between smartphone applications of user and the main microcontroller of the system. Furthermore the status of the system either to operate the system manually or automatically will be controlled from the application. In addition, this system also included with function to calculate the power consumption of household appliances which will also displayed in the smartphone application if no fault occurred. Thus, this system is successfully upgraded more than the previous system with new function and capabilities.**

Keywords*— *smart recovery system; power monitoring; blynk application; online monitoring;

I. INTRODUCTION

The presence of breakers in electrical field is extremely vital to prevent fires and harms from the electrical shock by opening or disrupting the electrical system when problem appear in the circuit system. From the statistic that accidents happen due to the electrical fault result in Malaysia, there are 405 accidents occurs and 191 people died due to that accident [1]. For the updated accidents is in 2016, about 3 accidents that trigger off by electricity occur in the first three months due to the electronic device malfunction or short circuit when managing the main electrical component [2]. Therefore, the Malaysian Government has already taken action by providing an understanding upon electrical protection and threat to the people community for their safety in daily activities. Instead of that action, a very good defense device also needs to be counted for the electrical safety.

The protection component as the Earth Leakage Circuit Breaker (ELCB) are commonly used for disconnecting circuit system when the component detects an unstable current between the neutral conductor and live conductor. This protection device also can help to prevent from electric shock to the human body. Even better, the ELCB would cut off the electrical supply to the house if some leakage current to the earth from any electrical device strike. However, all the systems that created would have their difficulties that will give problems to the user of the system. What the weaknesses of this protection system are that it is a lack of effectiveness because when the ELCB in tripping state means that manually power supply restoration are needed to execute. So in terms of safety and effectiveness still need to be developed more. As we know that the safety of human being is the uppermost priority in any situation, but typically we haven't concerned about it until an unforeseen event have appeared, either it is caused by faulty appliances, overload and even a lightning strike. In order to prevent that from occurring, an automated system has been planned. This project proposal serves to improve the efficiency of current protection system and to enhance more the ways to discover the fault that strikes.

In addition, in our modern daily life the continuous supply of electricity and power dependability is really vital for the consumers and even critical to the industrial area. These are because they have electrical appliances and equipment which need to be endlessly supplied even though when there is no one there to manage the system. For example, security alarm system, refrigerator, and even the aquarium ventilation system. Furthermore, regularly the domestic area has machine that they need to run 24hours, so in term of continuousness supply is critically important for them because they may loss profit worth a thousand dollars if there is no electricity cause of tripping condition

II. LITERATURE REVIEW

A. Common Electrical Fault

Electrical fault is an unusual situation, caused by failures in equipment such as transformers, environmental conditions, rotating machines and human errors. Besides that, usually the electrical devices in an electrical system will operate at normal voltage and current ratings under safe or normal operating situations. However, the current and voltage values will varies from their actual scales when the fault in a device or circuit takes place [3].

All this failure has caused damage of electrical devices or machine, interruption of electricity flows and even lead to the death of humans and animals. In addition the faults in power system also cause under voltage, over current, phase unbalanced, high voltage surges and even reversed power. This results cause by the breakdown of electrical devices, disruption of the normal process of the network and flames from the electrical system [4].

B. *Earth Leakage Circuit Breaker (ELCB)*

An Earth Leakage Circuit Breaker (ELCB) is a device which is able to detect leaking current to earth of electrical system and then disconnect it from power supply. Two type of ELCB that are used in domestic are which is the first is voltage operated ELCB and secondly is current operated ELCB.

For voltage operated ELCB, the danger of electric shock will occur and can cause dissimilarity between load body voltage and earth when the voltage of the load body is increase. An electric current from the load metallic body passes through the relay loop and finally to earth will occur due to the voltage dissimilarity. However voltage operated ELCB is presently not been consumed in domestic wiring since the current ELCB operated is more dependable to be mounted in household [5]. In normal state for current operated circuit breaker (IELCB), total current operated to the load is uniform with overall current out of the load. This happen because of the stability of in and out of current, plus it does not influence the current transformer device. Besides that, the in and out of current will no longer in balance, if there is any earth current leakage affected by earth damage. In addition, destabilize current phenomenon will also generate the current. Then the ELCB will jerked and cut off the supply if the current surpassed the approved rate. Fig. 1 shows the diagram of ELCB tripping mechanism [6].

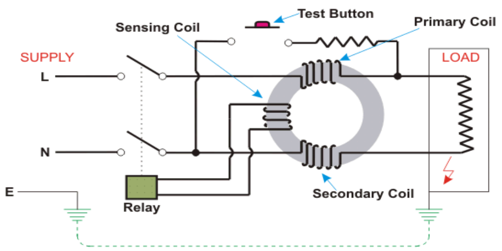

Fig. 1. ELCB Tripping Mechanism

C. *Method that Already Implemented to ELCB*

Yukinori Hirooka [7] have implemented an invention called as automatic breaker re-closing device which will recovered the system cause of the malfunction of load or abnormal load and caused by the lightning surge automatically. The automatic breaker re-closing device contains with breaker unit, control unit, and drive unit. The main function of control unit is to detect either the breaker is in open situation or closed situation. The advantage of this project is that it will determine whether the cause is the abnormality in load or lightning strike only when the breaker is open position. The device will automatically re-close only if the breaker triggered from an abnormality in load and for the cause of lightning surge, the automatic breaker will not proceed to re-closing the breaker. The disadvantage of this system is that there is no display showing the activation count, so the activation history of the device cannot be checked.

Next is Ahmad Firdaus [8] have designed the automatic earth leakage circuit breaker (AELCB). The benefit of this project is to design a system that can alert the house's owner if the earth leakage circuit breaker (ELCB) trip occur at home especially when nobody at home. Moreover, the user can send SMS to command the system reclose the ELCB. Furthermore, it can prevent some of the problems from becoming serious after the ELCB trip. However the project was not fully succeeded because there is problem with the GSM modem. The GSM modem cannot interface with the PIC microcontroller which cause by careless in writing a C programming and understanding about the operation of GSM modem not very clear enough.

From the previous project, Chong Mie Jie [9] improved the project by identifying the GSM problem and solve it. By focusing more on the GSM modern working operation, the project that was not successful before was completed this time. However there is some improvement that was recommended by resetting back the ELCB for about three times only. After the third tripping, the ELCB will be a permanent tripping and it means that the system will not reset back but it will miscall the user mobile phone to inform the user to take action on the ELCB condition.

Siti Hajar Binti Md Halid [10] have proposed an automatic Earth Leakage Circuit Breaker integrated with Arduino that will reclosed the circuit breaker after tripping occur. The advantages of this design is that it also implemented with system that can send alerts to the house's owner if tripping occurs more than three times consecutively. This project was design based on different method than before that is using servo motor to control the movement of the ELCB switch. Besides that, Arduino UNO was used as microcontroller of the system since Arduino UNO consist of two parts which is hardware and software. Furthermore, the Arduino that she used also available with add on board which will allow multiple Arduino boards to communicate wirelessly. However the project only used basic switch as the indicator of ELCB not using the real ELCB.

Last but not least, Mohamad Hafiza Bin Mohamad [11] have invented an automatic earth leakage circuit breaker system that using Internet as backup if the system malfunction. The prototype of this project was designed by using an Arduino Ethernet Shield and Arduino UNO as the main microcontroller that will control all of the system including with communication between user and the ELCB. The benefit of this system than other is that the use of internet in this system which is to inform the user and to reclose the ELCB in large range. For example if the user cannot reclose the ELCB if they are not at home, the driver will send the information to user through email if the ELCB having problem and the user will control the ELCB through internet by clicking the link provided in the email. This link will turn on back the ELCB. However, this system need to be improved in term of the method used because this project used two number of microcontroller which is the first one for the system and the second for the connection with user since it will combine with the Ethernet Shield. So more effort needed to program both microcontroller.

III. PROJECT METHODOLOGY

Fig. 2 below show the planning flow of the whole work from the first semester until the second semester for this project.

Fig. 2. The project flow diagram of this project

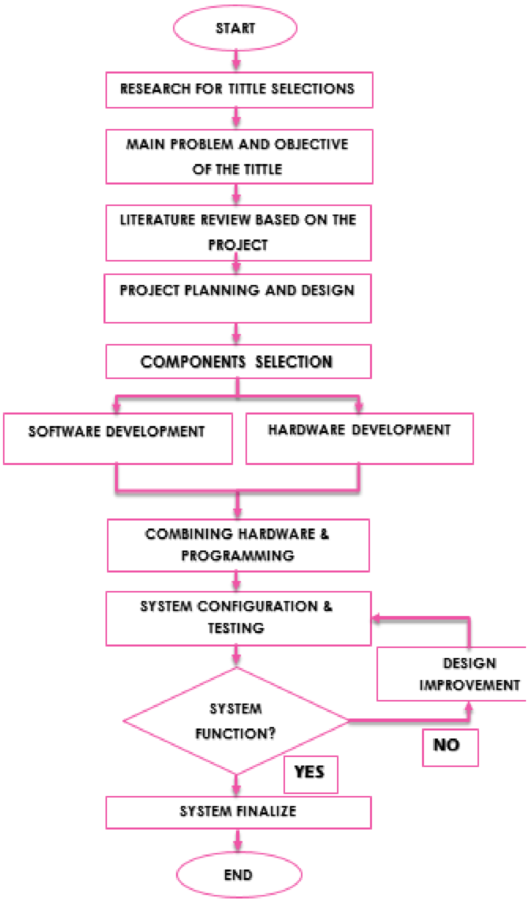

A. System Flow Description

In the project planning and designing, an automatic power recovery system is designed for the domestic electrical protection system. This system operates in two parts that is the power recovery system and power consumption meter. Fig. 3 show the design for the automatic power recovery system.

Power recovery system is a process where the part for power turning on back after the power is shut down as result of faulty or tripping in the three phase protection system. An automatic ELCB resetting system using Wi-Fi connection with smartphone application is designed to cover back the main system to restore the supply system. This system is important because there are certain electrical devices or appliances that require continuous supply to avoid from damage or harm others. For example refrigerator, house security system, water pump for aquarium and many more. For current domestic electrical system, all the operation to recover power supply is manually done. Sometime unexpected accident will occur cause of untrained or unexperienced person to handle the system even though it seem simple.

For second part is the power monitoring system and this part where it is operated when there is supply to the system or no tripping occur in the distribution board. The current flow through the distribution board will be measured by using the current sensor. The amount of power and energy usage can be monitored on the LCD display which also included at the main controller. In addition, consumer also can monitored this from the smartphone application since this system are using wireless connection to the main controller.

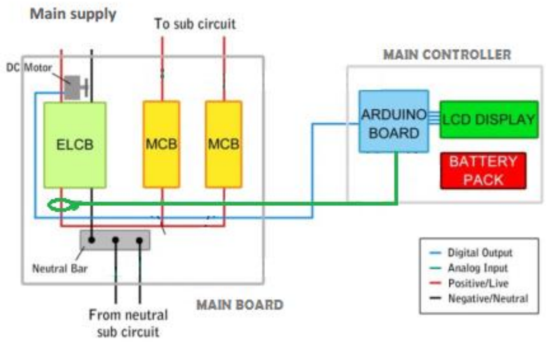

Fig. 3. Circuit Diagram of the Prototype

B. Hardware Implementation

1) Current Sensor

The function of current transformer is to convert high current into regulated values for control devices as meters and relays. In electrical power industry, it is used in protective relay and metering especially where they are facilities the protected amount of large currents including for high voltages. Besides that, it also use for circuitry control from excessive voltages that existing on the circuit being measured [12].

For this project, it is crucial to have suitable current sensor with correct sensitivity and rating as to measure accurately and obtain the current value. Thus it is preferable to have current sensor that able to detect up to 100A for domestic usage.

2) Espresso Lite V2

Microcontroller is the most crucible part in this project. Since it is function to control whole system, so Espresso Lite V2 is used as the main part of this project. The reason why Espresso Lite V2 is chosen because it has its own software to communicate with computer and included almost everything needed to support the programs. In addition, it also has digital and analogue ports for connection with many type of sensors, motors, module and switches. Furthermore, this microcontroller also included with Wi-Fi module which will be used for wireless connection with the smartphone application.

3) Servo Motor

For this project to success, DC servo motor is required to switch on the trip ELCB. The selection of this DC servo motor is important because it will be required enough mechanical force to rotate and to pull the handle of ELCB and MCB. This servo motor is controlled by sending a pulse width modulation (PWM) or electrical pulse through the control wire. The electronic part in the servo motor has the function to translate this PWM signal into position value and instructed the servo motor to rotate [13].

4) LCD Display

A liquid-crystal display (LCD) is an electronically modulated optical device that uses the light-modulating properties of liquid crystals. It is available to display arbitrary images or fixed images with low information content, which can be displayed or hidden such as preset words and digit [12]. For this project, LCD display is used to display the condition or process of the system including the measured power and energy usage.

C. Software Implementation

1) Arduino IDE Programmer

For Arduino programs, it is possible to be written in any programming language with a compiler which will produce binary machine code. In addition, the Arduino board is open source which refers to a hardware that is reasonably priced and the software is free from the internet. The interface of Arduino is shown in Fig.4.

2) Proteus Design Suite

The Proteus Design Suite is an Electronic Design Automation (EDA) tool that include with simulation, PCB Layout modules and schematic capture. PCB Layout modules is used for this project to design the circuit diagram. This PCB Layout module is automatically given with connectivity information in form of netlist from schematic capture module. By applying this information, it can assist with error free board design.

IV. Result and Discussion

A. System Operating Process

1) Power Recovery System

The process of an actual auto-reset ELCB function by using the prototype designed as shown in Fig. 4 is tested. During tripping condition, the LED will light off to indicate that fault condition is occurred. Thus the ELCB will undergo maximum of two times reset testing to recover the power supply. In tripping condition, the ELCB will be in OFF position and ON position after reset operation. While the LCD will function to display the reset sequence which indicate number of reset test that already has done. This system is developed with current sensor which is function to check the current flow after each auto-reset ELCB processed. In detail description, after reset test sequence of ELCB completed, the current sensor will check for the electrical power supply. However if the current sensor does not detect any power supplied, then the servo motor will go for next reset sequence. But if the power supply is restored after the first or second trial, thus the system will operate back the power monitoring system.

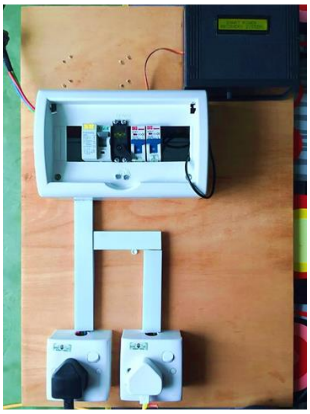

Fig. 4. Completed Prototype of this Project

Last but not least, if the auto-reset ELCB failed again to recover power supply, thus the alert system will be operated. This alert system will send a notification to the user smart phone directly to notify the user permanent electrical fault had occurred as shown in Fig. 5. Thus, even though user is not at home, they still can know how the power status and directly take an action for their home safety. Another thing about this system is that it can be controlled manually or automatically, which means the user is able to try resetting back the ELCB on their by using the slider widget in the Blynk application on their smartphone as shown in Fig. 5.

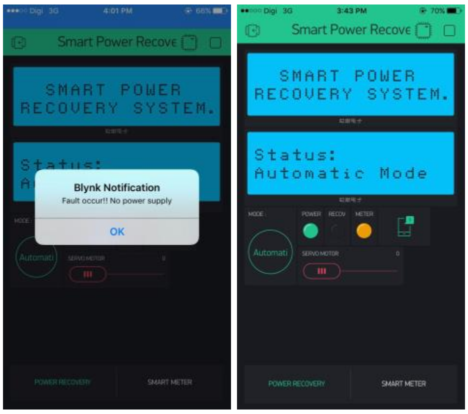

Fig. 5. Interface of Notification and Slider in Blynk

2) Power Monitoring System

Power monitoring system is a system that designed to measure the power consumed by domestic devices or household appliances by clamping the current sensor to the distribution board. This system will only be operated when there is no tripping occur to the ELCB. The power and amount of energy usage from the monitored distribution board is displayed on the LCD display.

Since this system included with wireless connection to the Blynk application, so the value of power and amount of energy usage will updated to this application every second. Fig. 6 below shows the interface of the power monitoring system in

Blynk application. Thus the user will always get the updated data on their power and energy usage of their home.

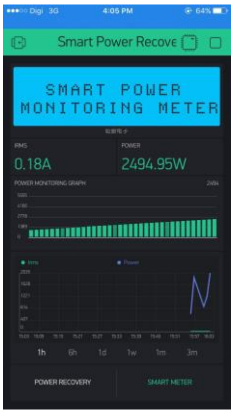

Fig. 6. Interface of the Blynk Meter

B. Angle of Servo Motor Analysis

Servo motor works on PWM (Pulse Width Modulation) principle, where its angle of rotation is controlled by the duration of pulse to its Control Pin on the Espresso Lite V2. The controller circuit in the servo motor will read the waveform from the programming and translate it in term of motion by motor and gearbox. For this project the servo motor that used is the type that can rotate maximum 180°. Thus this angle of servo motor will determine whether it is able or not to pull up the ELCB switch. Table I show the result on different type of angle for the servo motor to success this project.

TABLE I. RESULT ON THE ANGLE OF SERVO MOTOR

Angle of Servo Motor	Number of Tested	Success	Failure
30°	10	0	10
60°	10	1	9
90°	10	3	7
120°	10	5	5
160°	10	10	0
180	10	10	0

C. Power and Current Analysis of Selected Load

To verify the functionality of this system especially the current sensor, a test with selected load had been carried out. The test is done with using the trainer machine which represent the power system flow from the transmission line until to the distribution state that included with load bank as the load of this system. The load bank consists of certain numbers of resistance and inductive loads. The current measurement is taken by using current sensor and this current value can be read through the serial display of the microcontroller as the result of the load. Besides that, the value for power usage and total energy usage also included in the serial display as shown in Fig. 7.

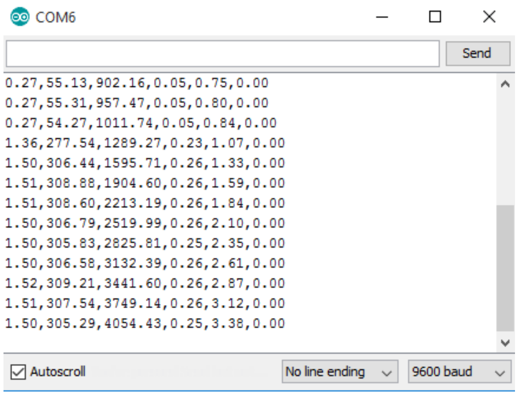

Fig. 7. Sample Results from Serial Display

There are two types of measurement that were taken which is actual value and measured value. Measured value is the value that taken from the power monitoring system while for the actual value is that taken from the power analyzer device. Power analyzer which is an instruments for measuring various parameters of an electrical power distribution system such as for single phase systems voltage, power factor, instantaneous power in watts, frequency, energy in watt-hours and others. Thus the value that gathered from the serial display will compared with the power analyzer to make sure this system is valid to be used as measurement device in this project. From the result in Table II, the reading of current sensor for monitoring meter for the system designed almost the same as the reading from the power analyzer. Furthermore the percentage error of the current measurement is lower than 5% based on Table III. Thus this system is valid to be used as the measurement device for energy consumption in this project. In addition, it is also valid to be used as the measurement device to sense whenever tripping occur in at ELCB.

TABLE II. DATA BASED ON DIFFERENT LOAD

Load		Power Monitoring Meter	Power Analyzer
R_1L_2	Current(A)	0.83	0.85
	Power(W)	163.92	172
R_1L_3	Current(A)	0.88	0.87
	Power(W)	170.77	189
R_1L_4	Current(A)	0.89	0.90
	Power(W)	173.76	203
R_2L_3	Current(A)	1.54	1.53
	Power(W)	298.58	297
R_2L_4	Current(A)	1.64	1.65
	Power(W)	325.43	340
R_3L_4	Current(A)	2.21	2.20
	Power(W)	429.57	405

TABLE III. PERCENTAGE ERROR OF THE DATA

Load	Percentage Error (%) of Current(A)
R_1L_2	2.35
R_1L_3	1.15
R_1L_4	1.11
R_2L_3	0.65
R_2L_4	0.61
R_3L_4	0.45

V. CONCLUSION

As a conclusion, the objectives of this project has been successfully achieved. A prototype of smart power recovery for consumer application was develop and had been used to reset the ELCB using the Wi-Fi connection. By using an Espresso Lite V2 as the main microcontroller and current sensor as the device to measure the current value, it will be able to sense whenever tripping occur at ELCB. In addition, this system able to connect with the smartphone application which can be used to monitored and controlled the system. Control the system means that this system is already enhanced by making the system of two-way communication system which make this system able to be operated manually and automatically depends on the user. This system also can send notification to the user by using the Wi-Fi module when temporary or permanent fault occur in the system. Furthermore, this system is successfully improved than before because it also included with power monitoring system. This additional function make the system to be able to measure the power and energy consumption for the whole house of user since the current sensor is clamped at incoming live wire at the distribution board. Main reason of this additional function is to acknowledge the public on how to manage the energy usage of their home. Since it is combined system, so the cost to develop this energy meter is low and easy to handle by the user. In addition, user can monitored their energy usage with the simple use of a smartphone application at everywhere as long they have the internet connection. Thus it is very compatible to be used by user because nowadays internet and smartphone is everything to the user. Last but not least, the data of the energy usage also can be used by student or researcher for further study in decreasing the energy usage of consumer.

REFERENCES

[1] "191 Mati Akibat Kejutan Elektrik", Newspaper Article, 2011. http://ww1.utusan.com.my/utusan/info.asp?y=2011&dt=0415&pub=Utusan_Malaysia&sec=Dalam_Negeri&pg=dn_10.htm

[2] " Tiga kes kematian babitkan elektrik ", Sinar Harian Newspaper, 2016.

[3] H. (2016). Types of Faults in Electrical Power Systems. Retrieved December 10, 2016, from http://www.electronicshub.org/types-of-faults-in-electrical-power-systems/

[4] What are the Different Types of Faults in Electrical Power Systems? (2016). Retrieved December 18, 2016, from https://www.elprocus.com/what-are-the-different-types-of-faults-in-electrical-power-systems/

[5] Mohd Tarmizi Bin Rahim, "Development Of Earth Leakage Circuit Breaker With An Auto Re-Closer Unit", Bsc. Dissertation . Universiti Malaysia Pahang May 2009

[6] Shahful Bakhtiar Bin Shahiran, "Development Of Auto Re-Closer Earth Leakage Circuit Breaker (AR-ELCB)", Faculty Of Electrical & Electronics Engineering Universiti Malaysia Pahang April 2009.

[7] Hirooka, Y. (2011). Automatic re-closing devices for breaker. 2011 7th Asia-Pacific International Conference on Lightning. doi:10.1109/apl.2011.6111071

[8] Ahmad Firdaus Bin Razali, "Automatic Earth Leakage Circuit Breaker (AELCB)", Bsc. Dissertation .Universiti Teknologi Malaysia (2009).

[9] Chong Ming Jie, "Intelligent Earth Leakage Circuit Breaker", Bsc. Dissertation .Universiti Teknologi Malaysia (2010).

[10] Siti Hajar Binti Md Halid, "Automatic ELCB Integrated With Arduino", Bsc. Dissertation .Universiti Teknologi Malaysia (2014).

[11] Mohamad Hafiza Bin Mohamed, "Reclose Earth Leakage Circuit Breaker By Using Internet", Bsc. Dissertation .Universiti Teknologi Malaysia (2015).

[12] Ahmad Zakwan Hariz Bin Abd Azzis. "Automated Electrical Protection System (Auto-Epros)", Bsc. Dissertation .Universiti Teknologi Petronas (2012).

[13] Mohd Azraie B Suarin, "Automatic Tester Device For Earth Leakage Circuit Breaker", Bsc. Dissertation .Universiti Malaysia Pahang

Design of Wave Energy Converter Equivalent Circuit Model and Implement it in Malaysia

Mohammad Razalie bin Ahmad Murad
Faculty of Electrical Engineering
Universiti Teknologi Malaysia
Johor Bahru, Malaysia.
rzlmrdjalie@gmail.com

Abdullah Asuhaimi bin Mohd Zin
Department of Electrical Power Engineering
Faculty of Electrical Engineering
Universiti Teknologi Malaysia
Johor Bahru, Malaysia.
asuhaimi@utm.my

***Abstract*—Renewable Energy source, unlike conventional fuel burning, naturally widely distributed and can be set up in a limited way around the globe in different courses. The use of fossil fuels in power generation led to the pollution problem in many states. In this report, the scope and opportunity to develop ocean wave power generation scheme that is sustainable. The equivalent circuit method can be effective modelling techniques to examine the system of Wave Energy Converter (WEC). The general approach presented in this paper to obtain the entire circuit model of mechanical-electrical subsystems that is to say from the buoy to the generator. Power converter is employed to convert electrical energy from single phase to three phase. Overall WEC equivalent circuit model was produced in the MATLAB/Simulink environment. The electrical parameters of WEC model have been described that include output voltage, current and power. This paper also presents a feasibility study of wave energy in different locations in Malaysia, including the calculated sum of power available from the ocean environment in Malaysia.**

Keywords—wave energy; equivalent circuit; wave buoy; synchronous generator; power converter; Simulink

I. INTRODUCTION

Development of a country is dependent on energy management that is efficient and effective. Success factors to the implementation of wave energy has to do with the policy, the economy and environment of a country. Renewable Energy (RE) is the best alternative which is less affected and the impact on the environment. Wave energy is an eco-friendly RE and easily available in the ocean.

WEC technology has been employed to convert wave power into electricity, but they are no longer commercially feasible. To attain this, control engineering is believed to take on an important part in this area. There are a large number of concepts for WEC. Despite the great variation in design, WEC usually categorized by location and type.

Among the types of WEC, the type of point absorber has the potential to offer a great amount of energy in a relatively small device [1]. It is as well recognized as the buoy technology. Conversion of force to the electrical elements is used to hold a series RLC circuit to conduct wave buoy [2]. Additional model generator circuit, the equivalent circuit WEC developed with all significant parameters [3]. There are different configurations of WEC uses different converter design. This converter is employed to set the input voltage varying system compared to the desired output voltage [4].

Wave buoy, synchronous generators and power electronic converters are connected to the production of the WEC system. This paper is a simplified equivalent circuit for the WEC system can continue to be used in system optimization and reliability analysis. It also describes the use of the equivalent circuit as common modelling language. By modifying the physical elements into electrical components, one can execute the overall WEC system analysis by simulating an electrical circuit model.

II. DESCRIPTION OF THE SYSTEM

A WEC in this system consists of a single buoy body, generators, and power electronics. The buoy absorbs the wave impact force. This force is then transformed into the oscillating electrical energy. The production of the generator is oscillating. To eliminate unnecessary oscillation of output power, AC to DC converter block is incorporated with the system and consequently the DC output is changed over to the corresponding frequency using inverter block. Fig. 1 representing an overall block diagram of the system studied.

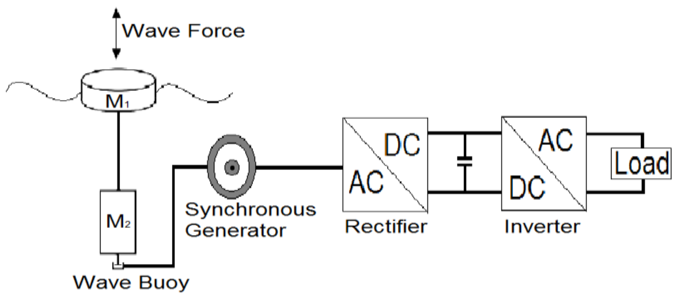

Fig. 1. WEC Parts In This System

III. WAVE DATA ANALYSIS IN PERSPECTIVE MALAYSIA

Five locations were chosen for this investigation. These locations are Straits of Malacca (L1), Tioman (L2), Kuching (L3), Labuan (L4) and Sulu (L5) Waters. In this section the wave height, wave period and wave power are expressed for different months of a twelvemonth. The data are obtained by the Malaysian Meteorological Department for 2016 [5]. The mean output wave power from these five locations are estimated and submitted in tabular forms in Table 1.

Table 1. Wave Data Analysis

Location	Average Wave Height (m)	Average Wave Period (s)	Average Wave Power (W/m)	Average Wave Force (N)
L1	0.5	6.625	1632	21622
L2	0.854	7.167	5152	43225
L3	0.938	6.417	5557	38032
L4	1.021	7.042	7230	49872
L5	1	9.25	9114	84302

Wave power given by [6]:

$$P=\frac{\rho g^2 H^2 T}{32\pi} \tag{1}$$

where, ρ is the mass density of water (1000 kg/m^3 for fresh water or 1030 kg/m^3 for salt water), g is the acceleration due to gravity (9.807 m/s^2), H is the wave height (m) and T is the period of wave (s). From Equation (1) it is clean that the square of the wave height is directly relative to the wave period because other parameters of the equation are constant.

Power, as a mapping of time, is the pace at which work is performed. Because work is a force applied over a length, this can be rewritten as:

$$P=\frac{W}{T}=\frac{FH}{T} \tag{2}$$

Wave force given by:

$$F=\frac{PT}{H} \tag{3}$$

Based on analysis of this data in Table 1, it can be concluded that there was an annual average wave power at sea Malaysia is (1632 + 5152 + 5557 + 7230 + 9114) / 5 = 5737 W/m which have the highest potential of wave power annually in Sulu Waters estimated 9114 W/m.

IV. WEC Equivalent Circuit Model

Equivalent circuit model for a comprehensive WEC system can be depicted in this division.

A. Approximation and Electrical Model of Wave Buoy

The equivalent circuit model of a wave buoy WEC system is constructed based on the system force analysis. Fig. 1 illustrates the scenarios of the linear WEC model for force analysis. In summation to the layout of the circuit, one of the most important steps is to find out the corresponding equivalent electrical components. By comparing each term force of the voltage drop over different RLC components, conversion relationship can be obtained. They are summed up in Table 2 [7].

Table 2. The Main Conversion Relationship

Terms Appear In Force Equations	Electrical Equivalents
mass = *M*	inductor = *M* henries
viscous damper = f_v	resistor = f_v ohms
spring = *K*	capacitor = 1/*K* farads
applied force = *f(t)*	voltage source = *f(t)*
velocity = *v(t)*	mesh current = *v(t)*

To obtain the equivalent circuit model in terms of force, generally five steps necessary [2]:

i. Converts each physical quantity in the equivalence of force to electrical parts.
ii. Discern if electrical components have a fixed rate or variable.
iii. Identify the electrical circuit layout, determine if it is parallel or series connected between components.
iv. Determine the direction when setting the electrical portion, when it causes positive and negative poles.
v. Add a switch in an electrical circuit in which deformation forces equation.

Parameters such as buoy mass, hardness of the spring or other means fixed parameters for a set of WEC units. They can be fed into the electrical circuit model with the same value in SI units. Based on the Fig. 1, the equivalent circuit model presented in Fig. 2.

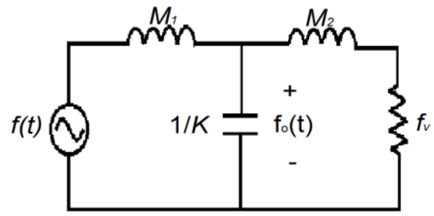

Fig. 2. Approximated Wave Buoy Equivalent Circuit Model

Follow the convention that the force is equal to the voltage drop, because all the force requirements can be composed in the form of Ohm's law.

B. Equivalent Circuit of Synchronous Generator

Model generator can be obtained from the equivalent circuit as presented in Fig. 3. This is a beginning point for the establishment of an important equation. A synchronous machine as the name suggests must be spinning in a unique synchronous speed related to supply frequency. Stator winding is a three phase, but the rotor winding carrying a direct current. Equivalent circuit per phase synchronous generator stator links and run the rotor windings.

Main elements of equivalent circuit are stator and rotor resistance (R_s, R_f), stator and rotor leakage inductance (L_{ls}, L_{lf}), core-losses resistance (R_m) and magnetizing inductance (L_m), supply (stator) voltage (V_s), excitation or speed EMF (V_f), stator and field (rotor) current (I_s, I_f), magnetizing current (I_m) [3].

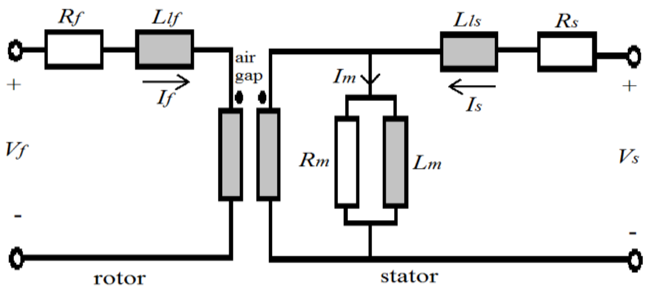

Fig. 3. Equivalent Circuit Per Phase Of Synchronous Generator

C. Power Converter

A phase converter used in this study. A phase converter is a device that changes electrical energy supplied as a single phase to multi-phase or vice versa. The majority of the phase converter is employed to generate three-phase electric power from a single phase source. Circuit diagram explains the conversion as shown in Fig. 4 [8].

Phase converter typically consists of a, single phase diode rectifier, DC link capacitor and three phase inverter. The single phase rectifier is applied to change AC voltage to DC voltage. Three-phase inverters is used to change DC power to AC power of variable voltage and frequency.

A DC link capacitor is a capacitor connected in DC link between the rectifier and the inverter circuit converter. These capacitors serve to filter out transients that might arise from the inverter and also help smooth the output DC waveform. In general the DC link capacitor is designed as a high value so that the organization sustains a constant DC link voltage.

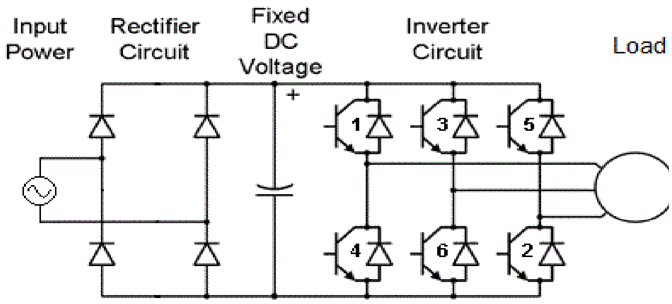

Fig. 4. Working Method Of Single Phase To Three Phase Converter

V. SIMULATION RESULTS & DISCUSSIONS

The simulation is done using MATLAB/Simulink R2016a and computer PC with the following specs: Windows 7 Home Premium 64-bit SP1, Intel Pentium CPU P6200 @ 2.13GHz, 2.0GB RAM, AMD Radeon HD 6470M.

From Table 1, the highest average wave force and average wave period is from Sulu Waters with the value is 84302 N and 9.25 s. Fig. 5 shows the simulation results of wave excitation force, wave buoy force and velocity. The wave buoy have been used with the resistance value $f_v = 3\ \Omega$, inductance value $M_1 = 4$ H, $M_2 = 2$ H and capacitance value $1/K = 1/5$ F.

The output from wave buoy then going to synchronous generator to convert wave power into electric power. Fig. 6 shows the output voltage of the synchronous generator. The synchronous generator have been used with the resistance value $R_s = R_f = 10^{-1}\ \Omega$, $R_m = 10^{-3}\ \Omega$ and inductance value $L_{ls} = L_{lf} = 10^{-2}$ H, $L_m = L_{ag} = 10^{-4}$ H. It is clear from the graph that, at the beginning the voltage goes up to high values before stable at normal value around 45 V.

The output voltage from generator then going to single phase diode rectifier. Fig. 7 shows the DC output voltage from generator after converted from single phase diode rectifier. The DC link capacitor have been used with the capacitance value C = 1 nF. The output voltage start to increase until reach the final around 180 V.

Fig. 8 shows the phase to phase (V_{ab} (top), V_{bc} (middle) and V_{ca} (bottom)) voltages of the three phase inverter. Fig. 9 shows the phase to neutral voltages (V_{an} (top), V_{bn} (middle) and V_{cn} (bottom)) at the load side before using RLC filter. It is clear from the graph that the maximum positive or negative peak of the phase to neutral voltage is 2/3 of the maximum positive or negative peak of the phase to phase voltage shown in Fig. 9.

The phase to phase voltage shown in Fig. 8 has been redrawn in Fig. 10 after RLC filter was used. The RLC filter have been used with the resistance value R = 1 Ω, inductance value L = 1 mH and capacitance value C = 1 mF. As shown in the Fig. 10, it is clear that the system has some variation under various loads.

The phase to neutral voltage shown in Fig. 9 has been redrawn in Fig. 11 after RLC filter was used. The RLC filter have been used with the resistance value R = 1 Ω, inductance value L = 1 mH and capacitance value C = 1 mF. As shown in the Fig. 11, it is clear that the system has some variation under various loads.

Fig. 12 shows the output power of the WEC. It is clear from the graph that, at the beginning the power goes up to high values before stable at normal value around 6 kVA. From the developed circuits from the previous sections, an equivalent circuit model for a comprehensive WEC system can be shown in Fig. 13.

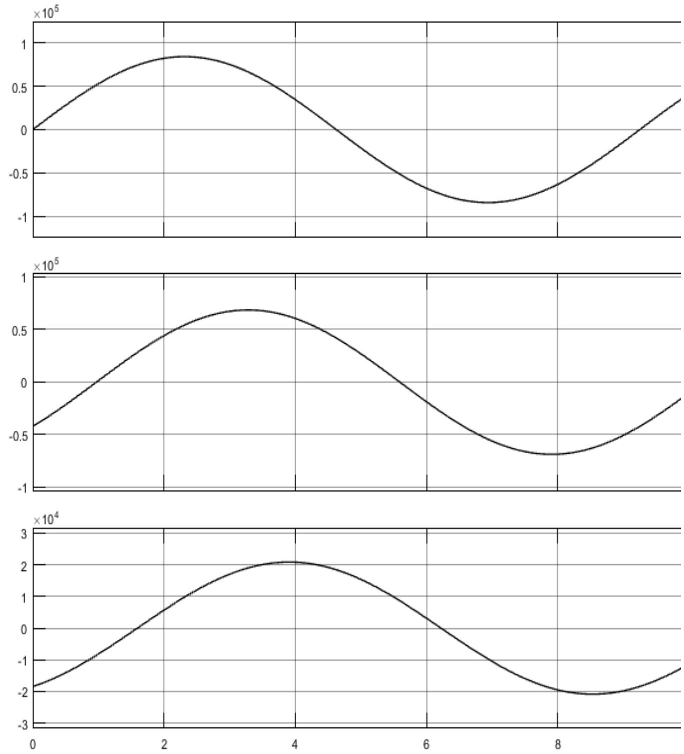

Fig. 5. Wave Excitation Force (Top), Wave Buoy Force (Middle) And Wave Buoy Velocity (Bottom)

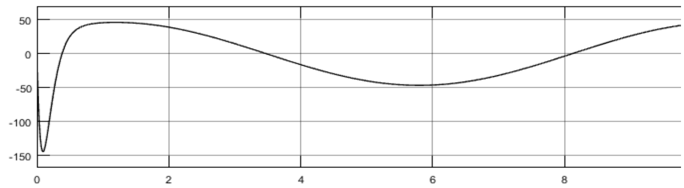

Fig. 6. Output Voltage From Generator

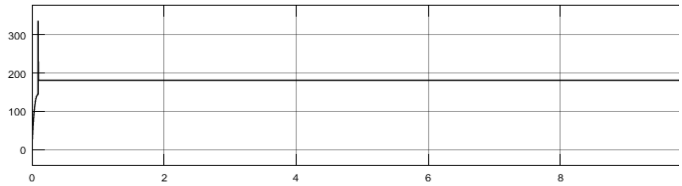

Fig. 7. DC Output Voltage From Generator After Converted From Single Phase Diode Rectifier

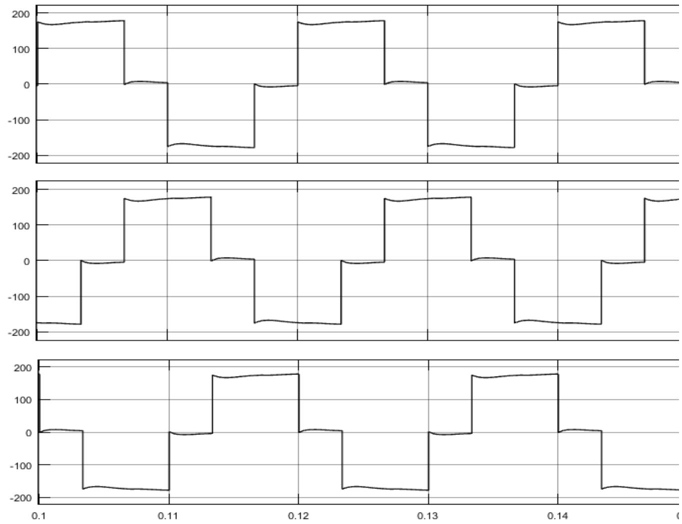

Fig. 8. Phase To Phase Voltages Of The Three Phase Inverter (V_{ab} (Top), V_{bc} (Middle) And V_{ca} (Bottom))

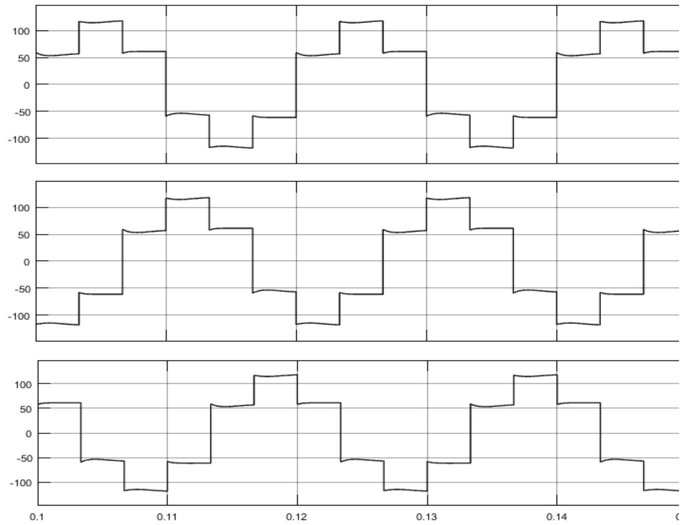

Fig. 9. Phase To Neutral Voltages Of The Three Phase Inverter (V_a (Top), V_b (Middle) And V_c (Bottom))

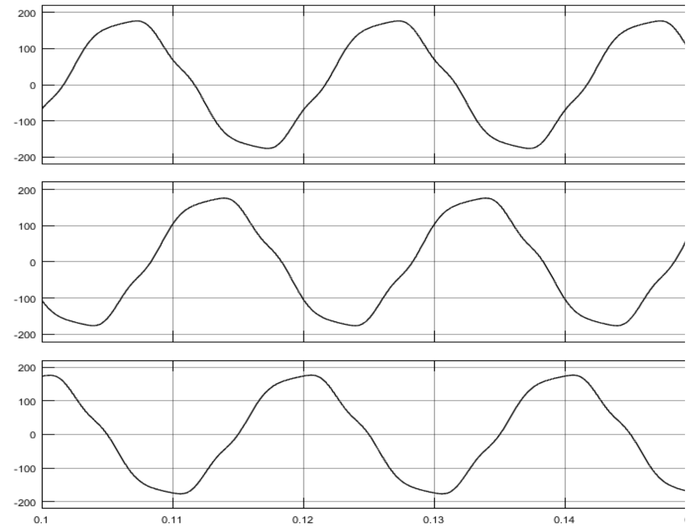

Fig. 10. Phase To Phase Voltages Of The Three Phase Inverter (V_{ab} (Top), V_{bc} (Middle) And V_{ca} (Bottom)) After Using RLC Filter

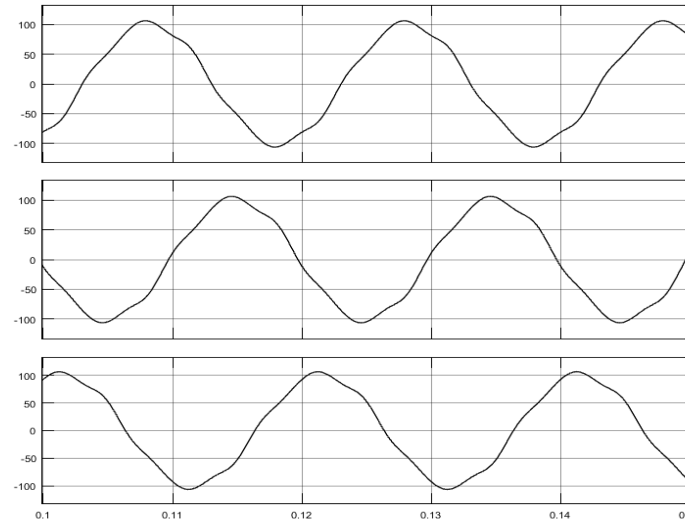

Fig. 11. Phase To Neutral Voltages Of The Three Phase Inverter (V_a (Top), V_b (Middle) And V_c (Bottom)) After Using RLC Filter

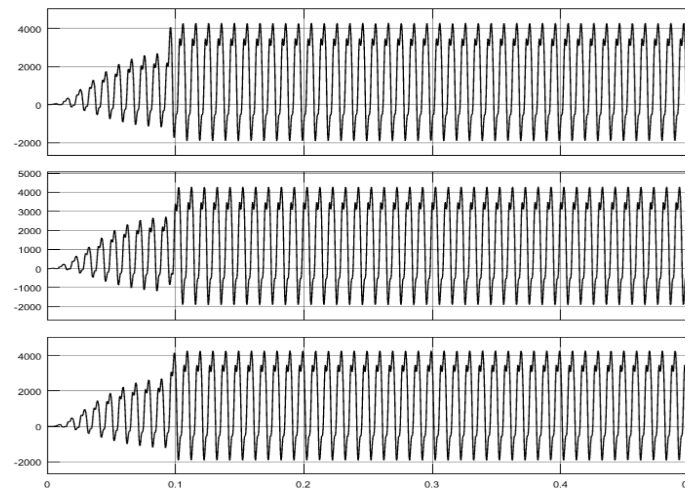

Fig. 12. Output Power Of The WEC

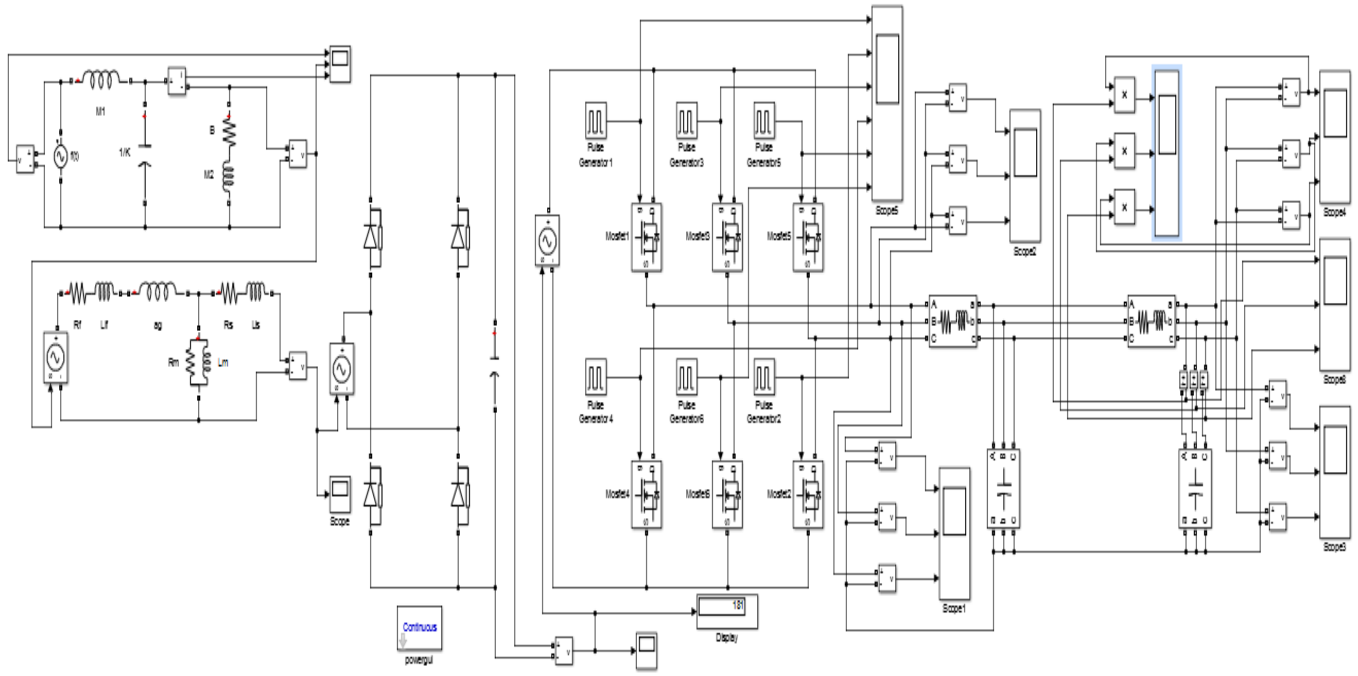

Fig. 13. Overall WEC Equivalent Circuit Model In MATLAB/Simulink

VI. Conclusion

This paper expands on the methodology of setting up a nonlinear equivalent electric circuit model to be utilized as a system modelling tool for point absorbing WEC systems. Validation of a simple model to bring out the good forecast the average electrical power captured can be awaited from this model. This rapid modelling method will simplify the design, fitting and optimization of certain key parameters and system-wide wave power. To realize the wave energy in Malaysia, a special study on energy generator waves to do with the depth of get the maximum possible amount of energy. Further inquiry is needed to explore more about the problem of checking the output voltage of the converter and specific problems of grid connected power electronic converter under grid voltage distortion.

References

[1] Drew, Benjamin, Andrew R. Plummer, and M. Necip Sahinkaya. "A Review of Wave Energy Converter Technology," J. Power Energy, vol. 223, pp. 887–902, 2009.

[2] L. Hai, M. Göteman and M. Leijon, "A Methodology Of Modelling A Wave Power System Via An Equivalent RLC Circuit," in IEEE Transactions on Sustainable Energy, vol. 7, no. 4, pp. 1362-1370, Oct. 2016.

[3] Špoljarić, Željko, Krešimir Miklošević, and Vedrana Jerković. "Synchronous Generator Modelling Using MATLAB". SiP 2010 28th International Conference Science in Practice. 2010.

[4] K. H. Mohamed, N. C. Sahoo and T. B. Ibrahim, "Design Of Converters for Wave Energy Conversion System," 2012 4th International Conference on Intelligent and Advanced Systems (ICIAS2012), Kuala Lumpur, 2012, pp. 491-496.

[5] M. Kamaruzaman M. A., Nursalleh K. C., Dr. Fariza Y. And M. Helmi A. "Long Term Monthly Mean of Wave Height and Period over Malaysian Waters and Its Adjacent Seas". Research and Technical Development Division, Malaysian Meteorological Department. Technical Note No. 4/2016.

[6] N. H. Samrat, N. B. Ahmad, I. A. Choudhury and Z. Taha, "Prospect of Wave Energy in Malaysia," 2014 IEEE 8th International Power Engineering and Optimization Conference (PEOCO2014), Langkawi, 2014, pp. 127-132.

[7] Nise, Norman S. "Control System Engineering, John Wiley & Sons." Inc., New York (2011).

[8] Mariyammal, Harikumar, Lakshminarayanan, Raja & Dharmalingam. "Phase Conversion Using MOSFET Technology with an Embedded System". Best: International Journal of Management, Information Technology and Engineering (Best: IJMITE) Vol. 1, Issue 2, Nov 2013, 43-48.

Automation Analysis of Power Theft Detection using Machine Learning

Mohamad Syuib B Johari
Faculty of Electrical Engineering
Universiti Teknologi Malaysia
Johor Bahru, Malaysia.
syuib_09@yahoo.com

Dato` Profesor Dr Ahmad B Darus
Department of/ Centre of
Faculty of Electrical Engineering
Universiti Teknologi Malaysia
Johor Bahru, Malaysia
eahmad@utm.my

***Abstract*— The analysis of power system data required a vast usage of intelligent data analysis tools in order to accurately classify the desired results for the system. This paper presents an approach towards the detection of power theft faced by Tenaga Nasional Berhad (TNB) Malaysia by using support vector machine (SVM) as the main classifier and neural fuzzy inference system to further classify the probabilities of uncertain data. The main motivation of this research is to provide Tenaga Nasional Berhad (TNB) Malaysia with a user-friendly data analysis platform especially in detecting the electricity theft cases amongst the customers by using intelligent data analyzer. There are two platforms involved – EXCEL dashboard and MATLAB analyzer – created for this system. Then remote meter reading (RMR) data which consist of total energy consumption (kWh) and others important parameter are being used in order to verify the developed system. There are also several additional data i.e. Energy audit parameter and some economic indicator, being manipulated by using the same system which helps to maintain the validity of the results obtained regarding the suspected customers hit rate through variety of data. With the implementation of this platform, Non-Technical Losses (NTL) activities of the customers in TNB Malaysia are expected to be reduced effectively especially in the cases of electricity theft.**

Keywords—Nontechnical losses, Electricity theft; SVM, Fuzzy logic; Intelligent systems.

I. INTRODUCTION

The electricity demand in Malaysia has stated quite a large difference which comprised of Peninsular Malaysia (97.2TWh) and also in Borneo (12.1TWh). According to Zulkiflee Umar, Head of Demand Side Management Unit at the Energy Commission, as the time faded, the pattern of energy consumption demand kept on increasing from 85,260GWh to around 116,087.5GWh after 10 years consecutively. [1]

Power theft is considered as one of the non-technical losses (NTL) either at the transmission department or at the distribution department. Hence, it greatly affects the quality of supply, increasing the generation capacity in order to fulfill the excessive load demand and also affected the future tariff.

Based on the Energy Malaysia Magazine, Tenaga Nasional Berhad (TNB) have lost nearly RM14 million due to electricity theft. [2]

Hence, a lot of research was done in order to create a suitable intelligent system to be implemented in electrical system analysis which will then become the updated system in handling this power theft cases.

The researches includes the used of Statistical Methods, Decision Trees, Artificial Neural Networks (ANNs), Knowledge Discovery in Databases (KDD), and Multiple Classifiers using cross identification and voting scheme. [3]

But in taking consideration of the mostly being used method as the solution, load profiling which means the screening of the customer load profile patterns are stated as the one that most famously being implemented. [3]

This is also some of the preventive steps that could be taken by utility so that they could surpass the existing power quality and avert mischief from kept on happening either in transmission or distribution. [4]

II. SVM BASED FUZZY INFERENCE SYSTEM

A. Support Vector Machine (SVM)

In late 1960s, Vapnik had introduced the support vector machine (SVMs) concepts. [3] It is a special machine learning categorization tools which is very good in manipulating the concept obtained by inference from specific areas.

Their classification errors value is minimized based on the following equation [3];

$$f(x) = sgn\ (g(x)) \tag{1}$$

where $g(x)$ = decision boundary between 2 classes

This condition is achieved after undergoes the method of structural risk minimization (SRM) as explained in [3].

SVMs have proven to be an effective concept in linear and non-linear classification of data by considering the established method on reducing the training data points that involved in explaining the detail of the roots of the polynomial used as a function in the developed system.

Hence, these resulted in the reduction of unclassified data in introducing a classifier which also minimized the participating data points, known as support vectors. By implementing this process, the formation of noises could be avoided thus giving more capability on the generalization of the system training data.

SVM have its own advantage in automatically choosing their model capacity and optimizing the margin of separation. It used up kernel function for non-linear classification problems. But SVM also have its cons which cause by their black box nature. This is because it does not allow the extraction of interpretable inference obtained from the final classification models made by user. It also deteriorates once non-informative features being used as the system inputs. Besides, SVM alone will suffer computational cost and will not search for the optimal feature subset.

The SVM is one of the important interfaces created in order to produce the most optimum decision function through the classifications processes. These include the accuracy in predicting the invisible data into two main classes namely hyperplane that separate the classes.

B. Adaptive Neuro Fuzzy Inference System

Fuzzy Logic is a unique knowledge recognized as one of the most effective ways in qualifying probabilities and possibility in uncertain set of data which taking into the consideration of linguistic concepts besides acting also as the universal approximator, especially in manipulating nonlinear relationship of inputs and system outputs. It divides into three main concepts which is the theory of fuzzy set, fuzzy if-then rules and fuzzy reasoning. [5]

Fuzzy rules are considered to be among the closest computer languages with the linguistic feature made by human interpretation. It also at the best in defining non-linear functions and allowing the extraction of knowledge from the initial row of data such as High Risk and e-CIBS data from Tenaga Nasional Berhad.

As being mentioned in [5], the accuracy of fuzzy inference system (FIS) greatly depends on the number of the samples being trained and tested.

Despite of that, fuzzy have quiet low performance in term of classification, over fitting and the absence of generalization properties.

ANFIS which stand for Adaptive Neuro Fuzzy Inference System is a type of hybrid artificial intelligent system. It is the combination of two types of intelligent system which is artificial neural network and fuzzy inference system. Basically, ANFIS will manipulate some types of important components such as memberships function (MFs), rules and parameters.

C. Support Vector Machine-Fuzzy Inference System (SVM-FIS)

SVM-FIS is a type of hybrid machine learning which combine both support vector machine system and fuzzy inference system in order to get the desired classifications of data.

The analysis being done in [6] have proven that the precision of the SVM analysis can be reduced by adjusting the parameter of the memberships function (MFs) in the fuzzy inference system.

TABLE I. COMPARISON BETWEEN DIFFERENT MODELING APPROACHES

No of Fuzzy Rules	Methods				
	ANFIS-0	ANFIS-1	RBF	SVM	Proposed SVM-FIS
170	$<10^{-10}$	$<10^{-10}$	0.0042	0.0540	$<10^{-10}$
6	0.0034	0.0023	0.0082	0.0509	0.0076
5	0.0041	0.0024	0.0086	0.0635	0.0090
4	0.0050	0.0030	0.0091	0.0748	0.0091
3	0.0074	0.0034	0.0141	0.1466	0.0092
2	0.0087	0.0041	0.0191	0.1955	0.0099

Table I above proved that the proposed methodology in [7] is better than SVMs alone by showing the least probability of effectiveness in data classification.

SVM is providing a special framework in order to extract the supports vector for the application on the fuzzy rules. It would greatly resolve the issues regarding the interpretability and complexity. [7]

III. The Proposed System Architecture

In order to implement a special EXCEL Dashboard to be used by Utilities Company such as TNB, SESB and SESCO at the field, an integrated platform have been created by using Microsoft Excel as database and MATLAB as the data analyzer.

The framework shown in Figure 1 basically is made up from the previous research in [8]. But, in order to fulfill the desired total of input by means of increasing the hit rate of power theft detection, 3 main input have been added up to the framework which is economic parameter, BEI/GBI data and energy audit data.

By doing this, the system would be targeted to narrow down the probabilities of fraud more detailed than previous research. This is because the expectation of greater accuracy with more data being trained by ANFIS will contribute to higher hit rate detection on the power theft suspects.

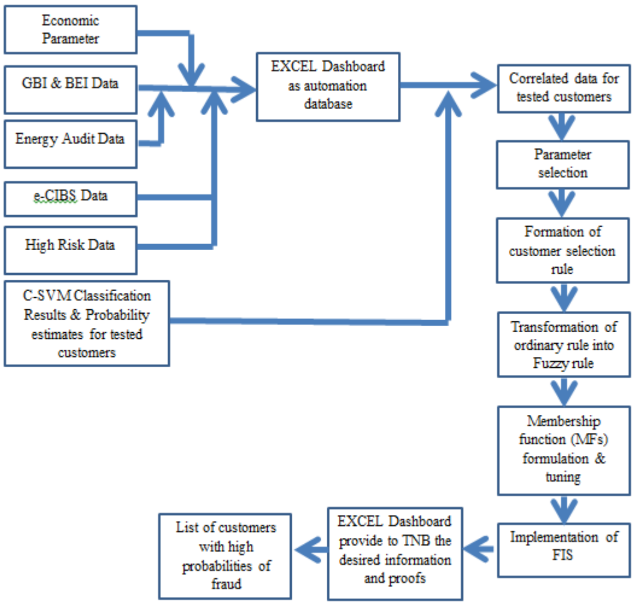

Fig. 1. Flowchart of the improved system by using Excel dashboard as the database for SVM and FIS classifier.

Figure 1 shows the preprocessed flowchart of the non-technical losses (NTL) mainly in the detection of electricity theft by considering some chosen internal parameter i.e. e-CIBS data, and also some external factor i.e. national gross domestic products (GDP) and oil prices, that have been classified as one of the contributing factors that affects the electricity tariff in Malaysia. [9]

Before the data being classified by C-SVM classifier, past research has been referred regarding Green Building Index (GBI) calculator concept in [10] so that GBI, Building Energy Index (BEI) and energy audit data would be categorized first before accumulated the data with e-CIBS and High Risk data. By doing so, it would be easier for SVM system to classify the data logged before entering the fuzzified stage. But in this project, the GBI, BEI and energy audit data just being placed in the database as future implementation in term of adding up the parameters to be trained. This is because these data have to be retrieved from each company. Hence, a lot of critical constraints have to be considered in taking the GBI and BEI data as the respective parameter in detecting the fraud.

Other than that, a new platform has been added in the framework for the implementation of database dashboard in order to give better hands-on experience for power utility in detecting power theft especially in short period of time and hence giving them enough proofs and analysis to suspect the fraud on the shortlisted customers.

A. Excel Dashboard and Automation

As for the means of big amount of data stored, a unique Excel dashboard has been built in order to provide reliable database for the data collected. This dashboard consists of all the data and parameter needed in order to classify the suspected customer committing the power theft.

The parameter included electricity consumption (kWh), sales (RM), recent crude oil and their refined products prices, annual Gross Domestic Product (GDP), premise and electrical equipment types that being used by the specified customer. These data are the collection of the data from year 2015 to 2016 except for both premise and electrical equipment because it has to be retrieved from each of the customers by conducting onsite inspection. Hence, the existence of both parameters in the dashboard will act as future platform for the system.

The dashboard also contained 3 different sheets of data analysis display which is input data, SVM analysis results and fuzzy inference system analysis results. They have been included in the dashboard in order to display and visualize the expected results produce from SVM-FIS classifier by using the MATLAB software.

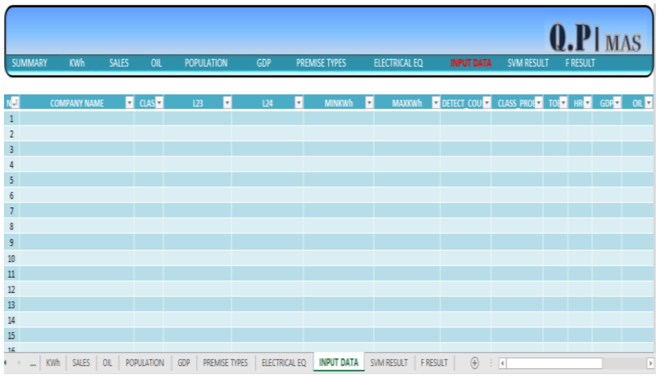

Fig. 2. Excel dashboard which being used as database before the data analyzed in th Matlab through SVM and FIS.

Figure 2 shows the Excel dashboard which known as the QP (MAS) which stand for Quest Power (Malaysia). This is the unique name created for the database, based on the project conducted. The figure displayed the input data sheet which consist of some basic parameter to be analyze using the SVM in Excel XLSTAT before fuzzified by the fuzzy inference system in MATLAB.

There is also a sheet named as Summary which comprised the visualization of all data collected in charts and these data will then be self-updated by using the latest results. The dynamic concept by using some of the function in EXCEL will create a self-updated graph and charts in order to visualize the latest results.

B. *Support Vector Machine Classifier*

SVM is one of the machines learning techniques that being used in separating between 2 classes of data so that the idea of getting bigger separation for more reliable classification of the data could be achieved.

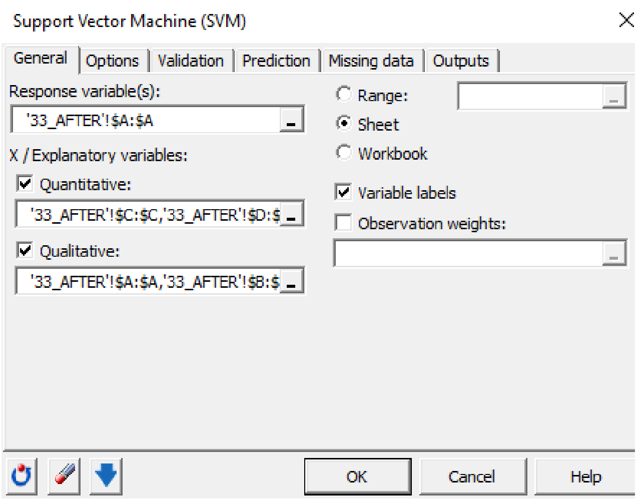

Fig. 3. SVM editor in Excel software by using XLSTAT as the add-in

Figure 3 shows the support vector machine (SVM) editor used to conduct the analysis of the data collected. This editor is one of the latest add-in function in Excel utilized the used of XLSTAT software, a well proven scientific analytical software. It provides the user with some intelligent data analyzer including support vector machine (SVM) classifier.

This editor mainly use linear kernel function in its SVM classifier in order to achieve the best fit on the data trained. But in order to obtain the interpretable fuzzy model by using support vectors, the number of support vectors stated have to be equivalent to the number of rules in fuzzy model.

C. *Neuro Fuzzy Designer*

There is some different toolbox prepared in the MATLAB that can be used in order to analyze the data by using fuzzy inference concept. For this project, the toolbox chosen is neuro-fuzzy designer. This toolbox applied Sugeno-type fuzzy and provide the user with ANFIS Editor. This editor will then be used in the determination of the selection rules

Figure 4 shows the adaptive neural fuzzy inference system (ANFIS) editor in the MATLAB. This editor is being used in order to analyze deeper the customer's data profiles by considering the formation of inputs, outputs and selection rules.

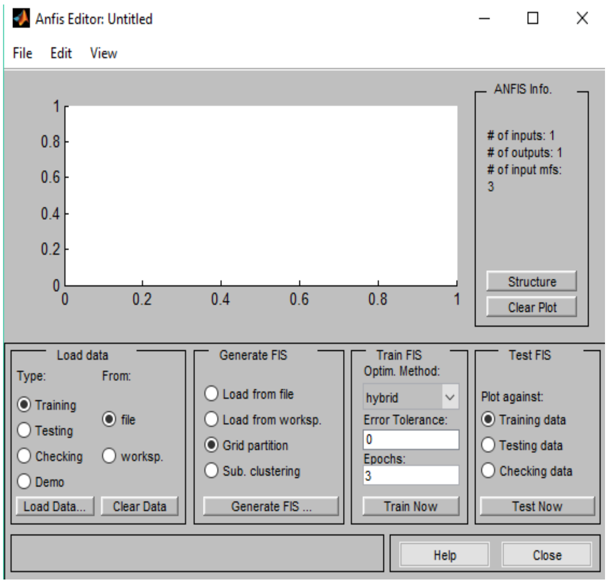

Fig. 4. ANFIS editor in Matlab

Figure 4 shows the adaptive neural fuzzy inference system (ANFIS) editor in the MATLAB. This editor is being used in order to analyze deeper the customer's data profiles by considering the formation of inputs, outputs and selection rules.

Sugeno-type fuzzy inference being used instead of Madani-type as the methods in constructing the fuzzy model for this system. This is because Sugeno-type theoretically proven to be effective in applying together the optimization techniques as well as adaptive techniques. By the means of the continuity of output surface, Sugeno-type is the better choice compared to Mamdani-type in term of mathematical analysis.

IV. Experimental Result

Confusion matrix for the training sample (detected- 0 / 1):

from \ to	0	1	Total	% correct
0	482	81	563	85.61%
1	118	262	380	68.95%
Total	600	343	943	78.90%

Confusion matrix for the validation sample (detected - 0 / 1):

from \ to	0	1	Total	% correct
0	44	13	57	77.19%
1	16	27	43	62.79%
Total	60	40	100	71.00%

Fig. 5. 1st SVM training result in Excel XLSTAT

Performance metrics (detected - 0 / 1):

Statistic	Training set	Validation set
Accuracy	0.789	0.710
Precision	0.803	0.733
Recall	0.856	0.772
F-score	0.829	0.752
Specificity	0.278	0.270
FPR	0.722	0.730
Prevalenc	0.511	0.440
Cohen's k	-0.032	-0.015
NER	0.597	0.570

Fig. 6. 1st SVM training statistics in Excel XLSTAT

Confusion matrix for the training sample (detected - 0 / 1):

from \ to	0	1	Total	% correct
0	475	98	573	82.90%
1	218	152	370	41.08%
Total	693	250	943	66.49%

Confusion matrix for the validation sample (detected - 0 / 1):

from \ to	0	1	Total	% correct
0	52	9	61	85.25%
1	17	22	39	56.41%
Total	69	31	100	74.00%

Fig. 7. 2nd SVM training result in Excel XLSTAT

Performance metrics (detected - 0 / 1):

Statistic	Training set	Validation set
Accuracy	0.665	0.740
Precision	0.685	0.754
Recall	0.829	0.852
F-score	0.750	0.800
Specificity	0.161	0.220
FPR	0.839	0.780
Prevalenc	0.504	0.520
Cohen's k	-0.189	-0.097
NER	0.608	0.610

Fig. 8. 2nd SVM training statistics in Excel XLSTAT

Figure 5 to Figure 8 above shows the results of SVM classifier used to trained the data. In this initial data training, a total of 1300 backdated load profile for customers in Kulai, Johor are taken randomly from the sample of 88000 customers in year 2015 to 2016. These 1300 customers are shortlisted based on their Theft of Electricity (TOE) tagging and High Risk Customer (HRC) tagging, given by the TNB Metering Department in Petaling Jaya, Selangor.

After conducting some series of data training on the same sample, the accuracy of the detected customers on the fraud are recorded simultaneously once the training are done. The statistics of the data training are also being displayed on the same sheet.

It is found that on the first 1st training result, 71% of accuracy are recorded. The accuracy kept on increasing after 2nd training being done which 74% of the training accuracy are recorded. These results proved that this system is reliable in detecting the potential customers committing the electricity theft by comparing it with the results in [8].

V. Conclusion

Based on the results analyzed by this system, the detection hit rate of the potential customer recorded are classified as reliable based on the onsite inspection that have been done by TNB SEAL in year 2015 to 2016. The accuracy issue kept on happening even in the past research because in the detection of electricity theft amongst thousands of customers, there are a lot of aspects that should be considered. For this research, by considering the effects of economic status in Malaysia, the oil prices and gross domestic product (GDP) on the respective years are being considered as one of the additional parameter. This system should increase the detection hit rate on the fraud. Moreover, by expanding deeper insight in machine language, the database still could be upgraded to a better system in order to ease the utility companies such as Tenaga Nasional Berhad in reducing the non-technical losses (NTL) especially in Malaysia.

References

[1] Ahmad Fauzi Hasan. (2015,Vol 6). Leading public adoption. *Energy Malaysia*[Online].Available:http://www.st.gov.my/index.php/ms/downloads/category/112-energy-malaysia?download=585:energy-malaysia-volume-6-2015

[2] Ahmad Fauzi Hasan. (2014,Vol 4). Keeping watch. *Energy Malaysia* [Online].Available:https://www.google.com/url?sa=t&rct=j&q=&esrc=s&source=web&cd=2&cad=rja&uact=8&sqi=2&ved=0ahUKEwjwvsPdyuzTAhWBPRoKHULjDOgQFggnMAE&url=

[3] Jawad Nagi, Keem Siah Yap, Sieh Kiong Tiong, Syed Khaleel Ahmed, and Malik Mohamad, "Nontechnical loss detection for metered customers in power utility using support vector machines", IEEE TRANSACTIONS On POWER DELIVERY, Vol. 25, No. 2, 2010.

[4] Soma Shekara Sreenadh Reddy Depuru, Lingfeng Wang, Vijay Devabhaktuni, "Electricity Theft: Overview, issues, prevention and a smart meter based approach to control theft", Energy Theft (2011), pp . 1007-1015.

[5] Michael Negnevitsky, Hybrid Intelligent System, 2nd ed, Artificial Intelligence, 2005.

[6] Jongcheol Kim and Sangchul Won, "New fuzzy inference system using support vector machine", Conference of Decision and Control, 2002.

[7] Duc-Hien Nguyen and Manh Thanh Le, "Improving the interpretability of support vector machines-based fuzzy rules", University of DaNang, 2014.

[8] Jawad Nagi, Keem Siah Yap, Sieh Kiong Tiong, Syed Khaleel Ahmed, and Farrukh Nagi, "Improving SVM-based ontechnical loss detection in

power utility using the fuzzy inference system", IEEE Transactions on Power Delivery, Vol. 26, No. 2, 2011.

[9] Norasibah Abdul Jalil, "The impact of oil price on the Malaysian economy', 2010.

[10] Nur Hazirah Zainal, "A Study of Building Energy Index and Energy Audit for Commercial Building", Universiti Teknologi Malaysia (UTM), 2013.

Smart Solar Powered Ventilation System for Vehicles

Wan Nur Azira Binti W Yahya
Faculty of Electrical Engineering
Universiti Teknologi Malaysia
Johor Bahru, Malaysia.
wannurazirawyahya@gmail.com

Prof Dr Ahmad Bin Darus
Department of / Centre of
Faculty of Electrical Engineering
Universiti Teknologi Malaysia
Johor Bahru, Malaysia.
eahmad@utm.my

***Abstract*— Solar energy is the most promising backup energy sources of clean and environment friendly energy sources that derived from the sun that can be exploited directly to generate electricity and has the potential to be developed in coming years in Malaysia. The temperature inside the car cabin will tremendously increases when they park their cars under the scorching sun and been there more than one hours especially in the afternoon. Many problem can be occur by this situation. The purpose of this study is to develop and design a simple ventilator using solar energy, which inhales fresh air from outside into the car and remove hot air to the outside without operates the car's engine. In this paper, the development, design and component for this smart solar powered ventilation system is described briefly. To complete this simple cooling system, the component that have been combined are solar cell, rechargeable battery, brushless fan, temperature sensor, current sensor, microcontroller, LCD 16x2 and data logging shield. Based on result, it is demonstrated that this research were conducted were given a positive feedback because it has successful reduce hot air from inside cars and maintain the temperature. In addition, due to its capability in improving the quality and quantity of air inside the cars that can provides comfort to user from this simple system that were proposed.**

Keywords*— *car ventilation system; solar cell; brushless fan; cabin temperature;

I. INTRODUCTION

The energy demand is expected to increase in Malaysia since the population for Malaysia is estimated to be 32.374 million by the year 2020. The global environmental concerns created the awareness to use clean energy [1]. Nowadays, renewable energy has been widely growing. Solar energy is the most promising backup energy sources of clean and environment friendly energy sources that derived from the sun that can be exploited directly to generate electricity and has the potential to be developed in coming years in Malaysia. The photovoltaic (PV) solar panel that can generate green electricity that has been growing rapidly and increasingly globalized. Photovoltaic convert solar energy directly to electricity [2]. Malaysia has been high PV energy production since it is located in the second largest solar radiation region as shown in Figure 1 and has daily average solar radiation of 4000–5000 Wh/m2 [3-4]. Malaysia is an equatorial country which is located in 4.2105° N and 101.9758°E; makes Malaysia's temperature is generally uniform throughout the year, with high humidity and heavy rains and with an average of sunshine daily of 12 hours that abundant of the sunshine throughout the year.

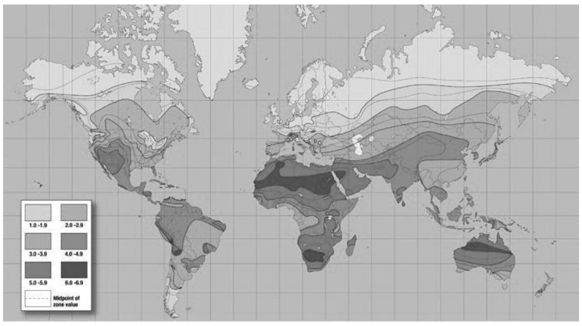

Fig. 1. Global surface solar radiation.

As the number of private transportation increased day by day, it caused so many problem because sometime cars needed to park in opening area. Because of limited space for indoor parking area and during peak hour, the needs of parking space are getting critical and most of drivers are having difficulty to get an indoor or roof parking space will automatically choose the alternative choice that is parking or leave their car in open parking space area where it is directly exposed to the sunlight. In this situation, the temperature inside the car cabin will tremendously increases. Moreover after the vehicles been in exposed to the sun for long period of time, this experience causes the driver and passengers feel very uncomfortable entering their vehicle [5]. Today, there are hundreds of children cases that being left in cars and experience varying degrees of heat illness and dead [6]. The main cause of this drastic rise in temperature inside car cabin can be attributed to conduction, convection and radiation but the most influencing factor in heating are radiation. There are several methods that can prevent solar radiation such as using sunshades when it is sunny, and installing the solar reflective films or window tints but cannot maintain comfortable temperature inside the car compartment [6].

Usually the simple way to reduce the high temperature and to maintain comfort in their vehicles is by running the air conditioner at high speed [7]. By using the air conditioning system to reduce the temperature will take some time and it will increase fuel consumption of the car to consumes a lot of power and will increase as well as carbon dioxide, CO2 . Hence, it need ventilation system to remove unwanted heat to help reduce all this kind of problem. There are many factors that can also influenced the behavior of the temperature such as ambient wind velocity, natural conduction, natural convection and radiation [8]. In general, the purpose of ventilation system not only for to remove the unwanted air but also can reduce unwanted smell at any place at any time. Ventilation system is a process which remove hot air in car cabin to the outside and inhales fresh air from outside into the car cabin without using or operates the car's engine and been done through proper design. Ventilation is very important because it can bring fresh air, circulated air flow and removed hot air from the car and provide the fresh air inside the car cabin that give comfortable to passenger even after been exposed to sunlight.

The temperature inside the car cabin increases tremendously even if the windows leaving slightly opened, the temperature inside the car not change much because the decreases of temperature is between 3 ºC to 5 ºC only. For this project, the main question is "How to design, develop and employ a simple and yet an effective system that can manage in and out of the air flow inside the car cabin." This may cause a various problem such as while entering the car the hot air inside the car cabin can make passenger became uncomfortable, it also can bring damage to the things, food, human and pet that found in the car and causing car aging problem. The purposes for this project are to determine, measure and analyses the temperature behavior inside car cabin that was expose under the direct sunlight with and without ventilations system and then design a simple ventilator using solar energy, which inhales fresh air from outside into the car and remove hot air to the outside without operates the car's engine.

II. Literature review

A. *Ventilation System*

In general, the purpose of ventilation system not only for to remove the unwanted air but also can reduce unwanted smell at any place at any time. Ventilation system is a process which remove hot air in car cabin to the outside and inhales fresh air from outside into the car cabin without using or operates the car's engine and been done through proper design. Ventilation is very important because it can bring fresh air, circulated air flow and removed hot air from the car and provide the fresh air inside the car cabin that give comfortable to passenger even after been exposed to sunlight. The usage of air-conditioning system in vehicle must be seriously considered since the air-conditioning system of the vehicles consumes a lot of power if want to improve vehicles mileage per charge [9]. By modifying the air inlet and outlet configurations can change the temperature inside the vehicles by modify low air circulation in the cabin [10].

B. *Thermal Comfort*

Nowadays, many research about the thermal comfort inside the vehicles has been carried out. Heating, Ventilation and Air-Conditioning (HVAC) is maintained the thermal comfort for the passenger of the vehicles [11]. The main parameters that control the thermal comfort of a passenger are relative humidity, air-flow temperature and velocity cabin temperature and the number of vents. When the relative humidity value is 50%, it is the optimal for thermal comfort sensation and if the values are in the range of 30 % to 70 %, humidity fluctuations play a minor role [12]. By measurements of the flow velocity and temperature at different operating conditions using equivalent temperature index were been studies in the thermal comfort in a car cabin [13]. Dependent on heat conduction, convection, radiation and evaporative heat loss, the thermal comfort is also a subjective term [10].

C. *Greenhouse Effect*

The greenhouse effect happens when the car park with all the windows closed for many hours that were been expose to the direct sunlight the thermal radiation from the sun were absorb by the greenhouse gases trapped inside a passenger car and re-radiate it inside in all direction [11]. Because of that, temperature inside the car cabin and external ambient temperature created a lot of difference between this two of temperature. By using the air conditioning system to reduce the temperature will take some time and it will increase fuel consumption of the car to consumes a lot of power and will increase as well as carbon dioxide, CO2 .The challenging problem is to saving overall cost for car, user of fuel and engine, reduce greenhouse effect and to save the environment.

D. *Solar Radiation*

The most instantaneous phenomena of energy transfer is radiation [6]. The solar irradiation enter the cabin through the windshield glass and hitting on the cabin interiors because of the reflection angle between the windshield glass and the sun ray than the interiors absorb the solar thermal radiation energy and eventually re-radiate the heat in vehicles [9]. The accumulated heat will affect many interiors inside the vehicle cabin for example electronic components, materials of the dashboard and the leather covers [14]. The main cause of this drastic rise in temperature inside car cabin can be attributed to conduction, convection and radiation. However, the most influencing factor in heating are radiation. The basic concept of radiation can be divided into three phenomena that is conduction, convection and radiation are shown in Figure 2 [15].

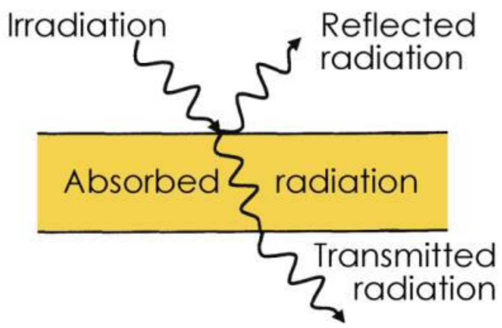

Fig. 2. Absorption, reflection, and transmission on real surface.

By using the sunshade can prevent solar radiation from entering the vehicles also can reduced the heat accumulation beside than opening the window slightly on both sides of the vehicles. Three effect were investigated between the relation of solar radiation and thermal comfort and the effect are the intensity of direct solar radiation from sunlight, spectral content of solar radiation and the glazing type on human thermal sensation responses that they concluded than the specific wavelength of the radiation is the critical factor affecting thermal comfort when total intensity of solar radiation is increases [16]. The radiation absorbed and emitted by the interiors of the cabin and the thermal radiation exchanged between the environment and body of the car can influence the temperature variation inside the car [6].

E. Solar Energy

Solar energy can be used to run the ventilator, and to charge the battery simultaneously. Figure 3 show the cross section of solar panel.

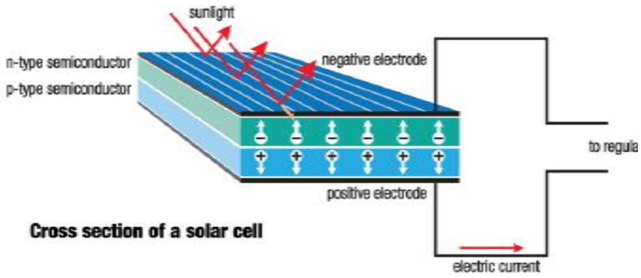

Fig. 3. Cross section of a solar panel.

III. METHODOLOGY

This project will be designed in order to determine the most efficient design of ventilation system using solar energy. This project is about how to keep ventilator system function when the vehicle is parked under the sunlight or in the cloudy day even if the vehicle engine is turned off. There are two parts of experimental methodology adopted in the current project. The first part are developing and testing the temperature measurement devices inside the vehicles cabin and then the temperatures are taken and record without ventilation system that have been two cases, closed all window and slightly open for both front window. In the second part is to design and develop a simple standalone solar PV ventilation and also to investigate cabin air temperature rise with developed the solar P.V ventilator. The best position of exhaust and the blower fan placed diagonally opposite to each other as shown in Figure 4. With this position of two fan, it has the non-existence of the dead zone and a better distribution of airflow compared to both other position such as the two fan placed opposite with each other and the two fan placed on the same side [17].

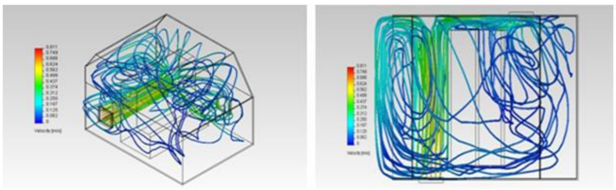

Fig. 4. Two fan placed diagonally opposite to each other.

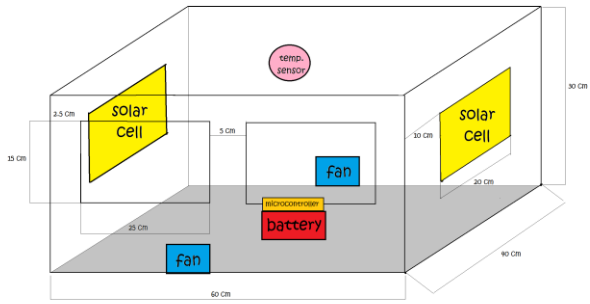

Fig. 5. Dimension for prototype model and position of component.

From Figure 5, one sensor was place at centre and upper inside the car to measure the temperature. The system will start operate and both fan will start working if temperature is more than 35°C that been powered by solar energy and rechargeable battery.

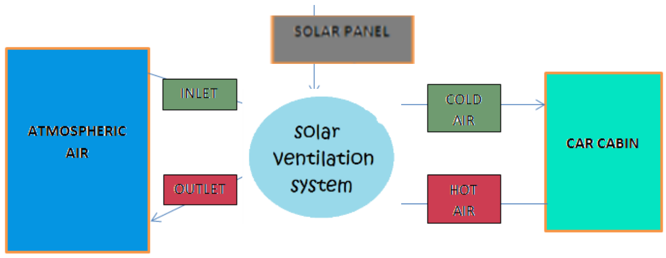

Fig. 6. Simple block diagram of solar ventilaton system.

The figure 6 shows the simple block diagram of solar ventilation system. This device consists of two brushless fans for inlet and the other for outlet. The fresh air is circulated in the car cabin due to inlet fan force and the warm cabin air is pushed out through the outlet of the device. The primary source of power for the operation is harnessed from solar panel. The main problem and challenge for this project are to develop, design and install the ventilation system that should not obstruct any of vehicles utility inside the vehicle cabin.

A. Design Specifications

The component that were used in this design employs exhaust fan, blower fan, rechargeable battery, temperature sensor, current sensor, LCD, data logging shield and a microcontroller. In this ventilation system consists of two fan for circulation of inhales fresh air inside and blower hot air outside of the car. In this project, the Arduino Uno use as a microcontroller and with the help of temperature sensors that senses the temperature inside the car and become switches for the exhaust and blower fans to turn on or off. The power for running the fans was generated by a two 3W solar panel with back up rechargeable battery. In Table 1 are shown the components were used in designing and fabrication of a simple standalone Smart Solar Power Ventilation System For Vehicles.

TABLE I.

Component	Specification
Solar Cell	12V, 0.25A, 3W, 220mm x 120mm x 2mm
Microcontroller	Arduino Uno
Temperature Sensor	SN-LM35DZ Low-cost on board temperature sensor Calibrated directly in Celsius
LCD Blue Backlight	16 x 2 characters LCD display Blue backlight white character
Data Logging Shield	SD card interface works with FAT16 or FAT32 formatted cards. Built in 3.3v level shifter circuitry. Real time clock (RTC) keeps the time going even when the Arduino is unplugged.
Rechargeable Battery	12V, 7.0Ah 150mm x 63mm x 94 mm ~2.324kg
Brushless Fan	12V, 0.24A
Current Sensor	ACS712 20A Module

Figure 7 show the circuit that has been design and conduct for this project. this design also been tested using Multisim to test whether the circuit is working.

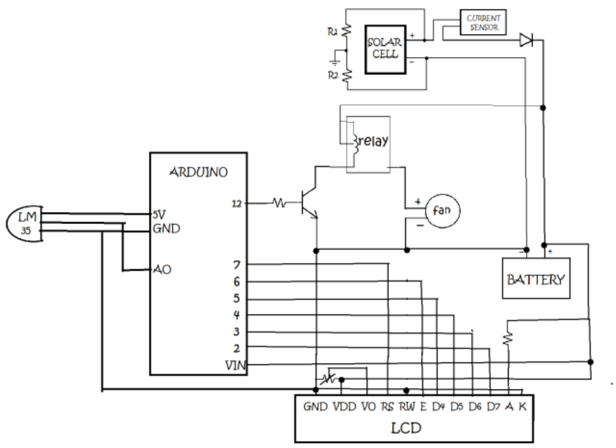

Fig. 7. Circuit and connection

IV. Result

For the result, the objective of the experiment is to obtain and measure the temperature inside of the vehicles with and without slightly open window of both side at front car that has been exposed to the sunlight at all direction, with no major shadows on any of them and also with or without solar ventilation system. The experiment were conducted at open space area that has been expose to direct sunlight. Table 2 and 3 show the details about testing this project and the case conditions that has been done.

TABLE II.

TEST DETAILS	
CAR MODEL	Perodua Myvi
DATE	1.5.2017 – 8.5.2017
VENUE	Parking S23, KTC, UTM
TIME START	9 AM
TIME END	7 PM

TABLE III.

CASE	SYSTEM DETAIL
I	Vehicle without both window slightly open and without ventilation system
II	Vehicle with both window slightly open and without ventilation system
III	Vehicle with both window slightly open and ventilation system

The temperature inside the car from three different case conditions was measured between 9 O'clock in the morning until 7 O'clock in the afternoon about 10 hours per days and were been conduct in 1 week and all temperature were compared together to get the characteristics and behavior temperature and air in that vehicles. The data obtained were then analyzed. The result are shown in Figure 8.

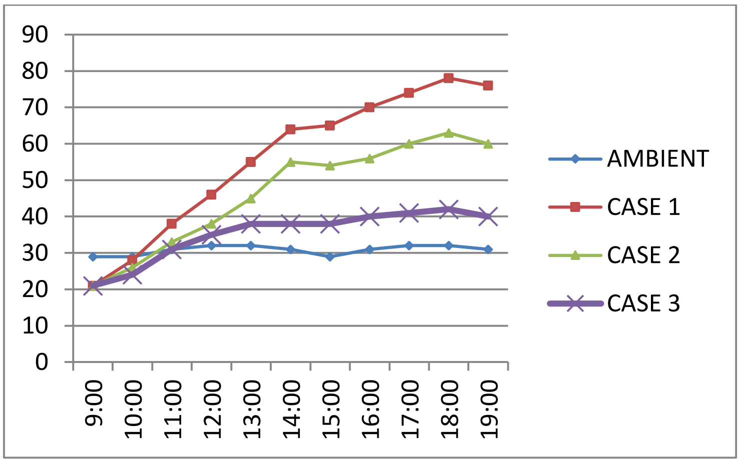

Fig. 8. Characteristic and behavior on temperature in diffrents case

From the graft, we can observed that the peak hours between of 1 o'clock and 2 o'clock in the afternoon has the higher temperature inside the vehicles cabin. from 9 o'clock in the morning readings taken is slightly increase until 12 o'clock in the afternoon. However, the temperature readings is rapidly increased after an hour later. after than the temperature readings decreased at a slower rate between 3 o'clock and above in the afternoon.

From the result, it shows that the solar ventilation system was tested with different condition. This can be conclude that the most effective system is in case III based on the average temperature in the car is lower than other case but also it can maintain the temperature close to ambient temperature.

V. CONCLUSION

This project uses solar energy for ventilation system that is to start and drive the fan and also to charge battery for backup supply. This project should be able to reduce the temperature inside the vehicles that were placed at an open parking and were expose to direct sunlight during the day. From result, it shows that the vehicles cabin temperature can reach up to 60°C after 1 o'clock in the afternoon that were been exposure to direct sunlight at various sunlight intensity. The highest temperature difference was obtained when all window was closed. This is shown that by improving the airflow inside the vehicles cabin can affect the temperature inside the vehicles cabin. It is suggested that if in that vehicles were add the ventilation system that use solar energy inside the cabin, were will be accelerated decreases in the cabin temperature. This project works successful and completely on green energy. At case III showed that the temperature was maintained inside the car cabin and within a short period showed an average of 10°C reduction. Further study for this project are by develop and design how to overcome the overheating problem, such as proper planning of the battery or energy management, a study of the design of fans, radiation effect and battery charging time, power produced from the solar panel and the evaluation of a control strategy.

REFERENCES

[1] K. Sopian, M.Y.Othman, B. Yatim, and W.R.W. Daud, "Future Directions in Malaysian Environment Friendly Renewable Energy Technologies Research and Development," ISESCO Science and Technology Vision, Vol. 1, pp. 30-36, 2005.

[2] Wu, Yupeng., Eames, Philip C. and Smyth, and Mervin, "Optical Analysis of Asymmetric Compound Parabolic Photovoltaic Concentrators (ACPPVC) Suitable for Building Façade Integration," 4th International Conference on Solar Concentrators for the Generation of Electricity or Hydrogen, 2007.

[3] Ahmed Belhamadia, Muhamad Mansor, and Mahmoud A. Younis, "A Study on Wind and Solar Energy Potentials in Malaysia," International Journal of Renewable Research, Vol. 4, No.4, pp. 1042-1048, 2014.

[4] S. Mekhilef, A. Safari, W.E.S. Mustaffa, R. Saidur, R. Omar, and M.A.A. Younis, "Solar energy in Malaysia: Current state and prospects," Renewable and Sustainable Energy Reviews, Vol. 16, pp. 386– 396, 2012.

[5] A. Grundstein, V. Meentemeyer, and J. Dowd, "Quantifying the Heat-Related Hazard for Children in Motor Vehicles," Bulletin of the American Meteorological Society, 91(9), pp. 1186-1191, 2010.

[6] R. Saidur, H. H. Masjuki, and M. Hasanuzzaman, "Performance of an Improved Solar Car Ventilator," International Journal of Mechanical and Materials Engineering (IJMME), Vol. 4, pp. 24 -34, 2009.

[7] A. Grundstein, V. Meentemeyer, and J. Dowd, "Maximum vehicle cabin temperatures under different meteorological conditions. International journal of biometeorology," Vol. 53(3), pp. 255-261, 2009.

[8] M.S.F. Mansor, U.Z. Abd Rahman, M.S. Zainal Abidin, M.Z. Md Zain, and M.R. Md Yusof, "Variation of Car Cabin Temperature Influenced by Ventilation Under Direct Sun Exposure," Journal of Mechanical Engineering and Sciences (JMES), Vol. 6, pp. 1014-1023, 2014.

[9] Y.-A. Yan, C.-Y. Tseng, and J.C. Leong, "Feasibility of Solar Powered Cooling Device for Electric Car," 2nd International Conference on Advances in Energy Engineering (ICAEE), Energy Procedia 14, pp. 887-892, 2011.

[10] Om Prakash Singh, Rohit Raut, Mrinmoy Biswas, and Ramji Singh, "Effect of Dynamic Vents on the Thermal Comfort of a Passenger Car," Journal of Mechanical Engineering 61, pp. 561-570, 2015.

[11] A. Alexandrov,V. Kudriavtsev, and M. Reggio, "Analysis of Flow Patterns and Heat Transfer in Generic Passenger Car Mini-Environment," The 9th Annual Conference of the CFD Society of Canada. Kitchener, pp. 27–29, 2001.

[12] R. Musat, and E. Helerea, "Parameters and models of the vehicle thermal comfort. Acta Universitatis Sapientiae," Electrical and Mechanical Engineering, vol. 1, pp. 215-226, 2009.

[13] Martinho, N.A.G., M C.G. Silva, and J.A.E. Ramos, "Evaluation of thermal comfort in a vehicle cabin," J. Automob. Eng., pp. 159-166, 2004.

[14] Hussain H. Al-Kayiem, M. Firdaus Bin M. Sidik, and Yuganthira R.A.L Munusammy, "Study on the Thermal Accumulation and Distribution Inside a Parked Car Cabin," American Journal of Applied Sciences 7, Vol. 6, pp. 784-789, 2010.

[15] L. B. Theodore, S. L. Adrienne, P. L. Frank, and P. D. David, Fundamentals of heat and mass transfer, Vol. 7th ed., New Jersey: John Wiley & Sons, 2011

[16] S. G. Hodder, and K. Parsons, "The effect of solar radiation on thermal comfort," Int. J Biometeorol, Vol. 5, pp. 233-250, 2007

[17] Gaurav Kumar Jaiswal, Mohit Gandhi, Sanket Phalgaonkar, Harshal Upadhyay, Ankit Agrawal, Vasudevan Rajamohan, and K Ganesan, "Design of a smart automotive ventilation system for a parked car," International Journal on Theoretical and Applied Research in Mechanical Engineering, Vol. 1, pp. 83-88, 2012.

Thermography Analysis ANN-based for Determining the Ageing Level of Glass Disc Insulators

Nurafiq Akmal Norazam
Faculty of Electrical Engineering
Universiti Teknologi Malaysia
Johor Bahru, Malaysia.
afiqnaa@gmail.com

PM. DR. Zulkurnain Abdul Malek
Institute of High Voltage and High Current
Faculty of Electrical Engineering
Universiti Teknologi Malaysia
Johor Bahru, Malaysia.
zulkurnain@utm.my

***Abstract*—It is known that thermography analysis is popular nowadays for monitoring electrical equipment. In this world, thermography analysis and artificial neural network were used in determining the ageing level of glass disc insulators. The thermal profile of the insulators was represented by several parameters to be used as training in the artificial neural network. The insulator conditions were identified as good, moderate and damaged. Results are quite promising. More measurements and trainings can be made in future to increase the accuracy and precision of the network.**

Keywords—Thermography; Artificial Neural Network; Glass Disc Insulator; Ageing Severity

I. INTRODUCTION

Glass insulators have been used in transmission and distribution lines with good performance nowadays. The use of glass disc insulators in high voltage installations has been intensified in last decades because of their advantages such as low cost, constructive simplicity, impact resistance, competitive price and easy installations. Despite having lots of benefits, they also come with some disadvantages, and the worst of them is the difficulty to detect the defect of the insulators. In many previous situations, it is only possible to detect the damage and ageing severity after a fault has occurred. It is necessary to make continuous evaluation of these devices through an efficient and good monitoring technique. It is well known that condition monitoring techniques have a great significance in future inspection and maintenance. From time to time, it has been increasingly importance to prevent failure or deterioration of electrical equipment using this technique. Condition-based maintenance (CBM) is a technique in which preventive intervention is conducted after symptoms of impending failure have been detected. CBM is a maintenance process which decides maintenance actions using the information collected through condition monitoring. It is based on the understanding that a piece of equipment goes through multiple degraded states before its failure. The health conditions of the equipment can be monitored and predicted, and optimal maintenance actions can be scheduled for preventing equipment breakdown and minimizing total operation and maintenance costs (Tian et al., 2009). One of the ways for monitoring insulator condition is using the thermography technique. The thermal inspection has been used for other equipment such as zinc oxide surge arrester. The ageing level of the equipment can be determined using the artificial neural network (ANN) technique after several key parameters have been set up for the classification purposes.

In high voltage systems, overvoltages can occur through switching operations, fault currents and lightning strikes. The function of insulators is to protect the equipment from sudden rise of current which can lead to damage of the equipment. Overvoltages and flashovers can cause major disturbances to the energy transmission and distribution lines when failure of the overhead insulator occurred. These insulators still undergo ageing by time due to the long-term low and high current discharge. Thus, these insulators must be inspected to determine the condition of the devices whether it has a bad, good or moderate condition. Unfortunately, the condition of the glass disc insulator is hard to be determined with currently available methods. It is because the breakdown maintenance method is to wait the insulator to fail and actions were taken after that. Such schemes are not efficient enough due to our level of technology. Thus, thermal inspection is needed for inspection because the method is efficient. The thermal inspection technique is a simple method as it can be monitored from farther and safer place. It can detect whether the insulator is good, moderate or bad condition at very early stage. This work aims to provide a new technique of glass disc insulator ageing detection using thermal images.

II. BACKGROUND

A. Thermography

Thermography technique is a process that thermal images can be produced from the temperature or the thermal profile body of the subject. As an example, an infrared camera is used to measure the temperature variations on the surface of the glass disc insulator so thermal images of the object can be produced. Basically, the thermal image is taken by an infrared camera which can convert the infrared radiation emitted by the objects that are being focused, into a color scale which indicates level of temperature. In other words, in thermal image, the temperature of the objects is identified by its color. Besides that, an abnormality of the equipment might be indicated by the increase or decrease of the surface temperature of the equipment such as cracking.

B. Artificial Neural Network

Artificial Neural Network (ANN) is information processing software that is inspired by the way of biological nervous systems, such as the brain that we used to process information. ANN is popular because of its potential to link input and output data together. The neural networks require both input and target data to study the relationship between those parameters. This process is called as 'training'. Those input data were selected to match the target data in attempts to predict. During the training process, specialized training algorithm is used to adjust certain parameters in the network to increase its assumptions power network. In other words, ANN is like just like a human that learn by examples.

III. METHODOLOGY

A. Thermal Image Capturing

The experiment carried in the laboratory and the equipment used was set up as in Figure 1. Several glass disc insulators test samples were used. A portable thermal imaging camera model H-2640 was used to capture the temperature of the glass disc insulator. The camera distance must be constant and placed at safe distance.

Fig. 1. Experimental setup of the image capturing

For capturing the image, the thermal imager orientation was faced directly towards the targeted insulator surface in order to make an exact measurement. The space was set between 1 to 1.5 m and the emissivity value was set at 0.95 as generally recommended for electrical equipment thermography. The original images from the thermal camera is shown in Figure 2.

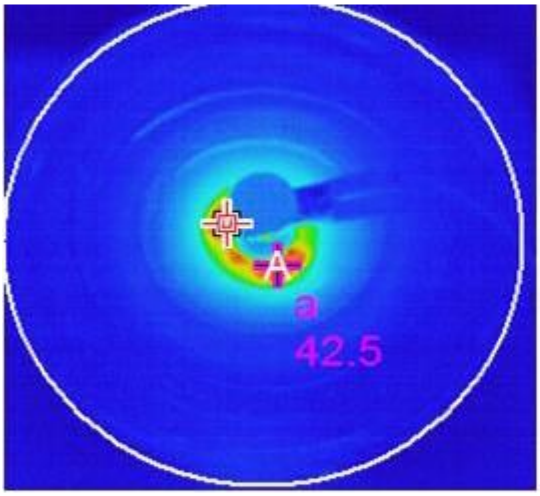

Fig.2. Sample of image from the thermal camera

B. Image Segmentation

Using MATLAB image processing toolbox, the dilated and eroded images were applied to the binary image. After all boundaries line image were connected to each other, the region of interest in this case was the glass disc insulator, which were filled with white colors using "imfill" function in the toolbox to make them contrastive to the background. The last segmentation process functioned to remove all connected lines and background of the insulator. The segmented image would leave only the insulators with white color and all background with black color.

C. Extraction of Data

This data was extracted using MATLAB and Infrec analyzer. The original image was in a RGB color format. The "rgb2gray" MATLAB function was used to converts RGB images to grey scale images for simplicity and data reduction. In MATLAB, the image must be in segmented image form in order to extract data such as mean, variance and standard deviation. The Infrec analyzer can extract the maximum and minimum temperatures. Later, the data were being normalized by dividing them with the highest value in each element to get the range of -1 (minimum) to +1 (maximum) datasets for training precision purposes.

D. Training Network

A feed forward back propagation neural network with Levenberg-Marquadt which consists of two layers with 128 neurons at the first layer is used for training purposes. The network had been set with maximum epoch up to 1000 and 0.01 learning rate. The training tool is shown in Figure 3. After the network had been trained for several times, validation of the output was tested using some of the samples. Outputs of the network versus the actual target were made. An error between the target and actual output target was then calculated.

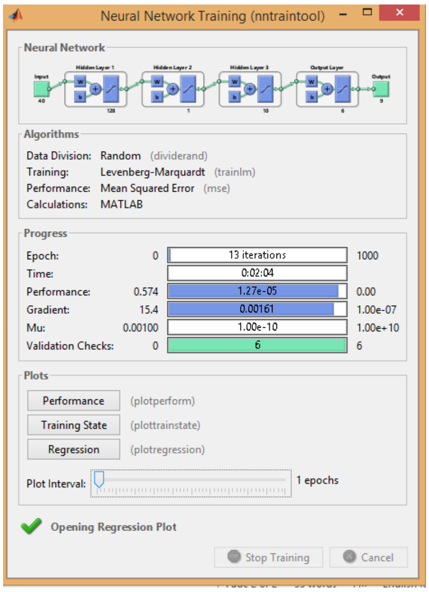

Fig. 3. Neural network training tool

IV. Results

The first training and performance results are shown in figure 3. The best training performance is 0.0009721 after 1000 epochs as shown in Figure 4. The number of epochs 1000 is a large number and this indicates that the time to achieve the required minimum error is long.

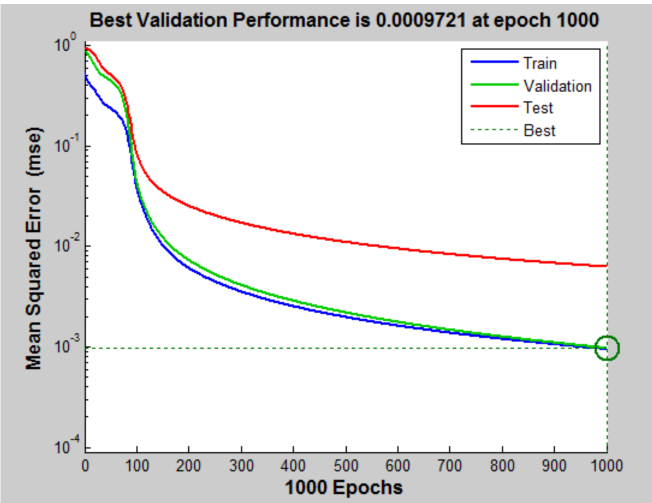

Fig.4. Training performance of the network for the first time

Figure 5 shows the regression value for the first training of the neural network classification. These linear regression values indicate the correlation between the target of the neural network and its output. In this case, the linear regression value is 0.88289 which indicates that the correlation is not so strong. The training value must be at least 0.93 to show the correlation of the target and output data is strong. Thus, training must be done again to get the desired training value.

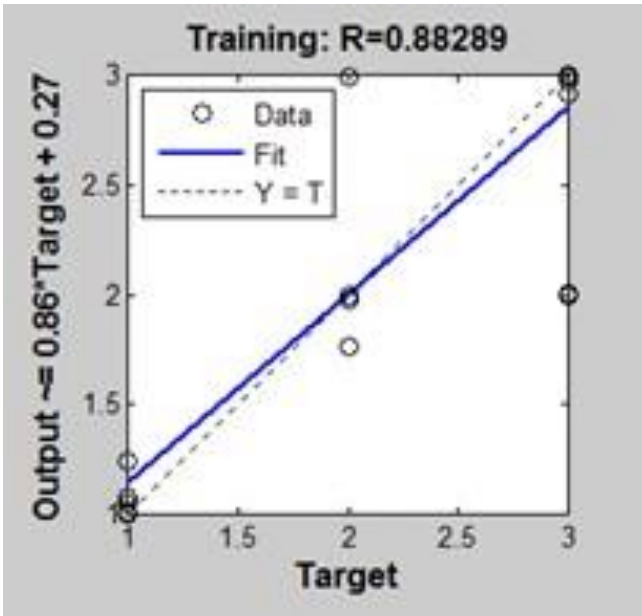

Fig.5. Linear regression value of the first training of the neural network.

The network is being trained until three times. The best training performance is 0.00083225 after 1000 epochs as shown in Figure 6. The number of epochs 1000 is a large number and this indicates that the time to achieve the required minimum error is long.

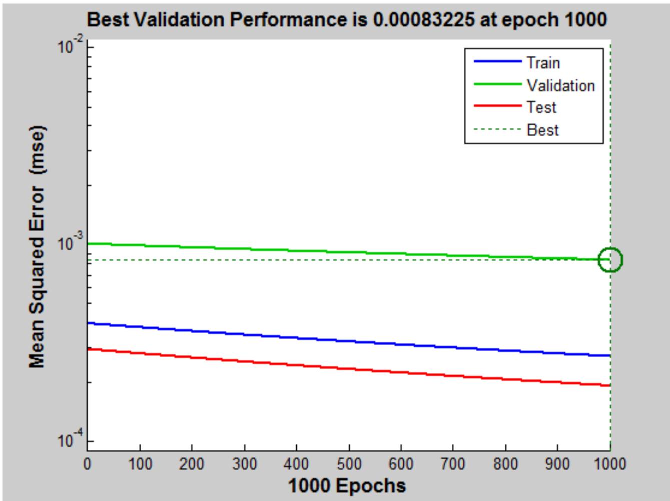

Fig.6. Training performance of the neural network after third time training

Figure 7 shows the regression value for the third training of the neural network classification. As shown in the figure, the training value is 0.99951 which indicates the correlation between the output and the target data is strong compared to the first training. In other words, the network precision increases after the third time training.

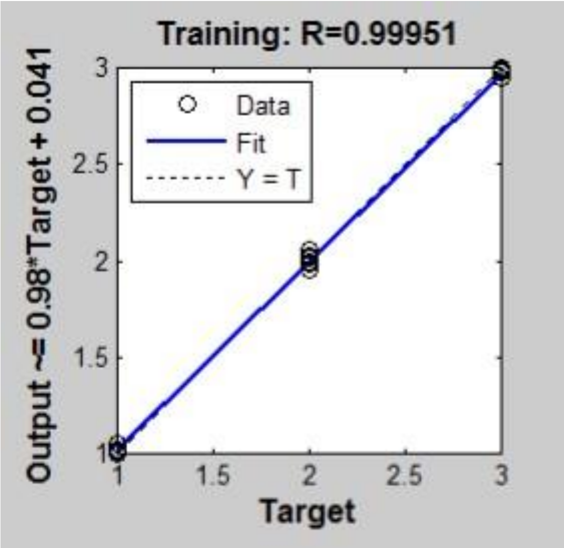

Fig.7. Linear regression value of the third training of the network

After the training phase had been completed, testing and validation should be done to test out the network precision. Figure 8 shows the comparison between the ANN and actual output that is plotted using Excel. There is a slight error on classification on samples 6 and 7. Out of 9 samples tested, 7 samples were correctly classified.

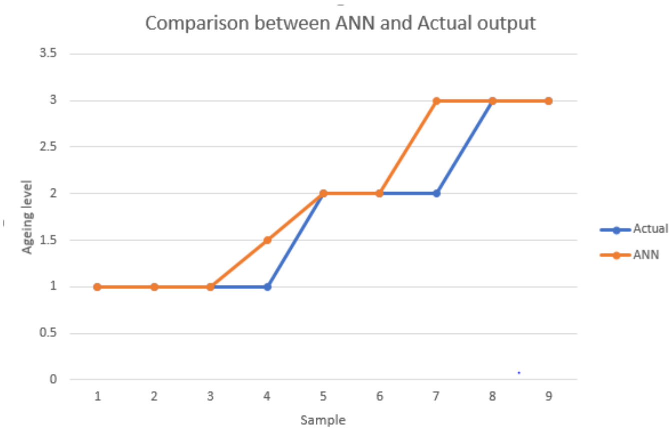

Fig.8. Comparison between ANN and actual outputs

From the results shown, there is small difference between the actual and the calculated output, which means an error which equals to 16.67%. For this network, the value of error is relatively small as it shows the minimum classification error. From the results obtained, it can be concluded that there is still more room for improvement to increase the output of the neural network. The accuracy can be increase using samples.

V. CONCLUSION

Based on the results, neural network classification methods for determining the condition of glass insulator have been successfully developed and tested. The regression, validation and testing of the neural network developed are directly proportional to the numbers of training. In other words, the linear regression value increases when the number of training of the network is increased. The number of epoch, regression linear value and testing error were used to evaluate the training network performance as well as testing performance. Results show that there is small difference between the actual and the calculated output. Determination of the ageing level of glass disc insulator using thermography analysis and artificial neural network is successful.

REFERENCES

[1] Edson G. da Costa, Tarso V. Ferreira, Max G.G. Neri, Isaac B. Queiroz and Andre D. Germano, "Chracterization of Polymeric Insulators using Thermal and UV Imaging under Laboratory Conditions", IEEE Transactions on Dielectric and Electrical Insulations, August 2009.

[2] Azmat and D. J. Turner, "Infrared thermography and its role in rural utility environment", pages B2/1–B2/4, May 2005.

[3] Baoshu, Z. Xiaohui, Z. Shutao, and N. Wendong, "HV Power Equipment Diagnosis Based on Infrared Imaging Analyzing In Power System Technology 2006", PowerCon 2006 International Conference on, pages 1–4, 2006.

[4] Ying-Chieh and Y. Leehter. "Automatic Diagnostic System of Electrical Equipment Using Infrared Thermography. In Soft Computing and Pattern Recognition", 2009. SOCPAR '09. International Conference of, pages 155–160, 2009.

[5] Niancang, "The infrared thermography diagnostic technique of high-voltage electrical equipments with internal faults", volume 1, pages 110–115 vol.1, Aug. 1998.

[6] Muhr, S. Pack, S. Jaufer, and H. Lugschitz, "Thermography of aged contacts of high voltage equipment", e & i Elektrotechnik und Informationstechnik, 123(12):537–543, 2006. URL http://dx.doi.org/10.1007/s00502-006-0393-4.

[7] Novizon, "Condition Monitoring of Zinc Oxide Surge Arrester using Correlation between Thermal Image and Leakage Current", Universiti Teknologi Malaysia, 2015.

[8] Muhammad Bin Abdullah, "Thermography analysis using artificial neural network in determining the ageing level of metal-oxide arrestor", Universiti Teknologi Malaysia, 2011.

[9] Tamal Dutta, Jaya Sil, Paramita Chottopadhyay, "Condition Monitoring of Electrical Equipment using Thermal Image Processing", 2016 IEEE First International Conference on Control, Measurement and Instrumentation (CMI), 2016.

[10] Christine Kar-Ling Gee, Chin Kuan Ho and Somnuk Phon-Amnuaisuk, "Prediction of Thermal Profiles using Artificial Neural Network", November, 2010.

[11] N. Bashir, "Ageing of Transmission Line Insulators: The Past, Present and Future", 2nd IEEE International Conference on Power and Energy (PECon 08), 1-3 December, 2008.

Condition Monitoring of Overhead Line Glass Disc Insulator using Infrared Emission Measurement

Muhammad Asraf Romainor, Zulkurnain Abdul Malek

Faculty of Electrical Engineering

Universiti Teknologi Malaysia

Johor, Malaysia

***Abstract*— Insulation is the essential part in power system. Nowadays, glass disc insulator has become a global research hotspot because of its increasing application in high voltage AC overhead transmission and distribution systems. However, glass disc insulator under continuous stress voltage may deteriorate due to excessive heating thus may lead to its failure. Therefore, condition-based monitoring research is necessary for diagnosis purpose. An experimental setup to be work for a simulated ageing condition test and for a contamination test was established to monitor the condition severity of the glass disc insulator based on its surface temperature. Thermography analysis was carried out for applied AC voltage from 10 kV to 28 kV on insulator samples. Such a preventive intervention allows for detecting the potential problems through temperature characteristic at their very earliest stages. Measurements of insulator surface temperature had been made using infra-red camera to find the correlation between the surface temperature and the applied voltage, and also the pollution levels through thermal image processing. The thermal image captured was filtered and segmented so that the feature data extracted was more accurate to be used in the diagnosis tools. Once the selected parameters are detected, the condition of the glass disc insulator can be predicted based on the thermal image alone. Results show that the maximum temperature is the parameter suitable for the classification theory, however more samples are needed before a definite conclusion can be made.**

Keywords—glass disc insulator, high voltage transmission lines, infra red emission, thermography, temperature discharge, severity classification

I. Introduction

The overhead conductors are important in power transmission and distribution system. However, there must be an insulator between tower and current carrying conductors as it mechanically support the conductor and electrically isolate the conductor from the ground structure [1]. Glass disc insulators are used in power transmission and distribution system for insulating purpose with the advantages of low thermal expansion coefficient, high resistivity and dielectric strength. Toughened glass insulator also known to be less affected by ageing compared to porcelain or polymer insulator.

Nevertheless, the glass insulator still absorbs part of the electrical energy and convert it to the thermal energy. A long term low-current discharge activity may eventually damage the insulator surface. If this increase in temperature is not been detected and controlled wisely, it might cause a significant increase in the flashover thus risking the power system and affecting the safety of people nearby [2]. However, the intensity of thermal discharge emitted from the overhead lines glass disc insulator is still unknown [3]. Hence, a study to investigate the thermal discharge emitted from the glass insulator is deemed necessary for diagnostic purposes especially in maintenance work.

This paper is important because the thermal parameters in the surface temperature file can be used for severity detection without measuring the glass insulator's leakage current as in the conventional technique. In particularly, the correlation between the thermal image parameters captured and the voltage applied as well as the pollution levels is desired to be determined. The severity of the insulator's pollution layer can be classified into three levels, namely, good, moderate and heavy. Lastly, the result are presented and discussed to achieve the objective of the research then verified and improved the method used.

II. Background

A. *Overhead Line Glass Disc Insulator*

In transmission and distribution systems, an overhead glass disc insulator is usually required between the tower body and current carrying conductors. Several derived properties are high dielectric strength and insulation resistance, lower coefficient of thermal expansion and mechanical ability to withstand the tension and weight of conductor.

Previous research has shown that an insulator contamination remains as a serious technical problem which may cause flashovers. This contamination induced flashover happen when the surface of insulator become sufficiently coated with a wet conducting film containing dissolved unwanted deposits such as salts, dust, and cements [3]. In the course of the flashover, the heat produced by arcing, may directly affect the insulator ageing.

B. *Condition Monitoring Using Thermography Images*

Thermography analysis is a non-destructive monitoring technique (NDT), which has been used for a long time in analyzing transmission lines and electrical equipment. For example, the thermal image processing based on statistical methods and morphological image processing technique for identifying the hotspots and reference temperature had been practiced by Ying-Chieh and Leehter in 2009. A qualitative and quantitative analyze were carried out on the gathered information. The results showed about 91 % accuracy and 9 % error, including 8% over caution and 1 % lack of caution [4].

Besides, to measure the discharge temperature along with low current discharges, the "Best-fit" method of optical emission spectroscopy analysis has been well applied. The relationship between the temperature discharge and its current discharge has been shown to be linear as in Figure 2.2, but only if the supply circuit is constant [5]. Therefore, a thermal imaging based condition monitoring can be developed for severity monitoring of the glass disc insulator.

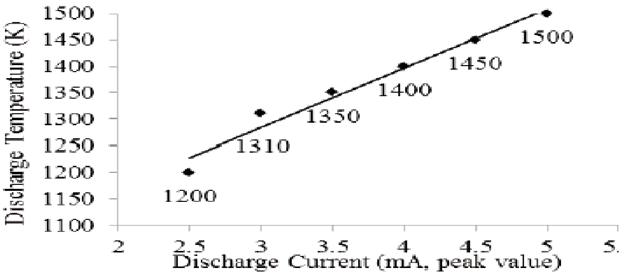

Fig. 2.1: *Correlation between discharge current and discharge temperature [5].*

C. *Artificial Accelerated Ageing Test*

Artificial tests performed on insulators fog chambers have been standardized by the International Electro-technical Commission (IEC) for both ceramic and polymeric insulators [6]. Two types of methods are employed, the salt fog and clean fog. For the salt fog method, a cleaned insulator is contaminated with saline fog at a measured pollution index and high voltage is applied for 60 minutes or when flashover occurs. A withstand flashover voltage is obtained after 3-4 tests have been carried out. In the clean fog method, the insulator is pre-contaminated with kaolin and voltage applied either while the insulator is still wet or dry.

D. *Aging and Failure of Outdoor Insulator*

The term aging refers to degradation of an insulator by a generation of continuous discharges by exposing the energized insulator to various environmental conditions. In tropical environments, where the climatic conditions are characterized by permanently high relative humidity (>80%), corrosion can lead to failure of ceramic insulator [7]. In particular conditions, the skewness and the kurtosis of the leakage current (LC) pattern appear to be very sensitive to discharge generated damage of the surface [8]. Consequently, treeing and surface erosion takes place on the skirt of the insulator at later stages as shown in Figure 2.2. The eroded surface causes more contaminants deposited on the surface of the insulator [9].

Fig. 2.2: *Surface discharge of glass disc insulator [8].*

E. *Equivalent Salt Deposit Density (ESDD)*

ESDD is a method to determine the pollution degree on the insulators that been removed from the transmission lines or field testing stations. It been defined as the equivalent deposit of NaCl in mg/cm² on the surface area of an insulator, which will have an electrical conductivity equal to that of the actual deposit dissolved in the same amount of water [10]. This method involves checking the temperature of the solution, liquefying the surface deposits in a known quantity of water with a low conductivity and calculating the ESDD from the volume of water, measured conductivity and the insulator surface area. The advantages of this technique are it can be carried out on actual insulators with shed profile performance that can be assessed.

III. METHODOLOGY

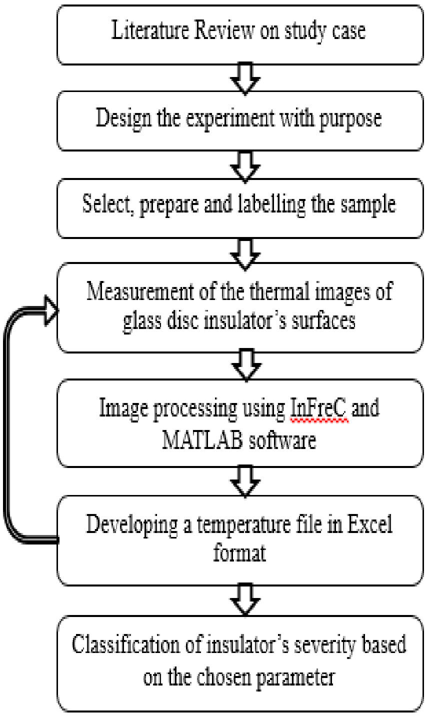

Fig. 3.1: *Overall flow of research methodology*

This section describes the research procedure used and how it has regulated the data collection, data analysis and further expansion of the theories. Two main sub-sections are the description on the thermography image data collection and the description on the thermography image features extraction. The gathered data can be used later in presenting the classification of glass disc insulator severity using an artificial neural network (ANN). Figure 3.1 shows the overall flow of the research methodology. The three major tasks are accelerating aging test, capturing the thermography image, and analyzing the thermal parameter.

A. *Samples Preparation*

Two used standard profile overhead line glass disc insulator which are EIV type and SEDIVER type were utilized in this work as shown in Figure 3.2 Both were the toughened glass for AC application in distribution and transmission line from just a few kV up to 33 kV HVAC. The samples were obtained from TNB without return any identification on the location.

(a) (b)

Fig. 3.2: *Overhead line glass disc insulator; (a) EIV type and (b) SEDIVER type.*

B. *Field Measurement*

The simulated ageing condition and contamination test was carried out in IVAT laboratory and the equipment to be used was set up as Figure 3.3 based on IEC 61109 Annex C standard. The set up consisted of a flexible voltage source, a voltage regulator type 1225 C, a 220 V/100 kV step up transformer, HVAC test meter and test object.

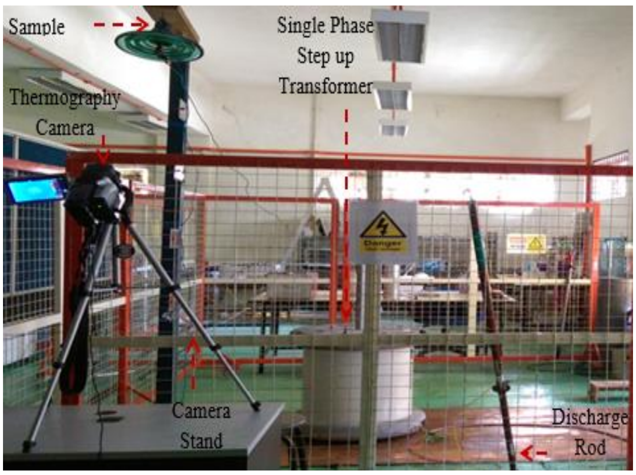

Fig. 3.3: *Experimental set up for accelerated aging test.*

The thermography measurement was performed by injecting 10 kV to 28 kV with 2 kV step every 10 minute. Each step consists of five minute breaks before capturing an image to allow more or less steady state surface temperature condition. In every step, the thermal images of the surface insulator were captured in a dimension of 640 – 480 pixels using a NEC AVIO H2460 thermography camera with fusion technology. The camera was placed about 1.5 m perpendicular to the insulator surface. The ambient temperature was from 27°C to 31°C while the emissivity value was set at 0.95 [11]. All images were saved in a database system.

C. *Thermography Processing*

Segmentation is a process of distinguishing or partitioning the region of interest (ROI) from its background. Image processing MATLAB toolbox was used to segment the image while the InfRec analyzer software was used to determine the scale of temperature and also to set the ambient temperature and emissivity value of visual image before obtaining the coordinate of maximum and minimum temperature. The segmentation showed only a region of the glass disc insulator surface block without background areas. After the pixel coordinate of segmented image is obtained, the matching process was used to determine the temperature file of segmented image [12]. From the temperature of segmented image, the histogram of temperature can be built and the features is obtained.

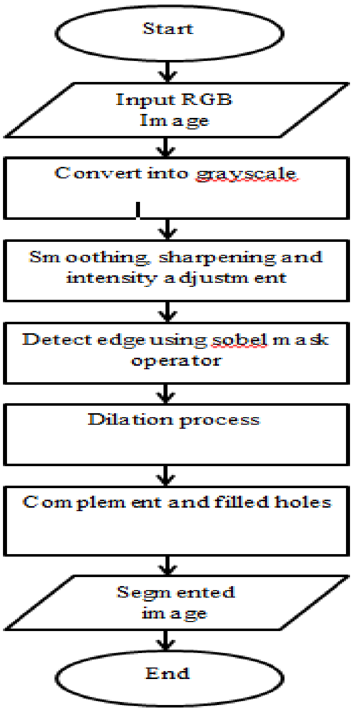

Figure 3.4: *Flowchart of image segmentation technique.*

Figure 3.4 shows the flowchart of image segmentation method using edge detection with Sobel mask operator. Sobel edge detection help in converting the grey scale image to binary image, denoted as 1 for white color for all boundaries edge image, and 1 for black colors for the rest of image. Firstly, the RGB image must be converted into grey scale images which contain only 8 bits data using ‘‘rgb2gray’’ MATLAB function so the image gradient as well as a threshold can be calculated and applied to create a binary gradient mask in segmentation process later.

Secondly, the filtering process was carried out. The intensity values of the gray scale image were adjusted using "imadjust" MATLAB function. Then "roifilt2" MATLAB function calls filter2 to return an image that consists of filtered values for pixels in locations where BW contains 1's for all pixels that are in the region of interest (ROI) part, and unfiltered values for pixels in locations where BW contains 0's, assumed as the background image. To find the local maxima in binary image, "imdilate" MATLAB function was used in dilation process which resulted in dilated gradient mask images.

For the complement and filled holes process, an excessive part in dilated gradient mask image is removed using "imfill" MATLAB function to make them contrastive with the surrounding. Lastly, the pictures that are not desirable were deleted using ''imclearborder'' MATLAB image segmentation function toolbox. The black color surrounding the disc insulator images was indicated by 0 and the white color was indicated by 1 (ROI). Hence, the coordinates of disc insulator surface could be obtained by using the 'find (img == 1)' in MATLAB toolbox image processing. Figure 3.5 shows the example result of image processing from RGB image to segmented image for EIV type.

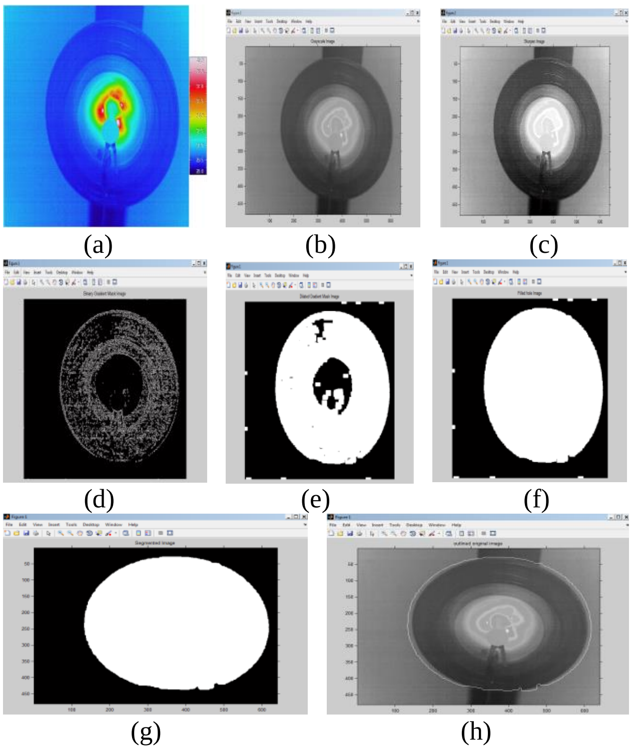

Fig. 3.5: *An example result from image processing of clean EIV sample; (a) RGB image, (b) Grayscale image, (c) Filtered image, (d) Binary gradient mask image, (e) Dilated gradient mask image, (f) Filled holes image, (g) Segmented image, and (h) Outline original image.*

D. Features Extraction

With the aim of finding a smooth and practical transform of the original object, a feature extraction is one of the most importance methods used for condition monitoring and fault diagnosis. Important features contained in region of interest of thermography image can be extracted from the temperature histogram as shown in Figure 3.6. The selected features are the major factor that determines the success of severity classification process. There are various methods that can be used for feature extraction and selection. In this research, the first order histogram features such as maximum, minimum, mean, variation and standard deviation were extracted from temperature file as thermal parameters classification also as the input of neural network classification [12].

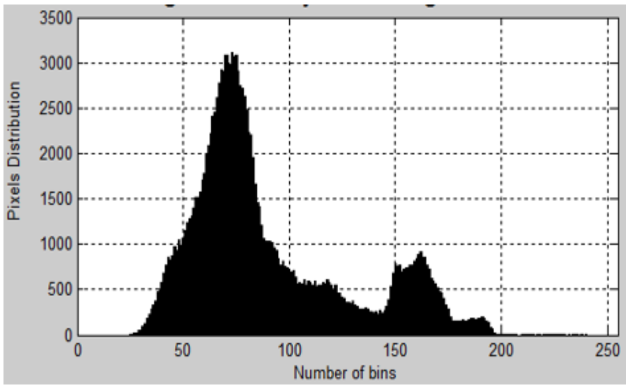

Fig. 3.6: *An example of the temperature histogram for segmented block of clean EIV sample with applied voltage.*

IV. Results

In this section, the parameters of the thermal image extracted from the temperature histogram will be discussed to determine the best parameter in presenting the correlation between surface temperature and applied voltage, and also the pollution levels.

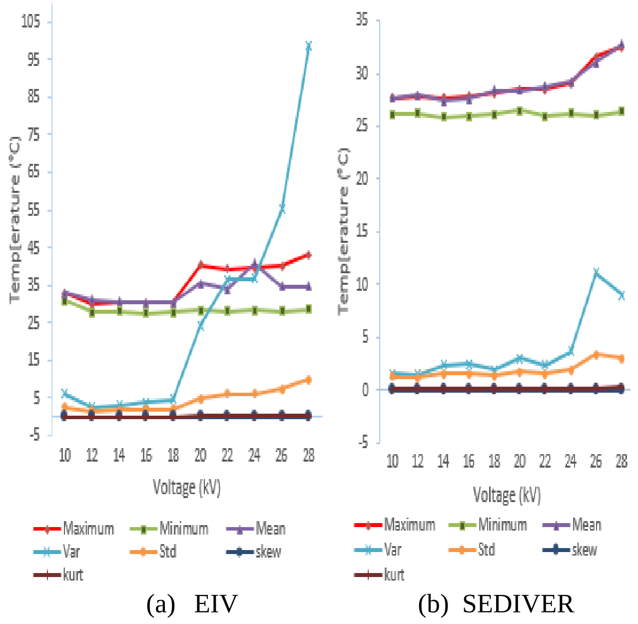

Fig. 4.1: *The maximum, minimum, mean, variance, standard deviation, skewness and kurtosis of temperature variations for EIV and SEDIVER clean test samples with applied voltage.*

For clean test results shown in Figure 4.1, both insulators had shown that the increasing in voltage stress lead to the worst condition of insulator due to its temperature increased. However, the EIV type obviously showed a sharp increase in maximum temperature between 18 kV to 20 kV while the SEDIVER type only show a regularly increase at the same stress voltage. So the EIV insulator is more aged compare to SEDIVER insulator. Although the variance and standard deviation had shown an increased in value for both types, the skewness and kurtosis seem not much affected by the applied voltages. Based on maximum parameter characteristic performance, the SEDIVER insulator is more effective with voltage application compared to EIV as it needs higher voltage to exhibit higher excessive heat.

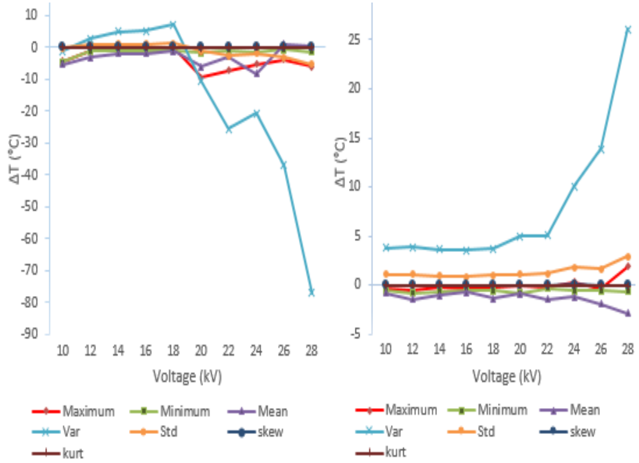

(a) EIV (b) SEDIVER

Fig. 4.2: *The changes in the maximum, minimum, mean, variance, standard deviation, skewness and kurtosis of temperature variations for EIV and SEDIVER polluted (2.85 mol/L test sample) with applied voltage.*

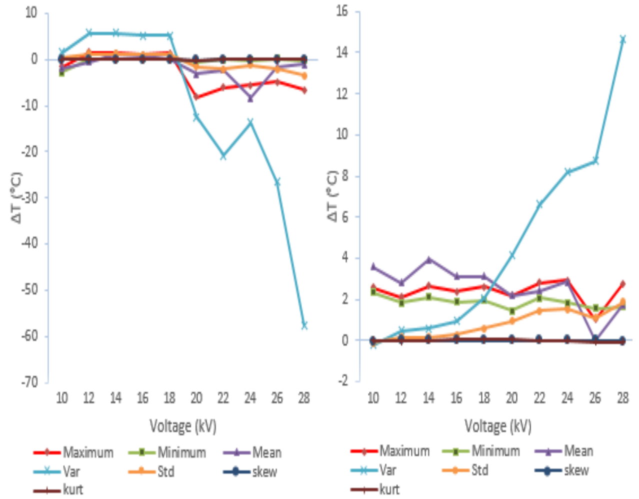

(a) EIV (b) SEDIVER

Fig. 4.3: *The changes in the maximum, minimum, mean, variance, standard deviation, skewness and kurtosis of temperature variations for EIV and SEDIVER polluted (5.7 mol/L test sample) with applied voltage.*

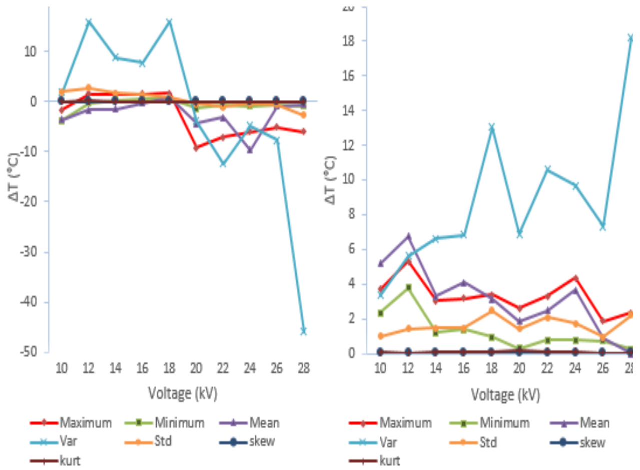

(a) EIV (b) SEDIVER

Fig. 4.4: *The changes in the maximum, minimum, mean, variance, standard deviation, skewness and kurtosis of temperature variations for EIV and SEDIVER polluted (8.56 mol/L test sample) with applied voltage.*

Based on the salty polluted test result shown in Figures 4.2, 4.3 and 4.4, the maximum and average temperatures of EIV had shown a negative changes in temperature, ΔT at 28 kV. However, for SEDIVER, its maximum temperature constantly show a positive changes in temperature, ΔT starting from 10 kV onwards. The changes of minimum temperature for both types seem not to alter much by the applied voltage followed by the skewness and kurtosis. Considering the SEDIVER as the better insulator, the maximum parameters can be used to correlate with the applied voltage due to its direct proportional relationship and positive ΔT with the support of lower standard deviation, positive skewness and kurtosis.

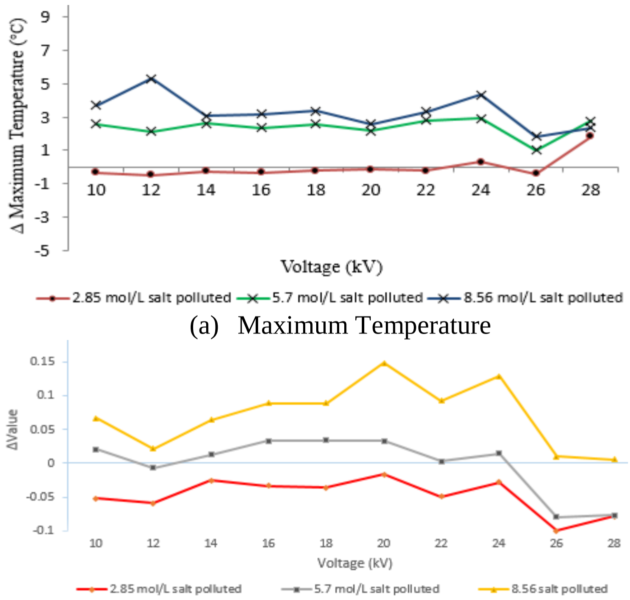

(b) Kurtosis

Fig. 4.5: *Variation of changes in (a) maximum temperature ΔT and (b) kurtosis, ΔValue with applied voltage for three different pollution levels for SEDIVER.*

Referring to Figure 4.5, there is a difference in the result of changes in temperature, ΔT for three different salt polluted samples. SEDIVER insulator with 8.56 mol/L salt, had the highest positive ΔT along the applied voltage, and the 2.85 mol/L salt polluted sample showed the lowest ΔT. This result verifies the interaction between pollution level and temperature discharge of the insulator surface that is the increasing in pollution levels will cause the temperature discharge to increase. This correlation confirmed by the characteristic of the changes in value, ΔValue of the standard deviation, skewness and kurtosis for this three different salt polluted tests which showed almost the same trend as maximum temperature.

V. Conclusion

It is shown by the result of this paper that an increase in applied voltage across the insulator above and beyond its normal operating voltage can also be used as a simulated increase in ageing condition since a corresponding increase in surface temperature is observed. The work has successfully shown this theory and the corresponding correlation between the simulated ageing level and thermal emission.

Besides, higher levels contaminations on the glass surface lead to poorer condition of the insulator and hence higher surface temperature. The work has successfully shown a correlation between the insulator surface condition and the thermal emission. Once the correlation is obtained, the condition of glass disc insulator is classified into good, moderate and heavy severity. In short, the infra-red thermal emission measurements using a NEC AVIO H2460 thermography camera can be a potential condition monitoring technique for glass disc insulators.

Acknowledgment

The research is carried out using the grant from Universiti Teknologi Malaysia under a code number 106HL.

References

[1] A. P. Mishra, R. S. Gorur, S. Venkataraman and D. Kingsbury, "Condition assessment of porcelain and toughened glass insulators from residual strength tests," *2006 IEEE Conference on Electrical Insulation and Dielectric Phenomena*, Kansas City, MO, 2006, pp. 413-416.An Xiao, Simon M. Rowland, Xin Tu and J. Christopher Whitehead, "*Thermal Features of Low Current Discharges and Energy Transfer to Insulation Surfaces*". IEEE Transactions on Dielectrics and Electrical Insulation Vol. 21, No. 6; December 2014.

[2] A. Rodriguez, H. Nour, F. Wang and S. J. Dale, "Effect of insulator surface temperature on the flashover voltage of outdoor insulators," *1985 EIC 17th Electrical/Electronics Insulation Conference*, Boston MA, USA, 1985, pp. 56-61.

[3] A. C. Baker *et al*., "Insulator Selection for AC Overhead Lines With Respect to Contamination," in *IEEE Transactions on Power Delivery*, vol. 24, no. 3, pp. 1633-1641, July 2009.

[4] Ying-Chieh and Y. Leehter, "Automatic Diagnostic System of Electrical Equipment Using Infrared Thermography". In Soft Computing and Pattern Recognition, 2009. SOCPAR '09. International Conference of, pages 155–160, 2009.

[5] A. Xiao, S. M. Rowland, X. Tu and J. C. Whitehead, "Thermal features of low current discharges and energy transfer to insulation surfaces," in *IEEE Transactions on Dielectrics and Electrical Insulation*, vol. 21, no. 6, pp. 2466-2475, December 2014.

[6] British Standard Institution. Artificial Pollution Tests on High-voltage Insulators to be Used on A.C. Systems. London, BS EN 60507. 1993.

[7] Parraud, R. and Dumora, D. "Corrosion Mechanism of Insulators in Tropical Environment". *CIGRE Symposium CAIRNS*. September 200 I. ClGRE: 200 I, Paper 300-04. 1-5.

[8] M. Amin, M. Akbar and M. N. Khan, "Aging Investigations of Polymeric Insulators: Overview and Bibliography," in *IEEE Electrical Insulation Magazine*, vol. 23, no. 4, pp. 44-50, July-Aug. 2007.

[9] Houlgate, R.G. and Swift, D.A. "*Composite Long Rod Insulators for AC Power Lines: Electrical Performance of Various Designs in a Coastal Station*". IEEE Trans. on Power Delivery, 1990.5(4): 1944-1955.

[10] G. Montoya, I. Ramirez and J. I. Montoya, "Correlation among ESDD, NSDD and leakage current in distribution insulators," in *IEE Proceedings - Generation, Transmission and Distribution*, vol. 151, no. 3, pp. 334-340, May 2004.

[11] Z. Azmat and D. J. Turner, "Infrared thermography and its role in rural utility environment," *Rural Electric Power Conference, 2005*, San Antonio, TX, USA, 2005, pp. B2/1-B2/4.

[12] Novizon. "Condition Monitoring Of Zinc Oxide Surge Arrester Using Correlation Between Thermal Image And Leakage Current". Faculty Of Electrical Engineering Universiti Teknologi Malaysia, AUGUST 2015.

Energy Saving Strategy for Residential Sector using Load Signature Approach

Mohd Nazrin Bin Mohd Tola
Faculty of Electrical Engineering
University Teknologi Malaysia
Johor, Malaysia

Professor Dr.Mohammad Yusri Hassan
Centre of Electrical Energy Systems (CEES)
Institute of Future Energy
University Teknologi Malaysia
Johor, Malaysia

***Abstract*—Electrical appliances have its own behavior consumption pattern of which can be translated as load signature. Load signature is the unique consumption pattern implicit to each individual electrical appliance of equipment which express in graphical form. Exploring on load signature is the fundamental of practical technologies for load monitoring, which involves the identification of the operating state of electrical appliances. This paper focuses on obtaining the electricity consumption pattern using load signatures. Through the load signature result, we can propose the strategies or intelligent ways of operation when using electrical appliances and suggest latest technology can be used to achieve minimum energy consumption. This paper presents the basic concept of load signature, methodology, the observation of load signature and analysis of load signature. The highest and the lowest energy consumption are measured.**

Keywords—load signature, load monitoring

I. INTRODUCTION

Nowadays, developed technologies promise to strengthen the link between utility and their customers by providing a better understanding of the usage and consumption of electric power [15]. Each electrical appliance has their own behavior and its operating state when using the power which can be translates in graphical form which known as a load signature. Energy monitoring helps the process of obtaining the load signature. Energy monitoring is the act of collecting real-time or interval energy data which very useful to obtain the parameter of the appliance including current, voltage and power. Monitoring appliances can be performed by placing a sensor between the appliance and power outlet. This method is generally called “intrusive” monitoring.

Energy monitoring is initially aimed to find out information about the amount of energy use but energy monitoring actually is one method to achieve the huge scale of energy reduction. Monitoring appliances is a condition for efficient energy management by providing energy consumption of each appliance to the customer. Energy monitoring provides the energy usage information of the appliances. The energy saving strategy can be achieved when the customer know the behavior or the operating state of the appliance used.

Load signature of the electric appliances presented in graphical form where the power consumption varies with time, depending with on their state and mode of use [10]. The current wave-shape can be seen as a unique signature. Thus, the interpreting of the load signature will help to provide the strategies on achieving better energy utilization.

Knowledge of electric load signatures is the foundation of practical technologies for load monitoring, which involves the identification of an electric appliance and the determination of its operating state [15]. This knowledge can provide benefits to the customers, utilities appliances manufactures and stakeholders. The utility sector can develop and improve their products and services, such as give the explanations and provide the strategies should be taken based on the load signature while the manufacturers should provide more effective and efficient products [15]. Thus, the customers will earn the benefits from reduced costs and other improvement in power consumption and reliability even for further enhance the value of electricity by knowing the behavior when it consume electricity and know more on how to use it more efficiently.

There are three main objectives of this paper which is to investigate the behavior of the electrical appliances based on the load signature, to provide energy saving strategies opportunities for enhancing the energy efficiency and to define which appliances suit for energy efficiency at residential sector.

This paper first explains the concept of load signatures and load monitoring. Then, the electrical energy activities in Malaysia been introduced which include energy efficiency, energy management and energy labeling. The methodology of using the software and hardware until obtain the result is presented. Energy saving strategy then proposed and suggest latest technology can be used to achieve minimum energy consumption discuss in the result and discussion part.

II. CONCEPT AND DEFINITIONS

A. *Load Signature*

Load signature is the unique consumption pattern intrinsic to each individual electrical appliances of equipment. Each electrical appliance contains unique features in its consumption behavior [5]. This behavior is limited to what can be monitored at a point of interest. The variables which usually measure include voltage, current and power consumption. Load signature can be used to disaggregate a composite load signal. Load signature can be classified into two levels which are micro and macro level. The micro level is a detailed view of load signature which requires the sampling interval shorter than 1 second while macro level load signature refers to the data with a sampling interval of longer than 1 second. Traditionally, load signature studies and disaggregation research mainly focused on macro level load signature [7].

B. Load Monitoring

Load monitoring is a process obtaining the amount of energy use depends on the parameter required such as current, voltage and power. Load monitoring can be classified into two methods which are “intrusive” and “non-intrusive” load monitoring []. Obtain the power consumption individually by placing a sensor between appliance and power outlet explains the method of intrusive while non-intrusive measure the power consumption signals at the entry point of the main electrical panel of a building and then disaggregate it into the power consumption of individual appliances or in other words without the need to have access to individual sockets.

C. Energy Efficiency

The efficient of energy consumption same like energy efficiency which means use the energy with the efficient and productive for completing the same tasks [13]. The goal of energy efficiency is to reduce the amount of energy required to provide products and services.

D. Energy Management

Energy management is a management and technical activities which are controlled energy usage in the organization [13]. This activity did not affect a certain function, user comfortable, and productivity. The primary objective of energy management for the user is to reduce the consumption of power per unit hour (kWh) as well as to reduce the energy total and electric bills

E. Energy Labelling

Energy label provides information about the specification and efficiency of the electrical appliances depends on the star rating given as shown in figure 1. The higher the number of the star, the efficient the appliances. The specification such as the energy performance, the cost to run and how efficient the appliances all are included in the energy rating. The energy consumption figure and the star rating are the two kinds of information on it. The Energy Rating Label provides an estimate of how much energy (in kilowatt-hours or kWh) the appliance will use over a year. This is based on assumptions about ‘average usage’.

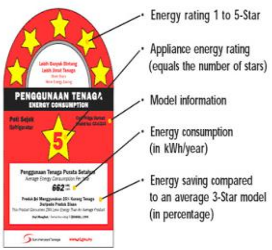

Figure 1: Energy Efficient Label

STAR	Nilai STAR Index
5	+25%= STAR Index
4	+10%= STAR Index <+25%
3	-10%= STAR Index <+10%
2	-25%= STAR Index<-10%
1	STAR Index <-25%

Figure 2: The Comparative Star

F. Inverter Technology

The inverter technology is the latest evolution of technology concerning the electro motors of the compressors. The role of the inverter is to control the speed of the compressor motor which it will continuously regulate the temperature. The variable frequency drive (VFD) act as the main role for this technology, comprises an adjustable electrical inverter to control the speed of the electromotor, which means the compressor and the cooling or heating output. The process of the drives start from the incoming of AC current to DC and then through modulation in an electrical inverter produces current of desired frequency[12].

Nowadays, inverter technology mostly implements in heating and cooling appliances such as air-conditioner and refrigerator. The implementation of the inverter technology help in reducing the power consumption up to 30% to 50%[12].

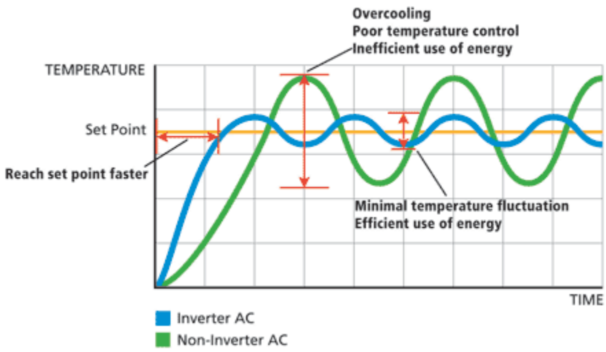

Figure 3: The difference in power consumption for inverter and non-inverter

III. METHODOLOGY

Figure 4 shows the general block diagram of the project which explain the flow and sequence to conduct this project until the output achieve.

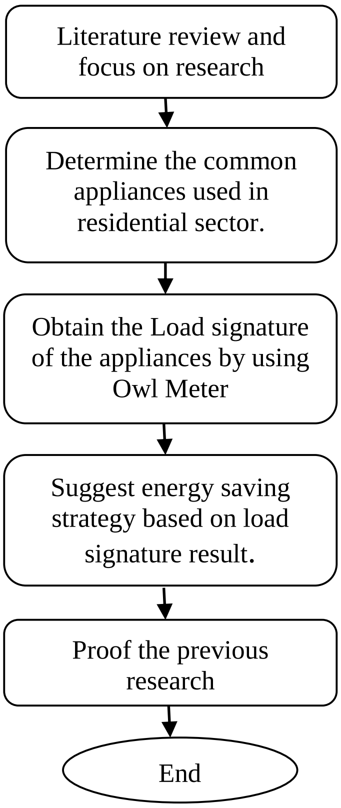

Figure 4: General Block Diagram of the Project

At first, literature review based on journal, thesis, books and the internet to find the information related to the topic especially about the behavior of electrical appliances when it operate and how to save energy based on load signature result. Understanding which appliances contribute more in power consumption and study the performance of the appliances based on the specification.

Then obtain the load signature of the appliances used in the residential sector using Owl meter and The Owl software. Finally, suggest the energy saving strategy based on load signature result.

IV. CONCEPTUAL MODELLING AND IMPLEMENTATION

Figure 5 shows the steps to obtain the load signature of the appliances with the aid of Owl meter and The Owl software. There are three elements that The Owl software can extract from the appliance which are the value of power (P), current (I) and cost. All of these values presented in table form in Microsoft Excel and the value will be capture every 6 second as shown in figure 6. The power value will be used to draw the load signature graph as shown in figure 7 where the graph shows time against power.

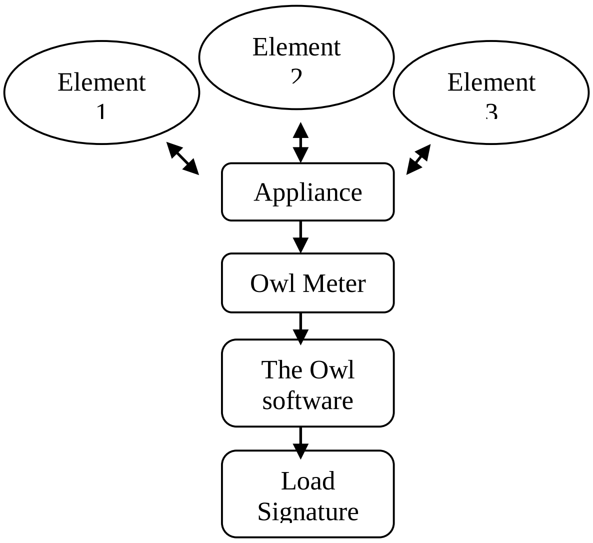

Figure 5: The steps obtaining Load Signature

	A	B	C	D	E	F
1	Device	Time	Tariff_Cost	Amps_Raw_Data	kW_Raw_Data	Cost_Raw_Data
2	Iron	22:28:06	1.36	0	0	0
3	Iron	22:28:00	1.36	0	0	0
4	Iron	22:27:53	1.36	0	0	0
5	Iron	22:27:47	1.36	3.99	917.7	124807
6	Iron	22:27:41	1.36	3.99	917.7	124807
7	Iron	22:27:35	1.36	0	0	0
8	Iron	22:27:29	1.36	0	0	0
9	Iron	22:27:23	1.36	0	0	0
10	Iron	22:27:17	1.36	0	0	0
11	Iron	22:27:11	1.36	0	0	0
12	Iron	22:27:05	1.36	0	0	0
13	Iron	22:26:59	1.36	0	0	0
14	Iron	22:26:53	1.36	0	0	0
15	Iron	22:26:47	1.36	0	0	0
16	Iron	22:26:41	1.36	0	0	0
17	Iron	22:26:34	1.36	0	0	0
18	Iron	22:26:28	1.36	0	0	0
19	Iron	22:26:22	1.36	4.06	933.8	126997
20	Iron	22:26:16	1.36	4.06	933.8	126997
21	Iron	22:26:10	1.36	0	0	0

Figure 6: Table form data

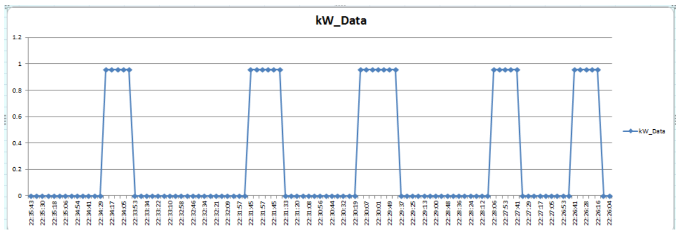

Figure 7: The load signature of the appliance

To measure the power consumption, there are two methods to clamp the sensor either at the individual live cable or at the live cable on outgoing meter as shown in figure8 and figure 9. The difference between these two methods is at the starting process. When the sensor clamp at the outgoing cable meter, all of the appliances at the house need to turn off except the appliance need to be test to ensure there is only the tested appliances' current flow. This method usually used for large power consumption appliance such as air-conditioner. Different when the sensor clamp at the individual live cable where the tested appliance need to plug at the modified socket and then test.

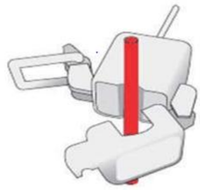

Figure 8: Clamp sensor at individual live cable

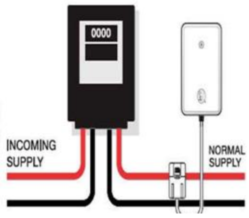

Figure 9: Clamp sensor at outgoing cable meter

V. RESULT AND DISCUSSION

The common electrical appliances used at residential sector are tested and they include:-

- Refrigerator
- Iron
- Air-conditioner
- Light bulb :-
  - Incandescent Bulb
  - CFL Bulb
  - LED Bulb
- Television :-
  - Cathode Ray Tube(24')
  - LCD (50')
  - LCD (25')
- Washing Machine :-
  - Automatic
  - Manual

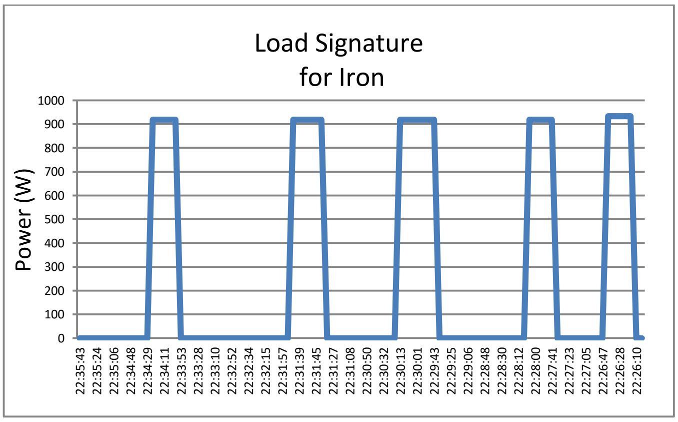

Figure 10: Load Signature for Iron

From the load signature result for iron shown in figure 10, it shows fluctuation graph which explained that iron has on and off state. The advantage that we can take from this result, we can used the iron without using any power because the iron still hot in off state condition. So, the benefit from this result is we can iron the clothes without using power when it in off state. This is the reason why the government encourage ironing the clothes in many portions for one time.

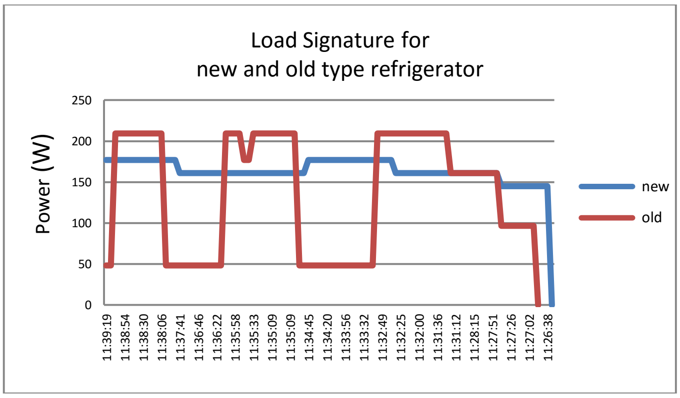

Figure 11: Load Signature for two type refrigerator

Figure 11 shows the load signature for two different type of refrigerator where new refrigerator install with inverter technology while the old refrigerator didn't come with any technology. The major difference is the behavior of the refrigerator when it consumes energy. The new refrigerator shows the optimum operation where it use low power consumption. This happen due to the compressor only produces the power when it is required at the optimum condition.

The compressor will never switch off even the temperature already stabilizes but runs at a slower speed to maintain the temperature inside the refrigerator. Overcooling and poor temperature control happen on the refrigerator without inverter technology at ones shows inefficient use of energy. Change the refrigerator to the latest technology is the best strategy can be taken.

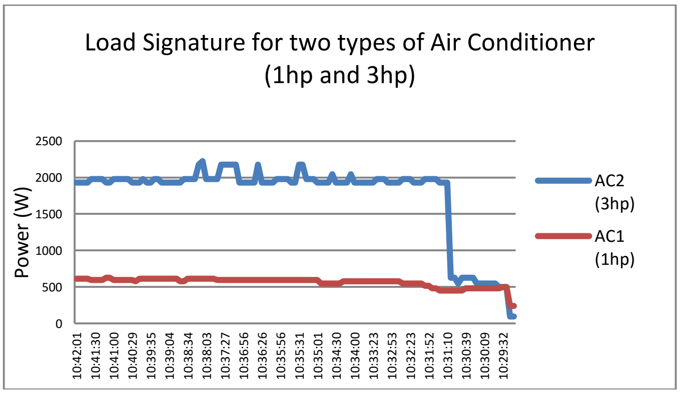

Figure 12: Load signature for two different type air-conditioner

Based on the load signature result for two different types of air-conditioner shown in figure 12, the 3HP air-conditioner shows higher power consumption compared to 1HP air-conditioner. Both air-conditioner test at the optimum temperature (24°C) and both come with inverter technology.

The role of this technology is to control the speed of the compressor. It will give more power when the air-conditioner needs more power and produce less power when low power required. The compressor will always in ON state but less power consumption. The power consumption depends on the temperature of the incoming air and the level set on the thermostat. This technology also has a sensor which adjusting the power according to the current temperature.

Different with the air-conditioner without an inverter technology. The air-conditioner just operates based on the temperature set and throws cool air. It operates in ON and Off state which shows fluctuation load signature when controlling its temperature and this causes the compressor run at full power at all time it ON.

Therefore, switch or buy the air-conditioner embedded with inverter or other latest technology which result optimum power consumption is the best strategy can be taken for energy saving and reduce cost for long term. Other than that, the place for installing the air-conditioner needs to emphasize. The smaller the size of the room, the lower the power of the air-conditioner.

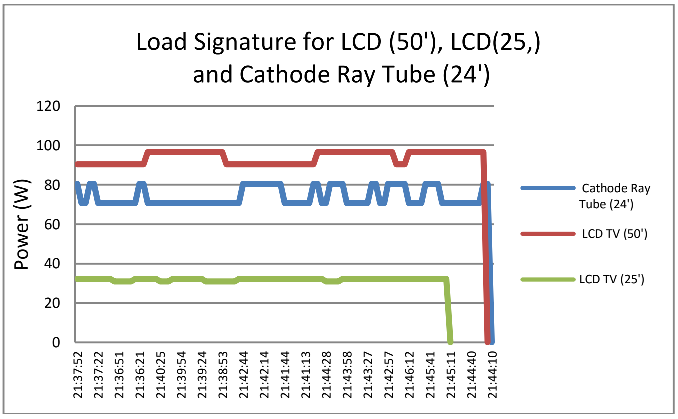

Figure 13: Load signature for 3 different type of Television

LCD television shows low power consumption compared to Cathode Ray Tube as shown in figure 13. This due technology install for displaying images on the screen known as TFT LCD (thin film transistor liquid crystal display) different with the Cathode Ray Tube used CCF (cold cathode fluorescent) where it less power efficient result in high power consumption.

Another case when comparing the television on the same screen type but different in size. The bigger the size, the higher the power consumption. Therefore, the strategies should be taken is when choosing the television. Choose a display size which you are comfortable with and obviously the latest technology shows the low power consumption. So, consumer should turn to the latest technology television for long term saving.

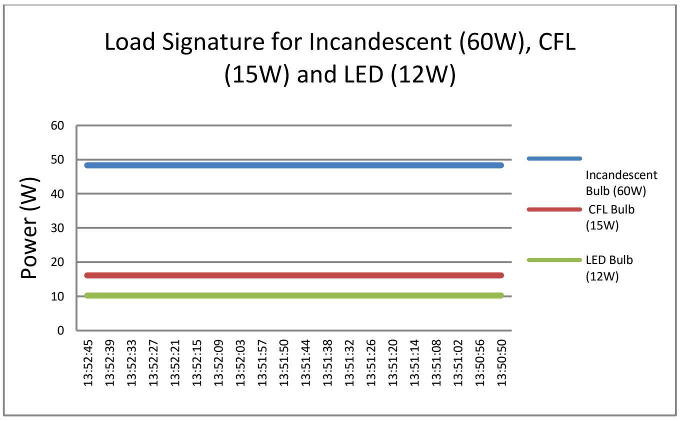

Figure 14: Load signature for 3 different type of Bulb

Figure 14 shows the load signature for three different bulbs with the same brightness. The Incandescent bulb shows the highest power consumption followed by CFL bulb and LED bulb. The incandescent bulb is like miniature electric resistance heaters, in fact, 90% of the energy consumed is given off as heat, while 10% of the energy produces light [3] cause it inefficient.

The electrical discharge method which operates on CFL bulb is far more efficient than the resistance method of Incandescent bulb. It produces 4 to 10 times more lumens per watt. It also last 10 to 15 times longer and this method gives less heat for the same unit of light. CFL bulb uses 25% to 35% less energy than Incandescent. For LED bulb it used at least 75% less energy and 25 times longer than Incandescent. The less dependency from the need of reflector and diffusers that can trap light. LED also emits little heat which is more efficient compared to Incandescent which release 90% heat. LED bulb only needs 2-17 Watts of power which is 1/3 of CFL bulb and 1/30 of Incandescent Bulb.

Therefore, the usage for LED and CFL bulb shows more profitable compare to Incandescent Bulb. Changing to the LED and CFL bulb from Incandescent bulb is the best strategy that the consumer must take for long term saving.

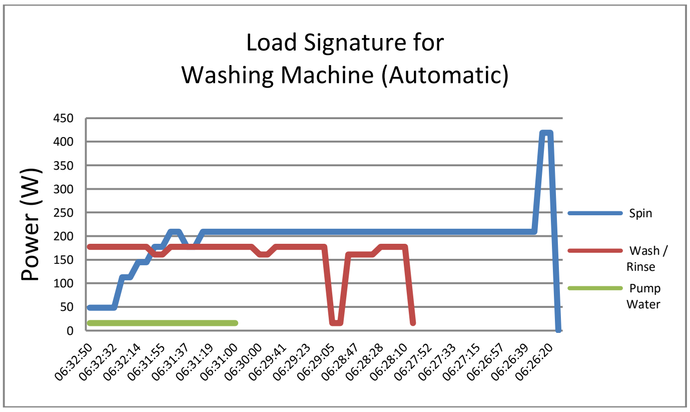

Figure 15: Load signature for Washing Machine (Automatic)

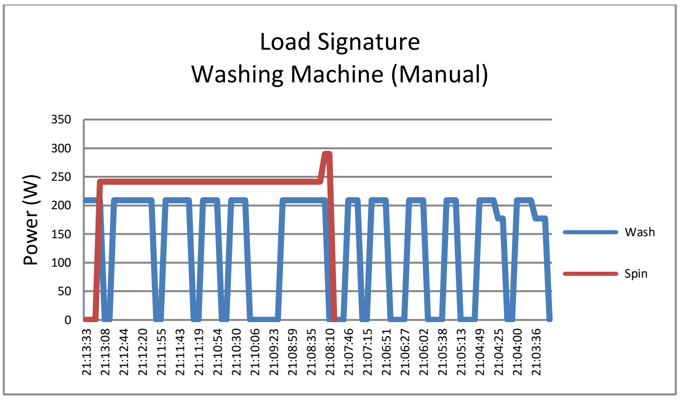

Figure 16: Load signature for Washing Machine (Manual)

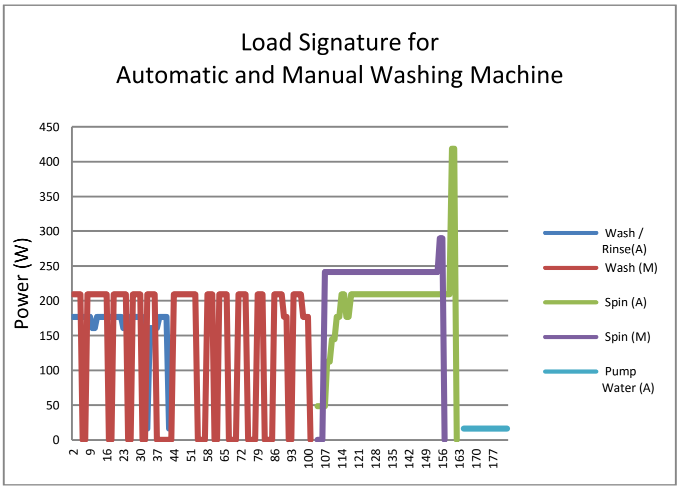

Figure 17: Load signature for two different type of Washing Machine

Figure 17 shows the load signature for two different type of washing machine where the automatic washing machine install with inverter technology while the manual washing machine didn't has any technology inside. The comparison for this two different washing machine based on two processes which are wash and spin process. Pump water is the extra process in automatic washing machine. Pump water shows constant power consumption and the time depends on the water level been choose. Based on the load signature result shown in figure 15 and figure 16 show that spin process consume more power when they operate compared to wash process.

The automatic washing machine shows optimum ways on operation and used less power consumption compared to manual washing machine. The load signature for wash process at manual washing machine shows ON and OFF state which result inefficient power utilization. The inverter technology inside the automatic washing machine has a sensor which detects the load of the washing machine. When the load detected, it will determine the optimum speed on which the motor should operate and run to optimize the power consumption. This technology able to predict the actual or optimum power needed. It converts the incoming power which is a fixed voltage and frequency to the variable value.

The washing machine without inverter technology will operate and consume power same for all load. Either the load for the washing machine is full or not the electricity usage still the same. This is because it doesn't have a sensor to detect the load and able to calculate the optimum power usage.

Once again the inverter technology proved that optimum power utilization and the consumer should take an advantage from this technology because it really helpful in saving although this technology more costly at the beginning but save for long term.

VI. Conclusion

In this paper, all the concept of load signature has been defined and the load signature of each appliance has been taken individually. Based on the load signature result, the energy saving strategies proposed and investigated. All the strategies taken by the government and utility sector to reduce the power consumption has been stated.

Acknowledgment

Firstly, I would like to extend much appreciation and many thanks to my supervisor, Prof. Dr. Mohammad Yusri Hassan who gave many lessons, assistance, guidance, as well as advice that was priceless throughout this semester. With a tight of schedule did not prevent his from being the most important advisor in the completion of this project. Finally, thank everyone that was involved directly or indirectly in the success of this project

References

[1] Robinson, S., & Dubin, F. S. (1978). The energy efficient home: A manual for saving fuel and using solar, wood, and wind power. New York: New American Library
[2] Bertoldi, P., Ricci, A., & Almeida, A. T. (2001). Energy efficiency in household appliances and lighting. Berlin: Springer.
[3]Thorpe, D. (2014). Energy management in buildings: The Earthscan expert guide. London: Routledge, Taylor & Francis Group, Earthscan from Routledge.
[4] Harbuck, S., & Harbuck, D. D. (2014). Residential energy auditing and improvement. Lilburn, GA: The Fairmont Press.
[5] Liang, J., Ng, S., Kendall, G., & Cheng, J. (2010). Load signature study ¡V part I: Basic concept, structure, and methodology. IEEE PES General Meeting. doi:10.1109/pes.2010.5589406
[6]Liang, J., Ng, S., Kendall, G., & Cheng, J. (2010). Load signature study ¡V part II: Disaggregation framework, simulation, and applications. IEEE PES General Meeting. doi:10.1109/pes.2010.5589424
[7]Cheng, J. W., Ng, S. K., Liang, J., & Zhong, J. (2012). An alternative use of power quality information - Load signature studies & applications. 2012 IEEE 15th International Conference on Harmonics and Quality of Power. doi:10.1109/ichqp.2012.6381297
[8]Iksan, N., Sembiring, J., Haryanto, N., & Supangkat, S. H. (2015). Appliances identification method of non-intrusive load monitoring based on load signature of V-I trajectory. 2015 International Conference on Information Technology Systems and Innovation (ICITSI). doi:10.1109/icitsi.2015.7437744
[9] Learn About LED Bulbs | ENERGY STAR. (n.d.). Retrieved December 10, 2016, from https://www.bing.com/cr?IG=27F2B6F04C9E418A8FF3F6E9CC67327E&ID=271B785C905C69EC3E0171AD916D685B&rd=1&h=nPW5fyRUgwNkoy_z0pdOZPN-JeTs0UA8CB-

Kb4xtod0&v=1&r=https%3a%2f%2fwww.energystar.gov%2fproducts%2flighting_fans%2flight_bulbs%2flearn_about_led_bulbs&p=DevEx,5099.1
[10] Variable Frequency Drives - Questline. (n.d.). Retrieved December 11, 2016, from http://www.bing.com/cr?IG=66324077192C44ABA9A4BA7FA8D785FC&CID=23043EA895D4630C3A26375994E56241&rd=1&h=wCJmuE89MM7GoQdaBKWrUybECAbADl9CQScxK11e3s&v=1&r=http%3a%2f%2fmembers.questline.com%2fpresentations%2f20111025EcovaVariableFreqDrives.pdf&p=DevEx,5117.1
[11] Labelling | Energy Rating. (n.d.). Retrieved December 18, 2016, from http://www.bing.com/cr?IG=4ABDE26E1A1B4793B03F1DD485CCEEFC&CID=1C81D9C7DC5D64991525D036DD6C65D4&rd=1&h=Losqhasd5L_YtRCXDJGum3hivN-toCJJaGUqYz4iMGM&v=1&r=http%3a%2f%2fwww.energyrating.gov.au%2fabout%2fwhat-we-do%2flabelling&p=DevEx,5170.1
[12] What is the Inverter technology in air conditioners ... (n.d.). Retrieved December 21, 2016, from https://www.bing.com/cr?IG=41DD963EA2064435887DEF724006C6C3&CID=0483601FFC0B6CAF1AE469EDFD3A6D74&rd=1&h=bvAFhnpBTiLi8vBDnQD4yVTn9rbf33DYvtvyMo9RbG0&v=1&r=https%3a%2f%2fwww.inventorairconditioner.com%2fblog%2ffaq%2fwhat-is-the-inverter-technology-in-air-conditioners&p=DevEx,5191.1
[13] Energy Efficiency for Industrial Sector in Malaysia (Unpublished master's thesis). Universiti Teknologi Malaysia. (2007).
[14] Potential Of Electricity Savings and CO2 Reduction from the Implementation of Energy-Efficient Refrigerator and Air-Conditioner Program for Residential Sector In Malaysia(Unpublished master's thesis). Universiti Teknologi Malaysia. (2009).
[15] Lee, W. K., Lam, H. Y., & Y, F. H., Chan. (2004). Exploration on load signature. Retrieved December 21, 2016.
[16] Times, N. S. (n.d.). Technology can reduce energy cost 60 percent. Retrieved Jan. & Feb., 2009
[17] ENERGY STAR® | Department of Energy. (n.d.). Retrieved December 13, 2016, from http://www.bing.com/cr?IG=080FA94F968042EEAD1AE562540F69B4&CID=1ED740396A9966B1085749CB6BA867FD&rd=1&h=zMziaZ05IvP-vJu6UXBVMDQhptCO4ilW_0byQX0RXSc&v=1&r=http%3a%2f%2fwww.energy.gov%2feere%2fbuildings%2fenergy-star&p=DevEx,5147.1

Optimal Placement and Sizing of DVR for Voltage Sag Mitigation using Firefly Algorithm Optimization

Mohd Safwan bin Abdul Latip
Faculty of Electrical Engineering
Universiti Teknologi Malaysia
Johor Bahru, Malaysia.
mohdsafwanabdullatip@gmail.com

Prof. Dr. Ahmad bin Darus
Department of / Centre of
Faculty of Electrical Engineering
Universiti Teknologi Malaysia
Johor Bahru, Malaysia.
eahmad@utm.my

***Abstract*—This paper represents implementation of Firefly Algorithm(FA) to optimize the placement and sizing of Dynamic Voltage Restorer (DVR) for voltage sag mitigation within a radial distribution system. The objective function implemented into FA was designed to minimize effect of voltage sag and to minimize total investment cost of DVR. For this study, the algorithm is implemented on IEEE 33-bus radial distribution system using MATLAB software. Objective of this study is to obtain certain location and capacity for DVR in order to restore voltage profile during fault to its voltage profile before fault. This is to ensure distribution system reliability and protect sensitive component from malfunction. Expected result is voltage profile of the distribution system return to normal after a fault occurred.**

Keywords—Firefly Algorithm; Dynamic Voltage Restorer; Voltage Sag; MATLAB)

I. Introduction

Voltage sag is one of the most frequent power quality problem and the most severe problem where the bus experience a short duration of decrease in voltage level [1]. There are many ways to reduce or mitigate the effect of voltage sag in a distribution system and one of them are by introducing custom power device (CPD). Custom power device is divided into two categories, that is compensating type and network reconfiguring type. Compensating type such as Distributed Static Synchronous Compensator (DSTATCOM), Dynamic Voltage Restorer(DVR), and Unified Power Quality Conditioner (UPQC) will make fast adjustment and compensate the disturbance to ensure almost constant nominal voltage level.

Evolutionary algorithm has been used for so many optimization application in various field of work. Popular algorithm such as Genetic Algorithm (GA), Particle Swarm Optimization (PSO) are used widely in finding optimized solution through a set of instructions and function that help to select and choose the best solution available. The difference between each algorithm is the flow and function used to choose the best solution. Recently, a study has performed by [2] shows the superiority of Firefly Algorithm (FA) in finding better solution, accuracy, and shorter convergence time compared to GA and PSO. FA is a nature type algorithm that follow the characteristic of firefly and introduced by [3].

Optimization on placement of static compensator (STATCOM) and DVR for voltage sag mitigation was implement based on niching type of GA [4]. Technical parameters regarding FACTS devices was implemented into Particle Swarm Optimization (PSO) with objective to minimize generation cost and power losses [5]. Another optimization algorithm, binary gravitational search algorithm was implemented to maximize reliability and improve voltage profile due to voltage sag within a distribution system [6]. Optimization which involving both GA and PSO was used in [7] with objectives to obtain optimal placement and sizing of Distributed Generation (DG).

In this project, the voltage sag is mitigated by introducing DVR into the best location in which the most sensitive load located. Location of the most sensitive load are determined by using Firefly Algorithm (FA) method. A single objective function is designed to minimize effect of voltage sag and improve voltage profile. The FA capabilities in optimizing placement and sizing of DVR is experimented on 33-bus radial distribution system, and the result obtained from FA will be tested on SIMULINK to observe voltage sag mitigation on the given placement.

II. Literature Review

A. *Objectice Function*

Minimization Voltage Deviation

This objective function formulated from [8] to show voltage deviation of all bus within the distribution system from the reference voltage. Voltage Deviation Index holds the value which indicate how good voltage profile of the distribution system which can be obtained by;

$$V_{dev} = \sqrt{\sum_{i=1}^{B}(V_{i-ref} - V_i)^2} \tag{1}$$

Based on the objective function, V_{ref-i} indicate the reference voltage before voltage sag occur, V_i represent measured voltage after voltage sag occur and B is the total bus.

Investment Cost of DVR

Cost of investment formulated from (3) is influenced by number of device (DVR) that used and the size of the device (capacity). The cost parameter is from [9], and shown below.

$$C_{DVR} = DVRCapacity * \$300$$

$$C_{initialcost} = \$750000$$

$$C_{TotalCost} = C_{initalcost} + C_{DVR} \quad (3)$$

Based on (3), C_{DVR} is the cost for capacity used by DVR. While, $C_{initialcost}$ is the total initial cost for installment of DVR, and $C_{Totalcost}$ is the total cost for one DVR.

B. Problem Constraint

Bus Voltage

To ensure optimization to be in the optimum range of voltage. For this study, minimum voltage constraint is the after-fault voltage, and maximum voltage constraint is the before fault voltage. This because, DVR main objective is to compensate voltage sag so that it returns to its normal voltage

$$M_{min} < M < M_{max} \quad (4)$$

Where M is bus number under study, while M_{max} is the bus voltage before fault, and M_{min} is the bus voltage after fault.

DVR Capacity

DVR Capacity should be limited to certain range of value during the optimization process which specified as;

$$S_{DVR-min} < S_{DVR} < S_{DVR-max} \quad (5)$$

Likewise, $S_{DVR-min}$ is the least capacity value under study, and $S_{DVR-max}$ is the maximum capacity value under study.

C. Overall Objective Function

In-order to meet all constrain and objective function, a method from [8] known as weighted method is used to simplify optimization process. This method allows FA to treat it as single objective optimization instead of multi-objective optimization. The following formula is modified from [8].

$$F = f_1 + wf_2 + \varphi \sum_{i \in M} \max\left(V_i - V_{beforefault}, 0\right)$$

$$+\max(V_{beforefault} - V_i, 0) + \quad (6)$$

$$\varphi \sum_{i \in M} \max(S_i - S_{DVR-max}, 0) + \max(S_{DVR-min} - S_i, 0)$$

Where, f_1 is the (1), w is the relative fixed weight factor, designed to normalize the value to its maximum base value, f_2 is equation (3), and φ is a penalty multiplier, which containing large number. So, if the constraint is violated, the output cost function from that violation will be far greater than the other output cost function, this helps to eliminate constraint violated output since this is optimization process.

D. Firefly Algorithm

Firefly Algorithm (FA) was founded by Yang [3] which an algorithm that created based on firefly mating behavior and it movement. Firefly Algorithm is a metaheuristic algorithm that has proven in [3] on its effectiveness in obtaining better and faster result compared to GA and PSO. Basically, the framework of FA was designed based on differences of light intensity, I and the attractiveness, β. Attractiveness is an important component in FA. Attractiveness are defined by the observer which is among fireflies. So, attractiveness is affected by two main components, which is distance between attracting firefly and attracted firefly, and medium which the light travel through. This because, the attractiveness decreases as distance increase, and light absorbed by medium may cause the light became dim and not attractive anymore. Equation (4) show the relationship attractiveness with distance and fixed light absorption

$$\beta(r) = \beta_0 e^{-\gamma r^2} \quad (6)$$

Likewise, r is the distance between observing firefly and firefly that being observed, β_0 is the attractiveness of an individual firefly at r=0, and γ is the fixed light absorption coefficient.

Distance between firefly i and firefly j which located at location x_i and x_j can be obtain using Euclidean distance as shown (4);

$$r_{ij} = \sqrt{\sum_{k=1}^{d} (x_{i,k} - x_{j,k})^2} \quad (7)$$

Where x_{i-k} is the *k*-th component if the spatial coordinate x_i of the *i*-th firefly, and d is the dimension of the problem.

Movement of firefly i is attracted toward more attractive firefly j is determined by equation (6). The first component in equation (6), is the current location for x_i, the second component is due to attraction and the third component is for randomization component.

$$x_i^{k+1} = x_i^k + \beta_0 e^{-\gamma r^2}(x_j - x_i) + \alpha(\xi) \quad (8)$$

Where, rand is the random number generator uniformly distributed within range from 0 to 1 and α is the randomization parameter.

E. Firefly Algorithm Implementation Pseudocode

```
Insert the objective function f(x), x = (x1, x2, …,xd)^T
Initialize the fireflies population xi, i = 1, 2, …,n)
Determine the light intensity Ii at xi using f(xi)
Set light absorption coefficient γ, randomize coefficient α
while (t < MaxGeneration)
        for i = 1 : n    all n fireflies
                for j = 1 : n
                        if (Ii < Ij), Move firefly i towards j ; end if
                        Vary attractiveness with distance r via exp[−γr^2]
                        Evaluate new solutions and update light intensity
                end for j
        end for i
        Rank the fireflies and find the current global best
end while
Print results
```

Figure. 1. Firefly Algorithm Implementation Pseudocode

III. METHODODOLGY OF IMPLEMENTATION FA FOR OPTIMIZATION OF DVR PLACEMENT AND SIZING.

For this project, FA optimization method is implemented to solve placement and sizing problem for DVR. To solve this problem, FA is used to minimize the objective function (6). To initialize optimization, distribution system data such as line data and bus data is inserted into FA as an input. Whilst, the variable for this optimization is the sizing and placement of the DVR. Then, backward/forward sweep power flow method [11] is used as load flow algorithm to determine changes in bus voltage as DVR is placed randomly into the distribution system by FA. Thus, result from the load flow will be used as data and inserted into objective function (6). The objective function is then ranked according to its value, and the best of each iteration is stored and will be compared to the next iteration solution. Since this is minimization of voltage deviation, the smallest value of (6) will be the best solution.

IV. RESULT AND DISCUSSION

A. Introducing Fault to Simulate Voltage Sag

To implement the FA framework into determining best placement and sizing for DVR within a distribution system, a radial distribution modified 33-bus distribution system is used as the test distribution system as shown in Fig. 2 [10]. In-order to simulate voltage drop due to three phase fault, heavy load is added to 31th bus of the test distribution system. This cause voltage drop across bus that connected to bus 31, when backward/forward sweep load flow is executed. Load data and line data is shown at appendix.

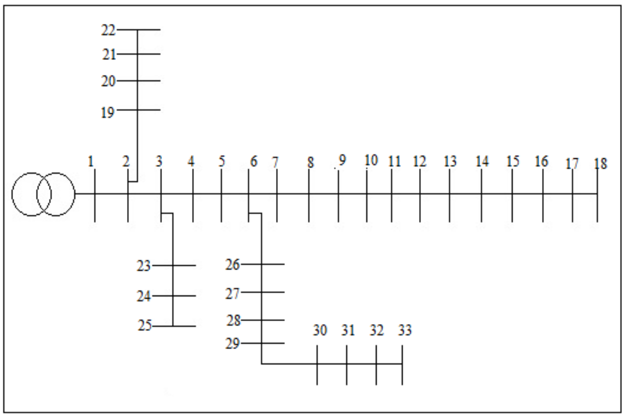

Figure. 2. IEEE 33-bus radial distribution system

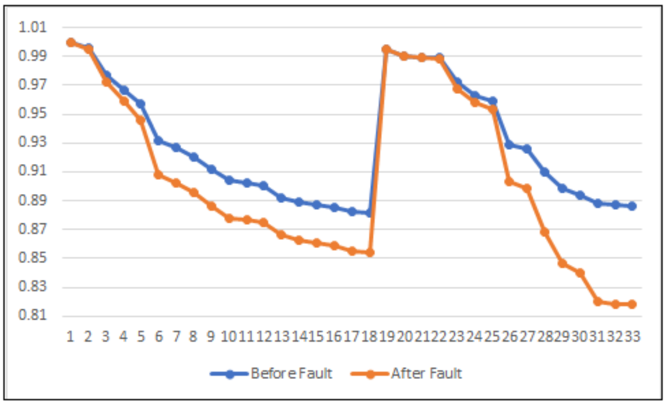

Figure. 3. IEEE 33-bus voltage before and after fault

As shown in Figure. 3., it is observable that voltage drop occur across the distribution system after heavy load introduced at bus 31 Bus voltage data is calculated by backward/forward sweep load flow [11]. The voltage drop is treated as a voltage sag since voltage sag also related to voltage drop but happen at very small time interval [1].

B. Firefly Algorithm

For this study, proposed number of possible solution created is 100, and number iteration is 100 iteration. In-order to ensure the output is the best solution, number of iteration should be kept to a large number so that FA can achieve convergence.

TABLE I. FIREFLY ALGORITHM PARAMETER

Parameter	Value
α	0.2
β_0	2
γ	1
α_{damp}	0.95

Based on Table. I., the parameter used is the basic parameter for FA.

TABLE II. FA OUTPUT

Maximum Capacity	Location	Capacity Size(KVa)	Cost Function	Total Investment Cost
1000	**33,1,31,18**	**137.6560,0,633.9488,5.6118**	**1.0545**	**$3233200**

Table II. show output result from FA optimization. Maximum capacity is the maximum allowed capacity for individual DVR. Location is the DVR placement in the distribution bus, and capacity size is the sizing of DVR optimized by FA. Cost function is an output from FA which indicate the objective function and the constraint, which voltage profile and total investment cost of DVR is minimized and optimized by FA. Also, shown the total investment cost which is considered optimum by FA. However, bus location 1 have 0 capacity, this is resulted from FA optimization procedure where it must minimize voltage profile index and total investment cost. Total investment cost is shown (3). Although bus location 1 DVR has 0 capacity, it still has initial cost of $750000. The capacity cost calculated need to be updated since bus location 1 has no use. Thus, new total investment cost is $3233200−$750000 = $2483200.

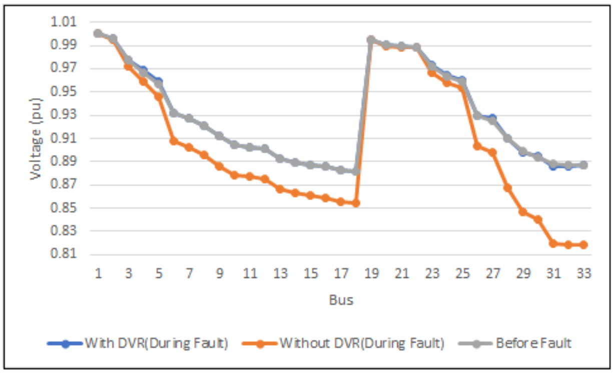

Figure. 4. Voltage Profile of IEEE 33-Bus Distribution System.

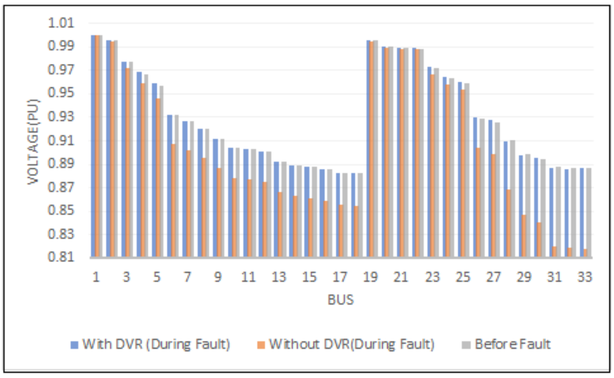

Figure. 5. Voltage Profile of IEEE 33-Bus Distribution System.

Figure. 4. and Figure. 5 shows result of optimization regarding specific capacity and placement of DVR to achieve total restoration of voltage profile of affected distribution bus system. Figure. 4 shows overlap between line before fault and line during fault with DVR, and to make it observable, Figure. 5 shows comparison in term of voltage magnitude in pu.

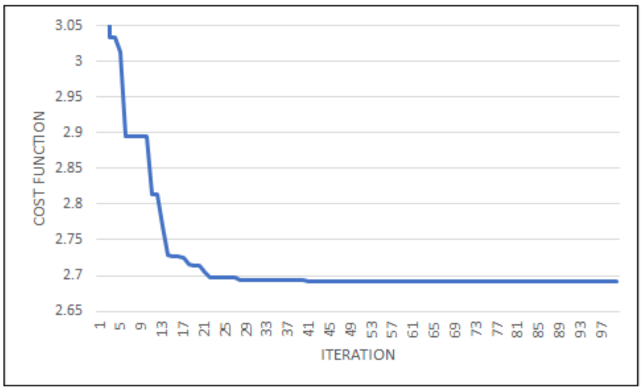

Figure. 5. Convergences of FA

Figure. 5. Shows the rate of reaching global optima which required about 60 iteration. However, rate of convergences can be manipulated by changing the parameter of FA.

a.

CONCLUSION

Using FA optimization method, placement and sizing problem for DVR can be solved. Through optimization, most optimal solution can be achieved and reduce time required for a repetitive experiment to find the best solution. Through this study, IEEE 33 bus radial distribution system is used as case study and using MATLAB software to implement FA to find the optimal placement and sizing for given fault location is presented. Minimization of investment cost of DVR and compensation of voltage sag is implemented as the objective function which enable FA to find the best solution according to the objective function needs.

REFERENCES

[1] Math H.J. Bollen,” Voltage sags: effects, mitigation and prediction”, Power Engineering Journal June 1996.

[2] Masoud Farhoodnea, Azah Mohamed, Hussain Shareef,” Power Quality Enhancement in Distribution System by Optimal Placement of Dynamic Voltage Restorer”, 2013 IEEE Student Conference on Research and Development (SCOReD).

[3] X.-S. Yang, "Firefly Algorithm," in Engineering Optimization, ed: John Wiley & Sons, Inc., 2010, pp. 221-230.

[4] Y. Zhang and J. V. Milanovic, "Global Voltage Sag Mitigation With FACTS-Based Devices," IEEE Transactions on Power Delivery vol. 25, pp. 2842-2850, 2010.

[5] A. Parastar, A. Pirayesh, and J. Nikoukar, "Optimal location of FACTS devices in a power system using modified particle swarm optimization," in 42nd International Universities Power Engineering Conference (UPEC), 2007, pp. 1122-1128..

[6] N. Salman, A. Mohamed, and H. Shareef, "Reliability Improvement in Distribution Systems by Optimal Placement of DSTATCOM Using Binary Gravitational Search Algorithm," PRZEGL ẠD ELEKTROTECHNICZNY, vol. 88, pp. 295-299, 2012.

[7] M. Moradi and M. Abedini, "A combination of genetic algorithm and particle swarm optimization for optimal DG location and sizing in distribution systems," International Journal of Electrical Power & Energy Systems, vol. 34, pp. 66–74, 2011

[8] M. Farhoodnea, A. Mohamed and H. Shareef, "Power quality enhancement in distribution systems by optimal placement of dynamic voltage restorer," 2013 IEEE Student Conference on Research and Developement, Putrajaya, 2013, pp. 111-115.

[9] Mahmoud A. El-Gammal, Amr Y. Abou-Ghazala and Tarek I. El-Shennaw, "Costs of Custom Power Devices Versus the Financial Losses o International Journal of Computer and ElectricalEngineering, Vol. 2, No. 5, October, 2010.

[10] K Dharageshwari, C Nayanatara, "Multiobjective Optimal Placement of Multiple Distributed Generations in IEEE 33 Bus Radial System Using Simulated Annealing", 2015 International Conference on Circuit, Power and Computing Technologies [ICCPCT].

[11] T. Jen-Hao and C. Chuo-Yean, "Backward/Forward Sweep-Based Harmonic Analysis Method for Distribution Systems," IEEE Transactions on Power Delivery, vol. 22, pp. 1665-1672, 2007.

Experimental Kit of Controlling the Brush Direct Current (DC) Motor Speed with Pulse Width Modulation(PWM) Method by using Arduino Microcontroller

Muhamad Nazarudin Bin Yahaya
Faculty of Electrical Engineering,
University Technology Malaysia, Johor, Malaysia
muhamadnazarudin_94@yahoo.com

Associate Prof. Dr. Nik Rumzi Bin Nik Idris
Faculty of Electrical Engineering,
University Technology Malaysia, Johor, Malaysia
nikrumzi@fke.utm.my

***Abstract*—Nowadays, the brush direct current (DC) motor used in industrial application have increased rapidly due to its characteristic that make it ease of controllability that meets the user's needs. This journal paper exposed the method of controlling the speed of brush DC motor by pulse width modulation (PWM) on Arduino microcontroller. This project is to implement the experimental kit for students learning about the DC motor specification, operation, and information related to the DC motor and the hardware components such as the Arduino microcontroller, blanking/dead time circuit, gate/motor driver, and power electronic converter. The PWM output generated from Arduino connected to blanking time circuit that will make the signal delay, then to the gate driver for stepping up the voltage, then to power electronic converter (in this project, MG8Q6ES42 converter was used) and finally to the DC motor.**

***Keywords*— DC motor, Arduino Microcontroller, Pulse Width Modulation(PWM), dead/blanking time circuit, gate driver, power electronic converter**

I. INTRODUCTION

Technologies have grown drastically, including the DC motor. It has been used widely in the industry and many application for example from toys to push-button adjustable car seats. Brushed DC motors are inexpensive, easy to drive, and are readily available in all sizes and shapes. DC motor produced mechanical energy from the electrical energy supplied. DC motors have the potential for very high torque capabilities. It is generally a function of the physical size of the motor, are easy to miniaturize, and can be throttled via adjusting their supply voltage. DC motor not only the simplest but the oldest electric motors. A DC Motor uses direct current. In other words, the direction of current flows in one direction.

There are two primary advantages of DC motors which is speed variation and torque. Speed variation can be achieved by changing either the armature voltage or field voltage, or a combination of both. The voltage input for the armature is directly proportional to the speed of the motor which is when the higher voltage and current is supply, the speed will increase according to its supply. The other advantage is torque. Torque can be defined as a turning force that tends to produce rotation on a shaft. The primary advantage of the DC motor is that it can develop constant torque over a wide speed application.

Although there are many applications of DC motor in daily life, there are still many do not know about its operation and how it works. Students need to study and learn about it including the specifications of the motor, how it works, how to control it and also how to handle and run the DC motor.

II. LITERATURE REVIEW

There are four main components of the DC motor which is Stator, Rotor, Commutator and Brushes.

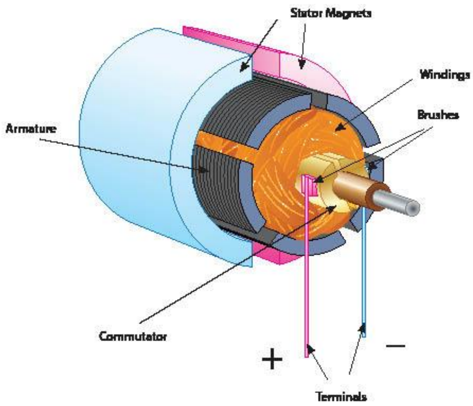

Fig. 1. Brush DC motor

The stator generates a stationary magnetic field that surrounds the rotor. This field is generated by either permanent magnets or electromagnetic windings.

The rotor, also called the armature, is made up of one or more windings. When these windings are energized they produce a magnetic field. The magnetic poles of this rotor field will be attracted to the opposite poles generated by the stator, causing the rotor to turn. As the motor turns, the windings are constantly being energized in a different sequence so that the magnetic poles generated by the rotor do not overrun the poles generated in the stator. This switching of the field in the rotor windings is called commutation.

Brush DC motors do not require a controller to switch current in the motor windings. Instead, the commutation of the windings of a BDC motor is done mechanically. A segmented copper sleeve, called a commutator, resides on the axle of a BDC motor. As the motor turns, carbon brushes slide over the commutator, coming in contact with different segments of the commutator. The segments are attached to different rotor windings, therefore, a dynamic magnetic field is generated inside the motor when a voltage is applied across the brushes of the motor. It is important to note that the brushes and commutator are the parts of a BDC motor that are most prone to wear because they are sliding past each other.

III. METHODOLOGY (HARDWARE DESIGN)

A. Arduino UNO Microcontroller (ATmega328P)

Arduino UNO is a microcontroller board based on the ATmega328P. It has 14 digital input/output pins (of which 6 can be used as PWM outputs), 6 analog inputs, a 16 MHz quartz crystal, a USB connection, a power jack, an ICSP header and a reset button. It contains everything needed to support the microcontroller; simply connect it to a computer with a USB cable or power it with an AC-to-DC adapter or battery to get started.

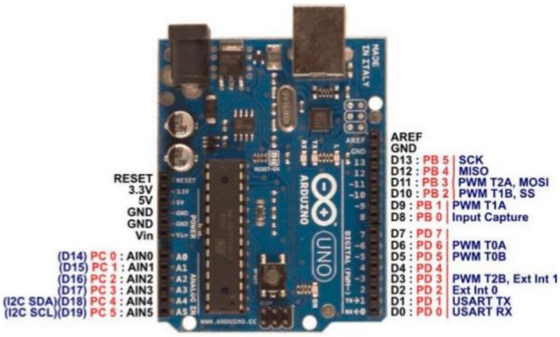

Fig. 2. Arduino UNO microcontroller (ATmega328P)

In this project, the PWM signal was generated by the Arduino as an input for the gate driver before the motor.

B. Gate Driver

Fig. 3. Gate Driver

The gate driver will step up the voltage signal from the Arduino from 5V to 15V. There is 6 input from the Arduino that will be receive.

C. Power Electronic Converter (Toshiba MG8Q6ES42)

For the Power Electronic Converter, there are 6 IGBT switches but only 4 need to be used. This Power Electronic Converter allows only 2 switches on.

Fig. 4. Power Electronic Converter (Toshiba MG8Q6ES42)

D. Dead/Blanking Time Circuit

To avoid the simultaneous turn-on of two switches in the same bridge arm, an extra circuit is needed to provide dead-time insertion. The diode-R-C circuit at the first stage of the circuit is inserted to provide a time delay for the input signals. The time interval between the input signal and the output signal is determined by the RC time constant and the threshold voltage of the Schmitt trigger inverter, noting that the output voltage of the Schmitt trigger inverter is established after the voltage of the capacitor reaches the threshold value.

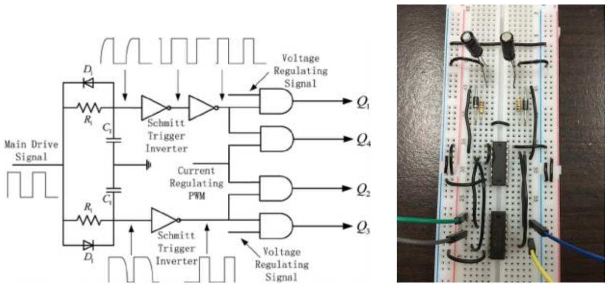

Fig. 5. Dead/Blanking Time Circuit

For the experimental kit, there are several stages for the signal from the Arduino going through before reach the motor to operate. Below is the process of the operation.

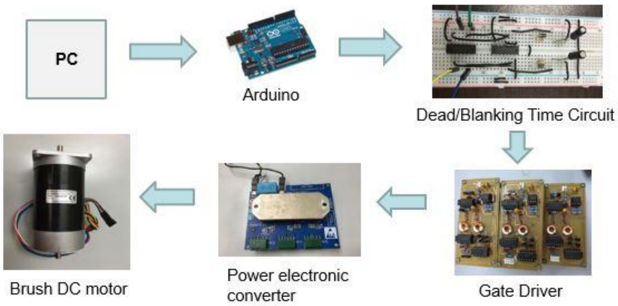

Fig. 6. Operation of Brush DC Motor

In the first place, the PWM signal will be generated by Arduino from the coding and the signal's duty cycle generated can be control by adjusting the potentiometer whether high percentage of duty cycle or low. The duty cycle will affect the value of voltage.

Then, the signal will enter the dead/blanking time circuit in order to generate dead time to avoid the simultaneous turn-on of two switches in the same bridge arm. The next stage is gate driver which is increase the voltage signal because the signal produce from Arduino is weak ad low. For example, the gate driver was tested by using the voltage 5V, the output of the gate driver was 15V. After that the signal will turn the 2 switches of the power electronic converter ON while another 2 is OFF to allow current flow only one direction of the motor.

IV. Results And Discussion

As a result of the project of implementation of the experimental for controlling the speed of the brush DC motor by Arduino as microcontroller, there are some results obtained. The first result is the PWM signal from Arduino that can be control its duty cycle by potentiometer.

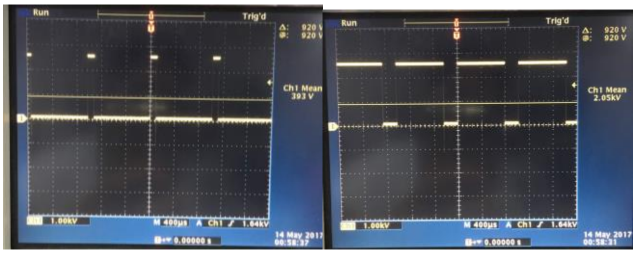

Fig.7. The PWM signal generated by Arduino microcontroller.

Figure 7 above shows the PWM signal generated by Aduino and the duty cycle can be control by using potentiometer whether from 0% to 100% which is from 0V to 5V voltage.

The next result is the dead/blanking time circuit implementation for the delay of the signal. The results of the signal is shown in Figure 8 below.

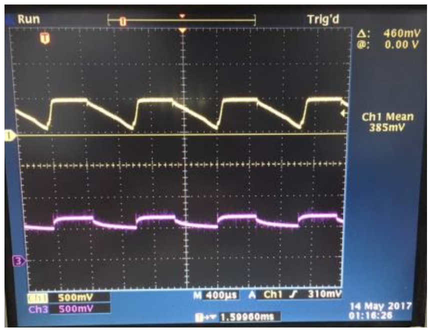

Fig. 8. The delay generated by Dead time circuit

The delay produce by the circuit is about 400 microseconds. Based on the results, it is not suitable for the signal to run the motor. Hence, the circuit need to be adjust and change the parameter to obtain the desire delay which is about 2 to 3 microseconds.

Besides, the voltage from Arduino have been tried directly to the gate driver to test the voltage. Figure 9 below shows the result of the voltage.

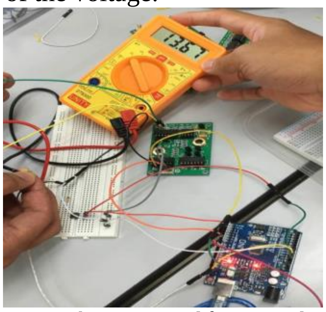

Fig. 10. Voltage acquired from gate driver

The voltage reading output from the gate driver obtained was 13.67V from 5V input direct from the Arduino. This shows an increase of voltage from the Arduino through the gate driver to drive the motor but there still need the delay for the signal to avoid the simultaneous turn-on of two switches in the same bridge arm.

V. Conclusion

All in all, from the beginning, this experimental kit will help students learn about the fundamentals of Brush Direct Current Motor including how it works, what are the specification of the motor, and how to control its speed. Other than that, this experimental kit also will help students to generate signal from Arduino UNO by coding. The next things to be learn is about the dead time generator. This dead/blanking time circuit is very important to generate delay signal to avoid the simultaneous turn-on of two switches in the same bridge arm, otherwise, the motor will not run. In this project, the delay from the dead time circuit was not achieved the desired value of 2-3 microseconds that stunted the motor from running. In order to achieve that, other circuit needs to be design and the parameter of RC circuit need to meet the specifications.

VI. References

[1] y. S. E. Ali, S. B. M. Noor, S. M. Uashi and M. K Hassan, “Microcontroller Performance for DC Motor Speed Control System” National Power and Energy Conference (PECon) 2003 Proceedings

[2] Norazuin Md Ayob, Modelling and Control of DC Motor, January 2013, pp. 2-3

[3] J T. Castabnet and J. Nicolai, "Digital Control for Brush DC Motor," IEEE Transaction Oil Industry Application", Vol, 30, No 4, July/August 1994.

[4] J Krishnan and Thadiappan, "Speed Control of DC Motor Using Thyristor 0",,1 Converter," IEEE Trans., Vol, T-IECI, pp, 391-399, Nov. 1976.

[5] A. II. M. S. Ula and J. W. Steadman, "Design and Demonstrate of a Microcontroller Control for an Industri.1 Sized DC Motor," IEEE Transaction of Energy Conversion, Vol. 3, No. I, March 1988

[6] J. Nicolai and T. Castagnel, "A Flexible Microcontroller Based Chopper Driving a Pcrmanent Magnet DC Motor," The Europeoll Po",er Elec/rallies Applicalioll. 1993.K. Elissa, “Title of paper if known,” unpublished.

[7] Moleykutty George. Speed Control of Separately Excited DC Motor, American Journal of Applied Sciences 5, 2008 Science Publications

[8] Anonymous , Speed and Direction Control of DC motor Using PIC Microcontroller Using PWM and H-Bridge. Available http://wineyard.in/wp-content/uploads/2011/12/WK605.pdf

Real-Time Water Quality Monitoring System Powered by Solar Energy

Abdul Zakir Ajasman
Faculty of Electrical Engineering
Universiti Teknologi Malaysia
Johor Bahru, Malaysia.
azakirjasman21@gmail.com

Hasimah Abdul Rahman
Centre of Electrical Energy System (CEES)
Faculty of Electrical Engineering
Universiti Teknologi Malaysia
Johor Bahru, Malaysia.
hasimah@fke.utm.my

***Abstract*—Water pollution nowadays have become common problems in our daily life. This is because water is one of the crucial things in our life. There are a lot of reasons why water are being polluted by humans although they need it. Water that are being polluted actually will affect a lot of things in the earth such as humans, animals, and plants. With the polluted water, many species of plants and animals will die because they cannot use the polluted water for their daily life cycle. For humans, polluted water cannot being used for drinks and daily life use because polluted water are dangerous that may cause illness to the humans. There are many ways for detecting water pollution for fast response in giving water treatment to the polluted area and to avoid the pollution spread in bigger area. In this project, three sensors are being used to determine the quality of water for fast response if water pollution occur. The data from these sensors are being transmitted to the user by using GSM module for faster response. These sensors and GSM module are controlled by Arduino microcontroller and powered by solar energy.**

I. INTRODUCTION

Nowadays, the occurrence of water pollution in the river and oceans are frequently happen. There are so many factors that lead to this problem. One of the factor is oil spills because oil is the crucial things in our daily life.

For the oil spills in the river, usually it is occur due to the industrial and commercial waste that flows into the river. This is because the lack of awareness for conserving the river from water pollution. Sometimes, it is also due to reducing their operation cost. Thus, without disposed the waste that contains oil into the right place, they just dump it into the river.

Next, for the oil spills in the oceans, it is usually occurred due to the spills of oil during the transportation and the spills of oil from the oil rig. For the transportation, the oil may spills into the oceans because of the collision between the oil tanker and the other ships or technical problems within the oil tanker. For the oil rig, the oil spills may be occurring due to natural disaster or technical problem.

Water pollution is defined as the water that contains excessive amounts of hazardous substance that causing the water not suitable anymore to be use for drinking, bathing, cooking or other uses [1].As we know, water that contains oil spills are categorized as polluted water. This is because this water is not safe anymore to be use in our daily life. Besides, it is also killing the habitat that lives within it. Normally, the water pollution not only detected by the presence of oil in the water but by detecting the hazardous substance in the water.

Thus, the oil spills detector has been developed for faster detecting the presence of the oil in the water. Usually, the oil spills in the river is caused by the waste from the industrial and commercial. They just dump the waste that contains oil into the river without give the treatment to the waste to be free from pollution. For the oil spills in the oceans, one of the main causes is the oil spills from oil tanker. With the needs of the oil, we need to transport it. One of the way to transport the oil is by using oil tanker. As we know oil tanker are carrying a lot of oil especially crude oil. This oil sometimes spills out from the oil tanker for some of reasons such as collision between two ships or maybe technical problem from the ship itself.

Next, the other causes to oil spills into the oceans come from the oil rig. As we know the oil rig use to dig into the oceans to find the crude oil. Sometimes, the crude oil from oil rig may spills into the oceans due to natural disaster or technical problem from the oil rig itself. The impacts of the oil spills into the oceans and the river are very bad. This is because it will cause water pollution that will affect the marine ecosystems. In general, the effects of the oil spills into the oceans and the river are including habitat degradation, smothering, fouling of gill structures, impaired reproduction, growth, development, feeding, immune response, respiration, and disturbance of the food web [2]. One of the examples for oil spills from oil rig is the Deepwater Horizon oil spills tragedy. This tragedy causes about 4.6 to 4.9 million barrels of oil entered the Gulf of Mexico. The tragedy affects the marine ecosystem including estuaries, beaches, barrier islands, tidal mud flats, and mangrove stands [2]. Therefore, these problems must be solved because it will affect the marine ecosystem in a long term that will lead to the extinction of the rare species in marine ecosystem.

One of the way to solve this problem is by using early oil spills detection sensor. This is because the early steps taken when oil spills occur is very important. The early steps taken when the oil spills occur will avoid the oil spills from spread to big area. Thus it will make the problems to be solved easier. Besides, with the little area only that involve during the oil spills, only small portion of the marine ecosystem will get involve too. When water pollution especially oil spills occur, the response need to be fast to avoid the oil spills from spread at larger area.

This is because when faster response, the area that need for treatment process is smaller thus reducing the cost and time used. There are several ways to detect water pollution and oil spills that are being used right now.

Firstly, the method that being used is Wireless Sensor for Continuous Real-Time Oil Spill Thickness and Location Measurement. This method use a devices that placed on board oil tankers and offshore drills. These devices will be thrown into the oil spills area and it will give the information about the oil spills [3].

Next, the method that are being used to detect oil spills is by using SAR Imagery and GIS. This method basically use satellite to detect the oil spills that occur. The oil spills are detected through the images of the dampening capillary waves on the ocean's surface that will be dark in contrast with background radar signal [4].

Then, mid-IR spectroscopy and supervised recognition techniques also being used for detecting water pollution and oil spills. This technique use infrared to detect the oil in the water through the wavelength [5]. The wavelength of the water that contains oil and does not contains oil is not same.

Basically, all of the techniques above have their own advantages and disadvantages. Thus, these disadvantages needs to be overcome by designing new technique in detecting water pollution and oil spills. This conducted study is for helping in solving the water pollution and oil spills problem that occur both in the sea and the river as the water pollution will affect the ecosystem of the aquatic and will lead to the extinction. By using this monitoring system, the water pollution will be detected earlier and can avoid it from spread at larger area. By earlier detection of water pollution, this water quality monitoring system will help the water treatment process become easier and cheaper. Furthermore, this system device is cheaper and simpler to be develop compared to the other methods of detecting water pollution and oil spills. Thus, this system device can be used widely.

II. LITERATURE REVIEW

A. Introduction

Water pollution is defined as the water that cannot be drink or use by human, animals and plants while oil spills is defined as the release of a liquid petroleum hydrocarbon into the water due to human activities or natural disasters [6]. In our daily life, there are so many water pollution and oil spills that occur in the oceans and the river.

B. Related Works on Water Pollution and Oil Spills Detection

There are so many techniques in detecting water pollution and oil spills in the water such as Wireless Sensor for continuous Real-Time Oil Spill, Oil Spills Emergency Response using SAR and GIS, Screening Oil Spills by Mid-IR Spectroscopy and Supervised Pattern Recognition Techniques, and Oil Spill Detection using Electrode Microfluidics System. These techniques are keep improving by using new technologies to give the better result in detecting water pollution. However, these techniques have their own limitations since there are so many obstacles when detecting water pollution and oil spills.

C. Real-Time Water Quality Monitoring System Powered by Solar Energy

Real-Time Water Quality Monitoring System Powered by Solar Energy basically consists of three sensors. These sensors are turbidity sensor, pH sensor and conductivity probe. All of these sensor are being used for monitoring the water quality. The data that are gained from these sensors then will be send to the responsible authorities/stakeholder by using GSM module. These sensors and GSM module are controlled by Arduino microcontroller and powered by battery that being charged by solar panel.

a) Turbidity Sensor

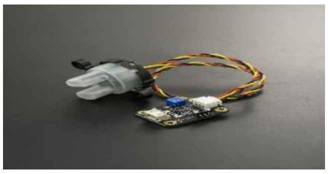

Fig. 1. Turbidity Sensor

Turbidity sensor use to measure the quality of water by measuring levels of turbidity. It uses light to detect suspended particles in water by measuring the light transmittance and scattering rate, which changes with the amount of total suspended solid (TSS) in water. TTS is directly proportional to liquid turbidity level.

b) pH Sensor

Fig. 2. pH Sensor Probe

pH sensor basically have three components, which are measuring electrode, reference electrode, and temperature sensor. The measuring electrode that is sensitive to hydrogen ion, develops a potential (voltage) directly related to hydrogen ion in the solution. The reference electrode provides a stable potential against measuring electrode thus comparison can be made.

c) Conductivity Probe

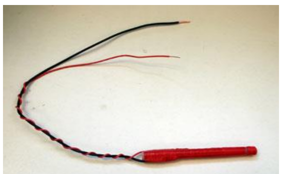

Fig. 3. Conductivity Probe

The conductivity probe use the resistance in the solution for measuring the conductivity. The solution will complete the circuit at the probe. If the resistivity of the solution is high, the output voltage is low. With this measurement, we can know what the content in the solution is because every solution have different conductivity.

d) GSM Module

Fig. 4. Sim900A GSM Module

For this project, Global System for Mobile Communication (GSM) act as a medium to transmit data. GSM have gone through many evolutions to become better with the improvement in performance and spectral efficiency. To fulfil the demand of higher data rates, many efforts have been made for the evolution of GSM [11]. GSM basically is the cheapest way in transmitting data with widely coverage. In this project, GSM will be used to send the data about the water quality thus help to track water pollution easier.

e) Arduino Microcontroller

Fig. 5. Arduino Uno Microcontroller

Arduino is the microcontroller that are able to read inputs and produce outputs. Basically, the Arduino microcontroller need to be programmed before can be used to read inputs and produce outputs. The programming is by using Arduino programming language and Arduino software (IDE) [12]. For this project, the Arduino will be microcontroller that receive signals from the sensors and then convert it into analog or digital signals before send the signals to the user through GSM module. The Arduino powered by the solar energy.

f) Solar Kit

Fig. 6. Solar Kit Set complete with Battery

Nowadays, solar energy have been used widely since it's provide daily free energy. Solar energy is the free energy that are affordable, inexhaustible, and clean [13]. For this project, solar energy being used to provide power to the sensors, GSM module, and Arduino microcontroller. This is because by using solar energy and rechargeable battery, all of the electronic devices used does not need frequent changing battery since the rechargeable battery will be charged by the solar panel.

III. RESEARCH METHODOLOGY

A. Flowchart for Research Process

Research flowchart is very important as it work as a reference for the flow of this project. It also work as a guidance for doing the work step.

Firstly, in doing this project, the research is on the current technique in detecting water pollution and oil spills. The current technique will show their own way in detecting the oil spills. After that, the research on the current technique also find the advantages and disadvantages of the current technique. This is for finding the best solution for detecting oil spills.

Next, the research proceed to the finding the suitable component and system for this project. In this part, the electronic component such as sensors, GSM module, Arduino microcontroller, and solar kit are chosen. These components are chosen to be work together. GSM module being chosen as a medium to transmit data because it is the cheapest way to transmit data and have widely coverage.

After that, the designing process is being done. In this process, the system are being design for being suitable with the scopes. The design also include the container that hold the electronic component.

When the design part have been done, the testing for this project being conducted. This testing process being done by putting the electronic parts container on the water. If the system of the electronic parts works, the research continue to the next part which is documentation. If the system does not works, it will goes to the troubleshooting process.

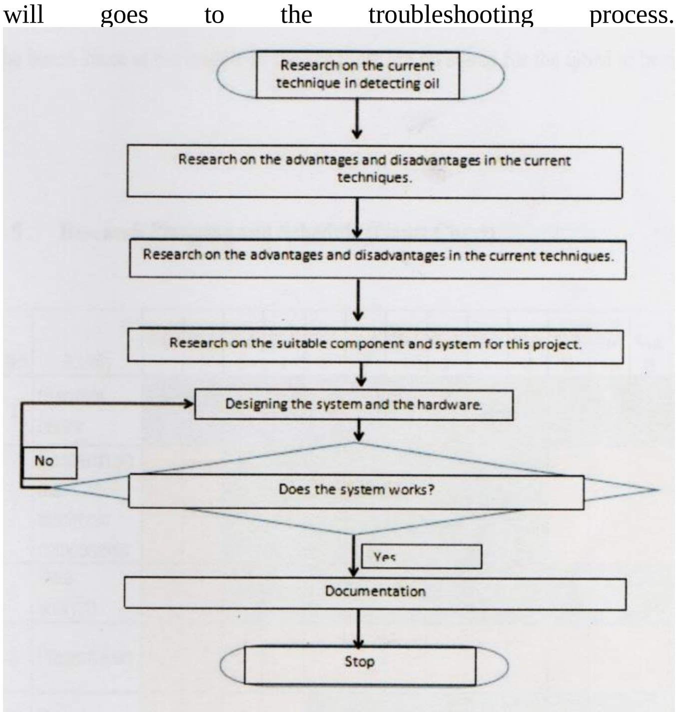

Fig. 7. Flowchart for the Research Process.

B. The Approach in The Research

The approach in this research is for better understanding in this project. Besides, it helps to identify the advantages and the disadvantages in this project through the experiments, qualitative research, and rational.

C. Assumptions and Limitations

The assumptions for this system is that it will works both in the oceans and in the river. It will helps to detect water pollution and oil spills for providing faster response in water treatment/cleaning process. For the limitations, the system have the limits in the distance from the beach or in the middle of the forest since at these place there are no signal for the GSM to be operate.

D. Summary

For this chapter, all research methodology are being discussed as it describe the steps that are being taken when developing this project. In this project, three sensors are being used to determine the quality of water whether it is polluted or not and these sensors are powered by solar energy.

IV. RESULT AND DISCUSSION

For this project, the results are shown as below.

Solution	Voltage(V)	Turbidity(%)	pH
Mineral water	4.1	9	7.0
Oil(lubricant oil)	2.8	53	-
River water	3.8	88	6.8

Fig. 8. Result of the experiments.

The experiments that have been done show the comparison between the solution. In this experiment, the mineral water and the river water are not polluted. This data were transmitted to the user through GSM module. This results shows every solution have different resistivity, turbidity, and pH value. This is because the content in the solution will determine all of these value. All of these value will be used to determine whether the water are being polluted or not by referring to base value.

V. CONCLUSION

As a conclusion, this Real-Time Water Quality Monitoring System Powered by Solar Energy being developed to improve the way on detecting water pollution and oil spills. Besides, this monitoring system also have less maintenance features that will be user friendly since it use solar energy as the power source. Lastly, this monitoring system will help to make faster response from responsible authorities/stakeholder when water pollution or oil spills occur thus avoiding the pollution from spread at larger area.

REFERENCES

[1] Owa, F.D Water Pollution ; Sources, Effects, Control and Management. Mediterranean Journal of Social Sciences, September 2013.

[2] Michele Blackburn, Celeste A.S. Mazzacano, Candace Fallon, Scott Hoffman Black. Oil in Our Oceans, A review of the Impact of Oil Spills on Marine Invertebrates, 2014.

[3] Hovig Denkilkian, Student Member, IEEE, Agop Koulakezian, Student Member, IEEE, Rostom Ohannessian, Student Member, IEEE, Milad S. Chalfoun, Mohamad Khaled W. Joujou, Ali Chehab, Senior Member, IEEE, and Imad H.Elhajj, Senior Member, IEEE. Wireless Sensor for Continuos Real-Time Oil Spill Thickness and Location Measurement. Instrumentation and Measurement, IEEE Transactions on, 2009. 58(12): p.4001-4011.

[4] H. Assilzadeh & Y. Gao, Oil Spills Emergency Response mapping for Coastal Area Using SAR Imagery and GIS in OCEANS. 2008.

[5] M.P. Gomez-Carracedo a, R. Fernández-Varela a, D. Ballabio b, J.M. Andrade a, Screening Oil Spills by mid-IR spectroscopy and supervised pattern recognition techniques. (Chemometrics and Intelligent Laboratory Systems). 2012.

[6] Pu Li, Qinhong Cai, Weiyun Lin, Bin Cheng*, Baiyu Zhang*. Offshore Oil Spill Response practices and emerging challenges. Marine Pollution Bulletin. 2016

[7] Jonny Beyer, Hilde C. Trannum, Torgeir Bakke, Peter V.Hodson, Tracy K.Collier. Environmental effects of the Deepwater Horizon oil spill: A review. Marine Pollution Bulletin. 2016

[8] Norfarahanim Binti Suhaimi. Oil Spill Detection Using Electrode Microfluidics System. (UTM).2014.

[9] https://www.nohken.com/overseas/product/other/impedance/lz.html [Access November 2016]

[10] Silviya Korpilo, Tamo Virtanen, Susanna Lehvävirta. Smartphone GPS tracking-Inexpensive and efficient data collection on recreational movement. (landscape and Urban Planning).2016.

[11] Wolfgang Gerstacker, Robert Schober, Raimund Meyer, et al,. GSM/EDGE: A mobile communications system determined to stay. (international Journals of Electronics and Communications (AEŰ).2011.

[12] Retrieve from https://www.arduino.cc/en/Guide/Introduction, [Access December 2016]

[13] Balasubramaniam Viswanathan, Chapter 7- Solar Energyy: Fundamentals. Energy Sources. Fundamentals of Chemical Conversion Process and Applications, 2017.p. 139-147.

Wind Charger for Rider

Akmal Nuriqram Bin Rosli
Faculty of Electrical Engineering
Universiti Teknologi Malaysia
Johor Bahru, Malaysia.
akmal.nuriqram@gmail.com

***Abstract*—The buck-boost converter is a power electronic circuit that have two mode, buck and boost which can step down and step up the input voltage based on desired output voltage. In this paper, the buck-boost converter use variable input voltage and current because the values depending fully on wind speed. The range for the input voltage is varies while the output is fix so, voltage sensor is needed to sense the input voltage and match it with the suitable duty cycle that had been calculated earlier. The buck-boost converter switching, duty cycle and frequency are fully control by the Arduino MEGA board. As for the load, mobile phone or power bank are the most suitable since the amount of voltage and current to charge them suit the system output voltage and current. At the end of this paper, the desired output power is not as expected due to losses at the load and also during the conversion of kinetic energy to electrical energy at the input source.**

Keywords— Buck-Boost Converter; Power Electronic; Voltage Sensor; Arduino MEGA Board; Kinetic Energy; Electrical Energy.

I. Introduction

Nowadays, electricity become one of the most important element needed by the people around the world since the technology develop drastically. Almost all appliances and equipments exist nowadays need electricity to be turned on because it can reduce man power and functioned automatically just by pressing some particular buttons. The electrical appliances and equipments can be powered up easily when there is dependent source of electricity which connected to the distribution part from the national grid but, it will be a big problem when there is no dependent source such as the outdoor environment.

The outdoor environment mentioned involving the forest, mountain, remote area and on road. All of these places need an independent source to supply electricity to the users since sometimes in urgent condition they need it. To create an independent source, energy from the nature can be used to generate the electricity and this energy known as renewable energy. Renewable energy is the source of energy that can get freely from the nature with unlimited usage. There are various type of renewable energy such as wind, water (hydro), biomass, photovoltaic (solar), geothermal and wave [1]. All of the energy can be harvested anytime and anywhere without the permission from the authority. This free-harvested energy usually use to supply electricity but need some mechanism to convert it and cannot be use directly.

This project consist of three objectives. The first objective is to recycle wind as source to generate electricity. The second objective is to study the conversion of kinetic energy to electrical energy by using DC motor as generator. Wind energy are move in mechanical principle which include the velocity and speed, a device is needed to undergo the conversion process. In order to find the most suitable device, the DC motor will be the one. The third objective is to implement power electronic technology in controlling the energy conversion process. Inconsistent nature of the output makes the current and voltage unpredictable and unstable. Power electronic technology has many circuit to control the behavior of the electrical parameter like voltage and current. However, the type of current use will determine which circuit can be use as the most suitable controller in this system.

This study covers the usage of renewable energy and how to use it as the source in generating electricity. Renewable energy like wind energy need to undergo energy conversion process which lead to the conversion of mechanical energy to electrical energy. The unstable output voltage and current at the generating need to be control by the power electronic circuit which can adjust the output voltage to be fix in value. All these three elements had been covered and discussed in this paper.

II. LITERATURE REVIEW

A. Wind Power System Operation

Wind energy usually implemented at the places that has the highest wind speed in the country. In Malaysia, Mersing and Kuala Terengganu are rank for the highest wind speed area because their geographical coordinate facing the South China Sea [2]. The high speed of wind flow through the propellers or fan to rotate the rotor of the turbine generator. The operation involves many aspects and principles related to the mechanical and electrical engineering study. The mechanical engineering apply the kinetic energy which is exist due to the rotation of the propellers by the wind flow [3]. The propeller then connected to the rotor of the turbine generator to induce the generation electricity. When the propeller and rotor are connected [4], the electrical engineering application will take place where the rotation of the turbine rotor produce electricity at the output of the generator.

There are two types of wind turbine that can possibly be use, horizontal axis type [5] and vertical axis type [6] as shown in Fig. 1 and Fig. 2 where the efficiency for each of them are different. The horizontal axis wind turbine are mostly in use for the wind turbine implementation around the world because of its efficiency to generate electricity are higher. Higher efficiency in generating electricity is because of the factor of larger surface area for the size of the propellers and larger size of propellers can trap more wind flow. However, this type also have major weakness where it is not suitable to be implemented for the small scale wind turbine. For the vertical axis wind turbine, the efficiency quite low compared to the horizontal axis type because the size of the propellers cannot be large in size. Although the size of propellers are small, the rotation of propellers are not too slow [3]. The vertical axis coordination limit the size of the propellers and this type of wind turbine is suitable for the small scale wind turbine.

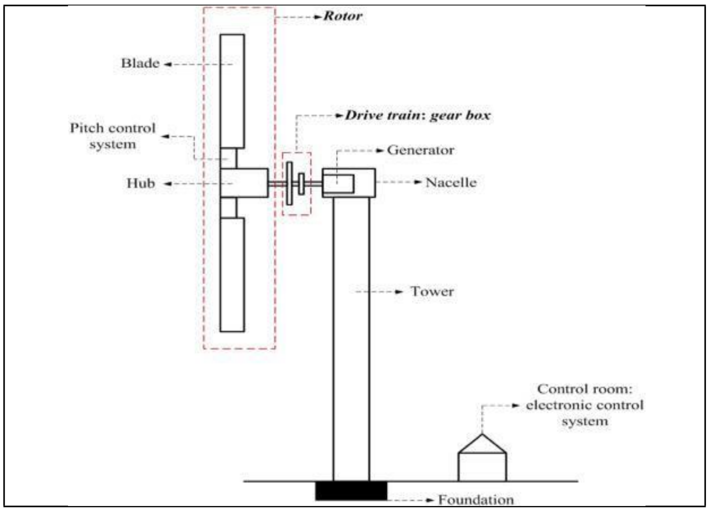

Fig. 1. Horizontal Axis Wind Turbine.

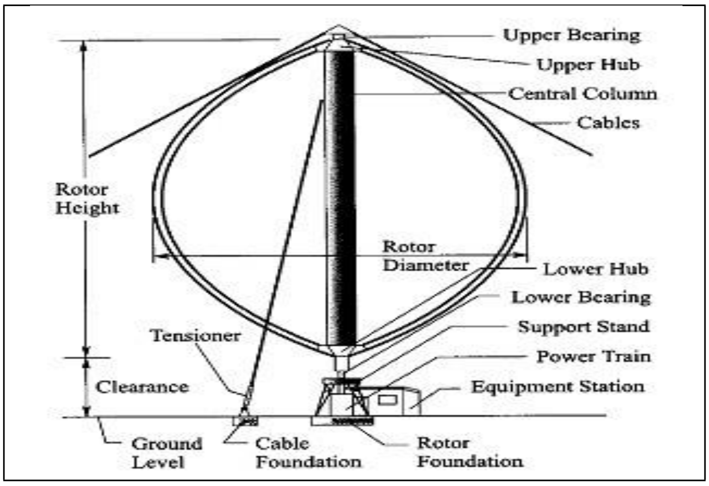

Fig. 2. Vertical Axis Wind Turbine.

B. DC Motor

Direct current (DC) permanent magnet (PM) motor is a device that use electromagnetic principle to produce mechanical rotation. The DC motor function can be reverse and change to DC generator. In this particular type of generator, the permanent magnet places horizontally inside the chassis and the magnetic fields are in horizontal position. The rotation of the rotor basically follows Faraday's Law of induction which states that the induced voltage in any closed circuit is equal to the time rate of the magnetic flux through the circuit [7]. Means that the cutting process of the magnetic field by the rotor winding at the rotor produce induce voltage at the output terminal.

C. Pulse Width Modulation Signal

Pulse Width Modulation (PWM) signal is a rectangular signal that use for controlling the switching for low frequency operation [8]. For a low frequency and small system, the PWM signal source usually get from the Arduino board and integrated circuit (IC) which have PWM output pin and specially design for switch controlling. The purpose of using PWM signal is because it easier to control the duty cycle since the wave are in rectangular waveform. Other advantages of using PWM signal are it can suppress chaos and subharmonic oscillation [9] or in the other word can reduce noise. Fig. 3 show how PWM signal control the duty cycle.

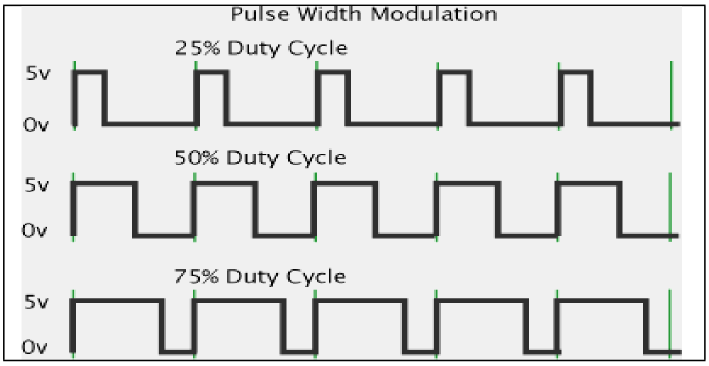

Fig. 3. Pulse Width Modulation Graph.

D. Buck-Boost Converter

Buck-Boost Converter is a combination of two DC-DC converter, Buck Converter and Boost Converter. A simple buck converter can only produce output voltages lower than the input voltage, and a boost converter, only output voltages higher than the input. To provide smaller and larger output voltages a circuit known as a buck-boost converter is required. The Buck-Boost Converter circuit is shown in Fig. 4.

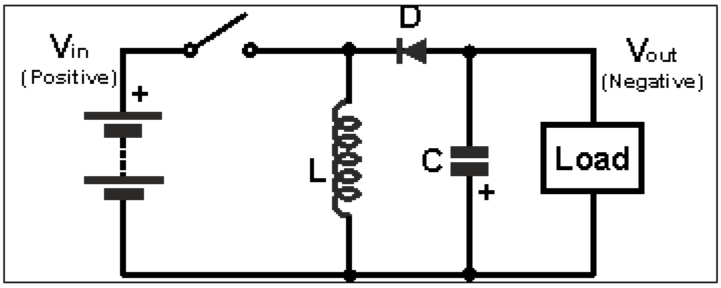

Fig. 4. Pulse Width Modulation Graph.

In producing lower and higher range of output voltage, frequency and duty ratio play an important part in controlling the switching process. As frequency and duty ratio increase, the switching mode will decrease Fig. 5. The duty ratio control depends on many factors and has different effects on each parameters. The parameter involves are output voltage, output current, minimum inductance and also minimum capacitance [10]. For the output voltage and output current, the relationship between them and duty ratio are linearly increase [10] as shown in Fig. 6 but different from minimum inductance and capacitance. The value of minimum inductance is inversely proportional to the duty ratio where the value of minimum inductance decrease as the duty ratio increase [10]. The next parameter is minimum value of capacitance. Minimum value of capacitance increase as the duty ratio increase [k] but the value is negative and both minimum inductance and capacitance are shown in Fig. 7. All the information and data were collected from the research and study about the duty ratio behavior. To get a fix output voltage, switching period and duty ratio play an important role in controlling the circuit operation. The ripple factor must be lower than 5% to achieve constant stability.

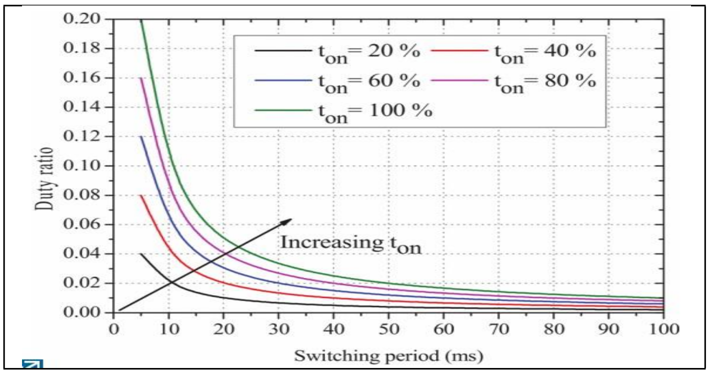

Fig. 5. Relationship Between Switching Period and Duty Ratio.

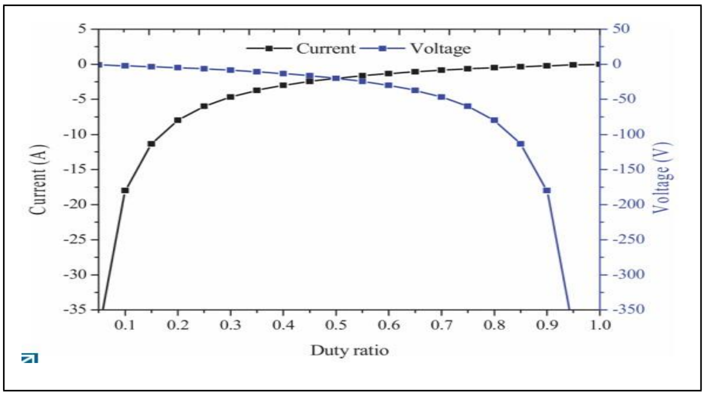

Fig. 6. Relationship Between Duty Ratio and Output Current/Output Voltage.

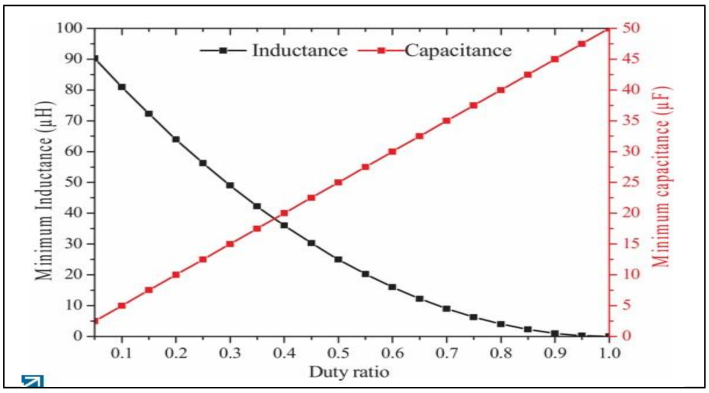

Fig. 7. Relationship Between Duty Ratio and Minimum Capacitance/ Minimum Inductance.

III. RESEARCH METHODOLOGY

In this paper, many thing were discussed regarding the design and research about the product that will be produce at the end of the study. To do research and designing work, a suitable work flow need to be plan so the progress will be smooth and align with the objectives. The work flow was planned at the beginning of the research since many information need to be gather and compile. By following the work flow, the work progress will be more organized and can avoid wasting time for something that not related to the research. In Fig. 8 show the work flow for the research progress.

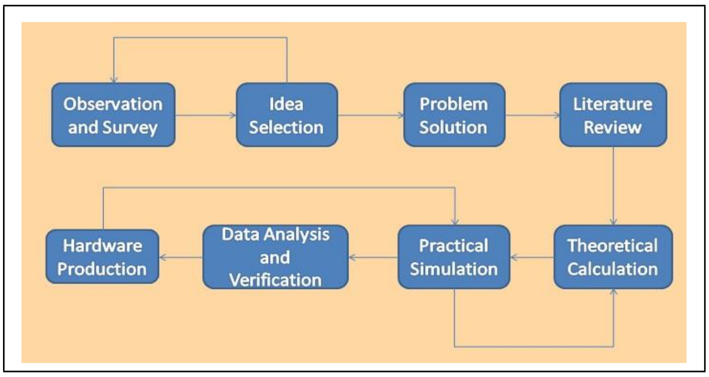

Fig. 8. Work Flow for Research Progress.

A. *Overall System Operation*

Basically, wind turbine generate electricity from the cutting process of the magnetic field by the rotor winding at the rotor and produce induce voltage at the output terminal. In this project, the turbine is replace with DC motor and the application is just the same. Wind energy are gathered from the movement of the motorcycle and rotate the propellers which directly connected to the DC motor shaft. The rotation produce induce voltage as the output for the DC motor. The output voltage from DC motor then transferred to the voltage sensor and buck-boost converter simultaneously as the voltage sensor connected to the Arduino MEGA board in order to control the switching and duty cycle. Duty cycle produced from the Arduino MEGA board are in Pulse Width Modulation (PWM) signal which can control the ratio from 20% to 90% depends on the input voltage from the DC motor. Through the buck-boost converter circuit, the output voltage is fix to 5V and connected to mobile phone or power bank. The overall system operation and system design are shown in Fig. 9 and Fig. 10.

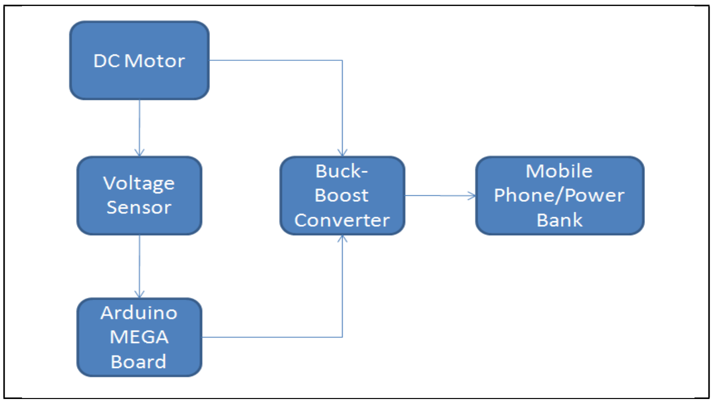

Fig. 9. Overall System Operation Flowchart.

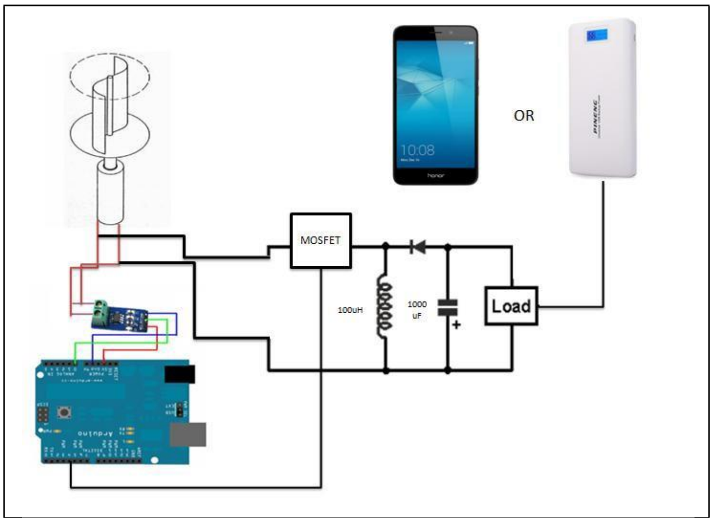

Fig. 10. System Design.

B. *Theoretical Calculation*

In this part, the parameters for the buck-boost converter were calculated by using the theoretical formula. The parameters that had been calculated are, duty ratio, input voltage, effective impedance, minimum inductance. All the calculation use the formulas as follows:

- Since the output voltage, V_o was fixed to 5V thus, the input voltage, V_d and duty ratio, D can be determine by using this formula:

$$V_o = -V_d \frac{D}{1-D} \quad (1)$$

- By assuming 5W load, the voltage and current are 5V and 1A thus, the effective impedance, R = 5Ω:

$$P = IV = I^2R = \frac{V^2}{R} \quad (2)$$

- The minimum inductance, Lmin is equal to 26.65µH and calculated by using the following formula:

$$L_{min} = \frac{(1-D)^2R}{2f} \quad (3)$$

- The capacitance calculated are 900µF and output voltage ripple, ΔV_o are assumed to be 0.005.

$$C = \frac{V_o D}{\Delta V_o f R} \quad (4)$$

C. *Practical Simulation*

The simulation was ran by using Simulink software and some theoretical parameters values were change in order to get the correct data for the analysis. The simulation figure are as shown in Fig. 11.

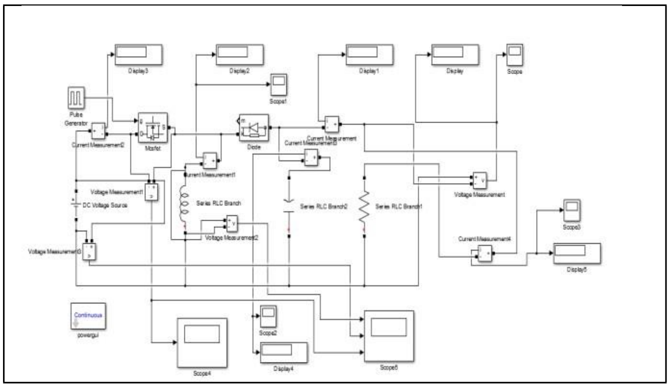

Fig. 11. Simulation Circuit.

Value for inductance were change from 22.65µH to 100µH because the amount of energy stored inside the inductor are insufficient and far from the targeted amount. The capacitance value were also changed from 900µF to 1000µF . By changing those values, the desired output voltage with a particular duty cycle can be achieve .

D. Pulse Width Modulation Signal Generation

Pulse Width modulation (PWM) signal play an important part in maintaining the output voltage for buck-boost converter. PWM signal basically control the switching of the MOSFET by using the Arduino MEGA board as the processor to set the duty cycle. On the Arduino MEGA board, there are 12 PWM signal output pin designed for many purpose depending on the users. Before setting the duty cycle, the frequency for the PWM signal generation need to be set and the desired value is 50kHz. As the frequency was set, about 20 duty cycle were assigned under one PWM signal output pin, pin 9 with range from 26% to 90% and inversely proportional to the input voltage from the DC motor. The value for the duty cycle with their particular input voltage will be shown in chapter IV.

IV. RESULTS AND DISCUSSION

In this chapter, the simulation and hardware results will be discussed further with different approaches.

A. Simulation Result

The output of this system is 5W with 5V voltage and 1A current values. The result shown below is sampled from one calculated duty cycle only which is 0.26. All the output voltage and current result are in positive because the polarity for the measurements are reverse from the actual circuit.

In controlling buck-boost converter, the inductor current is very important in order to make sure the system operate in continuous current mode. To reach continuous current mode, the inductor current value must not drop below zero and stable. Fig. 12 show the continuous current mode range from 0.82A to 1.59A.

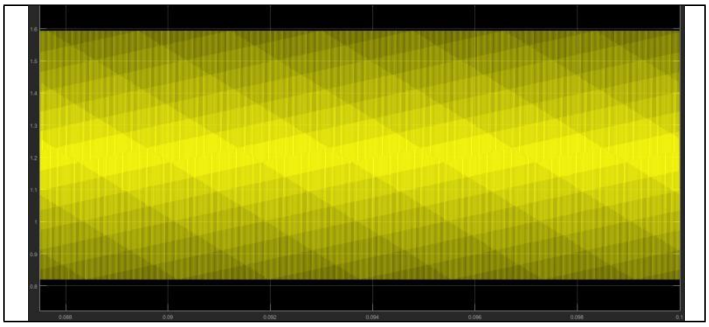

Fig. 12. Inductor Current.

From the previous chapter, the input voltage for this system is varies from 0V to 15V respectively depending on the wind speed. The desired values for inductance and capacitance are 100µH and 1000µF. The chosen values are different from the calculation due to unsufficient energy stored and availibility in market. Time setting to run the simulation is set at 100ms. Output voltage in this project is set in between range of 4V to 5V. Fig. 13 and Fig. 14 below shows the waveform of output voltage and output voltage ripple.

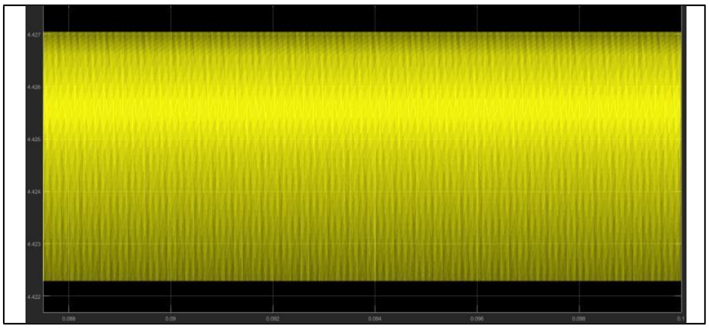

Fig. 13. Output Voltage.

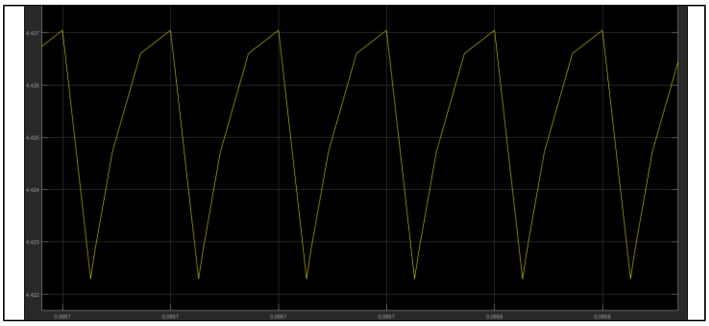

Fig. 14. Output Voltage Ripple.

From Fig. 13, the output voltage is 4.427V and for Fig. 14, the output voltage ripple recorded is 5mV.

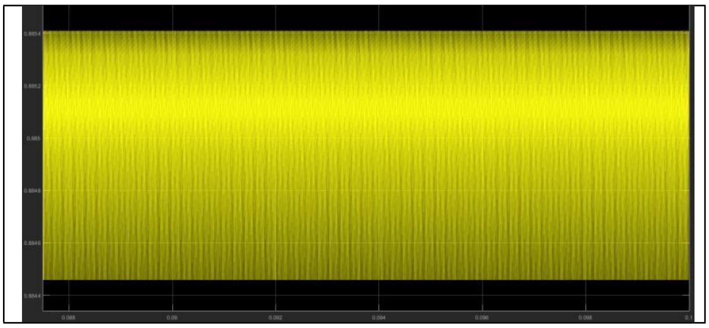

Fig. 15. Output Current.

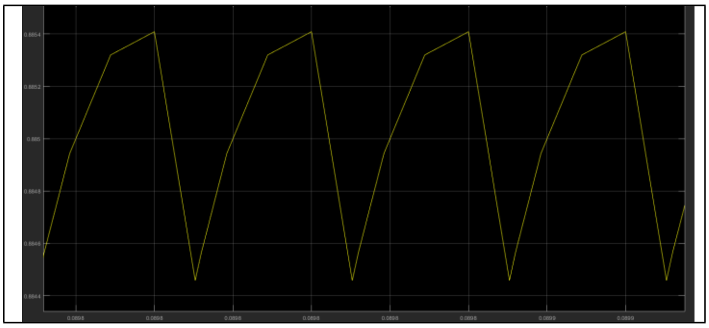

Fig. 16. Output Current Ripple.

For output current waveform in Fig. 15 and Fig. 16, the value of the current is 0.885A and current ripple about 1mA. The total output power for this simulation is 4W.

B. *Hardware Result*

Since the hardware were tested on road thus the waveform of the output voltage cannot be shown in the paper. The result were tabulated and as shown in TABLE 1 below.

TABLE I. HARDWARE RESULT

Speed (km/h)	Duty Cycle (%)	Input Voltage (V)	Output Voltage (V)
20	75	2.0	5.06
40	60	3.5	4.82
60	45	6.6	4.95
80	33	11.4	5.11
100	26	14.6	4.43

As in the table, the speed of wind is directly proportional to the input voltage and inversely proportional to the duty cycle. The current value practically is about 0.5A to 0.8A respectively, so the average output power for the hardware is around 2.5W to 4W.

C. *Discussion*

The power obtained are not reach 5W due to losses in energy conversion, kinetic energy to electrical energy. In order to improve the output power, the system need Proportional Differential (PD) controller to send feedback to control the switching if the output voltage not reach 5V. PD controller cannot be implement in this system because the switching is already connected to the Pulse Width Modulation (PWM) signal and if combine both, the switching period will be overlap. For mobile phone with battery capacity of 3100mAh, the time taken to fully charge is around 3 to 4 hour depend on the current value.

V. CONCLUSION

In this project, the frequency generated by Arduino MEGA board are fixed to 50kHz and using Pulse Width Modulation (PWM) switching to control the circuit switching. The buck-boost converter managed to operate well and produce suitable output voltage and current. The output power is lower than expected because the voltage drop at the load and also energy loss during the conversion of kinetic energy from the propellers to electrical energy.

REFERENCES

[1] Alexandros Gasparatos, Christopher N.H. Doll, Miguel Esteban, Abubakari Ahmed, Tabitha A. Olang, Renewable and Sustainable Energy Reviews, vol. 70, pp. 161–184, April 2017.

[2] Lip-Wah Ho, Renewable and Sustainable Energy Reviews, vol 53, pp. 279–295, January 2016.

[3] Ghulam Ahmad, Uzma Amin, Renewable Energy, vol. 101, pp. 286–292, February 2017.

[4] Changduk Kong, et al., “Structural Design of Medium Scale Composite Wind Turbine Blade”, 13th International Conference on Composite Materials (ICCM-13), Beijing, China, pp.561, 3–8, July 2001.

[5] Chi-Jeng Bai, Wei-Cheng Wang, Renewable and Sustainable Energy Reviews, vol. 63, pp. 506-519, September 2016.

[6] Wei-Hsin Chen, Ching-Ying Chen, Chun-Yen Huang, Chii-Jong Hwang, Applied Energy, vol. 185, Part 1, pp. 223-232, 1 January 2017.

[7] J.R. Bumby, R. Martin, Axial-flux permanent-magnet air-cored generator for small-scale wind turbine, IEE Proc. Electr. Power Appl., 152, issue. 5, pp. 1065–1075, Sept 2005.

[8] Weibo Li, Yoshitaka Niimi, Yuichiro Orino, Shinnosuke Hirata, Minoru Kuribayashi Kurosawa, IEEE Transactions on Circuits and Systems II: Express Briefs, vol. 61, issue. 4, April 2014.

[9] Jose D. Morcillo, Daniel Burbano & Fabiola Angulo, IEEE Transactions on Power Electronics, vol. 31, issue. 7, July 2016.

[10] Barnam Jyoti Saharia & Bani Kanta Talukdar, Energy, Power and Environment: Towards Sustainable Growth (ICEPE), 2015 International Conference, IEEE Xplore, July 2016.

Power Light Emitting Diode Dimmer using Buck Converter

Zakiah Anim bt Zainal Abidin
Faculty of Electrical Engineering
Universiti Teknologi Malaysia
Johor Bahru, Malaysia.
zakiahanim88@gmali.com

***Abstract*— High power LED dimmer using Buck converter is an LED driver which the brightness of LED can be controlled. The Buck converter is a DC-DC converter that used to step down voltage (while stepping current) from its input (supply) to its output (load). The voltage output can be change by varying the duty cycle. The method use to varying the duty cycle is using Arduino UNO which then produced square wave with 31.2 kHz switching frequency and 5V peak voltage. The output square wave then connected to a gate driver which used 12V power supply to step up the switching square wave to 10V. LEDs are arranged in two in series. Then the result obtain from practical will be compared with theory and discussion and recommendations are made based on the result obtained.**

Keywords—buck converter; high switching frequency; PWM controller with Arduino UNO.

I. INTRODUCTION

About 20% usages of electricity in the world is consumed for lighting applications, therefore there is high demand for efficiency of lamps [1]. The Annual Energy Outlook reports that the demand for electricity generated is used for illumination, and this pattern is repeated worldwide [6], [7]. The high power light emitting diode (HP LED) have become the competitor to replace conventional lights in various applications, such as automotives light, office lighting, traffic light, home lights as they use less energy consumption better than fluorescents and incandescent lamps. The smallest power consumption of HP LED is 1-3 W rated devices usually run at 350mA which have luminous flux of 115 lm which takes for incandescent lamp to operate more than 10W to have same luminous flux.

Several factors that contribute the use of HP LED nowadays in lighting and their wide ranging advantages over conventional light sources. These benefits including : (i) lifetime, (ii) high brightness, (iii) low power consumption, (iv) small size, (v) fast response (iv), and high reliability [2], [3], [4]. Besides these advantages, LED light is also visible even under the sunlight [5].

Mainly LED drivers usually have a rectifier to convert incoming AC power to DC power and continue to step down or step up the voltage specified to voltage rating and current of the LED. Nevertheless, this project was much more focus on how to control brightness of HP LED by varying duty cycle of Pulse Width Modulation (PWM) generate by Arduino UNO.

However, the frequency of the PWM signal on most pins of Arduino is approximately 490 Hz. On the Arduino Uno and similar boards, pins 5 and 6 have a frequency of approximately 980 Hz [9]. Thus the frequency of PWM need to be change to at least 30kHz to achieved high switching of the MOSFET.

There are many various methods that can be use as LED driver, one of it is Buck Converter. A buck converter-type switched mode power supply technology is a specific type of DC-DC power electronic converter which its goal to efficiently step down the DC voltage to a lower level [1].

II. LITERATURE REVIEW

LED is current controlled devices meaning that the intensity of the light is depends current passing through them. The current through LED should never exceed the device's nominal rating [10]. LED is better in efficacy. It is estimated that by 2020, the simple replacement of conventional light sources by LEDs will provide a decrease of 50% of the total amount spent on electricity for lighting, and a decrease of 11% of the total electricity consumption [6], [3]. In the US, it is estimated that if LED lighting technology fulfills its promises of efficiency, service life, and price, the illumination by LED lights would generate savings in electricity consumption of 46% by 2030 [8].

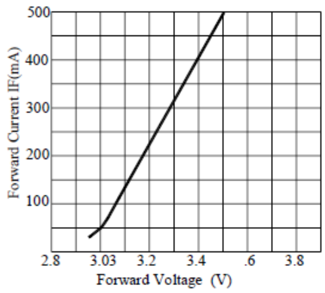

Fig. 1. IV characteristics of the HP LED

Based on IV characteristics shown above, it is crystal clear that any further increase of voltage after reaching threshold voltage of LED, will lead to increase of DC forward current [1]. Since LED's are very fast devices, if there is any variations in forward voltage, even for very short time, it will cause big variation in current which may damage the LED [1].

Nevertheless, without a proper LED driver circuit, LED may become too hot and unstable, leads to poor performance or failure of LED lights. Therefore, the development of correct power supply to power up the HP LED is mandatory.

A. *Buck Converter*

Buck converter is a specific type of DC-DC power electronic converter which the goal is to step down input voltage to a lower level with minimal ripple. In the Buck converter, a power Metal Oxide Field Effect Transistor (MOSFET) is usually used to switch the supply ON and OFF. In the Buck converter circuit, the inductor is use to store energy when the MOSFET is turn ON, then this energy will be use to provide current for the load when MOSFET is turn OFF. A diode is use to provide return path of current from the load during MOSFET is turn OFF [1]. The circuit of Buck converter is shown in Figure 2 below.

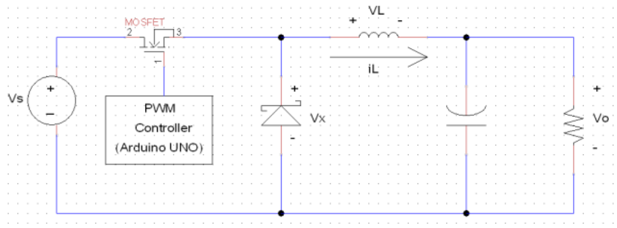

Fig. 2. Buck converter circuit

The voltage across the conductor is

$$V_L = V_s - V_o = L\frac{di_L}{dt}$$

Rearranging,

$$\frac{di_L}{dt} = \frac{V_s - V_o}{L}$$

Since the derivative of the current is a positive constant, the current increases linearly. The change in current while the switch is closed is computed by modifying the preceding equation.

$$(\Delta i_L)_{closed} = \frac{(V_S - V_O)}{L}DT$$

When the switch is open, the diode becomes forward biased to carry the inductor current and the equivalent circuit of Figure 3 applies.

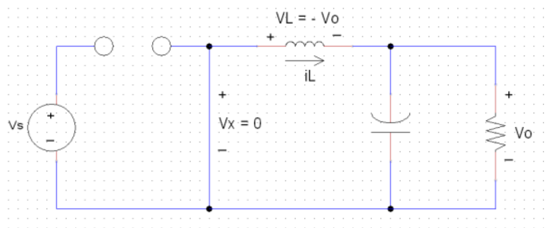

Fig. 3. Buck converter circuit equivalent circuit when switch is open

The voltage across the inductor when the switch is open is

$$V_L = -V_o = L\frac{di_L}{dt}$$

Rearranging,

$$\frac{di_L}{dt} = \frac{-V_o}{L}$$

The derivative of current in the inductor is a negative constant, and the current decreases linearly. The change in inductor current when the switch is open is

$$(\Delta i_L)_{open} = -\frac{-V_O}{L}(1-D)T$$

Steady-state operation requires the inductor current at the end of the switching cycle is same as the beginning, then the sum of inductor current over one period is zero. This requires

$$(\Delta i_L)_{close} + (\Delta i_L)_{open} = 0$$

$$\frac{(V_S - V_O)}{L}DT - \frac{V_O}{L}(1-D)T = 0$$

Solving for V_o

$$V_o = V_s D$$

Maximum inductor current,

$$i_{Lmax} = V_O\left[\frac{1}{R_L} + \frac{(1-D)}{2Lf_S}\right]$$

Minimum inductor current,

$$i_{Lmax} = V_O\left[\frac{1}{R_L} - \frac{(1-D)}{2Lf_S}\right]$$

Minimum value of inductor,

$$L_{min} = \frac{(1-D)R}{2f}$$

The output voltage depends only on the input and the duty ratio, D. If the input voltage fluctuates, the output voltage can be regulated by adjusting the duty ratio appropriately.

B. *Switching Frequency*

In power electronics, there are several types of switches that can be use such as diodes, thyristors, and transistors, All these switches are different in terms of size of current and voltage that they can withstand, controllability, switching speed and its power losses.

As we can see in Buck converter schematic circuit in Figure 2 MOSFET from transistor family is used as a switch. MOSFET is chosen as a switch because it is better at switching speed and lower switching losses compare to Bipolar Junction Transistor (BJT). MOSFET works by voltage compare to BJT which works by current. Which means, when voltage is apply between Gate and Source (V_{GS}), current is allowed to flow from Drain to Source (I_{DS}). MOSFET is kind like variable resistance control by voltage. Which mean depending on V_{GS}, the resistance between the Drain and Source (R_{DS}) will vary. When low voltage is apply at the Gate, the R_{DS} will be very high like an open switch. As we increase the V_{GS}, pass the threshold voltage ($V_{GS(th)}$)the R_{DS} will drop (R_{DS}=0) very quickly, and it is kind like a closed switch. All these values can be obtain from the datasheet of the MOSFET (IRF540).

The gate of the MOSFET is usually control by Pulse Width Modulation (PWM). The PWM signal can be generated by using IC microcontroller or Arduino. Then, the PWM generator, Arduino UNO, must be isolated from the MOSFET. In this project, Optocoupler MOSFET gate driver is used for isolation of the PWM generator, so that MOSFET switches can be prevented from damage [1].

III. METHODOLOGY

A. Buck Converter Parameters

Before the calculation were made, we have to studied the important parameters of High Power Light Emitting Diode (HP LED) from the datasheet. This is important because everything that we have designed was respected to output needs. The model of HP LED that will be use is 703-0148 Power LED and the number of LED will be use is four. These LEDs will be arranged in two parallel paths. In each path, two HP LED are arranged in series. The configuration is shown in Figure 3.1.1(a). A current limiting resistor is put to ensure that the current in each parallel path is equal. The current limiting resistor can also help avoid over-current at those LEDs.

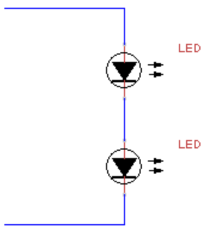

Fig. 4. HP LED arrangement

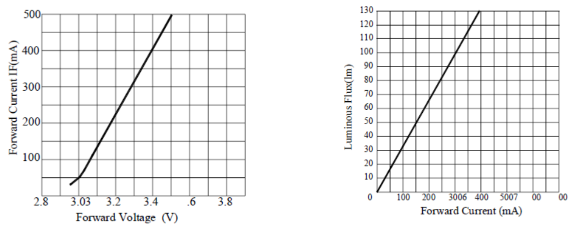

Forward Current VS. Applied Voltage   Forward Current VS. Luminous Flux

Fig. 5. HP LED model 703-0148 characteristics

TABLE I HP Led parameters collected from datasheet

Parameter	Value
DC Forward Current	350mA
Reverse Voltage	5V
Forward Voltage	3.2V
Thermal Resistance	15 ºC/W

Parameter	Value
Color	White

TABLE II Buck Converter Parameter

Symbol	Parameter	Value
f	Switching frequency	31kHz
V_S	Input voltage	12V
V_O	Output voltage	6.4
i_o	Output current	700mA
Δi_L	Inductor ripple current	0.232A
L	Inductor	500uH
C	Capacitor	40uF

B. MOSFET Rating

They are many types of MOSFET in the market which categorized as Enhancement Mode and Depletion Mode MOSFET. The MOSFET use is IRF540 which have parasitic body diode across it. The most important parameters that needed to know $V_{GS(th)}$ and $R_{DS(on)}$ from there we can determine power dissipation of the MOSFET.

TABLE III MOSFET ratings

Parameter	Value
$V_{GS(th)}$	10V
$R_{DS(on)}$	0.077Ω

C. Pulse Width Modulation

The method approached to produce the PWM in this project is by using Arduino UNO. However, the default frequency for the Arduino pin number 9 and 10 is 490 Hz. However, the PWM needed in switching technique must be higher than 20kHz, so the frequency chosen was 31kHz. Several modifications need to be adjust on the original coding of mine. The modification was done on Timer 1 base on setting shown below:

```
Setting     Divisor     Frequency
0x01        1           31372.55
0x02        8           3921.16
0x03        64          490.20    <--DEFAULT
0x04        256         122.55
0x05        1024        30.64

TCCR1B = (TCCR1B & 0b11111000) | <setting>;
```

Fig. 6. Timer 1 in phase-correct PWM mode setting

The duty cycle is varies by using a potentiometer that connected to the input of Arduino Uno. The potentiometer used has value 1kΩ and connected to 5V DC supply from pin Arduino Uno. The Arduino will read the analog reading from pin A0 which read the voltage drop across the potentiometer. Therefore, as potentiometer varies, the voltage drop across the potentiometer will be varies as well. From there, certain coding and calculation has been made to produce the PWM signal for each duty cycle needed in the buck converter (40%, 60% and 80%). The part of coding is as shown below:

```
if (voltage==2){
  analogWrite(led,pwm);
  pwm = 102;//for duty ratio 40%
  Serial.println("duty ratio = 40%");
}
```

Fig. 7. Coding for produce 40% duty cycle from voltage drop of 2V across potentiometer at the input of the Arduino Uno.

The coding shown above are repeated for 60% and 80% duty cycle with different value of SerialValue. The value of SerialValue or "pwm" is being calculated by using the formula shown below:

$$Duty\ cycle\ \times 255 = SerialValue$$

D. Gate Driver circuit

The most important part in order to make sure the MOSFET can switch in higher switching frequency is the voltage amplitude of PWM supplied to gate of MOSFET is higher or equal to $V_{GS(th)}$ which in IRF540 the value is 10V. In order to step up 5V amplitude of PWM signal from Arduino, we need a gate driver circuit. The circuit is obtained and modified based on the recommended circuit provided in the datasheet of HCPL-3180.

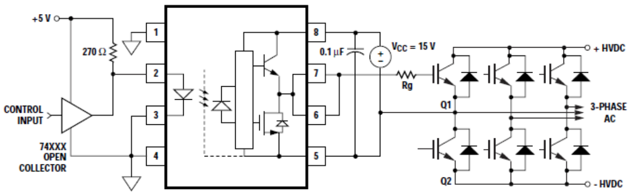

Fig. 8. Recommended LED drive and application circuit for HCPL-3180 from the datasheet

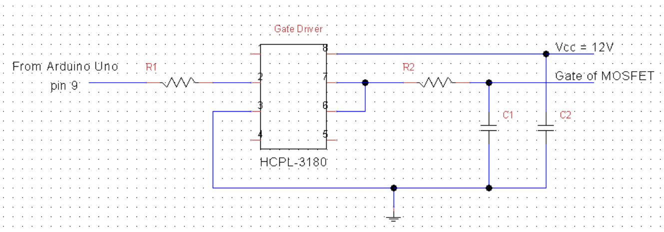

Fig. 9. HCPL-3180 Optocoupler circuit design

The value of R1 at pin number 1 of HCPL 3180 is to limit the current from the Arduino Uno output pin. The current needed to turn on the LED inside the optocoupler is 10mA(min) and 16mA(max) from the datasheet, therefore we can determine value of R1 needed as follows:

$$R1_{(min)} = \frac{V}{I} = \frac{5V}{10mA} = 500\Omega$$

$$R1_{(max)} = \frac{V}{I} = \frac{5V}{16mA} = 312.5\Omega$$

$$R1_{avg} = \frac{500 + 312.5}{2} = 406.25\ \approx 500\Omega$$

Then value of R2 is connected to pin number 6 an pin 7 where to minimize the IGBT switching losses as discussed in the datasheet. To calculate R2, using the given equation and parameter in the datasheet, with external DC source 12V, the gate resistor R2 can be calculated as follows:

$$R_g \geq \frac{V_{CC} - V_{OL}}{I_{OLpeak}} = \frac{15 - 3}{2} = 8.5 \approx 20\Omega$$

As for C1, it is use to decouples any high frequency signal and C2 is act as a bypass capacitor. The value for C1 is 1nF and C2 is 0.1uF.

IV. Result and Discussion

The buck converter is simulated using Proteus Professional ver. 8. The inductor current, output current and output voltage is observed. The frequency response for power stage switching switch around 31kHz are obtained by using Arduino UNO is also simulated by the software. The simulation was done by using the following parameters (parameters which are similar to hardware component except for 1N5711W).

- 12V Power Supply
- High switching MOSFET, IRF540
- Schottky diode, 1N5711W
- Torroidal inductor, 500uH (3A)
- Capacitor, 40uF
- LED, $I_F = 350mA\ and\ V_F = 3.2V$

A. PWM test

The PWM signal obtained from Arduino UNO with modification of build-in Timer in Arduino has been done in simulation and as well as hardware implementation. The result of the PWM signal obtained as follows:

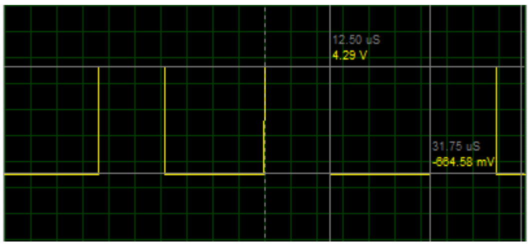

Fig. 10. PWM signal by using Proteus at 40% duty cycle

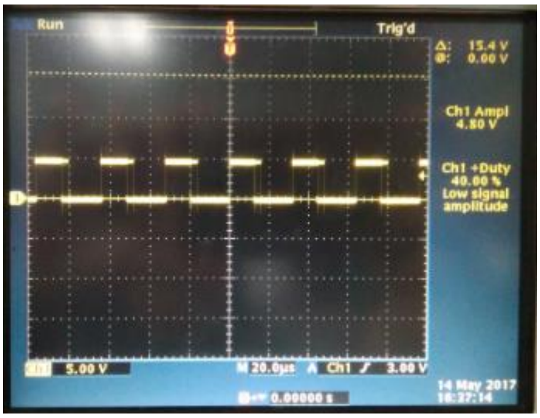

Fig. 11. PWM from Arduino Uno to oscilloscope at 40% duty cycle

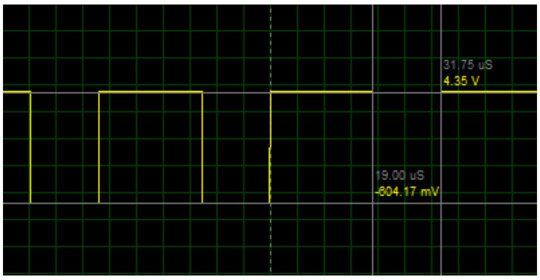

Fig. 12. PWM signal by using Proteus at 60% duty cycle

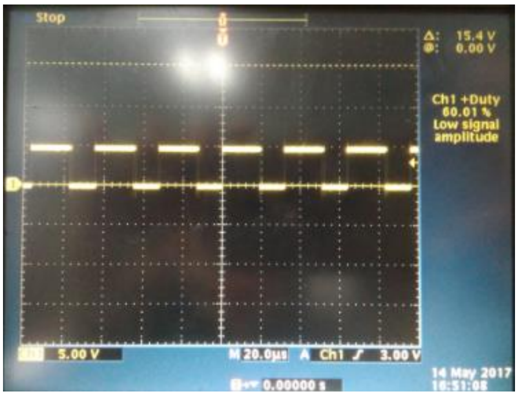

Fig. 13. PWM from Arduino Uno to oscilloscope at 60% duty cycle

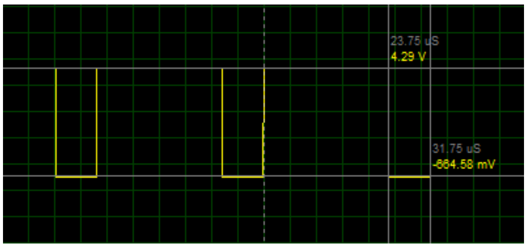

Fig. 14. PWM signal by using Proteus at 80% duty cycle

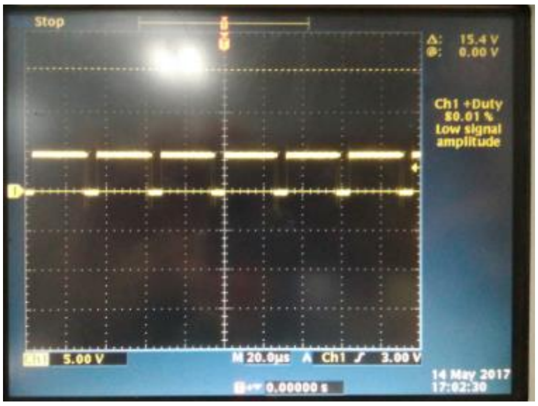

Fig. 15. PWM from Arduino Uno to oscilloscope at 80% duty cycle

B. Gate Driver circuit output

The most important part to drive MOSFET is the gate driver circuit. Gate driver is use to interface between the PMW sginal from Arduino Uno which have low voltage (5V) with gate of the MOSFET. However, the $V_{GS(th)}$ in order for IRF540 MOSFET to operate is minimum 10V, the PWM signal from Arduino may not enough to make the MOSFET operate. Therefore, the gate driver (HCPL-3180) is needed to step up the voltage to 10V. The gate driver circuit has been arranged according to the recommended circuit provided in the datasheet. However, the circuit is not being simulated, instead it has been implemented to hardware to the designed circuit as mentioned in methodology. The waveform of signal from the gate driver is as shown below:

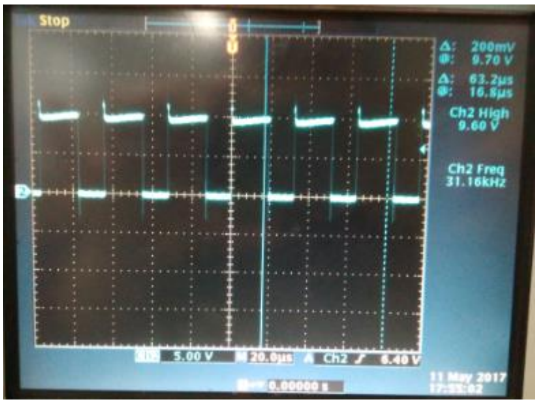

Fig. 16. Waveform from output HCPL-3180 at 60% duty cycle

C. Buck converter output

Buck converter for this circuit is designed to step down voltage of 12V DC power supply to 6.4V (max) for the LED. The output current and output voltage is varied by varying the duty cycle (40%, 60% and 80%) from Arduino Uno. Table below shows the comparison of output voltage between theoretical and practical. The waveform shown below is only for output voltage, the waveform V_L *and* I_L will be shown in the full thesis.

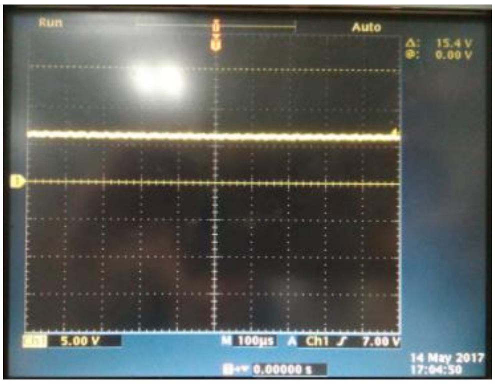

Fig. 17. Output voltage for duty cycle 80%

TABLE IV Comparison between output voltage in theoretically, simulation and practical and brightness of the LED.

	Fixed input voltage with 12V and varies duty cycle		**Brightness**
Duty cycle	**Vo (Theoretical)**	**Vo(Practical)**	
40%	4.8V	5.64V	
60%	7.2V	6.40V	
80%	9.6V	7.00V	

From the tabulated data shown, the result from theoretical and hardware is slightly different. The difference is due to the result of a worn component has a value of its own range of safety components.

V. CONCLUSION

In conclusion, the objectives of the project are completely achieved. From the result obtained it can prove that the buck converter can be operated following the existing theory. The outputs were successfully performed well with high power LED brightness control using Arduino Uno to control duty cyle.

There are a few recommendation in the future to improve the project, one of it is to use high switching frequency compare to 31kHz by using SG3525A PWM modulator as it can achieve higher frequency compared to Arduino Uno as the higher the switching frequency the more stable the output. Besides that use exact value capacitor to the required value instead of combining 3 different types of capacitor in parallel in order to obtain smooth output voltage and output current.

REFERENCES

[1] 1. Amruta Thomas and Aju S Nair, Driver Design and Simulation for 6W LED Bulb with PWM Dimming, 2015.

[2] 2. Y. Uchida and T. Taguchi, Lighting Theory and Luminuous Characteristics of White Light Emitting Diode,Optical Engineering, v.44, p. 124003, SPIE, 2005.

[3] 3. R. Lenk and C. Lenk, Practical Lighting Design with LEDs, Wiley-IEEE Press, New Jersey, 2011.

[4] 4. X. Luo, H. Liu, Z. Lu and Y. Wang, Automated Optimization of an Aspheric Light Emitting Diode Lens for Uniform Illumination, Applied Optics, v. 50, n. 20, pp. 142, 1997.

[5] 5. D.L. Evans, High Luminance LEDs Replacement Incandescent Lamps in New Applications, in Proceeding of Society of Photo-Optical Instrumentation Engineers, v. 3002, pp. 142, 1997.

[6] 6. E.D. Jones, Light Emitting Diodes (LEDs) for General Illumination, OIDA – Optoelectronics Industry Development Association, 2001.

[7] 7. U.S. Department of Energy, Adoption of Light Emitting Diodes in Common Lighting Applications: Snapshot of 2013 Trends, Office of Energy Efficiency and Renewable Energy, Building Technologies Program, 2013.

[8] 8. U.S Department of Energy, Solid State Lighting Research and Development : Multi-Year Program Plan, 2012.

[9] 9. Adjusting PWM Frequencies : http://playground.arduino.cc/Main/TimerPWMCheatsheet

[10] 10. N. Badalan, P. Svasta and F. Draghici, Constant Current versus Pulse Current for Power Supplies on High Power LED, 2015 IEEE 21st International Symposium for Design and Technology in Electronic Packaging (SIITME), Brasov, 2015, pp. 263-266.

[11] 11. Hart W. Daniel, Power Electronics, 2011 : McGraw Hill

[12] 12. Comparison Chart, LED Lights vs. Incandescent Light Bulbs vs. CFLs : http://www.designrecycleinc.com/led%20comp%20chart.html

[13] 13. IRF540, Power MOSFET, Vishay Siliconix, 2011

[14] 14. 1N5817, Schottky Barrier Plastic Rectifier, Vishay Siliconix, 2013.

[15] 15. HCPL-3180, A. Tecnologies, Editor, 2009.

[16] 16. Basic Calculation of a Buck Converter's Power Stage, Application Report, Texas Instruments, 2011.

[17] 17. 703-0148 High Power LED, Multicomp, 2012.

[18] 18. Travis Meade, Pulse Width Modulation Using an Arduino, 2014.

[19] 19. Gerald Recktenwald, Basic Pulse Width Modulation, EAS 199, 2011.

Autonomous Solar Powered Movable Aerator by Air Bubble Technique

Luqman Hakim Bin Noresham
Faculty of Electrical Engineering
Universiti Teknologi Malaysia
Johor Bahru, Malaysia.
luqmanhakim.noresham@gmail.com

Nik Din bin Muhamad
Department of Energy Conversion
Faculty of Electrical Engineering
Universiti Teknologi Malaysia
Johor Bahru, Malaysia.
nikd@fke.utm.my

***Abstract*—Dissolved oxygen is the most important thing when conducting a fish pond or lake. Adequate level of dissolved oxygen in a pond is required to be maintained as the aquatic life need it for respiration. This dissolved oxygen can be increased by using aeration. The typical aeration system used in Malaysia is stationary and surface type aeration system. The subsurface aeration system is better than surface type aeration system where the dissolved oxygen produced is higher. The aeration system is set to be movable thus the dissolved oxygen can be increased rather than the stationary aeration system. Arduino microcontroller is used in this project to make the aerator to be movable. The aerator can be controlled by using smartphone application and can be set to be move autonomously. The rate of dissolved oxygen produced is experimented for stationary and movable. The differences of dissolved oxygen produced in various depth also is determined and compared. The rate of dissolved oxygen produced when the aerator is set to be movable is found much higher than it set to be stationary. The control method of this movable aeration system is explained in this paper.**

Keywords—dissolved oxygen; aeration; subsurface aeration system

I. INTRODUCTION

Aeration is an important process need to be done when conducting a fish pond or lake. Aeration is a process of increasing the oxygen saturations of water which is done by bringing the air and water into intimate contact. It consists of ventilation of air on the water surface by passing an amount of air through the water. This process needed to eliminate the dissolved gases or unwanted gases contain in the water such as carbon dioxide, methane and hydrogen sulphide [1]. Naturally, this aeration process is done by the air breeze. But, when the biochemical oxygen demand (BOD) of the water is high, natural aeration cannot support the demand [4]. Thus, artificial water aeration is created.

II. LITERATURE REVIEW

A. Introduction

Mostly aeration system used in Malaysia is surface aeration system. This system can only aerate only the surface of water or cannot aerate the entire water column. So, the bottom of the water will be held still and no aeration will be done in it. Furthermore, the system used also cannot be move or stationary. Thus, the oxygen transfer rates will be accumulated around the aerator only. These will make the ponds suffer from poor water quality [6].

B. Dissolved Oxygen and Aeration System

Dissolved oxygen is a major contributor to determine the water quality and the healthiness of ponds or lakes [1]. The dissolved oxygen indicates the availability of oxygen can be found in the water. This dissolved oxygen is needed not only by the fish and aquatic life, but also the aerobic bacteria who help to decompose the organic matters in the water [2]. Without this dissolved oxygen, all the aquatic life will be affected [5]. This dissolved oxygen can be increased through aeration [3].

Naturally, the aeration process is done by the winds and rain. As example, the winds will aerate the surface of water. Thus, oxygen will be exchange through diffusion process. But, without the winds or rain, the water will be unaerated. According to [1], the dissolved oxygen will be supplied by the surface-dwelling phytoplankton through photosynthesis in some ponds or lakes. But, the photosynthesis product from the phytoplankton is proportional to the light intensity. During daytime, the biochemical oxygen demand (BOD) can be supplied. The problem is raised when the oxygen supply in night time cannot meet the demands since the phytoplankton need light intensity to do photosynthesis.

C. *Previous Paper*

From the research that has been conducted by [5] and [6], the subsurface aeration system is the best among the other type of aeration. The dissolved oxygen is really needed by the aquatic life for their respiration as well as it can affect their growth. These effects have been proved by [6]. Another research on the effect of aeration rates toward the aquatic life has been conducted by [7] where the authors defined the aeration rates will affect the growth of aquatic life. This research support the conclusion made by [6].

III. METHODOLOGY

A. *Introduction*

In this chapter, the method and procedure implemented for the project is discussed. The knowledge obtained from the literature review is used in order to get better result. The project will be divided into two subprojects which are operation using Android application and autonomous operation using ultrasonic sensor. The application and features of the aerator, hardware development and software development are listed in Table 1 below.

TABLE I. PROJECT DESCRIPTION

Parameter	Description
Application	Autonomous Solar Powered Movable Aerator by Air Bubbler Technique using Arduino and Android Application
Feature	• The aerator can be controlled by using smartphone. • The aerator will be moved automatically when no Bluetooth connection available.
Platform	Arduino Uno that based on ATmega328
Programming Language	Arduino programming language and block diagram
Actuator and Driver	DC motor and Motor Driver L293D
Communication Technology	Bluetooth
Sensor	Ultrasonic Sensor
Smartphone Platform	Android

B. *Proposed System Design*

The aerator basically has two part of operations which are operation using Android application and autonomous operation using ultrasonic sensor. For the first part, the aerator is connected to the android smartphone via Bluetooth. In this type of operation, the aerator will wait for the instruction given by the application. If the instruction is not given, the aerator will be stationary. But, the motor used for air pump will still operate accordance to previous instruction given. For the second type of operation, the aerator will be moved across the ponds automatically by using ultrasonic sensor as the guidance so that the aerator will not collide with the riverbank. The project operation flow is illustrated in Fig 1.

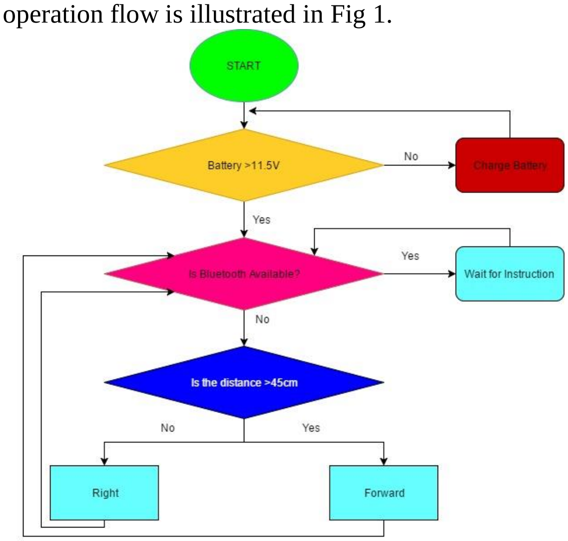

Fig. 1. Aerator System Flowchart

C. *Hardware Component*

1) *Aerator Model*

The aerator is designed by using plastic container. The plastic container as shown in Fig 2 is selected due to robustness and water resistant material. The propeller is attached to the aerator so that the aerator can be moved to the desired location. All the components such as Arduino, Bluetooth module, ultrasonic sensor, battery and motor driver will be put inside the aerator as shown in Fig 3. The solar panel which is used to charge the battery will be put on top of the aerator. The finished design model is shown in Fig 4 below. The aerator is attached with polyvinyl chloride (PVC) pipes that act as the buoys to ensure the aerator will kept float. PVC pipes is selected due to its ability to float and robustness in watery condition.

Fig. 2. Aerator Design

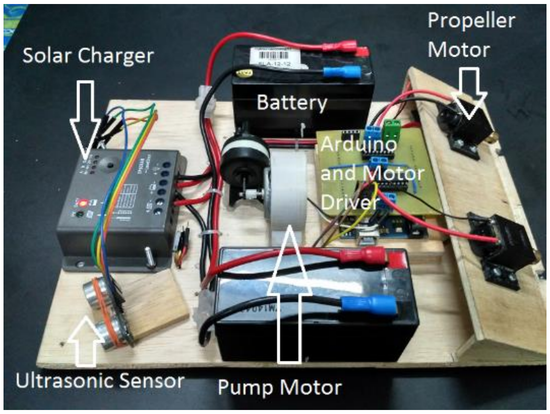

Fig. 3. Aerator Components

Fig. 4. Aerator Finished Design

2) Circuit Connection

In this project, the Bluetooth module HC-06 is used as a communication between the Android smartphone and the aerator. The Bluetooth module TX pin will be connected to the RX0 pin of Arduino while the RX pin of Bluetooth module will connect to the TX1 of the Arduino to ensure two-way data transfer can be achieved.

The ultrasonic sensor which acts as the guidance in the autonomous mode will be also connected to the Arduino. The ECHO pin of HC-SR04 will be connected to pin 10 while TRIG pin will be connected to pin 11 of the Arduino.

The motor driver L293D is used to control the propeller motor and aerator pump motor. The output pins from the motor driver will then connected to the Arduino Uno. The description of connection detailed in Table 2 and Table 3. The complete diagram of all components to the Arduino is as shown in Fig 5.

TABLE II. CONNECTION OF ARDUINO UNO AND PROPELLER MOTOR DRIVER L293D

L293D Pin	Arduino Pin
EN A (Motor A Enable)	5
EN B (Motor B Enable)	6
IN 1 (Motor A positive terminal)	A2
IN 2 (Motor A negative terminal)	A3
IN 3 (Motor B positive terminal)	A4
IN 4 (Motor B negative terminal)	A5

TABLE III. CONNECTION OF ARDUINO UNO AND AERATOR PUMP MOTOR DRIVER L293D

L293D Pin	Arduino Pin
EN A (Motor Enable)	3
IN 1 (Motor positive terminal)	7
IN 2 (Motor negative terminal)	8

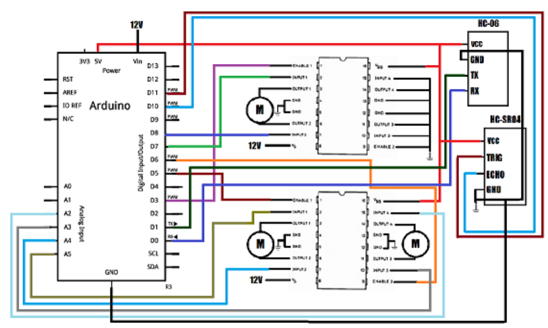

Fig. 5. Connection between Arduino Uno and Both Motor Drivers

3) Measurement Method for Dissolved Oxygen

The method of measurement for the dissolved oxygen is needed to be well-maintained as the dissolved oxygen contained in the water can be increased easily even with a small shaking force is applied towards the container. The experiments were conducted using UTM's Lake Water. The experiments were conducted in the Environmental Lab which is located at C07, Faculty of Civil Engineering by using a 30 litre container. The tip of the hose for the aerator pump was connected with the air stone. The air stone is used to create smaller air bubble thus the dissolved oxygen can be increased easily [5]. The motor used for the aeration pump for both experiments was set to be same which is operated at voltage of 3.8V. The temperature for tested water is set to be maintained at 20.9°C.

Two types of experiment were completed to analyze the behavior of dissolved oxygen under different circumstances. First, the air stone was set to be stationary while the depth will be tested in various levels which are at the top, middle and the bottom of the container. Every selected depth is increased by factor of 2 respectively. Second, the air stone was set to be movable with the depth has been manipulated same as in the first experiment. The experiments conducted in the container were illustrated in Fig 6. The experiment is set up as shown in Fig 7 and Fig 8.

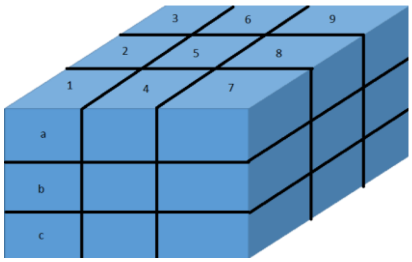

Fig. 6. Dissolved Oxygen Measured Point

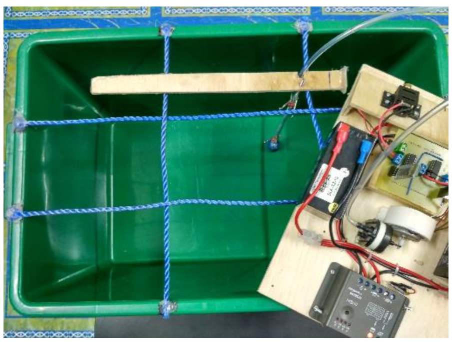

Fig. 7. Experiment Setup (Top View)

Fig. 8. Experiment Setup for Depth (Inside View)

IV. Result and Discussion

A. Stationary with Different Level of Depth

In this experiment, the dissolved oxygen produced in the container was measured in every 5 minutes interval. From the result obtained, the dissolved oxygen measured from each of the point is divided by time. By these, the rate of dissolved oxygen produced from each point can be analyzed.

From the experiments conducted, the rate of dissolved oxygen for depth C is the best where the rate of dissolved oxygen produced is the highest among the various depth tested in the experiment. So, the experiment conducted by [6] has been proved. The author had suggested that the dissolved oxygen can be increased by increasing the depth of the air stone.

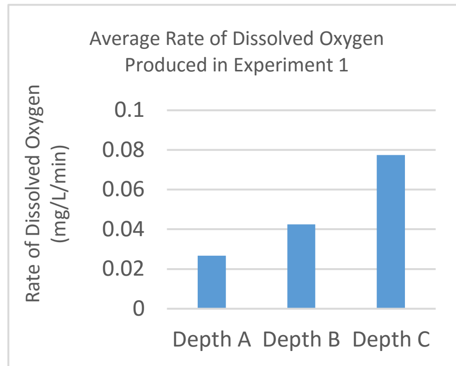

Fig. 9. Average Rate of Dissolved Oxygen Produced in Various Depth

B. Movable Air Stone with Different Level of Depth

In this type of experiment, the air stone of the aerator pump is set to be movable. The depth of experiment is set to be same as experiment 1 which is the depth will be increased by factor of 2 respectively and will be tested on the top (depth A), middle (depth B) and bottom (depth C) of the container.

From the experiments, it is found that the average rate of the dissolved oxygen produced in the tested water at the lowest depth, depth C is the highest among all the tested depth. By increasing the depth of the air stone, the rate of dissolved oxygen produced can be increased up to 50%.

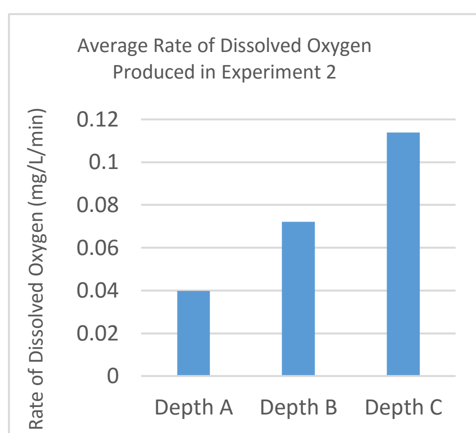

Fig. 10. Average Rate of Dissolved Oxygen Produced in Various Depth

Based on the finding, it can be concluded that when the air stone is set to be movable, the dissolved oxygen contains in the water can rise much more quickly rather than the air stone is set to be stationary. It is also found that the rate of dissolved oxygen produced at each point is different unlike the experiment 1 which is the rate of dissolved oxygen produced is almost the same at every point. The average rate of dissolved oxygen for both experiments conducted in various depth are compared in Fig 11.

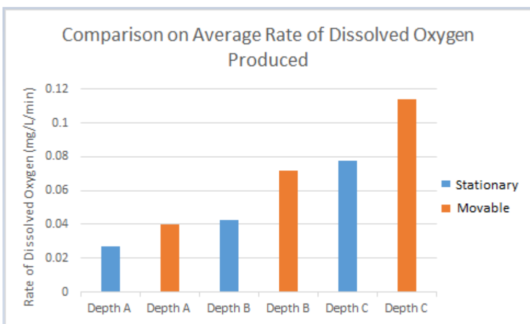

Fig. 11. Comparison of Average Rate of Dissolved Oxygen Produced

V. Conclusion

The movable and controllable aerator by using coarse bubble technique is successfully design. The subsurface aerator which consists Arduino, Bluetooth module, motor, air pump and powered by solar panel is successfully build. The aerator can be controlled by using smartphone application. The dissolved oxygen produced when it is put stationary and it is set to be movable are analyzed. It is found that, the dissolved oxygen can be increased when the movable aeration system is used.

References

[1] M. R. W. Association, M. D. o. Health, M. T. Coalition, and U. S. O. o. D. Water, Minnesota Water Works Operations Manual: Minnesota Rural Water Association, 1994.

[2] S. Culberson and R. Piedrahita, "Aquaculture pond ecosystem model: temperature and dissolved oxygen prediction — mechanism and application", Ecological Modelling, vol. 89, no. 1-3, pp. 231-258, 1996.

[3] J. Park, Y. Kim, S. Kim, H. Hwang, Y. Cho, Y. Lee, C. Song and J. Yun, "Effect of aeration rate on the mycelial morphology and exo-biopolymer production in Cordyceps militaris", Process Biochemistry, vol. 37, no. 11, pp. 1257-1262, 2002.

[4] Kannel, Prakash Raj, et al. "Application of water quality indices and dissolved oxygen as indicators for river water classification and urban impact assessment." Environmental Monitoring and Assessment 132.1-3 (2007): 93-110.

[5] Hidayat, Kurniawan W., et al. "Effect of three simple design micro-pore aeration on growth and survival of hybrid catfish Pangasius sp." (2016).

[6]Mahmoud, Ahmed, et al. "Development of a solar updraft aeration system for pond aquaculture in resource-constrained environments." Global Humanitarian Technology Conference (GHTC), 2015 IEEE. IEEE, 2015.

[7] Mallya, Yovita John. "The effects of dissolved oxygen on fish growth in aquaculture." The United Nations University fisheries training programmer, Final project, pp30 (2007).

Potential of Biomass on Electricity Generation in Malaysia

Nurfatin Anis Binti Ismail
Faculty of Electrical Engineering
Universiti Teknologi Malaysia
Johor Bharu, Johor
fatinanis_09@yahoo.com

Ms. Faridah Binti Husin
Faculty of Electrical Engineering
Universiti Teknologi Malaysia
Johor Bharu, Johor
faridahh@fke.utm.my

.

***Abstract*— Electricity demand is increasing throughout the world. This due to population growth and the sources needed for generating electricity should be increased in this period of time. Fossil fuels are the main source on generating electricity. The availability of fossil fuel sources are decreasing and need long term to produce. Besides, the price of fossil fuels having a fluctuation due to the unstable economic growth and lead to increasing cost of electricity generation. Energy consumption has risen in past two decades because of the combination of urbanization and industrialization. The growing of energy demand and prices of fossil fuels has to cater with alternative sources such as renewable energy sources. This problem had brought to this project which to identify biomass residues that have a huge energy potential to produce electricity, to identify electricity production from certain amount residues by using Homer Pro, to study the process and treatment of biomass waste from some ASEAN countries, and advantages of using biomass compare to fossil fuel in generating electricity. This project is focusing on biomass residue from palm oil and municipal solid waste. The result suggests that biomass sources could be one of the alternative sources of fossil fuels in generating electricity. The paper concludes with discussion on waste treatment is useful to keep environment clean.**

Keywords—demand; urbanization; industrialization; renewable soource; biomass;fossil fuel; treatment;

I. Introduction

The population in Malaysia has increased from 23 million in 2000 to almost 31 million in 2016 [1]. Rising of the population could lead to increasing the number of waste production in recent years and it becoming a big issue to handle because those wastes have to be manage wisely to ensure everyone living in a healthy environment. From Urban Development Series-Knowledge Papers, municipal solid waste (MSW) generation is 1.3 billion tons per year and this number is expected to rise up 2.2 billion in 2025. Moreover, each person is estimated producing wastes from 1.2 kg to 1.42 kg per day and its increasing from year to year. This show large amount of energy is produced and could be useful to generate electricity if that energy is being utilized. Process of wastes in landfill produce 40% of energy and can be collected as useful energy to human daily life.

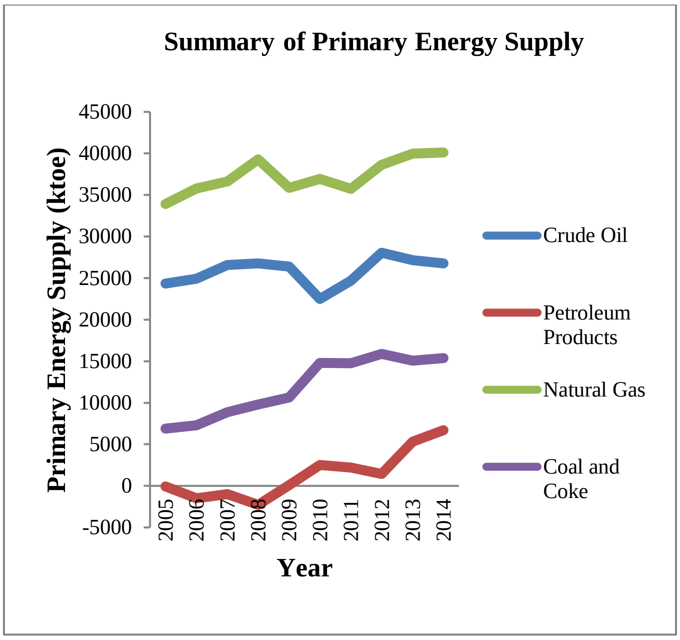

Fig. 1. Primary Energy Supply

Based on Fig. 1, the primary energy supply such as crude oil, petroleum products, natural gas and coal and coke are increasing over ten years' time. The availability of those sources decreasing and some steps on replacing the sources that give green and environmental friendly should be applied. There are some renewable energy sources that already practicing in our daily life such as solar energy, biomass, hydroelectric generator and wind energy. Wind energy could not be applied in Malaysia due to it received small average amount of wind besides others sources that can be supplied over long period of time. As the population increase, the electricity demands to power up appliances is high, besides moving the electrical vehicles, producing a variety of product and increasing production of agriculture plantation are all needs electricity to be functioned.

In Fig. 2, the pie graph shows Malaysia renewable energy consumption in recent years. Renewable energy has the least energy consumption compared to petroleum, coal, natural gas and nuclear electric power. Only 8% from the energy consumption is from renewable energy and 50% is of renewable energy from biomass. Biomass has the highest energy consumption among the renewable energy and this include for electricity and heating purposes. Biomass becomes one of the resources energy that can be processed to produce

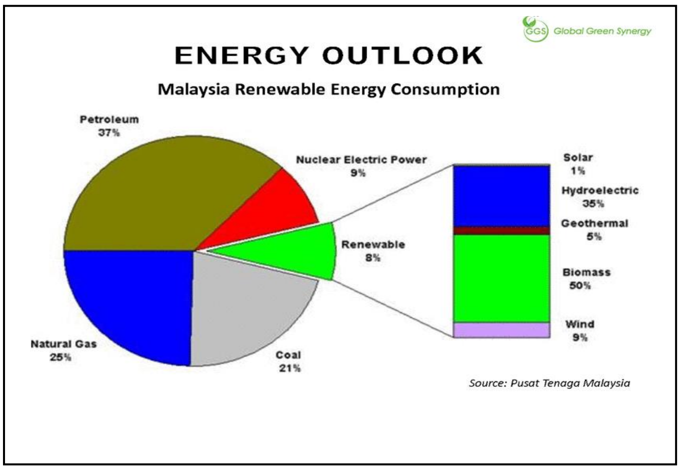

Fig. 2. Primary Energy Supply

car fuels, cooking purposes, electricity, as a heater and many more. Biomass is a resource that comes from tress, grasses, algae, agricultures and forest waste and municipal solid waste. To prevent the world from air pollutions, global warming, dependency of oil import and a weak of farm economy, these waste should be recycled to become a useful energy.

II. LITERATURE REVIEW

A. Electricity Supply and demand

Electricity demand is rising about 10% every year with the increasing number of population in Malaysia. Malaysia producing electricity from different resources such as combustion of fossil fuel, trapping solar energy, speeding of turbine for hydroelectric generation and biomass energy. This generation of electricity based on the availability of resources in Malaysia.

Fossil fuel is one of the main sources on every country in this world in producing electricity. The usage of fossil fuel in generating electricity is about 60% in Malaysia, 67% in United State, compared to solar energy, hydro energy, wind energy and others [1]. The process of generating electricity using fossil fuel is by using a combustion process which could emit some gaseous such as carbon dioxide, carbon monoxide, sulphur dioxide, nitrogen dioxide and nitric oxide. Even all those gaseous are colorless and cannot be seen, it could affect health problems, greenhouse effect and global warming.

B. Biomass Resources

1) Agricultural Waste

Agricultural waste is a waste that exists from agricultural residues, food processing residues, animal wastes and animal renderings. In California, agricultural waste is second largest of bio energy sources useful for generating powerful sources either for electricity purposes of transportation purposes. The agricultural waste is comes from vineyard residues, seed crops, corn residues and soybeans [2]. Besides, animal residues are one of the agricultural wastes that exist to supply useful power to customers.

Malaysia has abundant supplies of biomass sources and plantation residues and agricultural residues are the main sources of biomass Malaysia. Palm oil residues give higher percentage production on generating electricity due to it produced 20,000,000 t in 2013 which is the second largest palm oil producer in the world after Indonesia. About 60% of palm fibers and shells are considers as a waste and the lowest of moisture content of each residues in palm oil will combust more effectively than the higher moisture content. The ascending orders of moisture content of palm oil are shells, palm fibre and EFB [9]. Only 10 % of palm oil would become oil and the 90% of the palm oil production is a biomass waste [10].

2) Municipal Solid Waste

Municipal solid waste can be classified as a waste produce from human daily activities such as food, paper and plastic. But, only waste that produce from renewable sources is considered as biomass residues. In Malaysia, average of per person produces waste in between 0.5 and 0.8 kg/day and about 1.7 kg/day for people living in cities. In addition, the total waste produce is 168 million tons per year. In MSW, both organic and non-organic materials can be used to generate electricity.

C. Biomass Conversion Technologies

1) Direct Combustion

Direct Combustion is the most widely use and establish application of solid biomass compared to gasification and pyrolysis processes. It contributes 97% of power production and most of countries such as China, California, Nigeria, Germany and United State use combustion process for burning biomass to produce heat and electricity. Combustion is used to convert biomass energy into hot gases with temperature around 800-1000 °C [7]. Practically, combustion process is more suitable for biomass that content less than 50% of moisture. In addition, more than 90% efficiency can be achieved by a modern combustion plant and boiler with minimal environmental effects [8]. Direct Combustion can be categorized into three main system; fixed bed combustion, fluidized bed combustion and dust combustion. Those categorize works depend on the type of biomass.

2) Gasification

Gasification is one of the biomass conversion technologies that transform raw solid biomass material feedstock into a mixture of gaseous products with existing of oxidation agent (air, oxygen, water, carbon dioxide, etc.) by chemical reaction at high temperature in an enclosed chamber called as reactor. Gasification involved for processes; drying, pyrolysis, reduction and combustion. The gaseous produced from gasification is called producer gas or syngas [5]. Syngas can be used in more efficient combined cycle of power generation system which combines steam and gas turbine [4]. Gasification is applied by some countries; Denmark, Japan, United Kingdom, Austria, Germany, and Switzerland to process wood residues such as wood pellets, wood chips and lignocelluloses. In Nigeria, Carbo Consult and Engineering (Pvt) Ltd. is a company that has been assigned to conduct the gasification technology in a few areas in South Africa and other countries for commercial purposes [3].

3) Pyrolysis

Pyrolysis is a process that converts biomass into liquid form of product. This process going through subset of gasification systems and biomass degrade without oxidation process. The formation of liquid bio-oil is through partial combustion at lower temperature which between 450°C to 600°C [6]. Pyrolysis produce energy fuels that making the most efficient process of biomass conversion with non-renewable fossil fuel resources. Pyrolysis can be divided into three subclasses; slow pyrolysis, fast pyrolysis and flash pyrolysis. Pyrolysis oil can be used to generate electricity.

4) Anaerobic Digestion

Anaerobic digestion is microbiological processes that produce biogas through natural process or under control environment and residues digestate without present of oxygen. AD needs certain bacteria for a natural breakdown of organic matter. Bacteria would help to decompose feedstock into a smaller size but these processes need some times to produce the product. Biogas is gaseous that consist of methane gas, carbon dioxide and some other gaseous. Methane gas is useful for heating and generating electricity purposes. Biogas and residues digestate have some steps to be produce such as decomposition of livestock, conversation of decomposed materials into organic acid and formation of biogas. In addition, residues digestate could be a good fertilizer after passing through appropriate treatment. AD is commercially used as biomass technologies in certain countries such as Nigeria, United State and Malaysia. This technology is one of the continuous processes that need a constant feedstock supply [10].

D. Treatment of Biomass

1) Thailand

Thailand is an agricultural based country that received high solar irradiation potential. The renewable sources that available in Thailand are solar power, biomass, hydro power, wind power, biogas and municipal solid waste [12]. Thai government introduced scheme of feed-in-tariffs in 2015 for waste is 5.6 Baht/kWh with subsidiary of 10 years and feed-in-tariffs for biogas is 3.76 Bath/kWh with subsidiary of 20 years to promote the management of biomass in the country. Conversion of waste into electricity was being introduced to reduce cost of electricity production and carbon dioxide emissions. Waste conversion is being processed with several technologies such as anaerobic digestion, fermentation, gasification and incineration.

Besides, different waste is treated with different treatment. Bangkok and other urban areas (municipalities' areas) contribute about 61% of MSW and 39% from rural areas in Thailand. About 64% of MSW is organic waste from food and followed by plastic and paper 17% and 8% [11].

2) Singapore

In Singapore, waste to energy initiative programs have been practices and about four incineration plants had been built. Waste management system in Singapore focuses on collection, recovery and treatment. Besides, Singapore has very limited land in providing landfill areas, government had introduced several strategies such as push toward zero landfill, minimizing waste through reducing, reusing and recycling, and developing waste management industry and positioning Singapore as a center for waste management technology in the region [13].

There are three main types of biomass residues available and it is useful for recycle, reuse and being process such as farm waste, plant waste and used oil from cooking food. In Singapore, there are two farms had setting up for biogas plant in 2014 that turns bird poo into electricity. The electricity that produced meets the total energy demand in the chicken farm. This could reduce farm's operating cost and provide a return on their investment within 5 to 6 years [13].

3) Indonesia

Biomass sources in Indonesia come from forestry waste, agricultural waste and municipal solid waste. The utilization of biomass in electricity generation is still low in percentage. The government focuses on recycling program which need low expenses and convenient to the society. For example, biomass waste is use for household cooking, fertilizer and rural electrification. Besides, Indonesia is the biggest supply of palm oil production in the world for agricultural industry. Production of palm oil increasing yearly and amount of palm oil residue to be treated should be increasing. One way to manage palm oil residues is process of gasification to generate electricity. People live in rural areas are the highest society using biomass resources in Indonesia where the necessity for them to live is very limited and difficult to get. Biomass residues that produce from forestry and agriculture are important for the residences in rural area to generate electricity.

4) Malaysia

Biomass residues that produce in Malaysia can be classified into five main sources; municipal solid waste, palm oil residue, bagasse, woody residue, and rice husk. Palm oil residue is the highest of biomass resources contributor follow by municipal solid waste. Process of biomass in Malaysia consists of anaerobic digestion, pyrolysis, gasification and esterification. The process is based on the biomass sources that produce in Malaysia. Basically, government has given incentive to investor who applying Fit-in-Tariff (FiT) on renewable energy. About 0.67 per cent of total biomass resources are provided by government to encourage private companies and society aware the important of biomass treatment in Malaysia [15].

E. *Barriers of Implementation on Biomass Energy*

1) *Financial*

Electricity generation cost depends on variable cost and investment cost which are including fuel cost, capital cost, operational and maintenance cost. Additional effects of power generation in biomass cost are power capacity, heat and electricity efficiency, power plant life time and load factor. For developers to overcome biomass cost in power generation, they must continue to exploit emerging technologies and take a long term view that can reduce electricity generation cost [4]. European Union (EU) provided some fund for energy projects in ASEAN countries including renewable energy. Four categories had introduced; market awareness, institutional frameworks, feasibility studies and demonstration project [31]. But, the process of implementing biomass in society need time to be considered. In addition, market of biomass utilization is relatively limited.

2) *Policy*

Feed-in-Tariff has been introduced in Malaysia since 2004. This is one of ways to encourage people in producing their own electricity from renewable resources that exist in our environment. But, awareness among society is still in low level. Many commercial investors have unattractive to invest in renewable resources power generation because of conventional energy is cheaper than RE. Information about RE among different national agencies that have implemented power generation from biomass resources are insufficient. Flaws in program design cause investors do not taking any risk [4].

3) *Technical*

Barriers in technical part can be categorized into five types; no local expertise for efficient biomass energy conversion, lack of technical knowledge has led to poor quality product, lack of new technology, insufficient education, training and sharing experiences among investors, and no local manufacturers for the efficient conversion of biomass to energy [4]. Government and privatization sectors should play their role to overcome the barriers to ensure RE can fully utilize for society.

III. METHODOLOGY

There are three method used in this project which are collecting data from government agencies for palm oil production and municipal solid waste production in Malaysia, calculation and simulation using Homer Pro for electricity production. The data of palm oil and municipal solid waste provided by Malaysian Palm Oil Board (MPOB) and Perbadanan Pengurusan Sisa Pepejal dan Pembersihan Awam (SWCorp).

A. *Equation*

$$COE\ (i, N) = \frac{C_{ann,tol}}{E_{prim}+E_{def}+E_{grid,sales}} \qquad (1)$$

Where,

E_prim and E_def are total amount of primary and deferrable loads respectively

E_(grid,sales) is amount of energy sold to grid per year

IV. RESULT AND DISCUSSION

A. *Result*

1) *Simulation Design*

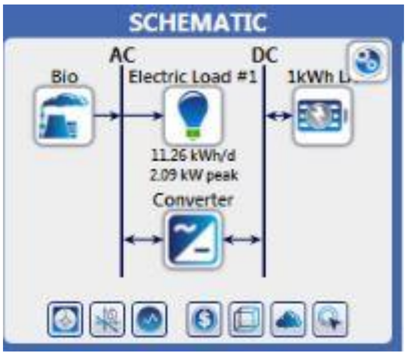

Fig. 3. Schematic Diagram of Design .

Fig. 3 shows that the schematic diagram of biomass simulation in Homer Pro. There are several components are used in the simulation as listed below:

a) Biogas Genset 500kV: to produce electricity from biomass residues.

b) Electric Load 11.26 kWh/d:to

c) Converter: to convert alternating current supply to direct current supply

d) 1kWh Lithium ion: to store excess power generated in high density capacity of battery.

2) *Simulation Result*

Fig. 4. Production of Palm Oil Residues per day

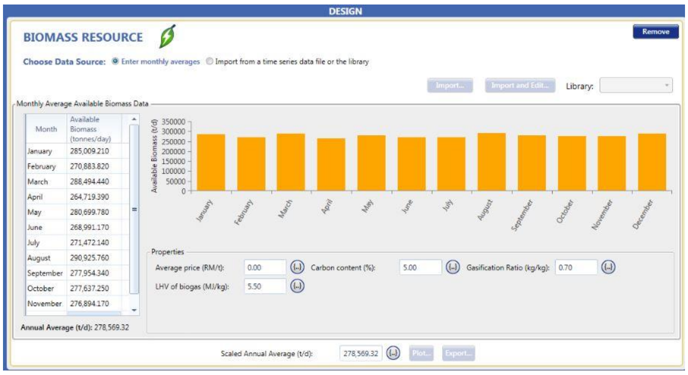

Fig. 5. Production of MSW per day

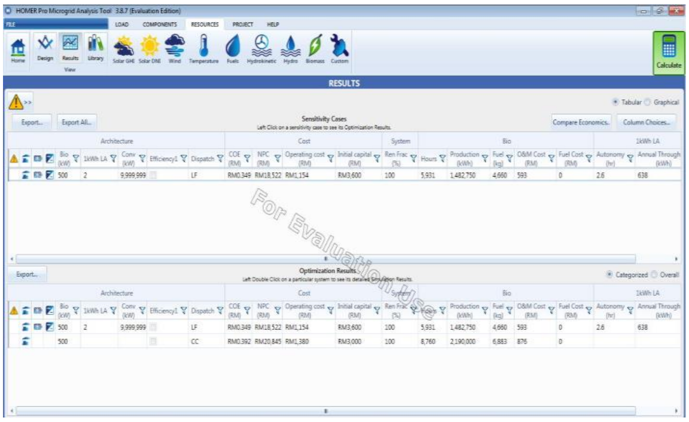

Fig. 6. Simulation Result for Palm Oil Residues

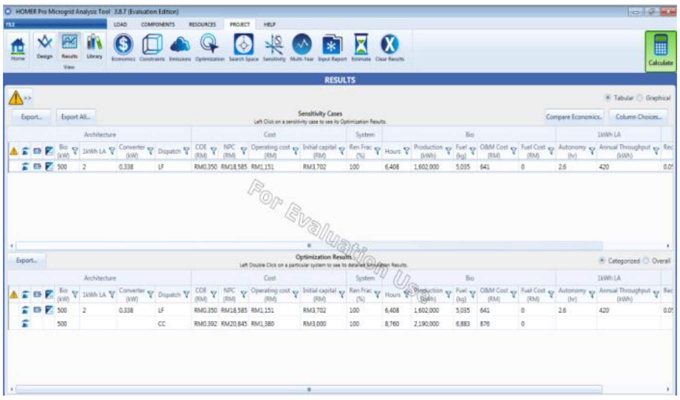

Fig. 7. Simulation Result for MSW

Table. 1.Simulation Result for MSW

Biomass	COE (RM)	Operating Cost (RM)	Production (kWh)	Hours
Palm Oil Residue	0.349	1,268	1,482,750	5,931
MSW	0.188	1,154	1,815,500	7,262

B. *Discussion*

Palm oil residues and MSW are the largest contribution of biomass energy production in Malaysia besides forestry, rice husk and bagasse. Based on simulation result, the average production of palm oil residues is 10,476 tons/day while the average production of MSW is 278,569.32 tons/day. The amount of palm oil residues production are contributed by all state in Peninsular Malaysia while production of MSW is from all state in Malaysia except Seremban, Nilai, Port Dickson and Pasir Gudang. Electricity produce by palm oil residues and MSW are 1,482,750 kWh and 1,815,500 kWh. The estimation operating cost for palm oil residue is RM 1,268 while MSW is RM 1,154.

Malaysia's per household electricity consumption is 251 kWh per month which equal to 171.68 kg carbon dioxide released in a month. Estimation of total residence that would get electricity supply from biomass production is 13,140 household per month. The total amount of electricity production from palm oil residues and MSW could supply 12 per cent of total electricity demand per year by residential areas in Malaysia.

CONCLUSION

As a conclusion, electricity production from biomass energy can supply 13,140 household per month. Carbon dioxide emission is about 2,255,875.2 kg compared to fossil fuel which produced about 32% from burning of fossil fuel. In tropical countries, palm oil production is the main waste production in Thailand, Indonesia and Malaysia. The process of biomass conversion technologies used is combustion, gasification and pyrolysis. While in Singapore with limited areas for palm oil plantation, the government introduced a program that producing electricity from farm waste production. It can be concluded every countries is trying increase production of electricity by managing the waste production on each country.

REFERENCES

[1] Zia Haq, "Biomass for Electricity Generation", California, USA, 2002.

[2] Richard Germain and Ryan Katofsky, "Recommendation for Bioenery Plan for California", Navigant Consulting, inc.April 2006.

[3] S. Dasappa , "Potential of Biomass Energy for Electricity Generation in Sub-Saharan Africa", Centre for sustainable Technologies, Indian Institute of Science, Bangalore, India, 2010.

[4] S.M. Shafie, T.M.I. Mahlia, H.H.Masjuki, A. Ahmad-Yazid, " A Review on Electricity Generation based on Biomass Residue in Malaysia", June 2012.

[5] Y.S Mohammaed, A.S. Mokhtar, N. Bashir, R.Saidur, "An Overview of Agricultural Biomass for Decentralized Rural Energy in Ghana", Universiti Teknologi Malaysia, April 2012..

[6] International Renewable Energy Agency, Biomass for Power Generation Volume 1: power sector Issues 1/5, June 2012.

[7] McKendry P. Energy production from Biomass (part 2): Conversion technologies. Bioresoure Technology 2002;83(1): ppg 47-54.

[8] Leskens M. LBMv Kessel, Bosgra OH. "Model Predictive control as a tool for improving the process operation of MSW combustion plants: Waste Management", 2005; 25;ppg 78-98.

[9] Onochie et al, "Caloric value of palm oil residues for energy utilization", Volume 4, Issue 4, ISSN: 2277-5668, International Journal of Engineering Innovation & Research, 2015.

[10] Rizky Fauzianto, “Implementation of Bioenergy from Palm Oil Waste in Indonesia”, Technische Universität München, School of Forest Science and Resource Management, Germany.

[11] Chak Cherdsatirkul, “Generation and Disposition of Municipal Solid Waste Management in Thailand”, Department of Earth and Environment Engineering, Columbia University, April 2012.

[12] PrachuabPeerapong and Bundit Limmeechokchai, “Waste to Electricity Generation in Thailand: Technology, Policy, Generation Cost, and Incentives of Investment”, Sirindhorn International Institute of Technology, Thammasat University,2016.

[13] International Enterprise Singapore, Waste Management: World-Class Environmental and Waste Management Services [Brochure]. Singapore, Mar 2012.

[14] Climate Change SG. (2014, January). Making Waste Work for Us. Retrieved from https://www.nccs.gov.sg/climatechallenge/issue08/Waste-To-Energy-Initiatives.html

Air-Condkit: Generate Electricity from Air Conditioning Compressor Fan using Wind Energy Concept

Abu Muaz Bin Mohd Adid
Faculty of Electrical Engineering
Universiti Teknologi Malaysia
Johor Bahru, Malaysia.
abumuaz123@gmail.com

Faridah binti Hussain
Department of power
Faculty of Electrical Engineering
Universiti Teknologi Malaysia
Johor Bahru, Malaysia.
faridahh@fke.utm.my

***Abstract*— primary source likes coal, oil, natural gas and wood are reduce year by year. It will decrease dramatically than human expectation. Nowadays, investor and engineer are rushing to use renewable energy as future main electricity. But in this case study will focus on generate electricity from home appliances by using its output. For the example generate electricity from heat of lamp, wind speed of fan or rotational air conditioner compressor. So, air conditioner compressor is chosen because it's not human uses compare to lamp and fans. Speed of the compressor will turn of generator. DC motor used as compressor and 3 types of DC motor will turn into generator. The objective is to ensure this project will generate electricity at least light up one LED bulb. LM2596 dc-dc buck converter will help to give different value of power supply.**

Keywords—Brushless dc motor; Tamiya Motor, Brush motor; LM2596 dc-dc buck converter

I. INTRODUCTION

Wind energy outshines all other renewable energy resources due to the recent technological and construction improvement. This is because, wind energy can generate electricity up to 8MW or more for the one oscillation from its turbine. So it is worth to spend a lot of cost to get huge amount of energy for people. Moreover, wind energy is one of the renewable energy that satisfied the needs of energy for people without causing reduction of the nature energy resources swiftly and harms the environment [1]. Of course there several renewable energy such solar, hydro, geothermal, tides and waves. But wind energy is the high courage by engineer and investor.

The cost to install wind turbine in Malaysia, it takes Million Ringgit Malaysia for the each. By the way, several "display" wind turbine located at Perhentian Island, Terengganu because they are not working at all. Poor wind speed and maintenance technician in Malaysia causes wasting huge cost of investment. In Malaysia, wind turbine is not suitable because of the slowest wind speed. Data recorded form Malaysia Meteorology Department says that wind speed is around 3 -5 m/s. While the potential of blades spin to reach the power rated is up to 10-15 m/s.

In my case study, rather than we use wind speed to spin the blades for producing electricity, the existing fan/turbine that found surrounding such as air-conditioner condenser can be applied into wind turbine concept. There are two sources that can be used, first is the wind produce form spinning blades and second is the rotation of the compressor. The main idea is, from kinetic energy from the working fan will convert to mechanical energy that connected to equipment and devices to produced electrical energy.

The weather is now getting hot and because of that, Malaysian start to install air conditioner inside their house, either in bedroom or living room. Based on observation, most household in Malaysia have air conditioner. From that observation, air conditioner compressor is chosen in generate electricity in new phase of innovation. The vision that bring this idea is "use output to get an input".

II. LITERATURE REVIEW

A. How wind turbine works

Inductions generators or synchronous generators can be used on wind turbine as electrical generators [2]. At high wind speed, the nameplate rating of a wind turbine which usually indicates the maximum power output of the turbine in kilowatts (kW). Power output will raise perpendicular to the wind speed. In other words, when wind speed is increase that make the blades rotating at high speed. The power output will be high as limit of the power rated. But, when there is very high wind speed. Wind turbine must be shut down according to the certain period to make sure no critical damage on turbine.

Cabinet placed a lot of switches for other system that allocate near to the door of wind turbine building. By the way, transformer is the next equipment after the switch box. Transformer is an apparatus designed which can convert alternating current from one voltage to another. To make it clear, it designed to "step up" or "step down" voltage plus it works on the magnetic induction principle [3]. Next, that equipment is connected to the substation.

B. Daikin Air conditioning

In real practical, wind speed sensor is used to measure wind speed of air condenser fan. Value of horsepower is directly proportional to the wind speed. In other word, fan will spin faster to produce high wind when use large horsepower. Table below shows data that have been recorded in term of wind speed on certain horsepower with different distance. Distance meant, the gap between sensor and air condenser.

TABLE I. WIND SPEED WITH DEFFERENT GAP AND AND ANGLE USING SAME HORSEPOWER

	AIR1, 3.0 HP	**AIR2, 3.0 HP (45° angle)**
Distance, m	***Wind speed, m/s***	***Wind speed, m/s***
0	4.8	6.0
0.1	3.8	5.7
0.2	3.0	4.7
0.3	1.8	3.2

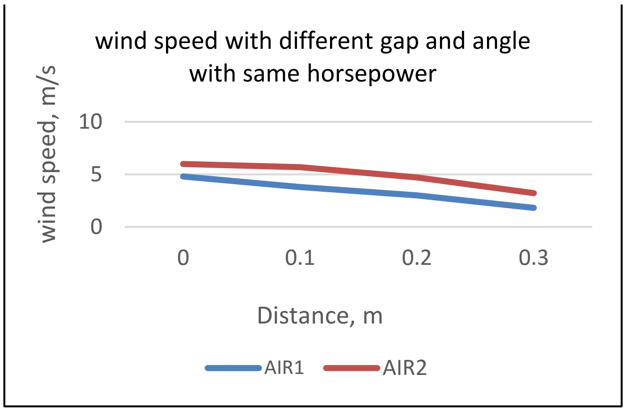

Graph 1, chart for the wind speed with different gap and angle with same horsepower

C. Turn motor into generator

There are few things or option than should consider when selecting dc motor will depend upon the accessibility of manufacturers and suppliers and the range of machines that they stock [4].

1) Efficiency: Usually, it is slightly lower efficiency when dc motor operate as generator than as motors. However, to improve the efficiency is by changing the operating voltage and frequency. Some manufacture has increase the amount of copper used in the windings and the quality of the steel in the stator and rotor cores to produce range of high effieciency motor.

2) Power rating: The higher operating temperature of the generator is depend on the greater the power drawn from it. So the life of its winding getting short. Therofore, so ensure long winding life when the motor act as a generatir, the machine should be kept below its full load operating temperature as a motor.

3) Voltage rating: When selecting a motor the voltage rating is a very foremost consideration. But for dc motor it can be used directly as a generator. Because some of the cases need fews modification to the windings will be specified.

4) Speed rating: Basically the generator suppose be directly driven by the turbine or other shaft connection. Power rated is a mark point where speeds affects generator to generate electricity. Ideally the speed of the motor or generator in revolution per minutes (rpm) or meter per second (m/s) unit. Limitation the radial load must be taken seriously to avoid damage and good bearing life.

III. METHODOLOGY

There a lots of hardware including machinery, equipment or tools used around the world. Technology is getting dramatically demand year by year. So, engineer rushing to ensure hardware is used in advance and making people life easier. In this project, basic hardware or tools like 12V DC power supply, voltage regulator, 3V DC Tamiya motor, brushless motor, DC wattmeter and battery storage are used to complete Air-CondKit. But there are only prototype shown how they work actually.

A. Flow chart

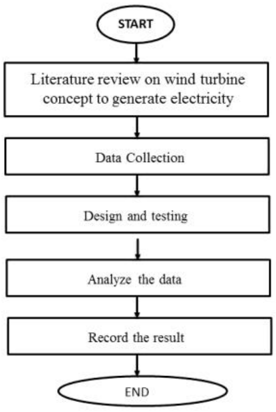

Fig. 2, Flow chart

Here are details of every single equipment or tools that very important in the project:

B. 12V DC power supply

DC motor which is presented as air conditioner compressor is used to make dc generator work. Therefore, power supply must in DC form. Back to back connection concept is where mechanical turn to electrical form. 12V, 0.5A DC power supply by using voltage regulator is to control the input of the voltage. Where the input can be varies by turning the adjustable resistance.

Note: the lower air conditioning temperature makes the compressor work faster. In voltage regulator, the higher voltage injected, the faster the motor will run.

Therefore, LM2596 DC-DC converter is used as a voltage regulator.

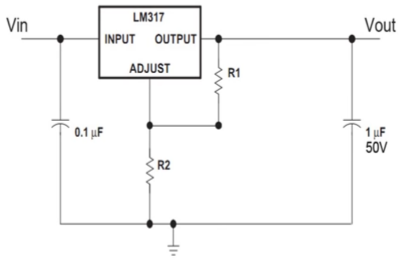

Fig. 1, LM2596 dc-dc converter circuit

$$V_{out} = 1.25 \text{ x } (1 + R2/R1) + 50\mu(R2) \quad (1)$$

This formula is figure out how to calculate the output voltage. If R1 is 510Ω and R2 is 10kΩ variable resistance, the supply can be adjusted from 1.25V to 25V output voltage. Putting couple of capacitances about 0.1µF and 1µF is to ensure the output voltage is stable in any situation.

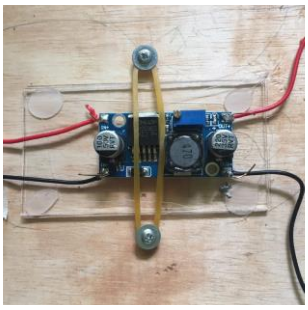

Fig. 3, LM2596 dc-dc converter

This LM2596 dc-dc converter have input and output. Positive input receiving current from the supply and will flow out to the positive output.

Moreover, this converter is actual acting as air conditioner remote control. The purpose of the remote control is to control temperature either to make it cool or warm. Based on observation, when temperature is low, compressor of air conditioner will run faster to make room cooler. So, more current will supply to the compressor so that it can make room temperature cool just in a minutes. Same thing goes to this converter by controlling the current from power supply. Then, dc motor will run according to the converter.

C. Motor Tamiya

Tamiya motor been act as air conditioner compressor. Compressor is motor that used in operation air conditioner. Wind speed test had been recorded (result) with two type of angle in same air conditioner compressor. The purpose is to know the capability of the wind speed from the compressor to transferring wind energy to the generator.

Unfortunately, data shows very poor wind speed that came out from the compressor. Therefore, second method will be used.

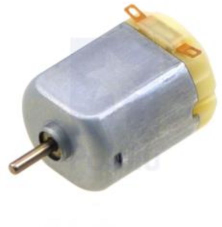

Fig. 4, Tamiya motor

The voltage can be supply for this Tamiya motor in range 1.5V-3.0V. The speed of motor without any load can be reached about 12,300 rpm. The stall torque at 3V about 36 g-m and the stall current at 3V is about 0.70mA [5].

Back to back connection by implement shaft between compressor and generator. The fan speed of compressor is enough to turn on Air-condkit’s generator. For the prototype of the compressor, Tamiya motor is chosen.

D. DC wattmeter

DC wattmeter is an instrument for measuring the electric power (or the supply rate of electrical energy) in watts of any given circuit. Besides, it can measure the value of voltage, current, power (Watts) and charge (Amp-hours). Dc wattmeter is a digital instrument and the data will appear digitally.

Fig. 5, DC wattmeter

DC Watt meters will helps to predict the model setup’s time flight and choose the best propeller or gearing with the appropriate motor. Moreover, it also can check the condition and usability of the battery, measure power and energy consumption of the device with a battery and ensuring the operating currents are safe for the motor, wiring and connector.

E. Generators

For this case study, dc motor is used as a dc generator which it can give dc output. Those 3 types of motors are:

1. RK-370cc-14230 dc brush motor
2. DC brushless motor
3. DC Tamiya motor

Generator 1	Generator 2	Generator 3

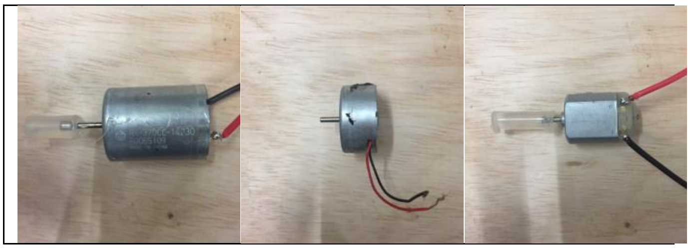

Fig. 5, Types motor used as generators

Some of the advantages using dc machine as generator including availability, cost and robustness. Different types of dc generator will give differ output value. For sure the specifications of each generator are not same. For generator 1, the voltage is in range 12V – 30V and it can produce current about 0.11A. The speed without any load can reach 20,700 rpm which mean, the faster it run, the higher the current and voltage. For generator 2, it more easily to generate electricity compare than others. While generator 3 need a large supply to generate small amount of electricity. Refer to analysis part for the result.

F. LED bulb

By using LED bulb as a load for this project is parallel to achieve of the main objective state. At least one LED bulb will light up to make sure this method success. The reason why LED bulb is chosen because, electricity that generate from the dc generator very small and suitable for the bulb been tested.

Fig. 6, White LEDs bulb

Typically indicator LEDs are designed to produce with no more than 30-60 mill watts (mW) of electrical power. High efficiency is one the key advantages of LED-based lighting. However, white LED quickly matched and overtook the efficiency of standard incandescent lighting systems [6].

IV. ANALYSIS

The impact of injection of power supply to the motor assisting the dc generator produces electricity. The winding inside the motor will determine how fast the motor run. Since Tamiya motor is used to operate the system, there are 3 types of dc generator will be tested with single white LED bulb as a load. Those of them had been mentioned in hardware parts where they are RK-370CC-14230 brush dc motor, brushless motor and Tamiya dc motor.

RK-370CC-14230 brush dc motor is the first dc generator been tested. The power supply for three dc generator is increasing orderly starting from 2.00 volt. Among important data that have been recorded are input and output of voltage, current and power.

To calculate the power, the formula is:

$$P = IV \tag{2}$$

TABLE II, GENERATOR 1

	Stage 1	Stage 2	Stage 3
Input Voltage, V_{in} (V)	2.00	2.50	3.00
Input Current, I_{in} (mA)	0.62	0.78	0.91
Input Power, P_{in} (mW)	1.24	1.95	2.73
Output Voltage, V_{out} (V)	2.94	3.35	3.51
Output Current, V_{out} (mA)	0.04	0.06	0.07
Output Power, P_{out} (mW)	0.1176	0.201	0.2457

What can be described from the table 2, output current voltage can be seen increasing when the injection voltage rise. Therefore, the power can get by using equation 1. Addition of power supply must be considered because it need very be careful while controlling the converter. Multi meter is used to measure the input and output.

TABLE III, GENERATOR 2

	Stage 1	Stage 2	Stage 3
Input Voltage, V_{in} (V)	2.00	2.50	3.00
Input Current, I_{in} (mA)	0.36	0.49	0.61
Input Power, P_{in} (mW)	0.72	1.225	1.83
Output Voltage, V_{out} (V)	2.93	3.28	3.57
Output Current, V_{out} (mA)	0.03	0.06	0.09
Output Power, P_{out} (mW)	0.0879	0.1968	0.3213

For generator 2, the output voltage and current are look similar. This is because; brushless motor can generate electricity easily. At 1.41V of output voltage, LED bulb already lighting up. Compare to the generator 1, it is a bit late to make LED bulb work.

TABLE IV, GENERATOR 3

	Stage 1	Stage 2	Stage 3
Input Voltage, V_{in} (V)	2.00	2.50	3.00
Input Current, I_{in} (mA)	0.38	0.39	0.41
Input Power, P_{in} (mW)	0.76	0.975	1.23
Output Voltage, V_{out} (V)	1.06	1.58	2.02
Output Current, V_{out} (mA)	0.00	0.00	0.00
Output Power, P_{out} (mW)	0.00	0.00	0.00

By the way, generator 3 give very small amout of current, unfurtunately it cannot light up even a single LED bulb at stage 3. What can say here is, tamiya motor are not suitable act as generator for the compressor.

V. Conclusion

Generation planning should requires an assessment of appropriate capacity of conventional either it need to be supply mainly or on the other hand. Because of Back to Back connection method used, types of generation must be selected wisely and effectively to avoid performances of the air conditioner compressor (DC motor) affected. Another importance factor that should be in observation is torque of generator. Lower torque will lead to efficient way in order get great input and output of the voltage. As a backup plan if the compressor stops working, battery bank must be in there to supply the electricity. It is also important to consider generating electricity that the load used must follow the limit of the generation. Avoiding overload will not forcing compressor and generator work beyond limitation.

References

[1] Performance Analysis of Wind Turbine As A Distributed Generation Unit In Distribution System. Ramadoni Syahputra, Imam Robandi, Mochamad Ashari, Department of Electrical Engineering, Faculty of Industrial Technology. Institute Technology Sepuluh November, Surabaya, Indonesia. Department of Electrical Engineering, Faculty of Engineering, Universitas Muhammadiyah Yogjakarta, Yogjakarta, Indonesia.

[2] L.L Amuhaya, M. J. Kamper, Design analysis of a hybrid-PM synchronous generator for wind energy applications, Dept. of Electr. & Electron. Eng., Stellenbosch Univ., Stellenbosch, South Africa.

[3] Georgy Jose, Rani Chacko, A review on wind turbine transformers, Dept of Electrical and Electronics Amal Jyothi College of Engineering Kanjirappilly, Kerala, India.

[4] Nigel Smith, Motors as Generators for micro-hydro Power, 2rd ed., Practical Action Publishing, 2008, pp.11-15.

[5] Pololu company, Tamiya motor datasheet, database, in website.

[6] Efremov, A. A. et al. (2006). "Effect of the joule heating on the quantum efficiency and choice of thermal conditions for high-power blue InGaN/GaN LEDs". R. Nicole, “Title of paper with only first word capitalized,” J. Name Stand. Abbrev., in press.

Light Emitting Diode (LED) Strip 5050 Driver using LDR Sensor

Muhammad Izwan Bin Ton Karim
Faculty of Electrical Engineering
Universiti Teknologi Malaysia
Johor Bahru, Malaysia.
Muhdizwan_94@yahoo.com

En. Nik Din Bin Muhamad
Department of Electrical Power
Faculty of Electrical Engineering
Universiti Teknologi Malaysia
Johor Bahru, Malaysia.
nikd@utm.my

***Abstract*— Light Emitting Diode (LED) are widely used in lighting application nowadays due to it low power consumption and high efficiency with long lifetime hours. LED strip is one of the LED that are surface mounted to make it more flexible and convenient for lighting application. The main objective for this project is to design LED driver that can be controlled by Light Dependent Resistor (LDR) depending to the light intensity through it. LDR that being used for this project is for an automatic switch for this system. An AC supply being convert to DC mode by using rectifier and current flow being transferred to Flyback transformer. Flyback transformer are used for this project in terms of its smaller size and switching device is Viper 50 that connected to the auxiliary pin of the transformer. Viper 50 consist of oscillator that will generate the PWM signal, comparator to power up the PWM signal and MOSFET that connect to the primary pin of the transformer. This thesis includes the design and flow of the project include the calculation of the parameter that being taken throughout this project. Result that being taken had being analzse and troubleshoot being made if the objective of this project is not achieved.**

I. INTRODUCTION

Light emitting diode (LED) have been used for conventional light for daily application especially for lighting due to longer lifetime hours faster response in smaller size [1]. In early 1962, LED are used as practical electronics components that emitted low intensity infrared light. Throughout the years as the time passed, researches had made a lot of improvement on LED to make it more conventional by making it has visible wavelength with high brightness [2].

LED become the most component in lighting application by replacing fluorescent lamp because of the same brightness being transmitted with lower energy consumption, longer lifetime, smaller size and faster switching. One of the innovation of LED is LED strip. This LED strip are surface mounted diode and its commonly used in accent lighting, backlighting and decorative lighting applications. This LED strip are very flexible are can be designed freely due to its flexibility that can bend without harm the connection of the led strip.

Configuration for this driver consist of rectifier with DC-DC converter. Rectifier will convert current or voltage in ac mode to voltage and current that purely dc [4] while DC-DC converter will provide a regulated output from DC voltage that have different voltage level [4]. For the rectifier, the ac voltage and current from residential electrical supply will be convert to dc mode and DC-DC converter that being used for this system is Switch Mode Power Supply (SMPS) which is an isolated transformer that called Flyback converter. There are others dc converter like buck, boost and buck boost but this type of dc converter has the advantage in terms of efficiency being produced. Output power that being produced by Flyback converter are around 5 Watt to 150 Watt. This shown that that Flyback converter can be used for high power application.

II. LITERATURE REVIEW

Theories of concept, software uses and hardware are explained in this chapter. This chapter also included the component operation and the principle that will be used in this project.

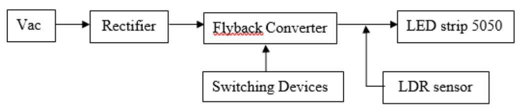

Figure 2.1 shows block diagram of LED strip 5050 driver using LDR sensor.

A. *Flyback Converter*

In this chapter, the topology of knowledge about Flyback converter during switch on and switch off, switching technique transformer are explained.

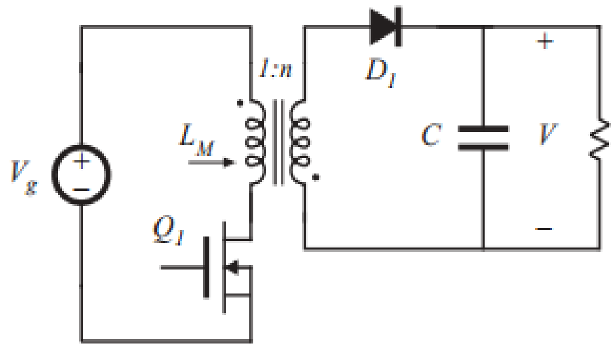

Figure 2.2: Flyback converter

One of the Switched Mode Power Supply (SMPS) is Flyback converter. This converter being function to produce output DC voltage from lower or higher supply input DC voltage. Flyback converter are DC to DC converter with buck-boost design and consist of inductor split transformer for additional isolation. This converter store energy in the air gap that located in the core and this converter is a multi-winding coupled inductors. Figure 2.2 above shows the configuration of Flyback converter.

This converter consists of 2 mode of functioning process which are during switch ON mode and switch OFF mode. Figure 2.2 below shown the configuration Flyback converter during switch ON mode. Based on this configuration, current flow at the primary side from the voltage source but the current does not flow at the secondary circuit due the diode in reverse biased mode. Primary winding of the transformer being magnetized and energy stored in the air gap during switch ON mode.

Derivation for switch closed analysis:

$$V_s = V_1 = L_m\frac{diLm}{dt}$$

$$\frac{diL_m}{dt} = \frac{\Delta iL_m}{\Delta t} = \frac{\Delta iL_m}{DT}$$

$$Vs = L_m\frac{\Delta iLm}{DT}$$

$$\frac{Vs}{Lm} = \frac{\Delta iLm}{DT}$$

Therefore, the current change in magnetizing inductance [6]:

$$(\Delta i_{Lm})_{\text{closed}} = \frac{VsDT}{Lm}$$

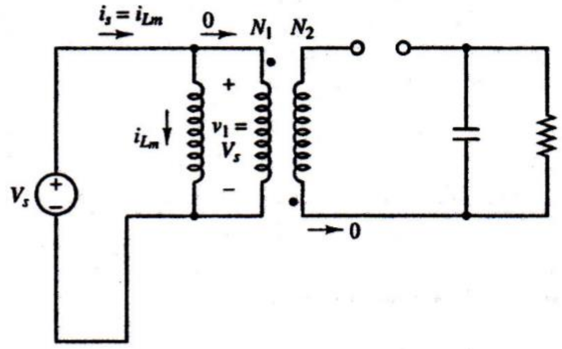

Figure 2.3: Closed circuit Flyback converter [4]

For the derivation for open switch circuit, current flow in the circuit cannot change immediately in inductance L_m, conductance path should flow through primary turns of ideal transformer. Current I_m at the primary winding enters undotted terminal and exit at secondary winding through undotted terminal and this will allow current flow through diode since its forward biased. Energy stored that being stored in the air gap during switch ON mode have been released to secondary winding through the forward biased diode and complete the circuit. Figure 2.3 below shows the configuration switch OFF mode for Flyback converter:

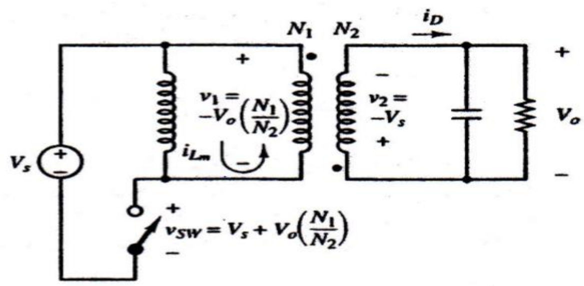

Figure 2.4: Opened circuit Flyback converter [4]

Derivations for switched opened analysis:

Since the voltage for V_2 is become $-V_0$ due to current flow to opposite direction, current and voltage during open switch:

$$V_2 = -V_0$$

$$V_1 = -V_0\left(\frac{N1}{N2}\right)$$

$$V_1 = V_2\left(\frac{N1}{N2}\right) = -V_0\left(\frac{N1}{N2}\right)$$

$$L_m\frac{diL_m}{dt} = V_1 = -V_0\left(\frac{N1}{N2}\right)$$

$$\frac{diL_m}{dt} = -\frac{V_0}{L_m}\frac{N1}{N2}$$

$$\frac{\Delta iLm}{\Delta t} = \frac{\Delta iLm}{(1-D)T} = -\frac{V_0}{L_m}\left(\frac{N1}{N2}\right)$$

Total current over one period is equal to zero for steady state equation [6]. Therefore, the equation will be:

$$(\Delta i_{Lm})_{closed} + (\Delta i_{Lm})_{open} = 0$$

$$\frac{VsDT}{Lm} - \frac{(1-D)TV_0}{L_m}\left(\frac{N1}{N2}\right) = 0$$

The output voltage will become:

$$V_o = V_s\,\frac{1-D}{D}\,\frac{N2}{N1}$$

B. Switching Technique

Heart of power electronic circuit contain semiconductor switching network and there will have 2 mode which are ON mode and OFF mode [7]. Bipolar Junction Transistor(BJT), Metal Oxide Semiconductor Field Effect Transistor (MOSFET), Gate Turn-off Transistor(GTO) are some of the examples of power electronics switches. These switches have their own capability in terms of switching speed, limitations of their current and voltage, and power losses. MOSFET are used for this electronic circuit due to low losses and high efficiency compared with the other electronic devices.

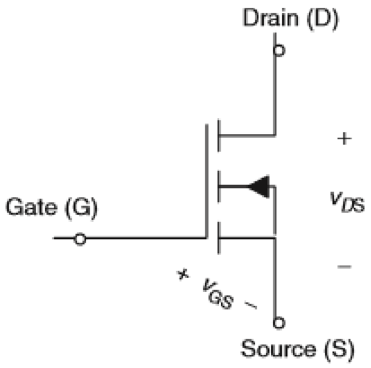

Figure 2.5: Configuration of n-channel MOSFET

Figure above shows the configuration of n-channel MOSFET that consist of three terminals that known as Gate(G), Source(S) and Drain(D). Supplying voltage through its gate eventually turned ON the MOSFET. This MOSFET consist of 3 operating regions for its operation which are triode region (linear region), saturation region (active region) and cut-off region. For the switch mode, triode region and cut-off region will be used for this operation while the saturation region are used for amplifier. V_{gs} must be lower than V_{th} (threshold voltage) to maintain the MOSFET in cut-off region while in triode region, V_{ds} should be less than $V_{gs} - V_{th}$ and the device will act like constant resistance, R_{ds} (on).

C. Rectifier

A rectifier will convert AC waveform input to DC waveform input and its consist 2 configurations which are half wave rectifier and full wave rectifier. Full wave rectifier will be focusing for this research due to inherently less ripple than half wave rectifier [6] and the configuration for full wave rectifier are shown in figure 2.7 below:

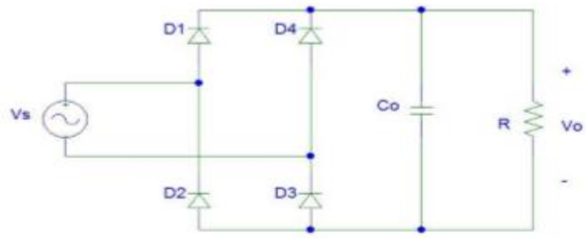

Figure 2.7: Full bridge rectifier

As seen from figure above, the circuit consist of 4 power diodes, capacitor and resistor(load). The function of diode is making the flow of current flow in one direction. The function of capacitor will act as voltage stabilizer for the output of rectifier to produce nearly DC waveform [6]. Inductor and capacitor output filter can improve the quality of DC output and peak current can be reduce [6]. Figure 2.8 below show the output of rectifier voltage:

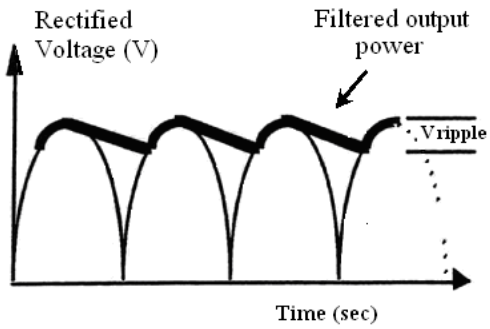

Figure 2.8: Rectifier output voltage

All diodes are assuming ideal for the analysis for full-wave rectifier:

$V_o(\omega t) = |\,V_m \sin \omega t\,|$ one diode pair on

$= (V_m \sin\theta)\, e^{-(\omega t-\theta)/\omega RC}$ diodes off

Where θ is angle of the diode become reverse biased

$$\theta = tan^{-1}(-\omega RC)$$

$$= tan^{-1}(\omega RC) + \pi$$

At boundary point, maximum output voltage, V_m and minimum output voltage can be determined when $\omega t = \pi + \alpha$

$$(V_m \sin\theta)\, e^{-(\pi+\alpha-\theta)/\omega RC} = -V_m \sin(\pi + \alpha)$$

$$(\sin\theta)\, e^{-\frac{\pi+\alpha-\theta}{\omega RC}} - \sin\alpha = 0$$

Difference between maximum and minimum voltage or ripple voltage

$$\Delta V_o = V_m - |V_m \sin(\pi+\alpha)| = V_m(1 - sin\ \alpha)$$

In practical circuits where $\pi \ll \omega RC$

$$\theta \approx \pi/2$$

Minimum output voltage for diodes off at $\omega t = \pi$

$$v_o\left(\pi+\alpha\right) = V_m e^{-\left(\pi+\frac{\pi}{2}-\frac{\pi}{2}\right)/\omega RC} = V_m\, e^{-\pi/\omega RC}$$

Approximation for ripple voltage with capacitor filter

$$\Delta V_o \approx V_m(1 - e^{-\frac{\pi}{\omega RC}})$$

Peak to peak ripple voltage

$$\Delta V_o \approx \frac{V_m\,\pi}{\omega RC} = \frac{V_m}{2fRC}$$

III. METHODOLOGY

This chapter will cover about progress project planning and operation flow to complete this project. Besides that, this chapter will give an explanation about the implementation of software simulation and hardware design for LED 5050 driver. Calculation and simulation results were analysed and compared.

A. *Project Workflow*

This part will present about the workflow in order to complete this project. Flowchart project planning are shown in figure 3.1. This flowchart as a guide for design and development for this project.

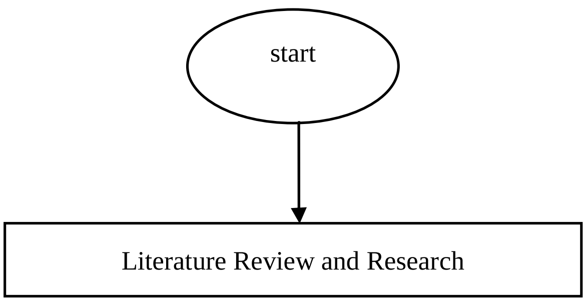

.

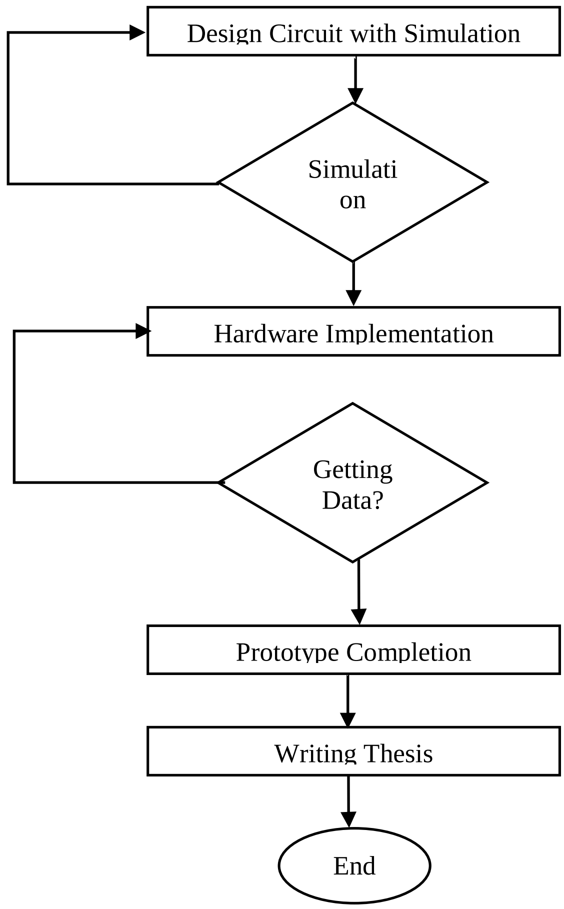

B. *Component Parameter Calculation*

The construction for this project have to understand the operation of Flyback converter and knows the switching devices that compatible with the transformer and find exact parameter that needed for the application. Table 3.1 below show the parameter value that needed for Flyback converter circuit. Value that be used to determine the rating of the component will be discuss in this topic.

PARAMETER	SYMBOL	VALUE
Input Voltage	Vs	240 VDC
Switching Frequency	F	100k Hz
Duty Cycle	D	0.5
Inductance	L	500uH
Primary Turn	N_1	50
Secondary Turn	N_2	7
Output voltage	Vo	12V DC

IV. RESULT

A. Simulation

Simulation of this project have been done through Pspice software in order to implement to hardware. Pspice software that being used for this project is ORCAD Capture CIS (Lite). There are few step that need to do to design the simulation for this project. First, profile of the project must be create and identify the location for the project file in computer. This step is shown in figure 3.3 below: -

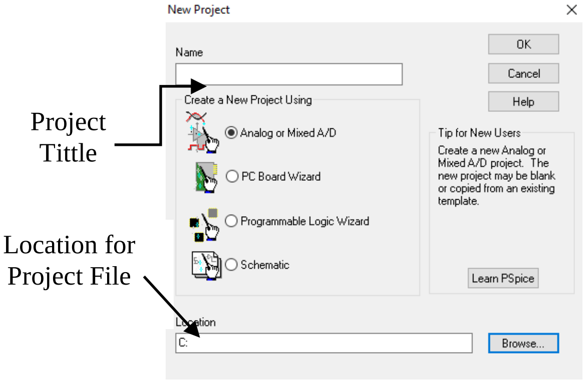

Figure 3.3 Simulation Profile

After the project file have been done, the circuit simulation must be created according to the parameter specification that being stated in table above. Circuit design for this project using Pspice shown in figure 3.4.

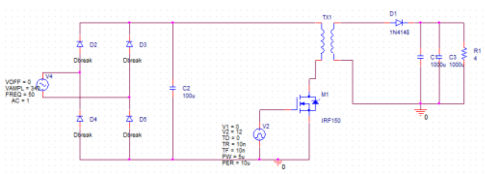

Figure 3.4: Circuit Design in Pspice Simulation

The simulation have been done in Psipice and the output voltage are based on the figure below:-

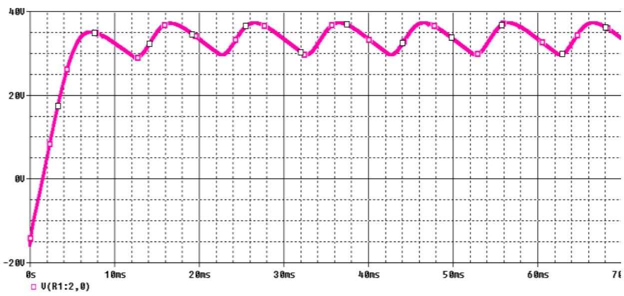

Figure 3.5: Output Voltage

The output voltage above showing that the output of the simulation is approximately around 33V. Which is are above from the needed voltage by the LED strip to turned ON. This means that the output of the flyback transformer need a voltage regulator that give output 12V using LM7812 component. This device can give the desired output that required by the LED strip 5050 to be turned ON.

V. CONCLUSION

This project should be convert from 240 VAC to 12VDC using rectifier that convert from AC to DC and using Flyback converter for the DC-DC converter. The switching device that should be used must be 100k Hz frequency according to the specifications of the flyback transformer. At the end of the result, this driver should be able to light up LED strip 5050 with LDR sensor that will act as automatic switch.

REFERENCES

[1] Ray-Lee Lin, Yi-Chun Chang, and Chia-Chun Lee. Optimal Design of LED Array for Single-Loop CCM Buck–Boost LED Driver. IEEE Transactions on Industry Applications, vol. 49, no. 2. 2013

[2] Held, Gilbert (Ed.). (2009). Introduction To light Emitting Diode Technology and Applications. London, UK: Taylor & Francis Group,LLC.

[3] Picard, J., Under the Hood of Flyback SMPS Designs, in 2010-2011 Power Supply Design Seminar. 2011, Texas Instruments.

[4] Daniel, W. Hart (2011). Power Electronics. McGraw. Hill International Edition.

[5] Ghani, I.A., P.I. Khalid, and S.H. Ruslan, Electronic Circuits Teaching Module. 2011: Faculty of Electrical Engineering, Universiti Teknologi Malaysia

[6] Daniel W. Hart. Power Electronics. Valparaiso. Americas, New York, N.Y.: McGraw-Hill. 2011

[7] M.H. Rashid. Power Electronics: Circuits, Devices, and Applications. 3rd. ed. Upper Saddle River, N.J.:Pearson Education, Inc. 2004

[8] C. Mathas.(2012).Light Sensors: An Overview. Electronic PRODUCTS URL: http://www.digikey.com/en/articles/techzone/2012/sep/light-sensors an overview

[9] Light Dependent resistor, Data pack F, RS data sheet, issued March 1997, 232-381

Design of Power LED in Automotive Headlight using Buck Converter

Nur Atiqah binti Ahmad Bakhtiar
Faculty of Electrical Engineering
Universiti Teknologi Malaysia
Johor Bahru, Malaysia.
atiqah.bakhtiar@yahoo.com

En. Mohd Zaki Daud
Electrical Power Eng. Department
Faculty of Electrical Engineering
Universiti Teknologi Malaysia
Johor Bahru, Malaysia.
mdzaki@utm.my

***Abstract*—This paper presents high power LED driver for automotive headlight low beam system. High power LED is a current control device that needs to be regulated for long life operation. The proposed regulator is switching regulator instead of linear regulator for high efficiency system. Buck converter is used to step-down the 12V car battery voltage to LED voltage requirement, 6.8V which consists of 2 LEDs connected in series in a string. However, 12V car battery always fluctuates from 9V to 16V, so it needs to be regulated first; hence a boost converter is used in front of the buck converter for handling the voltage variation problem. Simulation have been done using OrCAD Pspice software and results of inductor voltage and current, voltage across Gate and Source of MOSFET, output voltage and current have been analysed. The propose circuit design is implemented, and the result is nearly same as calculation and simulation.**

Keywords—low beam system, Buck Converter, MOSFET, LED

I. Introduction

The study of controlling the flow of electrical energy with the help of electronic circuits is defined as Power Electronics [2]. Electronics or properly called linear electronics, often deals with semiconductor devices that are linear. Linear electronics priority is to process information at low power level [1]. It involves in gain and bandwidth contrast to power electronics, which focus more on efficiency and distortion [2]. Linear electronics is about processing information, but power electronic is about processing electric energy. Basically, power electronics use electronics to convert high power supply and control the parameters involved to user end load.

The growth of power electronics is sloping upward into many industry fields of converting one energy into another, including automotive industry. Not only that, the technology of Light Emitting Diode (LED) is raising upward, and one of the technology is headlight system in automobiles. The latest technology is the application of high power LED, which gives the highest production of luminous flux than any other lighting devices. This allows many applications applicable for the uses of power LED especially in automotive headlight.

However, most conventional automobiles headlight use linear mode lighting like Halogen light. The light is fairly bright and has low efficiency with high consumption of power. Continuous use of the bulb makes the bulb consume high enough power for shorten the bulb lifetime. Hence, it can burnt out easily and need to be frequently replaced. Therefore, the maintenance cost of the headlight alone is high. People need to pay on something that is trifling but since it involves in road safety, and the convenience when driving at nights, it is quite necessary for them to replace the burnt lamp even the headlight bulb only last for a short period of time. Thus, the alternative way is by using switching mode lighting, LED.

This project focuses on the development of the high power LED driver for front headlight of automobile. The objectives of this project are to learn the basic concept of switching regulator; Buck converter, and PWM microcontroller, to design a step-down (Buck) converter for driving high power LED for automotive headlight system, to simulate the designed circuit using OrCAD Pspice, and to develop hardware for the application of power LED in automobiles.

II. Literature Review

A. The Arising of High Power LED in Automotive Lighting

Back then, halogen is used as headlight lamp. Halogen lamp has same principle as incandescent lamps but it has 500 to 1000 hours of lifetime, it is also low in efficiency because it has lots of energy loss as heat [6], but most car makers choose halogen lamps because of its low instalment and replacement cost compared to others [4].

Then, High Intensity Discharge (HID) type of lamp is used. HID have a lot more lumens than halogen, with lifetime of 2000 hours which is longer than Halogen, but it needs high ignition which draws a lot more of power before reaching full brightness; more than 2000V [3]. Drawing more power means that increasing the torque of the car alternator and makes fuel consumption increases every turning on of the headlight. HID lamp's maintenance cost is costlier to be compared to Halogen lamps. This is because HID is more complex as it need ballast for the circuit [4].

After all, these recent years, LED was introduced and since it can last about 15000 hours, it is more preferable than Halogen and HID [3]. LED is made on semiconductor materials of P and N type regions, holes exist in P-type region and electrons exist in N-type region. As one electron from N-type region combines with one hole from P-type region, one photon of light is emitted

[5]. This process happens thousands of time in a split second, hence the continuous bright light [4].

B. *High power LED vs. ordinary LED*

High power LED is chosen over ordinary LED is based on few causes. One of the causes is low power consumption, and others are higher efficacy, have higher luminous flux, higher brightness, and have ability to reach maximum brightness in a millionth of second.

Brightness of LED is dependent on amount of current, since low power LED only deals with small amount of current which is tens of mA, hence small luminous flux, but for high power LED, it can be driven ups to hundreds of mA and to more than 1A [9], thus high luminous flux and higher brightness. High power LED is a growing technology because it consumes a small amount of power, which is 1 to 10W only.

The most important point of using Power LED is because of its reliability. It can last about 100,000 hours, which is 11 years of continuous operation and 22 years if 50% of operation [7], hence less maintenance. In addition, it turns on quicker than conventional lighting; 130ms for LED and 200ms for bulbs [8]. If it is applied at brake lights, the reaction time increases equate to a car length, thus this is the major contribution to road safety and reducing car accidents.

On the side of brightness, ordinary LED can supply efficiency of luminous flux 50 lm/W but for high power LED, it can reaches until hundreds of lm/W.

C. *Conceptual of power LED*

Power LED is a current control device, its output depends on forward current and that is why power LED or power LED arrays need a current regulator. High power regulators also use switching converters for efficient system. Switching converters is chosen instead of linear converter because linear output voltage is always less than input voltage, although the forward current of linear regulators is good as it keeps at low level, but the efficiency dropping as the current increase, while switching regulators keep high efficiency in any condition [6].

High power LED can be drives by high amount of current and that causes high temperature and high loss, this is the part where heat sink is crucial for heat dissipation for avoiding LED damaged instantaneously. Halogen and HID emits heat to surrounding, which is the one reason of their high losses and low efficiency, but high power LEDs do not emit heat to surrounding, it emits heat at the bottom of the LED (Emitter side) and also the electrical circuit chip. For daytime running light and tail light, heat sink is not needed because they do not need power as much as headlamp.

D. *Automotive Lighting System*

As for automobile headlight, it generally has two different beams; low beam (dip beam) and high beam (main beam). The connection is as shown in Fig. 1.

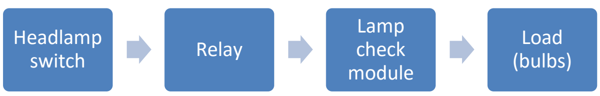

Fig. 1. Flow process of electricity in an automotive headlight.

In the lamp check module block, there is supply power plug and the driver for the load [8], which in the case of high power LED, the process is straight away from switch to lamp check module which consists of high power LED driver, and to load.

E. *High Power LED Driver*

LED driver have to give fixed desired light output within the target range. For LED driver, switching regulator is preferred, which the simple regulator for DC-DC converter is sufficient; buck converter, boost converter, and buck-boost converter [6].

In this project, Buck converter is used to deliver constant low voltage levels regardless of power changes to load, thus ensure constant current to load.

1) *Buck Converter*

The Buck Converter, or in other names, step-down converter, is a switching regulator that produces lower output voltage than the input voltage supply. Basically, Buck converter consists of a power semiconductor switch, a diode, an inductor, and a capacitor. The basic circuit is as shown in Fig. 2.

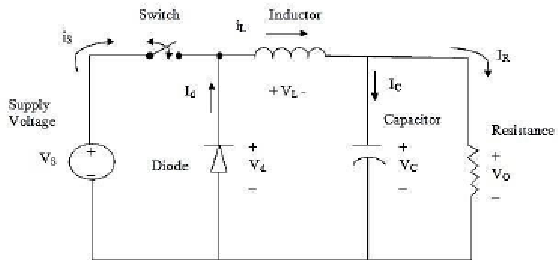

Fig. 2. Buck converter circuit.

As in Fig. 2, the V_o should be lesser than V_s due to the step-down process (voltage chopped) by the presence of voltage drop in Inductor, V_L. Semiconductor switch is commonly use transistor that is operated in switched-mode. When the switch is closed (transistor signalled 1), it is fully on and operated in saturation region, current flows but no voltage drop occurs and when the switch is open (transistor signalled 0), it is fully off and operated in cut-off region, no current flows at the transistor.

a) *Switch is close*

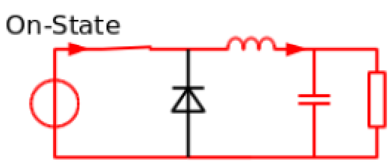

Fig. 3. The ON state circuit.

When the switch is closed, diode is in reverse biased, therefore it acts as open circuit. Thus, current flows from source to inductor, L, and produced inductor voltage, V_L and inductor current increase linearly.

$$V_L = L\frac{di_L}{dt} \quad (1)$$

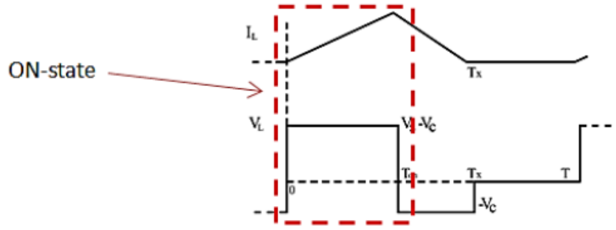

Fig. 4. The inductor current and inductor voltage during switch is closed.

Inductor voltage, V_L in Fig. 4 is the subtraction between input voltage supply, Vs and load voltage, V_O as stated in (2).

$$V_L = Vs - Vo \quad (2)$$

Since the time taken or period, T of one cycle is on ON-state and OFF-state condition, time for ON-state is DT, and time taken for OFF-state is T- DT. Hence, the inductor current increase linearly with time as shown in (3).

$$\Delta i_L|switch\ closed = \left(\frac{Vs - Vo}{L}\right)(DT) \quad (3)$$

b) Switch is open

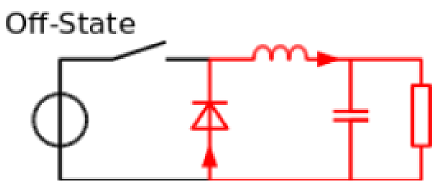

Fig. 5. The OFF state circuit.

When the switch is open as in Fig. 5, i_L from the inductor L flows to diode. Hence, diode is in forward biased and acts like a short circuit. Thus, load, receives current. At this time, inductor voltage is negative to load voltage.

For switch opened condition, time taken is, $\Delta t = (1-D)$T. Thus, Fig. 6 shows the decreasing of inductor current as in (4).

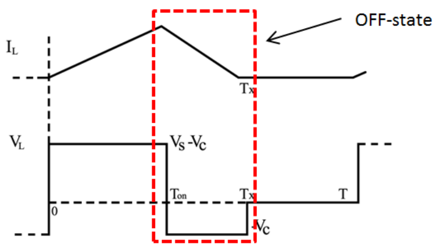

Fig. 6. The inductor current and inductor voltage during switch is open.

$$\Delta i_L|switch\ open = \left(-\frac{v_o}{L}\right)(1-D)T \quad (4)$$

c) Steady-State Operation

Steady-state operation is when i_L at the end switching cycle is the same at the early of the next cycle which made the change of i_L for one period is zero. The equation is as shown in (5).

$$V_o = DV_s \quad (5)$$

d) Modes of Operation

Buck converter can be operated in two modes, one is Discontinuous Conduction Mode (DCM) and another one is Continuous Conduction Mode. If the converter is operated in CCM, the minimum value of Inductor can be determined by calculation in (6).

$$L \geq L_{min} = \frac{(1-D)}{2f} \cdot R \quad (6)$$

III. Methodology

This section focuses on the methodology process on designing Buck Converter, the hardware selection to build buck converter circuit and PWM controller circuit.

This project focuses only on low beam lighting. Fig. 7 shows the sub-circuit of this project which contains the controller part of the Buck Converter, and the converter itself.

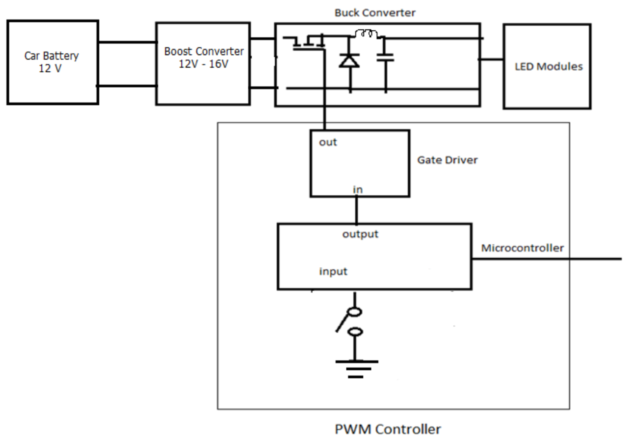

Fig. 7. Sub-circuit of Automotive Headlight LED driver.

12V DC car battery has nominal value of 12V but it fluctuates in the range of 9V to 16V due to load changes. This is where boost regulator in front of the buck converter plays its role; to handle input voltage variation for making input voltage of the buck converter constant.

Switching frequency of this Buck Converter is chosen to be high frequency, 50 kHz for decreasing the size of Buck Converter with smaller value of inductor, L and capacitor, C.

The load is chosen to be a string of two LEDs in series. The LEDs will have typical forward voltage and current of 3.4V and 350mA respectively. Since LED is current control device, CCM mode is chosen for driving the current to be constant.

A. Selection of Buck Converter Components

The Buck Converter design involves the selection of the inductor, the capacitor and the power switch.

To select the value of inductor, duty cycle of the Buck Converter must be calculated first. Knowing the maximum and the minimum value of supply voltage, minimum and maximum duty cycle can be analysed.

For the string of the LEDs, the output voltage is 6.8V. Based on (5), maximum duty cycle is determined by the minimum input voltage, 9V, and the maximum input voltage. 16V is selected for minimum duty cycle,. Therefore the maximum and minimum duty cycle is as shown in (7) and (8) respectively.

$$D_{max} = 0.756 = 75.6\ \% \tag{7}$$

$$D_{min} = 0.425 = 42.5\ \% \tag{8}$$

For CCM mode of operation, (6) is used to calculate the minimum value of inductor in the buck converter. $L_{min}\ is\ 47.41\ \mu H$, so the chosen inductor value is 330 μH which is 7 times bigger of minimum inductor value to ensure buck converter runs in CCM. For best design of buck converter, the selections of the components are based on maximum duty cycle, 75.6%. The minimum current rating for the inductor is the maximum peak current of the inductor, calculated using equation in (9), which gives $I_{L(max)}$ = 468.5mA. Hence, toroidal iron core 330μH inductor with the current rating of 3A is chosen.

$$I_{L(max)} = I_L + \frac{\Delta i_L}{2} \tag{9}$$

To choose the output capacitor value, peak to peak output ripple voltage is chosen to be 20mV. Therefore, based on equation in (10), the capacitor value is 6.1 μF and the chosen output capacitor value is slightly higher than calculated value, 10 μF.

$$C = \frac{(1-D)V_O}{8Lf^2\Delta V_O} \tag{10}$$

For power switch, common choices are usually between MOSFET, IGBT and BJT. Since MOSFET is a voltage control device and have simple gate driver, and BJT needs high base current and expensive also complex base drive circuit. MOSFET is chosen to be the power switch for this project.

The buck converter diode is chosen to be a schottky diode, 1N5822 because of its fast reverse recovery time and low forward voltage, 0.525V.

B. Selection of PWM Controller Circuit

The power switch of buck converter, MOSFET need switching signal to drive the Buck Converter and the switching signal chose is PWM signal.

Since the luminance of the LED is dependent with the duty cycle, duty cycle for low beam lighting is to be the minimum duty cycle.

The generation of PWM signal is from microcontroller which for this project, microcontroller PIC16F877A is chosen over Arduino and AVR microcontroller. Even though Arduino is easy to use, but it used non-standard terminology and has poor substitute for real schematic, and for AVR, it will have one cycle jitter while PIC's interrupt is constant and AVR's device configuration is a mess.

MOSFET needs about 10V to 20V to ON, therefore a gate driver is needed for amplifying the voltage of 5V PWM switching signal to 12V PWM switching signal. For this project, gate driver of IR2112 from International Rectifier is chosen to amplify 5V switching signal to 12V switching signal. The connection of the driver is based on the datasheet and capacitor between V_S and V_B is a bootstrap capacitor to ensure Gate and Source of MOSFET always receives positive voltage.

IV. Results and Analysis

A. Simulation Results

Circuit design and simulation have been conducted using ORCAD Pspice software. Since this project only focuses on low beam lighting, only the minimum duty cycle, 42.5% is used for generating PWM switching signal. The circuit is as shown in Fig. 8.

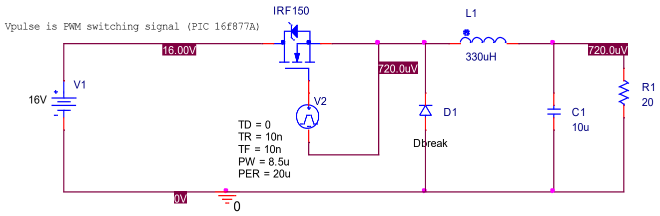

Fig. 8. Buck converter circuit.

The Pulse Width (PW) value of the simulation, 8.5 μs is the time when switch is ON. Equation (11) is used to calculate the time.

$$D = \frac{T_{ON}}{T_{ON} + T_{OFF}} \tag{11}$$

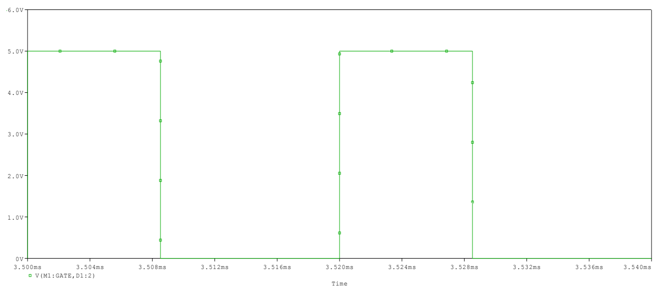

Fig. 9. Voltage of gate to source of MOSFET, Vgs.

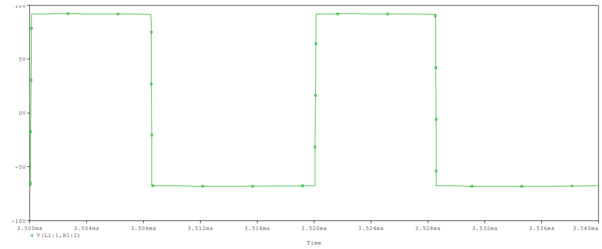

Fig. 10. Voltage across Inductor, V_L.

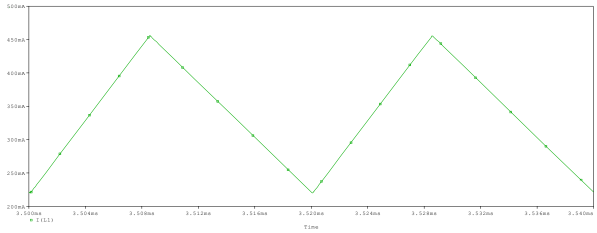

Fig. 11. Inductor current, I_L.

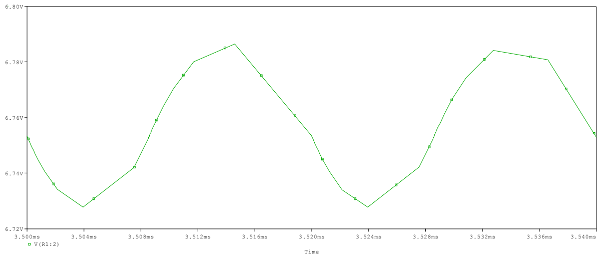

Fig. 12. Output Voltage, V_O .

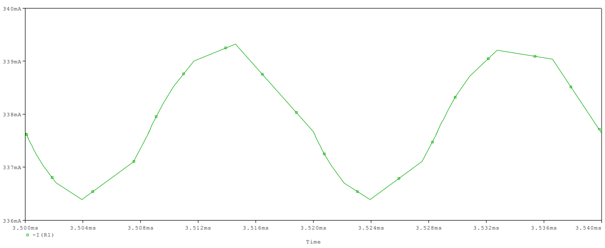

Fig. 13. Output Current, I_O.

The Vgs in Fig. 9 is the PWM switching signal with 5V amplitude and 8.5 μs pulse width. Since the input voltage is 16V, the peak value of voltage across inductor, V_L according to (2) is 9.2V as in Fig. 10. Fig. 11 shows the peak to peak inductor current with Δi_L of 235mA, $I_{L(max)}$ of 460mA, and $I_{L(min)}$ of 225mA. These value of Δi_L, $I_{L(max)}$, and $I_{L(min)}$ are approximately the same as calculation using (3), (9) and (12) which are 237mA, 468.5mA, and 231.5mA respectively.

$$I_{L(min)} = I_L - \frac{\Delta i_L}{2} \tag{12}$$

For the output, the simulation result in Fig. 12, is 6.75V to 6.79V which is almost as the same as desired voltage, 6.8V. The output current, I_O in Fig. 13 shows current of range 337.5mA to 339.5mA and it is nearly 350mA as desired.

B. Hardware Results

The simulation results focuses only on buck converter with PWM signal of 5V amplitude, but for hardware, the power switch; MOSFET, needs a gate driver (IR2112) who will amplify the 5V of PWM signal to 12V to ensure MOSFET is switching. Circuit is implemented and results are observed from oscilloscope. Fig. 14 shows the PWM signal from PWM output pin of PIC 16f877A microcontroller and from the high side output of IR2112 gate driver. The value of voltage across inductor V_L is as shown in Fig. 15.

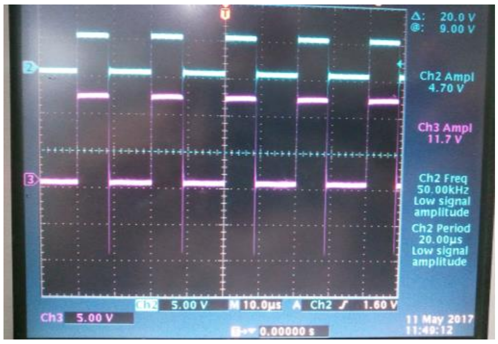

Fig. 14. PWM signal. Channel 2: PWM from PIC16f877A Channel 3 : PWM from IR211

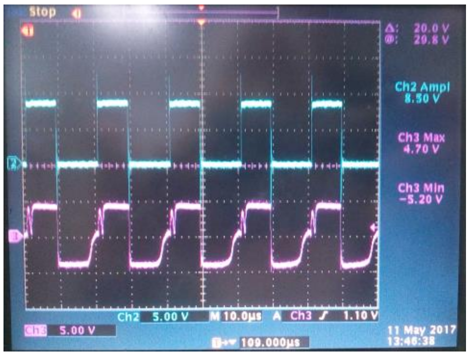

Fig. 15. PWM signal and voltage across inductor, V_L. Channel 2 : PWM from IR2112 Channel 3 : voltage across inductor, V_L

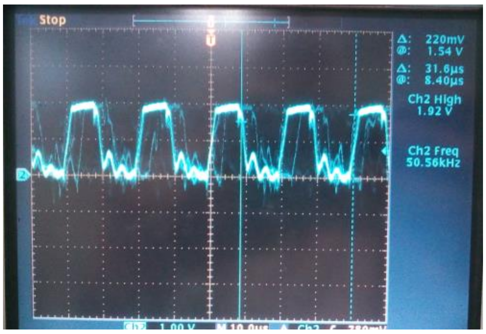

Fig. 16. Voltage across Gate and Source of MOSFET, V_{GS}.

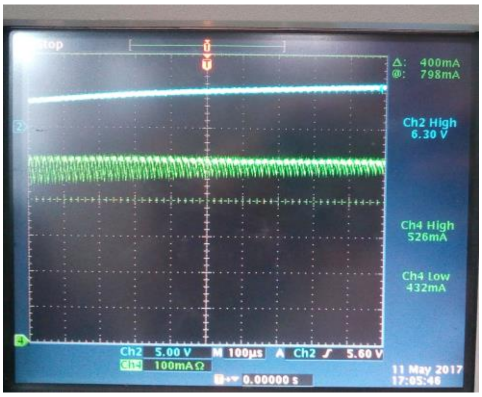

Fig. 17. Output voltage, V_O and inductor current, I_L. Channel 2 : V_O Channel 4 : I_L.

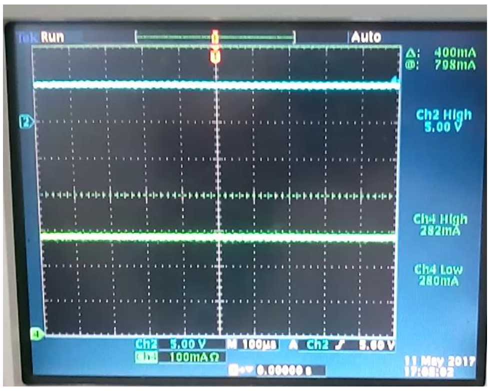

Fig. 18. Output voltage, V_O and output current, I_O. Channel 2: V_O Channel 3:I_O.

Based on Fig. 14, the PWM signal from channel 3 is as desired (12V of PWM signal with duty cycle of 42.5% to ensure MOSFET is on ON state).

In Fig. 15, the V_L on channel 3 shows the positive inductor voltage is 4.70V and the negative inductor voltage is -5.20V. The negative inductor voltage is nearly as simulated (-6.8V), but for positive inductor voltage, the value of 4.70V have about 4.5V mismatch from calculation and simulation result (9.2V).

Voltage across Gate and Source of MOSFET, V_{GS} is supposed to get 5V amplitude with duty cycle of 42.5% and T_{ON} of 8.5μs, but in Fig. 16, V_{GS} is only receives 1.92V amplitude with T_{ON} of 8.5μs. Implementation of hardware gives loss of 61.6% to V_{GS}. The value of Δi_L in Fig. 17 which is 94mA is not the same as simulation and calculation. It differs about 143mA from the calculation and 141mA from simulation.

V_O from Fig. 17; 6.20V is practically same as desired output voltage but it is before load is connected. When load; 2 high power LED of 1W connected in series in a string, is connected parallel with output capacitor, the output voltage drops to 5.00V with maximum peak current of 282mA as shown in Fig. 18.

V. Conclusion

The designed Buck Converter for automotive LED headlight, low beam lighting is successfully developed. In this system, input voltage of buck converter is from boost converter and the buck converter receives PWM switching signal for step-down the voltage to 6.8V of two high power LED rated 3.4V each connected in series in a string.

To conclude, the project is completed successfully and objectives are achieved.

References

[1] Khanchandani, M. D. (2007). *Power Electronics 2nd Edition.* New Delhi: Tata McGraw-Hill Publishing Company Limited

[2] *What is Power Electronics*. (2015, January 1). Retrieved October 2, 2016, from Power Electronics A to Z: http://www.completepowerelectronics.com/what-is-power-electronics/

[3] M.A Juarez, P. M. (2014). *Analysis of Buck Converter Control for Automobile LED headlight Apllication.* Retrieved September 25, 2016, from IEEE Xplore: http://ieeexplore.ieee.org/stamp/stamp.jsp?tp=&arnumber=7036298

[4] Popa, B. (2016, January 21). *Battle of the Headlights: Halogen vs. Xenon vs. LED vs. Laser vs. Conversion Kits.* Retrieved October 3, 2016, from Autoevolution: http://www.autoevolution.com/news/battle-of-the-headlights-halogen-vs-xenon-vs-led-26530.html.

[5] Kitai, A. (2011). *Principles of Solar Cells, LEDs and Diodes.* United Kingdom: John Wiley & Sons, Ltd

[6] D. Gacio, A. C. (2008). *SUITABLE SWITCHING CONVERTER TOPOLOGIES FOR AUTOMOTIVE SIGNAL LAMPS AND HEADLAMPS USING POWER LEDS.* Spain: IEEE.

[7] Ming, L. G., (2007). Boost Converter for Automotive LED lighting (Bachelor thesis). Retrieved from Perpustakaan FKE . (Call No. TK7871.89.L53 L56 2007 raf

[8] Denton, T. (2004). *Automobiles Electrical and Electronic Systems.* Burlington: Elsevier Butterworth-Heinemann.

[9] Ambastha, S. (2016, May 16). *How to identify the right high power LED*. Retrieved October 14, 2016, from electronicsb2b: http://electronicsb2b.efytimes.com/headlines/identify-right-high-power-led/

Improvement of Moisture Assessment in Power Transformer using Frequency Dielectric Spectroscopy

Raihan Binti Sulaiman
Faculty of Electrical Engineering
Universiti Teknologi Malaysia (UTM)
Johor, Malaysia
raihansulaiman94@gmail.com

Zuraimy Adzis
Department of Electrical Power Engineering
Universiti Teknologi Malaysia (UTM)
Johor, Malaysia
zuraimy@fke.utm.my

***Abstract*—This project aims to provide prevailing method of assessing moisture content in oil-paper insulated power transformers. The effect of high moisture content due to existing of water can leads to three dangerous effects: it decrease the dielectric withstand strength, accelerates cellulose aging and causes the emission of gaseous bubbles at high temperatures. The moisture content can be determined by using dielectric dissipation factor test (tan δ) measurement. From tan delta measurement, the condition of solid/liquid insulation can be determined. However, from tan δ measurement, the causes of moisture assessment cannot be determine either it is from paper or oil. Frequency dielectric spectroscopy (FDS) measurement is one of dielectric response test to determine the moisture content in oil-paper transformer by using new technique of analysis with Omicron DIRANA. This new method is based on the comparison of onsite FDS measurement with a modeled dielectric response of the database from the software and measurement on oil and paper samples for control result by injecting 200 V of AC voltage with frequency of 0.1 mHz.**

Keywords—Power transformer, moisture content, frequency dielectric spectroscopy, FDS measurement.

I. INTRODUCTION

Power transformer are the most expensive equipment in the transmission network for electrical energy in order to supply electrical energy from generation to the users [1]. However, probability of failure occurs increase due to components deteriorate as the transformer ages. Dryness and ageing state of the oil-paper insulation level are important to determine the reliability of the transformers since moisture has deleterious effect on dielectric and insulation ageing [2].

Most of electrical equipment need to undergo maintenance service to ensure the effectiveness of the equipment. There several diagnostic tests for power transformer. Since this research are more focusing in moisture assessment, the preferable tests would be dielectric response test of frequency dielectric spectroscopy measurement that also known as FDS measurement. Today, Omicron DIRANA software is the best analyzer for FDS measurement.

Moisture content problem will affects the reliability and contribute to the ageing process of the power transformer. Before this, conventional method was used to determine the moisture content of power transformer by using the moisture equilibrium diagram. However, this conventional method may not be able give accurate data such as an over estimated value of moisture content and inapplicable to calculate the moisture in paper and oil.

There are several tests method to determine the moisture content in power transformer. Usual diagnostic test to monitor transformer oil-paper insulation condition such as dielectric dissipation factor also called as tan δ measurement cannot identified the causes of moisture content, either it is from paper or oil.

The effect of both moisture assessment method above will lead to inappropriate maintenance action might be performed in power transformer due to leak of information on analyzing data of the moisture content. Basically, there are two method to perform maintenance service to recover moisture content problem in transformer. If the moisture content in cellulose, transformed need to dried up and if the moisture content in oil, the transformer need to filter up remove the impurities in oil.

This project focused on improvement of moisture assessment using frequency dielectric spectroscopy (FDS) measurement. The database of the dielectric response of real transformer using Omicron DIRANA software was analyze and experimental on real transformer oil (new and ageing) and pressboard only conducted.

II. LITERATURE REVIEW

A. *Dielectric Dissipation Factor (tan δ)*

Dielectric dissipation factor also known as tan δ measurement is one of routine diagnostic test for power transformer performed by the manufacturer and related industry up until now. The purpose of this measurement is to monitor the condition oil-paper insulation. The data collected from this measurement will give the rate of deterioration of the health of insulation in power transformer [4]. However, tan δ only measured the dielectric loss but can determine the dielectric strength. This measurement was performed on each winding to ground and each winding to all other windings in the transformer in order to evaluate the insulation system. Parameter that will measured was current leakage through the insulation and dissipation power factor calculated as the ratio of the watt-loss to the apparent power input.

In order to determine the condition of oil-paper insulation in transformer, the percentage of tan δ must not exceed 1% to consider the transformer is dry. Otherwise, the transformer will estimate as in wet condition and need proceed to suitable maintenance service. However, from this measurement, the causes of the moisture content cannot be determine either it is from paper or oil.

B. Conventional Methods

- Moisture equilibrium

This method consist of three steps: (1) Sampling of oil under services conditions, (2) Measurement of water content by Karl Fisher Titration and (3) Deriving moisture content in paper through equilibrium diagrams from moisture in oil [1]. Percentage of moisture content in oil-paper insulation of transformer was analyze as figure below.

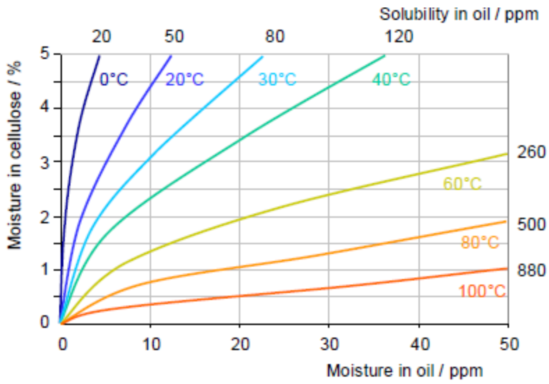

Fig. 1 Moisture Equilibrium [1]

Unfortunately, this approach is not been reliable due to sampling and analysis errors, unequal moisture distributes between cellulose and oil and also equilibrium condition are rarely achieved because it is depends on temperature after hours/days/months. [1], [5].

- Moisture in Oil Measurement

Previously, moisture in oil measurements was used to estimate the dryness of transformer. Essentially, the condition of oil-paper insulation can be interpret according to tables below.

Table 1 Interpretation of % saturation of water in oil, published by [6]

% Water Saturation of oil	**Condition**
0-5	Dry insulation
6-20	Moderate to wet. Lower numbers indicate fairly dry to moderate levels of water in the insulation, whereas values towards the upper limit indicate moderately wet insulation
21-30	Wet
>30	Extremely wet

Table 2 Interpretation of % moisture by dry weight of paper, published by [6]

% Moisture by dry weight in paper	Condition
0-2	Dry paper
2-4	Wet paper
>4.5	Excessively wet paper

After determine the moisture content in oil at certain temperature, the corresponding moisture content for the paper may be estimated from Fig. 2. Percentage of moisture by dry weight of cellulose insulation can be determine by following these five steps: (1) Determine PPM of H2O, (2) Determine temperature of the bottom sample, (3) add 5°C in the temperature of the bottom sample, (4) From graph using the temperature, get the value of correlation multiplier and (5) Percentage of moisture by dry weight of cellulose insulation will determine after multiply PPM of H2O by correlation multiplier [6]

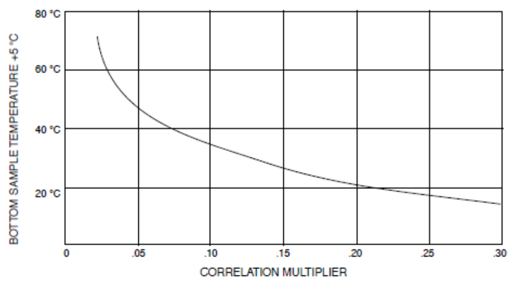

Fig. 2 Percent moisture of dry weight of cellulose insulation [6]

However, water content in the oil and oil condition are very dependent on temperature. Hence, overestimation of moisture content might be occurs during the analysis.

C. Frequency Dielectric Spectroscopy (FDS)

Frequency dielectric spectroscopy (FDS) is one of dielectric response methods that most suitable to determine moisture content power transformer. The fundamental of FDS measurement is to measure the dissipation factor (tan δ) and complete capacitance as a function of frequency [7]. FDS will measure the response from sinusoidal excitations at different frequency where the frequency range of the measurements are from 0.1 mHz to 1 kHz [5]. This method also allows the measurement of the composite insulation capacitance, permittivity, conductivity and loss factor based on frequency [8]. Complex capacitance is assume as test object and current I (ω) can be measured from the relationship complex capacitance and applied voltage V (ω) as follow:

$$I(\omega) = j\,\omega\,C(\omega)\,V(\omega) \tag{1}$$

$$I(\omega) = j\,\omega\,[C'(\omega) - C''(\omega)]\,V(\omega) \tag{2}$$

where C’ (ω) is the real component and C” (ω) is the imaginary part of the dielectric capacitance. Besides that, complex relative permittivity ε’ (ω), real and ε’ (ω), imaginary at the frequency of applied voltage are enables [5], [8]. Thus, the loss factor tan δ in FDS can be defined as follow:

$$\tan\delta = \frac{\varepsilon''(\omega)}{\varepsilon'(\omega)} = \frac{C''(\omega)}{C'(\omega)} \quad (3)$$

The value of tan δ against frequency will determine the condition of oil and paper of the power transformer. Fundamentally, if the value tan δ and capacitance are higher at lower frequencies, the higher the temperature and water content in power transformer [8]. FDS measurement have various type of technique to perform. Previously, FDS measurement by using Insulation Diagnostics System IDA 200 from GE Energy and analyze the database with MOD V.1.5 software [3]. However, this approach take around 11 hours to complete which is need more time consuming to monitor.

D. Omicron DIRANA

Firstly, the new dielectric response method use Omicron DIRANA (Dielectric Response ANAlyzer) equipment to conduct FDS measurement [9]. The combination of time domain and frequency domain is one of the advantage of Omicron DIRANA which is can reduces the measurement time compared to existing techniques since there are two input channels in this equipment.

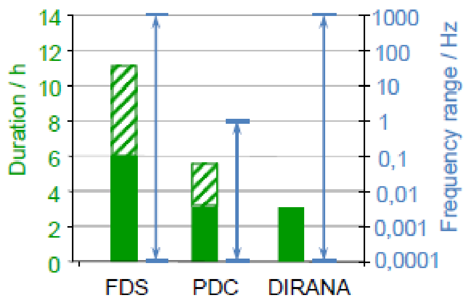

Fig. 3 Time duration required and frequency range acquired for different measurement approach [9]

Other than that, Omicron DIRANA can provide high accuracy and precise measurement at all temperature level and determine the moisture content in oil-paper insulation in order to give accurate condition assessment [10]. Moreover, this technique is based on international standard, IEC 60422 to analyze moisture assessment in power transformer.

Omicron DIRANA also come up with DIRANA software which is easy to use and very efficient. The software give user choice either to choose basic moisture assessment for beginner or extended moisture assessment for experts [10]. This software will give reliable even though the FDS measurement data was collected from aged oil-paper insulation of power transformer. The benefits of using this analyzer, moisture content and oil conductivity are automatically analyze and compensation for temperature and insulation geometry.

III. Project Methodology

In the real transformer, FDS measurement was performed on each winding to ground and each winding to all other winding in transformer. The database from FDS measurement will evaluate the condition of the insulation system with the plotted graph of tan δ against frequency. Capacitance between HV and LV winding (CHL) give valuable information to determine the water content of the main insulation but the value of moisture content that have measured between low voltage winding to ground (CL) and high voltage winding to ground (CH) are recorded as the references during the analysis of the data.

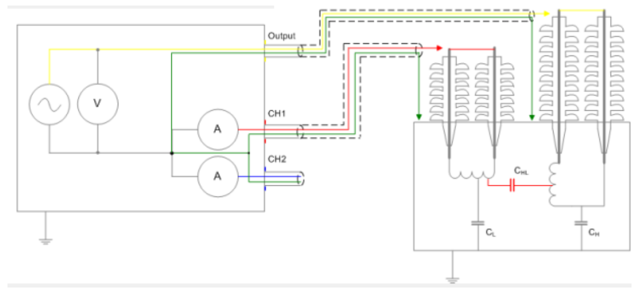

Fig. 4 Configuration of FDS measurement on real power transformer

Based on FDS measurement conduct by TNBR in real transformer, the data was analyze using Omicron DIRANA software. The guidelines to interpret the results of FDS measurement followed by IEC 60422 standard as shown in table 3 and table 4 [10].

Table 3 Percentage of moisture in cellulose on power transformer

Moisture Categories For Cellulose	
Dry	≤ 2.2 %
Moderately wet	2.2 % up to 3.7 %
Wet	3.7 % up to 4.8 %
Extremely wet	≥ 4.8 %

Table 4 Value to analyze the oil conductivity in power transformer

Oil Conductivity		
Very good	0 pS/m up to 16 pS/m	
Good	17 pS/m up to 110 pS/m	
Satisfactory	120 pS/m up to 320 pS/m	
Unsatisfactory	≥ 330 pS/m	

By referring both tables, the condition of oil-paper insulation system on power transformer can be determined and the suitable maintenance service for power transformer due to existence of moisture content can be performed.

A. Experimental flow

According to flowchart that illustrate in Fig. 5, new and ageing oils of real transformer, mineral oil (Hyrax oil) was impregnated with new and immersed pressboard (thickness of pressboard: 1 mm) for control results of FDS measurement in laboratory.

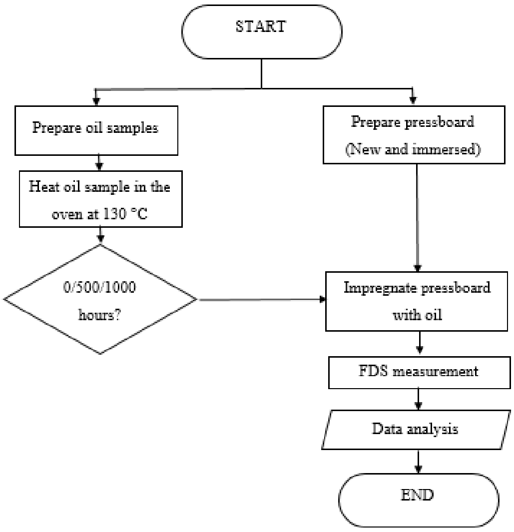

Fig. 5 Experiment flowchart

B. Sample preparation of oils and pressboard

- Hyrax oil was prepared as in Fig. 6, Fig. 7, Fig. 8 and Fig. 9.
- Oils sample undergo process of thermal ageing process with temperature of 130°C for 500 hours and 1000 hours of ageing process.
- New pressboard and immersed pressboard was prepared as fig. 10 and fig. 11.

Fig. 6 Transfer oil samples to measuring jug

Fig. 7 Filtered oil samples before inserted to the glass bottle

Fig. 8 Filled argon gas to the oil samples

Fig. 9 oil samples are heated in an oven

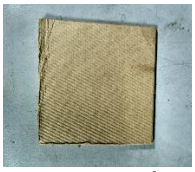

Fig. 10 New pressboard

Fig. 11 Immersed pressboard

C. Experimental setup

Basically figures below are the experimental setup of FDS measurement.

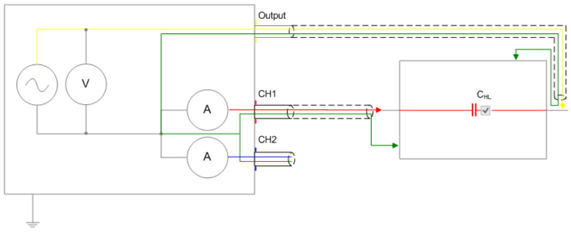

Fig. 12 FDS measurement schematic circuit diagram

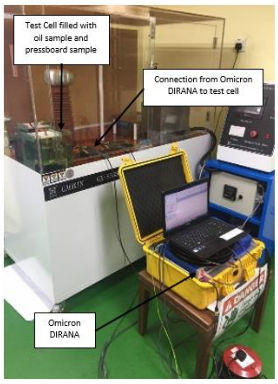

Fig. 13 FDS measurement setup

D. Measuring procedure

To perform the experiment, procedure below must being followed;

- The oils sample and pressboards sample were prepared.

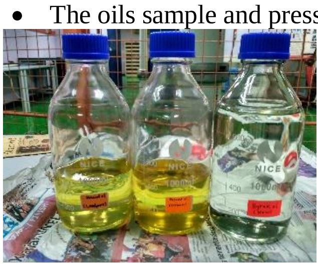

Fig. 14 Oil samples

Fig. 15 pressboard with 1 mm thickness

- New Hyrax sample and new pressboard were placed in the test cell.

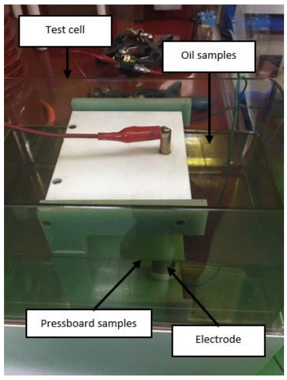

Fig. 16 Test cell use to impregnated oil samples and pressboard samples

- The test cell was placed on the test table. The test cell was connected to grounding wire and voltage wire.

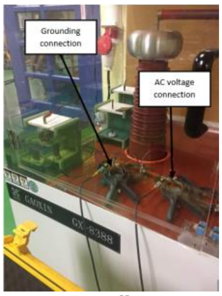

Fig. 17 Test cell connection

- Through Omicron DIRANA software, 200 V of AC voltage was injected at 0.1 mHz and its took around 3 hours to complete the measurement.

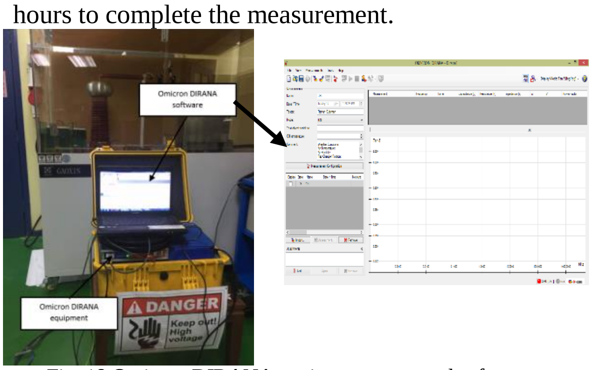

Fig. 18 Omicron DIRANA equipment setup and software

- All steps above were repeated for 500 hours and 1000 hours oil samples with new and immersed pressboard for control results.

IV. Result And Discussion

This project begins with analyzing the data of FDS measurement on power transformer from TNBR to prove reliable method to determine the existed of moisture content in the power transformer. As for control results, the main insulation of power transformer which are oil and paper were used as variable in the experimental. The sample of real oil transformer (Hyrax oil which also known as mineral oil) with the sample of pressboard to be undergo FDS measurement.

A. FDS measurement data from TNBR

Table 5 Data analysis of FDS measurement from TNBR

Type of Transformer / **Characteristics and results**	**P**	**Q**	**R**	**S**
Manufacturer	MTM	MTM	MTM	Bonar long com.
Year manufacturer	2009	1998	1997	1978
Rated voltage	33/11 kV	33/11 kV	33/11 kV	22/6.6 kV
Rated capacity	30 MVA	30 MVA	30 MVA	12.5 MVA
Moisture content (%)	1.6	3.6	3.8	4.8
Condition	Dry	Moderately wet	Wet	Extremely Wet

Oil conductivity (pS/m)	5.4	85	69	88
Condition	Very good	Good	Good	Unsatisfactory

The data from table 5 shows the results of FDS measurement for real power transformer. By referring to Fig. 19, lower frequency range indicates cellulose dielectric loss is the main factor while at medium frequency range, oil conductivity is the dominant contributor of the moisture content. Next, at higher frequency range, the cellulose and the oil volume determine the dielectric loss which the moisture content in power transformer may be due to both factor. The graph for each FDS measurement result from table 5 was plotted according the reading of moisture content and oil conductivity. From graph, the factor moisture content can be identified. As for oil, the conductivity of oil must be near to 0 pS/m because oil in power transformer is act as insulation and heat should not be released from oil.

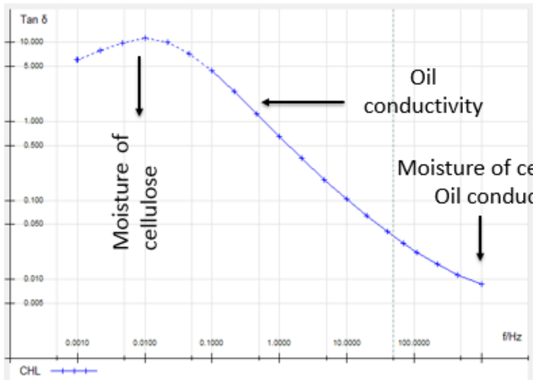

Fig. 19 Graph for FDS measurement analysis

B. Control results from oil and pressboard samples

Table 6 Data analysis for control results

Type of oil	**Type of paper**	**Moisture content (%)**	**Condition**	**Oil Conductivity (S/m)**	**Condition**
New	New	4.7	Wet	100 p	Unsatisfactory
New	Immersed	3.5	Moderately wet	3.7 n	Unsatisfactory
500 hours	New	3.5	Moderately wet	3.5 n	Unsatisfactory
1000 hours	New	4.6	Wet	160 p	Unsatisfactory
1000 hours	Immersed	3.7	Wet	1.9 n	Unsatisfactory

From table 6, results for new oil sample and new pressboard shows that for moisture content, the condition considered to be wet. Fundamentally, the condition of paper insulation should be dry since the pressboard sample not undergo any immersed process with oil. However, there are a few factor that might be effect the result for the new pressboard sample. By referring to oil conductivity condition illustrated all oil conductivity in unsatisfactory condition. Hence, due to oil conductivity condition, the condition for moisture content in paper might be affected. As for result for oil conductivity, the oil might have contamination in oil samples since there are liquid above Hyrax oil tank before taking to transfer to the glass bottle that lead to the results in table 6.

CONCLUSION

FDS measurement method help most of electrical power industrial to monitor the condition of the insulation in power transformer. By using Omicron DIRANA software, the result of the moisture assessment in power transformer is more reliable than previous method. As for control result that have been conducted in this project, the effect of the oil condition might give inaccurate results. However, FDS measurement method is practically perform in real power transformer and it was proven by most of industrial company that perform services in electric power.

REFERENCES

[1] M. Koch. (2008). Reliable moisture determination in power transformer. Stuttgart: Stuggart University.

[2] S.M Gubanski, P.Boss, G. Csepes, V. Der Houhanessian, J. Filippini, P. Guuinic, U. Gafvert, V. Karius, J. Lapworth, G. Urbani, P.Werelius, W. Zaengl. (2002). Dielectric response methods for diagnostics of power transformer. Paris: Cigre 254.

[3] M. Koch, S. Tenbohlen, M. Kruger, A. Kraetge. (n.d.). Improved moisture analysis of power transformer using dielectric response methods. Stuttgart: Mat Post 07.

[4] B.D. Malpure, K. Baburao. (2007). Failure analysis and diagnosis of power transformer using dielectric dissipation factor. Mumbai: IEEE

[5] S.M. Gubanski, J. Blennow, B. Holmgren, M. Koch, A. Kuenchler, R. Kutzner, J. Lapworth, D. Linhjell, S. Tenbohlen, P. Werelius. (2010). Dielectric response diagnoses for transformer windings. Cigre 414.

[6] IEEE Std 62-1995. (1995). IEEE Guide for diagnostic field testing of electrial power apparatus- Part 1: Oil filled power transformers,regulators and reactors, 37-39.

[7] J H Yew, T K Saha, A J Thomas. (2006). Impact of temperature on the frequency domain dielectric spectroscopy for diaagnosis of power transformer insulation. Queensland: IEEE.

[8] A. Setayeshmehr, I. Fofana, C. Eichler , A. Akbari, H. Borsi and E. Gockenbach. (2008). Dielectric spectroscopy measurements on transformer oil-paper insulation under controlled laboratory conditions. Hanover: IEEE.

[9] M. Koch, S. Raetzke, M. Krueger. (2010). Moisture diagnostics of power transformer by a fast and reliable dielectric response method. Klaus: IEEE.

[10] DIRANA: Dielectric response analysis and moisture in oil-paper dielectrics (OMICRON L2277). (2016). Klaus: OMICRON.

Characterisation of Arcing in Malaysia Domestic Wiring

Norshafiza binti Moktar
Faculty of Electrical Engineering
Universiti Teknologi Malaysia
Johor Bahru, Malaysia.
shafizamoktar@gmail.com

Dr. Zuraimy bin Adzis
Institute of High Voltage & High Current
Faculty of Electrical Engineering,
Universiti Teknologi Malaysia,
81310 Johor Bahru, Malaysia.
zuraimy@fke.utm.my

***Abstract*— Arcing is one of the most dangerous phenomenon that can occur in domestic wiring as it can cause fires, injuries, death and property losses. This paper discuss the characterisation of arcing which is series and parallel that occurs in domestic wiring. For this project, the series and parallel arcing is generated using 240Vrms single phase power supply. The voltage characteristics of these arcing is monitored using oscilloscope. There is a voltage drop during both parallel and series arcing.**

Keywords—series arc; parallel arc; arc voltage; arc fault; characteristics

I. Introduction

In this era of development, the electrical protection system for domestic application has become more important for the safety of the residents and the electrical equipments that is the necessities in people's lives such as computers, refrigerator and air conditioners [1]. The current electrical safety devices (circuit breakers) used in Malaysia domestic wiring are Miniature Circuit Breaker (MCB) and Residual Current Circuit Breaker(RCCB) that protects from overcurrent and ground faults which is common in single-phase power system [2]. However, one of the most dangerous phenomenon that can occur in domestic electrical system is arcing fault. Defined by UL1699, arcing fault is “an unintentional arcing condition in a circuit” which is the flow of current through the air between phase conductors or neutral or ground [3][4]. In USA, home electrical fires that are associated with arcing is high according to United States Fire Administration (USFA), with more than 40,000 fires each year that lead to injuries, death, damages and property losses [5].

There are many factors that causes arcing in domestic wiring which is loose connection, accidental cut on the insulation, stressing an extension cord on a single point, natural aging and etc that will lead to electrical fires since current circuit breaker cannot interrupt the circuit during arcing. It is identified that conventional protecting technique is unable to break a circuit in the situation when a brief arc fault occurs and the arc current is below thermal or instantaneous trip levels. Due to this, Arc Fault Current Interrupter (AFCI) is introduced and implemented in countries such as USA and Canada to prevent electrical fires [6][7].

This paper describes the experiment carried out to determine the characteristics of series and parallel arcing in Malaysia domestic wiring.

II. Literature Review

A. Arc Fault

According to studies, low arc fault current which is in between 2A and 10A can cause a high temperature (2000℃~4000℃) that can lead to home electrical fire [1]. Arc is a "continuous luminous discharge of electricity across an insulating medium"[7]. There are two types of arc fault which is parallel and series arc fault which can be seen from figure below.

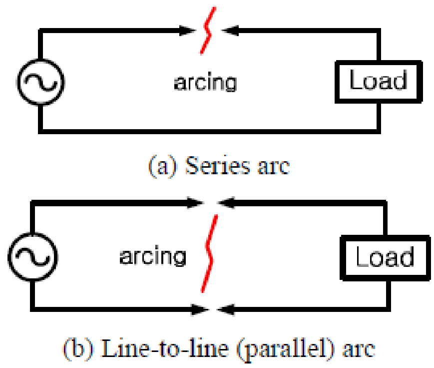

Fig. 1. Series and Parallel arcing

Conventional circuit breaker that is used in domestic wiring cannot detect arc fault current.

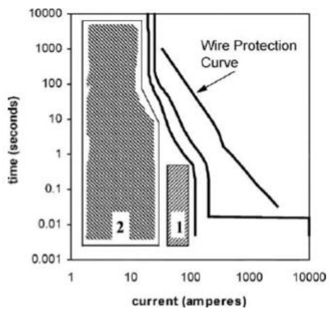

Fig. 2. Time-Current characteristics for a 20A circuit breaker

From Figure 2, the shadowed area represents the range where arc fault current occur. During arc fault, the circuit breaker does not interrupt the circuit since the area is not included in the protection curve. However, the energy from arc fault in region 1 and 2 is ample in causing ignition in flammable materials or organic insulation in a short time despite the small current [1]. Arc fault in region 2 is a series arc that occur in series with load while arc fault in region 1 is a parallel arc fault which occur between live and neutral.

There are many typical characteristics of arc fault waveform such as the difference in sinusoidal waveform of normal AC current and AC arcing current with the presence of 'shoulders' at zero crossing which can be seen in Figure 3 [8].

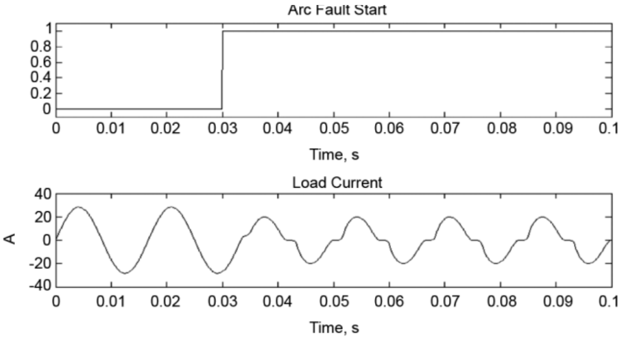

Fig. 3. Waveform when arcing occur

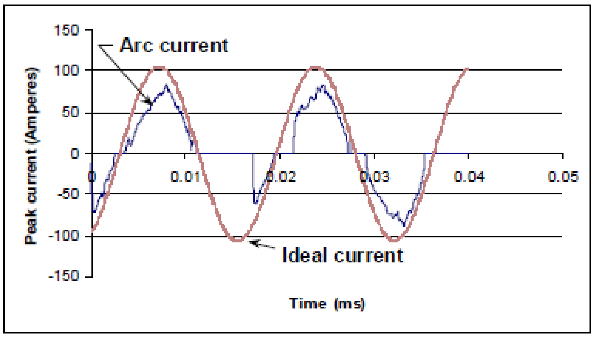

Fig. 4. Normal and parallel arc waveform

B. AFCI

Since the conventional circuit breaker is not effective in detecting arc fault current, Arc Fault Current Interrupter (AFCI) has been introduced to overcome this problem and supported by institutions like Consumer Product Safety Commission (CPSC), National Association of State Fire Marshals (NASFM), the Department of Housing and Urban Development (HUD), and National Electric Manufacturers Association (NEMA) . However, there are certain institutions and individuals that have been questioning the usage of AFCI claiming that the technology has not been proven to be an effective solution to residential electrical fires [4]. Even so, this arc fault detection technology has been accepted and required in new construction.

Apart from detecting arc fault current, AFCI can distinguish the hazardous arc and intended arc. In our home, there are many household appliances that will create arcing like waveform during operation. These arcs are the safe arcs where it will not cause harmful effects to the equipments and will not lead to electrical fire. Thus, AFCI will not trip when arcs caused by normal working appliances such as drills, computer, vacuums and etc occurs.

The ability to detect the harmful arc is the key requirement for the operation of AFCI. Per the 2005 NEC, AFCI combination devices will be required in bedroom circuits beginning January 1, 2008 [4]. The branch/feeder AFCI provides for detection of arcing faults that can occur line-to-line, line-to-neutral and line-to-ground while Combination AFCI has the same protection as branch/feeder AFCI but with additional function that provides for series arc detection down to 5 amperes and beneficial to detect lower level arcing in both branch circuits and power supply cords. From figure, branch/feeder AFCI protects region 1 while combination AFCI protects both region [9].

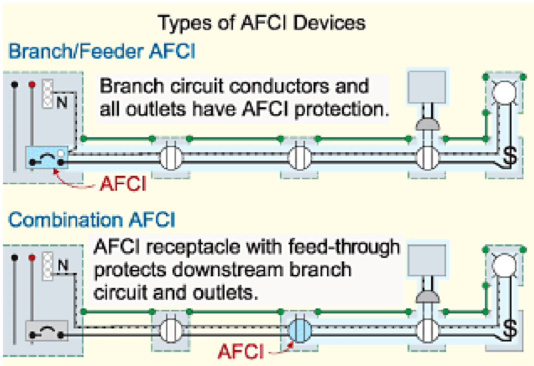

Fig. 5. Types of AFCI devices

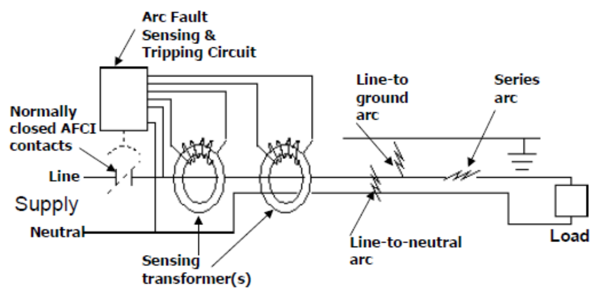

Fig. 6. The AFCI arrangement for arcing detection

III. METHODOLOGY

A. Preparing the workbench

Before doing the experiment to determine the characteristics of parallel and series arcing, a workbench was set up. The workbench consists of main switch, 1 residual current circuit breaker (RCCB), 10 miniature circuit breakers (MCBs), 3 switch for 3 light bulb, 2 3-pin switch, and 3 switch for fault buttons. The circuit connection for the workbench can be seen as the figure below.

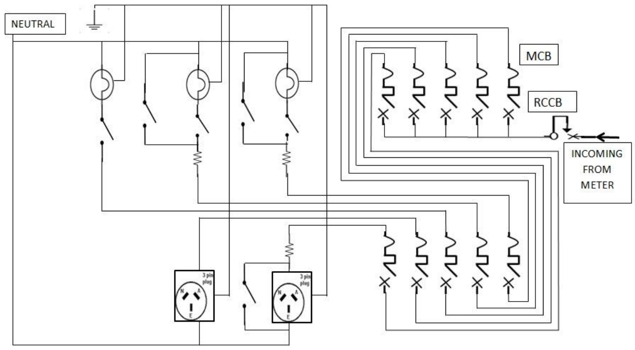

Fig. 7. Circuit connection for the workbench

Fig. 8. Workbench

The workbench is a prepared based on the domestic wiring in Malaysia. This experiment is carried out on a workbench as one of the protection to prevent the arcing from causing damage to the normal working appliances.

B. Generating series and parallel arc

To determine the characteristics of arcing, two types of arcing must be generated which is series and parallel arcing. For parallel arcing, live and neutral wire is used which is parallel to the load while for series arcing, live wire is used that is in series with the load. The load that is used for this experiment is a light bulb. To generate these arcs, vernier caliper is used to close the gap between the wires slowly so that the sparking during arcing can be seen. Besides, the gap need to be close slowly to prevent the wires for touching as it can cause tripping. The setup for generating arcing is shown in the figure below.

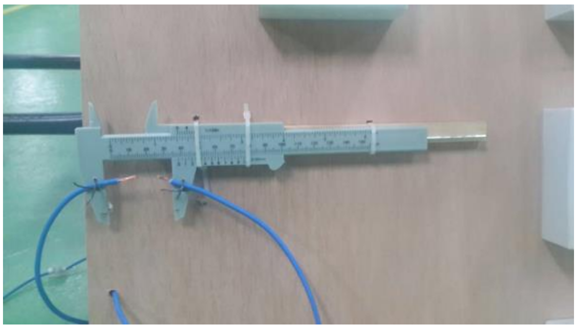

Fig. 9. Setup for generating arcs

C. Characteristics of the arcing

During the generation of the arc, the characteristics of the voltage can be monitored using oscilloscope. Potentiometer is used to reduce the voltage before it is connected to the oscilloscope.

IV. RESULT AND DISCUSSION

For this experiment, when there is no arcing in the circuit, the oscilloscope show normal sinusoidal wave for voltage 240Vrms. During arcing occurrence, there is a significant voltage drop that is monitored through the oscilloscope that is connected in parallel with the point of arcing. These voltage drop is monitored during both series and parallel arcing. The characteristics of the voltage drop for both series and parallel arcing is compared.

During the generation of the arc for parallel arcing, when live and neutral wires are touching, the sparking occur and the MCB tripped. This is due to the high current during arcing which is quite dangerous. To prevent MCB from tripped during parallel arcing, the gap between the wires must be close enough only to get the arcing voltage waveform. The light bulb which is connected parallel to the point of arcing did not light up since the connection is short-circuited. When series arcing occurred, the light bulb flickered as the load is in series with the arc.

V. CONCLUSION

Arcing in domestic wiring is dangerous as it can lead to electrical fires which can bring damage, injuries and even death. For this experiment, the voltage drop between the arcing is compared. For better characterisation of these arcing, the current measurement can be included in the experiment. From the characterisation of these arcing, a low cost indicator that can differentiate and indicate the arc fault can be developed to improve the protection system in domestic wiring since arcing is considered a dangerous occurrence. This development can be an improvement for domestic wiring protection in the future.

REFERENCES

[1] Y. Wu, Z. Song, and J. Wang, "A Method for Parallel Arc Fault Detection and Identification," in Proceedings of the 2nd International Conference on Computer Science and Electronics Engineering, 2013.

[2] A. A. Azzis, N. M. Nor, and T. Ibrahim, "Automated Electrical Protection System for domestic application," in Power Engineering and Optimization Conference (PEOCO), 2013 IEEE 7th International, 2013, pp. 23-28.

[3] D. A. Lee, A. M. Trotta, and W. H. King Jr, "New Technology for preventing residential electrical fires: Arc-fault circuit interrupters (AFCIs)," Fire technology, vol. 36, pp. 145-162, 2000.

[4] D. Li, Z. Song, J. Wang, Y. Geng, H. Chen, L. Yu, et al., "A method for residential series arc fault detection and identification," in 2009 Proceedings of the 55th IEEE Holm Conference on Electrical Contacts, 2009, pp. 8-14.

[5] J. Swart, J. Loud, and D. Slee, "Arcing and fires-case studies," in Product Compliance Engineering, 2009. PSES 2009. IEEE Symposium on, 2009, pp. 1-6.

[6] C. E. Restrepo, "Arc fault detection and discrimination methods," in Electrical Contacts-2007 Proceedings of the 53rd IEEE Holm Conference on Electrical Contacts, 2007, pp. 115-122.

[7] J. A. Wafer, "The evolution of arc fault circuit interrupters," in Proceedings of the Fifty-First IEEE Holm Conference on Electrical Contacts, 2005., 2005, pp. 156-161.

[8] G. Artale, A. Cataliotti, V. C. S. Nuccio, D. Di Cara, G. Tiný, and G. Privitera, "A set of indicators for arc faults detection based on low frequency harmonic analysis," in Instrumentation and Measurement Technology Conference Proceedings (I2MTC), 2016 IEEE International, 2016, pp. 1-6.

[9] G. D. Gregory, K. Wong, and R. Dvorak, "More about arc-fault circuit interrupters," in Industry Applications Conference, 2003. 38th IAS Annual Meeting. Conference Record of the, 2003, pp. 1306-1313.

[10] W. S. Moon, J. C. Kim, A. Jo, S. B. Bang and W. S. Ko, "Ignition characteristics of residential series arc fault in 220V HIV wire," 2014 IEEE Industry Application Society Annual Meeting, Vancouver, BC, 2014,pp.1-5.

Experimental Study of Intended Arcing Characteristic in Single Phase 240V Domestic System

Mohamad Mafazi Bin Mohd Mazlan
Institute of High Voltage and High Current
Faculty of Electrical Engineering
University Teknologi Malaysia
81310 Johor Bahru, Johor
mohamadmafazi@yahoo.com

DR. Zuraimy bin Adzis
Institute of High Voltage and High Current
Faculty of Electrical Engineering
University Technology Malaysia
81310 Johor Bahru, Johor
zuraimy@fke.utm.my

Abstract*— This paper aims to characterize voltage and current waveform during arc occurrence in domestic system. A work bench was designed and constructed for the experiment. The electrical loads used in this experiment were the hammer drill and arc welding. An analysis was done by observing the current waveform through the oscilloscope for both loads during operation. An arc current signature was calculated and plotted in Ms-Excel based on the voltage waveform obtained across the shunt resistor. Each voltage and current waveforms for hammer drill and arc welding have different characteristics observed from their wave-shape. Voltage waveform for hammer drill displayed the peak of waveform being chopped when voltage drop during the arcing. For arc welding exist slope for both positive and negative cycle which result from the arc occurrence. The wave shape for both arc current signatures showed slight difference from the sinusoidal and the hammer drill had sharp peak while arc welding had dull shape. These uniform arcing currents in every cycle and the wave shape of current signature will be used to distinguish intended arc against unintended arc.

Keywords—arc current; ; hammer drill; arc welding;

I. INTRODUCTION

Every house in Malaysia use Miniature Circuit Breaker (MCB) and Residential Current Circuit Breaker (RCCB) as electrical protection in low voltage system. The MCB and RCCB is a safety device for distribution circuit between power source and load in domestic household. In Malaysia, from year 2005 to 2011, there are 405 accidents due to electrical fault event, and 191 people died due to electrical accidents [1]. Another statistic of electrical accident from year 2002 to 2010 showed that about 536 accident cause by electrical been reported. Figure 1 displayed the number of cases reported according to state.

In China, typical distribution systems operate with full grounded for its favorable position of compensating capacitive component of fault current and diminish the speed of recovery voltage of faults. Since single-phase arcing faults is the most regular establishing issue in grounding fault in distribution systems [3].

While in Korea as indicated by the information given by Korea Electrical Security Corporation. Moreover, around 21.3% (9351) flames were created by electric arc. An examination of the causes of electrical flames demonstrates that short circuits because of protection disintegration represented 2287 (24.5%) fires, and unidentified short circuits brought on 2245 (24%) fires. Besides, 722 (7.7%) flames happened because of open circuit, and short circuit because of following brought about 668 (7.1%) fires. In this way, electrical flames because of arc fault represent around 73.2% or 6844 cases [4]. Regarding this statistic, there is no device been created to prevent the electrical cause the fires [5]. A proper electrical safety device should be produce instead rising awareness on electrical safety and hazard to the public.

II. PROBLEM STATEMENT

There are many cases reported on injuries and death to human caused by electrical accident which are about 50.9% reported died and another 49.1% injured. Figure 1.2 showed a pie chart about the percentage of causes for electrical accident over years 2002-2010. The total numbers of cases is 536 with 582 victims involved. The highest number cause the electrical accident happen was improper installation with total of 198 cases follow by working procedure not followed with 166 cases. These two causes should be aware and prevent because it may lead to short circuit fires which very dangerous to people and environment.

About 81 cases happened in domestic between 2002 and 2010. This paper aims to prevent this accident occurred by experimental study to characterize intended arcing in 240V domestic system which can be used for future development electrical protection in south east region.

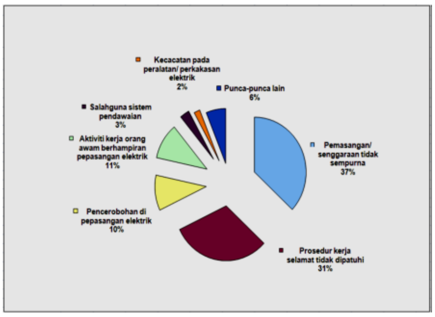

Figure 1: causes for electrical accident over years 2002-2010

III. METHODOLOGY

Flow chart is one way to design this project movement. Figure 4 show the project flow this project from the start until the end. The method uses in this project are measurement of voltage by oscilloscope to observe the behavior sinusoidal wave when arc fault occur and current by using equation ohm's law.

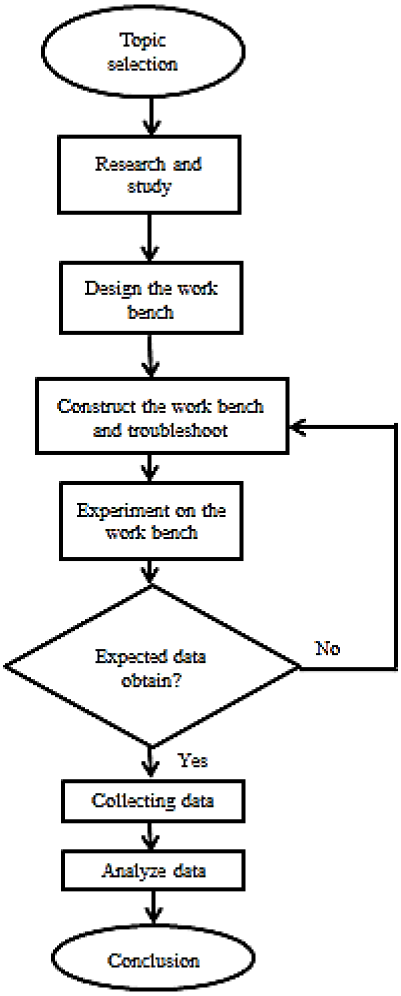

Figure 2: project flow

A. Designed circuit diagram and work bench

Figure 3 show the designed circuit diagram which implement on the work bench. This circuit designs according to wiring for single phase in domestic home.

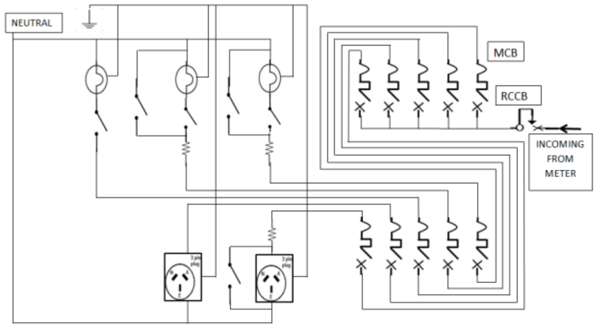

Figure 3: circuit diagram

Figure 4: work bench constructed

B. Point measurement

In this project, an oscilloscope used as measurement tool to observed the waveform of the load when testing. A rheostat also include in this project which is in series with the socket. This rheostat act as resistor with fixed value of resistor, 110Ω. The measurement point was located before and after the rheostat with two probes and both grounds grounding to the ground at distribution board. The design showed in figure 5 and the connection in Figure 6.

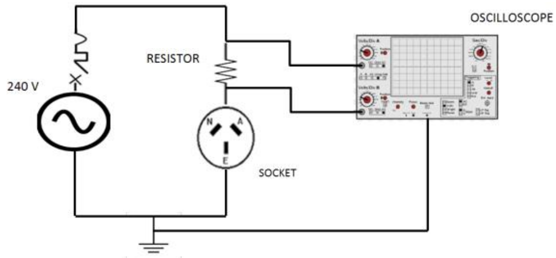

Figure 5 measurement design

Figure 6 measurement set up

Experiment set up

There are two electric load will apply on this experiment which are hammer drill and arc welding.

- Hammer drill: the method use in this experiment is an oscilloscope which to observe the behavior of wanted arc. Hammer drill act as load is plug into the 3 pins socket outlet. The first probe and second probe of oscilloscope connects to before and after the rheostat as the oscilloscope parallel to the load.

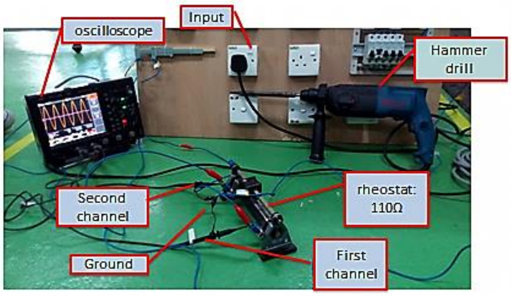

Figure 7: first experiment set up

- Arc welding: for arc welding, the set up same with the hammer drill and just replace the hammer drill with arc welding.

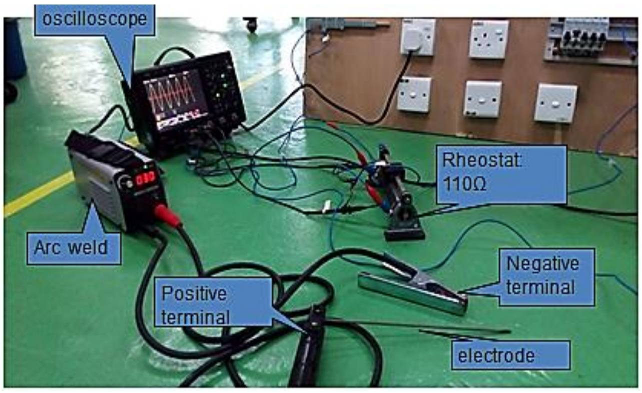

Figure 8: second experiment set up

IV. RESULT AND DISCUSSION

results gained by observing the waveform pattern behavior when the load operating.

A. Hammer drill

A hammer drill was plug to the socket at work bench and observe the voltage waveform when the drill running. Figure 8 show flow of the waveform pattern for the hammer drill.

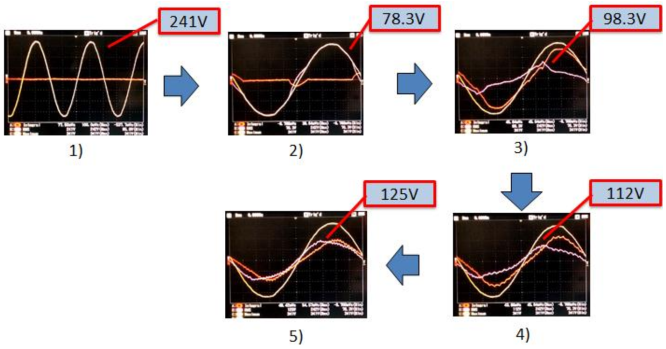

Figure 9: flow of the waveform when operating

The oscilloscope captured a different wave shape from sine wave. Focus on the pink waveform, the peak of the voltage's waveform drop like a peak of mountain being cut into half. This non-sinusoidal shape called harmonic distortion. The waveform corresponded to the sum of different sine waves with the different magnitude and phase, having frequencies that are multiples of power-system frequency.

Table 1: data obtained for hammer drill

Figure	Condition	Voltage Supply (V_{rms})	Voltage across the load	
			V	V_{rms}
1	Before running (open circuit)	240	341	241
2	Current start to draw	240	110.73	78.3
3	Drill gained speed	240	139.02	98.3
4	Before reach maximum speed	240	158.4	112
5	At maximum speed and rotation	240	176.78	125

The arcing phase can be see when focus into the commutating current waveform. From the graph show the current progression is non-sinusoidal wave which indicates that the brush resistance affects the electrical time constant of the commutating circuit during arcing.

The value of current flow calculated using the equation:

$$V=IR \quad (1)$$

Rearrange the equation (1) to get the current by divided the voltage drop across the load with the load (R).

$$I=V/R \qquad (2)$$

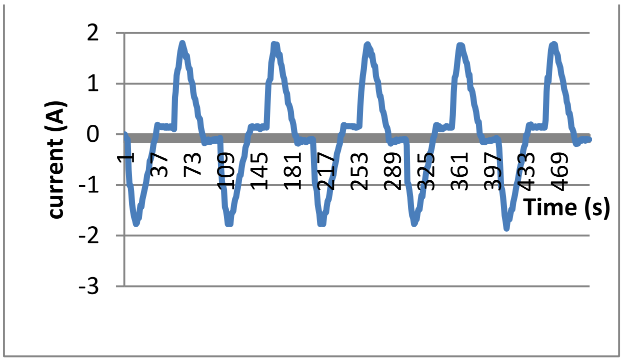

Figure 10: Arc current signature for hammer drill

B. Arc welding

This welding has two terminals which are positive and ground. During welding, the user can set the amperage according to the type of electrode use and the thickness workload. In this experiment, the amperage set to 30 only because the experiment did not use any metal plate and only tapping between the tip of electrode with ground terminal.

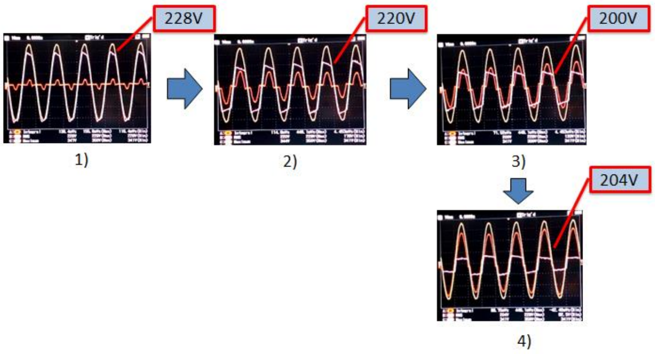

Figure 11: waveform pattern for arc welding

Table 2: data obtained for arc welding

Figure	Condition	Voltage Supply (V_{rms})	Voltage across the load	
			V	V_{rms}
1	Before running (open circuit)	240	322.44	228
2	First tapping	240	311.13	220
3	Second tapping	240	282.84	200
4	Third tapping	240	288.5	204

The oscilloscope captured a different wave shape from sine wave. Focus on the pink waveform, the peak of the voltage's waveform like a slope. In AC welding, the polarity alternated every half cycle. Welding current becomes null at the crossover and reignites in the following half cycle. This arc voltage is called reignition voltage, A. The reignition voltage, A is higher than usual arc voltage, B. In an open circuit voltage of a power source from yellow waveform, must be higher than the reignition voltage, A for AC arc to be sustained.

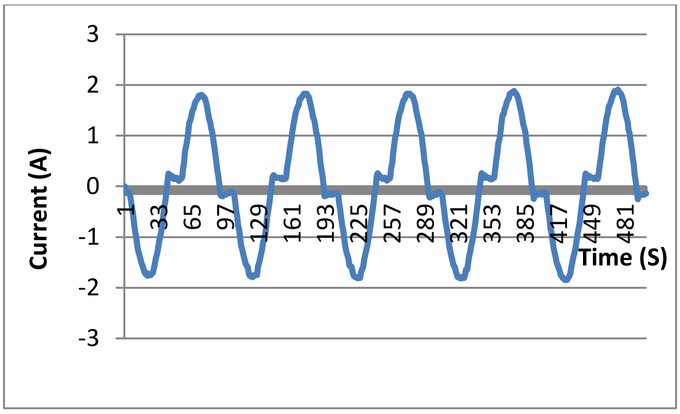

Figure 12: arc current signature for arc welding

Figure 14 showed the instantaneous power graph plotted using Ms-excel based on calculation made. Firstly the data retrieved need to be convert in time based since it was in point form. An interval for a cycle of the waveform equal to 0.02s where the frequency used is 50 Hz. The average power for arc weld is 121.96 Watt and the energy calculated using area under graph is 0.00614 joules. The result of area under graph done by divided the area into small trapezium and totaled all values. The energy produced in positive indicates that arc weld release the energy and the value is small because it happen in very short period.

Comparison between these waveforms for hammer drill and arc welding showed each voltage waveform had their own characteristic. Voltage waveform for hammer drill displayed the peak of waveform had been cut to half because of voltage drop during the arcing. For voltage waveform for arc welding had slope for both positive and negative cycle which result from the arc occurrence. The value of power and energy also different because there is rectifier and capacitor installed in hammer drill which energy is absorb while for arc welding is release the energy. The wave shape for both arc current signatures showed slightly different from the sinusoidal and the hammer drill had sharp peak while arc welding had dull shape. These uniform arcing currents in every cycle and the wave shape of current signature will be used to distinguish intended arc against unintended arc.

V. CONCLUSION

In conclusion, based on the objectives of the study, the experiment conducted to determine the pattern of voltage and current waveform when arcing occur achieved. Arc current signature was constructed successfully in this project by using Ms EXCEL. The outcome of this experimental study was attained to achieve the objectives of this project which are:

i. To study and review on application and properties of electric arc

ii. Construct and experiment on the work bench to characterize the arcing

iii. Observe the waveform pattern in application manifest arcing and measure the voltage and current when arc occur

A review had been made and found that almost none of electrical protection for arcing in the south East Asian region. Mostly in US region, they already develop a devise to prevent the arcing named Arc Fault Current Interrupter (AFCI). A workbench successfully and used the work bench to experiment and testing. . The observation made through the potentiometer which in series the socket where the load plug in. the data obtained from the oscilloscope characterized by the uniform arcing current and the current wave shape of the current signature. These uniform arcing currents in every cycle and the wave shape of current signature will be used to distinguish intended arc against unintended arc.

References

[1] "191 Mati Akibat Kejutan Elektrik", Utusan Newspaper Article, 2011.

[2] “Analisa Kemalangan Elektrik di Malaysia bagi tahun 2002 hingga 2010, Jabatan Kawalselia Keselamatan Elektrik,” Suruhanjaya Tenaga,2010.

[3] Bo Zhang, Qing Yang, Wenxia Sima, Ming Yang, Jiaquan Ran, “Automatic Suppression of Single Phase Arcing Fault In AC Distribution systems ” National Natural Science Foundation of China (51477018)

[4] “A Statistical Analysis on the Electrical Accidents in 2011,” Korea ElectricalSafety Corporation, Seoul, Korea, 2012

[5] Won-Sik Moon, Jae-Chul Kim, Ara Jo, Sun-Bae Bang, “Ignition Characteristic of Residential Series Arc Fault in 220-V HIV Wires, ” IEEE Transactions on Industry Applications, Vol. 51, NO. 3, May/June 2015

[6] Antoni Sawicki, “Approximations of arc voltage-current characteristics in electrotechnological device,” Biuletyn Instytutu Spawalnictwa, Faculty of Electrical Engineering, Czestochowa University of Technology, No. 6, 2013.

[7] V. Terzija, V. Koglin, “A new approach to arc resistance calculation,” Journal of Electrical Engineering, Volume 83, Issue, 187-192, 2001.

[8] V. Terzija, V. Koglin, “ A novel on the modeling of long arc in still air and arc resistence calculation,” IEEE Transaction on Power Delivery, 1102-1107, 2004.

[9] Jonathan Andrea, Patrick Besdel, Olivier Zirn and Marc Bournat, “The electric arc as a circuit component,” IEEE, IECON2015-Yokohama, 2015

[10] C. E. Restrepo, "Arc fault detection and discrimination methods," in Electrical Contacts-2007 Proceedings of the 53rd IEEE Holm Conference on Electrical Contacts, 2007, pp. 115-122

[11] Wu, Z. Song, and J. Wang, "A Method for Parallel Arc Fault Detection and Identification," in Proceedings of the 2nd International Conference on Computer Science and Electronics Engineering, 2013

[12] G. Artale, A. Cataliotti, V. C. S. Nuccio, D. Di Cara, G. Tiný, and G. Privitera, "A set of indicators for arc faults detection based on low frequency harmonic analysis," in Instrumentation and Measurement Technology Conference Proceedings (I2MTC), 2016 IEEE International, 2016, pp. 1-6

[13] Abdillah Fashiha Ilman, Dimas Anton Asfani, Yuslistya Negara, Daniar Fahmi, “ Design of Low Voltage Arcing Identification Based on Wavelet Transform, ” International Seminar on Application for Technology of Information and Communication 2016.

[14] G. D. Gregory and G. W. Scott, “The Arc-fault circuit interrupter: An Emergency product,” IEEE Trans. Ind. Appl., vol. 34, no. 5, pp.928-933, Sep. /Oct. 1998.

[15] Wu,Yuan, "A Method for Arc Fault Detection Based on the Analysis of Signal's Characteristic Frequency Band with Wavelet Transform". International Conference on Electric Power Equipment, Japan.2013. Hal 1-4

[16] J. Swart, J. Loud, and D. Slee, "Arcing and fires-case studies," in Product Compliance Engineering, 2009. PSES 2009. IEEE Symposium on, 2009, pp. 1-6.

[17] D. A. Lee, A. M. Trotta, and W. H. King Jr, "New Technology for preventing residential electrical fires: Arc-fault circuit interrupters (AFCIs)," Fire technology, vol. 36, pp. 145-162, 2000.

[18] G. D. Gregory, K. Wong, and R. Dvorak, "More about arc-fault circuit interrupters," in Industry Applications Conference, 2003. 38th IAS Annual Meeting. Conference Record of the, 2003, pp. 1306-1313.

Development of Permanent Fault Indicator for Miniature Circuit Breaker

Mohamad Nasharuddin Bin Mohamad Rosli
Faculty of Electrical Engineering,
Universiti Teknologi Malaysia,
81310 Johor Bahru, Malaysia
nasharuddin_90@yahoo.com

Dr Zuraimy Bin Adzis
Institute of High Voltage & High Current
Faculty of Electrical Engineering,
Universiti Teknologi Malaysia,
81310 Johor Bahru, Malaysia
zuraimy@fke.utm.my

***Abstract*— Ability of miniature circuit breaker (MCB) to cut-off the circuit when there was a fault could safe many lives in homes instead industrial areas from electrocuted. That is why it needs to be applied in every single wiring system. This research was conducted to develop a prototype for permanent fault indicator (PFI) that will stick to the MCB. This PFI could improve the performance of MCB where it can last for a long time and reduce the time require when doing maintenance. Current design of MCB was taken as a template to build a retrofitable PFI which it can easily attach to and detach from the MCB. A test for reliability was conducted by turn on and off the MCB until the indicator cannot be used and the time MCB was turned on-off is counted and recorded. The output of the test is that when the fault occurs in the circuit, the indicator will light up and continue to light up until the fault is repaired. This is also an indicator for maintenance officer to not turn on yet the MCB. The PFI also is reliable which it does not easily broken even one hundred times turn on-off the MCB. Development of PFI able to increase the life span of the MCB by reducing vibration caused by turning on-off of the MCB.**

Keywords—miniature circuit breaker; permanent fault; retrofitable; reliability; maintenance.

I. INTRODUCTION

Miniature Circuit Breaker (MCB) is famously used in commonwealth country like Canada, Britain and other include Malaysia. Generally, MCB is widely used for household and any similar installations [10]. The purpose of the MCB is to protect people and the electrical appliances from damaged when there is a permanent fault which is live wire and neutral wire shorted or overload occur in the circuit that cause thermal effects. Either those cases occur, the MCB should be able to break the circuit. Theoretically, when the circuit is shorted the resistance would get to zero and by Ohm's law the current will go to infinity or very high.

Basically, MCB will be tripped if current value reaches around 16 Ampere and some trips at 10 Ampere depend on the characteristic of the MCB. Trip coil inside the MCB will be heated and at some point it will disturb the latch point and cause the MCB trip. Malfunction of circuit breaker will allow the fault occur freely in the circuit, increase current flow and affect user's energy usage. This was a money-waste which the user needs to pay more for the energy that they not even used it. This will cause the household to be broken and sometime it would explode and start a fire. Sometime it has a delay to cut the circuit or the lever goes down (trip) while the circuit still complete. The worst case may happen that it exploded and break the device, and hurt people around it.

There were many factors that lead MCB to be malfunction and one of them is vibration. The vibration that occur to the MCB if happen continuously can cause the mechanical parts getting loose and this reduce its effectiveness to break the circuit well. Miniature Circuit Breaker construction is simple and it has no replacement parts which it is simply replaced when the unit goes badly [3]. Due to its important function, performance of the circuit breaker needs to be improved. So, reliability of the MCB should be in high grade.

By locating an indicator at MCB will improve the reliability of MCB by giving a signal whether the circuit already repaired yet. The indicator will light up if the fault still exists in the circuit. Maintenance works should be easier to be done than before which you need to turn on-off the MCB to know whether the circuit is repaired yet.

A. The objectives of the project are as follows:

- To design a retrofitable prototype for Permanent Fault Indicator (PFI).
- Fabricate and testing the prototype of Permanent Fault Indicator.
- Run reliability test for Permanent Fault Indicator for Miniature Circuit Breaker.

B. Scope of the project is as follows:

- Miniature Circuit Breaker design is used as model in this project for sizing Permanent Fault Indicator.
- Neon lamp is used as indicator for permanent fault
- Design software like Solidwork is used to design the Permanent Fault Indicator.
- Reliability of Permanent Fault Indicator will be tested by recording how many lever turn until the neon lamp broken.

II. LITERATURE REVIEW

Research will be cover an analysis on miniature circuit breaker and fault indicator exists on distribution system.

A. Analysis on Miniature Circuit Breaker

MCB today become an alternative to fuse since it does not need replacement if overload or fault is detected. MCB is not practical in America because they use different wiring system which T-N system means supply from transformer and neutral at home or end user while at commonwealth country use T-T system means supply from transformer and neutral at transformer. The purpose of miniature circuit breaker is cut-off the circuit to ensure the safety of the households and people. If the circuit still complete to allow the current flow, the households will break and sometime explode and can cause worse case to occur like starting a fire and hurting people around the broken items.

Theoretically, existence of fault in the circuit will cause the current goes very high and even more than the rated current of MCB, mostly were designed to trip if exceeding 10 Ampere. It has minimum time-delay for MCB to trip after high current detected which is 10 millisecond [6]. The construction of MCB also is simple. It has no replacement parts but if the device breaks, it is required to replace with the new one [3].

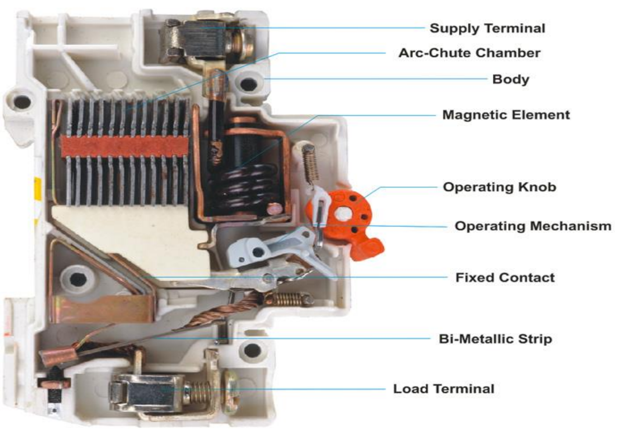

Fig. 1. Cross section of miniature circuit breaker

The trip coil is sensitive to heat. This part acts to protect the conductors and other parts inside the MCB. Existence of fault will cause the current goes very high and influence the temperature in the cable to goes high. At certain temperature later heat the trip coil to expand and disturb the latch point that cause the circuit breaker to trip. Miniature circuit breaker also has probability to work fail.

1) There are 3 types of failure [10]:

a) Operational failure (Heading 4): The miniature circuit breaker cannot break the circuit if it is tripped manually or automatically which high current still flow through the circuit.

b) False operation: Unexpected behavior of the circuit breaker to trip even there is no fault or overload exists in the circuit.

c) Refusing operation: Trip part in miniature circuit breaker does not break the circuit instantaneously.

2) Mechanisms of failure of miniature circuit breaker as follow [9]:

a) The burned failure of the switch: The arc-shaped screw terminal is not fitted with the arc-shaped gasket that cause the contact is not tight enough. The contact will then become loose effect of force from outside or vibration (turn on-off the lever also causes vibration to the device). Later, the contact resistance will increase and wiring terminal is burned.

b) Aging of the switch: This factor is a common cause to all defection of electronic and mechanical device. As the time goes on, the reliability of the material become worse.

c) The electronic component failure: There are resistors, capacitors, diodes, and other elctronic components on the board. Break of stuffs like those components will make the circuit breaker to turn off.

d) Burned failure of the printed circuit board: Affect of very high temperature of resistances on the printed circuit board lead the circuit to burn.

e) Corrosion of the Printed Circuit Board: Because of aging and electrolyte, electrical conductivity of the board surface is increased in the damp air that causes leakage current also increases. Along with the leakage, electrochemical reaction corroded the metals and insulation materials and at last they are destroyed.

B. Current fault indicator exist in distribution system

Fault indicator in distribution system already widely used around the world but in different method for different country and need. One of the methods proposed by [2] was Improved Binary Shuffled Frog Leaping Algorithm (IBSFLA) to find a better place to put the fault indicator in the distribution networks. Locating fault indicators can be done accurately by minimizing of cost function.

Other method is using Global System for Mobile communication (GSM) technology. This technology sends fault information to the center station and then spread the information to the maintenance worker. Next method is by improving the fault localization process. The user will analyze the fault using certain algorithm to detect which devices were defected. Other method that was used in distribution network is Chirp Zeta Transform (CZT) [5]. Basically we need stationary signal to be analyzed and fault signal is non-stationary. With CZT, the non-stationary signal of fault can be transformed to stationary signal.

III. METHODOLOGY

A. Set up the workbench:

First of all, a workbench was prepared. The workbench consist of 1 main switch, 1 residual current circuit breaker (RCCB), 10 miniature circuit breakers (MCBs), 3 switch for 3 bulb, 2 3-pin switch, and 3 switch for fault buttons. All of those were attached to a board. Solidwork software was used to design the permanent fault indicator (PFI). Measurement on MCB should be made carefully in order to make the prototype could fit the MCB well. The prototype was created by 3D printing. Holes were set to the printed for LED and its wiring.

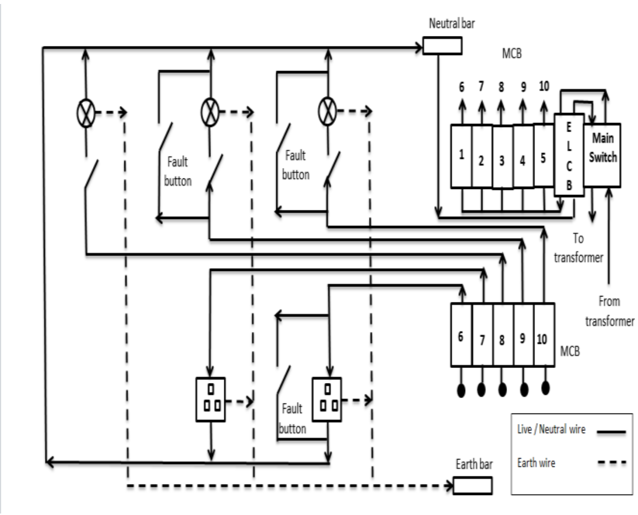

Fig. 2. Wiring for workbench

Fault buttons were connected parallel to the load. Circuit for fault button does not connected to any material or device, still only with resistance of wire. This is to ensure the current will not flow to the load as fault button is turned on. No power at load and the load will malfunction as no current source flow through it. High current will flow to the MCB and tripped because current flow beyond the current limited by the MCB which ten Ampere.

B. Testing for Permanent Fault Indicator (PFI)

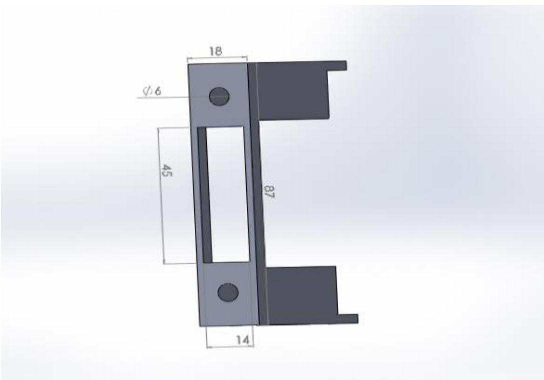

Fig. 3. Design for prototype of permanent fault indicator

Bulb is connected between the incoming and outgoing source of MCB. PFI was attached to one of the MCB. Circuit that connected to the MCB with PFI was tested and shorted by pushing the fault button. The MCB does not trip if no fault occur in the circuit and the indicator does not light up. Lever of MCB will goes down when there is fault in the circuit and automatically turn on the indicator until the fault is being repaired.

Testing for reliability of PFI need more time. Reliability test is done to make sure the PFI can still longer and just like to test for its quality. MCB is turned on and off for multiple times while PFI is attached to it. The times of MCB is turned on and off is counted and recorded. Theoretically, PFI should not be broke easily because PFI only involve bulb and connection wire. PFI could work as long as the MCB could work.

IV. RESULT AND DISCUSSION

Many solutions were created in order to build a retrofitable Permanent Fault Indicator (PFI). Finally, a design of PFI for latest design of MCB successfully built. The PFI could fit exactly as the size of MCB which is it does not take more space than what is prepared for it. This would be easily for anyone to use it and did not need to think much about the other aspect to make the PFI works well.

$$I = V / R \quad (1)$$

$$\alpha + \beta = \chi. \quad (1)$$

(1)

After doing many tests, the data was collected and the result showed as expected. Neon bulb which acts as indicator light up when there is a fault exists in the circuit. When fault occur, high current will flow through the MCB beyond its limit and cause the lever of Miniature Circuit Breaker (MCB) tripped down and this will turn on the indicator. Based on the formula (1), when the circuit shorted the resistance would be very low approach to zero and cause the current went very high. Current is inversely proportional to resistance. Lever of MCB acts as a switch for indicator to turn on-off automatically. If the lever of MCB goes up, the bulb light up, and vice versa.

TABLE I. CONDITION OF ITEMS

Item	**Condition of Item in Stated Situation**	
	Normal	***Fault***
Lever of the MCB	Up	Down
Bulb (Indicator)	Light off	Light on

When the fault occurs, the current will flow through the indicator and cause the bulb light up. The MCB was turned on and off many times. This is because to test for the reliability of the PFI. The result from the reliability test showed that the PFI could stand for a long time even the MCB was turned on-off and does not break easily as it only works electrically compared to the MCB which works consist of electrically and mechanically. Mechanical parts of MCB is broken easily in most cases. The vibration that occur when doing maintenance need to be reduced to minimum. PFI was created to fulfill that demand.

V. CONCLUSION

The design of prototype of permanent fault indicator would increase the performance of Miniature Circuit Breaker. The indicator (neon lamp) gives a hint to the user if they are not repair the fault yet. The user can reduce their energy and time to turn on the MCB by looking at the indicator. This would increase the lifespan of MCB. The prototype also was designed to be retrofitable which it can easily attach to and out from the MCB even normal people can do it by themselves (DIY – Do It Yourself). It is not a big problem if the user wants to repair the fault themselves without wrong-use the circuit breaker. The prototype is predicted can stand for a long time to detect the existence of fault after the reliability test was done.

ACKNOWLEDGMENT

The authors would like to thank Universiti Teknologi Malaysia (UTM), for the use of facilities and supervisor for guiding to finish the project.

REFERENCES

[1] A. Vukojevic, P. Frey and M. Smith, "Making a Smart Grid Case: Fault circuit indicators," 2013 IEEE Power & Energy Society General Meeting, Vancouver, BC, 2013, pp. 1-5.

[2] A. Kimiyaghalam, A. Ashouri and M. Beykverdi, "Application of IBSFLA and BSFLA approaches for locating of fault indicators in distribution networks," 2012 Proceedings of 17th Conference on Electrical Power Distribution, Tehran, 2012, pp. 1-7.

[3] D. Pop, L. Neamt, R. Tirnovan and D. Sabou, "3D finite element analysis of a miniature circuit breaker," 2013 8TH INTERNATIONAL SYMPOSIUM ON ADVANCED TOPICS IN ELECTRICAL ENGINEERING (ATEE), Bucharest, 2013, pp. 1-4.

[4] Feijin Peng, Yuan Qincheng and Yue Liu, "Research and application of new type fault indicator in smart distribution grid," 2014 China International Conference on Electricity Distribution (CICED), Shenzhen, 2014, pp. 67-69.

[5] G. Artale, A. Cataliotti, V. C. S. Nuccio, D. Di Cara, G. Tinè and G. Privitera, "A set of indicators for arc faults detection based on low frequency harmonic analysis," 2016 IEEE International Instrumentation and Measurement Technology Conference Proceedings, Taipei, 2016, pp. 1-6.

[6] H. W. Wolff and T. G. F. Atherton, "Design, performance and application of miniature circuit-breakers," in Proceedings of the IEE - Part A: Power Engineering, vol. 102, no. 3, pp. 364-373, June 1955.

[7] Li Wenhua, Wu Xiaoyong, Zhang Xiaoyan and Yao Fang, "Research on the reliability test control system's design of the miniature circuit breaker," 2009 IEEE International Symposium on Industrial Electronics, Seoul, 2009, pp. 1380-1384.

[8] M. Raphaël and B. Raison, "A probabilistic fault localization method for distribution networks using fault indicators," 2013 IEEE Grenoble Conference, Grenoble, 2013, pp. 1-6.

[9] Y. Xue et al., "Analysis on failure modes of miniature circuit breaker," 2016 IEEE International Conference on Power System Technology (POWERCON), Wollongong, NSW, 2016, pp. 1-4.

[10] YanYan Luo, JianGuo Lu and ZhiGang Li, "Study of reliability test and analysis for miniature circuit breakers," Proceedings of the Forty-Eighth IEEE Holm Conference on Electrical Contacts, 2002, pp. 80-85.

Effect of Pollution and Profile Design on Glass Disc Insulator

Hazreen Elina Nur Ali Za[1], Zulkurnain Abdul-Malek[2]
Institute of High Voltage and High Current
Faculty of Electrical Engineering
Universiti Teknologi Malaysia
Johor Bahru, Malaysia.
[1]hazreenelina@gmail.com, [2]zulkurnain@utm.my

***Abstract*—This paper presents electric potential distribution and electric field stress along the surface of a glass disc insulator subjected to polluted environment and changes in shed region. In this work, the electric potential and field distribution on clean and polluted glass disc insulators were obtained using COMSOL Multiphysics. In addition, the shed of glass disc insulator had been changed to the semi-flat shape to determine the effect on electric field stress on the glass insulator. The simulation results show that the voltage distribution concentrated on the insulator cap. The electric field stress of original profile and semi-flat glass insulator results show that the horizontal electric field stress are the same for both cases while vertical electric field stress of original profile is higher than the vertical electric field stress of semi-flat glass insulator.**

Keywords—glass disc insulator; pollution; semi-flat glass insulator; electric potential; electric field stress

I. INTRODUCTION

Insulators play important role in high voltage performance. In transmission system, the overhead conductors are generally supported by supporting towers or poles. The towers and poles are properly grounded. Therefore, insulators must be placed between tower or pole body and current carrying conductors in order to prevent the flow of current from conductor to the earth through the grounded supporting towers [1]. In this project, glass disc insulator was used as insulating material on the overhead transmission line. This is because in Malaysia, Tenaga Nasional Berhad (TNB) used glass disc insulator on the transmission system. Glass insulator was the earliest insulator used in power transmission system other than polymer or porcelain insulator [2].

Nowadays glass insulator has become popular in transmission and distribution system by many countries including Malaysia [3]. Tough glass insulator is used for insulating purpose. There are a lot of advantages by using glass disc insulator over conventional porcelain insulator [4]. Firstly, glass disc insulator has very high dielectric strength its resistivity is also very high compared to porcelain insulator [1]. Besides that, glass disc insulator has higher tensile strength compared to porcelain insulator [5]. This shown that glass disc insulator is quite tough rather than porcelain insulator. After all, glass disc insulator is cheaper than porcelain insulator [6] that is why it is preferable to use on the power transmission system in Malaysia to have good performance over the years according the environmental condition. Unfortunately, the insulator will having failure after a certain amount of time. In conclusion, a study needs to be done to determine the relationship between environmental conditions together with insulator performance.

Although glass disc insulators have a good performance over the years, failures can and do occur due to inferior design and materials, improper manufacturing, misapplication of the insulator for its intended service environment or extreme stresses linked to weather, vandalism, wildlife or mishandling [7]. The insulators need enough mechanical resistance to maintain the weight, wind and temperature of the surrounding [8]. These strength characteristics are needed for the insulator to withstand the voltage level applied which it can be operated at rated voltage of 11 kV.

Potential distributions on the glass insulator are different according to the surrounding condition as the charge on the surface of glass disc insulator are not the same. The potential distribution will affect the insulator located across the end next to the high voltage transmission line because this insulator has higher voltage value [8]. Once a section of insulator at the end has broken down, the full voltage is applied across the remaining length, therefore the breakdown will occur quickly from the high voltage end to the other, and a flashover arc will start immediately.

The relationship between pollution and profile design of glass disc insulator together with electric potential and electric field stress has not been clarified. Therefore, this project is purpose to study on the electrical potential and electric field stress on several type of glass disc insulator which is clean, polluted and semi-flat glass insulator. As the shape and condition of the glass insulator has been changed, the electric potential and electric field stress can be observed on every point that we want.

II. BACKGROUND

A. Electrical Insulator

Insulators play important role in high voltage performance. An insulator performs dual functions which are mechanically and electrically. For mechanical Function, it holds the conductor or busbar at a certain distance from ground and electrically it also provides the necessary insulation. Insulator prevents unwanted flow of current to the earth from its supporting points [8]. In overhead transmission line, the conductors are usually supported by supporting towers or poles which are properly grounded. An insulator is required between the tower and conductor to prevent the flow of current from conductor to earth through the grounded supporting towers [8].

High voltage transmission line insulator can be divided into two types which are ceramic and non-ceramic insulator. Non-ceramic insulator is also known as polymeric insulator. Organic material is used in ceramic insulator while inorganic material is used in non-ceramic insulator. Ceramic insulator consists of glass and ceramic structure while non-ceramic insulator consists of composite insulator and cast cycloaliphatic epoxy resin insulator [8]. The insulators will be further explained in the following subsections.

B. *Glass Insulator*

Glass insulator is popular nowadays among other insulator [9] as shown in Fig. 1 since it has a lot of advantages. Glass insulator can withstand very high mechanical strength under pressure and hardness. It has very high dielectric strength compared to porcelain and since it is transparent, it will not be heat up by surrounding temperature as compared to porcelain. The properties of glass insulator are shown in Table 2.1

TABLE I. PROPERTIES OF GLASS INSULATOR [1]

Properties	**Approximation Value**
Dielectric Strength	140 kV/cm
Compressive Strength	10 000 kg/cm^2
Tensile Strength	35 000 kg/cm^2

Fig. 1. Glass Disc Insulator

C. *Analysis on Electric Potential and Electric Field on Insulator*

Othman et al. (2014) presented the result of simulation of potential and electric field distribution for high voltage glass disc insulator. The simulation result for potential distribution of clean glass insulator is shown in Fig. 2 while polluted glass insulator in Fig. 3. The distribution of voltage gradually increases from the insulator cap to the insulator pin. Analysis of voltage and electric field distribution is essential in charge study since it articulates the distribution of charges in the material [9].

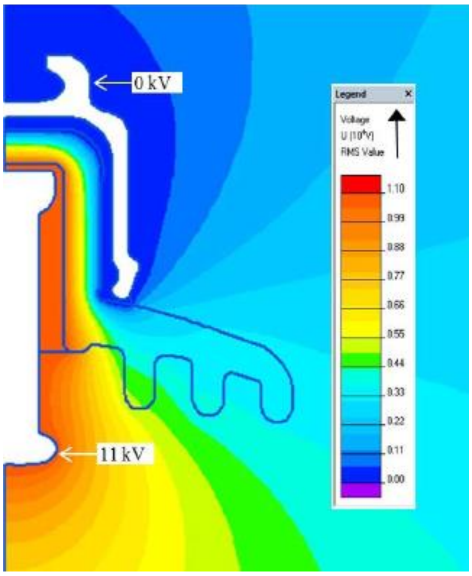

Fig. 2. Potential Distribution of Clean Glass Insulator [9]

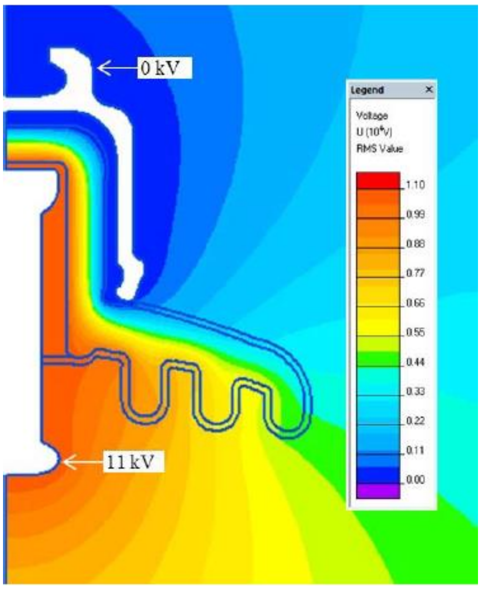

Fig. 3. Potential Distribution of Polluted Glass Insulator [9]

For the electric field distribution, it is shown that the electric field is high at the triple junction regions which consist of air, cap and glass. This is believes due to the imperfections [9]. The electric field stress of clean insulator is shown in Fig. 4.

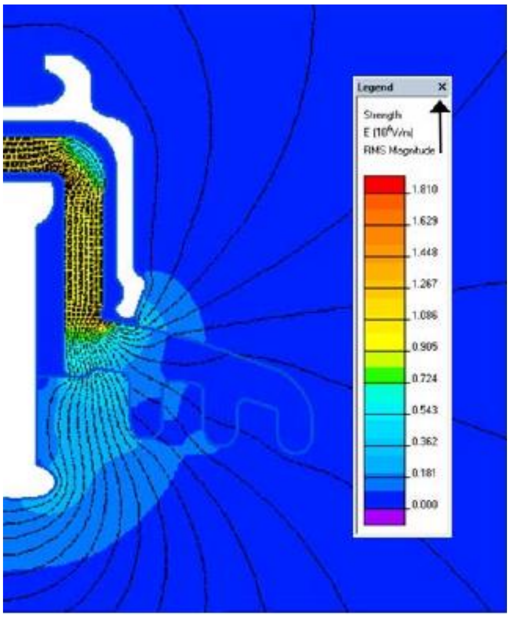

Fig. 4. Electric Field Distribution of Clean Glass Insulator [9]

III. METHODOLOGY

Glass insulator has been modeled by using several parameters. The glass insulator has been modeled and design by using AutoCAD Software. Then, the model was imported to COMSOL Multiphysics to add the parameters. The glass insulator has been modeled according to Fig. 5. There are five separate regions are assigned for modeling such as cap (G1), cement between cap and glass (G2), glass (G3), cement between glass and pin (G4) and insulator pin (G5). The modeled of glass insulator by using COMSOL Multiphysics shown in Fig. 6.

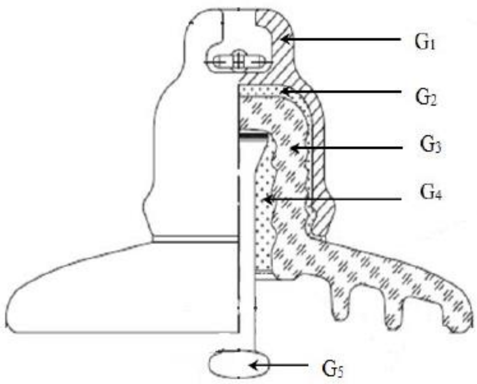

Fig. 5. Glass Insulator Model [9]

Glass insulator is made up by different materials which are glass, cast iron, and cement. For each material, the relative permittivity and electric conductivity are different. Table II shows the materials properties used for the simulation which are inserted in the materials properties of COMSOL Multiphysics.

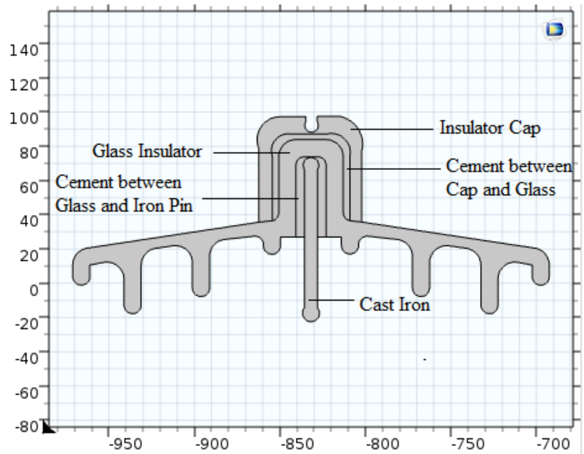

Fig. 6. Glass Insulator Model on COMSOL Multiphysics

TABLE II. PARAMETERS OF GLASS INSULATOR

Type of Material	Relative Permittivity [F/m]	Electric Conductivity [S/m]
Cement (G2 and G4)	15	1×10^{6}
Glass (G3)	4.2	10×10^{-12}
Cast Iron (G1 and G5)	14.2	1×10^{10}
Pollution Layer	81	0.003

Since the project is to determine the potential distribution of the glass insulator with pollution layer, the parameter for the pollution layer also has been added on COMSOL Multiphysics. Besides that, the shape of glass disc insulator has been design to form a new model which is semi-flat model to determine the electric field stress on the glass insulator as shown in Fig. 7.

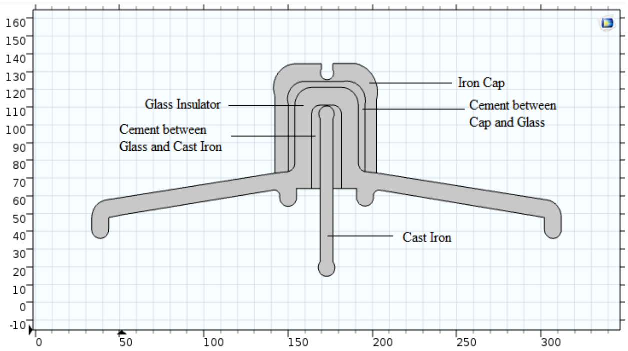

Fig. 7. Semi-Flat Glass Insulator Model on COMSOL Multiphysics

As all the parameters have been added to the software, COMSOL Multiphysics will run the simulation and give the electrical potential and electric field stress distribution.

IV. RESULTS AND DISCUSSION

The potential distribution of clean, polluted and semi-flat glass insulator shown that the voltage distributed gradually decrease from insulator pin to insulator cap [9] since the power supply is connected on the pin while the cap is grounded.

Potential distribution of clean glass insulator shown in Fig.8 while polluted glass insulator are shown in Fig.9. The changes of voltage can be seen clearly in the glass part.

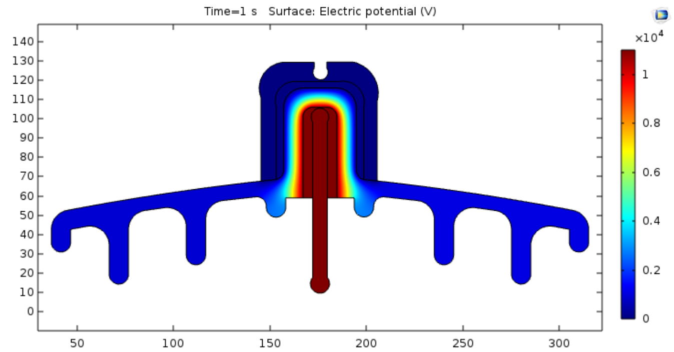

Fig. 8. Voltage Distribution of Clean Glass Insulator

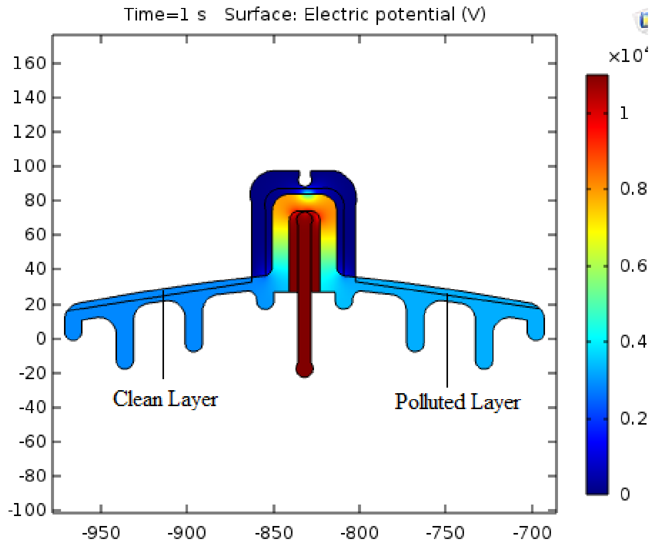

Fig. 9. Voltage Distribution of Polluted Glass Insulator

Meanwhile the voltage distribution of semi-flat glass insulator in Fig. 10 can be seen in the cement part between glass and cast iron.

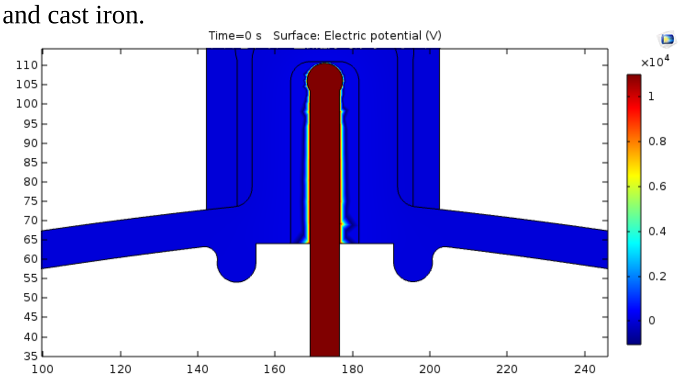

Fig. 10. Voltage Distribution of Semi-Flat Glass Insulator

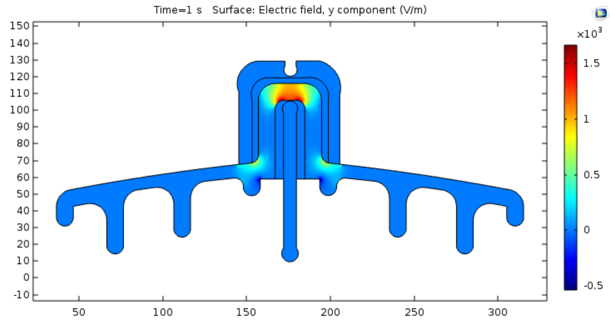

Fig. 11. Vertical Electric Field Distribution of Clean Glass Insulator

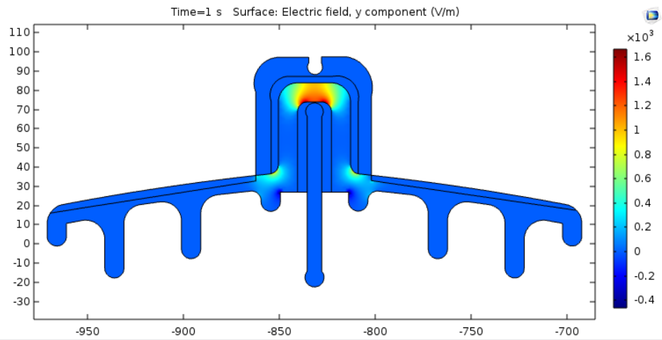

Fig. 12. Vertical Electric Field Distribution of Polluted Glass Insulator

Fig. 11 and Fig 12 show the electric field distribution of clean and polluted glass insulator respectively. The pattern of the electric field distribution for both cases are the same their maximum values are different. The maximum electric field of clean glass insulator is 1.5 kV/m while the maximum electric field of polluted glass insulator is 1.6 kV/m. it is shown that the maximum electric field of polluted glass insulator is slightly higher compared to maximum stress of clean glass insulator.

Fig. 13 shows vertical electric field stress inside the glass of clean glass insulator while Fig. 14 shows vertical electric field stress on the polluted layer of glass insulator and Fig. 15 shows vertical electric field stress of semi-flat glass insulator. It is shown that vertical electric stress of clean glass insulator increase from zero V/m until it reached maximum stress at about 15 meter length before it goes down to zero V/m again at 30 meter arc length. Vertical electric stress along polluted layer of glass insulator reduces rapidly from 0.15 V/m to zero V/m at about 2 meter distance and increases back to 0.02 V/m. The stress then reduces slowly until it completely reaches zero V/m at 20 meter distance. Vertical electric field stress of semi-flat glass insulator increase from zero V/m until it reached maximum stress at about 15 meter length before it goes down to zero V/m again at 30 meter arc length. The shape of graphs for original profile and semi-flat glass insulator are the same but the maximum values are different where the maximum stress of original profile is about 235 V/m while the maximum stress of semi-flat glass insulator is about 215 V/m.

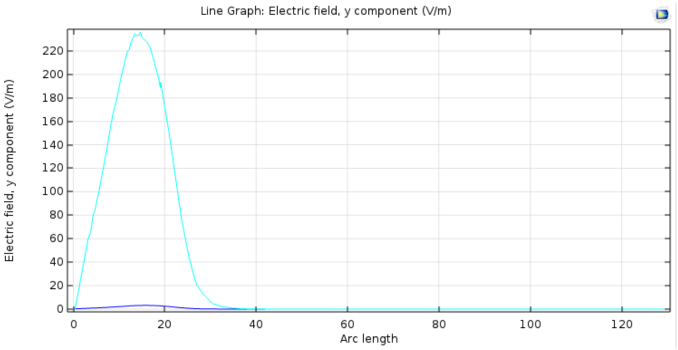

Fig. 13. Vertical Electric Field Stress inside the Glass of Clean Glass Insulator

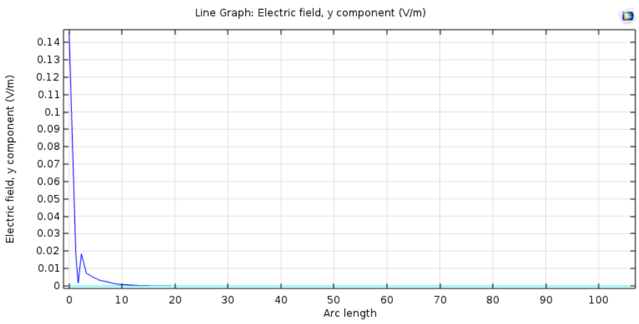

Fig. 14. Vertical Electric Field Stress on the Polluted Layer of Glass Insulator

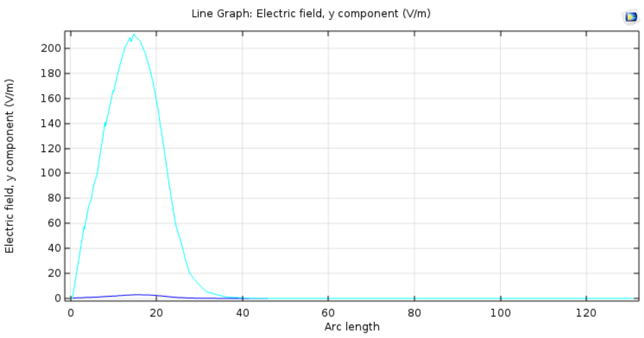

Fig. 15. Vertical Electric Field Stress inside the Glass of Semi-Flat Glass Insulator

In order to investigate the shape of glass insulator together with electric field stress, the stress was observed on the cut part of the insulator. Fig. 16 shown the observed part of clean glass insulator while Fig. 18 shown the observed part of semi-flat glass insulator. The horizontal stress of clean glass insulator shown in Fig. 17 shows that the stress increased from 10 V/m until it reached maximum stress of 119 V/m at 5 meter distance and reduced to 20 V/m at 10 meter distance.

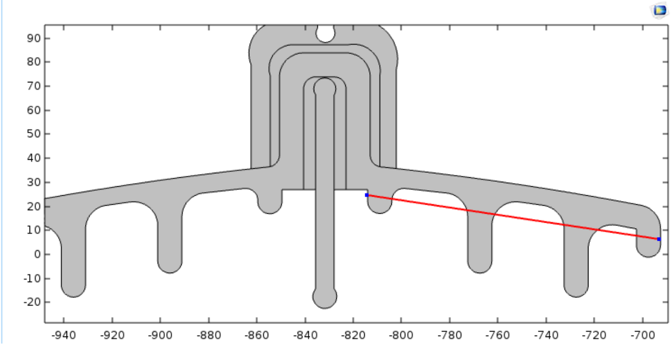

Fig. 16. Part of Stress Observed on Clean Glass Insulator

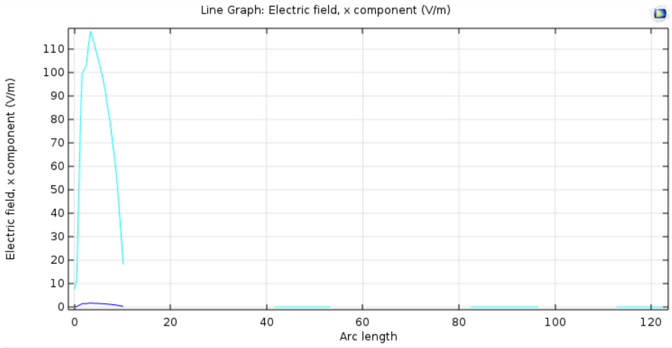

Fig. 17. Horizontal Electric Field Stress of Clean Glass Insulator

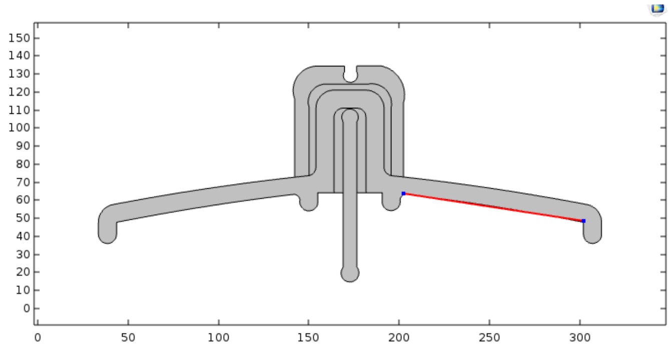

Fig. 18. Part of Stress Observed on Clean Glass Insulator

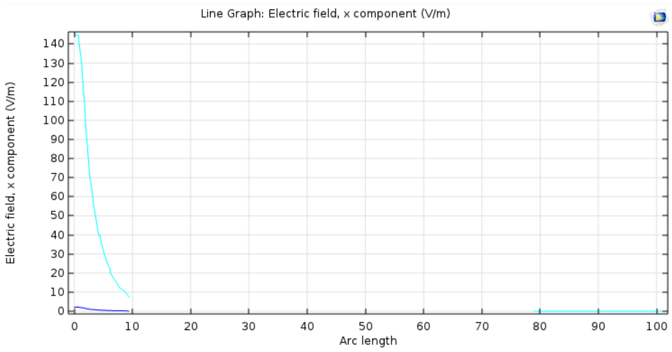

Fig. 19. Horizontal Electric Field Stress of Semi-Flat Glass Insulator

Fig. 19 shows that the horizontal electric field stress of semi-flat glass insulator reduced from it maximum value of 145 V/m to 10 V/m at 10 meter distance. It is shown from the graph of Fig. 17 and Fig. 19 where the maximum stress of semi-flat glass insulator is higher compared to the maximum stress of clean glass insulator. This is due to the glass shape has been cut off until it become semi-flat.

V. CONCLUSION

An attempt to simulate the distribution of voltage between clean and polluted glass insulator and electric field between clean and semi-flat glass insulator using COMSOL Multiphysics is conducted in this paper.

From this study, it was found that the voltage distributed from insulator pin to the insulator cap since the pin is connected to the power supply while the cap is grounded for all cases considered. The electric field stress of semi-glass insulator is higher compared to standard clean glass insulator. There, careful attention must be considered when design all type of insulators especially for high voltage purpose.

ACKNOWLEDGMENT

This work was supported by a project grant 106H1 from University of Technology Malaysia (UTM)

REFERENCES

[1] Online Electrical Engineering Study Site, "Electrical Insulator," [Online]. Available: http://www.electrical4u.com/electrical-insulator-insulating-material-porcelain-glass-polymer-insulator/, [Accessed December 9, 2016]

[2] N. A. Othman, M. A. M. Piah, Z. Adzis and H. Ahmad, "Measurement of surface charge distribution on glass insulator using steel mesh," 2014 IEEE International Conference on Power and Energy (PECon), Kuching, 2014, pp. 105-108.

[3] M. H. Zainuddin, "DC Pollution Flashover Performances of Glass and Porcelain Insulator" Degree of Bachelor Thesis, University of Technology Malaysia, June 2015.

[4] M. Sivaraman and J. Sivadasan, "Comparison of pollution flashover performance of various insulators," 2014 International Conference on Circuits, Power and Computing Technologies [ICCPCT-2014], Nagercoil, 2014, pp. 148-152.

[5] B. Zhang et al., "Voltage and electric field distribution along porcelain long rod insulator string in AC 500kV transmission line," 2016 IEEE International Conference on High Voltage Engineering and Application (ICHVE), Chengdu, 2016, pp. 1-4.

[6] M. Raju and N. P. Subramaniam, "Comparative study on disc insulators deployed in EHV AC and HVDC transmission lines," 2016 International Conference on Circuit, Power and Computing Technologies (ICCPCT), Nagercoil, 2016, pp. 1-4.

[7] INMR, "Insulator Failure," [Online]. Available: http://www.inmr.com/examples-insulator-failure/, [Accessed September 22, 2016]

[8] F.H. Basri, "Analysis of Potential Distribution of a Glass Insulators String with Different Number of Broken Units," Degree of Bachelor Thesis, University of Technology Malaysia, June 2015.

[9] Engineering Forums, "High Voltage Transmission," [Online]. Available: http://www.eng-tips.com/viewthread.cfm?qid=417941, [Accessed December 23, 2016]

[10] N. A. Othman, M. A. M. Piah, Z. Adzis, H. Ahmad and N. A. Ahmad, "Simulation of voltage and electric-field distribution for contaminated glass insulator," 2013 IEEE Student Conference on Research and Developement, Putrajaya, 2013, pp. 116-120.

Enhancing Dielectric Properties of Low Density Polyethylene by Adding Boron-Nitride Nanofiller

Nurul Humaira Binti Muhd Zaimi
Faculty of Electrical Engineering
Universiti Teknologi Malaysia
81310 UTM Johor Bahru, Malaysia
nhumaira@utm.my

Zulkarnain Bin Ahmad Noorden
Institute of High Voltage and High Current (IVAT)
Universiti Teknologi Malaysia
81310 UTM Johor Bahru, Malaysia
zulkarnain-an@utm.my

***Abstract*—Electrical insulation plays an important role in the power cables nowadays as it helps the conducting part of the equipment separate electrically from each other and from earthed components. Recently, there is a new technique introduced in order to enhance the dielectric properties of insulator by incorporating nanofillers. In this project, Boron Nitride has been chosen to be added to the Low Density Polyethylene to improve dielectric strength, as well as dielectric constant for the polymer nanocomposite insulator. All the samples are tested for dielectric properties with Dielectric Spectroscopy Measurement according to ASTM d150, and AC breakdown test, in accordance to ASTM D149. Based on the results, it can be seen that for the breakdown strength, at 63.2 % breakdown probability, 1wt% and 3wt% BN has higher dielectric strength compared to the unfilled polymer. However, for the 5wt% BN, it has lower dielectric strength compared to unfilled polymer. It is also revealed that, the improvement of dielectric strength is due to the high surface area of nanocomposite and the reduction of permittivity is due to the immobililty of polymer chain.**

Keywords— Low Density Polyethylene; Nanofiller; Breakdown strength; Dielectric constant; Dielectric loss

I. INTRODUCTION

In electric power transmission, high voltage cable is frequently used to transmit electric power at high voltage. The cable consists of a conductor and insulation. Besides, as an insulation material, it should have high dielectric strength in order to withstand high voltage stress, tracking or even electric discharge which produces ozone in air. It should also has low dielectric loss and dielectric constant Nowadays, many electrical industries are using the polymeric insulating materials in high voltage equipment especially in the power cables [17]. This is due to many improvements of the polymer properties itself. However, just like any other insulating material, polymeric insulating material might also undergo failure due to subjected by different type of electrical discharges during the operation of the equipment [12]. The failure of insulating material might result in the failure of the whole electrical system. One of the factors that contribute to the failure of insulating material in power cables is breakdown phenomenon. Moreover, the high voltage components might need to be replaced when breakdown occur which in the end lead to high cost in order to buy a whole new component or even when doing maintenance.

Many researches have been done in order to improve the dielectric properties of the polymeric insulating material such as breakdown strength, dielectric loss and permittivity.. Hence, one of the methods is by adding nanofiller into the polymeric material. It has been found that the addition of nanofiller results in a good performances of the material including better dielectric strength [6-7],[9-10], [15] and better heat handling capacity. Other than that, the addition of nanofiller could also enhance mechanical, chemical and electrical properties [14],[18] without affecting the process of manufacturing the component. A good insulating material should have low dielectric loss and low permittivity [27]. It also was found that by incorporating nanofiller, it could lower both dielectric constant and dielectric loss of the materials [27-31]. The decreasing of the permittivity is said to be due to the immobility of the polymer chain, while the decrement in the tangent delta is due to the inhibitions in the charge carries transport. [23] Hence, with the improvement of the polymeric insulating material, a longer life span could be obtained and thus the cost for maintenance will also be reduced.

II. LITERATURE REVIEW

A. Polymer Nanocomposite

Nanotechnology is nowadays one of the most important methods in the development of technology. Many researches have been conducted on nanocomposites due to its enhanced properties as an insulating material for high voltage equipment. Polymer nanocomposite is actually a new improved insulating material due to the results of generation of insulating material with the addition of nanofiller. A study by Zulkifli et al. said that nanoparticle that has been added to a matrix in order to enhance the properties of the material is called nanocomposite (2016) [17]. Based on previous studies, it has been found that nanocomposite is chosen as the new insulation due its excellent performance in electrical, mechanical and also chemical properties. The addition of nanofiller will actually enhance and improve the dielectric properties such as dielectric breakdown of the insulator. A research survey by Ghouse et al, states that by mixing the proper amount of nanofillers in dielectric materials will result in an improvement of breakdown strength and voltage endurance (2013) [10]. Breakdown voltage has always been a major phenomenon in high voltage equipment that leads to the failure of the whole electrical system. Because of that, many researches have been finding the solution of introducing insulation material which could withstand electrical stress at longer time and require low cost. As a result, they come out with polymer nanocomposites. The addition of inorganic nanofiller to the polymer could improve the electrical properties of polymer and forming new materials which is called polymer nanocomposite (Ossama et al., 2014) [15]. Another study shown by Li et al., observed that addition of nanofiller could actually improve the characteristic of the insulating material (2010) [7]. Polymer nanocomposite with better dielectric strength and voltage endurance are slowly emerging in high voltage application and becoming more popular due to it overcomes the drawbacks of traditional insulating material.

Polymer matrix can be categorized into three categories which are thermoplastics, thermoset and elastomers. Next, for nanofiller, it can be categorized by the type of dimensions which are one dimensional, two-dimensional and three dimensional. The most common used nanofiller for insulator are the one dimensional which are Silicon dioxide (SiO2), Boron Nitride (BN), Aluminium Oxide (Al2O3), titania (TiO2), and many more. For this experiment, the nanofiller that will be added to the Low Density Polyethelene are Boron Nitride and Silicon dioxide. The reason of using these nanofiller is to improve the dielectric strength of the insulator. On the other hand, the interfacial area between the filler and the matrix are called interaction zone. [1]

B. Dielectric Breakdown and Strength

The Dielectric breakdown voltage or also known as breakdown voltage is one of the characteristic of an insulator that indicate the maximum voltage which can be applied across the material before the insulator ruptures and conduct electricity. There are several types of breakdown voltage in mechanism of polymers which are avalanche, thermal and electromechanical breakdown (Mattias) [8]. While, dielectric strength can be defined as a measure of the electrical strength of a material as an insulator. It indicates the maximum voltage required to produce dielectric breakdown through the material. The quality of an insulator is represented by its dielectric strength and a better quality of insulator has a higher dielectric strength. The formula for dielectric breakdown strength is as follow:

$$E = Vbd/ d \text{ (V/mm)} \quad (1)$$

Where Vbd is breakdown voltage and d is the sample thickness.

In order to obtain a better quality of insulator, many methods have been done which includes adding nanofiller to the dielectric material. This is because; the addition of nanofiller can improve the physical, chemical and electrical properties of the material [16, 19].

C. Dielectric Spectroscopy

The Dielectric spectroscopy is one of the popular methods used to identify the dynamical behavior of a sample through the analysis of its frequency dependent dielectric response. Through this method, the dielectric properties of the material can be obtained. Capacitance that has been sandwiched between two electrodes is measured as a function of frequency. [22]

Besides, through this technique also, tan delta, which also known as loss factor can be determined from the test. Dielectric spectroscopy is based on the interaction between the applied field and the electric dipole moments throughout a sample. Through dielectric spectroscopy, the information of the mobility of the polymers can be provided by testing the dielectric properties. [19]. For the test, the tan delta and permittivity over a range of frequency, were measured. The sample will be cut into a circle with certain diameter and will be applied with a voltage of 1 Vrms. The room temperature was maintained during all measurements. [16,19].

Dielectric spectroscopy is most suitable used to measure the dielectric properties of thin sample. [22] It is also an experiment method which is characterizing electrochemical systems. This method will measure the impedance of a system over a range of frequency. Hence, energy storage and dissipation properties, which are the frequency response of the system is revealed. Data often will be obtained graphically in a bode plot or nyquist plot by electrochemical impedance spectroscopy (EIS). [23]

Figure1. Sample test cell for dielectric spectroscopy measurement [19]

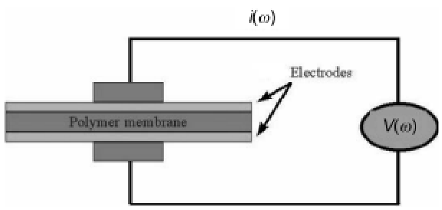

D. Dielectric constant and Tangent Delta

In Dielectric properties such as dielectric constant and tangent delta have an important role in determining the reliability of an insulating material in nowadays. Dielectric constant, also known as permittivity measures the ability of a material to store electrical charge/energy in it. It is better for a material that will be used as an insulator to have lower dielectric constant. [27]

According to research, due to the low chain mobility and tangled chain structure, it can be found that polymers have relatively low dielectric constant including Low Density Polyethyene, that have permittivity which is between 2.3 – 2.4. On the other hand, Boron Nitride has permittivity of 4. The dielectric constant of a material could actually be increased or decreasedby adding nanofiller. [23] Dielectric constant can be obtained through the following equations: [15,22,23]

$$\varepsilon' = Cp/C_0 \quad (2)$$

$$\varepsilon'' = 1/\omega RpC_0 \quad (3)$$

Whereas Cp is the capacitance measured by the Gamry and Co=(εo x π x r^2)/d is the capacitance of the empty sample cylindrical capacitor, d is thickness of sample and r the electrode radius. ω is 2πf and εo is the permittivity of vacuum (εo = 8.854 x 10-12 F/m).

The complex dielectric constant of materiall are as below:

Tangent delta also known as loss factor is another dielectric properties which measurred a material’s inherent dissipation of electromagnetic energy. When an electrostatic is applied to a material, dielectric loss will occur. As a result, there will be a formation heat in the material. This heat will then raise the temperature and causing deterioration occurs faster. [27] Hence, a material with low dielectric loss must be selected in

$$\varepsilon_r^* = \varepsilon_r' - j\varepsilon_r''$$

order to get a good insulating material. Tangent delta can be obtained through the following equation:

$$\text{Tan } \delta = \varepsilon'/\varepsilon'' \quad (4)$$

III. METHODOLOGY

This chapter discusses of the experimental process for the research methodology. This research covers the methodology to obtain the experimental results, which including preparation of sample, the experimental flow for AC breakdown voltage test according to ASTM D149. Next, the dielectric spectroscopy measurement according to ASTM D150 was also shown in this chapter. The three main parts of the methodology for the study consists of:

- Preparation of sample
- Dielectric spectroscopy measurement according to ASTM D150
- Experimental flow for AC breakdown test according to ASTM

A. Preparation of sample

For this project, the material to be used is Low Density Polyethylene (LDPE) employed with several different percentages of nanofiller. The base polymer material that will be used is LDPE due to its excellent thermal, mechanical and electrical properties, high breakdown strength and resistivity and also easy to be mix with nanofiller through simple melt mixing. The type of nanofiller that will be added is Boron Nitride (BN). Firstly all the materials will be obtained from the supplier such as Lotte Chemical Titan, Nanostructured &Amorphous Materials and also Sigma Adrich. Next, all the materials will be dried to remove the moisture content. The process of drying will be done by using a vacuum at 105ºC for duration of 24 hours. Then, LDPE was added to the nanofiiler to produce LDPE nanocomposite. The LDPE nanocomposites will be next compounded using a Brabender mixer and mix for 2 minutes for each sample. After that, the mixed sample will be granulated or pelletized into small pellets for 5 minutes by using Samchin Plastic Granulation model, SLM50FY. In this step, the pellets size sample then had been compression molding to obtain a specific thickness. Lastly, the LDPE nanocomposite sample will be compressed by using 80 ton Hydraulic Hot Press in Polymer Laboratory at Faculty of Chemical Engineering. For the compression process, the machine will be set at temperature of 160°C for both upper and lower plates. A stainless steel mold with dimension 25cm x 25 cm will be used. Then, the sample will be fully compressesed for 5 minutes. After that, the mold should be placed inside the hydraulic cold press machine for cooling process. Lastly, a sheet of LDPE nanocomposites sample with 100u thickness will be obtained by using hot press air.

The steps on using hot press sir to prepare for all the samples are firstly, the hot press air is turned on, next, the temperature is assigned to 160 C and is then allowed to reach 160 C. Each sample is then cut in pieces in order to obtain a weight of 0.5g to 0.6 g. The sample is then put between two OHP papers, before being sandwiched by two plates, to undergo pressing. The sample is then pressed (without any pressure applied to it) and was left for 3 minutes. Next, the sample was applied with pressure of 2 tonnes and left for 3 minutes. After all the steps have been done, the sample is checked for any impurities presence and the thickness is measured. If there are any impurities present, a new sample will be made.

B. Dielectric Spectroscopy Measurement

Figure below shows the experimental set up for dielectric spectroscopy measurement. The Gamry interface is connected to the computer via Universal Serial Bus (USB), while between Gamry interface and solid insulation test cell, it is connected by using Gamry lead. Then, the prepared sample is sandwiched between the electrodes, and AC voltage of value 1 Vrms is applied over frequency of 10mHz to 1Hz with 10 points per decade. Before the sample is placed between the electrode, acetone is used to clean the electrodes surface. The tests are run at room temperature and are in low noise mode to avoid interference to the test results.

Figure 2. Dielectric Spectroscopy Set Up [23]

The experiment has taken a few hours in order to complete it. The data obtained by electrochemical impedance spectroscopy (EIS) is in term of bode plot (impedance spectrum) and nyquist plot. It has taken several hours to complete the experiment. The result of data has been obtained in term of impedance spectrum and nquist plot. The data was then tabulated and calculated using the permittivity equation using microsoft excel before plotted using excel. The experiment was then repeated for different percentage of nanofiller.

C. AC Breakdown Test

The experiment for AC breakdown test was carriedout at IVAT laboratory of Faculty of Electrical Engineering, UTM, Skudai. The experiment was set up as follow:

Figure 3. Schematic Diagram for AC breakdown test [21]

The sample is sandwiched between two stainless steel electrodes which have a diameter of 6.4mm. The test cell is put inside a transformer oil to avoid the flashover from occur.

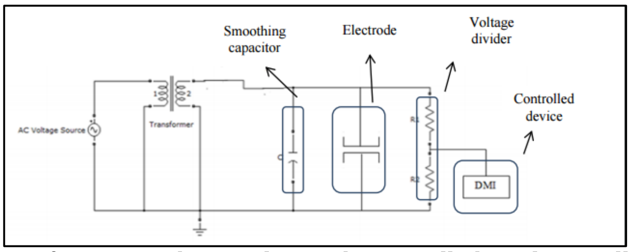

After putting the sample into the test cell, the voltage will be applied and increased at a rate of 2000 V/s (according to ASTM D149) for every 20 s until breakdown occurs. The breakdown voltage of the sample will be recorded. Five breakdown tests will be done and recorded for each sample and all the procedures will be repeated for different type of LDPE nanocomposites. All the obtained result will be recorded.

IV. RESULT AND ANALYSIS

In this chapter, it will show the complete result of dielectric properties which are dielectric constant, dielectric loss and dielectric strength for each sample with different percentage of Boron Nitride nanofiller. The results are presented in terms of table, graph and line chart plot for breakdown strength. While, for the permittivity the results are presented in terms of line chart using excel. Next, the results will be further discussed in this chapter.

A. Breakdown Strength

Dielectric breakdown can be seen improving for all the samples except for sample Low Density Polyethylene with 5wt% BN nanofillers. At 63.2% of breakdown probability, both 1wt% and 3wt% has higher dielectric strength compared to the unfilled polymer. This is due to the small size of nanocomposite, it results in high surface area which will lead to the high interaction of polymer matrices with filler that could affect the polymer chain motion leading to the adjustment of the properties of the insulating material. For the 5wt% BN nanofiller is lower than unfilled polymer due to the presence of impurities in the sample during the preparation of sample. Impurities will cause the sample's dielectic properties to be affected.

Figure 4. Breakdown Strength of nanocomposite

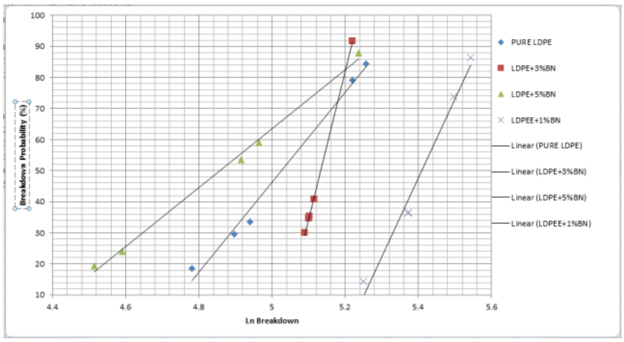

B. Dielectric Constant

Based on the result below, it can be seen that for both 3wt% and 5wt% Boron Nitride, at certain frequency, some of the permittivity is higher than the dielectric constant of the pure LDPE and some are lower than the Pure LDPE. Not much changes can be seen from the result. Based on researches, the addition of nanofiller should result in a lower dielectric constant.

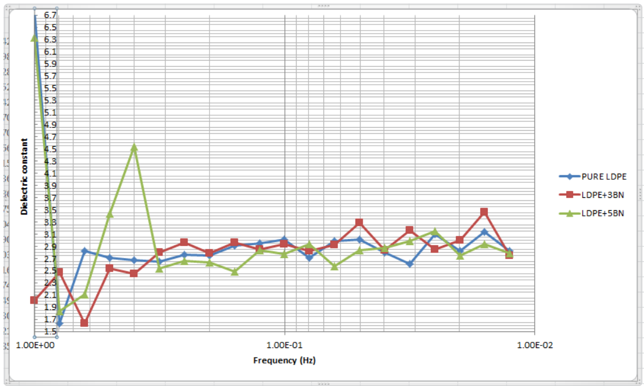

According to report, the effective dielectric constant of nanocomposites can be reduced or increased compared to the unfilled polymer, depending upon the combination interaction of the chain immobilisation and the rate of dielectric constant enhancement in the material with respect to the fillers loading [23]. Due to this, it explain why the permittivity is lower at certain frequency and higher at other frequency compare to the unfilled polymer.

Figure 5. Dielectric constant of Polymer nanocomposite

V. CONCLUSION

Based on the results, it can be concluded that all the objectives have been answered. The first objective is to determine the effect of adding nanofiller on the dielectric strength of the insulator. It can be seen tha 3wt% Boron Nitride exhibit the highest dielectric breakdown followed by1wt%, and 3wt% compared to unfilled polymer. 5wt% BN has lower dielectric strength than unfiled polymer due to the presence of impurities. For the second objective, which is to determine the effect of adding nanofiller on the dielectric contant, has also been achieved. It can be seen that for both 3wt% and 5wt% Boron Nitride, at certain frequency, some of the permittivity is higher than the dielectric constant of the pure LDPE and some are lower than the Pure LDPE. Not much changes can be seen from the result. This is due to the combination interaction of the chain immobilisation and the rate of dielectric constant enhancement in the material with respect to the fillers loading.

.

REFERENCES

[1] W. A. Izzati, Y. Z. Arief, Z. Adzis, and M. Shafanizam, "Partial Discharge Characteristics of Polymer Nanocomposite Materials in Electrical Insulation: A Review of Sample Preparation Techniques, Analysis Methods, Potential Applications, and Future Trends," Sci. World J., vol. 2014, pp. 1–14, 2014.

[2] Equipotentials and Electric Field Lines. Retrieved November 5, 2016, from Appalachian State University: https://physics.appstate.edu/laboratory/quick-guides/equipotentials-and-electric-field-lines, n.d.

[3] N. A. Awang, Y. Z. Arief, S. Yahya, K. Y. Lau, M. H. Ahmad, N. A. Muhamad, N. Bashir, S. H. Rhaif, and A. Z. Abdulameer, "Experimental investigation on partial discharge characteristics of epoxy-nanocomposite as high voltage insulation material," in 2014 IEEE International Conference on Power and Energy (PECon), 2014, pp. 146–149.

[4] K. N. Izzati , "BREAKDOWN STRENGTH OF NANOFILLED POLYETHYLENE BLEND," Malaysia: Universiti Teknologi Malaysia,2015.

[5] C. W. Kit, " BREAKDOWN STRENGTH AND VOLUME RESISTIVITY OF POLYMER NANOCOMPOSITE MATERIAL," Malaysia: Universiti Teknologi Malaysia, 2011.

[6] D. Edison Selvaraj, S. Usa, C. Pugazhendhi Sugumaran, " Comparative Analysis of Dielectric Properties of Enamel Filled with Various Nanofillers such as ZrO2, Al2O3, CNT and ZnO,"in International Journal of Science and Engineering Applications (IJSEA),pp. 51-55, 2012.

[7] Li. Zhe, K. Okatomo, Y. Ohki, & T. Tanaka, " Effects of nano-filler addition on partial discharge resistance and dielectric breakdown strength of Micro-Al2O3 Epoxy composite," in IEEE Transactions on Dielectrics and Electrical Insulation, pp.653-661, 2010.

[8] M. Karlsson, "Investigation of the dielectric breakdown strength of polymer nanocomposites," Sweden: Uppsala University,2014.

[9] M. M. S. Shirazi, H. Borsi, E. Gockenbach, " Effect of TiO2 Nanofillers on Electrical, Thermal and Mechanical Parameters of Epoxy Resin," in Conference Record of the 2012 IEEE International Symposium on Electrical Insulation (ISEI), pp. 69-72,2012.

[10] S. M. Ghouse, S. Venkatesh, R. Rajesh, S. Natarajan, "Effects of SiO2and TiO2 Nano Fillers in Enhancing the Insulation Breakdown Strength of Epoxy Nano Composite Dielectric under Divergent Electric Fields," in International Journal on Electrical Engineering and Informatics, pp. 501-518, 2013

[11] U. Sreedhar, B. Somashekar, N. Lakshmipthy, "Breakdown Test on Solid Insulators Using Rod Gap ," in International Journal of Emerging Technology and Advanced Engineering,pp. 66-74, 2008

[12] P. Preetha, M.J. Thomas, "AC Breakdown Characteristics of Epoxy Nanocomposites," in IEEE Transactions on Dielectrics and Electrical Insulation , pp.1526-1534,2011

[13] G. Iyer, R. S. Gorur, R. Richert , "Dielectric Properties of Epoxy based Nanocomposites fo High Voltage Insulation," in IEEE Transactions on Dielectrics and Electrical Insulation,pp. 659-666, 2011

[14] M. Praeger, A.S. Vaughan, S.G. Swingler, "Phase dispersion of filler and its influence on dielectric properties. UK: University of Southampton,2013

[15] E. G. Ossama, F.M. Sohair, A. E. Ahmed, S. H. Ahmed, "Improving the Dielectric Properties of High Density Polyethylene by Incorporating Cay-Nanofiller," in World Journal of Engineering and Technology,pp. 290-297,2014

[16] S. S. Linda, J.K. Nelson, C. Calebrese, T. Alice , " High Temperature Breakdown Strength and Voltage Endurance Characterization of Nanofilled Polyamideimide," in IEEE Transactions on Dielectrics and Electrical Insulation, pp. 2090-2101, 2012

[17] N.H. Zulkifli, N. A. M Jamail, M. A. A. Azmi, M. I. H. Razali, N. A. A. N. Zarujhan , " Effect of TiO2 Nanofiller on the AC and Impulse Characteristic for HV Application," in ARPN Journal of Engineering and Applied Sciences, pp. 10806-10813,2016

[18] C. H. John, L. S. Daniel, G. Guido, "Improved Electrical Properties of Epoxy Resin with Nanometer-Sized Inorganic Fillers," in International Power Modulator Conference,pp. 1-3, 2006

[19] Q. Wang, G. Chen, " Effect of nanofiller on the dielectric properties of epoxy nanocomposite," in Advances in Materials Research, pp. 93-107,2012

[20] N. Syazwan , " Modelling the ELectric Field on Solid Dielectric Material under High Voltage Stress using COMSOL Multiphysics," Malaysia: Universiti Teknologi Malaysia, 2015

[21] E. Norfarhana, "BREAKDOWN STRENGTH OF NANO FILLED HIGH DENSITY POLYETHYLENE," Malaysia: Universiti Teknologi Malaysia, 2015

Electrochemical Properties of Activated Carbon Electrode with Atmospheric Plasma Treatment

Noor Ameera Binti Zakaria
Faculty of Electrical Engineering
Universiti Teknologi Malaysia
81310 UTM Johor Bharu, Malaysia
mierazack94@gmail.com

Zulkarnain Bin Ahmad Noorden
Institute of High Voltage and High Current (IVAT)
Universiti Teknologi Malaysia
81310 UTM Johor Bahru, Malaysia
zulkarnain-an@utm.my

***Abstract*— Activated carbon layered on the nickel form as electrodes treated by atmospheric plasma. Plasma treatment applies fixed alternating current 8 kV voltage supply and 50 Hz frequency for 4 sample with different of times as parameter in ranges 1minute – 15minute. After that, the performance of supercapacitor analyses by obtained electrochemical properties of electrodes which are comparing between untreated and treated sample was carried out using cyclic voltammetry (CV), galvanostatic charging-discharging (GCD) and electrochemical impedance spectroscopy (EIS) with 0.1 mol sulfuric acid (H_2SO_4) solution and glass wool as separator. In addition, prove the improvement of supercapacitor based on the highest specific capacitance achieved is 5.46 F/g at 1 minutes sample which is examine by galvanostatic charging-discharging measurement at scan rates 2 mA.**

Keywords* — *activated carbon; atmospheric plasma; electrochemical ; supercapacitor

I. INTRODUCTION

Supercapacitor also known as electric double layer capacitor or ultracapacitor which is developed other initiative power supply system using new kind of power sources [1]. Moreover, supercapacitor are group of energy storage device which give good result of their short charging time, high power density and long cycling life. Recently, energy storage devices offering a promising that high power and energy capabilities are not far apart to the physical and chemical properties of thin film layer electrode [2].

The role as supercapacitor are achieved due to the integration of the two electrode with short distance that separates the different charges as labeled by electric double layer and great porous electrodes that manifest prominent surface area. To upgrade the supercapacitors electric specifics, the capacity and charging-discharging cycles the secondary layer is applied. The layer can be composed of metal oxide; copper oxide, nickel oxide or conductive polymers and of carbon. The layer surely increases the sufficient surface area, less thickness and stabilizes electrical charges. Thus, activated carbon electrode is used for this application [1].

The physical and chemical of carbon electrodes are closely related with the power and energy potential. Carbons are currently preferred other than other material as the electrode because of high surface areas, less cost and good conductivity. The characteristics of the electrodes have a primary effect on the supercapacitor parameters. In this project, the material used for electrodes is activated carbon; from the raw carbon undergoes process of with two methods of activation like steam activation and chemical activation. The result shows the increment of the surface area from the absorption and chemical reaction [3].

Plasma treatment is numerously used in treating surface of the materials like coating, printing or stickiness application. Nowadays, many method of plasma has been discovering like for example in argon, hydrogen and oxygen gas for material treatment. Hence, this research focuses on the investigation of the behavior and performance of supercapacitor with atmospheric plasma treatment carbon electrode. In this project, experimental is conducted on activated carbon electrodes which is undergoes the surface modification by using atmospheric plasma technique to deliver significantly improved performance of supercapacitors [4, 5].

This project concentrates on the effect of the activated carbon after it being treated through the atmospheric plasma treatment and H_2SO_4 as electrolyte. The electrochemical properties test were conducted in order to analyze and determine the performance of activated carbon is in form of thin film and decided all undergo the laboratory tests. The test involved such as cyclic voltammetry (CV), galvanostatic charging-discharging (GCD) and electrochemical impedance spectroscopy (EIS).

II. LITERATURE REVIEW

A. Activated Carbon

The activated carbon (AC) is very useful composite material for purify liquids and gases in many applications such as purification of dye wastewater, industrial pollution control and water filter [6]. Moreover, activated carbon is the one of the main important material for supercapacitor that plays as the electrodes in the industry which are contains high carbon content that produce from the natural sources such as coal, coconut shell and wood. To becoming the activated carbon the raw material need to undergo the physical modification and thermal decomposition in furnace. The outcome may produce the higher surface area and large porous of the structure of the material.

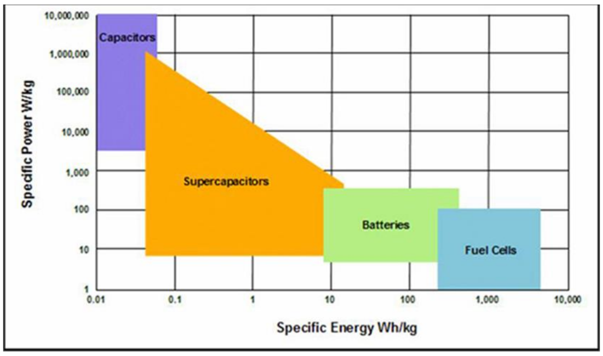

Fig. 1. Energy and power density various energy storage device

Activated carbons widely used as electrode of supercapacitor, its physical properties are involved in this project. Because the supercapacitors are capability in higher power, better cycle life and better performance rather than the batteries in Fig 1 [7].

B. *Atmospheric Plasma Treatment*

Refer to other research, many kind of the plasma treatment approaches have been analyze and widely applied for application in industry for example argon plasma treatment, hydrogen, oxygen plasma treatment. But the most preferred is argon plasma treatment because it generated in low pressure vacuum chamber and used for plasma cleaning, surface activation and etching. In addition, this treatment often referred to as micro-sandblasting [8].

For this project, the atmospheric plasma treatment will be conducted. Atmospheric plasma treatment is a functional tool that has been applied in various fields. This technique can be also be used in the small scale. From the experimental, in atmospheric shows the discharges form in filamentary purple glow that extract the plasma at the surface of the electrode [9].

C. *Evaluation of Supercapacitor*

The performance of the supercapacitor based on the CV curve of the activated carbon electrodes that display a quasi-rectangular shape [1]. The integrated area of the curve indicates the behavior of the supercapacitor. Significantly, the large area of the quasi-rectangular specify as the excellence capacitive attitude and high rate capability [10].

The supercapacitors are evaluated based on the rate of the performance at different current densities. The results come out which is the Galvanostatic charge-discharge can determine the voltage drop of the discharge curve. From the research has made, with large voltage drop may affect the capacitance value due to the increment of the discharge current densities and that lead to the decrease of specific capacitance.

III. METHODOLOGY

Activated carbon widely used of applications and industrial scale. Firstly, preparation of electrode with activated carbon sheet by using epoxy glue as binder. Epoxy glue mostly used in relation to adhesives, coating and electronics [11]. The characteristic of the epoxy glue that can stand with 1 mol of hydrochloric acid allows proceeding as electrode of the supercapacitor. 7 gram of blended activated carbon that is in form of powder was mixed with epoxy glue and the mixture having volumetric fractions 7:3, which are 7 g activated carbon and 3 g epoxy glue respectively. After that, the mixture layered spread evenly on the surface of nickel form. In addition, the conductivity of nickel better than iron or carbon metal which less resistive. The sample was pressed by hydraulic press in 6 min at 25 Celsius (room temperature) become thinness layer [12].

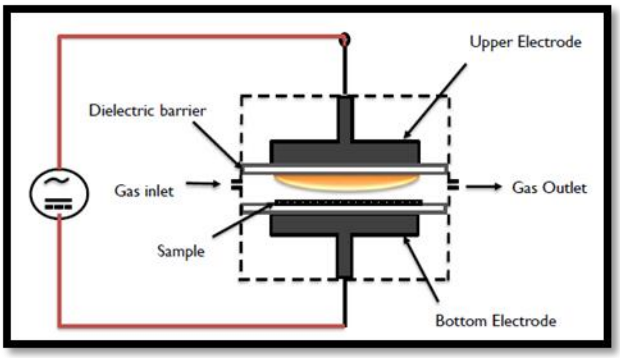

Fig. 2. Plate-to-plate arrangement Dielectric Barrier Discharge (DBD).

Fig. 2 shows the equipment called plate-to-plate reactor or dielectric barrier discharge chamber used for treat the electrode. In this part, activated carbon sheet with weight 0.85 gram was used and it was treated under plasma discharge within air surrounding. Moreover, the experiment conducted in 8 kV AC voltage supply, frequency of 50 Hz with 4 sample with different of time such as 1 min, 5 min, 10 min and 15min. The electrodes were places between the glass plate and the chamber were connected with high voltage and ground electrode. Fig 3 show the oxygen plasma treatment, but for atmospheric plasma treatment does not used oxygen gas therefore assemble of connection still same [13].

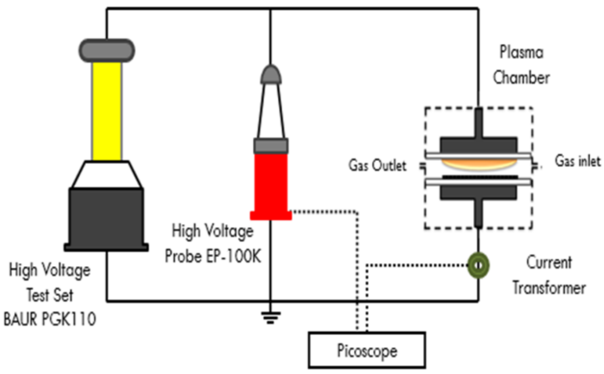

Fig. 3. Plasma treatment arrangement.

Activated carbon treatment under atmospheric plasma and electrochemical measurement was studied based on the literature review of the journals, articles and books [14]. This project more focuses on the performance of the supercapacitors of it electrochemical properties by using Gamry Interface 1000.

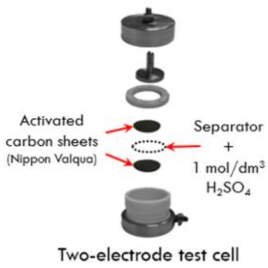

Fig. 4. Two electrode test cell connected to Gamry Interface 1000.

In this project, 1 mol H_2SO_4 was used as electrolyte solution and the activated carbon sheet were used to form ionization process in supercapacitor. Meanwhile for the separator, the glass wool paper was used to avoid the short circuit between the electrodes [15]. To test the electrochemical behavior of supercapacitor, the test cell is the tools measurement which is in the cylindrical shape. So, the electrodes and glass wool paper was in manually cut into circular shape and the test cell connected with Gamry Interface 1000 to collect the data like in Fig 4 [16].

The performance of the supercapacitor were analyze based on the data collected from cyclic voltammetry (CV), galvanosatatic charging-discharging (GCD) and electrochemical impedance spectroscopy (EIS) tests. For CV measurement is carried out with three different scan rates which are 5 mV/s, 10 mV/s and 50 mV/s. the information that can find out in CV is the voltage window, capacitance and the life cycle. The voltage limits entered in setup were 0 to 1 V and the data analyze based on 10^{th} cycle. The low scan rates results shows the longer duration to charge and discharge process meanwhile high scan rate results fast process and need short time testing.

Galvanostatic charging-discharging (GCD) measurement was conducted in three different constant current which are 2 mA, 5 mA and 10 mA in 20^{th} cycle. The information can be define from GCD is to test the behavior and cycle-life of the supercapacitor. Based on the curve, the waveforms shows the different time taken the system charge-discharge depends on the scan rates. The higher the scan rates prove the time taken to charge and discharge even quickly than lower scan rates. EIS rate ranges are 1m Hz to 100 kHz [15, 17].

IV. Result And Discussion

In this project, five set of 0.85 g for each set of activated carbon sheet were used. The activated carbons were treated under atmospheric plasma treatment, which is using air surrounding. It can seen that the plasma forms the filamentary discharge in purple color [18]. Besides, it is depended on how much the voltage applied and the gas used to make the plasma showed. Fig 5 shows the applied voltage and power at 8 kV_{rms} and 3 W respectively. The performance of supercapacitor can be identified by getting data from cyclic voltammetry (CV), galvanostatic charging-discharging (GCD) and electrochemical impedance spectroscopy (EIS).

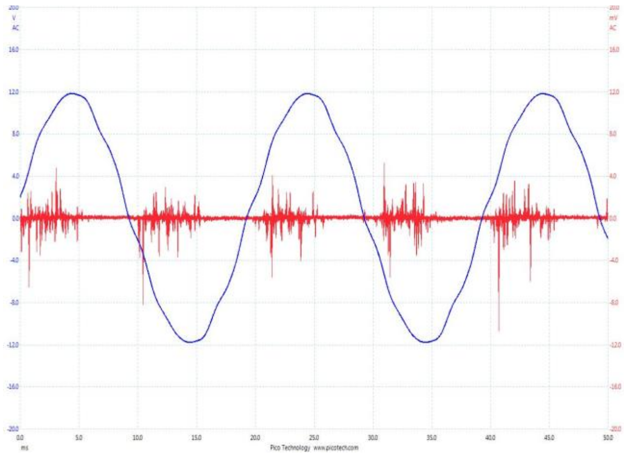

Fig. 5. Atmospheric plasma treatment waveform from picoscope

Cyclic voltammetry (CV) for activated carbon electrodes are shown in Fig. 6 the CV curve show the reversible charging discharging behavior of electrodes. The shape of curve similar to the conventional CV of activated carbon on different time of treatment undergoes plasma [19]. This relates that the properties of the composite electrodes are defined by the electrochemical behavior of the activated carbon sheet. At scan rates 5 mV/s shown in Fig. 7 the highest static specific capacitance is 1.2 F/g. The capacitance value was obtained from CV curves according to the equation:

$$Cs,cv = \frac{\int_{v_1}^{v_2} I(V)\, dV}{\frac{dV}{dt}(V_2 - V_1)} \; x \; \frac{4}{m} \tag{1}$$

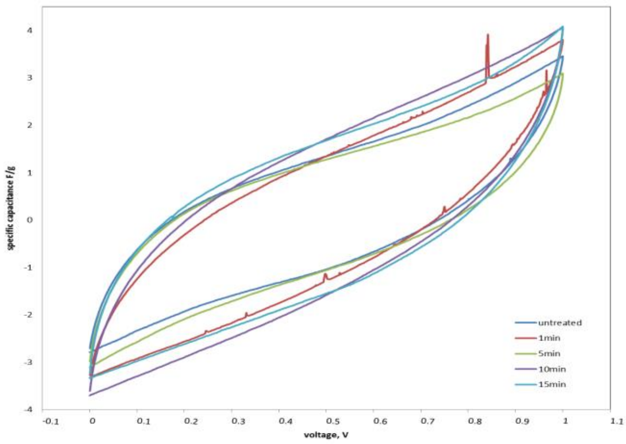

Fig. 6. CV with different treatment time.

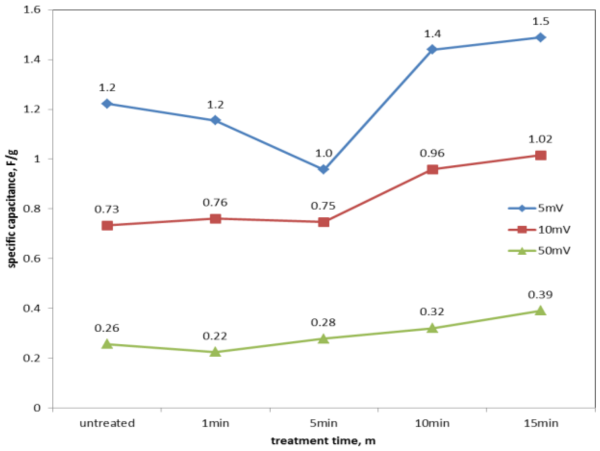

Fig. 7. Static specific capacitance from CV with different scan rates.

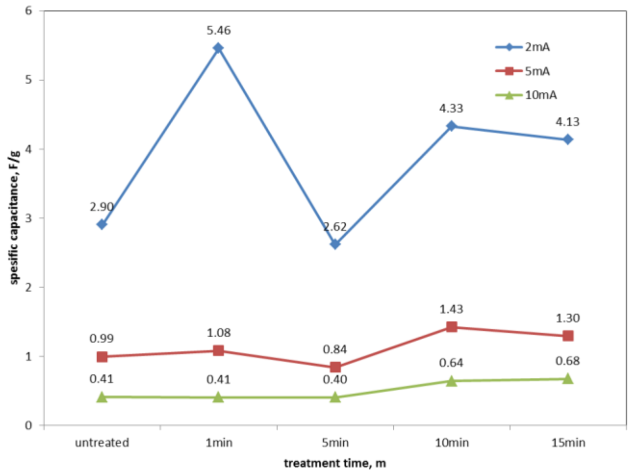

Fig. 9. Specific capacitance with scan rates at 2, 5 and 10mA

The performance of the electrodes shown in Fig. 8 the sample treated in 10 minutes better performance than others different time or even compared with untreated sample. In addition, it is take longest time to charging and discharging which specify the highest capacitance [20]. The specific capacitance of the activated carbon electrodes was analysed by galvanostatic charging-discharging (GCD) with different current densities of the untreated and plasma treated activated carbon electrodes sample. The specific capacitance shown in Fig. 9 can be calculated based on the following equation:

$$Cs, g = \frac{Id\ \Delta t}{\Delta v}\ x\ \frac{4}{m} \tag{2}$$

Where I_d refer to the discharge current (A), dV/dt is the change of voltage excluding calculation of voltage drop and the change of time during discharging. At scan rates 2 mA/s highest specific capacitance is 5.46 F/g which is treatment time at 1 minute.

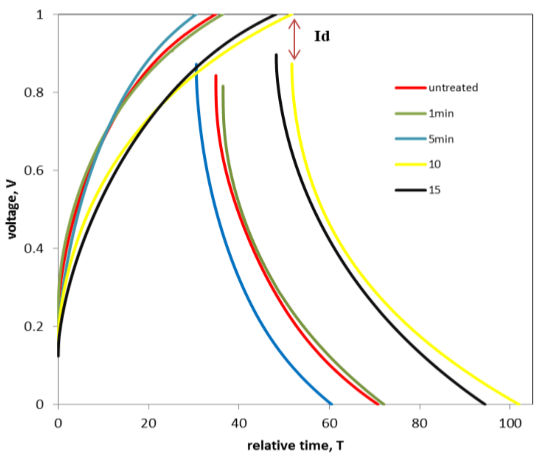

Fig. 8. Galvanostatic charging-discharging with various of sample

More detailed estimation of the electrochemical properties of activated carbon supercapacitors can be obtained by analysis of the electrochemical impedance spectroscopy (EIS). Nquist plot response as shown in Fig. 10 at frequency 1 mHz to 100 kHz the supercapacitor behavior and test the impedance whether higher or not which are the higher value of impedance contribute decreasing capacitance [21]. Fig. 11 close view of high frequency 100 kHz that 15 minute sample improved sample resistance of 4.16 Ω compared to untreated sample 12.47 Ω.

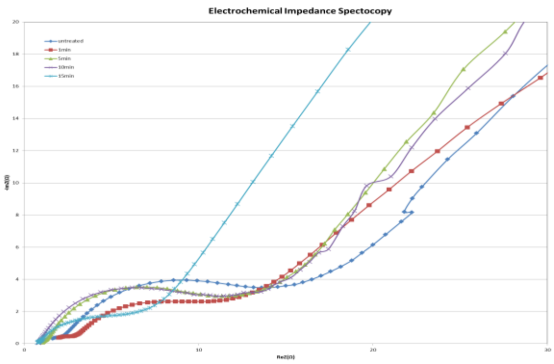

Fig. 10. Nquist plot of untreated sample and different treatment time

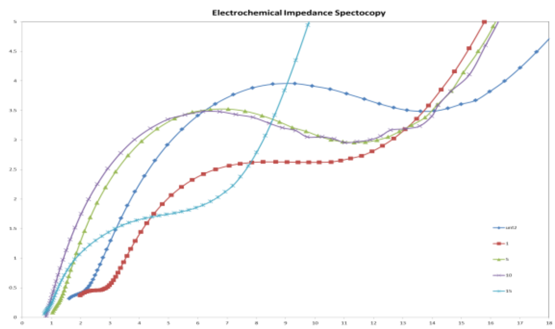

Fig. 11. Close view high frequency region

Based on the galvanostatic data, other parameter can be obtained such that equivalent series resistance $R_{esr,g}$ (Ω) in Fig 12. The reason resistance is calculated to find the power density of the supercapacitor. The result can be identifying by the formula below:

$$Resr = \frac{Vdrop}{\Delta I} \tag{3}$$

Where V_{drop} *(V)* represents as voltage drop and ΔI is the current change during charging and discharging process.

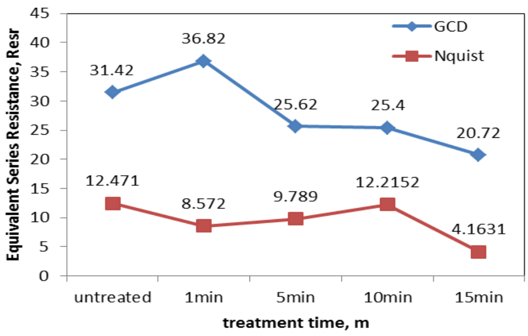

Fig. 12. Equivalent series resistance againts nquist plot and GCD

Energy storage is the importance parameter to decide the capability of supercapacitor work as energy storage. Based on the galvanostatic curve, the power and energy density can be calculated in order to exposes the supercapacitor performance shown in Fig 13 and Fig. 14.

$$P = \frac{V^2}{4\,R_{esr}} x \frac{1000}{m} \tag{4}$$

$$E = \frac{CV^2}{2} x \frac{1}{3.6m} \tag{5}$$

Where V is the charging-discharging voltage range, R_{esr} represented the equivalent series resistance from GCD and C is the absolute capacitance.

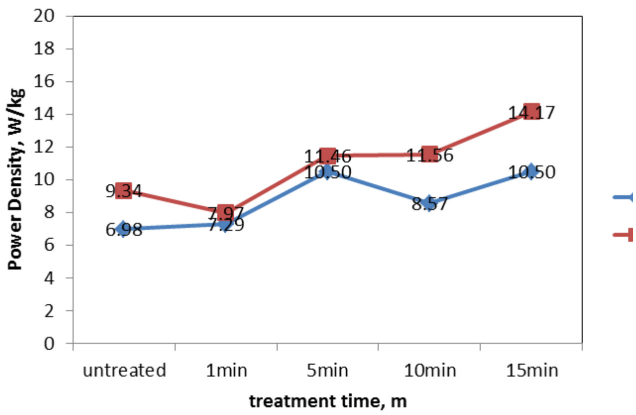

Fig. 13. Power density againts scan rates 2mA/s and 5mA/s

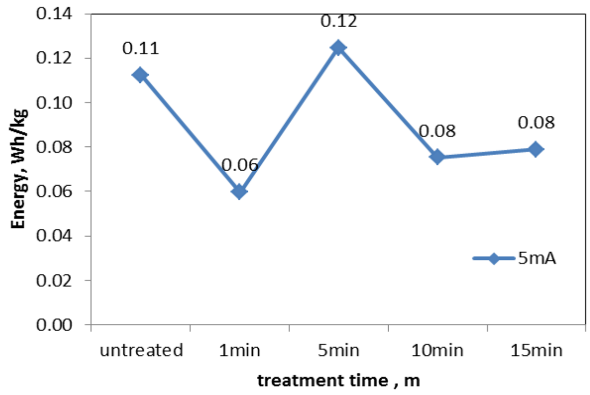

Fig. 14. Energy density at scan rates 5mA/s.

V. Conclusion

This project demonstrates activated carbon layered on the nickel form as supercapacitor undergoes atmospheric plasma treatment by using plate-to plate dielectric barrier discharge (DBD). Four sample treated by plasma at 8 kV with different treatment time as 1 min, 5 min, 10 min and 15 min. Using the atmospheric or air prove that can improve the ability of ion transfer, reduces the internal resistance of the electrode and increase the value of specific capacitance from 0.99 to 1.41 F/g which is untreated electrode and 10 minute treatment sample respectively at 5 mA/s. This prove that material used undergoes atmospheric plasma treatment modified the surface material of sample which effective technique to boost the specific capacitance, performance rate and developing high energy storage supercapacitor.

References

[1] R. Kötz and M. Carlen, "Principles and applications of electrochemical capacitors," *Electrochimica Acta*, vol. 45, pp. 2483-2498, 5/3/ 2000.

[2] V. V. N. Obreja, "On the performance of supercapacitors with electrodes based on carbon nanotubes and carbon activated material—A review," *Physica E: Low-dimensional Systems and Nanostructures*, vol. 40, pp. 2596-2605, 5// 2008.

[3] D. Tashima, R. Hirakawa, T. Sakoda, and M. Otsubo, "Electrochemical capacitances of carbon powder treated with dielectric barrier discharge," in *2011 Annual Report Conference on Electrical Insulation and Dielectric Phenomena*, 2011, pp. 109-112.

[4] T. G. Enercon, "Atmospheric Plasma - What is it and what is it good for," 2016.

[5] A. K. S. 1, 1B. S. Dotel, R. S. S. Dhungana, 1H. B. Baniya, 1U. M. Joshi, 1D. P., and Subedi, "SURFACE MODIFICATION OF POLYCARBONATE USING MESH ELECTRODE AT ATMOSPHERIC PRESSURE DISCHARGE AT 50 HZ," vol. Vol 10, November 2014.

[6] M. Zhi, F. Yang, F. Meng, M. Li, A. Manivannan, and N. Wu, "Effects of Pore Structure on Performance of An Activated-Carbon Supercapacitor Electrode Recycled from Scrap Waste Tires," *ACS Sustainable Chemistry & Engineering,* vol. 2, pp. 1592-1598, 2014/07/07 2014.

[7] W. Huang, "Asymmetric supercapacitors based on nano-architectured NiO/graphene foam and hierarchical porous nitrogen-doped carbon nanotubes with ultrahigh-rate performance," 2013.

[8] N. Theophile and H. K. Jeong, "Reduction of Graphite Oxide by Using an Atmospheric Pressure Plasma," *New Physics: Sae Mulli,* vol. 66, pp. 637-641, 05 2016.

[9] I. C. Cheng, C. Jian-Zhang, and H. Cheng-Che, "Rapid atmospheric-pressure-plasma processed nanomaterials for electrochemical energy harvesting and storage devices," in *2016 Progress in Electromagnetic Research Symposium (PIERS)*, 2016, pp. 954-954.

[10] B. E. Conway. (1999). *Testing Electrochemical Capacitors Part 1: CV, EIS, and Leakage Current*. Available: http://www.gamry.com/application-notes/battery-research/testing-electrochemical-capacitors-cyclic-voltammetry-leakage-current/

[11] A. E. Eltom, M. P. Fournier Lessa, M. J. da Silva, and J. C. da Rocha, "Production & Characterization of Activated Carbon Membranes," *Journal of Materials Research and Technology,* vol. 1, pp. 80-83, 2012/07/01 2012.

[12] X. Feng, R. Li, Z. Yan, X. Liu, R. Chen, Y. Ma, *et al.*, "Preparation of Graphene/Polypyrrole Composite Film via Electrodeposition for Supercapacitors," *IEEE Transactions on Nanotechnology,* vol. 11, pp. 1080-1086, 2012.

[13] P. F. Riccardo d'Agostino, Christian Oehr, Michael R. Wertheimer. (june 22-27 2003). *Plasma Processes and Polymers*.

[14] R. Jozef and M. S. Daniel, "The transition from a filamentary dielectric barrier discharge to a diffuse barrier discharge in air at atmospheric pressure," *Journal of Physics D: Applied Physics,* vol. 38, p. 547, 2005.

[15] Z. Lin, Y. Liu, Y. Yao, O. J. Hildreth, Z. Li, K. Moon, *et al.*, "Surface engineering of graphene for high performance supercapacitors," in *2011 IEEE 61st Electronic Components and Technology Conference (ECTC)*, 2011, pp. 236-241.

[16] G. Instuments. (2016). *Two, Three and Four Electrode Experiments*. Available: http://www.gamry.com/application-notes/electrodes-cells/two-three-and-four-electrode-experiments/

[17] H. G. Liuyang Zhang, "Improvement in flexibility, volumetric performance for supercapacitor application and effect of Ni-Fe ratio on electrode behaviour," 2015.

[18] S. J. Kim IH, Kwon TY, Kim KH, "Effect of Atmospheric Plasma Treatment to Titanium Surface on Initial Osteoblast-Like Cell Spreading," January 2015.

[19] V. Khomenko, E. Frackowiak, and F. Béguin, "Determination of the specific capacitance of conducting polymer/nanotubes composite electrodes using different cell configurations," *Electrochimica Acta,* vol. 50, pp. 2499-2506, 4/15/ 2005.

[20] K. Naoi, "New Material and New Configurations Advanced Electrochemical Capacitors," *Journal of the Electrochemical Society (JES),* vol. 17, pp. 34-37, 2008.

[21] S. H. Kim and W. Choi, "A method for performance evaluation and optimal sizing of the supercapacitor module by the Electrochemical Impedance Spectroscopy," in *INTELEC 2009 - 31st International Telecommunications Energy Conference*, 2009, pp. 1-6.

Ergonomic Design Of Ozone-based Surgicial Equipment Sterilizer

Muhamad Fazrol Iman B. Ishak
Faculty Of Electrical Engineering
Universiti Teknologi Malaysia
Johor Bahru, Malaysia.
Fazrol.Ishak@Gmail.Com

Assoc. Prof. Dr. Zolkafle B.Buntat
Department Of Power
Faculty of Electrical Engineering
Universiti Teknologi Malaysia
Johor Bahru, Malaysia.
zolkafle@fke.utm.my

***Abstract*—This paper discuss about solving the current problem face by surgical equipment sterilizer process. Ozone-based sterilizer machine is one of the latest approach to increases the effectiveness and efficiency of sterilization process. The method used to developed ergonomic design of ozone based surgical equipment sterilizer is divided into three process. The final result of these project include complete system of the design and the ability of the system to produce high level concentration of ozonated water.**

Keywords—ozone;sterilizer;ergonomic design; design process

I. INTRODUCTION

As the increases in human population, it also mean increasing number of patients. So the system in the hospitality need to be improve. Sterilization process for the surgical equipment is one of the important process in the hospital system. This process is important to prevent the growth and spread of disease by surgical equipment. Sterilization is a procedure of destruction of all types of living microorganisms and spore from a substance. These materials include medications, plant, surgical equipment, food, and so forth [1].

Furthermore, There are several method uses to sterilize surgical equipment such as steam, ethylene oxide, dry heat, microwaves, formaldehyde gas, hydrogen peroxide plasma, chemical solution, and ionizing radiation. Steam sterilization is the most generally utilized processes for sanitizing instruments, trays, and tapes. According to the CDC, steam under pressure is the procedure of decision at whatever point conceivable as it is viewed as safe, quick, and the most practical for health care facilities. Steam sterilizers come in a wide range of sizes and sterilizer cycles can differ among producers. The cycle a sterilizer runs can commonly be found in the sterilizer manual [2].

The following are examples of standard cycle parameters (AAMI ST79, AORN) for packaged instruments. The specification of standard cycle parameters (AAMI ST79, AORN) for bundled Unwrapped instruments is at 121°C for 20 minutes at 15 PSI above climatic weight or at 134°C for 3–4 minutes at 30 PSI above environmental pressure and for bundled Wrapped instruments at 121°C for 30 minutes at 15 PSI above climatic weight or at 134°C for 15 minutes at 30 PSI above environmental pressure [2].

However, for heat sensitive surgical instrument this method cannot be applied. Another method needs to be used such as chemical method. Chemical method basically is sterilization by utilizing dangerous gasses. The gas infiltrates rapidly into the material like steam. In this way, the sterilization is successful. However, the odds of the blast and cost elements are to be considered. The gasses utilized for disinfection are extremely poisonous. The regularly utilized gas is ethylene oxide with a blend of carbon-dioxide. Carbon dioxide is added to minimize the probability of a blast [1]. Besides, hydrogen peroxide also been used to sterilize heat sensitive surgical equipment. However, this method had been proving failed under some condition, especially which equipment has complex shape [3].

This is very beneficial if the multipurpose surgical equipment sterilizer which can be used for both heat sensitive equipment and also non-heat sensitive equipment to be produced. So buyer can pick more powerful and beneficial surgical equipment sterilizer and also with less cost.

The objective of this project are to design ergonomic architecture of Ozone-based surgical equipment sterilizer using Solidworks software, to arrange the equipment of complete sterilizer system structure suitable for ergonomic design, and to develop electrical system model for these project using Arduino as microcontroller.

II. LITERETURE REVIEW

Ozone usually be delivered in nature by lightning. It is unstable particles that acquire three ions of oxygen that reinforced together and O3 is symbolized to it. It is one of nature's most capable oxidizers. The stratosphere level at atmosphere where most of the ozone can be found. This region is up to 50 kilometers, located around 10 km to 16 km from the surface of the earth. It also has a high level of ozone concentration. It usually being refers as the ozone layer.

In the atmosphere, ozone particles have a low relative abundance and there are generally a couple of thousand ozone atoms for each billion air particles. Most air particles contain oxygen (O2) and nitrogen (N2) atoms. Ozone is even less abundant when it close to the surface of earth. In spite of the fact that ozone high up in the stratosphere gives a shield to ensure life on Earth, the ground level, additionally known as the troposphere that brought on by the human exercises diminish the limited ozone in the Earth's surface.

Ozone was accounted for to be viable in eliminating microscopic organisms, infections or algae (Glaze, 1987). The resistance of microorganisms takes after the expanding request is microscopic organisms, infections then cysts [4]. Bacteria Escherichia coli was discovered ozone enters the cell layer and respond with cytoplasmic substances, this is explored by (Bringmann, 1954; Holluta and Unger, 1954; Katzenelson et al., 1974; Burleson et al., 1975; Hunt and Mainas, 1997). (Ishizaki et al. 1987). As indicated by Mc Guire and Davis in 1988, ozone is capable in evacuating Escherichia coli bacteria and inactivate poliomyelitis virus. In 1988 Shinriki et al found that ozone assaulted both protein coat and ribonucleic acids in the tobacco mosaic virus. In 1984 Wickramanayake et al. reported that ozone is by all accounts more effective for cyst inactivation than free chlorine. In 1992 Labatiuk reported that he found by utilizing ozone for Cysts (Giardia Muris) can be inactivated quickly with contact time below 2 min and Wolfe et al in 1989 reported 5 min were required for inactivation of microorganism in the surface waters [4]. An ozone concentration as low as 0.1mg/l is fit for inactivating 99.9% of bacterial suspension inside 1 min [5].

As ozone reported was an extremely viable oxidizing operator to eliminate microscopic organisms and viruses, it is broadly utilized as a part of numerous applications. A common use of ozone as recorded is drinking water treatment, wastewater treatment, angle incubator ozone applications in the sustenance business, ozone applications in soil sterilization, and ozone applications in polymer surface adjustment [6].

The capability of ozone to sanitize contaminated water was perceived by de Meritens in 1886 and the quantity of ozonated drinking water became accelerate in 1914 [6]. Other, wastewater treatment using ozone is varied into two categories which are industrial and municipal. Ozone has additionally self-disintegrated into nontoxic oxygen and solid antimicrobial ability makes it extremely valuable in nature of food [7]. Nowadays, soils defilement is generally brought on by PAHs, basically because of fuel oil slicks. Effective treatment utilized for soils contaminated with low sub-atomic weight PAHs were found, that is Biodegradation technic [8].

Ergonomic word is actually from two Greek words, which is ERGO which mean work and NOMOS which mean laws. In logical significance, ergonomic is an investigation of science concentrates on human variability. In other word, it means human fit and diminished weakness and uneasiness through design of the product [9]. Ergonomic design is very important, especially in the work station. This is because of some condition such as rehashing a similar movement all through the workday, working in clumsy or stationary positions, lifting substantial or clumsy things, using intemperate constrain to perform tasks, and being presented to over vibration or extreme temperatures [10]. The basic comprehension of ergonomics investigation to identify end-user need is anthropometry, posture, repetitive movement, and workspace configuration [9].

The end user of the product comes in many sizes and shapes. In this manner, it is essential to gauge the range of body size in population. This measure procedure is known as anthropometry. There are basic posture found in the workplace environment that can be considered when designing workplaces items or space. This measurement of posture is divided into standing, sitting, reaching, and moving [9]. The repetitive movement also needs to be considered in ergonomic design. The product design with this requirement will lead to higher working efficiency. Workspace configuration also needs to consider when designing an ergonomic product. In this project the survey of common use product such as Tuttnauer product been conducted to gain suitable configuration in the workplace.

III. Project Methodology

This chapter will discuss the development of the ergonomic design of ozone-base surgical equipment sterilization machine. The developments of this project included the design of the main structure of the machine by using solidwork software and design the operation of the machine. After the design of the structure and operation of the machine complete, the component use in the machine will be determined according to the operation of the machine. Next, the component will be arranged inside the machine. The arrangement of the component is the most crucial process to ensure the machine ergonomically and efficiently.

The methodology to build up this machine is isolated into three processes. To begin with is a design process, second is development process and the final process is experimental process.

A. Design Process

1) Design the basic structure of the machine.

Design basic structure of the machine is the crucial part to ensure the project achieves ergonomic design. The design was conducted by using Solidwork software. The basic structure of the machine is consisting of the dimension of the machine, height of the panel, the dimension of the sterilizer chamber and any other dimension. As has been explained before, to achieve ergonomic design, 4 category need to be considering is anthropometry, posture, repetitive movement, and workspace configuration.

In this project, anthropometry measurement is focused on Asian female. This is because the main purpose of this project is to develop a sterilizer machine for the hospital. Sterilizer process in the hospital is inside the job scope of worker. As known, most of the workers in this sector usually female. Second category need to be considered is posture. This means the posture of the worker while executes sterilizer process. In this project, the posture of the worker is standing. So, all the design measurement will consider the worker was standing.

Next, the third category is a repetitive movement. However, this project does not require a lot of worker interface. This is because, the product in this project is built to operate automatically by using microcontroller. Thus, this category isn’t affecting much on the design. Finally, fourth category is workspace configuration. In this category for this project, the workspace considers is sterilizer room. The design need to consider current used sterilizer machine as reference to avoid the need of workspace renovation when the user decide to use this project as sterilizer machine.

2) Design the operation of the machine.

To design the operation of the machine, the skill of the user need to be considered. The best way is ensure minimum skill need to operate the machine. The operation of the machine is from after the surgical equipment was washed until the surgical equipment been stored in proper and suitable storage

B. Development Process

1) Determine component

The component of the system was determined according to the operation of the machine that had been designed before.

2) Design control system of the machine

The system of the machine was divided into three systems. That is a water flow system, air flow system and also electrical system. The water flow system is considered from distilled water that flow into the machine until the waste water use to sterilize is settled. While the air flow system is considered from the normal air that flow into the machine until the end of the process. Next, electrical system of the machine. This system will consider wiring of the supply to the machine and wiring of the control system of the machine to control the component.

3) Arranged component of the machine in the basic structure.

After all the design is complete and all the components used had been determined, the component was arranged in the basic structure while not disturbing the ergonomic design of the structure and to compact the component as possible.

C. Experimental Process

In this process, experiment to investigate the concentration of ozone by using this system was conducted. The purpose of these experiment is to ensure this system can be used to sterilize surgical equipment successfully. The experiment was done by using sample of ozonated water from the same system used to produce ozonate water in this project. Then the sample was tested by using UV spectrophotometer. The reading from this meter is in absorbance to concentration (ABS). Then this reading was converted into milligram per liter by using ozone concentration measurement equation (1).

$$O_3\left[\frac{m}{l}\right] = \frac{2(48)(ABS)(1000)}{(1)(3100)} \tag{1}$$

This process was repeated three time and the average value was recorded.

IV. Result And Discussion

A. Design Process

1) Design the basic structure of the machine.

The design of basic structure is show in Fig. 1 and Fig. 2. All the dimension is in millimeter. The height of the machine is 1000mm because this height is suitable to ensure the worker easily handle the equipment to be sterilize. While the depth of the sterilizer chamber is 700mm and diameter of 340mm, this dimension was choose by observe current use sterilizer machine.

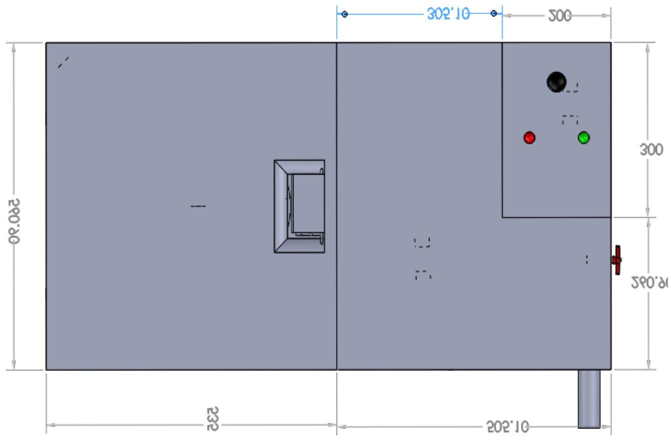

Fig. 1: Top view of basic structure

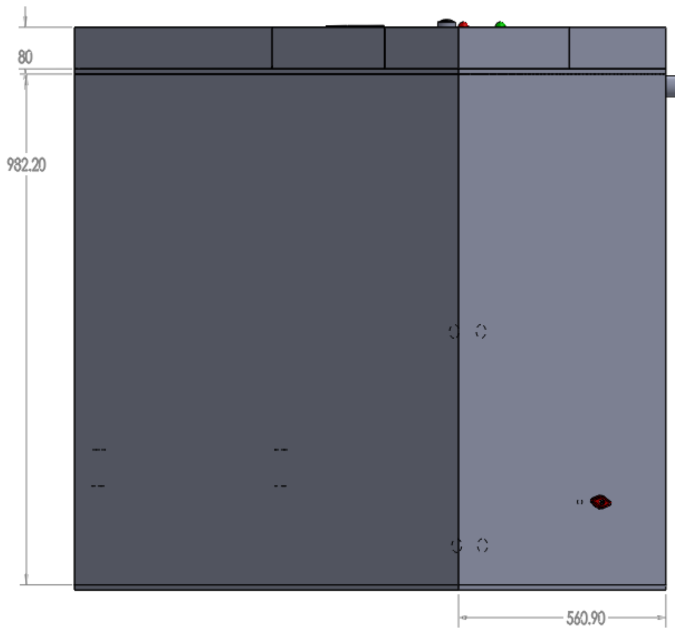

Fig. 2: 45^0 view of basic structure

2) Design the operation of the machine.

The operation of the machine is best be elaborate in flow chart. Fig. 3 shows the flow chart of operation of the machine. The flow chart start with supply of the machine is on. The green indicator will light on to indicate the machine is ready to sterilize. When the process running the indicator will turn to red and back to green when the process end.

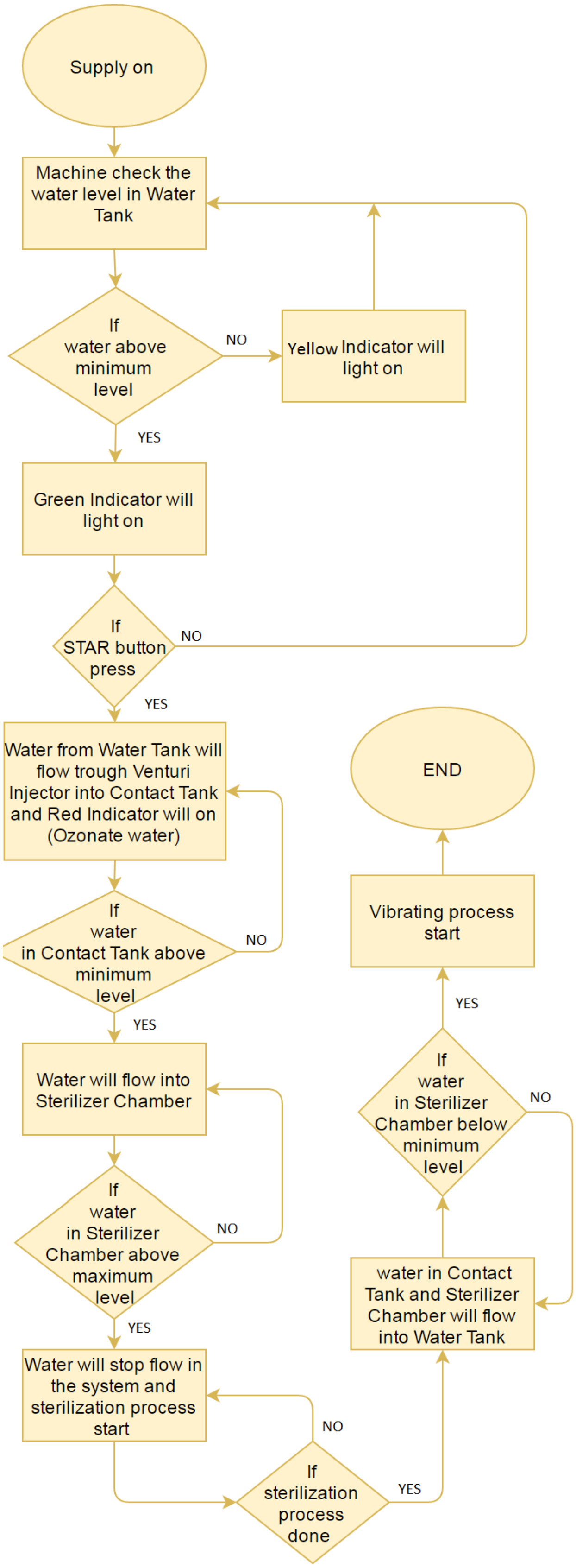

Fig. 3. Flow chart of operation.

B. Development Process

1) Determine component

a) Control Box

Consist of Arduino as microcontroller and relay to connect the equipment to power supply.

b) Ozone destructor

To destroy the remaining ozone gas in the system before releases into the air

c) Ozone generator

To generate ozone gas

d) Water tank

Storage of water in the system

e) Water valve

To control the flow of water in the system

f) Water pump

To control pressure of the water in the system

g) Air valve

To control the flow of ozone in the system

h) Venturi injector

To inject ozone gas into the water

i) Contact tank

Where the mixing of ozone and water occur

j) Vibration motor

To dry the surgical equipment after sterilization process

k) Sterilizer chamber

Where the ozonated water sterilize the surgical equipment. Consist of vibrating mechanism.

2) Design control system of the machine

This system include three system that is wiring system for electrical, water piping, and gas piping for ozone gas. Fig 4 shows block diagram of all three system. Blue line is for electrical wiring system, red line is gas piping, and black arrow is for water piping.

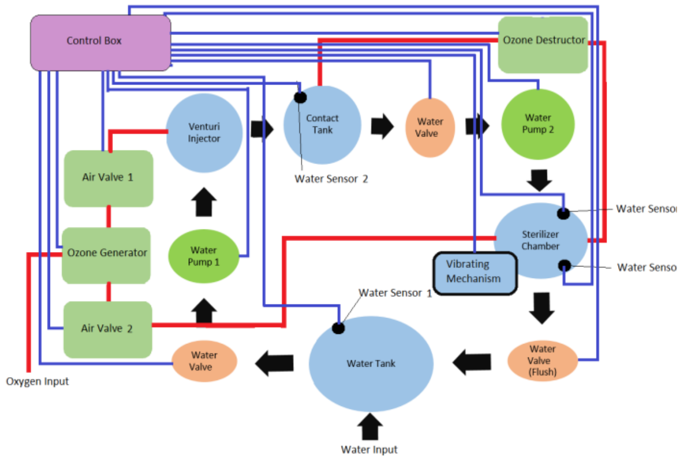

Fig. 4.Block diagram of complete system

3) Arranged component of the machine in the basic structure.

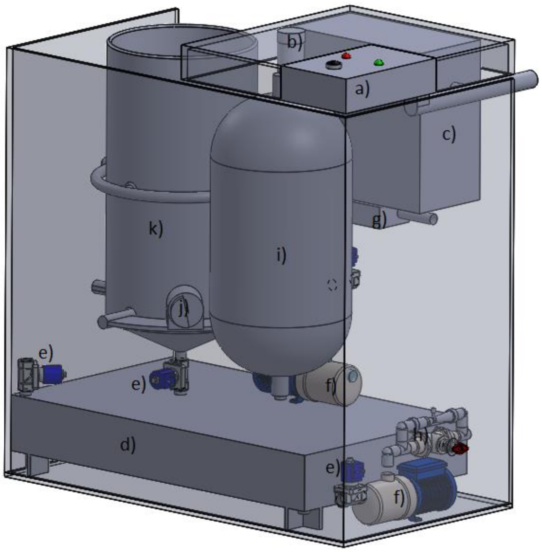

Fig. 5: Arrangement component of the machine in the basic structure

The arrangement of the component of the system without any piping or wiring to give clear vision of the arrangement is shows Fig. 5.

C. *Experimental Process*

The result of ozone concentration from the experiment was 24.85 mg/l when convert to ppm the value is 24.88ppm this reading is more than 800 mV in ORP value, this value is in range high concentration ozone and 800mV is requirement ORP level for water sterilization.

For this project system, the sterilizer process will use distilled water and ozone bubble will be produce continuously, then the concentration of ozone must be very high and more than enough to kill microorganism.

V. CONCLUSION

The project is relevant to the public's health, especially to the worker, which conducts the surgical sterilizer process. Otherwise, the project will increase the productivity and efficiency of the sterilizer process because of the ergonomic design. For the environmental impact, this project will reduce the usage of hazardous gas in sterilizer process. Finally, this project also do not harm the environment in any perspective.

REFERENCES

[1] H. Khan, "Study read," in Microbiology, Ramesh, 2015. [Online]. Available: http://www.studyread.com/what-is-sterilization-methods. Accessed: Dec. 20, 2016.

[2] H. Schein, "The Six steps of instrument Reprocessing - Henry Schein medical," 2016. [Online]. Available: http://www.henryschein.com/usen/OBGYN/ResourceCenter/Instrument ReprocessSixSteps.aspx. Accessed: Dec. 20, 2016.

[3] K. Kanemitsu et al., "A comparative study of ethylene oxide gas, hydrogen peroxide gas plasma, and low-temperature steam formaldehyde sterilization," Infection control and hospital epidemiology., vol. 26, no. 5, pp. 486–9, Jun. 2005. [Online]. Available: https://www.ncbi.nlm.nih.gov/pubmed/15954488. Accessed: Dec. 20, 2016.

[4] V. Camel and A.Bermond, 1998, the use of ozone and associated oxidation process in drinking water treatment, water research, Vol. 32, No. 11 pp.3208- 3222, Publisher 1998 Elsevier Science Ltd.

[5] Ballantine B, Morris T and Turner P ed., 1995 "General and applied Toxicology", abridged edition, The MacMillan Press Ltd.

[6] Charles, G.H., Jr., et al., Ozone Treatment, in Encyclopedia of Chemical Processing (Print Version). 2005, CRC Press. p. 1993-2001.

[7] Kim, J.-G., A.E. Yousef, and S. Dave, Application of ozone for enhancing the microbiological safety and quality of foods: a review. Journal of Food Protection®, 1999. 62(9): p. 1071-1087.

[8] Masten, S.J. and S.H. Davies, The use of ozonation to degrade organic contaminants in wastewaters. Environmental science & technology, 1994. 28(4): p. 180A-185A.

[9] S. Openshaw and E. Taylor, Ergonomics and Design A Reference Guide, G. Minder, W. Witherow, T. Long, and M. Ford, Eds. Muscatine, Iowa.: Allsteel Inc., 2006.

[10] Ergonomics: The Study of Work. New York: U.S. Department of Labor Occupational Safety and Health Administration, 2000.

Portable Electrocardiogram Monitoring Device with Android Based Analysis and Cloud Storage Facility

Lee Chee Fan
Faculty of Electrical Engineering
Universiti Teknologi Malaysia
Johor Bahru, Malaysia.
leecheefan0317@hotmail.com

Tan Chee Wei
Department of Electrical Power Engineering
Faculty of Electrical Engineering
Universiti Teknologi Malaysia
Johor Bahru, Malaysia.
cheewei@utm.my

***Abstract*—Cardiovascular diseases (CVDs) constitute 31% of global deaths making it the leading cause of death. Electrocardiogram (ECG) is the most readily available and immediate tool to diagnose CVDs. There are a lot of ECG devices available in the market but most of them are only ECG recorders where patients need to go to hospital so that ECG data can be retrieved for further diagnosis. Therefore, this project is to develop a portable ECG device that used Arduino Uno as the microcontroller which can transmit ECG data wirelessly to Android Smartphone via Bluetooth connection. Then an Android application is developed by using Android Studio to receive and record the raw ECG data, display them in real time graphical form and upload them to cloud storage so that any authorized person can access the ECG data online. Lastly a real time ECG analysis algorithm is developed by using MATLAB and implemented on the same Android application where the algorithm is capable to calculate the heart rate and detect two types of heart diseases (premature ventricle contraction and supra ventricle tachycardia). The algorithm is designed by using Pan and Tompkins method to detect R peaks of the ECG wave and other ECG parameters such as P, Q, S and T waves are extracted by local search around R peaks detected on the wavelet filtered ECG signal. Then diagnosis is done based on the heart rate and QRS complex duration. At the final stage, the algorithm developed is tested by using twelve ECG data downloaded from MIT-BIH Arrhythmia Database. It shows that the ECG analysis algorithm have a high value of accuracy up to 99.69% on R peaks detection of the ECG wave. Besides, the algorithm is able to detect PVC and SVT accurately as well where the sensitivity and specificity of PVC detection are 95.14% and 99.08% respectively while for SVT are 95.83% and 99.99% respectively.**

Keywords—Electrocardiogram (ECG); ECG parameters; Bluetooth; ECG analysis; heart rate; QRS complex duration

I. INTRODUCTION

Cardiovascular diseases (CVDs) constitute 31% of global deaths making it the leading cause of death [11]. It is very important to get public's heart check for an early disease detection as some of the CVDs are asymptomatic. Electrocardiogram (ECG) is a representation of the heart's electrical current activity in a graphical form [10]. It is the most readily available and immediate tool to diagnose CVDs [9]. ECG is an important component in cardiology as it gives an accurate diagnosis of the CVDs [7].

Holter is the most traditional portable ECG device that can record the patients' ECG for 24 to 48 hours outside hospital. However, Holter may not pick up the irregular heart rhythms for diagnosis during the period patients wear the Holter because symptoms happen unpredictably [5]. Holter only functions as a ECG recorder but no immediate action is taken to help patients when a major incident occurs during the monitoring period [3]. The patients need to report to hospital so that the ECG data recorded can be retrieved and then analyzed by their cardiologist [3]. Besides, wearing Holter device can cause physical discomfort as it is burdensome to patients because they have to bear its weight in few days over their neck or on a belt underneath their shirt with many dangling wires [2]. There are many other products in the market apart from Holter. Although some of them consist of personal computer (PC) software to analyze ECG data, most of them are only ECG recorders same as Holter and patients need to go to hospital for further diagnosis [4].

Therefore, a real time analysis on ECG signal is very important as immediate action can be taken if anything abnormal heart rhythm is detected. Besides, the real time analysis algorithm also can assist cardiologist to make better decisions because cardiology needs higher accuracy levels of diagnosing in comparison to some of the other medical areas [7].

This project is to develop a portable ECG device which can transmit ECG data wirelessly to the Android Smartphone via Bluetooth by using Arduino Uno as the microprocessor while Olimex ECG shield and ECG sensor are used to measure the ECG signal. At the same time, an Android application will be developed by using Android Studio to receive and record the raw ECG data, display them in real time graphical form for monitoring purpose and upload them to Google Drive cloud storage so that any authorized person (such as cardiologist) can access the ECG data online. Lastly, a real time ECG analysis algorithm will be developed by using MATLAB and implemented on the same Android application. Fig.1 shows the overall of the project descriptions.

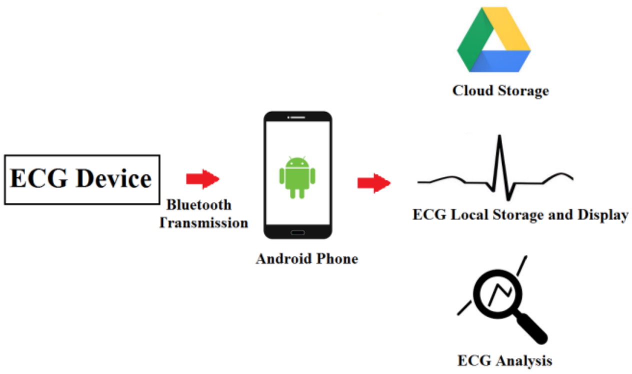

Fig. 1. The overall of the project descriptions.

II. LITERATURE REVIEW

ECG waveform is a representative of electricity activity from various regions of the heart where the electricity is produced due to the heart muscle cells in the atria and ventricles contract [10]. Fig. 2 shows the resultant ECG waveform where the isoelectric line indicates that no heart electrical activity occurs or the activity is too weak to measure [13].

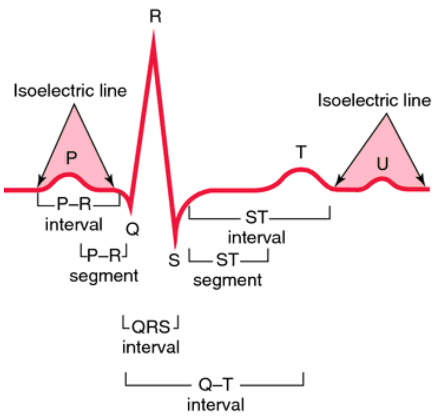

Fig. 2. Resultant ECG waveform.

Each portion of a heartbeat produces a different deflection on the ECG. These deflections are recorded as a series of positive and negative waves [13]. On a normal ECG, there are typically up to five visible waveforms which are P, Q, R, S and T wave as shown in Fig 2.

The ECG can be split into different segments and intervals which relate directly to phases of cardiac conduction [13]. The segments and intervals are PR interval, PR segment, QRS interval, QT interval, ST segment and RR interval as shown in Fig 2. Limits can then be set on these to diagnose deviations from normality [1].

8-steps method is suggested to analysis or interpret an ECG as follow [13]:

- The regularity of heart rhythm is analyzed in step one. Atrial rhythm is regular if intervals between P waves are consistent while ventricular rhythm is regular if RR intervals are consistent. Q waves of consecutive QRS complexes are used if the R waves are not present.
- In step two, the heart beating rate is analyzed. The number of QRS complexes in a period of 6 seconds are counted and this number is then multiplied by 10. The final value will be the heart beating rate because ten 6-seconds represent one minute. According to [1], rate below 60 indicates bradycardia and rate above 100 indicates tachycardia.
- In step three, the P wave is analyzed. A few characteristics of the P waves are considered in this analysis which are existence, configurations normality and similarity of the P waves.
- In step four, the duration and consistency of the PR interval are determined. The normal duration for PR interval is between 0.12 to 0.20 seconds [1].
- In step five, the duration, similarity and consistency of the QRS complex are determined. The normal duration for QRS complex is between 0.06 to 0.10 seconds [1].
- In step six, the T waves is analyzed. A few characteristics of the T waves are considered in this analysis which are existence, configurations normality, similarity and deflection of the T waves.
- In step seven, the duration of the QT interval is determined. The normal duration for QT interval is between 0.36 to 0.44 seconds [1].
- In the last step, ectopic beats, ST segment and other abnormalities are analyzed. After that, the types of arrhythmias can be determined by referring to the origin of the rhythm, rate characteristics and rhythm abnormalities.

III. PROJECT METHODOLOGY

There are three parts in this section namely hardware development, software development and ECG analysis algorithm development.

A. Hardware development

This section will discuss on development of portable ECG device with Bluetooth data transmission which can transmit data to the Android Smartphone. Fig. 3 shows the connections between components in the ECG device.

The main part of the device is Arduino Uno. Arduino Uno is used in this project as a microcontroller that process analog signal by using 10-bit analog-to-digital (ADC) conversion with digital range from 0 to 1023 [12]. This means that Arduino Uno receives the analog ECG data and convert them into digital form where the converted data is then available for further processing.

ECG sensor is connected to Olimex ECG shield and it is used to capture the ECG signal from patients. While Olimex ECG shield is connected to Arduino Uno to send it the captured ECG data. In order to send the ECG signal through Bluetooth data transmission to the Android Smartphone, a Bluetooth module known as BlueBee is used in this project where it is connected to Arduino Uno.

Rechargeable Li-ion 3.7V battery with 4800mAh capacity is used in this project as power supply to the ECG device. While, charger module which is known as TP4056 is used to recharge the battery. The battery is connected to a designed boost converter to boost up to voltage level of 5V before it is used to power up the Arduino Uno which is the input voltage required by Arduino Uno. Designed boost converter is used to replace the low efficiency of the built-in linear regulator of Arduino Uno by using LM2621 chip (a step-up DC-DC switching regulator). The boost converter circuit diagram is shown in Fig. 4.

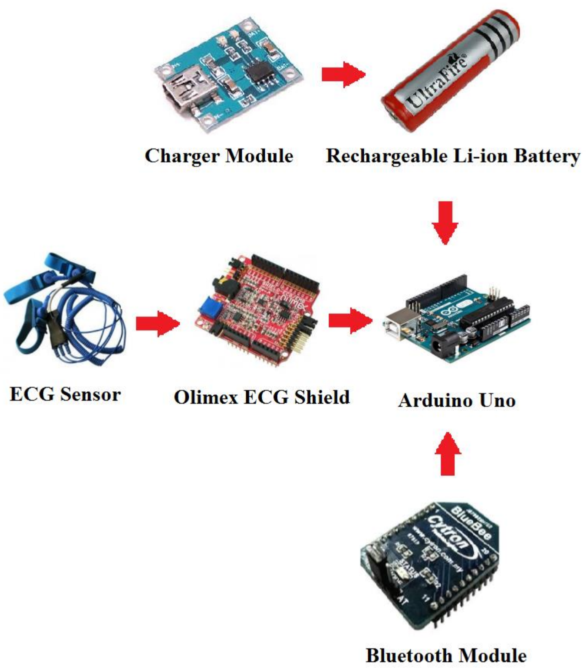

Fig. 3. Connections between components in the ECG device

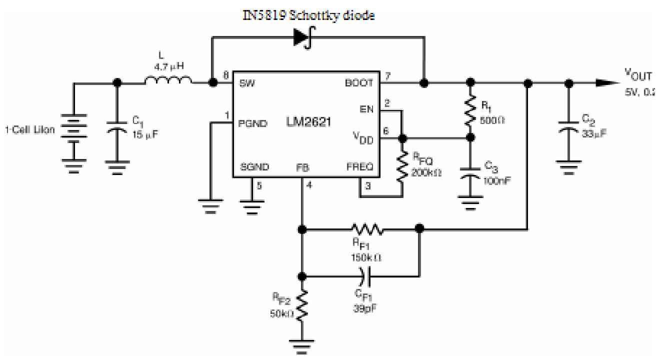

Fig. 4. Boost converter circuit diagram

B. Software development

This session focus on software development on Arduino Uno as well as Android application. Arduino Uno is programmed to receive the ECG data and control the data transmission between BlueBee and Smartphone. While Android application is developed to receive ECG data from Arduino, display ECG data in graphical form, upload ECG data to cloud storage and to implement ECG data analysis algorithm.

The flowchart of Arduino Uno software development is shown in Fig. 5 and it is divided by two parts as follow:

- First part of the programming is to receive the ECG data measured from ECG sensor. There are three analog inputs connecting to the Arduino Uno from the ECG sensor. The ECG data transmit to the Arduino through the analog inputs and converted into digital form.
- The second part of the programming is to transmit the digital form of ECG data to the Smartphone via Bluetooth connection. BlueBee is programmed to standby for a connection from a Smartphone and BlueBee is starting to transmit data if it is connected to a Smartphone and a transmitting command is detected. On the other hand, the data transmission is stopped if stopping command is detected by Arduino Uno.

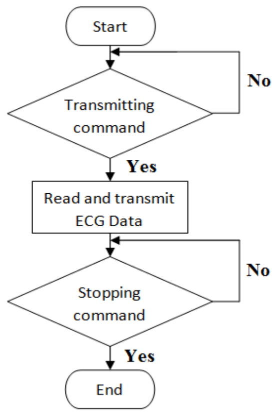

Fig. 5. Flowchart of Arduino Uno programming.

There are few parts in software development on Android application as follow:

- The first part of the programming is to receive ECG data from the Arduino Uno and record them on comma-separated values (CSV) files. The application will start to search for the BlueBee and connect to it after a connection command is given. After the connection between Arduino Uno and Smartphone is established via Bluetooth, a transmitting command is sent to Arduino Uno to order it to start the ECG data transmitting process. Then, the application will record the received ECG data on CSV files. On the other hand, a stopping command must send to Arduino Uno from the application in order to stop the transmitting process.
- The second part of the programming is to display the digital ECG data in real time graphical form. In this case, one of the Android charting library is used to draw the digital ECG data from the CSV files in real time graph. The library used is named as GraphView.
- The third part of the programming is to upload the ECG data in CSV files to cloud storage. In this case, an application known as FolderSync Lite is opened programmatically and it used to upload the files to Google Drive cloud storage.

- The last part of the programming is to implement the ECG data analysis algorithm into the Android application. The analysis algorithm is developed by using MATLAB where the algorithm is then converted to Java language before implementation of the algorithm into Android application.

C. *ECG Analysis Algorithm development*

In order to analysis ECG signal and diagnose heart diseases digitally, the characteristics or parameters of the ECG waveform (P wave, Q wave, R wave and so on) must be extracted. Therefore, an algorithm is developed by using MATLAB to extract those components from ECG waveform. The overall block diagram of the algorithm is shown in Fig. 6.

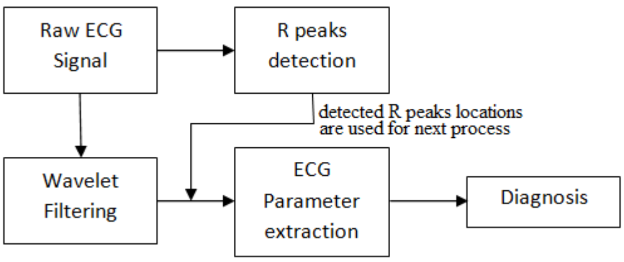

Fig. 6. Flowchart of Arduino Uno programming.

R peak is determined at the first place because it is the easiest component to be determined in ECG waveform since it has the highest amplitude. In this project, Pan and Tompkins algorithm is used for R peaks detection since it is easy to be implemented and its failed detection only up to 0.675% [8]. Basically the algorithm consists of a few ECG signal processing steps which are band-pass filtering, differentiation, squaring, moving window integration and thresholds adjustment [8]. The R peaks can be detected by regarding to analysis of the slopes, amplitude and width of the ECG signal [6].

After the R peak is determined, the other ECG parameters can be extracted by local search around the detected R peak. In this case, wavelet band-pass filtering is done on the raw ECG signal by using Daubechies wavelet and this filtered signal is then used for ECG parameters extraction. Wavelet filtering method is used to maintain the shape or position of the original signal so that parameters extraction can be done more accurately [14].

The local search interval for other ECG parameters are shown in Table I. The types of points (maximum or minimum point) of interest in searching are also indicated in the same table. The symbols definition from the search interval equations are as follow:

- i is indicate the numbering of the current parameter.
- RR is the interval between two consecutive R waves.
- Qon is the Q wave onset point.
- Q, R, S and T are corresponding to Q, R, S and T wave respectively.

After successfully extraction of ECG parameters, diagnosis can be one on those parameters to detect various types of heart diseases. In this project, algorithm is only developed to detect two types of heart diseases which are premature ventricle contraction (PVC) and supra ventricle tachycardia (SVT). Detection of these two diseases require information of heart beat rate per minute (BPM) and QRS complex duration where theses two components can be calculated from the previous ECG parameters. PVC is detected when heart rate is greater than or equal to 100 BPM and QRS complex duration is greater than or equal to 100 ms. While SVT is detected when heart rate is greater than or equal to 150 BPM and QRS complex duration is between 40 ms and 100 ms.

TABLE I. LOCAL SEARCH INTERVAL FOR ECG PARAMETERS

Parameters	Starting Point	End Point	Type
P wave	0.71 * RR(i) - 7	Qon(i) - 12	Maximum
Q wave	RR(i) - 25	RR(i) - 7	Minimum
Q onset	Q(i) - 12	Q(i) - 5	Maximum
S wave	R(i) + 6	RR(i) / 5 - 10	Minimum
T wave	S(i) + 15	RR(i) / 2	Maximum
T onset	0.7 * (T(i) - S(i))	T(i) - 10	minimum

IV. RESULT AND ANALYSIS

A. *Android Application*

An Android application is developed and it has following functions:

- Able to receive and record ECG signal wirelessly.
- Able to view the ECG signal in real time graph.
- Able to upload the ECG signal to Google Drive cloud storage.
- Able to perform analysis on ECG signal recorded.

Fig. 7(a) shows the main user interface of the application developed. The "BLUETOOTH CONNECTION" button as shown from the figure is used to established connection with ECG device. After Bluetooth connection is established, users can start to receive and record the ECG signal by click on the "START RECORDING" button.

The recorded ECG signal is stored as three CSV files (named as Data_1, Data_2 and Data_3) in folder named according to the date and time the users started the recording. Users can click on "DATA STORAGE" button to view the recorded files and the user interface after the button is clicked is shown in Fig. 7(b). In this user interface, users allow to perform two actions which are "CHART" and "UPLOAD". Users can click on the "CHART" button to view the real time graph of the ECG signals received as shown in Fig. 7(c). On the other hand, users also can upload the ECG files to Google Drive cloud storage by click on the "UPLOAD" button. Once the button is clicked, an Application which is known as FolderSync Lite (as shown in Fig. 7(d)) is opened and users are now available to perform actions to upload their desired files.

Besides, users also can perform analysis on ECG signal recorded by click on the "ECG ANALYSIS" button from main user interface. After the button is clicked, user interface for folder selection is came out as shown in Fig. 7(e). After users selected the desired folder for ECG analysis, ECG files to the corresponding folder is listed out as shown in Fig. 7(f). Now users can click on the "ANALYSIS" button to perform analysis on the corresponding ECG file and the analysis results can be view by click on the "RESULT" button. Fig. 7(g) shows a sample of analysis results that tell users the total heart beat detected, BPM, and number of PVC and SVT detected.

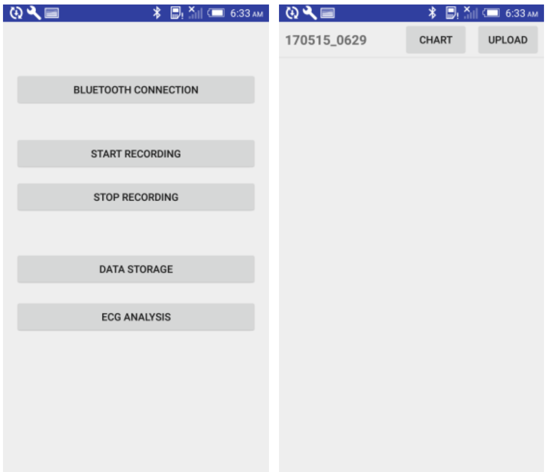

(a) (b)

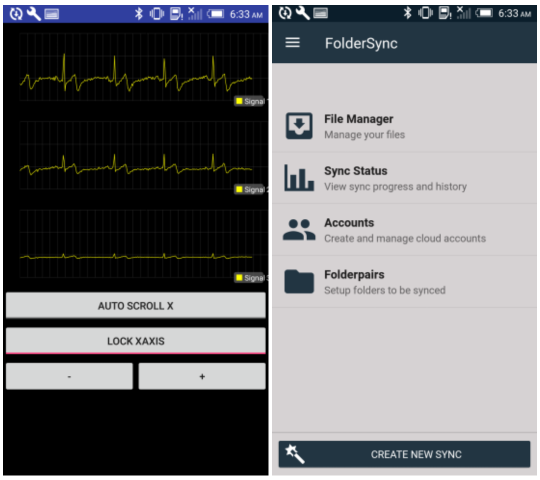

(c) (d)

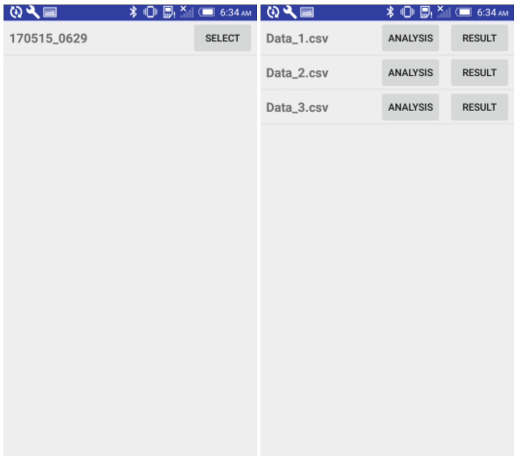

(e) (f)

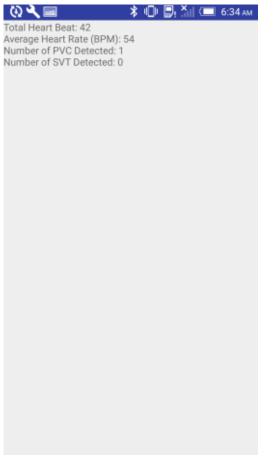

(g)

Fig. 7. (a) Main user interface. (b) Data storage user interface. (c) Graph view of ECG signal. (d) FolderSync Lite application. (e)User interface for folder selection for ECG analysis (f)User interface for file selection for ECG analysis (g) Result of ECG analysis.

B. ECG Analysis Algorithm

The accuracy of the algorithm developed is tested by using ECG data downloaded from MIT-BIH Arrhythmia Database. Twelve ECG data are selected from the database which are 102, 106, 109, 111, 116, 119, 121, 200, 208, 214, 221 and 223.

Firstly the R peaks detection or total number of heart beats detection accuracy is determined. The percentage of accuracy is calculated based on the ratio of the total number of R peaks detected by algorithm to total number of heart beats recorded in the MIT-BIH Arrhythmia Database. The average accuracy of the algorithm to detect R peaks on ECG signal is up 99.69% and the results is shown in Table II.

Lastly, the sensitivity and specificity of the algorithm developed to detect PVC and SVT are determined as well by using the following equations where TP, TN, FN and FP are stands for true positive, true negative, false negative and false positive respectively. The result is shown in Table III. The result shows that PVC detection average sensitivity and specificity are up to 95.14% and 99.08% respectively. Besides, it also shows that SVT detection average sensitivity and specificity are up to

TABLE III. SENSITIVITY AND SPECIFICITY OF PVC AND SVT DETECTION.

ECG Data	PVC Detection		SVT Detection	
	Sensitivity (%)	Specificity (%)	Sensitivity (%)	Specificity (%)
102	100.00	100.00	100.00	100.00
106	94.62	100.00	100.00	100.00
109	71.05	100.00	100.00	100.00
111	100.00	100.00	100.00	100.00
116	100.00	100.00	100.00	100.00
119	97.52	100.00	100.00	100.00
121	100.00	100.00	100.00	100.00
200	100.00	95.89	100.00	100.00
208	100.00	95.36	50.00	100.00
214	94.14	100.00	100.00	99.91
221	100.00	97.74	100.00	100.00
223	84.36	100.00	100.00	100.00
Average	95.14	99.08	95.83	99.99

95.83% and 99.99% respectively. High values of these sensitivity and specificity indicates that the algorithm developed is able to detect PVC and SVT in high accuracy.

TABLE II. R PEAKS OR TOTAL NUMBER OF HEART BEAT DETECTION ACCURACY.

ECG Data	R Peaks or Total Number of Heart Beat Detection Accuracy (%)
102	100.00
106	99.85
109	99.80
111	99.48
116	99.17
119	100.00
121	99.89
200	100.00
208	98.82
214	99.87
221	99.84
223	99.54
Average	99.69

$$Sensitivity = TP/(TP+FN) \quad (1)$$

$$\alpha + \beta = \chi. \quad (1)$$

(1)

$$Specificity = TN/(TN+FP) \quad (2)$$

$$\alpha + \beta = \chi. \quad (1)$$

(1)

V. CONCLUSION

ECG is a main tool to diagnose CVDs. This project is successfully developed a portable ECG device which can transmit ECG data wirelessly to the Android Smartphone via Bluetooth. At the same time, an Android application is developed to receive and record the raw ECG data, display them in real time graphical form for monitoring purpose and upload them to Google Drive cloud storage so that any authorized person (such as cardiologist) can access the ECG data online.

Lastly, a real time ECG analysis algorithm is also developed by using MATLAB and implemented on the same Android application. The ECG analysis algorithm have a high value of accuracy up to 99.69% on R peaks detection of the ECG wave. Besides, the algorithm is able to detect PVC and SVT accurately as well where the sensitivity and specificity of PVC detection are 95.14% and 99.08% respectively while for SVT are 95.83% and 99.99% respectively.

The real time analysis ability on ECG signal is very important as immediate action can be taken if anything abnormal heart rhythm is detected. Besides, the real time analysis algorithm also can assist cardiologist to make better decisions because cardiology needs higher accuracy levels of diagnosing in comparison to some of the other medical areas [7].

REFERENCES

[1] Becker, D. E. (2006). Fundamentals of Electrocardiography Interpretation. Anesthesia Progress, 53(2), 53-64.

[2] Kai, L., Zhang, X., Wang, Y., Suibiao, H., Ning, G., Wangyong, P., Chen, H. (2011). A system of portable ECG monitoring based on Bluetooth mobile phone. 2011 IEEE International Symposium on IT in Medicine and Education.

[3] Leijdekkers, P., & Gay, V. (2007). Personal Heart Monitoring System Using Smart Phones To Detect Life Threatening Arrhythmias.

[4] Lobodzinski, S. S., & Laks, M. M. (2012). New devices for very long-term ECG monitoring. Cardiology Journal, 19(2), 210-214.

[5] Mathur, N., Seutter, R., & Levine, G. N. (2014). Holter Monitors, Event Monitors, Ambulatory Monitors, and Implantable Loop Recorders. Cardiology Secrets, 60-67.

[6] Mohamed B., Besma K. & Abdennaceur K. (2007). Analysis and Parameter Extraction of P Wave Using Corellation Method. The International Arab Journal of Information Technology, Vol.6, No.1.

[7] Nallaperuma, D., & Lokuge, K. (2012). Cardiology Predictor: Cardiology Interpretations for Medical Diagnosis. Sri Lanka Journal of Bio-Medical Informatics, 2(4).

[8] Pan, J., & Tompkins, W. J. (1985). A real-time QRS detection alogarithm. IEEE.

[9] Rampal, L. (2016). The Medical Journal of Malaysia.

[10] Shade, B. R. (2013). Fast & easy ECGs: A self-paced learning program. New York, NY: McGraw-Hill.

[11] Soman, S., Kar, S. S., Satheesh, S., & Ramalingam, A. (2016). Cardiovascular Disease Risk Profiling Among First Degree Relatives of Coronary Artery Disease Patients Admitted in Cardiology Ward of JIPMER, Puducherry. Journal of Cardiovascular Disease Research, 7(3), 108-111.

[12] Wheat, D. (2011). Arduino Software. Arduino Internals, 89-97.

[13] Wolters K., Lippincott W. & W. (2011). interpretation made incredibly easy.

[14] Zahra G. (2015). Classification of ECG Signal by Using Wavelet Transform and SVM.

Operational Performance Monitoring of Photovoltaic System through IOT

Chua Hai Siang
Faculty of Electrical Engineering
Universiti Teknologi Malaysia
Johor Bahru, Malaysia.
haisiang.chua@gmail.com

Dr. Tan Chee Wei
Department of Electrical Power Engineering
Faculty of Electrical Engineering
Universiti Teknologi Malaysia
Johor Bahru, Malaysia.
cheewei@utm.my

***Abstract*—The increase in installation of small-scaled photovoltaic system has present the need to monitor the performance of the system. By taking advantage of the development of Internet of Things (IOT) in recent years, the monitoring system is built to be able to upload data to the Internet. The sensors used to collect the data are voltage sensors, current sensors, temperature sensor, and irradiance sensor. The voltage sensor is built using a voltage divider circuit while the ACS712 Hall Effect sensor is chosen as the current sensor. The temperature sensor chosen is the DS18B20 temperature sensor. The irradiance sensor is built using three SFH203P photodiodes. Raspberry Pi is used as the microcomputer of the monitoring system. ADS1115 Analog-to-Digital Converter (ADC) is used to convert analog input to digital values. The Internet of Things platform used in this system is Ubidots, which also have built is notification system to alert users. The IOT monitoring system has been built and successfully implemented. It is able to collect real time data from the panels and upload it to Ubidots for display.**

Keywords—photovoltaic; monitoring system; Raspberry Pi; Internet of Thing; Ubidots

I. INTRODUCTION

Small-scaled residential electrical power generation system using solar photovoltaic (PV) systems has become a tempting option for many households [1]. While this can be partly due to the technological advancement that have reduced the cost of PV system, various programs such as the Feed-in Tariffs (FIT) are also spurring the growth of residential photovoltaic generation system. Under Feed-in Tariff, electric utilities or grid companies are obliged to purchase all PV-generated electricity that a household produces at a set price for a given number of years [1].

The Feed-in Tariff has attracted many homeowners to invest their money in photovoltaic generation system. The capital investment for a photovoltaic system is not cheap, and it will take some time before a return of investment is obtained. Since PV system is so expensive, it should be obvious to protect the system from any sort of failures and permanent damages. Hence, a monitoring system for the PV system is proposed to counter this problem.

The Internet of Things (IOT) is a paradigm shift that affects the way human interact with everyday objects. The basic idea of this concept is the pervasive presence around us of a variety of things or objects, such as Radio Frequency Identification (RFID) tags, sensors, actuators, and mobile phones, which, through unique addressing schemes, are able to interact with each other and cooperate with their neighbors to reach common goals [2]. For IOT to take the desired shape of global connectivity, each and every small object in the world needs to be connected in sensory and intelligent manner [3].

To take advantage of the connectivity and benefits of IOT, the monitoring system of the solar panel should be connected to the Internet. Internet connectivity will boost the functionality of the system. Furthermore, since the data are uploaded to the Internet, it will be accessible from anywhere and anytime as long as there is Internet connection.

Monitoring of PV plants to quantify the energy yield and detect failures has assumed a relevant role in recent years [4]. Various monitoring solutions are already present, however, the system circuits are quite complex and often require a cumbersome installation [4]. Some system require additional cables for data transmission [5], while others require a power stage and Power Line Communication (PLC) [6], which reduce the system performance . These solutions however, does not allow for monitoring of individual panels. According to [7], the panels contribute up to 15% of the total failure.

Furthermore, current alternatives of monitoring system are for large scale application such as a PV farm. Since the numbers of residential PV system is growing, there is a need to monitor each of their individual output. The lack of a remotely operated monitoring system will hinder early detection of fault by homeowners as they lack the required knowledge. Internet connectivity is required for the measured performance parameters to be made available anywhere and anytime. The system must also be low cost as to not add on to the already costly capital investment.

II. LITERATUE REVIEW

A. Temperature and irradiance effect

Cell temperature and solar irradiance have a pronounce effect on the performance of photovoltaic cells as they relate to the system efficiency and output energy. Temperature effects are the inherent characteristic of silicon-based cells [8]. They will have a higher voltage when the temperature decreases and the voltage will drop as the temperature increases. At the same photocurrent I_{PH}, the output power will decrease due to the lower voltage.

The temperature increase will cause the band gap of the semiconductor to shrink, therefore decreasing the open circuit voltage V_{OC} as seen in the diode factor q/kT. As temperature increases, the band gap of the intrinsic semiconductor shrinks, meaning more incident energy is absorbed because a greater percentage of the incident light has enough energy to raise charge carriers from the valence band to the conductance band. A larger photocurrent results; therefore I_{SC} increases. This effect would raise the theoretical maximum power given by (1).

$$P_{max} = I_{SC} \times V_{OC} \tag{1}$$

The effect of temperature and irradiance on cell characteristic is shown in Fig. 1. From Fig. 1. (a), the increase of irradiance causes the open circuit voltage to increase logarithmically, while the short circuit current increases linearly. The temperature has a major effect on the open circuit voltage, which decreases linearly with the cell temperature, causing the cell efficiency to drop [8]. Short circuit current, on the other hand only increases slightly as the temperature increases.

B. *Wireless photovoltaic monitoring system*

In [9], a design methodology for in-situ solar panel monitoring system based on wired and wireless sensor network technologies is proposed. The system utilized low power wireless sensor nodes to transmit performance parameters to a remote coordinator. The characterization of each individual PV panel is carried out. The I-V data are collected and then transmitted wirelessly to the park coordinator. In addition to that, the temperature and humidity of the panel is also measured. The irradiance level is also measured using a photodiode.

The methodology proposed in [9] combines computation and communication technologies to determine the performance of PV panels. The paper demonstrated the possibility of monitoring individual panels to determine their performance. The data is also transmitted wirelessly and viewed through a web application.

In another paper, a system to track and monitor the performance of the solar panel is developed. The system can set the maximum power point of the solar panels, monitor its instantaneous power output, and transmit and receive data and commands from an operator at a remote location using wireless medium [10]. In addition, the system is also able to alert the homeowners in the event of any operational problem, such as panel shading due to fallen tree branches.

The system consists of various sensors, the sensor input reader, the load control unit and the wireless communication unit. After the measurement data are collected by the remote units, they are transferred wirelessly via Zigbee to the coordinator unit located inside the house. The coordinator then transferred the data via a USB to serial cable to the computer [10]. All the collected data are stored in the computer.

III. System Design

The proposed system consists of a microcontroller collecting data from sensors and sending them to the server. Four sensors are used to measure the operational parameters of the Photovoltaic (PV) panel. The sensors used are voltage sensor, current sensor, temperature sensor, and irradiance sensor. The system is used to monitor the performance of a standalone PV system. The microcomputer is powered by the PV system through a buck converter.

A. *Sensors*

The current sensor and the temperature sensor are bought and can be used right out of the box without further hardware design. The current sensor used is the ACS712 Hall Effect sensor while the temperature sensor used is the DS18B20. On the other hand, the voltage sensor is designed and built using a voltage divider configuration.

$\alpha + \beta = \chi$. (1) (1)

A 100Mohm and a 100kohm resistor are used to form the voltage divider. A large resistance is chosen to reduce the loading effect of the sensor. Usually, irradiance is measured using a pyranometer. However, a pyranometer is way too expensive for the budget of this system. An alternative way of measuring irradiance is employed by using the SFH203P photodiode. Three photodiode are connected in series to increase the voltage output of the sensor. The ACS712 is a Hall Effect sensor module which produces voltage levels at its output corresponding to the measured current. A voltage divider circuit is also used at its output to limit the voltage to suitable level for the system.

The irradiance sensor and temperature sensor are mounted externally while the voltage sensor and current sensor are integrated into the circuit of the PV system. The irradiance sensor is placed next to the PV panel. The temperature measured is the panel temperature not the ambient temperature, hence the sensor is placed at the back in contact with the panel. The voltage sensor is connected in parallel with the output of the PV panel while the current sensor is connected in series as shown in Fig. 1.

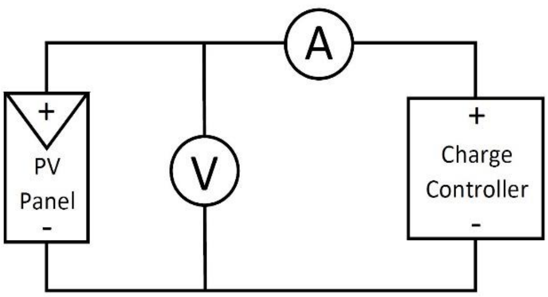

Fig. 1. Voltage sensor and current sensor connected to the PV system.

B. *Data Acquisition*

The Raspberry Pi is chosen as the microcomputer of the system. It has more than enough computing power to cater to the needs of the whole system. Furthermore, it has a built in Wi-Fi and ethernet port that enabled it to connect to the Internet. However, the Raspberry Pi does not have analog input

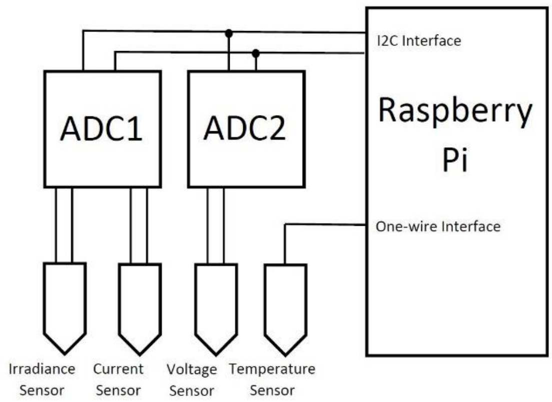

Fig. 2. Block diagram for the data acquisition interface.

built in. Due to that, the ADS1115 Analog to Digital Converter (ADC) is used. It provides high resolution conversion as it uses 16-bit conversion. The ADS1115 can accept four single ended inputs or two differential inputs. For this project, the differential input is used as it is less susceptible to noise. Since there are three inputs from the sensors, two of the ADC are required. The output of the temperature sensor does not require conversion as it produces digital values.

The ADS1115 communicate with the Raspberry Pi through the Inter-Integrated Circuit, or commonly known as I2C interface. Both ADC connects to the same bus and is selected through an addressing scheme. The temperature sensor is connected to the Raspberry Pi though the One-Wire interface. As the name suggests, only a single wire is required. The block diagram of the data acquisition interface is shown in Fig. 2.

C. *Support System*

An SSD1306 OLED (Organic Light Emitting Diode) display and two pushbuttons are also included as support components for the system. The OLED display provides an easy way for the user to view the status of the system. On the other hand, the pushbuttons are used to change the mode of the display and to start or stop the program. The mode of the display is shown in Table I.

D. *IOT Platform*

The IOT platform selected for the monitoring system is Ubidots. It is a convenient platform to host the collected data and display them in real time. First, an account is created. Next, a device is created with the name 'Raspberry PV'. Under the device, the variables are created. The variables are power, voltage, current, temperature, and irradiance. Data uploaded from the Raspberry Pi are stored in these variables. Ubidots provide a useful feature called 'Dashboard' to display all the variables in real time, which is set up by selecting the variable to display.

To upload data from the Raspberry Pi to Ubidots, the Application Programming Interface (API) key and the variable id are required. The API key is unique to every user, while the variable key is unique to each variable. Using the API key and variable id, the Raspberry Pi is able to identify which user and which variable to upload data to. Both of them are generated automatically by Ubidots.

TABLE I. DISPLAY MODE

Mode	Display
0	All parameters
1	Power
2	Voltage
3	Current
4	Temperature
5	Irradiance
6	Raspberry Pi temperature

E. *Programming the Raspberry Pi*

The program language used in Raspberry Pi is written in Python. First, the program is initialized by declaring all the relevant libraries, such the ADS1115 library and the SSD1306 library. The main program starts by reading data from the sensors through the ADC. The data from the temperature sensor however are taken directly. Next, the collected data are processed to convert them from digital values back into analog form. Equation (2) is used for the conversion.

$$V_A = V_D \times S \times R_{vd} \times k \quad (2)$$

Where V_A is the analog value, V_D is the digital value, S is the sensitivity of the ADC expressed in mV/count, R_{vd} is the voltage divider ratio of the sensor and k is the conversion factor. The sensitivity, S for the 16 bit ADS1115 is 125mV/count. The voltage divider ratio, R_{vd} is 11 for voltage sensor, 2 for current sensor, and 1 for irradiance sensor. The conversion factor, k is only applicable for the current sensor which is 185mV/A.

After the data are processed, they will be displayed on the OLED display. A conditional branch will check if 5 minutes have passed. If yes, the data will be uploaded to the server. Conversely if the condition is not fulfilled, the program will continue to read data from the sensors and displaying them on the OLED display. The flowchart of the whole program is shown in Fig.3.

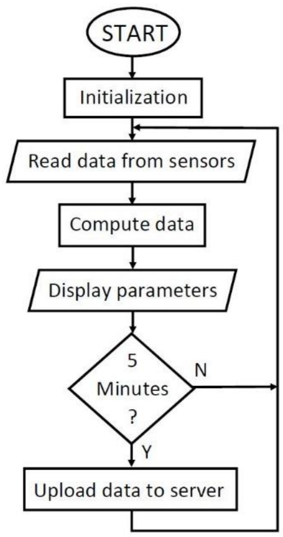

Fig. 3. Flowchart for the program

F. Buck Converter

The buck converter is used to step down the PV system voltage, which is 12V to 5V. It is used to supply power to Raspberry Pi. The design is centered on the LM2596, which could produce switching action at 150kHz. The schematic diagram of the buck converter is shown in Fig. 5. A 1N5822 Schottky diode is used as it is rated at 3A, which is the rated current of the LM2596. Since the input voltage and output voltage are known, the duty cycle calculated is 0.42. Using the frequency and duty cycle, the inductance can be calculated. The L_{min} is found out to be 10µH. L is chosen to be 10 times greater than L_{min}, hence 100µH is chosen as the inductor value. Following that, the C_{out} can be found. By allowing a ripple factor of 1%, the C_{out} is found out to be 3.2µF. A capacitor with a larger capacitance, 220µF is chosen.

Lastly, the C_{in} is chosen to be an arbitralily large value at 680µF as the capacitance of C_{in} is less important than its voltage rating. The voltage rating must be more than the input voltage. The voltage rating of C_{in} is 25V. The schematic diagram of the buck converter is shown in Fig. 5.

IV. Results and Discussion

After the design have been verified through testing of each part of the system, the circuits are transferred to the Printed Circuit Board (PCB). The ADCs, voltage sensor, and current sensor are placed on the PCB called the main board. The main board also have connectors to connect to components that are not on the board such as the temperature sensor and the irradiance sensor. The buck converter is etched on a separate board as shown in Fig. 4. Fig. 4. Shows the completed system with the main board, Raspberry Pi, buck converter, and OLED display visible.

The completed monitoring system is used to monitor a 20W PV panel. The panel is connected to the charge controller and battery. The Raspberry Pi is connected as load to the charge controller. During a 30 minutes test, the monitoring system is able collect performance parameters of the PV panel. The parameters are then uploaded to Ubidots through Internet connection. The system worked well as intended.

All the collected data, the voltage, current, temperature, and irradiance are displayed on the Dashboard page of Ubidots.

Fig. 4. Completed photovoltaic monitoring system

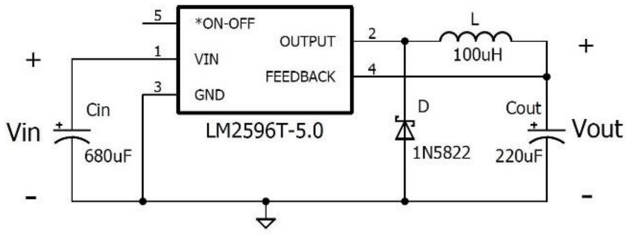

Fig. 5. Schematic diagram of the buck converter

The power and temperature of Raspberry Pi are also displayed on the Dashboard. The power is calculated using the voltage and the current data. The temperature of the Raspberry Pi is obtained from built in sensor in the microcomputer itself. Once the monitoring system is running, real time data will be updated and displayed on the Dashboard page as shown in Fig. 6 to Fig. 10.

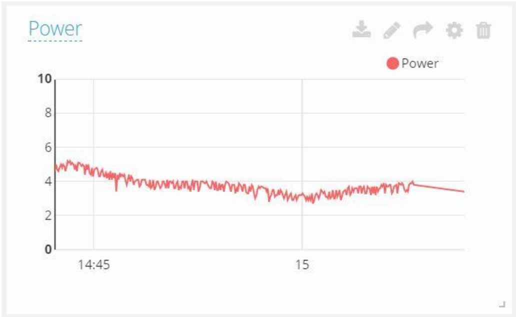

Fig. 6. Dashboard page of the Ubidots showing power data

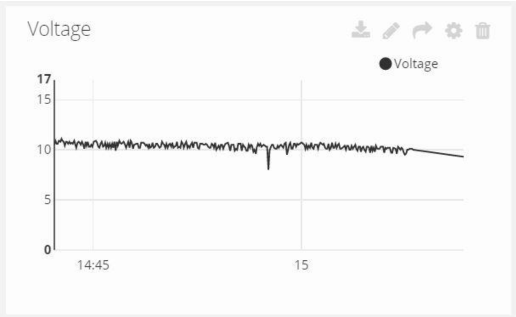

Fig. 7. Dashboard page of the Ubidots showing voltage data

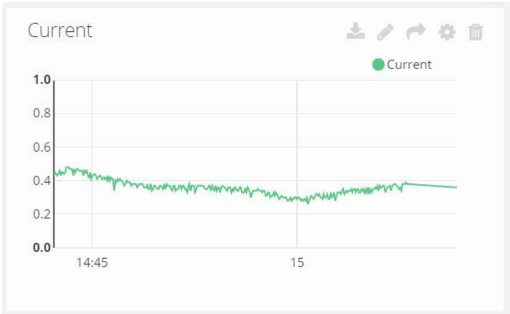

Fig. 8. Dashboard page of the Ubidots showing current data

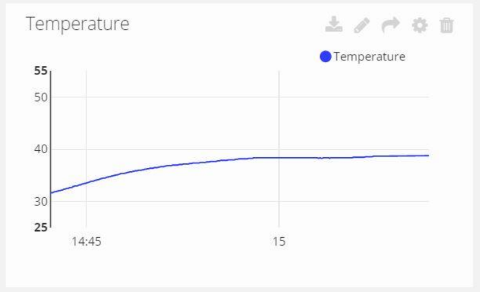

Fig. 9. Dashboard page of the Ubidots showing panel temperature data

Fig. 10. Dashboard page of the Ubidots showing irradiance data

Based on the collected data, it is clear that the voltage output of the PV panel is affected by the device temperature. As temperature rises, the voltage drops slightly as shown in figure. The output current of the PV panel on the other hand, is affected by the irradiance. The higher the irradiance, the higher is the output current. The dependency of current on irradiance can be seen in Fig. 11, where the waveform of the current follows the irradiance. As the irradiance decreases, the current decreases as well. Furthermore, the dip in the irradiance also translate onto the current dip.

The alert system in Ubidots is called 'Events'. An event must be first setup by the user. The notification to alert users of abnormal parameters is set up in the Event page in Ubidots as shown in Fig 12. In this case, if the power output of the PV panel is less than 0.5W, the system will automatically generate a Telegram message to the specified user. The screenshot of the received message is shown in Fig. 13

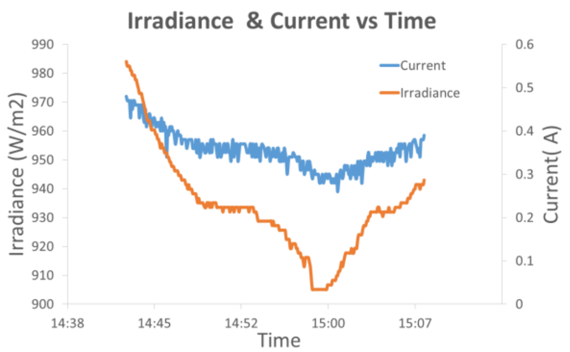

Fig. 11. Graph showing dependence of current on irradiance

Fig. 12. Event page of the Ubidots

Fig. 13. Telegram alert received on a mobile phone

CONCLUSION

The emergence of IOT in recent years have changed the interactions between users and devices. By taking advantage of the IOT platform available, an IOT monitoring system of the PV panel is designed and implemented. A notification system is also included in the system whereby a Telegram message will be sent to user in the event of abnormalities in the measurements. This is an indicator that the PV panel is not performing as it should.

With the exception of the irradiance sensor, all the sensors are readily available in the market and can be incorporated into the system with minimal additional components. Photodiodes are used to replace pyranometer as irradiance sensor. The resulting measurements are comparable to that of the pyranometer.

REFERENCES

[1] Y. Yamamoto, "Pricing electricity from residential photovoltaic systems: A comparison of feed-in tariffs, net metering, and net purchase and sale," Solar Energy, vol. 86, pp. 2678-2685, 2012.

[2] D. Giusto, A. Iera, G. Morabito, and L. Atzori, "The Internet of Things," ed: Springer-Verlag, 2010.

[3] S. Agrawal and M. L. Das, "Internet of Things – A Paradigm Shift of Future Internet Applications."

[4] M. Gargiulo, P. Guerriero, S. Daliento, A. Irace, V. d'Alessandro, M. Crisci, et al., "A novel wireless self-powered microcontroller-based monitoring circuit for photovoltaic panels in grid-connected systems," in SPEEDAM 2010, 2010, pp. 164-168.

[5] N. Forero, J. Hernández, and G. Gordillo, "Development of a monitoring system for a PV solar plant," Energy Conversion and Management, vol. 47, pp. 2329-2336, 2006.

[6] E. Roman, R. Alonso, P. Ibañez, S. Elorduizapatarietxe, and D. Goitia, "Intelligent PV module for grid-connected PV systems," IEEE Transactions on Industrial electronics, vol. 53, pp. 1066-1073, 2006.

[7] U. Jahn and W. Nasse, "Operational performance of grid-connected PV systems on buildings in Germany," Progress in Photovoltaics: Research and applications, vol. 12, pp. 441-448, 2004.

[8] M. E. Meral and F. Dinçer, "A review of the factors affecting operation and efficiency of photovoltaic based electricity generation systems," Renewable and Sustainable Energy Reviews, vol. 15, pp. 2176-2184, 2011.

[9] P. Papageorgas, D. Piromalis, K. Antonakoglou, G. Vokas, D. Tseles, and K. G. Arvanitis, "Smart Solar Panels: In-situ Monitoring of Photovoltaic Panels based on Wired and Wireless Sensor Networks," *Energy Procedia*, vol. 36, pp. 535-545, 2013.

[10] C. Ranhotigamage and S. C. Mukhopadhyay, "Field Trials and Performance Monitoring of Distributed Solar Panels Using a Low-Cost Wireless Sensors Network for Domestic Applications," *IEEE Sensors Journal*, vol. 11, pp. 2583-2590, 2011.

Effect of Non-Idealistic Components on Boost-Inverter

Nur Addinni Binti Mohamad Azhar
Faculty of Electrical Engineering
Universiti Teknologi Malaysia
Johor Bahru, Malaysia.
addinniazhar@gmail.com

Dr. Shahrin Bin Md. Ayob
Department of Electrical Power
Faculty of Electrical Engineering
Universiti Teknologi Malaysia
Johor Bahru, Malaysia.
shahrin@fke.utm.my

***Abstract*— Boost-Inverter is an integrated circuit that have been widely used to convert small DC input obtained from battery or renewable energy such as Photovoltaic (PV) system or even DC source into higher AC output. In theory, most of power electronic circuits and applications are assumed to be ideal for a simple understanding. However, when applied it in practical, there are many things that need to be consider. Each electrical circuit may encounter with the unavoidable existence of parasitic elements due to magnetic field created by flow of current in the circuit. This paper represents the analysis of output voltage and current of boost-inverter with the presence of parasitic elements. The design and simulations of the circuit are done by using MATLAB Simulink. The parasitic elements have been placed in series with inductor in boost converter circuit and in series connected between boost converter and inverter circuit. The both parasitic elements are varying to compare the output voltage and current for each parameter. The performance of non-ideal boost-inverter is likely reduced compared to ideal boost-inverter. The results obtained are different between the changes of parasitic resistance (RESR) and changes of parasitic inductance, (LS).**

Keywords—boost converter; inverter; parasitic elements; boost-inverter; equivalent series resistance (ESR)

I. INTRODUCTION

A power converter that converts direct current (DC) to alternating current (AC) is called inverter. Boost converter is a DC-DC power converter that is used to have a larger output from a small input. Boost-inverter is integrated circuits between boost converter and inverter where it is function to produce a larger output of AC from a small DC input. In theory, for understanding of these power converters, the presence of non-idealistic components such as stray inductance or parasitic inductance are usually is neglected. The operations of the power converters are assumed to be in ideal cases.

Parasitic inductance or stray inductance is an unintended and unwanted inductance in a circuit which happened because of magnetic fields that are created from the flow of current in any wires or components leads. [1] These stray inductances are always present and it can interrupt the flow of current in a circuit. [2] The stray inductance should be as low as possible where it can be avoided from affecting the efficiency of power electronic devices. The existence of these stray inductances, there might be some effect occurred in the circuit. In this project, the focus is to identify the effects that might happen with the existence of these non-idealistic components in the circuit.

II. LITERATURE REVIEW

A. Parasitic Elements

Stray inductance or parasitic inductance also known as source inductance is mainly come from printed circuit board (PCB) or device package. The existence of magnetic field inside the PCB produced an unwanted or unintended inductance that may cause severe effect in many performances. The performances that may include are the switching performance, the flow of current in the circuit and the output value of a circuit. [1, 2, 3, 9]

In the perspective of switching performance, this parasitic inductance may cause EMI noise, overshooting of signal and energy loss in switching. The effects shown are from the impact of MOSFET switching characteristics. Switching in a circuit involved frequency and with the increasing of the switching frequency, the effect on the performance of the system will increase. [12] However, some study shows that the effects of these parasitic elements may improve model accuracy such as modeling of DC-DC power converter, the efficiency study and the dynamic performance of the system though it resulting in nonlinear voltage and current waveforms.

In practical DC-DC converter, two major of parasitic inductance may be found as shown in Figure 1. There are the source power current path and gate drive loop from the drain which sharing with the inductance in the circuit are also known as common source inductance, Ls, and high frequency power loop inductance, L_{LOOP}, that the positive terminal of the input capacitance to the power commutation loop and comprised of the parasitic inductance.

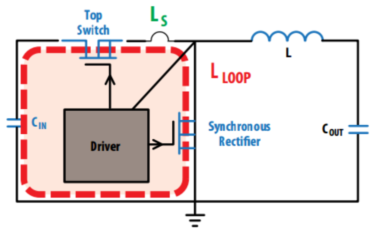

Fig. 1.The DC-DC converter with parasitic inductance.

There are methods to reduce an effect of parasitic inductances in a circuit. Some of the methods is the parasitic inductances need to be kept in small value so that it can improve a long term reliability. In order to calculate the value of the parasitic inductance, two techniques have been used in the past which is the impedance measurement where it is more simple and straightforward and the time domain reflectometry (TDR) measurement where this method requires software, complicated experimental measurements and special hardware (TDR/sampling head). [11]

III. SIMULATION DESIGN

For the early stage of this project, an ideal boost converter and inverter are designed by using MATLAB Simulink. Both designed circuits are then integrated so that it can be boost-inverter circuit as it required in the project. The exact parameters of each component for both boost converter and inverter are clarifying before simulated to achieve the objectives of this project.

From the ideal boost-inverter circuit, a non-ideal circuit of boost-inverter is designed by adding parasitic elements in the circuit. Similar to the ideal circuit, the non-ideal boost-inverter exact parameters of each component need to be clarified before simulated it. Then, both output results from ideal and non-ideal boost-inverter will be analyzed. Figure 3.1 shows the project flow for the whole project.

In this simulation, an ideal boost-inverter circuit is designed by integrate the boost converter circuit and unipolar PWM inverter circuit. As for the non-ideal boost-inverter circuit, there is addition of parasitic elements into the ideal boost-inverter which is RESR and LS. The parameters are followed by the circuits; boost converter and inverter, before there been integrate. Figure 2 shows the circuit of an ideal boost-inverter circuit and non-ideal boost-inverter for Figure 3.

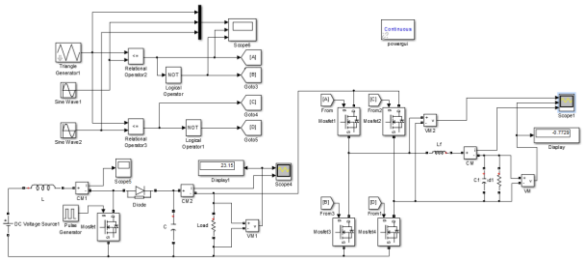

Fig. 2. *The circuit of ideal Boost-Inverter.*

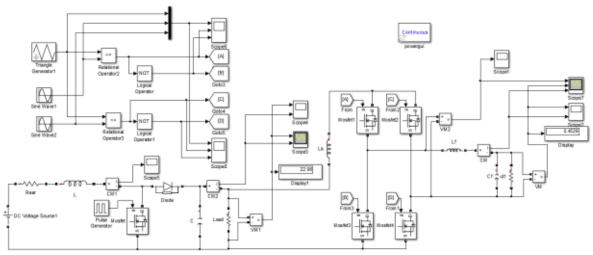

Fig. 3. *The circuit of non-ideal Boost-Inverter.*

B. Boost Converter

Boost converter is used to boost a low DC input to higher DC output. The output of boost converter will be the input of inverter circuit. The required parameters for boost converter is calculated by using Equation (1) until (4) and the information in Table 1.

$$D = 1 - \frac{V_{in}}{V_{out}} \quad (1)$$

$$R = \frac{{V_{out}}^2}{V_{in} I_{in}} \quad (2)$$

$$L_{min} = \frac{D(1-D)^2 R}{2f} \quad (3)$$

$$C = \frac{D}{R\frac{\Delta V}{\Delta V_{out}} f} \quad (4)$$

TABLE I. PARAMETERS FOR BOOST CONVERTER

Input Voltage, V_i	12V
Switching frequency, f	30kHz
Duty Cycle, D	0.5
Resistance, R	57.6Ω
Inductor, L	150µH
Capacitor, C	57.87µF

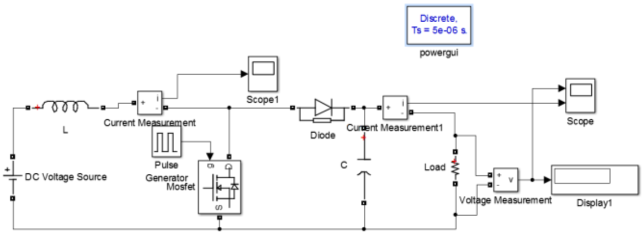

Fig. 4. *The circuit of Boost-Inverter.*

C. Single Phase of Unipolar PWM Inverter

For the inverter circuit, full bridge inverter is used for this project with unipolar switching PWM for switching signal generator. Figure 5 shows the circuit of full bridge inverter circuit. The ratio of amplitude modulation, ma is set to be 0.9. The frequency reference, fsine and the frequency carrier, ftri are 50 Hz and 10 kHz respectively. The load apply to the inverter is 100Ω.

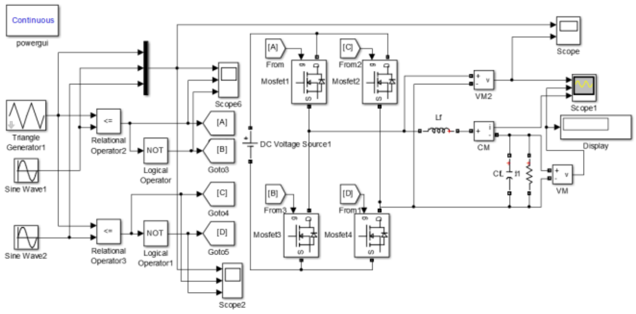

Fig. 5. *The circuit of Inverter.*

D. Filter Circuit

The filter circuit is constructing to filter the pulse width modulation (PWM) so that it becomes sinusoidal for the overall output. The filter used is LC filter and been calculated by using the Equation (5). The cutoff frequency has been chosen which is 2 kHz. The capacitor and inductor obtained from the calculations are C = 0.563 µF and L = 11.25 mH.

$$f = \frac{1}{2\pi\sqrt{LC}} \tag{5}$$

IV. RESULTS AND DISCUSSIONS

The results and discussions from the simulation will be shown in this chapter. There are results from simulations of boost converter, inverter and boost-inverter circuit with ideal and non-ideal components. There are also the analysis and discussions of the effects for non-idealistic components in boost-inverter.

A. Boost Converter

The results obtained for output voltage and current of boost converter is 23.78V and 513.51mA. The results are almost similar to the calculation. The ripple of the output voltage is almost unseen. Although there are some overshoot from the early few seconds, but it quickly become constant. The Figure 6 shows the output voltage of boost converter.

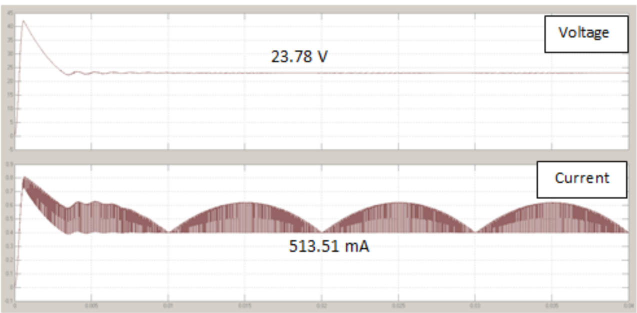

Fig. 6. The output voltage and current of boost converter.

B. Single Phase Unipolar PWM Inverter

From the designed inverter circuit, the input voltage is assumed to be 24 V before it integrate with boost converter circuit since the boost converter produced 23.78 V for the output voltage. The output voltage and current of PWM are shown in Figure 7. The output voltage obtained is about ± 24 V with the amplitude modulation, ma = 0.9.

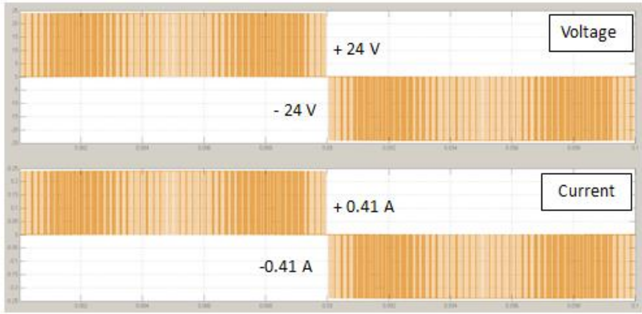

Fig. 7. The output voltage and current of inverter.

C. Ideal Boost-Inverter

The integrated circuit, boost-inverter has result differently from the individually simulation. The parameter of each component from boost converter and inverter circuit is still the same when it is integrate. Figure 8 shows the output voltage and current of the ideal boost-inverter after the filter circuit. The output voltage and current obtained from this circuit are 21.82V and 218.6mA.

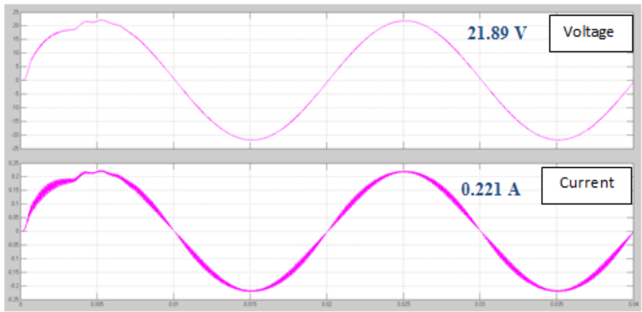

Fig. 8. The output voltage and current of ideal boost-inverter.

D. Non-Ideal Boost-Inverter

For the non-ideal boost-inverter circuit, the parasitic elements that been used are parasitic resistance, R_{ESR}, at the source of boost converter and parasitic inductance, L_S, at the source of inverter. The parameters of R_{ESR} and L_S are been varied for analyzing the output voltage and output current that obtained from the changeable of non-idealistic components. Table II shows the output voltage and current obtained from boost converter and boost-inverter with the variable of R_{ESR} while Table III shows the outputs with the variable of L_S. To be precise, the parameter in both table for $V_{Inveter}$ and $I_{Inverter}$ are the RMS value of the result from boost-inverter..

TABLE II. OUTPUT VOLTAGE AND CURRENT WITH VARIABLE OF PARASITIC RESISTANCE

L_s (H)	R_{ESR} (Ω)	V_{Boost} (V)	I_{Boost} (mA)	$V_{Inverter}$ (V)	$I_{Inverter}$ (mA)
0.001	0	23.482	545.68	10.67	215.19
	0.001	23.474	545.42	10.66	215.12
	0.005	23.461	545.16	10.65	215.05
	0.01	23.444	544.64	10.65	214.87
	0.05	23.311	541.73	10.599	213.88
	0.1	23.153	538.08	10.531	212.54
	0.5	22.079	513.58	10.085	203.55
	1	21.013	488.83	9.606	193.79

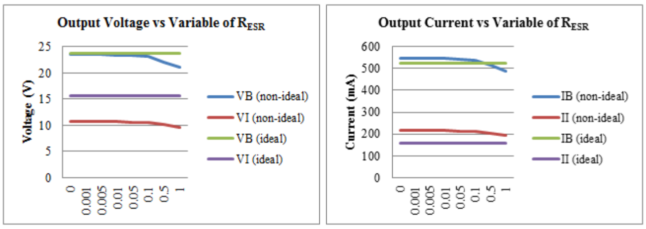

Fig. 9. Differences of output voltage and current of ideal and non-ideal with the variable of R_{ESR}

TABLE III. OUTPUT VOLTAGE AND CURRENT WITH VARIABLE OF PARASITIC INDUCTANCE

L_s (H)	R_{ESR} (Ω)	V_{Boost} (V)	I_{Boost} (mA)	$V_{Inverter}$ (V)	$I_{Inverter}$ (mA)
0	0.001	23.566	608.64	15.557	311.25
0.001		23.473	545.42	10.661	215.12
0.005		23.479	469.79	4.722	95.70
0.01		23.491	444.61	2.81m	56.51
0.05		23.656	420.53	0.695	13.73
0.1		23.503	413.99	0.405	7.99
0.5		23.541	411.90	0.211	4.20
1		23.340	407.98	0.180	3.60

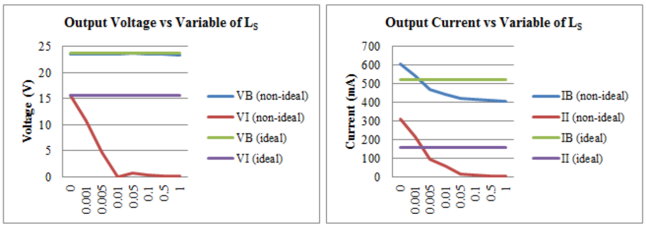

Fig. 10. Differences of output voltage and current of ideal and non-ideal with the variable of L_S.

As we can see from both Figure 9 and Figure 10, with the presence of R_{ESR} and L_S, the performance of the boost-inverter is decreased. During the presence of parasitic resistance at the boost converter, the output voltage of boost-inverter from the beginning can be seen that it is 10 V rather 15 V. As for the output current, it is higher than the ideal boost-inverter which is 215 mA rather than 156.77 mA. Different with boost converter, both output voltage and output current started to slumped down when the R_{ESR} = 0.1 Ω.

For the presence of parasitic inductance at between boost converter and inverter, the output voltage obtained from the boost-inverter is reduced drastically from 15 V to below than 5 V although the output from the boost converter is the same. The output voltage reduced as the load current reduced as shown in the Figure 10. On the other hand, the output current reduced for both boost converter and boost-inverter are almost the same.

V. CONCLUSION

The presence of non-idealistic components such as parasitic inductances and parasitic resistance in a circuit cannot be avoided but it should be kept minimized. There are several techniques that had been introduced in some study in minimizing the stray inductances; however, this study is not on how to minimize the stay inductance. This study is the study on the effect of these parasitic inductances and the equivalent series resistance (ESR) value in affecting the performance of boost-inverter circuit. As for the improvement from this project, although the effects from the parasitic elements on the boost-inverter can be seen clearly, but there still no mathematical justification to prove that which parasitic elements between R_{ESR} or L_S are affecting more on the boost-inverter. Other than that, the parameters of the parasitic elements in this project are quite high that it is not really suitable for low voltage. Since parasitic elements also known as stray inductance, it is also meant that the parasitic elements are small parameters. The parameters used for this project may be happened in high voltage.

REFERENCES

[1] What is Stray Inductance? (n.d). Retrieved December 6, 2016, from http://www.learningaboutelectronics.com/Articles/What-is-stray-inductance.php

[2] Kathiriya Shrikantkumar Mithabhai, Vinod Patel, ."Effect of Parasitic Inductance on Inverter Module Performance", Volume 3, Issue V, International Journal for Research in Applied Science and Engineering Technology (IJRASET) Page No: , ISSN : 2321-9653,www.ijraset.com

[3] Elbanhawy, Alan. "Effects of parasitic inductances on switching performance." Proc. PCIM Eur (2003): 251-255.

[4] Meade, T., O'Sullivan, D., Foley, R., Achimescu, C., Egan, M., & McCloskey, P. (2008, February). Parasitic inductance effect on switching losses for a high frequency Dc-Dc converter. In Applied Power Electronics Conference and Exposition, 2008. APEC 2008. Twenty-Third Annual IEEE (pp. 3-9). IEEE.

[5] Shen, Y., Jiang, J., Xiong, Y., Deng, Y., He, X., & Zeng, Z. (2006, July). Parasitic inductance effects on the switching loss measurement of power semiconductor devices. In 2006 IEEE International Symposium on Industrial Electronics (Vol. 2, pp. 847-852). IEEE.

[6] Hart, D. W. (1997). Introduction to Power Electronics. Upper Saddle River, NJ: Prentice Hall.

[7] Arinah Binti Arsah. Implementation Of Dc-Dc Boost With High Efficiency And Low Ripple Voltage. Bachelor Degree Thesis. Universiti Teknologi Malaysia, 2013.

[8] Nymand, M., & Andersen, M. A. (2010). High-efficiency isolated boost DC–DC converter for high-power low-voltage fuel-cell applications. IEEE Transactions on Industrial Electronics, 57(2), 505-514.

[9] Chen, Z., Boroyevich, D., & Burgos, R. (2010, June). Experimental parametric study of the parasitic inductance influence on MOSFET switching characteristics. In Power Electronics Conference (IPEC), 2010 International (pp. 164-169). IEEE.

[10] B. Yang, J. Zhang, “Effect and utilization of common source inductance in synchronous rectification,” in Proc. IEEE

APEC’05, Mar. 2005, vol. 3, pp. 1407–1411.

[11] Chen, J. Z., Yang, L., Boroyevich, D., & Odendaal, W. G. (2004). Modeling and measurements of parasitic parameters for integrated power electronics modules. In Applied Power Electronics Conference and Exposition, 2004. APEC'04. Nineteenth Annual IEEE (Vol. 1, pp. 522-525). IEEE.

[12] Ning Dai and F. C. Lee, "Characterization and analysis of parasitic parameters and their effects in power electronics circuit," PESC Record. 27th Annual IEEE Power Electronics Specialists Conference, Baveno, 1996, pp. 1370-1375vol.2.

Fault Location at Radial Distributed Network by using Monitoring Placement

Mohamad Ikmal Bin Karim
Faculty of Electrical Engineering
Universiti Teknologi Malaysia
Johor Bahru, Malaysia.
eikmal94@yahoo.com

Dr. Saifulnizam Bin Abdul Khalid
Department of Electrical Power Engineering
Faculty of Electrical Engineering
Universiti Teknologi Malaysia
Johor Bahru, Malaysia.
nizam@fke.utm.my

***Abstract*—this paper presents a method for monitor placement for fault localization in radial distribution systems. The proposed method is based on the fault current sensitivity of system buses and topology consideration of the system. By considering bus fault current sensitivity and system topology, a systematic procedure is developed and tested with IEEE 34 bus of radial distribution network. Balanced 3-phase fault was applied in the system to obtain the total outflow current of the system. This system divided into a several zone based on a bus which have many decedents and high propriety of the total outflow current. The results shows that only 5 monitors are required for finding the faulty feeder in the system instead of placing monitors at each bus. This method can be further extended for exact location of fault in the distribution systems.**

Keywords—Fault location; Monitor placement; Current sensitivity; System topology

I. INTRODUCTION

The connections between electric power system and consumer are defined as power distribution system [12]. In Malaysia there are several level voltages for distribution system networks from 400/230 V, 6.6 kV, 11 kV, 22 kV and 33 kV [13]. Electric power distribution systems are complex and approximately 80% of overall faults in power distribution system come from a wide range of phenomena including equipment failure, natural disaster such as landslide [12], severe weather such as lighting, storm, down tree and human factors [11]. In the case of failure to the system, the maintenance to disconnect the fault must be restored as soon as possible to prevent any damage to the consumer.

This scenario will make the engineer are in a difficult situation which is need to locate the fault location in the distribution system. To detect exact location of fault in distribution cable especially underground cable and distribution system a very difficult because too large variation of fault impedance compare to the other part of power system [14]. Therefore, identifying the fault location are very important to make sure the maintenance process running quickly and smoothly. So far many fault location methods has been reported in the literature [1] and it can be broadly classified into impedance [2] high frequency travelling wave [3] and artificial intelligence based methods [4]. The techniques and method with fast and accurate to detect fault locations in distribution system are important to improve and to normalize the system of supply which is one requirement for modern society [13].

In this recent year, the most popular method to detect fault location in transmission line and distribution system are using artificial neural network and fuzzy logic. However, the speed of this method is not suitable for fast and accurate fault location because for intelligence based method, they need to train first and it depends on the input data from the monitoring devices [1]. So, the most important thing to locate the fault location are the monitoring device. Thus, for the intention of better fault location in distribution system, meter placement must be designed to accurately fault locations considering fault characteristics [1]. By using monitoring placement, fault current levels in different points and the topology of the system need to consider in order to determine the fault location in radial distributed network.

Based on the topology consideration, it follow the Kirchhoff's Current Law, which is the fault current always flow from the source to the fault location. Considering tree structure, if a monitor is placed at a bus with many descendants in the tree, the monitor can cover more extensive areas than a monitor place bus with few descendants and it can more accurately verify whether the fault location is coming from upstream or downstream [1]. Therefore, components with many descendants must receive more attention in monitor placement for fault location purpose [15]. While, based on fault current level consideration are the total monitoring bus outflow current changes in its descendent branches must be monitor to determine the fault location in radial distributed network [1].

II. PROPOSED MONITOR PLACEMENT METHOD

In order to determine the monitor positions for fault location in radial distribution networks it is impotent to consider fault current levels in different points and the topology of the system. The following subsections highlight the importance of these two factors.

A. Topology consideration

Based on Kirchhoff's Current Law, in a radial distribution system, the fault current always flows from the source to fault location. Considering tree structure, if a monitor is placed at a bus with many descendants in the tree, the monitor can cover more extensive areas than a monitor place bus with few descendants. Furthermore, if the outflow currents are monitored from a monitoring bus with many decedents, it can more accurately verify whether the fault location is coming from upstream or downstream. Therefore, components with many descendants must receive more attention in monitor placement for fault location purpose [15].

B. *Fault current level consideration*

The principle of determining the monitor placement must also consider total monitoring bus outflow current changes in its descendent branches, if a ground fault occurs, in the system. The buses with the most significant total outflow currents can be observed and utilized to decide the monitor positions for fault location in radial distribution system. In the proposed method, total bus outflow current changes in its descendent branches are considered as one of the guideline for the motor placement. The basic procedures to obtain the bus outflow currents from bus i due to fault at bus k can be obtained as follows in paper [10].

III. LITERITURE REVIEW

Before this, there are many researchers have proposed many method to detect the location of the fault and many method to identify the type of the fault that happened in distribution and transmission line. Fault location problem has more importance and is more difficult to solve in distribution field compared to transmission line and generation system because due to large variations of fault impedance and also because applying of underground cable are growing now days [3]. Nowadays, the common method that used to solve this problem are using one of the intelligent system technique which is Artificial Neural Network. But, the fault location method and their accuracy general depends on the device or instrumentation used for monitoring the system.

Distribution network differ with transmission network because the number of branches and sources is much higher in distribution network compared to transmission network [7]. That's why distribution system are less closely monitored and it is important to have an instrumentation and monitoring system at every branch of the system for accurate fault location at the distributed system [1]. From the past study which is done by Siti Hajar Ibrahim, they have mention that accuracy of intelligent based method depends on input data from the monitoring devices and size of training data [1]. The result from the study also show that by using monitoring placement at every branch of the distributed system, the fault location can be determine accurately.

For the literature, there are a number of efficient and reliable method to locate the fault location at distribution system and transmission system such as impedance based method, travelling based met8hod (high frequency travelling wave) and artificial intelligent based method [2, 3, 4]. In 2014, paper [1] developed the method of fault location at radial distribution network using monitoring placement. Yuan Liao said that in paper [5] which is currently there are very few research works related to meter placement for fault location in distribution systems. Thus, for the intention of better fault location in distribution system, meter placement must be designed to accurately fault locations considering fault characteristics [1]. There are two important factor to determine the fault location by using monitoring placement which is topology consideration and fault current level consideration [1].

Other than monitoring placement to detect the location of fault, there are several method to detect the fault location such as based impedance method. In paper [2] impedance based method was used to locate the fault location and in this paper also do the comparison for the power distribution system. Impedance based method obtain the location of fault by calculating the impedance from the measurement of voltage and current. However, this method is unreliable because the electrical distance from the measuring point may be identical in a multi feeder network [2]. But to solve this problem, in 2003 fault sensor devices was used which detect and distinguish abnormal current and voltage events at the overhead power lines [1].

Travelling wave method also another method to locate the fault. In paper [3], this method was used to determine the location of the fault in distribution system. The incoming voltage or current surges are detected at both ends of the line and the time of arrival of the surge is used to locate the fault [8]. However this method is difficult to adopt in distribution feeders because of short feeder lengths and several discontinuous points said by Thomas itself in paper [3].

Nowadays, the famous method to locate the fault location are using artificial intelligence based method such as artificial neural network and fuzzy logic. In 2012, Gastaldello said that in his paper [7] artificial intelligence application such as neural networks and fuzzy logic is a powerful tools in the fault location and received much interest. Ziolkowski [4] used the artificial intelligence based method to identify the fault location in power system. In paper [9], Sadeh proposed a new and accurate fault location algorithm using ANFIS in a combination between transmission line and underground cable. Considering the structure and training algorithm of the ANFIS, the speed of this method is not suitable for fast and accurate fault location. Moreover, accuracy of intelligent based methods depends on input data from the monitoring devices and size of the training data [1].

In 2003, Yuan Liao [5], present the fault location observability analysis and optimal meter placement based on voltage measurement. However, too many measurements may not be economically possible. Also too few measurements may lead to multiple possible fault locations depending on the meter locations [5]. In paper [1] also proposed the finding an appropriate location to install monitor for fault location purpose in distributed network.

Prakash, K [6] presented the topological and primitive impedance based load flow method for radial and weakly meshed distribution system. in this paper, the data for simulation for 33 bus system was taken because compare to another data, in this paper the data for 33 bus system are more relevant compared to another one and another reason are this data are more to up to date because this paper was published in 2011 and the data still valid.

IV. METHODOLOGY

In the purpose method, 10-bus, 33-bus and 34-bus of radial distribution system are taken as the sample of the test case to locate the fault location. All the sample are totally different from the voltage bus, load and the line resistances. All the data for this system are obtained from the IEEE previous paper.

A. Software Implementation

The purposed method in this project is using Power World Simulator Software to inject the fault in the radial distribution system and to get the power flow analysis. The 34-bus of radial distribution system are designed and the simulation is run. After that, bus fault was injected and the voltage and the line current of the system are recorded. The result obtained from the monitor placement that we place on at every zone. Based on the result obtained, the analysis is done to locate the fault location at the system.

B. 34-bus radial distribution network

The proposed method for fault location has been implemented to a 34-bus radial distribution test system. Line and load data for 34-bus distribution test system can found in [18]. The single-line diagram of the 11 kV, 34-bus system is illustrated in Fig. 1. The total installed peak power is 5.4MVA, with an average power factor of 0.85. All the calculations have been carried out in the per unit system with the three-phase base S, = 100MVA,VB = 11 kV.

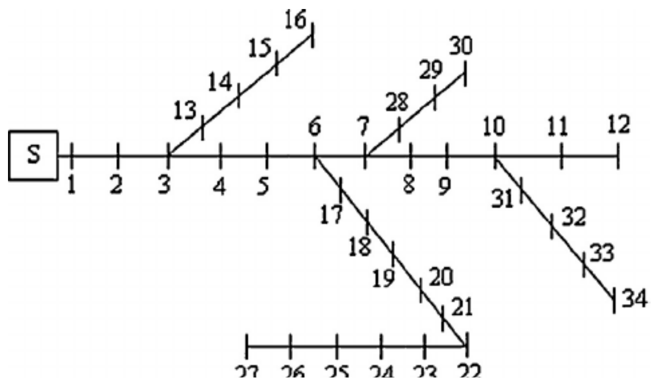

Fig. 1. 34-bus distribution network line diagramTable Styles

V. RESULT AND DISCUSSION

The proposed monitor placement method for fault location is tested on IEEE 34 bus test system. It is an 11kV voltage balanced three-phase system consisting of 34 bus and 33 lines as shown in Figure 1. All the loads are fed from the substation located at Bus 1. The system has 33 loads with total 4.4 MW and 2.73 MVAr, real and reactive power loads, respectively [18]. The simulation model is built in Power World software and balanced three phase fault at each bus is applied to obtain bus outflow current as explained in the previous section. Table below shows the result of three phase fault analysis which indicates the total accumulated bus outflow current due to faults at every in the system.

According to the procedure, zones are created from a bus which have many decedents and high propriety is given to the bus with highest outflow currents. In this case, considering the topology of the system, Buses 3, 6, 7 and 10 are selected as priority buses for monitor placement fault location.

Next, other buses which are not included in the zones are scanned for higher outflow currents which are greater than the lowest outflow bus currents which is already been selected. In this case, Bus 1 has a large total outflow current compare to the other buses. Thus Bus 1 is selected for monitor placement. Therefore, for IEEE 34 bus radial distribution test system, 5 monitors at Buses 1, 3, 6, 7 and 10 are required for fault location purposes. Below are the table of the result for fault that has been injected at bus 5, 9, 12, 22 and 33.

TABLE I. FAULT AT BUS 5

Monitor	**Voltage and Line Current**		
	Voltage (pu)	***Line 01_02***	
Monitor 1	0.92135	1.96731	
Monitor 2	***Voltage (pu)***	***Line 03_04***	***Line o3_13***
	052901	1.96446	0.00155
Monitor 3	***Voltage (pu)***	***Line 06_07***	***Line 06_17***
	0.00208	0.00558	0.01063
Monitor 4	***Voltage (pu)***	***Line 07_08***	***Line 07_28***
	0.00354	0/00457	0.00101
Monitor 5	***Voltage (pu)***	***Line 10_11***	***Line 10_31***
	0.00620	0.00160	0.00098

TABLE II. FAULT AT BUS 9

Monitor	**Voltage and Line Current**		
	Voltage (pu)	***Line 01_02***	
Monitor 1	0.96696	0.68103	
Monitor 2	***Voltage (pu)***	***Line 03_04***	***Line o3_13***
	0.83158	0.67703	0.00214
Monitor 3	***Voltage (pu)***	***Line 06_07***	***Line 06_17***
	0.57444	0.66295	0.01516
Monitor 4	***Voltage (pu)***	***Line 07_08***	***Line 07_28***
	0.42626	0.66237	0.00129
Monitor 5	***Voltage (pu)***	***Line 10_11***	***Line 10_31***
	0.00046	0.00162	0.00099

TABLE III. FAULT AT BUS 12

Monitor	**Voltage and Line Current**		
	Voltage (pu)	***Line 01_02***	
Monitor 1	0.97677	0.55875	
Monitor 2	***Voltage (pu)***	***Line 03_04***	***Line o3_13***
	0.86511	0.55455	0.00219
Monitor 3	***Voltage (pu)***	***Line 06_07***	***Line 06_17***
	0.64898	0.53702	0.01637
Monitor 4	***Voltage (pu)***	***Line 07_08***	***Line 07_28***
	0.51708	0.53607	0.00131
Monitor 5	***Voltage (pu)***	***Line 10_11***	***Line 10_31***
	0.10595	0.53557	0.00077

TABLE IV. FAULT AT BUS 22

Monitor	**Voltage and Line Current**		
	Voltage (pu)	***Line 01_02***	
Monitor 1	0.98352	0.62448	
Monitor 2	***Voltage (pu)***	***Line 03_04***	***Line o3_13***
	0.85955	0.62024	0.00214
Monitor 3	***Voltage (pu)***	***Line 06_07***	***Line 06_17***
	0.61423	0.00758	0.60971
Monitor 4	***Voltage (pu)***	***Line 07_08***	***Line 07_28***
	0.61228	0.00133	0.00489
Monitor 5	***Voltage (pu)***	***Line 10_11***	***Line 10_31***
	0.60946	0.00217	0.00135

TABLE V. FAULT AT BUS 33

Monitor	**Voltage and Line Current**		
	Voltage (pu)	***Line 01_02***	
Monitor 1	0.98084	0.50093	
Monitor 2	***Voltage (pu)***	***Line 03_04***	***Line o3_13***
	0.88070	0.49665	0.00221
Monitor 3	***Voltage (pu)***	***Line 06_07***	***Line 06_17***
	0.68582	0.47755	0.01714
Monitor 4	***Voltage (pu)***	***Line 07_08***	***Line 07_28***
	0.56567	0.47643	0.00137
Monitor 5	***Voltage (pu)***	***Line 10_11***	***Line 10_31***
	0.20875	0.00107	0.47511

To demonstrate how these 5 monitors can be used for fault location, consider three phase faults at Buses 5, 9, 12, 22 and 33. Table 1, 2, 3, 4 and 5 shows the recorded fault current by the monitors at Bus 1, 3, 6, 7 and 10 during the faults. From the table it is clear that current recorded at particular monitor is relatively high when the fault happens in the respective zone of the monitor. For example when the fault happens at Bus 5, monitor at Buses 1 and 3 register vary high current at branch between Buses 1 and 2 as well as branch between Buses 3 and 4 compare to the recorded current at other monitor location. Therefore the fault location is expected to be between Bus 3 and 5. For fault at Bus 9, monitor at Bus 1, 3 and 6 are show the high current compare to the other. Based on the current sensitivity, the fault location are between Bus 7 and 9 because from the Table 2, we can see that the fault current flow from the source to the fault location. Lastly, when fault happen at Bus 33, all the monitor at Bus 1, 3, 6, 7 and 10 are show with a high current but we can see the different of the line current at the monitor buses. Therefore, the fault location is expected to be between Bus 10 and 34.

VI. CONCLUSION

This paper illustrates a method for monitor placement for fault location purpose in radial distribution system. It considers system topology and the fault current sensitivity levels at various system buses. The result shows that the method can be used to identify the faulty feeder in the system by using only few monitors. The simulation with IEEE 34 bus test system show that only 5 monitors at Buses 1, 3, 6, 7 and 10 are required for fault location.

REFERENCES

[1] Siti Hajar Ibrahim, Hussain Shareef , Azah Mohamed , Ahmad Asrul Ibrahim, 2014"Monitor Placement for Fault Location in Radial Distributed Network Based on Current Sensitivity and System Topology".

[2] Mora-Fl`orez, J., J. Mel´endezand G. Carrillo-Caicedo, 2008. "Comparison of Impedance Based Fault Location Methods For Power Distribution Systems" Electric Power Systems Research, 78: 657-666.

[3] Thomas, D.W. P., R.J.O. Carvalho and E.T. Pereira, 2003. "Fault location in distribution systems on traveling waves" presented at the IEEE Bologna Power Tech Conf., Bologna, Italy.

[4] Ziolkowski, V., I.N. da Silva and R.A. Flauzino, 2007. "Automatic Identification of Faults in Power Systems Using Neural Network Technique" 16 IEEE International Conference on Control Applications: Singapore.

[5] Yuan Liao, 2009. "Fault location observability analysis and optimal meter placement based on voltage measurements" Electric Power Systems Research, 79: 1062-1068.

[6] Prakash, K. And M. Sydulu, 2011. "Topological and Primitive Impedance Based Load Flow Method for Radial and Weakly Meshed Distribution Systems" Iranian Journal of Electrical and Computer Engineering, 10(1).

[7] Gastaldello, D.S., A.N. Souza, C.C.O. Ramos, P. da Costa Junior and M.G. Zago, 2012. "Fault location in underground systems using artificial neural networks and PSCAD/EMTDC" INES 2012 IEEE 16th International Conference on Intelligent Engineering Systems, Lisbon, Portugal.

[8] Bo, Z.Q., G .Weller and M.A. Redfern, 1999. "Accurate fault location technique for distribution system using fault-generated high-frequency transient voltage signals," Proc. Inst. Elect. Eng., Gen. Transm. Distrib., 146: 1.

[9] Sadeh, J., H. Afradi, 1999. "A New and Accurate Fault Location Algorithm for Combined Transmission Lines Using Adaptive Network-Based Fuzzy Inference System" Journal of Electric Power System Research.

[10] Chang, G.W., J.P. Chao, S.Y. Chu and C.Y. Chen 2007. "A New Procedure for Tracking the Source Location of Voltage Sags" Power Engineering Society General Meeting. IEEE Mediterranean Conference on Electro technical.

[11] Marusic, A., Gruhonjic, S. Ferhatbegovic, 2006. "A Computerized Fault Location Process for Overhead Radial Distribution Feeders" IEEE Mediterranean Conference on Electro technical.

[12] Coser, J., D. T. do Vale, et al. "Artificial Neural Network based Method for Fault Location in Distribution Systems". Intelligent Systems Application to Power Systems. Proceedings of the 13th International Conference on. 2005.

[13] Amirul Hisham, 2012. "Analyze And Detect Fault Location In Distribution System"

[14] Javadian, S. A. M., A. M. Nasrabadi, et al. "Determining fault's type and accurate location in distribution systems with DG using MLP Neural networks". Clean Electrical Power. International Conference on. 2009.

[15] Won, D.J. and S.I. Moon, 2008. "Optimal Number and Location of Power Quality Monitors Considering System Topology" IEEE Transactions on Power Delivery, 23(1): 288-295.

[16] Taha, F.M. and Khairuddin, A. Asas Kejuruteraan Kuasa, Johor, Electrical Engineering Faculty, Universiti Teknologi Malaysia. 2006.

[17] Glover, J. Ducan. Power System Analysis and Design 3rd edition, Pacific Grove, CA. 2002.

[18] M. Chis, M. M. A. Salama and S. Jayaram, "Capacitor placement in distribution systems using heuristic search strategies," in IEE Proceedings - Generation, Transmission and Distribution, vol. 144, no. 3, pp. 225-230, May 1997.

Buck Converter Using Microcontroller With P , PI , PD and PID Feedback

Muhammad Hafiz bin Idris
Faculty of Electrical Engineering
Universiti Teknologi Malaysia
Johor Bahru, Malaysia.
hafizidris1994@gmail.com

Dr Mohd Rodhi Sahid
Department of Electrical Power Engineering
Faculty of Electrical Engineering
Universiti Teknologi Malaysia
Johor Bahru, Malaysia.
rodhi@utm.my

***Abstract*— This project is about power electronic conversion techniques for switch mode power supply of Buck converter topology. Buck converter in this project is dc - dc converter that steps down the voltage 15V dc voltage to the 5V. In order to get high efficiency converter, the best controller has been chosen in between P , PI , PD and PID controller base on stability and steady state error, compared in simulation MATLAB and implementing in microcontroller. Microcontroller is used to drive MOSFET that act as switch in Buck converter, dsPIC4011 is chosen because its can produce less noise PWM for MOSFET and has medium 16-Bit processing speed that suitable for closed loop Buck converter to got stable output of 5V even disturbance is applied.**

Keyword—Buck converter; PID controller; MATLAB; Microcontroller; Mosfet.

I. INTRODUCTION

Nowadays DC to DC converter is widely used in industry and daily life. DC converter can be found in most of a house appliance like a battery charger for phone, laptop charger and most of electronic device have a DC converter inside it. There two main function DC converter, to convert voltage whether step down or step up and the other function is as isolation circuit between main circuits to the source.There are two types of DC converter, linear voltage regulator and switching regulator. Linear voltage regulator is commonly used in industry because it is cheap, small and easy to use, however linear voltage regulator not so efficient and it also got so many losses in term of heat so even it is small in size, but need a large heat sink for ensuring system, don't get damaged and it also can only convert from high voltage to low voltage, in other words linear voltage regulator just can step down the voltage compare to switching regulator, it can step down and step up[1]. Switching regulator has high efficiency in voltage converter and emitting low heat[1,4]. Switching regulator consists non-linear element that operates in saturated region and cutoff region, which is why make more efficiency and got less losses compare to linear voltage regulator that only operate in active mode which is between saturated region and cutoff region.Buck converter is switching regulator that can step down voltage, but it was a medium complex circuit consist switch, power diode, inductor, capacitor and resistor, but need a controller to drive switch to ensure Buck converter fully operate. In other word, need a modern controller to transmit PWM signal to switch to get desired output voltage at Buck converter.There are two types of controller that can be used, analog controller and digital controller. Analog controller is a complex circuit and easy affected by noise, but it is rugged system and make a better efficiency of output PWM in high power level. Digital controller is a very simple circuit with a good efficiency at low power level and easy to modify the desire criteria[7].

II. LITERATURE REVIEW

A. Buck Converter

Buck converter is one of DC converter that commonly used and easy to design, it is switching regulator that can convert from high to low voltage. Buck converter needs two state to fully operate which is ON state and OFF state. By using semiconductor devices as switch such as bipolar junction transistor BJT, metal oxide semiconductor field effect transistor MOSFET or insulated gate bipolar transistor IGBT[3,4]. Buck converter has two modes which are discontinuous current mode (DCM) and continuous current mode (CCM). In practical, Buck converter needs to be a CCM to ensure voltage output got the less ripple and constant. Switching frequency need to be medium high and the value of the minimum need to calculate to ensure Buck converter always operates at CCM. Buck converter consists switch, power diode, inductor, capacitor and resistor as shown in Figure 1.

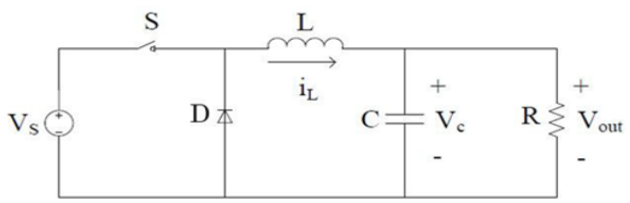

Fig. 1. Buck Converter Circuit

B. Closed Loop Buck Converter

Buck converter can be controlled using duty cycle of switching frequency that transmitted to switch. But in real life input voltage not always regulated and cannot be expected, so we need a feedback with a good compensator and with set point or voltage reference desire output voltage will be obtained.

Figure 2.3.1 shows that block diagram for closed loop Buck converter.

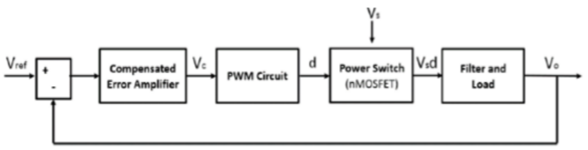

Fig. 2. Closed Loop Converter

Stability of closed loop system can be obtained from analysis of the open loop Buck converter, stability is important to achieve steady state and less resonant for output. There are two things that affect stability of system, crossover frequency or bandwidth and phase margin. Bandwidth at least need to greater than the switching frequency over 10, in this project switching frequency is 20 KHz so the bandwidth would be 2 KHz or 12.6K rad per second. Phase margin needs to be at least 45 degrees to achieve stability of transient response[2,5,12].

C. *Controller*

In this project,comparison between proportional P , proportional derivative PD,proportional integral PI and proportional integral derivative PID controller are made to determine which of the controller type suitable to use and implement in the microcontroller.

Proportional controller or can be known as a gain controller is a very simple controller, which has just included Kp term. This controller just adjusts the gain of the plant to achieve to get the desired output .Gain adjustment can choose a better transient response , but however, the gain can be limited to those responses that exist along the root locus only.

The proportional derivative controller also a simple controller, same with P controller, but this controller has a derivative term which can use to improve transient response of system and maintaining the steady state error. In other word, PD controller will give not much resonant and constant output[5].

The proportional Integral controller can make the system better with the improvement of the steady state error, this controller will minimize the steady state error by adding an open loop pole at origin system and will increase the system type by one. But this will make change a root locus of the system , to solve this a zero close to the pole has to add. Thus, steady state error can be improved without changing transient response[5].

Proportional integral derivative controller is an implementation of PI and PD controller. This controller has a good performance compared to the previous controller because it improves steady state error and transient response of the system by adding two poles and one zero at origin system[12].

D. *Microcontroller*

DsPIC microcontroller is the combination of the digital signal processor with a microcontroller. This dsPIC is made by microchip technology and the architectures modified from Harvard architecture.DSPIC18F3011 is 16-bit digital signal controller that have 24- bit wide instruction and 16-bit data path. This dsPIC also have 48 Kbyte flash memory, 2 Kbyte data RAM and 1 Kbyte of nonvolatile data EEPROM. DSPIC30F4011 consist of 40 pins that have 5 I/O port, six PWM channel that can be divided into two which are complementary or independent output modes and 2 external timer clock. The rest of the pins are an interrupt, reset and pin for the input source. Furthermore, the peripheral of this microcontroller has an analogue to digital conversion (ADC) and a comparator for output function to make the programming of the system can be minimized[4,6].

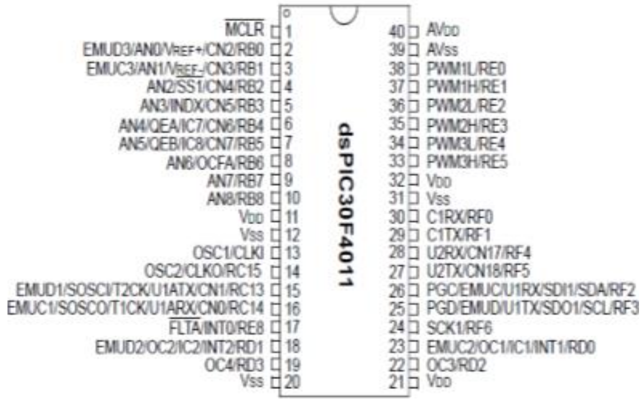

Fig. 3. dsPIC30f4011

E. *MPLAB X IDE*

MLAB X IDE is software made from microchip that can be used to program almost PIC and dsPIC family . This software can be downloaded free from the official microchip website. This project using MLAB X IDE to implement a PID controller to microcontroller and by using X16 compiler program can burn to dsPIC.

F. *PIC KIT 3*

Pic kit 3 is a tool to connect between dsPIC and programmer. This debugger executes code like others device with built in emulation circuitry. There are 3 pins that active to debug the program, pin 1(Vpp/MCLR), 5(PGC) and 4(PGD). Pin 2 and pin 3 are connected to supply source for the circuit to complete[4,14,15].

III. METHODOLOGY

This project started with studying and doing research about switching regulator which is Buck converter and how to drive its switch, after that comparison between analog and digital , digital controller was chosen because it more suitable. Then ,the project proceeds about parameter calculation for Buck converter and parameter chosen based on available on the market . Simulation for the open loop Buck converter has done to verify parameter that had chosen, software used for simulation is MATLAB 16a.

Next , study about filter transfer function for Buck converter because need to tune controller base on Buck converter transfer function .Then proceed with controller development, P, PD, PI and PID controller and make comparisons in term of stability to see which one is suitable to implement to Buck converter. Each of controller was tuned and implement to Buck converter by simulation to make the comparison again and verify which one is the best.

Then , study about C program that will be used in MPLAB X IDE and all that related to PWM and PID feedback in term of coding. After that, make a research about hardware that will be used , dsPIC30F , PIC kit 3 and gate driver . Programing for PWM with desired duty cycle base on theoretical calculation and simulation and programing for PID controller and test it on board dsPIC30 by oscilloscope. Lastly, make a whole circuit by implementing controller and Buck converter circuit and test it with an oscilloscope and see the stability of output when the voltage source regulated.

A. *Buck Converter Design*

The main important things in the design Buck converter are voltage source and desire voltage output , from these two values of parameter , duty cycle can calculate . The other things are switching frequency for power switch , high switching frequency is best for ensuring Buck converter operated in CCM and lower the value of the inductor. In this project 20K Hz switching frequency was used, voltage source 15v,desired output 5V and voltage ripple less than five percent. With this parameter that decide , other parameter was calculated .

Vs	15V
V0	5V
R	2.5Ω
fs	20K HZ
I	2A
D	0.33
L	220µH
C	300µF

Table. 1. Parameter for Buck Converter

Table 1 shown that parameter and the criteria that the design of Buck converter .The next parameter will be verified in simulation Simulink as an open loop converter to see whether Buck converter can operate in CCM with this parameter and desired output stable or not.

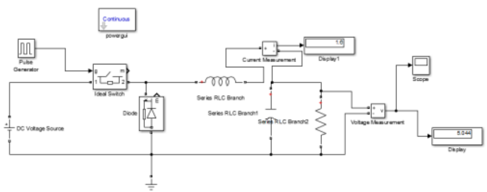

Fig. 4. Simulation for Buck converter

B. *Controller Design*

For closed loop Buck converter needs a feedback with a good controller to get a desired stable output voltage. The controller was designed with two criteria , bandwidth 2k Hz and phase margin atleast 45 degree. First , each of controller , P , PI , PD and PID design with Ziegler Nicholas method and then verified with auto tune in MATLAB apps. By using transfer function of Buck converter, a bode plot of the plant was made by using MATLAB because the Ziegler Nicholas method needs to find crossover frequency and gain margin of plant first.

$$\frac{15}{6.6e^{-2}s^2+8.8e^{-5}s+1} \tag{1}$$

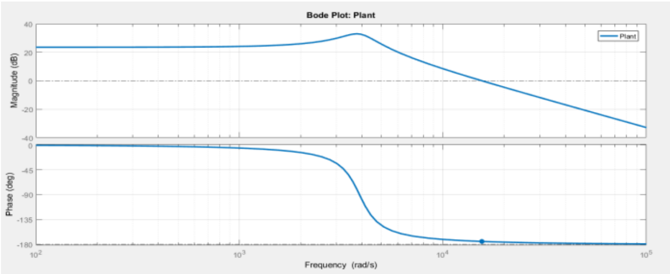

Fig. 5 Bode Plot for Plant

After getting crossover frequency and phase margin from a bode plot of Buck converter, ultimate gain and ultimate period calculated by using given formulae.

$$Ku = 10^{(-\frac{GM}{20})} \tag{2}$$

$$Pu = \frac{2\pi}{\omega} \tag{3}$$

Then, gain for each controller calculated using the table or Ziegler Nichols:

Controller	Kp	Ki	Kd
P	Ku/2	-	-
PD	Ku/1.25	-	(0.6Ku.Pu)/8
PI	Ku/2.2	0.54Ku/Pu	-
PID	Ku/1.7	1.2Ku/Pu	(0.6Ku.Pu)/8

Table. 2. Zieller Nicholas Table

To verify the controller that has been designing , auto tune MATLAB apps was used . Ziegler Nichols is a manual tuning method use theoretical calculation, so result from it will not be so accurate.

Fig. 6. Auto Tune Apps

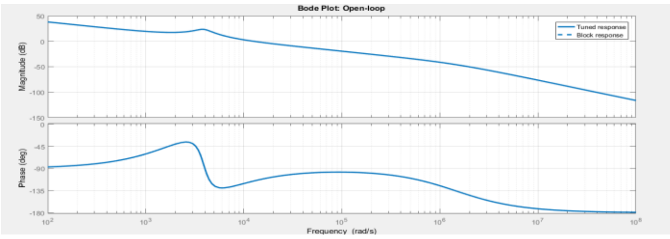

Fig. 7. Tuned Bode Plot

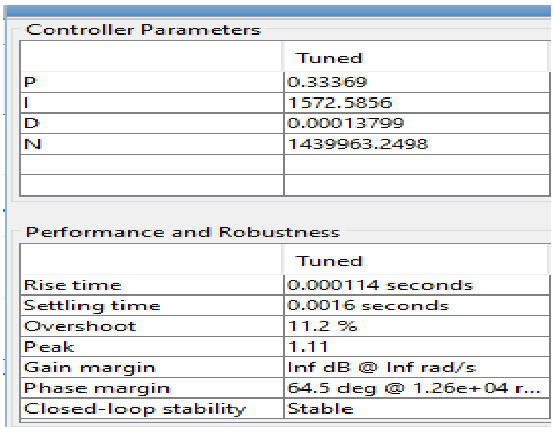

Controller Parameters

	Tuned
P	0.33369
I	1572.5856
D	0.00013799
N	1439963.2498

Performance and Robustness

	Tuned
Rise time	0.000114 seconds
Settling time	0.0016 seconds
Overshoot	11.2 %
Peak	1.11
Gain margin	Inf dB @ Inf rad/s
Phase margin	64.5 deg @ 1.26e+04 r...
Closed-loop stability	Stable

Fig. 8. Controller Criteria

Figure 6 shown that auto tune apps from MATLAB that has been used and with phase margin and bandwidth 60 degrees and 12.6K radian per second which equal to 2K Hz have chosen. Figure 7 and 8 shows bode plot of the plant after tuned and stability criteria of controller which include all parameters such as , gains Kp Ki Kd ,rise time , settling time , overshoot , gain margin and phase margin.

C. *Implementing PID to microcontroller*

Below is the programming for PID control to generate suitable PWM signal to produce 5V regulated voltage. In this, the duty cycle of PWM signal is set from 0.2 to 0.7 because to avoid the large current and voltage flow in the microcontroller [15,21,10].The operating voltage for the microcontroller is range from 2.5V to -5.5V.The set point of this microcontroller is 5V which compare with the output voltage from buck converter. This two value will give error value that uses to determine the error, integral and derivative part. From this 3 parameter, the output of the system which is the duty cycle can be calculated. This process will repeat to give the suitable duty cycle to the system.

```
while(1)
{
    while(_T2IF == 0); // wait for start of next cycle
    _T2IF = 0;

    setpoint = read_analog_channel(0);
    measured_value = read_analog_channel(1);

    error = setpoint - measured_value;
    integral = integral + error*dt;
    derivative = error - previous_error /dt;
    output = Kp*error + Ki*integral + Kd*derivative;
    previous_error = error;

    duty_cycle = output;
    if (duty_cycle > 0.8) duty_cycle = 0.8;
    if (duty_cycle < 0.2) duty_cycle = 0.2;

    OC1RS = (int)(duty_cycle * Ton);
    OC2R = OC1RS + dead_time;
}
```

Fig. 9. PID programing

D. *Printed Circuit Board*

The PCB of each circuit are designed on PROTEUS software after all the parameter is identified. There is three circuits layout which are PWM circuit in Figure 10, a gate driver in Figure 11 and buck converter in Figure 9.

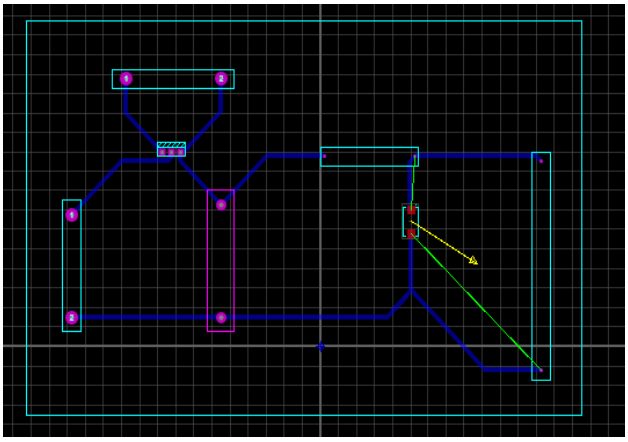

Fig. 9. Buck Converter PCB

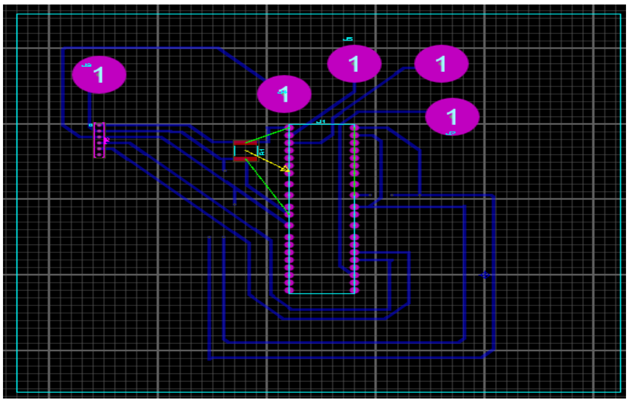

Fig. 10. PWM Circuit PCB

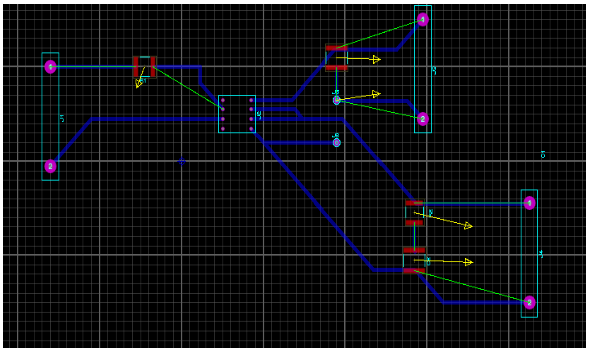

Fig. 11. Gate Driver Circuit PCB

After the PCB layout design is completed, it is then printed using a laser jet printer on the glossy paper. The printed layout in glossy paper is patched with the copper board and been laminated using the laminating thermal machine. After one hour, the ink in the glossy paper will strongly stick to the PCB copper board. The board is put into acid liquid for several minutes to remove the unwanted copper that does not stick with ink. After this process is completed, the PCB board is drilled and components are implemented into it. The components are soldered based on their respective location.

IV. RESULT SIMULATION

Result simulation for open loop Buck converter and closed loop Buck converter. For closed loop converters, they're divided by four categories with different controller, P , PI , PD PID.

A. *Open Loop*

Figure 12 shown that current in the inductor by using parameters that decided and simulate using Simulink. Current got the small ripple and not fall to zero , which is proved that its operate in CCM mode. And Figure 13 indicates voltage output for open loop , with 0.33 duty cycle that has been calculated , voltage output got approximately 5V.

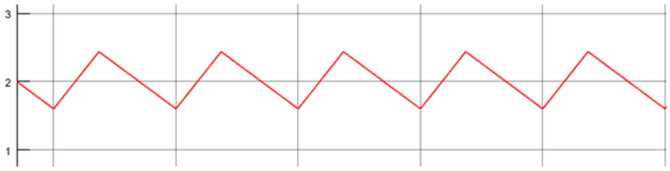

Fig. 12. Inductor Current

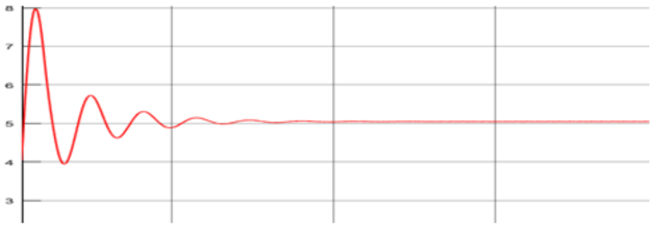

Fig. 13. Voltage Output

B. *Closed Loop*

Buck converter needs a feedback and a good controller to ensure the system stable and voltage output stay 5v even voltage source regulated. Four types of controller were compared to see which one gives a good performance when implement to Buck converter. A comparison was done by using simulation Simulink.

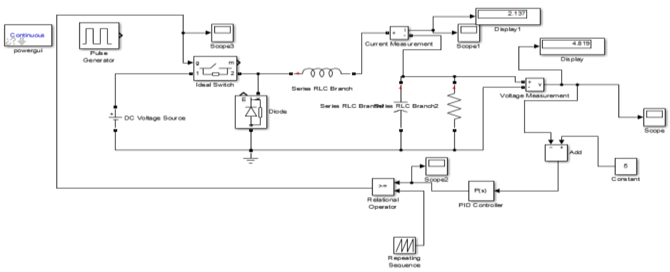

Fig. 14. Feedback Ciruit

Figure 14 shows that the feedback Buck Converter circuit connected to controller simulated with software MATLAB Simulink . The result of output voltage for controller P, PD, PI and PID is shown in figure 15 ,16 ,17 and 18 respectively.

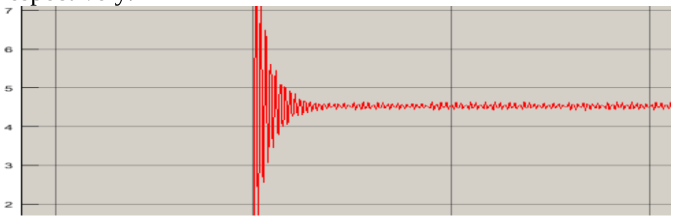

Fig. 15. Output of P controller

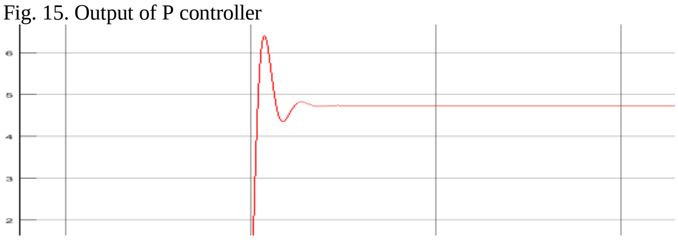

Fig. 16. Output of PD controller

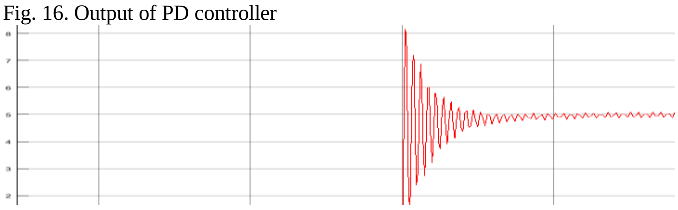

Fig. 17. Output of PI controller

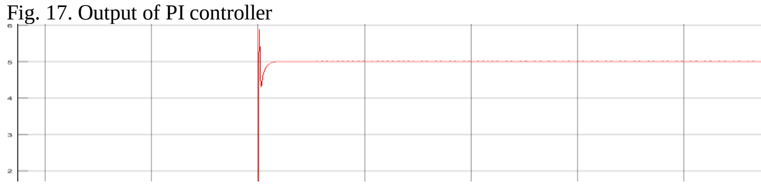

Fig. 18. Output of PID controller

Output of P controller start with high resonant and only achieved 4.8V at steady state. For PD controller output a more stable because PD controller can improve transient response, but still not achieved desired setpoint which is 5V. For PI controller setpoint 5V achieved at steady state condition but still got more resonant and not stable because PI controller only eliminating error but not improve transient response.And PID controller can improve both transient response and eliminating error ,Figure 18 shows that voltage output most stable and achieve desired setpoint compared to other controller.

V. CONCLUSION

As a conclusion of the first part of this project , an expected outcome was achieved, which is PID controller make a better performance as a feedback for Buck converter, so the PID controller has chosen to implement as feedback in real circuit in next semester. Buck converter was successful develop and 15V to 5V step down voltage was successful based on simulation.

REFERENCES

[1]. Jin, S. S. 2015 Design Of Closed Loop Power Supply Controller Using Buck Converter, 2015.

[2]. Yuan, Y., Chang, C., Zhou, Z., Huang, X. and Xu, Y. Design of a singleinput fuzzy PID controller based on genetic optimization scheme for DCDC buck converter. Next-Generation Electronics (ISNE), 2015 International Symposium on. IEEE. 2015. 1–4.

[3]. Bessegato, L., Modeer, T. and Norrga, S. Modeling and control of a tappedinductor buck converter with pulse frequency modulation. Energy Conversion Congress and Exposition (ECCE), 2014 IEEE. IEEE. 2014. 3672–3678.

[4]. Sefa, I., Battal, F. and Balci, S. Modeling and implementation of dsPIC based interleaved buck converter. Power Engineering, Energy and Electrical Drives (POWERENG),2013Fourth International Conferenceon.IEEE. 2013. 1652– 1657.

[5]. Valenti, C. Implementing a pid controller using a pic18 mcu. Microchip Technology, 2004.

[6]. Microchip dsPIC30F4011/4455/4550 Data Sheet

[7]. Weissbach, R. S., & Torres, K. M. (n.d.). A noninverting buck-boost converter with reduced components using a microcontrol

[8]. Trip, N. D., & Dale, S. (2010). Digital Control for Switched Mode DC-DC Buck Converters, 99–102.

[9]. Dusan Gleich, Mira Milanovic, Suzana Uran, Franic Mihalic.“Digitally controlled buck converter” IEEE power electronics society ISCAS-2004, pp-V944-V947.

[10]. Tarun Gupta, R.R. Boudreaux, R.M. Nelms and John Y Hung, “Implementation of a fuzzy controller for DC-DC converters using an inexpensive 8-bit Microcontroller”, IEEE Transactions on Industrial Electronics, Vol. 44, No.5, October 1997.

[11]. Mouhadjer, S., Chermitti, A., & Neçaibia, A. (2012). Comprehensive and field study to design a buck converter for photovoltaic systems, 15, 321–330.

[12]. Guo, L., Hung, J. Y., & Nelms, R. M. (2002). PID Controller Modifications to Improve Steady-State Performance of Digital Controllers for Buck and Boost Converters, 00(c), 381–388.

[13]. Wang, S., Wang, M., Ma, Y., & Hong, H. (2009). Series Connected Buck-Boost Type Solar Power Converter Based on Microcontroller, 2642–2646.

[14]. Bowling,S. An introduction to AC induction motor control using the dsPIC3ds mcu. 2005.

[15]. Elliott, C. and Smart Power Solutions, L. Using the dsPIC30F for Sensorless BLDC Control. Microchip Technology, 2004.

Transmit A Data To The Different Outputs With A Energy Meter

Siti Zulaikha Binti Saadon
Faculty of Electrical Engineering
Universiti Teknologi Malaysia
Johor Bahru, Malaysia.
zulaikhajue@gmail.com

Dr. Rasyidah Binti Mohamad Idris
Department of Electrical Power Engineering
Faculty of Electrical Engineering
Universiti Teknologi Malaysia
Johor Bahru, Malaysia.
rasyidahidris@utm.my

Abstract—**Every building in this world will have more than one electrical appliance whether at office, home, or shopping complex. These appliances are quite annoying if there is only one switch to control the turn on and off for one appliance only. Therefore, to make the situation becomes easier, one remote controller is needed to control more than one electrical appliance regardless AC or DC load. In this case, Radio Frequency (RF) Module is the best match to implement into the remote controller as it is a wireless communication component. RF Module is divided into two, there are transmitter (TX) and receiver (RX). Transmitter will implement on remote controller, while receiver will implement on appliance.The main benefit of using RF Module is it can communicate even if there are walls and other obstructions. The power and energy consumption that are implemented in receiver circuit will make this appliance becomes more great because people can know the energy that has been used as the increase of energy consumption will increase the price of the bill of the appliance. The ACS712 Current Sensor and Adapter are used to find Current RMS (A) and Voltage RMS (V) respectively. These values will result of finding Power and Energy Consumption of AC Load. For the DC load, the load is just implemented together to the receiver circuit because receiver circuit uses DC voltage and current.**

Keywords—RF Module; Energy Consumption; ACS712 Current Sensor; AC Load; DC load

I. INTRODUCTION

In this era of globalization and technology, the electrical appliances become more advanced year by year. Due to that, it makes humans' life becomes easier. It can be said, humans will not be spared from their relationship with the electrical appliances. It cannot be denied, every building in this world will have more than one electrical appliance whether at office, home, or shopping complex as right now, this world is in the era of technology. These appliances are quite annoying if there is only one switch to control the turn on and off for one appliance only. So that, to make it easier, one remote controller is needed to control more than one electrical appliance. The identification code must be installed on each of the receiver circuits (connected to the load) to make sure only that appliance will turn on or off and the other appliances will not be affected.

Knowing more about the electrical appliance such as power and energy consumption will make this appliance becomes more great because people can know the energy that has been used as the increase of energy consumption will increase the price of the bill of the appliance. Therefore, admin can make an energy saving for the electrical appliance. Besides, it is just a knowledge for the people to know the power that will be used. Therefore, admin can make a comparison among the electrical appliances.

Radio Frequency (RF) Module is the best match to implement into the remote controller as it is a wireless communication component.[1] RF Module is divided into two, there are transmitter (TX) and receiver (RX).[1] Transmitter will implement on remote controller, while receiver will implement on appliance. RF Module has a lot of benefits, and the main benefit is it can communicate regardless of the fact that there are walls and other obstructions. The minimum range of distance of RF Module is six meters when the antenna is connected to the RX.

The power and energy consumption must be implemented in the RX circuit as the load is interfacing to the RX circuit. Time is implemented also because the calculation of energy in kWh includes a time. Furthermore, the admin also can know how long his appliance has been switched on. Some electrical appliances have three or two pin plug to be connected to AC Source. Some appliances do not have plugs as they just have battery as a main supply and they are a DC Source. Therefore, the benefit of this project is all the electrical appliances can be used regardless AC or DC load.

The ACS712 Current Sensor and Adapter are used to find Current RMS (A) and Voltage RMS (V) respectively.[4-5] These values will result of finding Power and Energy Consumption of AC Load.[7-8] For appliance that has DC supply, it will just directly connected to the receiver circuit but must be connected to the voltage regulator first to decrease the voltage as the operating voltage at receiver circuit is 5V.

II. Literature Review

A. Radio Frequency (RF) Module

Radio frequency (RF) and infrared (IR) waves are Wireless communication without cables or cords. Radio Frequency is any frequency within the electromagnetic spectrum that is able to propagate through space associated with radio wave propagation[1]. This RF uses the principle of Amplitude Shift Keying (ASK) modulation. The RF Module has the pair of transmitter and receiver (Tx/Rx) [2]. ASK is a form of coherent digital bandpass modulation (converted signal to sinusoidal waveform) that represents digital data as variations in the amplitude of a carrier wave. The level of amplitude of ASK represents binary logic 0s and 1s. In the modulated signal, logic 0 is represented by the absence of a carrier,so the signal makes the switch turn off. While, binary 1 is vice versa to the binary 0[1,9-10].

Fig. 1. RF Module

Figure 2 and figure 3 show the block diagram of transmitter and receiver of RF Module.

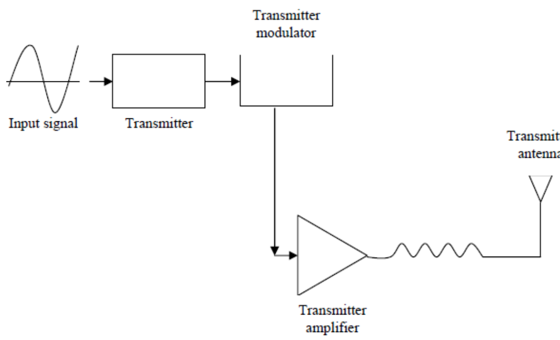

Fig. 2. Transmitter Block Diagram[1]

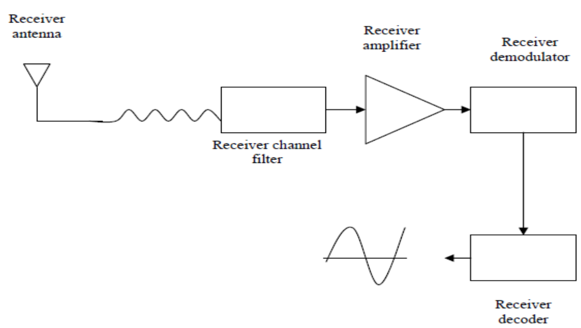

Fig. 3. Receiver Block Diagram[1]

B. ACS712 Current Sensor

ACS712 current sensor is based on the principle of Hall-effect, which was discovered by Dr. Edwin Hall in 1879.[3-4] When a current carrying conductor is placed into a magnetic filed, a voltage is generated across its edges perpendicular to the directions of both the current and the magnetic field. A thin sheet of semiconductor material that is called Hall element will carry a current and placed into a magnetic field (B) that is perpendicular to the direction of current flow. The presence of Lorentz force will make the distribution of current is not uniform when across the Hall element. Therefore, a potential difference, known Hall voltage is created across its edges perpendicular to the directions of both the current and the field. The voltage is directly proportional to the magnitudes of I and B.[3]

Fig. 4. ACS712 Current Sensor

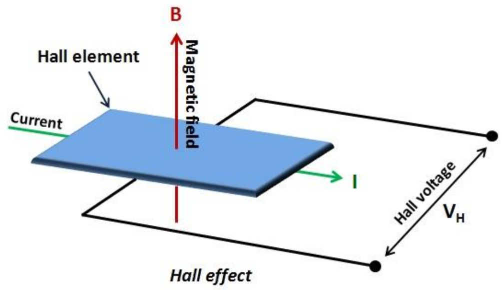

Fig. 5. Principle of Hall-effect[3]

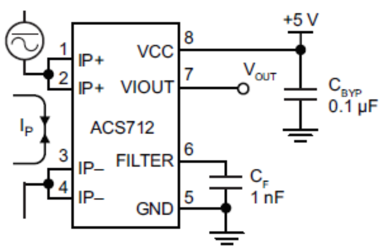

Fig. 6. ACS712 outputs an analog signal[4]

III. METHODOLOGY

A. *Test the Radio Frequency*

Before starting the project, RF module should be tested first to know whether it can function smoothly or not. RF Module is the main component of the project, and it has two frequencies, there are 315MHz RF Module and 433MHz RF Module. The different type of frequency will make the RF Module cannot transmit a signal. For instance, transmitter that using 315MHz RF Module cannot transmit the signal to the receiver 433MHz RF Module. So, one experiment is needed by testing the RF Module.

B. *Design and build the circuit*

The transmitter circuit and two receiver circuits have been designed. For the transmitter circuit, it has two push buttons because for the first button, it will switch on and off the DC Load. While, the second button will switch on and off the AC load. DC load is implemented in first receiver circuit and the buzzer is selected to be DC Load. At AC Load, it has time, power and energy consumption. Those are implemented at second receiver circuit. The Current (A), Voltage (V), Power (W) and energy (kWh) will display at LCD Display. The ACS712A current sensor is used to sense the current.[3] While, adapter arduino is used to sense the voltage.[5] The circuits were design using Proteus 8 software. Build the circuit according to its design.

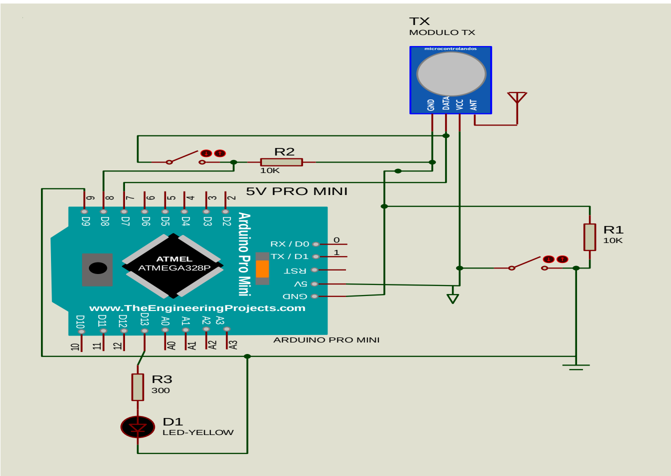

Fig. 7. Transmitter Circuit

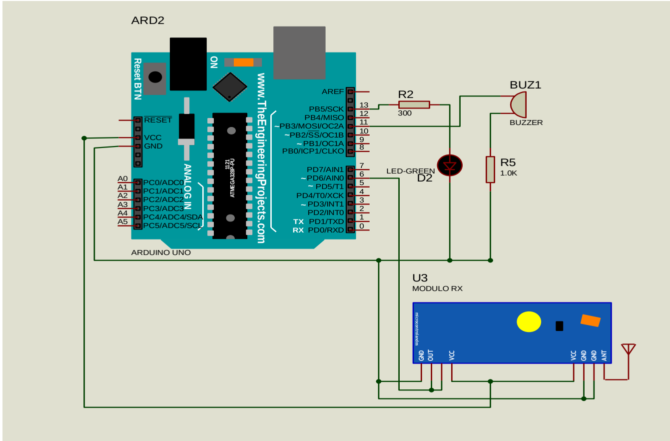

Fig. 8. Receiver Circuit 1 : DC Load

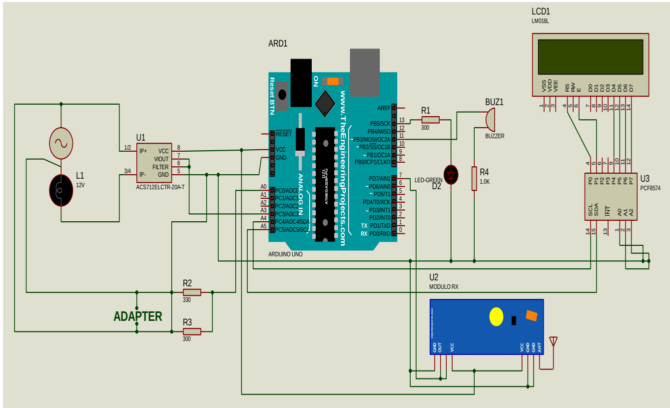

Fig. 9. Receiver Circuit 2 : AC Load

C. *Upload and test the coding*

The coding of each of the components should be tested first and should be run smoothly before compiling all the coding to be one coding. Upload the coding to the circuit and record the result if the circuit is function according to the objectives. If the circuit not function smoothly, troubleshoot the coding or the circuit.

D. *Make and antenna for RF Modules*

The antenna is made by using jumper (copper wire). the wavelength of the antenna should calculate first before interfacing the antenna to the RF Modules. The formula of the antenna is[6] :

$$\lambda = \frac{1}{4}\left(\frac{C}{f}\right) \qquad (1)$$

Where,

λ = wavelength of antenna

C = Velocity of light (3×10^8 ms^{-1})

f = frequency of RF Module (315 MHz)

After that, do the experiment of the range of distance between transmitter and receiver circuit with or without the antenna. When without antenna, will have a shorter distance compared to with antenna. In theoretically, the distance between transmitter and receiver circuit that interfacing with antenna must be equal or more than six metres.

IV. Result And Discussion

The result of the project is divided into two. First is RF Module and the second one is Power and energy Consumption.

A. RF Module

Each of the RXs will have the identification code itself. That is why when the first button at transmitter (TX) circuit pushes, only DC load will turn on as its identification code is same as first button. The AC Load will not turn on as it has different identification code.

Graph in figure below showed the RX signal when received the data from TX, that was when the button has been pushed, after that, TX transmitted its data to the RX immediately and RX received the data. The signal was modulated when received the data. The graph was plotted by using serial plotter IDE Software.

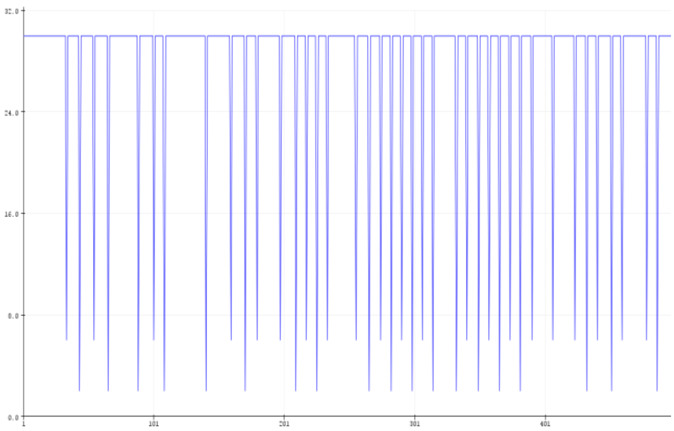

Fig. 10. RX signal when received the data from TX

Graph in figure below showed the RX signal when no data received from TX, that was when the button had not pushed, TX was not transmitted its data to the RX. The signal was not modulated because no data was received. The graph was plotted by using serial plotter IDE Software.

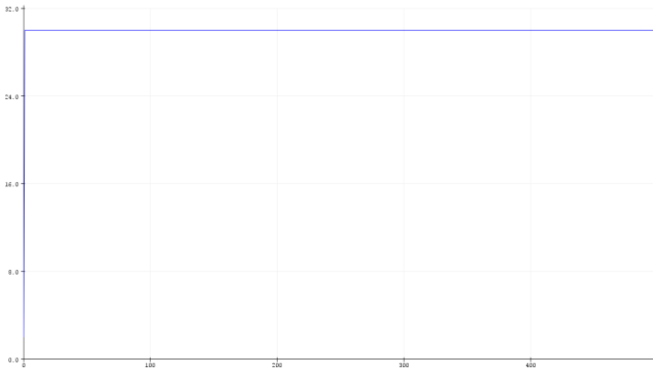

Fig. 11. RX signal when no data received from TX

For the antenna, after calculated its wavelength, the antenna was experimented to know the distance between RX and TX.

Calculation of the antenna[6,11] :

$$\lambda = \frac{1}{4}\left(\frac{300M}{315\,M}\right)$$

$= 0.24$ m

$= 24$ cm

Therefore, the wavelength that has been built was 24 cm. Figure below shows RX with and without antenna.

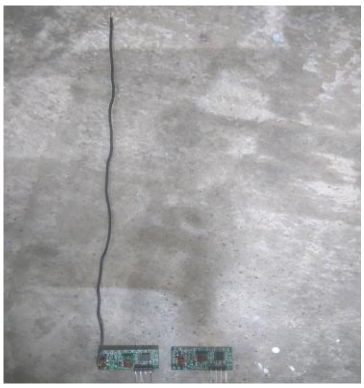

Fig. 12. RX with and without antenna

The distance between RX and TX without antenna was as shown in figure below and its distance was 86.5 cm or 0.87 m. tape measure was used to measure the distance.

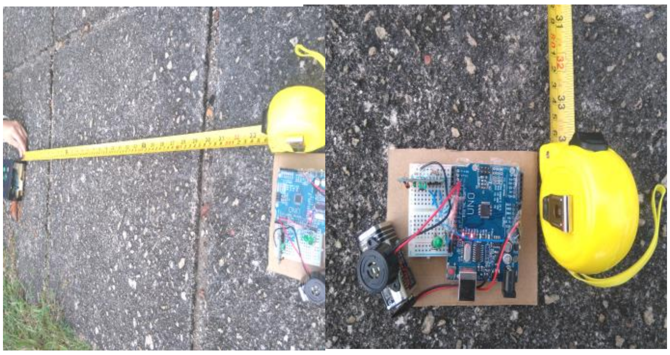

Fig. 13. Distance between RX and TX without antenna

The maximum distance between RX and TX with antenna was as shown in figure below and its distance was 883 cm or 8.83 m. in this case, because of the distance quite long and the tape meter only can measure 5m, therefore, the tape measure was used two times.

Fig. 14. Maximum distance between RX and TX with antenna

B. Power and Energy Consumption

The comparison of power consumption of the electric kettle result between Power Fluke Meter and coding were shown in figures and table below :

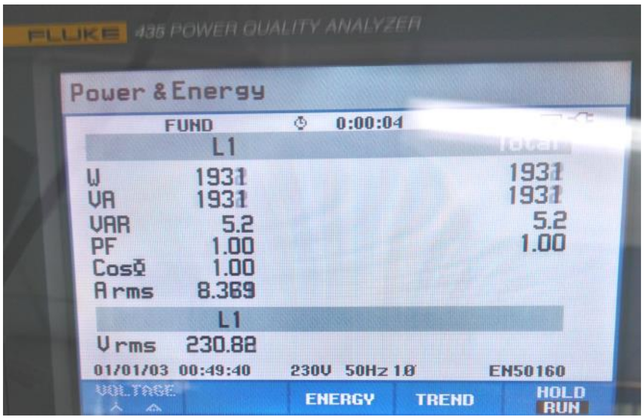

Fig. 15. Power Consumption using Power Fluke Meter

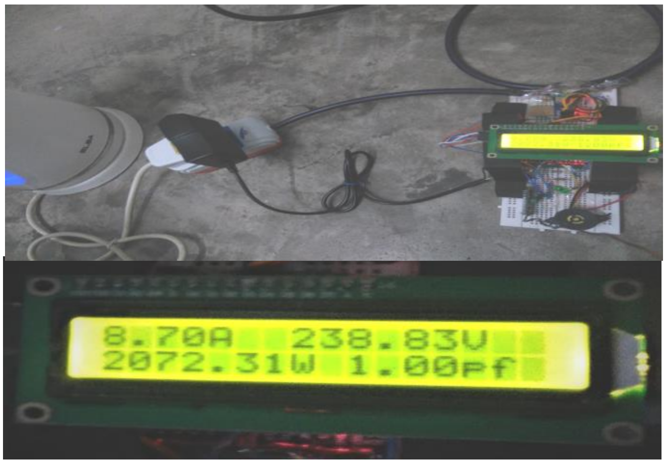

Fig. 16. Power Consumption using Coding

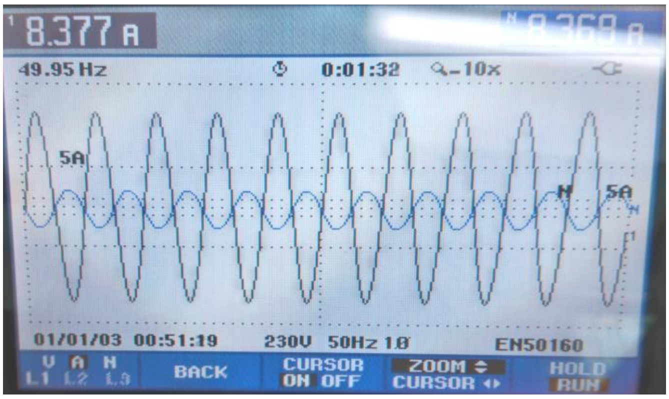

Fig. 17. Graph of Current RMS using Power Fluke Meter

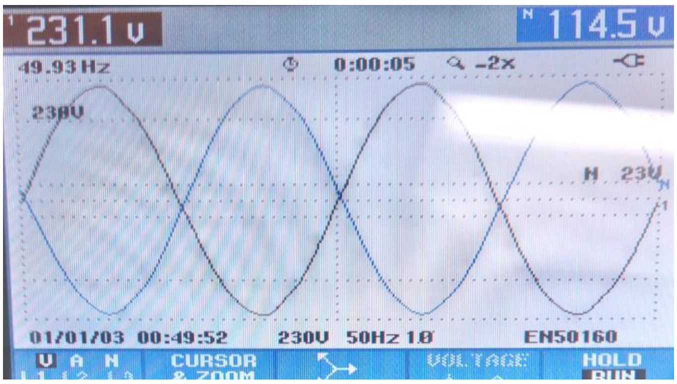

Fig. 18. Graph of Voltage RMS using Power Fluke Meter

Table 1 below shows the comparison result of power consumption of the electric kettle between using the Power Fluke Meter and the coding.

TABLE I. POWER CONSUMPTION OF THE ELECTRIC KETTLE

The result above shown that by using the coding, current RMS and voltage RMS was quite larger than using Power Fluke Meter. This was because, for the voltage, it might be the AC source of the building. The coding was done in the hostel, while, the power fluke meter was done in the Advanced Power Laboratory. But, for the current, the current was measured by using multimeter in the hostel, the result was 8.74 A as shown in figure below. Current RMS by using the coding and multimeter was slightly same.

Fig. 19. Current RMS using Multimeter

The comparison of AC loads using the coding shown in table below :

TABLE II. POWER CONSUMPTION OF AC LOADS USING CODING

Power Reading	**Power Consumption**		
	Electric kettle	***iron***	***solder***
Current RMS (A)	8.70	4.45	0.12
Voltage RMS (V)	238.83	239.06	239.77
Real Power (W)	2072.00	1060.25	27.61
Power Factor	1.00	1.00	0.97

Next, the energy consumption of solder was calculated. The solder was chosen because it can turn on more than one hour compared to electric kettle and iron. The formula of energy[7] :

$$Energy = \frac{P \times t}{1000} \quad (2)$$

Where,

P = Real Power (W)[8]

t = time taken in hour (h)

Power Reading	**Power Consumption of the Electric Kettle**	
	Power Fluke Meter	***Coding***
Current RMS (A)	8.377	8.700
Voltage RMS (V)	231.10	238.83
Real Power (W)	1931	2072
Power Factor	1.00	1.00

According to the coding, the real power was 27.61 W and one hour was taken as a time. Energy of solder :

$$Energy = \frac{27.61 \times 1}{1000}$$

$$= 0.028 \text{ kWh}$$

When compared the result between calculation and coding, the energy was 0.03 kWh. Therefore, the coding of energy consumption was successful. Figure below shown the result of using coding in 1 hour and 4 seconds :

Fig. 20. Energy of Solder using Coding

V. CONCLUSION

RF Module can used to transmit a data to from the transmitter to the receiver regardless of obstacles between them.[1] With the antenna (implemented to the receiver module), the data can transmit more than six metres. ACS712 Current Sensor is used to get the Current RMS reading.[3-4] While, adapter is used to get Voltage RMS reading. From these reading, the power and energy consumption can be determined. For the DC

load, the load is just implemented together to the receiver circuit because receiver circuit uses DC voltage and DC current.

REFERENCES

[1] Khuzaimah Bt Mohd Ali. "Electronic Security Device (ESD) Alert System", Malaysia : Universiti Teknologi Malaysia, May 2007,pp 1 -88.

[2] Weiming et al. "RF Based Wireless Remote using RX-TX MODULES (434MHz.)".,2016, pp 1 - 10.

[3] R-B "A Brief Overview Of Allegro ASC712 Current Sensor Part 1," [Online]. Available : http://embedded-lab.com/blog/a-brief-overview-of-allegro-acs712-current-sensor-part-1/. Embedded Lab. [Accessed November 21, 2017], January 12, 2015.

[4] “Fully Integrated, Hall Effect-Based Linear Current Sensor IC with 2.1 kVRMS Isolation and a Low-Resistance Current Conductor”, Datasheet, United States of America : Allegro MicroSystems, LLC,2013, pp 1 - 15.

[5] “How to build an Arduino energy monitor - measuring mains voltage and current,” [Online]. Available : https://learn.openenergymonitor.org/electricity-monitoring/ctac/how-to-build-an-arduino-energy-monitor?redirected=true, Open Energy Monitor,2017.

[6] John Erickson,“Planck’s Equation”, 2005, pp 1.

[7] “Electrical Meter Reading,” Rural Areas Electricity Company S.A.O.C, 2017, pp 1 -7

[8] Charles K. Alexander and Matthew N. O. Sadiku “Fundamental Of Electric Circuits,” United States Of America : Mc Graw Hill, fifth edition, pp 458 - 488, 2013.

[9] John W. M. Rogers, Calvin Plett, and Ian Marsland “Radio Frequency System Architecture and Design, ” United States of America : Artech House, pp 12 -13, 2013

[10] Erick C. John, and Christopher A. Chong “RFID in Logistics. A Practical Introductions,” Broken Sound Parkway NW : Taylor and Francis Group, LLC, pp 428 - 430, 2008

[11] “Antenna Basic Concepts,”Pulse Electronics : Larsen Antenna ,2017, pp 1 - 9

Solar Tracker Dual-Axis with Additional of Mirrors and Cooling System

Muhammad Amin bin Mat Yusof
Faculty of Electrical Engineering
Universiti Teknologi Malaysia
Johor Bahru, Malaysia
muhammadamin5367@yahoo.com

Dr Rasyidah binti Mohamad Idris
Faculty of Electrical Engineering
Universiti Teknologi Malaysia
Johor Bahru, Malaysia
rasyidahidris@utm.my

***Abstract*—Nowadays, renewable energy is a need since the amount of fossil and oil decreased by year. One of the best choice of renewable energy to generate electricity is solar energy since it has unlimited resources and categorized as green energy. But, the utilization of solar panel as tools to convert the light energy to electrical energy were not used at maximum usage. This paper present the development of solar tracker dual-axis system using Arduino as microcontroller. This system used four Light Dependent Resistor (LDR) and two servo motor to track and pivot the solar panel perpendicular to the sun. With additional of mirror as reflector, the amount of light capture can be increased, hence the efficiency of solar panel will be increased. The design and system of solar panel will be described briefly in this paper. The result of power gain by solar panel will be compared with three different situations; passive solar panel, solar tracker dual axis without and with additional of mirror. The value of power obtained by parallel the solar panel with resistance and measured the value of current and voltage. One of the obstacles that may interrupt the system is the sensitivity of LDR. At the end of this paper, the result obtained showed that this model helped the solar panel gain more power than passive solar panel. It proved that by pivoted the solar panel to the sun and with helped of mirror as reflector assisted the solar panel to gain more power.**

Keywords—solar panel, solar tracker, mirror, servo motor, LDR, power gain.

I. Introduction

Solar tracking become a new phenomenon nowadays. Almost every country around the world that received abundance of solar radiation utilize this system either a single-axis nor dual-axis. Each of them scrambled over the technologies to gain maximum power from the unlimited resources for electricity generation, the Sun. Based on research study by Rebecca Harrington, 2016, the top ten of the countries that leading the world in solar energy were South Korea, Belgium, Australia, Spain, France, United States, Italy, Japan, China and the top one is Germany with 38,250 MW.

Even nowadays, many countries already used the solar panel, but they should know the advantages of having a smart tracker. For an example, a company from Germany, SunPower Corporation that expert in solar power systems. The company designed a single-axis tracker that move from east to west in order to increase the productivity of power output. As the results, they gain at least 30% more power than static solar panel that facing the south. In addition, a company named Spectrolab developed a smart dual-axis tracker with a new technology that uses mirror to focus the sunlight to their solar panel. The results were surprising the world with very high efficiency of production that more than 40% of power produced.

Fig. 1. Spectrolab company use miror to focus the sun.

Hence, it can say that solar tracking could be a new future that will save the world. Besides, it can increase the efficiency of power production by maximize the input radiation from the sun. In addition, by choosing the solar energy as main source, the pollution that usually came from the used of fossil and oil can be avoided.

II. Literature Review

A. Solar Energy in Malaysia

Solar energy is one of the best renewable energy that could be used to generate electricity. There were so many advantages of using this energy since solar energy was categorized as green energy. One of them, it was harmless and free pollute. Compared to other resources for example fossil fuel, it caused the air pollution which harm the health of humanity. Besides, it also has unlimited sources unlike the fossil fuel that has limited resources. In different point of view, it also can be a good investment for corporate company since the payback period is not more than five years. That's why the implementation of solar energy as main resources brings more pros than cons.

Malaysia is one of countries that located close to the equator and receives a lot of solar radiation. The duration of the sunshine was quiet long which range six to eight hours per day. The normal temperature is consistently high extending from 26°C to 28°C every year, with plentiful of rainfall and high humidity. In view of the mean solar radiation per month, is it adequate for the operation of solar panel, which the major towns show a good review. The range of solar radiation were between 400-600 mWhcm-2 where dominated by northern states. The mean of solar radiation in Malaysia per day are 4.21 kWh/m² to 5.56 kWh/m² annually. For yearly analysis, the solar radiation varies between 1400-1900 kWh/m² which dominated by Bayan Lepas and Kota Kinabalu with 1809 kWh/m² and 1900 kWh/m² respectively. [2]

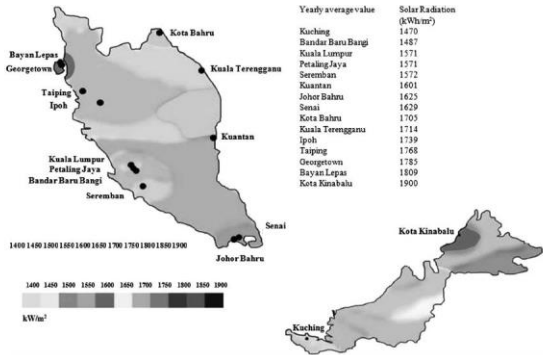

Fig. 2. Solar radiation in Malaysia.

B. *Concept of Solar Radiation*

The amount of energy produced by solar panel was determined by the solar radiation. The quantity of solar energy that absorbed by solar panel for a certain period is called as solar radiation or known as solar irradiation. The solar radiation can be divided into three parts, direct radiation, diffuse radiation and reflect radiation. The production of energy by solar panel limited whenever it cannot absorb sufficient of solar energy to generate the electricity especially when it is cloudy and wet weather.

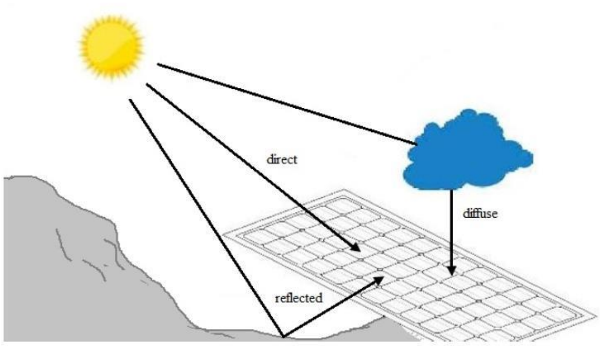

Fig. 3. Types of solar radiation.

Direct radiation is a direct strike of solar radiation on solar panel without any disturbance while the diffuse radiation is indirectly radiation which basically hit the cloud at first before absorbed by solar panel. Only 10% of solar energy carried by diffuse radiation while the rest is carried by direct radiation. During a sunny day, almost all the solar energy become direct solar radiation due to absence of cloud on the sky. Another radiation was reflected radiation. Reflected radiation refer to direct radiation that hit the earth first and then reflect to the solar panel. Hence, the global radiation on solar panel refer to the combination of all types of radiation as mention above. [4]

At a point of view, the solar panel was facing an efficiency problem to generate maximum power from the sun. One of the way to solve this problem was by applying the solar tracking concept. The system of solar tracking is implied to maintain the position of solar panels always perpendicular to a direction of sun radiation. [7]. Basically, solar tracker does track the position of the sun during a shiny day and automatically aligned the angle of the solar panel perpendicular to the sun at all times. The efficiency of the conversion system may be increase by the orientation of the solar panel. [10].

C. *Factors That Affect Power Gain by Solar Panel*

There are several factors that affects the efficiency of power gained by solar panel. One of them is the incidence angle between the sun and the solar panel. As the value of incidence angle decrease, the efficiency of solar panel will increase. Hence, the solar trackers were proposed to decrease the value of incidence angle all the time. Besides, the clean solar panel will produce more energy compared to dirty solar panel. Usually, the dirty panel covered by dusts. These dusts will block the solar radiation to be absorbed by solar panel directly. By cleaning the panel, the panel can work more efficient. Other than that, the ambient temperature could be a factor that affect the efficiency of power gained. The optimum temperature for normal solar panel to operate is 25°C. If the temperature rise over the optimum temperature, it will decrease the production of energy.

Next, the weather of daily could cause the inconsistency of energy production. During the cloudy day, the sun was block by the cloud cause the tracker will lose sight of the sun. That's the reason why solar panel does not work on raining or cloudy day. The position of solar tracker could be one of the factors. If a solar panel was placed behind a tree, at a certain time the production will drop because the solar panel was blocked by the shadows of the tree. The animal also can be a threat to the safety of solar panel. They probably can damage the solar panel with rock or something else. Sometimes a little squirrel climbed on the solar panel and scratched it.

III. METHODOLOGY

Before started developing the solar tracker, the study about solar tracker was performed to identify all of the components involves with details specification. All factors were considered in order to obtain the best results. Then, the design of the circuit and model solar tracker were sketched followed the suitable specifications. Next, all of the components were connected properly to the Arduino UNO which acts as microcontroller.

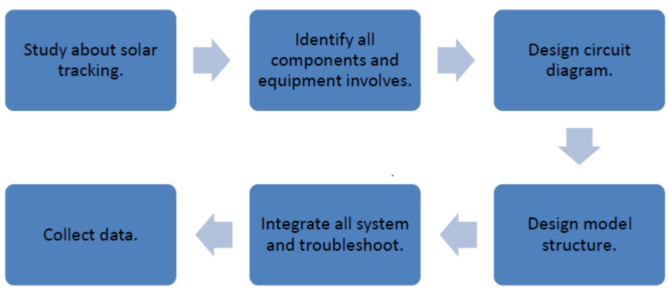

When the model was built up, the program of the system is tested and troubleshoot to get the desired output. At this stage, the most difficult thing is to stabilize the position of solar tracker. It is because the value of each LDR are not equal even at the normal condition. A lot of troubleshoot required to make sure the solar panel facing perpendicular to the sun.

A. Flowchart of Tracking System

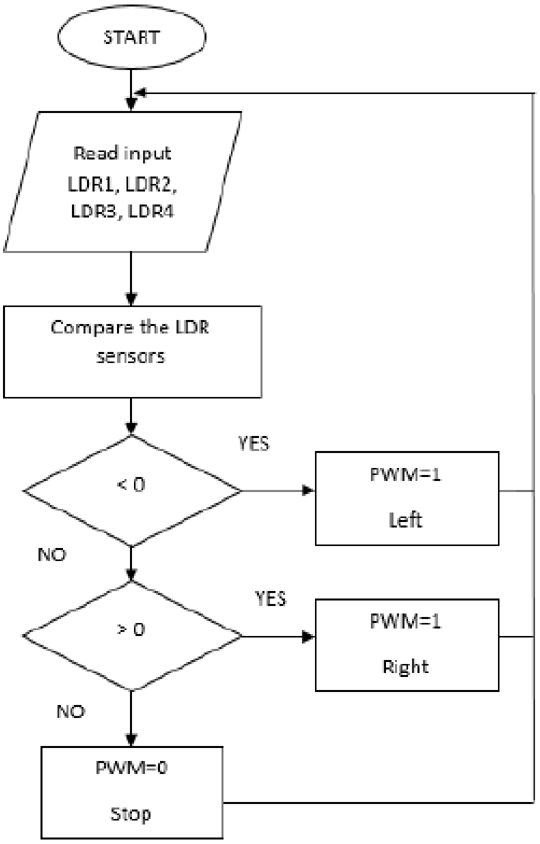

A simple explanation for this flowchart. There are four LDR sensors where LDR1 will compare with LDR2 and LDR3 will compare to LDR4. Whenever the difference of the pair LDR consume negative value, the motor will rotate to the left until the difference is zero. Same goes to another one, whenever the difference of the pair LDR consume positive value, the motor will rotate to the right until the difference is zero. Then it will keep read the data input from LDR. If there is any difference, the motor will rotate.

B. Circuit Design

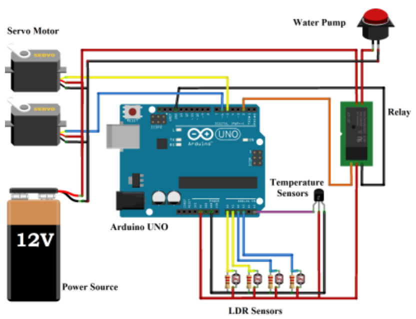

Fig. 4. Complete circuit design for whole system.

For the circuit design in dual-axis tracking system, the components and hardware that involves in development of the model include the solar panel, Arduino UNO as microcontroller for the systems, the LDR sensors as the input for the system, servo motors to pivot the movement of solar panels and power source. Basically, the movement of solar panel were pivoted by two servo motor with two different angle; azimuth angle and altitude angle. Each of this servo were controlled by two LDR sensor. Hence, the movement of solar panel depends on different of these LDR sensor at each servo.

This dual-axis model was equipped with another feature which is the mirror and cooling system. The mirrors were attached around the solar panel to collect more sun radiation by using the concept of reflection. For cooling system, hardware that involves were temperature sensors, water pump and tube which utilize standard pump system with intelligence method. The water pump will trigger whenever the temperature of solar panel exceeds the optimum range value of solar panel.

C. Hardware Implementation

1) Arduino UNO

- The Arduino UNO was the brain for this system. It received data from LDR sensors, interpret and then send data to the motors. It controlled the movement of the solar panel based on the input received.

2) Light Dependent Resistor (LDR)

- Four LDR were used and placed on top of the solar panel. The idea was two LDR sensors will control one motor. The difference of intensity between these two LDR will determine the movement of motor either to rotate right or left. Whenever the amount of intensity for both LDR is same, then the motor will stop.

3) Servo Motor MG995

- This type of servo was chosen because it used metal gear which is more durable compare to MG90. Besides, it has high torque 10 kgf·cm (6 V).

4) Solar Panel

- 10 Watt solar panel was chosen to carry out this project. The size and weight of solar panel were considered to suit the torque that can carried by servo.

5) Temperature Sensor LM35

- Small size and easy-use were one of the factors LM35 was selected. It can operate over a -55°C to 150°C.

6) Water Pump

- DC water pump 12V was chosen since the power source was 12V lead acid battery. It allows 350 liters per hour for the maximum flow. The diameter of out water pump is 7mm which smaller than in water pump 8mm. It gave high pressure for water to flow.

7) Relay 5V

- Relay function as auto switch for water pump. Its operate at 5V and can withstand with up to 250VDC. One of pin IN in the relay will connected to the Arduino to gain the instruction from the masterpiece.

IV. Result and Discussion

In order to calculate the value of voltage and current from solar panel, a fixed resistance was connected parallel to the solar panel. Then, a multimeter was connected parallel to the load for voltage value and connected series for current value. The experiment was conducted at evening to get different value for comparison between passive solar and solar tracker. The experiment was conducted from 7.00a.m until 7.00p.m at different situations. The three different situations were;

(a) Passive solar panel without tracking and mirror.

(b) Dual axis tracking system without mirror.

(c) Dual axis tracking system with mirror.

Then, the data the value of power were calculated by using this formula (1):

$$P = VI \tag{1}$$

TABLE I. Data For Passive Solar Panel

NO	Time	Voltage (V)	Current (A)	Power (W)
1	0700	13.64	0.28	3.8192
2	0800	14.78	0.33	4.8774
3	0900	15.08	0.39	5.8812
4	1000	15.47	0.42	6.4974
5	1100	15.74	0.45	7.0830
6	1200	15.97	0.47	7.5059
7	1300	15.82	0.46	7.2772
8	1400	15.73	0.45	7.0785
9	1500	15.38	0.40	6.1520
10	1600	15.11	0.37	5.5907
11	1700	14.83	0.33	4.8939
12	1800	14.62	0.31	4.5322
13	1900	13.92	0.29	4.0368

TABLE II. Data For Dual Axis Without Mirror

NO	Time	Voltage (V)	Current (A)	Power (W)
1	0700	14.81	0.33	4.8873
2	0800	15.42	0.37	5.7054
3	0900	15.73	0.41	6.4493
4	1000	15.81	0.46	7.2726
5	1100	16.01	0.48	7.6848
6	1200	16.13	0.49	7.9037
7	1300	16.04	0.48	7.6992
8	1400	15.97	0.47	7.5059
9	1500	15.73	0.44	6.9212
10	1600	15.48	0.41	6.3468
11	1700	15.33	0.39	5.9787
12	1800	14.98	0.35	5.2430
13	1900	14.64	0.31	4.5384

TABLE III. Data For Dual Axis With Mirror

NO	Time	Voltage (V)	Current (A)	Power (W)
1	0700	15.55	0.35	5.4425
2	0800	15.84	0.39	6.1776
3	0900	16.14	0.44	7.1016
4	1000	16.31	0.48	7.8288
5	1100	16.34	0.50	8.1700
6	1200	16.52	0.51	8.4252
7	1300	16.41	0.49	8.0409
8	1400	16.29	0.48	7.8192
9	1500	16.08	0.46	7.3968
10	1600	15.83	0.45	7.1235
11	1700	15.64	0.42	6.5688
12	1800	15.37	0.38	5.8406
13	1900	14.82	0.32	4.7424

Hence, we can see that by implying the dual axis tracker with additional of mirror gives highest output of power compare to another situation. The value of power output can be achieved at 8.4252W compare to passive model, 7.5059W during noon. A huge different can be seen at 1600 between passive solar panel and both tracker system (with and without mirror). It proved the advantages of using tracker.

If we see the data collections in all the tables, the data looks not consistent for every situation. It is because of several factors during the measurement was taken. One of them was whenever the measurements taken, there were certain times that the sun was sheltered by the cloud and it gave low value of voltage and current. Besides, another factor is the inconsistent value of LDR as mention before. The disadvantage of using LDR is it does not have same exact value each other even at the normal condition. Then, it will affect the position of solar panel to the sun. In addition, the cooling system during this experiment does not trigger since the temperature sensors does not read the proper values that will trigger to the water pump.

V. Conclusion

As a conclusion, the development of solar tracking dual axis with additional of mirror and cooling system can maximize the usage of solar panel. It proves with the data collection in section result and discussion. The model showed that it can gain more power at least three times compare to the passive solar panel. With help of mirror as a reflector, it helps the solar panel gain more radiation and help it produces more electric energy.

References

[1] Stamatescu, I., G. Stamatescu, N. Arghira, I. Fagarasan, et al. Fuzzy Decision Support System for Solar Tracking Optimization. 2014 IEEE International Conference on Development and Application Systems (DAS). May 2014, Suceava: IEEE. 2014. 16-20.

[2] Ahmad, S., Shafie, S., Kadir, M.Z.A.A. A High Power Generation, Low Power Consumption Solar Tracker. 2012 IEEE International Conference on Power and Energy (PECon). Dec 2012, Kota Kinabalu: IEEE. 2012 366 - 371.

[3] Alexandru, C. The Design and Optimization of a Photovoltaic Tracking Mechanism. 2009 International Conference on Power Engineering, Energy and Electrical Drives. March 2009. Lisbon: IEEE. 2009. 436–441.

[4] Usta, M.A.; Akyazi, O.; Altas, I.H. Design and Performance of Solar Tracking System with Fuzzy Logic Controller Used Different Membership Functions. 2011 7th International Conference on Electrical and Electronics Engineering (ELECO). Dec 2011. Bursa: IEEE. 2011. 381–385.

[5] Zhang, X., Li, X. and Lu, K. Research on an Intelligent Solar Tracking System Based On LPC2131. 2012 3rd IEEE International Conference on Network Infrastructure and Digital Content (IC-NIDC). Sept. 2012. Beijing: IEEE. 2012. 429 – 432.

[6] Ahmad Amshar bin Azman. A Solar Tracking System With Multiple Parameter Input For Maximize Efficiency. B. Degree Thesis. Universiti Teknologi Malaysia; 2014

[7] Sebastian Bader, Bengt Oelmann. Enabling BatteryLess Wireless Sensor Operation Using Solar Energy Harvesting at Locations with Limited Solar Radiation. 2010 Fourth International Conference on Sensor Technologies and Applications. July 2010. Venice: IEEE. 2010. 602-608.

[8] Huang, Y.J., Wu B. C., Chen C. Y., Chang C. H., et al. Solar Tracking Fuzzy Control System Design using FPGA. 2009. I (1): 1–5.

[9] İ. Sefa, M. Demirtas, and İ. Çolak. Application of One-Axis Sun Tracking System. Energy Conversion and Management. 2009. Vol. (50): 2709-2718.

[10] Chin C. S., Neelakantan P., young H. P. and Teo K.T. Optimisation of Fuzzy Based Maximum Power Point Tracking in PV System for Rapidly Changing Solar Irradiance. 2011. Vol. 2: 2229-8711.

[11] Shrivastava, S.M. Dual Axis Solar Tracker. B. Degree Thesis. Gautam Budh Technical University; 2013

[12] H. Mousazadeh, A. Keyhani, A. Javadi, H. Mobli, K. Abrinia, and A. Sharifi. A Review of Principle and Sun-Tracking Methods for Maximizing Solar Systems Output. Renewable and Sustainable Energy Reviews. 2009. Vol. 13: 1800-1818.

[13] Tianze L., Hengwei l., Chuan J., Luan H., et al. Application and Design of Solar Photovoltaic System. Journal of Physics: Conference Series. 2011. Vol. 276: p.012175.

[14] Clifford M. J. and Eastwood D. Design of a Novel Passive Solar Tracker. Solar Energy. 2004. Vol. 77: 269-280.

[15] Abdallah S. and Nijmeh S. Two-Axis Sun Tracking with PLC Control. Energy Conversion and Management. 2004. Vol. 45: 1931-1939.

Application of Led Technology to Reduce Energy Consumption for Street Lighting

Muhamad Safwan Md A Halim
Faculty of Electrical Engineering
Universiti Teknologi Malaysia,
Johor Bahru, Malaysia.

Dr. Rasyidah Mohamad Idris
Faculty of Electrical Engineering
Universiti Teknologi Malaysia
Johor Bahru, Malaysia.

***Abstract*— The 'Light Emitting Diode' (LED) is not a new technology, however, it is used widely in many related products and being adopted in our daily life. However, for the street lighting system, LED technology is not fully accepted at the moment to replace the 'High Pressure Vapour Sodium' (HPSV) street light which has been used throughout the country. Due to sudden increment in operating costs and energy supply tariff, this technology starts to gain its consideration because of its ability in saving the energy. The street lighting system involves relative complex specification especially in terms of safety. Therefore, the LED street light is still at its initial level. In Universiti Teknologi Malaysia, the first project in implementing the LED street lighting system was installed at Dataran Ilmu and Senai-Exit 2-lane single carriageway. The project focuses on the structure of the road, pole distances, height of pole and several of LEDs that will be investigated for replacing HPSV in order to reduce power consumption. The aim of this paper is to study on the ability to identify whether the LEDs street light can meet the specification requirements mentioned in MS-825. In this study, the changes of pole distance and height of pole will give the performance of street lighting more efficient and improving the quality of light. By maintaining the existing street light structure in UTM, the comparison is made between HPSV and LEDs. As a result, 90 watt of LED is capable to satisfy the specification requirements. In addition, from the 'Return on Investment' (ROI) shows that the paybacks cannot be achieved within 5 years which under warranty period by the manufacturer or supplier. This proves that the proposed of replacing HPSV with LED street light is not reasonable. (*Abstract*)**

Keywords— LED technology; road lighting; HPSV; return on investment

I. Introduction

Source of light has been through a lot of changes from the time since Thomas Edison introduced the incandescent lamp. The outdoor lighting applications used nowadays are mainly discharge lamps, but new technologies like light-emitting diode (LED) are coming into the market with promising different perspectives. According to Fusheng Li, Dahua Chen, Xianjie Song & Yuming Chen (2009)[1], there are two main reason why LED are good than discharge lamp. There are luminaire efficacy and dimming & intelligent control. For the luminaire efficacy must be evaluate in full of functioning of both the source light and the fixture, including power suppliers and other electronics and optical elements. Furthermore, LED light output more efficiently because of the light is emitted downward, thus avoiding wasteful reflections inside the luminaire by Vitor C. Bender, Fernanda B. Mendes, Tiago Maggi, Marco A. Dalla Costa and Tiago B. Marchesan (2013) [2]. Additional advantage LED street lighting is also have good colour rendering of white LED chips state by Kostic (2011) [3]. In Malaysia, electrical energy is created from burning fuels, gas and coal fired burning that will cause carbon dioxide emission (CO_2) to atmosphere. The more electrical energy being utilized, the more CO_2 will be transmitted to the air space and will bring about worldwide temperature alteration. This effect could be reduced with less energy consumption. One of the applications in energy saving solution is through replacing the existing street lighting using LED. In designing street lighting, there are several components need to be considered which is an optical system, structural system and electrical system. Over the past decade, street lighting commonly used High Pressure Sodium Vapour (HPSV) lamp due to lower capital cost instead of Light Emitting Diode (LED) that have a high capital cost but consume less power. The most existing road lighting at UTM using HPSV lamp while the first application of LED street lighting at Senai exit and Dataran Ilmu. There are many researches done in the LEDs lighting system especially in term of the efficiency. This shows that this system has expanded rapidly. Therefore, this study is made to determine the effectiveness of LED lighting which is said to provide brighter lighting and at the same time reduce the power consumption. In addition, analyses were performed to assess the lighting performance and the return-on-investment (ROI). This study is important due to its influence in high investment matters and to compare the effectiveness of LEDs versus HPSV lighting system which have been long established in road lighting. At the same time, the maintenance aspect is also one of the important factors which involve the cost need to be identified. The benefit of this study is to determine the following:

1) *To compare the LED and HPSV optical system based on efficiency and effectiveness.*
2) *To determine the compatibility of both HPSV and LED street lighting comply the road specification at UTM according MS-825 that recommended by JKR.*

3) To determine return on investment (ROI) for replacement of HPSV with LED street lighting

II. LIGHTING ANALYSIS

There were three main processes adopted in this project. First, the design of HPSV street lighting which is has been used in UTM campus. Second, the comparison of measurement result between the existing of HPSV with LED in difference structure and position of street lighting. Lastly, calculation of the ROI. The road profile modeling for the case study will adopt the ME3 road classes which is the standard used for urban and not congested roads.

A. Simulation on HPSV

The simulation data of HPSV were compared with the measurement data of LED street lights, since HPSV has been installed in UTM campus. The simulation was done using the HPSV model. Before that, there are few parameters need to be set and fulfilled as shown in Table I.

B. Measurement Data (LED Street Lighting)

The step of measurement follows the CIE–140: Road Lighting Calculation [4]. However, the study focuses on the illuminance measurement according to the designing of road lighting. The measurements were recorded based on the height of pole, pole distances and various of lamp in term of power usage in order to saving energy consumption.

C. Analysis

From both simulations on HPSV and LED measurement data, the comparison was done by comparing the luminance of light with MS-825 requirement. Algorithm of the data analysis process is illustrated in Fig. 1

D. Return on Investment (ROI)

The ROI is used to calculate the payback period. Based on the ROI, it will show whether the LED street light is worth to replace HPSV street light. For that purpose, there are three measurements were taken; capital cost, operation cost and maintenance cost, respectively.

The wattage of the LED light needed to be considered as well. Therefore, surveys from the manufacturers and suppliers were done earlier. Based on the outcome from the survey, the suitable LED wattage for road profile using ME3 is model from Nikkon manufacture. There are three types of lamps of that have to be investigated which are 90, 80 and 60 watt and should be compatible with MS-825 requirement.

1) Capital Cost.

The capital (some refers this as initial cost) is related to the money that needs to be invested for buying the product i.e. LED lights. Its included the installation cost to replace HPSV with LED.

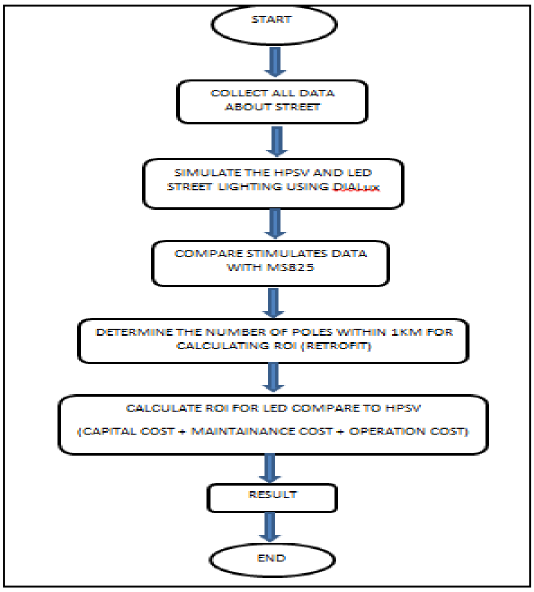

Fig. 1: Algorithm of data analysis process

Table 1: Data for simulation

Information	***Value***
Classes of road	ME3
Road surface classification	R3
Lane Width	7m
Lane	2
Pole arrangement	Single sided arrangement
Spacing Pole to pole	25m
Height of pole	10m
Maintenance factor	0.8
Overhang	3

.

2) Operation Cost.

The operation cost is included in the monthly electricity bill. Based on the previous years, the electricity bill has been updated since 2014 by power utility. Figure 2 shows the street lighting tariff that will be charge on the users based on the option of user whether including the maintenance or not.

TARIFF CATEGORY	CURRENT RATE (1 JAN 2014)
TARIFF G - STREET LIGHTING TARIFF	
For all kWh (including maintenance)	30.5 sen/kWh
For all kWh (excluding maintenance)	19.2 sen/kWh
The minimum monthly charge is RM 7.20	

Figure 2. Tariff for street lighting

3) Maintenance Cost.

Maintenance cost for both HPSV and LED lantern are depending on their components. Besides that, the machinery and labour cost also need to be considered as maintenance cost.

$$\text{Payback Period} = \frac{\text{Initial cost}}{\textit{Annual saving Operation Cost} + \textit{Maintenance Cost}}$$

III. RESULT AND DISCUSSION

A. Calculation of Simulation

The simulation was done using the specification in Table I as the parameter which follows the road profile model. The summary of simulation result for HPSV as shown in Fig. 4.

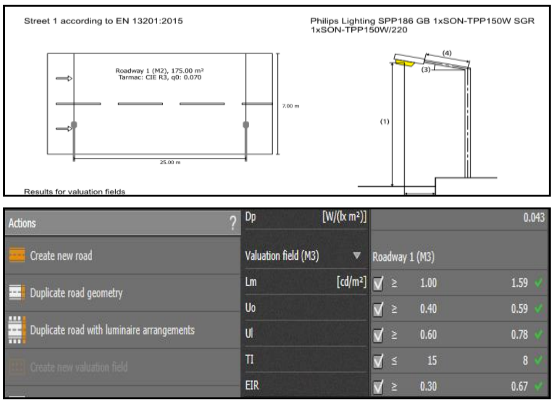

Fig 3. Summary of simulation result for HPSV

B. Measurement Data for LED Street Light

The luminance measurement has been done in the difference cases using DiaLux software which are concerning the pole distance, height of pole and the wattage usage of lamps to be investigated. There are four cases to be investigated to obtain the best quality of light in designing street lighting. . In according to fulfill the requirement MS-825 standard, the height pole and pole distance were changed to identify the suitable method could be used to improve quality of light in order to reduce power energy consumption.

C. Comparison Between HPSV & LED

The purpose of comparing between HPSV and LED is to make sure both street lights comply the standard MS-825. Table V shows the comparison between HPSV & LED toward the MS-825 standard.

Horizontal illuminance [lx]										
6.417	22.2	19.0	15.2	12.4	11.1	11.1	12.4	15.2	19.0	22.2
5.250	23.7	20.0	15.7	12.7	11.2	11.2	12.7	15.7	20.0	23.7
4.083	24.1	20.3	15.9	12.8	11.2	11.2	12.8	15.9	20.3	24.1
2.917	23.4	19.9	15.7	12.5	11.0	11.0	12.5	15.7	19.9	23.4
1.750	21.0	18.4	14.5	11.6	10.2	10.2	11.6	14.5	18.4	21.0
0.583	17.9	16.1	13.0	10.5	9.33	9.33	10.5	13.0	16.1	17.9
m	1.250	3.750	6.250	8.750	11.250	13.750	16.250	18.750	21.250	23.750

Figure 4. Sample result for Horizontal illuminance of LED

Case 1 : Height of pole 10 meter / Pole distance 25 meter

Table 2. Result from simulation software

ME3	Luminance Of The Road Surface Of The Cariageway For dry Road Suraface Condition				
Characteristics	MS-825	HPSV	LED 90W	LED 80W	LED 60W
Pole distance (m)	-	25	25	25	25
Luminance max, L_{max}	30	39.5	24.1	20.6	16
Luminance min, L_{min}	10	9.93	10.1	8.38	6.76
Luminance average, L_{avg} (cd/m²)	≥ 1.00	1.59	0.95	0.81	0.63
Overall Uniformity, U_o	≥0.40	0.59	0.65	0.63	0.63
Longitudinal Uniformity, *UL*	≥0.70	0.78	0.78	0.75	0.79
Threshold Increment, *TI* (%)	≤10 %	8	5	5	5

For HPSV, the isolux pattern in figure 5 shows that in front of light with the maximum illuminance about 39.5. It's value obviously above the road specification according to MS-825 which is maximised to 30. It can be concluded that there is excess of lighting, which means the HPSV light power is too big and it is a waste of energy. The performance of LED 90 watt is better compare to others lighting which are 80 and 60 watt. Based on standard MS-825 light distribution of street lighting luminaires should be in range between 10-30 cd/m² and just only one can be approved that fulfill the specification which is 90 watt. For both 80 and 60, the values below the range of illuminance and not appropriate used to replace the HPSV lighting.

a.

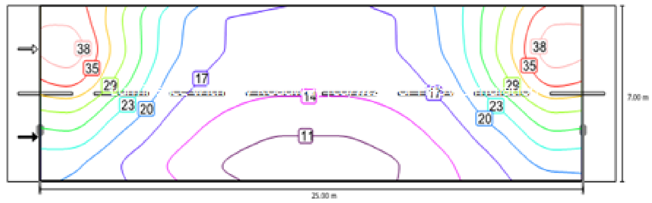

Figure 5. Isolux for HPSV road lighting

Case 2 : Height of pole 10 meter / Pole distance 20 meter

Table 3. Result from simulation software

ME3	Luminance Of The Road Surface Of The Cariageway For dry Road Suraface Condition			
Characteristics	MS-825	LED 90W	LED 80W	LED 60W
Pole distance (m)	-	20	20	20
Luminance max, L_{max}	30	26.2	22.3	17.5
Luminance min, L_{min}	10	14.8	12.4	10.0
Luminance average, L_{avg} (cd/m²)	≥ 1.00	1.19	1.01	0.76
Overall Uniformity, U_o	≥0.40	0.66	0.65	0.66
Longitudinal Uniformity, *UL*	≥0.70	0.85	0.85	0.88
Threshold Increment, *TI* (%)	≤10 %	4	5	4

Two results for application of led able to fulfill the ME3 requirement due to average luminance are above than the minim um value 1.00 cd/m^2. It indicates the value is 1.19 increased by 0.24 for led 90 watt. While for 80 and 60 watt, the value of average luminance is 1.01 and 0.76 increased by 0.2 and 0.13 respectively. For 60 watt led application is not able to fulfill the ME3 requirement due to lack of average luminance, but smaller the spacing from 25m to 20m between luminaries will give a street lighting more efficient and improving the quality of light at a particular area. As can be seen there is an obvious improvement of the quality of street lighting that can be summarized by an increasing in the minimum illuminance (lm/cd^2) from 10.1 to 14.38 for 90 watt, from 8.38 to 12.4 for 80 Watt, and from 6.76 to 10.0 for 60 watt. . It can be concluded that if the project implementation are carried out by applying the spacing between luminaries become smaller it will helps to improve the quality of lighting.

Case 3 : Height of pole 8 meter / Pole distance 25 meter

Table 4. Result from simulation software

ME3	Luminance Of The Road Surface Of The Cariageway For dry Road Suraface Condition			
Characteristics	MS-825	LED 90W	LED 80W	LED 60W
Pole distance (m)	-	25	25	25
Luminance max, L_{max}	30	34.6	29.6	23.5
Luminance min, L_{min}	10	10	7.84	6.46
Luminance average, L_{avg} (cd/m^2)	≥ 1.00	1.13	0.97	0.77
Overall Uniformity, U_o	≥0.40	0.64	0.65	0.64
Longitudinal Uniformity, *UL*	≥0.70	0.88	0.86	0.87
Threshold Increment, *TI* (%)	≤10 %	7	7	6

The lamp of 90 watt LED is the only one can fulfill the criteria of requirement compare to the other two applications. The lack of average illiuminance for 80 watt LED is slightly different compare to requirement of JKR which is 0.97 approaching to 1.00 cd/m^2 and can be considered in designing street lighting. In this case, two type of lighting can be chosen to implement the road lighting which is fulfilling the specification of JKR. But due to lack of minimum illuminance which is 8.9 lux in the middle of measurement area, 80 watt lamp is not suitable to be implemented. Therefore, 90 watt of LED has been chosen if the project implementation is carried out

Case 4 : Height of pole 8 meter / Pole distance 20 meter

The average illuminance for 60 watt LED is approaching to 1.00 cd/m^2 and fulfills MS-825 requirement. So, there are 3 types of lamp compatible the standard. The purpose of the investigation is replacing HPSV to LED and reduces the operation cost of street lighting

Table 5. Result from simulation software

ME3	Luminance Of The Road Surface Of The Cariageway For dry Road Suraface Condition			
Characteristics	MS-825	LED 90W	LED 80W	LED 60W
Pole distance (m)	-	20	20	20
Luminance max, L_{max}	30	37.6	32.2	25.2
Luminance min, L_{min}	10	13.8	11.5	10
Luminance average, L_{avg} (cd/m^2)	≥ 1.00	1.42	1.21	0.96
Overall Uniformity, U_o	≥0.40	0.63	0.65	0.66
Longitudinal Uniformity, *UL*	≥0.70	0.77	0.86	0.80
Threshold Increment, *TI* (%)	≤10 %	6	6	5

In this case, the best lighting to be implemented in order of quality of lighting and saving energy is 60 watt LED. It can be concluded that reducing the pole distance and height of pole give the best performance in designing road lighting**.**

D. Calculation of Return on Investment (ROI)

The research not just to prove that the LED street light can meet the standard, but calculation of ROI also need to be considered to see whether by implementing the LED technology is power consumption saving and economical. The calculation is focused on retrofit installation at existing road and not for the new design of street light. The component and the calculation of profit are based on price list provided by the local authority.

1) Capital Cost

The LED technology is growing rapidly with the increasing in demand that makes the price of LED street light very competitive. This is the reason this research implement the ROI based on the current price. According to the research from Onaygil et al. [6] to determine the optimum design conditions, capital cost should be chosen with lower luminaire prices and high efficiency factor of LED. Thefore, the capital cost of this research has chosen the most economical lantern which is 224 watts at a price RM 3,500. Fig. 5 and Fig. 6 show the design of LED street light and the result for calculating the ROI.

- Number of Poles in 1km with twin central installation
  = 1000 meters / 25 spacing between pole to pole
  = 40 poles

- Number of lantern = 40 pole x 1 (single sided)
  = 40 lanterns

- Cost of new LED lantern = RM 3,500 / per lantern

- Cost of installation :
  (sky lift rental price / per day + labor cost / per day) x (20 lantern/per day) /54 lantern
  = (RM 450 + RM 300) x (54 / 20 lantern) / 54
  = RM 37.50

- Initial cost for 1 lantern = (RM 3,500 + RM 37.50) + 10% profit
  = RM 3891.25

- Total initial cost = RM 3,561.25 x 40
  = **RM 155,650**

2) Annual Saving Operation Cost

Saving energy = HPSV luminaire – LED luminaire
= 150W – 90W
= 60W

Annual saving energy :

40 lantern x 12 hour per day x 365days per year x 60W saving energy x 30.50 sen/Kwh
= **RM 3206.16**

3) Annual maintenace cost

The HPSV street lighting maintenance cost calculate by follow the JKR practice where the total of maintenance cost need to multiply with 35% as maintenance factor because from the JKR previous record show that 35% of the lantern will fail before the next maintenance cycle. The components that need to be replacing for HPSV lantern are ignitor, capacitor, ballast and bulb. Below is an annual saving maintenance cost calculation of HPSV.

- Cost of lamp and component :
  ignitor + capacitor + ballast + bulb
  = RM52.10 + RM55.60 + RM87.20 + RM46.80
  = **RM 241.70/ lantern**

- Cost of installation :
  (sky lift RM 450/ day + labour RM 300/ day) x (20 lantern/ day)/80
  = (RM450 + RM300) x (80/20) / 80
  = **RM37.50 lantern**

- Initial cost for 1 lantern :
  = (RM241.7 + RM 37.50) + 10% profit
  = **RM 307.12**

- Total cost :
  = (RM 307.12 x 40 lantern) + 35%
  = **RM 16,584.48**

$$Payback\ Period = \frac{\text{Initial cost}}{\text{Annual saving operation cost} + \text{annual saving maintenance cost}}$$

$$= \frac{\text{RM } 155560}{\text{RM } 3206.16 + \text{RM } 16584.48}$$

= 7.86 years / 8 years

Table 6. The ROI for LED lantern

Year	Initial Cost (RM)	Annual saving (maintenance + operation cost)	Payback Period
1st	RM 155650	RM19790.64	RM 135859.36
2nd	RM135859.36	RM19790.64	RM 116068.72
3rd	RM116068.72	RM19790.64	RM 96278.08
4th	RM96278.08	RM19790.64	RM 76487.44
5th	RM 76487.44	RM19790.64	RM 56696.80
6th	RM 56696.80	RM19790.64	RM 36906.16
7th	RM 36906.16	RM19790.64	RM 17115.52
8th	RM 17115.52	RM19790.64	RM 2675.12

The ROI more than 5 years are not recommended to be done. High value of ROI due to the high capital cost for LED lantern. There are cheaper price can be obtained at the market with half price of the lantern will be used that can tremendously reduce the ROI value. At the same time, the quality of the product need to be consider that cause the lamp to have longer lifetime but expensive. However, even with long payback period, energy saving program still being done for the reason of climate change.

IV. Conclusion

From the simulation of HPSV and LED street light proves that the value of illuminance is depending on the road profile and the design of the lighting. To achieve the standard requirement, the designer needs to adjust a distance and the height of the pole. With the comparison between LED and HPSV street light, it is found that the HPSV street light can be replaced by LED using 90 watt and comply the standard requirement with the ME3 standard. The 5-year warranty product by supplier or manufacturer is not reasonable because the maintenance will starts on the 8th year. Therefore, the ROI calculation should meet the 5-year payback (ROI) and without maintenance requirement. With the fast moving technology in LED industry, the lumen of the LED only need very low power consumption and the same time, the cost will be reduced.

Acknowledgment

The author would like to thank local authority, suppliers and manufacturers and Universiti Teknologi Malaysia for the facilities provided and support during completion of this research work.

REFERENCES

[1] Fusheng Li, D. C. LEDs: a Promising Energy-Saving Light Source For Road Lighting. IEEE, , 2009, 1-3.

[2] Vitor C.Bender, Fernanda. B. Mendes, Tiago Maggi, Marco A. Dalla Costa and Tiago B. Marchesan, 2013.

[3] Design Methodology For Street Lighting Luminaires Based On A Photometrical Ana Kostic, M. D. LEDS In Street And Ambient Lighting - Two Case Studies. CIE 27th Session, 2011,pg 358-365.lysis. IEEE.

[4] Illumination, I. C. CIE140: Road Lighting calculation, 2000.

[5] Tenaga Nasional Berhad. (2014). Tariff Rates. Available : http://www.tnb.com.my

[6] Onaygil, Guler O, Erkin. Cost Analyses Of LED Luminanires In Road Lighting. CIE 27th Session, 2011, Pg 723 -729.

[7] LITE-ON GROUP. (n.d.). A Municipal Guide For Converting To LED Street Lighting. Available: http://www.leotek.com

Comparison on Lower- and Higher-Adjustable Factor Filter in an Internal Model Control (IMC) Design

Noor Hafizah Abdul Rahman,
POWER Department,
Fakulti Kejuruteraan Elektrik, Universiti Teknologi Malaysia,
81310 Johor Bahru, Malaysia.
hafizah_abdulrahman@yahoo.com

Norzanah Rosmin* and Siti Maherah Hussin
POWER Department, Centre of Electrical Energy System (CEES),
Fakulti Kejuruteraan Elektrik, Universiti Teknologi Malaysia,
81310 Johor Bahru, Malaysia.
norzanah@fke.utm.my, maherah@fke.utm.my

Aede Hatib Musta'amal@Jamal
Fakulti Pendidikan, Universiti Teknologi Malaysia,
81310 Johor Bahru, Malaysia.
aede@utm.my

***Abstract*— The internal model control (IMC) structure offers more benefits than the classical design in terms of the controller design procedure, in which the IMC is more direct and natural than the classical control. The main purpose of this study is to develop an internal model control (IMC) design for a squirrel-cage induction generator (SCIG) for a wind turbine system. In this study, research has been focused on the power regulation of such system using IMC design but still using proportional-integral (PI) tuning rule. During the controller design, the effect of low and higher order filter for the PI-IMC design has been compared. From the simulation study, for the speed and torque controller, it has been observed that lower adjustable factor (λ) filter could provide easier, faster and smoother power regulation. While, for flux controller, it has been found that higher λ filter could provide easier, faster and smoother power regulation.**

Keywords*— Hiher-order filter, internal model control (IMC), first-order filter, wind turbine; Proportional-Integral (PI) controller.

I. Introduction

Renewable energy comes from the source that won't run out. Example of renewable (RE) energies is such as wind, solar, geothermal, hydroelectric and tidal. Industrial wind turbines are known as a complex RE production due to the high installation and operation and maintenance (O&M) costs [1-5]. Wind turbine industry requires high investment due to the factors of capital cost, logistics, engineering, testing, insurance, experimental work and etc [6-8]. Pitch-regulated wind turbine is the more popular than stall-regulated wind turbine. Stall-regulated is typically used in fixed-speed operation and its operation is depends on aerodynamically blade controlled, in particular during high wind speeds. For a modification from running in fixed speed into variable speed, a reliable aerodynamic blade control and rotor speed control are vital. If this is possible, such turbine has a potential to be commercialized better than pitch-regulated wind turbine due to its less in capital, operation and maintenance costs since lack of electronic actuators and parts [1-5]. Fig.1 depicts a classical design control loop for a wind turbine. Three loops of PI control are used in this model. The first loop is rotor flux control, the second loop is stator current control of the quadrature-axis and the third loop is speed loop control. In this method, the flux control is used as a single closed loop control. While, the speed loop and the torque loop are cascaded. For the cascaded system, the speed loop is considered as the outer loop, while the torque loop is considered as inner loop.

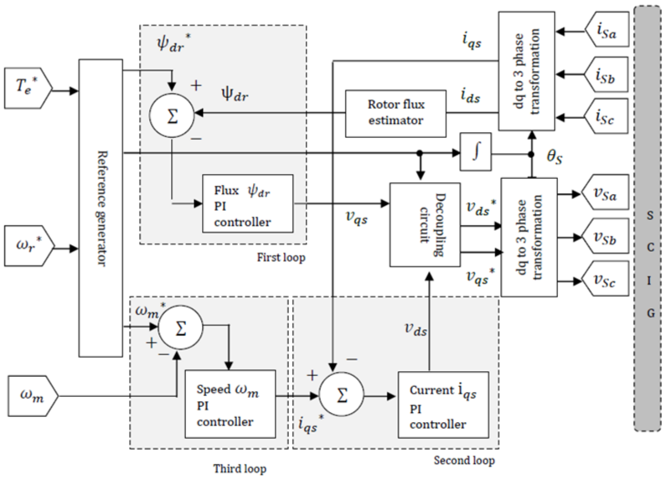

Fig.1 Standard Indirect Vector Control for a wind turbine

The design of each feedback controller must follow some form of a model for the process that is to be controlled and /or the dynamics of the exogenous signal that affecting the process. Therefore, the terms of 'model-based' is always used in simulation work. Internal model control (IMC) that has been presented by Garcia and Morari [10] is a controller that was designed based on model based controller design algorithm. IMC can be developed upon the internal model principle where we could combine the process model and the external signal dynamics. The process design of the IMC controller is quite extensive and diverse. IMC controller develops a number of forms that could be in the forms of multiple-input, multiple-output (MIMO) formulation, single-input single-output (SISO), the design process of an unstable open-loop system, continuous-time and discrete-time design process, combining with feedback-feedforward IMC design and etc. To design an IMC controller, understanding its basic requirement is important for IMC evaluation and feedback control. The impact on control performance with the existence of non-minimum phase element (delay and right half plane zero), the order of the model and control performance requirements based on its complexity are also important [11].

There are many tuning techniques could be used in IMC design. One of the popular and well-established tuning methods is using the proportional and integral (PI) method. PI control could meet the target of most of the control capacity, while proportional-integral-derivative (PID) has widely used in control industry nowadays. For the IMC controller based on PI controller, to obtain the best performance, there is an optimal filter structure that must be searched for each specific process model [12-14]. IMC-PI controller is designed as an inverse process model in series with a low pass filter. The filter then depends on the adjustable factor (λ) values. For the λ value, many approaches are available to find its optimum one. Different rule of the λ selection provides a different performance of a system.

In section II, the procedure on how to implement an IMC design in a stall-regulated wind turbine system is explained. The tuning procedure for the λ adjustment will be given in section III before demonstrate the results and conclusion in section IV and V, respectively.

II. INTERNAL MODEL CONTROL (IMC) DESIGN

Internal model control (IMC) has been presented by Garcia and Morari [10]. IMC can be developed upon the internal model principle to combine the process model and external signal dynamics. The block diagrams of the classical and IMC feedback control structure are shown in Fig. 2(a) and (b), respectively. As shown in Fig. 2, Gp represents the process, $\widetilde{qc}$ represents the process model and qc is the IMC controller. The internal model control (IMC) structure offers more benefits than the classical design in terms of the controller design procedure, in which the IMC is more direct and more natural than the classical control. The necessary of solving the root of the characteristic polynomial 1+GpGc does not implement where only a simple examination of the poles of qc (IMC controller) is required.

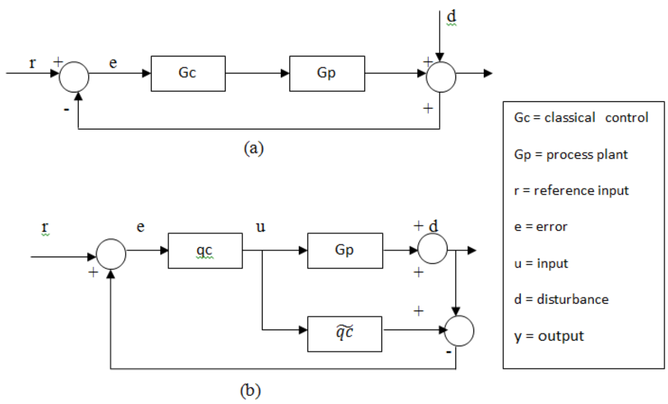

Fig. 2 (a) Classical feedback structure and (b) IMC structure [12]

For optimal design of IMC design procedure, there is two main steps must be fulfilled.

Step 1

The process plant model decomposed into two parts [15]:

$$\text{Gp(s)} = \text{Gp-(s)Gp+(s)} \qquad (1)$$

where Gp-(s) is an invertible minimum phase and Gp+(s) is the noninvertible part contains all non-minimum phase elements such as the zeros of the right half plane (RHP) and delays. Firstly, the process model Gp must be obtained. The most commonly process model Gp is modeled as first order plus time delay (FOPTD) dynamics as

$$\text{Gp(s)} = \frac{K}{\tau s+1} e^{-\theta s} \qquad (2)$$

It can also be express as

$$\text{Gp(s)} = \frac{K(-\theta s+1)}{\tau s+1} \qquad \theta,\tau>0 \qquad (3)$$

The inputs are step under the assumption, where K is the gain, τ is the time constant and θ is the time delay of the FOPTD model of the plant transfer function. Thus,

$$\text{Gp+} = -\theta s + 1 \qquad \text{Gp-} = \frac{K}{\tau s+1} \qquad (4)$$

The IMC controller is known as

$$\widetilde{qc}(\text{s}) = \text{Gp-}(s)^{-1} \qquad (5)$$

This is more causal and stable. Thus,

$$\widetilde{qc}(\text{s}) = \frac{\tau s+1}{K} \qquad (6)$$

Step 2

Augment $\widetilde{qc}$ with an IMC filter(s) is the final of the IMC controller. The IMC controller is designed by [15]

$$\text{qc(s)} = \text{Gp-}(s)^{-1}\text{f(s)} \qquad (7)$$

$$\text{f(s)} = \frac{1}{(\lambda s+1)^r} \qquad (8)$$

where the lambda parameter of λ is an adjustable parameter for the trade-off between the robustness and performance of the inner loop. When, the values of the λ increases, the closed loop time constant will increase and slow the speed of the response. The larger the values of the λ, the higher the robustness the control system. While, decrease the parameter of the λ provide a faster response but at the expense of more active control inputs. The selection of large enough of the filter order r is important to create a (semi) proper IMC controller qc. However, the filter order r is must be properly selected because the order of the filter is depends on the plant of the system.

The IMC controller qc that related to the conventional feedback controller Gc is given in equation (9).

$$\text{Gc(s)} = \frac{q(s)}{1-Gp(s)q(s)} = \frac{\tau s+1}{K}\frac{1}{(\lambda s+1)^r} \qquad (9)$$

From this conventional feedback controller, this controller is not in the form of the PI controller. Therefore, PI controller can be obtained by applying the Maclaurin series expansion formula. The approximate of the Gc that given in equation (10) as

$$Gc(s) = \frac{1}{s}[f(0) + f'(0)\,s + \frac{f''(0)}{2}s^2 + \ldots..] = Kc(1 + \frac{1}{Tis} + Tds) \quad (10)$$

where f(s) = sGc(s). Usually, PI controller or P controller can be obtained using only the first two terms or the second term, respectively. Thus, the gain for the PI controller can be written as in equation (11) where Ti = τ.

$$Kp = \frac{\tau}{K(\theta+\lambda)} \quad (11)$$

III. SELECTION OF ADJUSTABLE FACTOR (λ)

The adjustable factor, λ tuning is important in order to give non-oscillatory response and faster response time that required by a plant. Several approaches of λ tunings are available in the literature such as Tham [16], Rivera [17] and Shahrokhi and Zomorrodi (SnZ) [18]. In this study, these three tuning approaches were considered.

A. *Tham*

For the selection of adjustable parameter λ of a filter, Tham rule has been applied since 1985. Tham method offers simplicity approach where it ignores the use of parameter that need to be obtained from the estimator to calculate the self tuning control system. This method adjusts the values of the λ based on some closed loop stability of the system. Using this rule, the selected λ is set as twice as fast as the open loop respond. The adjusting of the λ is proportional to the 2r [16],

$$\lambda = 2r \quad (12)$$

B. *Rivera*

Rivera rule was developed in 1986. This method can be used to measure the robustness of the closed loop system. The performance of the signal is obtained from variation of the λ as a function shown in equation (13). By varying λ in the filter, smoother closed loop respond could be achieved [12]. Note that by using Rivera rule, the value of the parameter λ can be used as [17]

$$\frac{\lambda}{\theta} > 1.7 \quad (13)$$

C. *Shahrokhi and Zomorrodi (SnZ)*

Shahrokhi and Zomorrodi (SnZ) rule has been introduced in 2013. The adjusting of the parameter λ is done for optimization purpose and to smoothing further the signal of the closed loop system. The performance of the system depends on the values of the λ. If λ value is smaller, the system performance become larger and if the λ value is larger, closed loop system becomes more robust. The rule selection of λ based on SnZ can be implemented as shown in equation (14) [18].

$$\frac{\lambda}{\theta} > 0.2\tau \quad (14)$$

Table 1 list the summary of λ selection towards the methods that were introduced by Tham, Rivera and SnZ.

Table 1 Controller Parameters

	Tham	Rivera	SnZ
Rule	λ = 2r	λ/θ>1.7	λ/θ>0.2τ
Flux	λ = 2	λ>1.7 *10^-4	λ>1.4*10^-7
Torque	λ = 2	λ>1.06	λ>0.162
speed	λ = 2	λ>1.1	λ>0.177

IV. RESULTS AND DISCUSSION

Fig. 3, 4 and 5 show the flux, torque and speed responses when λ is adjusted in the range of rule that was proposed by Rivera and Shahrokhi & Zomorrodi (SnZ), as shown in Table 1. For Tham rule, λ is fixed to 2. From Fig. 3, 4 and 5, it can be seen that the adjusting factor of λ influences the flux, torque and speed performance of the SRVSWT system. Among these three methods, SnZ provides the worst flux performance as clearly depicted in Fig. 3. This is also shown in Table 2 where flux signal reached 60% of overshoot and significant experience of noise. Torque and speed signals also experience overshoot; however, they only reach up to 10% of overshoot. However, when the λ is increased to be 1.2 and 1.9, the flux signal becomes better, where the noise and oscillation can be totally removed. The response for torque and speed are also improved when the λ was increased. However, among these three methods, Rivera provides the smoothness and robust performance. Compared to Tham, there is actually no significant difference for the torque and speed signals when λ is set to 1.2 and 1.9.

However, in terms of settling time, Rivera shows better robustness in all signals compared to Tham. As shown in Table 2, Rivera achieves faster settling time and rise time compared to other methods. For torque response, Rivera required only 3.8s to settle down. Meanwhile, Tham and SnZ took quite sometimes to settle down. For flux and speed response, they can settle in 1s and 3.5s, respectively when Rivera is used.

Table 2. Results for different adjusting factor (Tham, Rivera and SnZ methods) in IMC-PI design.

Tuning Method	Controller	Steady state	Percentage Overshoot (%)	Settling time (s)	Rise time (s)
Tham (λ = 2r)	**Flux**	0.0216	0	6.2	5.2
	Torque	2.938	0	3.98	2.1
	Speed	0.125	0	4.8	4.58
Rivera (λ/θ>1.7)	**Flux**	0.0032	0	1	0.8
	Torque	2.848	0	3.8	1.9
	Speed	0.108	0	3.5	0.7
SnZ (λ/θ>0.2τ)	**Flux**	0.000864	60	1.42	0.02
	Torque	2.56	10	5.9	1.4
	Speed	0.08996	10	4	1

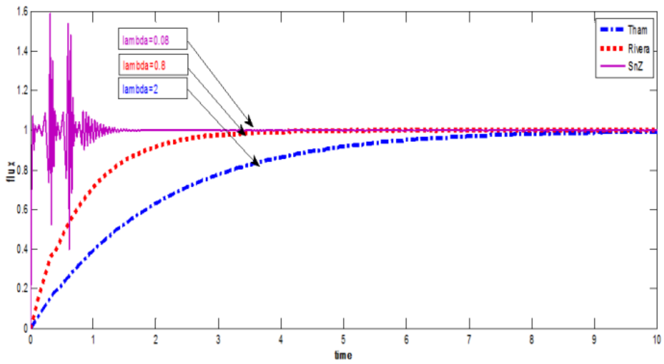

Fig. 3 Flux response

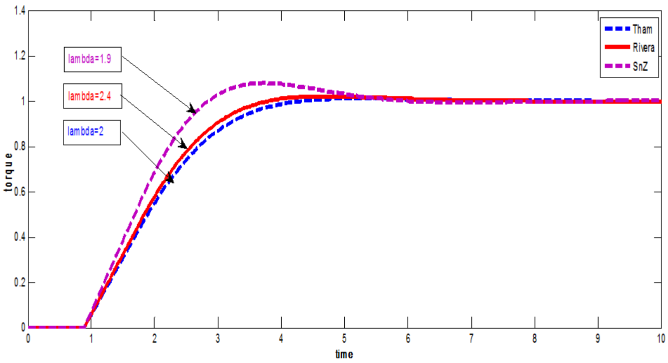

Fig. 4 Torque response

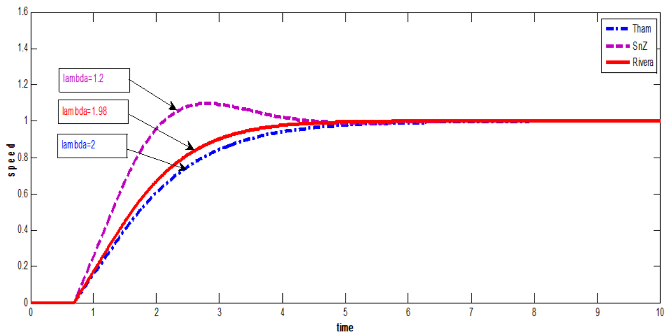

Fig. 5 Speed response

V. CONCLUSION

An IMC structure design using different adjustable factor λ of the filter for a squirrel-cage induction generator (SCIG) of a stall-regulated, variable-speed wind turbine (SRVSWT) system that coupled with a full-rated power converter of a small (25kW) has been presented in this paper. The comparison performance of the SRVSWT system is also given when Rivera, Tham and SnZ methods are employed. From the simulation study, it can be conclude that using IMC-PI design, the λ of the filter that used in proposed controller could be applied easier. Besides, for the proposed IMC-PI in SRVSWT system, it can be said that for the speed and torque controller, it has been observed that lower λ filter could provide easier, faster and smoother power regulation. While, for flux controller, it has been found that higher λ filter could provide easier, faster and smoother power regulation. Among the three methods (Rivera, Tham and SnZ), Rivera shows the best performance for all response (flux, torque and speed).

ACKNOWLEDGEMENT

Thanks goes to CEES, Power Department, FKE, UTM and the Ministry of Higher Education Malaysia for the sponsored grant 12H00 and 4F794.

REFERENCES

[1] N.Rosmin and S.J. Watson, "Power Limitation at high wind speed for a Variable Speed Fixed Pitch Wind Turbine using Close-Loop Scalar Control," Renewable Energy & Power Quality Journal (RE & PQJ) 2010; 8:1-4.
[2] S.Heier, Grid integration of wind energy conversion systems, West Sussex: John Wiley &Sons, Ltd.2006.
[3] N.Rosmin and S.J. Watson, "Power Limitation at high wind speed for a Variable Speed Fixed Pitch Wind Turbine using Close-Loop Scalar Control," in int. Conf. Renewable Energy & Power Quality Conference(ICREPQ12), Granada, Spain, 2010, pp. 1-4. March.2010.
[4] J.F. Manwell, J.G. McGowen, and A.L. Rogers, Wind energy explained: theory, design and application (West Sussex:UK, John Wiley & Sons Ltd, 2002.
[5] Rosmin N, Samsuri S, Hassan MY, Rahman HA.Power Optimization for a small-sized Stall-regulated Variable-speed Wind Turbine, IEEE International Power Engineering and Optimization Conference 2012(PEOCO2012), Melaka, Malaysia, pp 373-378, 6-7th June 2012.
[6] A. Albers, O&M Cost Modelling, Technical Losses and Associated Uncertainties, The proceedings of EWEC 2009, Pare Chanot, Marseille, France, 16-19 March 2009.
[7] Hofmann, Matthias. "A Review of Decision Support Models for Offshore Wind Farms with an Emphasis on Operation and Maintenance Strategies. "Wind Engineering 35.1(2011): 1-16.
[8] Rosmin N, Watson S.J, Mustaamal AH. Stall-regulated Variable-speed Wind turbine Simulink Model, IEEE International Power Engineering Malaysia, 2-3th June 2012. Already accepted and will be presented.
[9] Bianchi, F. D., et al.(2007). Wind Turbine Control Systems. Principles Modeling and Gain Scheduling Design (1st ed), Springer, ISBN 9871846284922, London UK
[10] Garcia, C. E. and Morari, M., "Internal Model Control - Unifying Review and Some New Results", Industrial Engineering Chemical Process Design and Development, vol. 21,1982.
[11] Bahram, S. & Hassul, M., Control System Design, Prentice-Hall, NJ, 1993.
[12] Krishnaswamy P.R., B.E Mary Chan.,and G.P, Rangaish; "Closed- Loop Tuning of Control Systems", Chem.Eng.Sci.42,2173(1987)
[13] Lee J.;"Online PID Controller Tuning For A Single Closed Test", AIChe J, 32(2), 329(1989)
[14] Lee J., W. Cho;"An Improved Technique for PID Controller Tuning from Closed Loop Tests", AIChe J,36,1891(1990)
[15] Norzanah Rosmin, "Internal Model Control (IMC) Design for a Stall-Regulated Variable-Speed Wind Turbine System," Doctoral Thesis, 2015.
[16] Tham KW, Croxford B, Young A, et al. 1999. A study of local electrostatic filtration and main prefiltration on airborne and surface dust levels in air conditioned office premises Proceedings of the 8th International Conference on Indoor Air Quality and Climate - Indoor Air '99, Vol 2, pp 12-17. Edinburgh - Indoor Air '99.
[17] Rivera, D.E., M. Morari, and S. Skogestad, "Internal Model Control 4. PID Controller Design," Ind. Eng. Chem. Process Des. Dev. 25, 252, 1986
[18] Shahrokhi, M. and A. Zomorrodi (2013). "Comparison of PID Controller Tuning Methods." Department of Chemical & Petroleum Engineering Sharif University of Technology.

Photovoltaic Cell based LLC Resonant DC-DC Converter for DC Motor

Jazlyn Andriana Bt Mahadzir
Faculty of Electrical Engineering
Universiti Teknologi Malaysia
Johor Bahru, Malaysia.
jazlyn.andriana@yahoo.com

Dr. Norjulia Binti Mohamad Nordin
Department of Power Electronics
Faculty of Electrical Engineering
Universiti Teknologi Malaysia
Johor Bahru, Malaysia.
norjulia@fke.utm.my

***Abstract*—This paper explains the implementation of the LLC resonant tank into the DC-DC converter whereby its voltage source is obtained from the photovoltaic cell in order to run a DC Motor. The LLC resonant converter is known for having high power density and produces excellent efficiency. In the other hand, photovoltaic cells are prominent in developing clean energy without inducing pollutions. The details of the design of parameters used are explained in this paper. A simulation of this design is carried out using MATLAB Simulink. An output voltage of 400v is obtained and verified through the simulation.**

***Keywords*—Photovoltaic Cells; LLC Series Parallel Resonant Converter; DC Motor**

I. INTRODUCTION

The industrial demand for the higher density power converters is growing rapidly, causing the switching frequency of the power converters to be increased in order to catch up with today's technology. If the power converters are able to cope with a greater switching frequency, the size of any electrical circuits could be dramatically reduced, thus inducing an ergonomic, compact and a more cost-effective circuit. However, the switching frequency of a power converter corresponds to the switching losses, hence it will partially degrade the system's efficiency. In other words, increasing the switching frequency would lead to an increase of the switching losses.

Switching devices absorb power when they are turned on and turned off, this is due to a transition which happens when the current and voltage are non-zero. In order to solve this problem, a resonant tank is introduced into the system. A resonant switching circuit avoids simultaneous transitions of current and voltage, whereby the switching will take place when the current and/or voltage are zero. This method would eliminate the switching losses caused by the transitions.

The applications of this resonant based power converter are substantial, anywhere ranging from controlling a DC motor to a power optimizer for the photovoltaic power systems. The application varies upon the configurations, but this paper focused more on the DC motor application. The objectives of this paper are as follows:

- To study the working mechanism of the resonant converter
- To implement an LLC resonant tank into a DC-DC converter
- To design and construct a circuit for the photovoltaic cell based DC-DC converter to run a DC motor.

II. METHODOLOGY

First of all, the parameters of the LLC Resonant Converter need to be identified in order to design the circuit. The desired input voltage and the desired output voltage have to be pre-determined before calculating the rest of the parameters. In this paper, an input voltage range of 18V to 36V is decided since that is the average voltage range of one photovoltaic panel which contains 72 solar cells. The output voltage has been set to 400V so that this circuit can also be connected to the grid if a DC motor is not connected to the load.

$$V_{in} = 18V - 36V \tag{1}$$

$$V_{in(nominal)} = 33V \tag{2}$$

$$V_{out} = 400V \tag{3}$$

After the input voltage and output voltage has been determined, the transformer ratio, n can be calculated. The transformer turn ratio are calculated as shown in (4).

$$\begin{aligned} n &= \frac{Vin(nominal)}{Vout}\, x\, M_{nominal} \\ &= \frac{33V}{400V} \times 1 \\ &= \frac{1}{12.12} \end{aligned} \tag{4}$$

The transformer ratio is 1:12.12 assuming the nominal gain equals to 1. The maximum and minimum gain is then determined as shown in (5) and (6).

$$\begin{aligned} M_{max} &= \frac{Vin(nominal)}{Vin(minimum)}\, x\, M_{nominal} \\ &= \frac{33V}{18V} \times 1 \\ &= 1.833 \end{aligned} \tag{5}$$

$$\begin{aligned} M_{min} &= \frac{Vin(nominal)}{Vin(maximum)}\, x\, M_{nominal} \\ &= \frac{33V}{36V} \times 1 \end{aligned}$$

$$= 0.91667 \qquad (6)$$

The maximum and minimum gain values would provide a suitable value of Q and k [2]. The selected values of Q and k are 0.4 and 6 respectively. These values best suit the design requirements. The equivalent AC resistance is calculated in (7).

$$R_{ac} = \frac{8}{\pi^2} \times \frac{n^2 {V_{out}}^2}{P_{out}}$$

$$= \frac{8}{\pi^2} \times \frac{\left(\frac{1}{12.12}\right)^2 400^2}{500}$$

$$= 1.763\ \Omega \qquad (7)$$

The resonant tank consists of the resonant inductor, Lr resonant capacitance, Cr and the magnetizing inductor, Lm. These parameters can be determined through the simultaneous equation method as shown in (8), (9) and (10).

$$Q = \frac{\sqrt{L_r/C_r}}{R_{ac}}$$

$$0.4 = \frac{\sqrt{L_r/C_r}}{1.763}$$

$$L_r = 0.4988\ C_r \qquad (8)$$

By inserting the resonant frequency = 100kHz,

$$f_r = \frac{1}{2\pi\sqrt{L_r C_r}}$$

$$100kHz = \frac{1}{2\pi\sqrt{L_r C_r}}$$

$$L_r = \frac{2.533 \times 10^{-12}}{C_r} \qquad (9)$$

Substituting (8) into (9) will result in the values of resonant inductor, Lr and resonant capacitance, Cr. The calculated values are $L_r = 1.124\mu H$ and $C_r = 2.25\mu F$. Substitute $L_r = 1.124\mu H$ into (10),

$$k = \frac{L_m + L_r}{L_r}$$

$$6 = \frac{L_m + 1.124\mu H}{1.124\mu H} \qquad (10)$$

Solving equation (10) would result in the value of $L_m = 5.95\mu H$. After obtaining all of the parameters, the simulation can be conducted using MATLAB Simulink.

III. Simulation Results

In this simulation, the LLC DC-DC converter is designed using a software named MATLAB/ Simulink. This circuit is simulated using the ode23tb solver(stiff/TR-BDF2) with the relative tolerance of 1e-4. First, the photovoltaic panel needed to be modeled according to the parameters in the datasheet. The solar panel used in this experiment is the Hyundai Solar HiS-S325TI monocrystalline series.

The solar panels are modeled by placing 72 of the solar cells in series. The short circuit current, Isc of each cell are set to 9.2A while the open circuit voltage, Voc are set to 0.65V. The irradiance used for the measurements are $1000W/m^2$. The quality factor has also been set to 1.5.

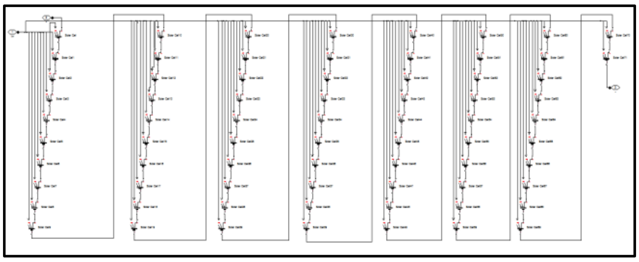

Figure 1: 72 Solar Cells Connected in Series

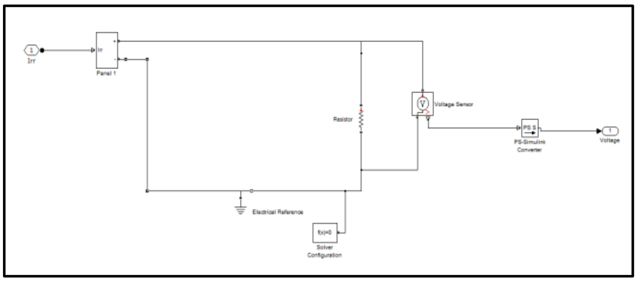

Figure 2: Solar Panel Modelling

After the modelling of photovoltaic panels has finished, it can be connected to the LLC resonant converter as a DC voltage source. The design of the circuit is as shown in Figure 3. The parameters of each components are set up according to the calculations earlier. A DC motor are also placed at the end of the circuit as a load.

The DC motor used in this simulation is the separately excited DC motor. This separately excited configuration is chosen because it is the most widely used DC motor in the market at this moment.

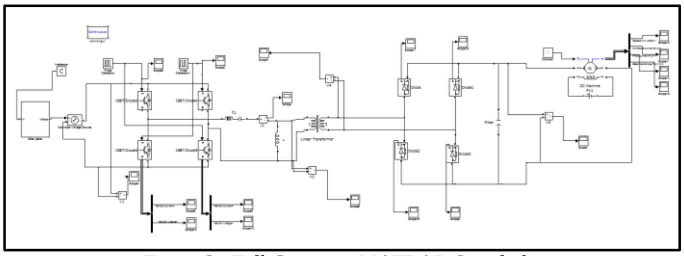

Figure 3: Full Circuit in MATLAB Simulink

The solar panel DC voltage will first go through an inverter whereby the inverter would convert the DC voltage to AC voltage. The AC voltage would then undergo the resonant tank where the resonant tank would increase the AC voltage before going through the transformer. The simulated results of the solar panel DC voltage and the AC voltage after going through the resonant tank is shown in Figure 4 and 5 respectively.

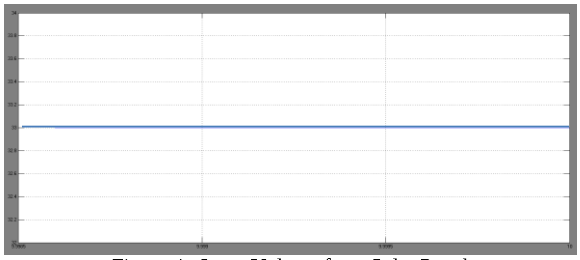

Figure 4: Input Voltage from Solar Panel

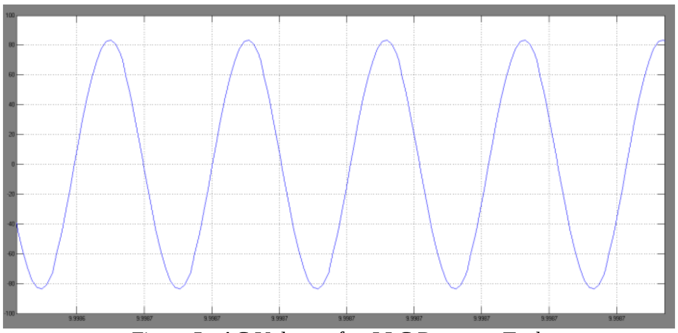

Figure 5: AC Voltage after LLC Resonant Tank

The AC voltage has increased from 33V to 83V after going through the LLC resonant tank. After that, this AC voltage will go through a step-up transformer which will then produce AC voltage of 400V. However, the simulated results differ from the calculated results. The simulated output of the transformer appears to be around 415V. This is due to the existing magnetizing inductor present in the transformer that has been neglected during the calculation procedures.

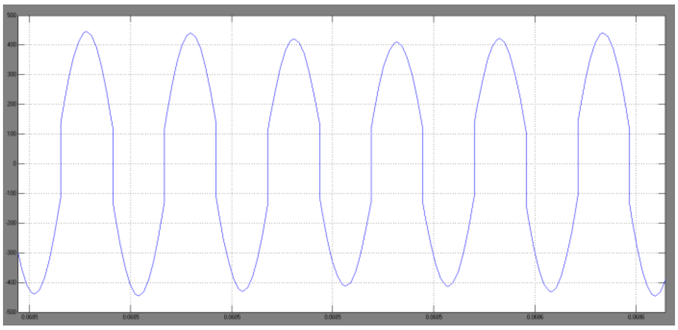

Figure 6: Transformer Output

The AC voltage output of the transformer will then go through a rectifier whereby the AC voltage would be converted to DC voltage in order to fed the DC motor. The output of the rectifier is shown in Figure 7 below. The output voltage of the rectifier is in DC form and have a ripple factor of 0.00004.

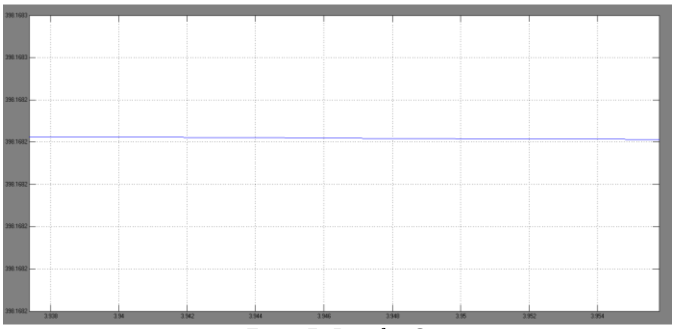

Figure 7: Rectifier Output

The output of the rectifier will then fed the DC separately excited motor. The DC motor's speed, armature current, electrical torque and field current are as shown in Figure 8, Figure 9, Figure 10 and Figure 11 below.

Figure 8 shows that the simulated motor speed is equals to 1750 rpm which is the rated speed of the motor. However, the photovoltaic cells voltage varies because the value of irradiance is uncontrollable. Therefore, a feedback system is introduced in order to ensure the output voltage stays at 400V. The feedback system is made out of a multiport switch with three different pulse generators controlled by an embedded MATLAB function block. Each of the pulse generators contains different switching frequency. The feedback system will detect the output voltage of the rectifier before it enters the DC motor. The embedded MATLAB function will then decide which pulse generator to be used for the inverter before the resonant tank.

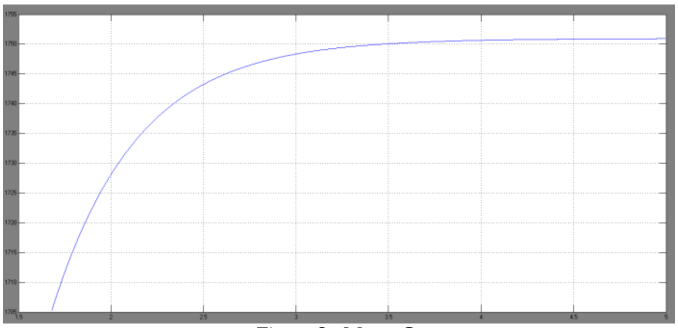

Figure 8: Motor Output

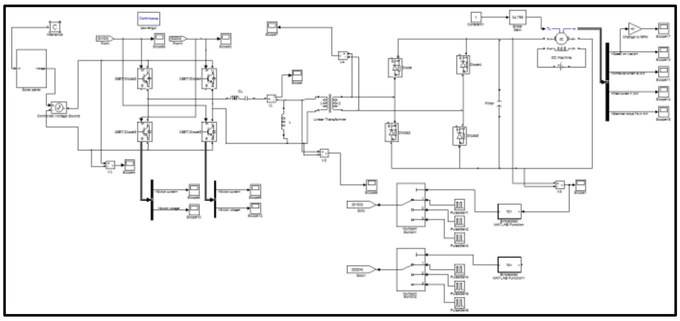

Figure 9: Complete circuit with feedback system

IV. Conclusion

The steps of designing a photovoltaic based LLC DC-DC converter with DC motor circuit has been identified. The values of all the parameters are calculated according to the design specifications. The working mechanism of the resonant converters has been studied and the LLC resonant tank has been implemented into the dc-dc converter circuit.

ACKNOWLEDGEMENT

The author would like to thank her supervisor, Dr. Norjulia Binti Mohamad Nordin who helped so much in this journal. Dr. Norjulia explained in detailed whenever the author is unsure about the components and give insights on which the author could never get from the textbook. The author of this experimental report is very grateful to Dr. Norjulia for providing encouragement and dedication to conduct this study.

References

[1] T. Jiang, J. Zhang, X. Wu, K. Sheng, and Y. Wang, "A Bidirectional LLC resonant converter with automatic forward and backward mode transition," IEEE Transactions on Power Electronics, vol. 30, no. 2, pp. 757–770, Feb. 2015.

[2] N. M. L. Tan, T. Abe, and H. Akagi, "Design and performance of a bidirectional isolated dc–dc converter for a battery energy storage

system," IEEE Trans. Power Electron., vol. 27, no. 3, pp. 1237–1248, Mar 2012.

[3] F. Z. Peng, H. Li, G.-J. Su, and J. S. Lawler, "A new ZVS bidirectional dc–dc converter for fuel cell and battery application," IEEE Trans. Power Electron., vol. 19, no. 1, pp. 54–65, Jan. 2004.

[4] G. Ma,W. Qu, G. Yu, Y. Liu, N. Liang, and W. Li, "A zero-voltage switching bidirectional dc–dc converter with state analysis and soft switching oriented design consideration," IEEE Trans. Ind. Electron., vol. 56, no. 6, pp. 2174–2184, Jun. 2009.

[5] X. Fang, H. Hu, Z. J. Shen, and I. Batarseh, "Operation mode analysis and peak gain approximation of the LLC resonant converter," IEEE Trans. Power Electron., vol. 27, no. 4, pp. 1985–1995, Apr. 2012.

[6] J.-H. Jung, H.-S. Kim, J.-H. Kim, M.-H. Ryu, and J.-W. Baek, "Design methodology of bidirectional CLLC resonant converter for high-frequency isolation of dc distribution systems," IEEE Trans.Power Electron., vol. 28, no. 4, pp. 1741–1755, Apr. 2013.M. Young, The Technical Writer's Handbook. Mill Valley, CA: University Science, 1989.

[7] K.Wang, C. Y. Lin, L. Zhu, D. Qu, F. C. Lee, and J. S. Lai, "Bi-directional dc/dc converters for fuel cell systems," in Proc. IEEE Trans. Power Electron., Oct. 1998, pp. 47–51.

APPENDIX

Embedded MATLAB Code

```
function y = fcn(u)
y=1;
if (u>=270)
  y=1;
elseif (u<270) && (u>=200)
  y=2;
elseif (u>200)
  y=3;
end
```

Educational Kit for Overvoltage Protection in House

Nur Syuhadah Binti Mohamad Isa
Faculty of Electrical Engineering
Universiti Teknologi Malaysia
Johor Bahru, Malaysia.
syuhadah.mohamadisa@gmail.com

Dr Noor Azlinda Ahmad
Institute of High Voltage and High Current
Faculty of Electrical Engineering
Universiti Teknologi Malaysia
Johor Bahru, Malaysia.
azlinda@fke.utm.my

***Abstract*— Overvoltage is the phenomena that occur when voltage in power system is suddenly increased over system rated voltage. It can damage the equipment connected to power system in just a second and also can cause fatal injury to the human. Thus, the aim of this project is to increase awareness among people about the importance of overvoltage protection by building an educational kit that can demonstrate the overvoltage protection in house. This project consist of three important parts which are voltage input generation, development of Surge Protection Devices, circuit breaker that act as second protection and load. The SPD has been tested and the result shown that SPD that used MOV as main suppress materials is suitable for lightning strike protection and not for temporary overvoltage protection.**

Keywords—Surge Protection Devices (SPD), Metal Oxide Varistor (MOV), Temporary Overvoltage (TOV), Distribution Board (DB)

I. INTRODUCTION

An overvoltage is the phenomena that occur when voltage in power system is suddenly rise over 110% of the nominal rated voltage [1]. This extremely high voltage can lead to insulation failure of the equipment connected in the system and can cause malfunction of the equipment [1]. Overvoltage can be divided into two types which are external overvoltage and internal overvoltage [2]. For external overvoltage, it is occur due to atmospheric disturbances usually due to lightning strike either indirect or direct strike [2]. Meanwhile, internal overvoltage happens due to changes in power system operational for example temporary overvoltage (TOV) [2].

Lightning is one of the natural phenomena that look artistic when the light stroke the ground, but behind the beauty it is actually discharges tens million voltage and several thousand amperes to the ground that the effect is deadly [3]. According to IEEE standard, lightning is the phenomena that caused by large separation of electrical positive charge and negative charges. When an air between the charges gets larger and breakdown to the ground, it is result to the lightning which is the current that ionizes in the air and glow brightly. Meanwhile thunder is the pressure wave that occurs due to the sudden increasing of the temperature in the air [4]. There are four ways in which lightning strike can damage houses.

1. *Strike to power or communication lines.*
2. *Strike to or near equipment outside house.*
3. *Strike to nearby object like a tree.*
4. *Direct strike to the structure at the house.*

In addition, temporary overvoltage (TOV) is one of the types of overvoltage that usually occur due to high voltage switching and fault. For lightning surge, the overvoltage will last longer for only a few micro second but the peak value is high. Besides, for temporary overvoltage, it can last a few seconds and a few cycles with much lower peak value [5].

This two type overvoltage can lead to equipment damages and fatal injury. According to Ronald [4], lightning strike can cause fatal injury to the human and damage the house appliances. Based on statistics of annual fatality of the human injury due to lightning strike, Malaysia shows the second highest rate among Asian countries behind Singapore [4]. Meanwhile, 60% to 80% internal overvoltage (TOV) occurs in Malaysia [6]. Although this overvoltage occurs within the facility, it also has the same effect as lightning strike and can lead to electric shock for human.

All the statistics of cases occur for both overvoltage types which are lightning strike and temporary overvoltage (TOV) shows the increasing value. This due to less knowledge in public about the importance of overvoltage protection for house or building and less awareness about safety, risk and treatment when overvoltage cases happen. Thus, it is important to start educate people about this.

In this paper, the fundamental of overvoltage protection according to IEEE standard will be explained. The suitable suppress materials for overvoltage protection also will be described in details. In addition, the method of constructing an educational kit for overvoltage in house will be explained and lastly the result will be recorded and analyzed.

II. LITERATURE REVIEW

A. Surge Protection Device (SPD)

Surge Protection Devices is an appliance that has been designed to protect electrical or electronic equipment from surge or transient over-voltage resulting from lightning or switching sources. These devices are often used for low voltage protection and communication network. These devices consist of two state of operation. The first state is called as non-conductive states which there are no over-voltage passes through it. These devices will become highly conductive (low value of resistance) when transient over-voltage exceeds its threshold voltage and it will limit overvoltage to a safe level for protected equipment by divert the large current to ground through earth conductor system [7].

The component that can be used as suppress materials in SPD are Metal Oxide Varistor (MOV), Gas Discharge Tube (GDT), Silicon Avalanche Diode (SAD) or combination of these components [8]. In this project, MOV is chosen as main suppress materials for SPD because it has high energy capability as the disc size is increased compared to SAD that has low energy capability [9]. Beside, MOV is easy to get and inexpensive compared to GDT and SAD. MOV also has a good mechanical connectivity which means that it can be connected parallel or series to improve the performances [9]. For AC system, most common suppress materials that been used is MOV because GDT is not suitable due to its poor reliability [9].

B. *Metal Oxide Varistor (MOV)*

These devices are made by mixing zinc oxide with small amount of other metal oxide. These mixture is then undergoes certain process which begin with granulated, and then it need to be dried and pressed it into disc shape and lastly sintered it [10]. In sintered process, the mixture will become polycrystalline ceramic which give a characteristics of voltage-dependent resistor (VDR) of varistor [11]. The zinc oxide grains has a low resistivity and it been surrounded by high resistive oxide called as granular layer and is strongly bonded together. Due to that, MOV has high energy absorption capability thus it also increase the surge current handling capability.

In addition, varistor operate equivalent to back-to-back zener diode operation which mean when small voltage is passes through the varistor, there are small leakage current that flow through the diode junctions because during this condition, varistor has high resistance. While, when surge over-voltage passes through these devices, it will become conductive and can conduct high current to flow through it to go to the earth conductor system. In simple sentences, MOV has high resistance at low voltage and low resistance at high voltages [12].

The electrical characteristic of MOV can be determined based on the I/V curve. From the I/V characteristic, when current less than 1mA is known as “high-resistance” condition, where constant leakage current passing through MOV. When overvoltage event occur, the curve shows increasing passing current through MOV. This is because, during this condition MOV become highly conductive thus it can conduct high current. The 1mA line is generally used as standard reference or also known as “dividing line” [13].

III. METHODOLOGY AND IMPLEMENTATION

A. *Overall circuit diagram*

Fig. 1 shows the overall project diagram for this project. Basically, the circuit can de divided into three important parts. The first part is input where the lightning impulse voltage and temporary overvoltage is fed to the circuit in order to test the performance of the overvoltage protection that has been design. When the input voltage is greater than rated voltage of the system, SPD will become main device to divert excess voltage to ground and the electrical appliances are safe from damages. Next is distribution (DB) and finally load. Circuit breaker in DB will act as backup protection incase SPD fail to protect the system and load is the part that will complete the system.

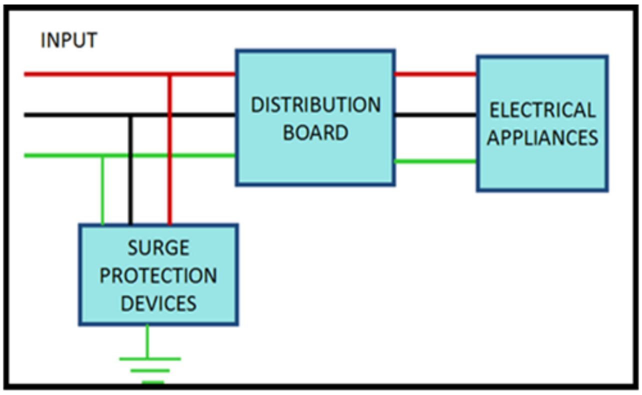

Fig. 1. Overall circuit diagram.

B. *Distribution and load circuit diagram*

Fig. 2 shows the circuit diagram for this part.

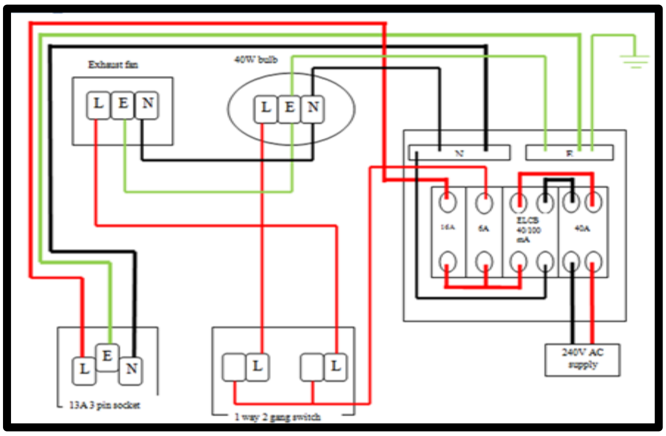

Fig. 2. DB and load circuit diagram [14].

The power distribution grid will deliver power to the houses from power plant. The power deliver from power plant (usually 240V AC) must been distribute to the electrical appliance at house. An electrical appliance is design to limit the current flowing through it for safety purposes. Too much current flow will heat up the appliances and building’s wire and worst case can lead to the fire [15].

Thus, circuit breaker is needed to be install because it act as a protection for the house. Circuit breakers will cut-off the supply whenever there is sudden current increment above the safe level in the circuit [15]. Fig. 3 shows the mechanism of circuit breaker.

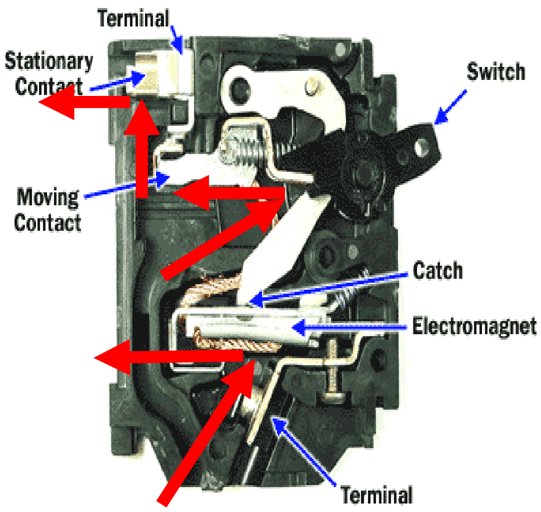

Fig. 3. The mechanism of circuit breaker [15].

When the switch is ON, under the normal condition the current will flow from terminal below that has live wire connect on it and passes through electromagnet, then flow through the moving contact, across to the stationary contact and lastly out to the upper terminal [16]. The red arrow shows the current flow through the circuit breaker.

Under protection condition, when the current flow is above the safety level, electromagnet will heat up and it will pull down a metal lever that been connected to switch and moving contact will move away from the stationary contact to break the circuit [15].

Table 1 below shows the function of each circuit breaker used.

TABLE 1: THE SPECIFICATION OF CIRCUIT BREAKER.

Type	Specification
ELCB (Earth Leakage Circuit Breaker) [14].	• Detect current leakage in wiring and appliances. • ELCB will cut off the connection of power supply when it detect leakage current exceed its preset value. • Rated current used is 40A/100mA.
MCB (Miniature Circuit Breaker) [17].	• A type of electrical protection device that is commonly used to protect cable and system against overload and overheating. • Used Single Phase Neutral (SPN) with rated current 16A (for socket) and 6A (for fan and bulb). • Used 63A MCB for incoming supply.

Next, to complete the protection system in house, it is important to have load. The electrical appliances that has been chosen in this project is the most common appliances used in typical house which are 40 Watt bulb, 240V AC mini ventilation fan (replacement of celling fan), 13A 3 pin socket and 1 way 2 gang switch. Size of the cable is depending on the appliances.

C. SPD circuit diagram

In this project, SPD Type 2 is constructed and basically it consists of two fuses, two LED indicators, metal oxide varistor as main protection and 1.5 mm2 cable wires (red, black, and green). The function of the fuse is to limit current that enter the SPD and LED acts as indicator to alert user if SPD is in good condition or need to be replaced. Fig. 4 below shows the circuit diagram of SPD.

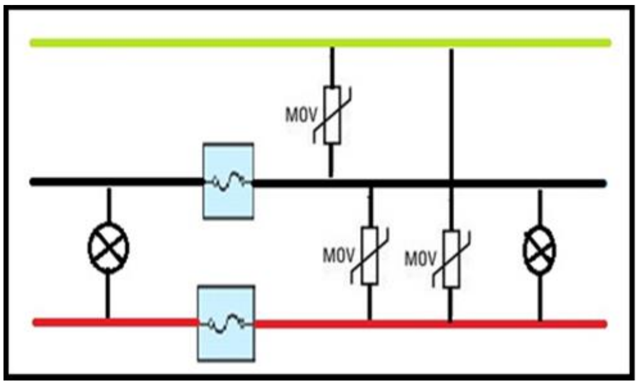

Fig. 4. The circuit of SPD [18].

D. Testing

There are three type of testing in this project. First testing is continuity testing. In this testing, 3 phase power supply with rated voltage 415 V is used. An input part on SPD is connected to the supply and output part is connected to multimeter to monitor the voltage output. The voltage input will be varied starting from 200 V to 400 V. The objective of this testing is to make sure the connection of SPD is functioning well. The result is recorded and will be analyze in section IV. Fig. 5 shows the equipment setup.

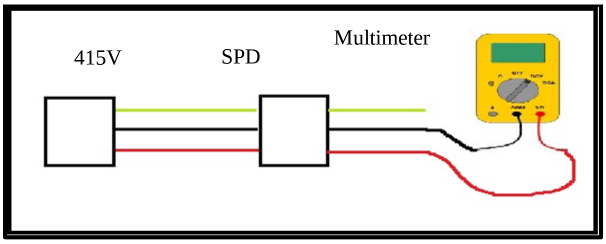

Fig. 5. Continuity testing setup.

Next is lightning impulse voltage testing. This testing is to monitor the performances of MOV during lightning. The MOV is put inside the safety cage of PSurge and oscilloscope is connected to the equipment to monitor the clamping activity of MOV. All data is recorded and will be analyze in section IV. Fig. 6 shows the PSurge equipment used.

Fig. 6. Psurge equipment.

Lastly is temporary overvoltage testing. During temporary overvoltage, the voltage in the system is suddenly rises above rated voltage of the system as had been explained in section II. Thus, this testing will simulate the same situation when overvoltage occurs. By using high voltage supply, the voltage is generated above the clamping voltage of the MOV and the performance of SPD is monitored. All data is recorded and will be analyze in section IV.

IV. Result and Anaysis

In this part, the data of the project will be described and analyzed to see if the desired output is achieved. The data presented is from three type of testing which are continuity testing, lightning impulse voltage testing and temporary overvoltage testing.

A. Hardware development of overall circuit diagram

Fig. 7 shows the development of overall circuit.

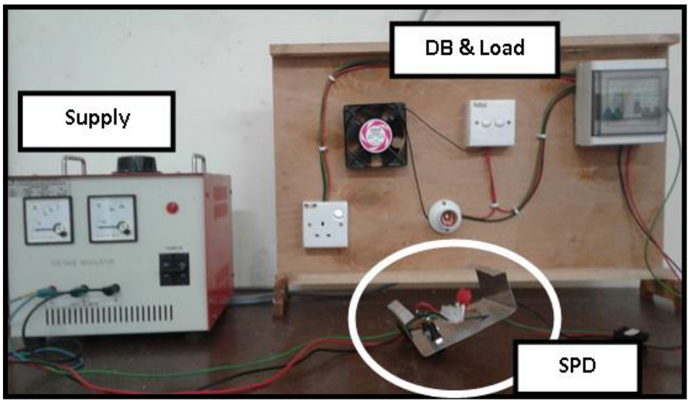

Fig. 7. Hardware development of overall circuit.

From the figure above, the three important part of this project had been constructed successfully. The first part is voltage supply. Two type of input voltage is successfully generated and had been supplied to the circuits. The second part is SPD circuit. There are some changes made during the development of SPD circuit and will be explained in details in C. Lastly is DB and load. This part also had some changes and will be explained in brief in B.

B. Hardware development of DB and load circuit

Fig. 8 shows the development of DB and load circuit.

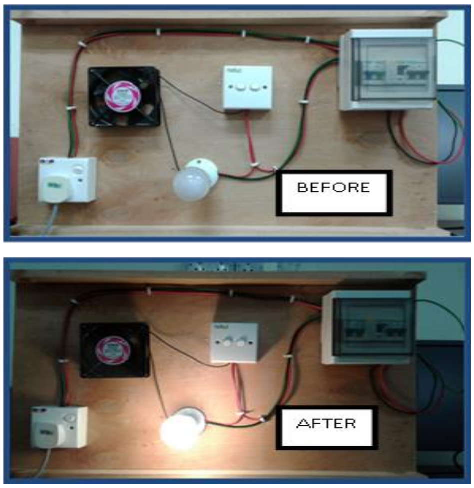

Fig. 8. Hardware development of DB and load.

From Fig. 8 shows that the circuit of DB and load is functioning well after the 240V AC supply is given. The brightness of the bulb also shows that it get enough supply to light up. Besides, the cable size that had been used for main circuit is actually 2.5 mm^2. The standard cable size for main or sub main circuit is 10 mm^2 or 16 mm^2 due to high wattage for typical houses. But, in this project, 2.5 mm^2 is enough to withstand 240V AC supply because the value of wattage required by the load is smaller.

C. Hardware development of SPD circuit

Fig. 9 shows the development of SPD circuit.

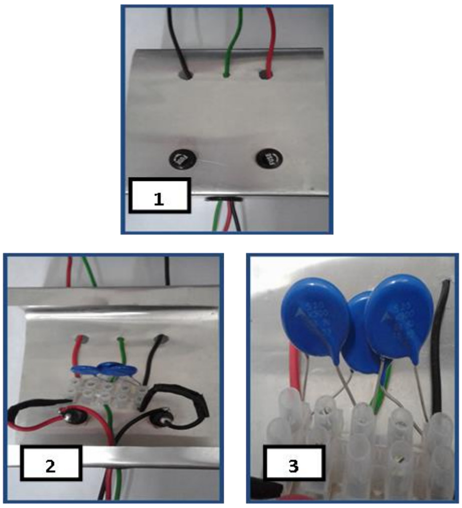

Fig. 9. Development of SPD.

The first picture shows the development of SPD circuit but without LED indicator. The other component is constructed according to the circuit that had been explained in section III. At first, during purchasing the component, the intention is to buy LED indicator with high rated voltage (1 kV and above) but due budget limitation and size of the indicator, the SPD is constructed without LED indicator.

D. Continuity testing

Table 2 shows the result from this testing.

TABLE 2: DATA FROM CONTINUITY TESTING.

INPUT VOLTAGE (V)	OUTPUT VOLTAGE (V)
200V	200V
300V	300V
400V	400V

The first input voltage that been supplied to SPD is 200 V and the multimeter shows the value of output voltage is same. Same goes to the second and third value of input voltage. From the data, it shows that the circuit of SPD is functioning well because it gives the value of output voltage

In addition, the input voltage that been supplied is actually below the clamping voltage of MOV which are 775 V. According to I/V characteristics of the MOV, when the voltage that passes through MOV is below its clamping voltage, MOV is in its normal condition which mean the resistance in the MOV is high, thus it will not clamp any voltage [12]. Thus, the value of the output voltage will be the same as the value of input voltage.

Thus, in this testing, it shows that circuit of SPD is functioning well but, MOV is not start clamping any voltage.

E. Lightning impulse voltage testing

Three value of lightning impulse voltage is injected to MOV and all the three values are above the value of MOV clamping voltage. First value is 1 kV and then it gives output voltage 0.8 kV which mean MOV clamp 200 V of the input voltage. The next value given is 3 kV and MOV clamp around 2 kV and its give output voltage 1.01 kV. The third value also has similar value with the second value which is input voltage is 5kV and output voltage is 1.21kV. Thus, from this data, the graph of percentage of voltage clamping against input voltage is constructed as shown in Fig. 10.

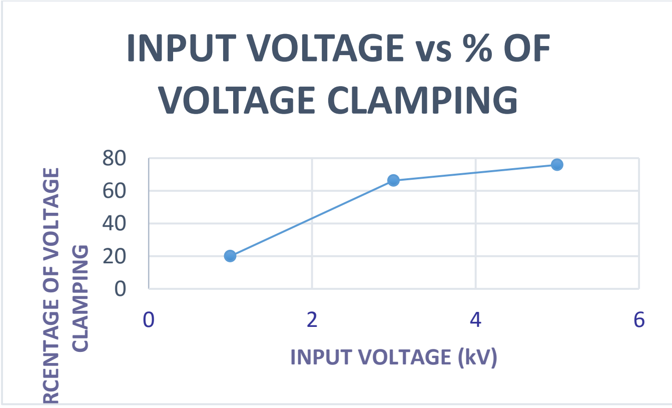

Fig. 10. Graph % of voltage clamping against input voltage.

Based on the graph above, when input voltage is 1 kV, MOV clamp the voltage about 20%. While, when 3 kV input voltage is injected, MOV clamp about 66.3% and lastly when 5 kV is given, the percentage of clamping is 75.8%. This pattern shows the higher the lightning impulse voltage given to MOV (must above its clamping voltage value), the higher the percentage of voltage clamping by MOV. Thus, it prove the theory of MOV which are when the sudden high value of lightning impulse voltage enter the MOV, the resistance value in the MOV will start to decrease and it starts to conduct excess current to the ground [12]. It will also clamp the excess voltage for the safety of the equipment. Thus, it protects the equipment from damages.

F. TOV testing

The high voltage supply is setup and the desired input voltage is the same as lightning impulse voltage testing which are 1 kV, 3 kV and 5 kV. However, when try to increase the input voltage to 1 kV, the input voltage just can go up to 480 V and the output voltage is 440 V, but the output current starts to increase as the input voltage increase.

After doing some analysis and research, this situation occurs due to the SPD circuit which is not suitable for high voltage supply equipment. The designed SPD has three inputs and three outputs while for high voltage supply consist of two inputs and one output.

Thus, the SPD performances during temporary overvoltage cannot be monitored. However, according to IEEE guide for surge protection [3], SPD that uses MOV as main suppress materials cannot withstand temporary overvoltage. This is because, the duration of TOV is too long compared to lightning impulse. MOV will dissipate more heat and can lead to thermal runaway effect that can degrade the age of MOV and worst case can lead to fire.

V. CONCLUSION

The fundamental of overvoltage protection according to IEEE standard has been studied. The most suitable protection for overvoltage especially for lightning strike and temporary overvoltage is Surge Protection Devices (SPD) that used Metal Oxide Varistor (MOV) as main suppresses materials.

Besides, the basic operational and performance of MOV also has been studied. MOV has excellent performances to suppress lightning impulse voltage or current due to its characteristics like back-to-back zener diode. However, during temporary overvoltage, the performance of MOV is easily degraded due to thermal runaway effect. Thus, MOV is not suitable to protect temporary overvoltage.

In addition, an educational kit for overvoltage protection also had been built successfully. All the part especially SPD has been constructed. It also undergoes three type of testing and passes two of the testing. Thus, the SPD circuit that had been built is functioning well to suppress the lightning impulse voltage.

ACKNOWLEDGEMENT

First of all, thanks to God because giving me the strength and patience during the journey of Final Year Project until its finish successfully.

Next, I would like to thanks my supervisor, Dr Noor Azlinda Ahmad for her guidance, opinion, encouragement, words of advice and patience throughout the whole semester of final year project.

Besides, I also would like to express my gratitude to those who help me to finish this final year project especially to technician of IVAT and Basic Machine Lab that spent much time and effort to give opinions about the project even though many obstacles occur during the project.

In addition, I would like to thanks my family for moral and financial support in order to complete this project. Last but not least, I would like to thanks to lecturers and all my friends who always give an opinion and encourage word when I face a challenge in order to completed this project with title "Educational kit for overvoltage protection in house"

REFERENCES

[1] V.S Pawar, S.M Shembaker (2013). *Transient Overvoltage in Power System.* Volume 2, Page 60. International Journal of Science, Spirituality, Business and Technology (IJSSBT).

[2] Causes and effect of overvoltage in power system, (2016). Retrieved 12 March, 2017, from My Tech Info website, http://www.mytech-info.com/2013/05/causes-and-effects-of-over-voltages-in.html

[3] Richard L. Cohen, Doug Dorr, James Funke, Chuck Jensen, S. Frank Waterer (2005). IEEE Guide for Surge Protection of Equipment connected to AC Power and Communication Circuits. *How to protect your house and its content from lightning: Surge Protection.* Page 10-31. Standard Information Network IEEE Press.

[4] Ronald L. Holle (2015). *Some aspect of global lightning impacts.*

AMS Annual Meeting, Phoenix 7 th Conf. Met. Appl. Ltg. Data, Paper 4.1.

[5] Geoff Cronshw (2011). *Surge Protection*. Page 24-26. IET Wiring metters.

[6] *Malaysia third highest in lightning strikes*. (2016, May 22). The Star Online. Retrieved12 March, 2017, from http://www.thestar.com.my/new/nation/2016/05/22/msia-third-highest-in-

[7] Schneider Electric- Electrical installation guide. *Overvoltage protection.*Schneider Electric. (2015).

[8] What is surge? What is transient voltage surge, (2013). Retrieved 15 March, 2017, from LEONICS website, http://www.leonics.com/support/article2_7j/articles2_7j_en.php

[9] Ramya Srinivasan, Vishal Sapru, Transient Voltage Surge Suppressor – Technology and Key Drivers in the industry, (2004). Retrieved 20 March, 2017, from Frost & Sullivan Market Insight website, http://www.frost.com/prod/servletmarket-insightprint.pag?ocid=26763556

[10] Overvoltage Protection, (2016). Retrieved 10 December, 2016, from Schneider Electric website, http://www2.schneiderelectric.com/resources/sites/SCHNEIDER_ELECTRIC/content/live/FAQS/277000/FA277471/en_US/Surge%20protection%20devices%20SPD.pdf

[11] SIOV metal oxide varistors, (2011). Retrieved 12 November, 2016, from EPCOS website, https://de.tdk.eu/download/185716/f161044d6457589b36ad1cacfc0815e1/siov-general.pdf

[12] Mohammad Reza Meshkatoddini (2011). Advances in Ceramics – 330 Electric and Magnetic Ceramics, Bioceramics, Ceramics and Environment. *Metal Oxide ZnO-Based Varistor Ceramics*. Page 1-9. Intechopen.com.

[13] Mohd Muridza Yaacob (2005). *The behavior and performances of MOV under the application of multiple lighting impulses.* (PHD Thesis). PRZS, UTM. (TH9057 M034 2005).

[14] Electrical Installation Wiring Pictures, Retrieved 14 April, 2017, form website,http://electricalinstallationwiringpicture.blogspot.my/2010/02/1-phase-elcb-connection-pictures.html

[15] IEEE Standard for High-Voltage testing Techniques, USA, 2013.

[16] Mohamed Samir, "Generation of High A.C Voltages," Available: http://eedofdit.weebly.com/uploads/7/3/2/6/7326910/notes_tee024_hv_unit2_cascaded_transformer_2011-12.pdf, [Accessed May 12, 2017]

[17] What is differences between MCB, MCCB, ELCB and RCCB, Retrieved 13 May, 2017, from Electrical engineering website, http://electrical-engineering-portal.com/what-is-the-difference-between-mcb-mccb-elcb-and-rccb

[18] *Lightning Surge Protection Modules Design and Installation Guide*. Page 3-17. Littlefuse Inc, (2016).

Speed Controller of DC Motor (Experimental Kits)

Mohamad Faiez bin Rohani
Faculty of Electrical Engineering
Universiti Teknologi Malaysia
Johor Bahru, Malaysia.
faiezutm@gmail.com

PM DR. Nik Rumzi
Department of Electronic
Faculty of Electrical Engineering
Universiti Teknologi Malaysia
Johor Bahru, Malaysia.
Supervisor's email address

***Abstract*— DC motor system is rapidly used in this era nowadays. Many company or industry use DC motor to handle the machine and system to create their product and also to help human works become easier. The important thing the user should know the fundamental of DC motor especially student to understand how DC motor works. In this paper, experimental kit for student learning is done to make student more understand about the principle of DC motor. The speed of DC motor can be control by using microcontroller. The gate driver is driven by a high frequency PWM signal. Controlling the PWM duty cycle is equivalent to controlling the motor terminal voltage and adjust directly the motor speed. Experimental result have been obtain that kit can be use by student for learning purposes about the DC motor.**

Keywords—dc motor, microcontroller, pwm, speed control,

I. INTRODUCTION

Permanent magnet (PM) direct current (DC) motor are important part of industry today. DC motor converts direct current electrical energy into mechanical energy and the direction of current flows in one direction. DC motor widely used in majority of household applications and electronic devices such as CD player, computer, remote control and others. The most important parts of DC motor are rotor, stator, armature and commutators with brushes. DC motor is the simplest types of motor used in electrical appliances compare to AC motor.

In this work, the good understanding of principle of DC motor is needed to implement the knowledge to develop hardware which is experimental kits for students to make students understand about the principle of DC motor in their daily life. This experimental kits include all the important component and their own characteristics. The main function for this experimental kits are for learning purposes for students. It is because DC motor are one of the motor types rapidly gaining popularity in world.

A microcontroller is needed to control the speed of the DC motor. In this research, Arduino Microcontroller is chosen to be install in experimental kits. Arduino Microcontroller is the most suitable microcontroller for learning purposes in university. This microcontroller commonly used by students in their studying. This will make a better understanding to understand the DC motor principle.

II. LITERATURE REVIEW

A. Dc motor

There are several basic component to construct DC motor, there are stator, rotor and auxiliary component, Fig.1 [1]. Stator is stationary part of a rotary system in DC motor that have field windings and fixed magnetic field. Rotor is represent a moving component of electromagnetic system that cause mechanical rotation, the rotation is interaction between windings and magnetic fields which produce a torque around the rotor. Rotor and stator are separated by small air gap and size of air gap is depend on motor power [2]. Then, auxiliary component similar to brush or commutator and the main function is to relay the current from the main to the armature windings [1].

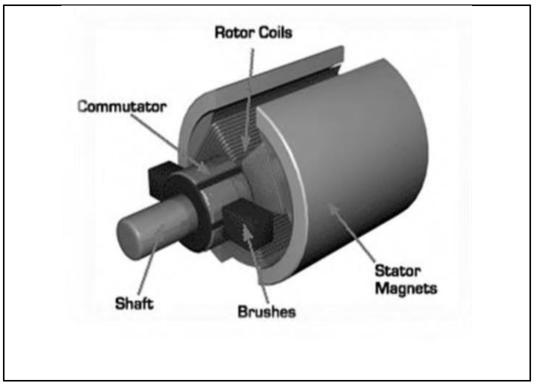

Fig. 1: Construction of DC motor

Dc motor is a machine that convert electrical power to mechanical energy through the interaction of two magnetic field. One field is produced by an electrical current flowing in the motor windings and another field is produced by a permanent magnet assembly. Both of the field result in a torque which tends to rotate the rotor. When the rotor start to turn, a continuous torque output is produced because current in the windings is commutated. The switching current between coils within the motor cause the movement of the magnetic field. At this action, commutation occur. The operation and direction of the force, magnetic field and current is given by Fleming's left hand rule, Fig. 2 [5].

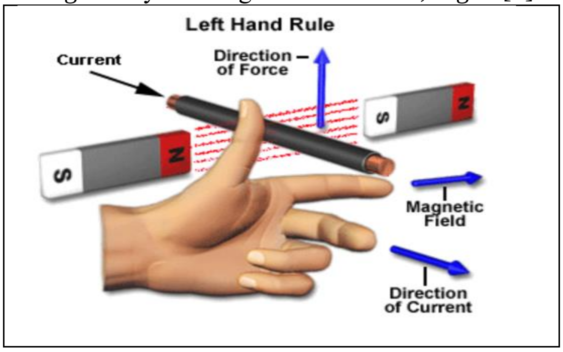

Fig. 2: Fleming's left hand rule

B. Microcontroller

Microcontroller widely used in industrial and control design from year to year over the past decade [2]. Many appliances become smaller compare to previous design and easy to use because improvement of the hardware and programming. In this current technology, microcontroller is made with possible to store hundreds of thousands of transistors inside it [2].

For this research, Arduino Uno, Fig. 3 is used to develop the experimental kits. Arduino software is available for Windows, MacOX and Linux. This microcontroller was chosen because the programming is simple and students enable to understand the system [6]. Furthermore the cost of Arduino microcontroller is lower compare other and easy to find it. Arduino is open source, it is because the hardware is in reasonable priced and the software is free [7].

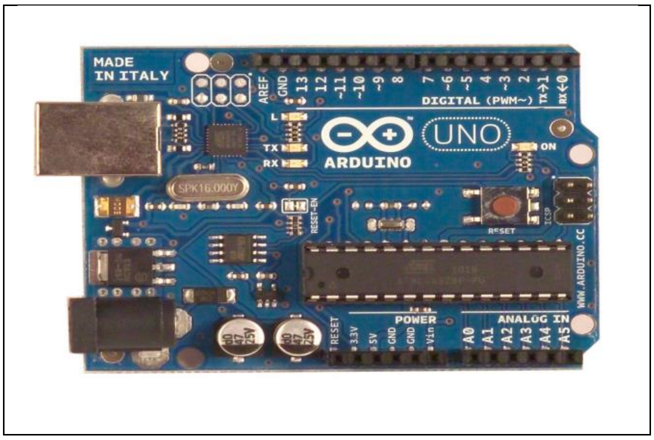

Fig. 3: Arduino Uno

C. Pulse Width Modulation (PWM)

Pulse Width Modulation (PWM) is a signal that generated from microcontroller, and the duty cycle of PWM is control by microcontroller depend on it speed. The PWM signal is used to motor driver to vary the voltage supply to motor to maintain at constant speed [3]. Dead time is used in PWM to avoid short from high and low power device. Dead time function in output voltage loss and current distortion and the impact is relevant as switching frequency increase and voltage become low [4].

The main advantage of PWM is that power loss in the switching devices is very low. When a switch is off there is practically no current, and when it is on and power is being transferred to the load, there is almost no voltage drop across the switch. Power loss, being the product of voltage and current, is thus in both cases close to zero. PWM also works well with digital controls, which, because of their on or off nature, can easily set the needed duty cycle.

The term duty cycle describes the proportion of 'on' time to the regular interval or 'period' of time, a low duty cycle corresponds to low power, because the power is off for most of the time. Duty cycle is expressed in percent, 100% being fully on.

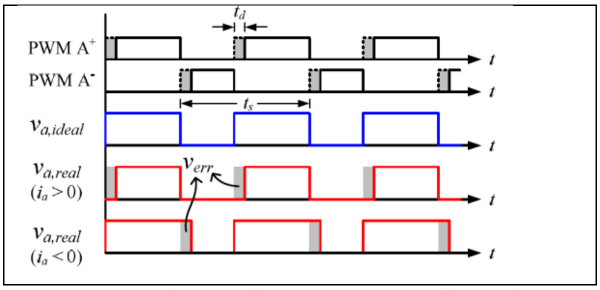

Fig. 4: Pulse Width Modulation with dead time

D. H-bridge

An H-bridge is an electronic circuit that enables voltage applied across a load in either direction. The allow DC motor to operate in forwards and backwards. An H-bridge is built with four switches with specific characteristics. According to Fig. 5 below, if S1 and S4 switches is closing and S3 and S4 is open, the positive voltage will produce and motor will operate in forward. Motor will operate backward if S1 and S4 is open, while S2 and S3 is closing, reverse voltage will produce [8].

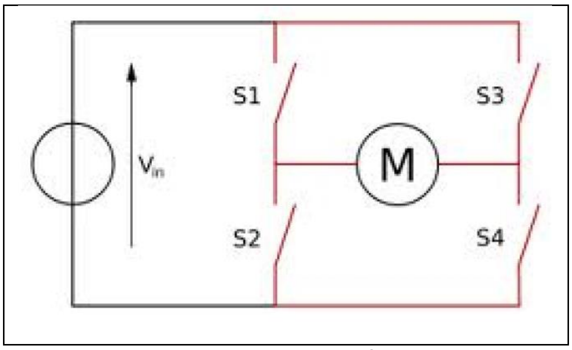

Fig. 5: H-bridge Configuration

III. METHODOLOGY

In this stage, method or flow of the project will be discuss briefly. Method to develop the experimental kits for student also will be explain in this stage.

Before connection of circuit is made, the fundamental of each device should be understand first, it is because each of the device are very complicated and to understand the fundamental is the most important thing how it's working. There are many device should be explore, there are Arduino, dead time circuit, gate driver, power electronic converter and dc motor.

Oscilloscope needs to calibrate first before experiment is doing. Oscilloscope function to show the waveform of PWM from the device that needs to calibrate. Multimeter is used to measure the output voltage, to check whether the voltage increase or not in gate driver.

Microcontroller should be program and study because pulse is generated from Arduino microcontroller. After programming is done, program is compiling and uploading to Arduino board before connection of circuit is doing. Potentiometer is used as adjustable of speed. Potentiometer is the input for Arduino and function to control the duty cycle of the pulse width modulation. Input voltage for this project is 5V supply to Arduino gate driver and power electronic converter before motor can operate.

IV. RESULT AND DISCUSSION

In this section, result and discussion about the project will be explain briefly according to the experiment result. After connection circuit to the device is done in laboratory, there are some result that obtain from the experiment. Fig. 6 shows the dead time circuit. Dead time circuit or blinking time circuit function is to avoid short of the motor. This circuit need two integrated circuit (IC), there are IC7414, Schmitt trigger gate and IC7404, not gate. The input of blinking time circuit is the PWM from Arduino. The output from this circuit is shown in Fig. 8. Oscilloscope is used in this experiment to see the waveform for each output. Before that, oscilloscope should be calibrate first to know whether the oscilloscope in good condition or not.

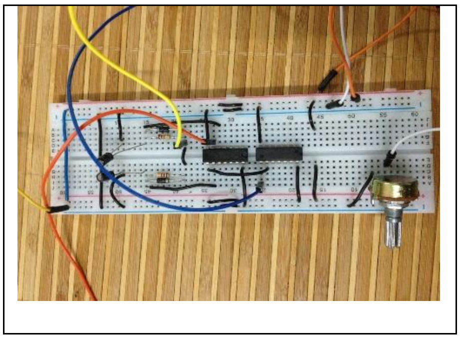

Fig. 6: Blinking Time Circuit

Fig. 7 shows the duty cycle that controlled by potentiometer. Potentiometer as the input for Arduino to control duty cycle of the PWM. When potentiometer is rotated the duty cycle will change synchronous with the pulse from the Arduino. The changes of duty cycle can be measured by using oscilloscope only. Positive terminal of oscilloscope is connected to pin 6 of Arduino, and negative terminal is connected at ground of
breadboard. Only pin 3, 5, 6, 9, 10 and 11 of Arduino board can generate PWM.

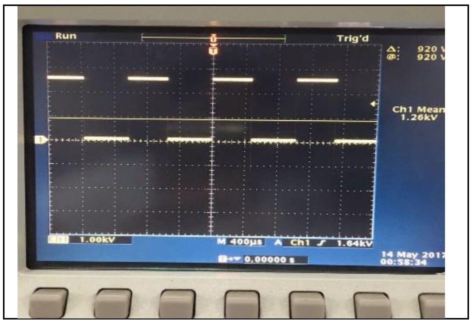

Fig. 7: Duty Cycle from Potentiometer and Arduino

From Fig. 8, waveform of PWM from blinking time circuit, this pulse is used in gate driver to increase the output voltage of gate driver before connected to power electronic converter. Signal PWM with 5V will increase to 15V in the gate driver device. In power electronic converter, the switch will on and off with different time, it is because the delay from blinking time circuit. The PWM from gate drive will on and off the switch before the motor start to operate.

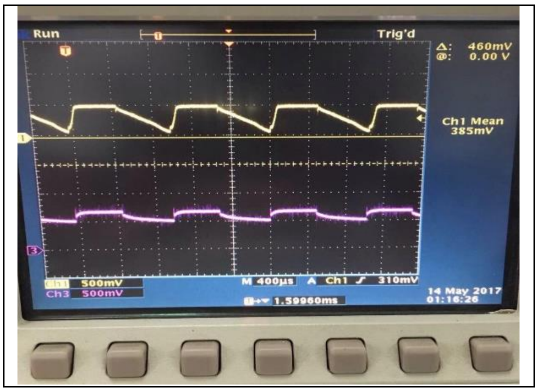

Fig. 8: Pulse from Blinking Time Circuit

V. CONCLUSION

In conclusion, from the result obtained in above, DC motor only will operate with pulse width modulation (PWM), without PWM motor will not operate. H-bridge of dc motor allow motor to operate forward and backward operation. Based on the goal of the project, since the experimental kits is not fully complete yet, so student enable to use it for study. By using this experimental kits, student able to study and understand the fundamental and working principle of dc motor.

REFERENCES

[1] Salih, M. F., & Danapalasingam, K. A. (2014). Real time model validation and control of DC motor using matlab and USB (Unpublished master's thesis).

[2] Aziz, A. A. (2006). Speed control of induction motor using microcontroller (Unpublished master's thesis). Project Paper (Sarjana Muda Kejuruteraan (Mekanikal)) - Universiti Teknologi Malaysia.

[3] Mr S.M.Rangdal, Prof. G.P.Jain. Speed control of DC motor using microcontroller. 2014 International Journal of Advanced Technology in Engineering and Science. Vol no. 2.

[4] Lin, Y., & Lai, Y. (2009). Dead-time elimination method and current polarity detection circuit for three-phase PWM-controlled inverter. 2009 IEEE Energy Conversion Congress and Exposition. doi:10.1109/ecce.2009.5316468.

[5] (n.d.). Retrieved May 14, 2017, from http://www.studyelectrical.com/.

[6] Thomas E. Murphy, Introduction to The Arduino Microcontroller, June 17 – 29, 2012.

[7] Arduino Microcontroller Guide,W. Durfee, Arduino Microcontroller Guide, University of Minnesota, Ver. Oct-2011.

[8] Vignesh Subramaniam, Matthew Kaye, and Parth Chopra. H-bridge motor control. 2012 University of Pennsylvania.

[9] Agung, I. R., Huda, S., & Wijaya, I. A. (2014). Speed control for DC motor with pulse width modulation (PWM) method using infrared remote control based on ATmega16 microcontroller. 2014 International Conference on Smart Green Technology in Electrical and Information Systems (ICSGTEIS). doi:10.1109/icsgteis.2014.7038740.

[10] Ali, Y., Noor, S., Bashi, S., & Hassan, M. (n.d.). Microcontroller performance for DC motor speed control system. *Proceedings. National Power Engineering Conference, 2003. PECon 2003.* doi:10.1109/pecon.2003.1437427

[11] Lin, Y., & Lai, Y. (2009). Dead-Time Elimination of PWM-Controlled Inverter/Converter Without Separate Power Sources for Current Polarity Detection Circuit. IEEE Transactions on Industrial Electronics, 56(6), 2121-2127. doi:10.1109/tie.2009.2014305

[12] Norazuin binti Md Ayob (2013). Modelling and Control of DC Motor (Unpublished master's thesis).

[13] Valery Vodovozov and Raik jansikene. Power electronic converters.

Wavelet Analysis of the Electric Field Pulse Emitted by Return Stroke at 3-30 MHz, 60 MHz and 2.4 GHz

Nuraishah Binti A. Ghani
Faculty of Electrical Engineering
Universiti Teknologi Malaysia
81310 UTM Johor Bahru,
Johor Darul Takzim, Malaysia
nuraishah.ghani@yahoo.com.my

Mona Riza Binti Mohd Esa
Faculty of Electrical Engineering
Power Electrical Engineering Department
81310 UTM Johor Bahru,
Johor Darul Takzim, Malaysia
monariza@fke.utm.my

***Abstract*—Wavelet analysis known as a powerful tool where it's able to present signals in the time-frequency domain. In this study, the electric field measurement at 3-30 MHz, 60 MHz and 2.4 GHz emitted by a return stroke is done and analysed using wavelet transformation. Electric field measurement is conducted in IVAT Lab, UTM, using three receiver antennas with the range of frequencies 3-30 MHz, 60 MHz and 2.4 GHz. From the analysis, it is found that the energy of the electric field emitted by the return stroke that captured by 60 MHz receiver antenna is higher compared to 2.4 GHz and 3-30 MHz receiver antenna. While the bandwidth or localized frequencies for the spectral and spread regions of the energy of the electric field captured by these three antennas are found to be almost similar.**

I. Introduction

Lightning is known as one of the deadliest natural occurrences where it creates temperatures hotter than the sun's surface and radiate shock waves in all directions. Lightning occurs when the electric potential between two regions of space and the resistance of medium between these two regions are sufficiently high [1]. In some case, lightning can cause danger where many injuries and damage have been reported due to lightning. The danger caused by lightning can be classified into three categories which are direct strike, power surge and radiation [2].

The direct strike related to human and property that typically happen when human or building is directly struck by lightning. For the second cause of danger which is power surge happened when lightning strikes the transmission line tower. High current carries by the lightning cause damage to equipment connected to the transmission line. The third causes which are radiation is related to electromagnetic interference (EMI). Interference is electromagnetic in nature; it can result in the magnetic and radio frequency disruption [3]. As lightning is one of the sources of interference, a study is conducted to analyse the behaviour of lightning, especially in the higher frequencies region.

Wavelet analysis is a powerful method in have been widely used in the lightning analysis [4]. As it has been used in the analysis of initial half and the overshoot of bipolar pulse, negative return stroke, positive return stroke, first return stroke and subsequent return stroke. This is because it is able to present signals in the form of the time-frequency domain. From wavelet analysis method, all the frequency components that present at a time can be exactly known [5].

In this paper, analysis of electric field emitted by a return stroke at frequencies 3-30 MHz, 60 MHz and 2.4 GHz is conducted to identify the high frequency components that occur before the formation of return stroke by using wavelet analysis method.

II. Literature Review

A. Wavelet Analysis Theory

Wavelet is an analysis where the signal is in time-frequency representation. In other word, the frequency component present at a certain moment in time can be exactly known [5]. There are two types of wavelet, which are discontinuous and continuous wavelet. Discontinuous wavelet usually used for decomposing and filtering a signal. Continuous wavelet usually used for power spectrum analysis [4].

Continuous wavelet is transformed into the form of translation and dilation of a fixed function called mother wavelet [6]. It can be described in the equation below:

$$\gamma(s,\tau) = \int f(t) \;\; \Psi^{*}_{s,\tau}(t)\, dt \qquad (1)$$

From equation (1), * demotes complex conjugation. Ψ(s,τ)* (t) is called as wavelet. Wavelet are generated from a single basic wavelet called as the mother wavelet, ψ(t) by using the scaling and translation [5].

$$\Psi^{*}_{s,\tau}(t) = \frac{1}{\sqrt{s}}\, \Psi\left(\frac{t-\tau}{s}\right) \qquad (2)$$

In choosing mother wavelet, there are two parameters that need to be considered which are width and shape. In order to obtain good time resolution, narrow wavelet function is needed. However, this will result in poor frequency resolution. While shape, it should reflect the type of features presented in time series [4].

B. Paper I

Wavelet characteristics of the first electric field pulse of negative cloud-to-ground flash, positive cloud-to-ground flash, cloud flash and isolated breakdown flash were investigated. The measurement was done by using electric field broadband antenna system that consist of three parts which are antenna, buffer and recording unit. The data obtained were categorized based on their characteristic of the wavelet power spectrum either multiple-peaks multiple-spreads, single-peaks multiple-spreads, multiple-peaks single-spread and single-peaks single-spreads. Then the spectral region and spread region were identified and the result was represented in box plot. From this paper, one of their findings is they found that both single peak and multiple peak pulses of negative cloud-to-ground and cloud flashes radiated energy at higher frequencies and gain larger bandwidth [7].

C. Paper II

In order to get the comparative idea of frequency content and their relative energy, preliminary breakdown pulses, stepped leader, first return stroke and subsequent return stroke were used. For the measurement, parallel plate antenna that connected to buffer were used to sense the lightning activities. In choosing wavelet for wavelet analysis, the Derivative of Gaussian (DOG) were chosen as it is stated that DOG is not critical for the computation of the wavelet power spectrum. They also stated that, time space for DOG wavelet is narrower. This comes to an agreement where, in choosing wavelet, narrow wavelet is preferable. The spread region and spectral region for every wavelet power spectrum were analysed. It is found that for return stroke, at a lower frequency return stroke are the strongest source of energy. It also found that subsequent return stroke also radiate predominantly at lower frequency [8].

III. METHODOLOGY

A. Experimentation

In-lab electric field measurement was conducted to measure electric fields emitted by a return stroke generated by an impulse generator. The measurement was conducted in the High Voltage Laboratory, Institute Of High Voltage and High Current (IVAT), Universiti Teknologi Malaysia (UTM). This measurement consists of two parts. The first part is the impulse generating unit where the impulse generator is used. The second part is the sensing unit where several high frequency electric field antennas were deployed.

1) Impulse Generating Unit

For this measurement, the impulse that needs to be generated is 80kV. The set up to generate the impulse is shown in Figure 1.

2) Sensing Unit

To measure electric field emitted by the return stroke generated by impulse generator, high frequency antenna is used. This system consists of three subparts which are antenna, filter and recording system is shown in Figure 2.

The antenna is made of two parallel rectangular plates of copper with effective height 0.3m. The area of the plate is 8.5×12.8 cm. The upper plate is connected to filter while the bottom plate is connected to ground. As there are three antennas were used in this project, connected to the three different filters. Recording system that used in this measurement is LeCroy WaveJet 354A with sampling rate 2 Giga sample per second. From filter to the recording system, it is connected via RG58 coaxial cable.

There are three different filters have been used in this measurement for three different antennas. But basically, the filter consists of a Low Noise Amplifier (LNA) and a Band Pass Filter (BPF). Three BPF of three different frequencies, which are 3-30MHz, 60MHz and 2.4GHz is used.

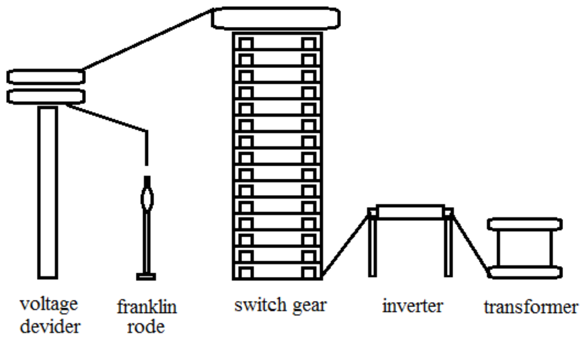

Figure 1. Impulse generator arrangement

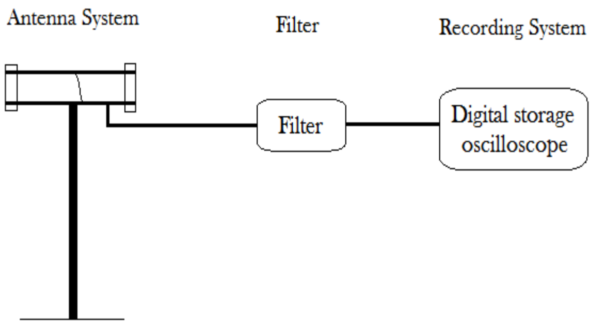

Figure 2. High frequency antenna system

B. Analysis

The waveforms obtained from the measurement were filtered and then were waveletly transformed. The contour and image of the wavelet power spectrum were analysed to identify the spectral region, spread region and the peak of the power spectrum.

Spectral region is defined as the region where predominant energy radiate. It can be identified by the area bounded by the light-blue color contour, or it is the area that has color bar value of 0.3 and above. Spread region is part of spectral region. This is the region that having the most intense energy radiation. It can be identified by the area bounded by the dark-red color contour or the area with color code 0.9 and above [7]. Power spectrum peak is the maximum value of the power spectrum radiates by each waveform.

The analysis is focusing on the bandwidth and time spread of both spectral and spread regions described above. The bandwidth is calculated by taking the maximum and minimum frequencies bound of both regions. Whereas, the time spread is the starting and ending time of both regions.

IV. Result and Discussion

From the measurement, a total of sixteen waveforms was captured and repeat for 4 times. There are four categories of data, first is impulse waveform, second is waveform obtained from the 3-30 MHz receiver antenna, third is the waveform obtained from the 60 MHz receiver antenna and the fourth category is the waveform obtained from 2.4 GHz receiver antenna. The example of waveforms for every category is shown in Figures 3 to 6.

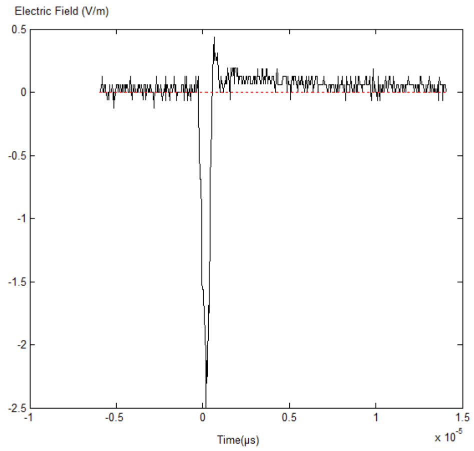

Figure 3. Impulse waveform

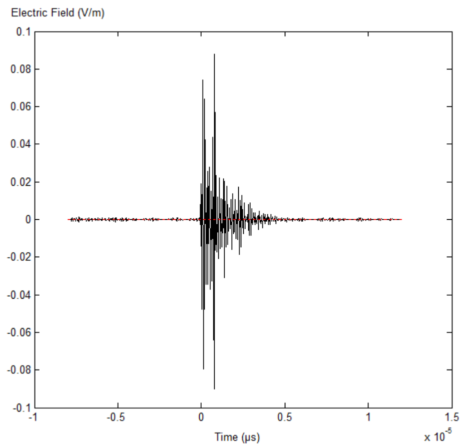

Figure 4. Waveform obtained from the 3-30 MHz receiver antenna

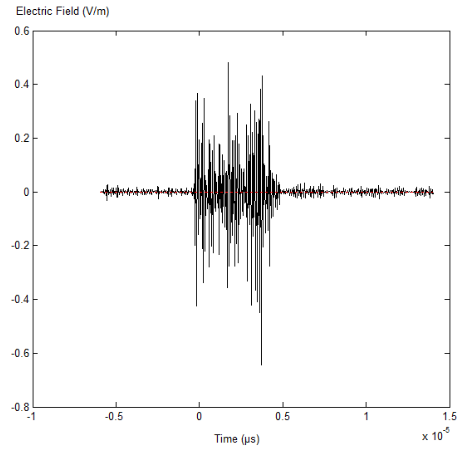

Figure 5. Waveform obtained from the 60 MHz receiver antenna

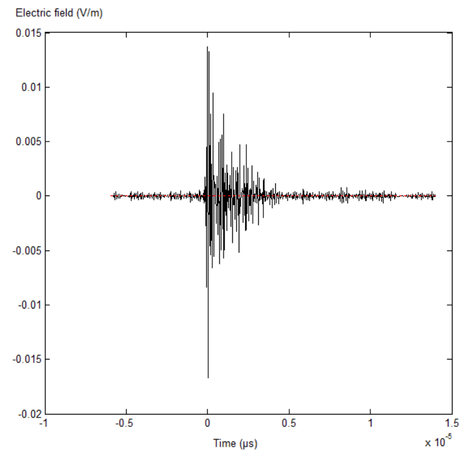

Figure 6. Waveform obtained from the 2.4 GHz receiver antenna

The example of the wavelet power spectrum for every category is shown in Fig. 7, Fig.8, Fig.9 and Fig.10.

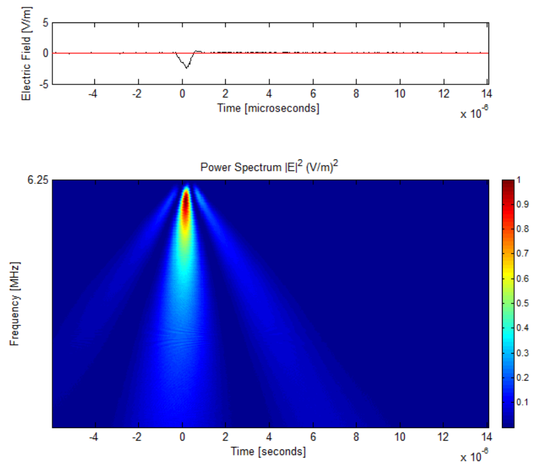

Figure 7. Wavelet power spectrum of impulse

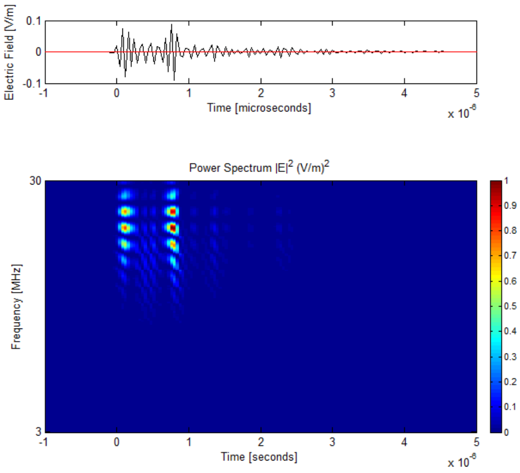

Figure 8. Wavelet power spectrum of 3-30 MHz

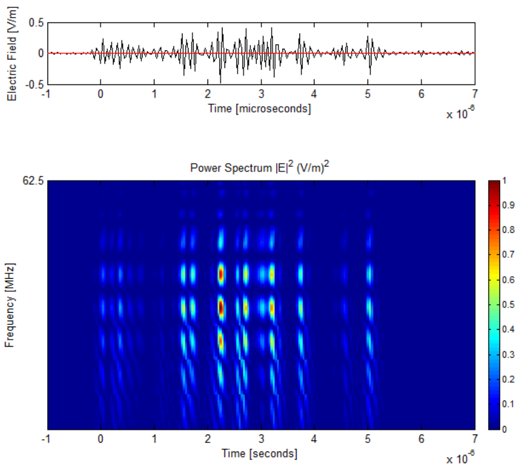

Figure 9. Wavelet power spectrum of 60 MHz

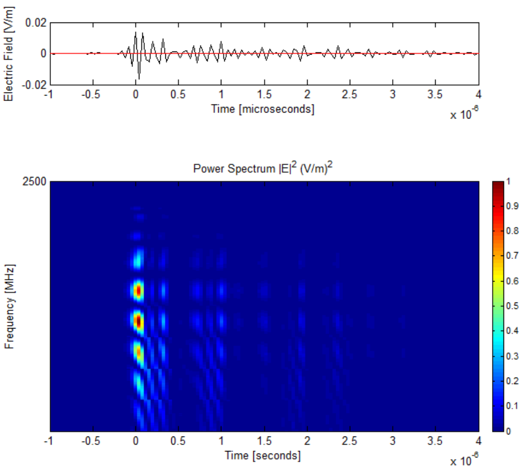

Figure 10. Wavelet power spectrum of 2.4 GHz

The value of the peak power spectrum, the frequency and time boundaries of spectral and spread regions for every wavelet power spectrum are then identified. Based on the data collected, the peak power and the frequency boundaries will be discussed in details as follows:

A. Peak power

The average peak power for every category is calculated and is presented using a box plot as shown in Fig.11.

TABLE 1. THE AVERAGE PEAK POWER SPECTRUM

	Peak power (V^2/m^2)		
	Maximum	***Minimum***	***Average***
3-30MHz	0.017	0.003	0.006
60MHz	1.582	1.502	1.539
2.4GHz	0.859	0.383	0.548

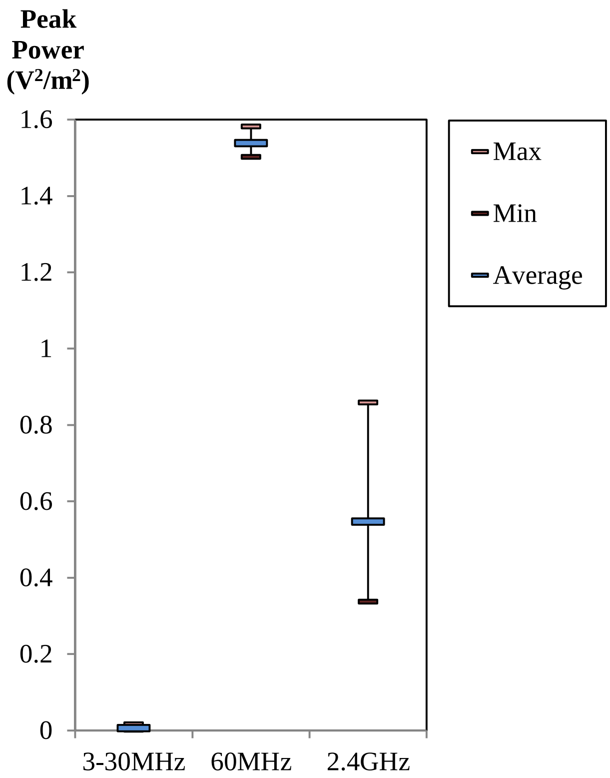

Figure 11. Distribution of power peak for 3-30 MHz, 60 MHz and 2.4 GHz

Figure 11 shows that a significant difference between the value of average power peak for three different receiver antennas. The 3-30 MHz gains the lowest average value of peak power while for 60 MHz shows the highest average of peak power. Interestingly, both have a small maximum to the minimum range of power peak. Compared to 2.4 GHz, the average of the peak power is in between 3-30 MHz and 60 MHz, which is 1.539 $(V/m)^2$. In contrast, the range of power peak for 2.4 GHz antenna is wider when compared to 3-30 MHz and 60 MHz.

B. *Frequency boundaries of spectral and spread region*

The frequency boundaries for spectral region and spread region for electric field captured by 3-30 MHz, 60 MHz and 2.4 MHz are tabulated in Table 2. Then it is presented in a box plot as shown in Fig.12 and Fig.13.

TABLE 2. MEAN OF MINIMUM AND MEAN OF MAXIMUM FREQUENCIES BOUNDARIES FOR SPECTRAL AND SPREAD REGIONS

	Frequency Boundaries (MHz)			
	Spectral region		Spread region	
	Max. Mean	*Min. Mean*	*Max. Mean*	*Min Mean*
Impulse	0.129	0.003	0.834	0.4509
3-30MHz	7.793	19.612	10.869	11.406
60MHz	7.186	19.374	10.875	11.410
2.4GHz	7.351	20.577	10.884	11.416

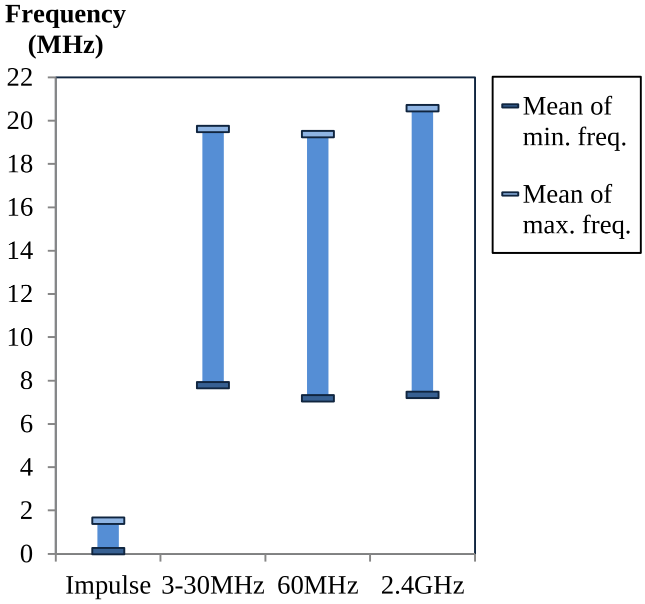

Figure 12. A localized frequency of spectral region for impulse, 3-30MHz, 60MHz and 2.4GHz

From Figure 12, the frequency boundaries of the spectral region for the impulse are small. The mean of minimum and maximum frequencies where energy radiate predominantly are also low. Thus, the energy of impulse radiate predominantly at low frequency.

However, the finding obtained from 3-30 MHz, 60 MHz and 2.4 GHz receiver antenna have a considerably difference from the impulse. It is found that for three different receiver antenna, the electric field emitted by the return stroke captured are radiate predominantly at quite the same frequency boundaries which are between 7 MHz and 22 MHz compared to the impulse which radiate energy between 0 and 2 MHz.

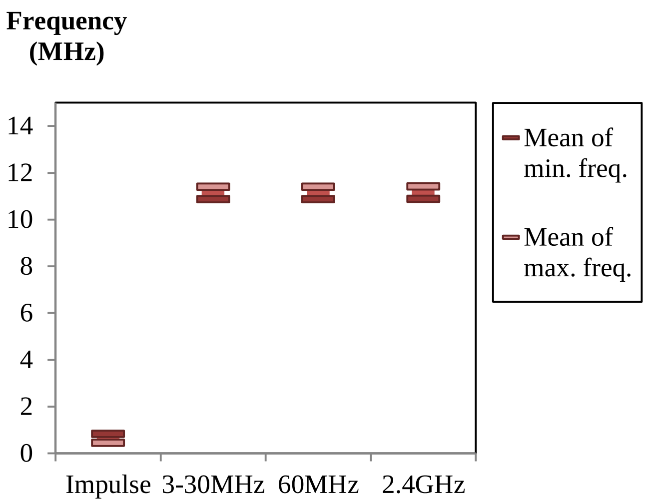

Figure 13. A localized frequency of spread region for impulse, 3-30 MHz, 60 MHz and 2.4 GHz

Same goes to spread region, it is found that the most intense energy radiated by the return stroke captured by three different receiver antenna is at the same frequency boundaries which are between 10 MHz to 12 MHz.

V. CONCLUSION

As a conclusion, there are several ideas to be suggested based on the result obtained. First, the energy of the electric field emitted by the return stroke that captured by 60 MHz receiver antenna is higher compared to 2.4 GHz and 3-30 MHz receiver antenna. While the energy of electric field captured by the 3-30 MHz receiver antenna is low. Second, the frequency boundaries of the spectral and spread region of the energy of electric field captured by all three receiver antennas are the same. This may be due all antennas capturing the same source of electric field which come from a return stroke.

VI. ACKNOWLEDGEMENT

The authors would like to express the gratitude to Dr. Mohd Riduan Bin Ahmad from Universiti Teknikal Malaysia Melaka (UTeM), Melaka for his contribution in providing extra knowledge and using the facilities in his laboratory. We also would like to thank Mr Dinesh and Mr Haziq for their help to the first author’s final year project. The research work was funded by the PAS grant from Universiti Teknologi Malaysia (UTM).

VII. REFERENCES

[1] "Lightning - The Most Deadly Natural Occurrence.". N.p., 2017. Web. 10 Dec. 2016.

[2] Ahmad, Mohd Riduan. Interaction of Lightning Flashes with Wireless Communication Networks: Special Attention to Narrow Bipolar Pulses. Diss. Acta Universitatis Upsaliensis, 2014.

[3] Burrell, James. Disruptive effects of electromagnetic interference on communication and electronic systems. Diss. George Mason University, 2003.

[4] Miranda, F. J. "Wavelet analysis of lightning return stroke." Journal of Atmospheric and Solar-Terrestrial Physics 70.11 (2008): 1401-1407.

[5] Valens, Clemens. "A really friendly guide to wavelets." ed.Clemens Valens (1999).

[6] Torrence, Christopher, and Gilbert P. Compo. "A practical guide to wavelet analysis." Bulletin of the American Meteorological society 79.1 (1998): 61-78.

[7] Esa, Mona Riza Mohd, Mohd Riduan Ahmad, and Vernon Cooray. "Wavelet analysis of the first electric field pulse of lightning flashes in Sweden." Atmospheric research 138 (2014): 253-267.

[8] Sharma, S. R., et al. "Temporal features of different lightning events revealed from wavelet transform." Journal of Atmospheric and Solar-Terrestrial Physics 73.4 (2011): 507-515.

High Power Light Emitting Diode Automatic Dimmer

Hafizuddin Jamaluddin
Faculty of Electrical Engineering
Universiti Teknologi Malaysia
Skudai, Johor Darul Takzim
jamaluddinhafizuddin@gmail.com

Mohd Rodhi Sahid
Faculty of Electrical Engineering
Universiti Teknologi Malaysia
Skudai, Johor Darul Takzim
rodhi@utm.my

***Abstract*— Nowadays, usage of power LED has drastically replaced the conventional light in the lighting system because it has reduces a lot of power consumption to operate compared with the old conventional light. To have more efficient lighting system, this project will design a driver circuit with pulse width modulation (PWM) dimming of power LED by automatically control the power LED light intensity due to light intensity demand in the particular room. The input source of electricity for this project is from the utility power supply which is 240V AC. Therefore, the driver consists of rectifier and Flyback converter in order to step down the voltage at the particular value which is 10V DC. As this project uses 9 units of power LED, the driver will produce about 10Watt of power. The driver implementing the PWM technique by adjusts the duty cycle value of the switching frequency. In this project, power MOSFET (IRF820) is used as switching device to reduce switching losses. The switching signal of PWM is generated by using PWM control circuit (SG3525) and Arduino Uno microcontroller at specific value of frequency. The signal then will be amplify by using gate driver (TC4428) in order to drive the MOSFET. Full-wave bridge rectifier and Flyback converter design parameter are known through calculation and circuit simulation using Matlab. The circuit design is tested and all results are presented.**

Keywords—Light Emitting Diode (LED); Pulse Width Modulation (PWM); Alternating Current (AC); Direct Current(DC); Metal Oxide Semiconductor Field Effect Transistor (MOSFET); Light Dependent Resistor (LDR); Cadmium Sulphide (CdS); Switched Mode Power Supply (SMPS); Intergrated Circuit (IC); Continuos Current Mode (CCM); Timing Resistor (Rt); Timing Capacitor (Ct).

I. INTRODUCTION

To increase the energy saving, low power consumption device need to be used. Today, to light up some space such as office, classroom and laboratory, majority of the commercial building still use fluorescent lamp as lighting source. However, this lighting device used high power consumption compare with power LED.

In addition, the fluorescent lamp used is not dimmable and less applied with daylight energy harvesting. The lamp that placed near to the window is still at maximum output although there is natural light enter the room through the windows. At first, to convert the AC voltage supply to DC voltage, full-waves bridge rectifier with filter capacitance was used. However, the output from a bridge rectifier is a high DC voltage and this do not suitable to operate the power LED. To step down the DC voltage to suitable power LED operating voltage, Flyback converter was used. Output from a Flyback converter has a variable DC voltage due to the transformer inside the Flyback converter and its can be design for suitable voltage to operate the power LED.

For this project, the scopes can be divided into parts which are software and hardware. This project will use the utility power supply which is 240V AC. This AC voltage was converted into DC voltage by full-waves bridge rectifier. To have a better DC voltage that suitable with power LED which 10V DC, Flyback converter was used in this project. On the other hand, to sense the ambient light intensity, LDR is used as the light sensor. Signal from LDR sensor is the input for this system. Then, Arduino Uno is implements as a microcontroller to control the output for the system due to the corresponding input signal.

For the software part, programing of Arduino Software codding will be design to digest the input signal from LDR and produce the variables duty cycle automatically depend on the stages of signal receive to control brightness of LED base on PWM dimming method. On the other hand, Matlab/Simulink software is used to simulate and verifies the circuit that have been design with calculated parameter.

II. RELATED WORKS

A. *Light Sensor (Photo-conductive Cell)*

The photoconductive light sensor used electromagnetic radiation such as visible light, gamma radiation, ultraviolet light, or infrared light will make the material becomes more electrically conductive due to the radiation effect. Cadmium Sulphide (CdS) which is sensitive to light in the visible spectrum is the most commercially available photoconductive cells [1]. LDR was design by using semiconductor material known as Cadmium Sulphide (CdS) photoconductive cells [2]. LDR is device that sensitive to the light intensity. The resistance value if LDR can vary due to light intensity that falls to it surface which it can reach a very high resistance about 10 MΩ when not illuminated [1].

B. *PWM Dimming*

PWM dimming operate at a constant DC peak value and it dimming control was based on the switching of the power LED [2].The power LED will light up when the switching frequency has applied to the system. Hence, the power LED will light up in ON and OFF state continuously and make the light produce in flicker frequency. As the operation of PWM will result the constant rated LED current, this will not affect the color shift of the power LED. The power LED lamp can be dimmed by using low-frequency of PWM [2].However, human eyes will notice the light is in not in continuous light up when the power LED is dimmed below the flicker frequency. In order to make human eyes do not notice the flickering and to avoid the stroboscopic effect the minimum dimming frequency can be used is 120 Hz [2]. However, the minimum dimming frequency recommend so that the human eye does not perceive the light pulses at least frequencies above 200, 300, or even 400 Hz for some applications [2].

C. Power Light Emitting Diode (LED)

Light emitting diode (LED) is basically a diode but it will produce light when the current flow through it in forward direction [4]. The operation principle of power LED is the same as diode and it have be made by using semiconductor based. The power LED will emits light and conduct the current when the forward voltage Vf is reached and it will block the current in reverse biased mode.

D. Flyback Converter

Flyback converter is one of the Switched Mode Power Supply (SMPS) topologies that introduce to produce variable level of DC output voltage which it can be higher or lower than input voltage. On the other hand, Flyback converter also has several advantages compared to the other SMPS topologies and one of its simple and easy to design [3].By using Flyback converter, the output sides were isolated from the input side due to the present of transformer in this topology and thus give a better safety for the system. The relative polarity of the coupling inductance can be identify by referring to the dot sign at the primary side and secondary side represents From the circuit figure below, it shows that the relative polarity of the coupling inductance is different of each other [5-7]. For the Flyback converter circuit, the analysis can be categories into two parts which are the analysis during ON state condition and analysis during OFF state condition.

E. Switching Technique

MOSFET can be control to turn ON by applying voltage to its gate. In other word, MOSFET will be turn OFF when the gate is no longer supplied with voltage. The gate of the MOSFET is usually controlled by Pulse-Width Modulation (PWM). In the practical way, PWM signal can be produced by using integrated circuits (IC) such as LM2743, SG3525, SG3524, SG3526, and many more. By adjusting the reference voltage, pulse width of PWM can be controlled.

F. Rectifier

The main proposed of using rectifier circuit in this project was to convert the AC voltage supply to the DC voltage that suitable for power LED lighting system operation. Direct current can be defined as a current which flows only in one direction, such as the current drawn from battery sources [7].

G. Literature Review

Few related research works on a light emitting diode (LED) dimmer are presented. These works form the basis of the proposed system design. Dimming led using LDR sensor by Muhammad Nor Al-Hafiz used 48V DC voltage source and step down it by using Flyback converter. By using a multilevel output at the secondary side of the transformer, it consists of 3 stages of LED output brightness with 1Watt each.

Buck-Boost Converter for Light Emitting Diode (LED) Driver Circuit with Arduino PWM Control by Mohd Faiz Zamri used buck-boost converter as a main driver for the LED. Two 1Watt power LED was used and it brightness was control by adjusting the duty cycle of PWM signal that generated from Arduino microprocessor.

High brightness light emitting diode dimmer using Flyback converter by Mohd Hafiz Adenan used a combination of AC transformer and the Flyback converter. The utility voltage supply was step down to 23V AC before it covert to DC voltage by using rectifier. The DC voltage then was step down by using Flyback converter. The parallel output of this Flyback was connected to high brightness LED with a 3 stages of brightness controlled by PWM signal.

III. PROJECT METHODOLOGY

This section discusses in detail about the methodological approach in design and development of high power light emitting diode (LED) automatic dimmer. The methodology includes the overall system and the codding flowchart.

A. Methodology

The project started with the calculation of all the parameter that involved in the rectifier and Flyback converter. By considering the output power, the current and the voltage of overall system can be calculated so that the ratings of component are correct. After have identified all the parameter, the system circuit was test and simulate by using computer software which is Matlab. After all the waveform of the system in the simulation result was correct, the project then proceeded to the hardware part. The hardware of this system was testing and measured so that every single waveform was same as theory.

B. System Flowchart

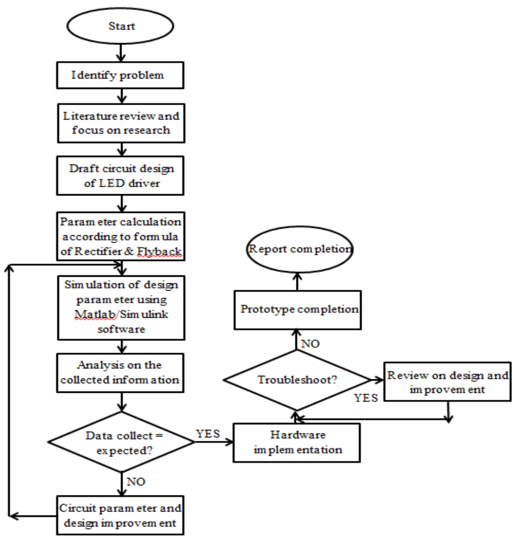

Fig. 1. Flow chart of the workflow in this project

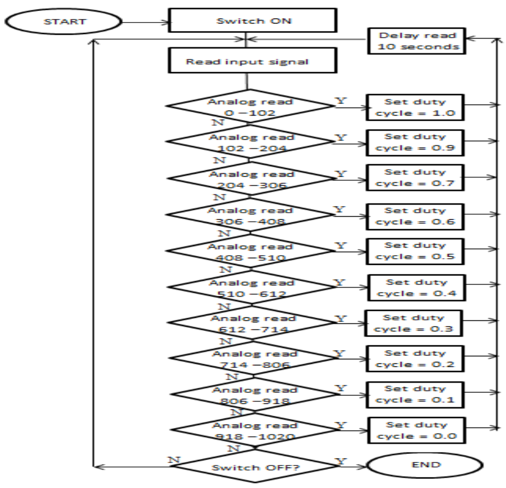

Fig. 2. Flow chart of the automatic dimming power LED

C. *Design and Parameters Calculation*

All the design and the calculation parameter were made by using the studied theory. This part will explain the design of Rectifier and Flyback converter, and design of pulse width modulation generation circuit.

Before starting to calculate all the parameter that involved in the bridge rectifier circuit, the properties of the output of this project needs to be considered which is power LED. This is very important because everything that wills design must base on it output demand. At the first part, the number of and the arrangement of power LED used need to be determined to calculated the required power for this power converter design.

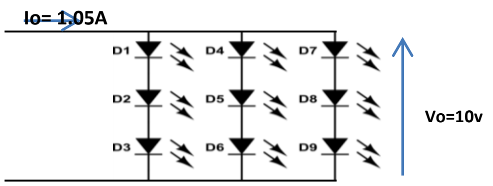

Fig. 3. Power LED arrangement for this project

In design the full-waves bridge rectifier, some parameter need to be calculated in order to do simulation on Matlab. The parameter that need to be identify and calculated in this rectifier are, voltage source, percentage ripple of output voltage, frequency, load resistance, filter capacitance and output voltage. All this parameter need to be design based on power load requirement. However, to put some safety of this rectifier component, all the calculation will make based on power rating of this rectifier which is higher than power load required which 15W.

Table 1 The parameters of the rectifier circuit

- Voltage source = Vm = 339V
- Percentage ripple output voltage = 5%
- Frequency = 50 Hz
- Load resistance = 7.7kΩ
- Capacitance filter = 13uF
- Output voltage = 322-339V

All the design parameter of Flyback converter circuit has shown in the table. By using these values, the calculation to obtain the component rating can be easy made.

Table 2 The specification of the Flyback converter

Parameter	Symbols	Value
Input voltage	Vs	330V DC
Output load	R	9.5Ω
Frequency	F	100kHz
Output voltage	Vo	10V
Duty cycle	D	0.5
Output power	Po	10.5W
Output Current	Io	1.05A

D. *Software for Simulation*

After calculated all the parameter that related to circuit design which are bridge rectifier and Flyback converter, this circuit design needs to be simulated before proceed to build up

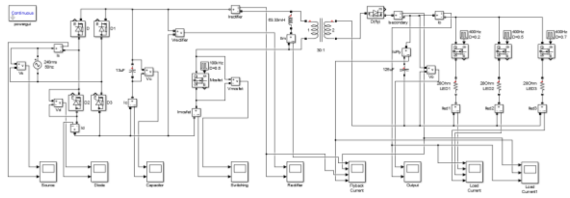

the hardware part. The purpose of do the simulation is to verify that the circuit design and all parameter that have be calculated are current, make sure that every single step of operation in the correct condition and to make sure that the output obtain was same as the calculation. For this simulation part, software Matlab was chosen to be used in getting the result for analysis due to this software easy to handle. The output waveform obtain from the simulation will be discuss on the next chapter of this report.

Fig. 3. The entire circuit on MATLAB simulation

E. *Hardware Assembly Design*

As the characteristic of diode that allow current flow only in one direction, power LED operate in DC voltage and current. The rectifier was used to convert 240V AC to the 330V DC. Flyback converter has been chosen to be used in step down voltage from 330V DC to 10V DC using transformer. To produce the pulse signal operates the MOSFET at the primary side of the Flyback converter, SG3525 PWM generator chosen to be used in this project. For the input part, LDR will be connected to the analog input of Arduino that connected in series with 10kΩ resistor.For the output part, MOSFET will be connected to the PWM output of Arduino that will control the ON and OFF of the power LED.

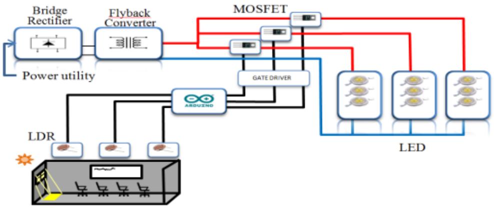

Fig. 4. The concept on automatic power LED dimmer

For the design and the testing section, all the connection will be implement to the breadboard. To used LDR as the input light sensor, some simple circuit that used of voltage divider principle need to the design. The LDR device needs to connect in series with the resistor, R1. This is because the value of voltage drop at the R1 will be determined by the resistance value of LDR. Therefore, resistor, R1 will able to generate different voltage drop across it that will represent the light intensity input. In the way to operate the Flyback converter, the pulse signal needs to be supply to the MOSFET in high frequency. To generate the PWM pulse signal in this project, SG3525 was chosen as pulse modulation controller chip. Without this pulse signal, the high frequency switching of the MOSFET for Flyback converter cannot be done thus make the overall circuit does not function. In the practical application, PWM signal must connected to gate driver circuit in order to amplify the voltage signal. To adjusted the value of duty cycle in the PWM signal, a variable resistor need to install in the connection of the circuit.

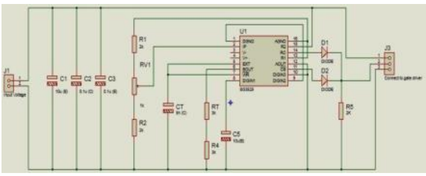

Fig. 5. The PWM pulse generator circuit

Based on the datasheet, the pulse generated from SG3525 controller chip will produce from 5V voltage. However, this value of voltage no enough to trigger the MOSFET because the MOSFET that will be used in this project needs at least 10V DC voltage to operate. Therefore this pulse needs to be amplifying by using the gate driver. In this project, Gate Driver Circuit TC4428 has been choosing to amplify the pulse signal. To use this gate driver in practical world, some circuit connection need to be design to make it operate. Then the output pin of this gate driver will directly supply to the MOSFET used.

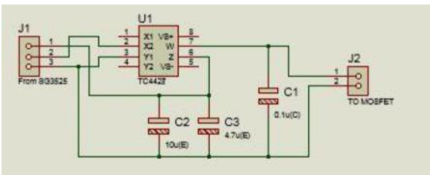

Fig. 6. The circuit for gate driver

IV. Result And Discussion

In this chapter, all the result that obtains from simulation and hardware will show and explain. For this project, the output can be divided into two parts which are on rectifier circuit and the Flyback converter. On the other hand, this chapter will also discuss the process that related to this work progress and the result obtained.

A. Result Simulation of Rectifier

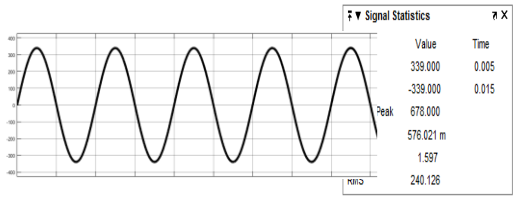

Fig. 7. The waveform of voltage source

From this waveform, it shows that the voltage supply in this project is 240V(rms) which equal to the 339V(peak) of the AC voltage. It also clearly shows that the waveform of this voltage source is a perfect sinusoidal shape which is same as the utility voltage supply. Therefore, this product can be run by using the standard utility power source without need the external DC or AC converter.

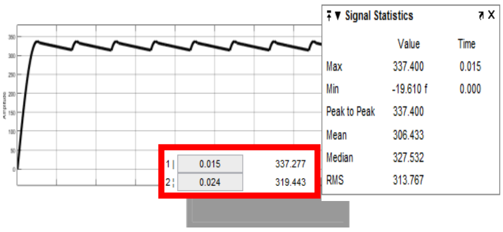

Fig. 8. The waveform of output voltage

From the output voltage of rectifier waveform shows as above, the range of output voltage is 320-337V DC. This output voltage obtain were similar to the calculation which is have output ripple voltage at 5% from its peak voltage. Therefore, from the simulation, the AC voltage was successfully had be converting to DC voltage by using the calculated value of diode and capacitor values.

B. Result Simulation of Flyback converter

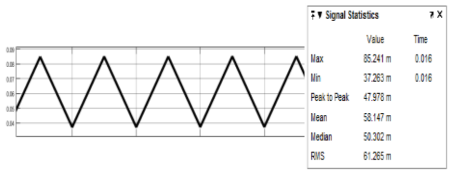

Fig. 9. The waveform of inductor current

The figure above show the waveform of the current through the magnetizing inductor it the primary side of the Flyback converter. As the minimum value of this current is always positive, the mode operation of this design circuit was in CCM mode. Besides that, the average inductor current obtains from the simulation approximately 58mA which is closed to the calculated value which is 64mA. From this waveform, the calculated inductance value of the transformer can be use in this project because it gives the correct simulation inductor current waveform.

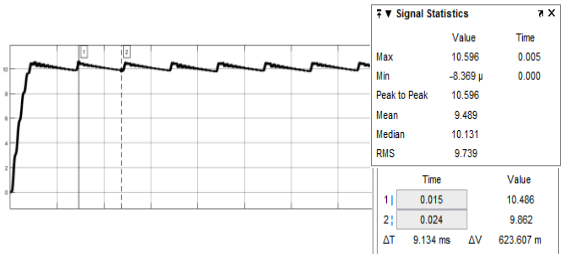

Fig. 10. The waveform of output voltage of Flyback converter

From the waveform above, it's shown that the output voltage from the Flyback converter is 9.5V and this value was close to the calculated output voltage which is 10V. The value of this output voltage was slightly drop because of some of the energy have drop in the circuit due to each of the components in the circuit has their internal resistance. It can be conclude that the practical situation will affect the theoretical voltage and current value. The output ripple voltage obtains in simulation for the Flyback converter was also near to the calculated values which is 5% of its peak value. Therefore, this pattern of output DC voltage was suitable for the load used which in power LED.

C. Result Simulation of PWM switching control of power LED

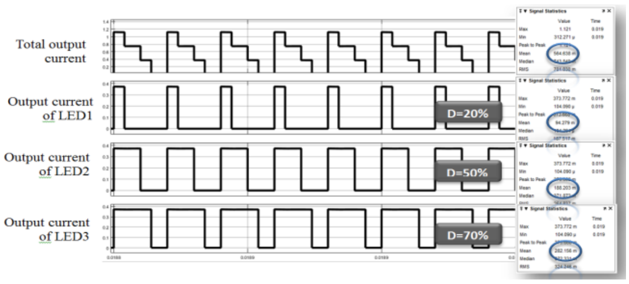

Fig. 11. The waveform of output current and each out power LED current

The important thing that need to observed in order to control the dimmer of the power LED is the current through its. From the output current waveform, it's shown that the duty cycle of the PWM output from the Arduino can control the current value of power LED. For the output current LED1, when the duty cycle was set into 20%, the positive cycle of the waveform will 20% from its period. This current also shows the average current of power LED1 is 94mA. When the duty cycle has been increase as the power LED 2 condition, the average current produce was also increased. From this observation, its clearly prove that duty cycle value played a big role in controlling the brightness of the power LED. Therefore, the higher the duty cycle, the higher the current flow through the power LED and the brighter the power LED light.

D. Transformer design

By identify the value of load power, primary current, frequency, primary inductance and flux density, the number of turn for the primary winding was calculated. For this project, to obtain the 11.13mH value of inductance, the calculated number of primary turns is 231.

The bobbin and clips for this project were selected according to the dimension and type of the ferrite cores used. For the primary side, the diameter of the enamel copper wire used was determine by the value of current flow through it which is 0.2mm. This enamel copper wire was wrapped around the bobbin by 231 turns. For each layer of the winding was isolated by using polyester tape to ensure so current leak for one layer to other layer.

For the secondary winding, the number of turn was determining by using the turn ratio of the transformer that had calculated before. The number of turns for the second winding is 15 turns. As the voltage at the secondary side less that the primary, the current for the secondary side should be higher that primary in order to maintain its power transfer. Therefore the diameter used for the secondary winding should be higher that primary winding. The diameter of wire required to withstand the current value for secondary is 0.7mm. By considering the skin effect of the copper wire when dealing with high frequency, the 0.6mm enamel copper wire was twisted in pair to produced two strands of wire.

After complete wrapped around the primary and the secondary winding, the ferrite cores were place in the bobbin and the polyester tape was used to tight up the ferrite cores to avoid air gap. Then the value of inductance produced from the primary winding was measured by using LCR meter.

Fig. 12. The transformer winding and measurement

E. PWM Hardware Result

From the calculation of the Flyback converter, the frequency used for the switching in this Flyback converter was 100 kHz. Regarding to the formula used in determining the value of component used in this project, the value of the component used such as capacitor and inductor will decrease when the frequency of switching increase. Therefore, 100 kHz was chosen in this project in order to obtain the small value of component to make this project compact and more economic.

To produce the 100 kHz PWM signal, the SG3525 controller chip was used in this project. By referring and understanding to this SG3525 datasheet, this SG3525 can produce the a variable frequency up to 400 kHz by controlling the values of timing resistor (RT) and timing capacitor (CT). As a result, the 5nF capacitor and the 5kΩ variable resistor were used in this project in order to produce 100 kHz PWM frequency. In the other hand, this SG3525 was also can produce a variable duty cycle of the PWM value by controlling the resistance value on pin 13, pin16 and pin 2. However, this project used a fixed value of duty cycle which is 0.5. Therefore, 5kΩ variable resistor was used to obtain the required duty cycle for this project.

The pulse generated by the SG3525 chip was produce the 5V voltage. However, as this project used IRF820 MOSFET, it's required at least 10V voltage to operate. Therefore, the MOSFET will be not operating if the signal was supply directly to the gate of the MOSFET. To overcome this problem, this PWM signal needs to amplify by using a gate driver. The TC4428 low side gate drive was chosen in this project as it can amplify the signal voltage from 5V to 15V.

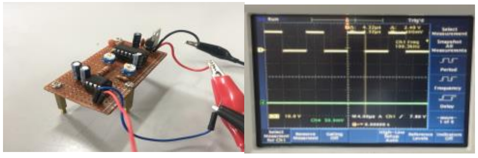

Fig. 13. The PWM circuit and output waveform

F. Hardware Result

All the waveform obtains from the hardware circuit were observed and recorded as below:

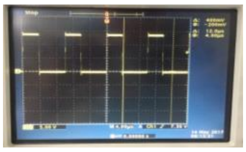

Fig. 14. The PWM circuit and output waveform

Figure 14 shows the waveform that had been amplified by gate driver. The signal voltage signal was increase from 5V to 15V after had been amplified. The PWM signal also operate at high frequency which is 100kHz as the period from the oscilloscope show about 10uS.

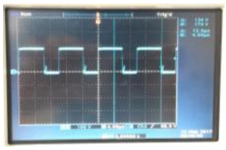

Fig. 15. Voltage waveform of MOSFET

Figure 15 shows the voltage waveform between Drain-Source terminal and Gate-Source terminal of MOSFET. When the switch is on, the voltage of Vgs should be zero and Vds is high. Turn off situation of the switch made the Vds is 0V when the Vgs is 15V amplitude. This result show that the MOSFET is functioning well.

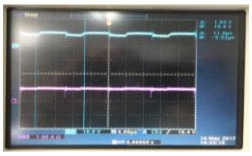

Fig. 16. Output voltage and current for Flyback converter

Figure 16 shows the voltage of output voltage (blue waveform) and the output current (pink waveform) of the Flyback converter. The voltage and current produced were same as the calculation and the simulation which are 10V and 1A. As the result produced was same as calculation, the output power obtain was also same as calculation which is 10Watt.

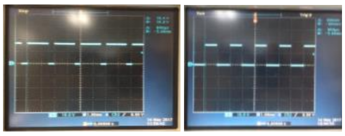

Fig. 17. The duty cycle of PWM signal

Figure 17 shows the voltage of the PWM signal from Arduino through the gate driver. This signal will used to control the current for the power LED output. The waveform shows the duty cycle of the PWM signal will varies when the level of light intensity sense by LDR sensor changed.

V. Conclusion

In designing a driver for automation dimming of power LED by using LDR sensor with the utility power source, the designer needs to understand the working principle of rectifier and Flyback converter. The driver for power LED has been designed to control the brightness of power LED automatically in order to increase its efficiency. Knowledge from journals and books helps a lot in designing the circuit in this project. The AC input voltage was converting into DC voltage by using rectifier circuit with the calculated value of components. The switching frequency for the Flyback converter is generated by SG3525 chip and for the average power LED current is generated by Arduino with PWM method. From the data collected, by adjusting the duty cycle value of PWM signal, the average output current will varies which is smaller duty cycle value produce less average output current while higher duty cycle will produce high average output current. As LDR sensor detect the light intensity, the signal the sent to the Arduino Uno microprocessor to covert the signal to the PWM signal by using instruction of developed codding that uploaded to the Arduino. Based on the PWM output, the duty cycle was varies automatically when the LDR sense different level of light intensity.

References

[1] C. Mathas.(2012).Light Sensors: An Overview. Electronic PRODUCTS

[2] Gacio, D., Alonso, J. M., Garcia, J., Campa, L., Crespo, M. J., & Rico-Secades, M. (2012). PWM series dimming for slow-dynamics HPF LED drivers: the high-frequency approach. 59(4), 1717-1727.

[3] P.D. MASO. (28 Februiary 2012) Strategic Efficient dimming for LED lighting Marketing Manager,Texas Instrument.

[4] C. DiLouie (Fri,10 Dec 2014).Controlling LED lighting systems: introducing the LED driver. LED Magazine, Lighting Control Association.

[5] Xu, L., Zeng, H., Zhang, J., & Qian, Z. (2011, March). A primary side controlled WLED driver compatible with TRIAC dimmer. In Applied Power Electronics Conference and Exposition (APEC), IEEE.

[6] Hassan, M. Y., Abdullah, H., Rahman, H. A., Abdullah, M. P., Hussin, F., & Bandi, M. (2013, December). IEEE.

[7] Badamasi, Y. A. (2014, September). The working principle of an Arduino. InElectronics, Computer and Computation (ICECCO), 2014 11th International Conference on (pp. 1-4). IEEE.

Automated Number Plate Recognition System for Parking Management

Norsailaniza Bt Mohamad
Faculty of Electrical Engineering
Universiti Teknologi Malaysia
Johor Bahru, Malaysia.
norsailaniza@gmail.com

Dr Mohd Fadli Bin Rahmat
Department of Electrical Power Engineering
Faculty of Electrical Engineering
Universiti Teknologi Malaysia
Johor Bahru, Malaysia.
mfadli@utm.my

***Abstract*—Nowadays, the community own their own vehicle to keep pace with the modern and fast lifestyle. With the increasing number of vehicle on the road, parking has become a huge problem for people in urban area as the usage of the parking facilities increased. Hence, a good management of the parking area with the latest technology to reduce the processing time is necessary to ensure that the traffic flow entering or exiting the parking area is smooth and under control. Therefore, an automated parking system, which is using the Number Plate Recognition System is developed to increase the quality of parking management especially in safety aspect. Generally, number plate recognition system is used to recognize car plate numbers, which can be used in many areas such as parking control system, traffic light control and speed-limit enforcement. The aims of this project are to model and design the automated number plate recognition system for parking management for authorize user only and also to enhance its performance. This system will recognize Malaysian's plate number especially on normal car. By developing this system, it can be very useful to help the administrator of parking area to keep the user's information on database for any purposes. It also will reduce the criminal case occurs during the parking space. So it can increase the confidence and reassurance of users to park their car.**

Keywords—Parking, Plate Number and Database

I. Introduction

Generally, a parking management systems is a system that is use to help users find parking spots quickly, thereby reducing frustration and also avoid from parking difficulties. This is because of time, health and cost are the main reasons for human beings to have a good life. It is very important to implement at a large building due to the increasing numbers of vehicles on the road. This parking management systems is designed to develop an automatic parking system that will increase convenience of the parking lot with minimum human involvement. This system use the technologies, which are Wireless Sensor Network (WSN), Radio Frequency Identification (RFID), Programmable Logic Controller (PLC), Supervisory Control and Data Acquisition (SCADA), Global Positioning System (GPS), Number Plate Recognition (NPR) and many mores to help the system to make the whole process of parking management become fast operating system and useful for both users and administrators [1].

In short, this project proposed an implementation of Automated Number Plate Recognition (ANPR) system for parking management, which is to faster the time processing to enter the parking area. By the implementation of ANPR, the parking system will become more manageable because the manager and administrator of parking area can keep the all data of the vehicles by their plate numbers during entering the parking lots.

II. Literature Review

A. *Background of Parking Management System*

Basically, parking management system is developed at the main entrance, which is the part that allow access to a place. It is very important to convince people that the place is secured from any criminal cases or accident when accessing the place. Basically, parking management system is installed at the company's building, hospital, sport complex, residential area, parking area and other enclosed structure.

Before the systematic parking system introduced, the people would simply park their vehicle at roadside and leave them until they use them again, which means no specific system is employed yet to that place at that time. Nowadays, when security and safety turn into a fundamental piece of human life, most of entrance system of parking area apply standard vehicle gate or barrier to assist advanced vehicle entry concepts including license plate recognition, vehicle type and model recognition, detecting vehicle colour or capturing drivers face by integrated closed circuit televisions (CCTV) system. All those advanced functions allowing the fulfill needs wherever where security is must [4-5].

For the gated and guarded concept area, the entrance of parking system has few security facilities in order to guarantee the security of resident, which is barrier gate with the help of security guards, central base monitoring system, 24-hour guard services, and CCTV. For the residents of gated and guarded societies, they are given an electronic access card and car sticker. The residents need to scan their card at the entry and exit of the housing areas. While for the non-residents or visitors they are compulsory to enrol themselves at the security guard house by leaving their identification documents such as driving license. The security guards are in charge to record the necessary information of the visitor in the daily logbook.

Simultaneously, they have to get the permission the owner before approved the visitor to enter the residential area [6].

B. Purpose of Parking Management System

Although the parking management system when through several of advancement, but the purpose is always unchanged, which are to assists users to park their vehicle at the provided parking lot in manageable and simplest way. Besides, the parking management system have various specialty to all customers. For example, it has function to provide a guidance where the user can know the vacant of the parking slot from far by seeing at the light at each slots. Apart from that, it will make the parking process fast and users will not waste their time to find the parking slots. Parking system also provide an area that ensure the vehicles are safe because safety is the most important factor that need to be aware when using the parking space [7]. It can affect the user's enjoyment. So, many thing need to be concerned about will be discuss in next topic.

C. Advantages and Disadvantages of Parking Management System

The benefits of parking system includes users can simply find the parking lots and can know the availability of parking lots. Thus, it can solve the problem of unnecessary time consumption to find the parking lot. With the aid of this system, it can manage, monitor and watch over the parking facilities from any vandalism. The parking area also become fast operating parking-lot system with the automated payment of parking charge, where the users do not have to line up. Besides, the managers and administrator can aware the illegal mobility of the car parking and able to get the data about the parking area [8].

In the other hand, the parking systems also have the weakness such as not all of the parking system can improve the security feature and some of them are not design for car management system. The intelligent parking system that use the video sensor is very costly and the use of video sensor can produce a very large amount of data, which can be very difficult to transfer in a wireless network [9]. The system also cannot manage how to accurately detect the mobility of automobile, especially when the vehicles move in high speed. Other than that, sometimes it is not effective for visitors, which only allows the authorized vehicles that are registered. There are some system that is not systematic because they are manually managed.

D. Development of ANPR System

1. History and Overview of ANPR

Police Scientific Development Branch in the United Kingdom established the Number Plate Recognition (NPR) in 1976. Model of the systems were functioning by 1979 and allowed to construct industrial systems, first at EMI Electronics and then at Computer Recognition Systems (CRS) in Wokingham, UK. Early tested systems were deployed on the A1 road and at the Dartford Tunnel [10]. By having thirty years of practical involvement, the newest invention of Vysionics ANPR systems apply the most excellent in camera, processor, software and illumination technologies, offering the application specialised solutions for a large variety of traffic monitoring. In 2013, the vector integrated ANPR camera was commenced, providing very capable, standard platform for the toughest of ANPR projects. In November 2014. Vysionics market heading ANPR and normal speed enforcement solutions will now help from exposure to the global market place [11].

First, the car reach at the barrier gate of parking system. The infrared sensor will sense the presence of the car at the barrier gate. The sensor also send signal to camera to snap the image of number plate. The number plate image of the car will go through a process to convert the image of number plate into text. Then, it will stored in a database that can easily accessed by the administrator of parking area for any purposes. After that, the barrier gate will lift up. The same process is occur at both entry and exit gate of parking area.

Character recognition is the important step needed in this system. This technique is used to recognize the characters and numbers in the picture captured by webcam because the digital image unable to transform into text yet although after done the plate localization step. For that reason, this step is required in order to detect the plate number image and turn into text, which can be shown on computer monitor. The details of this technique are discussed in the following sub-chapter.

2. ANPR Using Quick Response (QR) Code

The QR code is identified as a 2-dimensional computerized image by a semiconductor picture sensor and then digitally analyzed by a programmed processor. The processor locates the three distinctive squares at the edges of the image, and standardized image size, orientation, and angle of viewing, assisted by a smaller square close the fourth edge. The small dots are then changed to binary numbers and authority checked with an error-correcting code. This code offer a brand new way for people to interact with simple, pleasing and secure facility [12].

Bhupendra [13] proposed the installation QR Code system; where at the slow lane level, the CCTV (Closed Circuit Television) cameras capture image of the car including QR code in it. Otherwise, a small optical QR code scanner are mounted for on spot detection. When vehicles go through under the camera or scanner, their QR codes are computerized recorded. Then, the embedded information (image/video/QR code) is sent together with date and time to the main computer. The QR code recognition technique is made at the software part and involves of the several steps: If straightforward information is sent from lane level, then continue for finding the record in database at the same time. Otherwise if image or video support is obtained, then focus the QR code recognition software part for the QR code accepted to retrieve the data and then search the record.

Prof. Pritesh A. Patil [14] suggested the the similar method that capture live images from camera. It acquires estimated region of QR code, and apply for positioning for QR image based on pattern detector to get accurate position as its alignment pattern. Subsequently, this code can read and recognize by computer using machine vision system containing of cameras and software to interpret QR code. Binarization technique is used for decoding the QR code. Then, the translated file is saved in database. For searching data, SQL Query is used. After information is pair with precompiled database of vehicle to identify and display this information on monitor.

3. ANPR Using Optical Character Recognition (OCR) Process

The website article [15] recommend about OCR process that also contain the identification process to verify the country and state of origin of the vehicle number plate. For segmentation phase, the license plate is placed within the input. The region is indicated by the red shading. The region that consist the license plate is binarized, where the foreground is separated from the background of image. The region are considered to be foreground are colored black and specified with the green marking. The algorithms created use the general knowledge of the layout to ensure high recognition performance, better backgrounds and fonts to be discovered on the variety of plate styles used in the nations. Lastly, each foreground character is categorized, the specific meaning of every graphical symbol is defined. This results in the final determined license plate number together with the classified plate style and matching layout.

Bhupendra [13] also studied about the process of OCR. Firstly, the image of plate number is captured by the camera at the entry gate. The isolation of the number plate from the captured is begin, which is called plate localization technique. After that, move to plate orientation and sizing step, which is the isolated number plate is then resized and rotated as required by the recognition software. At character segmentation, each character on the number plate is separated by illustrating horizontal and vertical edges and thus form rectangles around each character. Normalization step is done after character segmentation, the brightness and contrast of the image is adjusted until the background of image is look white. Each character is then recognized by the software at character recognition. The software implements the technique of pattern matching to identify the characters, thus pairing the characters with the recorded samples. The characters are then combined together to form full number plate.

Aarti Soni [16] applied the ANPR system using OCR that is used to obtain the alphanumeric characters exist on the number plate. First of all, it uses a series of image manipulation techniques to detect, normalize and enrich the image of the number plate. Two components are used in the system, which are cameras at the front-end and the remote server at the back-end. In this system, efficiency can be increased by using the two cameras. The cameras will captured the images of number plates and transfer it to the remote computers to perform further process such as optical character recognition on the stored images forwarded by the cameras. A server farm is used to process the high amount of images stored, which involves of several computers working at the same time. The remote computers are linked with the database that stores the details of the car owners and other required information

III. Methodology

A. Project Description

At entry gate, when IR Sensor 1 detect a vehicle that entering into the parking area, it will send the signal to the PC to activate the webcam to capture that vehicle's plate number. After capturing the plate number, the image will be sent to the PC where it will processed through OCR process and the data will be stored. The process is done if the plate number match with the authorize plate number that exist in the database of the system. Then, this sensor will trigger the servo motor to lift up the barrier gate by 90°. Thus, the vehicle can park in any available space at parking area. However, the barrier gate is not lift up if the plate number of vehicle after OCR process is not match with existing plate number in the database. After that, the barrier gate closed after car pass through it. For this project, a parking area model as shown in Figure 1 has been created to give a clear view on how ANPR System is running. The model does not have parking lots because this project only focus on entry and exit gate only.

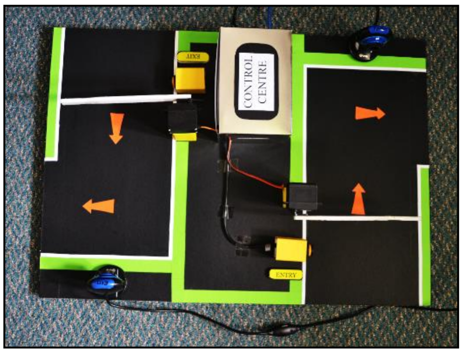

Fig. 1 Prototype Model

On the other hand, when IR Sensor 2 detected a vehicle is going out from the parking area, it will send the signal to the PC to inform the webcam to capture that vehicle's plate number. After capturing the plate number, the image will be sent to the PC where it will be processed through OCR process same as at entry gate. Therefore, this sensor again will inform the servo motor to lift up and car pass through it and lastly the barrier closed. .

B. Hardware Devices

1. Webcam

In this project, there are two same webcams being used. The webcams used in this project, which is Megapixel 10X digital zoom f3.85mm can capture up to 8.0 megapixels images and connected using USB port to laptop. The higher pixels of image will ensure the quality of the picture captured and hence will avoid the error during the OCR process. This webcam also equipped with microphone, night vision LEDs, snap short button, lens, flexible tube and multi-functional clamp.

2. Infrared Sensor

Infrared sensors will be used as the input for the webcams where the sensors will detect existence of car approaching the barrier gate. The signal will be sent to the webcam to capture the image of number plate as the sensor is triggered. The detection distance is 3-80 centimetres and it has better immunity to ambient light and light disturbance. In the other word, it also known as infrared transmitter and receiver, which operate together become a photoelectric sensor. The sensor has a lengthy detection distance and the interference by visible light is very less because it has modulated infrared light. It also has a screwdriver adjustment to set the detected distance, then gives a digital output when it senses object within its range [28].

3. Servo Motor

The purpose of the servo is to receive a control signal that represents a desired output position of the servo shaft, and apply power to its DC motor until its shaft turns to that position. It is controlled by sending an electrical pulse of variable width, or pulse width modulation, through the control wire. There are two ball bearings help reduce friction and improve performance. In this project, servo motor is used to lift up and down the barrier gate that is programmed by Arduino IDE.

4. Arduino UNO Board

Arduino UNO is a microcontroller board that will be used to implement and programmed the parking system. Arduino is a device that leads by Atmel microcontrollers. It has digital and analogue input output ports to connect many sensors, switches, motors and modules.

C. Software Used

1. Arduino IDE

This software is a very simple and easy to use by the users. The Arduino IDE is open-source, which means it is fairly priced and its development software is free. The Arduino programming language is an easy version of C/C++.

2. Visual Studio 2017

Visual Studio 2017 is a software to create the graphical user interface together with database system to manage and convey data in a professional way. By using this software, the table can be created for users of parking system with each record containing the user's ID, vehicle plate number, date and time.

IV. RESULT AND ANALYSIS

In this chapter, the system operating process together with the result obtained from the hardware and software developed will be discussed. The hardware developed represented by the prototype model of parking system with entry and exit gate that has IR sensors and barrier gates. Then, the hardware and software are assembled to show the output of the system that must achieve the objectives of this research and prove the system was successful implemented.

1. Character Recognition Analysis

In this project, there are 40 samples of vehicle plate number used to analyse the optical character recognition process. From the result obtained, it show this system successfully can convert all the character on plate number image into text and number with no error. Each sample take about 10 second to pass through OCR process and then enter the parking area to park their vehicle.

Table 1: Character Recognition Result

No	Plate Number	Success	Fail	No	Plate Number	Success	Fail
1	QWE901	/		21	PDK4526	/	
2	MAN7485	/		22	WHP2163	/	
3	ABC1234	/		23	NCE9842	/	
4	JKL4567	/		24	MBG9522	/	
5	NBE2518	/		25	MDE2468	/	
6	BGB2368	/		26	TAM9870	/	
7	PLL7396	/		27	TBB4841	/	
8	KDH3857	/		28	AGU783	/	
9	THJ5931	/		29	PHT5622	/	
10	WLW88	/		30	SAA2155	/	
11	JGG2241	/		31	CCT3039	/	
12	SAB211	/		32	CBX7639	/	
13	NBF4542	/		33	PFQ3294	/	
14	WSY23	/		34	JEK7877	/	
15	JKS1176	/		35	JMQ995	/	
16	TAW789	/		36	BFL6897	/	
17	JET482	/		37	JKR6325	/	
18	BGN667	/		38	JQJ1994	/	
19	JBY9500	/		39	WA3693	/	
20	WFM5723	/		40	DCH373	/	

2. Angle of Plate Number

The angle of vehicle plate number also analysed to identify the maximum angle of plate number compatible for OCR process in this system. The angle is tested from 0 degree until 20 degree and it show the maximum angle for OCR process is only at 15 degree. At that angle, OCR process took 2 second longer than normal condition. Thus, if the plate number of vehicle is titled more than 15 degree, the vehicle cannot park in the parking area because the OCR process failed to recognize the plate number. Therefore, user must ensure the position of their plate number is only at 0 degree or up to 15 degree. The plate number will adjusted to below to get the maximum angle suitable for this system.

Table 2: Angle of Plate Number

Angle	Tested Sample	Success	Fail	Average Time Taken
0/180°	40	/		10 seconds
5°	40	/		10 seconds
10°	40	/		10 seconds
15°	40	/		12 seconds
20°	40		/	Failed

3. Rare Font of Plate Number

Sometimes, there are few vehicle that use different type of font of plate number, which mean the font that rarely used in this country. So, an analysis for that type of font is done by choosing five type of rare font to know whether this system capable to recognize the character on that fonts. Based on result obtained, only two out of five type of font are successfully recognize and the bold and italic font are failed to recognize by the OCR process. Besides, the curly font like Lucida Handwriting font also failed because character 'B' is recognize as '13' and character 'G' as '16'. In order to avoid from that situation, those user who have different font or using the illegal font, they are not be allowed to register as authorize user in this system. This is because, they will having difficulties to enter and exit from the parking area due to failure of OCR process. However, time taken is unchanged as normal plate number, which is 10 second and it show that time taken is not influenced by the rare fonts.

Table 4.3: Rare Font of Plate Number

Type of font	Number Plate	Success	Fail	Time Taken
Forte	7HJ5931		TH69311Y	Failed
Bauhaus 93	QWE901		0111EQM	Failed
Kristen ITC	PLL7396	/		10 Seconds
Segoe Script	KDH3857	/		10 Seconds
Showcard Gothic	WLW88		Not Detected	Failed
Bradley Hand ITC	MAN7845	/		10 Seconds
Lucida Handwriting	BGB2364		1316132364	Failed

V. CONCLUSION

In conclusion, ANPR System for Parking Management is believe to provide a more comfortable, convenience and easier handling parking system to the parking user. The users do not need to do anything when they enter the parking area until the barrier gate is open. The system will provide automatic solution from getting the vehicle plate number that is stored in the database. In short, the project scopes and objectives have been fulfilled. The system is able to read the car plate number automatically when the car enters the parking area and determine the number of empty parking lots left in the parking area as well as keep the information in parking database.

REFERENCES

[1] Parking Management System, Traffic Tech Group (Middle East/bulf): http://www.traffic-tech.com

[2] PIC16F877A:http://www.microchip.com/wwwproducts/en/PIC16F877A

[3] What is OCR and OCR Technology: https://www.abbyy.com/en apac/finereader/about-ocr/what-is-ocr/

[4] Parking Management System - HaSaM International. Retrieved October 21,2016,fromhttp://www.hasam.eu/enus/products/identificationsystems/ parkingmanagementsystem.aspx

[5] Parking systems, entrance and exit gates and doors, etc. Retrieved October 21, 2016, from http://web.ntd.cz/en/parking-systems-entrance-and-exit-gates-and-doors etc

[6] Z.Shamsudin and E.Y.Ying, "The Safety Level of Gated and Guarded Community

[7] Schemes in Malaysia", International Soft Science Conference. eISSN: 2357-1330

[8] Parking Management System, Somfy India Private Limited - December 2014: http://www.somfy.co.ln

[9] Advanced Parking Management System: A Cross Cutting Study. January 2007: http://www.its.dot.gov

[10] Mingkai Chen, Tainhai Chang, "A Parking guidance & Information system based on Wireless Sensor Networks", IEEE International Conference on information & Automation Shenzhen, China, June 2011.

[11] Shriram Kishanrao Waghmare, A. K. Gulve,Vikas N.Nirgude "Automatic Number Plate Recognition (ANPR) System for Indian conditions using support vector machine (SVM)" [ISSN 2250 - 3765] International Journal of Computer Science and its Applications

[12] Our History: http://www.jenoptik.co.uk/about-us/our-history

[13] Parking Fee Payment Made Easy With QR Code: www.beqrioustracker.com/parking-fee-payment-made-easy-with-qr-code/

[14] Bhupendra Moharil, Vijayendra Ghadge, Chaitanya Gokhale, Pranav Tambvekar, "

[15] An Efficient Approach for Automatic Number Plate Recognition System Using Quick Response Codes", International Journal of Computer Science and Information Technologies (IJCSIT). ISSN: 0975-9646, Vol. 3 (5), 2012, Pp5108 – 5115.

[16] Prof. Pritesh A. Patil, Aniket P. Gaikwad, Pallavi P. Bendale, Anita M. Turkane, Chaitanya S. Ambardekar, "Vehicle Identification Using Android Enabled Mobile Devices", Department of Information Technology. IJSART – Vol.2 Issue 3 –MARCH 2016, ISSN [ONLINE]: 2395-1052, Pp 1-3

Smart Energy Meter

Mohamad Abdul Bari Bin Mohamad Razali
Faculty of Electrical Engineering
Universiti Teknologi Malaysia
Johor Bahru, Malaysia.
abdulbari_094@yahoo.com

Dr. Mohd Fadli Bin Rahmat
Department of Electrical Power Engineering
Faculty of Electrical Engineering
Universiti Teknologi Malaysia
Johor Bahru, Malaysia.
mfadli@utm.my

***Abstract*—this paper presents a design of smart energy meter for monitoring and proper management of power consumption in residential area. This project has been conducted in order to study the energy consumption measurement on customer side. The most vital components in this product are microcontroller Arduino Uno, current sensor SCT 013-000, AC voltage sensor ZMPT101B and GSM Sim 800L. The formula of power consumption and the billing price are programmed and uploaded in the microcontroller. Both current sensor and voltage sensor are used to measure the current flow to the loads and the voltage supply respectively. Besides, this smart energy meter can display the real time power consumption and the billing price on the LCD display and also can send the energy consumption information to the consumer by using the GSM Sim800L. This smart energy meter is only available for the residential area with single phase supply only. Thus, by using this meter, consumers can easily monitor their power consumption so that there will be no unwanted usage which is due to their lack of usage management.**

Keywords—Power consumption; Energy meter; Current sensor; Voltage sensor;

I. Introduction

Gradually smart grids and smart meters are closer to the home consumers. A few nations has developed researches concentrates in the effects emerging from the introduction of these technologies and one of the fundamental are related to the effectiveness of energy, observed through the awareness of the population on behalf of a more efficient consumption [5]. So, smart energy meter is one of the alternative ways in order to increase the awareness of the consumer towards monitoring and reducing their energy consumption.

Compare to the conventional meter which can only displaying the total power consumption, the smart meter is a device that can measure the power consumption through the measurement of the current and voltage and compute the power usage using the microcontroller. Then, it will display the power consumption in kilowatt-hour (kWh) and the billing price on the LCD display. The billing price is based on the latest tariff rate stated by the Tenaga Nasional Berhad (TNB).

The relation between the consumer and the smart meter is vital because the main key factor for their future cash reserve funds and for the advantages of the whole energy chain is depended on the involvement of the customers in controlling their energy consumption [6]. The relation between the consumer and the smart meter can be achieve with the aids of the Global System for Mobile communications (GSM) which can transmit the energy consumption information to the consumer via Short Message Service (SMS). With the aids of this system, the consumers can control and monitor their power consumptions by themselves. Thus, they can save their money rather than paying for the electricity that they do not use.

II. Literature Review

In order to determine the monitor positions for fault location in radial distribution networks it is impotent to consider fault current levels in different points and the topology of the system. The following subsections highlight the importance of these two factors.

A. Electrical Energy

In this modern era, the consumption of electricity is very vital in our daily life. All of the people rely on the electricity in all of our daily activities such to do work, cooking and supply for our household appliances. In a simple word, electricity helps to make our life easier and simpler. Since, all of us use the electricity in our daily life; the demand in electricity is keep increasing from day to day. In addition, the rapid growth in both population and the technologies also result to the increasing of the electricity demand.

But, based on the research, the demand can be reduce if the consumers reschedule the time to use the electrical appliances from the peak periods to the off-peak periods. This program is included in the demand side management program. The demand side management program is implemented in order to reduce the energy consumption by shifting the use of electrical energy from peak to off-peak time depending on customer's choice [5]. Peak time is referred to when the residential consumers use high electricity and the off-peak time is the vice versa. Furthermore, usually the rate charge of electricity during peak time is much expensive compare to the off-peak time.

To know the appliance's energy used, we use a formula;

$$Energy\ Consumption = \frac{Watt\ x\ Hours\ Used\ Per\ Day}{1000}$$

(2)

$$\alpha + \beta = \chi. \qquad (1)$$

(1)

1) Energy Consumed

Energy consumption is referred to the amount of electrical energy used by the customers. Nowadays, the energy consumption is keep increasing due to the development of technologies. As the technology is continually developed, many researchers and inventors create or invent new products. So, it resulted to the increasing of household appliances as the customers or users buy the new products in the market. Thus, the energy consumption in their home is increasing due to this factor. Based on the statistics, about 49% of the residential electricity demand in U.S. has increased over the last twenty years due to the increasing in the household electrical appliances [15]. Besides, high energy consumption is also because of the inrush current during the starting of appliances that lead to the additional starting power [7]. Basically, many loads consume additional power which is called as the starting watts. This starting watts occurs for a short period which is when the transition of the appliances from off state to the on state.

Besides, since the advancement of technology, people nowadays want to live in more better and comfortable ways. For example, they want to have television in every room in their house. Indirectly leads to the increasing of loads in their home. Besides, because of their carelessness such as forgot to switch off their unused household appliances leads to the unwanted usage of electricity. If they consumers do not care or realize about this situation, they will be wasting their energy consumption and also their money.

2) Electricity Bill

Electricity bill is the bill of charge for the electrical energy consumption for a month. Usually the utility bill tells the customers about the total energy consumption, total cost of energy consumption and the tariff rate. It is important for all customers to get know about the calculation of the total bills of their energy consumption. One approach to comprehend these charges is by referring to the tariff rate that applies to the bill and recalculate the total costs by using the energy consumption data from the bill such as the rated charges for the first two hundred units of kilowatt-hour (kWh).

Kilowatt-hour or kWh was utilized for standard charging of electrical power. It is calculated by multiplying the total power used (kW) by the total of time interval of the power used (h).

kWh = kW x hours (1)

$$\alpha + \beta = \chi. \quad (1)$$

(1)

The energy bill is depended on the total number of units recorded in a one month. Some utilities charge the all of the energy consumption in a same tariff rate, but some utilities do not. They charge different tariff rate based on the total energy consumption. For instance, in Malaysia, the power provider Tenaga Nasional Berhad (TNB) charges the first 200 kWh for 21.88 $cent/kWh$. The next kWh used will be charged differently as shown in Table 1.

TABLE I. TENAGA NASIONAL BERHAD ELECTRICITY TARIFF

Energy Used	***Rate (Cent/kWh)***
For the first 200 kWh (1 - 200 kWh) per month	21.80
For the next 100 kWh (201 - 300 kWh) per month	33.40
For the next 300 kWh (301 - 600 kWh) per month	*51.60*
For the next 300 kWh (601 - 900 kWh) per month	*54.60*
For the next kWh (901 kWh onwards) per month	*57.10*

So, based on the table, the rate tariff is increasing as the power consumption is increasing. If the electricity consumers do not care on monitoring and controlling their energy consumption, then they will lose their money for an unwanted usage.

B. Smart Energy Meter

A smart energy meter is a digital device that is used to measure the electrical energy consumption and the billing price at certain time intervals. This product is the improvement of the traditional power meter which can only measure the total of energy consumption. The smart energy meter is able to provide the energy consumption information to the users whether through SMS or through Wi-Fi. Besides, it also can alert the user by sending the SMS to the user when the energy usage is exceeds or when it receives any demand side requests [2]. There are many types of smart energy meter. This type is depending on the controller of the energy meter such as using the energy meter chip for the controller or using the other microcontroller. For instance, Arduino power meter is a power meter that is using the Arduino as the microcontroller. Basically, the microcontroller is needed in order to process all the signals or data from the inputs such as the current and voltage sensor. Then, it will calculate the power consumption based on the formula that are been uploaded into the microcontroller. Next, it will display the output and send the energy consumption information to the user. So, the main objective is to educate the consumer about the effective use of household appliances for energy saving.

C. Environmental Issues

In this modern day, people cannot live without electricity. With the existence of electricity, their works become easier and simpler. But, do all of us realize that the electricity that we are using today will bring effect to the environment? High energy consumption will lead to the increasing of the carbon intensity and greenhouse effect. Mostly the increasing of energy consumption in our home is due to air conditioning, lighting, heating and refrigeration. So, consumers must be aware to this environmental issue since all of share the same Earth. So, all of us must take initiatives to reduce our energy consumption by monitoring our energy usage.

1) Carbon Intensity of Energy Supply

Carbon intensity is a measure of the amount of CO2 that is released into the atmosphere for every unit of energy produced. Based on the studies, in 2014, 25% of the greenhouse gas emissions are due to the electricity production. In addition, about 65% of our electrical energy generate by the power generation station comes from the combustion of the fossil fuels such as coals and natural gases.

2) Greenhouse Effect

Greenhouse effect is the process of absorption and reemission of long wave radiation by the greenhouse gases in the atmosphere [13]. Gases such as carbon dioxides (CO2), methane (CH4), chloro fluoro carbon (CFC), nitrous oxide (N2O), Ozone (O3), water vapor are some of the greenhouse gases. Based on the research, it is found that 66% of the total magnitude of the greenhouse effect is contributed by the carbon dioxide gases alone [13]. That is why the controlling of the emissions of carbon dioxide gases is important in order to reduce the greenhouse effect. So, the overall gain in monitoring and controlling the energy usage is to have better energy efficiency and low greenhouse gas emissions.

III. METHODOLOGY

Figure 1 below shows the planning flow of the whole work for first semester and second semester for this project.

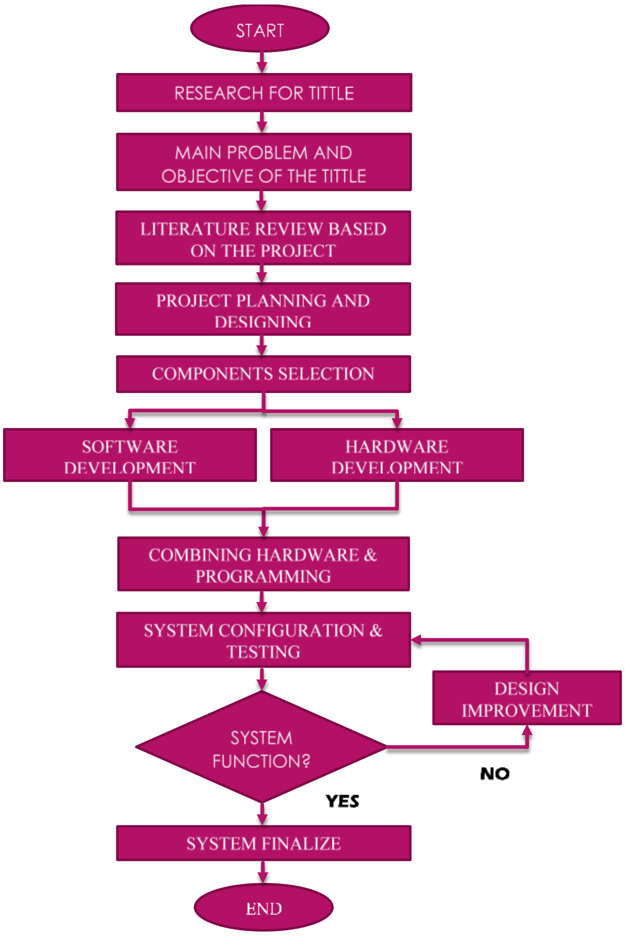

Fig. 1. The project flow diagram for entire research study

A. Hardware Implementation

1) Microcontroller Arduino Uno

Microcontroller is the most crucible part in this project. Since it is function to control whole system, so, Arduino UNO is used as the main component in this project. The reason why Arduino UNO is chosen because it has its own software to communicate with computer and included almost everything needed to support the programs. In addition, it also has digital and analogue ports for connection with much type of sensors, motors, module and switches.

2) Current Sensor SCT 013-000

The split core current transformer SCT-000 is used to measure the current flow to the loads. This current sensor can measure up to 100A. It consists of primary winding, magnetic core and secondary winding. It is a clamped-type sensor which can be clipped directly on either the live or neutral wire coming into the appliances or buildings.

3) AC Voltage Sensor ZMPT101B

ZMPT101B voltage sensor module is a voltage sensor made from the ZMPT101B voltage transformer. It has high accuracy, good consistency for voltage and power measurement and it can measure up to 250V AC. It is simple to use and comes with a multi turn trim potentiometer for adjusting the ADC output.

4) Global System for Mobile Communication (GSM) Module SIM800L

GSM module is a wireless modern that works with a GSM wireless network. It requires a SIM card from wireless carrier to operate like a GSM mobile phone. Furthermore, it supports an extended set of AT commands and with this extended action such as sending SMS.

5) Liquid Crystal Display Module

This 16X2 LCD display was used to display the power consumption and the billing price. Compared to other electronic display modules, LCD display is simple and easy to handle. This module is also familiar to be used with Arduino.

B. Software Implementation

1) Arduino Programmer

For Arduino programs, it is possible to be written in any programming language with a compiler which will produce binary machine code. In addition, the Arduino board is open source which refers to a hardware that is reasonably priced and the software is free from the internet.

IV. RESULT AND DISCUSSION

A. Completed set up of Smart Energy Meter

The smart energy meter that was completely developed is used to measure the energy consumption of the electrical appliances in houses or buildings by clamping the current sensor directly to the loads and connecting the voltage sensor probes parallel to the source of loads. Even though this device was safe to use by anybody, the user must take the precious step during conduct this device especially when clamping the current sensor on live wire. Figure 2 below shows the completed Smart Energy Meter.

Fig. 2. Completed Smart Energy Meter

Before this meter can be used to measure the power consumption, it needs to calibrate in order to get more accurate current and power values. The calibration takes place at the laboratory where a load bank was used to measure the power consumption. Then, after the Smart Energy Meter is calibrated, the loads were increased by switch on the load at the load bank. Figure 3 below shows the setup of smart energy meter during the calibration test.

Fig. 3. Calibration process using power analyzer

After that, the amount of energy usage and the billing price is displayed on the LCD display and the power consumption information is sent to the user automatically when the power consumption is reached certain value as it was programmed. Figure 4 below show the information of power consumption and the billing price sent to the consumer via GSM Sim800L.

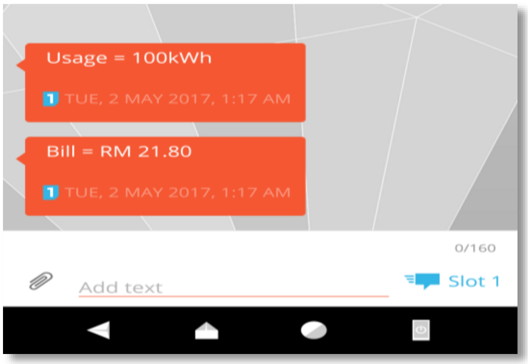

Fig. 4. Power consumption information and billing price

B. *Energy Consumption Usage by Selected Appliance*

Power analyzer is an instruments for measuring various parameters of an electrical power distribution system such as sing phase system voltage, power factor, instantaneous power in Watts, frequency, energy in Watt-hours and others.

There are six loads measured by the power. The real time information of energy consumption and billing price can be indicated from the LCD display. There are two types of reading were taken during the test which are actual value and measured value. Actual value is the value of parameters measured by the power analyzer while the measured value is the value of parameters measured by the smart energy meter. The current, voltage and power measured by both of the meters were collected and compared in Table 4.4 below.

TABLE II. COMPARISON OF CURRENT , VOLTAGE AND POWER READINGS FROM TWO DIFFERENT METERS.

Load		*Irms (A)*	*Vrms (V)*	*Power (W)*
R_1L_2 (pf = 0.91)	Actual	0.83	232	175
	Measure	0.85	230.28	165.85
R_1L_3 (pf = 0.95)	Actual	0.88	233	195
	Measure	0.86	231.10	169.22
R_1L_4 (pf = 0.97)	Actual	0.90	234	205
	Measure	0.89	233.52	176.92
R_2L_3 (pf = 0.85)	Actual	1.53	227	298
	Measure	1.50	225.73	288.64
R_2L_4 (pf = 0.91)	Actual	1.65	228	342
	Measure	1.62	226.47	311.12
R_3L_4 (pf = 0.84)	Actual	2.21	224	411
	Measure	2.18	223.19	414.40

TABLE III. THE PERCENTAGE ERROR OF CURRENT AND VOLTAGE READING

Load	Percentage Error (%)	
	Current Error	*Voltage Error*
R_1L_2	2.410	0.741
R_1L_3	2.273	0.815
R_1L_4	2.222	1.150
R_2L_3	1.961	0.559
R_2L_4	1.818	0.671
R_3L_4	1.357	0.362

From the result in Table II, the readings from the current sensor and voltage sensor approximate to the readings from the power analyzer. There are small errors in the measurement of current and voltage which leads to small error of power consumption measured. Based on the collected data, most of errors of measurement are less than 5%.

V. CONCLUSION

As a conclusion, smart energy meter is successfully designed where it can display the power consumption and the billing price. The pattern of power consumption and the bill price can be seen clearly on the LCD display and also via sending message to the consumer. It helps the consumer to understand their power usage and bills. By showing the electricity consumption and bill price is the best way to increase the consumers' awareness about the power usage, hence encourage them to reduce the energy consumption in their daily life.

REFERENCES

[1] Md. Masudur Rahman, Noor-E-Jannat, Mohd. Ohidul Islam and Md. Serazus Salakin, "Arduino and GSM Based Smart Energy Meter for Advanced Metering and Billing System", Electrical Engineering and

Information Communication Technology (ICEEICT), 2015 International Conference, 2015.

[2] Himshekhar Das and L.C. Saikia, "GSM enabled smart energy meter and automation of home appliances", Energy, Power and Environment: Toward Sustainable Growth (ICEPE), 2015 International Conference, 2015.

[3] Arif, A., et al. Experimental study and design of smart energy meter for the smart grid. in Renewable and Sustainable Energy Conference (IRSEC), 2013 International. 2013. IEEE.

[4] G. Aurilio, D. Gallo, C. Landi, M. Luiso, V. Cigolotti and G. Graditi, "Low cost combined voltage and current transducer for Smart Meters", Instrumentation and Measurement Technology Conference (I2MTC) Proceedings, 2014 IEEE International, 2014.

[5] Haroldo L. M. do Amaral, André N. de Souza, Danilo S.G., Filipe F. and Zita V., "Smart meters as a tool for energy efficiency", Industry Applications (INDUSCON), 2014 11th IEEE/IAS International Conference, 2014.

[6] I. Opris and L. Caracasian, "The relation between smart meters and electricity consumers", 2013 12th International Conference on Environment and Electrical Engineering, 2013.

[7] Nattachart Tamkittikhun, Thitinan Tantidham and Puwadech Intakot, "AC Power Meter Design Based On Arduino: Multichannel Single-Phase Approach". Computer Science and Engineering Conference (ICSEC), 2015 International, 2015.

[8] Nattachart Tamkittikhun, Thitinan Tantidham and Puwadech Intakot, "AC Power Meter Design For Home Electrical Appliances". Electrical Engineering/Electronics, Computer, Telecommunications and Information Technology (ECTI-CON), 2015 12th International Conference, 2015.

[9] Muhammad Bilal Khan and Muhammad Owais, "Automatic Power Factor Correction Unit". Computing, Electronic and Electrical Engineering (ICE Cube), 2016 International Conference, 2016.

[10] Fransiska R.W. , Septia E.M.P. , Vessabhu W.K. , Frans W. , Abednego W. , and Hendro"Electrical Power Measurement Using Arduino Uno Microcontroller And Labview". Instrumentation, Communications, Information Technology, and Biomedical Engineering (ICICI-BME), 2013 3rd International Conference, 2013.

[11] Vinayak Sonandkar, Arun Bhati, Dheeraj Gupta, Shivdayal Chouhan, Nandkishor Kinhekar, and Narayana Prasad Padhy, "Power Measurement Using Arduino For Effective Demand Response". Power Systems (ICPS), 2016 IEEE 6th International Conference, 2016.

[12] Bryce J. Griffler, "Hômenergy: A System To Reduce Home Energy Usage For Systems And Information Design Symposium". Systems and Information Engineering Design Symposium (SIEDS), 2010 IEEE, 2010.

[13] Patrick Gougeon, Kostas Andriosopoulos and Othman Cole, "Improving Carbon Efficiency: Is Economic Growth So Favourable?". European Energy Market (EEM), 2012 9th International Conference, 2012.

[14] 14. R. Samuel Selvaraj and V. Sivamadhavi, "Magnitude Of Green House Effect And The Contribution Of Carbon Di Oxide View Document". Recent Advances in Space Technology Services and Climate Change (RSTSCC), 2010.

[15] 15. Naimah Binti Mohammad. (2014). Smart Power Meter, Universiti Teknologi Malaysia (UTM).

[16] P. Zhang, "CHAPTER 5 - Microprocessors," P. B. T.-A. I. C. T. Zhang, Ed. Oxford: William Andrew Publishing, 2010, pp. 155–214.

[17] J. M. Pearce, "Chapter 4 - Open-Source Microcontrollers for Science: How to Use, Design Automated Equipment With and Troubleshoot," J. M. B. T.-O.-S. L. Pearce, Ed. Boston: Elsevier, 2014, pp. 59–93.

[18] 18. J. Sarik and I. Kymissis, "Lab kits using the Arduino prototyping platform," Frontiers in Education Conference (FIE), 2010 IEEE. pp. T3C–1–T3C–5, 2010.

Static Shielding Analysis for Improving String Efficiency of Glass Insulators in Transmission Line

Anis Syahidah Mohd Rahim
Faculty of Electrical Engineering
Universiti Teknologi Malaysia
Johor Bahru, Malaysia.
anisss.rahim@gmail.com

Dr. Mohamed Afendi Mohamed Piah
Department / Center of High Voltage and High Current
Faculty of Electrical Engineering
Universiti Teknologi Malaysia
Johor Bahru, Malaysia.
fendi@fke.utm.my

***Abstract*—This paper presents the effect of static shielding that also known as grading ring on the performance of voltage distribution along glass insulators in transmission line system. This is because of the non-uniformly of voltage distribution occur along the glass insulator string. It is found that after static shielding implemented to the system, the string efficiency of glass insulator strings are increased from 30.77% to 42.75%, 42.21%, and 43.03% according to the different design of guard ring respectively.**

Keywords—static shielding; transmission line; glass insulator; string efficiency

I. INTRODUCTION

Insulator acts as a device which is used on the electricity supply network system. This device completely resists the flow of the electric charge. There are several types of insulator which are pin insulator, suspension insulator and strain insulator. Insulator plays a significant role in the transmission line. The overhead insulator is an insulator that support the live wire to the transmission tower and at the same time avoiding any current flowing through it [1]. This transmission tower is a tall structure that is made up of steel lattice. Voltage level of transmission line systems is depending on the number of insulators in a string as shown on the TABLE 1.

TABLE I. NUMBER OF INSULATORS IN SUSPENSION STRING [2]

Voltage (kV)	33	66	132	230	400	750
Number of Units	3-4	5-7	9-11	14-20	18-21	30-35

The information of voltage distribution within high voltage insulators is very significant and helpful for engineers to design and plan the insulation of power lines. In addition, it contributes many advantages such as voltage distribution may valuable to detect inflated insulators in a string [3].

The operational voltage or the voltage distribution along glass insulator string is affected by the existence of stray capacitance, which may cause a non-uniform voltage distribution. This problem may lead to flash over or insulator breakdown of the system as well as affecting to the operation of transmission lines [4]. Moreover, the issue also effect the string efficiency of glass insulators. In order to explain these activities and phenomena clearly in this research, two equivalent circuit that take the insulator material properties and the stray capacitance is analysed using in the Multisim Analog Device software. The simulation is conducted to analyse the voltage distribution along the insulator string with and without guard ring. During experimental procedure, the voltage distribution and string efficiency need to be measured and calculated among without and with guard ring with different design of guard ring.

II. METHODOLOGY

During this project, several methodologies have been come out to analyze the data. Firstly, design of project flow is created for investigating the sequence of task that need to be done for these two semesters. There are two approaches in completing the data analysis, which are simulation approach and experimental approach.

A. Simulation Approach

The simulation software that used to simulate the circuit diagram of five glass insulators in transmission line systems is Multisim Analog Software. In this simulation, it highlights the the clean suspension glass insulators condition. There are two different circuits for simulation which are circuit without guard ring and circuit with guard ring. Voltage distribution across each insulator has been measured and string efficiency of glass insulators is calculated by using string efficiency formula. Hence, the data of voltage distribution and string efficiency have been compared between equivalent circuit without guard ring and with guard ring as well as the performance of the string insulator supposedly should be improved.

B. Experimental Approach

Experiment for this project was conducted at high voltage laboratory In this experiment, voltage distribution of string glass insulators was measured in several conditions. First, measuring voltage distribution when the string glass insulators without installing guard ring. Next, voltage distribution also measured when the string glass insulators connected to guard ring with different design of guard ring. For the measurement purpose, voltage divider method was used in this experiment. Thus, the string efficiency of the glass insulators was calculated for the both conditions and the value of stray capacitance was determined. Fig. 1 shows the sample of glass insulators and different types of guard rings that used in the experiment are shown in Fig.2-4:

Fig. 1. Sample of glass insulators

Fig. 2. Design 1 of guard ring

Fig. 3. Design 2 of guard ring

Fig. 4. Design 3 of guard ring

The five glass insulators need to be cleaned before setting up the experiment in order to prevent from contamination problem. Then, the insulators were arranged in suspension (series) form. A voltage divider 100 μF and 1000 kVA was used for measuring the voltage across each insulator. Fig 5. shows the setup of the experiment:

Fig. 5. Experimental set up for insulator string without guard ring

The experiment was conducted on three different design of guard rings. Fig. 6 shows the experimental set up for insulators string with guard ring installed at high voltage electrode.

Fig. 6. Experimental set up of insulator string with guard ring

The measured voltage across each insulator string were used to calculate the string efficiency. The higher the string efficiency the more uniform voltage distribution of each insulator [5]. The calculation of the string efficiency is shown in equation (1).

$$\text{string efficiency} = \frac{\text{voltage across insulator}}{\text{n (voltage insulator nearest to line)}} \qquad (1)$$

where n is the number of insulators in a string [5].

Fig.7 exhibits the schematic diagram with the voltage to be measured.

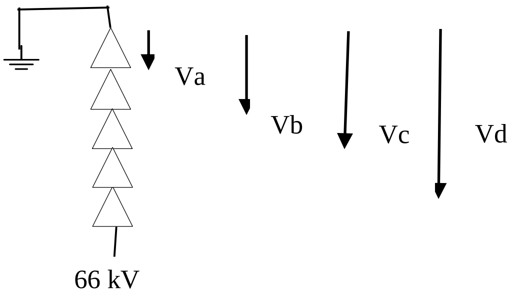

Fig. 7. Schematic diagram of insulator string

Voltage distribution across each insulator is calculated by using equation (2)-(6), where V_1 is for insulator nearest to the high voltage line.

$$V_1 = 66\,kV - V_d \qquad (2)$$

$$V_2 = V_d - V_c \qquad (3)$$

$$V_3 = V_c - V_b \qquad (4)$$

$$V_4 = V_b - V_a \qquad (5)$$

$$V_5 = V_a \qquad (6)$$

III. Result and Discussion

The results from experimental and simulation are illustrated using graphs and charts. A 66 kV of AC voltage wa applied to the insulator string. Insulator 1 is the one that nearest to the high voltage line and insulator 5 is nearest to the ground. All of results of voltage distribution are used to calculate the string efficiency of insulators.

A. Simulation Result

Based on the simulation work of Fig. 8, the voltage distribution along the insulators is non-uniformly. The value of U1 which the insulator nearest to the line conductor is the highest voltage among the others while value of U5 is the lowest. This is because of the existence of stray capacitance in the system that influence on the measurement of voltage distribution.

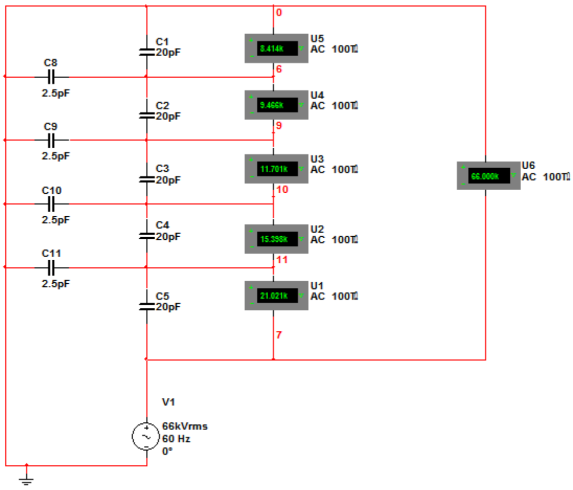

Fig. 8. Simulation analysis of insulator string without guard ring

After installation of guard ring to the circuit which is represent as a shunt capacitance, the voltage distribution become more uniformly. The values among the five insulators almost same and do not have a lot of difference between them.

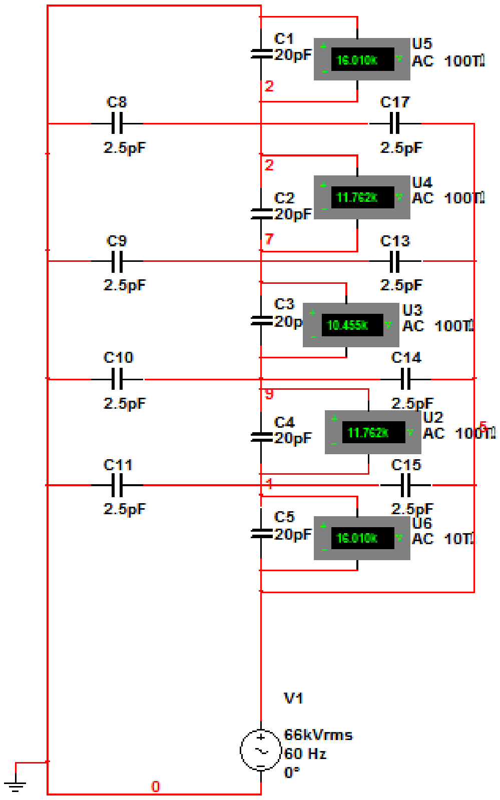

Fig. 9. Simulation analysis of insulator string with guard ring

B. Experimental Result

During the experiment, the values of voltage that recorded are inject voltage and measuring voltage of the glass insulator string. From the data obtained, calculation need to be done to get the voltage across each insulator. Each experiment is repeated until three times in order to obtain the accurate value.

According to the Fig. 10-13, the values across each insulator in each experiment are illustrated as a chart. Even though the data obtained for the glass insulator string with guard ring are not have a big difference to the glass insulator without guard ring, there still show the pattern of the voltage distribution along the glass insulator become more stable compared to without guard ring. It is due to the presence of shunt capacitance that can eliminate the stray capacitance in the system.

The voltage distributions across the string insulators with and without guard ring are exhibited in Fig. 10 to Fig. 13. Generally, the existing of guard ring will improve the string efficiency of the insulators. However, the results obtained are not very convincing due to the not properly clearance of the test objects that set-up in the laboratory.

1) For Glass Insulator String without Guard Ring

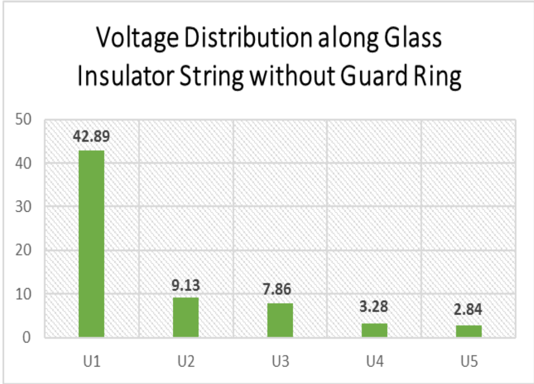

Fig. 10. Voltage distribution across each insulator without guard ring

2) For Glass Insulator String with Guard Ring

a) Design 1

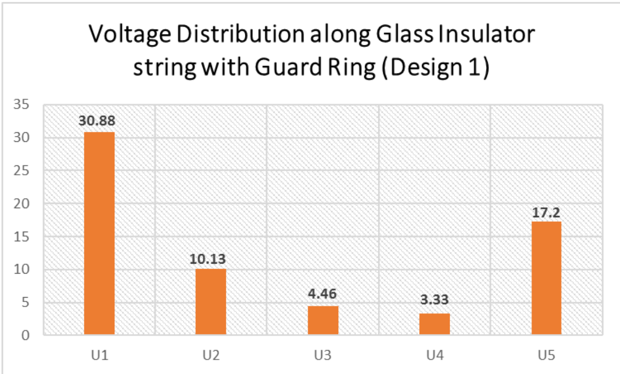

Fig. 11. Voltage distribution across each insulator with guard ring (Design 1)

b) Design 2

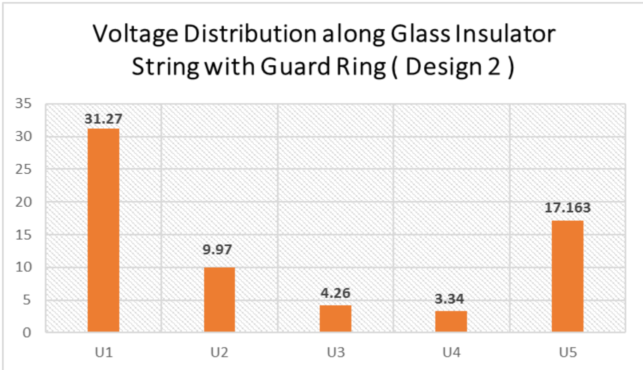

Fig. 12. Voltage distribution across each insulator with guard ring (Design 2)

c) Design 3

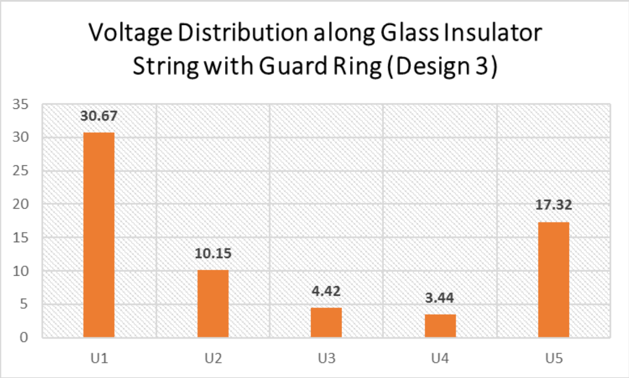

Fig. 13. Voltage distribution across each insulator with guard ring (Design 3)

Regarding to the result obtained, the string efficiencies are calculated using equation (1) and illustrated in the chart form as shown in Fig. 14. The result demonstrates that the string efficiency shows some improvement when the guard ring is installed at the string insulators. The string efficiency is increased from 30.77 % to 42.75 % (design 1), 42.21 % (design 2) and 43.03 % (design 3) respectively.

It concludes that the guard ring with Design 3 gives the best result in string efficiency compared to other design. Also shows that different design of guard ring would give different effect to the voltage distribution of transmission line string insulators system.

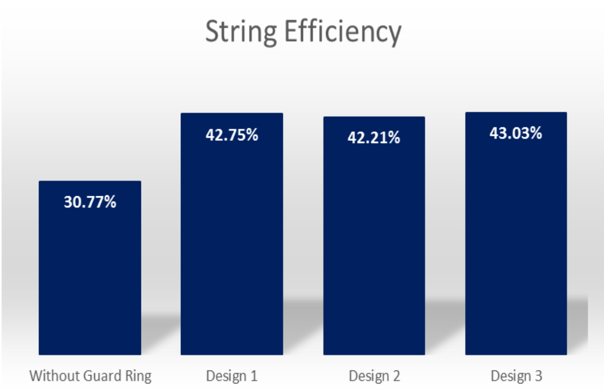

Fig. 14. String efficiency of each experiment

IV. CONCLUSION

It has been observed that the capacitance values can adjust the voltage distribution on insulator string units up to the desired level as expected. The voltage on a string of suspension insulators does not distribute itself uniformly across each insulator due to the existence of shunt or stray capacitance. The disc nearest to the high voltage conductor has maximum voltage across it. The string efficiency can be improved by introducing guard ring. This static shielding would improve the effectiveness of the insulator string in transmission line by introducing the effect of shunt capacitance and thus making voltage distribution across each insulator more uniform.

V. ACKNOWLEDGEMENT

The authors would like to thank Universiti Teknologi Malaysia (UTM), for the use of facilities and by awarding the research grants under vote number of 12H07 from UTM and 4F751 from Malaysia Ministry of Higher Education (MOHE).

REFERENCES

[1] MB Asadpoor, “Simulation and measurement of the voltage distribution on high voltage suspension Porcelain insulator string under pollution condition,” *Int. J. Appl. Sci. Eng. Res.*, vol. 1, no. 1, pp. 165–175, 2012.

[2] B. Wireless and A. Systems, “IEEE Standards,” *Access*, vol. 2004, no. October, 2004.

[3] N. Tonmitr, E. Kaneko, K. Tonmitr, A. Kaewrawang, and A. Suksri, “The Measurement of the Voltage Distribution along High Voltage Suspension Porcelain (5-6-7 Insulator)/String in Case of Clean Condition,” *Appl. Mech. Mater.*, vol. 752–753, pp. 1133–1138, 2015.

[4] S. Kumar, P. Anil, K. Kori, and J. E. College, “Evaluation of String Efficiency and Voltage Distribution of 400 KV over a String of Glass Suspension-Type Insulator in Different Atmospheric Condition,” vol. 4, no. 5, pp. 694–699, 2016.

[5] E. Akbari and M. Mirzaie, “I NVESTIGATING THE E FFECTS OF D ISC I NSULATOR T YPE AND C ORONA R ING ON V OLTAGE D ISTRIBUTION OVER 230- KV I NSULATOR S TRING U SING 3-D FEM,” vol. 3, no. 1, pp. 1–8, 2012.

[6] E. A. Cherney *et al.*, “Evaluation of and replacement strategies for aged high-voltage toughened glass-suspension insulators,” *IEEE Trans. Power Deliv.*, vol. 30, no. 3, pp. 1145–1152, 2015.

[7] A. B. Patel, “G LOBAL J OURNAL OF E NGINEERING S CIENCE AND R ESEARCHES INVESTIGATION OF CERAMIC AND NON-CERAMIC SUSPENSION INSULATOR,” vol. 2, no. December, pp. 77–84, 2015.

[8] F. Hanani *et al.*, “UNIVERSITI TEKNOLOGI MALAYSIA DECLARATION OF THESIS / UNDERGRADUATE PROJECT Name of Supervisor : Date,” vol. 16, no. June, 2015.

[9] N. A. Othman, M. A. M. Piah, Z. Adzis, and H. Ahmad, “Measurement of surface charge distribution on glass insulator using steel mesh,” *Conf. Proceeding - 2014 IEEE Int. Conf. Power Energy, PECon 2014*, pp. 105–108, 2014.

Smart Switch for Home Automation Application

Nabilla Wahida binti Khalid
Faculty of Electrical Engineering
Universiti Teknologi Malaysia
41310 Skudai, Johor, Malaysia
nabillawahida@gmail.com

Dr. Md. Pauzi bin Abdullah
Faculty of Electrical Engineering
Universiti Teknologi Malaysia
41310 Skudai, Johor, Malaysia
mpauzi@utm.my

***Abstract*—A smart switch that is equipped with wireless technology that are able to communicate with each other seamlessly is proposed to correspond in home automation application. The wireless technology produces an alternative way to connect the smart switches without a call for restructures the wiring system in homes. Generally, home with automation system will require a new wiring installation that fit the specifications of the system, which can cost you a fortune. To test the effectiveness of the communication medium, several wireless technology have been taken into account including Bluetooth, Wi-Fi, ZigBee, Infrared, and Power Line Communication. In addition, the wireless technologies are classified in term of its capabilities and compatibilities to home automation application.**

Keywords—smart switch; home automation; wireless technology; Arduino.

I. INTRODUCTION

In the modern era that is advancing very rapidly, everything is getting smarter from the littlest thing as our watch to the big home we live in. Smart home innovations seem to be everywhere lately, whether it is smart security, energy, entertainment or automation that helps in simplifying our daily lives. Consumers increasingly expect technology to provide them with seamless experiences that improve their lives. Whilst security system outstrips the chart of the appeal category of smart home solutions, the home automation catches up as the second place with the idea of having our home under control at the tip of our finger. Over and above, the system can be assessed anywhere at anytime of our likings.

Despite our ignorance in this matter, home automation technology has been around for up to several decades now. The home automation technology is getting common in our everyday use for it helps in simplifying our everyday life, allowing us to take more control with advanced automation solutions. However, the industry as a whole has been slow to take off due to the clunky, hard-to-use system with very expensive cost that required professional installation.

On top of acquiring home automation system, proper wiring is an essential phase so that all of your devices can communicate with each other seamlessly. Professional experiences are needed to do so and they, of course, do not come with low prices. Though enthusiasts do not mind paying a fortune installing home automation in existing home, it is going to cost a whole lot less before the walls go up. Nevertheless, this does not mean that someone with existing home should not consider of having smart home. It just costs a whole heap and that is the major reason of why home automation has not received much demand and attention, adding to the complexity of installing it and configuring it.

Fig. 1. Existing home wiring system that requires new installation to meet the specifications of automation system.

II. LITERATURE REVIEW

The study will cover on the overview of home automation system to get more idea of how the system works. On top of that, the study will also go through different type of microcontrollers that will be then used as the ‘brain’ of the smart switches. Besides, several mediums of communication technology have also been studied.

A. Home Automation System

Home Automation is not a really a new thing in this era of information technology. Even so, none of the arrangement or specification has made it into the standard yet. Home Automation is amongst the branches of the broad term – Smart Home. Slightly more focus, home automation particularly referred to appliances in the household that are programmable to function automatically. Past years show the automation was only on the basic appliances of the household, but the rapid change of the recent technology spread the functionality of home automation to a more advance level. The possibilities ranges to a wider scope of appliances: from lights, locks, cameras and even coffee makers [15]. The idea of home automation gives a remote interface to home appliances via the home computerization through phone lines or Internet.

B. Microcontroller

Any devices that can be remotely controlled contain at least one microcontroller and can have as many as six or seven. Basically, a microcontroller is a cheap, small version of computer and the devices that are implemented with this component are capable of interacting with its user.

Microcontrollers are commonly applied in embedded system to employ automation in its applications.

1) Raspberry Pi

The Raspberry Pi is a credit-card-sized SoC device that plugs into a monitor and a keyboard. It is entrusted for the use in many electronic projects due to its capability as a little computer [1]. There is not much different to other fully functioned computer, Raspberry Pi requires an OS to operate. Basically, Raspberry Pi runs on Raspbian, which is a specially designed Linux operating system for the device, to enable its functionality. Raspbian is the official OS where other third party operating systems can be installed on.

Just like any other computer, Raspberry Pi has memory, processor, USB ports, audio output, a graphic driver for HDMI output and as it runs on Linux, most of the Linux software applications can be installed on it. [2] Several models and revisions of the device are Raspberry Pi, Raspberry Pi 2, Raspberry Pi 3, and Raspberry Pi Model B+. Further characteristics of Raspberry Pi will be discussed more in the next subtopic.

2) Arduino

Arduino is often used in building electronic projects through its open-source platform with a physical board base or better known as microcontroller and IDE to program the physical board. Unlike Raspberry Pi, Arduino functions well with just several lines of code without any OS and software application [2] but are not as much powerful as the Raspberry Pi. The commonly used versions of Arduino board that are available in the current market are Arduino UNO, Arduino PRO, Arduino MEGA, and Arduino DUE. Arduino boards read inputs and turn it into an output. In fact, the board can interact with buttons, LEDs, motors, GPS units, the Internet and even any smart devices.

3) Raspberry Pi vs. Arduino

Both Raspberry Pi and Arduino are quite different in each and every discipline. Though some of the difference gave disadvantages to one side, some others might be the strength of the other. The following table comprises the comparison between the Arduino and Raspberry Pi.

TABLE I. COMPARISON OF ARDUINO AND RASPBERRY PI

Criteria	Arduino	Raspberry Pi
Simplicity	Very easy to interface analog sensors and other electric component	Need to install some libraries and softwares for interfacing the components
	Simpler coding	Needs to have knowledge of Linux and its command
Robustness	Can be turned ON and OFF at any point of time without any risk damage	Must be properly shut down before turning OFF the power, otherwise, the OS and applications might get corrupted
Power Consumption	Less power	Continuous 5V supply
	Easily powered using battery pack	Difficult to run on batteries
Price	Cheaper	More expensive
Powerfullness	Less capable of doing multiple task	More capable of doing multiple tasks and 40 times faster
Networking	Needs external hardware or shield to connect to networks	Has built in Ethernet port which can be directly connected to

C. Wireless Technology

1) Power Line Communication (PLC)

As the name goes, the idea of how this technology works is obviously predictable – Power Line. Unlike other communication technology that will be compared in this project, Power Line Communication is not actually wireless but it does not need any new wires. Power Line Communication or Power Line Carrier, is a system that enables sending data over existing power cables that is also used for electric power transmission [5].

Beyond our concern, the inception of PLC in actuality is not as relatively recent as we thought but around 1890's [6]. As a matter of fact, the first power line signaling was proposed in the United Kingdom. Generally, PLC can be classified into two parts and that is Narrowband PLC and Broadband PLC. The following Table 2.4.1(a) shows the difference between these two types of PLC.

TABLE II. NARROWBAND PLC VS. BROADBAND PLC

Narrowband PLC	Broadband PLC
Lower frequencies (3-500 kHz)	Higher frequencies (1.8-250 MHz)
Lower data rates (up to 100s of kbps)	High data rates (up to 100s of Mbps)
Longer range (up to several kilometers)	Shorter range applications

2) Wi-Fi

Unlike PLC, Wi-Fi is a wireless technology designed for WLAN that requires no wire or cables, be it the new or existing. Wi-Fi provides a network connection via radio waves. A wireless adapter is needed to establish a Wi-Fi connection by creating hotspots or areas in the wireless router locality that are connected to the network and allow users to access Internet services [8].

Wi-Fi is the most common wireless network used in computer networking for its ultimate characteristics which is fast connection, high data rate, secure and satisfactory range [14]. Wi-Fi is more appropriate to use in large data rate application. This wireless network offers dynamic rate functionalities with data rates of 11Mbit/s.

3) ZigBee

ZigBee is quite a new network that is developed recently. Though, its application in smart home is so wide despite the number of years it is being established. The popularity of this network outgrows most of the well-established existing wireless network in so many ways. The ZigBee is commonly used in low-power WLANs that cover huge vicinity region via a mesh network specification.

The low duty cycle of the network and its power consumption makes it the best consideration to provide high data throughput in applications. Its wide application in industrial automation and physical plant operation makes it familiarly associated with M2M communication and the IoT [9]. There are three ZigBee specifications that are available in current market, which are ZigBee, ZigBee IP and ZigBee RF4CE.

4) Bluetooth

Bluetooth made its first appearance as a consumer technology in 2000 and it is still going strong even after more than a decade. The standard of this wireless network continues to improve, speeding up the transfer times and reducing the power use, which is much favorable in portable devices such as smartphone and smart watch. Bluetooth is a wireless communication protocol to connect devices through the air. Even though it is not as powerful as Wi-Fi but the setup is much simpler, and is usually preferred for device-to-device transfers [10].

Suitable for the usage in ad hoc network, Bluetooth uses the unlicensed band of 2.4 GHz and implement frequency hopping to resist interference and selective fading. The network devices detect and connect to one another automatically and can handle up to eight of them at one time. The network implements the frequency hopping when two devices want to talk but the other is already taken, thus it randomly switches to one of the others. In order to minimize the risks of interference from other electrical appliances and improving its security, pairs of devices constantly shift the frequency they are using up to thousands of times a second [11].

5) Infrared

This wireless technology conveys data through infrared radiation. Unlike any other wireless technology, IR wireless cannot penetrate through walls and this is its major weakness. However, it widely used in control and automation of electrical appliances in houses, but in a short range within the limited room of its locality. Therefore, the network is generally not possible to establish between different rooms in a house, or between different houses in a neighborhood. Despite of the disadvantage, IR wireless is more private that offer a level of security comparable to that of hard-wired systems [12].

6) Characteristics of ZigBee, Wi-Fi and Bluetooth

TABLE III. ZIGBEE, WI-FI AND BLUETOOTH CHARACTERISTICS

Criteria	ZigBee	Wi-Fi	Bluetooth
Data Range	250 kbps	11 & 54 Mbps	1 - 2.4 Mbps
Range	10 - 100 m	50 -100 m	10 m (can be extended)
Complexity (Device & App Impact)	Low	High	High
Power Consumption	Low	High	Medium
Cost	High	High	Medium

III. METHODOLOGY

The commencement of the project work is done with the execution of research on several wireless technologies that might be compatible for the home automation usage. The research comprises the related works that have been done by graduates of UTM and other related researchers.

As for the beginning, a relay switching circuit was designed to enable the load controlling by using the Arduino module. The loads are represented by a light bulb and will be turned ON and OFF to show the switching process. The controlling of the automation is done using the IR controller at the first stage. The circuit developed is used for the next part of the project, which is the Two-Way Switching Circuit development.

Upon completing the relay and two-way switch development, labor on both PLC transmitter and receiver shall proceed. On top of that, a home automation system should be developed as for the end product presentation. Once the hardware has been completed, it will be tested and troubleshooted if there is any error or problem occurs in the system.

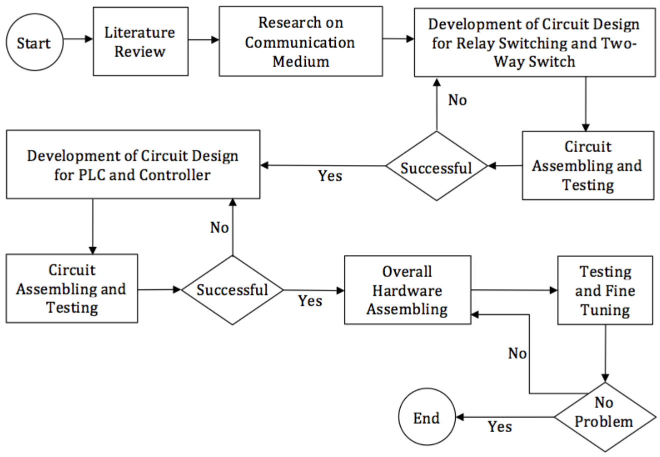

Fig. 2. Overall overflow for the development of the smart switch.

IV. RESULT AND DISCUSSION

The following describes the hardware implementation of the whole system.

A. 5V Supply for Relay and Arduino Use

The Arduino and relay used in the project are only functioning when there is voltage supplied. Both of the components needed supply of 5V DC while the rated voltage supplied to houses in Malaysia is 240V AC. The voltage supply can be obtained from dry cells or batteries. Nevertheless, the use of batteries in this project is not applicable and inconvenient. Nobody would want to change batteries of the wall-mounted switch every now and then. Thus, the alternative is to convert 240V AC to 5V DC via converter just like the one we have to charge our laptop and smartphones.

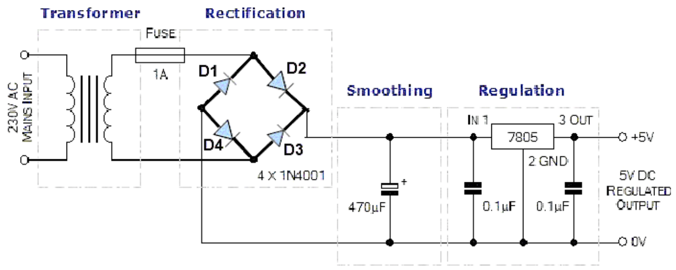

Fig. 3. The circuit used for 240V AC to 5V DC Converter.

B. Two-Way Switching

Two-way switching allows you to control from two locations. Basically, this two-way switch is widely used to control lamp in a number of places, particularly hallways and stairs. As stated in previous chapter, the switch should be remotely controlled both wirelessly and manually (normal way to turn ON and OFF appliances). Thus, two-way switch circuit is implemented to enable the function. The difference is the other switch is the relay switches that for the automation control. The following figures are the conditions of lamps for different position of switch in two way switching.

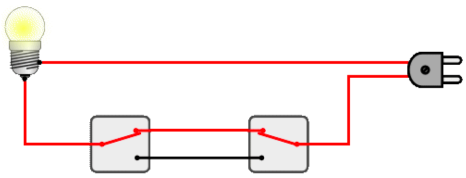

Fig. 4. Switch Position I – Lamp ON

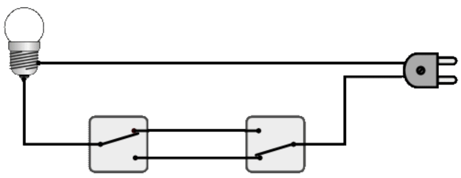

Fig. 5. Switch Position II – Lamp OFF

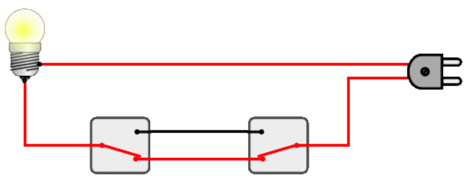

Fig. 6. Switch Position III – Lamp ON

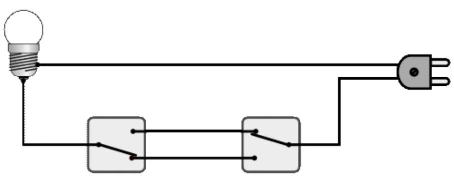

Fig. 7. Switch Position IV – Lamp OFF

C. Relay Module

The developed relay switching circuit is as provided in the Figure 8 below. As we can see in the figure, the power supply for the Arduino and the relay module is not of the same power supply. This is done to isolate the Arduino and the relay if any voltage spike or any unwanted event occurs. The isolation is done to protect the Arduino from damage due to such events. The role of the optocoupler IC in the relay module is to transfer the electrical signals between the two isolated circuits. Other than that, optocoupler also prevents high voltages from affecting the system receiving the signal.

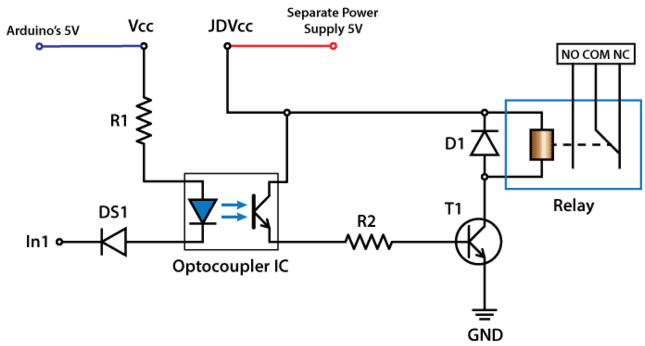

Fig. 8. Relay Switching Circuit

D. Arduino UNO Program Code

For the Arduino UNO to board to interact with the application of this project, a certain program code is required to be implemented to the Arduino UNO. As for the early stage of the project, the Arduino UNO is used to read the inputs from the IR receiver to turn ON and OFF the light bulb. In this early stage, the wireless IR is used to perform as a home automation system and for the purpose of affirming whether the designed relay switching circuit needed to be troubleshoot or not for further use.

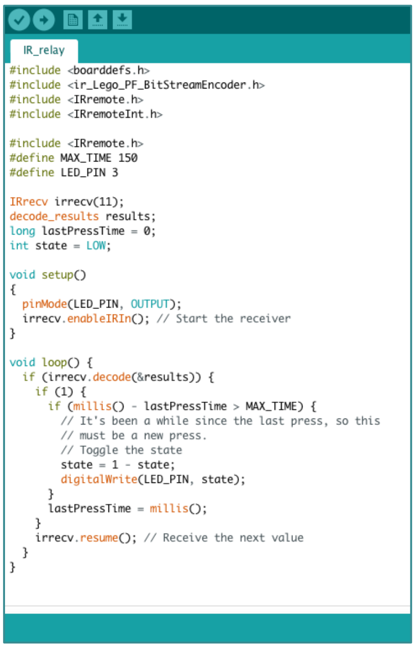

IR_relay

```
#include <boarddefs.h>
#include <ir_Lego_PF_BitStreamEncoder.h>
#include <IRremote.h>
#include <IRremoteInt.h>

#include <IRremote.h>
#define MAX_TIME 150
#define LED_PIN 3

IRrecv irrecv(11);
decode_results results;
long lastPressTime = 0;
int state = LOW;

void setup()
{
  pinMode(LED_PIN, OUTPUT);
  irrecv.enableIRIn(); // Start the receiver
}

void loop() {
  if (irrecv.decode(&results)) {
    if (1) {
      if (millis() - lastPressTime > MAX_TIME) {
        // It's been a while since the last press, so this
        // must be a new press.
        // Toggle the state
        state = 1 - state;
        digitalWrite(LED_PIN, state);
      }
      lastPressTime = millis();
    }
    irrecv.resume(); // Receive the next value
  }
}
```

Fig. 9. Arduino UNO Program Code for IR controller

CONCLUSION

The project aims to develop a smart switch that is equipped with wireless technology to communicate with each other seamlessly without restructuring the home wiring. The design of the smart switch for home automation application was completed for hardware implementation. Basically, the scope of this thesis is more on the usage in home automation. This concept will provide some benefit especially in term of cost, which the wiring installation cost, could be reduced by taking an alternative way using wireless communication technology to connect the system seamlessly.

REFERENCES

[1] FAQS – Introduction: What is Raspberry Pi. Retrieved from https://www.raspberrypi.org/help/faqs/#intro

[2] Jayant. Arduino vs Raspberry Pi: Differences between the two. Retrieved from http://circuitdigest.com/article/arduino-vs-raspberryp-pi-difference-between-the-two

[3] Margaret Rouse. (2006, April). Wireless. Retrieved from http://searchmobilecomputing.techtarget.com/definition/wireless

[4] Ahmed Sirajuddin Ahmed Alhaj. (2015, June 23). Home Automation System using Arduino. Universiti Teknologi Malaysia: Tesis Sarjana Muda.

[5] Muhammad Hafidzuddin Mazlan. (2009, May 15). Power Line Communication for Home Automation. Universiti Teknologi Malaysia: Tesis Sarjana Muda.

[6] Gilbert Held. (2006). Understanding Broadband over Power Line. New York, Auberbach Publication.

[7] Niovi Pavlidou, A.J. Han Vinck, Javad Yazdani & Bahram Honary. (2003, April). Power Line Communications: State of Art and Future Trends. IEEE Communication Magazine, 34-40.

[8] Christina. (2016, February 3). What is WiFi and How Does It Work? Retrieved from http://ccm.net/faq/298-what-is-wifi-and-how-does-it-work

[9] Margaret Rouse. (2015, March). Internet of Things: ZigBee. Retrieved from http://internetofthingsagenda.techtarget.com/definition/ZigBee

[10] David Nield. (2016, June 13). How To: What is Bluetooth? Retrieved from http://www.techradar.com/how-to/computing/what-is-bluetooth-1323284

[11] Chris Woodford. (2016, June 13). Bluetooth. Retrieved from http://www.explainthatstuff.com/howbluetoothworks.html

[12] Margaret Rouse. (20015, September). IR Wireless. Retrieved from http://searchmobilecomputing.techtarget.com/definition/IR-wireless

[13] (2011, August 17). EE Times – What is Power Line Communication? Retrieved from http://www.eetimes.com/document.asp?doc_id=1279014

[14] Sahrul Arif & Suhono Harso Supangkat. Simulation and Analysis of ZigBee – Wifi Interference.

[15] Ry Crist. (2015, March 3). Home Automation Buying Guide. Retrieved from https://www.cnet.com/news/smart-home-buying-guide-home-automation/

Energy Efficiency and Renewable Energy for Household

Ameera Wahida Solikhudin
Faculty of Electrical Engineering
Universiti Teknologi Malaysia
Johor Bahru, Malaysia.
aameerawahida7986@gmail.com

Dr. Law Kwan Yiew
Institute of High Voltage and High Current (IVAT),
Faculty of Electrical Engineering
Universiti Teknologi Malaysia
Johor Bahru, Malaysia.
kwanyiew@utm.my

***Abstract*—Solar is an alternative energy resource which are clean, inexhaustible, and environmental friendly. This study aims to save energy by using wide ranges of technologies and solutions for a conventional domestic building leading to green building. These include high efficiency lightings and installation of photovoltaic system. The system configurations comprise of 100% grid dependent and photovoltaic (PV)-grid connected system for two different of load profiles. HOMER software was used for the analysis of economic performance, electricity, and emission of pollutant gases. The result proved that, using high efficiency appliances for the domestic building with PV system are saved more energy and environmental friendly.**

Keywords—PV-grid connected; photovoltaic; lighting system; energy saving; power converter; domestic

I. Introduction

The analysis of final energy consumption by sectors show that residential and commercial sector is at third place after industrial sector and transportation [1]. From 1993, this sector contributed 11.7% of the energy consumption and roses by year until 2013 about 14.4% show that exploitation of non-renewable energy sources increasing [1]. Research proved that buildings consumes up to 40% can cause up to 1/3 of global contamination which is released of greenhouse gas (GHG) through fossil fuels burning in generating electricity [2]. For domestic building, lighting and air conditioning are dominant loads followed by ventilation, heating, and various plug loads. But, low efficiency of appliances used causes higher energy consumption and emission of pollutant gases. Hence, various approach need to be study such as using renewable energy sources and replacement of high efficiency appliances. The objectives of this project are; to compare on efficiency of different type of electrical appliances in reducing energy consumption; to investigate different method for reducing the electricity consumption of a bungalow house; and to simulate and analyze the economic performance of renewable system by using HOMER Software.

Lighting or illumination is an application of light to achieve some aesthetic or practical effect by includes the use of both artificial light source such as lamp and natural illumination of interiors from daylight [3]. Nowadays, a modern commercial building is likely dependent on artificial lighting. Artificial lighting is most commonly provided today by electric lights such as florescent lamp, light bulb, halogen lamp, LED types and more. Thus, interior lighting system is the dominant consumer of electrical energy which give impact as internal heat [3]. Recently developed energy efficient lighting equipment such as compact fluorescent lamps and electronic ballast can be used to help cutting down lighting operational costs by 30% to 60% while enhancing lighting quality, reducing environmental impact and promoting health and work productivity [4].

Photovoltaic (PV) panel is a capable material for converting the energy contained in photons of light into an electrical voltage and current. The direct current is produced from photovoltaic system and it can be convert to alternating current by using the inverter or power conditioning unit (PCU) or connected to grid connection. In other hand, photovoltaic system can operate as a stand-alone system with battery storage and a generator. The power requirement, location, and the available space on site will determine the size of the photovoltaic system. Using the renewable energy also benefits the user as nowadays Malaysia has taken steps to further clean energy deployment by mandating adoption of a renewable energy feed-in tariff (FiT) mechanism under the country's 2011 Renewable Energy Act. The FiT implementation process was designed to support rapid renewable energy deployment while also enhancing energy security and addressing climate change challenges [5].

II. Methodology

A. Defining Test System for Case Study

A domestic building of 2-level bungalow is used as the test system. It consists of five bedrooms with a bathroom, a formal living, two store rooms and a shoe room, a dining living, a kitchen, a laundry area, a music room, a family living, and a study room. The building's layouts consist of lighting system are drafted by using AutoCAD Software. To maximize the PV system performance, the annual peak sun hour (PSH) of the test system location must be high enough. Hence, the test system is conducted in Bayan Lepas, Pulau Pinang which at coordinated of 5˚18' N, 100˚ 15' E. The choice of test system was determined by the following factors:

- Availability of electrical appliances data
- A domestic building which consume high electricity
- High possibilities the owner can supported PV system installation cost
- Suitable location with high annual peak sun hour (PSH)

B. Data Collection of Proposed Electrical Appliances Used

For this domestic building, the load efficiency improvement only focused on the lighting system as it already specified in the layout. Specifications of each type are determined based on the datasheets from the manufacturers. While, the data of daily consumption for home electrical appliances are determined and analysed from TNB website [6]. All the conventional of lightings used were compared with the advanced lightings which consume less energy. The realization of efficiency of lighting system can be improved by replacement of the conventional light bulb with light emitting diode (LED) lamps and compact florescent lamps (CFLs). The comparison of data is showed in Microsoft Excel. The calculation of energy consumption and cost electrical bill are made to help analysing the daily load profile, as in

$$\text{Energy consumption (Wh/day)} = \text{Number of appliances x Power rating (W) x Usage hour} \quad (1)$$

$$\text{Cost of electrical bill (RM/day)} = \frac{\text{Total energy consumption (Wh) x Tariff A (RM/kWh)}}{1000} \quad (2)$$

C. HOMER Software

HOMER Software is a software application which has evolved in to a very robust tool for modelling both conventional and renewable energy technologies. It is a tool to use for designing renewable energy base system and most data can be extract as it commonly used to analyse for photovoltaic systems. The inputs of this software are load demand or load profile, resources such as solar irradiation, component details and cost for examples the size of the solar panel and its cost, and constrains. While, the outputs of this software including optimal sizing, net present cost(NPC), and cost of energy(COE), capital cost, capacity shortage, excess electricity, and renewable energy fraction.

D. Defining the Power System

Test system is proposed to use renewable energy by installing the photovoltaic system. Fig. 1 shows the equipment needs and the configuration of the system by using HOMER software. Grid connected is selected to support this photovoltaic system. For PV grid connected system, the battery component does not need as local grid can supply the electricity if the system cannot fully support the demand especially during night. Also, the excessive electricity can sell back to the grid based on Feed-in-Tariff (FiT).

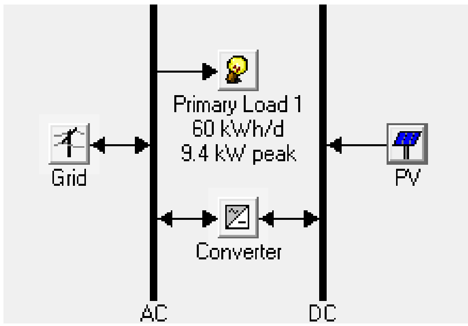

Fig. 1. Configuration of PV grid-connected system

By using HOMER software, the configuration can be design for different components including multiple loads, grid option, photovoltaic arrays and converters. The cost of each equipment used is determined based on Table I.

TABLE I. PV COMPONENTS PRICING [7]

Components	**Cost (RM)**
PV panel	5/Wp
Inverter	1/W
Installation	10% of PV cost
Operation and maintenance	2% of PV cost

E. Solar Resource Input

Database of solar resources are imported directly by HOMER from the NASA Surface Meteorology and Solar Energy database by entering the GPS coordinates. Using the coordinates from the Wind Resource section, the annual solar radiation of the selected location is 4.85 kWh/m²/day. The trend of monthly solar radiation shows almost constant which peak radiation only in February, 5.341kWh/m²/day and March about 5.356 kWh/m²/day. While, the lowest radiation is 4.571 kWh/m²/day in November. But, for the rest months show that the average radiation almost has constant trend from 4.663kWh/m²/day to 5.162kWh/m²/day. Hence, it proved that the selected location is suitable to run this project as all the annual radiation above 4.0kWh/m²/day which can give a reliable source of power coming from the photovoltaic panels.

F. Defining the Load Profile

To run the simulation in HOMER software, it is important to determine the primary load inputs. Common electrical appliances are used to model the daily load profile such lightings, refrigerator, washing machine, iron, kettle, television, ceiling fan, and air conditioning. Other electrical appliances are ignored because the energy usage is not significant and is hard to estimate. All the rating power of electrical appliances proposed are referred based on the datasheets. The data of daily energy consumption are determined hourly using Microsoft Excel.In this project, two different of the daily load profile are proposed for each case study,

- Case study 1: Conventional daily load profile; and
- Case study 2: Advanced daily load profile.

G. PV array sizing

Sizing is the process of matching number of modules in series and parallel with an inverter. First, the total daily consumption need to consider. Next, solar array voltage is determined based on the DC voltage input of the power converter. The large the PV system, the higher the solar array voltage. So, based on datasheet of Sunny Tripower 12000TL/15000TL, the rated input voltage of power converter used is 600V. Hence, the total output current from PV array can be determined using equation (3).

$$\sum output\ current\ of\ PV\ array(A) = \frac{Energy\ consumption(kW\square)}{solar\ array\ voltage\ (V) x\ bright\ sunshine\ period\ (h/\ day)} \quad (3)$$

Normally, Malaysia has 12 hours of daylight but the optimum bright sunshine period is about 9 hours from 8.00am to 5.00pm. The actual possible number of modules can be installed is computed by using equation (4), (5), and (6).

$$No.\ parallel\ strings = \frac{\sum output\ current\ of\ PV\ array(A)}{Impp(A)} \quad (4)$$

$$No.\ panels\ series\ per\ string = \frac{solar\ array\ voltage(V)}{Vmpp(V)} \quad (5)$$

$$Proposed\ no.\ panels\ used = no.\ parallel\ strings\ x\ no.\ series\ per\ string \quad (6)$$

The solar panel proposed to use is Sunmodule SW250 and all the specifications are referred from the datasheet. Hence, total power production to be achieved is estimated based on equation (7).

$$Size\ of\ PV\ system\ (kW) = Voc\ (V)\ x\ No.\ parallel\ strings\ x\ No.\ panels\ in\ series\ per\ string\ x\ Impp(A) \quad (7)$$

Hence, the size of PV array for both cases is 12kW. The PV input for HOMER simulation shown in fig. 2.

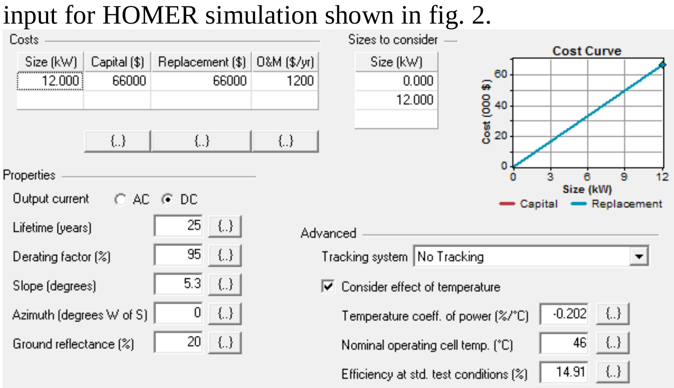

Fig. 2. PV array input

H. Grid Input or Rates

The rate of grid price is obtained from TNB website which stated that the usage cost of electrical appliances at home based on an average usage is RM 0.2847/kWh [7]. Based on Feed in Tariff rates provided by SEDA Malaysia, the basic FiT rates having installed capacity of above 4kW and up to and including 24kW is RM0.7243/kWh. Since, the proposed size of PV system is 12kW, the sellback price is RM 0.7243/kWh. All the rates and costs onward that been inserted in HOMER simulation are using Ringgit Malaysia (RM) currency.

I. Power converter sizing

The total of power AC load is identified earlier in data load analysis. For both cases, the size of power converter should be higher about 25% to 30% of its value or 15% to 30% smaller than the size of PV array. The range of power converter size is estimated as,

$$Power\ converter\ size = 1.25\ x\ Total\ power\ AC\ load\ (kW) = 0.85\ x\ Size\ of\ PV\ array\ (kW) \quad (8)$$

Hence, the calculated size of power converter in case study 1 is 15kW and 12kW for case study 2. The variation size is determined for 4kW, 8kW, 10kW, 12kW and 15kW. Fig. 3 shows the entered input for power converter in HOMER simulation.

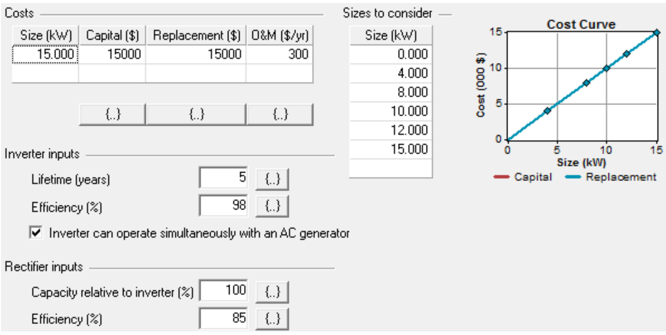

Fig. 3. Power converter input

III. RESULTS AND DISCUSSION

The results of load improvement as well as the reduction of electricity bills are presented. From HOMER simulation results, the net purchase cost, cash flow, electricity production and renewable fraction are discussed to compare three different condition:

- 100% grid dependent system.
- Case study 1: PV grid connected system with conventional load profile.
- Case study 2: PV grid connected system with advanced load profile.

A. Analysis of energy saving by replacement of appliances

Lamps or bulbs are essential for each part of building especially during night side for lighting purpose. The bungalow is installed various type of lightings which used 94 units at ground level, and top level, also, only 34 units at outside area. Hence, during the daytime, power consumption for lighting is 22kW. At night time, the usage of lighting system is higher due to the absence of sunlight. From Fig. 4, it shows there are three major daily energy consumption loads which consumed high electricity. The highest of energy consumption is about 28.8kWh contributed from a refrigerator, followed by the washing machine, 26.11kWh, and conventional lightings, 21.0kWh. After changing the conventional lightings with advanced lightings, it proved in Fig. 5 as more energy is saved as the lightings system does not categorized in major consumption.

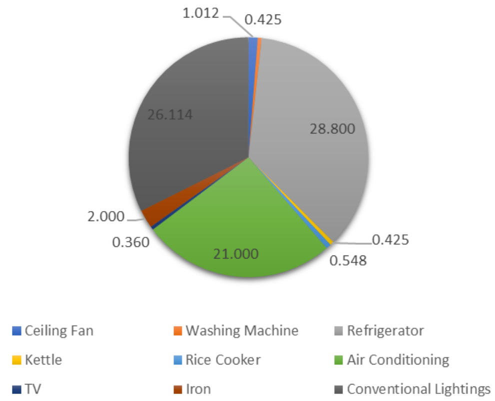

Fi ... *Wh)*

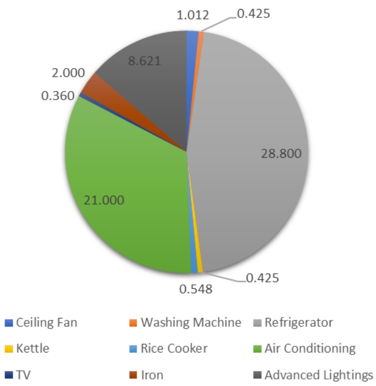

Fig. 5. Daily energy consumption of advanced load(kWh)

B. Analysis of Proposed Load Profile

Fig. 6 shows that the electricity consumption is high from 7.00am to 9.00am and from 8pm to 10pm, hence, most of house appliances are used during that time intervals. While, the usage of electricity is low as owners at the workplace from 9.00 am to 6.00 pm and from 1.00 am to 7.00 am is sleeping period. Other than that, the usage of electricity is average for house chores activities.

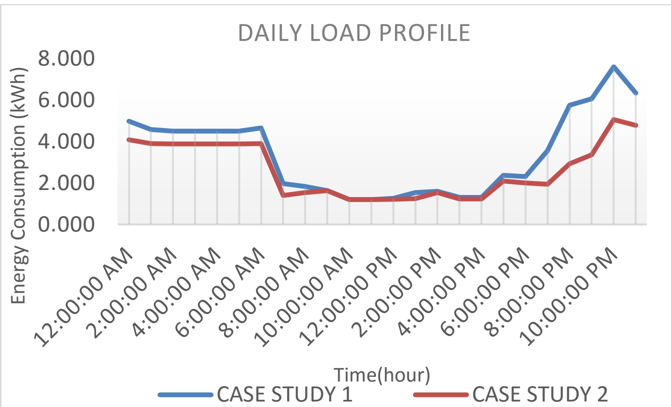

Fig. 6. Daily load profiles

However, the total of energy consumption is dependent on the awareness of energy and owner's. The consumption patterns in different building types, especially in households are unique. The awareness and consumer's attitudes towards energy consumption have also an influence on energy use, especially in households.

C. Analysis of 12 kW PV system using various sizes of power converter

A simulation has been conducted based on an annual interest of 8% and a 25-year projection. As the calculation made earlier, the test system is suitably installed with 12kW PV array and 12kW to 15kW of power converter for both cases. Various size of power converter is considered to determine the most efficient PV grid connected system.

From Table II, it shows that the total electricity production of case study 1 is higher than case study 2. The electricity production from PV array is same about 19,577kWh/year as both case study using same size of PV array. But, the test system of case study 1 need to purchase more electricity from local grid about 23,611kWh/year to support the daily consumption of 80.4kWh/day. While for case study 2, only 17,413kWh/year are purchased from grid to support the daily consumption of 62.6kWh/day.

TABLE II. ELECTRICITY PRODUCTION

Electricity Production	PV array (kWh/yr)	Grid purchases (kWh/yr)	Total (kWh/yr)
case 1	19,577	23,611	43,188
case 2	19,577	17,413	36,990

Fig. 7 shows that using above 12kW of power converter can maximize the efficiency of PV grid connected system as the excessive electricity is nearly 0.0%. Also, it proved that nearly 100% of electricity production are used either by the AC loads or sell back to the grid. The higher of the electricity production, the bigger size of power converter need to minimize the waste. But, if the size of power converter too bigger than size of PV array, the cost of energy maybe higher than 100% grid dependent. Otherwise, the negative cash flow is affected on having longer period of the return of investment.

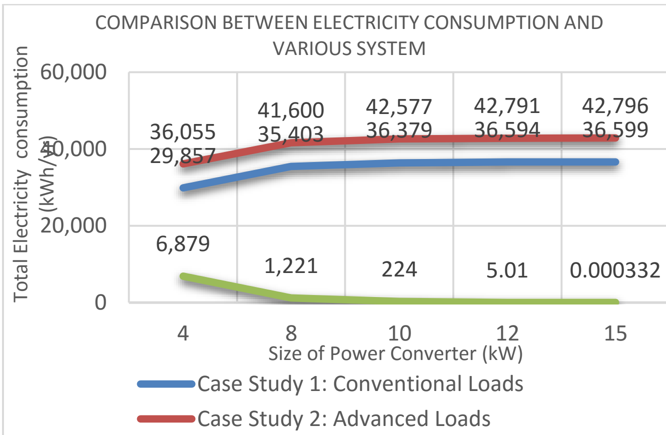

Fig. 7. Electricity consumption

From Fig. 8 and Fig. 9, the trendline for the total net purchase cost (NPC) and the cost of energy (COE) are analysed. Fig.12 shows that COE using 12kW and 15kW of power converters for both case studies are lower than the COE of 100% grid dependent, RM0.285/kWh. But, 12kW power converter is selected as the COE of system much lower than the system with 15kW. For case study 1, the cost of energy is RM0.219/kWh while, for case study 2 is only RM0.195/kWh.

Sensitivity variables

Primary Load 1 (kWh/d) 80.4 Global Solar (kWh/m²/d) 4.85

Double click on a system below for simulation results.

PV (kW)	Conv. (kW)	Grid (kW)	Initial Capital	Operating Cost ($/yr)	Total NPC	COE ($/kWh)	Ren. Frac.
12	10	1000	$ 76,000	131	$ 77,669	0.207	0.45
12	8	1000	$ 74,000	480	$ 80,132	0.214	0.45
12	12	1000	$ 78,000	334	$ 82,264	0.219	0.45
12	15	1000	$ 81,000	867	$ 92,089	0.245	0.45
		1000	$ 0	8,355	$ 106,803	0.285	0.00
12	4	1000	$ 70,000	3,780	$ 118,315	0.315	0.45

Fig. 8. Overall simulation result of case study 1

Sensitivity variables

Primary Load 1 (kWh/d) 62.6 Global Solar (kWh/m²/d) 4.85

Double click on a system below for simulation results.

PV (kW)	Conv. (kW)	Grid (kW)	Initial Capital	Operating Cost ($/yr)	Total NPC	COE ($/kWh)	Ren. Frac.
12	10	1000	$ 76,000	-1,851	$ 52,341	0.179	0.53
12	8	1000	$ 74,000	-1,502	$ 54,804	0.188	0.53
12	12	1000	$ 78,000	-1,648	$ 56,935	0.195	0.53
12	15	1000	$ 81,000	-1,114	$ 66,761	0.229	0.53
		1000	$ 0	6,505	$ 83,157	0.285	0.00
12	4	1000	$ 70,000	1,798	$ 92,987	0.318	0.53

Fig. 9. Overall simulation result of case study 2

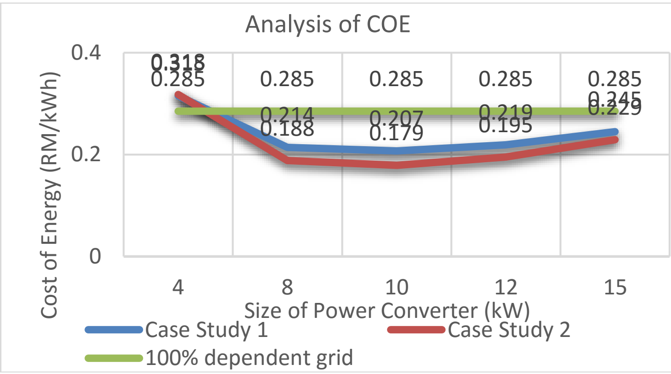

Fig. 10. Analysis on cost of energy (COE)

On the other hand, the trendline in Fig. 11 shows that using 4kW power converter contributed the highest of NPC as both case study still need to purchase more energy from local grid. While, the trendline of NPC started increased from 10kW power converter onward. The system using 10kW power converter shows the lowest NPC, but it is not too efficient since present the waste of excessive electricity. Hence, the system with 12kW power converter is the most efficient as its net present cost lower than the system with 15kW power converter. Compared with case study 1, the net present cost of case study 2 is reduced from RM82,264 to RM56,935. The comparison of COE and NPC for both case study proved that using advanced loads more energy and cost are saved than using conventional loads. So, the most suitable PV grid connected system for both case study is 12kW PV array with 12kW power converter.

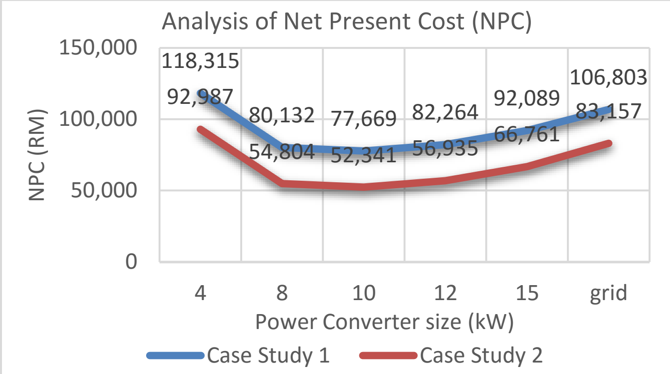

Fig. 11. Analysis of net present cost(NPC)

D. Economic analysis of Selected PV system

As the 12kW of PV-grid connected system with 12kW power converter is selected for both case study, the economic analysis is discussed in this section. From Fig. 12 and 13, it shows that RM78,000 of capital cost and RM24,417 of replacement cost are same for both case study because used same size and types of components. The operation and maintenance fee for grid in the case study 1 is RM38,561 while, for cases study 2 is estimated at around RM63,889. This is because both the systems are supported by local grid and still need to buy the electricity from local grid especially during night day. Also, the excessive electricity which generated by PV system is sold back to the local grid as the system does not supported with battery storage system. Hence, for case study 2, the excessive electricity is higher than case study 1 as the system operated for smaller loads. So, the operational and maintenance for grid is much higher as more excessive electricity need to be sold all times especially during day side. But, the negative cost shows the operational and maintenance cost for grid is barred fully by the local grid company.

Component	Capital ($)	Replacement ($)	O&M ($)	Fuel ($)	Salvage ($)	Total ($)
PV	66,000	0	15,340	0	0	81,340
Grid	0	0	-38,561	0	0	-38,561
Converter	12,000	24,417	3,068	0	0	39,485
System	78,000	24,417	-20,153	0	0	82,263

Fig. 12. Cash flow summary for case study 1

Component	Capital ($)	Replacement ($)	O&M ($)	Fuel ($)	Salvage ($)	Total ($)
PV	66,000	0	15,340	0	0	81,340
Grid	0	0	-63,889	0	0	-63,889
Converter	12,000	24,417	3,068	0	0	39,485
System	78,000	24,417	-45,481	0	0	56,935

Fig. 13. Cash flow summary for case study 2

As shown in Fig.14 and 15, the cash flow for the current system is higher than the ones existing at the beginning, this is due to the high startup cost needed to install the photovoltaic system. For case study 1, the difference between the two systems started to show significantly after the first year where the annual worth about RM1,920 while RM2,051 for case study 2. This trend continues until the 5th year, 15th and 20th year where the inverters needed to be replaced. Compared to the grid only configuration, the negative cash flow always constant for 25 years as the system need to buy 100% from the local grid. Hence, from simulation result, the return of investment for case study 1 is 10.3% as 10.3 years of the simply payback after 15.6 years of the discounted payback. While, for case study 2, the return of investment is lower about 10.4% with shorter simply payback by 8.41 years and 15.2 years of the discounted payback.

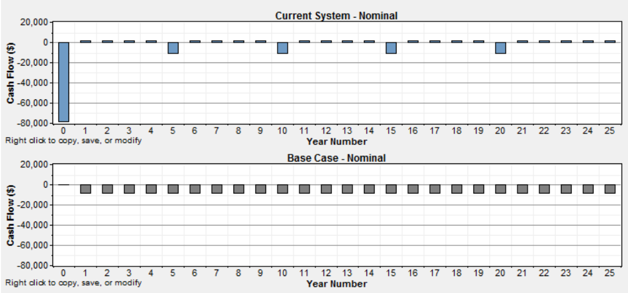

Fig. 14. Comparison of yearly cash flow between case study 1 and 100% grid dependent system

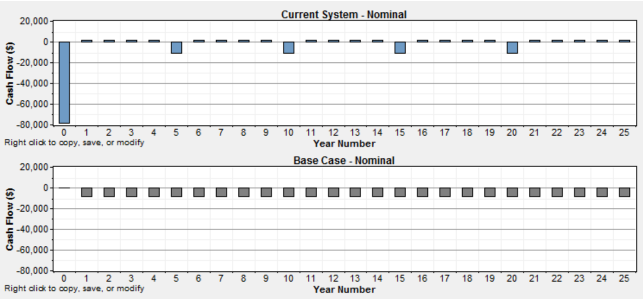

Fig. 15. Comparison of yearly cash flow between case study 2 and 100% grid dependent system

E. Comparison of Renewable Fraction and pollutant factor

The simulated results show that the benefit of installing the PV-grid connected system are not only limited to the operating cost, in fact it would also reduce the carbon emission notably. Table III shows that when the system in case study 1 only relies 100% on the grid, it produces 18,547 kg/year of carbon dioxide, 80.4 kg/year of sulphur dioxide and 39.3 kg/year of nitrogen. While, if compared with case study 2, about 14,441 kg/year of carbon dioxide, 62.6 kg/year of sulphur dioxide and 30.6 kg/year of nitrogen oxide is much lower due to low energy consumptions. These pollutant emissions are contributed because the energy from the grid is mainly generated by fossil fuels and the combustion of fossil fuels emits greenhouse gasses.

On the other hand, after installing the PV system, the carbon dioxide reduces tremendously to 6,425 kg/year, 28 kg/year of sulphur dioxide and 14 kg/year of nitrogen oxide for case study 1. While, for case study 2, these pollutant emissions are the lowest which are only contributed 2,318 kg/year of carbon dioxide, 10.1 kg/year of sulphur dioxide and 4.92 kg/year of nitrogen oxide. The PV grid connected system with advanced loads has reduced the emission of greenhouse gasses about 14,333.68 kg/year. Moreover, the renewable fraction for case study 2 is 0.53, higher than case study 1, 0.45. It proved case study 2 need the least electricity supply from the grid compared to case study 1. Hence, the PV grid connected system with advanced loads is not only beneficial in energy and cost saving, but the system also more environmental friendly as the system is used renewable energy at maximum.

TABLE III. EMISSION OF POLLUTANT GAS

	Case study 1		**Case study 2**	
Emissions Pollutant(kg/yr)	***PV-grid connected***	***Grid***	***PV-grid connected***	***Grid***
Carbon dioxide	6,425	18,547	2,318	14,441
Carbon monoxide	0	0	0	0
Unburned hydrocarbons	0	0	0	0
Particulate matter	0	0	0	0
Sulphur dioxide	28	80.4	10.1	62.6
Nitrogen oxides	14	39.3	4.92	30.6

IV. CONCLUSION

Based on the load profiles and the availability of solar resources, the proposed PV-grid connected system with two options of daily load profiles were simulated using HOMER software. The simulation results were discussed show that the case study 2 of PV-grid connected system with the 12kW power converter is produced the lowest energy cost, greatest reduction of CO^2 emission, least excessive electricity, highest positive cash flow, and largest fraction of renewable energy. However, these results required the expensive initial capital cost. But, the owner will get profit after a few years as the return of investment is estimated. Hence, simulation results show the performances of the test system with renewable energy sources and advanced loads were used maximally which helps in energy and cost saving.

REFERENCES

[1] Malaysia Energy Statistics Handbook 2015, Malaysia: Energy Commision of Malaysia, 2015.

[2] R. Z. W. O. M. Z. A. M. A. L. S. M. M. R. M. Z. N. A. Z. Shahrul Nizam Mohammad, "Potential of Solar Farm Development at UTM Campus for Generating Green Energy," *Applied Mechanics and Material*, 2014.

[3] F. B. A. BAKAR, "Green Building Design For Energy Conservation," Universiti Teknologi Malaysia, Johor, Malaysia, 6 August 1986.

[4] B. S. David, "Energy Efficient Lighting," David Nelson & Associates, United Stated, 2015.

[5] "Malaysia Establishes Feed-in Tariffs to Accelerate Renewable Energy Deployment," Clean Energy Ministerial, 16 January 2016. [Online]. Available: http://www.cleanenergyministerial.org/News/malaysia-establishes-feed-in-tariffs-to-accelerate-renewable-energy-deployment-59786. [Accessed November 2016].

[6] T. N. B. (TNB), "Tenaga Nasional Berhad (TNB)," 2017. [Online]. Available: https://www.tnb.com.my/residential/energy-savings-at-home. [Accessed November 2016].

[7] H. A. R. Nur Dalilah Nordin, "An Optimization Method for Designing Stand Alone Photovoltaic System Using Iterative Method," in *Smart Energy Grid Engineering (SEGE), 2015 IEEE International Conference, Oshawa, ON, Canada*, Universiti Teknologi Malaysia, 2015.

Breakdown Strength of Low Density Polyethylene With Different Nanofillers

Muhammad Shafiq Bin Baderol Hisam
Faculty of Electrical Engineering
Universiti Teknologi Malaysia
Skudai, Johor
shafiqbaderol@gmail.com

Dr. Lau Kwan Yiew
Faculty of Electrical Engineering
Universiti Teknologi Malaysia
Skudai, Johor
kwanyiew@utm.my

Abstract*—In this research, the combination of polymer and nano filler which is called nanocomposite that widely used in high voltage electrical insulation system for the past few years was investigated. The most important parameter that would always be the main topic is the ability for the insulation materials to endure high breakdown voltage. Each and every properties and characteristic of nanocomposites needs to be investigated before it can be applied to the high voltage system in order to make sure the usage of the material is safe and suitable. In this project, low density polyethylene (LDPE) was chosen as the polymer matrix. Meanwhile, the use of nano silica (SiO2) and nano magnesia (MgO) were chosen as the nano fillers. For the fabricaton of the materials, eight type of samples which are the pure LDPE, LDPE filled with 0.3 wt%, 0.5 wt%, 1.0 wt% of nano silica, LDPE filled with 0.3 wt%, 0.5 wt%, 1.0 wt% of nano magnesia and LDPE filled with 1.0 wt% of the mixture of nano silica and nano magnesia were prepared using a two-roll mill machine and compressed by using a hot press machine. For the testing, DC breakdown testing was conducted towards all samples by using the spherical gap electrode configuration. The testing conducted was based on ASTDM D149 test standard. From the experiment conducted, the obtained data were analysed using the Weibull distribution graph. Based on the graph the results showed that the addition of 1 wt% of nano silica into the polymer matrix give the sign of degradation compared by adding 0.3 wt% of nano silica. However, the addition of nano silica into the polymer matrix give the most degradation in term of breakdown strength compared to nano magnesia.

I. INTRODUCTION

Electric power transmission is the movement or flow of the electrical energy from a generating site or also known as power plant, power station or power house. These type of industrial facility responsible on generating electrical power for consumer's uses which is it need to be distribute to electrical substation first. Substation then will change the voltage supplied from high to low. Basically, the movements of the electrical energy from generating until consumers are in the term of high voltage which means the current carried is lower for the same amount of power transmitted. Therefore, it required smaller wires which will be beneficial to the system. However, there are many factors that need to be focus on especially to deliver electricity via high voltage transmission. One of the factors is the use of insulation materials.

Insulation materials are very important in high voltage industries. Insulation is an act or process of protecting something by surround it with material that capable of reduces, prevents or block the transmission of sound, heat or electricity. Insulation medium can be divided into four categories which are air, solid, liquid and vacuum. In term of electricity, most of the equipment, apparatus or machine use oil as the medium of insulation especially in high voltage application. However, the used of insulation medium may varied depends on the situation or the equipment itself.

On the other hand, polymer is the material that used widely in the high voltage industries as a material for protection. Furthermore, the use of nanodielectric in the polymer can improve its properties. Basically, nanodielectrics are a class of materials containing at least one phase at the nanometer scale and their advantages come in the form of increase endurance and enhanced breakdown strength of the insulation materials. In the other words, by adding nanoparticles into the matrix of polymeric materials can produces nanodielectrics that can greatly improve the thermal, mechanical and electrical properties of the polymeric composites [1].

Many researches has eventually advanced with the technologies that grow rapidly and past few years researches give a full attention into the application of nanodielectric in the field of electrical insulation [2]. It has proven that by mixing nanoparticles into polymeric material with a proper way and method will give beneficial result in its dielectric strength.

In this world there is no such thing as perfect insulator. It is because every insulator contain at least small amount of mobile charges (charge carriers) inside it. When this insulator suddenly becomes electrically conductive due to the sufficiently large voltage applied, the electric field will be able to tear the electron away from the atoms. Therefore, the mobile charge inside the insulator will carry the electron. When there is the movement of electron, that's mean the insulator reaches its material limitation. This phenomenon called as breakdown voltage of an insulator.

Nowadays, researches still struggle to investigate and to improve the breakdown strength of the insulation materials. Even though there are many experiment conducted but still cannot come out with the best solution. Thus, this project will investigate the pure low density polyethylene (LDPE) and compare it with a mixture of different nano fillers to see the improvement in term of breakdown strength.

II. Literature Review

A. Insulation material

An electrical insulator is a material whose electric charges inside the material does not move freely and therefore make it nearly impossible to conduct electric current under the influence of an electric field [4]. This characteristic is different with other materials such as semiconductors and conductors which known to conduct electric current more easily. The property that differentiates an insulator with the rest of the materials is its resistivity. It is because insulators have higher value of resistivity compared to semiconductors and conductors. High resistivity material such as glass is classified as very good electrical insulators. A much bigger class of materials, even though they have the lower type resistivity, but are still good enough to prevent current from flowing. This includes plastics and rubber-like polymers.

B. Polymers and its classification

A polymer is defined as a large molecule composed of many repeated subunits [11]. Just because of their broad range of properties, both synthetic and natural polymers play an important role in everyday life [12]. Polymers are created via polymerization of many tiny molecules also known as monomers. Polyethylene is one of the polymer matrixes that being widely used in electrical industry. It is a good electrical insulator which is offers good tracking resistance. It was also the first flexible polymer to achieve the ideal electrical properties [5].

For the classification of polyethylene, there are several of types but the basic and always being used widely in the industry are high density polyethylene (HDPE) and low density polyethylene (LDPE).

High density polyethylene (HDPE) has a low degree of branching which is the mostly linear molecules that pack together very well. Thus, its intermolecular forces are stronger compared to others highly branched polymers. HDPE also consist of 90% of crystalline configuration which make it mechanically stable, stiffer and stronger [5]. The strength of HDPE makes it applicable in products and packaging such as detergent bottles, garbage container and water pipes.

Low density polyethylene (LDPE) has been used in many researches as the polymer especially polymer nanocomposites. It is because LDPE is among the cheapest polymer. Even though it has lower tensile strength and increased on ductility but it has the material's ability which it can be stretched into a wire or cable.

C. Polymer nanocomposites

Polymer nanocomposites consist of polymer that having nano fillers or nanoparticles dispersed into the polymer matrix. According to Lau et al. [14], polymer nanocomposites are defined as the composites which have small amounts of nano fillers that dispersed homogenously in polymers by several weight percentages (wt%). As defined, the amount of the nano fillers that added into the matrix of polymer is very small in quantity, which is less than 10 wt%.

D. Breakdown in solid state insulator

Electrical breakdown or also known as dielectric breakdown is the reductions in the resistance of the insulation materials when certain amount of voltage applied across it exceed its peak value (breakdown voltage). These phenomenon occur will result in the insulator sudden changing in properties which is become electrically conductive. Basically, electrical breakdown is the momentary event that could be end if the protective device can function to interrupt the current flow. Otherwise it will result a permanent damage to the insulator if the device fail to react.

E. Dielectric strength test

The dielectric strength test is the test that required by the electrical safety testing standard especially for the high voltage applications before it can be used. The variable value that needs to be measured is a current value which has to be lower than the value that has been indicated by the international standards [17].

According to [17], the dielectric strength test is performed in AC and DC with the increasing of voltage that varies from some hundred volts to several tens of kilo volts. The value of the test voltage is determined by the standard which it's going to be applied to the product tested.

III. Methodology

In this chapter, the process of the fabrication of the materials, the procedure and the materials preparation are briefly explained. The tables, figures and block diagram of the project are going to be presented in detail to provide better understanding about the whole project through the Final Year Project 1&2.

A. *Materials preparation*

From the materials that already prepared, it will be sent for blending process to mix the materials accordingly. Eight types of samples with different mixture of substances were produced and tabulated in Table 3.1.

Samples	LDPE, 35g (%)	Nano silica (wt%)	Nano magnesia (wt%)
1	100	0.0	0.0
2	100	0.3	0.0
3	100	0.5	0.0
4	100	1.0	0.0
5	100	0.0	0.3
6	100	0.0	0.5
7	100	0.0	1.0
8	100	0.5	0.5

Table 3.1: Eight different types of samples

B. *Fabrication process*

The fabrication process was done in the Faculty of Chemical Engineering using the Polymer Testing Laboratory.

For the process of making the samples, the LDPE, nano silica and nano magnesia were weight first accordingly by referring the scale that already been decided in Table 3.2 for each samples. After the weighting of the materials complete, it will put in to small plastic bag and labelled so that it won't cause any confusion due to the materials itself have the exact characteristic between each other especially nano silica and nano magnesia. After all samples have been packed and labelled nicely, then it can proceed to the blending process.

Figure 3.1: Two Roll Mill machine

Figure 3.2 shows the Two Roll Mill Machine that used for the blending process. The machine is automatic but it need human to perfectly blend the samples. Thus before the blending process happen, the temperature of the machine must be reach 142 degree Celsius to make sure the blending and melting process of LDPE and nano fillers runs smoothly.

C. *Compression process*

In this process, Hydraulic press was used to compress the samples into the circular shape with the thickness of 100µm. One sample is used to make four circular shapes. The reason behind it is one circular shape can be used up to four times for the testing. The detail explanation about it will be much elaborate in the testing part.

The hydraulic press consist of the hydraulic, steel plates and also installed with heating system to make it easier for the compressing of the samples. The temperature that needed to perfectly compress the samples is about 160 degree Celsius and the weight that needs to be applied to the samples during press in order to get the thickness of 100µm was about 1.5 tonne.

D. *Testing process*

For the testing process, the activity was conducted in Institute of High Voltage and High Current (IVAT) at Faculty of Electrical Engineering, UTM. The testing process is necessary in order to get the results and also for analysing the samples.

The aim of the testing process was to require the breakdown strength of each samples by simply measured the thickness of the sample and also it breakdown voltage. Each of the samples has their own breakdown voltage when high voltage is applied into it. For testing, there are two method that can be used either DC test or AC test. These two will give the same result which is the breakdown strength of the samples. The different between it is, the circuit configuration

For the breakdown voltage measurement, there are two device used as controller devices which are Digital Measuring Instrument (DMI 551) and Operating Terminal (OT 276). These two devices basically used for AC, DC and impulse measurement. However, this research only covered completely the DC part.

IV. Result and Discussion

In this chapter will discuss about the results obtained during the research especially during testing and also based on the Weibull distribution graph method after the data was collected.

A. *DC breakdown voltage test*

Breakdown voltage test is the test that used to determine the breakdown strength of the insulation material to see whether or not it can withstand a high voltage. During the experiments that have been conducted, the breakdown strength was determined by simply measured and recorded the thickness of the sample and its breakdown voltage. In order to calculate the breakdown strength of the tested sample, the formula below was introduced.

$$\frac{Breakdown\ Voltage}{Sample\ Thickness} = Breakdown\ Strength\ (\frac{kV}{mm})$$

The experiments consist of 8 samples with different nano fillers. The experiment conducted using DC breakdown voltage test and then it repeated to finally get 10 readings for each samples. The data collected were gathered and calculated by using the formula above. After that, it was plotted in the Weibull Distribution Graph. The advantages of using this method is the graph give a better understanding yet a simple graphical solution. In this method there were two parameters that need to be considered which are the Weibull Cumulative Failure Probability (%) and the breakdown field (kV/mm).

The tables shown below are the data collected from every sample with an increasing in breakdown strength for 10 readings

Table 4.1: LDPE (unfilled)

Pure LDPE	
no. of reading	Breakdown Field (kV/mm)
1	**194**
2	**236.36**
3	**280**
4	**290**
5	**290.91**
6	**300**
7	**300**
8	**316.67**
9	**325**
10	**336.36**

Table 4.2: LDPE+SiO2 (1 wt%)

LDPE + SiO2 (1%)	
no. of reading	Breakdown Field (kV/mm)
1	**163.62**
2	**180**
3	**190**
4	**190.91**
5	**191.67**
6	**200**
7	**200**
8	**220**
9	**222.22**
10	**230**

Table 4.3: LDPE+SiO2 (0.5 wt%)

LDPE + SiO2 (0.5%)	
no. of reading	Breakdown Field (kV/mm)
1	**163.64**
2	**168.42**
3	**218.18**
4	**218.18**
5	**220**
6	**226.09**
7	**226.09**
8	**227.27**
9	**227.27**
10	**260**

Table 4.4: LDPE+SiO2 (0.3 wt%)

LDPE + SiO2 (0.3%)	
no. of reading	Breakdown Field (kV/mm)
1	**218.18**
2	**218.18**
3	**220**
4	**227.27**
5	**230**
6	**230**
7	**233.33**
8	**245.45**
9	**250**
10	**250**

Table 4.5: LDPE+MgO (1 wt%)

LDPE + MgO (1%)	
no. of reading	Breakdown Field (kV/mm)
1	**209.09**
2	**220**
3	**230**
4	**236.36**
5	**236.36**
6	**240**
7	**245.45**
8	**250**
9	**270**
10	**270**

Table 4.6: LDPE+MgO (0.5 wt%)

LDPE + MgO (0.5%)	
no. of reading	Breakdown Field (kV/mm)
1	**227.27**
2	**227.27**
3	**236.36**
4	**236.36**
5	**240**
6	**240**
7	**245.45**
8	**250**
9	**260**
10	**260**

Table 4.7: LDPE+MgO (0.3 wt%)

LDPE + MgO (0.3%)	
no. of reading	Breakdown Field (kV/mm)
1	**140**
2	**218.18**
3	**240**
4	**254.55**
5	**254.55**
6	**272.73**
7	**272.73**
8	**290.91**
9	**300**
10	**320**

Table 4.8: LDPE+SiO2+MgO (1 wt%)

LDPE + SiO2 + MgO (1%)	
no. of reading	Breakdown Field (kV/mm)
1	**241.67**
2	**245.45**
3	**245.45**
4	**250**
5	**250**
6	**254.55**
7	**254.55**
8	**263.64**
9	**266.67**
10	**272**

B. Weibull distribution analysis

Based on the figure 4.1, the graph shows the pattern of distributed data where the different between samples can be seen. A comparison between unfilled LDPE, LDPE with 1 wt% nano silica, LDPE with 1 wt% nano magnesia and LDPE with the mixture of 1 wt% nano silica nano magnesia was made to see which samples is better with the same amount of nano filler. The unfilled LDPE was needed there as a reference sample.

From the graph it proves that the most degradation occurs when nano silica added into LDPE compared to by the addition of nano magnesia and the mixture of nano silica and magnesia. Even though all samples shows degradation in breakdown strength when compared to unfilled LDPE. However, the LDPE with the mixture of nano silica and magnesia shows the positive sign of increasing in breakdown strength compared with the others samples.

From this observation, there are two things that can be conclude which are nano silica negatively affect the breakdown strength of the polymer nanocomposites and second, is by the mixture of another nano filler with the nano silica it somehow can improve its properties and increase the breakdown strength of the LDPE.

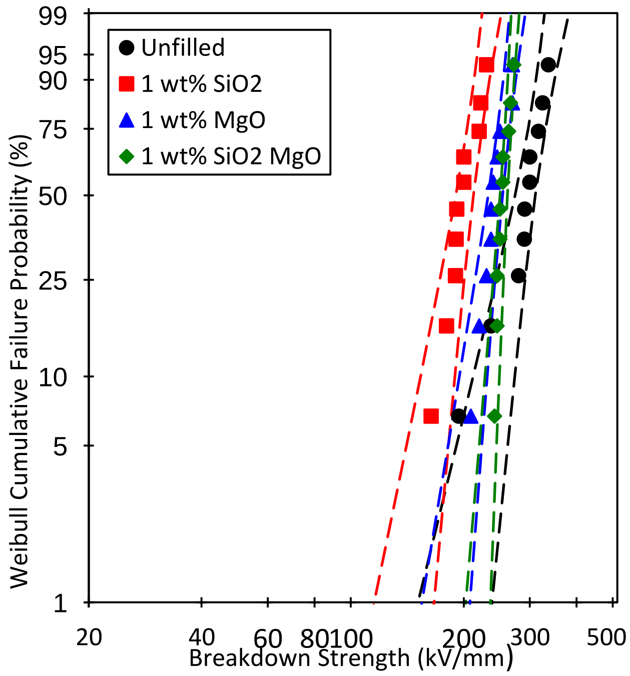

Figure 4.1: Weibull distribution graph

CONCLUSION

As the conclusion, the fabrication process plays the important role to determine whether the samples developed can give the better result or at least shows some significant in term of improvement of the dielectric strength of the compound.

The form of agglomeration in the compound during the blending process may occur and can give the bad result for the project and it cannot be undone. However, the previous studies have been state that there are many ways to overcome agglomeration inside the compounds. It's either the suitable materials especially nanoparticles used or the process to fabricate the materials that need to be varied to avoid the agglomerate in the compounds.

Apart of that, based on the observation of the result it can be concluded that, the unfilled Low Density Polyethylene (LDPE) is better compared to the LDPE with nano silica ($SiO2$). It was prove not just in this experiment but also in the previous researches. Furthermore, the addition of 0.3 wt% of nano magnesia (MgO) into the polymer matrix shows a positive sign of increment in term of breakdown strength. Thus, in the near future, the used of nano fillers such as magnesia (MgO) can be worth investigate.

REFERENCES

1. S. S. Banji, A. Bulinski and M. Abou Dakka. *Nanodielectric Materials For High Voltage Devices*. Institute for National Measurement Standards. 2006
2. Y. Cao and P. C. Irwin. *The Electrical Conduction In Polyimide Nanocomposites.* IEEE CEIDP, Albuquerque, USA, pp-116-119. 2003.
3. United State Department of Energy. (2008, December 26). Final report on the August 14, 2003 blackout in the United States and Canada. Retrieved from the website: http://www.ferc.gov/industries/electric/indus-act/reliability/blackout
4. M. S. Naidu and V. Kamaraju. *High Voltage Engineering Third Edition.* McGraw Hill Publishing Company Limited. 2004.
5. R. W. Sillars. *Electrical Insulating Materials and Their Application*. Peter Penegrinns Ltd. 1973.
6. Henrikh Hillborg. Senior Principal Science. ABB Corporate Research. *Polymer Nanocomposites As Electrical Insulation In High Voltage Applications.* ABB Group. 2010.
7. Kwabena A. Narh, Ahmed-Tijani Agwedichan and Laila J. Jallo. *Influence Of Deagglomeration States Of Carbon Nanotubes On The Thermal And Mechanical Properties Of Carbon Nanotube-Reinforced Polyethylene Oxide*. World Scientific Publishing Company. International Journal of Nanoscience. 2009. Vol. 8: 23-27.
8. Christof Sumereder, Petru V. Notingher, Sandra Schlogl and Michael Muhr. *Propertiesof Polymer Composites Used In High Voltage Applications*.MDPI.2016.
9. *Electrical Porcelain Insulator*. Product spec sheet. Universal clay products, Ltd. 2008.
10. Cotton, H. *The Transmission And Distribution Of Electrical Energy*. London: English Univ. press. Copied on insulator usage, A. C. Walkers. Insulation information. 1958.
11. Panter, Paul C, Coleman, Michael M. *Fundementals Of Polymer Science: An Introductory Text*. Lancester, PA. Technomic Pub.Co. P. 1. ISBN 1-56676-559-5. 1997.
12. McCrum, N. G. Buckley, C. P. Bucknall, C. B. *Principal Of Polymer Engineering*. Oxford. New York, Oxford University Press. P. 1. ISBN 0-19-856526-7. 1997.
13. Kwan-Chi Kao. *Dielectric Phenomena In Solids: With Emphasis On Physical Concepts Of Electronic Processes*. Academic Press.2004.
14. K. Y. Lau, M. A. M. Piah. *Polymer Nanocomposites In High Voltage Electrical Insulation Perspective*: A review. Malaysian polymer journal, 2011. Vol. 6, No. 1, pp 58-69.
15. Osama Gouda, Ahmed Thabet. *Thermal Experimental Dielectric Characterization Of Cost-Fewer Low Density Polyethylene Nanocomposites. Advances In Electrical And Electronic Engineering*. 2014. Vol. 12, no. 5.
16. Tanaka, T. Montanari, G. C., and Mulhaupt, R., *Polymer Nanocomposites As Dielectrics And Electrical Insulation-Perspectives For Processing Technologies, Materials Characterization And Future Applications*. IEEE Transaction on dielectric and electrical insulation, 11(5). 763-784. 2004.
17. Dielectric strength test. Retrieved from: www.sefelec.com/en/dielectric-strength-test.php
18. Spherical electrodes configuration. Retrieved from: https://www.researchgate.net/figure/electrode-configuration-for-the-determination-of-the-dielectric-breakdown
19. Y. Wang, Y. C. Chan, Z. L. Gui, D. P. Webb, and L. T. Li. *Application Of Weibull Distribution Analysis To The Dielectric Failure Of Multilayer Ceramic Capacitors. Materials Science And Engineering B47*. ELSEVIER Ltd. 1997.
20. Y. Murata, Y. Murakami, M. Nemoto, Y. Sekeguchi, Y. Inoue, M. Kanaoka, N. Hozumi and M. Nagao. *Effect Of Nano-Sized Mgo-Filler On Electrical Phenomena Under DC Voltage Application In LDPE. Annual Report Conference On Electrical Insulation And Dielectric Phenomena*. IEEE. 2005.

21. Ahmed Thabet Mohamed. *Experimental Enhancement For Dielectric Strength Of Polyethylene Insulation Materials Using Cost-Fewer Nanoparticles. Electrical Power And Energy Systems*. Elsevier Ltd. 2014. 469-475.
22. Y. Murata, Y. Sekiguchi, Y. Inoue, and M. Kanaoka, *"Investigation Of Electrical Phenomena Of Inorganic-Filler/LDPE Nano Composite Material"* Proc. 2005 ISEIM, pp: 650-653, 2005.

Effects of SiO_2 and MgO Calcination on the Breakdown Strength of Polyethylene Nanocomposites

L. R. Kumaran and K.Y. Lau
Institute of High Voltage and High Current, Faculty of Electrical Engineering
Universiti Teknologi Malaysia, 81310 Johor Bahru, Malaysia.
E-mails: leshan93@yahoo.com; kwanyiew@utm.my

***Abstract*—Nanocomposites are developing technology for the dielectrics community, where nanofillers have been incorporated into polymers in attempts to improve the electrical performances of cables for power transmission. However, the presence of water in nanofillers has been found to degrade the electrical performances of nanocomposites. This paper focuses on the effect of high temperature treatment (calcination) of nanofillers (silica (SiO_2) or magnesia (MgO) on the breakdown strength of the subsequent polyethylene nanocomposites. The nanofillers were calcined at 600°C and 1200°C before the subsequent nanocomposite samples were subjected to DC breakdown testing. The results showed that filler calcination at 1200°C resulted in more water loss compared to filler calcination at 600°C. Meanwhile, the breakdown strength for the nanocomposites was similar for those containing uncalcined nanofillers and nanofillers calcined at 600°C; nanofiller calcination at 1200°C showed adverse breakdown effects. Nevertheless, the nanocomposites containing MgO had higher breakdown strength compared to SiO_2 under the uncalcined and calcined conditions.**

Keywords*—blend polyethylene; SiO_2; MgO; calcination; breakdown strength

I. INTRODUCTION

Nanocomposites are composites in which polymers have small amounts of fillers dispersed uniformly in the size of nanometer (less than 100 nm) [1]. The incorporation of nanofillers into polymers often improves the mechanical and thermal characteristics of the nanocomposites. However, some studies showed that the use of nanocomposites negatively affected the electrical breakdown strength of the materials. In this regard, the effect of water or moisture content on nanocomposites has not been fully understood.

Although many studies have stated that the addition of nanofillers into polymers has improved its overall properties such as resistance to water, fire retardancy and wear resistance, most of the results were reported without considering the surrounding condition and the sample storage condition in detail. For example, even though polyethylene itself is hydrophobic, the addition of nanofillers such as silica (hydrophilic) into polyethylene may cause the resulting nanocomposites to tend to absorb water. This situation becomes worse when the polymer itself is hydrophilic (prone to water absorption). For instance, epoxy matrix itself is hydrophilic and the combination of the material with a hydrophilic filler may result in to more water absorption for the resulting nanocomposites.

The presence of water in nanocomposites is often contributed by the presence of nanofillers [2]. The big specific surface area of the filler [1] and its hydrophilic nature allows water to be absorbed by the nanocomposites. The interface region between the polymer and the filler is said to be the favorite places for water accumulation. Meanwhile, one of the factors that influences the breakdown strength of nanocomposites which is water absorption. Hosier et al. [3] in an investigation on the influence of moisture absorption on the dielectric properties of nanosilica/polyethylene stated that the water absorption led to a reduction in the breakdown strength of nanocomposites.

Yang et al. [4] found that water absorption still happened in nanocomposites upon nanofiller surface treatment. This was because of partial surface treatment of the nanofiller which could not remove the overall water content of the nanofiller, since nanofiller surface treatment might not remove all the hydroxyl (OH) group on its surface. However, Yang et al. stated that temperatures of higher than 200°C could be used to remove the bonded water molecules entirely. In another experiment, Praeger et al. [5] showed that the nanocomposite samples containing calcined nanosilica (calcined at 1050℃ under dry nitrogen for 10 hours) showed negligible weight change upon water immersion testing, as compared with nanocomposite samples containing uncalcined nanosilica (as received). This shows that nanosilica's surface, hence nanocomposites may be rendered more hydrophobic upon nanofiller calcination.

II. METHODOLOGY

A. Materials

The polymer used for this study was a polyethylene (PE) blend composed of low density polyethylene (LDPE) and high density polyethylene (HDPE) in the ratio of 80: 20. The nanofiller used was either silica (SiO_2) or magnesia (MgO), with 5 wt% loading.

B. Sample Preparation

The fabrication of materials was divided into three parts, which were calcination, mechanical blending and hot pressing. Calcination of the nanofiller (SiO_2 or MgO) was carried out using the Carbolite-Gero furnace at 600°C or 1200°C for four hours. After that, the nanofiller and the matrix was blended at

TABLE I. MATERIALS INVOLVED

Type	Sample
A	PE
B	PE/Uncalcined SiO_2
C	PE/Uncalcined MgO
D	PE/Calcined SiO_2 (600°C)
E	PE/Calcined MgO (600°C)
F	PE/Calcined SiO_2 (1200°C)
G	PE/Calcined MgO (1200°C)

140°C using a two-roll machine. There were seven types of materials used for blending, as shown in Table I. The nanocomposite lump produced from the mechanical blending process was hot pressed into disc-shape samples of ~100 µm thickness using a hydraulic press at 160°C and 2.5 ton load.

C. DC Breakdown Test

DC breakdown testing was carried out according to the guidelines set in the ASTM D149 standard. The sample was immersed in mineral oil and subjected to step-by-step voltage with 2 kV increase every 20 s until breakdown occurred. The breakdown voltage was recorded and analyzed using the Weibull distribution to determine α (breakdown strength) and $ß$ (shape parameter).

III. RESULTS

A. Calcination

The percentage of reduction in the mass of the nanofiller, which represented the amount of water removed after calcination, is shown in Fig. 1.

Calcination at a temperature of 600°C resulted in a mass reduction of 7.83% and 15.88% for SiO_2 and MgO, respectively. Meanwhile, calcination at a temperature of 1200°C resulted in a mass reduction of 10.89% and 20.49% for SiO_2 and MgO, respectively. It can be seen that SiO_2 had lost 3.06% more water when calcined at 1200°C compared to 600°C. On the other hand, MgO has lost 4.61% more water when calcined at 1200°C compared to 600°C. The results of calcination showed that calcination at 1200°C can remove a higher amount of water. From Figure 1, MgO lost a higher amount of water compared to SiO_2. Calcination led to water loss in the nanofillers. More losses in mass could mean the MgO nanofiller has a high level of initial water content compared to the SiO_2 nanofiller [5].

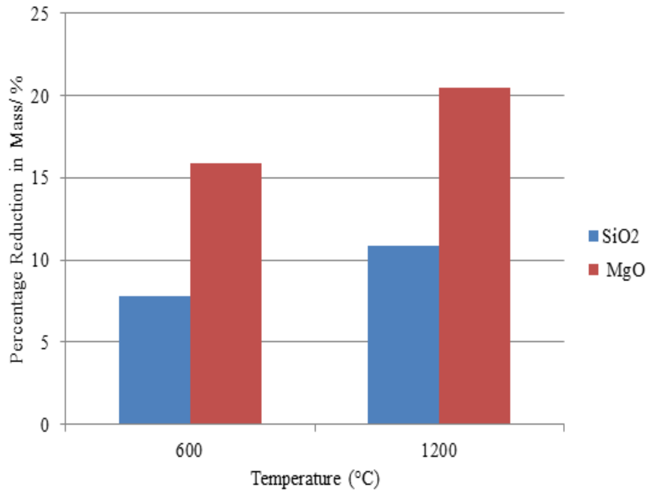

Fig. 1. Percentage reduction of mass after filler calcination

According to the manufacturer's datasheets for SiO_2 and MgO, calcination at a temperature of 850°C for two hours could result in SiO_2 to lose more water than MgO, but the results in this study showed otherwise. The difference in the current experimental results and the information provided from manufacturer's datasheet may be due to the elimination of residual impurities of MgO that was higher.

B. Weibull Analysis

Fig. 2 shows the Weibull plot of the unfilled PE and the nanocomposites containing uncalcined and calcined SiO_2 or MgO. The unfilled PE shows the highest breakdown strength of 251 kV/mm while the samples containing SiO_2 and MgO nanofillers shows lower breakdown strength. The breakdown strength of the samples containing uncalcined SiO_2 and MgO were 164 kV/mm and 182 kV/mm, respectively. The breakdown strength of the samples containing calcined SiO_2 (600°C) was slightly higher than the samples containing uncalcined SiO_2. The samples containing MgO calcined at 600°C was also slightly higher than that containing uncalcined MgO by 5 kV/mm. Meanwhile, the breakdown strength of the samples containing calcined SiO_2 (1200°C) and calcined MgO (1200°C) was the lowest. The breakdown strength of the samples containing calcined SiO_2 (1200°C) was 61 kV/mm while the breakdown strength of the samples containing calcined MgO (1200°C) was 139 kV/mm.

Table II shows the results generated from Weibull analysis. The nanocomposites containing uncalcined MgO and calcined MgO at 600°C have a similar $ß$ value of 6. The unfilled PE had a lower $ß$ value of 5. The breakdown strength of the nanocomposites containing calcined MgO (1200°C) had a $ß$ value of 4.

Fig. 3 shows the comparison of the breakdown strength for the nanocomposite samples containing SiO_2 and MgO. Generally, it could also be stated that the samples containing MgO had higher breakdown values compared to SiO_2.

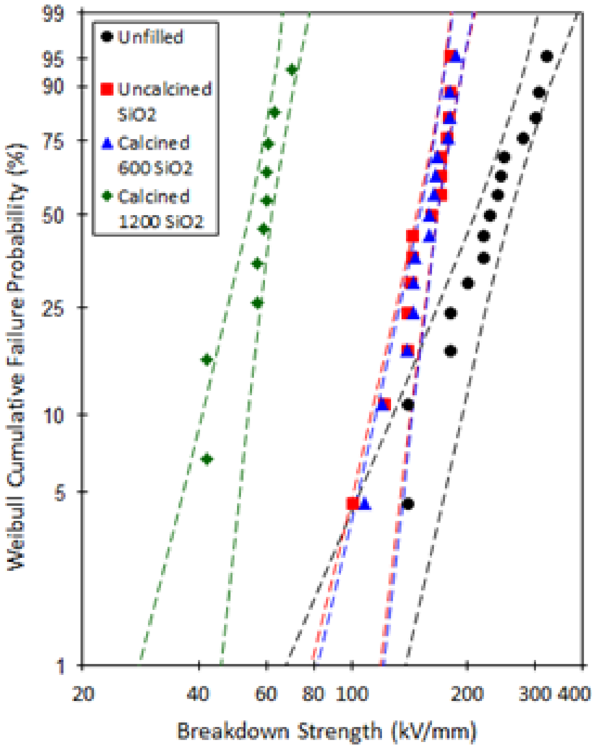

(a)

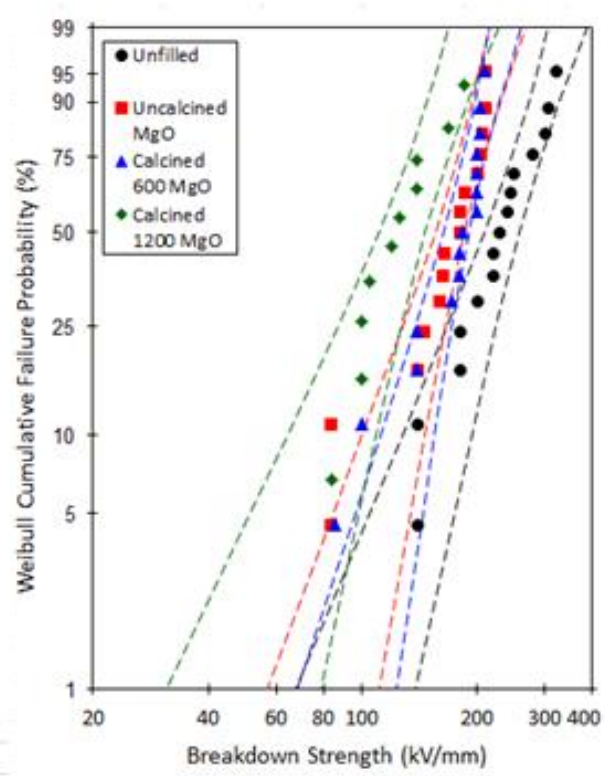

(b)

Fig. 2. Weibull plots for nanocomposites containing (a) SiO_2, (b) MgO

TABLE II. WEIBULL PARAMETERS FOR DC BREAKDOWN TEST

Sample	α (kV/mm)	ß
PE	251 ± 25	5 ± 2
PE/Uncalcined SiO2	164 ± 9	9 ± 3
PE/Uncalcined MgO	182 ± 15	6 ± 2
PE/Calcined SiO2 (600°C)	166 ± 8	9 ± 4
PE/Calcined MgO (600°C)	187 ± 14	6 ± 3
PE/Calcined SiO2 (1200°C)	61 ± 4	9 ± 4
PE/Calcined MgO (1200°C)	139 ± 18	4 ± 3

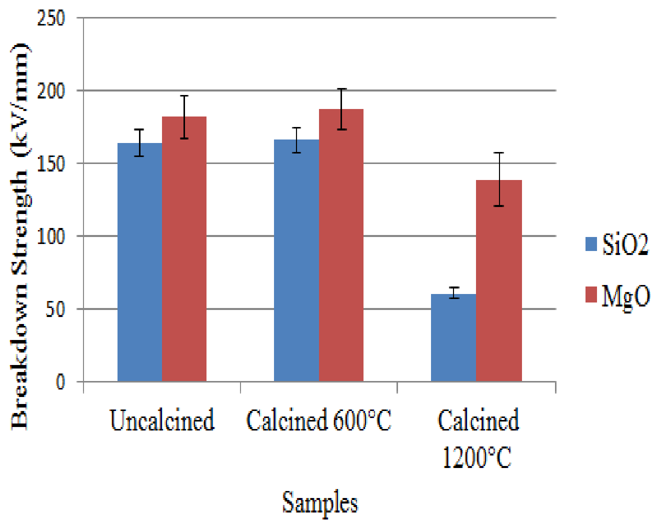

Fig. 3. Comparison of breakdown strength of samples containing uncalcined and calcined nanofillers

IV. DISCUSSION

The nanocomposite samples containing calcined SiO_2 (600°C) and calcined MgO (600°C) showed slightly higher breakdown strength compared to the samples containing uncalcined SiO_2 and uncalcined MgO. It is believed that, upon filler calcination at 600°C, the hydroxyl groups on the surface of SiO_2 and MgO was still present on the both the nanofillers. Therefore, the breakdown strength of the nanocomposites was not significantly improved.

On the other hand, for filler calcination at 1200°C, the breakdown strength of the nanocomposites containing the calcined SiO_2 (1200°C) and calcined MgO (1200°C) deteriorated. There could be several reasons that led to these results. According to Bergna et al. [6], temperature above 1000°C was required to remove the water completely from the SiO_2 nanofiller. However, another study by Gaber et al. [7] showed that as the calcination temperature increased from 300°C to 1050°C, the size of the nanoparticle became bigger, and the agglomeration of the nanoparticles became more obvious. This could be the case in the current work.

As the calcination temperature became too high, it could lead to the agglomeration of nanoparticles. Agglomeration is a factor that leads to the poor electrical characteristics of nanocomposites. While calcination was done mainly to remove water on nanofillers, much higher calcination temperatures (e.g. 1200°C) could otherwise lead to nanofiller agglomeration. Although mechanical blending is used to melt and mix polymers and nanofillers, homogenous dispersion of nanoparticles remains a major concern [8]. Nanoparticles agglomeration is common due to the small size nanofillers that tend to clump easily, where the nanoparticles are attracted to each other by interaction forces between them [9].

Meanwhile, the nanocomposite samples containing MgO nanofiller under all the uncalcined and calcined conditions showed higher breakdown strength compared to SiO_2 nanofiller. This could be attributed to higher amounts of water loss by MgO compared to SiO_2 upon calcination at 600°C and 1200°C. In addition, agglomeration was less obvious in the investigated nanocomposites containing MgO compared to SiO_2. Reduced water contents and less nanoparticles agglomeration in nanocomposites containing MgO led to better breakdown strength of the materials compared to SiO_2.

V. CONCLUSIONS

Calcination at high temperatures was done to remove water from the nanoparticles. This was evident with higher weight loss of the SiO_2 and MgO nanofillers at a calcination temperature 1200°C compared to 600°C. This implies that higher amounts of water can be removed at very high temperatures. It was expected that nanofiller calcination at high temperature could improve the breakdown strength since water could be effectively removed, but the current work showed otherwise. Since more nanoparticles agglomerations could be formed in nanocomposite samples containing SiO_2 and MgO calcined at 1200°C compared to 600°C, nanoparticles agglomeration upon nanofiller calcination needs to be looked into. Nevertheless, the nanocomposite samples containing MgO showed higher breakdown strength under all the uncalcined and calcined conditions, compared to SiO_2. This shows that filler calcination can have different effects for different types of nanofillers.

VI. ACKNOWLEDGEMENTS

The authors thank the Ministry of Higher Education, Malaysia and Universiti Teknologi Malaysia for their financial sponsorships and the research grants 13H12 and 03G66.

REFERENCES

[1] Tanaka, T., Montanari, G. C., & Mulhaupt, R. Polymer nanocomposites as dielectrics and electrical insulation-perspectives for processing technologies, material characterization and future applications. IEEE Transactions on Dielectrics and Electrical Insulation. 2004.11(5): 763-784.

[2] Kochetov, R., Andritsch, T., Morshuis, P. H. F., & Smit, J. J. Impact of postcuring and water absorption on the dielectric response of epoxy-based composites filled with MgO nanoparticles. 2011 Annual Report Conference on Electrical Insulation and Dielectric Phenomena (CEIDP). October 16-19, 2011. Cancun: IEEE. 2011. 342-345.

[3] Hosier, I. L., Praeger, M., Holt, A. F., Vaughan, A. S., & Swingler, S. G. Effect of water absorption on dielectric properties of nano-silica/polyethylene composites. 2014 IEEE Conference on Electrical Insulation and Dielectric Phenomena (CEIDP). October 19-22, 2014. Des Moines, IA: IEEE. 2014. 651-654.

[4] Yang, J., Wang, X., Zhao, H., Zhang, W., & Xu, M. Influence of moisture absorption on the DC conduction and space charge property of MgO/LDPE nanocomposite. IEEE Transactions on Dielectrics and Electrical Insulation. 2014. 21(4): 1957-1964.

[5] Praeger, M., Hosier, I. L., Vaughan, A. S., & Swingler, S. G. The effects of surface hydroxyl groups in polyethylene-silica nanocomposites. 2015 IEEE Electrical Insulation Conference (EIC). June 7-10, 2015. Seattle, Washington, USA: IEEE. 2015. 201-204.

[6] Bergna, H. E., DuPont, & Wilmington. Washington, DC: American Chemical Society. 1994.

[7] Gaber, A., Abdel- Rahim, M. A., Abdel-Latief, A.Y., & Abdel-Salam, M. N. Influence of calcination temperature on the structure and porosity of nanocrystalline SnO2 synthesized by a conventional precipitation method. International Journal of Electrochemical Science. 2014. 9(1): 81-95.

[8] Moniruzzaman, M., & Winey, K. I. Polymer nanocomposites containing carbon nanotubes. Macromolecules. 2006. 39(16): 5194-5205.

[9] Šupová, M., Martynková, G. S., & Barabaszová, K. Effect of nanofillers dispersion in polymer matrices: a review. Science of Advanced Materials.2011.3(1):1-25.

Smart House System for Energy Monitoring

Mohammad Sobree
Faculty of Electrical Engineering
Universiti Teknologi Malaysia
Johor Bahru, Malaysia.
mohammad.sobree@gmail.com

Hasimah Abdul Rahman
Centre Of Electrical Energy Systems,
Institute of Future Energy,
Universiti Teknologi Malaysia
Johor Bahru, Malaysia.
hasimahar@utm.my

***Abstract*— The project served to provide each house's socket electricity consumption to the user. This information can be accessed using a smartphone. The Blynk software used as user interface within the smartphone and communicate through the internet. At the same time, the power consumption will be calculated according to tariff set. Through this data, user able to decide whether they want to turn on or turn off that particular device(s). The project consists of Arduino as the controller, ACS 712 as a current measurement device and Relay Module as switch based on Arduino input. The ESP8266 in this project will act as a wireless network module which used to connect the system to the internet. Through this system, the user able to know their bill for each particular socket that connected to the system.**

Keywords— Smart House System; Energy Monitoring; IoT; Blynk; ESP8266;

I. INTRODUCTION

Electricity was first discovered in 1767 by Benjamin Franklin through his famous kite experiment during thunderstorm lighting. The evolve of Electrical Engineering was started in the early of 1990 by famous scientist such as Alexander Graham Bell, Thomas Edison and Nikola Tesla. Since the early 2000, the current trend shows that the global electricity consumption keeps on rising. As recorded by The World Bank, Electricity Consumption for the worldwide in 2010 is 2956.762 kWh per capita and in 2011 is 3021.38 kWh per capita. While in 2012 it grows to 3047.213 kWh per capita and in 2013 is 3104.382 kWh per capita. [1] While in Malaysia itself, the similar occasion occurred. Based on statistic made by Suruhan Jaya Tenaga (Energy Commission) Malaysia, the total electricity consumption generated Tenaga Nasional Bhd (TNB), Sabah Electricity Sdn Bhd (SESB), Sarawak Energy Sdn Bhd (SEB), for the year 2011 is 104474 GWh. This value increase in 2012 to 109299 GWh and 116089 GWh in 2013. Finally, in 2014, the electricity consumption reached 121699 GWh. [2]

Smartphone is currently one of devices that connected to people's daily life. Starting from people who lived in the cities until the village area, from youngster to the elderly, from high class society to the lower-class society. As technology advances and more features able to be performed on smartphone, this device has integrated into the society's daily life. A statistic conducted by statista.com recorded that in 2014, there were 1.57 billion mobile phone users worldwide. This number increase to 1.86 billion by 2015 and expected to reach 2.1 billion in 2016. [3]

With the rapid changes in technology and innovation, new demands created based on the current society needs. Home automation or Smart House System is one of the rising demand to increase our life's quality. There are 2 types of Smart House System based on its medium, which are wired and wirelessly connected. Wired connected automation usually has several remote attached in the wall throughout the house to control the electrical appliances. Users need to go to the remote device in order to set or adjust the Smart House System. While the wire also needs to be connected to the device manually, which would be a main weakness of wired connected Smart House System when users want to expand their system. Wireless connected Smart House System could overcome this problem and at the same time has even wider network range through the implementation of Internet of Things (IoT). Through the IoT, users able to control their system through the application of a smartphone.

The Powermeter is one of the common measurement devices for calculating the power energy in electricity. While Powermeter is able to be implemented in Arduino module, but there is still a little amount of research to combine power meter to the Smart House System. The implementation of power meter in Smart House System could provide users regarding the usage data of their electricity consumption. As the Smart House System connected with a smartphone, a user would be able to control their household easily and monitored their electricity consumption in any location.

II. LITERATURE REVIEW

As rapid changed and development of technology innovations in various fields, for example, telecommunication, electronic devices and renewable energy, over the couple of years, smart house system has become even more reliable and affordable for the household usage. There are 3 requirements in smart house system architecture. First is the requirements of measuring the conditions of the house. Next is processing the instrumented data. Last would be monitoring home appliances. The common approach in smart house system is microcontroller-enabled sensors which used to measure home condition and microcontroller-enabled actuators to monitor the household electrical appliances. [4]

One of the widely-used processing unit is Arduino. Arduino system able to send and receive commands to most of electrical devices. Arduino also able to send information in a specific device through the internet. It is supported with many input and output modules, indicators, sensors, motors, displays, and more making it able to interact easily with other electrical devices. [6] Arduino contained Atmel AVR processor with an open hardware design, which makes it can be build or modify by third party. Arduino used standard programming language which is simplified C++, in a processing-based IDE. The programming command, then compiled and uploaded to the Arduino device. [7]

With the help of microcontrollers and microcontroller platforms, Internet of Things (IoT) is becoming one of a bridge between computing and communication. IoT is a new IT technology developed where everything communicates and connected to each other through internet platform. These things are not bound only to electrical devices, but to everything that surround us. The IoT might also define as to utilize systems and devices connected intelligently based on data obtained from sensors and actuators embedded in machines or other physical objects. The main process of IoT is through data harnessing and analyzing to increase productivity and decrease costs. [12]

Through IoT, devices able to be controlled and sensed remotely while still performing the process. For example, coffee maker can produce coffee without needing the user's to be near the device. Everything in IoT able to communicate with each other through the Unique Identification that embedded within it. This device was identified through IPv6 address as it able to have vast devices registered compared to IPv4 with maximum 4.3 billion registered devices. IoT can monitor, search for anything present in the world, manage and control things automatically. Besides that, in entertainment, IoT able to play with things around us. For example, converting real world environment for gaming through the mobile phone's camera. [13]

While most Smart House System developed only limited to controlling the household electrical appliances, most of users still unaware with their electricity consumption. Thus, in order to help users in controlling their own electricity consumption, smart house system should also report the current energy usage in the house itself. By integrating this information to the smart house system through the concept of IoT, hopefully the energy consumption could be used even more efficient and effectively.

III. METHODOLOGY

This chapter emphasizes on the approach to create and develop the smart house energy monitoring system. The design approach has been divided into six phases which consist hardware and software implementation. The first phase would be project preliminary study, which used to provide necessary information and existing innovation and technologies related to the project. The next phase is designing the system's in term of hardware and software. The third phase is the hardware's systematic creation and implementation based on designs created. Their test also needs to be conducted in order to ensure the hardware able to provide desired output. In the fourth phase, the software based, which used in Android smartphone, will be developed using Blynk. Finally, in the last phase, the integration between Hardware and software.

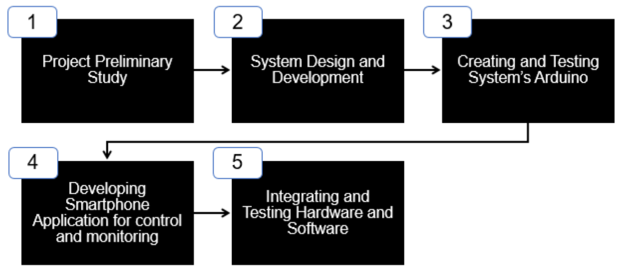

Fig. 1. Project Flow of the System Design and Implementation

In order for the controller to function correctly, the external module and hardware need to be connected to the controller. For this project, there are 2 crucial parts needed by controller, which is the current sensor (ACS712) and relay breakout board. This system used Arduino MEGA as the main controller of the system. While ESP8266 act as a wireless network module to communicate between the Arduino MEGA with internet network.

A. Arduino Mega

Arduino mega is based on ATMega2560 which used as a microcontroller unit in a system. This unit has a 16MHz crystal oscillator, 64 digital input/output pins, ICSP header, a USB connection, a reset button and a power jack. It also supports most of module and shields available and able to manage it. Arduino MEGA is chosen as it contains many pins which could help in further development.

Fig. 2. Arduino Mega

B. ACS712 – 30A (Current Sensor)

ACS712 is one of the current sensor module that suitable to be adopted in Arduino microcontroller including Arduino MEGA. The current sensor module is based on the Allegro ACS712ELC-30A chip. There are 3 pins in the ACS712 which is GND to ground, VCC to 5V and Out to any analog pin. For the specification, the supply voltage needed is 5Vdc Nominal. While the measurement range starting from -30 to +30 Amps. The scale factor would be 66 mV per Amp. [20] As current meter need to be connected in series with the circuit, the 3 terminals in ACS712 need to be inserted by series in the desired connection.

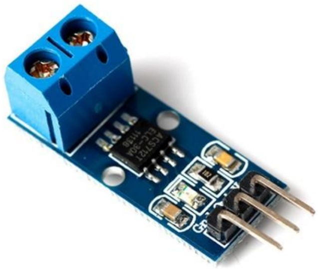

Fig. 3. ACS712 Current Sensor

C. *Relay Breakout Board*

By using the relay breakout board, the microcontroller can easily manipulate and control the relay by using 5v. There are 3 inputs in this module. The first is VCC which needed to connect with a 5V supply. Second is GND which required ground input. Finally the IN port from assigned digital pin. There are also 3 terminals which are COM, NO, and NC which acts as a switch for the connected circuit. There are many applications of this module such as, controlling high current load or voltage, solenoid valves, and AC load. [21]

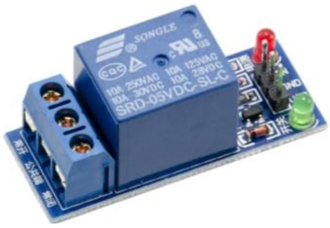

Fig. 4. 5V Relay Breakout Board

D. *Wireless Network Module*

The common WiFi module used in Arduino is ESP8266 WiFi Module. It able to provide any microcontroller an access to WiFi network through its integrated TCP/IP protocol stack. This module able to create its owned WiFi Network or connecting to an existing network. The ESP 8266 contained pre-program AT command set firmware causing it able to connect to any Arduino microprocessor. This module also powerful enough to run its owned program and devices due to its processor and on storage chip implemented. The ESP 8266 able to support Bluetooth module and APSD for Void Application. [11]

Fig. 5. ESP8266, Wi-Fi Module

IV. RESULT AND ANALYSIS

A. *Result*

Smart House System for Energy Monitoring prototype has been designed and created. The final design of the system can be seen in Figure 6. The system was tested to ensure that the final output suited with little error.

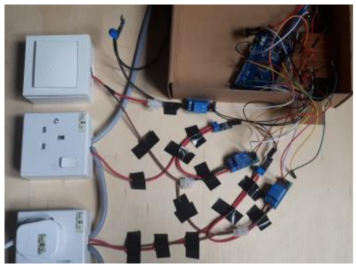

Fig. 6. Smart House System for Energy Monitoring

The smartphone interface for the Energy monitoring system is shown in Figure 7. It consists of switch button, display meter for power consumption and display meter for price expense. Each of the socket connected to the system will have this interface.

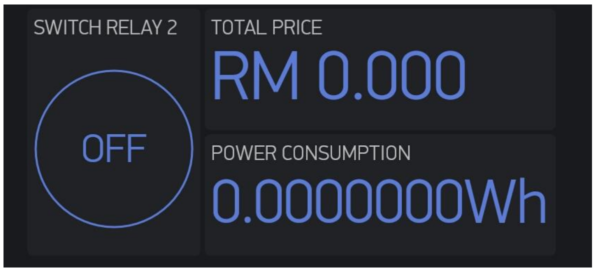

Fig. 7. Smartphone Interface

The control module in this system is the Relay Breakout Board. Relay will be acting as a switch in order to decide whether the system will turn on or turn off. In the circuit connected, Relay Breakout Board is connected in series along with the ACS712 current sensor. This will help the user to manipulate the circuit without needing to have physical contact with that particular socket.

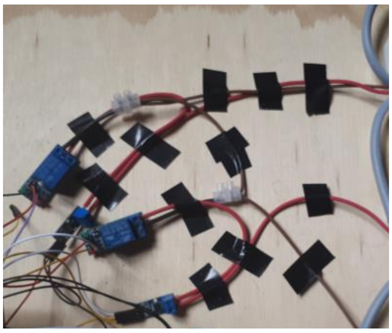

Fig. 8. Relay Breakout Board and ACS712 in series with circuit

B. Analysis

As the current measured in ACS712 is in AC current, the RMS current is used and need to be calculated based on the sensor's reading. As the sampling rate of this system is in 1 second, the microprocessor unit needs to ensure that the reading is the peak value in that particular circuit. In order to ensure that, comparison coding need to be done before finalizing to the reading.

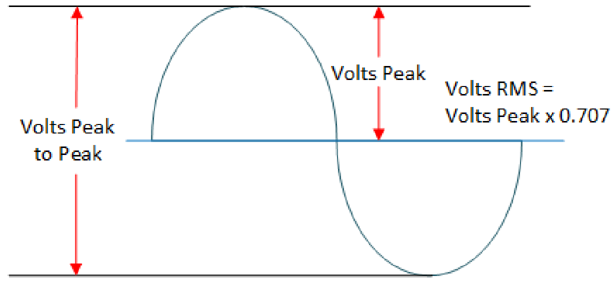

Fig. 9. AC Voltage Signal

There are several steps needed to convert the reading of sine wave form to RMS current form. The first step would be getting the peak to peak voltage. The result is obtained from peak to peak voltage will be inserted into the equation (1).

$$V_{RMS} = \frac{Vpeak\ to\ peak}{\sqrt{2}\ x\ 2} \quad (1)$$

The ACS712 module used in this system has a maximum range of 30A. As we already calculated the V_{RMS}, the scale factor need to be considered in order to find the I_{RMS} value. For the range of 30A, in order to find I_{RMS}, equation (2) will be used.

$$I_{RMS} = \frac{VRMS\ x\ 1000}{66} \quad (2)$$

In a single-phase house system, the power factor (PF) and V_{RMS} usually do not change much. Based on TnB information, the assumption no voltage and PF drop for this system, the PF would be 0.85 and residential voltage supply would be 240V. [22] While equation (2) already calculated the I_{RMS} value, the equation (3) is used to calculate Energy consumption per hour.

$$\text{Energy (Wh)} = \frac{\text{VRMS x IRMS x PF x t (sec)}}{36000} \quad (3)$$

By substituting in equation (3) with V_{RMS} equal to 240V and PF equal to 0.85, equation (4) is obtained.

$$\text{Energy (Wh)} = \frac{\text{240 x IRMS x 0.85 x t (sec)}}{36000} \quad (4)$$

After finding the Energy rate, the value is substituted to equation (5) where the price calculation started. In this system, the assumption tariff is made only from the first 200 KWh consumption, which is RM 0.218 / KWh. [23] As the unit in previous equation is Wh, the tariff become RM 0.000218 / Wh. Using this information, equation (5) is obtained which used to calculate the tariff.

$$\text{Tariff (RM)} = \text{Energy x 0.000218} \quad (5)$$

Before directly be used, calibrated would also needed in order to create an accurate measurement. The first 5 seconds should be a no-load condition, and the peak current measured should be recorded. This information will be used to get an offset value in that particular sensor.

Based on laboratory simulation and measurement, the actual current and the reading received by the system is as in Table I.

TABLE I. CURRENT MEASUREMENT WITH LOAD

No of Reading	Type of Measurement	
	Multimeter Measurement (mA)	*ACS712 – Current Sensor Measurement (mA)*
1	503	547
2	3000	2946
3	3546	3624
4	3570	3789
5	8150	7983
6	8610	8749

One of the limitation in this project would be the in term of data send and receive. As Blynk is a free hosting provider, the amount of information to be sent or receive in one second is limited to one. This could cause a delay when sending or receiving a data and instruction. Blynk also unable to record previous data each time the connection is disconnected, so the Arduino will start with initial information for each of the parameters set.

V. CONCLUSION

This project focused on smart house system which solely used Energy monitoring as the topic. The objectives of this study is to create a system that is able to notify users regarding their electrical consumption and at the same time making them able to control it. The Arduino MEGA serves as the microcontroller together with ESP 8266 creating a wireless network system. This makes them able to establish internet connection with android smartphone making them become much more convenient.

As the monitoring system is one of the basic functions, the project could still be improved in the future. More parameters can be included such as automated control and synchronizing virtual and physical switch in one command and helpfully help user to minimize their power consumption further.

REFERENCES

[1] World Bank. (2014). Electric Power Consumption. Retrieved November 12, 2016, from http://data.worldbank.org/indicator/EG.USE.ELEC.KH.PC?end=2013&start=2010

[2] Suruhan Jaya Tenaga (Energy Commission). (2015). Malaysia Energy Statistics Book 2015. Putrajaya, Malaysia: Malaysia Energy Information Hub Unit.

[3] Statista. (2016). Number of smartphone users worldwide 2014-2020. Retrieved November 12, 2016, from https://www.statista.com/statistics/330695/number-of-smartphone-users-worldwide/

[4] Soliman, M., Abiodun, T., Hamouda, T., Zhou, J., & Lung, C. (2013). Smart Home: Integrating Internet of Things with Web Services and Cloud Computing. 2013 IEEE 5th International Conference on Cloud Computing Technology and Science. doi:10.1109/cloudcom.2013.155

[5] Boxall, J. (2013). Arduino workshop: A hands-on introduction with 65 projects. San Francisco: No Starch Press.

[6] Badamasi, Y. A. (2014). The working principle of an Arduino. 2014 11th International Conference on Electronics, Computer and Computation (ICECCO). doi:10.1109/icecco.2014.6997578

[7] D'Ausilio, A. (2011). Arduino: A low-cost multipurpose lab equipment. Behavior Research Methods, Vol. 44, no. 2, 305-313. doi:10.3758/s13428-011-0163-z

[8] Ahmed Alhaj, A. S. (2015). Home Automation System Using Arduino (Degree's thesis, Universiti Teknologi Malaysia). Skudai: Faculty of Electrical Engineering.

[9] Molly Edmonds & Nathan Chandler. How Smart Homes Work. 25 March 2008. HowStuffWorks.com. <http://home.howstuffworks.com/smart-home.htm> 19 November 2016

[10] Han, D., & Lim, J. (2010). Smart home energy management system using IEEE 802.15.4 and zigbee. IEEE Transactions on Consumer Electronics, Vol. 56, no. 3, 1403-1410. doi:10.1109/tce.2010.5606276

[11] Thaker, T. (2016). ESP8266 based implementation of wireless sensor network with Linux based web-server. 2016 Symposium on Colossal Data Analysis and Networking (CDAN). doi:10.1109/cdan.2016.7570919

[12] Thiyagarajan, M., & Raveendra, C. (2015). Integration in the physical world in IoT using android mobile phones. 2015 International Conference on Green Computing and Internet of Things (ICGCIoT). doi:10.1109/icgciot.2015.7380576

[13] Kaur, J., & Kaur, K. (2016). Availing Internet of Things in Industrial Decision Making - A Survey. 2016 International Conference on Electrical, Electronics, and Optimization Techniques (ICEEOT). doi:10.1109/ICEEOT.2016.7755075

[14] Al-Fuqaha, A., Guizani, M., Mohammadi, M., Aledhari, M., & Ayyash, M. (2015). Internet of Things: A Survey on Enabling Technologies, Protocols, and Applications. IEEE Communications Surveys & Tutorials, 17(4), 2347-2376. doi:10.1109/comst.2015.2444095

[15] Shabtai, A., Fledel, Y., Kanonov, U., Elovici, Y., Dolev, S., & Glezer, C. (2010). Google Android: A Comprehensive Security Assessment. IEEE Security & Privacy Magazine, 8(2), 35-44. doi:10.1109/msp.2010.2

[16] Xie, B., & Abelson, H. (2016). Skill progression in MIT app inventor. 2016 IEEE Symposium on Visual Languages and Human-Centric Computing (VL/HCC). doi:10.1109/vlhcc.2016.7739687

[17] Pokress, S. C., & Veiga, J. J. (2013). MIT App Inventor: Enabling Personal Mobile Computing. PRoMoTo 2013 Proceedings.

[18] Madhumetha, M., Athiya, G., Raveena, R., & Banupriya, N. (2016). Hybrid Sensing System for Monitoring Air Quality. Middle-East Journal of Scientific Research. doi:10.5829/idosi.mejsr.2016.24.IIECS.23172

[19] Vani, P. D., & Rao, K. R. (2016). Measurement and Monitoring of Soil Moisture using Cloud IoT and Android System. Indian Journal of Science and Technology, 9(31). doi:10.17485/ijst/2016/v9i31/95340

[20] H. (2017, February 06). ACS712 Arduino AC Current Tutorial. Retrieved May 13, 2017, from http://henrysbench.capnfatz.com/henrys-bench/arduino-current-measurements/acs712-arduino-ac-current-tutorial/

[21] Cytron. (n.d.). Single channel 5V relay breakout board. Retrieved May 13, 2017, from https://www.cytron.com.my/p-bb-relay-5v-01

[22] TNB. (n.d.). Power Factor. Retrieved May 14, 2017, from https://www.tnb.com.my/commercial-industrial/power-factor

[23] TnB. (n.d.). Pricing & Tariffs. Retrieved May 13, 2017, from https://www.tnb.com.my/residential/pricing-tariffs/

Arduino based Harmonic Analyzer

Akmal Afiq Yusri
Faculty of Electrical Engineering
Universiti Teknologi Malaysia
Johor Bahru, Malaysia.
aafiqyusri@gmail.com

Dalila Mat Said
Centre of Electrical Energy System
Faculty of Electrical Engineering
Universiti Teknologi Malaysia
Johor Bahru, Malaysia.
dalila@utm.my

***Abstract*—Due to non-linear electric loads, it could result to harmonic voltages and currents in an electric power system. While frequent cause of power quality problems in the power grid caused by harmonic frequencies. Harmonics in power systems result in increased heating in the equipment and conductors that could lead to equipment failure. Furthermore, harmonic distortion also causes torque pulsations in motors and misfiring in variable speed drives. Early detection of harmonics is considered desirable since it can avoid any further damage to the equipment. Fluke 435 is multipurpose meter that is widely used for harmonic distortion detection. Nevertheless, Fluke 435 is a very complex device and expensive. Moreover, it takes a longer time to set up this device. In this project, a prototype of Arduino Based Harmonic Analyzer will be designed to approve that the system can detect the harmonic distortion. The goal of this project is to propose a solution for detection of harmonic distortion in the early stage. Besides cheap and much simpler, it is easy to set up. By clamping the device to the harmonic source, it can display the output waveform.**

Keywords—Total harmonic distortion; Liquid crystal display; Current transducer

I. INTRODUCTION

In this era of globalization, every building and electrical equipment need to in good condition in order to avoid accident or losses in damaged equipment. A perfect equipment usage without any problem is expected from every company yet it is impossible where there is no such thing perfect electrical equipment that can perform well for the next 5 years without any problem. The reality case is the real voltage and current waveforms are distorted.

These distortions can occur for few reasons such as non-linear load in a system, a rotating machine, power supply of semiconductors and thyristor controlled reactors and the arcing device. Thus, when distortion rise the Total Harmonic Distortion (THD) will increase too. This can damage electrical equipment in the building itself.

The frequency of standard building's load is 50 Hz or 60 Hz (fundamental frequency). The first harmonic will belong to fundamental frequency of 50 Hz, the 2nd harmonic is 100 Hz, and the 3rd harmonic is 150 Hz, and so on. This harmonic component will increase and as it increases, it will strengthen the nonlinear load by consumers. Thus with the largest value of frequency current produced by nonlinear loads, it can damage equipment and make sudden failure from sustained overheat.

Fig. 1. Example of damaged equipment due to distortion

These problems are actually have a long term effects focusing in transmission lines and wires where skin effect occurred with the operation of protection circuit. Thus, it is critical to solve this problem as soon as possible of harmonic distortion in order to avoid the damage and to preserve the safety of customer, device and also quality of the systems, yet also can save the spending on replacing the damaged device or fix it.

A. Problem Statement

Distortion of harmonic can caused damage to any electrical equipment due to several conditions such as the harmonic impact is enhanced, resonant condition and capacitor banks damaged. The damage equipment not only involved the first party but the worst case is it can affect other electrical equipment on the system. This actually can be prevented by being able to detect the distortion as soon as possible, yet the device used to detect this is expensive and take time to set up the device itself also known as FLUKE 435. This could be one of the reasons why the common problem cause by distortion is frequently occurs with or without the person in charge to this matter.

Fig. 2. Example of commercialize multipurpose meter (FLUKE 435)

B. *Objective*

The specific objectives of this project are:

a) To investigate the type of load that produce harmonic.

b) To design and develop the system of Arduino based harmonic analyzer.

c) To validate the proposed harmonic analyzer with FLUKE 435.

C. *Paper Outline*

This paper is organized as follows: in Section I, an introduction along with the problem statement and objectives was addressed. Section II describes the literature review related to the project. In addition, Section III explained the project methodology to develop the proposed system. In the last two sections, results and analysis were tabulated and discussed followed by the conclusion section.

II. Literature Review

This chapter will explain in details about the source of harmonics, harmonic distortion effects on electrical equipment, effects of harmonic and economical harmonic analyzer compare to Fluke 435.

A. *The Source of Harmonic*

There are various sources of harmonics in power systems, it share a common characteristic which is a non-linear voltage-current operating relationship. The fluctuation of load causing the current does not correspond to applied voltage waveform [1].

Next, there are much more common sources come from applications of solid-state devices. These also conclude:

a) *Rectifier output control*

b) *Frequency conversion*

c) *Diode (simple rectifier)*

Other examples of non-linear loads include common office equipment such as computers and printers, Fluorescent lighting, battery chargers and also variable-speed drives [8].

B. *Effects of Harmonic*

The negative effects of harmonic are usually unnoticed until problematic things happen such as failure of equipment [12]. These harmonics has a catalyst factor such as non-linear loads due to high demand nowadays as the world growth in economy as well as technology [1].

Harmonics also tend to slowly to increases due to eddy current loss [2,3]. Furthermore, harmonic can be neglected on any cases yet it also cannot be freely increases because the result of that usually turns bad [7].

C. *Harmonic Distortion Effects on Electrical Equipment*

“The impact of harmonics is enhanced, with damaging results.”[2].This phrase shows that if the harmonic distortion is not being contained, it would cause a damaging effect to the equipment and then it can affect the neighborhood equipment. As a more critical condition, substantial damage can occur due to harmonic resonance [4].

In addition, harmonic can actually be transmitted from one facility to another especially if it share it common transformer [7]. These also another critical damage cause by harmonic distortion. Still, 2nd, 5th and 8th harmonic create a negative torque on motor running [6]. This is totally a disadvantage of this problem.

D. *Economical Harmonic Analyzer Compare to Fluke 435*

A great harmonic analyzer should be easy to use and able to show you graphically the problem of your component harmonics and as a bonus should be able to show more information for example you’re Total Harmonic Distortion (THD) [10].

III. Methodology

After In this chapter, method to conduct this project is briefly explained. The general block diagram and the flow chart of the project are presented. There is example of device Fluke 435 that is act as comparison to the project device. Also, review on the structure that the CT sensor, LCD and Arduino combined. This aim of this chapter is to give an overview of the project that lead to the final result.

A. *Project Design*

Basically, this project required a controller, sensor and display to be able to display the harmonic display. For this project Arduino will act as controller, CT sensor as the sensor (clamping to the wire) and LCD display 128x64 as the display platform.

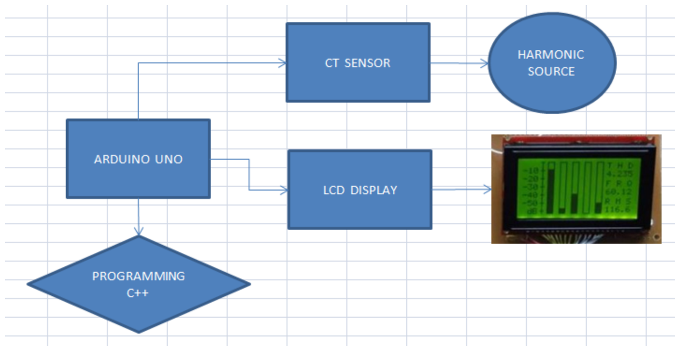

Fig. 3. Basic flow chart

This flowchart is the basic structure of the project where starting from a harmonic sources then usage of CT sensor to detect the harmonic up to 5th harmonics. Arduino act as the controller with a programming set to the arduino and display it on the LCD display.

B. *Components and devices used*

The benefits of the conducted project show that besides design and develop a new Arduino based harmonic analyzer, it is an improving way of designing a much simpler and cheaper device for a similar functional of harmonic analyzer. By detecting the distortion in the early stage, there is a chance to avoid all the possibility of electrical equipment been damage by the distortion. This project is focusing on single phase harmonic producer, to be exact the project focusing on single phase lamp. The various type of lamp will be further explained on preliminary result. Harmonic output generated will be compared with the commercial harmonic analyzer. If the comparison process resulting the same display, the project consider succeed and the problem statement is solved with prove.

Fig. 4. ACS 712 (CT sensor)

Fig. 5. Arduino UNO

Fig. 6. Light crystal display (LCD) 128x64

C. *Operational Framework*

With only single phase harmonic source, the measured harmonic cannot measure a three phase harmonic. In addition, this project would have an unstable display because of the device usage and frequency differential between device and harmonic sources. Compare to Fluke 435, this project only can display harmonic whereas Fluke 435 can measure three phase, voltage, current and many more. Yet, it is understandable that it is really complicated to design or duplicated such device.

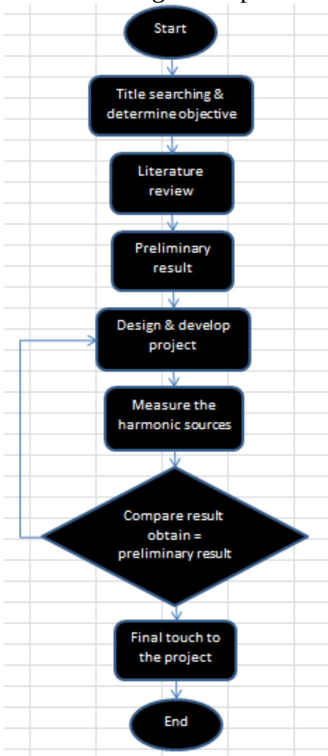

Fig. 7. Operational flowchart

IV. RESULT & ANALYSIS

At the end of this project, the Arduino based Harmonic Analyzer is expected to display the same harmonic form as the FLUKE 435 display. Thus, that proved that this project successfully replace the FLUKE 435. The preliminary result that has been experiment has 4 variables such as LED (36W), T8 lamp, T5 lamp and CFL.

A. *Preliminary result*

Figure 8 & 9 shows the output display along of the first until fifth harmonic by the FLUKE 435. The measurement use the LED, T8 lamp, T5 lamp and also CFL as the source of harmonic.

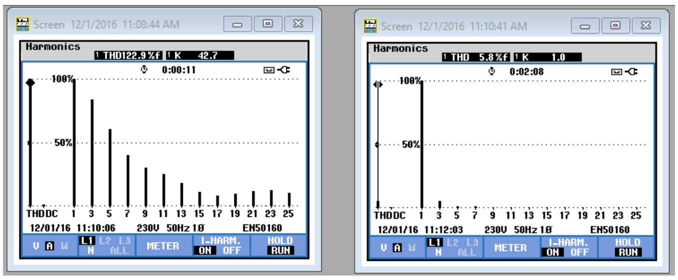

Fig. 8. Harmonic pattern of LED & T8 lamp

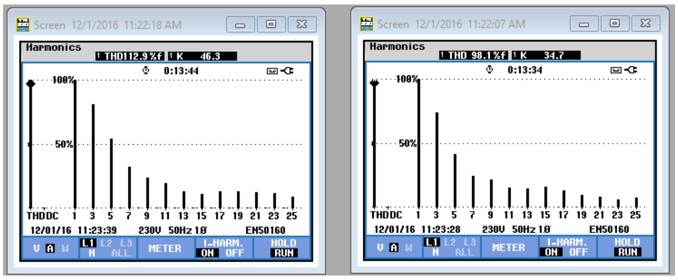

Fig. 9. Harmonic pattern of T5 lamp & CFL

B. *Project result*

This project was only able to be carried out for CFL as the stability of the project is not stable and due to some component the usage is limited. Here is the LCD display that have benn measured by the project.

Fig. 10. CFL harmonic display

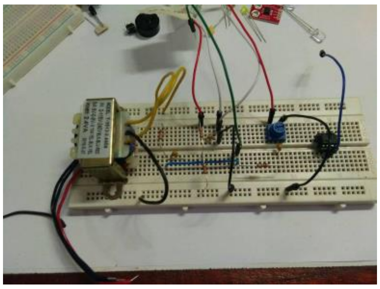

Fig. 11. Project circuit

As the display measure show the harmonic pattern, the result show a slight different between second and forth hamonic where the LCD preview a different display from FLUKE 435. Thus, this prove the project is still unstable for the time being.

V. Conclusion

This project was able to achieve the objective to duplicate the function of harmonic display by FLUKE 435 from 4 sources of harmonic.

As for the future work and plan, the project can be design and upgrade it with a harmonic analyzer using Arduino Uno as the controller and CT sensor act as the clamp mechanism to measure the harmonic and LCD display (128x64) will act as display device. On the other hand, a programming for the Arduino will be using a C++. With an improvement of additional function for example voltage display, current display and so much more. Thus, an additional circuit also would be needed to implement the CT sensor to the Arduino. Furthermore, the design will be tested frequently to be able to display the same harmonic as FLUKE 435 obtained in the preliminary result. Then, a compact casing will be design for the closure of the circuit and device as the finishing touches for this project.

VI. Acknowledgement

I would like to start my appreciation and deepest gratitude to almighty Allah for provide me the health, commitment and the strong will to finish my final report 1 in semester 1 and be able to done this report within the due date. A great and highest thanks to my supervisor, Dr. Dalila binti Mat Said, who has been really supportive and continuously guide me for where sometimes I am lost regarding to this project. I really appreciate all the suggestions and comments to drive me on the right track for this project to be success. Not forgetting, a millions thanks and love to all my family members for always support and keeps me going throughout the project. Also, I would like to express my deepest thanks to all my friend who help me directly or indirectly throughout this semester whether sharing ideas or support me when I am lost.

References

[1] N.senthilnathan, Virtual harmonic analyzer harmonic analysis and estimation of thd using LabVIEW, 2009.

[2] Sung W. P., A new portable harmonic analyzer based on MSP430, 2014.

[3] Hamdan Daniyal, Arduino based power meter using instantaneous power calculation method, 2015.

[4] Hammack B., Albert M., Harmonic analyzer, 2014.

[5] Christopher M., Arduino based wireless power meter, 2010.

[6] Mohd Zawawi M. F., Comprehensive analysis of economic impact on distribution transformer due to harmonic, 2015.

[7] Robert G. E., Power system Harmonic: A reference guide to causes, effects and corrective measures, 2001.

[8] Said D. M. & Nor, K. M. . Effects of harmonics on distribution transformers, 2008.

[9] Naja'a amalina binti ilias, Improving power quality by reducing the harmonics distortion in distribution area, 2015.

[10] Ahmad Ali I., Comparison of several types of compact flourescent lamp in terms of harmonic and illumination, 2011.

[11] Mohd Hafifi R., Impact of compact flourrescebt lamp in term of total harmonic distortion, 2011.

[12] Ming-Yin Chan, A Case Study Survey of Harmonic Currents Generated from a Computer Centre in an Office Building, 2007.

[13] Alan G. Smith, Introduction to Arduino, A piece of cake, 2011.

[14] Chris Trane T., Arduino Energy meter, 2014.

[15] Maswood, I. A. & Haque, M. H., Harmonics, sources, effects and mitigation techniques, 2002.

[16] Power P., Power Quality and Harmonics: Causes and Effects, 2015.

Solar Sun Tracker with Energy Monitor

Muhammad Nasrul Bin Mohammad Radzi
Faculty of Electrical Engineering
Universiti Teknologi Malaysia
Johor Bahru, Malaysia.
mnasrulradzi@gmail.com

Dr. Awang Bin Jusoh
Department of Electrical Power Engineering
Faculty of Electrical Engineering
Universiti Teknologi Malaysia
Johor Bahru, Malaysia.
awang@fke.utm.my

***Abstract*—Nowadays, energy demand keeps increasing year by year while fossil fuels and other raw materials used to generate energy are decreasing fast. On the other hand, renewable energy is our hope to continue to supply us with the energy needed so that we can use it in our daily life. Photovoltaic system is one of the renewable energy and is widely adopted all around the world. Even though it is not widely implemented in Malaysia, photovoltaic system is considered one of the most suitable type of renewable energy in this country since the statistic of solar irradiance in Malaysia is high. This project aims to construct a photovoltaic system that has more efficiency to absorb the sunlight and generate electricity. The dual-axis sun tracker by using the LDR sensor is capable of following the direction of sunlight accurately hence increasing the solar panel exposure towards sun light. Also, an energy monitor has been designed to ensure that it is suitable to be used with a photovoltaic panel and it is the one of innovation. It can help the user to monitor the energy generated by the solar photovoltaic system day by day and improve the system based from the data collected. This dual-axis photovoltaic panel is using the sunlight energy to supply power to the controller and the actuators. Hence, this system becomes a fully independent system that can improve the energy quality in our country.**

***Keywords*—solar panel; sun tracker; arduino; servo motor; energy meter; bluetooth.**

I. INTRODUCTION

Solar energy is a form of renewable energy which means that it will never run out. This is because the source of solar energy is the sun or more specifically the UV ray that is produced by the sun. The solar panel is equipment that made up from solar cells which capture the sunlight and convert it in form of electrical energy by using photovoltaic effect. Photovoltaic effect is the process of converting sunlight to voltage or electricity and it involve both of the physical and chemical reaction. Firstly, when the sunlight is absorbed by a material and it excites the electrons inside it causing the electrons to break free from their atoms into higher energy states. For this case, the separation of the charges will cause a potential difference. The sunlight has to have enough energy to overcome the excitation barriers for this process to happen.

There are two ways to make the solar tracker which are single axis solar tracker and dual axis solar tracker. Single axis solar tracker only move the solar panel horizontally or vertically and usually it is used for large photovoltaic system such as solar farm but dual axis solar tracker move the solar panel both horizontally and vertically and it is suitable for small system especially for residential usage.

Whilst the system efficiency can be solved, we need to ensure that the system can run independently. This means that all the components and actuators that related to the sun tracker must use the energy generated from the photovoltaic solar system. Other than that, the power and energy produced should be monitored so that the system performance can be tracked and improvement can be made to increase the output productions.

The scope for this project is designed hardware of solar photovoltaic system with dual-axis sun tracker and fully independent system. This is the first step to get the best design for use in this project. Besides that, this project also builds the monitoring system for the power generated by the solar panel so that user can monitor energy and apply further improvement based from the data collected. Lastly, this project also needed to understand the characteristic of light dependent resistor and the characteristic of the actuator used. This project is focus on the mechanical part and the electrical MPPT will not be used

II. LITERATURE REVIEW

Solar panels refer to the equipment that absorbs or uses sun's rays to generate electricity or heating. Solar modules use light energy which is photon emitted from the sun to generate electricity using the photovoltaic cells through photovoltaic effect. However, the main challenge is on how to maximize the sunlight shines on the solar panels to maximize the electricity produced [1]. A solar panel works by allowing light particles (photons) from the sun to knock electrons free from atoms, generating a flow of electricity. Many cells are linked together make up a solar panel. Photovoltaic cells are made from layers of semi-conducting material, usually silicon. When light shines on the cell it creates an electric field across the layers. The stronger the sunshine, the more electricity is produced [2]. Electrical connections are made in series to achieve a desired output voltage or in parallel to provide a desired current capability. The cells must be connected electrically to one another and to the rest of the system. Photovoltaic power systems are generally classified according to their functional and operational requirements, their component configurations, and how the equipment is connected to other power sources and electrical loads. The three principal classifications are grid connected system, hybrid systems and stand-alone systems [4]. Photovoltaic systems can be designed to provide DC and/or AC power service, can operate interconnected with or independent of the utility grid, and can be connected with other energy sources and energy storage systems.

It has been found out that the solar panel efficiency improved by 30-60 percent when we use tracking system instead of fixed solar panels [6]. Sun trackers direct solar panels or modules toward the sun. These devices change their orientation throughout the day to follow the sun's path to maximize energy captured. Single-axis sun trackers only rotate on one axis in a single direction. There are three different types of single-axis sun trackers include horizontal, tilted, and polar aligned (azimuth) [1]. Dual-axis trackers continually face the sun because they can move in two different directions and it has two types which are tip-tilt and azimuth-altitude. In single axis horizontal trackers, a long horizontal tube is supported on bearings mounted on the frames. The axis of the tube is on a north–south line. Panels are mounted upon the tube, and the tube will rotate on its axis to track the apparent motion of the Sun through the day. Vertical single axis trackers axis of rotation is vertical with respect to the ground. These trackers rotate from East to West over the course of the day. All trackers with axes of rotation that is between horizontal and vertical axes are considered tilted single axis sun trackers. Singles axis sun tracker is implemented widely in solar farm at all around the world while dual axis sun tracker is implemented for household or small usage. The dual axis sun tracker gives freedom to the solar panels to be moved anywhere perpendicular to the sun direction. Dual axis trackers used to gain optimum solar energy levels due to their ability to follow the sun vertically and horizontally.

Renewable energy is still in development in Malaysia. But we have taken steps that it further deployment in our country by adopting a renewable energy feed-in tariff (FiT) mechanism under the country's 2011 Renewable Energy Act. FiT implementation purposes are to support and enhance the growth of renewable energy development in Malaysia while also enhancing energy security and addressing climate change challenges. Mainly, FiT implementation is focused on review and improvement of rates for solar photovoltaic system, small hydropower, biomass, and biogas system. Other than that, FiT also focusing on analysis of other potential policy mechanisms to support large-scale deployment of solar photovoltaic system such as auction and tendering purposes. Also, FiT support for design of a geothermal energy based from experiences and benchmarks in other country. We must know that FiT is not only applied to solar photovoltaic system but to all types of renewable energy. With this new policy, Malaysia is targeting that 11% of renewable energy capacity to be installed by 2020 [7]. Other than that, to supporting solar photovoltaic FiT, Malaysia has launched a new net metering policy (NEM) in January 2016. The NEM purpose is to support tendering approaches for larger scale system

III. PROJECT METHODOLOGY

The main objective of this project is to design dual-axis solar tracker that follow the movement of the sun precisely using microcontroller. In order to achieve that objective, the prototype of that sun tracker is design using four light dependent resistors (LDR) and using Arduino UNO. The source code of the Arduino programming is included in the appendix A at the end of this report. The general block diagram of the sensor is shown in figure 1. The sun tracker is the most important equipment in this project because it will detect the sun position and give the controller direction to rotate. However, the materials and components needed for the sun tracker is very easy to find. This makes the sun tracker easy to be built. Table below shows the materials needed to build the sun tracker.

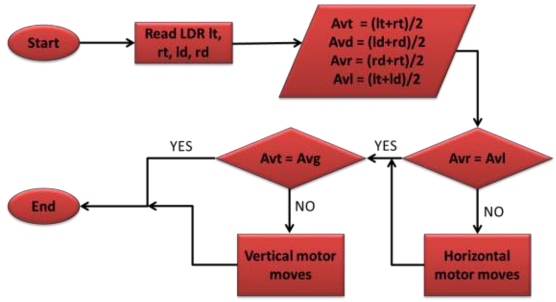

Figure 1: Sun Tracker Flowchart

A. *Overall SystemsDesign*

These project subprojects are to make a sun tracker and energy monitor. For that purposes, a proper plan will be needed to ensure that all the works will run smoothly. The main components of this project will also needed to be specified early so that they can be finished early compared to other components. Basically, the main components of this project are the sun tracker, energy monitor system and the actuator implementation. In this topic, we will review all the main components design and their system.

The actual sun tracker sensor body is designed same as the prototype, but instead of being on its own, it will be attached to the solar panel holder. This means that the servo motor in the actual design will not be attached directly to the sun tracker. This is to ensure that the motor can work perfectly to move the solar panel, not only the sun tracker. Other than that, all of its function and working principle remain the same as the prototype version. For the solar panel movement, it will be done by two 9g servo motors. One will act as the horizontal motor and the other as vertical motor. Servo motor can rotate from 0 degree to 180 degree circular motion. Besides, since I am using Arduino as the controller, servo motor can be directly attached to the Arduino without any motor driver. This will save some budget for the project. The motors will be attached to the hardware that will be made with 3mm plywood. Other than plywood, we also can design the hardware using 3D printing. The upsides are our hardware become lighter and more precise. But the downside is that this project cost will increase drastically because 3D printing is very expensive.

For the energy monitor design, two 5V solar panels will be used and connected in parallel. This will make the output voltage remain as 5V but the current produce will be bigger. Hence, the power generated also will be bigger. Both solar panels will be connected to two current sensors to measure the current and it will be directed to the voltage divider circuit to measure the output voltage produced. All of this information will be connected to the Arduino microcontroller and the controller will then calculate the power generated and energy produced and it will display the result via the LCD screen connected. Other than that, the Arduino controller will be connected to the Arduino bluetooth module so that the user can surf the data via their mobile phone using Arduino RC application. This application will enable the user not only to keep track with the power generated, but it also enable user to directly control the whole system and save the data gained into their mobile phone. The figure below shows the overall system operation overview and proposed hardware design.

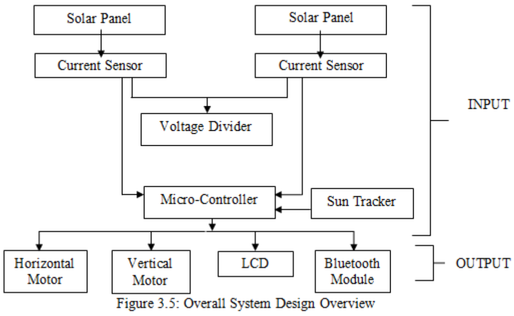

Figure 2: Overall system flowchart

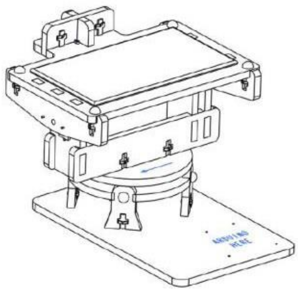

Figure 3: Hardware Design

B. Hardware Development

Based from previous part, the construction of the system is still the same, but instead of using 3D printed material, I used 3mm plywood. The reason that I choose 3mm plywood is that it is lighter than 3D printed materials. Also, we can save much money and time because the plywood is much cheaper and I can cut the plywood myself to save time.

The hardware consists of three parts which are base, middle and top part. The base part will be to place the horizontal motor while the vertical motor will be placed at the middle part and also the middle part used to connect both the motors to the solar panel holder which is located at top part. The top part must be strong so that the system will not collapse. The actual parts will be shown in the figures below.

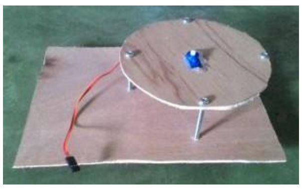

(a)

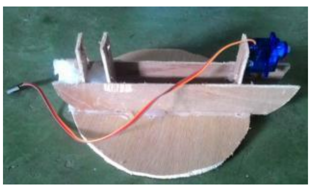

(b)

(c)

Figure 4: base (a), middle (b), top (c)

C. Circuits connection

Both servo motors are connected to the Arduino directly. But the vertical servo motor will need jumper wire to make their movement smoother and prevent any accident. The signal wire of the servo motors wi8ll be connected to PWM pin of the Arduino. For horizontal motor, it is connected to PWM pin 9 and for vertical motor it is connected to PWM pin 10. The diagram of t5he connection is as below.

Light dependent resistor (LDR) on the other hand will be connected to analog input pin of the Arduino. One pin of LDR is connected directly to the 5V voltage supply of the Arduino and another pin is connected series with 10 KΩ resistors and connects direct to ground. Between connection of the LDR and resistor, a jumper wire is connected the pin to analog input pin of the Arduino. Figure below shows one connection of LDR and another three LDR follow the same step. The connections are listed in the table below.

The voltage divider circuit and current sensor circuit is made to be as simple as possible. T5he current sensor used ACS712 current sensor module than can be connected to the Arduino directly. This current sensor will detect the amount of current produce by the solar panels. Also, this current sensor must be connected to an electrical load for it to be functioning well. For the voltage divider circuit, I used a simple voltage divider principle using two 10 kΩ resistors connected from the solar panel and into the Arduino. The diagram of the circuit is shown below.

Last but not least, the connection for LCD and Bluetooth module acted as user interface. Basically, the connection of the Bluetooth module is so simple because it only has 4 pins which are Vcc, Gnd, Tx and Rx. The Bluetooth module is connected to Arduino based of their respective pins. Vcc and Gnd are connected to Arduino Vcc and Gnd and the Tx and Rx pins are connected to Arduino Tx and Rx pins which are the Digital Input pin number 0 and 1. For the LCD connection, it is a bit complicated because lcd consist of many pins that need to be connected to the Arduino. So I will explain the connection using diagram of the complete circuit connection below.

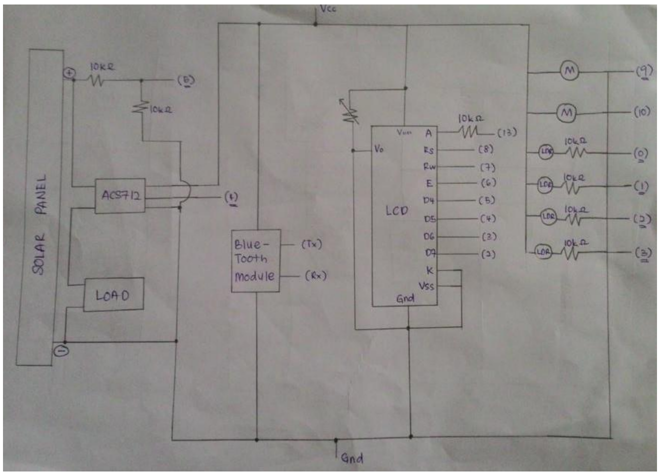

Figure 5: Complete circuit connection

All of the connection will be connected using printed circuit board (PCB). This is so the circuit can be troubleshooting easily and it can last longer. The PCB development will be discussed after this in the next subtopic.

D. Printed Circuit Board (PCB)

The processes for designing a PCB begin by designing the circuit by using Proteus software. Because of in this project the PCB used both top and bottom circuit on the same copper board, this condition must be factored in the software designer tool so that it can differentiate between top and bottom connection. Generally, for the top connection was used for the peripherals to Arduino connection and the bottom connection was used for the power supply connection.

After the designing the PCB circuit was done, the circuit must be printed on a laser jet printer on specialized glossy paper. This is because to ensure that the ink printed are able to stick on the copper board after press heating process. The copper board that has copper on both sides of the board was used to make the dual layer PCB. After that, the process was continued with the press heating process. For the press heating process, the laminate machine needed to be heated at 200°C for about 15 minutes. Also, for dual layer PCB, several references point must be created to ensure that the top and bottom PCB will be parallel and match each other. If not, the top and bottom PCB will not be connected and this will be a waste of time and money.

Next step is the removing of the glossy paper from the board carefully leaving only the carbon layer circuit on the copper board. The carbon layer is used to protect the copper layer that it covered so in the next part, only unnecessary copper will be removed. One reminder for this step, after removing the glossy paper, check the circuit thoroughly and ensure there is not missing or discontinued carbon connection for the circuit. If there is discontinued carbon connection maybe due to rash paper removal step, the connection need to be created or to be more accurate, sketched back on the copper board using carbon ink pen. For the next step, the unnecessary copper need to be removed from the board by using specialized acid solution. This process is called etching process and it will take the longest time. To help speed up the process, the PCB was shook inside the solution so that the useless copper will be removed faster.

Finally, the PCB is finished and needed to be cleaned by using clean water to ensure no external materials still attached to the board. After this, the point created on the PCB was drilled using small point driller and this step was done very carefully to ensure nothing happened to the copper connection. After the drilling step is done, the component was placed on the PCB and soldering process was done. One reminder for the soldering process makes sure that the bottom components are soldered to the bottom circuit and vice versa so that the circuit is connected. If the components need to be connected to top and bottom circuit, solder it to both top and bottom PCB.

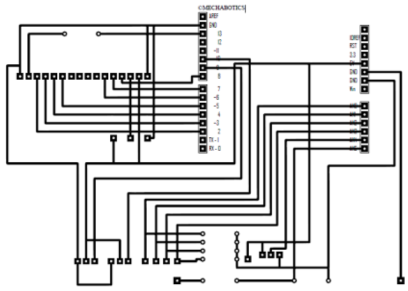
Figure 6: Complete PCB circuit printed

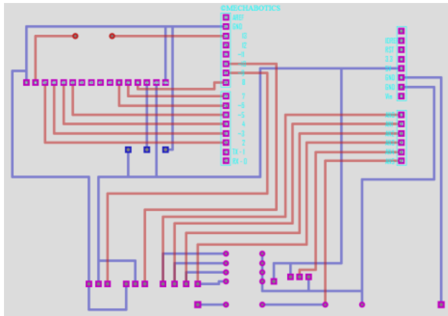
Figure 7: Complete PCB circuit designed, (top = red, bottom = blue)

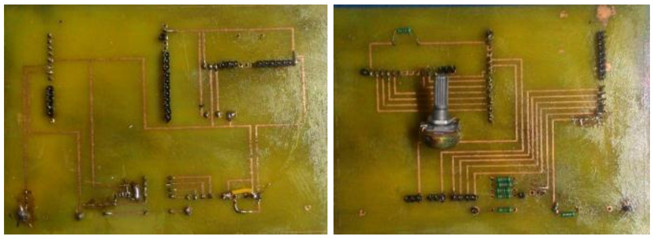
(a) (b)

Figure 8: bottom layer (a), top layer (b)

IV. RESULT AND ANALYSIS

A. Sun Tracker Results

The sun tracker sensor works perfectly because it follows the sun movement or in this case torchlight was used and directed at the sensor to move the sensor around. The sensors that are attached to the plane which is the same as solar panels will ensure that the solar panels will also face the direction of the light source directly. The actuator which are the horizontal servo motor and vertical servo motor have no trouble moving the solar panels and the plane because of the load applied on them is still light.

The motor was set to move slowly because in the real situation, sunlight movement during the day is very slow. So as the motor also move slowly and this will give more accurate placement and avoid any overshoot. Both of the servo motors have been limited to only rotating from 0 degree to 180 degree. This is to ensure that the wire from the motor and sensor will not be tangled.

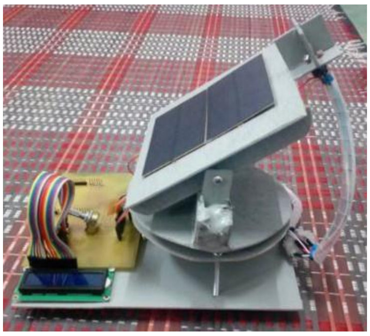

Figure 9: Initial condition of the solar panel (side view)

Figure 10: Initial condition of the solar panel (front view)

Figure 11: Right side sun tracker testing

Figure 12: Left side sun tracker testing

The energy meter is only capable of displaying the data that the microcontroller provides. It does not have the capabilities to store the data or transfer the data to other device. This will make the system much simpler and lighter. But for large scale system, data of the energy generated needed to be recorded and transferred to another device because the value is large. Also it can make the system easier to manage because it is a large scale system rather than a small scale system like this one.

At the end of this project there is three expected outcome that need to accomplish. Firstly, the solar tracker designed can follow and track the sun movement precisely to improve the solar photovoltaic system efficiency. Secondly, the power generated can be displayed and monitored by user so that the system can be improved from time to time. Lastly, the solar photovoltaic system with sun tracker will be an independent system and its entire component only used the energy produced by the solar panels aside from the solar panels produce energy for the household.

V. CONCLUSION

This report discussed the design of solar photovoltaic system with dual-axis photovoltaic tracker. The dual-axis tracker is design by using software solid work and Arduino UNO. This project is to make sure the dual-axis tracker will able to move perpendicular based from the light (sunlight) direction. The prototype design by using the micro servo motor, hope the dual-axis tracker rotation or movement will be in smooth condition. With a high sensitivity of light dependence resistor, it will make sure the dual-axis tracker can operate with more effective.

Besides that, the actuators use the energy generated by the solar panels to be powered up hence it make the whole system independent. When it is night time, the system will shut down automatically because there is no power to be supplied to the actuators. Other than that, energy monitoring system will allow the users to detect any problems or to improve the system based from the energy data collected.

REFERENCE

[1] Nader Barsoum. Fabrication of Dual-Axis Solar Tracking Controller Project. in Intelligent Control and Automation, on 2011, 2, 57-68.

[2] Tri Bui, Tuyen Bui, Christopher Davis, Stephen Holman. Portable Solar Tracker. in Senior Design 1, on 2010.

[3] Qi-Xun Zhang, et al. A Solar Automatic Tracking System that Generates Power for Lighting Greenhouses. in energies, on 21 July 2015.

[4] Muhammad Nurhanudin Bin Baharudin. Dual-Axis Photovoltaic Tracker With Motorized Surface Panel Cleaning. in Final Year Project Thesis of UTM, on June 2016.

[5] Tan Jin Huat. Development Of Solar Tracker And Charger System. in Final Year Project Thesis of UTeM, on May 2012.

[6] Shreyasi Chakrabory, et al. Microcontroller based Solar Tracker system using LDRs and Stepper Motor. in International Conference on Microelectronic Circuit and System on. 2015.

[7] Sustainable Energy Development Authority Malaysia (SEDA). National Survey Report Of PV Power Application in Malaysia. in Photovoltaic Power System Programme, on 2014.

[8] Muhd.Ikram Mohd. Rashid, et al. Dual-Axis Solar Tracking System for Maximum Power Production in PV Systems. in Nigerian Journal Of Technological Development, Vol. 12, No. 2 December 2015 on. 2015.

[9] Liping Guo, Jingbo Han and Andrew W. O.. Design and Simulation of a Sun Tracking Solar Power System. in 120th ASEE Annual Conference & Exposition on. 2013.

[10] Lakeou S., Ososanya E., Latigo B. O. and Mahmoud W.. Design of a Low-cost Solar Tracking Photo-Voltaic (PV) Module and Wind Turbine Combination System.

[11] Soumen Ghosh and Nilotpal Haldar. Solar Tracking System using AT89C51 Microcontroller and LDR. in International Journal of Emerging Technology and Advanced Engineering on. 2014.

[12] Muhammad Faheem Khan and Rana Liaqat Ali. Automatic Sun Tracking System (ASTS). in Research Gate on. 2005.

[13] Syed Arsalan. Sun Tracking System with Microcontroller 8051. in International Journal of Scientific & Engineering Research, Volume 4, Issue 6, June-2013 on. 2013.

[14] Azman Zainal Abidin, KS Kannan and Asfaazam Kasbani. Malaysia Rapid Assessment And Gap Analysis For Sustainable Energy For All (Se4all) Initiative. in A Report by the UN Country Team Malaysia on. 2012.

[15] J. A. Beltran, J. L. S. Gonzalez Rubio, C.D. Garcia-Beltran: Design, Manufacturing and Performance Test of a Solar Tracker Made by an Embedded Control, CERMA 2007, Mexico.

[16] O. Stalter, B. Burger, S. Bacha, D. Roye: Integrated Solar Tracker Positioning Unit in Distributed Grid-Feeding Inverters for CPV Power Plants, ICIT 2009, Australia.

[17] M. A. Panait, T. Tudorache: A Simple Neural Network Solar Tracker for Optimizing Conversion Efficiency in Off-Grid Solar Generators, ICREPQ 2008, Spain.

[18] A. M. Morega, J. C. Ordonez, P. A. Negoias, R. Hovsapian: Spherical Photovoltaic Cells – A Constructal Approach to Their Optimization, OPTIM 2006, Romania.

[19] A. M. Morega, A. Bejan: A Constructal Approach to the Optimal Design of Photovoltaic Cells, Int. Journal of Green Energy, pp. 233-242, 2005.

[20] J. Horzel, K. De Clerq: Advantages of a New Metallization Structure for the Front Side of Solar Cells, 13th EC Photovoltaic Solar Energy Conference, France, 1995.

[21] P. I. Widenborg, G. Aberle: Polycrystalline Silicon Thin-Film Solar Cells on AIT-Textured Glass Superstrates, Advances in OptoElectronics Journal, Vol. 2007.

[22] P. A. Basore: Manufacturing a New Polycrystalline Silicon PV Technology, Conference Record of the 2006 IEEE 4th World Conference on Photovoltaic Energy Conversion, pp. 2089-2093, 2006.

[23] Arindam Bose, Sounak Sarkar, Sayan Das "Helianthus –a Low Cost High Efficient Solar Tracking System Using AVR Microcontroller", International Journal of Scientific & Engineering Research, Volume 3, Issue 10, October-2012.

[25] K.S.Madhu, B.R.Wadekar, Finavivya Chiragkumar.V, Gagan.T.M "Intelligent Two Axis Solar Tracking System with Mechanical Application", International Journal of Scientific & Engineering Research Volume 3, Issue 9, September-2012.

[26] Shen, C.L.; Tsai, C.T. Double-linear approximation algorithm to achieve maximum-power-point tracking for photovoltaic arrays. Energies 2012, 5, 1982–1997.

[27] Liu, K.H. Dynamic characteristics and graphic monitoring design of photovoltaic energy conversion system. WSEAS Trans. Syst. 2010, 10, 239–248.

[28] Nayak,S.R.; Pradhan, C.R. Solar tracking application. IOSR J. Eng. 2012, 2, 1278–1281.

[29] Lee, C.Y.; Chou, P.C.; Chiang, C.M.; Lin, C.F. Sun tracking systems: A review. Sensors 2009, 9,3875–3890.

[30] Rubio, F.R.; Ortega, M.G.; Gordillo, F.; Lopez-Martinez, M. Application of new control strategy for sun tracking. Energ. Conv. Manage. 2007, 48, 2174–2184.

[31] Blanco-Muriel, M.; Alarcon-Padilla, D.C.; Lopez-Moratalla, T.; Lara-Coira, M. Computing the solar vector. Solar Energy 2001, 70, 431–441.

[32] Chong, K.K.; Siaw, F.L.; Wong, C.W.; Wong, G.S. Design and construction of non-imaging planar concentrator for concentrator photovoltaic system. Renewable Energy 2009, 34, 1364–1370.

[33] Grena, R. An algorithm for the computation of the solar position. Solar Energy 2008, 82, 462–470.

[34] Reda, I.; Andreas, A. Solar position algorithm for solar radiation applications. Solar Energy 2004, 76, 577–589.

[35] Sproul, A.B. Derivation of the solar geometric relationships using vector analysis. Renewable Energy 2007, 32, 1187–1205.

[36] Abdallah, S.; Nijmeh, S. Two axes sun tracking system with PLC control. Energy. Conv. Manag. 2004, 45, 1931–1939.

[37] Saravanan, C.; Panneerselvam, M.A.; Christopher, I.W. A novel low cost automatic solar tracking system. Int. J. Comput. Appl. 2011, 31, 62–67.

[38] Arbab, H.; Jazi, B.; Rezagholizadeh, M. A computer tracking system of solar dish with two-axis degree freedoms based on picture processing of bar shadow. Renewable Energy 2009, 34, 1114–1118.

[39] Arturo, M.M.; Alejandro, G.P. High-Precision Solar Tracking System. In Proceedings of the World Congress on Engineering, London, UK, 30 June–2 July 2010; pp. 844–846.

[40] Berenguel, M.; Rubio, F.R.; Valverde, A.; Lara, P.J.; Arahal, M.R.; Camacho, E.F.; Lopez, M. An artificial vision-based control system for automatic heliostat positioning offset correction in a central receiver solar power plant. Solar Energy 2004, 76, 563–575.

[41] Barsoum, N. Fabrication of dual-axis solar tracking controller project. Intel. Control Autom. 2011, 2, 57–68.

[42] Barsoum, N.; Vasant, P. Simplified solar tracking prototype. Global J. Technol. Optimiz. 2010, 1, 38–45.

[43] Bajpai, P.; Kumar, S. Design, Development and Performance test of an Automatic Two-Axis Solar Tracker System. In Proceedings of 2011 Annual IEEE India Conference, Hyderabad, India, 16–18 December 2011; pp. 1–6.

[44] Ponniran, A.; Hashim, A.; Joret, A. A design of low power single axis solar tracking system regardless of motor speed. Int. J. Integr. Eng. 2011, 3, 5–9.

[45] Chong, K.K.; Wong, C.W. General formula for one-axis sun tracking system and its application in improving tracking accuracy of solar collector. Solar Energy 2009, 83, 298–305.

[46] Ponniran, A.; Hashim, A.; Munir, H.A. A Design of Single Axis Sun Tracking System. In Proceedings of the 5th International Power Engineering and Optimization Conference, Selangor, Malaysia, 6–7 June 2011; pp. 107–110.

[47] Dasgupta, S.; Suwandi, F.W.; Sahoo, S.K.; Panda, S.K. Dual Axis Sun Tracking with PV Cell as the Sensor, Utilizing Hybrid Electrical Characteristics of the Cell to Determine Insolation. In Proceedings of 2010 IEEE International Conference on Sustainable Energy Technologies, Kandy, Sri Lanka, 6–9 December 2010; pp. 1–5.

Mitigation of Voltage Sag and Harmonics using Unified Power Quality Conditioner

Syukur Bin Sulaiman
Faculty of electrical engineering
Universiti Teknologi Malaysia
Johor Bahru, Malaysia
syukur.sulaiman11@gmail.com

Ahmad Safawi Bin Mokhtar
Department of power
Faculty of electrical engineering
Universiti Teknolgi Malaysia
Johor Bahru, Malaysia
safawi@utm.my

***Abstract*—Power quality has become a main concern among electrical industry. The demand from the electrical user is high quality power supply continuously. Therefore, it is very important to protect the system from any disturbance so that the quality and reliability of the power system can be maintained. Voltage sags and harmonics are among the power quality problem that commonly occurred in distribution power system. These disturbances are caused by the increasing use of sensitive electronic equipment and non-linear load in electrical system which leads to the negative impact on distribution power system. Unified Power Quality Conditioner (UPQC) is one of the device that can offer the system to retain its power quality. Unified Power Quality Conditioner (UPQC) has the ability to mitigate most of the issues on the power system immediately with high speed precise response. The main purpose of this report is to implement the UPQC device with a proper controller to mitigate voltage sags and harmonics. MATLAB Simulink are used to shows that UPQC device has the potential to deal mutually with both supply voltage and load current imperfection. By implementing UPQC device, there is a reduction of percentage in sagging and total harmonic distortion to the value within the range set by IEEE standards. This show that the UPQC are able to restore sags and improve the current harmonics.**

Keywords—harmonics, voltage sag, modelling of UPQC, simulation

I. INTRODUCTION (*HEADING 1*)

Nowadays, power quality issue has drawn attention from both utility side and the end user itself. This is because the increasing of usage of sensitive electronic equipment which is the biggest factor in the power quality problems. It is inconvenience to experience the power outages which affecting domestic, commercial, and industrial customer. This problem also could bring great financial losses especially for the industrial customer and also utility companies. It would be an operation interruption and cause the product quality reduction which results a lot of losses. On the side of utility companies, they need to supply a high quality of power supply to the consumers so that they would not experience any losses. Therefore, the expectation regarding the reliability of electrical power supply is necessary at this point.

Voltage sag and harmonics are the most common power quality problem that occur in the power system. These disturbances may affect the functionality of the equipment which is in a worst case it also could damage the system equipment. Power quality disturbances are come from the quality of current drawn by the load and the quality of supply voltage. Voltage sags occurred due to the fault in the distribution of transmission system while harmonics are caused by non-linear load.

There are several ways to improve the power quality in power system. Passive power filters is one of the method that can reduce the unwanted disturbance. Passive power filter are more economical to implement and it is a convenient way to suppress harmonics in distribution system. Furthermore, they can introduce some resonance in power system. As the result, Active Power Filter (APF) was introduced to overcome these problems.

However, they have some flaws in their performance which is limited to a certain type of load as they were custom designed for application [4] [5].

The ability of APF able to mitigate the voltage sags or swells and also reactive power in the distribution system and also harmonic suppression. APF are related with Custom Power Device. The most well-known CPD are Dynamic Voltage Restorer (DVR), Distribution Static Compensator (DSTATCOM) and Unified Power Quality Conditioner (UPQC) [7].

The best and most advanced device in CPD is UPQC as it is a combination between DVR and DSTATCOM. It has two voltage source inverter (VSI). One of VSI is connected in series and the other one is connected in shunt. UPQC is probably the best proposed device to deal with the both low quality of supply voltage and load current.

II. LITERATURE REVIEW

A. Voltage Sag

The voltage sags is defined as the reducing of the root means square (rms) voltage in the range between 0.1 and 0.9 per unit at the power frequency for the period of

0.5 cycles to 1 min by according to the IEEE standard 1159-1995 [9]. Voltage sags also can be defined as a temporary reduction between 10% and 90% of rms voltage at the power frequency for duration of 0.5 cycles to 1 minute [7] [8] [9] [10] [11]. Voltage sags is one of the most regular disturbance that is experienced by consumer. It is normally caused by short circuit or fault which can caused equipment failure in a network system. The energizing of heavy machines also can be the cause of voltage sag [12]. The fault happened in the distribution system can caused consumers to experienced voltage sag even the location of fault is far away. Voltage sag waveform, can be shown clearly in Figure 1

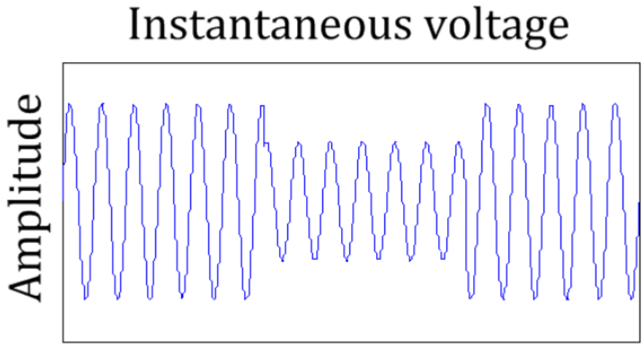

Figure 1: voltage sag waveform

B. *Harmonics*

Rapid used of non-linear load equipment can cause the electrical equipment to generate current harmonics [13]. WHEN non-linear load equipment connected with power system, the current waveform will transform to non-sinusoidal. This non-sinusoidal current waveform are the reasons for the voltage drop to the network system and produce voltage distortion [4] [16]. Basically, these harmonics produced from the combination of different frequency of various sine waves [5]. It causes the harmonics in the waveform and the waveform become distorted. Figure 2 show the harmonics distortion.

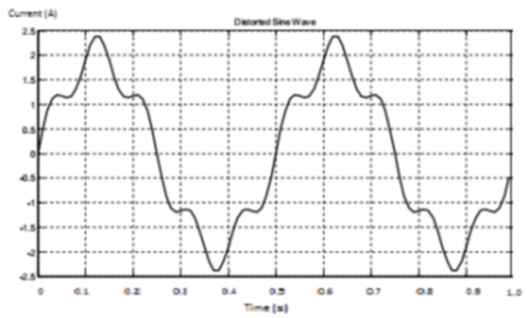

Figure 2: Harmonics Distortion

C. *Unified power quality conditioner (UPQC)*

Unified Power Quality Conditioner has excellent performance and widely used in the power system nowadays. It can deal with both voltage supply and load current imperfection mutually and it is the most advanced device in CPD. This is because UPQC is a combination between series and shunt Active Power Filter (APF). UPQC can solve various kinds of power quality issues such as harmonics, voltage sags, voltage swells, power factor correction, reactive power, power factor correction, and unbalanced current source [20]. Thus, this shows UPQC has the ability to overcome most of the problem related to power quality. UPQC has a precise identification of the disturbance signal and fast processing of reference signal and it show it reliability to improve power quality [3].

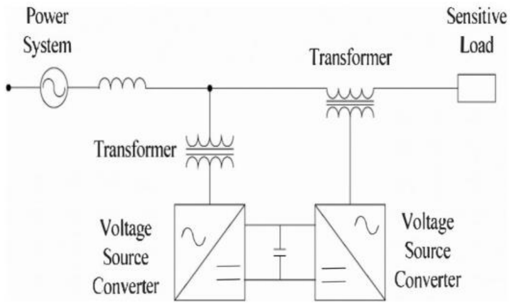

Figure 3: Basic Configuration of UPQC

Basic configuration of UPQC are shown in Figure 3. UPQC connected back-to-back with the DC capacitor and it consist of both series and shunt VSI. Other component in UPQC are high pass filter, low pass filter, and series and shunt transformer connected to power system.

VSI is connected in series in this system. It control voltage distortion by acting like DVR which is injecting voltage to the power system. In addition, it disable high frequency component produced by high frequency switching by using low pass filter and it used at series VSI.

On the other hand, shunt VSI is VSI shunt connected system. It has the ability to cancel harmonics currents at the load by acting like a current source and. It inject currents to the power system and also can correct the power factor and balance reactive current at load. High pass filter is apply with shunt VSI to absorb current switching ripple.

DC capacitor has two main purposes in this configuration which is to supply real power during the transient period by acting as energy storage elements and it is used to maintain DC voltage with a small ripple in steady state. Besides that, series and shunt transformer are being implemented in order to inject the compensation currents and voltage and make electrical isolation.

III. METHODOLOGY

A. *Flow Chart of Project*

Distribution system network can be design by using MATLAB Simulink. The network system is developed with the presence of fault and non-linear load and it will produce voltage sag and harmonics. Analysis can be done by using simulation. After that, the proposed device which is UPQC will be installed in the existing network. Lastly, UPQC and the controller will be execute with the existing network system to analyse the output. The project flow is shown in the flow chart in figure 4 below.

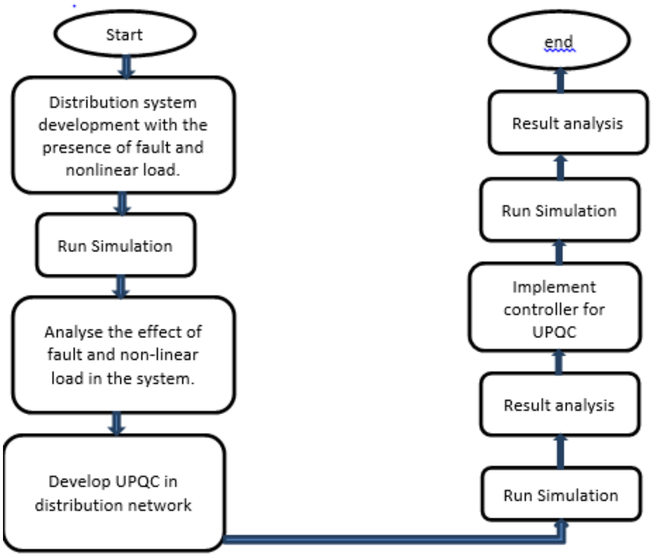

Figure 4: Research Flowchart

B. Simulation Model

Figure 5 below shows the single line diagram for network system with the addition of UPQC. This 3 bus system has been designed with Feeder A and Feeder B which are connected with different type of load. Feeder A connected to linear load while non-linear load is connected to the Feeder B. LG, LLG, and LLLG fault are introduced at Feeder. Hence, UPQC performance can be studied.

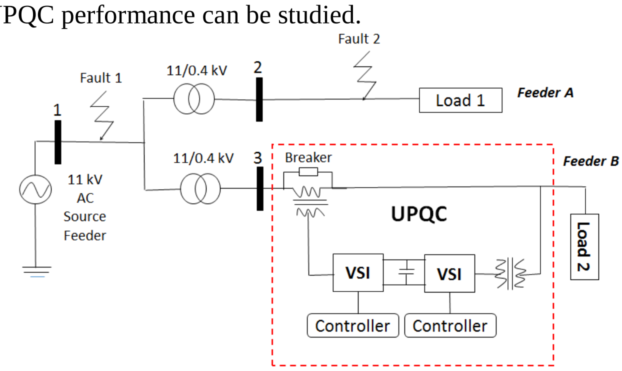

Figure 5: Single Line diagram for UPQC Model.

In this project, the system in single line diagram above is implemented into Simulink model in Matlab as shown in Figure 6. The simulation model is tested under 4 conditions which are normal condition (without fault and non-linear load), with fault condition (voltage sags), with non-linear load condition (harmonics) and lastly with UPQC condition. The voltage is measured at each feeder while load current is measured at Feeder B.

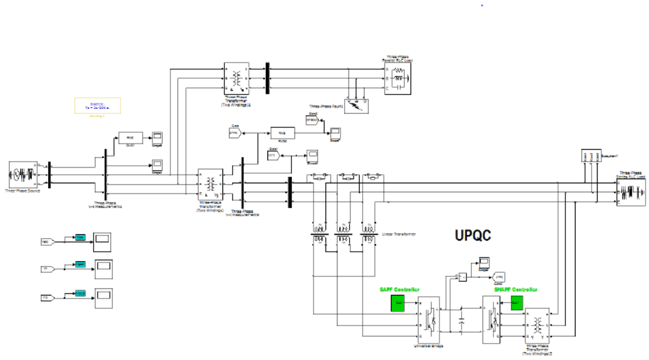

Figure 6: Simulink UPQC Model

C. Control Method for UPQC

Controlling method for UPQC for both shunt APF and series APF is same. The controlling method used is synchronous reference frame control or dq control. The controller configuration is shown as in the Figure 7. It uses abc to dq transformation to transform the current and voltage waveform at grid into a reference frame that rotates synchronously with grid voltage. The controlling would become easier as the control variables become dc values.

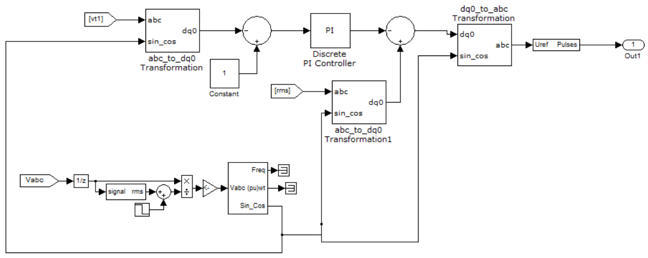

Figure 7: Series and Shunt APF Controller of UPQC

IV. SIMULATION RESULT

A. Effect of the three phase fault and non-linear load

Figure 8 shows the circuit of the system after three phase fault and non-linear load has been implemented.

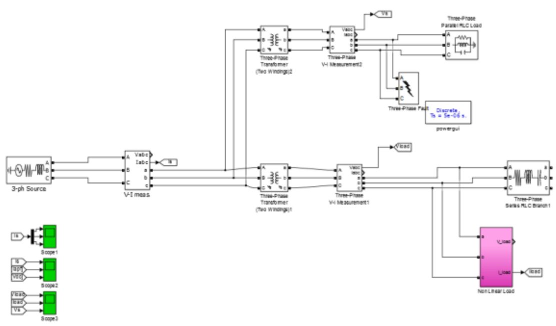

Figure 8: System with three phase fault and non-linear load.

Figure 9 and figure 10 below show the results of the waveform after implementation of three phase fault and non-linear load respectively.

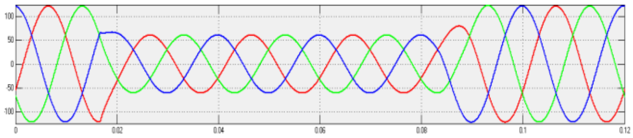

Figure 9: Voltage Sag Because Of the Fault

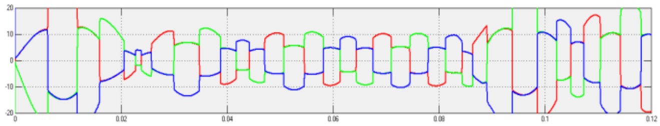

Figure 10: Harmonics Because Of Non-Linear Load

B. *Voltage sag and harmonics mitigation after UPQC*

Figure 11 shows the circuit of the UPQC with appropriate controller is being implemented in order to mitigate the voltage sag and harmonics

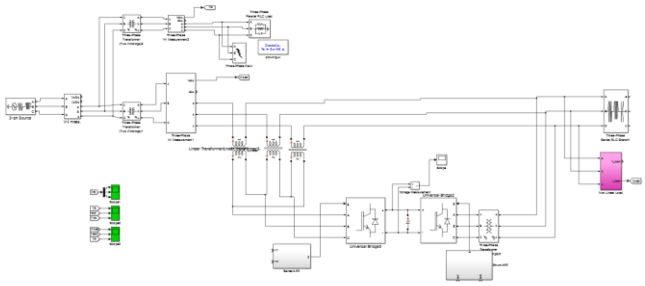

Figure 11: Circuit of UPQC Device

The figure 12 shows the result of the waveform of the system after UPQC device has been implemented into the system.

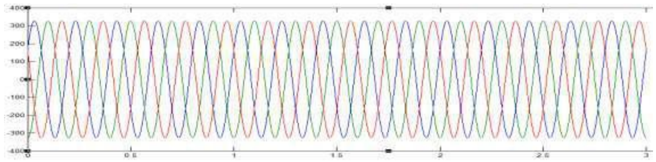

Figure 12: Voltage Waveform after UPQC

V. CONCLUSION

Furthermore, UPQC device has been successfully installed in the system in order to improve the power quality issues. The device has proved its ability to improve voltage sags and harmonics that are presented in the system. Results of the voltage and current waveform obtained by simulation show that UPQC can restore the sags of voltage and turned the non-sinusoidal current waveform back to the ideal waveform.

REFERENCE

[1] Dugan, R. C., McGranaghan, M. F and Beaty, H. W. Electrical Power System Quality. New York: McGraw-Hill, 1996. [2] IEC Std. 61000-2-1, Electromagnetic compatibility (EMC) - Part 2: Environment - Section 1: Description of the environment - Electromagnetic environment for low-frequency conducted disturbances and signalling in public power supply systems

[3] Faridullah Kakar. “Power Quality Improvement by Dynamic Voltage Restorer and Unified Power Quality Conditioner Using Fuzzy Logic”, Degree of Master, Universiti Teknologi Malaysia; 2015

[4] M.Izhar, C.M.Hadzer, Sfrudin M, S.Taib, S.Idris, National Power & Energy Conference (PECon) 2004 Proceedings, Kuala Lumpur, Malaysia, “Performance for Passive and Active Power Filter in Reducing Harmonics in the Distribution System”, 2004

[5] Anil Baitha, Dr Nitin Gupta, 2015 IEEE International Conference on Technological Advancements in Power & Energy, “A Comparative Analysis of Passive Filters for Power Quality Improvement”, 2015

[6] Joaquin Cicedo, Felipe Nararro, Edwin Rivas, Francisco Santamaria, Electromagnetic Compatibility and Interference Group (GEM) Universidad Distrital Francisco Jose de Caldas Bogota, Columbia, “Voltage Sag Characterization with Matlab/Simulink”, 2012

[7] Park Sang-Young, Park Jong-Keun, Power Engineering Society Winter Meeting, 2001, IEEE, “The Modelling and Analysis of Shunt Type Custom Power Device”, 2001

[8] Rosli Omar, Nasrudin Abd Halim, ARPN Journal of Engineering and Applied, “Mitigation of Voltage Sags/Swells Using Dynamic Voltage Restorer (DVR), vol.4, No. 4, June 2009

[9] IEEE Recommended Practice for Monitoring Electric Power Quality, IEEE Std. 1159, 1995

[10] E.Babaei, M. Farhadi Kangarlu, IEEE Electrical Power and Energy Conference, “Three Phase Cross-Phase Voltage Sag Compensator to Compensate Balance/ Unbalanced Voltage Sags and Phase Outages in Distribution Systems”, 2011

[11] IEEE Standards Coordinating Committee 22 on Power Quality. IEEE Std 1159. IEEE Recommended Practice for monitoring electric power quality. 1995

[12] Surya Hardi, I. Daut, The 4th International Power Engineering and Optimization Conf. (PEOCO2010), Shah Alam, Selangor, Malaysia, Sensitivity of Low Voltage Consumer

Equipment to Voltage Sags, 23-24 June 2010

[13] Ravi Kumar Jujjuvarapu, B.Basavaraja, International Journal of Power System Operation and Energy Management ISSN (PRINT): 2231 – 4407, Volume-1, Issue-4, “Modeling and Estimating Voltage and Current Harmonics of Variable

Speed Drive (VSD)", 2012

[14] Pinky Saxena, Rajan Chaudhary, Advance in Electronic and Electric Engineering.

ISSN 2231-1297, Volume 3, Number 4 (2013), pp. 503-508. Research India Publications, "Harmonics Modeling, Activity Analysis of Equipments with Switch Mode Power Supply and Reduction on Matlab/ Simulink", 2013

[15] K.R.Valluvan, A.Vetrivel, A.M.Natarajan, Jovitha Jerome, Proceedings of the 2008 International Conference on Computing, Communication and Networking (ICCCN 2008), "Minimisation of Harmonics Amplification Due to Resonance by Relocation of Capacitors Using ADALINE on a DSP", 2008

[16] K.R.Suja, Jacob Raglend, 2013 International Conference on Circuits, Power and Computing Technologies [ICCPCT-2013], "Fuzzy Based Unified Power Quality Conditioner for Power Quality Improvement", 2013

Wind Energy Harvesting using Piezoelectric

Poh Hung Sheng
Faculty of Electrical Engineering
Universiti Teknologi Malaysia
Johor Bahru, Malaysia.
hungsheng94@gmail.com

Ahmad Safawi bin Mokhtar
Department of Electrical Power Engineering
Faculty of Electrical Engineering
Universiti Teknologi Malaysia
Johor Bahru, Malaysia.
safawi@utm.my

***Abstract*—In today's world, we often heard about renewable and sustainability in our daily life. Wind energy is a type of renewable energy that is sustainable and useful to us. Generation of electricity using wind energy is common in foreign country such as the United States, Japan, Europe countries but not in Malaysia as Malaysia wind speed is low. Minimum wind speed is not reach to turn the wind turbine to produce electricity. Therefore, this work will focus on the generation of electricity using wind energy in Malaysia. Instead of using the standard wind turbine that has minimum operating wind speed, piezoelectric is used to convert the mechanical energy from wind to electrical energy. Piezoelectric can produce electricity through bending the structure therefore a low wind speed is enough for piezoelectric to produce electricity. A series of designs are used to test the wind capturing efficiency by measuring the output voltage and current. Designs are important in here as it influence greatly on the power output. Each piezoelectric used must produce at least 1mA current with 0-200V to get a satisfying output. In this project, due to budget constrain, a cheaper piezoelectric element is used as a material, therefore, the output of the result is not very satisfying. Although the piezoelectric element is not good but the design of this project is very good and easy to capture wind in all direction.**

Keywords—piezoelectric; electricity; generation; wind; renewable.

I. INTRODUCTION

In Malaysia, renewable energy is encouraged by the government since the 8th Malaysia Plan with five-fuel energy in 2005 [1]. It is a disappointment to say that until now, renewable energy is still at the low energy production side as Malaysia mainly still depending on non-renewable sources such as fossil fuel and natural gas [2]. Renewable energy failed to become popular as most of the people in Malaysia did not get to expose to this kind of knowledge.

Among the usage of renewable energy, solar and hydro are the two most widely used renewable energy in Malaysia. Malaysia is rich with natural resources such as water, minerals and ores but with the only disadvantages is Malaysia has low wind speed. Wind is produced by difference in temperature. Higher the difference of temperature, stronger the wind will blow. Wind in Malaysia mainly because of monsoon season [3]. Monsoon wind produced is based on the theory of Walker Circulation [4]. Wind energy did not play a main role because Malaysia has low wind velocity in turn makes the energy harvested using wind is low as well.

However, energy harvesting using wind energy can be done in many ways. Instead of using turbine, piezoelectric can be used as it converts mechanical vibration into electrical energy. Piezoelectric also called as Lead Zirconate Titanate (PZT) is a very sensitive element hence it can be used as a sensor or energy transducer [5]. Low wind speed can be detected and amount of energy harvested will be proportional to the wind speed. In this research, amount of energy harvested using piezoelectric will be studied. PZT will be used as a main energy harvester in this project along with circuit amplification and storing system. Therefore, the problem of low wind speed can be solved using PZT material.

Using piezoelectric to convert wind energy to electricity is useful to many places in the world as only low wind speed is required for it to operate. Piezoelectric is small in size, end product built using piezoelectric can be as small as solar panel. It is convenient to put on the rooftop to harvest energy without taking up much space. Besides, using piezoelectric to harvest wind energy can make sure birds is safe from harmed. It is eco-friendly yet sustainable to produce clean energy for usage.

In addition, wind energy harvesting can let people harvest energy during day and night. Unlike harvesting solar energy, wind blows all the time, energy can be harvested all the time as well. Moreover, using renewable energy to harvest energy is a plus for the future as the electricity prices are increasing from year to year contemplating with the decreasing of non-renewable sources on earth. Our electrical supplier TNB has been increasing electricity bill and renewable energy sources such as wind energy harvesting is another option for the users to decrease their electricity bill while conserving the mother earth.

II. LITERATURE REVIEW

Energy harvesting has been existed for a long time, there are many energy harvesting sources that can be found in the market such as wind turbine the harvest wind, solar panel to harvest light, thermoelectric to harvest heat and piezoelectric to harvest mechanical force (vibration). Using piezoelectric to harvest energy is a new technology as normally piezoelectric is just for small scale power device like buzzer.

Wind energy harvesting has been implemented using wind turbine decades ago. With the development of technology, wind turbine has been improving a lot in terms of efficiency of turbine and capturing the amount of wind energy [6]. Wind turbine has been designed to capture as much wind as possible to produce better output. There are horizontal and vertical axis of wind turbine according to different condition required. Both development aim to have maximum output power from the energy harvested [7,8].

Wind energy harvesting is one of the fastest development renewable energy generation in the world. It is because of its capability to generate a huge amount of electricity compared to the other sources. Figure 2.4 shows the model of turbine with the power output of the wind turbine. In wind energy harvesting, the stronger the wind, the greater the energy harvested. Therefore, turbines are built up high, wind blade are aerodynamic designed and rotor diameter is long to capture more wind as altitude proportional to wind speed [9,10].

Besides using wind turbine to harvest wind energy, piezoelectric is another option for wind energy harvesting purposes. The difference is piezoelectric can only able to produce small power [11]. Increasing in number of piezoelectric can increase the power output as well. The benefits of using piezoelectric is that it can produce electricity even in low wind speed unlike wind turbine which required much higher wind speed to turn the rotor. Since Malaysia has low wind speed in overall, piezoelectric is a better option than using wind turbine to harvest energy.

Basically, piezoelectric converts mechanical stress into electricity. Ceramic based piezoelectric is divided into 2 types which are lead zirconate titanate (PZT) and polyvinylidene fluoride (PVDF). PVDF piezoelectric can produce much higher voltage compared to PZT due to their characteristics [12,13]. The efficiency of PVDF is higher than PZT.

PVDF piezoelectric is a thin film with high sensitivity. It can be used in many field such as sensor as well as energy harvester. Cantilever type of method is chosen to set up the PVDF as it can fully let the piezo film to vibrate as wind passes by to harvest energy [5]. PVDF working principle is when mechanical force is applied to the surface of piezoelectric, the re-orientation of molecules arrangement causes charges to flow hence produces electricity. If deformation is done on piezoelectric material, higher voltage will produce due to greater change in polarization of piezoelectric material [14,15].

Mechanical structure needed to be considered thoroughly to suit the surrounding condition. In order to maximize the energy harvested, the mechanical structure must be able to turn according to wind direction. Mostly, people proposed to use wind sensor. Wind sensor using opto-isolator to convert mechanical signal to electrical pulses to calculate its speed and direction [16]. However, based on costing, developing a wind sensor is too costly for a simple energy harvesting system. Therefore, a simple mechanical bearing is used as its economical aspect and it can reduce the friction of rotational movement which can easily turn the structure around with minimum force [17].

III. Project Methodology

A. *Wind Energy Harvesting Device*

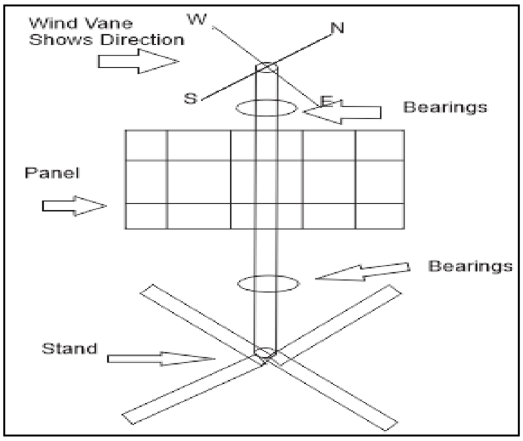

Fig. 1. Wind Energy Harvesting Device Design 1

The first design is designed in this way by getting the idea from the solar panel. The panel in the middle holds the piezoelectric and wind will vibrate the piezoelectric attached on the panel. The design fails as the panel is only facing one direction therefore, it is inefficient in harvesting wind energy. Wind from other direction will come into waste energy.

Fig. 2. Wind Energy Harvesting Device Design 2

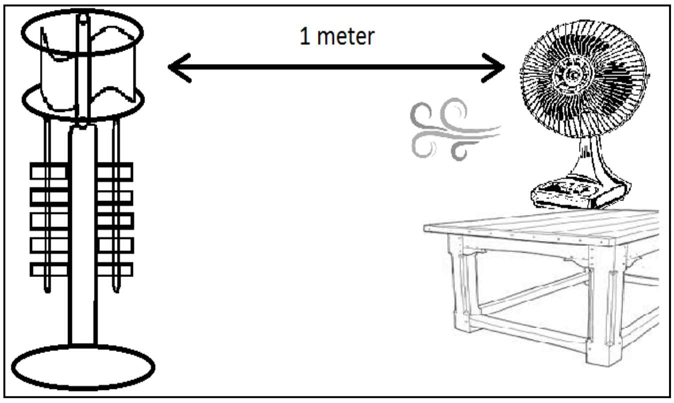

The second design is taken from the vertical wind turbine design. As the mechanical design required low cost and suitable efficiency in capturing wind. Savonius design is the best to apt the situation. Savonius design comes with 2 blades that captures wind from any direction. Wind flows into the blade will twist and turn and come out on the other side. This design in turn will make it turn solely in one direction only despite the incoming wind direction. 2 sticks below the savonius design are to hit the piezoelectric hence make the piezoelectric element bend and produce electricity. This method is more efficient and produces a greater amount of electricity compared to the first one.

B. *Workflow of the Project*

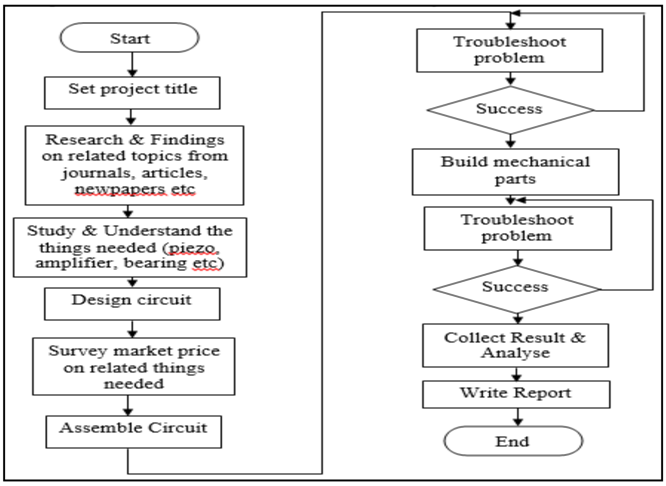

Fig. 3. Project Workflow

Researches and analysis are done before doing the project. The circuit of the project consists of rectifier, capacitors and load. It converts alternating voltage to direct voltage and hence store in the capacitor and supply to the load. Mechanical design is done by accessing the structure and build the most economical design with satisfactory output. Any design problem is troubleshoot and a better design is come out to overcome the problem previously. Results are collected to analyze after the circuit and mechanical design is done.

C. *Experiment Flow*

Steps of Conducting Experiment:

1. Place the assembled wind harvesting device on a flat surface.
2. Make sure the wind harvesting device have a stable base so that it will not flip over when wind blows. (Alternative way is to remove the base and bury part of the pole into cement wall.)
3. Place a wind generator at 1 meter away from the wind harvesting device.
4. A wind speed of 1.7m/s is turn on using the fan.
5. Multimeter are connected to the circuit to measure the output voltage.
6. Repeat step 4 by measuring output current.
7. Take the result and record it in a table.
8. Repeat step 6 for 10 times to get average result. (10 times are repeated as harvesting energy from surrounding is difficult and many energy lost, this can let the result more accurate.)
9. Repeat the experiment using different wind speed of 2.5m/s and 3.5m/s.

A table fan (wind source) is placed on top of a table to let the wind to blow directly proportional into the design of the wind energy harvester. The experiment is conducted this way to duplicate the actual wind blow as wind in the actual environment covers a large area. Besides, wind blows directly into the wind energy harvester model is the most effective way to make it turn.

A distance of 1 meter is set in between the wind energy harvester and the wind source to get the wind to cover larger area rather than a focused small area. This way of conducting experiment hence makes the result more reliable as well. An anemometer is used when the experiment is running to test the incoming wind speed changing from time to time. Hence, a graph of output voltage/current against time can be plotted.

Different wind speed is used to conduct this experiment to get the responding wind speed towards the output voltages and current. The 3 different wind speed use can be portrayed to the different wind speed throughout the year.

IV. Result and Analysis

The experiment is conducted with 3 different wind speed. 1.5m/s, 2.5m/s and 3.5m/s. The results below are for the experiment of 2.5m/s wind speed.

A. *Voltage Response*

TABLE I. INPUT AND OUTPUT VOLTAGE RESPONSE

Input Voltage (V)	Output Voltage (V)
0	0
5.64	0.46
13.93	0.96
20.45	1.68
23.54	1.76
29.79	2.23
27.64	1.96
28.53	2.04
28.19	2.15
26.88	1.92

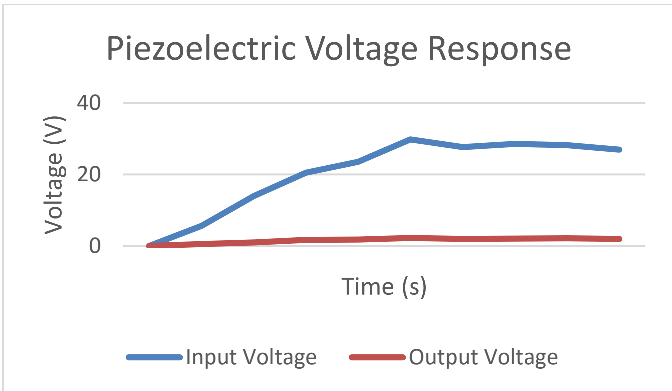

Fig. 4. Piezoelectric Voltage Response

Voltage is measured using multimeter at two different potential points. The input voltage is the rms of ac voltage while output voltage is dc voltage after being rectified. The voltage increases slowly to reach the average value when wind applied. Voltage will increase and decrease in a small value according to the bending rate and bending angle of the piezoelectric.

B. Current Response

TABLE II. INPUT AND OUTPUT CURRENT RESPONSE

Input Current (uA)	Output Current (uA)
0	0
4.56	2.34
5.11	3.54
5.94	4.06
8.64	5.78
10.53	7.88
14.57	9.13
12.36	8.55
16.77	9.89
14.02	8.96

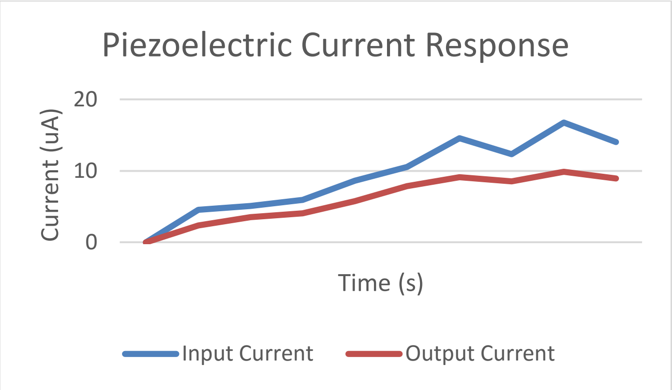

Fig. 5. Piezoelectric Current Response

Current is measured using a digital multimeter. The current flow is too small so that the multimeter must be able to measure current in microamperes. The input current is measured directly at the piezoelectric while output is measured after it is being rectified. The output current did not decrease too much from the input compared to the voltage.

V. CONCLUSION

Piezoelectric can produce a lot of voltages but only very low current. Power is a product of voltage and current. Therefore, piezoelectric is only suitable for small power application. There is a lot of different types of piezoelectric in the market, Different pricing will result in different quality. Some piezoelectric will even produce up to 100mA. Therefore, parallel the piezoelectric circuit is important as it will greatly help in boosting its current while series of the circuit can increase the voltage produced as well.

In short, piezoelectric is suitable to be used in energy harvesting but only limited to the field of small power such as lightings. It is difficult for piezoelectric to help in power generation in large scale.

REFERENCES

[1] Solangi, K. H., Badarudin, A., Kazi, S. N., Lwin, T. N. W., & Aman, M. M. (2013, April). Public acceptance of solar energy: The case of Peninsular Malaysia. In TENCON Spring Conference, 2013 IEEE (pp. 540-543). IEEE.

[2] Belhamadia, A., Mansor, M., & Younis, M. A. (2013, November). Assessment of wind and solar energy potentials in Malaysia. In Clean Energy and Technology (CEAT), 2013 IEEE Conference on (pp. 152-157). IEEE

[3] Webster, P. J., & Yang, S. (1992). Monsoon and ENSO: Selectively interactive systems. Quarterly Journal of the Royal Meteorological Society, 118(507), 877-926.

[4] Julian, P. R., & Chervin, R. M. (1978). A study of the Southern Oscillation and Walker Circulation phenomenon. Monthly Weather Review, 106(10), 1433-1451.

[5] Kim, H. S., Kim, J. H., & Kim, J. (2011). A review of piezoelectric energy harvesting based on vibration. International Journal of precision engineering and manufacturing, 12(6), 1129-1141.

[6] Kotzalas, M. N., & Doll, G. L. (2010). Tribological advancements for reliable wind turbine performance. Philosophical Transactions of the Royal Society of London A: Mathematical, Physical and Engineering Sciences, 368(1929), 4829-4850.

[7] Templin, R. J., & Rangi, R. S. (1983). Vertical-axis wind turbine development in Canada. IEE Proceedings A-Physical Science, Measurement and Instrumentation, Management and Education-Reviews, 130(9), 555-561.

[8] Yadav, A., Bhateja, A., & Mishra, V. K. (2016, March). Design, development and fabrication of horizontal axis wind turbine. In Electrical, Electronics and Computer Science (SCEECS), 2016 IEEE Students' Conference on (pp. 1-4). IEEE.

[9] Acciani, G., Di Modugno, F., Gelao, G., & Mininno, E. (2015, November). Shape optimization of cantilever beam for wind energy harvesting. In 2015 International Conference on Renewable Energy Research and Applications (ICRERA) (pp. 1207-1212). IEEE.

[10] Raj, A., Gurav, R. B., Saha, A., Chavan, D. S., Karandikar, P. B., & Sankpal, J. B. (2016, April). Study of output parameters of horizontal axis wind turbines using experimental test setup. In Computation of Power, Energy Information and Commuincation (ICCPEIC), 2016 International Conference on (pp. 363-368). IEEE.

[11] Sun, H., Zhu, D., White, N. M., & Beeby, S. P. (2015, April). A miniature piezoelectric energy harvester for air flows. In Design, Test, Integration and Packaging of MEMS/MOEMS (DTIP), 2015 Symposium on (pp. 1-3). IEEE.

[12] Vatansever, D., Hadimani, R. L., Shah, T., & Siores, E. (2011). An investigation of energy harvesting from renewable sources with PVDF and PZT. Smart Materials and Structures, 20(5), 055019.

[13] Malmonge, L. F., Malmonge, J. A., & Sakamoto, W. K. (2003). Study of pyroelectric activity of PZT/PVDF-HFP composite. Materials Research, 6(4), 469-473.

[14] Starner, T., & Paradiso, J. A. (2004). Human generated power for mobile electronics. Low-power electronics design, 1-35.

[15] Andre Preumont. Vibration Control of Active Structure, An Introduction. Berlin Heidelberg New York: University Libre de Bruxelles Active Structure laboratory

[16] Amin, M. R., Mishu, M. K., Al Faysal, A., & Nizam, M. R. (2016, December). Design and implementation of opto-isolator based low cost digital anemometer with wind direction monitoring system. In

Informatics, Electronics and Vision (ICIEV), 2016 5th International Conference on (pp. 133-138). IEEE.

[17] Bleuler, H., Cole, M., Keogh, P., Larsonneur, R., Maslen, E., Okada, Y., ... & Traxler, A. (2009). Magnetic bearings: theory, design, and application to rotating machinery. G. Schweitzer, & E. H. Maslen (Eds.). Springer Science & Business Media.

Overheat Protection for Electrical Enclosure using Internet of Things (IoT)

Alif Aminuddin Bin Mohd Aziz
Faculty of Electrical Engineering
Universiti Teknologi Malaysia
Johor Bahru, Malaysia.
alifaminuddinmohdaziz@gmail.com

Dalila Binti Mat Said
Centre of Electrical Energy System
Faculty of Electrical Engineering
Universiti Teknologi Malaysia
Johor Bahru, Malaysia.
dalila@utm.my

***Abstract*—Global warming turns into a genuine concern, the increase of surrounding temperature due to global warming makes the temperature inside the electrical enclosure issue becoming more critical. Electronic equipment is sensitive to temperature changes. The system developed should hold the temperature and humidity inside the electrical enclosure to be an ideal condition of electrical equipment to operate. All the extra feature that include Internet of Things expected to bring positive impact to the user. The system will ease the user for monitoring and control the temperature and humidity inside electrical enclosure.**

Keywords—Temperature, Humidity, Monitoring, Electrical Enclosure, Internet of Things.

I. INTRODUCTION

Electrical enclosure as shown in Fig. 1, is a cabinet for electrical or electronic equipment to mount switches, knobs and displays. Generally, the electrical enclosure holds the purpose to prevent electrical shock to equipment users and protect the contents from the hazarder and harsh environment conditions. The electrical enclosure come with variety involving material they made of, their size, and the type of system the electrical enclosure will hold and as well the location of the electrical enclosure [1], this will influence the outline design of the electrical enclosure in the area so it fills in as it needed.

Fig.1 Electrical enclosure

There is numerous system installed inside the electrical enclosure, for example, like telecommunications system, machine control system, electrical distribution system and switch system. Nowadays, the electrical system is revolving to more efficient and reliable. All this possible throughout the development of electrical equipment used in the system. Most equipment used today has been re- engineered from analogue to digital. This system re-building process have made the framework utilizing electronic hardware [2].

However, electronic equipment is sensitive to temperature changes. The designer must design the electrical enclosure to ensure the temperature inside the electrical enclosure to be ideal temperature of the equipment and not too hot. At high temperatures, drive execution is de-rated; I/C-based devices are unfavorably influenced by erratic yield/voltage migration, in addition to properties of silicone materials change with temperature extremes. In wiring protection, flexibility and quality are lessened; pliability increments incidentally [2]. Because of that, it is imperative to make the temperature inside the electrical enclosure an area with perfect temperature for the hardware to guarantee the framework inside the electrical enclosure in the area work legitimately.

There are many approaches to address the temperature change issue, one of them by utilizing a temperature controller. Temperature controller has been introduced to handle the temperature change inside the electrical enclosure known as thermostat control. However, current solution still has space for development for better control and more advanced feature. This project will tackle that space by providing a new way of solution to solve the issue will be use another type of controller. The controller and framework will be design all through the venture by coordinating equipment and programming. New features also will be added into the system in line with current technology and trend. This project will concentrate on electrical enclosure to ensure the temperature inside it in ideal temperature for the equipment to operate and work as it ought to.

II. METHODOLOGY

A. Design Method

In this project, development of overheat protection of electrical enclosure will be the main objective. The design method mainly focusing on active solution [3]. The system will act as a thermal control device and will force ventilation into the electrical enclosure to cool it off. Forced ventilation active went it needed only to reduce energy use. The system will cover for low voltage system only with maximum temperature recommended for industrial components not more than 35℃[1]. Airing and ventilation approach for temperature management using air-air exchanges by using fans will use [3].

Extra feature also will be added into the system to make it innovative and up to date relevant with today's trend. Humidity also will be considered in the system because it has an extraordinary impact on power electric field estimation [4]. Humidity also will cause condensation, rapid rusting and insulation failure [5]. Malaysia is tropical weather; humidity is a common feature here. It's not as critical as the temperature inside the electrical enclosure. However, in the system design, humidity will be considered to make it relevant to apply practically in the site. The sensor will be put inside and outside the electrical enclosure to collect data of surrounding temperature inside the electrical enclosure. The system will be linked to internet via Wi-Fi to apply internet of things (IoT). Throughout IoT system, users can access and gather data with the need to go to the site. It can save the operation cost while it will make the system more flexible. Data like current temperature and humidity, system status and send warning to the user if the condition of the electrical enclosure can't be handled by the system. This will give spare time to the user. Fig. 2 shows the prototype of the system. The smaller size of the model will be worked to demonstrate it can work, all things considered.

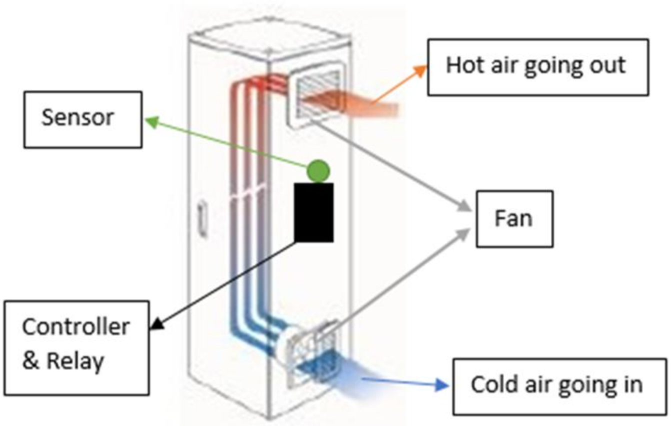

Fig. 2 prototype of the system

B. Hardware

There are four main components in this project required to build the model. The first component is controller with Wi-Fi module. This component is the heart of the system. It will control all the other component by receive and sent signal. Second component is sensor. Sensor is gadget that identifies or measures a physical property and records, shows, or generally reacts to it. In this case, the system will use temperature and humidity sensor. Third is fan. It will act as mechanical part. The fan function to make airflow in and out the model develops. Fourth is two channel relay. The relay act as switch to on/off the fan. It will react according to signal send by the controller.

NodeMcu Lua WIFI controller board will be used as a controller in this project. It will control the input for sensor and as output, it will send signals to fan if desire condition inside the electronic enclosure can't be achieved. It also will send data like current temperature and humidity, system status and send warning to the user if the condition of the electrical enclosure can't be handled by the system via internet to apply IoT [4] to the system. NodeMCU is an open source IoT stage. It incorporates firmware which keeps running on the ESP8266 WiFi SoC from Espressif, and equipment which depends on the ESP-12 module. The expression "NodeMcu" as a matter of course alludes to the filmware instead of the dev packs. The firware ESP8266 utilizes the Lua scripting dialect. It depends on the eLua extend, and based on the Espressif Non-OS SDK for ESP8266. It utilizes many open source activities, for example, lua-cjson and spiffs. NodeMcu with 9 input/output is capable to handle the system. The board just need 5V DC supply to operate. The complete data sheet for the product can be refer at the reference [6]. The NodeMcu will code with C++ using software Arduino IDE.

DTH11 will be used in the system to detect temperature and humidity change inside the electrical enclosure. It is an advanced temperature and humidity sensor that comes aligned and doesn't require extra parts to sense the air [7]. DHT11 Humidity Sensor Module is designed by using DHT11 which is able to detect the temperature and humidity of the surrounding environment. This module is compatible with Arduino, PIC, Raspberry pi and etc. DHT11 have three terminals that are VCC, DATA and GND. VCC is the supply terminal. To make the sensor operational it 3.3V DC supply. In this project it will be supply by controller. GND is ground that must be connected to ground at the board. DATA is importance information that the sensor will sent to the board. The sensor has measure range of 0℃ to 50℃ for temperature and 20%RH to 90%RH for humidity [7]. For it accuracy, temperature has ± 2℃while humidity has ± 5%RH [7]. This specification is acceptable to make the system operate efficiently. For more information of the sensor use, refer reference [7].

Fan will be choosing by considering the internal heat load in watt using 1 Watt = 3.4513 British thermal unit per hour (BTU/Hr). Then determine the temperature difference, ΔT (°F). Using formula to get CFM at Eq.1:

$$Volume\ Airflow\ (CFM), ft^3/\min = \frac{(3.16 \times Watts)}{\Delta T\ (°F)} \quad (1)$$

Every different ΔT (°F) with having different CFM. So a different kind of fan will be used. For this prototype, Ventilation Fan with 12cm x 12cm size, DC 12V powered and Net Weight: 150g will be used to valid the system concept [8]. The fan airflow is 28 CFM. By the specification given, the model could cool down 363 Watt system by temperature difference of 5 °C or 41 °F. This specification is enough to prove the system concept.

Relay module bolster two channel which mean it can associate up to two electrical utilizations [3]. The module is driven by opt coupler where it gives a detachment ground between your microcontroller and transfer. In the event that there are electrical separate, the microcontroller can be spare starting from the break. The two Channels Relay Module is a convenient board which can be used to control high voltage, high current load such as motor, solenoid valves, lamps and AC load. It is designed to interface with microcontroller such as Arduino, PIC and etc. The relays terminal COM, NO and NC is being brought out with screw terminal. COM stand for common, NO means normally open and NC means normally closes. It can control switching until 240V AC and 30V DC with current limited to 10A [8]. It also comes with a LED to indicate the status of relay. It will be used to on and off the fan. The connection will be shows and explained in circuit design.

The process of circuit design of this system will involve integrated all the component via connection to become integrated circuit. The process involves drawing circuit, testing, and soldering. Wire management also be done using cable tight. At the beginning, the controller circuit be solder to strip board. Then all the component be connected with wire. The connection of the component is show at figure 3. The system has two different supply to ON the system. The first supply is 5V DC that will ON the controller and relay module while the second supply that is 12V DC will ON/OFF the fan. Sensor DHT11 just need 3.3V DC to operate [7]. It can be supply by the controller. At figure 3, the red wire represent supply, green wire is ground, black wire for neutral and blue and yellow for data or signal. For relay, is connected to COM and NO.

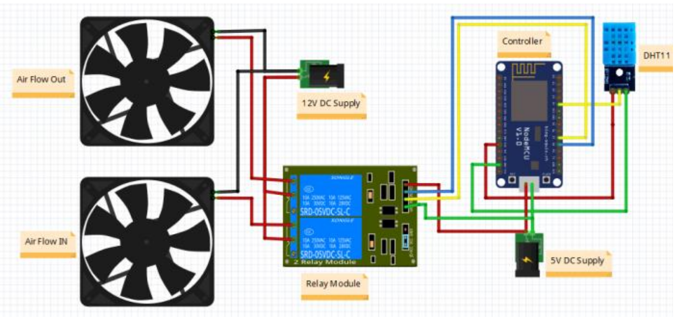

Fig. 3 Wiring circuit

Finally, after completed the circuit, the case of the model will be build. For the case, it will consist two. The first will hold the controller, sensor and relay module. The second will included the first case and fan. The second case actually represent the enclosure. The first case is having dimensions (Height × Width × Depth) of 12cm × 8cm × 4cm plastic material box. The Second case has dimensions (Height × Width × Depth) 35.5cm × 17.5cm × 42cm aluminum material case. The position of the fan is according to the design method. After the installation the model of the system as shows at Fig. 4. Cable management has been applied to ensure the neatness of the project box.

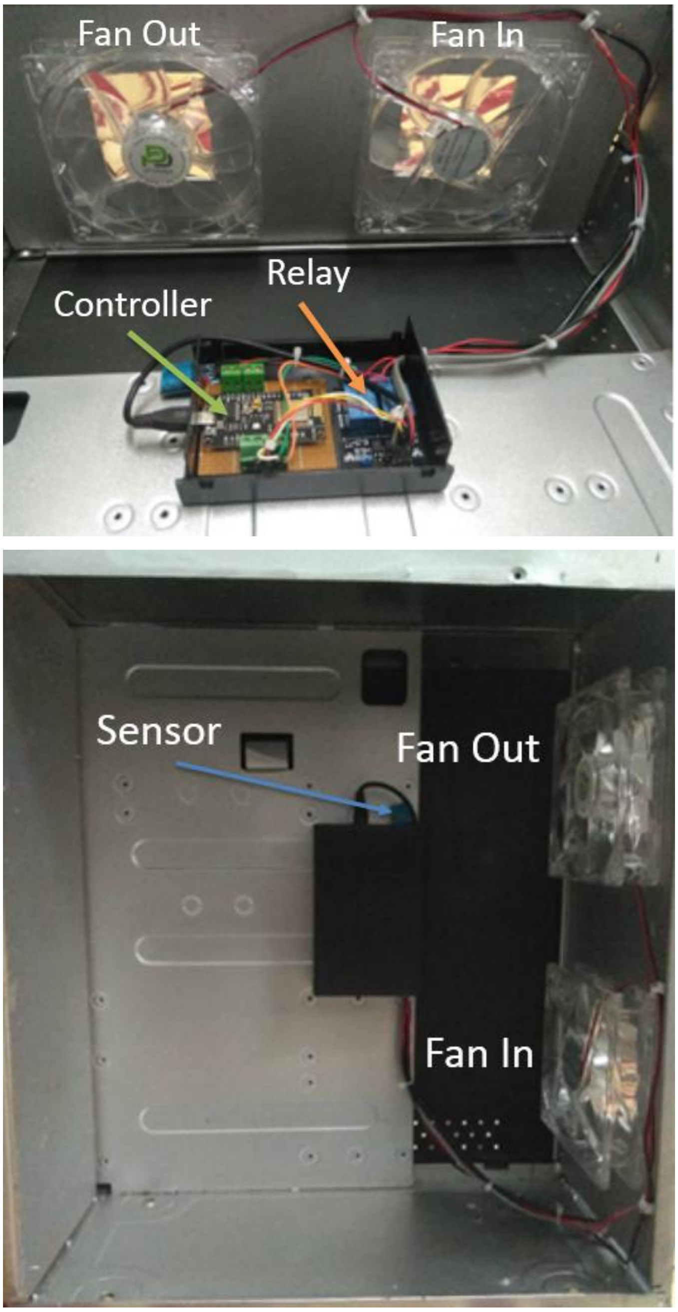

Fig 4 After installation

C. Software

This system using two type of software development. The first is Arduino IDE. Nowadays there are a lot of controllers can be used. However, Arduino IDE has offered feature that ease the user. The general purpose of the "Arduino Platform" is to take into consideration simple, quick and free prototyping due to they are open source [9]. Having the capacity to recently attach to various types of hardware [3] and have the capacity to show result on it in a matter of minutes, rather than hours, is just incredibly capable and helpful the user when they have a thought in mind and simply need to check whether their theory or idea works or not. For prototyping, the Arduino stage gives you a considerable measure of pre-wiring and free code libraries [9] that will give you a chance to focus on testing ideas and thought in practice. It also able user to investing the supporting hardware should be put into the model to improve the prototyping.

The second part of the software development is internet of thing (IoT). IoT offers the information gathering and control over the system. But, IoT is designed to be more flexible. The loT totally changes network from "at whatever time, any place" for "anyone" into "whenever, anyplace" for "anything" [4]. The loT can associate true components and implants the savvy in correspondence framework for astutely handle its particular data and self-governing choice. Consequently, IoT is a key empowering the distinctive sorts of valuable applications and administrations which can manage our economy, transportation, environment and heath that we as user never anticipated. It eases the user to monitoring and control the system via IoT.

For this part, Blynk has be choose to act as platform. Blynk was intended for the Web of Things. It can control equipment remotely; it can show sensor information. Furthermore, it can store information, and visualize it. The feature that make Blynk be selected are Blynk app, Blynk server and Blynk libraries. Blynk app permits to user make stunning interfaces for your tasks utilizing different gadgets Blynk give [10]. The app available for Android or IOS user. For Blynk server, it in charge of the considerable number of interchanges between the cell phone and equipment. Client can utilize Blynk Cloud or run your private Blynk server locally [10]. Its open-source, could without much of a stretch handle a large number of gadgets. The best feature is Blynk libraries. It has prepared libraries to empower correspondence with the server and process all the approaching and out coming charges for all the popular hardware platforms [10]. The Blynk working structure show at Fig. 5. The interface of the system also be design using Blynk. It functions of each widget show Fig 6.

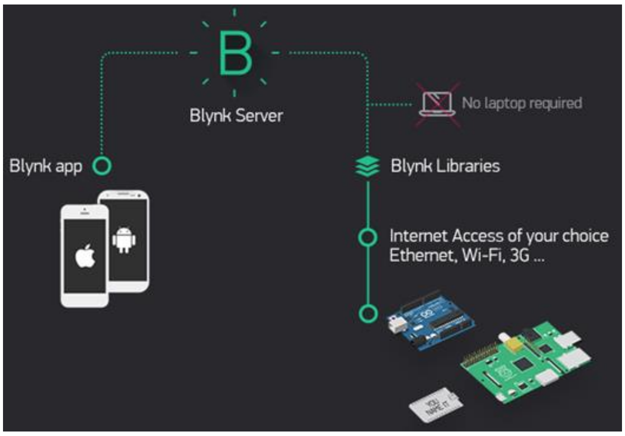

Fig. 8 Blynk working structure

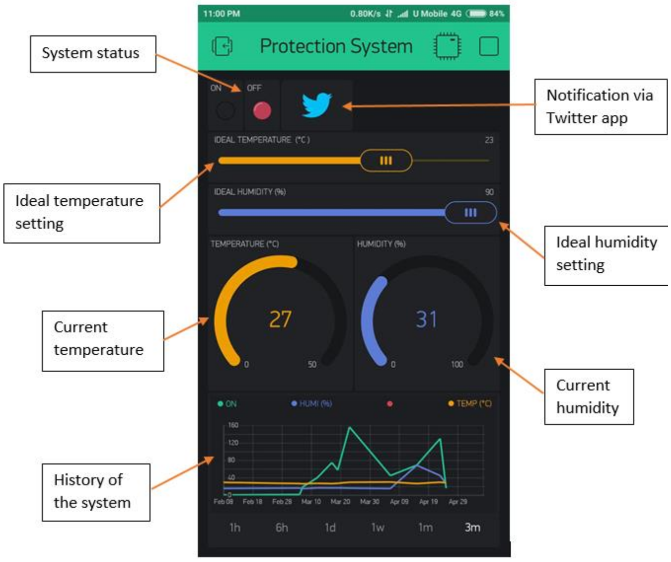

Fig. 9 System widget

III. RESULT

A. Sensor comparasion

The sensor that the system use has been compare will another device. To validate the design system using HD300 Thermo-Anemometer and HTC-2 Temperature and Humidity Meter with Probe Digital Clock Hygrometer, Digital Thermo Hygrometer, an experiment has been done to ensure the accuracy of the sensor. The result of the experiment is promising. All the devise shows almost the same value. It proves that the sensor is reliable. Fig. 10 show the result of the experiment.

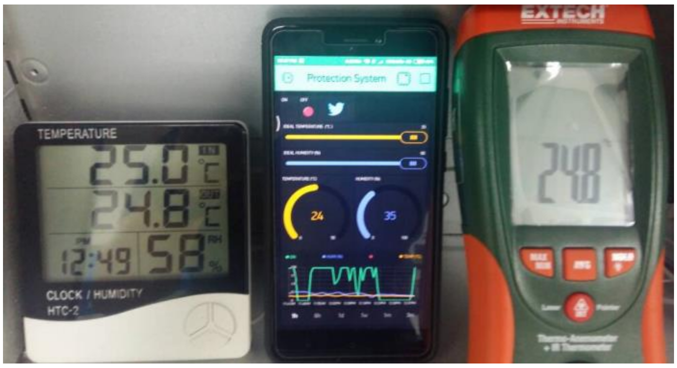

Sensor	Temperature (°C)
HTC-2 (At left)	24.8
DHT11 (System use at middel)	24
HD300 (At right)	24.8

Fig. 10 Sensor comparasion

B. System Performance

The system has been test by performing experiment to evaluate the performance of the system. The procedure of the

Surrounding Temperature = 30℃/ Humidity = 70% RH		
Start Condition	***End Condition***	***Time Taken to Achieve Thermal Equilibrium***
35 ℃/ 51% RH	30 ℃/ 60% RH	2 minutes 20 seconds
35 ℃/ 45% RH	30 ℃/ 51% RH	2 minutes 9 seconds
35 ℃/ 42% RH	30 ℃/ 53% RH	2 minutes 18 seconds
35 ℃/ 45% RH	30 ℃/ 55% RH	2 minutes 17 seconds
35 ℃/ 43% RH	30 ℃/ 53% RH	2 minutes 18 seconds

Table I Results of First Condition

Surrounding Temperature = 27℃/ Humidity = 59% RH		
Start Condition	***End Condition***	***Time Taken to Achieve Thermal Equilibrium***
32 ℃/ 41% RH	27 ℃/ 32% RH	24 minutes 2 seconds
32 ℃/ 17% RH	27 ℃/ 32% RH	25 minutes 18 seconds
32 ℃/ 18% RH	27 ℃/ 31% RH	25 minutes 48 seconds
32 ℃/ 19% RH	27 ℃/ 32% RH	26 minutes 12 seconds
32 ℃/ 19% RH	27 ℃/ 32% RH	27 minutes 10 seconds

Table II Results of Second Condition

experiment is beginning with detection of the surrounding temperature. Then, the temperature inside the enclosure is heat up using iron by 5℃ more that the room temperature. After that, the time of the enclosure become thermal equilibrium is recoded. The experiment can be done in two condition. First condition is when the fan of the system is fully operated. Second condition is when the fan of the system is not operating. The result of first condition been show in Table I and second condition show in Table II. From the experiment, it shows that with the present of the Overheat Protecting System accelerate the process of cooling down the condition inside the model enclosure to achieve desire condition. In this case, the desire condition is surrounding temperature. The different in time is almost 24 minutes different.

IV. CONCLUSION

The aim of this project is to protect electrical equipment that to cover for low voltage system only with the maximum temperature recommended for industrial components not more than 35℃ has been achieved. The system develops hold the temperature and humidity inside the electrical enclosure to be an ideal condition of electrical equipment to operate. All the extra feature brings positive impact to the user. The system will help the user to monitor and control the temperature and humidity inside electrical enclosure.

REFERENCES

[1] Panel Builders, Schneider Electrical East Mediterranean, Low Voltage Systems Newletter Issue #3 – September 2011.

[2] 2. Hoffman, Why Optimize a Cooling Set Point? White Paper, Pentair Equipment Protection, 2014.

[3] Ahmed Sirajuddin Ahmed Alhaj (2015). Home Automation System Using Arduino. Bachelor Philosophy, Universiti Teknologi Malaysia, Skudai.

[4] L. Coetzee, J. Eksteen. “The Internet of Things – Promise for the Future? An Introduction,” 1ST Africa 2011 Conference Proceedings (CSIR). 2011.

[5] W. l. He, B. q. Wan, C. m. Pei, J. g. Zhang and J. j. He, "Effect of humidity on transmission lines' power frequency electric field measurements," 2012 Asia-Pacific Symposium on Electromagnetic Compatibility, Singapore, 2012, pp. 289-292.

[6] "NodeMCU v2", 2017. [Online]. Available: https://lib.chipdip.ru/414/DOC001414363.pdf. [Accessed: 05- May- 2017].

[7] DHT11 Humidity & Temperature, D – Robotics, July 2010.

[8] “2 channel 5V 10A relay module”, 2017. [Online]. Available: http://www.energiazero.org/arduino_sensori/2_channel_5v_10a_relay_module.pdf. [Accessed: 05- May- 2017].

[9] "Arduino - Introduction", Arduino.cc, 2016. [Online]. Available: https://www.arduino.cc/en/Guide/Introduction. [Accessed: 08- Sep- 2016].

[10] "Blynk", Docs.blynk.cc, 2017. [Online]. Available: http://docs.blynk.cc/. [Accessed: 08- May- 2017].

Partial Discharge Detection and Measurement in Insulating Materials using Low Cost Rogowski's Coil

'Aifaa Nadirah binti Jefri
Faculty of Electrical Engineering
Universiti Teknologi Malaysia
Johor Bahru, Malaysia.
aifaanadirahjefri@yahoo.com

Mohd. Hafizi bin Ahmad
Department of Electrical Engineering (Power)
Faculty of Electrical Engineering
Universiti Teknologi Malaysia
Johor Bahru, Malaysia.
Mohdhafizi@utm.my

***Abstract*— This paper presents a low cost partial discharges detector with applying the implementation of Rogowski's coil. The induced currents produced from the Rogowski's coil are used to calculate partial discharge current and apparent charge by using a numerical integrator. Comparison of Rogowski's coil pulses produce is observed with a commercial partial discharge detector equipment pulses. The implementation of partial discharges detection and measurement in insulating materials such as void insulation using Low-Density Polyethylene (LDPE) sample and silicon rubber insulation in electrical treeing test, is performed. It is proved that the detection of partial discharge current as well as the apparent charge using the implementation of Rogowski's coil are successfully fulfill the measurement from the regular method.**

Keywords— Partial Discharge; Rogowski's coil; Current transformer; Insulating material.

I. Introduction

Partial Discharge (PD) test in insulating materials is normally conducted in order to define the insulation quality of high voltage equipment. Usually, the PD current and charge are detected by the commercial instrument based on IEC standard 60270 [1]. However, there have been attempts in applying the Rogowski's coil in detecting a high frequency current with a low amplitude such as partial discharges pulses [2]. Rogowski's coil is popular as an alternative method for partial discharge detection equipment. It has been noted that the rogowski's coil under developments has high sensitivity and wide bandwidth to detect the partial discharge pulses [2]. Apart from that, Rogowski's coil is a device that employs the voltage that is induced in a coil as a parameter for measuring such currents [3]. The Rogowski's coil is defined as a transducer which is able to convert a current to a voltage [4]. The induced voltage from the rogowki's coil is proportional to the rate of a change of a measured current to the time [4]. Nevertheless, the cost of the Rogowski's coil is high since it is require an expensive type of core such as ferrite. The cost of the device has been the crucial constrain in using Rogowski's coil as one of the testing equipment in high voltage laboratory.

In order to simplified PD detection with low cost approached, an air core Rogowski's coil are performed. Thus, the observation and measurement on the comparison between the Rogowski's coil PD detector measurement and commercial detector measurement is conducted in order to prove the effectiveness of the low cost Rogowski's coil design.

II. Methodology

A. *Rogowski's Coil*

Rogowski's coil is the sensor where a voltage is induced in a secondary circuit as response to the change in the magnetic flux produced around the current wire in the primary circuit [3]. The secondary circuit is an air coil. This kind of structure was proposed by Z. S. Zhang [2]. An equivalent circuit of the Rogowski's coil is shown as Fig. 1 [2].

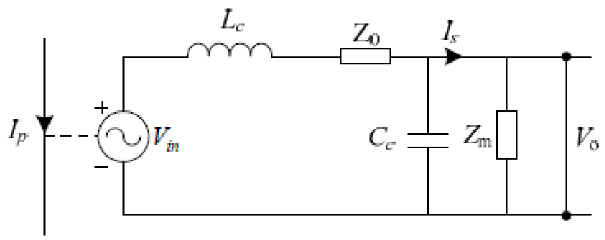

Fig 1. The equivalent circuit of Rogowski's coil [2].

I_p = Primary current o be measured
V_{in} = Induced Voltage
M_c = Mutual inductance between enclosed cable and coil
L_c = Self-Inductance of coil
C_c = Parasitic capacitance to the environment
I_s = Secondary current
Z_m = Secondry measurement impedance
V_o = Secondary Voltage
Z_o = Balance impedance

Modified Rogowski's coil using an air core placed around by the conductor, and induced voltage from the Rogowski's coil is mathematically integrated by a numerical integrator. The induced voltage and the integrated induced voltage can be written as equation (1) and (2) respectively [3].

$$V_{in}(t) = \frac{dM_c I_p(t)}{dt} \quad (1)$$

$$V_0(t)=\frac{1}{T_i}\int_0^t V_{in}(t)dt=\frac{M_c}{T_i}\left(I_p(t)-I_p(0)\right)=\frac{M_c}{T_i}I_p(t) \quad (2)$$

The Rogowski's coil model as shown in Fig. 2, shows that there is adjustable impedance Z_0 attached at one end of Rogowski's coil because it will increase the bandwidth and the sensitivity simultaneously in order to make the PD pulse detected.

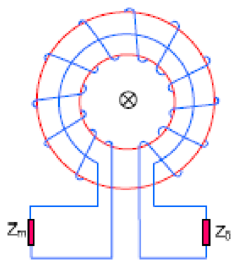

Fig. 3. Rogowski's coil model [2].

In the process of the measurement, the discharge current is received from an induced voltage. The Rogowski's coil will detect noise component and the induced voltage at the same time that will shows in the signal. As a result, the noise detected in the signal is required to be filtered. The system of the Rogowski's coil that include filter is shown in Fig. 4, which is developed for the PD measurement.

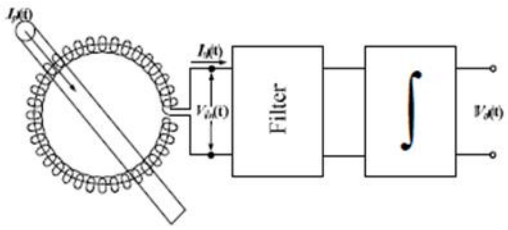

Fig. 4. The system for measuring current with Rogowski's coil [3].

From Fig. 5, it shows the Rogowski's coil that has been developed in order to perform the PD detection and measurement for this paper. This developed Rogowski's coil has 26 turns around the secondary circuit that has made up by using plastic material to create the air core. The impedance, Z_0 value attached at the end of the Rogowski's coil turns is 51 Ohm (Ω).

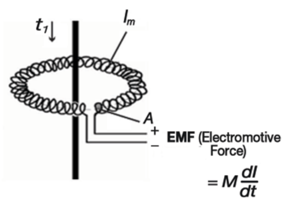

Fig. 5. The schematic diagram of the developed Rogowski's coil.

B. Experimental Setup

The experiment setup as in Fig. 7 is suitable for all three type of sample proposed in order to determine the ability of the Rogowski's coil to detect partial discharge pulse in various type of insulating materials. In this experiment, the insulating material that was tested are using Low-Density Polyethylene (LDPE) sample in order to detect PD in void insulation and needle plane sample for electrical treeing in order to detect PD in silicon rubber insulation.

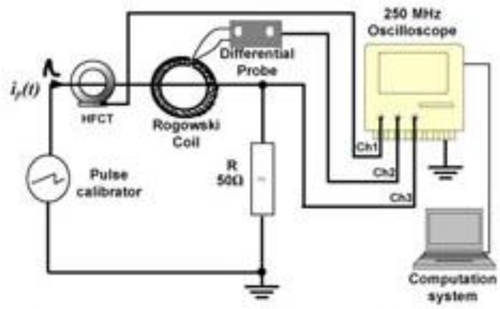

Fig. 7. The experimental setup of partial discharge test.

In Fig. 8, shows that the supply generated to the conventional circuit is getting through the developed system by placing the wire in the middle of the secondary circuit in order to transform secondary current on the developed system.

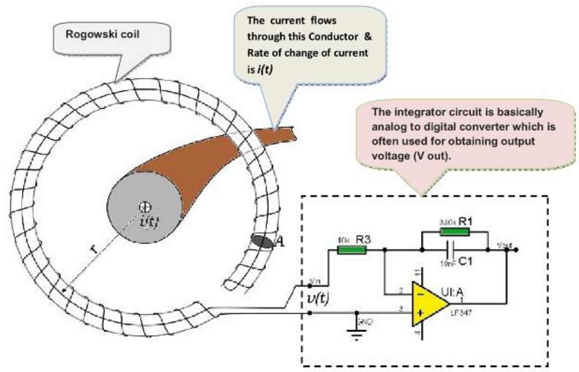

Fig. 8. The experimental setup of partial discharge test.

III. Results

In order to prove the ability of the developed Rogowski's coil in PD detection system, experiment on different type of insulating materials was carried out which are using Low-Density Polyethylene (LDPE) sample in order to detect PD in void insulation and needle plane sample for electrical treeing in order to detect PD in silicon rubber insulation.

The pulse of the PD detection produced by developed system will be compared to the pulse of the PD detection produced by commercial system in both type of insulating material. The data of the PD detected by the Rogowski's coil was observed and measured in order to determine the Rogowski's coil is functioning as a PD detector. Thus,

A. *Partial Discharge Detection on Void Insulation Sample using LDPE.*

Fig. 9, shows the experimental setup for void insulation sample using LDPE sample to test the PD detection ability of the Rogowski's coil. The LDPE sample was placed in the Cigre and attached to the coupling capacitor during the experiment.

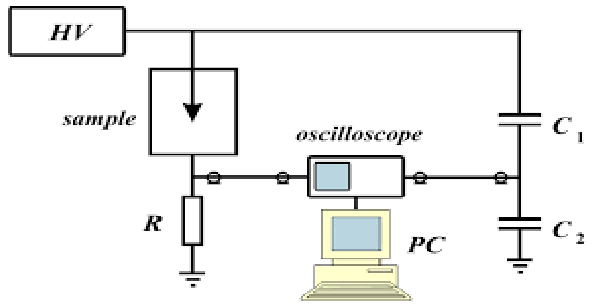

Fig. 9. The experimental Setup for PD detection on LDPE Sample using Cigre.

From the experiment, the pulse of the PD detection was observed by using oscilloscope with four channels. As in Fig. 10, channel 1 shows the supply voltage waveform in Voltage,V. Meanwhile, channel 2 shows the developed Rogowski's coil pulse detection of PD and channel 3 shows the pulse of PD detected by the commercial PD detector. As a result, the performance of the developed Rogowski's coil in PD detection agrees with the PD detection result of commercial PD detector according to the pattern of the PD pulse. However, the measurement of the PD pulse detected by the developed Rogowski's coil and the commercial PD detector are slightly different in amplitude value which are 310mV and 900mV respectively. This might be occurred because of the different number of turns of the secondary circuit of the developed Rogowski's coil from the commercial PD detector that effect in the change of the magnetic flux produced by the current from the primary circuit.

Since the developed Rogowski's coil is proved to be able to detect the PD pulse and provide the measurement data as commercial PD detector, therefore, Fig. 11 shows the PD phase resolved pattern gain from the developed system with the data recorded from the experiment.

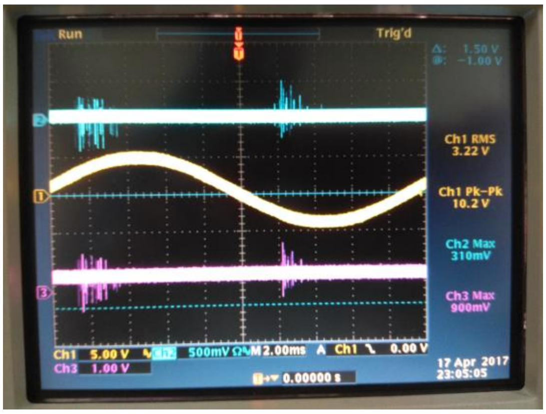

Fig. 10. The Partial Discharge Detection Pulse of LDPE Sample.

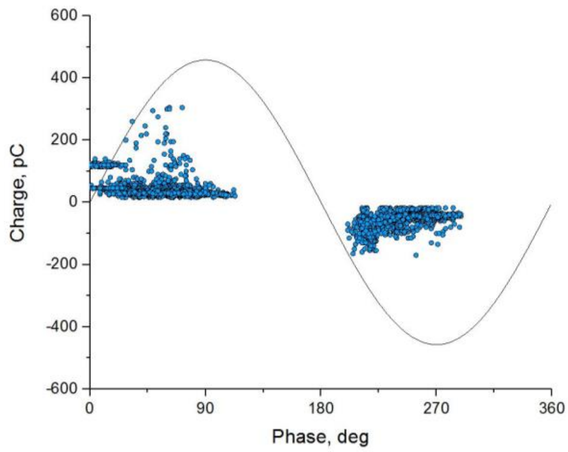

Fig. 11. The Partial Discharge Phase Resolve Pattern of LDPE sample.

B. Partial Discharge Detection on Silicon Rubber Insulation Sample in Electrical Treeing Test.

Fig. 11, shows the experimental setup for silicon rubber insulation sample using electrical treeing test in order to test the PD detection ability of the Rogowski's coil. The needle plane sample for electrical treeing test was placed under the microscope and attached to the coupling capacitor during the experiment. The treeing process was recorded while PD detection pulse was observed.

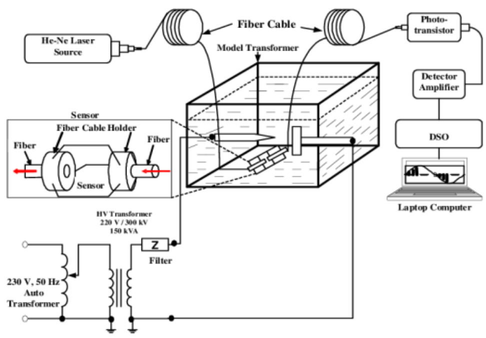

Fig. 13. The experimental Setup for PD detection on Silicon Rubber Insulation sample in Electrical Treeing Test.

Meanwhile, the experiment that involve electrical treeing test in order to observe PD detection pulse and measurement on silicon rubber insulation also using oscilloscope with four channels. As in Fig. 13, channel 1 shows the supply voltage waveform in Voltage,V. Meanwhile, channel 2 shows the developed Rogowski's coil pulse detection of PD and channel 3 shows the pulse of PD detected by the commercial PD detector. As a result, the performance of the developed Rogowski's coil in PD detection agrees with the PD detection result of commercial PD detector according to the pattern of the PD pulse. However, the measurement of the PD pulse detected by the developed Rogowski's coil and the commercial PD detector are slightly different in amplitude value which are 216mV and 710mV respectively. This might be occurred because of the different number of turns of the secondary circuit of the developed Rogowski's coil from the commercial PD detector that effect in the change of the magnetic flux produced by the current from the primary circuit.

Since the developed Rogowski's coil is proved to be able to detect the PD pulse and provide the measurement data as commercial PD detector, therefore, Fig. 14 shows the PD phase resolved pattern gain from the developed system with the data recorded from the experiment.

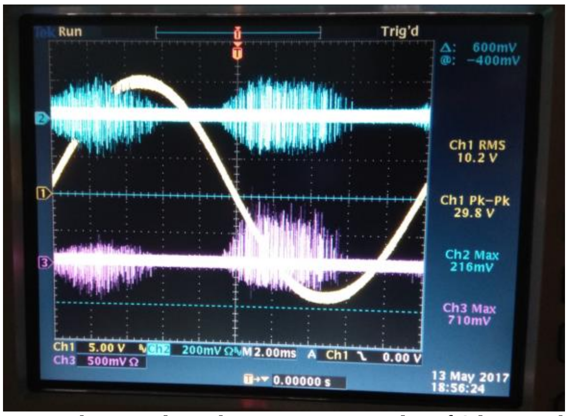

Fig. 14. The Partial Discharge Detection Pulse of Silicon Rubber Sample.

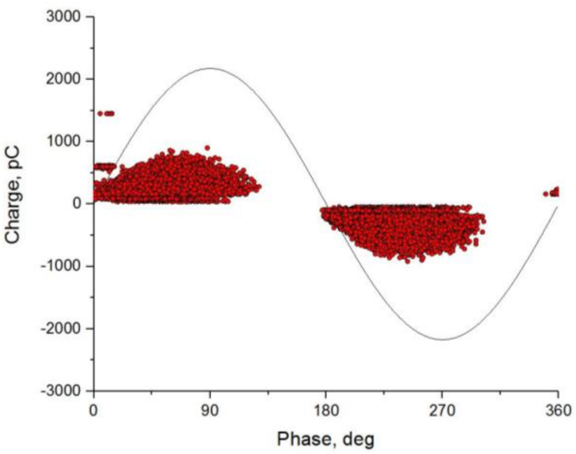

Fig. 14. The Partial Discharge Phase Resolve Pattern of Silicon Rubber sample.

IV. Conclusion

In this paper, a Rogowski's coil has been developed in order to prove the capability of the system in PD detection on insulating materials. The performance of the Rogowski's coil on PD detection and measurement has been evaluated by performed the experiment on two different types of insulation which are void insulation using LDPE sample in cigre and silicon rubber insulation in electrical treeing test using needle plane sample. From the experiment, it has been proved that the developed Rogowski's coil is able to perform as a commercial PD detector in PD detection pulse experiment on both types of insulating materials even though the amplitude of the results have a slightly different because of the effect from the different number of turns in the developed Rogowski's coil in ratio 3:1 to the commercial PD detector. In addition, the capability of the developed Rogowski's coil in provides PD detection data in term of pulse current measurement and apparent charges can be confirmed from the experiment. Therefore, the Rogowski's coil system proposed as an alternative for a low cost PD detector is accepted.

Acknowledgement

Authors would like to express their gratitude to Universiti Teknologi Malaysia (UTM), Faculty of Electrical Engineering and Institute of High Voltage and High Current (IVAT) in the form of research scholarships, research sources facilities and laboratory equipment sponsor.

References

[1] IEC60270 "High Voltage Test Techniques – Partial Discharge Measurement".
[2] Z. S. Zhang, D. M. Xiao and Y.Li, "Rogowski air coil sensor technique for on-line partial discharge measurement of power cables" IET Science, Measurement an Technology, Vol.3, Iss.3, pp. 187-196, 2009.
[3] B. Paophan, A. Kunakorn and P. Yutthagowith, "Implementation of a Rogowski's Coil for Partial Discharge Detection", 2016.
[4] D. A. Ward, J. La, and T. Exon, "Using Rogowski's coil for transient current measurements," Engineering Science Education Journal, Vol.2, No.3, pp. 105-113, 1993.
[5] Giscar F. C. Veloso, L. E. Borges da Silva, I. Noronha, G. Lambert Torres, J. Haddad Rondineli R. Pereira, Se Un Ahn, "Detection of Partial Discharge in Power Transformer using Rogowski coil and Multiresolution Analysis", 2019.

Electrochemical Performance of Supercapacitor using Aqueous Solution as Electrolyte with Glass Wool Separator

Zulisman bin Rahman
Faculty of Electrical Engineering,
Universiti Teknologi Malaysia,
Johor, Malaysia.
zulisman94@gmail.com

Zulkarnain bin Ahmad Noorden
Department of Electrical Power Engineering,
Faculty of Electrical Engineering,
Universiti Teknologi Malaysia,
zulkarnain-an@utm.my

***Abstract*—Electrolyte have been discovered as a one of components in supercapacitor's construction delivered a significant effect in the performance of electrochemical supercapacitors. This paper evaluate the electrochemical performance of supercapacitor using three different of electrolytes (H_2SO_4, KOH and NaOH) using cyclic voltammetry (CV), galvanostatic charge-discharge (GCD) and electrochemical impedance spectroscopy (EIS). With same material of activated carbon was assembly by sandwiching an electrolyte and at middle have glass wool as separator. The electrical properties in terms of specific capacitance, equivalent series resistance, power and energy densities have been reveal for the comparing performance of each electrolyte solutions. A sulphuric acid (H_2SO_4) show the an excellent characteristic with the highest specific capacitance value (72.36 F/g) and lowest equivalent series resistance (11.94 Ω), leads to higher rating of supercapacitor compared to KOH and NaOH electrolyte solutions.**

Keywords—supercapacitor; electric double layer capacitor; electrolyte; aqueous solution

I. Introduction

Energy storage is a device that captures the energy produced at one time and will use for at the later time. It is very necessary for harvesting from renewable such solar, wind, and hydro while it's become quietly needed. Recently, the issue of increasing a cost of fuel, the number of pollution and global warming needs to developing other method energy resources and improvement of storage technologies [1]. An effective utilization method of renewable sources and a better efficiency of transportation systems are goals to be pursued this issue.

Supercapacitors are also known ultracapacitor or electric double layer capacitor a new high technology of electrochemical energy storage due to the power energy density and fast charging-discharging cycles also can fulfill requirements of many application such an electric vehicle, memory backup systems, and solar energy system [1-6]. Supercapacitor already widely used in many kinds of electrical industry as energy storage compares to batteries or conventional capacitor.

The construction of supercapacitor made up from four significant part which are the current collector, electrode, electrolyte, and separator. Specific capacitance and equivalent series resistance (ESR) are two critical parameters that affected by that construction [1,7]. Activated carbon is commonly used as an electrode material because of having excellent chemical stability and large surface area while the low-cost electrolyte; the aqueous solution that capable produce high power density[1,]. Recently, ionic liquid and organic solution (ionic liquid with solvents) become a favorable development in a supercapacitor that provides wider voltage window and higher energy density instead of using the aqueous solution as an electrolyte that has low operating voltage [1,2,7,8,9]. However, the lower conductivity of solution affect the higher capacitance of supercapacitor also contribute better power density [9]. Besides that, glass wool has high conductivity and degree of porosity expose high specific capacitance and low ESR value when its in structure of supercapacitor [3].

The aim of this research to obtain the high performance of supercapacitor using glass wool separator in three different aqueous solutions as electrolyte. Besides, by using three techniques of testing; cyclic voltammetry, galvanostatic charge-discharge and electrochemical impedance spectroscopy the electrochemical performance of supercapacitor can be proved.

II. Experiment

A. *Seperator Materials*

The separator also a significant part of the construction of supercapacitor to separate the two electrodes for avoiding short circuit. Regularly, a separator uses a very porous material to reduce the equivalent series resistance (ESR). The separator has chemically inert to maintain the stability and conductivity of the electrolyte. Besides that, the separator is a medium for carry out the charges in the liquid electrolyte to the electrode.

From the previous research, the experiment was conducted to the performance of supercapacitor using various type of separator; polypropylene (PP) sheet, cellulose paper, fiberglass and glass wool in 1 mol/dm3 of H_2SO_4 [3]. The power and energy density, ESR, also especially specific capacitance as the parameter measured to obtained the performance of each type of separator.

From the testing experiment show that the glass wool separator has better performance with high specific capacitance (131 F/g), lowest ESR value (13Ω) also have highest power and energy densities compare to another separator. Glass wool also have high conductivity and porosity as shown in Table I [3]. Precisely, supercapacitor with glass wool separator compromises a better electrochemical performance.

B. Electrolyte

Electrolyte also is a significant part in the supercapacitor performance [1,7,8,9]. Apart from that the concentration of electrolyte has to be the high concentration for preventing the depletion problems called starvation effect especially for organic electrolyte [3]. The requirements properties of an electrolyte are involved the operating voltage window, higher conductivity, high stability, high ionic concentration, low toxicity, etc. [1,8]. The electrolyte might be in aqueous solution, ionic liquid, and organic. The aqueous solution is most widely used since it's low cost. However, the limitation of these electrolyte has low operating voltage (1 V) rather than organic (2.7 V or higher) and ionic liquid (up to 3.5 V). Regarding capacitance aqueous solution electrolyte shows that high value than organic electrolyte due to the higher concentration and lower ionic radius [1,3,8]. The organic electrolyte is familiarly used as solvents such as acetonitrile (ACN) and these electrolytes have better conductivity but high relative cost [8,10].

From the Lewandowski's study, supercapacitor using ionic liquid with same carbon electrode can operate up 3.5 V while for aqueous solution have high power density. In this experiment, the sulphuric acid (H_2SO_4), potassium (KOH) and sodium hydroxide (NaOH) as aqueous solution electrolyte with 1 mol/dm^3 of concentration for each electrolyte.

TABLE I. PROPERTIES OF SEPARATOR

Separator	*Density (g/cm^3)*	*Conductivity (mS/cm)*	*Porosity (%)*
Cellulose paper	0.39	8	36±8
PP sheet	0.22	25	51±6
Fiber glass	0.43	19	74±6
Glass wool	0.31	24	84±2

*Data taken from [3]

C. Test cell construction

Two symmetrical electrode test cell practically act as supercapacitor to figure out the characteristic of the real supercapacitor. This test cell was formed with anode and cathode terminal. Firstly, to prepared the materials inside this test cell by clean the inside part then keep in dry condition. At the same time, the glass wool was cut into a circular shape in form thin sheet-like. Next, the two activated carbon sheets already prepared and the mass was measured (73.3mg). For the establishing this test cell act entirely practically supercapacitor, a symmetrical two electrode was binding with two activated carbon sheets between the glass wool separator. Before the test cell was attaching with activated carbon sheets, the glass wool separator was immersed into 1.0 mol/dm3 of each electrolyte with the room temperature condition (25 ℃). Figure 1 show that the material used and two symmetrical electrode test cell.

Fig. 1. Materials used and two symmetrical electrode test cell.

D. Characterization

In order to obtained the the characteristic of supercapcitor, the CV, GCD and EIS were performed by using potentiostat (Gambry Interface 1000) on each contructed capacitor. The CV measurement was carried out with 2, 10 and 50 mV/s of scan rates at potential voltage 0 - 1 V for aqueous solution (H_2SO_4, KOH, NaOH). By using similiar potential voltage for GCD testing at various constant current at 5, 10, and 50 mA. The EIS measurement was conducted at 10 mV AC amplitude within 1mHz and 100kHz. The measurements was conducted under room temperature of each test cell contructed.

III. RESULTS AND DISCUSSION

A. Cyclic Voltammetry

Figure 2 shows the CV curves of the tested supercapacitor with various type of electrolytes at 10 mV/s and scan rates. The specific capacitance was directly obtained from equation (1) where I (in ampere) is the CV current measured, m (in gram) is mass of the activated carbon sheets and *dv/dt* represents as scan rate.

$$C_s = \frac{I}{dv/dt} x \frac{4}{m} \tag{1}$$

The CV curves of tested supercapacitor by using differents of aqueous solution electrolytes (H_2SO_4, KOH, NaOH) at constant scan rate of 10 mV/s as shown in Fig. 2. Each electrolyte showed ta rectangular, symmetric, reversible shape in potential voltage range of 0-1.0 V, illustrate an excellent behaviour of capacitor [10,11]. The voltage reached to 1.0 V when it is charging while back to 0 V when discharge process take place [11]. Beside, the absence of Faradaic peak (no reduction or oxidation processs) during the charge discharge process which will prove a higher cyclability of supercapacitor performance [3].

The static specific capacitance of each electrolytes of tested supercapacitor, $C_{s,cv}$ able to computed during charge discharge processes by using equation (2) [3,10].

$$C_{s,cv} = \frac{\int_{V_1}^{V_2} I(V)dV}{(dV/dt)(V_2 - V_1)} x \frac{4}{m} \tag{2}$$

Where V_1 and V_2 are lower and upper limit of the CV curves respectively. The specific capacitance value of each electrolyte is tabulated in Table II.

Based on the results, the strong acidic elecrolyte (H_2SO_4) delivered the highest $C_{s,cv}$ with 56.56 F/g at 10 mV/s followed by KOH and NaOH with specific capacitance 10.08 and 3.61 respectively. Due to high conductivity, H_2SO_4 is most frequently used for electrolyte in construction of supercapacitor, beside have lower equivalent series resistance, which lead to provide better power density of energy storage system (ESs). The increasing of ionic conductivity lead to higher specific capacitance of supercapacitor [8].

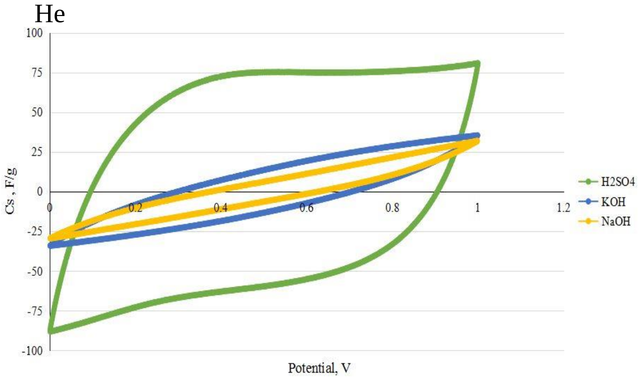

Fig. 2. Cyclic voltammetry at 10 mV/s scan rate

TABLE II. STATIC SPECIFIC CAPACITANCE OF VARIOUS ELECTROLYTE AT 10 AND 50 MV/S OF SCAN RATE

Electrolyte	**Cs,cv, F/g**	
	10 mV/s	**50 mV/s**
H_2SO_4	56.56	18.61
KOH	10.08	0.83
NaOH	3.61	0.27

CV measurement also conducted for each electrolyte with different value of scan rate for investigate the behaviour when tested supercapacitor higher scan rate as shown as Fig. 3 (a), (b), and (c). Even after the scan rate increases to 50 mV/s the CV response still maintained the symmetrical rectangular shape, almost ideal characteristic.The higher scan rates will cause faster charge-discharge process while the low scan rates show slow charge-discharge process with lower current applied. This finding show that the H_2SO_4 as electrolyte proclaim the best characrteristic of capacitor with the lower deterioaration occur in fastest scan rate of 50 mV/s in CV curve. The specific capacitance of each electrolyte tested supercapacitor was calculated corresponds to (2) and represented in Fig. 4 also the data is tabulated in Table II. From the results exposed clearly the highest $C_{s,\ cv}$ value (18.61 F/g) at highest scan rate of 50 mV/s belongs to H_2SO_4 electrolyte followed by KOH and NaOH with $C_{s,\ cv}$ values 0.83 and 0.27 F/g respectively. The specific capacitance decay at so high potential scan rate prove the performance of activated carbon is related to size of pore [8].

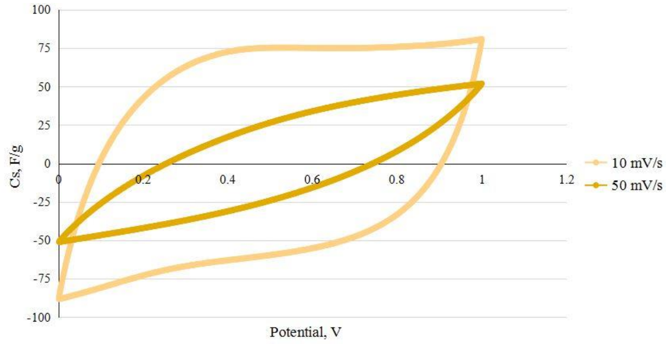

(a)

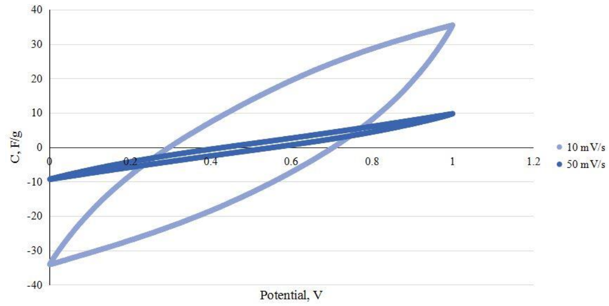

(b)

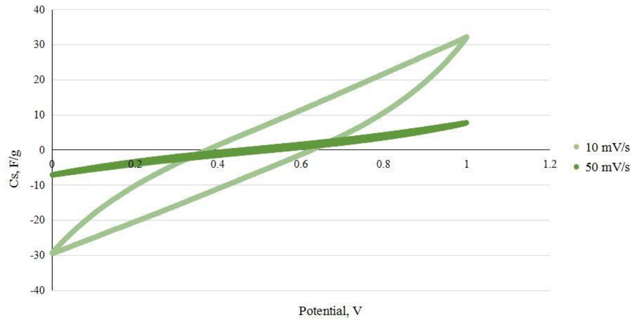

(a)

Fig. 3. Cyclic voltammetry curve of 10 mV/s against 50 mV/s by using (a) H_2SO_4, (b) KOH, (b) NaOH as electrolyte.

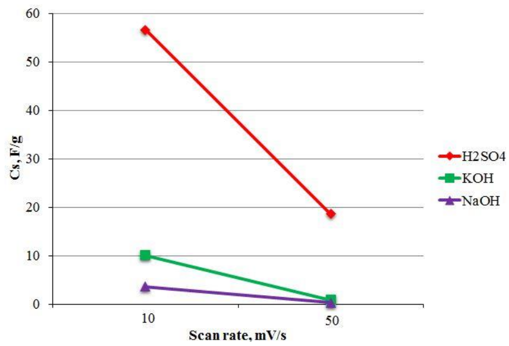

Fig. 4. Static specific capacitance of each electrolyte at 10 and 50 mV/s of scan rate.

B. Galvanostatic charge-disharge

In order to further investigation, the electrochemical performance of the three electrolytes of tested supercapacitor undergoes galvanostatic charge-discharge measurements from 0 - 1.0 V at 5 mA of constant current represent in Fig. 5. After 20 cycles of charge- discharge process, the graph show the linear variation (corresponds to the nearly CV curve) indicate the tested supercapacitor in excellent characteristic of supercapacitor for all this three electrolyte []. The values specific capacitance $C_{s,\,gcd}$ (F/g), equivalent series resistance $R_{esr,gcd}$ (Ω), power density P (W/kg) and energy density E (Wh/kg) obtained according equation (3)-(6). The calculation results was tabulated in Table III.

$$C_{s,\mathrm{gcd}} = \frac{I_d \Delta t}{\Delta V} x \frac{4}{m} \tag{3}$$

Where Id represent as discharge current, Δt and ΔV represent the time during discharge process and voltage shift.

$$R_{esr,\mathrm{gcd}} = \frac{V_{drop,\mathrm{gcd}}}{\Delta I} \tag{4}$$

Where $V_{drop,gcd}$ [V] is the voltage drop and I [A] is current change at the instance of charge–discharge transition.

$$P = \frac{V^2}{4R_{esr,\mathrm{gcd}}} x \frac{1000}{m} \tag{5}$$

$$E = \frac{1}{2} C V^2 x \frac{1}{3.6m} \tag{6}$$

Where V [V] represents as the voltage potential window for charge-discharge, $R_{esr,\,gcd}$ [Ω] represents the ESR value, m (g) is the total mass of activated carbon electrode, and C (F) stands for absolute capacitance of the supercapacitor during testing.

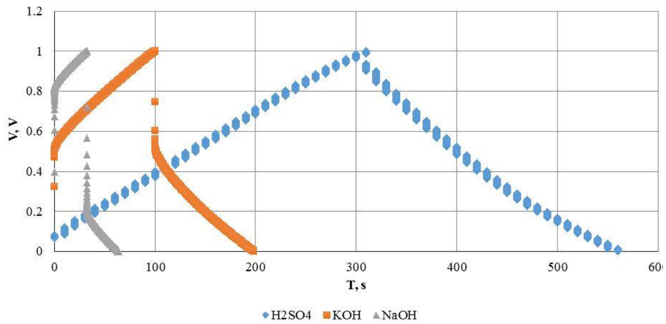

Fig. 5. Galvanostatic charge-discharge curve of tested supercapacitor by using various electrolyte with 5 mA constant current.

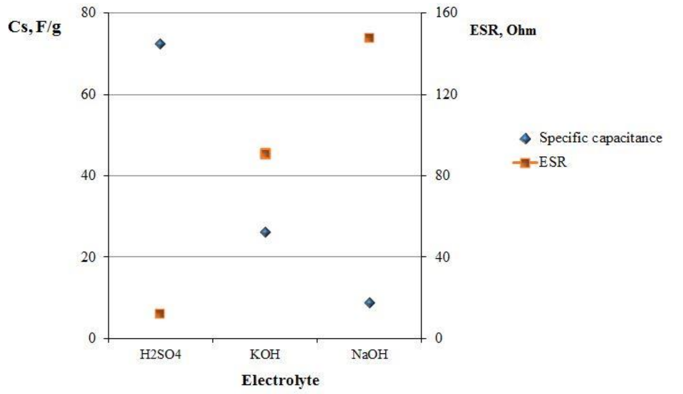

Fig. 6. Static specific capacitance and equivalent series resistance values from galvanostatic charge-discharge measurement of each tested supercapacitor.

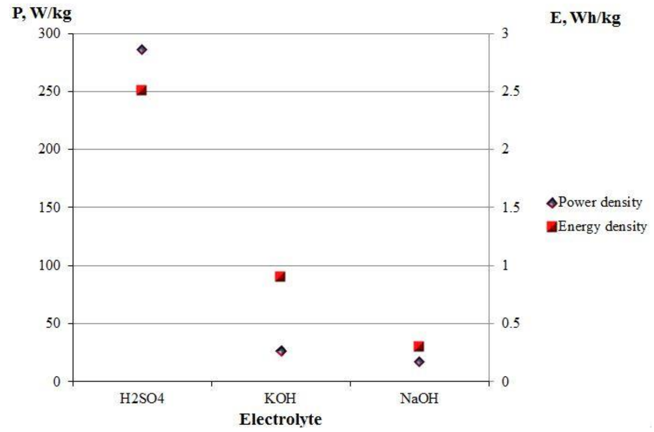

Fig. 7. Power and Energy densities values from galvanostatic charge-discharge measurement of each tested supercapacitor.

TABLE III. ESTIMATED SPECIFIC CAPACITANCE, EQUIVALENT SERIES RESISTANCE, POWER AND ENERGY DENSITIES FROM GALVANOSTATIC CHARGE-DISCHARGE MEASUREMENT

Electrolyte	C (F)	$C_{s,gcd}$ (F/g)	$R_{esr,gcd}$ (Ω)	P (W/kg)	E (Wh/kg)
H_2SO_4	1.33	72.36	11.94	285.65	2.51
KOH	0.66	26.03	91.10	27.09	0.90
NaOH	0.22	8.68	147.34	16.75	0.30

From galvanostatic charge discharge measurement, value of $C_{s,\,gcd}$ are in same agreement with the CV measurement where the H_2SO_4 gives the highest specific capacitance of 72.36 F/g followed by KOH and NaOH (26.03 and 8.68 F/g respectively) with large different values in 5 mA constant current. Another characteristic can be compare from this measurement is equivalent series resistance, which will contribute to the power density of supercapacitor performance [8]. Fig. 6 shows the graph of the value of $C_{s,\,gcd}$ and $R_{esr,gcd}$ against three different electrolyte used. The lowest $R_{esr,gcd}$ goes to H_2SO_4 (11.94 Ω)followed by KOH and NaOH with 91.94 and 147.34 Ω respectively. It can seen clearly at graph in Fig. 6, the lowest ESR value contributes highest specific capacitance of tested supercapacitor.

As shown as Table III and Fig. 7, the power and energy densities results from enhancement of specific capacitance and improved equivalent series resistance by using three different electrolyte used in tested supercapacitor. As expected, the highest power and energy densities belongs to H_2SO_4 with 285.65 W/kg and 2.51 Wh/kg respectively cause by having the highest $C_{s,\ gcd}$ and lowest $R_{esr,gcd}$. Sulphuric acid (H_2SO_4) as a strong acid electrolyte exhibit high conductivity have an advantages for lowering $R_{esr,gcd}$ and lead to better power density[3,8].

C. Electrochemical Impedance Spectroscopy

Fig. 8 illustrate the nyquist plot of the electrochemical impedance of tested supercapacitor with three different eletcrolyte used by using EIS measurement with frequency range is 1 mHz to 100 kHz. All the samples exhibit the ideal characteristic behaviour of supercapacitor the vertical lines occur at imaginary axis during the lower frequency applied while at the higher frequency region, a semicircle curve occur [2,3,10,12,13]. There are several reason of the semicircle present at high frequencies region are electrode porosity and the charge transfer of possible capacitor contributing to the total observed capacity [2]. The $R_{el,\ eis}$ (electrolyte-electrode interface resistance) value of each electrolyte used obtained from the intercept of the nyquist plot with Z_{real} -axis [3]. Table IV represents the estimation values $R_{el,\ eis}$, the H_2SO_4 shows the lowest $R_{el,\ eis}$ value with 0.18 Ω compared to 0.29 and 0.31 Ω from KOH and NaOH electrolyte solution respectively. The sequences of $R_{el,eis}$ corresponds with ionic conductivity of the aqueous solution [8]. The equivalent series resistance also show in Table IV, from the intercept of the extrapolation of vertical lines with Z_{real} -axis. As expected, the $R_{esr,\ eis}$ value obtained from EIS measurement almost same with galvanostatic charge-discharge measurments with the lowest value find from H_2SO_4 electrolyte solution used in tested supercapacitor with 6.71 Ω whereas KOH and NaOH solution have biggest value (81.55 and 107.6 Ω respectively). This is a good justification for tested supercapacitor corresponds of both measurements.

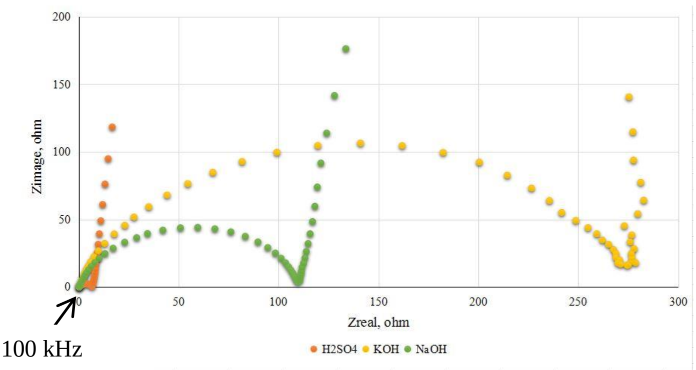

Fig. 8. Nyquist plot of impedance data

TABLE IV. EQUIVALENT SERIES RESISTANCE AND ELECTROLYE-ELECTROLYTE RESISTANCE FROM EIS MEASUREMENT

Electrolyte	$R_{esr,\ eis}$ (Ω)	$R_{el,\ eis}$ (Ω)
H_2SO_4	6.71	0.18
KOH	81.55	0.29
NaOH	107.6	0.30

IV. CONCLUSION

A supercapacitor with glass wool separator has been successfully performed by using two symmetrical electrode test cell and have been tested with Potentiostat Gambry Interface 1000. Cyclic voltammetry and galvanostatic charge-discharge technique were conducted on supercapacitor with glass wool separator in 1 mol/dm3 of H_2SO_4, KOH and NaOH electrolyte solution used to analyse its performance based on various of controlling variables. The result most likely as expected, cyclic voltammetry testing provide nearest ideal supercapacitor characteristic curve with no faradaic effect and the value of specific capacitance was affected by various scan rates at all electrolyte solutions [2,3]. For the galvanostatic charge-discharge technique, linear voltage responses based different amount of constant current were performed corresponds to the supercapacitor tested was similar to typical supercapacitor [2,3]. Same goes to EIS measurements, the ideal capacitive behaviour reveal by the present of vertical line on the nyquist plot. The difference of peformance of each electrolyte used of tested supercapacitor came when the specific capacitance, equivalent series resistance, power and energy densities were calculated. Sulphuric acid (H_2SO_4) give an excellent result with the highest specific capacitance (72.36 F/g)and lowest equivalent series resistance (11.94 Ω)due to high conductivity followed by KOH and NaOH respectively []. On the hand, with same operating voltage and concentration, the power and energy density (285.6 W/kg and 2.51 Wh/kg respectively) by using H_2SO_4 electrolyte solution.

REFERENCES

[1] Ander González, Eider Goikolea, Jon Andoni Barrena, Roman Mysyk, Review on supercapacitors: Technologies and materials, Renewable and Sustainable Energy Reviews, Volume 58, May 2016, Pages 1189-1206.

[2] Lewandowski A, Olejniczak A, Galinski M, Stepniak I, Performance of carbon-carbon supercapacitors based on organic, aqueous and ionic liquid electrolytes, Journal of Power Sources 2010; 195(17):5814–5819..

[3] Noorden, Z. A., Sugawara, S. and Matsumoto, S. (2014), Noncorrosive separator materials for electric double layer capacitor. IEEJ Trans Elec Electron Eng, 9: 235–240.

[4] Pandolfo A, Hollenkamp A. Carbon properties and their role in supercapacitors. J Power Sources 2006;157(1):11–27.

[5] R. Nicole, “Title of paper with only first word capitalized,” J. Name Stand. Abbrev., in press.

[6] M. S. Halper, J. C. Ellenbogen, Supercapacitor : A Brief Overview, MITRE Nanosystems Group (2006), Virgina USA.

[7] R. Negroiu, N. Bădălan, A. Vasile and C. Marghescu, "A research of the characteristics of materials used in the construction of EDLCs," 2015 IEEE 21st International Symposium for Design and Technology in Electronic Packaging (SIITME), Brasov, 2015, pp. 95-98.

[8] Zhong, C., Deng, Y., Hu, W., Qiao, J., Zhang, L., & Zhang, J. (2015). A review of electrolyte materials and compositions for electrochemical supercapacitors. Chem. Soc. Rev., 44(21), 7484-7539.

[9] M. Galinski, A. Lewandowski, I. Stepniak, Ionic liquids as electrolytes, Electrochimica Acta 51 (2006) 5567–5580.

[10] Z. A. Noorden and S. Matsumoto, Electrochemical Study of Hydrocarbon-Derived Electrolytes for Supercapacitors, Japanese Journal of Applied Physics 52 (2013).

[11] S. Kumagai, K. Mukaiyachi, M. Sato, N. Kamikuri and D. Tashima, "Roles of pore structure and type of electrolyte on the capacitive performance of activated carbons used in electrical double-layer capacitors," Proceedings of 2014 International Symposium on Electrical Insulating Materials, Niigata, 2014, pp. 511-514.

[12] Redondo, E., Goikolea, E., & Mysyk, R. (2016). The decisive role of electrolyte concentration in the performance of aqueous chloride-based carbon/carbon supercapacitors with extended voltage window. Electrochimica Acta, 221, 177-183.

[13] Tiruye, G. A., Muñoz-Torrero, D., Palma, J., Anderson, M., & Marcilla, R. (2015). All-solid state supercapacitors operating at 3.5 V by using ionic liquid based polymer electrolytes. Journal of Power Sources, 279, 472-480.

An Ergonomic Design and Development of Plasma Needle for Dentistry

Mohd Adi Luqman Bin Mohammed Hanafiah
Faculty of Electrical Engineering
Universiti Teknologi Malaysia
Johor, Malaysia

Zolkafle Bin Buntat
Institute of High Voltage & High Current (IVAT)
Universiti Teknologi Malaysia
Johor, Malaysia

***Abstract*— Development of plasma needle that used in biomedical field has become a popular topic in dentistry. Nowadays, mechanical drill and laser techniques are used by dentist to perform treatment process. This two common techniques give some negative effect which is patient feel vibration and pain during treatment process. Thus, developing for plasma needle to avoid negative effect and give comfortable condition during treatment. Besides, there are some previous design of plasma needle that have develop but flexibility of using the model design become difficult and not suitable for dentist. This paper described about the improvement of plasma needle design and also to verify the successfully operation of plasma needle by using new an ergonomic design using 3D printing model.**

Keywords—plasma needle, dentistry, treatment process, an ergonomic design,

I. INTRODUCTION

On earth, solid, liquid and gas are three states of matter that can be easily found. Human are very familiar with these three states of matter as they are facing them every day. In 1879, an English physicist, Sir William Crookes had identified a fourth state of matter where we call it as plasma now. The name plasma was first being applied by Dr. Irving Langmuir, an American chemist and physicist, in 1929.

Plasma comprises of free charge carriers (electrons and ions), active radicals and excited molecules and atoms which is similar to gas. High energy such as thermal, electrical, or light is needed to ionize its atom or molecules and this process will cause the gas to become electrically conductive. This electrically conductive, ionized gas is called plasma. The temperature for plasma electrons normally above 104 K while the temperature for neutrals and ions depend on type of plasma and have the range from room temperature to 107 K.

The current trend is more focus on plasma in bio-medical applications, usage on living tissues and even usage on human body. Non-thermal plasma has the capability of bacterial inactivation [1], non-inflammatory tissue modification [2] and healing effects on a living organism [3][4]. These capabilities led to the development of the plasma needle and many researchers glow their interest at the interaction between non-thermal plasmas and biological tissues.

In bio-medical especially in dentistry, plasma needle is used for deactivation of bacteria in caries or plaque disease. Caries form when bacteria in dental plaque. Mechanical drilling and laser technique is commonly techniques used during dental plaque treatment. This type of technique has several weaknesses where heating and vibration of structure are taking placed. This may cause pain on the patient. In addition, drilling may cause damage and destructive the structure of teeth.

II. LITERATURE REVIEW

A. Plasma

In 1879, Sir Wiliam Crookes was conducting his experiment by using his Crooks tube, he was discovering about the plasma. The real name of plasma was invented by Irving Langmuir when he comparing the ionized gas with blood plasma. Plasma is identified as a state of matter with enough free charged particles for its dynamics to be dominated by electromagnetic forces [5]. Inelastic collisions of highly energetic electrons or protons with neutral atoms and molecules will cause charge of particles was created. These collisions can be on two type of matter which is gaseous or fluid-like mixture that contains ions, free electrons, radicals, (excited) atoms and molecules.

There are common three state matters that all over the world know which are solid, liquid, and gas. The other fourth state matters that actually exist are plasma after giving more heat or energy to the gas. These fourth state matters are different depend on level on their energy level. The process from gas to become plasma is adding more energy to steam that will cause the gas becomes ionized. This ionization will push the gas to become electrically conductive when the breakdown voltage is reached and discharge. This electrically conductive is called plasma. Figure 2.1 shows the fourth state matters change process when heat or energy adding in the state matters.

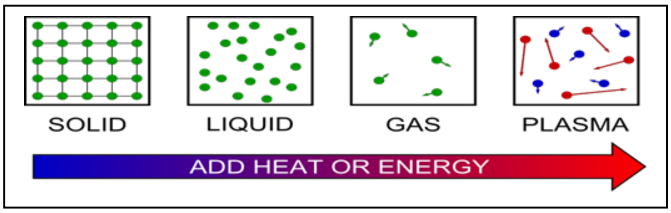

Fig. 2.1: *State of Matters*

Plasma also can be described into two main groups which is temperature (high and low) and atmospheric-pressure glow discharge. Charged particles that accelerated from low temperature plasma will collide with neutral particles, generating new charged particles and hereby causing a cascade of collisions. These phenomenal called low temperature plasma and for high temperature plasma, they are consists all other particles such as electron, ions, and natural particles that are in thermal equilibrium state each other. Besides, atmospheric pressure glow discharge can be obtained by diversity of electrical discharge. There are also has other partition when non-thermal atmospheric-pressure glow discharge which is corona discharge, atmospheric-pressure plasma jet, and dielectric barrier discharge.

B. *Plasma Needle Design*

In year 2002, there are some researches about plasma by Physicist Eva Stoffels and her team at Eindhove University of Technology in Netherland and they had come out with an innovative idea which is the plasma needle. Physicist Eva Stoffels and her team have developed a novel plasma needle which has to operate at atmospheric pressure by using the concept of radio-frequency discharges. It has a single-electrode configuration and operated with the presence of helium gas [6]. This kind of research allow plasma needle to be applied in bio-medical applications. The advantages using plasma needle in bio-medical application are do not cause pain and avoid destruction of the tissue yet allows treatment of uneven surface and has a small penetration depth. Figure 2.2 show the schematic drawing of plasma needle.

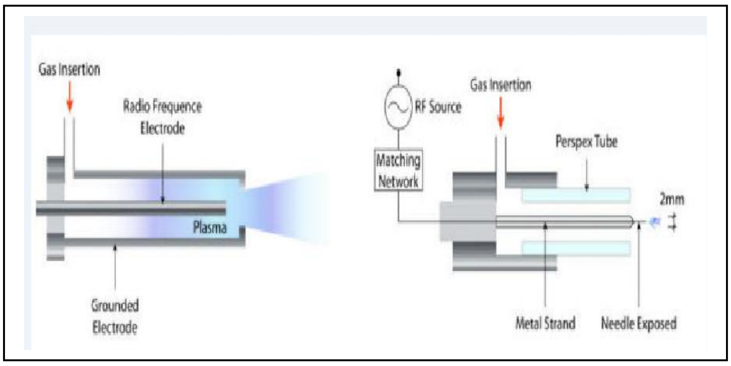

Fig. 2.2: *Schematic Drawing of Plasma Needle*

The cathode is a needle electrode made of tungsten or stainless steel with a 1 mm diameter connected to a RF source (13.56 MHz). The needle electrode lies within a quartz tube whereas the anode electrode is grounded. Depending on the application, helium or argon were mixed with various gases. In the former version, the needle was enclosed in a box and as a result, the samples had to be placed inside of the box to be treated. In the new version, the plasma needle consists of a 0.3 mm metal strand diameter with a sharpened tip inside of a Perspex tube. The length of the entire needle is 8 cm and 1.5 cm remains uncovered by the Perspex tube. The gas used most frequently is Helium due to its high thermal conductivity. The gas is then mixed with air at the needle tip where a micro discharge is created. Gases other than Helium are also used [7]. The diameter of the plasma glow generated is 2 mm. Micro plasma is created when RF power at 13.05 MHz ranging between 10 mW and several watts is applied to the needle. Its small size enables it to be used to treat small areas where accuracy is required like in dentistry [8][9].

C. *Previous design For Plasma Needle*

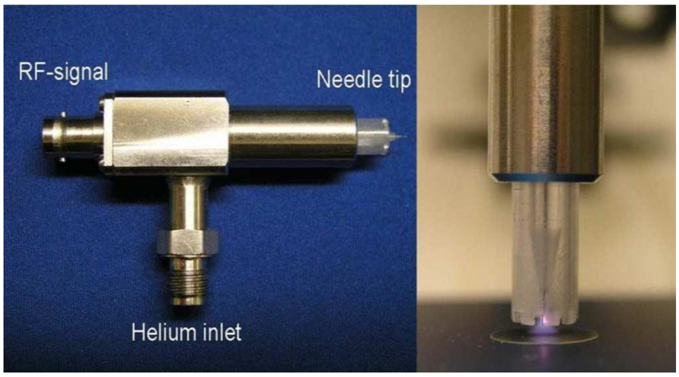

Fig. 2.3: *Practical Design of Plasma Needle*

The portable plasma needle consisting of a tungsten wire in a Perspex tube attached to a source of helium. The plasma needle (Figure 2.3) consists of a metal wire (0.3-mm diameter) with a sharpened tip and is confined in a Perspex tube (4-mm inner diameter). The helium flow is directed through the Perspex tube at a flow rate of 2 L/min, which is controlled by a mass-flow controller (Brooks Instrument, model 5850E). An RF voltage is applied to the tip of the needle at a frequency of

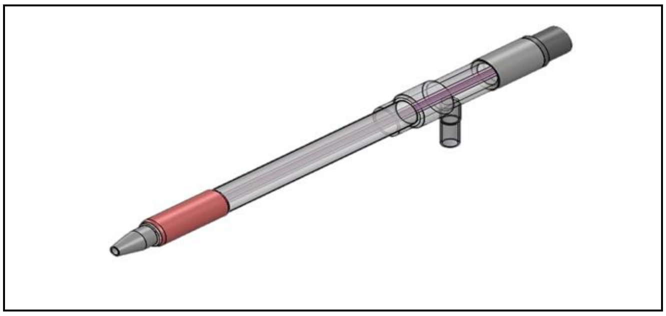

13.05 MHz [10].

Fig. 2.4: *Previous Design of Plasma Needle*

Casing body that has been involved in experiments for the existence of non-thermal plasma needle is a third design based on figure 2.4. There are time constraints, the third design was chosen for fabrication. Design features easy to handle or hold and suitable for pushing into the mouth for dental treatment. The body casing plasma size is almost like a pencil. This design looks simple but still follow the important features in the development of non-thermal plasma source.

This design was made in a real situation for the purpose of experimentation to complete a full production system non-thermal plasma at the end of the tungsten needle. The most important structure in the plasma needle is a tungsten wire and stainless steel to achieve the original goal of generating non-thermal plasma source. At the end of the plasma device, stainless steel attached on its end that acts as a grounding. End of Tungsten wire look like needle shape surrounded by stainless steel without touched each other.

III. RESEARCH METHODOLOGY

For this chapter, method will be explained briefly in order to get overview of the project. Methodology procedure included software used for project, all material used for developing plasma needle, and the circuit development of the project. To finish the design in a simple flow chart, methodology procedure will list out all necessary steps. Besides, this chapter also explains how problem statement was approached and solved based on the scope of project which is to find out the best way in fabrication of plasma needle design and also successful operation of plasma in the fabrication design in order to give the best performance for end-user which is dentist.

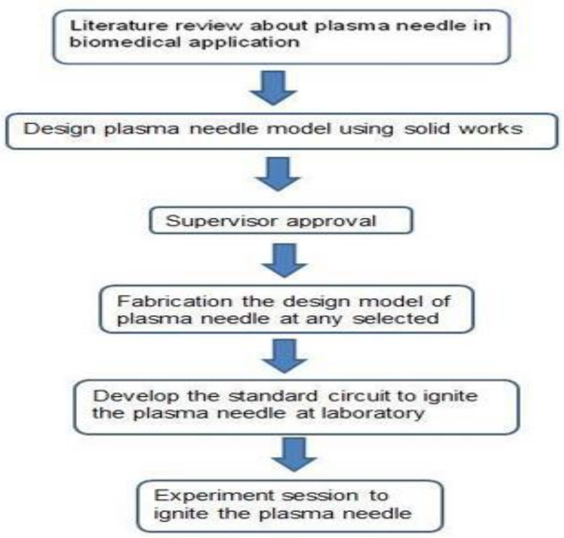

Fig. 3.1: *Flow Chart of research methodology.*

For flow chart of research methodology, it take several steps in order to finish the project. First of all, literature review about plasma needle need to be consider in research because we need to know about previous design, what kind of problem that happened before, and so on. Proceed to next step which is design plasma needle model using solid works. This step need some information about latest design, an ergonomic design for dentistry, and also need to be consider about safety during use the plasma needle model. After discuss with supervisor, we must move to the next step which is fabrication of plasma needle model. The combination of fabrication model with standard circuit of high voltage source will produce a significant plasma needle in the end of experiment. Last but not least, experiment session to ignite the plasma needle must be carried in order to achieve the objective of the project.

A. Software Used

In this project, the software used to complete the project is SolidWorks 2015. SolidWorks is the one of the software that engineer use for drawing and it helps the engineer to create 2D or 3D solid model without any complexity, faster, and in the cost effective way. There are many advantages using this software which is very easy to use, simple graphic user interface, and more friendly compared with other CAD solid modelling software. There are three types of the main function of SolidWorks which is part, assembly, and drawing. All three functions must be selected right before start drawing anything else.

Fig. 3.2: *Software SolidWorks 2015*

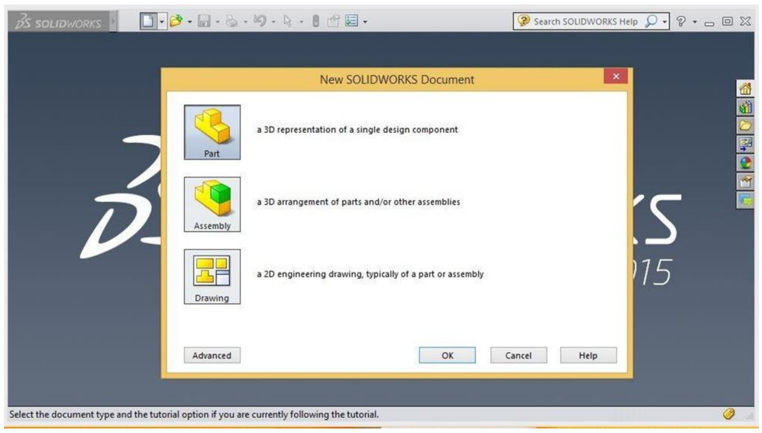

B. Material Used For Development Plasma Needle

Solid Works was selected for being an item for this project to design plasma needle. This software easy to understand and have too many reference video in YouTube. While developed the design, the learning process based on the video in YouTube was continues. Solid work learning process is a very enjoyable experience. In the process of drawing the shape for every part of plasma needle in this software, the measurement for every part of material must emphasize because Solid Work ask any measure of length, width, radius for each form that want painted.

There are several material that use for develop the plasma needle model which is glass, grounding, excitation gases, transmission cable, high voltage source, and electrode. Glass have the purpose to capsulate the tungsten wire so that the RF signal transmission or high voltage pulse transmission is not disturbed by the helium gas during the experiment and discharge processes occur only at the end of the needle. Besides, copper wire function as grounding for the aiming to produce the plasma light. The end of plasma device like nozzle is made up by the copper wire. Discharge phenomena will occur at the space gap between conductor and grounding item. Then, the glass in the plasma needle 3D printing was filled with helium gas. Helium gases delivered to fill the space of glass with flow rate that control by mass flow controller. The mass flow controller device used Brook Instrument, model 5850E. Flow rate of helium was varied to make sure the glow discharge non-thermal source ignite at the tip of the tungsten wire. The helium flow was mixed with small amount of air near the tip. The helium-air mixture is important for the intended application in dentistry because the plasma must be applied in air filled oral cavity. The presence of air guarantees the formation of active radical species that play an important role in sterilization.

IV. RESULTS

The final achievement of this project when the plasma needle have the ability to ignite the plasma glow discharge at the tip of needle. Before the final goal is achieved, the design of plasma needle must be ensured completion of plasma needle casing body fabrication. After that, focus more on laboratory experiments with the help of tools to ensure that non-thermal plasma-derived or form. Successful non-thermal plasma is generated even sporadic presence there. The larger signal is required to ensure that the resulting plasma was more consistent.

A. Fabrication Design of Plasma Needle

Most important part is ensure the completion of plasma needle casing body fabrication. This is because casing body that have created will be used for industrial and fabrication also show flexibility, ergonomic, and ability of functional the product itself. Figure 4.1 show the final design of plasma needle casing body in 3D solid works. Design features easy to handle or hold and suitable for pushing into the mouth for dental treatment. All material that will use in develop plasma needle such as glass, copper rod as electrode, copper wire as grounding, and helium gas can be found inside the fabrication design. This design looks simple but still follow the important features in the development of non-thermal plasma source.

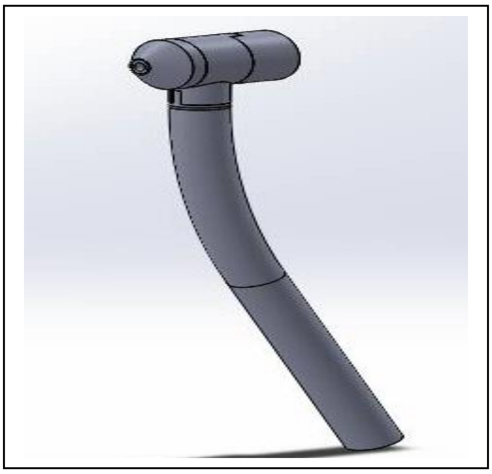

Fig. 4.1: *Design of Plasma Needle in SolidWorks*

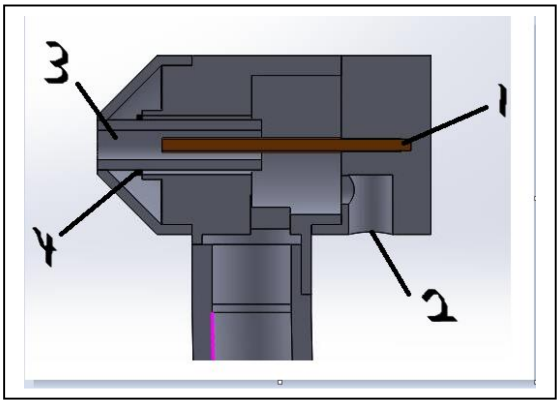

Fig. 4.2: *Inside Design of Plasma Needle.*

Development of plasma needle need to be consider the inside of the design because plasma needle will not produce if connection inside not channeling. Figure 4.2 show the inside of

fabrication design plasma needle. The following is the composition of the material involved 1) copper rod as electrode, 2) channel of helium gas flow, 3) glass, 4) copper wire as grounding.

Fig. 4.3: *Fabrication Design of Plasma Needle.*

Figure 4.3 show the real design of plasma needle in 3D printing design. The shape and size of design is suitable for entering mouth. The rate of helium gas supply is about 1liter/minute and use the high voltage supply to produce plasma emission. There are two wire inside the casing body which is red wire and black wire. Red wire represent high voltage transmission cable and black wire is the grounding transmission cable.

B. *Experimental to Ignite Plasma Needle*

Preparation equipment for experimental purposes are running smoothly. High voltage supply source will be connected to a red wire for the purpose of ensuring the maximum power transfer. While the red wire high voltage will be connected directly to the electrode in the plasma needle device casing body. In the plasma device is the space for the flow of helium gas. Helium gas will react chemically among space or gap. This area has been identified as a discharge area between the copper wire as grounding and copper rod as electrode. Figure 4.4 and 4.5 shows the plasma ignite at the end of glass with purple color appear.

Fig. 4.4: *Ignite of Plasma Needle.*

Fig. 4.5: *Ignite of Plasma Needle..*

V. CONCLUSION

In conclusion, the complete of fabrication model design of plasma needle was successfully developed because the design can entering the mouth area and suitable size for holding in dentistry application. Radio frequency or high voltage pulse generator are used to provide suitable waveform for the operation of plasma needle. This high voltage pulse source will make combination with helium gas during discharge process. Discharge process will occur at the end of plasma device between copper wire as grounding and copper rod as high voltage electrode. The presence of plasma gas that helps the appearance of such ultra violet light which is produce purple color in the end of the glass. Experiment to get the non-thermal plasma at the end of the needle has been carried out repeatedly. However, experiment can be carried out in the future with equipment capable of producing signal with a higher voltage and power. The common technique use in dental care especially in Malaysia can be improve by plasma needle project for biomedical field in the future.

REFERENCES

[1] M K Boudam, M. M., B Saoudi, C Popovici, N Gherardi and F Massines (2006). Bacterial Spore Inactivation by Atmospheric-Pressure Plasma In The Presence or Absence of UV Photons as Obtained with the Same Gas Mixture.

[2] Kieft, I. E., M. Kurdi, et al. (2006). Reattachment and Apoptosis After Plasma-Needle Treatment of Cultured Cells. Plasma Science, IEEE Transactions on 34(4): 1331-1336.

[3] Roxana Silvia Tipa, G. M. W. K. (2011). Plasma-Stimulated Wound Healing. IEEE Transactions On Plasma Science 39(11): 2978-2979.

[4] Laroussi, M. (2009). Low-Temperature Plasmas for Medicine? Plasma Science, IEEE Transactions on 37(6): 714-725.

[5] B.R.Rampadarath (2006). Design for 3DPlasma Needle Manipulation, DCT2006.050.

[6] E Stoffels, A. J. F., W W Stoffels and G M W Kroesen (2002). Plasma needle: a non- destructive atmospheric plasma source for fine surface treatment of (bio)materials. Plasma Sources Science And Technology 11: 383-388

[7] Li S-Z, Huang W-T, Zhang J, Wang D: Optical diagnosis of an argon/oxygen needle plasma generated at atmospheric pressure. Appl Phys Lett2009, 94:111501.

[8] Jiang C, Gundersen MA, Schaudinn C, Webster P, Jaramillo DE, SedghizadehPP, Costerton JW: An atmospheric pressure non-thermal

plasma needlefor endodontic biofilm disinfection. IEEE Int Confer Plasma Sci - ICOPS2011:1–1. doi:10.1109/PLASMA.2011.5993048.

[9] Sladek REJ, Baede TA, Stoffels E: Plasma-needle treatment of substrateswith respect to wettability and growth of Escherichia coli andStreptococcus mutans. IEEE T Plasma Sci 2006, 34:1325–1330.

[10] Raymond E. J. Sladek, Tom A. Baede, and Eva Stoffels (2006). Plasma-Needle Treatment of Substrates With Respect to Wettability and Growth of Escherichia coli and Streptococcus mutans. EEE TRANSACTIONS ON PLASMA SCIENCE, VOL. 34, NO. 4, AUGUST 2006.

Aquaculture Monitoring System using Internet of Things (IoT)

Muhamad Hazim Bin Ahmad Daud
Faculty of Electrical Engineering
Universiti Teknologi Malaysia
Johor Bahru, Malaysia.
hazimd94@gmail.com

Tan Chee Wei
Department of Electrical Power Engineering
Faculty of Electrical Engineering
Universiti Teknologi Malaysia
Johor Bahru, Malaysia.
cheewei@utm.my

***Abstract*— The project is designed to monitor water quality of aquaculture in aquarium tank by using the concept of Internet of Things (IoT) in the system. The project will include graphical interface for the monitoring by using smartphones. The platform involved in the monitoring is Blynk application provided that it is connected to the Internet. The project will also include fish feeding system that can be control by the user with smartphone. The purpose of this project is to be implemented to fish farm monitoring. The project is divided in two part with the first part involve monitoring system for water and the second part involve in fish feeding system. This project will compose of Arduino UNO as the controller, water sensing module (ultrasonic sensor, temperature sensor and potentiometer), and fish feeding system which consist of servo motor. The wireless sensor network use in this project is ESP8266 that will connect the system with Internet. The system will operate and give alert to the user if any of the parameter fall below optimum. The system should be easy to install, easy to maintain and able to adapt to variety of situation.**

Keywords*— IoT; Blynk; ESP8266; wireless transmission; feeding system

I. Introduction

Aquaculture development in Malaysia is undergoing rapid growth. The earliest beginning of aquaculture was not popular and small in size, but sizeable farms only began in 1950s. In 1992, total production was amounted to 79, 699 tons valued at RM 207.4 million [1]. The production was 23% higher than the previous year.

Like agriculture, aquaculture involves controlled culture and individual who own the crop. There is a different between fisheries and aquaculture but are involved in aquaculture. While fisheries involve hunting and general public accesses the crops, aquaculture involve in enhance fisheries by providing fish to restock streams, lakes and oceans [2].

Aquaculture is a relatively new word used to describe the business of producing aquatic animals and plants that are useful to humans. It is also categorized as a type of agriculture activity but the farming occurs at water instead of land [2]. For the past few years, aquaculture have undergoing considerable growth globally and it is possible because of many factors involved [1]. One of the factors is in the field of aquaculture engineering. It involves in the development and improvements of technology that allow reduced water consumption and development in re-use system [1].

Aquaculture engineering involves a very large area of knowledge and many engineering skills such as environmental engineering, mechanical engineering, monitoring, etc. Its primary aim is to implement and utilize technical engineering knowledge and principles in aquaculture [1]. With this, the production and economy will increase since the technology used can boost the production.

II. Literature Review

In recent years, aquaculture industry has become one of the most important industry for sources of protein, aquatic plant and can also generate income. It has the advantages of high yield, better quality, uses less water, various water or environmental parameters. These advantages can effectively detect and control in aquaculture and hence the develop the best environment for the growth and survival of the fish [3]. In traditional aquaculture, the farmer does not have reliable tools or system to monitor environmental parameters and this lead to lower yield and slower growth and survival of the fish. Moreover, domestic aquaculture uses data combined with farming experience for feeding decision but it is still a problem to minimize the cost to achieve best feeding [3]. This always lead to unnecessary wasted feed for fish.

As technology advance, the demand on food hygiene and quality have increase. For example, in consumer demand for aqua-farm product. By using Internet of Things concept, the sensors to monitor the aqua-farm is employed. With this technology, it will allow personnel to keep tabs on the facilities at anytime and anywhere [4]. Internet of Things (IoT) has manifest as a global Internet-based information architecture where it facilitates the exchange of goods and services [16].

Generally, it refers to the object that is connected and networked where it is often found in ubiquitous intelligence object [22]. The number of connected devices has increased in the recent years and is expected to exponentially grow as the number of people purchased the devices also increase [15]. Internet have become most powerful and important in our daily lives since the impact is already on education, business, communication, science, government and humanity. Many things can be achieved with the use of Internet [12]. Hence, machine to machine (M2M) communication is also possible and widely used through the Internet. It means, with minimal intervention from human, the machine can deliver the services that meet the needs of industry [15].

Aquatic organisms' survival and growth are critically dependent on water quality. Drastic changes in water quality such as temperature, oxygen and water level may affect the fish. Therefore, to achieve high economic and production efficiency, many sensors are necessary to monitor the status of the farm. Moreover, constant remote wireless water quality monitoring is important in ensuring the fish health and growth [5]. Water quality such as oxygen and temperature is not suitable for short-term since pathogen infection spread rapidly through water. Hence, by using a number of sensors to monitor status of fish farm environment, the efficiency can be increase [6].

III. METHODOLOGY

The hardware design is needed so that the programming of controller can be done. The design must follow the programming of the controller. In this project, the hardware part is divided into two which is for monitoring quality of water and for feeding system. The system uses Arduino MEGA as the processing of each sensing module, Wireless network module using ESP 8266 as a communication network.

A. Arduino Mega

Arduino Mega is a microcontroller board based on the ATMega2560. It has 64 digital input/output pins, a 16MHz crystal oscillator, a USB connection, a power jack, ICSP header and a reset button. It contains everything needed to support the microcontroller and is compatible with most shields and module. For this project, Arduino Mega is used because it is easy to shield it with wireless module ESP8266.

Fig. 1. Arduino Mega2560

B. Water Level Sensing Module

Water level is important so that the fish have enough supply of oxygen and increase the production. In this project, ultrasonic sensor HC-SR04 is used to monitor the level of water. It works by taking difference in distance by referring to a set point. The pulse is transmitted until an echo return after impacting object. The module will send out 8-cycle burst of ultrasound and raise its echo when supply a short 10µs. The range can be calculated through the time interval between transmission trigger signal and receiving echo signal [7].

Fig. 2. Ultrasonic Sensor, HC-SR04

C. Temperature Sensing Module

To monitor the temperature, DS18B20 temperature sensor is used since it is waterproof. The DS18B20 provides 9 to 12-bits temperature reading which indicate the temperature of the device. Its information is sent over 1-wire interface which means only one wire (and ground) needed to be connected to the controller.

Fig. 3. Temperature Sensor, DS18B20

D. Dissolved Oxygen Sensing Module

For this project, the oxygen level will be represented by resistance by using potentiometer as sensing module that act as a dissolved oxygen of water. The higher resistance shows high concentration of dissolved oxygen while low resistance shows low concentration of dissolved oxygen.

Fig. 4. Potentiometer

E. Fish Feeding

For this project, automatic fish feeder will be used and triggered by using IoT. The part consists of RC Micro Servo Motor. Servo are controlled by sending them a pulse with variable width. To send this pulse, signal wire is used and these pulse has minimum pulse, maximum pulse, and repetition rate. Given the rotation constraint of the servo, neutral position where the servo is the position where the servo has exactly the same amount of potential rotation in the clockwise direction as it does in the counterclockwise direction. Also, different servo will have different constraint in their rotation.

Fig. 5. RC Servo Motor

F. *Wireless Network Module*

The wireless communication network used for the system is ESP8266. The ESP8266 is a Wi-Fi module that is low cost compared with ESP32 with many functionalities. It used to add functionality of Wi-Fi to an existing controller via UART serial connection. The module can even be programmed to act as standalone Wi-Fi connected device. It also able to boot up directly from external flash when host the application and when it is the only application processor in the device.

Fig. 6. Wi-Fi Module, ESP8266

IV. Result And Discussion

Aquaculture monitoring system which consist of hardware and application was built. Figure 7 shows the final completion for the controller shielded with ESP8266 that have connectivity to Internet. The system was tested to see whether the parameter measured correctly with little error. The interface for the Blynk consists of water level, temperature and dissolved oxygen gauge to monitor water quality and a slider to control servo motor.

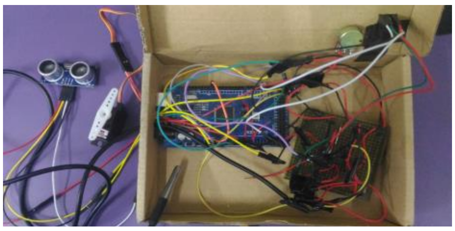

Fig. 7. Controller shielded with ESP826

The limitation of this project is that the notification takes quite some time to receive because of overloaded information with sensors parameter and notification setting. Another limitation is with Blynk connectivity where it is possible to disconnected automatically while monitoring. The coding is required to automatic reset if the Blynk disconnected. However, there is limitation of how long it can reset continuously.

A. *Water Level Monitoring*

Figure 8 shows the gauge for monitoring water level. The range is set from 0 to 1023 default. The controller will send the value of the distance detected by ultrasonic sensor to Blynk to display the water level.

Fig. 8. Gauge for Water Level

Ultrasonic sensor distance is calculated based on the duration of which pulse travelled. Equation (1) is used to determine the distanced travelled for the pulse. The time is the time when the echo pulse is high. Testing with ultrasonic sensor was done by comparing manual measurement with sensor measurement.

$$Distance = time/58 \tag{1}$$

Testing with ultrasonic sensor was done by comparing manual measurement with sensor measurement.

TABLE I. Testing On Ultrasonic Sensor

No of Reading	Type of Measurement	
	Manual measurement (cm)	***Sensor Measurement (cm)***
1	3.0	3.2
2	4.0	4.1
3	5.0	5.3
4	6.0	6.2
5	7.0	7.0
6	8.0	8.1
7	9.0	9.2
8	10.0	10.4

B. *Dissolved Oxygen Monitoring*

The potentiometer is used in this project to represent dissolved oxygen parameter because dissolved oxygen level in the market is too expensive. Figure 9 shows the gauge for dissolved oxygen monitoring where the unit used is in mg/L.

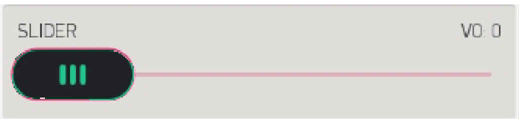

Fig. 9. Gauge for Dissolved Oxygen

C. *Temperature Monitoring*

Figure 10 shows the gauge for monitoring temperature. The range is set from 0 to 1023 default. The controller will send the value of the temperature detected by DS1820 temperature sensor to Blynk to display the temperature.

Fig. 10. Gauge for Temperature

D. *Fish Feeding*

Figure 11 shows the slider function to control the rotation of the servo motor. The range of rotation is set from 0 to 180 degree. Servo motor encounter a problem with inconsistency in the rotation because of the delay in Serial communication between Arduino and ESP8266. After connected to the controller, it rotates inconsistently for a brief of time.

Fig. 11. Slider for Servo Motor

V. Conclusion

The topic for this project is aquaculture based environmental monitoring system. the purpose of this study is to monitor the parameter involved in fish farm industry to grasp on what happen on the parameter of water. Arduino Mega and ESP8266 are used as the shield for building a wireless sensor network. The shield can connect with the Internet and can be used with Android mobile devices to increase overall system convenience.

This monitoring system using is only the most preliminary function. In the future, this study hopes to analyze more parameter, include load control and include more effective feed system for the fish farm industry to adjust the most suitable environment for the growth of farmed fish industry.

References

[1] Kechik I. A. (1995). Aquaculture in Malaysia. In T.U. Bagarinao & E. E. C. Flores, Towards Sustainable Aquaculture Development in Southeast Asia and Japan: Proceedings of Seminar-Workshop on Aquaculture Development in Southeast Asia, Iloilo City, Philippines, 26-28 July, 1994 (pp. 125-135). Tigbauan, Iloilo, Philippines: SEAFDEC Aquaculture Department.

[2] Rick Parker. Aquaculture Science. 2nd ed. Delmar: Thomson Learning, 2002.

[3] Zhao J. Research on Wireless Sensor Network in Aquaculture. (2014). http://www.scientific.net/AMM.686.397.pdf (Accessed 2016-10-6).

[4] Min Yang, Fang Tsou. Aquaculture Cloud Management System. Journal of Information Technology and Applications. doi: 10.7251/JIT1402075Y.

[5] Tsai Sung, Ho Chen, Chiun Huang, Hao Ju. Multisensors Realtime Data Fusion Optimization for IOT Systems. 2014 IEEE International Conference on Systems, Man, and Cybernetics.

[6] J. H. Chen, W. T. Sung and G. Y. Lin, "Automated Monitoring System for the Fish Farm Aquaculture Environment," 2015 IEEE International Conference on Systems, Man, and Cybernetics, Kowloon, 2015, pp. 1161-1166. doi: 10.1109/SMC.2015.208

[7] Marzuki Liyana. (2015). Ultrasonic System for Measuring Water Level. Degree's Thesis Universiti Teknologi Malaysia. Skudai: Faculty of Electrical Engineering.

[8] Aquaculture Fisheries Division. Fish Feed Management. Agriculture, Fisheries and Conservation Department. (2009). http://www.hkaffs.org/en/images/GAP1.pdf (Accessed 2016-10-6).

[9] N. E. Cater, "Smart ocean Sensors Web Enabled ocean sensors for aquaculture," OCEANS 2008, Quebec City, QC, 2008, pp. 1-9. doi: 10.1109/OCEANS.2008.5151870

[10] Satya Nagabhushana Rao Kamisetti and Arvind Dattatreye Shaligram, "Smart electronic system for pond management in fresh water aquaculture," 2012 IEEE Symposium on Industrial Electronics and Applications, Bandung, 2012, pp. 173-175. doi: 10.1109/ISIEA.2012.6496623

[11] Lekang, Odd Ivar. Aquaculture Engineering. 2nd ed. Wiley-Blackwell, 2013.

[12] Miazi Nazmus, Erasmus, Md Razzaque. Enabling the Internet of Things in Developing Country: Opportunities and Challenges. 2016 5th International Conference on Informatics, Electronics and Vision (ICIEV): 564-569. doi: 10.1109/ICIEV.2016.7760066.

[13] Prasad, Mamun, Islam, Haqva. Smart Water Quality Monitoring System. 2015 2nd Asia-Pacific World Congress on Computer Science and Engineering. (2015): 1-6. doi: 10.1109/APWCCSE.2015.7476234

[14] Roca, Nemirovsky, Rodolfo, Valero. Emergent Behaviours in the Internet of Things: The Ultimate Ultra-Large-Scale System. IEEE Micro. (2016): 36-44. doi: 10.1109/MM.2016.102.

[15] Rocus, Anthony. Internet of Things. New Jersey City, NJ: Clanrye International. 2015.

[16] Rolf H. Weber. Internet of Things. Springer, 2010.

[17] A. B. Kevin, "Power System Security," [Online]. Available: http://www.citeseer.ist.psu.edu/387125.html, [Accessed January 9, 2005]

Analysis of Air Termination System Using Rolling Sphere Method and Angle Protection Method at Building P19a, UTM

Muhammad Zul Naqib Bin Roslan, Dr. Noor Azlinda Binti Ahmad
Faculty of Electrical Engineering
Universiti Teknologi Malaysia
Johor Malaysia

***Abstract*—Lightning is one of the dangerous natural phenomena occur in this planet. Lightning also can be major damage toward a building, equipment and system which can be threat to human. To minimize the damage, lightning protection system was introduced. There are several method to design the lightning protection system but in this case study, rolling sphere method and angle protection method will be chosen to analyse with the aid of simulation. The design consists of selection of the level of protection, the number of the air termination rod to be installed on top of the selected buildings, height of air termination rod and method use for design. This case study are carry out at P 19A building, University of Technology Malaysia (UTM). Most of the simulation are using Autocad software. The result of angle protection method and rolling sphere method will be compare and discuss.**

Keywords*—Angle protection system, Lightning protection system, Rolling sphere method.

I. Introduction

Lightning is one of the natural phenomena that can cause heavy loss of human life. Is also one of the major sources of power interruption, communication and cause major damage to the building. Until now, lightning still cannot be predicted even our scientist. Malaysia is known as Asia Lightning capital. In terms of lightning density, Kuala Lumpur is ranked 5th in the world. Kuala Lumpur has 48.3 lightning strikes hit the ground for every square kilometre of real state, according to National Lightning Safety Institute of United State [1].

Since the electricity that contain in the lightning strike cannot be eliminated, the best way to prevent it from the lightning protection system.The lightning protection system is designed to protect an object, a building, or a system being struck by lightning and cause damage. There are several way to design the lightning protection system. Angle protection method and rolling sphere method are commonly use to design lightning protection system.

In UTM, most of the buildings are installed with lightning protection system including at building P19a, however fault still happen to the electric and electronic devices inside the building when lightning strikes.

In this case study, angle protection method and rolling sphere method had been analyse to determine the efficiency and the reliability of both method. Both method is applied and simulation with computer software were used in order to determine the unprotected area at P 19A building and from that, suitable lightning protection system design is proposed which consist of the number of air termination rod needed and the best position of rods to be placed.

The objective of this case study is study and understand the concept of both method, to analyse the efficiency of both method and propose a profound solution to improve the reliability of both method.

II. Literature Review

A. Lightning Protection System

lightning protection system can be defined as a complete system that can reduce or minimize physical damage on the structure, system and object due to lightning strike. Basically, it's made up by rod and conductor to protect structures against direct strike and damage [7]. The first protection system had been design by providing a small iron rod with such a length that one end being three or four feet in the moist ground, the other may be six or eight feet above the highest part of the building.

The complete lightning protection system consists of air termination, down conductor which is vertical wire to ground terminal which is buried grounding electrode. Beside protecting outer structure, electrical wiring and electronic equipment within the structure such as air conditioners and computer, should be protected from the voltage induce in those electric and electronic systems by lightning current flowing in the lightning protection system and electromagnetic effect by using surge suppression device [8].

Beside that, there are four lightning protection level. Each of them corresponds to a different value of lightning parameter. The important parameter for lightning protection are the magnitude of lightning energy. The priority or need for the structure to be protected will also affect the selection of lightning protection level. The maximum tolerable risk must always more than the risk of damage on the structure due to direct lightning strike. The annual frequency of direct lightning strike to the structure will be used to estimate the risk of damaged for the structure.

Lastly, there are several method to design the air termination rod position such as angle protection method, rolling sphere method, mesh method and electro-geometrical method.

B. Angle Protection Method

In empirical method, there is assumption being applied which is the air terminal can intercept all the lightning strike from make direct contact with protected structure if the air terminal can maintain a certain geometrical relation by means of separation distance and different in term of height to the protected structure[9].

The simplest method to apply those assumption is using angle protection method where the angle, α is describes as an inclined line that protect all objects below it.

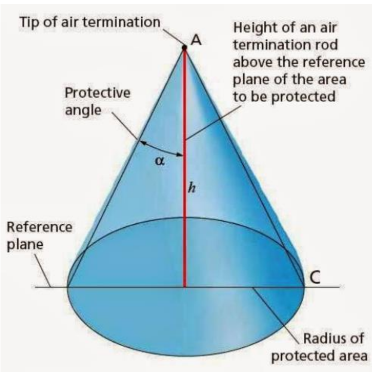

Figure 2: Angle protection method for vertical rod.

For vertical rod, the protection area of the air terminal is assumed as a conical surface and all objects covered by this surface are assumed to be protected against a direct lightning strike. But, note that empty space never be protected since lightning strike only hit objects or structures.

C. Rolling Sphere Method.

Rolling sphere method is the method that use to predict the probability of lightning strike position on the building whether it is a flat surface, a sharp point or an edge of corner of structure. Lightning travel to the ground as a step leader. The concept of this method is directly related to the electro-geometrical model, based on the assumption, which is a step leadder has to approach to a critical distance before it can attracted to the structure. In other word, this concept assume that there is a spherical region with radius equal to the striking distance and allocated around the tip of the step ledder. The grounded structure that enter into this spherical volume will be point of the attachment od the step leader [3].

This method also use to determine the positioning of air termination rod. There are four class to determine the radius of the imaginary sphere that use in the rolling sphere method. Each of the classes has different minimum interception current.

Table 3: Relationship between minimum interception current with striking distance[10].

Protection level	Sphere radius (m)	Minimum interception current (kV)
I	20	2.9
II	30	5.4
III	45	10.1
IV	60	15.7

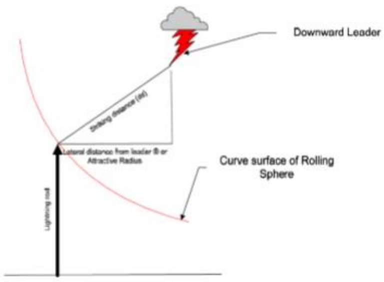

Figure 3: the relationship rolling sphere and the striking distance [11].

To identified the position of the air termination by using this method, the imaginary sphere will be roll on the structure, building or object. When the imaginary sphere touch some point of the structure, the point will be known as unprotected area. The air termination shall be placed at unprotected are since the are had expose to the lightning stroke. By placing air termination rod to the unprotected area, the lightning damage at that will be reduce.

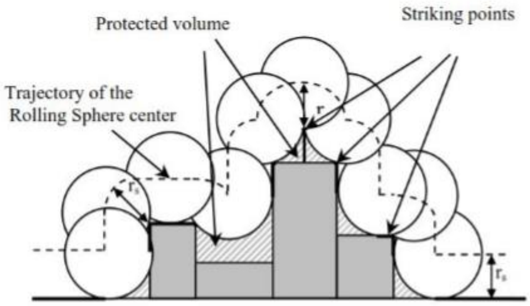

Figure 4: Illustrate of rolling sphere [11].

Furthermore, the lightning will strike the first object that touched by the rolling sphere method since the radius of the sphere is assume equal to the striking distance of the lightning. For the structure below than 60m, the side of the structure can be negligible [3].

D. Air Termination Rod.

Lightning can cause major damage to a building, equipment and other. One of the ways to reduce lightning strike a building is by install air termination rod, which are it will conduct lightning to the ground. Usually, air termination are made up by metallic material such as aluminium and copper.

There are several types of air termination rod such as a sharp pointed tip, blunt tip and standard tip. Sharp tipped Franklin rod is widely used all over the world. Researcher found that moderately blunt metal rod are better lightning strike receptor compared to the sharper rod and very blunt one [15].

Researcher also a stated that if there are two air termination rod with different height, the taller one will be more likely to attach by a lightning strike than the shorter one. But, if the air termination rod is extremely high, the lightning protection system will be inaccurate. For the sharpness, the moderate blunt metal rod is about 19mm [12].

Figure 6: Air termination rod.[11]

III. Methodology

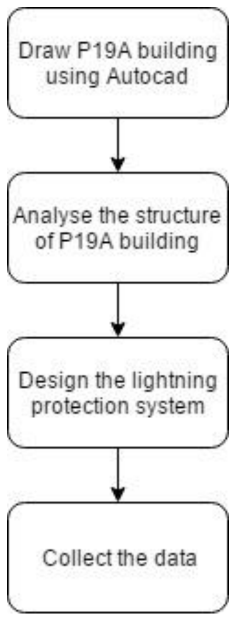

Figure 7: Flowchart for this case study

A. Angle protection method steps.

Figure () show the process from start to end of the process. Firstly, sketched the building by using Autocad. The drawing are base on the layout gave by Pejabat Harta Bina (PHB). Then, the drawing has been analyse to find hot spot or the area that lightning more attract to strike. Based on the building, there are three hot spot which is all the corner or edge of building since the building shape are triangle. Then, the area that unprotected are calculated. The total unprotected area is 3247.807 m^2.

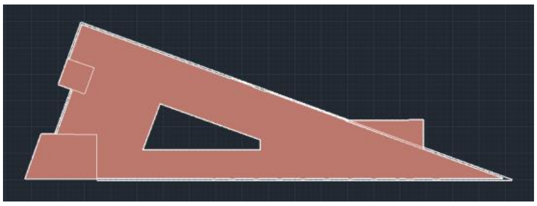

Figure 8: Top view of P 19a building.

After that, air termination rod are been placed based on the hot spot area. First, it only use three air termination rod. After that, it used 5 air termination rod. At air termination rod will be imaginary cone. One imaginary cone for one air termination. The imaginary will show the area that protected. The size are based on the graph.

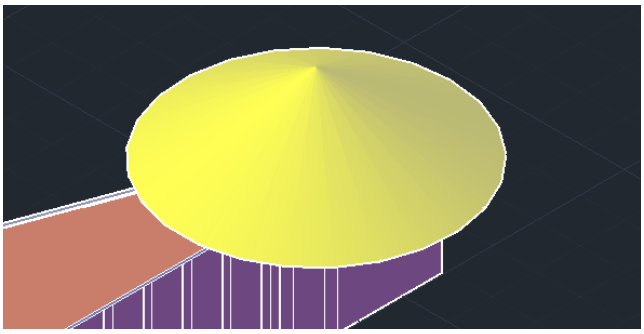

Figure 9: A imaginary cone for one air termination.

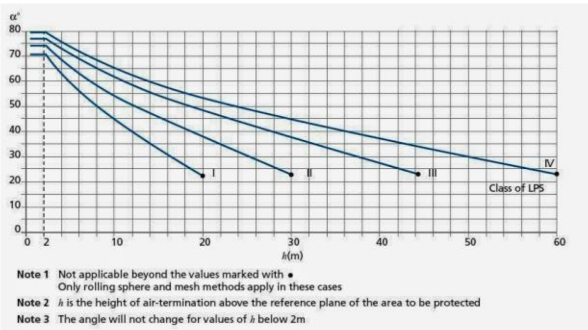

Figure 10: Angle of the cone against height of the air termination rod.

After the air termination been placed, the area that protected has calculated. The percentage of the protected area are calculated. The data are recorded.

$$\text{Protected area (\%)} = [\text{ Protected area } (m^2) / \text{ total of area } (m^2)](100)$$

B. Rolling Sphere Method Steps.

For rolling sphere method, it almost same with angle protection method step but it need to find unprotected area before the air termination are placed. To find the unprotected area, the imaginary sphere need to be roll against the surface of P19A building. This process occur when the drawing of P19a are completed. The imaginary sphere has different radius for different level.

Table 2: Relationship between minimum interception current with striking distance[10].

Protection Level	Sphere radius (m)	Interception current (kA)
1	20	2.9
2	30	5.4
3	45	10.1
4	60	15.7

After the unprotected a founded, air termination are placed. The first number of air termination are placed are 3. Then, the imaginary sphere will be roll again to find the new unprotected area.

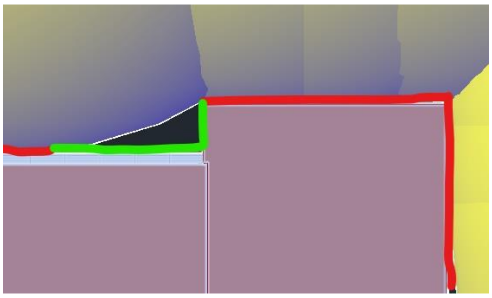

Figure 11: Rolling sphere method process to find unprotected area. Unprotected area(Red), protected area (Green).

The protected area are calculated. The data are recorded. After all process of rolling sphere method by using 3 air termination completed, the rolling sphere method process are repeated by using 5 air termination. The data are recorded.

IV. RESULT AND DISCUSSION

For this analysis, there are consists of selection of the level of protection, the number of the air termination rod to be installed on top of the selected buildings, height of air termination rod and method use for design. There are two method use to design the position of air termination.

A. *Selection of the level of protection.*

Level of protection for lightning protection system indicate the effectiveness of air termination rod or total amount current for air termination rod that can be intercept where the lower the current of the lightning, the shorter distant for current can travel from one point.

Figure 12 and figure 13 show analysis result using angle protection method. Blue line are 14 meter, orange line are 16 meter and green line are 18 meter. Based of the graph, it show by increasing the level of protection, α, the area protected are increasing. This is because of when the level of protection increase, the angle for imaginary cone will increase base on the graph of level of protection, α.

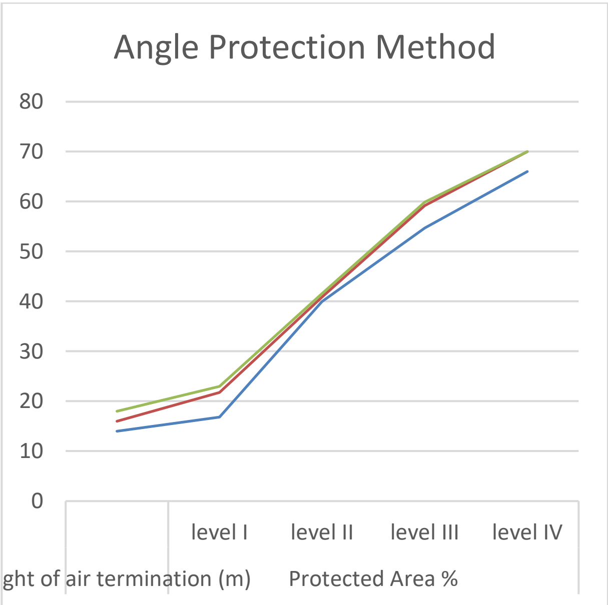

Figure 12: Graph for result analysis using 3 air termination rods.

Figure 14 and figure 15 show the graph result using rolling sphere method. Green line are 14 meter, orange line are 16 meter and blue line are 18 meter. Based on both graph, it show by increasing the level of protection, the protected area are increasing. This is because of when the level of protection increase, the radius of imaginary sphere also increase. Rolling sphere method has larger protected area than angle protection method.

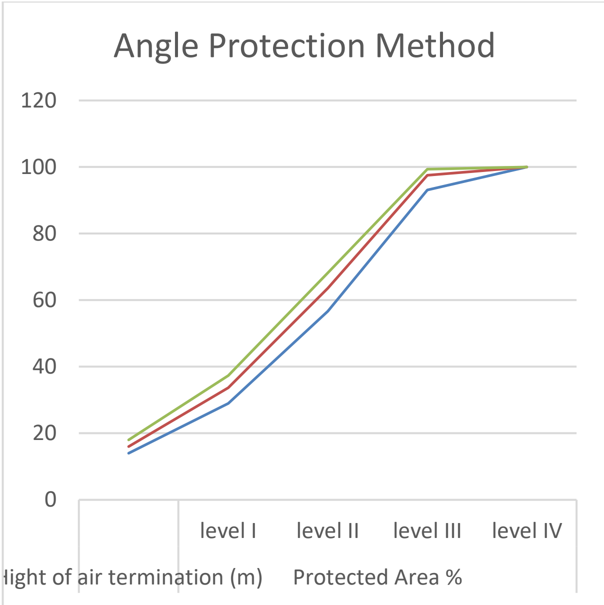

Figure 13: Graph for result analysis using 5 air termination rods.

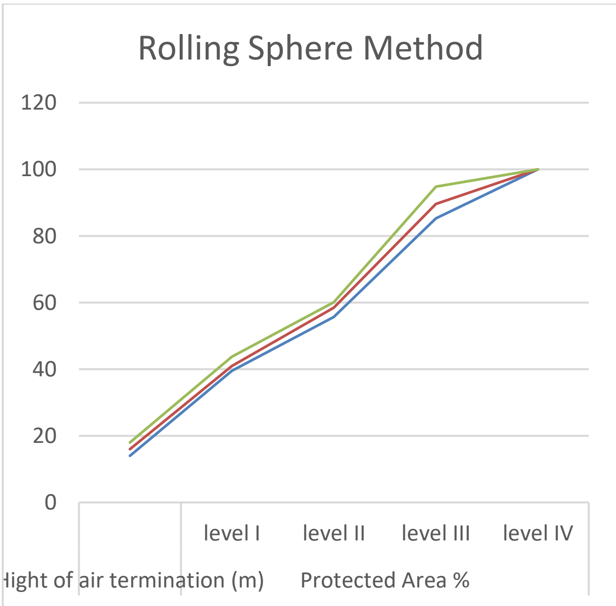

Figure 14: Graph for result analysis using 3 air termination rods

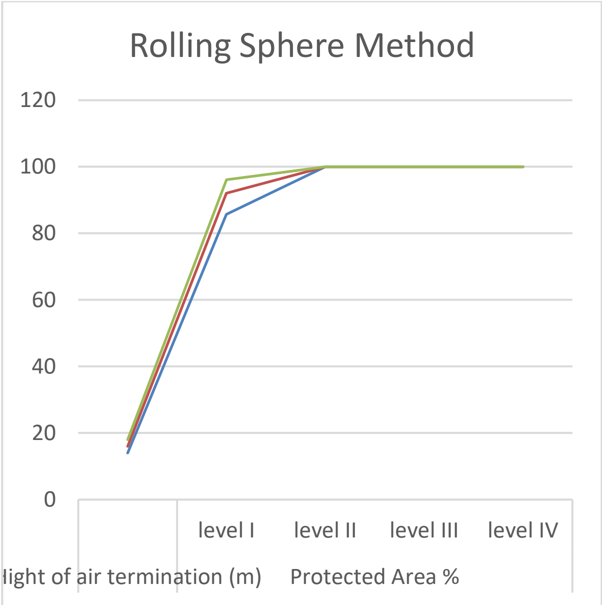

Figure 15: Graph for result analysis using 5 air termination rods

B. Number of air termination.

In this case study, there are different number of air termination rod. The first analysis are using 3 number of air termination rod and the second analysis are using 5 number of air termination rod. For both method, the are increasing in term of protected area when the number of air termination rod increasing from 3 to 5 number of air termination rods.

Air termination rod protect an area or object from lightning strike and cause harm. Based on figure (),(),() and (), rolling sphere method has increase steeply than angle protection method.

C. Height of air termination rod.

Height of air termination is one of the most important variable to increase the protected area. In this case study, height of air termination rod use is 14 meter, 16 meter, and 18 meter. The use of this height is because of to reduce the number of air termination use. If it use 3 meter of air termination rod, the number of air termination ill be increase in order to protect the whole unprotected area of P 19 A building.

Figure 16 and figure 17 show graph of analysis angle protection method using 3 and 5 air termination rods. Based on the both graph, it show that when height of air termination rods increasing, the efficiency for air termination intercept lightning are increasing while protected area increasing. This is because when height of air termination increasing, angle of protection ,α, are increasing.

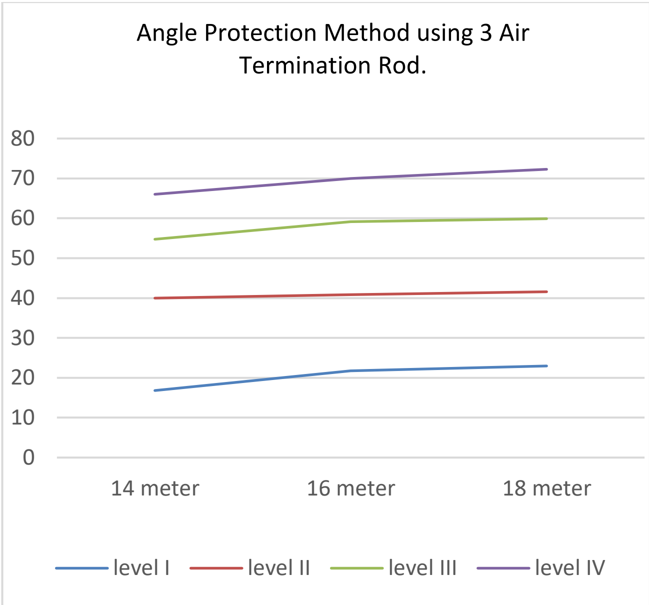

Figure 16: Graph for analysis the height of air termination rods.

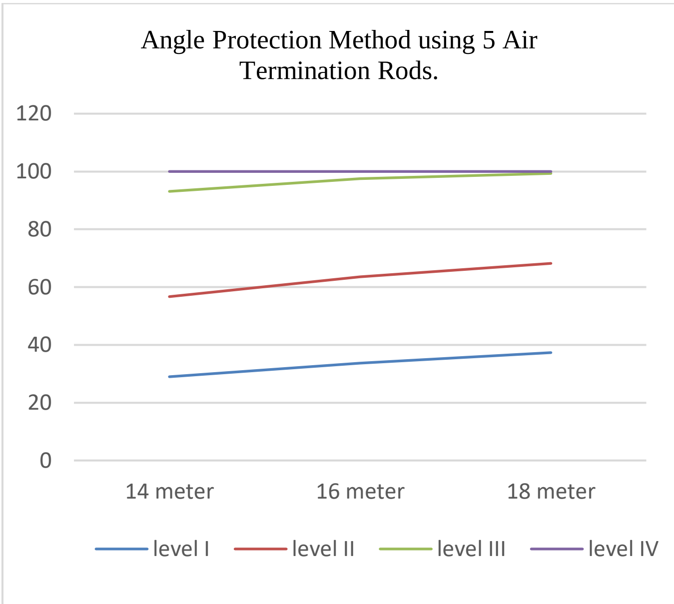

Figure 17: Graph for analysis the height of air termination rods.

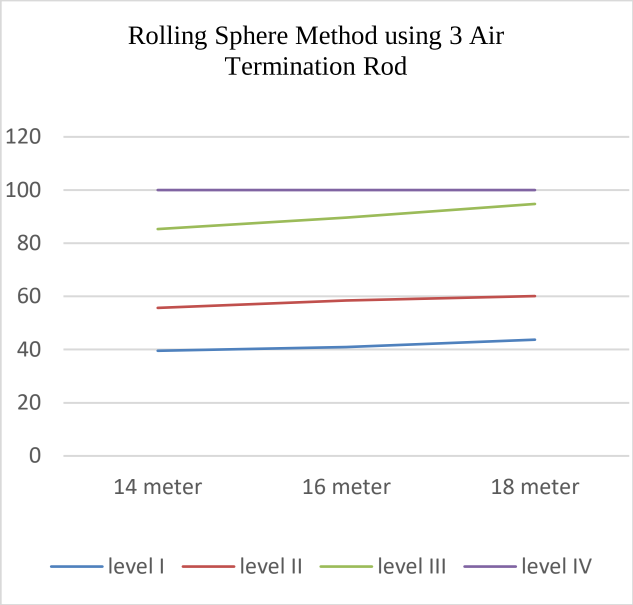

Figure 18: Graph for analysis the height of air termination rods.

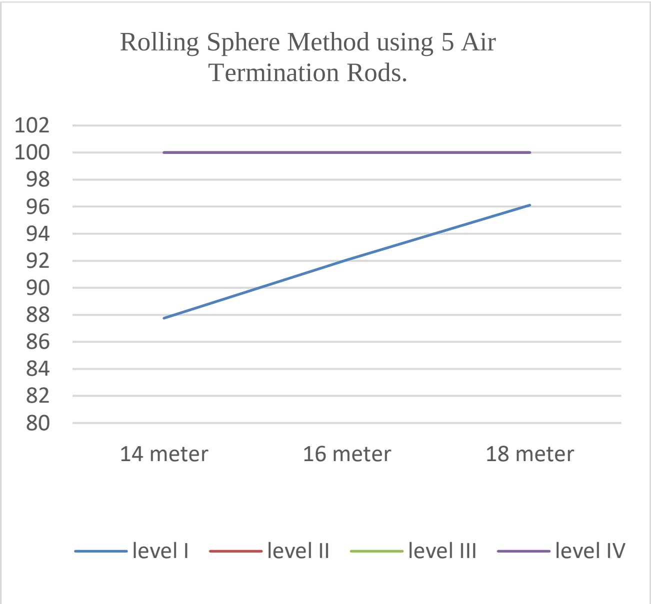

Figure 19: Graph for analysis the height of air termination rods

Figure 18 and figure 19 show graph of analysis rolling sphere method using 3 and 5 air termination rods. Based on both graph, it show by increasing height of air termination rod, area protected from lightning strike increase. This is due to radius of imaginary sphere. For level II, III, and IV, using 5 air termination and level IV, using 3 air termination, the whole surface of P 19 A building are protected from lightning strike. It because of for rolling sphere method, the protected surface area are larger that angle protection method.

V. CONCLUSION

As the conclusion, P 19 A building are more suitable using rolling sphere method than angle protection method. The rolling sphere method has larger protected area that angle protection method. Rolling sphere method may has longer step to analysis than angle protection method, but it has reduce the total of air termination use for protect P 19 A building from lightning strike.

ACKNOWLEDGEMENT

Alhamdulillah, praise is to Allah S.W.T for His enormous blessings, I manage to complete my final year project successfully.

I would like to take this opportunity to express my gratitude to my project supervisor, Dr. Noor Azlinda Binti Ahmad for his helpful effort and his important guidance throughout the accomplishment of this project.

My appreciation also goes to my family, who has been so understanding and supportive to me all these years. Thanks for their encouragement, love, and supports that they had given to me.

Last but not least, I would like to extend my appreciation to all staffs of the Pejabat Harta Bina (PHB), P19 A and my friends for their help and support and also to any other individual who have contributed to the success of this project.

REFERENCES

[1] Ahmad, N. A., Ahmad, N. A., & Adzis, Z. (2013). Study of Lightning Fatalities in Malaysia from 2004 to 2012. Jurnal Teknologi,66(1). doi:10.11113/jt.v66.1507

[2] M.K.Hassan, R. Z. Abdul Rahman, A. Che .Soh., M. Z. A. . A. K. (2011). Lightning Strike Mapping For Peninsular Malaysia Using Artificial Intelligence Techniques. Theoritical and Applied Information Technology, 471-472(2), 815–820.

[3] Cooray, V. (2010). Lightning protection. London: Institution of Engineering and Technology.

[4] R.H. Golde, "Lightning Protection", Edward Arnold 1973.

[5] Tibor Horváth, "Understanding Lightning and Lightning Protection: A Multimedia Teaching Guide", Research Studies Press Limited, John Wiley & Sons, 2006.

[6] Rosniza, Zainal (2013). A Study of Lightning Rod Shape and Its Striking Distance.

[7] Sigogne, C., Berger, G., Rees, T., & Ferron, A. D. (2013). May laboratory experiments explain how a lightning protection system works? 2013 8Th International Symposium On Advanced Topics In Electrical Engineering (Atee). doi:10.1109/atee.2013.6563443

[8] Beck, E. (1954). Lightning protection for electric system. New York, McGraw-Hill

[9] Yashin, A. M. (2009). A study on the secondary lightning protection system at wireless communication centre building (Unpublished master's thesis). Universiti Teknologi Malaysia.

[10] Nassereddine, M., & Hellany, A. (2009). Designing a Lightning Protection System Using the Rolling Sphere Method. 2009 Second International Conference on Computer and Electrical Engineering. doi:10.1109/iccee.2009.140

[11] FAHMEE, M. Z. (2016). ANALYSIS OF LIGHTNING PROTECTION SYSTEM FOR PRZS AND P19A USING ROLLING SPHERE METHOD. UNIVERSITI TEKNOLOGI MALAYSIA.

[12] Rison, W., Moore, C., & Aulich, G. (n.d.). Lightning air terminals - is shape important? 2004 International Symposium on Electromagnetic Compatibility (IEEE Cat. No.04CH37559). doi:10.1109/isemc.2004.1350045

[13] Mata, C. T., & Bonilla, T. (2012). Lightning Risk Assessment tool, implementation of the IEC 62305-2 standard on lightning protection. 2012 International Conference on Lightning Protection (ICLP). doi:10.1109/iclp.2012.6344320

[14] ERITECH. (2009). ERITECH Lightning Protection Handbook.

[15] Moore, C. B., Rison, W., Mathis, J., & Aulich, G. (2000). Lightning Rod Improvement Studies. Journal of Applied Meteorology,39(5), 593-609. doi:10.1175/1520-0450-39.5.593

Performance of Raspberry Pi as High Speed Camera in Identifying Discharge Processes

Siti Aishah binti Sabarudin
Faculty of Electrical Engineering
Universiti Teknologi Malaysia
Johor Bahru, Malaysia.
sitiaishahsaba@gmail.com

Mona Riza binti Mohd Esa
Institute of High Voltage and High Current
Faculty of Electrical Engineering
Universiti Teknologi Malaysia
Johor Bahru, Malaysia.
mona@fke.utm.my/monariza@utm.my

***Abstract*— This project is about testing the performance of Raspberry Pi camera module in analyzing the discharge process under lightning impulse. The breakdown in air was produced in a laboratory for a short gap distance in centimeter range. Commonly, the studying of lightning characteristics were done through signal analysis, thus, this project proposed that the analysis of the lightning pattern should be integrated using high speed camera that able to capture images at higher frame per seconds (FPS). In this project, positive polarity and negative polarity of discharges were tested with a voltage of 60 kV, 80 kV and 100 kV respectively. In addition, Haefly Hipotronics one stage divider impulse 140 kV was used to produce the voltages. The discharge process was captured using low cost high speed camera controlled by the Raspberry Pi board. The recorded videos were then translated into frames and redefined through denoising of image processing technique using OpenCv. In identifying the discharge pattern involving corona, streamer and leader process, a visual characteristic of each discharge process was done due to the limitation of the camera frame rate. The overall performance showed that the camera can captured a complete leader process in almost all of the voltages in both polarities, while only one streamer process can be observed. However, no corona process was able to be captured throughout the experiment.**

Keywords—Frame per second; Denoising; Raspberry Pi; Discharge process.

I. INTRODUCTION

The studying of lightning has long been done by the previous researcher as a way to improve the current protection system against lightning strike. In order to improve the current system, thorough understanding about the behavior of lightning is require prior to producing the solution. In order to further understand how lightning occurs, an artificial lightning can be replicate in a laboratory in a form of impulse to study the discharge process. According to A.Harfield Ltd, there are approximately 2,000 lightning storm around the world with over 100 strikes per second at one time. In Kerala, India there are reported 118 incidences of lightning accidents yearly which claimed the lives of 71 people in total[1]. As for Britain, among the 300,000 lightning strikes occurrences, 30 percent from it results in severe damage where 30 to 60 people are positively reported to have been struck by lightning. These incidents, occurs all over the world including in Malaysia. According to United States Lightning Safety Institution, Malaysia has the highest lightning activities where in its capital Kuala Lumpur, on average, there are 200 thunderstorm days per annum [2].Among 27 cases of fatal lightning strike that typically happens during the evening, 5 cases occurred in the month of December [3].

One of the reason for such findings is the monsoon seasons namely the Northeast and Southwest monsoon. The Southwest monsoon typically from late May to end of September brings the driest season while Northeast monsoon typically results in more rainfall. Rainfall increases the chances of lightning strike as the change of temperature in the air happens constantly and rapidly [3].

II. LIGHTNING FORMATION

The most common lightning formation theory begins with the collision of positively (+ve) and negatively (-ve) charged ions within the cloud [4]. The +ve usually consist of warm air that comes from ground and –ve consist of water droplets as a result of evaporation process within the ground and the heat from the sun. These two types of ions formed layers of charged ions within the cloud where the –ve ions were positioned at the bottom of the cloud as it is typically heavier than +ve ions. Strong winds from the air causes collisions between these two types of ions and triggers the avalanche of ions.

The avalanche creates a streamer at a velocity of one tenth the speed of light. As streamer usually last from 40μs or less, a second streamer appeared and this process was repeated a numbers of times with each step increase the channel by 10 to 200 m [4]. Due to the propagation of the streamer leading towards the earth, this process is known as stepped leader stroke. As the leader approaching the ground which contains massive amount of +ve ions, it will be attracted to the stepped leader as it was concentrated with –ve ions. As the two charges meets up at a certain point, an electrical discharged happens and electricity is produced. This electricity is known as lightning.

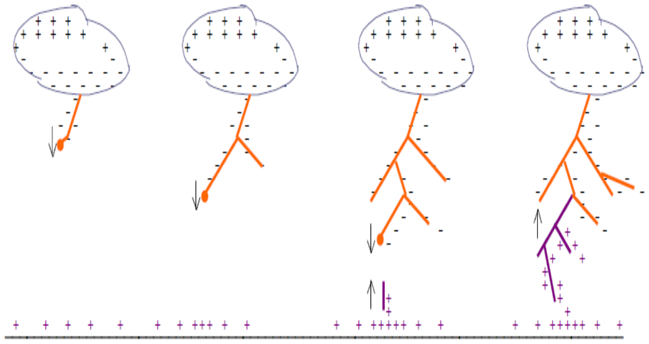

Fig. 1. Propagation of lightning channel [4].

A. *Positive Discharge*

The development of discharge with positive polarity is to represent positive cloud to ground phenomena (+CG). Positive cloud to ground happens when positively charged ions from the cloud propagate to the ground which has negatively charged ions. According to WeatherImagery, this type of discharge is known to have temperature 5 times hotter and can last 10 times longer than the negative discharge. Thus, generally, positive discharge is typically more dangerous. In laboratory generation, positive discharge is initiated by the formation of corona that consists of a number of narrow branches of streamers to form initial roots. During this stage, the electric field along the streamers is roughly around $5 \times 10^5 V/m$ [14]. When the potential at the tip of the electrode is high enough, the leader channels starts to propagate from the end of the corona roots and propagate continuously. In a stable propagation conditions, the electric field of leader is in the range of 1×10^5 V/m [14].The final process of discharge happens when the leader reaches the other end of the ground electrode which completes the breakdown process.

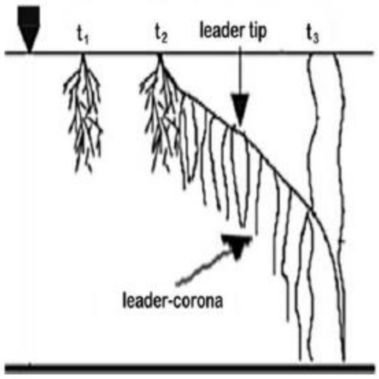

Fig. 2. The development of positive discharge [14].

B. *Negative Discharge*

In contrast with the positive discharge, negative discharge occurs when negatively charged ions from the cloud propagate to the positively charged ions on the ground. The phenomena is known as negative cloud to ground (-CG) in real life event. In laboratory generation, negative discharge formation begins with the initiation of negative corona, the same process as the positive discharge initiation but with different polarity.

The distinct difference between the two is that negative discharge is a non-continuous phenomenon which progresses through discrete and regular steps with an interval of 10 µs to 20µs [14]. After the corona extinction, a consequence of short interval of dark period takes place called pilot. At the end of the pilot inception point, space leader will be created to propagate as bi-directional discharge where positive end propagates to the cathode and negative end propagate to the anode. For negative streamer, the electric field lies in the range of 1×10^6 V/m to 2×10^6 V/m [15]. The next process involves the formation of negative leader from the negative electrode. The final stage of discharge occurs when the leader reaches ground electrode which completes the breakdown process.

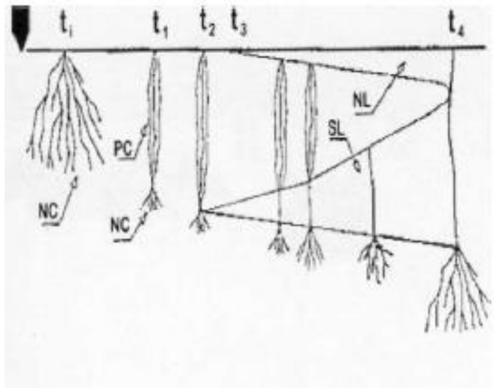

Fig. 3. The development of negative discharge[14].

C. *Raspberry Pi board*

In general, there are 4 different models of Raspberry Pi board namely Raspberry Pi 3, Raspberry Pi zero, Raspberry Pi 2 and Raspberry Pi A+. Among the four models, Raspberry Pi 3 is the latest version, released in the early 2016 that uses system on chip (SOC) of Broadcom BCM2387. The processor core type is Cortex A53-64 bit which has processing speed of 1.2GHz and internal memory, RAM of 1GB. As recording a video require some amount of memory storage and processing speed, the Raspberry Pi 3 memory and central processing unit (CPU) speed takes it all as this new model offers the largest memory and the fastest speed among all of the boards.

The downside of this model is the power consumption that is slightly higher as compare to other boards and its price of $45 each. However, because the board able to provide larger storage and faster speed, Raspberry Pi 3 was chosen for this project.

D. *Raspberry Pi camera module*

The Raspberry pi camera module is a compact camera which can capture still images as well as record a video in HD. The module has two different type of camera pixels, the 8MP and 5MP model. The 8MP model consist of Sony IMX219 8MP sensor which has better image quality in terms of colour, image quality and ability to capture at low light environment. While the 5MP model uses OmniVision OV5647 sensor, the ability for both camera is almost the same. Both cameras able to support 1080p at 30 FPS, 720p at 60 FPS and VGA90 video modes. However the lens focus for both models uses a fixed lens which makes it harder to capture an image or video in a long distance. The price for both of the cameras is within $25 range, however because the availability of the 5MP module is more abundant than the 8MP module, thus, for this project, Raspberry Pi camera module with 5MP was chosen.

E. Influence of temperature and atmospheric pressure

A different between temperature and atmospheric temperature in ideal condition (20 ºC,1013 Mbar) result in changes in air density of the environment where the testing are being conducted which result in a slight change in the actual value of generated voltage. This correction of air density (d) can be made by using this formula:

$$d = \frac{b}{1013} \times \frac{273+20}{273+t} \tag{1}$$

Where b is the atmospheric pressure in Mbar and t is the temperature in degree Celcius (ºC). The correction factor usually lies between 0.95 to 1.05. The divider ratio used for this experiment is 360.8 while the attenuator is 140. The divider ratio varies depending on the capacitance divider rating use in the experimental setup.

$$Actual\ generated\ voltag = Impulse\ voltage\ \times d \tag{2}$$

$$Impulse = peak\ voltage\ \times divider\ ratio\ \times attenuator \tag{3}$$

$$Impulse = peak\ voltage\ \times 360.8\ \times 140 \tag{4}$$

III. METHODOLOGY

Fig. 4. shows the experimental setup used to generate impulses ranges from 60 KV, 80 KV and 100 KV using One Stage Divider Impulse 140 KV of Haefely Hipotronics equipment. The variation of voltage can be obtained by manipulating the sphere gap at the discharge terminal. According to British Standard measurements (BSI), 1cm of separation between the spheres will generate approximately 30 KV of impulse. The increment of distance increase linearly with the voltage generated. Thus, for 60 KV impulse, 2cm gap was set prior charging the device.

The experimental setup in capturing the discharge processes were showed in Fig. 5. The camera module was set to be approximately 1 m apart from the sphere gap where the discharge process occurred. In order to control the camera module, a monitor and power supply connected to the Raspberry Pi board were put in place in order for the camera module to function properly.

Fig. 4. Haefely Hipotronics One Stage Divider Impulse 140 KV.

Fig. 5. Experimental setup for impulse generator and the camera module.

A. Operation of the equipment

The green columns located on the right side on Fig. 4 are the rectifiers which determine the polarity of the discharge generated. The output of the transformers is fed into the positive end of the rectifier to generate positive discharge and into the end of the resistor for negative discharge. The rectifier also serves as an AC/DC converter. The generated voltage then stored its energy in the capacitor (white column) until it is fully charged. For this setup, a 100pF of capacitor was used. The fully charged capacitor then discharged the energy through the sphere gap shown in Fig. 4. The two resistors located at the end of the system are responsible in generating the front time and the tail time of the discharge.

The 2400 Ω resistor was used to determine the tail time while 355 Ω resistor for the front time. The standardize front time value is known to be 1.2 µs and tail time of 50 µs with $\pm 30\%$ and $\pm 20\%$ acceptance level respectively. These two parameters plays an important role in getting the standard lightning waveform as the waveform should gives front and tail time within the acceptable limit only. The divider was placed at the end of the front time resistor to enable the measurements of voltage to be done.

The type of capacitive divider chosen needs to be taken into account into the digital measuring instrument (DMI) in the measurement process as it will determine the correct impulse level generated by the impulse kit. The equivalent circuit of the system is shown in Fig. 6, where C_1 is the charging capacitor, g is the sphere gap, R_t is the tail time resistor, R_f is the front time resistor, and C_2 capacitance voltage divider.

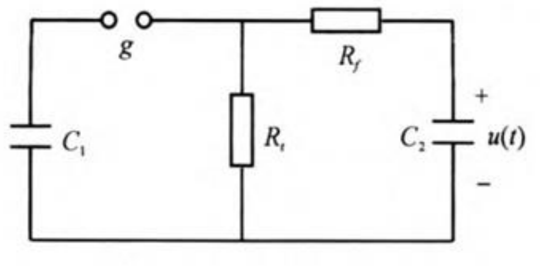

Fig. 6. Equivalent circuit of impulse voltage generator.

IV. Result And Discussion

From Table 1, it can be seen that the correction factor for air density (d) plays an important part in finding the actual impulse voltage generated. The difference in temperature and atmospheric pressure takes into account the time of the laboratory testing takes place. Because the testing takes place in the morning, the actual value of impulse voltages are not affected much, in approximation of 1 kV difference, but if taken in the evening, it is expected that the actual value will be approximate to 2 kV difference from the gathered information.

TABLE 1
IMPULSE VOLTAGE WITH INFLUENCE OF TEMPERATURE AND ATMOSPHERIC PRESSURE

Polarity	**Temp (ºC)**	**Pressure (Mbar)**	**Peak (V)**	**Impulse voltage (kV)**	***d***	**Actual Impulse voltage (kV)**
+60 kV	27.5	1015	1.26	63.6	0.98	62.3
+80 kV	28.4	1016	1.74	87.9	0.98	86.1
+100 kV	28.6	1016	2.2	111.1	0.97	107.8
-60 kV	28.8	1016	-1.44	-72.7	0.97	-70.5
-80 kV	30.0	1017	-1.72	-86.9	0.97	-84.3
-100 kV	30.5	1017	-2.02	-102.0	0.97	-98.9

For positive polarity waveform of 60 kV (blue), the front and tail time obtained is 0.67 µs/4.81 µs. This shows that it takes only 0.67 µs for the voltage to reach to its peak value, resulting a very steep front waveform. Same goes to the 80 kV (green) and 100 kV (red) impulse waveforms with 0.7 µs/6.02 µs and 0.6 µs/6.89 µs. All of the readings shows that the impulse generator could not provide a standardize value for both front and tail time as all of it occurred in a very fast instances below the acceptable range.

For negative polarity waveform of 60 KV, the front and tail time is 0.65 µs/4.64 µs. While 80 kV and 100kV result in 0.88 µs/5.49 µs and 0.85 µs/5.61 µs. All of the readings for tail time shows that the tail time suffers from the same problem as the positive polarity before. All of the tail time reduced significantly lower than the acceptable range. However, the front time for 80 kV and 100 kV voltage obtained, are within the acceptable range. This shows that the experimental setup is correct, but some of the components may be broken due to ageing effect.

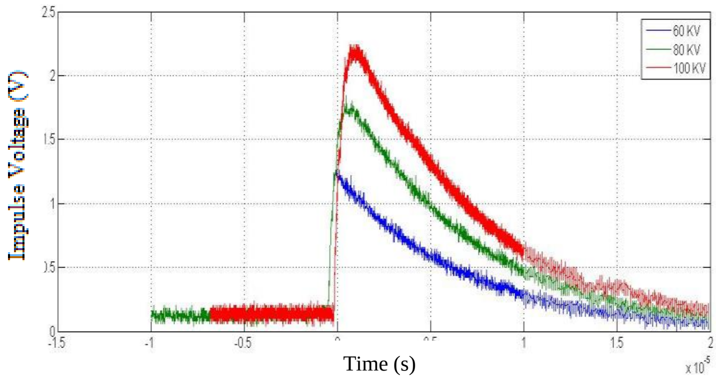

Fig. 7. Positive polarity impulse voltage.

A. Image Denoising

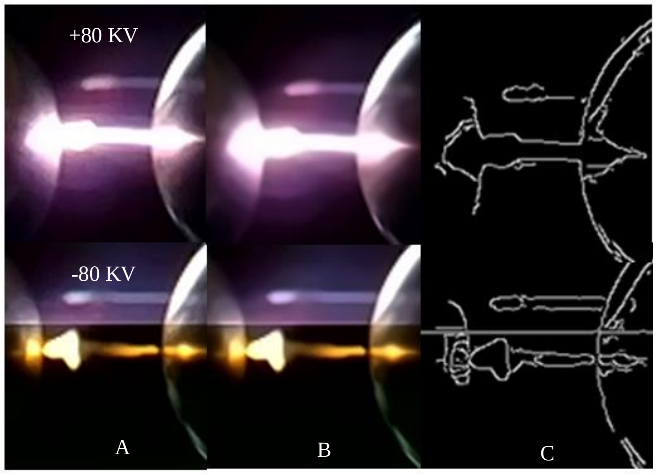

Fig. 8. Positive and Negative 80 kV denoising and canny edge.

Fig. 8 shows the result of denoising and edging process to refine the frame captured by the camera module. Image in A is the original frame where the pixels of the image can be seen to have rough surfaces due to low resolution of (640x480) in 90 FPS setting. The result of denoising technique in B, shown that the images were smoothen out to give better visualization of the process. In order to analyze the shape of the captured images, it was later undergoes canny edges filtration as shown in C. By analyzing the pattern obtain through the filtration, an identification of the discharge process can be made based on visual characteristics of corona, streamer, and leader process.

B. Positive and Negative Discharge

Normally, a complete discharge process takes within µs range. However, because the camera module maximum FPS is limited to 90 FPS, it can only captured in ms range for a single frame. This means that in a single video, it is difficult to capture different stages of discharge process, but it is possible to capture one of the discharge processes in a single video. Based on the characteristics of a leader process, it can be seen that for 60 kV, 80 kV and 100 kV of positive discharge, a clear leader process had been captured. A leader process is a result of the final jump of the streamer to the other side of the sphere polarity.

A complete jump produces a complete connection between positive and negative electrode. As the circuit is completed, a bright white light illuminates the leader indicating that all of the ions had been successfully transferred to the opposite electrode. At this moment, the maximum impulse voltage are generated which result in a complete discharge in air.

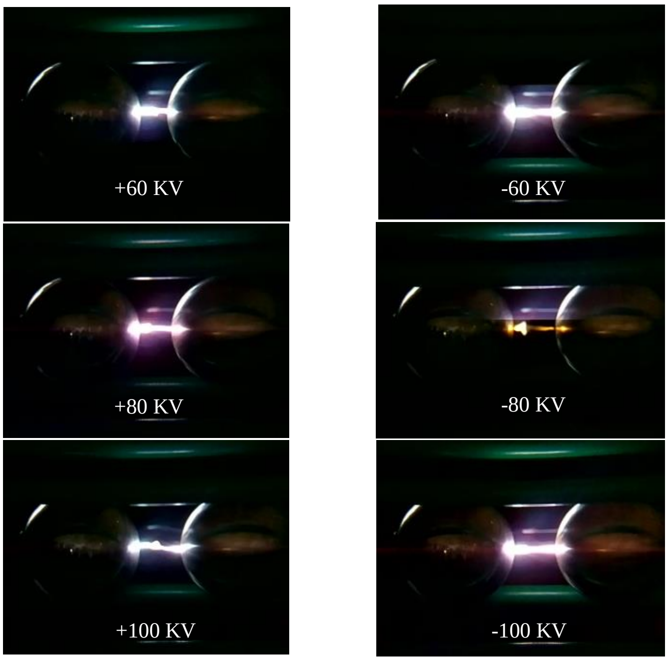

Fig. 9. Discharge process for positive and negative polarity.

In Fig. 9, for +80 kV leader process, it can be seen that the leader appears to be slightly reddish in colour compared to 60 kV and 100 kV which are more towards white. This is because, the frame obtained, captured the moment of the leader before it completely at its maximum temperature. When the temperature at its highest point, which is during the peak stage, bright white light will be produced as can be seen in 60 kV and 100 kV of discharge. As the gap between the sphere increases, the discharge process is most likely being affected by the surrounding ions in the environment. This explains the shape of the leader from 60 kV until 100 kV of discharge. For 60 kV discharge, the leader diameter appears to be almost consistently the same throughout the process. It can also be seen that the leader process travels in a straight line without diverting to the outer environment. However, for 100 kV discharge, the can be clearly observed that the leader formation is slightly crooked from the start point to the end point. This irregularity shows that during the streamer and branching of the leader, the avalanche of ions have higher tendency of collecting ions in the surrounding that is much further from the core of the leader[20].

For 60 kV and 100 kV of negative discharge, it can be seen that a complete leader process can be captured, same as in positive discharge. However, for 80 kV of discharge, it appears that the camera module captured a streamer process. Based on one of the streamer characteristics, streamer is a process of the avalanche of ions from the source electrode to the receiving electrode. This avalanche process will eventually create a droplet shape with its head travelling to the other side of electrode while its tail slowly follows from behind. As the captured frame was done for negative discharge, the head of the streamer consist of accumulated negative ions as it being attracted to the anode electrode. Positive ions that were less attracted to the anode will slowly reduce in speed, thus creating a trail behind the accumulated negative ions and creating a tail like shape[20].

As this was the only streamer process that the camera module could capture, it is difficult to compare and differentiate with the other two generated voltages. Fig. 9 however, shows no corona process can be capture in any of the videos as one of the factor of the inability, is due to the type of electrode use in the experiment. Corona process is highly likely to form when the surface of the electrode is sharp and pointy. These kind of surfaces provide an easy platform for the ions to accumulate due to the difference in surface area. In a visual and sound representation, a corona process starts when there exist a ‘hissing’ sound coming from the impulse generator. The sound indicates that the ions start to accumulate on the surface of the electrode. If this event was captured, it can be seen that on the surface of the electrode, a bluish bright light will starts to form directly. However, because of the limitation of the camera module, this process was unable to be identify throughout the experiment.

TABLE 2

OVERALL PERFORMANCE OF RASPBERRY PI CAMERA MODULE

Polarity	Corona	Streamer	Leader
+60 KV	-	-	✓
+80 KV	-	-	✓
+100 KV	-	-	✓
-60 KV	-	-	✓
-80 KV	-	✓	-
-100 KV	-	-	✓
Percentage of capturing the event (%)	**0**	**16.67**	**83.33**

V. CONCLUSION

The results showed that, by using Raspberry Pi camera module, the discharge process can be captured. However, not every process of the discharge can be observed due to the FPS limitation of the camera. The limitation affect the camera performance where it can only produce in larger time per frame compared to the discharge event that occurred. Thus, in a single video, only a single process can be captured at a time. The improvisation of the image captured through denoising also show minimal difference as the captured images were done in low light environment. The denoising technique was found to be suitable to be use for images which are exposed to high intensity of light as the differences would be more significant. Among the three discharge processes, the corona, streamer and leader, it was found that the camera was unable to capture any process involving corona. However, almost in all videos, the complete leader process can be observed and identify while only a single streamer process was able to obtained.

ACKNOLEDGEMENT

The authors would like to express the gratitude to Dr.Mohd Riduan Bin Ahmad frpm Universiti Teknikal Malaysia Melaka (UTem), for his contribution in providing extra knowledge and using the facilities in his laboratory. We also would like to thank Mr Fitri for their help to the first author’s final year project. The research work was funded by the PAS grant from Universiti Teknologi Makaysia (UTM).

REFERENCES

[1] R. Vishnu, V. A. Kumar, T. S. Sreekanth, V. N. S. Symon, S. M. Das and G. M. Kumar, "Formation of thunderclouds in a region of high lightning incidence, inferred from AWS, ceilometer and an electric field mill," 2011 7th Asia-Pacific International Conference on Lightning, Chengdu, 2011, pp. 135-139.

[2] M.K.Hassan, R.Z. Abdul Rahman, A.Che.Soh, M.Z.Abdul Kadir, *“Lightning strike mapping for peninsular Malaysia using Artificial Intelligence techniques*,Journal of Theoretical and Applied Infromation Technology, 2011, Vol.34. No.2.

[3] O. Murty, C. Kian, M. Ari Husin, R. a/l Nanta Kumar and W. Mohammed Yusuf, "Fatal Lightning Strikes in Malaysia", *The American Journal of Forensic Medicine and Pathology*, vol. 30, no. 3, pp. 246-251, 2009. [13] WeatherImagery, *“Two Types of Lightning – Positive and Negative*”, 2007, Extracted on 30 November 2016, http://www.weatherimagery.com/blog/positive-negative-lightning/.

[4] J R Lucas, “*High voltage Engineering”, Revised Edition,* 2001.

[5] I. Gallimberti, G. Bacchiega, A. Bondiou-Clergerie and P. Lalande, "Fundamental processes in long air gap discharges", *Comptes Rendus Physique*, vol. 3, no. 10, pp. 1335-1359, 2002. [15] Vernon cooray, *“An introduction to lightning”, Springer publication,* 2015.

[6] Nasim Mansurov, “*Understanding shutter speed- A beginner’s guide”,* 2015, Extracted on 23 August 2016, https://photographylife.com/what-is-shutter-speed-in-photography.

[7] Eben Upton, “*Raspberry Pi User guide”, John Wiley and Sons, Ltd publication,* 2012.

[8] Łukasz Staszewski, “*Lightning Phenomenon – Introduction and Basic Information to Understand the Power of Nature”*, 8th International Conference on Envronment and Electrical Engineering, May 2009.

[9] Kyle hill, “Your *brain has a frame rate and its pretty slow”,* 2014, Extracted on 16 August 2016, http://nerdist.com/your-brain-has-a-frame-rate-and-its-pretty-slow/.

[10] David Emanuel Ribeiro Gaspar, “Raspberry *Pi: a Smart Video Monitoring System”,* 2014.

[11] Thomas B. Greenslade, Jr. "*Nineteenth Century Textbook Illustrations XXI: The Camera*", *Phys. Teach.*, **16**, 162-163, 1978.

[12] Richard Trenholm, “*Photos: The history of the digital camera”,* 2007, Extracted on 5 August 2016, https://www.cnet.com/news/photos-the-history-of-the-digital-camera/).

[13] WeatherImagery, *“Two Types of Lightning – Positive and Negative*”, 2007, Extracted on 30 November 2016, http://www.weatherimagery.com/blog/positive-negative-lightning/.

[14] Ferris Jabr, “How *does a chicken tell time”,* 2014, Extracted on 16 August 2016, http://www.newyorker.com/tech/elements/how-does-a-chicken-tell-time.

[15] Vernon cooray, *“An introduction to lightning”, Springer publication,* 2015.

[16] H.Nguyen, T. Okinaka, Y. Takano, K. Takehara, V. Dao and T. Etoh, "Imaging with an ultra-high-speed video camera operating at 20 Mfps for for 300 kpixels", *Mechanical Engineering Journal*, vol. 3, no. 6, pp. 16-00286-16-00286, 2016.

[17] Q. Qi, W. Lu, Y. Ma, L. Chen, Y. Zhang and V. Rakov, "High-speed video observations of the fine structure of a natural negative stepped leader at close distance", *Atmospheric Research*, vol. 178-179, pp. 260-267, 2016.

[18] S. K S, L. H and H. Shivkumar, "Implementation of Image Processing on Raspberry Pi", *IJARCCE*, vol. 4, no. 5, pp. 199-202, 2015.

[19] P. Kuffel, W. Zaengl and P. Hammond, *High voltage engineering*, 1st ed.

[20] N. Hayakawa, K. Hatta, S. Okabe and H. Okubo, "Streamer and leader discharge propagation characteristics leading to breakdown in electronegative gases", *IEEE Transactions on Dielectrics and Electrical Insulation*, vol. 13, no. 4, pp. 842-849, 2006.

Effect of Surfactant on Breakdown Strength Performance and Thermal Conductivity of Transformer Oil-Based Nanofluids

Fatin Marlia binti Mohd Maulana
Faculty of Electrical Engineering
Universiti Teknologi Malaysia
Johor Bahru, Malaysia.
marliamaulana@gmail.com

Hafizi bin Ahmad
Department of High Voltage
Faculty of Electrical Engineering
Universiti Teknologi Malaysia
Johor Bahru, Malaysia.
mohdhafizi@fke.utm.my

***Abstract*—Mineral oil serves as an insulation & coolant for the transformer. The previous researchers have done a lot of effort to prolong the transformer's life. However the use of nanofluids as additive fillers has its drawbacks mainly on sedimentation & compatible issue. Therefore this research project proposes using CTAB surfactant to improve the sedimentation issues, breakdown voltage, thermal properties and electrical conductivity.**

Keywords—*nanofluids; CTAB; sedimentation; breakdown voltage; thermal properties*

I. Introduction

Transformer is the most significant and plays an important role in the power system. They help convert power to appropriate levels and helps in distribution of electric power. It is a static device without any direct electrical connection. With the aid of mutual induction between two windings it will transform electrical energy from one circuit to another circuit. Without it, the power grid simply would not be able to increase to meet the growing demand of electricity in future. It transforms power without changing its frequency but could be in varying voltage level.

Transformer uses a liquid as insulation which is known as transformer oil. This transformer oil is also known as mineral oil. Due to a good heat transfer rate and its self-healing mechanism, mineral oil has become the best choice for insulation of transformer (1). However, mineral oil that serving as an insulator could reduce the dielectric properties of the mineral oil due to aging and electrical stress.

Consequently, attempts have been made to improve the mineral oil characteristic by adding nanofillers but it caused the effect of sedimentation & agglomeration and thus resulting in incompatibility of mineral oil. It is noted that nanoparticle possess hydrophobic surface in nature. This increases the tendency of nanoparticles to aggregate and precipitate in a base fluid.

Therefore, this paper investigates the stability and effects of dialetric strength of nano-based mineral oil, subjected to the surfactants. The surfactants considered was Cetylmethylammoniumbromide (CTAB) which offered successful stabilization with metal nanoparticles (2). Recently, the use of CTAB surfactant is increasing for applications to obtain a stable nanofluids with an improvement of breakdown voltage, thermal properties and electrical conductivity.

A) Nanofluid

From another physics theory, the stability of nanofluids is based on two important things. The first one is its kinetic stability and the second one is its thermodynamic stability of a nanofluid. The temperature and pressure are influencing the thermodynamic stability of a nanofluid (3). Nanofluids are prepared by dispersing nanofillers into base liquids with or without dispersant such as ester oil, mineral oil, water, etc [20].In this research, alumina (AL2O3) nanofillers is investigated due to its insulation purpose.

B) Surfactant

The most common issue in producing nanofluids using the two step method is sedimentation.CTAB is one of the popular surfactant among the researchers.By adding a surfactant, the surface of nanoparticle will be modified to strengthen their grip to the base fluids (4). However, precaution should be taken on the amount of surfactant used.

C) Breakdown Voltage

One of the most important insulating components of oil is breakdown voltage. Breakdown voltage of oil is voltage which oil has not been able to resist the passage of electricity, and the electricity will pass through it.

D) Thermal Properties

It is known that the study of nanofluids has evolved over the decades. It was first discovered by Choi, (5) at Argonne National Laboratory that the presence of nanoparticles in fluids can enhance their thermal conductivity. Heat transfer performance of a thermal system can be improved through several methods. They are; maximizing heat transfer area, increasing temperature difference between the fluids, and improving thermal conductivity of the heat transfer fluid.

II. METHODOLOGY

The material selection for this study was based on the common materials used in electrical industry, the availability to get it, and also based on the criteria, suitability and functionality of the material itself.

A. Preparing of Nanofluids

The two step method was used for this project to prepare the nanofluids. Nanoparticles are obtained and synthesized separately as nanofillers before mixed up and dispersed into mineral oil. Both chemical and physical treatments were carried out during dispersion process. At early stage the optimum percentage of nanoparticles in the experiment was investigated before the experiment to get the optimum concentration of surfactants. This purpose is for having a better performance of insulation and breakdown strength when confront the second part of experiment.

B. Preparing of Nanofluids+ (CTAB) surfactant

The preparation of samples were repeated with a different concentrations of surfactant and selected percentage of nanoparticles at early stage. The samples need to be mixed with the surfactant first and stirred for 15 min before adding the nanoparticles so that the CTAB surfactant will be distributed all over the oil volume.

C. Testing/Experiments

All the samples were conducted in several experiments to investigate breakdown voltage and thermal properties. The experiment was AC test and thermal conductivity. At final stage, electrical conductivity which is the important parameters before performance analysis for industrial application was also conducted.

D. AC Test

The AC breakdown voltage was measured according to the IEC 60156 standard by IEEE Globalspec, (6) using a test vessels. There are two spherical brass electrodes in the test vessels, with gap distance between them is set to 2.5mm, according to the standards. The test vessel is very important to avoid any impurities and other subject, which is not needed, to be present inside the test vessel.

III. RESULTS

Table I shows that the result of four different samples that was prepared by using three different percentage of nanoparticle (Al2O3) that mixed with mineral oil and one base oil. The reading of breakdown voltage was taken six times according to IEEE 60156. The result obviously shows the nanofluids with 0.1% of Al2O3 has higher breakdown voltage compared to others. Therefore 0.1% of AL2O3 was chosen as nanofluid in further experiment due to its optimum concentration.This would lead to an significance improvement of breakdown voltage when surfactant is added

TABLE I: BREAKDOWN VOLTAGE OF NANOFLUIDS (AL2O3)

Reading	***Base Oil***	0.1% AL2O3	0.3% AL2O3	0.5% AL2 O3
Reading 1	18.05	32.47	28.85	37.76
Reading 2	21.76	44.48	36.27	29.76
Reading 3	21.85	51.07	29.07	24.95
Reading 4	21.67	51.45	14.78	32.09
Reading 5	30.42	29.19	20.19	18.75
Reading 6	32.87	44.15	27.46	37.02

TABLE II : BREAKDOWN VOLTAGE OF NANOFLUIDS (0.1 % OF AL2O3) WITH SURFACTANT

Reading	***Base Oil***	0.1% AL2O3 WITH 0.025% CTAB	0.1% AL2O3 WITH 0.050% CTAB	0.1% AL2O3 WITH 0.075% CTAB
Reading 1	18.05	50.79	41.16	36.64
Reading 2	21.76	48.86	40.22	35.96
Reading 3	21.85	51.90	39.18	34.16
Reading 4	21.67	49.88	37.54	36.02
Reading 5	30.42	50.60	41.06	38.90
Reading 6	32.87	51.42	40.14	35.12

From Table II, the results have a significant difference from the results in Table I due to ageing. This is because the base oil were been exposed to the air for a few days and this has made the oil itself already degraded before the samples were prepared. Basically the oil is subjected to the degradation because of the ageing, high temperature and chemical reactions such as oxidation.

However the result in Table II shows an expected outcome for this project. Breakdown voltage of Alumina with CTAB has an enhancement compared to only base oil. The result indicated that the AC breakdown voltage of base oil significantly decreased after applying impulse current, while this decrease is less in nanofluid samples and with CTAB surfactant. In other word, nanofluid with CTAB retains its strength against breakdown under impulse condition.

The highest breakdown voltage among the samples with CTAB surfactant is the sample with 0.025 wt% CTAB concentration, followed by sample with 0.075 wt% CTAB and lastly is the sample with 0.05wt%. An addition of CTAB surfactant contributes to a better breakdown voltage to the nanofluids. The sample with 0.025wt% CTAB concentration got 51.92kV, which is the highest among other samples.

However, the sample with 0.075wt% CTAB has lower breakdown voltage compared to the sample with no surfactant. The probability of breakdown voltage for an addition of CTAB in alumina also has fluctuating values.

TABLE II : THERMAL CONDUCTIVITY

Temperature (^{0}C)	Average Temperature (^{0}C)	Base Fluid (W/mK)	0.1 % of Alumina + 0.025% of CTAB (W/mK)	0.1 % of Alumina + 0.050% of CTAB (W/mK)	0.1 % of Alumina + 0.075% of CTAB (W/mK)
40	39.87	0.111	0.133	0.121	0.109
50	50.22	0.124	0.145	0.128	0.126
60	59.89	0.123	0.139	0.125	0.131
70	70.29	0.145	0.148	0.137	0.144
80	79.93	0.148	0.160	0.142	0.143

The KD2-Pro thermal analyzer was used to investigate the thermal conductivity of Alumina based nanofluids with surfactant at room temperature (~25° C). It works on the principle of transient line heat source (7).In order to minimize the errors during measurements and repeatability of results, an average leading from ten measurements was taken from each samples. In addition, the measurement was taken only after thermal equilibrium between the sensor and sample was achieved. This instrument has a specified accuracy of +-5%.

In table II It is noticed that there is no substantial thermal conductivity augmentation for the base fluids without surfactant. Thermal conductivity of 0.01wt% Alumina was not measured because the nanoparticles started to agglomerate right after the sonication process. Thermal conductivity of 0.075%wt CTAB with Alumina, there is only 0.3% thermal conductivity enhancement compared to that of base fluid. In this study, the average thermal conductivity of base fluid at 40° C is 0.111W/mK which is much lower compared to nanofluids with surfactant.

However, the percentage of thermal conductivity of Alumina based nanofluids with surfactant show convincing thermal conductivity improvement.It is found that 11.2%, 1.6% and 6.1% enhancement were observed at 60̊C for based nanofluids with 0.025%wt, 0.050%wt and 0.075%wt respectively. Therefore the thermal conductivity shows fluctuating trends when the weight percentage of CTAB increases.

IV. CONCLUSION

In this study, the effect of surfactant on breakdown voltage and thermal conductivity of Alumina based nanofluids has been investigated. The following conclusions can be derived from the present study.

Nanofluids often considered as a way to improve the breakdown voltage strength of conventional of mineral oil. Nanoparticles do have an effect to improve the breakdown Voltage of mineral oil. 0.1wt% of Alumina nanofluids dominates the highest breakdown voltage strength as compared to 0.3wt% and 0.5wt% of the samples and mineral oil. With the help of nanoparticles, nanoparticles play an important role to create a shallower trap to trap the electrons in mineral oil.

CTAB surfactant is used in this project for modifying the surface of nanoparticles to reduce the nanoparticles attractive energy. Different concentration of CTAB surfactant are used in this study which are 0.025wt%, 0.050wt% and 0.075wt% .The outcome of the experiments in this study proves that CTAB surfactant improves the breakdown voltage and thermal conductivity for Alumina nanofluids with surfactant compared to basefluid. It shows that the combined effects of Nanofluids with surfactant are required to produce sample with high thermal conductivity. However there is some issues on fluctuating values due to several factors such as humidity and viscosity.

REFERENCES

[1] **Moran, Robert B** *Guidelines for transformer application design.***.** s.l. : Penton, May 1, 1997.

[2] **Yue-fan, D.** *Effect nanoparticles on the breakdown strength of transfomer oil.* s.l. : Electrical Insulation, Conference Record of 2010, 2010

[3] **Yu-zhen, L,et al.** *Experimental Investigation of breakdown strength of mineral oil based nanofluids.* s.l. : Dielectric Liquids International Conference, 2011.

[4] ***Jin,H*** *AC breakdown voltage and viscosity of mineral oil based nanofluids***.**[ed.] Emerging Technologies. s.l. : Annual Report Conference, 2012, Electrical Insulation and Dielectric Phenomenon.

[5] **Argonne.**, *Enhancing Thermal Conductivity of fluids with nanoparticles.* [ed.] SUS Choi. s.l. : UNT Digital Library, October 1995, Vol. ii, p. 5. [

[6] **Mohanty, Akash.** *Dielectric breakdown performance of alumina/epoxy resin nanocomposites under high voltage applicatio.* Volume 47, Pages 711-716 : ELSEVIER, May 2013..

[7] ***Rafiq, Md Khan, and M.Ali***. Dielectric Properties of Transformer Oil based Nanofluids. s.l. : Power Generation System and Renewable EnergyTechnologies,2015

Electrical Breakdown Performance of Polyethylene Blends with Different Nanofillers

Mohamad Adli Bin Nor Zahid
Faculty of Electrical Engineering
Universiti Teknologi Malaysia
Johor Bahru, Malaysia.
mohamadadli8544@gmail.com

Lau Kwan Yiew
Institute of High Voltage and High Current
Faculty of Electrical Engineering
Universiti Teknologi Malaysia
Johor Bahru, Malaysia.
kwanyiew@utm.my

***Abstract*—This paper evaluated the DC breakdown strength of polyethylene blends based nanocomposites with different loading containing either magnesium oxide and silicon nitride. The presence of water increased the electrical conductivity of the nanocomposites. Under dry and ambient conditions, magnesium oxide surpass the breakdown strength of the base polymer. Moreover, this study shows that composition of polyethylene blends and magnesium oxide has the potential to improve the breakdown strength and less water absorption than silicon nitride. Thus, the used of magnesium oxide hold a promising potential in the application of HVDC cables.**

Keywords*—*Nanocomposites; water absorption; DC breakdown streght

I. INTRODUCTION

In 2002, Nelson and his co-workers demonstrated that nanodielectrics applications has a promising impact in insulation materials [1]. Since that, researchers have put a lot of effort in discovering the potentials of nanodielectrics as the next generations of high voltage cable, as addition of nanodielectrics may improve electrical breakdown strength of a polymer, also its mechanical properties [2]. Various study related to electrical breakdown of nanocomposites polymer have been done by the past researchers in introducing the next generations of high voltage cable. Distinctive parameters such as loading percentage of nanofillers, type of nanofillers, and temperature variations have been take into account in order to achieved promising result. A study done by Masuda [3] which concentrating on LDPE/MgO nanocomposites polymer have demonstrated a positive outcome. In view of his discoveries, it is found that the DC breakdown strength of LDPE increased with addition of MgO nanofillers as compared to without MgO nanofillers. Not only that, the addition of MgO nanofillers degrade the progression of short circuit tree length and its initiation.

The positive outcome on electrical breakdown strength then upheld by Murakami et al [4]. The study focusing on the space charge formations, and therefore the space charge formations degrades as addition of MgO nanofillers into polymer matrix. The study also concluded that addition of MgO nanofillers is suitable for DC insulating materials as in term of space charge formations. Furthermore, there is interesting finding in the recent study where the addition of MgO nanofillers into LDPE from 0.1%wt to 1%wt increased the electrical breakdown strength. However, the electrical breakdown strength decreased as the nanofillers at 2%wt [5]. Along these lines, the study inferred that low stacking of nanofillers into polymer matrix have better scattering rate. Also, the high-level loading of MgO nanofillers might result to agglomeration of nanoparticles. According to Lau et al [6], the research of nanocomposites performance not only on electrical properties, but in fact there are many researches concentrating in improving its mechanical properties such as water absorption performance as presence of water will affect the dielectric properties of a material. The water absorption is in fact of the challenges in nanodielectric field.

Based on previous research, addition of nanofillers into polymer matrix shows a great potential in extend the electrical breakdown strength. However, the nanocomposites polymer seemed vulnerable towards water absorption. For example, silica/epoxy nanocomposites absorbed more water as compared to unfilled epoxy [7]. While Zhang and Stevens [8] reported that the addition of alumina nanofillers into polyethylene have different amount of water absorption with unfilled polyethylene. The volume of water being exposed for both sample is the same. This has come to understanding that the area of nanoparticles in the base matrix is the potential area of water molecules. By mean of that, the interface between nanoparticles and base matrix become affected due to presence of water in that specific area [9]. Thus, the nanocomposites materials more likely become hydrophobic in presence of water.

However, the issue is currently being addressed thoroughly. The water absorbed into nanocomposites is gradually decreased as surface treatment is needed [10]. The study also shows the same outcome where the amount of water absorbed increases as the content of silica nanofillers being increase into polyethylene. The surface treatment of nanocomposites is able to reduce the diffusion of water into the interfacial of nanoparticles with the polymer matrix. Another study done Hosier et all [11] shown that the small amount of nanofillers have less water content being absorbed into polyethylene blends. Not only that, it is found that silicon nitride nanofillers have absorbed less water compared to silica nanofillers. Thus, this paper will present the breakdown performance of polyethylene blends with the addition of nanofillers with different loadings. Magnesium oxide and silicon nitride have been chosen, followed with their characteristic in different types of conditioning.

II. Methodology

A. *Sample Fabrications and Conditions*

Two type of nanofillers are used with two different loadings; 1% and 5%. Magnesium oxide and Silicon Nitride nanofillers are selected to be added into polyethylene blends (PE). While for the PE blends, a composition of 80% LDPE and 20% HDPE is chosen and the weight is fix at 65g. The small pellets of LDPE and HDPE were blended and melted by using two-roll machine at temperature of 140ºC. The blending process were strictly kept for 10 minutes for all the samples. Next, the sample will be transform into thin film, approximately 100µm and not more than 150µm in order to follow ASTM D149 by using hydraulic hot press at 160ºC and 2.5 tons of pressure. Three thin films were prepared for each sample which 1 grams of sample lumps is needed for one thin film. All the samples then undergo two weeks of conditioning (ambient, dry, wet) in order to evaluate the water contents and water absorption properties, and its effect on breakdown strength. Ambient conditioning was performed by exposing samples to ambient surroundings (27 ± 2 °c and 54 - 94 % RH) for 14 days. Dry conditioning was carried out by vacuum drying at room temperature. While, wet conditioning was conducted by immersion of all the samples into distilled water.

B. *DC Breakdown Test*

The sample thin films of each sample were enduring continuous step voltage until breakdown occur at rate of 2kV of increment for every 20s. Each of samples also undergoes 15 times of dc breakdown testing to ensure consistency in measurement. Then, all the measurements were analyzed by using Weibull Distribution method in determine the breakdown strength for each sample.

III. RESULTS

A. *Water Content Properties*

Fig. 1 present the change in mass of the composites after undergo dry and wet conditioning. In wet conditioning, there is 0.08% increased of mass of the unfilled sample. The amount of water absorbed is the lowest among all other composites. Between magnesium oxide and silicon nitride, it is clearly that magnesium oxide absorbed less water for both 1wt% and 5wt% as compared to silicon nitride. There are increase of 0.09% and 0.18% respectively for both 1wt% and 5wt% of magnesium oxide as compared to the unfilled sample. For 5wt% of magnesium oxide, the amount of water absorbed is double as compared to 1wt% of magnesium oxide. The 5wt% of silicon nitride is the most absorbed water as compared to other samples and the differences are very significant as the mass of the composite increased as much as 0.73% and 0.65% more than unfilled sample. While for 1wt% of silicon nitride, there is slight difference as compared to 5wt% of magnesium oxide and the change in mass is at 0.29%. In general, the least absorbed water is 1wt% of magnesium oxide and the most absorbed water is 5wt% of silicon nitride as compared to the unfilled sample.

The dry conditioning is purposely to evaluate the amount of water content in the composites. It is observed that there is no much difference in term of change in mass for unfilled sample with both 1wt% and 5wt% of magnesium oxide, as well as with 1wt% of silicon nitride. The mass of the composites reduced as much as 0.15%,0.16%,0.17% and 0.18% respectively. It is also shown that both 1wt% and 5wt% of magnesium oxide samples loss its mass due to water content at the rate which slower than unfilled sample. The 5wt% of silicon nitride sample loss as much as 0.26% of mass which is the most composite have the most water content as compared to other samples.

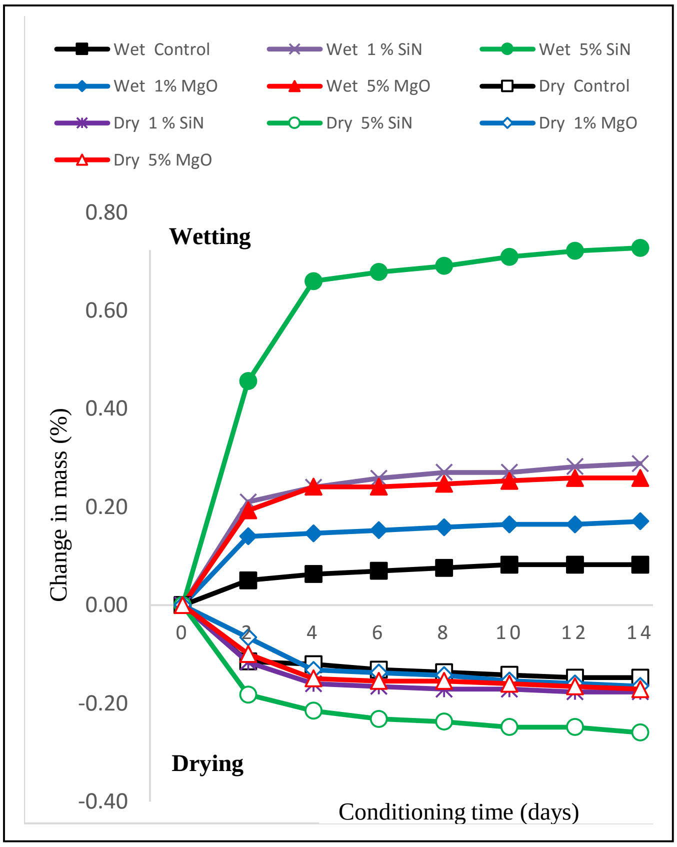

Fig. 1. Effect of conditioning on measured water ccontent

B. *Electrical Breakdown Performance*

Table I present the results of dc breakdown test of all composites in comparison with different types of conditioning. The control composite is taken as reference in evaluating the performance of nanocomposites polymer. While Fig. 2,3 and 4 illustrate the Weibull distribution of the breakdown strength for all 15 test breakdown voltages.

First, it is clear that presence of water content does affect the performance of dc breakdown strength of the composites. As addition of water being absorbed during wet conditioning, all of the samples show degradation as compared to the results on ambient condition. However, one nanocomposite containing magnesium oxide with 1wt% loading show a small degradation by 3 kV compared to the unfilled sample. While other samples are highly affected by the presence of water. This outcome also supported by the amount of water absorbed by the 1wt% MgO by referring Fig. 1 where it's the least nanocomposites that absorb water during wet conditioning. In comparison, for both silicon nitride nanofillers with 1wt% and 5wt% loadings proved that magnesium oxide nanofillers has the least water absorption that clearly have better dc breakdown strength.

In contrast to wet conditioning, removing any possible water content that normally in the form of moisture able to improve the breakdown strength of all composites. Based on Table I, the breakdown strength of all composites show improvement as compared with ambient and wet conditioning. This shows that presence of water weakens the breakdown strength of a composite. However, none of the nanocomposites able to show inferior breakdown strength than the unfilled sample when drying process take place. In this case, the breakdown strength of 1%wt of magnesium oxide shows similar breakdown strength with the unfilled sample with a slight difference of uncertainty.

Besides, nanocomposite containing 1wt% of magnesium oxide show a great dc breakdown strength as compared to the unfilled sample. Not only that, the 1wt% MgO also shows the best repeatability denotes by β parameter and consistency for all 3 conditionings. While the unfilled sample, the shape parameter (β) is lower than the 1wt% MgO which indicates increase in scattering measured data. Thus, it is clear to say that 1wt% MgO has the best performance as compared to other nanocomposites, also show promising improvement for both ambient and dry conditioning.

In overall, 1wt% loading of nanofillers into PE blends for both silicon nitride and magnesium oxide improve the breakdown strength in ambient condition. The breakdown strength of PE blends degrades when the loading of nanofillers reach to 5wt%. The presence of water inside the nanocomposites lead to detrimental effect that also been explained in the previous studies [6] and [11]. The presence of water weakens the interfacial between nanofillers with its polymer matrix that result in increase of conductivity which reduced the electrical strength or insulation properties.

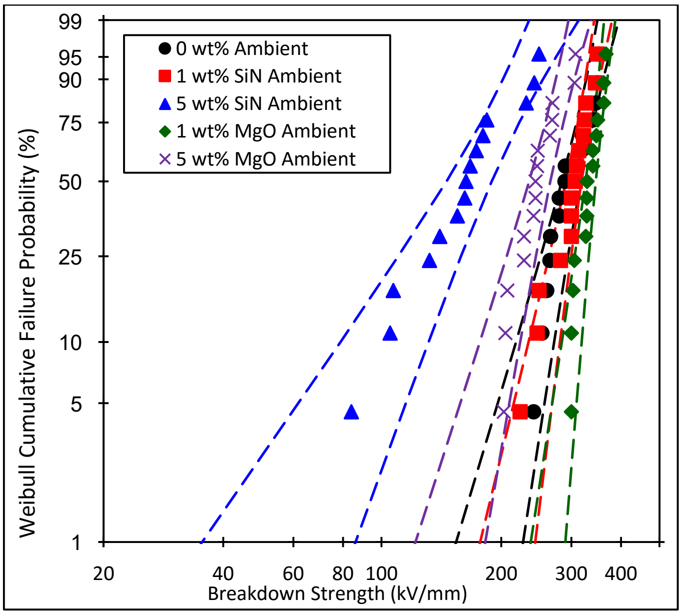

Fig. 2. Weibull distribution for ambient conditioning

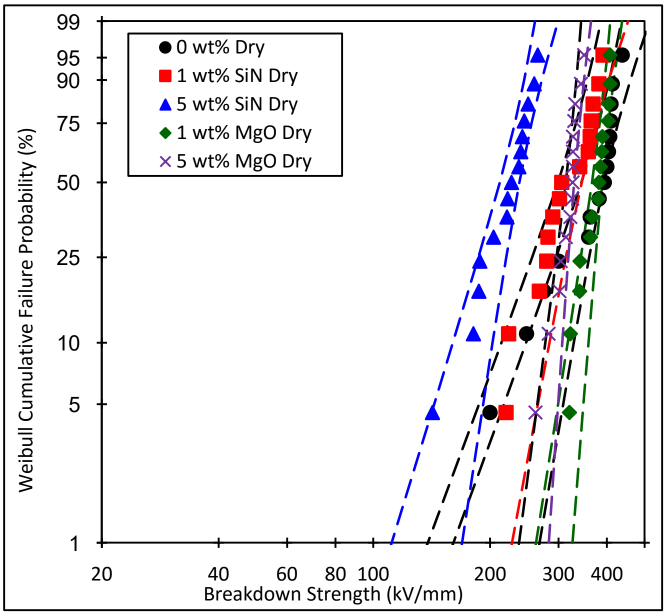

Fig. 3. Weibull distribution for dry conditioning

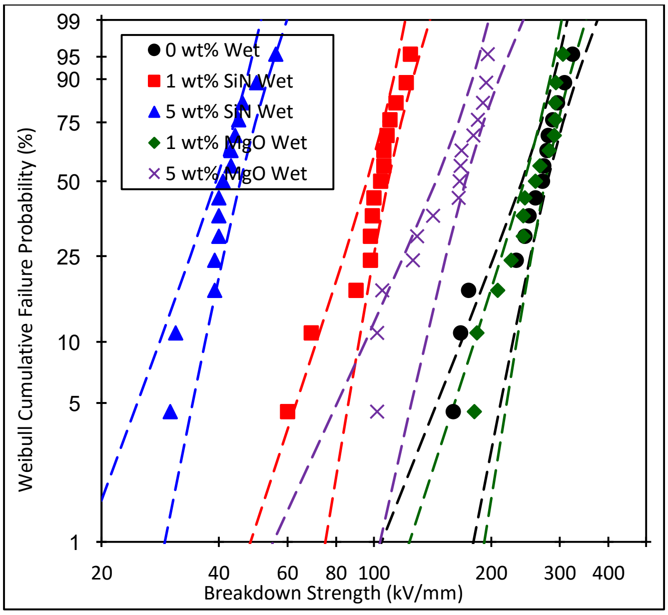

Fig. 4. Weibull distribution for wet conditioning

TABLE I. DC BREAKDOWN STREGHT OF NANOCOMPOSITES POLYMER

Composites	Weibull Result - kV/mm (β)		
	Dry	Ambient	Wet
Control	386 ± 24 (7)	313 ± 16 (9)	273 ± 19 (7)
1wt% SiN	338 ± 22 (7)	314 ± 13 (11)	107 ± 6 (8)
5wt% SiN	234 ± 13 (9)	183 ± 22 (4)	45 ± 3 (7)
1wt% MgO	386 ± 10 (17)	343 ± 9 (17)	270 ± 15 (8)
5wt% MgO	327 ± 8 (20)	261 ± 15 (8)	168 ± 13 (6)

IV. Conclusiion

In conclusion, four types of nanocomposites polymer were prepared with different level loadings. The DC breakdown strength improved at 1% silicon nitride or magnesium oxide under ambient condition. The DC breakdown strength highly affected in presence of water. However, by eliminating the water content through drying process, there is significant improvement of DC breakdown strength. Also, composites with 1% of magnesium oxide shows promising result as the DC breakdown strength greater than its host polymer for both ambient and drying condition. It is clear that magnesium is better than silicon in rejecting water molecule, thus has a significant potential in the application of the new generation of HVDC cable.

References

[1] J. K. Nelson, J. C. Fothergill, L. A. Dissado, and W. Peasgood, "Towards an understanding of nanometric dielectrics," 2002.

[2] J. K. Nelson, "Overview of nanodielectrics: Insulating materials of the future," in *2007 Electrical Insulation Conference and Electrical Manufacturing Expo*, 2007, pp. 229-235.

[3] M. Suguru, O. Shunsuke, K. Rudi, M. Yoshinobu, N. Masayuki, M. Yoshinao, *et al.*, "DC conduction and electrical breakdown of MgO/LDPE nanocomposite," in *2007 Annual Report - Conference on Electrical Insulation and Dielectric Phenomena*, 2007, pp. 290-293.

[4] Y. Murakami, T. Okazaki, M. Nagao, Y. Sekiguchi, C. C. Reddy, and Y. Murata, "Space charge formation in low-density polyethylene up to breakdown influenced by addition of MgO nano-filler under DC ramp voltage," in *2009 IEEE Conference on Electrical Insulation and Dielectric Phenomena*, 2009, pp. 685-688.

[5] S. Peng, J. He, J. Hu, X. Huang, and P. Jiang, "Influence of functionalized MgO nanoparticles on electrical properties of polyethylene nanocomposites," *IEEE Transactions on Dielectrics and Electrical Insulation,* vol. 22, pp. 1512-1519, 2015.

[6] K. Lau, A. Vaughan, and G. Chen, "Nanodielectrics: Opportunities and challenges," *IEEE Electrical Insulation Magazine,* vol. 31, pp. 45-54, 2015.

[7] C. Zou, J. C. Fothergill, and S. W. Rowe, "The effect of water absorption on the dielectric properties of epoxy nanocomposites," *IEEE Transactions on Dielectrics and Electrical Insulation,* vol. 15, pp. 106-117, 2008.

[8] C. Zhang and G. C. Stevens, "The dielectric response of polar and non-polar nanodielectrics," *IEEE Transactions on Dielectrics and Electrical Insulation,* vol. 15, pp. 606-617, 2008.

[9] S. Rowe, "Electrical ageing of composites: An industrial perspective," in *Proc. Int. Conf. Solid Dielectrics*, 2007, pp. 401-406.

[10] K. Lau, A. Vaughan, G. Chen, and I. Hosier, "Dielectric response of polyethylene nanocomposites: the effect of surface treatment and water absorption," in *Electrical Insulation and Dielectric Phenomena (CEIDP), 2012 Annual Report Conference on*, 2012, pp. 275-278.

[11] I. L. Hosier, M. Praeger, A. S. Vaughan, and S. G. Swingler, "Electrical properties of polymer nano-composites based on oxide and nitride fillers," in *2015 IEEE Electrical Insulation Conference (EIC)*, 2015, pp. 438-441.

Implementation of GSM Module In Energy Meter Reading for Household Appliances

Soraya Jasmine Yusof
Faculty of Electrical Engineering
Universiti Teknologi Malaysia
Johor Bahru, Malaysia.
myjasmine1994@gmail.com

Azhar Khairuddin
Department of Electrical Power Engineering
Faculty of Electrical Engineering
Universiti Teknologi Malaysia
Johor Bahru, Malaysia.
azharkhairuddin@utm.my

***Abstract*— Energy meter is used as a device to measure the amount of energy delivered to the consumers. The main purpose of this project is to develop an energy meter by using GSM module as a device that displays energy used and price of electrical energy used through smartphone. The device can help the people especially the household to monitor the electricity bills even though they are not at home. The scope of this project focuses on the electricity bill's calculations for the households in Malaysia which it will used the rate price of electrical energy used based on Tenaga National Berhad's Tariff. The first step of this work is to determine the suitability of current sensor SCT-013-030 and 240Vac to 9Vdc adapter which is used to measure current and voltage consumed by the load. The higher the power rating of the load, the higher the value of current. Then, load current value will be determined by microcontroller which has been programmed by using Arduino IDE's software. Then, the LCD display and GSM module will show the reading of current used, energy used and the price. The developed module can be useful for the household to check the price of energy used by using smartphone.**

Keywords—Smart Energy Meter; Arduino Nano Microcontroller; 240Vac-to-9Vdc adapter; LCD display; GSM module.

I. INTRODUCTION

Electrical energy is very important in our daily life nowadays. It is because many technologies in consumer appliances nowadays use electrical energy as power supply. Residential consumers use electrical energy for lights, kitchen appliances such as refrigerator and microwave, and entertainment appliances such as television and radio. Besides, commercial and industrial consumers use electrical energy for machine in producing appliances.

Electrical energy used by consumers is measured using energy meter. As we can see, every house has energy meter on the wall outside of the house. The energy meter is used to calculate the energy used by consumers in basic unit of kilo-Watthour (kWh) [1]. The energy meter is shown in Figure 1. The consumers will be charged for energy used based on the tariff from utility, where a bill will be produced each month based on meter reader that takes energy meter reading for the consumer.

Figure 1: Energy Meter

As for Malaysia, Tenaga Nasional Berhad (TNB) is a company which provides electrical energy to all consumers. The rate of electrical energy consumption is referred to as TNB's Tariff [2]. In this project, the tariff that will be used is the TNB's Tariff as shown in Figure 2.

	TARIFF CATEGORY	UNIT	CURRENT RATE (1 JAN 2014)
	Tariff A - Domestic Tariff		
	For the first 200 kWh (1 - 200 kWh) per month	sen/kWh	21.80
	For the next 100 kWh (201 - 300 kWh) per month	sen/kWh	33.40
1.	For the next 300 kWh (301 - 600 kWh) per month	sen/kWh	51.60
	For the next 300 kWh (601 - 900 kWh) per month	sen/kWh	54.60
	For the next kWh (901 kWh onwards) per month	sen/kWh	57.10
	The minimum monthly charge is RM3.00		

Figure 2: TNB's Tariff

Recently, there are efforts to develop a technology that enable the residential consumers to have their electrical bills through smartphones. It is used to display the price of electrical energy used and the power energy through consumers' smartphones. The objectives of the project are:

a) To develop an energy meter by using GSM module as a device that display the energy used and price of electrical energy used through smartphone.

b) To determine the calculation of TNB's Tariff that can display the current, energy usage and price accurately.

c) To design an energy meter that can enable consumers to check the current, energy usage and price of electrical energy used.

II. LITERATURE REVIEW

A. Arduino Based Smart Meter for Residential Load

Arduino is a microcontroller which can control any devices where it can read inputs such as light on a sensor, a finger on a button or a Twitter message. When it reads the inputs, then it will turn into an output which is activating a motor, turning on a LED, and publishing something online. Arduino is easy to be programmed [3].

Therefore, for this project, Arduino microcontroller is utilised to control the energy meter reading. Figure 3 shows the hardware configuration of the project. The project has used current sensor, Arduino UNO microcontroller, LCD display and bulbs as loads. The current sensor has been used to detect current flow through the live wire. The LCD displaycis required to display information given by the Arduino UNO microcontroller.

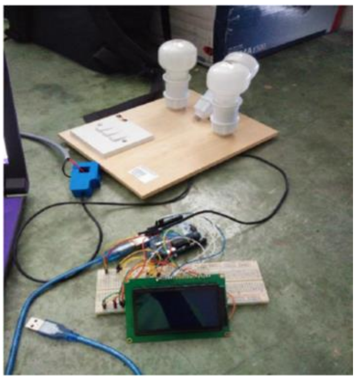

Figure 3. Arduino Based Smart Meter for Residential Load

Moreover, based on the Figure 3, when the load is on the current will flow through the live wire which had been clamped with current sensor. The current sensor detects the current flow through the live wire. Then, the microcontroller reads the current sensor continuously. After that, the microcontroller will send information to LCD display. LCD display will display the value of current used, power used and price of energy used.

B. Load Monitoring and Control by Using ZigBee Wireless Network

People nowadays do not aware with the power consumption when they are using electrical appliances at home. Sometimes, they just leave the appliances on without using them. It is just wasting the electrical energy and because of that, the electricity bills for their house will increase.

Therefore, Load Monitoring and Control by Using ZigBee Wireless Network is developed. The purpose of this project is to monitor and control loads in Kolej Tuanku Canselor, Universiti Teknologi Malaysia (UTM). Moreover, the focus for this project is to monitor energy consumption and control some electrical appliances at facility area such as corridor, bathroom and surau. So, the office management in Kolej Tuanku Canselor can monitor the power used in Kolej Tuanku Canselor [4].

Based on Figure 4, it shows the components used to develop this project. The ZigBee is a wireless device which used to send information to the office management. Therefore, the office management can easily monitor the power consumption. The current sensor is clamped to live wire and then, Arduino UNO microcontroller will read the input from current sensor. After the microcontroller completed read the input, it will send information to LCD display and ZigBee will send information to office management.

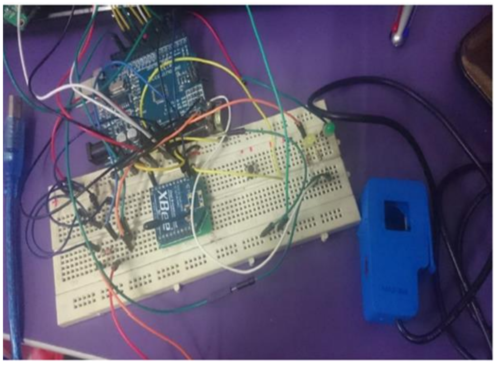

Figure 4. Load Monitoring and Control by Using ZigBee Wireless Network

III. METHODOLGY OF THE PROJECT

A. AC to DC Adapter Connection

First, the end of 240Vac-to-9Vdc adapter is connected to the voltage divider which has two resistors of 470kΩ in series, as shown in Figure 5. One of the resistor is to be the 5V output voltage terminal that is connected to analog pin 1 (A1) of the Arduino Nano microcontroller.

B. Current Sensor SCT-013-030

The current sensor SCT-013-030 is connected with additional circuit as shown in Figure 6. The circuit will be connected to analog pin 0 (A0) of the Arduino. Furthermore, the current sensor is clamped at the live wire of the extension wire.

C. LCD Display and GSM module

Then, LCD display and GSM module are connected to digital pin of the Arduino Nano microcontroller as shown in Figure 7(a) and 7(b).

D. *Arduino IDE Software*

The last part of the system is the Arduino IDE software that is used to program the coding in the Arduino Nano microcontroller. This software will enable the LCD display and GSM module to display the information sensed by the adapter and the current sensor.

E. *Power Meter*

Power meter is used to compare the results obtained from the Arduino system.

F. *Loads and Extension Wire*

The project is tested with two loads which are kettle and iron by connecting the load on the extension wire as shown in Figure 8.

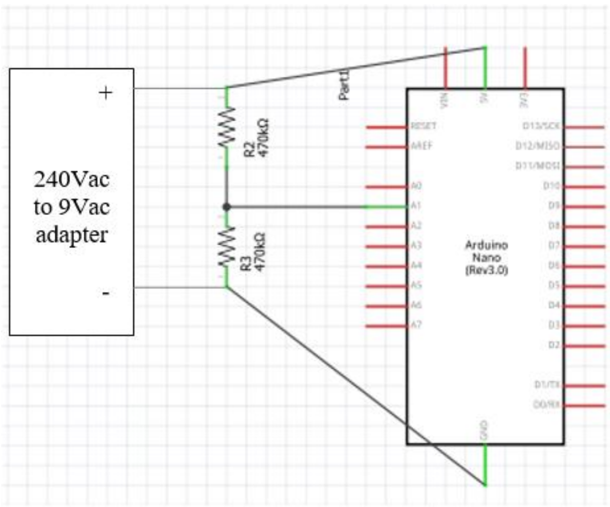

Figure 5. The Schematic Diagram of AC to DC Adapter to Arduino

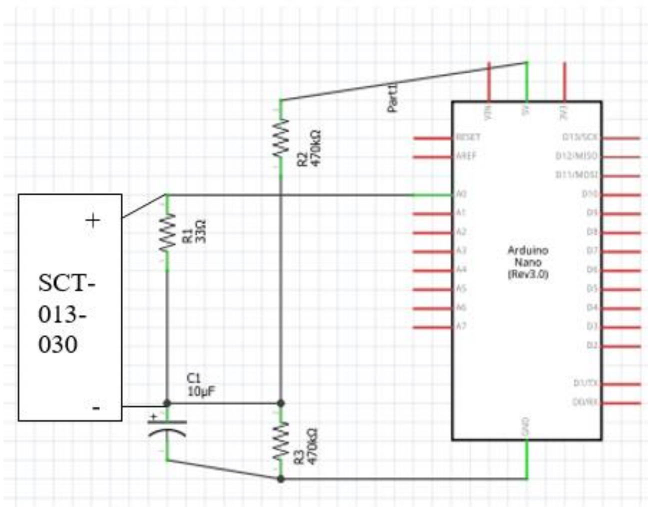

Figure 6. The Schematic Diagram of SCT-013-030 to Arduino

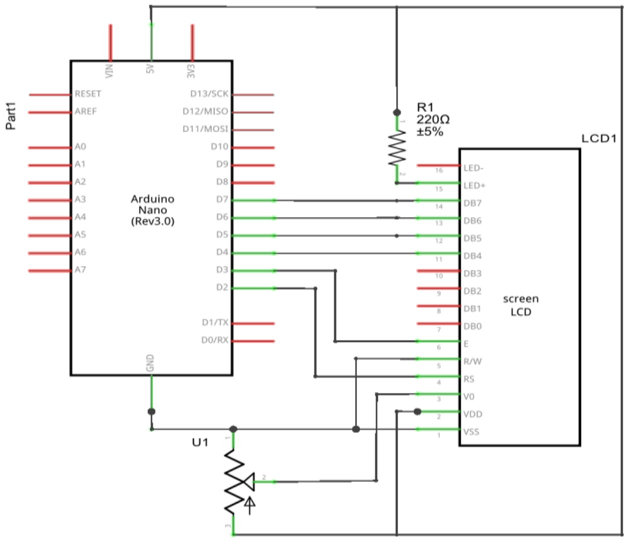

Figure 7(a): The Schematic Diagram of LCD Display to Arduino

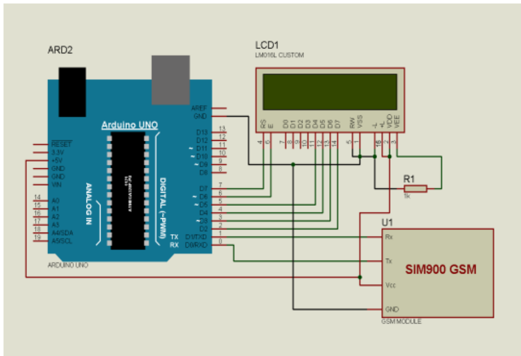

Figure 7(b): The Circuit Connection of LCD Display and GSM Module with Arduino.

Figure 8. Hardware of the Project

IV. Results and Discussions

The reading of voltage, current, power factor and power used by the load are recorded. The task flow for the project is shown in Figure 9. When the load is ON, the current sensor and adapter will sense reading of current flow and voltage to make sure that the microcontroller display the accurate information needed on the LCD display and smartphone.

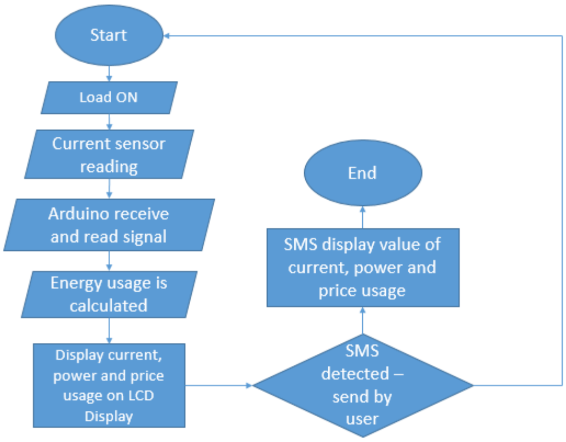

Figure 9. Flow of the project

A. *Iron as a Load*

Table 1 shows the results when iron is used as the load. The power rating for iron is 900W to 1100W. The value of energy and price is calculated after 31 seconds.

Table 1. The Percentage Error for Iron

	Power Meter	Arduino	Percentage Error, % error (%)
Voltage, V (V)	237.00	239.77	1.08
Current, I (A)	4.59	4.70	2.40
Power factor, pf	1.00	0.98	2.00
Power, P (kW)	1.088	1.104	1.47
Energy (kWs)	33.728	34.224	1.47
Energy (kWh)	0.009	0.010	0.11
Price (RM)	0.002	0.002	0.00

From Table 1, the percentage error for the value of voltage, current, power factor and power used by iron has been calculated. The percentage error shows that the reading of voltage, current, power factor and power in Arduino is acceptable when compared with the reading of those parameters in power meter with errors of 1.08%, 2.40%, 2.00%, and 1.47%, respectively.

B. *Kettle as a Load*

Table 2 shows the results when kettle is used as the load. The power rating for kettle is 1370W to 1630W. The value of energy and price is calculated after 31 seconds.

Table 2. The Percentage Error for Kettle

	Power Meter	Arduino	Percentage Error, % error (%)
Voltage, V (V)	237.00	239.77	1.17
Current, I (A)	6.51	6.69	2.76
Power factor, pf	1.00	0.99	1.00
Power, P (kW)	1.543	1.588	2.92
Energy (kWs)	47.833	49.228	2.92
Energy (kWh)	0.013	0.014	0.10
Price (RM)	0.003	0.003	0.00

From Table 2, the percentage error for the value of voltage, current, power factor and power used by kettle has been calculated. The percentage error shows that the reading of voltage, current, power factor and power in Arduino is also acceptable when compared with those in power meter, with errors of 1.17%, 2.76%, 1.00%, and 2.92%, respectively.

So, for both loads, all the readings are within the terror tolerances, which has been shown by using the calculation of percentage error. Even though the readings of voltage, current, power factor and energy have errors, these do do not greatly affect the total price of energy displayed by the system. It is already being proven in the Tables 1 and 2, where the percentage error for both loads are 0%.

V. Conclusions

In general, the project had achieved all the objectives that have been stated. The project can be used to display the energy used and price of electrical energy used through smartphone. Besides, the project can make household members to easily check the current, energy usage and price of electrical energy used with the display all the readings on the LCD display inside the house and through smartphone. Furthermore, the project is used the calculation based on TNB's tariff to show the current, energy usage and price accurately.

This project used current sensor and adapter to measure current and voltage. For future work, energy meter can be implemented instead of using current sensor and adapter. Moreover, the unit considered is kWs for energy unit due to the small power rating of the load. So, for future implementation, it can be adapted to high power rating of load for the energy in kWh.

REFERENCES

[1] T. Argawal, 2016. Edgefx.in Kits & Solutions. “Explain about 3 Basic Types of Energy Meters?” [Online]. Available: https://www.edgefx.in/introduction-on-energy-meter-different-types-of-energy-meters/, [Accessed 19th December 2016].

[2] Tenaga Nasional Berhad. “Tariff Rates,” [Online]. Available: https://www.tnb.com.my/residential/pricing-tariffs, [Accessed 19th December 2016].

[3] A. M. Muadz, “Arduino Based Smart Meter for Residential Load,” Universiti Teknologi Malaysia. Bachelor’s Degree Thesis, 2016.

[4] K. M. Amin, “Load Monitoring and Control by using ZigBee Wireless Network,” Universiti Teknologi Malaysia. Bachelor’s Degree Thesis, 2016.

[5] H. R. Zala, V. C. Pandya, “Energy Meter Data Acquisition System with Wireless Communication for Smart Metering Application,” International Journal of Engineering Research & Technology. Rev., vol. 3, pp. 1590-1595, 2014.

[6] M. M. Haque, M. K. Hossain, M. M. Ali, M. R. I. Sheikh, “Microcontroller Based Single Phase Digital Prepaid Energy Meter for Improved Metering and Billing System,” International Journal of Power Electronics and Drive System. Rev., vol. 1, no. 2, pp. 139-147, 2011.

[7] H. Mehta, 2015. Quora. “What is the difference between the Arduino Nano and the Arduino Uno?” [Online]. Available: https://www.quora.com/What-is-the-difference-between-the-Arduino-Nano-and-the-Arduino-Uno, [Accessed 19th December 2016].

[8] EFY group, 2016. Electronics for You. “All You Wanted to Know About GSM and GPRS Module,” [Online]. Available: http://electronicsforu.com/resources/what-is-gsm-module, [Accessed 19th December 2016].

[9] Advanced Wireless Planet, “GSM module GPRS module characteristics,” [Online]. Available: http://www.gsm-modem.de/gsm-module.html, [Accessed 19th December 2016].

[10] 2016, KTECHNICS SYSTEM, “30A SCT-013-030 Non-invasive AC current sensor Split Core Current Transformer AL,” [Online] Available: http://ktechnics.com/shop/30a-sct-013-030-non-invasive-ac-current-sensor-split-core-current-transformer-al/, [Accessed 19th December 2016].

[11] Instructables, “Interfacing 20x4 LCD with Arduino,” [Online]. Available: http://www.instructables.com/id/Interfacing-20x4-LCD-with-Arduino/, [Accessed 19th December 2016].

[12] SM, 2015. Arduino. “Arduino Software (IDE),” [Online]. Available: https://www.arduino.cc/en/Guide/Environment, [Accessed 19th December 2016].

[13] H. Das, L.C. Saikia, “GSM Enabled Smart Energy Meter and Automation of Home Appliances,” National Institute of Technology Silchar, India.

[14] G. Mostafa, “Development of a Bright Display Electrical Energy Meter using ATmega8 Architecture,” International Conference on Advances in Electrical Engineering. University of Science and Technology, 2015.

[15] Tae-Seop, Choi, Kyung-Rok, Ko, Seong-Chan, Park, Young-Sik Jang, “Analysis of energy savings using smart metering system and IHD (in home display),” Asia Pacific 2009 IEEE Transmission & Distribution Conference &Exposition, pp. 1-4, 26-30 Oct 2009.

[16] T. Tariq, “Smart energy management in a smart environment using a mobile device,” Global Summit on Computer &Information Technology, pp. 1-5, 14-16 June 2014.

[17] P. Prudhvi, D. Bhalodi, M. Manohar, V. Padidela, S. Adapa, “A Smart meter architecture in Indian Context,” 2012 11th International Conference on Environmental and Electrical Engineering (EEEIC), pp. 217-222, 18-25 May 2012.

[18] S. S. Ali, M. Maroof, S. Hanif, “Smart energy meters for energy conservation & minimizing errors,” PEDES, 2010, 2010 Joint International Conference on Power Electronics, Drives and Energy Systems, pp. 209-220.

[19] K. S. Choi, S. Hong, “New Design Approaches and Implementation of Smart Metering System,” ICSE, 2014, 18th International symposium on Consumer Electronics, pp. 1-2.

[20] S. D'Alessandro, A. M. Tonello, A. Monacchi, W. Elmenreich, “Home energy management systems: Design guidelines for the communication infrastructure,” ENERGYCON, 2014, 2014 IEEE International Energy Conference, pp. 805-812.

[21] V V. Das, “Wireless Communiaction System for Energy Meter Reading,” International Conference on Advances in Recent Technologies in Communication and Computing, pp. 896-898, 2009.

[22] R. Simpson, 2008. “ZigBee Smart Energy Profile,” ZigBee Alliance Std.

[23] T. Handa, A. Oda, T. Tachikawa, J. Ichimura, Y. Watanabe, H. Nishi, “Knives: A distributed demand side management system—Integration with zigbee wireless sensor network and application,” in Proc. 6th IEEE Conf. Ind. Informat, INDIN’08, 2008, pp. 324–329.

[24] L.C. Saikia, H. Das, D. N. B. Choudhury, T. Malakar, “GPRS Enabled Smart Energy Meter with In -Home Display and Application of Time of Use Pricing,” National Insttitute of Technology Silchar, India, IEEE, 2016.

[25] A. Datta, P. Mohanty, M. Gujjar, “Accelerated deployment of Smart grid technologies in India-Present scenario, challenges and way,” Innovative Smart Grid Technologies Conference, pp. 1-5, 19-22 Feb 2014.

[26] A. Arif, M. Hussain-Al, N. Mutariri-Al, E. Ammar-Al, Y. Khan, N. Malik, “Experimental Study and Design of Smart Energy Meter for the Smart Grid,” Renewable and Sustainable Energy Conference(IRSEC), pp. 515-520, 7-9 March 2013.

[27] R. Teymourzadeh, S. A. Ahmned, K. W. Chan, M. V. Hoong, A.B.M. Nasiruzzaman, “Smart GSM based Home Automation System,” ICSPC, 2013, IEEE Conference on Systems, Process & Control, pp. 306 – 309.

[28] M. S. Khandare, A. Mahajan, “Mobile Monitoring System for Smart Home,” ICETET, 2010, 3rd International Conference on Emerging Trends in Engineering and Technology, pp. 848-852

[29] E. Andrey, “Morelli J., Design of a smart meter techno-economic model for electric utilities in Ontario,” Electric Power and Energy Conference(EPEC), pp. 1-7, 25-27 Aug 2010.

[30] W. D. Hart, (2011). *Power Electronics*. New York, NY; McGraw-Hill.

Voltage and Frequency Regulation In An autonomous Microgrid Using Particle Swarm Optimization

Hafifi Fikri Bin Roslan
Bachelor of Engineering (Electrical)
Universiti Teknologi Malaysia (UTM)
Skudai, Johor, Malaysia
hafifi.fik@gmail.com

Prof.Ir.Dr. Mohd Wazir Bin Mustafa
Faculty of Electrical Engineering
Universiti Teknologi Malaysia (UTM)
Skudai, Johor, Malaysia
wazir@utm.my

Abstract— **Microgrids are new concept of electric power networks consisting of distributed generators, renewable energy sources and sensitive loads. Microgrid can operates in islanded mode and grid connected mode. However, in islanding mode the challenges are microgrid need to be establish the voltage and frequency to the system so that it can avoid the system collapse. This project represents the voltage and frequency regulation to maintain a better power quality in microgrid, where microgrid can improve the reliability of the power system by reducing the transmission losses and also continuing energy supply when there is interruption in power supply at the grid. Microgrid operates in islanded and under load change condition to improve the voltage and frequency regulation. An intelligent searching algorithm is applied in the power control parameters which is Particle Swarm Optimization (PSO). The idea and the strategy is that during the microgrid is islanded and under changes of load condition, the voltage and frequency in the system can be regulate by DG unit adopting Vf control mode. The results show that the proposed controller offers an excellent response and proves the validity of the proposed strategy.**

I. INTRODUCTION

Microgrid (MG) is a smaller version of conventional power system that the generation of the system aggregates a cluster of Distributed Generation (DG) [1]. It provide much closer proximity of generation and to the end user. Nowadays, RES are really importance in main component of MG especially in energy storage and main power source [2]. A MG itself have three mode of operations which are, grid connected mode, autonomous (islanded) mode and between these two modes dynamically[3]. Based on IEEE STD 1547-2003[4], islanding is a state which distributed generation solely energized the grid while that grid is disconnect and terminated by the national grid or other power system. In other word, the microgrid is supplied by the power and energy from DG without the presence of utility power from the grid. Microgrid can independently operate without connecting to the grid. Figure below show the operation during the islanding mode where Distributed Energy Resources (DER) still supplying the power even though the connection with the grid is disconnect[5] .

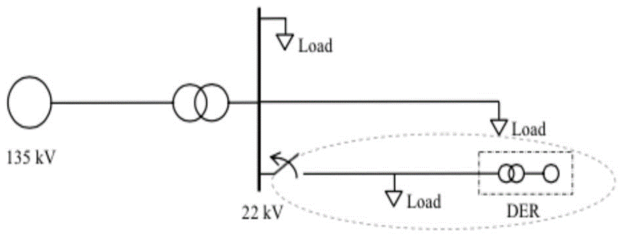

Fig. 1. Islanding Operation Mode[5]

The main problems in MG are involves power quality and stability of the system operation. Thus, the quality of powers supply is main concern in this project. The problem often occurs in both of the modes which grid connected and islanding mode. In grid connected mode, the problems are involves in active and reactive power while in islanding mode the main concern is voltage and frequencies are varies. Therefore, the variations of voltage and frequency can give severe negative impact especially on load requirement. Therefore, islanding mode control (IMC) is a need to reduce the effects of variations of voltage and frequency[6].

In this paper, the autonomous (islanding) mode is proposed to regulate the quality of the power supply through voltage and frequency regulation in the microgrid with the presence of DG based on Particle Swarm Optimization technique. The technique will find best parameters once the system are in islanding mode and during load changes on non-linear system. The remaining part of this paper is divide into 6 sections. Section 2 presents literature review of this project. In section 3, this paper will describes about methodology used in to achieved the objective of this project. Section 5 the result of the simulation is analysed and presented in this paper. Finally, the conclusion is outlined in section 6.

II. Literature Review

A. Inverter based DG

There are several type of DG supplying electrical power that need a conversion proses and can be categorized into three which are variable frequency, direct energy and high frequency as example of wind turbine, fuel cell and micro turbines respectively. The used of power electronic converter is vital as it is convert from DC to stable AC power frequency and voltage[7]. The most functional power electronic converter in this inverter based unit is called Voltage Source inverter (VSI). However, the characteristic of semiconductor component is nonlinear and resulting high switching frequency because of most of the sources are connected with Pulse-Width-Modulation (PWM)-VSI system[8]. For linear current controller, it is based on space vector PWM (SPVWM) which current error can be compensated by the proportional integrator (PI) or using predictive control algorithm. Thus, it can yield excellent steady state response, low current ripple and high quality sinusoidal form.

An efficient MG operation is depends on DG units control. Thus, current control strategy of PWM-VSI system is the important part to provide a better quality improvements. Therefore, the needs of the inverter based is to control the power quality by the imposed power command such as voltage and frequency. Current controllers have two categories which are nonlinear which closed loop PWM type and linear which are open loop voltage PWM[9].

B. Technique in Optimization Problem

To improve the operation of the microgrid, a design of microgrid is needed to alter the best parameters to use for the PI controller. An intelligent algorithm is required. Based on the literature review, several algorithm is compared and determine their limitation and the drawback to be used.

There are many techniques to solve the in the optimizations process in the non-linear problems. Type of the search space and function of the objective of the optimization's techniques can be classified as follows. Firstly, one of the simple method that uses only in linear objective and linear equality or inequality constraints in Linear Programming (LP) [10] . However, this techniques difficult to determine social, institutional, financial and other constraints. Besides that, it has problem to determine the relevant co-efficient values. Second technique is called Nonlinear Programming (NLP). It introduced for non-linearity objective function and constrains but the researchers have noticed that it is a difficult field, and also valuable results are only achieved when all constrains are linear, so it is referred as Linearly Constrained Optimization [11]. Another techniques is Dynamic Programming (DP) which this techniques is used widely in optimizations problems. However, this techniques requires more computational processes and it increase increases the probability of suboptimal results because of the dimensionality problems [12].

There are two techniques that are computational-intelligence based system to solve the problems. The techniques are called as Genetic Algorithm (GA) and Particle Swarm Optimizations (PSO). GA emulates the evolutionary biology to find the approximate optimal solutions by the search method [13]. Although GA is a good solutions, but it also have drawbacks such Converge moves toward local solution, sets of dynamic data are difficult to run and it is more complex.

Based on all the algorithm, they have their own drawbacks and limitation. As being reported in [14, 15], a suitable solution are achieved by using PSO algorithm that can be compared to other algorithm and optimizations technique. Compare to other methods PSO such as [16] :

1) With the used of PSO, it is easy for tuning with implement less parameters.

2) Each particle is able to remember its own previous best position and its neighbour's best. Thus, PSO has more effective memory capability compare to GA.

3) It is similar with community social behaviour because to move toward the best, the swarm used the most successful information. Therefore, PSO is more efficient to maintain the diversity of the swarm. On the other hand, GA abandon the worse solution and only used the good ones.

The advantages of PSO are [17]:

1) PSO can be applied in scientific research and engineering use.

2) PSO is produced best quality solutions in less time because PSO has no mutation and crossover calculation

3) PSO calculation is very simple compared to other optimization calculation.

4) PSO has less parameter to control.

5) PSO has less divergence.

Based on the literature review, the limitations of previous work is that the other method are more complex and requires more computational process. Thus, it requires more time than PSO. Advantages PSO tuned with the used of less parameters, PSO memory capability is more effective than GA and PSO is more efficient to maintain the diversity of the swarm.

III. Methodology

A. Modelling of Grid Connected VSI System

Fig. 2 shown modelling of LC filter three-phase grid connected VSI system where it consists of equivalent lumped resistance, Rs and inductance of the filter L_s , transformers coupling (if applicable) and grid which detected by the inverter. Besides that, C represents the filter capacitance and Vs represents grid voltage.

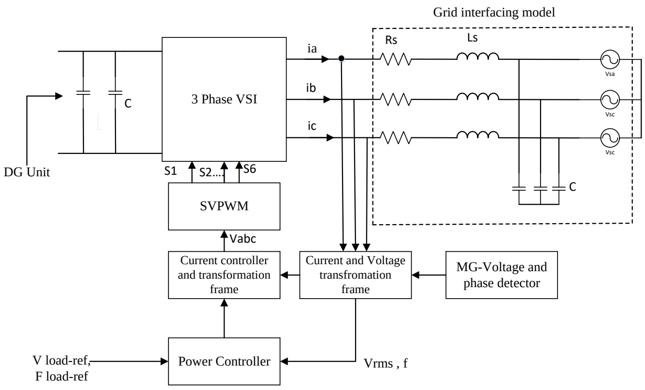

Fig. 2. Design of Autonomous Microgrid [16]

In the reference frame of abc, the equivalent system circuit can be given by as the equation of [17]:

$$\frac{d}{dt}\begin{bmatrix} ia \\ ib \\ ic \end{bmatrix} = \frac{Rs}{Ls}\begin{bmatrix} ia \\ ib \\ ic \end{bmatrix} + \frac{1}{Ls}\left(\begin{bmatrix} Vsa \\ Vsb \\ Vsc \end{bmatrix}\right) - \left(\begin{bmatrix} Va \\ Vb \\ Vc \end{bmatrix}\right) \tag{1}$$

By using Park's transformation in the equation (1), dq reference frame can be expressed as:

$$\frac{d}{dt}\begin{bmatrix} id \\ iq \end{bmatrix} = \begin{bmatrix} -\frac{Rs}{Ls} & \omega \\ -\omega & -\frac{Rs}{Ls} \end{bmatrix}\begin{bmatrix} id \\ iq \end{bmatrix} = \begin{bmatrix} \frac{1}{Ls} \end{bmatrix}\left(\begin{bmatrix} Vsd \\ Vsq \end{bmatrix} - \begin{bmatrix} Vd \\ Vq \end{bmatrix}\right) \tag{2}$$

$$i_{dq0} = Ti_{abc} \tag{3}$$

Where:

$$i_{dq0} = \begin{bmatrix} i_d \\ i_q \\ i_0 \end{bmatrix}, i_{dq0} = \begin{bmatrix} i_a \\ i_b \\ i_c \end{bmatrix} \tag{4}$$

$$T = \sqrt{\frac{2}{3}}\begin{bmatrix} \cos\theta & \cos\left(\theta - \frac{2\pi}{3}\right) & \cos\left(\theta + \frac{2\pi}{3}\right) \\ -\sin\theta & -\sin\left(\theta - \frac{2\pi}{3}\right) & -\sin\left(\theta + \frac{2\pi}{3}\right) \\ \frac{1}{\sqrt{2}} & \frac{1}{\sqrt{2}} & \frac{1}{\sqrt{2}} \end{bmatrix} \tag{5}$$

$\theta = \omega_s + \theta_0$, where θ_0 represents initial value in the equation of synchronous rotating angle.

B. *VSI Control Strategy of Microgrid Islanding Mode*

There are three types of DG energy source which are variable speed (wind energy), high frequency (Microturbines) and direct energy conversion source (fuel cell). Thus, it needs the VSI to interface the DG unit so that it can provide flexible operation. A power circuit of VSI based DG unit that had been connected with control structure.

To make microgrid in reliable operation, it is vital to ensure the transition from grid connected mode to islanding mode seen seamless and also keep a stable voltage and frequency regulation during islanding mode. The application to make the voltage and frequency within the threshold limit is shown in block diagram Figure 3. Microgrid Control Centre (MGCC) can defined locally the reference voltage and frequency values. Phase Locked Loop (PLL) application can measure the frequency that be given by:

$$V_{rms} = \sqrt{V_d^2 + V_q^2} \tag{6}$$

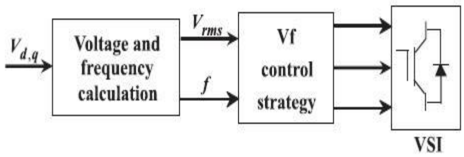

Fig.3. VSI base Vf power controller [18]

C. *Power Controller Strategy*

This power controlled strategy is to improve the quality of power supply by control the objective mode. Based on Figure 4, power controller is on the left side which the presence of two PI regulators. This controller generates two references current which are and . The control objective are achieved when slow change of reference current trajectory. Thus, it ensure that inverter output power is high quality. The main control objectives are to regulates voltage and frequency during islanding mode and load changes.Thus, Vf control strategy based on the PSO algorithm for the VSI based DG. During islanding mode and load changes, this controller regulates the voltage and frequency by the reference value of (V_{ref} and f_{ref}) and

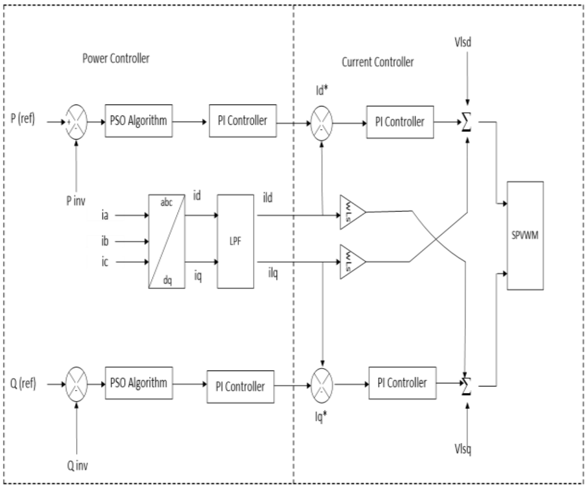

Fig.4. VSI base Vf power controller [19]

PSO acts as to provide optimum control parameters to give much optimum values of current vectors. Reference currents can be shows as [20]:

$$i_d^* = (V_{ref} - V)\left(K_{pv} + \frac{K_{iv}}{S}\right) \quad (7)$$

$$i_q^* = (f_{ref} - f)\left(K_{pf} + \frac{K_{if}}{S}\right) \quad (8)$$

D. Current Controller Strategy

This controller is to ensure that it can accurate tracking and short transient of the output current. Based on Figure 4, the right side of the model shows block diagram of the current control loop which the controls is based on the synchronous reference frame. The linear current controller based on SVPWM and open loop voltage type is utilised with the inner current feedback loop. This controller is usually used in a way that the voltage is applied to the inductive $R - L$ impedance, so that an impulse current in the inductor has a minimum error. The PLL block is required to detect the voltage phase angle in order to implement Park's transformation in the control scheme. Two PI regulators are used to eliminate current error, and both the inverter current loop and the grid voltage feed-forward loop are employed to improve the steady state and dynamic performance.

IV. Result and Analysis

The three phase model grid connected VSI system and the proposed controller are simulated by using Matlab/Simulink. The model are based on Fig. 4 and the PI controller is applied using Matlab/Simulink program. The parameter are defined as the table below. All the results are in per unit (pu) system.

Table 1. Model Parameters

Grid Parameters	
L_S	50mH
R_S	1.4Ω
f	50Hz
C	1500μF
DG Capacitor	5000μF
One DG unit Rating	50kW
Current Control Loop Parameter	
K_p	12.656
K_i	0.00215
SVPWM	
Switching Frequency	10kHz
Sampling Frequency	500kHz

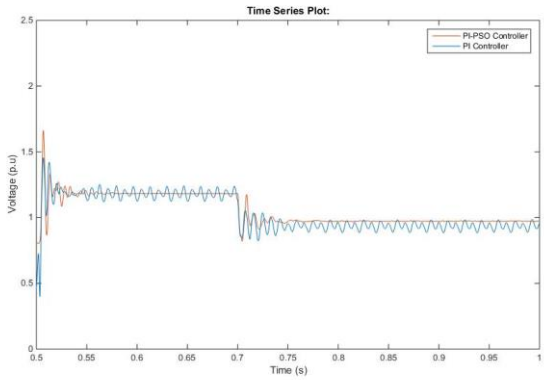

Fig.6. Microgrid voltage regulated by Vf regulator

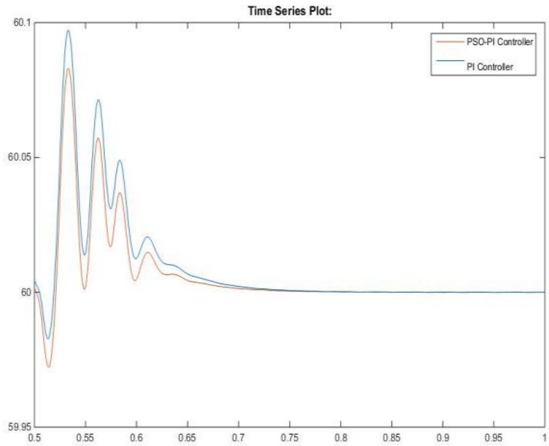

Fig.7. Microgrid voltage regulated by Vf regulator

The simulation at the beginning starts with grid connected mode as this period where the grid established the voltage and frequency. At 0.5s, the microgrid switched from the grid connected mode to islanding mode and at 0.7s the load of the system was increased to show that the variation of load changes in the system. The Vf power control mode based on PI controller and PSO algorithm adopts by DG unit in order to mitigate the voltage drop and unstable frequency due to islanding mode and load changes..

V_{ref} and f_{ref} of the proposed controller are set to 1.0 pu. Therefore as the result, Fig.6 and Fig 7 show the result of the controlled voltage and frequency and it shows the reaction between the proposed controller and PSO technique that had been applied. For example at 0.5s, the system are changing to islanding mode and it shows that frequency dropping at 0.52s. At this time, PSO algorithm playing its role by searching new power control parameters to make sure that the frequency are in the nominal threshold limit (±0.01p.u). Consequently, this processes act the same thoroughly during the islanding and load changes for voltage and frequency to make sure that both of voltage and frequency are between the respective nominal threshold limits.

V. Conclusion

In this paper, an optimal power control strategy has been proposed for an inverter based DG unit in order to improve the quality of the power supply in an autonomous microgrid operation. The proposed controller scheme consists of an inner current control loop and an outer Vf power control loop. The PSO algorithm has been incorporated into the Vf control mode to implement a real time self-tuning method in order to regulate the microgrid voltage and frequency, especially when the microgrid transits to the islanding operation mode or during load change. The simulation results show that the proposed controller offers an excellent response for regulating the microgrid voltage and frequency, and achieves short transient time. Consequently, this controller can be used by more than DG unit in a microgrid scenario.

VI. Acknowledgement

In the name of Allah the most mighty and the most merciful. Praise to All Mighty Allah for giving the opportunity for me to complete my degree and final year project within a certain period of time. Praise also to our prophet Muhammad, peace be upon him and his followers for showing the right path in my entire life.First of all, I would like to express my deepest gratitude to my supervisor, Prof. Ir Dr. Mohd Wazir Bin Mustafa for willingly accept and supervised me from the beginning until the end of my project. A big thanks to my mentor Mr Sajid Qazi for the guidance and encouragement in completing this project. Thanks to my parents and siblings for their motivation. Their encouragement and support made my journey by making this project enjoyable. To fellow colleagues, thanks for encouraging and gave me your time in helping me to do this project. I am pleased to have such wonderful people around me that made my world more meaningful.

VII. References

[1] D. E. Olivares, A. Mehrizi-Sani, A. H. Etemadi, C. A. Canizares, R. Iravani, M. Kazerani, *et al.*, "Trends in microgrid control," *IEEE Transactions on smart grid,* vol. 5, pp. 1905-1919, 2014.

[2] S. Heo, W. K. Park, and I. Lee, "Microgrid design with renewable energy sources and storage based on power conditioning system for autonomous island operation," in *2017 IEEE International Conference on Industrial Technology (ICIT)*, 2017, pp. 147-152.

[3] Z. Jizhong, "Optimization of power system operation," *United States,* 2009.

[4] I. Committee, "IEEE standard for interconnecting distributed resources with electric power systems," *New York, NY: Institute of Electrical and Electronics Engineers,* 2003.

[5] A. IZAM, "MODELLING HIGH PERFORMANCE AND OPERATION OF ANTI-ISLANDING PROTECTION DEVICE USING PASSIVE METHOD," UTM, 2015.

[6] M. Savaghebi, A. Jalilian, J. C. Vasquez, and J. M. Guerrero, "Autonomous voltage unbalance compensation in an islanded droop-controlled microgrid," *IEEE Transactions on Industrial Electronics,* vol. 60, pp. 1390-1402, 2013.

[7] S. Chowdhury and P. Crossley, *Microgrids and active distribution networks*: The Institution of Engineering and Technology, 2009.

[8] R. M. Strzelecki, *Power electronics in smart electrical energy networks*: Springer Science & Business Media, 2008.

[9] Q. Zeng and L. Chang, "Study of advanced current control strategies for three-phase grid-connected pwm inverters for distributed generation," in *Control Applications, 2005. CCA 2005. Proceedings of 2005 IEEE Conference on*, 2005, pp. 1311-1316.

[10] A. Schrijver, *Theory of linear and integer programming*: John Wiley & Sons, 1998.

[11] R. Byrd, J. Nocedal, and R. Waltz, "K nitro: An Integrated Package for Nonlinear Optimization," *Large-scale nonlinear optimization,* pp. 35-59, 2006.

[12] E. Díaz-Dorado and J. C. Pidre, "Optimal planning of unbalanced networks using dynamic

programming optimization," *IEEE Transactions on Power Systems*, vol. 19, pp. 2077-2085, 2004.

[13] M. Mohammadi, S. Hosseinian, and G. Gharehpetian, "GA-based optimal sizing of microgrid and DG units under pool and hybrid electricity markets," *International Journal of Electrical Power & Energy Systems,* vol. 35, pp. 83-92, 2012.

[14] W. Al-Saedi, S. W. Lachowicz, D. Habibi, and O. Bass, "Power quality improvement in autonomous microgrid operation using particle swarm optimization," in *Innovative Smart Grid Technologies Asia (ISGT), 2011 IEEE PES*, 2011, pp. 1-6.

[15] P. de Moura Oliveira, "Modern heuristics review for PID control," in *6th International PhD workshop on systems and control: a young generation viewpoint*, 2005, pp. 4-8.

[16] Q. Bai, "Analysis of particle swarm optimization algorithm," *Computer and information science,* vol. 3, p. 180, 2010.

[17] I.-Y. Chung, W. Liu, D. A. Cartes, and K. Schoder, "Control parameter optimization for a microgrid system using particle swarm optimization," in *Sustainable Energy Technologies, 2008. ICSET 2008. IEEE International Conference on*, 2008, pp. 837-842.

[18] W. Al-Saedi, S. W. Lachowicz, D. Habibi, and O. Bass, "Power flow control in grid-connected microgrid operation using Particle Swarm Optimization under variable load conditions," *International Journal of Electrical Power & Energy Systems,* vol. 49, pp. 76-85, 2013.

[19] W. Al-Saedi, S. W. Lachowicz, D. Habibi, and O. Bass, "Stability analysis of an autonomous microgrid operation based on Particle Swarm Optimization," in *Power System Technology (POWERCON), 2012 IEEE International Conference on*, 2012, pp. 1-6.

[20] W. Al-Saedi, S. W. Lachowicz, D. Habibi, and O. Bass, "Voltage and frequency regulation based DG unit in an autonomous microgrid operation using Particle Swarm Optimization," *International Journal of Electrical Power & Energy Systems,* vol. 53, pp. 742-751, 2013.

Wireless kWh Monitoring System for Residential Application

Mohamad Muslim Bin Rahim
Faculty of Electrical Engineering
Universiti Teknologi Malaysia
Skudai, Johor
muslimrahim94@gmail.com

Md Pauzi Abdullah
Department of Electrical Power Engineering
Faculty of Electrical Engineering
Universiti Teknologi Malaysia
Skudai, Johor
pauzi@fke.utm.my / mpauzi@utm.my

***Abstract*— Nowadays, the electrical energy usage is very high and the demand for electricity increased due to the modernity and technological advances. Therefore, the proper management and monitoring the electricity bill regularly can reduce the waste of electrical energy thereby reducing the negative impact to the earth. The project that has been conducted is a solution since this smart power meter able to read energy consumption and at the same time will display an electricity bills within domestic sector area. Microprocessor Arduino Uno, current detector SCT 013-000 and ESP8266 are the important device to develop this smart power meter. The programming that contain the calculations for the electricity and electric bill will be uploaded to the Arduino software to ensure the power meter can displays the desired information. In addition, the formula for the calculation of power and electricity bills referred to the latest TNB tariff. Then, the reading of electricity usage and electricity bills are focusing on overall energy usage in residential area. The energy and electricity bills will then be display on the LCD screen display. Besides, electricity readings and energy bills also can be displayed in the "Webpage" by the Ip address that has been set up from the beginning. The system that are used is a LAN (Local Area Network) which is computer network that interconnect computers within a limited area such as residence, school, laboratory, campus etc.**

Keywords—Arduino; LCD Display; ESP 8266; Current Sensor.

I. Introduction

The increasing of technology today due to the human need will lead to the creation of new electrical and electronic device. Since most of the new technology are using electrical as their main resource, it will lead to the usage of energy consumption and household power usage will increased drastically. This situation will contribute to the main problems of the modern world today which is the excessive energy consumption that will effect environment and also human being. For an example, huge amounts of energy consumption contribute to the pollution that leads to the ozone hole, which has a great deal with the greenhouse effect, that leads to the melting of ice and thus to the rise of sea levels and the extinction of rare species of fauna in the world.

Other than that, this problem also affecting the financial of the industrial and domestic use because usage of energy consumption are rapidly increasing and wasting the electricity was happen every year. This situation can be solve by reduce the energy consumption. To achieve that, an appropriate meter called Smart Meter is designed to solve this problem. Merely, the conventional power meter does not display the helpful information that can make the users aware about the electrical energy consumption. The result is users have very limited knowledge about the conventional power meter. Since the utility in Malaysia give one monthly reading for electricity use, the consumers cannot examine their electricity usage pattern. It is difficult for consumer to identify the source of energy use in homes in order to take effective action to reduce the future energy bills.

Consequently, this smart meter can display enough information to measure energy consumption and electricity bill and sent the information throughout the internet Wi-Fi at instantaneous time. The user will know how much they use the energy at any time and help them to realize the importance of reducing the energy used. Therefore, consumer can encourage themselves to reduce the electricity usage and understand clearly about the pattern of electricity usage.

II. Literature Review

A. Electrical Energy

Electrical power is an important resource required by the society for economic and daily activity since a lot advance technology and device today need electricity as a power supply. An electricity without interference proven that the component is difficult to be replaced to support a continued growth of economy [1]. In new era where dependency on science and technology always increase, in order to complete everyday routine, electricity energy become the most primary things needed in daily life. In other words, without electricity people, industry and most of the sector will having difficulty on their affair. The dependency of almost all fragments of the industry and different criteria of our life of electrical energy makes this enormous structure frame a strategic unit [2]. Besides, without electricity, internet and smartphone may not be used, security system and other appliances not working, at night building and house will be deserted without existence of electricity.

The amount of the electricity usage should be differ among the difference user. There are a few factors that lead to difference usage of electricity in a houses or building. This situation can be divided into 2 parts which is the type of appliances they use and how people living in the building use of these appliances [3]. Resident that used electrical equipment at a longer duration and those who use appliances with higher power rating will surely record a high energy consumption than the consumers that use appliances in a short duration and lower power rating. In fact, there is also other research that comes with the aim to develop a new sustainable electrical energy system for the individual consumer who can handle the problems and opportunities of the liberalized market [4]. The appliance's energy usage is calculated using the formula given below:

$$Daily\ Kilowatt\text{–}Hour\ (kWh\ )consumption= \frac{\text{Watt} \times \text{Hours Used Per Day}}{1000}$$

B. Smart Energy Meter

The smart power meter is an advanced energy meter that measures electricity consumption by providing the additional information for consumers rather than a conventional energy meter [5]. Smart energy meter is the application that can display the energy consumption and electricity billing which is operated based on the program uploaded to the microcontroller. In addition, it is often heralded as the key component supporting energy displays that can notify home occupants of their energy usage [6]. Smart energy meter are currently available in the market with a lot of design and speciation based on customer demanding. However, the price of these smart meter quite expansive and this application only can measure the energy consumption of the whole house with single phase only. They cannot tell which appliances in the household consume the most energy or are less efficient [7]. Due to that problem, a lot of research are done nowadays about displaying the electricity billing on smart energy meter and starting to be popular among the user. One of them is GSM Automatic Power Meter Reading where at the power provider side an eBilling system is used to manage all received SMS meter reading, compute the billing cost, update the database, and to publish billing notification to its respective customer through SMS, email, web portal and printed postage mailing [8]. Another application is using Arduino based wireless power meter. The difference is this application using an internet to transfer the data instead of SIM card. As a result, they can put the awareness on themselves and encourage people to do energy saving.

C. Existing Products on Markets.

There is a lot of product of Power Meter exist in the market. But, most of the product was came from developed countries such as Denmark, USA, Japan and many more. This is because the level of awareness about the energy waste and environmental problem was high. So that, a lot of device that contribute to the environment prosperity was develop including this energy meter.

III. METHODOLOGY

A. Project Method

Implementation of hardware and software are involved in this project. After studying from previous research that are related to this project, using Arduino Uno as a microcontroller is the best method to develop this project since Arduino Uno among simple and easiest device to handle. Besides, other component that are required for this project is current sensor, LCD display, potentiometer and esp8266. The first thing to do is writing the coding in Arduino software using the C programing language and uploaded it into the Arduino Uno. The instruction of programming language should be functioned same as the expected result based on the ATMEL ATmega328 8-bit microcontroller. USB cable is use to connect the Arduino Uno to the computer/laptop to ensure that the programming able to uploaded to the arduino Uno as mentioned above. A current sensor need to be connected to the Arduino UNO board through the analogue pin (A0). So that, the Arduino can reads the value of current from the current sensor and then pursue to the next step which calculating the value of the power used by load and billing price. Finally, the information of power and billing price will be send to the LCD display and web page. There must be an internet connection on the esp8266 and computer/laptop to display the information on webpage. To access the webpage, it will be given the Ip address that has been set up from the beginning.

B. Design Component.

The main component that are needed for this project are Arduino UNO, LCD display, current transformer, potentiometer, capacitor, resistor, voltage regulator and esp8266. All these components play an important role in this project. A minor component such as bread board, jumper, resistance and capacitance also the key to finish this project. The important is all these component are low cost, easier to purchase, easy to find and not dangerous for anyone who use these item. Besides, these component that are using for this project are simple connections easy to troubleshoot if anything is happening.

C. Arduino Uno

Arduino is a microprocessor incorporates most of the entire central processing functions on a single integrated circuit (IC) [9]. Arduino which is one of a microprocessor is a tool for making computers that can sense and control more of the physical world the desktop computer. An open-source single-board microcontroller, like the Arduino, acts as a light-weight brain for scientific automation-related tasks [10]. The platform is designed to be accessible to a wide range of students and easily adapted for other applications [11]. It is an open source physical computing platform based on a simple microcontroller board, and a development environment for writing software for the board [12]. Arduino also can be used to develop interactive objects, taking input from a variety of switches or sensors, and controlling a variety of light, motors and other physical outputs. Arduino projects can be stand-alone, or they can communicate with software running on the computer. The boards can be assembled by hand or purchased preassembled

Digital pin that use in this Arduino Uno for this project are 12, 11, 5, 4, 3, 2 and 16 which is connect directly to the LCD display. Meanwhile, analogue pin that use was (A0). This Arduino Uno have 5V and 3.3V pin. 5V is supplying LCD display and current sensor connection. ESP 8266 is get supply from 3.3V from Arduino which is cannot more than 3.3V or this device might be blown up. To make this Arduino project long lasting, this Arduino was supplied the power from the socket via AC-to-DC adapter..

IV. Result and Discussion

A. *Completed set up of Smart Energy Meter*

The smart power meter as shown in figure 1 was successful developed, so that it can be applied in distribution board, existence power meter in the house or any electricity appliance to measure the power used. Even though this device was safe to use by anybody, the user must take the precious step during conduct this device especially when clamping the current sensor on life wire. Based on figure below, adapter are used to supply the power to the device. Adapter was chosen because it was long lasting and can be used in long period of time. Compare to the other device such as battery or power bank, they need to be charge when they already out of power.

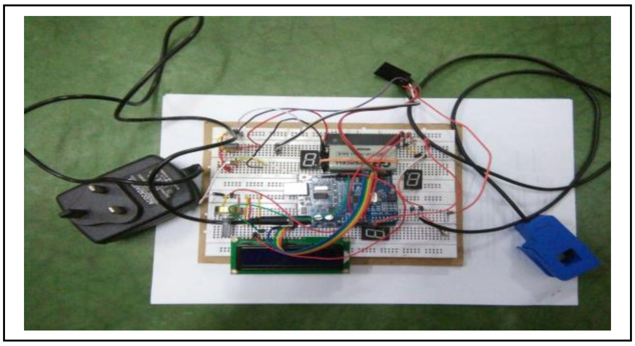

Fig 1: kWh Monitoring System

Since to apply this project to the existing energy meter quite hard, so that this power meter only can applied in two situation which is in distribution board and electricity appliance. Before conduct this project, make sure it is in good position and proper wiring connection to make sure the LCD clearly display, current sensor can detect the Irms current and ESP 8266 can connect wireless to the Wi-Fi. Figure 2 show the way to use this meter.

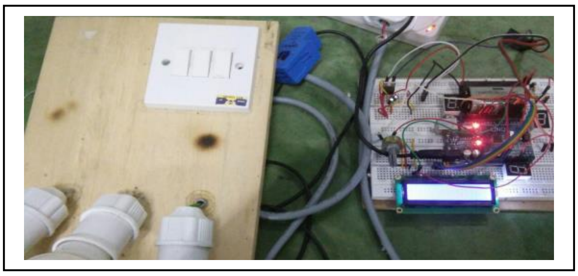

Fig 2:

Figure 2: Setup on Electrical Appliance

Connect the power meter to the adapter to turn it on. The power meter also should be calibrate in order to get the accurate current and power values. Then, clamp the current sensor carefully to the live wire of the appliance or distribution board. After that, turn on the load and let it measure the energy consumption and electricity billing from the load. The information of energy consumption and electricity billing can be seen directly at any time in LDC display. Besides, the user also can see the information form the web page as shown in figure 5 which is can access in the computer or hand phone as long there are in same internet connection.

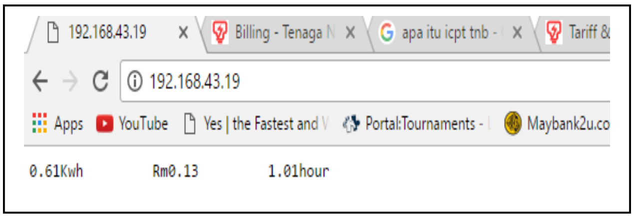

Fig 3: Interface of the web page to display the energy and billing price

B. *Energy consumption usage by selected appliance.*

There are five electrical appliance selected to be measure using this power meter. The information of energy consumption and billing price can be indicated from the LCD display and web page for every one minute. The selected appliance are three bulbs (rating: 180W), water heater (rating: 1900W), iron (rating: 1100W), hair dryer (rating: 1200W) and laptop charger (rating: 65W). The results are presented in Table 1 below.

TABLE 1.

NO	**STANDARD POWER(W)**	**M'METER READING(W)**	**KWH MONITORING METER(Wh)**		**ERROR (%)**
			30 MIN	**60 MIN**	
1	3 bulb (60W each)	243 x 0.79 = 191.79	90.52	181.79	-0.95
2	Water Heater	242 x 8.02 = 1940.84	952.50	1935.26	-1.86
3	Iron	241 x 4.9 = 1180.90	551.00	1133.52	-3.05
4	Hair Dryer	241 x 5.3 = 1077.3	501.09	1056.00	-4.67
5	Laptop Charger	240 x 0.28 = 67.2	32.50	65.70	-1.08

The data above show the comparison the power value of standard power, multimeter reading and kWh monitoring reading. The data was taken in 30 minute and 60 minute to get the absolute correction. The value of the standard power was already stated on the electrical appliance itself. For the multimete reading, it cannot directly get the value of power, but in separately way which is current and voltage. After that, multiple that both value to obtain the value power (W). To get value of current, the mutltimeter must be connect series on the live cable while value of voltage must be connect parallel to the load. Obviously, reading of kWh monitoring get from this project design using Arduino Uno.

The highest power and energy consumption is water heater. It take 1935W of energy in one hour. This appliance use high energy because it is heating element that are resistor made form copper. The second highest power is iron which is set in high temperature. Actually, the heating of the iron is not constant. The energy consumption depends on the temperature we are set. Electrical iron is just like another heating that has thermostat. Next is hair dryer that has heating element producing high energy followed by 3 bulbs and laptop charger.

Most of the electrical appliance have an error during conduct the experiment. The first one is this project is related to the internet, so that it may have some delay due to internet connection. Next is connection of the circuit on the proto board. The connection on the proto board is quite loose and easy to detach. This is due to the usage of several amounts of components without being soldered. Another error occurs is due to inaccurate reading. To overcome this problem, several readings are taken and the average value is calculated to get more accurate data.

V. Conclusion

In conclusion, this project was completely design and the objective has been achieve successfully. The development of this power meter was implemented and ready to use to get reading of power meter, so that it can show to the user how much they use the energy every day. Other than displaying the information on the LCD display, the user also can see the reading of power and billing price via computer or hand phone through the IP address that was given. Showing the electricity consumption and billing price is the best way to increase the consumers‟ awareness about the power usage, hence encourage them to reduce the energy consumption in their daily life. Managing energy consumption is an important element to be concerned nowadays since it is effecting the earth

Acknowledgment

Thank you to the lecturer who always giving the advice and idea to complete this project. Also thank to the UTM that a providing the facilities such as laboratory, component and others.

References

[1] Nagata, T. An electric power energy monitoring system in campus using an Internet. in Power Engineering Society General Meeting, 2006. IEEE. 2006.

[2] Pendram Samadi, Amir Hamed, Robert Schober, Vincent, and Juri, “Optimal real-time pricing algorithm based on utility maximization for smart grid,” Dept of Electric, British Columbia University, IEEE, 2010.

[3] Firth, S., Identifying trends in the use of domestic appliances from household electricity consumption measurements. Energy and Buildings, 2008 40: p. 926-936.

[4] A. Dusa, G. Deconinck, and R. Belmans, “Communication system for intelligent residential electrical installations,” Power Systems Conference and Exposition, 2004. IEEE PES. pp. 269–274 vol.1, 2004.

[5] S. S. S. R. Depuru, L. Wang, and V. Devabhaktuni, “Smart meters for power grid: Challenges, issues, advantages and status,” Renew. Sustain. Energy Rev., vol. 15, no. 6, pp. 2736–2742, Aug. 2011.

[6] S. Makonin, F. Popowich, and B. Gill, “The cognitive power meter: Looking beyond the smart meter,” Electrical and Computer Engineering (CCECE), 2013 26th Annual IEEE Canadian Conference on. pp. 1–5, 2013.

[7] M. Dong, P. C. M. Meira, W. Xu, and W. Freitas, “An Event Window Based Load Monitoring Technique for Smart Meters,” Smart Grid, IEEE Transactions on, vol. 3, no. 2. pp. 787–796, 2012.

[8] A. C. Tan, C. H. R. Lee, and V. H. Mok, “Automatic power meter reading system using GSM network,” Power Engineering Conference, 2007. IPEC 2007. International. pp. 465–469, 2007.

[9] P. Zhang, “CHAPTER 5 - Microprocessors,” P. B. T.-A. I. C. T. Zhang, Ed. Oxford: William Andrew Publishing, 2010, pp. 155–214.

[10] J. M. Pearce, “Chapter 4 - Open-Source Microcontrollers for Science: How to Use, Design Automated Equipment With and Troubleshoot,” J. M. B. T.-O.-S. L. Pearce, Ed. Boston: Elsevier, 2014, pp. 59–93.

[11] J. Sarik and I. Kymissis, “Lab kits using the Arduino prototyping platform,” *Frontiers in*

Education Conference (FIE), 2010 IEEE. pp. T3C–1–T3C–5, 2010.

[12] “What is Arduino.” [Online]. Available: https://learn.sparkfun.com/tutorials/what-is-an- arduino. [Accessed: 10-Nov-2013].

Optimal Location of Distributed Generation for Voltage Profile Improvement in Radial Distribution using Particle Swarm Optimization

Muhammad Mustaqim Bin Azaman
Faculty of Electrical Engineering
Universiti Teknologi Malaysia
Johor Bahru, Malaysia.
Mustaqim11.azaman@gmail.com

Mohd Hafiz Habibuddin
Faculty of Electrical Engineering
Universiti Teknologi Malaysia
Johor Bahru, Malaysia.
mhafiz@fke.utm.my

***Abstract*— This journal presents the impact of penetrating the distributed Generator (DG) on voltage profile in the distribution system. Remote area or rural places are having the problem in getting the electricity. The efficiency of distribution system is not good enough to provide the electric utility to rural area. Long distance between the power supply and rural area is the factor that cause the people not getting enough electricity. The DG technology is one of the solutions which give many positive effects like voltage profile improvement, thus can improve the efficiency of the system. However, the installation of DG at non optimal places can result bad effect to the system. In this journal, 33-bus radial distribution system is tested using Newton Raphson method and particle swarm optimization (PSO) to find the optimal location of the DG. Fixed size of type 1DGs are used in order to know the impact to the voltage profile. The system is simulated in Matlab simulation and analyse the voltage profile. The simulation results show the optimal place of DG will improve the voltage profile within the acceptable limit.**

Keywords— Distributed generator, Voltage profile, PSO, Matlab, Rural area

I. INTRODUCTION

The electrical power system is divided into 3 main systems which are generation system that provide the power, the transmission system that carries the power from generating centre to load centre and lastly the distribution system that distributed the power to all homes and individual customers.

The distribution system is the crucial part where it is the link in between the utility system and customers. As a result, the usage of the Distributed Generator (DG) is increasing everyday in order to improve the efficiency of providing electric power. DG can be defined as a small scale generation and it is active power generating unit that is connected at distribution level [1]. The usage of DG was implemented in many countries all around the world such as Malaysia, Spain, Argentina and United States (US) [2]. There many technologies used by the distributed generator such as fuel cell, micro turbine, wind turbines and photovoltaic (PV) [2]. In Malaysia, the inverter based DG such as PV is the most popular because of the availability of the sunlight [3]. There are some issues in the distribution system such as voltage drop and power losses that can be solved by penetrating the DG.

II. LITERATURE REVIEW

A. Distribution Generation

DG has becomes significant and a trend in the electricity industry, market, and power systems around the world. However, till now the definition of the DG is not consistent and from the most literatures, there are some definitions that can be considered common [4]. The DG also known as decentralized generation, dispersed generation and embedded generation [4-5]

The operation and installation of electric power generation units connected directly to the distribution network or connected to the network on the end user site of the meter is defined as the location of distributed generation [1]. Besides, Institute of Electrical and Electronics Engineers (IEEE) stated that the generation of electricity by the facilities sufficiently smaller than central plants, so as to allow interconnection at nearly any point in power system is known as distributed generator [6]. The rating the generation is up to 50MW [6].

The traditional power system does not include the distributed generator (DG) in distribution network and the power system nowadays uses the benefits of DG wisely. There are many technologies of DG that already implemented in many countries such as micro-turbine in Argentina, fuel cell in Spain and wind turbine in United States (US) [4]. The uses of renewable energy such as solar energy and wind energy as the sources of DG increase the interest of many countries to use the DG. The penetration of DG in the distribution system can improve the voltage profile, reduce power losses and improve the power quality [7]. The benefits of the DG are not guaranteed as long as the research and study about the optimal location and size of the DG are not done yet.

B. Benefits of DG

There are many benefits of using DG compare to the method in order to improve the efficiency for providing electricity to customers. The benefits of using DGs include environmental, economic and technical benefits [8].

Firstly, for environmental impact, the DG also uses the renewable energy as the sources. The renewable energy means it's green, clean and absolutely does not affect the environment. The renewable energy such as solar energy and wind energy are used widely all around the world.

Then, for economical point of view, the DG can supply small scale generation enough for customer by installing the DG in the certain location near to customers, thus it can reduce or avoid the need for building new transmission and distribution (T&D) lines, upgrade the existing power systems and reduce T&D networks capacity during planning phase [4]. The flexibility locations of DG also give positive impact in term of cost.

Lastly, for technical benefit, the DG can improve voltage profile, power quality and power losses reduction [9]. The reliability of power system increase as it can reduce the people affected when the failure of grid happen because the DG only use the microgrid [10].

C. *Types of DGs*

The types of distributed generator are divided into two, renewable energy and nonrenewable energy. The most common technologies of DG used nowadays are fuel cell, microturbine, and photovoltaic (PV) and wind turbine [11]. Besides, the types of DG also can be categorized as [12]

- Type 1: DG only capable of injecting real power, like PV and fuel cell.
- Type II: DG only capable of injecting reactive power, like compensator.
- Type III: DG capable of injecting both real and reactive power, like synchronous machine.

D. Particle Swarm Optimization

In 1995, Particle swarm optimization was first developed by Kennedy and Eberhart as an optimization method for continuous nonlinear functions [13]. The concept of the method is inspired by the social behavior of animals. The PSO is similar to the continuous GA as the random population process is the first step. The different between PSO and GA is the PSO does not contain evolution process such as crossover and mutation.

Each member of PSO population is called particle and each particles has a velocity and position. The position of a particle is a candidate solution and by using the current velocity, each of iteration is updated. Fitness function measures the quality of the position. The local best position is basically from the experience of each particle while the experience of the swarm is captured by the global best position [14]. Particle moves to new location based on the experience and the quality of new position. The formula of particle velocity and new position of particle are [15-16]:

$$V\ new = V\ old - c1 \times r1 \times (P\ local - P\ old) + c2 \times r2 \times (P\ global - P\ old) \quad (1)$$

$$P\ new = P\ old + V\ new \quad (2)$$

Where:

V new= New particle velocity
V old= Old particle velocity obtained in previous iteration
P new= New particle variables
P old= Old particle variables obtained in previous iteration
r1, r2= Are independent uniform random numbers
c1, c2= Learning factors
P local= Best solution found in previous iteration
P global =Best solution ever found the calculation

III. METHODOLOGY

A. *Model Radial Distribution System*

Fig. 1 shows system used in this project which is IEEE 33 bus radial distribution system. The characteristic of the system is [17]:

1) Number of bus = 33
2) Number of lines = 32
3) . Slack bus = bus 1
4) Base voltage=12.66KV
5) Base MVA=100MVA.

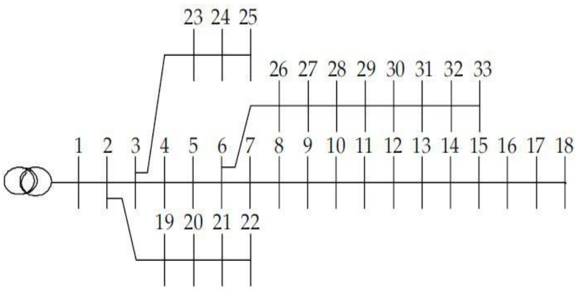

Fig.1. 33 Bus Radial Distribution System

B. Flowchart of the PSO

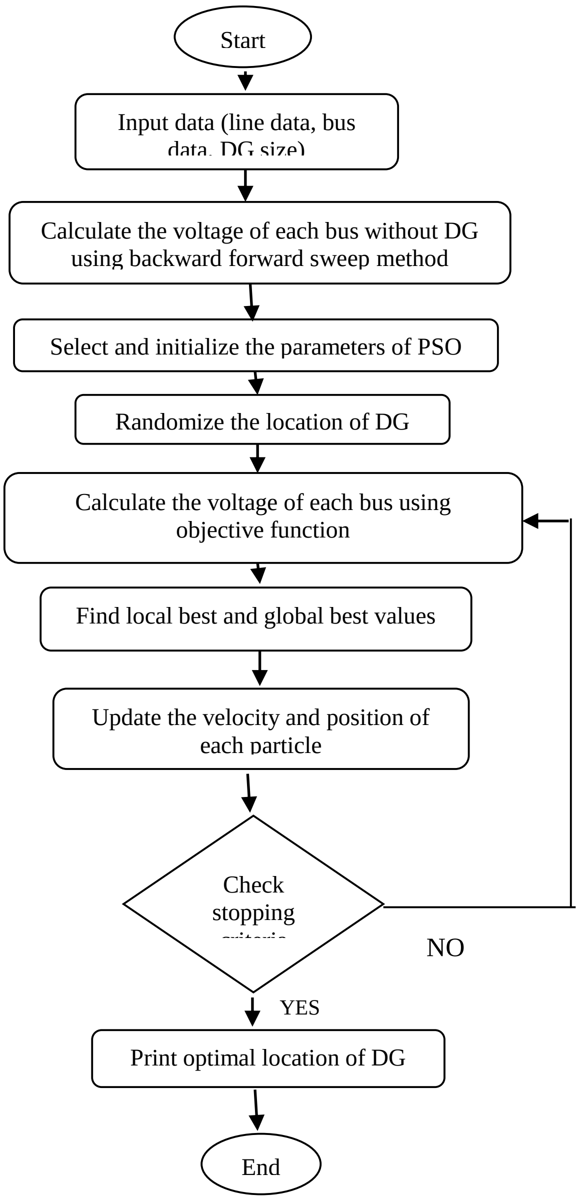

Fig 2. Flowchart of PSO

TABLE I Parameter of PSO

Parameter	Value
Population Size	50
Maximum iteration	100
Constriction factor c1 c2	2

The PSO technique will applies to the project in order to find the optimal place of the DG. First, the input data of 33bus radial distribution system such as line data and bus data are determined. The DG size which is 2MW and the limit voltage also are set before calculate the voltage of each bus using backward forward sweep method. Then, the parameters of PSO are initialized as shown as in Table I. The parameters of the PSO are population size, acceleration constants and inertia weight. The PSO process starts with a random population and random size of DG. After that, the objective function is designed for PSO. The voltage of each bus will be calculated using the objective function.

It proceeds with the update of velocity and new position of the particle. The best solution is recorded at each iteration. It is called the local best solution. All best solutions in the record are compared with each other and the best one is called the global best solution. These values have influence on the velocity and how particles move in the next iteration. The process proceeds until an assigned number of maximum iterations are met. The flow of method is shown in Fig. 2.

C. Objective Function

The objective of this work is to improve the voltage profile by putting the DG at the optimal place.

$$F = \sum_{1}^{n}(Vi - V_{ref}) \quad (3)$$

Where V_i = voltage at with DG

V_{ref} = voltage without DG

The constraint for PSO or limit for the voltage of each bus. The minimum voltage is 0.93p.u and the maximum voltage is 1.07p.u.

$$0.93\text{p.u} \leq Vi \leq 1.07p.u$$

IV. RESULT AND DISCUSSION

The proposed method to find the optimization is Particle Swarm Optimization (PSO). It is tested at the 33 bus radial distribution system. The size of t6he DG is fixed at 2MW which is approximately 53% of real power demand. The total load of the system is 3.715MW and 2.3MVAR

Two cases are analysed, case I and case II. Case I is the result of voltage of the system without DG and it was a reference case. Case II is the result of voltage when the DG was put at the optimal location using PSO method. The optimal location from the PSO algorithm is at Bus 6. Table II shows the voltage of each bus case I and case II. The results show that a significant voltage profile improvement after the installation of DG units in the system.

TABLE II Voltage of 33 Bus system with and without DG

No bus	Voltage without DG (case I)	Voltage with DG (case II)	No bus	Voltage without DG (case I)	Voltage with DG (case II)
1	1	1	18	0.9134	0.9436
2	0.997	0.9983	19	0.9965	0.9978
3	0.983	0.991	20	0.9929	0.9942
4	0.9755	0.9885	21	0.9922	0.9935
5	0.9682	0.9863	22	0.9916	0.9929
6	0.9498	0.9793	23	0.9794	0.9874
7	0.9463	0.9758	24	0.9727	0.9808
8	0.9415	0.9711	25	0.9694	0.9775
9	0.9352	0.965	26	0.9479	0.9774
10	0.9294	0.9594	27	0.9453	0.975
11	0.9286	0.9585	28	0.9339	0.964
12	0.9271	0.9571	29	0.9257	0.9562
13	0.921	0.9511	30	0.9222	0.9528
14	0.9187	0.9489	31	0.918	0.9487
15	0.9173	0.9475	32	0.9171	0.9478
16	0.916	0.9462	33	0.9168	0.9475
17	0.914	0.9442			

The voltage profile of the bus system with and without DG installation is illustrated in the Fig. 3. From the graph, the voltage profile of each bus is increase when the DG is installed. The lowest voltage before installation of DG is at bus 18 with 0.9133p.u. When the DG was put at bus 18, the lowest voltage profile is at bus 15 and 33 with 0.9475p.u. Installation of DG at the optimal place can improve the voltage profile of the bus system. The objective function was designed for PSO in order to find the optimal location of DG. The limit of the voltage also was determined to make sure the voltages that were got from the load flow is within the limit. Table III shows the comparison of the lowest voltage of each case.

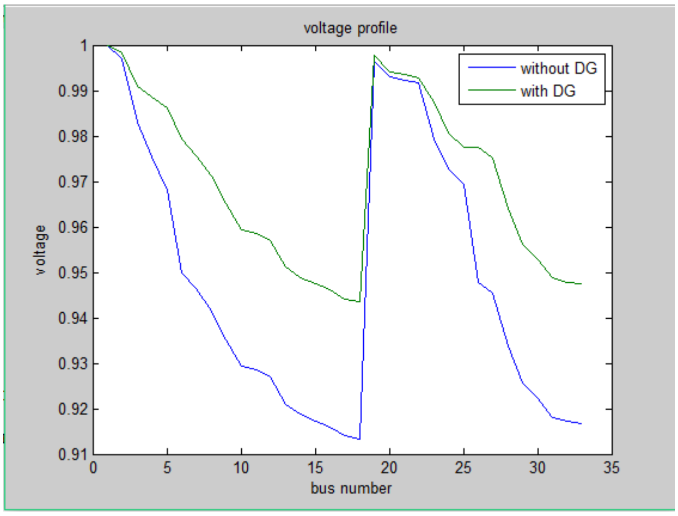

Fig 3. Voltage Profile of the System

TABLE III Comparison of Lowest Voltage

Case	DG Size	Location Bus	Lowest Voltage
I (without DG)	-	-	0.9133p.u @bus 18
II (with DG)	2MW	6	0.9475p.u @bus 15 and bus 33

V. CONCLUSION

Injection of the DG to the 33 bus radial distribution system is the crucial factor for voltage profile improvement.

Newton Raphson method is the method used to analyse the load flow of the system. The PSO algorithm is the proposed method to find the optimal location for the DG. An objective function is the important part in PSO algorithm to achieve the goal. The goal of the proposed method is to minimize the objective function and the bus 6 is the best or optimal location for the DG. 2MW of DG was put to the system and the voltage profile was analysed. The methodology used in this thesis can analyse the voltage profile before and after the penetration of the DG. A graph was plotted to compare the voltage profile with and without DG. The lowest voltage of the bus is increase from 0.9133p.u to 0.9475p.u. The method using PSO is very fast, simple and efficient. Therefore, by putting the DG at the optimal place can improve the voltage profile of the system.

REFERENCES

[1] Holtmeyer, M. L., Wang, S., & Axelbaum, R. L. (2013). Considerations for decision-making on distributed power generation in rural areas. Energy Policy, 63, 708-715.

[2] Duong Quoc Hung, NAdarajah Mithulanathan, R.c. Bansal " Analytical Expressions for DG Allocation in Primary Distribution Networks" IEEE Transactions On Energy Conversion, Vol. 25, No.3, Septembert 2010

[3] J. Kennedy and R. Eberhart. (1995). "Particle Swarm Optimization Proceedings". IEEE international conference on Neutral Network, 4, pp. 1942-1948.

[4] Reddy, S. C., Prasad, P. V., & Laxmi, A. J. (2012). Power quality and reliability improvement of distribution system by optimal number, location and size of DGs using Particle Swarm Optimization. 2012 IEEE 7th International Conference on Industrial and Information Systems (ICIIS).

[5] G. Celli, E. Ghaiani, S. Mocci, F. Pilo, " A Multiobjective Evolutionary Algorithm for the Sizing and Sitting of Distributed Generation, " IEEE Transactions on Power System, Vol. 20, 2005.

[6] H.L. W illis, "Analy tical Metho ds and Rule s of Thumb for Modeling DG Distribution Interaction," Proc. 2000 IEEE P ower Engineering Society Summer Me eting, Vol. 3, Seattle, WA, pp.16 43-1644, 200 0.

[7] X. Wu, Y. Wang, and T. Zhang, "An improved gapso hybrid programming algorithm," in 2009 International Conference on Information Engineering and Computer Science. IEEE, 2009, pp. 1–4

[8] Ackermann, T., Andersson, G., & Söder, L. (2001). Distributed generation: A definition. Electric Power Systems Research, 57(3), 195–204.

[9] Castilla, M., Mercado, P., Negroni, J., Gomes, M., Moreira, C., Sosa, J., & Souza, A. C. (2014). The growing state of distributed generation and microgrids in the Ibero-American region: A view from the RIGMEI network. 2014 IEEE PES Transmission & Distribution Conference and Exposition - Latin America (PES T&D-LA)

[10] Tang, J., Busrah, A., Hussin, A., & Wanik, M. (2014). Power system study for Distributed Generation interconnection to distribution network- A Malaysian case study. 2014 IEEE International Conference on Power and Energy (PECon).

[11] El-Khattam, W., & Salama, M. (2004). Distributed generation technologies, definitions and benefits. Electric Power Systems Research, 71(2), 119-128.

[12] Lopes, J. P., Hatziargyriou, N., Mutale, J., Djapic, P., & Jenkins, N. (2007). Integrating distributed generation into electric power systems: A review of drivers, challenges and opportunities. Electric Power Systems Research, 77(9), 1189-1203.

[13] Pepermans, G., Driesen, J., Haeseldonckx, D., Belmans, R., & D'Haeseleer, W. (2005). Distributed generation: definition, benefits and issues. Energy Policy, 33(6), 787-798.

[14] Marneni, A., Kulkarni, A., & Ananthapadmanabha, T. (2015). Loss Reduction and Voltage Profile Improvement in a Rural Distribution Feeder Using Solar Photovoltaic Generation and Rural Distribution Feeder Optimization Using HOMER. Procedia Technology, 21, 507-513.

[15] Abdel-Ghany, H. A., Azmy, A. M., Elkalashy, N. I., & Rashad, E. M. (2015). Optimizing DG penetration in distribution networks concerning protection schemes and technical impact. Electric Power Systems Research, 128, 113-122.

[16] Balamurugan, K., Srinivasan, D., & Reindl, T. (2012). Impact of Distributed Generation on Power Distribution Systems. Energy Procedia, 25, 93-100.

[17] Kuang, H., Li, S., & Wu, Z. (2011). Discussion on advantages and disadvantages of distributed generation connected to the grid. 2011 International Conference on Electrical and Control Engineering.

Voltage Sag Analysis in Distribution System Cause by Faults

Muhammad Amirul Izwan Bin Kamarudin
Faculty of Electrical Engineering
Universiti Teknologi Malaysia (UTM)
Johor Bahru, Malaysia
amirulizwann11@gmail.com

Zaniah Binti Muda
Department of Electrical Power Engineering
Faculty of Electrical Engineering
Universiti Teknologi Malaysia (UTM)
Johor Bahru, Malaysia
zaniah@fke.utm.my

***Abstract*— Nowadays, power quality is one of the most important aspects in power industry. There are numerous types of power quality issues but voltage sags became a major concern to the customers because it is one of the most harmful power quality disturbances. Voltage sag is sudden reduction of voltage, followed by a voltage recovery after a short period of time. Many industrial customers using sensitive equipment suffer a huge loss because of sag. Therefore in this project, the influences and consequences of voltage sags towards industrial customers will be verified. The radial distribution network is modeled by using the IEEE 13 Node Test Feeders. The voltage sag analysis is done using the PSCAD software that performing a fault simulation. The fault that will be simulated in this project is Single Line to Ground Fault and Three Phase Fault. Faults are introduced at various points in the system, which is near the buses and along the lines. Simulation covered on two parts which are simulation on normal condition and simulation on fault condition. There are 9 output voltages from the simulation results that were observed and analyze. From the simulation and analysis, voltage sag problems can be solved and mitigated thus provides a good power quality to the electrical system.**

Keywords—power quality; voltage sag analysis; chracterization; distribution system; fault location

I. Introduction

Malaysia is one of the developing countries in the world. Most the equipment used in the industrial process is high technology. In other to ensure the efficiency and productivity of the equipment, the good power quality need to be supplied and due from that, power quality become one of the main concern aspects in a power system nowadays. Most of the equipment or loads used in the industry are very sensitive to the power quality. The low power quality or power disturbances cause the sensitive equipment become malfunction and stop the operation process. It also can lead to financial losses and give the bad impact to the economy. Based on the Institute of Electrical and Electronics Engineers (IEEE), there are seven power quality disturbances which are transients, short duration variation, long duration variation, voltage unbalanced, waveform distortion voltage fluctuation, and frequency variation[1].Voltage sag is one of the most harmful power quality disturbances. Voltage sag is sudden reduction of voltage, followed by a voltage recovery after a short period of time. The faults occurred in the distribution system are the main cause of voltage sag. The MS IEC 61000 series define voltage sag as a sudden reduction in voltage to a value between 90% to 10% of nominal voltage, for duration of 10 ms. According to the IEEE Standard 1159-1995, the term “sag” is defined as a decrease in rms voltage to values between 0.1 to 0.9 p.u., for durations of 0.5 cycles to 1 min. Voltage sag becomes one of the most concern issues nowadays because it has a great economic and costly impact to the industrial customers. So, it is very important to have awareness about the consequences of voltage sag by analyzing their characteristics. To obtain the analysis of voltage sag in distribution system, PSCAD software is used to carry out the present study. This software is suitable to do the analysis about voltage sag happened in the distribution system.

II. Characteristics of Voltage Sags

Voltage sag is defined as a decrease in rms voltage at the power frequency for durations of 0.5 cycles to 1 minute. There are two aspects which is very important to determine voltage sag which is the rms voltage and duration. Sag magnitude is defined as the remaining voltage during the event. The reduction in rms voltage and the duration of the event are the main characteristics. This characterization is fine for single phase systems and three-phase balanced faults. In this instance the most affected phase is taken as sag magnitude [2]. These values can be determined by rms plots of the sampled data as shown in Figure 1. However, several studies have shown that some other characteristics associated with sags, such as phase-angle jump, point-on-wave of initiation and recovery, waveform distortion and phase unbalance, may also cause problems for sensitive equipment [2]. The magnitude of the voltage sag is determined by the position of the observation point (pcc) in relation to the site of the short circuit and the source of supply. The system can be represented by a simple equivalent circuit connecting the observation point to a single equivalent source and to the site of the fault as shown in Figure 2. The entire voltage (100%) is dissipated over the impedance between the source and the short circuit. The voltage drop to the observation point depends on the relative magnitudes of the two impedances connecting that point to the source and the short circuit. Depending on these impedances, the depth of the voltage sag can be anywhere in the range 0% to 100% [3].

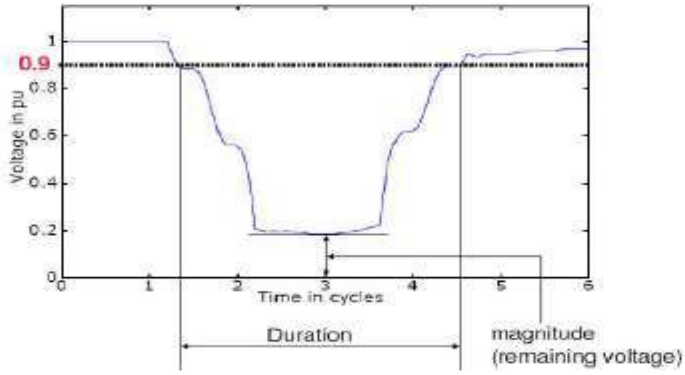

Fig. 1. RMS plot of simulated waveform showing sag magnitude and duration

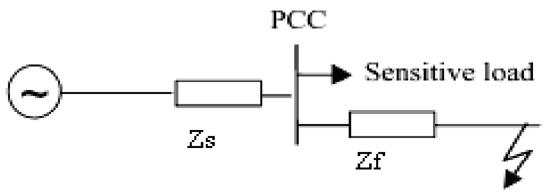

Fig. 2. Voltage divider model for sag magnitude calculation

$$V_s = \frac{Z_f}{Z_s + Z_f} E \qquad (1)$$

where:

Zf=Fault Impedance =

Zs=Source Impedance

E=Source

III. Causes of Voltage Sags

There are many cause of voltage sag which is fault on the transmission or distribution system, starting of large electric motor and transformers energizing [4].Voltage sags are typically caused by fault. Voltage sags can generally be characterized by sag magnitude, duration, and frequency [5].There are various fault occurred in power system that can lead to different type of sag such as single phase sags, phase to phase sags and three phase sags. The location of fault happened on a distribution system affects the magnitudes of the voltage. If the fault occurs near to the bus, the large magnitude of the voltage sags will be produced. Besides that, the magnitudes of the voltage sags are also depending on the fault impedance, pre-sag voltage level and the system configuration that is the system impedance and the transformer connections.

A. *Single Phase Sags*

Most of the fault occurred in utility system is single line to ground faults [6]. The lightning strike, tree branches and animal contacts is a fault that can produce single phase sag. The bus at substation will have a voltage drop and affect the others feeder that connected at the same bus. The voltage is back to normal if the faults were cleared.

B. *Three Phase Sags*

This type of system fault can be caused either by switching or tripping of a three phase circuit breaker. Switch or recloser also can create three phase voltage sag on other feeders from the same substation. Since it is three phase sag, the magnitude of each phase will be same. Consequences and Influences of Voltage Sag

IV. Consequences and Influences of Voltage Sags

Voltage sag is one of the power quality problems that happened in power system and it can give a very bad impact to the industrial customers. The equipment such as variable speed drive controls, motor starter contactor, robotics, programmable logic controller (PLC), controlled power supplies, and control relays that used in the industry is very sensitive to voltage sag [7]. Normally voltage sag does not cause damage to the equipment, but it can easily disrupt the operation of sensitive loads [8]. Due to its sensitivity, the equipment will trip and stop the operation and production of the product which result a major loss in term of money and time. Table I shows the equipment sensitivity that used in the industry. Different equipment has different sensitivity to voltage sag. For example, the machine that uses electricity to function will caused computer crashes or equipment lock-ups [9]. For personal computers, when voltage sag occurred, the data in volatile memory will totally loss and give a big problem to the user. Relays and starters that located in motor starters are very sensitive to voltage sag and operation process will stop when the voltage drop to 50% from normal operating voltage.

TABLE I. Typical Equipment Sensitivity [9]

Type of Equipment	**Remaining Voltage (%)**	**Time Duration (ms)**
Motors starter	50	40
Variable Speed motor with electronics	85	90
PLC I/O Device	50-90	8-20
Frequency inverter	82	1.5
Variable speed drive rectifier	50-80	2-3
Process controller	70	<8
Computerized numerical controlled lathe	70	<8
Direct current drive controller	88	<8
Personal computers	50-70	60-160
Contactors	50-60	20-30
Electromagnetic disconnecting switch	50	10
Electromagnetics relays	50-60	15-40
Medical equipment	60	130
Servo drives	80	50
Laser marker	90	100

V. VOLTAGE SAG ANALYSIS METHODOLOGY

The method used in the voltage sag analysis is described as below:

1. Choose a network for voltage sag analysis.
2. Use a model of IEEE 13 Node Test Feeder for the network.
3. Simulate the circuit and record the voltage magnitude. The recorded data will be the pre-sag values of voltage magnitude during normal condition.
4. Create and apply single line to ground fault and three phase fault at various locations.
5. For single line to ground fault simulation, create single line to ground faults for phase A at various points in the network and record the value of its voltage magnitude for 9 output voltages.
6. For three phase fault simulation, create three phase faults at various points in the network and record the value of its voltage magnitude for 9 output voltages.
7. Analyze the voltage sag occurred at monitoring equipment both faults.

VI. DESCRIPTION OF THE TEST SYSTEM

For this project, it will only focus on the distribution networks with radial systems. The IEEE 13 Node Test Feeders is used as a reference for distribution system. The performance study of sample system is carried out for detection and characterization of voltage due to power system faults. It is assumed that there are 9 faults are introduced at various points in the system, which is near the buses and along the lines as shown in Figure 4, and the fault duration is from 0.2 seconds to 0.3 seconds. There are 9 monitoring equipment are installed at the pcc that will produce 9 output voltages for each fault as shown in Figure 5.

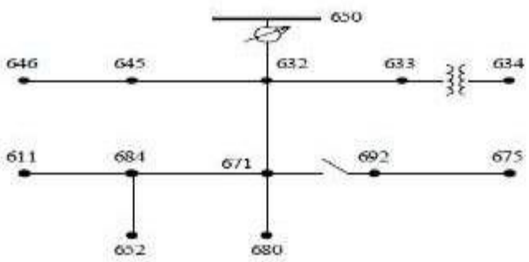

Fig. 3. Schematic Diagram of IEEE 13 Node Test Feeder

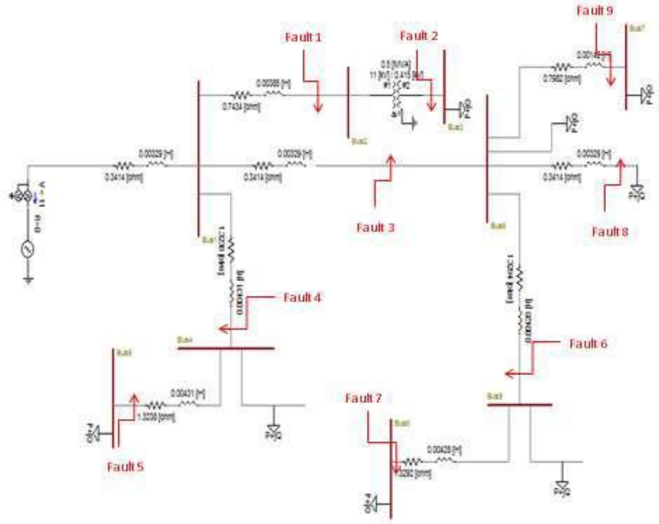

Fig. 4. IEEE 13 Node Test Feeder Circuit with Fault

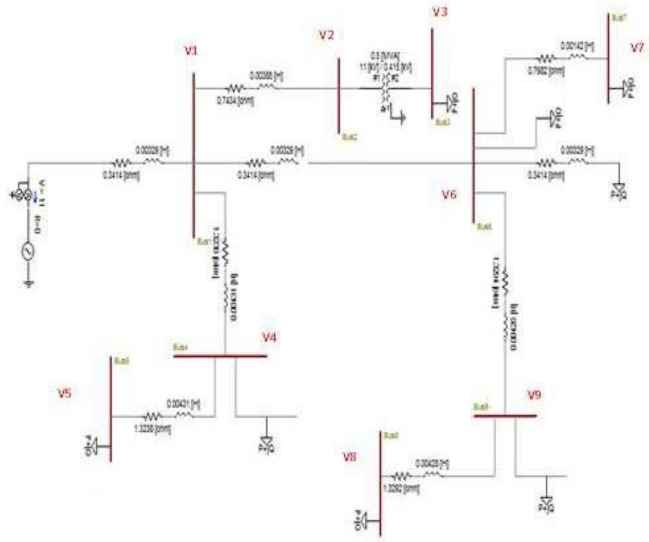

Fig. 5. Location of monitoring equipment

VII. SIMULATION RESULTS AND DISCUSSION

Simulation covered on two parts which are simulation on normal condition and simulation on fault condition. There are 9 output voltages from the simulation results that were observed and analyze in this project. These locations were selected in other to determine the effect of distance and fault location on voltage sags. The types of faults considered for the simulation were the single phase to ground fault and three phase fault.

A. *Normal Condition*

Simulation on normal distribution shows that all output rms voltages were approximately to the rated rms voltages. For 11 kV, the variation of nominal voltage is maintained within permissible limit which is ±5% and the variation of nominal voltage for 415V is maintained within -10% and +5%. Figure 5 shows the voltage waveform of V1 and Figure 6 shows the rms output voltage of V1. Since there is no fault occurred on the system, the voltage waveform and rms voltage are not affected. Table II shows the voltage at another 9 location during a normal condition. The voltage is maintained within a permissible limit for both 11kV and 415V [9].

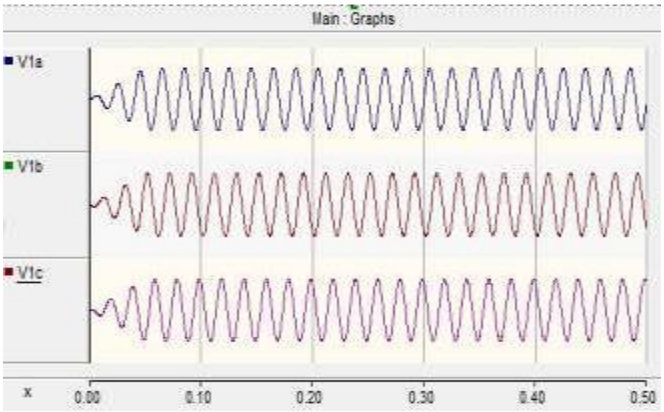

Fig. 6. Voltage Waveform of V1

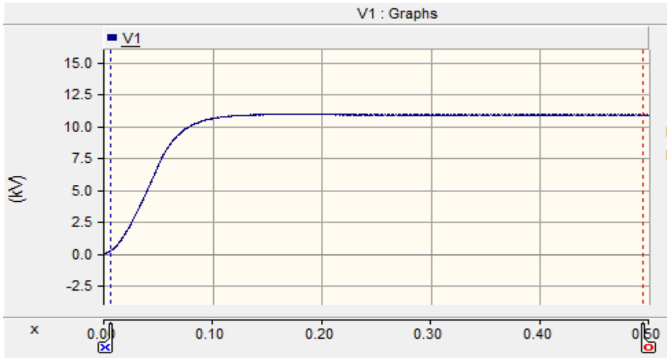

Fig. 7. RMS Output Voltage of V1

TABLE II. OUTPUT LINE RMS DURING FAULT 1

Output Line rms (kV)	
V1	10.906
V2	10.881
V3	0.403
V4	10.811
V5	10.742
V6	10.841
V7	10.834
V8	10.747
V9	10.780

B. *Single Line to Ground Fault*

Distribution circuit during fault was simulated to verify that the output line rms will drop during single line to fault. There are 9 simulations on fault condition that produced a total of 9 graphs of output voltages. For simulation, it is assumed that a single phase fault has appeared on phase A. The instantaneous voltages waveform of V1due to Fault 1 is shown in Figure 8 and Figure 9 shows the output line rms of V1 during Fault 1. The other values of rms output voltages during Fault 1 are transmitted into Table III.

The voltage on the faulted phase drops from a nominal values at the fault location, whereas the other two phase voltages remain more or less unchanged. This results in unbalanced voltage sag between phases. This imbalanced voltage sag is then transferred down to the equipment terminals within the industrial system. The sag experienced by the equipment is different to that observed on the utility network or service entrance due to the influence of the load in the industrial distribution system [10].

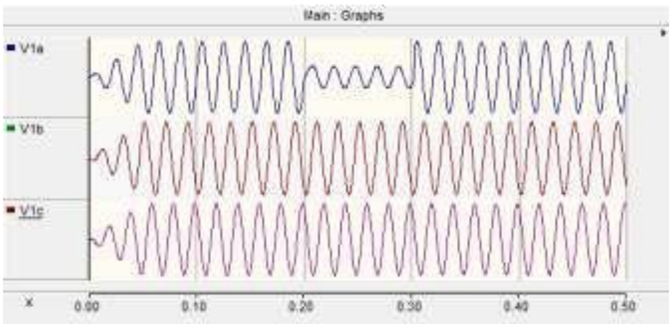

Fig. 8. Voltage Waveform of V1 during Fault 1

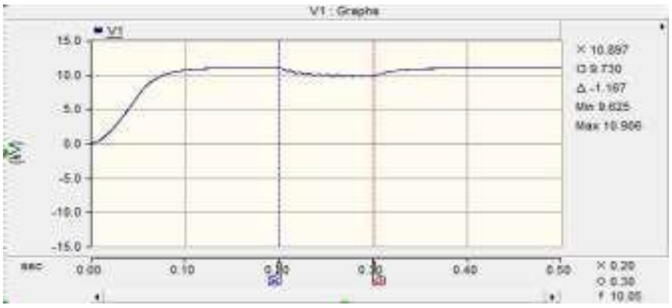

Fig. 9. Output Line rms of V1 during Fault 1

TABLE III. OUTPUT LINE RMS DURING FAULT 1

Output Line rms (kV)	
V1	9.625
V2	8.088
V3	0.294
V4	9.523
V5	9.467
V6	9.552
V7	9.543
V8	9.430
V9	9.473

TABLE IV. OUTPUT LINE RMS FOR ALL FAULT

Fault / Voltage rms (kV)	Fault 1	Fault 2	Fault 3	Fault 4	Fault 5	Fault 6	Fault 7	Fault 8	Fault 9
V1	9.625	10.831	9.419	9.849	10.182	10.019	10.264	9.784	9.804
V2	8.088	10.798	9.396	9.824	10.157	9.994	10.238	9.759	9.779
V3	0.294	0.395	0.344	0.360	0.372	0.366	0.375	0.357	0.358
V4	9.523	10.717	9.320	7.974	8.860	9.914	10.155	9.680	9.700
V5	9.467	10.654	9.265	7.926	7.714	9.855	10.906	9.623	9.643
V6	9.552	10.754	8.109	9.775	10.106	9.174	9.635	8.719	8.794
V7	9.543	10.739	8.101	9.765	10.096	9.165	9.626	8.710	7.967
V8	9.430	10.612	8.005	9.649	9.977	7.724	7.612	8.607	8.681
V9	9.625	10.660	8.041	9.693	10.022	7.760	8.551	8.646	8.720

Table IV shows the output line rms voltage for all faults applied in the distribution system. All the voltage sags shows in the results have a momentary decrease of rms (rated) AC voltage to a value between 90% to 10% of nominal voltage for a duration 0.1 seconds.

Based on results shows in Table IV, voltages close to the fault produce a large drop of rms voltage compared to other voltages in the circuit. For example, if Fault 1 occurred as shown Figure 4, V2 will have a large drop of rms voltage compared to other voltages. If Fault 7 occurs, therefore large drop of rms voltage will occur at V8.

The magnitude of voltage sags at a certain point in the system depends mainly on the type and the impedance of the fault, the distance to the fault and the system configuration. The calculation of the sag magnitude for a fault somewhere within a radial distribution system requires the point of common coupling (pcc) between the fault and the load. From (1), for fault closer to the pcc the sag becomes deeper (small Z_F). The sag becomes deeper for weaker supplies (larger Z_S) [11]. For example, when Fault 8 occurred in the sytem, output line rms for V6 is lower than V1 because fault impedance, Zf of V6 is smaller compared to V1.

Sag magnitude is high when there is a transformer between the pcc and the fault. Based on the result, the location of Fault 2 that located behind the transformer will have a high magnitude of voltage compared to other faults applied in the system. The sagged voltage will not collapse to a high degree because the transformer impedance is now on the load side of pcc.

C. Three Phase Fault

For three phase fault,, voltage sag can be characterized by the minimum RMS-voltage during the sag. If the sag is symmetrical, there will be equally deep in all three phases and the phase with the lowest remaining voltage is used to characterize the sag [12]. The instantaneous voltages waveform of Fault 1 for V1 shows in Figure 10 has the same magnitude of voltage for each phase. There are 9 simulations on fault condition that produced a total of 9 graphs of output voltages. Figure 11 show the output line rms of V1 during Fault 1. Values of rms voltages for other output voltages are transmitted into Table V.

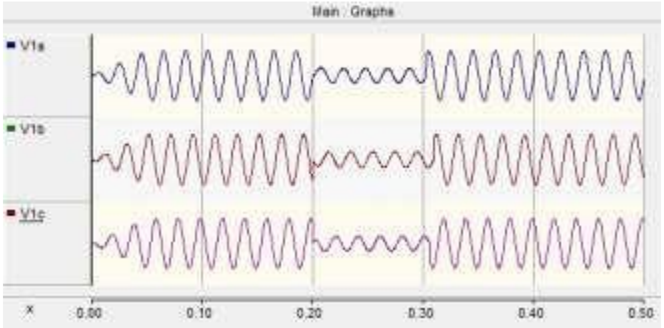

Fig. 10. Voltage Waveform of V1 during Fault 1

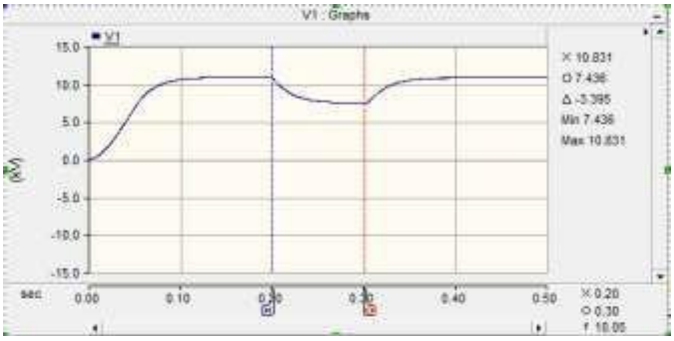

Fig. 11. Output Line rms of V1 during Fault 1

TABLE V. OUTPUT LINE RMS DURING FAULT 1

Output Line rms (kV)	
V1	7.436
V2	3.319
V3	0.122
V4	7.357
V5	7.313
V6	7.380
V7	7.373
V8	7.285
V9	7.318

TABLE VI. OUTPUT LINE RMS FOR ALL FAULT

Fault / Voltage rms (kV)	Fault 1	Fault 2	Fault 3	Fault 4	Fault 5	Fault 6	Fault 7	Fault 8	Fault 9
V1	7.436	10.84	6.806	8.114	9.017	8.529	9.224	7.801	7.951
V2	3.319	10.79	6.788	8.094	8.994	8.507	9.201	7.781	7.931
V3	0.122	0.395	0.249	0.297	0.33	0.312	0.337	0.285	0.291
V4	7.357	10.71	6.733	2.845	5.272	8.438	9.127	7.718	7.867
V5	7.313	10.65	6.693	2.827	1.87	8.389	9.073	7.672	7.82
V6	7.38	10.75	3.805	8.053	8.949	6.337	7.612	4.845	5.534
V7	7.373	10.74	3.802	8.046	8.941	6.331	7.605	4.838	2.872
V8	7.285	10.61	3.756	7.95	8.834	2.223	1.59	4.779	5.482
V9	7.318	10.66	3.773	7.986	8.875	2.234	4.462	4.801	5.487

Based on results show in Table VI, voltages close to the fault produce a large drop of rms voltage compared to other voltages in the circuit. The magnitude of voltage sags at a certain point in the system depends mainly on the type and the impedance of the fault, the distance to the fault and the system configuration. For fault closer to the pcc the sag becomes deeper and the sag becomes deeper for weaker supplies [11].

Sag magnitude is also high when there is a transformer between the pcc and the fault. Based on the result, the location of Fault 2 that located behind the transformer will have a high magnitude of voltage compared to other faults applied in the system. The sagged voltage will not collapse to a high degree because the transformer impedance is now on the load side of pcc.

Based on the result for single line to ground fault and three phase fault, it is apparent that single line to ground fault conditions results is much less severe voltage sag than three phase fault.

VIII. CONCLUSION

Good understanding of voltage sag characteristics can help all parties to solve the problems of this type of voltage variation. The magnitude and duration of the sags are the most important voltage sag characteristics. The voltage sag magnitude information at all parts of transmission and distribution networks and at particular customer of concern can be immediately obtained by making fault simulation. Voltage sags have been mainly characterized by magnitude and duration. This project presents a voltage sag characterization in terms of sag magnitude and sag duration by using PSCAD software which has been applied to the IEEE 13 Node Test Feeder. Simulation result has been presents in terms of the magnitude and duration due to single line-to-ground, and three phase faults.

REFERENCES

[1] Faisal, M. F. (2007). Voltage sag solutions for industrial customers

[2] Math H. J. Bollen, “Understanding Power Quality problems: Voltage Sags andInterruptions”, IEEE Press, 2000

[3] IEC 61000-4-30

[4] B. Tenaga, “A Guidebook on Power Quality-Monitoring, Analysis & Mitigations”, pages 1-61, 2006..

[5] M. H. J. Bollen, “Understanding power quality problems,” in VoltageSags and Interruptions. Piscataway, NJ: IEEE Press, 1999..

[6] Vima P. Mali, R.L Chakrasali and K S Aprameya (2015).A technicalinvestigation of Voltage Sag, American Journal of Engineering Research (AJER) M. Young, The Technical Writer’s Handbook. Mill Valley, CA: University Science, 1989.

[7] IEEE Recommended Practice for Monitoring Electric Power Quality, in IEEEstd . 1159-1995, New York, 2003, pp. IEEE, Inc.

[8] RadhaKrishna, C., et al. (2001). Impact of voltage sags in practical power system networks. Transmission and Distribution Conference and Exposition, 2001 IEEE/PES.

[9] Tenaga Nasional Berhad, Power Quality Guidebook: Voltage Sag Solutions for Industrial Customers. Pages 11-37, (2007).

[10] Magnus Ohrstrom and Lennart soder, “A comparison of two methods used for voltage dip characterization” IEEE Power Tech. Conference, Bologna, Italy, vol.4, June 23-26, 2003.

[11] Gülali Yalçinkaya, Math H. J. Bollen, and Peter A. Crossley,“Characterization of voltage sags in Industrial distribution systems,”IEEE Transactions on Industry Applications, Vol.34, No.4. pp. 682-688, July/August 1998.

[12] Ohrstrom, M. and Soder, L. (2003) A Comparison of Two Methods Used for Voltage Dip Characterization. IEEE

Application of Capacitor Bank in Distribution System

Muhammad Arazi Bin Deraman
Faculty of Electrical Engineering
Universiti Teknologi Malaysia
Johor Bahru, Malaysia.
razideraman@gmail.com

Dr. Saifulnizam Bin Abdul Khalid
Department of / Centre of
Faculty of Electrical Engineering
Universiti Teknologi Malaysia
Johor Bahru, Malaysia.
nizam@fke.utm.my

***Abstract*— This paper presents the application of capacitor bank at distribution system. The efficiency of both system are commonly related to the power factor installation. In order to make the power factor close to unity, the optimum size and location of capacitor bank should be considered. Normally, the system that have low power factor is due to the high inductive load. The low power factor will caused the system have voltage drop and power loss. Besides, the power penalties is imposed if power factor less than 0.85 for electricity supply below 132kV and less than 0.9 for electricity supply above 132kV. This rule is want to avoid highest cost incurred by Tenaga Nasional Bhd. (TNB) because more current must be transmitted than is actually used to perform useful work. Moreover, it can increased the bill from TNB due to lot of current transmitted to customer. Therefore, the objective of this project is want to minimize the voltage drop and power losses in the system. Next, to identify the optimum size of capacitor bank and the strategic location to install shunt capacitor in distribution system. This paper is focusing on 14 and 33 buses distribution system. These system are modelled by using Power World software simulation. After implementation of capacitor bank in these system, the voltage drop and power losses is reduced and the strategic location of capacitor bank is achieved based on simulation data. Thus, it is proven that by installing the optimum size and strategic location of capacitor bank can improve the efficiency of the system.**

***Keywords*—distribution systems; capacitor bank placement; voltage drop; power loss; power factor**

I. INTRODUCTION

The final stage of process transfer electric power is distribution system. This process of transfer electric power is carrying from transmission system to the consumers. In distribution system, there have a lot of inductive loads. For example of inductive loads are motors, transformers and lighting ballast. All of this loads have a winding due to it needs a magnetic field to operate. The electrical power in inductive load is divided into two which are real power (kW) and reactive power (kVAR). Real power or also called working power can be read by wattmeter and measured in kilowatts (kW). However, reactive power does not operate as a useful working power but it circulates between generator and loads. It also makes a heavier drain on distribution system. Real power and reactive power combine will provide the apparent power (kVA).

In order to make the distribution system work efficiently in electrical power used, the value of power factor must be closed to unity. The meaning of power factor is the ratio of working power to apparent power. The simple explanation for power factor can be seeing at power triangle diagram in Fig. 1. To achieve a better power factor for a system, the decrement reactive element must be made.

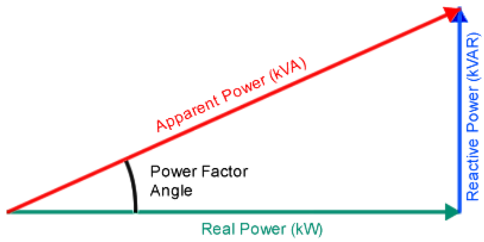

$$\text{Power Factor} = \frac{\text{Real Power (kW)}}{\text{Apparent Power (kVA)}} = \frac{kW}{\sqrt{kW^2 + kVAR^2}}$$

Fig. 1. Power Triangle Diagram

In Malaysia, there is company Tenaga Nasional Bhd. who are conducted electrical supply to all consumer. This had made a rule which is power penalties or it also called power factor surcharged. The low power factor will caused the system have voltage drop and power loss. Power surcharged is imposed if power factor less than 0.85 for electricity supply below 132kV and less than 0.9 for electricity supply above 132kV. This rule is want to avoid highest cost incurred by Tenaga Nasional Bhd. (TNB) because more current must be transmitted than is actually used to perform useful work. Moreover, it can increased the bill from TNB due to lot of current transmitted to customer. The power surcharged can be calculated as follows:

- 1.5% surcharge of the current bill – for every 0.01 less than 0.85 power factor.
- 3% surcharge of the current bill – for every 0.01 less than 0.75 power factor.

Moreover, there is some ways to improve power factor management. The first way is install capacitors (kVAR generators) such as capacitor bank, corrector, synchronous generators and synchronous motors. Other than that, the consumer also can reduce the operation of idling motors, prevent from operate the motor above its rated voltage and replace the motor that used more energy burning with energy efficient motors.

II. Literature Review

A. Power Factor Improvement

Capacitor bank installation is one of other method that can be used efficiently in order to improve power factor at plant distribution system. When apparent power (kVA) is greater than real power (kW), the utility must supply the excess reactive current plus the working current [2]. In order to reduce the current supply from utility system, the power capacitor bank must be installed. This because it act as reactive current generators. Fig. 2 will showed the benefit of installed capacitor on the system that will reduced the utility current supply.

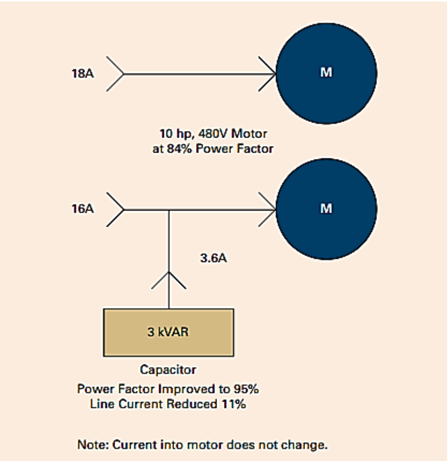

Fig. 2. Capacitor act as kVAR generators

The most efficient to install capacitor is directly at the motor where reactive power is used up. This is because it will reduced the current draw besides it can turn the motor into self-excited generator since the motor has a high inertia. Moreover, reactive power compensation is used to enhance the network capacity, keep the plant in long life, assist in voltage support and increase the power quality [5]. In addition, capacitor bank can be installed at service feeder due to make correcting at whole plant loads. However, when the capacitor bank installed at service feeder, the fused switch or circuit breaker must be provided in order to make a protection [1].

B. Benefit of Improving Power Factor

- Reduce the real power billing demand.
- Avoid from power factor surcharge.
- Increased the electrical system capacity and reduced losses.
- Increased the voltage level and make the motor working efficiently.

C. Capacitor Size and Location

There had some methods of voltage control by make an injection of reactive power [3]. For shunt capacitor connection, the location is effectively to apply at bus bar in distribution system. The reason is it will decreased the value of reactive power for generator and load. In addition, shunt capacitor connection also want to help the distribution system power factor maintaining to closer to unity [4]. Besides, to determine the effective size of capacitor bank must use in distribution is using the formula [10] shown in Fig. 3. This formula will calculated the effective size of shunt capacitor in order to increase the power factor of system and decrease the value of reactive power [7].

$$Q = P(\tan\theta - \tan\theta')$$

where,
Q is required KVAR.
P is active power in KW.
cosθ is power factor before compensation.
cosθ' power factor after compensation.

Fig. 3. The formula to determine size of shunt capacitor

III. Methodology

Fig. 4 shows the project flows from the start until end of the project research study. The method used in this project is by using simulation throughout Power World Software and calculation from literature review.

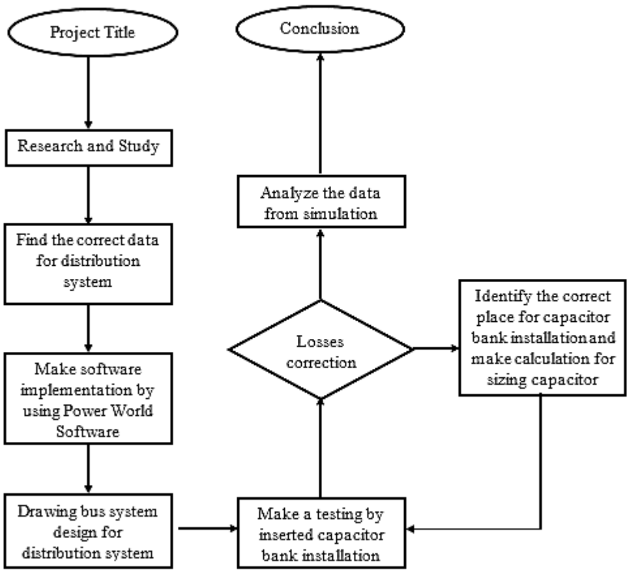

Fig. 4. The project flow diagram for entire research study

A. Software Implementation

The proposed method in this project is using Power World software and the location to install shunt capacitor bank is using trial and error method. The distribution system of 14 and 33 bus is designed and the simulation is run. In this simulation can earned the data either the size and location of capacitor bank is influence to the efficiency of distribution system or not. An important method of controlling bus voltage is by shunt capacitor banks at the buses of distribution levels along lines or at substations and loads [15].The data for these distribution system is specified in the following section.

1) 14-Bus System

a) Original System

The first test case for the proposed method is a 14-bus distribution system and the circuit is shown in Fig. 5. This system has rated line voltage is 132kV. The slack bus generator base apparent power is 100MVA. The details of the feeder and the load characteristics are given in Table I [12]. The details for line data of the system are given in Table II while Table III and Table IV are the transformer data and regulated bus data respectively.

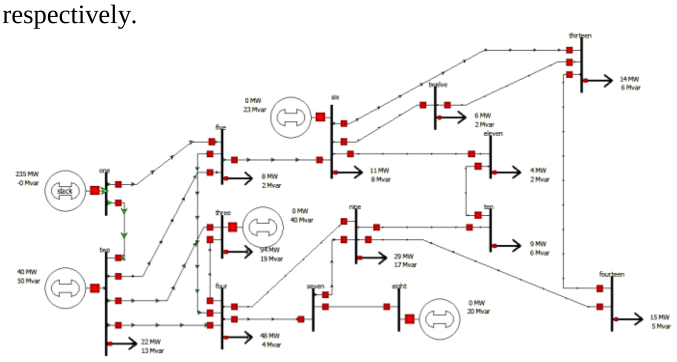

Fig. 5. 14-Bus system designed by using Power World Software

TABLE I. BUS DATA FOR IEEE 14-BUS SYSTEM

Bus No.	Bus Voltage		Generation		Load	
	Magnitude Per Unit	Phase Angle Degree	Real MW	Reactive MVAR	Real MW	Reactive MVAR
1	1.060	0.0	232.4	-16.9	0.0	0.0
2	1.045	-4.98	40.0	42.4	21.7	12.7
3	1.010	-12.72	0.0	23.4	94.2	19.0
4	1.019	-10.33	0.0	0.0	47.8	3.9
5	1.020	-8.78	0.0	0.0	7.6	1.6
6	1.070	-14.22	0.0	12.2	11.2	7.5
7	1.062	-13.37	0.0	0.0	0.0	0.0
8	1.090	-13.36	0.0	17.4	0.0	0.0
9	1.056	-14.94	0.0	0.0	29.5	16.6
10	1.051	-15.10	0.0	0.0	9.0	5.8
11	1.057	-14.79	0.0	0.0	3.5	1.8
12	1.055	-18.07	0.0	0.0	6.1	1.6
13	1.050	-15.16	0.0	0.0	13.5	5.8
14	1.036	-16.04	0.0	0.0	14.9	5.0

TABLE II. LINE DATA FOR IEEE 14-BUS SYSTEM

Line No.	Between Buses	Line Impedance		Half Line Charging Susceptance per unit
		R per unit	X per unit	
1	1 – 2	0.01938	0.05917	0.02640
2	2 – 3	0.04699	0.19797	0.02190
3	2 – 4	0.05811	0.17632	0.01870
4	1 – 5	0.05403	0.22304	0.02460
5	2 – 5	0.05695	0.17388	0.01700
6	3 – 4	0.06701	0.17103	0.01730
7	4 – 5	0.01335	0.04211	0.0064
8	5 – 6	0.0	0.25202	0.0
9	4 – 7	0.0	0.20912	0.0
10	7 – 8	0.0	0.17615	0.0
11	4 – 9	0.0	0.55618	0.0
12	7 – 9	0.0	0.11001	0.0
13	9 – 10	0.03181	0.08450	0.0
14	6 – 11	0.09498	0.19890	0.0
15	6 – 12	0.12711	0.25581	0.0
16	6 – 13	0.06615	0.13027	0.0
17	9 – 14	0.12711	0.27038	0.0
18	10 – 11	0.82050	0.19207	0.0
19	12 – 13	0.22092	0.19988	0.0
20	13 – 14	0.17093	0.34802	0.0

TABLE III. TRANSFORMER DATA

Transformer	Between Buses	Tap Setting
1	4 – 7	0.978
2	4 – 9	0.969
3	5 – 6	0.932

TABLE IV. REGULATED BUS DATA (P – V BUSES)

Bus No.	Voltage Magnitude per unit	Reactive Power Limit	
		Minimum MVAR	Maximum MVAR
2	1.045	-40.0	50.0
3	1.010	0.0	40.0
6	1.070	-6.0	24.0
8	1.090	-6.0	24.0

After the system had designed by using all the data above, the size of capacitor bank is calculated. For 132kV distribution system, the load power factor that below than 0.9 should be improved to become 0.9 and the size of capacitor is determined by using formula in Fig. 3. Table V shown the power factor for every load and size capacitor bank that want to improve the power factor to become 0.9.

TABLE V. POWER FACTOR OF LOADS AND SIZE CAPACITOR BANK NEEDED FOR 14-BUS SYSTEM

Load		Power Factor	Size Capacitor Bank MVAR
Real MW	Reactive MVAR		
0.0	0.0		
21.7	12.7	0.86	2.365
94.2	19.0	0.98	
47.8	3.9	0.99	
7.6	1.6	0.98	
11.2	7.5	0.83	2.419
0.0	0.0		
0.0	0.0		
29.5	16.6	0.87	2.449
9.0	5.8	0.84	1.458
3.5	1.8	0.90	
6.1	1.6	0.97	
13.5	5.8	0.92	
14.9	5.0	0.95	

Then, the size of capacitor bank 2.419MVAR will install at load that had highest voltage drop first. If it still cannot reduce the voltage drop, the size capacitor bank will increase by making addition one by one with 1.4580MVAR, 2.449MVAR and 2.365MVAR until found the optimum size to install in the system. The voltage drop and power loss before capacitor installation and after installation is analysed.

b) Increase 25% to All Loads

The 14-bus system loads had been increased by 25%. The voltage drop and power loss of the system is analysed and compare with original system.

2) 33-Bus System

a) Original System

The next test for the proposed method is 33-bus radial distribution system and the circuit is shown in Fig. 6. A distribution circuit normally uses primary or main feeders and lateral distributors [13]. This system has a main feeder and four laterals. The line and load data is given in Table VI [11]. The rated voltage of the system is 12.66kV. The slack bus generator base apparent power is 100MVA. Thus, for impedance base is 1.6028 ohm. Radial systems are popular because of their simple design and generally low cost [14].

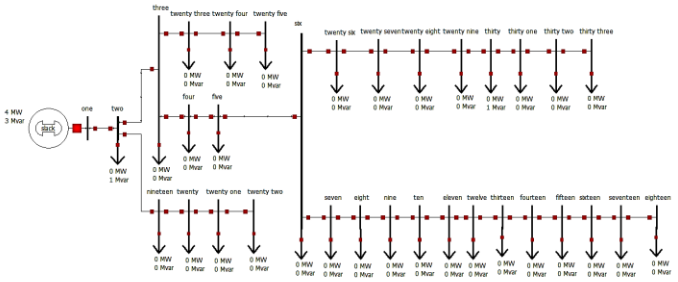

Fig. 6. 33-Bus system designed by using Power World Software

TABLE VI. LOAD POWER AND LINE IMPEDANCE DATA OF 33-BUS SYSTEM

Line no.	From Bus	To bus	R (p.u)	X (p.u)	PL (MW)	QL (MVAR)
1	1	2	0.0575	0.0298	0.10	0.60
2	2	3	0.3076	0.1504	0.09	0.04
3	3	4	0.2284	0.1163	0.12	0.08
4	4	5	0.2378	0.1211	0.06	0.03
5	5	6	0.5110	0.4411	0.06	0.02
6	6	7	0.1168	0.3861	0.20	0.10
7	7	8	1.0678	0.7706	0.20	0.10
8	8	9	0.6426	0.4617	0.06	0.02
9	9	10	0.6489	0.4617	0.06	0.02
10	10	11	0.1227	0.0406	0.04	0.03
11	11	12	0.2336	0.0772	0.06	0.03
12	12	13	0.9159	0.7206	0.06	0.03
13	13	14	0.3379	0.4448	0.12	0.08
14	14	15	0.3687	0.3282	0.06	0.01
15	15	16	0.4656	0.3400	0.06	0.02
16	16	17	0.8042	1.0737	0.06	0.02
17	17	18	0.4567	0.3581	0.09	0.04
18	18	19	0.1023	0.0976	0.09	0.04
19	19	20	0.9385	0.8456	0.09	0.04
20	20	21	0.2555	0.2985	0.09	0.04
21	21	22	0.4423	0.5848	0.09	0.04
22	22	23	0.2815	0.1924	0.09	0.05
23	23	24	0.5603	0.4424	0.42	0.20
24	24	25	0.5590	0.4374	0.42	0.20
25	25	26	0.1267	0.0645	0.06	0.03
26	26	27	0.1773	0.0903	0.06	0.03
27	27	28	0.6607	0.5825	0.06	0.02
28	28	29	0.5017	0.4371	0.12	0.07
29	29	30	0.3291	0.1613	0.20	0.60
30	30	31	0.6079	0.6008	0.15	0.07
31	31	32	0.1937	0.2258	0.21	0.10
32	32	33	0.2128	0.3308	0.06	0.04

The substation voltage for slack bus is take into 1.05 p.u with zero angle while for bus 2 until 33 the value of p.u voltage is 1.0 p.u with zero angle. After the 33-bus system had been drawing, the simulation is run and the data for the system was analysed. The load power factor that had below than 0.85 will improved to become 0.9. Then, the size of capacitor is calculated by using formula in Figure 2.3 Table VII shows the load power factor and the size of capacitor bank to improve power factor become 0.9.

TABLE VII. POWER FACTOR OF LOADS AND SIZE CAPACITOR BANK NEEDED FOR 33-BUS SYSTEM

Load		Power Factor	Size Capacitor Bank MVAR
Real MW	Reactive MVAR		
0.10	0.60	0.16	0.5683
0.09	0.04	0.91	
0.12	0.08	0.83	0.0226
0.06	0.03	0.89	
0.06	0.02	0.95	
0.20	0.10	0.89	
0.20	0.10	0.89	
0.06	0.02	0.95	
0.06	0.02	0.95	
0.04	0.03	0.83	0.0085
0.06	0.03	0.86	
0.06	0.03	0.86	
0.12	0.08	0.83	0.0226
0.06	0.01	0.99	
0.06	0.02	0.95	
0.06	0.02	0.95	
0.09	0.04	0.91	
0.09	0.04	0.91	
0.09	0.04	0.91	
0.09	0.04	0.91	
0.09	0.04	0.91	
0.09	0.05	0.87	
0.42	0.20	0.90	
0.42	0.20	0.90	
0.06	0.03	0.92	
0.06	0.03	0.92	
0.06	0.02	0.95	
0.12	0.07	0.86	
0.20	0.60	0.32	0.4954
0.15	0.07	0.91	
0.21	0.10	0.90	
0.06	0.04	0.83	0.0113

Then, the size of capacitor bank 0.5683MVAR will install at load that had highest voltage drop first. If it still cannot reduce the voltage drop, the size capacitor bank will increase by making addition one by one with 0.0226MVAR, 0.0085MVAR, 0.0226MVAR, 0.4954MVAR and 0.0113MVAR until found the optimum size to install in the system. The voltage drop and power loss before capacitor installation and after installation is analysed.

b) Increase 100% to All Loads

The 33-bus system loads had been increased by 100%. The voltage drop and power loss of the system is analysed and compare with original system.

IV. Result and Discussion

1) 14-Bus System

a) Original System

The system before capacitor bank installation had a voltage drop at bus 14 which is 0.93737 pu. This voltage is not in the range of -6% < V < +10%. The lowest pu voltage should be around 0.94000 pu only and the highest pu voltage is around 1.10000 pu. For this system, the highest voltage of the system is 1.00000 pu at slack bus due to near to generator. The location of bus 14 is far away from the generator and may effect to voltage drop and power loss. The total power generated is 274.89MW while the total power demand for the system is 259MW. Therefore, the power losses in the system is 15.89MW. Table VIII shows the voltage profile and power transmitted in the system.

TABLE VIII. Voltage profile and power generated in 14-bus system before shunt capacitor installation

Bus no.	Voltage (pu)	Voltage (kV)	Angle (Degree)	Load (MW)	Load (MVar)	Gen. (MW)	Gen. (MVar)
1	1.00000	132.000	0.00			234.89	-0.19
2	0.97975	129.327	-5.62	21.70	12.70	40.00	50.00
3	0.94923	125.298	-14.65	94.20	19.00	0.00	40.00
4	0.94023	124.110	-11.55	47.80	3.90		
5	0.94578	124.843	-9.90	7.60	1.60		
6	1.00000	132.000	-16.56	11.20	7.50	0.00	22.92
7	0.96438	127.298	-15.01				
8	1.00000	132.000	-15.01			0.00	20.22
9	0.94513	124.758	-16.86	29.50	16.60		
10	0.94002	124.082	-17.01	9.00	5.80		
11	0.98453	129.958	-17.33	3.50	1.80		
12	0.98106	129.500	-17.54	6.10	1.60		
13	0.97300	128.436	-17.56	13.50	5.80		
14	0.93737	123.732	-18.38	14.90	5.00		

After analyse this system, the capacitor bank 3.9MVar is installed at load bus 14 which has the lowest voltage. Then, the pu voltage at load bus 14 is increased from 0.93737 pu to become 0.94663 pu. Besides, the power generated is decreased from 274.89MW to become 274.78MW thus reduces the power loss in the system which is 15.78MW. This analysis had shown the size of capacitor bank is optimum and the location to install shunt capacitor bank is strategic. Table IX shows the voltage profile and power transmitted in the system after shunt capacitor connection.

TABLE IX. Voltage profile and power generated in 14-bus system after shunt capacitor installation

Bus no.	Voltage (pu)	Voltage (kV)	Angle (Degree)	Load (MW)	Load (MVar)	Generator (MW)	Generator (MVar)
1	1.00000	132.000	0.00			234.78	-0.95
2	0.98006	129.368	-5.63	21.70	12.70	40.00	50.00
3	0.94981	125.374	-14.64	94.20	19.00	0.00	40.00
4	0.94101	124.213	-11.56	47.80	3.90		
5	0.94635	124.918	-9.89	7.60	1.60		
6	1.00000	132.000	-16.50	11.20	7.50	0.00	20.40
7	0.96617	127.534	-15.03				
8	1.00000	132.000	-15.03			0.00	19.21
9	0.94856	125.209	-16.88	29.50	16.60		
10	0.94318	124.499	-17.03	9.00	5.80		
11	0.98526	130.054	-17.26	3.50	1.80		
12	0.98219	129.648	-17.49	6.10	1.60		
13	0.97511	128.715	-17.55	13.50	5.80		
14	0.94663	124.955	-18.55	14.90	5.00		

2) 33-Bus System

a) Original System

The system before shunt capacitor bank installation, there had lowest voltage profile below than 0.94000 pu voltage at load bus. The lowest pu voltage in this system is 0.90386 pu at bus 18 since the load the far away. The other lowest pu voltage is at bus 33 which is 0.91630 pu in the other lateral of the system. The total power transmitted is 3.93MW and the total load demand is 3.71MW. Thus, the power loss in the system is 0.22MW. Table X show the voltage profile and power transmitted in the system before shunt capacitor installation.

TABLE X. : The voltage profile and power transmitted in the system before shunt capacitor installation

Bus no.	Voltage (pu)	Voltage (kV)	Angle (Degree)	Load (MW)	Load (MVar)	Generator (MW)	Generator (MVar)
1	1.00000	12.660	0.00	0.00	0.00	3.93	2.98
2	0.99685	12.620	0.03	0.10	0.60		
3	0.98286	12.443	0.13	0.09	0.04		
4	0.97536	12.348	0.19	0.12	0.08		
5	0.96793	12.254	0.26	0.06	0.03		
6	0.94946	12.020	0.17	0.06	0.02		
7	0.94594	11.976	-0.07	0.20	0.10		
8	0.93230	11.803	-0.22	0.20	0.10		
9	0.92597	11.723	-0.29	0.06	0.02		
10	0.92013	11.649	-0.36	0.06	0.02		
11	0.91926	11.638	-0.35	0.04	0.03		
12	0.91775	11.619	-0.34	0.06	0.03		
13	0.91159	11.541	-0.43	0.06	0.03		
14	0.90930	11.512	-0.51	0.12	0.08		
15	0.90788	11.494	-0.55	0.06	0.01		
16	0.90650	11.476	-0.57	0.06	0.02		
17	0.90447	11.451	-0.65	0.06	0.02		
18	0.90386	11.443	-0.66	0.09	0.04		
19	0.99633	12.613	0.02	0.09	0.04		
20	0.99275	12.568	-0.05	0.09	0.04		
21	0.99204	12.559	-0.07	0.09	0.04		
22	0.99140	12.551	-0.09	0.09	0.04		
23	0.97928	12.398	0.10	0.09	0.05		
24	0.97261	12.313	0.01	0.42	0.20		
25	0.96928	12.271	-0.04	0.42	0.20		
26	0.94753	11.996	0.21	0.06	0.03		
27	0.94497	11.963	0.26	0.06	0.03		
28	0.93352	11.818	0.34	0.06	0.02		

29	0.92530	11.714	0.42	0.12	0.07		
30	0.92166	11.668	0.53	0.20	0.60		
31	0.91750	11.616	0.45	0.15	0.07		
32	0.91658	11.604	0.43	0.21	0.10		
33	0.91630	11.600	0.42	0.06	0.04		

The shunt capacitor size to install is 1.08MVar and the location is at two places which are at bus 18 and bus 33. The result is the value of pu voltage at both bus improve to 0.98860 pu for bus 18 and 0.96834 pu for bus 33. The total power transmitted is reduce to become 3.87MW and the power loss also decrease to 0.16MW. Table XI shows the voltage profile and power transmitted in the system after shunt capacitor installation.

TABLE XI. THE VOLTAGE PROFILE AND POWER TRANSMITTED IN THE SYSTEM AFTER SHUNT CAPACITOR INSTALLATION

Bus no.	Voltage (pu)	Voltage (kV)	Angle (Degree)	Load (MW)	Load (MVar)	Gen. (MW)	Gen. (MVar)
1	1.00000	12.660	0.00	0.00	0.00	3.87	0.71
2	0.99756	12.629	-0.04	0.10	0.60		
3	0.98719	12.498	-0.35	0.09	0.04		
4	0.98247	12.438	-0.59	0.12	0.08		
5	0.97797	12.381	-0.84	0.06	0.03		
6	0.97007	12.281	-1.62	0.06	0.02		
7	0.97104	12.293	-1.93	0.20	0.10		
8	0.96622	12.232	-2.83	0.20	0.10		
9	0.96522	12.220	-3.36	0.06	0.02		
10	0.96476	12.214	-3.88	0.06	0.02		
11	0.96436	12.209	-3.96	0.04	0.03		
12	0.96374	12.201	-4.11	0.06	0.03		
13	0.96608	12.231	-4.85	0.06	0.03		
14	0.96908	12.269	-5.16	0.12	0.08		
15	0.97154	12.300	-5.46	0.06	0.01		
16	0.97419	12.333	-5.81	0.06	0.02		
17	0.98492	12.469	-6.43	0.06	0.02		
18	0.98860	12.516	-6.76	0.09	0.04		
19	0.99704	12.622	-0.05	0.09	0.04		
20	0.99346	12.577	-0.12	0.09	0.04		
21	0.99276	12.568	-0.14	0.09	0.04		
22	0.99212	12.560	-0.16	0.09	0.04		
23	0.98362	12.453	-0.38	0.09	0.05		
24	0.97697	12.368	-0.47	0.42	0.20		
25	0.97366	12.327	-0.51	0.42	0.20		
26	0.96901	12.268	-1.66	0.06	0.03		
27	0.96767	12.251	-1.73	0.06	0.03		
28	0.96366	12.200	-2.08	0.06	0.02		
29	0.96104	12.167	-2.34	0.12	0.07		
30	0.95956	12.148	-2.45	0.20	0.60		
31	0.96283	12.189	-2.93	0.15	0.07		
32	0.96467	12.213	-3.08	0.21	0.10		
33	0.96834	12.259	-3.22	0.06	0.04		

V. CONCLUSION

Based on the analysis had made, by installing shunt capacitor bank may can be effect either positive or negative impact on the system. Sometimes, the power factor is improved but still had high power loss due to the size of capacitor no compatible or the location of capacitor bank installation not strategic. These also become the main reason why trial and error method was used in this project. However, there only had one configuration that can help to improve the voltage drop and power loss in the system and can increase the efficiency of the system. In addition, the installation of capacitor bank is a mandatory to the company or organisation from getting penalized by TNB. Moreover, by making power factor improvement, there is not only increase the efficiency of the system but also can help in reducing monthly electrical bill. This method by installing capacitor bank in the system may can give some benefit to the consumer to assist in net annual saving in initial investment.

REFERENCES

[1] Mohamed Fuad Bin Faisal, Medium Voltage Capacitor Bank Design, 1st ed. Petaling Jaya: BEM, 2008.

[2] "Power Factor Correction: A Guide For The Plant Engineer", Eaton, 2010. [Online]. Available: http://www.eaton.com/ [Accessed: 22- Sep- 2016].

[3] Dr. Mohamed Yusri Hassan, Power System Control, 4th ed. Johor Bahru, Johor, 2015.

[4] Ashish Chandra and Taru Agarwal, "Capacitor Bank Designing for Power Factor Improvement", International Journal of Emerging Technology and Advanced Engineering, vol. 4, no. 8, 2014.

[5] Marius Jansen, "Design Aspects of Medium Voltage Capacitor Banks".

[6] "TNB Better. Brighter.", TNB Better. Brighter., 2016. [Online]. Available: https://www.tnb.com.my/commercial-industrial/charges-penalties. [Accessed: 02- Dec- 2016]

[7] "Capacitor Bank | Reactive Power Compensation | Electrical4u", Electrical4u.com, 2016. [Online]. Available: http://www.electrical4u.com/capacitor-bank-reactive-power-compensation/. [Accessed: 02- Dec- 2016]

[8] R. Rao, S. Narasimham and M. Ramalingaraju, "Optimal capacitor placement in a radial distribution system using Plant Growth Simulation Algorithm", International Journal of Electrical Power & Energy Systems, vol. 33, no. 5, pp. 1133-1139, 2011.

[9] Hadi Saadat, Power Systems Analysis, 1st ed. McGraw-Hill, 2000.

[10] Mira Amalia, "Power Factor Management For Commercial Building", Universiti Teknologi Malaysia (UTM), 2015.

[11] Y. Qudaih and T. Hiyama, "Utilization of Energy Capacitor Systems in Power Distribution Networks with Renewable Energy Sources," Journal of Electromagnetic Analysis and Applications, Vol. 2 No. 4, 2010, pp. 244-251. doi: 10.4236/jemaa.2010.24030.

[12] Power Systems Test Case Archive - UWEE. [online] Available at: http://www2.ee.washington.edu/research/pstca/ [Accessed 10 Apr. 2017].

[13] Anwar Shahzad Siddiqui, Sheeraz Kirmani, and Md. Farrukh Rahman, “Optimal Capacitor Placement in Distribution System using Fuzzy Techniques”. (2010). Department of Electrical Engineering Faculty of Engineering and Technology Jamia Millia Islamia New Delhi-25, India.

[14] S.F.Mekhamer, S.A.Soliman, M.A.Moustafa and M.E.ElHawary, "Load Flow Solution of Radial Distribution Feeders: a new contribution", International journal of Electrical Power and Energy systems,24 (9),P.701707,Nov 2002.

[15] Siddiqui, A. and Rahman, M. (2012). Optimal Capacitor Placement to reduce losses in Distribution System. WSEAS TRANSACTIONS on POWER SYSTEMS, 7(1).

USB Bicycle Charger

Amalina binti Nordin
Faculty of Electrical Engineering
Universiti Teknologi Malaysia
Johor Bahru, Malaysia.
amalinanordin@gmail.com

Dr. Mohd Rodhi bin Sahid
Department of Power Electronic
Faculty of Energy Conversion
Universiti Teknologi Malaysia
Johor Bahru, Malaysia.
rodhi@fke.utm.my

Dynamo is usually used to generate electricity to light up bicycle's light during cycling. In this project, the generated electrical energy from dynamo will be harvested to charge portable devices. Since the output source of the dynamo is AC source, a rectifier is required to convert AC source to DC source. The voltage generated is depends on the speed of cycling, therefore the voltage produced is unregulated which is cannot directly connect to the portable devices. Thus, a DC-DC buck converter is used to step down the voltage from the rectifier to 5V. In order to produce an output of 5V, the DC-DC buck converter is designed in closed loop to regulate the variable of input voltage. Simulation of this project has been done through MATLAB to determine the parameter of buck converter and the hardware implementation as the prototype is constructed on a donut board.

Keywords— Bicycle Charger, Closed-loop buck converter, USB Bicycle Charger

I. INTRODUCTION

Generate electricity using bicycle dynamo have been discovered a long time ago for the purpose of light up the head lamp of the bicycle. The energy is harvested from the bicycle dynamo by converting the kinetic energy to electrical energy. Nowadays, most of the peoples in the world are practicing a healthy lifestyle which is one of the activity is cycling bicycle. By cycling, cardiovascular fitness can be increased, stress level can be decreased and many more benefits can be obtained from riding bicycle. Other than keep a healthy life, cycling also can help to reduce pollution and conserve our eco system. Furthermore, generating electricity using bicycle dynamo can be categorized as renewable energy due to the energy generated is clean, free and abundant. While conserving the green environment and having a great healthy lifestyle, at the same time electrical energy can be harvested by cycling and become an electrical source to charge a portable device such as power bank and mobile phone [1].

Therefore, a circuit to charge the power bank and LED safety light for the cyclist is designed in this work. The circuit consist of full bridge rectifier which is use to convert alternating current (AC) source from the dynamo to the direct current (DC) source. Besides that, there is a closed-loop buck DC-DC converter used to step down the unregulated input voltage to 5V.

The closed loop circuit design is using type III compensator due to commonly used of this type of compensator with buck converter and ability to provide phase boost. Buck converter is classified as switched mode DC-DC converter which is also called switching power supplies or switchers and it is more efficient compared to the linear regulator [2].

II. LITERATURE REVIEW

A. Bicycle Dynamo

Dynamo is a small generator which generates AC output when kinetic energy is converted to electrical energy. When the permanent magnet is rotating there are a changing of magnetic field. Thus, electricity is generated [3]. There are two types of dynamo which are hub dynamo and bottle dynamo. Hub dynamo is integrated into the hub of the wheel and cannot be installed on an already existing bicycle while bottle dynamo can be installed on an existing bicycle and the cost of dynamo is very affordable [4].

B. Full-Wave Bridge Rectifier

Full-wave bridge rectifier is used to convert AC output of the dynamo to DC source due to the source of the load is DC voltage. The rectifier is designed to follow the specification from the dynamo which is rated for 12V and 5.5W. Full-wave rectifier will convert the AC source to produce DC voltage or current [5].

The performance of dynamo need to be measured using oscilloscope to determine the frequency, voltage and current corresponding to the speed and the load [4]. The frequency of the dynamo need to be determined in order to properly design the rectifier circuit.

C. Buck Converter

Buck converter is a step down DC-DC converter circuit due to the output of buck converter circuit is lower than the input voltage. Buck converter consist of two type conduction mode which are continuous conduction mode (CCM) and discontinuous conduction mode (DCM). CCM occur when the inductor current is remains positive throughout the switching period while DCM, the inductor current is remains zero for some time in the switching period [6]. In order to reduces losses, the buck converter circuit must perform in CCM. Furthermore, CCM is more preferred for higher efficiency [7]. Generally buck converter circuit consist of switch, diode, inductor and capacitor. Fig. 1 shows a circuit diagram of the buck converter.

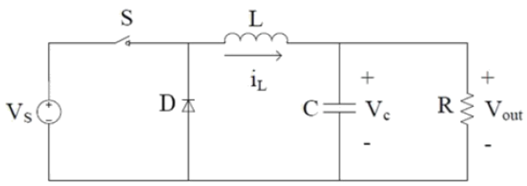

Fig. 1. Buck converter circuit diagram [8]

D. Power Switch

In designing buck converter, power switch is one of the main component of the circuit. Power switch consist of two states which are on and off. Since it having small losses, the application using switching device is desirable. In practical, during on state and when there is transitions between on and off state device will absorb some power. However, the efficiency of the circuit still high. Diode, thyristors and transistors are the examples of type of switch. Most of power supply application use transistor as a power switch. There are three types of transistor which are metal-oxide semiconductor field effect transistor MOSFET, bipolar junction transistor (BJT) and insulated-gate bipolar junction transistor (IGBT).

Selection of power switch is based on the characteristic of current, voltage and switching frequency. From the three types of transistor, MOSFET is the most suitable power switch for buck converter circuit. It is because MOSFET is a voltage-controlled device and have high switching frequency. MOSFET only require small amount of current to be turned on compared to the BJT which a current-controlled device and need a sufficient amount of current to turn on [2, 8, 9, 10].

E. Pulse Width Modulation (PWM)

Pulse width modulation (PWM) produce signal that compare sawtooth waveform and the error of amplifier output voltage which is shown in Fig. 2. Result from that, a duty cycle is formed and this signal is use as the reference to turn on and off the power switch [2, 8, 9, 10, 11].

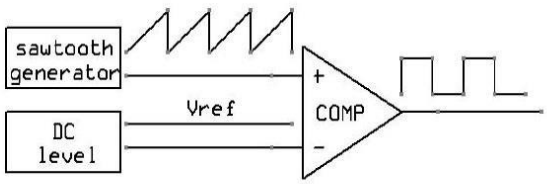

Fig. 2. PWM generator [2]

F. Gate Driver

Gate driver is used to amplify the output voltage from the PWM due to insufficient voltage produced which is unable to turn on the MOSFET [15]. For N-channel MOSFET normally the switch is rated at Vgs=10. Therefore, a voltage greater than 10V is needed to turn on the MOSFET [8].

G. Diode

Diode is a semiconductor device that allow current to flow in one direction. In buck converter, diode is reverse bias (open circuit) when the switch in buck converter is closed while diode will conduct forward bias (short circuit) when then switch is open. The inductor current cannot suddenly change [8, 9]. Diode is needed in order to ensure the current is flow to the inductor. In designing buck converter, a fast recovery diode is used due to handling the high switching frequency used

H. Inductor

In buck converter, the inductor value will limit the current slew rate. Inductor will limit the current inrush when the switch is closed (ON). The current of inductor cannot change suddenly. Inductor act as energy storage element which will determine whether the circuit is conduct in continuous mode or discontinuous mode [8, 9, 12].

I. Capacitor

In order to keep the output voltage constant in buck converter, a large capacitor is required. However, in practical the output voltage cannot keep perfectly constant due to the relation of the voltage-current relationship of the capacitor. Other than that, the function of capacitor is to store charge and minimize the output voltage ripple [2].

J. Power Supply Control

In this case of buck converter design, the input voltage is unregulated. Therefore, power supply control is needed to compare the output voltage of buck converter with a reference voltage which is the result will be converted into duty cycle ratio [2]. The duty cycle change respectively when the input voltage of buck converter is change in order to ensure that the output voltage is fixed and give the desired voltage. Fig. 3 shows feedback control of closed loop controller.

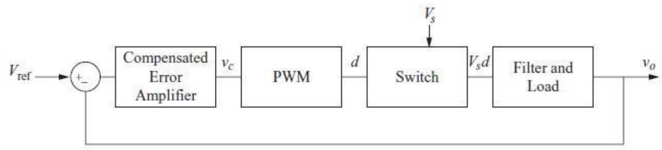

Fig. 3. Control representation of closed-loop controller [2]

III. METHODOLOGY

A. Output Voltage from Dynamo

An experiment has been done to measure the voltage output for the dynamo at certain speed with load and without load. The rated value of the dynamo used in this experiment is 12V and 5.5W and the load in this experiment is a head lamp of bicycle which is rated at 5W. Other than that, the duration is fixed to be 10 seconds to make sure the uniform cycle for each speed. The voltage at dynamo with and without load is tabulated in TABLE 1.

TABLE 1

AC output voltage from the dynamo

Rotation of pedal in 10 seconds	Voltage Without Load (V_{RMS})	Voltage With Load (V_{RMS})
7	8V	6V
9	9.4V	6.3V
11	11.2V	8V
13	12.3V	9.3V
15	15V	10.5V

Based on the result, the AC voltage is calculated to identify the value of the voltage after being converted to DC using rectifier to determine the converter that should be used. Voltage output that obtained from the dynamo is voltage in rms value. In order to determine the output voltage in DC, therefore the equation (1) is used since the usage of full-wave bridge rectifier in this project.

$$V_o = \frac{2V_m}{\pi} \quad ; V_m = V_{RMS}\, x \sqrt{2} \tag{1}$$

The nominal speed which is 7 rotational of pedal in 10 seconds is chosen because that is the normal speed which is a cyclist will use in real life. From the calculation result, the voltage is 7.2V without load and 5.4V with load. Therefore, the suitable DC-DC converter that should be used in this project is a buck converter.

TABLE 2

Average voltage produced by rectifier at nominal and maximum speed

Speed (Rotation of Pedal in 10 second)	Voltage Without Load	Voltage With Load
Nominal (7 Rotation of Pedal)	7.2V	5.4V
Maximum (15 Rotation of Pedal)	13.5V	9.45V

Buck converter will step down the voltage to yield the desire voltage for the load which is 5V. Other than that, a simulation for an open loop buck converter has been design to get the overview of the circuit and the parameters.

B. Power Stage Design

6V is choose as a reference voltage of input since it is a voltage from the nominal speed generated by the dynamo. Other than that, the switching frequency of this buck converter design is selected at 50kHz because the higher the frequency results in smaller of inductor and capacitor and it will reduce component size and reduce cost.

TABLE 3

Specification of Buck Converter Circuit

Vd	6V
Vo	5V
Frequency	50kHz
R	2.5Ω
ΔVo	5%
D	0.833
L	85µH
C	100µH
Io	2A
Δi_L	0.196

C. Compensator Design

Compensator is used to overcome the problem of the open loop buck converter circuit which is cannot regulate the output voltage due to the variation of input voltage [11]. In order to make the operation of feedback control successful, a proper design of compensator in PWM is required [12]. In control loops power converter there are two types of compensator that are widely used which are compensator type II and III [13]. Type II compensator consist of one origin pole, one zero and one high frequency and provide phase boost up to 90º while compensator type III, there are two poles and two zeros [11, 12]. In this closed loop design circuit, type III compensator is used. This is because, type III compensator can provide the required phase boost margin to maintain a reasonable phase margin [13].

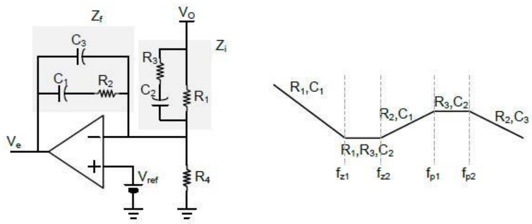

Fig. 4. Type III compensator with gain curve [14]

D. Closed-loop Buck Converter

In order to design the closed-loop buck converter, the linearize process of closed-loop buck is required. Figure 3.4 shows the linearization model of closed-loop buck converter.

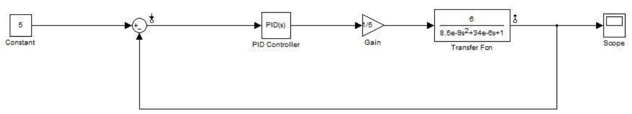

Fig. 5. Linearize model for buck converter

After implementing the linearized model of controller and
After implementing the linearized model of controller and
PWM to the buck circuit, the closed-loop buck converter is successfully designed and 5V is used as reference voltage to the PID controller.

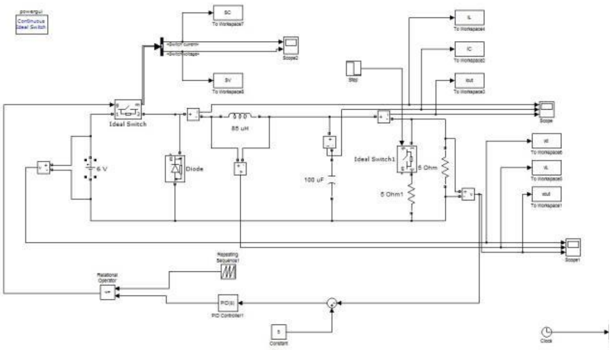

Fig. 6. Closed-loop buck converter circuit

E. *Hardware Implementation*

The hardware is implemented on a donut board. Th connection of the circuit is shows in Fig. 7 The IC socket is use because IC cannot resist the high temperature which can caus the IC to be damaged.

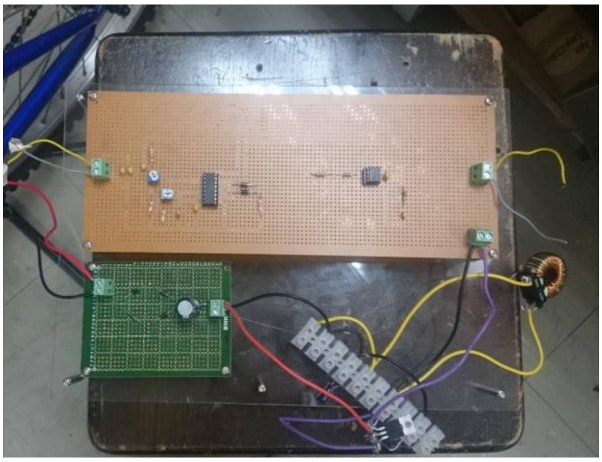

Fig. 7. Hardware implementation circuit

IV. Result and Discussion

A. *Full-Wave Bridge Rectifier*

Full-wave bridge rectifier is designed in the MATLAB simulation with the frequency of 50Hz and the selected voltage is 12V which is the maximum value rated for the dynamo. Fig. 8 and Fig. 9 shows the circuit design for the full-wave bridge rectifier with capacitance output filter of 680µF and the result of the simulation respectively. The result simulation indicates that the output voltage from the rectifier is nearly give purely DC output but there is ripples at the output voltage of the signal which is acceptable in designing a rectifier.

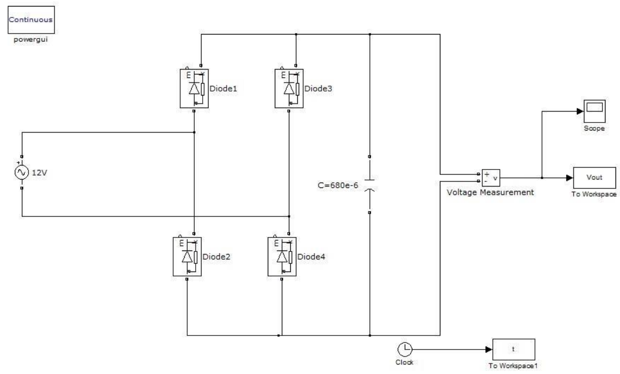

Fig. 8. Full-wave bridge rectifier design in MATLAB

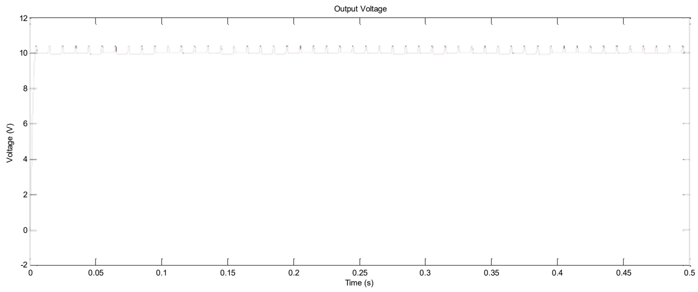

Fig. 9. Result simulation of full-wave bridge rectifier

B. *Closed-loop Buck Converter*

Fig. 10 shows the system respond of open-loop system and the system is not stable. To achieve the stability of system, the phase margin must be at least at 45º.

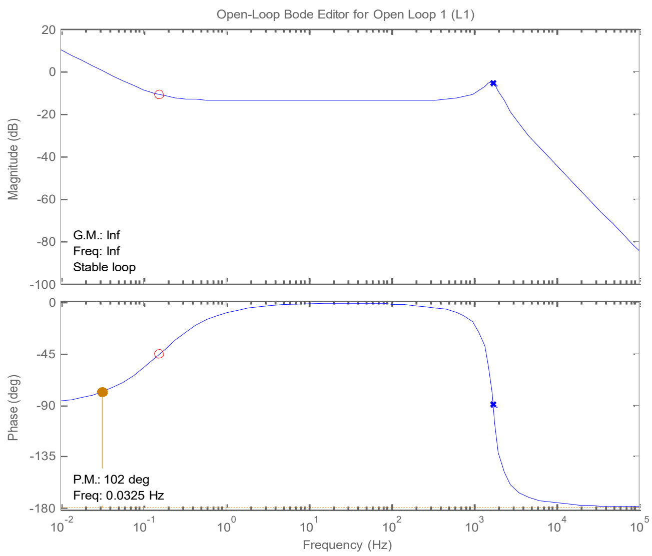

To obtain the desired respond, the system respond must be tuning to meet the criteria of 45º phase margin and 5kHz of crossover frequency. The crossover frequency is one decade below the selected switching frequency.

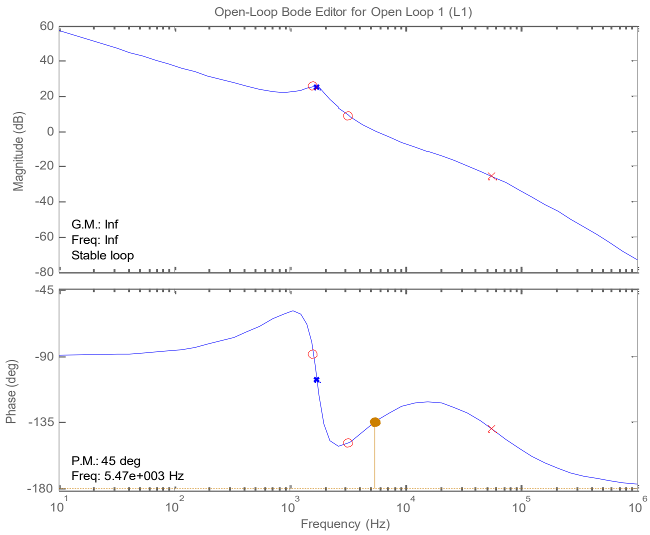

Fig. 11. System respond after compensator tuning

After completing the compensator tuning, a closed-loop buck converter circuit is designed as shown in the Fig. 12. The output voltage for closed-loop buck converter after the simulation is ran shown in Fig. 13 and the output voltage before 0.05 second shows the signal seems to be smooth. However, after 0.05 seconds the load is changes and it is shown that the signal produced is not very smooth and stable at 5V.

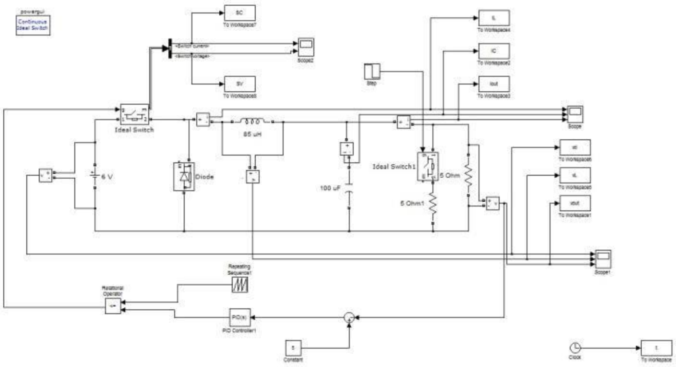

Fig. 12. Closed-loop buck converter design in MATLAB

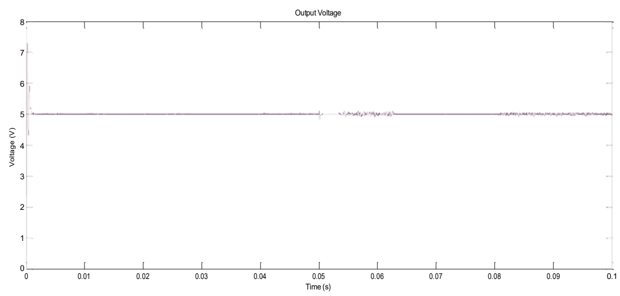

Fig. 13. Output voltage for closed-loop buck converter

C. Hardware Implementation Result

The prototype of this project is successfully implemented on a donut board. The data and result has been observed by using oscilloscope.

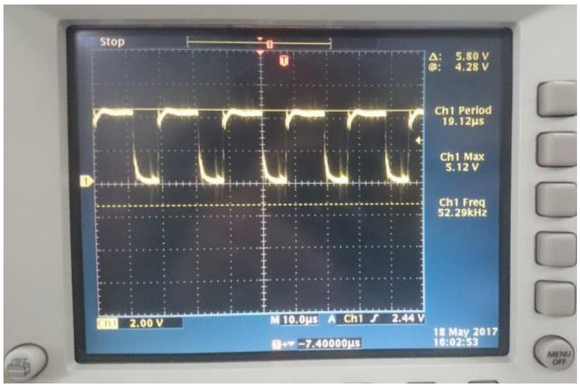

Fig. 14. Output from the PWM circuit

The PWM is supply with 15V and Fig. 14 shows the output of the PWM. The PWM is successfully design to meet the selected switching frequency which is 50kHz. However, the duty cycle cannot be adjust to D=0.833. This is because the resistor that should be in the design of PWM is removed due to the malfunctioning before do the test.

To turn on the MOSFET, the signal from PWM must get through the gate driver to boost the signal produced. The voltage from the PWM is amplified from 5V to 14.6V which is enough to turn on the MOSFET with Vgs=10V. Fig 15 shows the output from gate driver circuit.

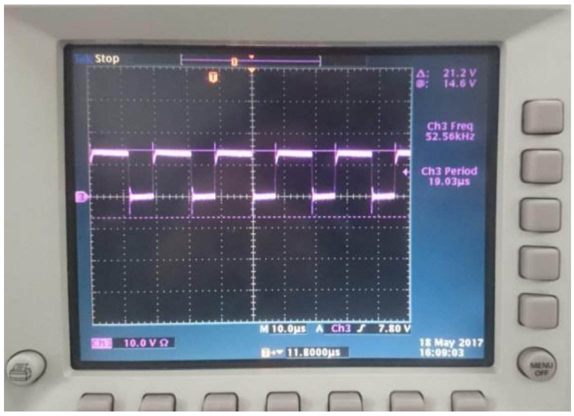

Fig 15. Output from gate driver circuit

The open-loop tested PWM and gate driver is connected to the buck converter. The output should produce 5V, since the duty cycle is cannot be adjusted further to D=0.833 the output of the open-loop buck converter is shown in Fig. 16.

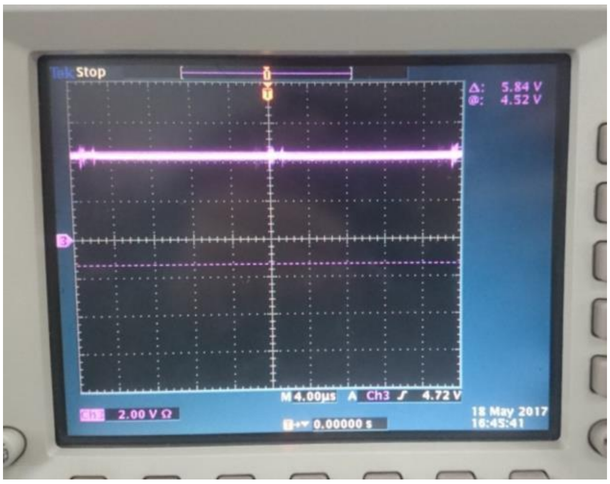

Fig 16. Output from buck converter

Unfortunately, the signal observation of open-loop buck converter cannot be further due to the malfunctioning of PWM. The possibility of this problem is due to the connection of the circuit on the donut board which is not properly solder.

V. Conclusion

In conclusion, the first objective of this project is achieved. However, the second objective is unsuccessful due to some error and mistake in doing the hardware implementation. The rectifier circuit for the hardware has been implemented, unfortunately the rectifier does not function. This problem is expected caused from the malfunction component used in the circuit. Other than that, the closed-loop buck converter circuit unsuccessfully completed is due to the damaged of the PWM.

References

[1] M. T Ullah, M. H. Uddin, M. A. Karim, G.M. Tauseef. (2015). Harvesting Green Energy from Wastage Energy of Human Activities Using Gymnasium Bicycle at Chittagong City. 2015 3rd International Conference on Green Energy and Technology.

[2] Hart, D. W. (2011). Power electronics. New York: McGraw-Hill.

[3] GCSE PHYSICS - Electromagnetism - What is a Bicycle Dynamo? . (2017, March). Retrieved from How does a Bicycle Dynamo Work? - GCSE SCIENCE: http://www.gcsescience.com/pme21.htm

[4] Megalingam, R. K., Nair, L. M., Viswanath, M., & Sugathan, S. (2012). Pedalite: Lighting up Lives in Un-electrified Villages. 2012 IEEE Global Humanitarian Technology Conference.

[5] (December, 2016). Retrieved from Full-wave Rectifier: http://www.eecs.tufts.edu/~dsculley/tutorial/diodes/diodes3.html

[6] Taufik, (2017, April). Retrieved from https://www.scribd.com/document/59252761/Taufik-Tutorial

[7] (2017, April). Retrieved from Sizing the Inductor of Buck Converter and Setting its Operation. (2017). ElectronicsBeliever: http://electronicsbeliever.com/sizing-the-inductor-of-buck-converter-and-setting-its-operation

[8] Azmi, H. S. (2016). Buck Converter Using DSPIC. Skudai, Johor: Universiti Teknologi Malaysia.

[9] Hassan, N. N. (2012). Design of Switched Mode: DC to DC Buck Converter. Skudai, Johor: Universiti Teknologi Malaysia.

[10] Zain, M. A. (2013). Buck Converter for LED Driver. Skudai, Johor: Universiti Teknologi Malaysia.

[11] Ramya H.S, Sangheeta.K, Shashirekha.M, Varalakshmi, Supriya.P, Assistant Professor. (n.d.). Design of Compensator for DC-DC Buck Converter. International Journal of Innovative Research in Technology & Science.

[12] Moktar, N. H. (2016). Solar Charger. Skudai, Johor: Universiti Teknologi Malaysia.

[13] Cao, L. (January 2011). Type III Compensator Design for Power Converter. 20-21.

[14] Lee, S. (July 2014). Demystifying Type II and Type III Compensators Using Op-Amp and OTA for DC/DC Converters.

Flyback Converter based LPG Leakage Detection Kit using GSM Module for Home Application

Thaventran A/L Panchanathan
Faculty of Electrical Engineering
Universiti Teknologi Malaysia
Johor Bahru, Malaysia.
thaven94@yahoo.com

Norjulia Binti Mohamad Nordin
Department of Electrical Power Engineering
Faculty of Electrical Engineering
Universiti Teknologi Malaysia
Johor Bahru, Malaysia.
norjulia@utm.my

***Abstract*— Liquefied Petroleum Gas (LPG) cylinder is a very common sight in most residential houses in Malaysia and it poses a great level of hazard when there is a leakage. This project proposes a Flyback converter based LPG leakage detection kit using Global System for Mobile communication (GSM) module for home application that can be powered from any ordinary electrical outlet (240V_{RMS}) of any household. The basic operation consists of three main modules: LPG leakage detection and level of leakage and transmission module. For early detection of LPG leakage, natural gas sensor MQ-4 is used and if the LPG level exceeds a safe threshold, fan will be activated for ventilation and solenoid valve will close, thus cutting the flow of LPG gas from the LPG cylinder. Then, user will be alerted by a message/call using GSM module. Flyback converter is successfully implemented with an output of 15 V_{DC} to power the solenoid valve, Arduino UNO, GSM module, natural gas sensor MQ-4, fan and buzzer. The main benefit of this system is fully automated thus requiring zero human intervention to operate and most importantly, it could save countless of lives from potential LPG leakage disaster.**

Keywords*— *Liquefied Petroleum Gas (LPG); Flyback converter; solenoid valve; Global System for Mobile communication (GSM) module; Gas Sensor MQ4

I. Introduction

It is very tough to imagine a life without Liquified Petroleum Gas (LPG), since most households use it for cooking. Although it is a common sight in every household, it is also very dangerous if the LPG is released in an uncontrolled amount. LPG for household applications consists of mixture of propane and butane which are flammable but nontoxic gases [1]. Now, since both propane and butane gases are odorless, ethanethiol a pungent gas is added so that whenever there is a potential gas leak, it would be possible for humans to detect by smelling otherwise it might go unrecognized. LPG is stored in a pressurized steel cylinders in liquid state to save space and evaporates at room temperature. LPG is even heavier than air so it tends to flow low points, therefore more prone to catch fire and explode if it leaks [2]. Another gas that is hazardous is the odorless and colorless carbon monoxide(CO) and is widely known as the ‘silent killer’ that can lead to asphyxiation and even in some serious cases, death [3]. CO gas is produced due to inadequate oxygen when fossil fuel is burned. The risk of CO gas is no different than LPG leak and steps to overcome it should be taken.

The effects of LPG gas leak and CO can be disastrous and could occur anytime anywhere, therefore, it is crucial to have a fully automated system that can monitor the LPG level and inform user if there’s any gas leak and take preventive measures to lower the LPG level. Proposed gas safety system method, a detection kit that can detect LPG and CO gas level that alerts the user if the gas level when above normal level and take preventive actions. The system comprises of three main parts; detection, action and transmission. Firstly, detection, it monitors the level of LPG gas and CO gas in the air using sensors MQ4 with MQ7 and if it is above normal, it takes action, turning OFF solenoid valve and turning ON exhaust fan and finally transmission, sends message or call the user to alert him/her. By turning OFF the solenoid valve, the flow of LPG from the cylindrical tank is cut off and turning ON the exhaust fan is to ventilate a room so that the concentration of LPG gas will be decrease. This system is very advantageous for those users who are physically far away from home, since the system is fully automated.

For this project, only Liquified Petroleum Gas (LPG) level will be detected whereas carbon monoxide gas level cannot be detected because CO gas is toxic and tough to obtain. An open loop Flyback converter is used to step down 240V_{rms} to 15V_{DC}. The output of the Flyback converter, 15V_{DC} which will power Arduino, LPG gas sensor MQ4, solenoid valve, buzzer and fan.

The goals of this project, requires stepping down 240V_{RMS} to 15V_{DC} using Flyback converter and with 555 Timer producing switching frequency of 31kHz coupled with Arduino as microprocessor. Besides, this project will be DC input independent, meaning it doesn’t require batteries or any form of DC input. Furthermore, this project aims to detect LPG and CO gas leakage and take preventive measures, closing of solenoid valve to stop flow of LPG from cylindrical tank and turning ON exhaust fan to ventilate the room. Lastly, this project is meant for residential/home where there is a LPG cylindrical tank.

II. Literature Review

There have many cases of Liquified Petroleum Gas (LPG) leak and in Malaysia such as housewife dies in cooking gas explosion [4], gas leak scare in Miri [5], gas leak victims were on vacation [6], elderly woman hurt in gas stove blast [7] and boy burnt in stove explosion [8]. According to the High Pressure Gas Safety Institute of Japan, from 2003 until 2015 the number of accidents for which includes LPG gas explosion and CO gas poisoning is still above 100 which is still high and annually the data either fluctuates higher than previous year or lower [9]. Therefore, LPG leak requires serious attention to avoid any LPG disasters.

Flyback Transformer, filter inductor and boost inductors are all members of the "Power Inductor" family. They all function by taking energy from the electrical circuit, storing it in a magnetic field, and subsequently returning this energy (minus losses) to the circuit. A Flyback Transformer is a multi-winding coupled inductors that have an air gap in the core to stored energy. The basic topology of the Flyback Converter is almost same as Buck-Boost converter. Flyback converter is in the category of Switch Mode Power Supply (SMPS) and has a higher operating efficiency in contrast with other DC-DC converters [10]. Flyback converters can be used as a step down or step up transformer based on the duty ratio and the ratio of primary turns with secondary turns.

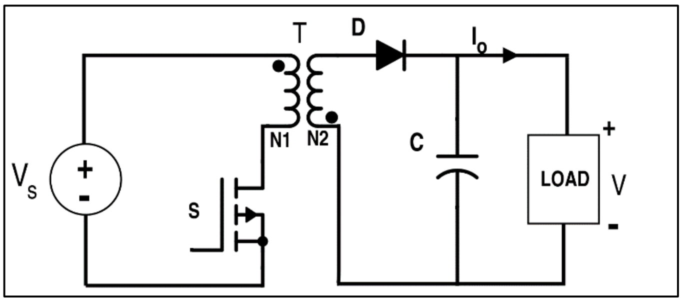

Fig. 1. Flyback Conveter Topology

Academic papers on gas leakage projects as follows, a Wireless Gas Leakage & Level Detection with Auto Renewal System by S.Sivajothi Kavitha is a gas leakage detection safety device that is wireless [11]. This device is meant to be utilised in households that use natural gas and LPG appliances. This framework additionally can be utilized for different applications as a part of the business or plants that rely on upon LPG and characteristic gas in their operations. The proposed remote home gas leakage framework comprises of three main modules: the gas leakage and level of exposure and transmission module (GSM/GPRS MODEM), and the receiver module (GSM Module). Continuous monitoring of the level of the LPG is done to detect the weight of the cylinder at the time of dispatch and throughout the usage. Auto restoration framework is alarmed when the barrel will be purged and auto booking is finished with the service station additionally giving the data to the customer.

Automatic Gas Alerting System by O. Mohana Chandrika and B. Alekya Hima Bindu proposed a Smart Gas cylinder machine is used to sort out all your problems associated with gas cylinder [12]. It will inform you through buzzer and SMS, gas leakage if any in the cylinder. SMS can be sent to the user as well as gas refilling agency when the gas level reaches below the threshold limit of gas around 2 kg so that the user can replace the old cylinder with new in time. If gas leakage is detected it will send SMS and immediately turn off the power supply which is most dangers for producing the spark leads to gas cylinder blast and it is indicated by buzzer to prevent fire accident.

An android based automatic gas detection and indication robot by Ch.Manohar Raju and N.Sushma Rani came up with an autonomous android based mobile robot for gas leak detection and localization in large industrial facilities [13]. The thought came up with a system that's able to perform scrutiny tasks in industrial facilities while not having to access unsafe areas directly - and while not requiring any human presence. The robot may be used for routine inspections of facilities or for targeted inspections of specific system components. The freelance quality of the system was enforced with varied navigation sensors and therefore the choice of manual intervention via device at any time.

III. Project Methodology

Basically, there are two circuits; main circuit and controller circuit. The controller circuit which starts with Timer555 will produce a switching frequency of 31kHz with an input from a $5V_{DC}$ adapter. Then the output of the 555 Timer will be stepped up to $15V_{DC}$ which is then fed to the MOSFET gate.

Next, is the main circuit whereby the input is an ordinary domestic 3-pin socket which is then connected to bridge rectifier which performs the AC to DC rectification. Then the output from bridge rectifier is connected to the Flyback converter which steps down DC to DC voltage and the output of the Flyback converter powers the load which includes Arduino, gas sensor MQ4, solenoid valve, buzzer and GSM module.

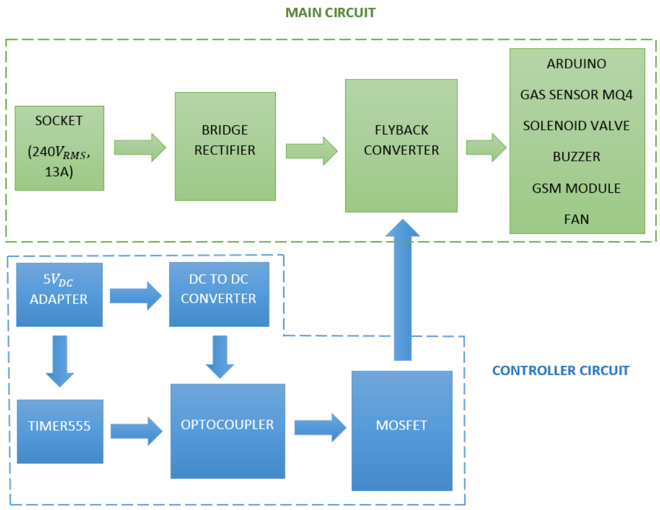

Fig. 2. Block diagram of the project

Based on the flowchart, this project depends on the input of the gas sensor MQ4, whereby if the level of CO and LPG leakage is found to be high, then the solenoid valve will be turned off and the exhaust fan with the buzzer will turn on followed by alerting the user via message or call.

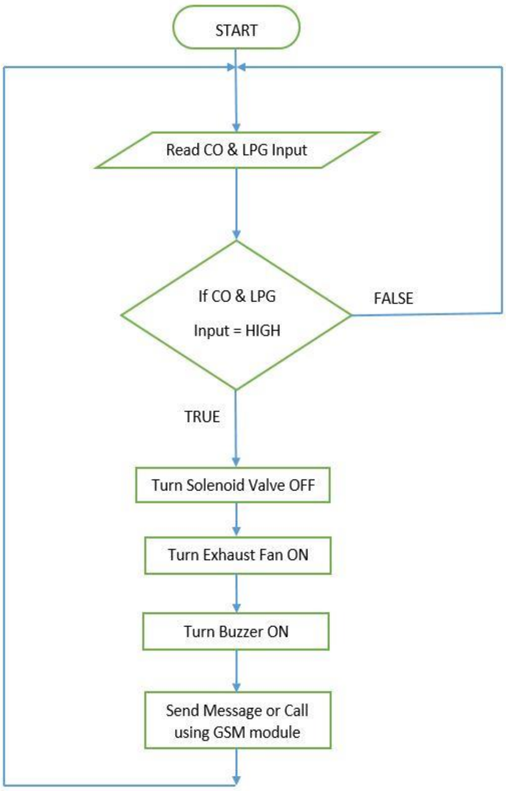

Fig. 3. Flowchart of the system

A. Simulation

From fig. 4, MATLAB is used to simulate the main circuit which consists of two parts, full wave rectification and Flyback converter. The first part, the input which is the domestic $240V_{rms}$, $13A$ is fed to diodes which converts AC to DC voltage. Then the output of the full wave rectification is connected to Flyback converter to step down the voltage to a desired voltage level and is then supplied to the load.

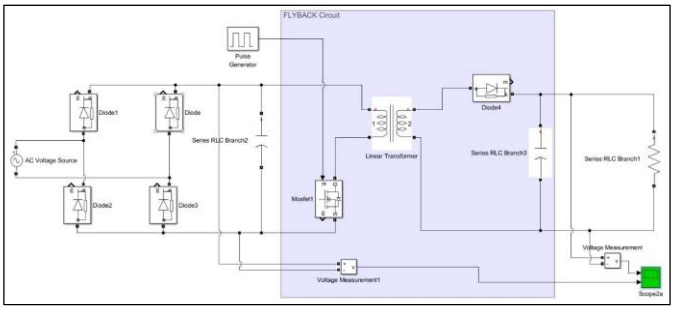

Fig. 4. Schematic circuit of simulation

TABLE I. FLYBACK CONVERTER SPECIFICATIONS

Specification	***Value***
Input Voltage, V_s	340 V_{dc}
Output Voltage, V_o	15 V_{dc}
Output Power, P_o	20 W
Switching Frequency, f	31kHz
Voltage Ripple, ${\Delta V_o}/{V_o}$	< 0.1 %
Winding ratio, ${N_1}/{N_2}$	17
Resistance, Ω	1

The required duty ratio,

$$V_o = V_s\left(\frac{D}{1-D}\right)\left(\frac{N_2}{N_1}\right) \quad (1)$$

Based on the specifications, D = 0.429

The required capacitor value, C_{min}

$$\frac{\Delta V_o}{V_o} = \frac{D}{RCf} \quad (2)$$

It is found the minimum capacitor value is $138.39\mu F$.

Minimum value of L_m,

$$L_m = \frac{(1-D)^2 R}{2f}\left(\frac{N_1}{N_2}\right)^2 \quad (3)$$

L_m = 9.42 mH

B. Hardware Setup

555 timer is an integrated circuit(IC) that is used widely in electronics due to its tough and reliable properties. Basically, it is a timing device that can produce highly accurate stable time delays or oscillation. For this project astable mode was used. In order to choose the right values of components, formulae need to be utilized to get desired output, 31kHz.

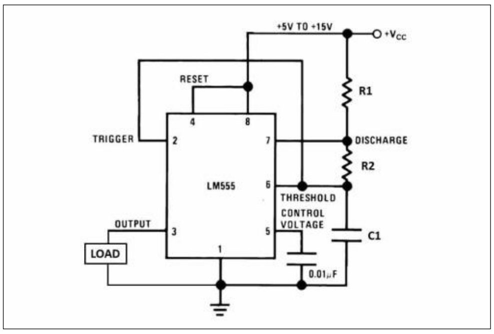

Fig. 5. 555 astable circuit diagram

The values of R1, R2 and C1 are used to establish the duty cycle, frequency, period and pulse length of the astable circuit. The formula to calculate frequency(f),

$$f = \frac{1.4}{(R1+2R2)\times C1} \quad (4)$$

Time period (T),

$$T = 0.69 \times (R1 + 2R2) \times C1 \quad (5)$$

Duty Cycle(D),

$$D = \frac{R2}{R1 + 2R2} \quad (6)$$

$$R2 = \frac{0.69}{f \times C1} \quad (7)$$

Subbing 31 kHz and 100pf into the equation gives 222.58 kΩ for R2 and R1 should be one-tenth of R2 value to obtain a duty cycle close to 50%. R1 is set to 22.26 kΩ.

Next is the optocoupler and it operates by transmitting electrical signals in the form of light from one isolated circuit to another. In this project, optocoupler is used to voltage from 555 Timer.

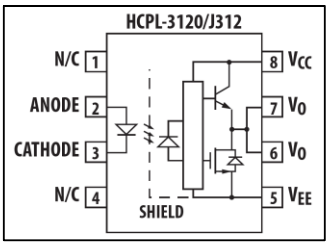

Fig. 6. HCPL-3120 pinout

The resistance that is needed for current regulation can be calculated using the formula as shown below,

$$R_g = \frac{(V_{CC} - V_{EE} + V_{OL})}{I_{OLPEAK}} \quad (8)$$

$$R_g = \left(\frac{15+5+2}{2.5}\right)$$

$$R_g > 8.8\ \Omega$$

$$R_g = 10\ \Omega$$

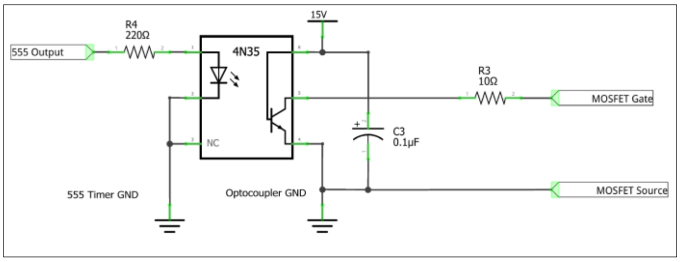

Fig. 7. Schematic diagram of HCPL-3120 circuit

Power switch MOSFET that is used in this project is IRFGB30 because it can handle fast switching up to nano seconds and the $V_{DS} = 1000\text{V}$, $I_D = 3.1\ A$, $R_{GS(on)} = 5\Omega$ at $V_{GS} = 20V$ and lastly it has maximum power dissipation of P_D= 125W.

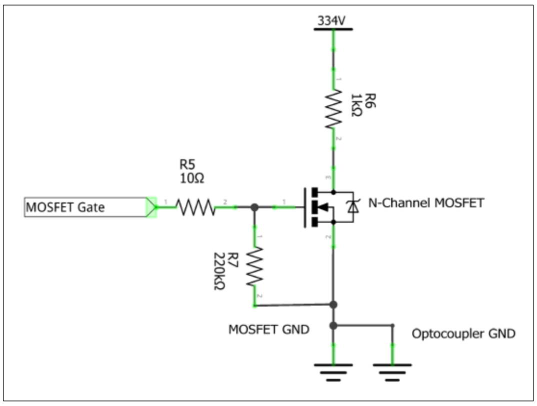

Fig. 8. Schematic diagram of N-Channel IRFGB30 MOSFET circuit

The main circuit which consists of Flyback transformer, capacitors, diode and loads. Loads are Arduino UNO, solenoid valve, GSM module, gas sensor MQ4, fan and buzzer.

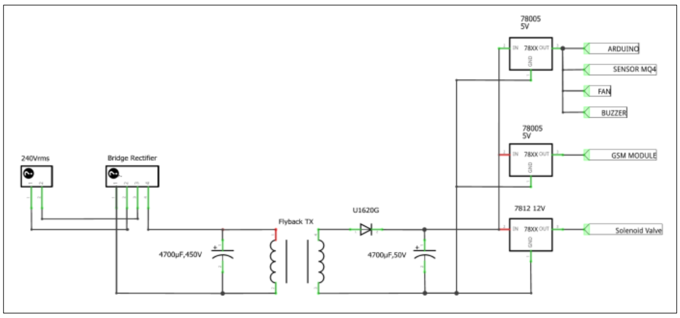

Fig. 9. Schematic of Flyback Transformer connected to loads

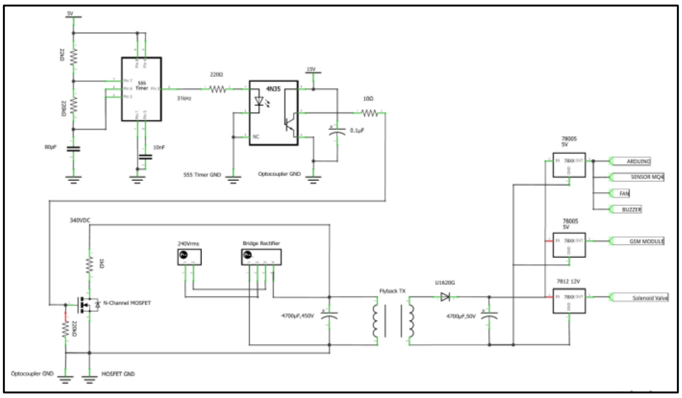

Fig. 10. The full schematic diagram of the whole project

IV. Results and Analysis

A. Simulation

From fig. 11, it can be seen that the Flyback transformer input which is from the rectification process is $340V_{dc}$ and the output of the Flyback converter is $15V_{dc}$

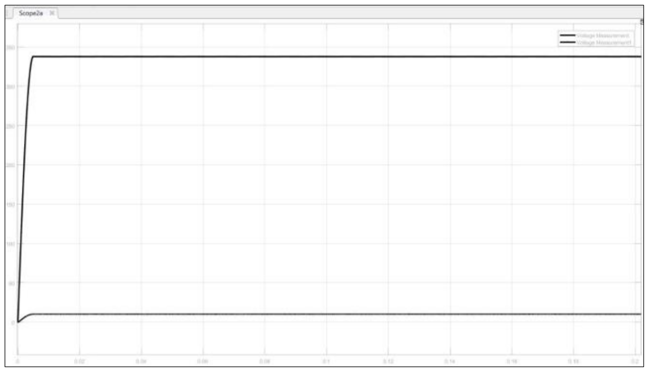

Fig. 11. Simulation Result at Flyback Input and Output

B. Hardware

After completing the wiring, output of the 555 Timer was observed using an oscilloscope, 555 Timer operates in astable mode produces a clock signal of close to 31kHz.

TABLE II. 555 TIMER

555 Astable 31kHz	
Component	***Value***
C1	80pF
R1	22kΩ
R2	220kΩ

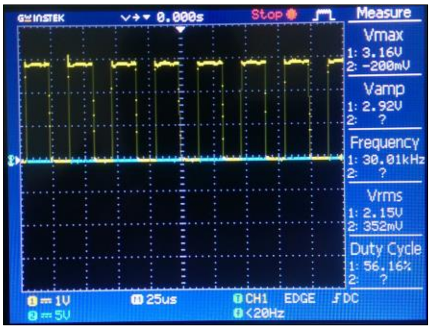

Fig. 12. Output of 555 Timer

After completing the circuit, the output of the octocoupler is observed using an oscilloscope, fig.13. It can be seen that the voltage is $17.2V_{DC}$ with a switching frequency of close to 31kHz.

Fig. 13. Output of optocoupler seen from oscilloscope

Flyback transformer was tested with loads such as Arduino UNO, GSM module, solenoid valve, gas sensor MQ4, buzzer and fan and the output measured across the secondary output of the Flyback transformer is shown in fig. 14.

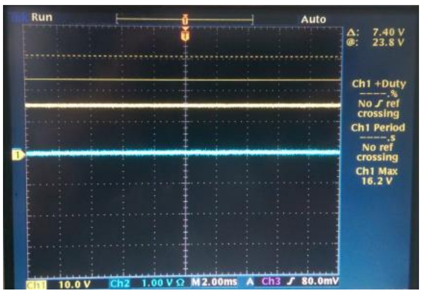

Fig. 14. Flyback transformer output voltage

As seen from fig. 14, the voltage produced is $16.2V_{DC}$. This shows that the Flyback transformer is working as expected..

TABLE III. FLYBACK TRANSFORMER PROPERTIES

Flyback Transformer	
Measurements	***Values***
Primary Voltage, V	339.00
Secondary Voltage, V	16.20
Primary Current, mA	33.00
Secondary Current, A	2.67
Primary Winding Resistance, Ω	87.74
Secondary Winding Resistance, Ω	4.36
Primary Winding Inductance, mH	159.27
Secondary Winding Inductance, mH	5.62

V. CONCLUSION

The Flyback transformer is able produce an output of $16.4V_{DC}$with 2.67A and is capable of powering Arduino UNO, GSM module, gas sensor MQ4, solenoid valve, buzzer and fan. In short, the goals of this project have been successfully executed that is stepping down $340V_{DC}$ to $15V_{DC}$ and powering Arduino UNO, LPG gas sensor MQ4, solenoid valve, buzzer and fan.

REFERENCES

[1] Woodford, Chris, " LPG (liquefied petroleum gas)," [Online]. Available: http://www.explainthatstuff.com/lpg.html.

[2] Abraham, John, "What is LPG and natural gas? | Energy Safety", *Energysafety.govt.nz*, 2016. [Online]. Available: http://www.energysafety.govt.nz/consumer/safe-living-with-gas-lpg/what-is-lpg-and-natural-gas.

[3] C.Kathy, " Carbon monoxide poisoning - NHS Choices," [Online]. Available: http://www.nhs.uk/Conditions/Carbon-monoxide-poisoning/Pages/Introduction.aspx#causes.

[4] W. Kong, "Housewife dies in cooking gas explosion," *Borneo Post Online* , 20-Mar-2012.

[5] "Gas leak scare in Miri," *Borneo Post Online*, 08-Aug-2014.

[6] K. A. Kili, "Gas leak victims were on vacation," *The Star Online*, 18-Mar-2015.

[7] A. Lai, "Elderly woman hurt in gas stove blast," *The Star Online*, 10-Feb-2015.

[8] "Boy burnt in stove explosion ," *The Star Online*, 21-Oct-2015.

[9] The High Pressure Gas Safety Institute of Japan(KHK). Annual Report on Liquefied Petroleum Gas (LPG) Related Accidents. 2016.

[10] Daniel Hart, W. (2011). *Power Electronics* (2nd ed.). New York: McGraw-Hill, 2011

[11] Senthilkumar, S. & Sivajothi Kavitha, S. (2015). A Wireless Gas Leakage & Level Detection with Auto Renewal System. *International Journal Of Advanced Research In Electrical, Electronics And Instrumentation Engineering*, *4*(4).

[12] Mohana Chandrika, O. & Alekya Hima Bindu, B. (2016). Automatic Gas Alerting System. *Imperial Journal Of Interdisciplinary Research (IJIR)*, *2*(6).

[13] Manohar Raju, C. & Sushma Rani, N. (2014). An Android based automatic gas detection and indication robot. *International Journal Of Computer Engineering And Applications*, *8*(1).

[14] L. Fraiwan, K. Lweesy, A. Bani-Salma and N. Mani, "A wireless home safety gas leakage detection system," *2011 1st Middle East Conference on Biomedical Engineering*, Sharjah, 2011, pp. 11-14.

[15] M. Rakesh and S. Dagadi, "Implementation of wireless gas leakage detection system," *2012 Sixth International Conference on Sensing Technology (ICST)*, Kolkata, 2012, pp. 583-588.

[16] R. Nicole, "Title of paper with only first word capitalized," J. Name Stand. Abbrev., in press.

[17] Y. Yorozu, M. Hirano, K. Oka, and Y. Tagawa, "Electron spectroscopy studies on magneto-optical media and plastic substrate interface," IEEE Transl. J. Magn. Japan, vol. 2, pp. 740-741, August 1987 [Digests 9th Annual Conf. Magnetics Japan, p. 301, 1982].

[18] M. Young, The Technical Writer's Handbook. Mill Valley, CA: University Science, 1989.

[19] A. B. Kevin, "Power System Security," [Online]. Available: http://www.citeseer.ist.psu.edu/387125.html, [Accessed January 9, 2005]

Energy Efficient of Intelligent Street Lighting System

Sunoorfatihah Binti Mohd Azman
Faculty of Electrical Engineering
Universiti Teknologi Malaysia
Johor Bahru, Malaysia.
sunoorfatihah@gmail.com

Abdullah Asuhaimi Bin Mohd Zin
Department of Electrical (Power)
Faculty of Electrical Engineering
Universiti Teknologi Malaysia
Johor Bahru, Malaysia.
asuhaimi@utm.my

***Abstract*— Street lighting is one of the important parts of a city's infrastructure where the main function is to illuminate the city's streets during the dark hours of the day. They make the society better and safer. High electricity consumption will cause an electricity crisis if not managed properly. One of the usages which consume electricity is public street lighting. This paper presents energy efficient of intelligent street lighting system which provides a safe night time environment for all road users. The main objective for this project is to improve the street lighting system performance, to reduce the power consumption of street lights that control by low-cost microcontroller which is arduino and to provide an automatic fault detector. Automatic street light is a simple and powerful concept, which uses Light Dependent Resistor and Passive Infrared sensors to switch ON and OFF the street light automatically. In addition, the Global System for Mobile Communication module will use in this system to send a message to the maintenance department when has damage lamp. This system operates during the dark day and focus is only for the one-way road at highway. By using this system, it is not only can reduce electric power consumption, but it also can remove manual works and faster repair a damage lamp. As a result, the system has been successfully designed and implemented as a model system.**

Keywords—Intelligent Street Lighting System; Arduino; PIR sensor; LDR sensor; Light Emitting Diode; GSM

I. Introduction

Nowadays, the number of streets increases rapidly with high traffic density in Malaysia. It became a serious issue when the electrical power wastage is higher due to the street lights. This is because the traditional lighting street lamps were controlled by manual control where the lamps "ON" and "OFF" based on a chronological time [1]. During the night, all the lights on the highway remain ON for the vehicles, but a lot of energy is wasted when there is no vehicle movement. Not all of the installation of street lights that existing today is perfect that give the intended result. Due to manual errors street lights not being switched OFF during the day time. The street lighting system must be improved because of Malaysian is the most populous country in the world that has the higher number of accidents on the road due to the lack of facilities on the roads and inefficiency of the street light system. Based on the statistical, index of death because of accidents on the road is increasing every year, which is 6615 people dead in 2013, 6674 people dead in 2014 and 6706 people dead in 2015 [2]. Besides, according to surveys it was found that 18% - 38% of the power wastage is due to the street lights [3]. So, the improvement of street lighting system must be considered. Thus, an automatic street light control system is of utmost importance to reduce power wastage and also to provide a safe night time environment for all road users.

II. SYSTEM AND METHODS

Hardware Specification

The system development starts with the design architecture of the proposed system. Almost 40% of the project consists of hardware part. Actually, this paper not only deals with the saving of energy, but also provides an automatic fault detector. The function of this project is to ON and OFF the street lights automatically based on the movement of vehicles that pass through the street during the dark day. The block diagram of this system is as shown in Figure 1. This project implemented "Intelligent Street Lighting System" by using Passive Infrared Sensor (PIR), Light Depends Resistance sensor (LDR), GSM module and Light Emitting Diode (LED). Each component has their role respectively.

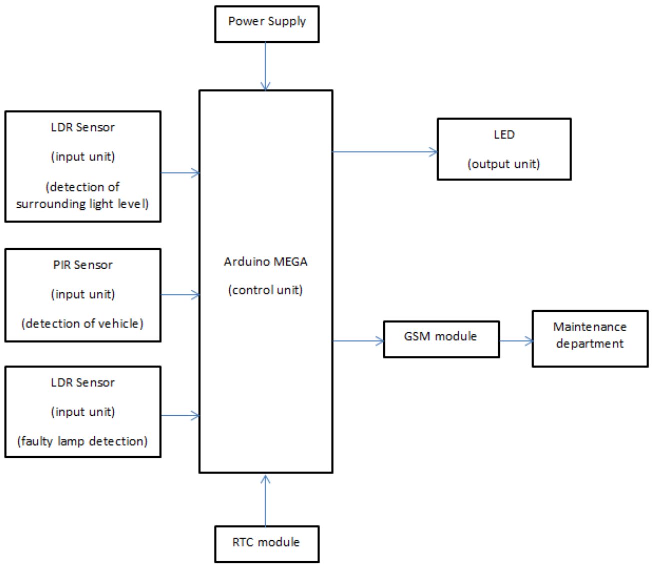

Fig. 1: The block diagram of intelligent street lighting system.

A. LDR Sensor

A Light Dependent Resistor (LDR) or a photo resistor is a device whose resistivity is a function of the incident electromagnetic radiation. Hence, they are light sensitive devices. LDR sensor is an electronic component that has a variable resistance that changes when it is exposed to light. The resistance of a LDR is not fixed and depends on the light intensity. A LDR has a high resistance in the dark, but a low resistance in the light [4].

In this project, LDR will use to detect the surrounding light level and also to send the signal to the microprocessor if lamp not glow on time. There are 13 LDR sensor used where the first LDR is used to activate the system to be ready to detect any object and vehicle by using Passive Infrared (PIR) sensor. This project focuses on 12 poles of lamp where each pole has one LDR to detect the faulty lamp that placed under the lamp. This LDR continuously sends signals to the microcontroller.

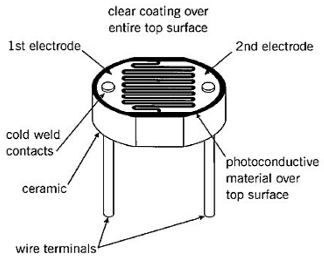

Fig.2: Parts of an LDR.

B. Passive Ir

A passive infrared sensor (PIR sensor) is an electronic sensor that measures infrared light radiating from objects in its field of view. They are commonly called simply "PIR", or sometimes "PID", for "passive infrared detector". The sensor is called “passive” because it does not send any signal outside to detect motion, but adjusts itself to record the infrared signature of the environment. Then it immediately probes the environment looking for any change. PIR sensors have many advantages, including quite in size, less expensive, possible to control the accuracy and easy to interface with. Other than that, PIR sensor is robust to surroundings in terms of temperature, humidity and electromagnetic noise [5]. In this project, PIR sensor will use to sense the vehicle that passes through the street. The sensor converts the resulting change in the incoming infrared radiation into a change in the output voltage, and this triggers the detection.

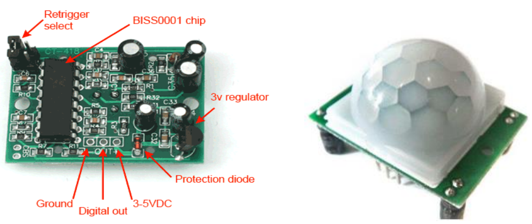

Fig. 3: Diagram of Passive Infrared Sensor.

C. Light Emitting Diode (LED)

A light-emitting diode (LED) is a two-lead semiconductor light source. LED is chosen for use in the street light technology nowadays because of many factors whether in term of size, energy consumption and environmental concerns. An LED street light is an integrated light-emitting diode (LED) light fixture that is used for street lighting as a one step towards energy saving. LED also has many advantages over incandescent light sources, including smaller in size that use low energy consumption, long and predictable lifetime, faster switching and more important is quick to turn ON and OFF [6]. Other than that, LED also can reduce glare, no need reflector that can send light in the desired direction and one more thing is LED does not contain mercury and do not release poisonous gases.

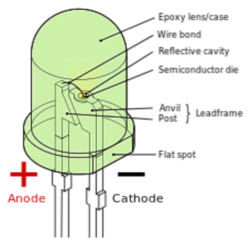

Fig. 4: Parts of an LED.

D. Global System for Mobile Communication (GSM) Module

The GSM mobile terminal provides us a communication channel that enables us to communicate with the world. GSM system was developed as a digital system using time division multiple access (TDMA) technique for communication purpose. A GSM digitizes and reduces the data, then sends it down through a channel with two different streams of client data, each in its own particular time slot. The features of GSM module have improved spectrum efficiency, international roaming, compatibility with integrated services digital network (ISDN), support for new services, SIM phonebook management, fixed dialing number (FDN), real time clock with alarm management, high-quality speech, uses encryption to make phone calls more secure and short message service (SMS) [7]. In this project, GSM will use to communicate between the street lamps and the main server.

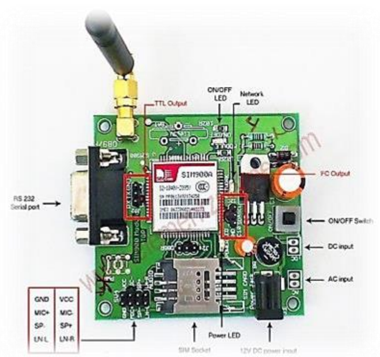

Fig. 5: Diagram of GSM module.

E. Real Time

A real-time clock (RTC) is a battery-powered clock that is included in a microchip in a computer motherboard. This microchip is usually separate from the microprocessor and other chips and is often referred to simply as "the CMOS" (complementary metal-oxide semiconductor). A small memory of this microchip stores system description or setup values - including current time values stored by the real-time clock. The time values are for the year, month, date, hours, minutes, and seconds. There are several advantages of RTC, including low power consumption, frees the main system for time-critical tasks and sometimes more accurate than other methods [8]. In this system, the RTC module was replaced with switch to set with mode for easier to demonstration.

Fig. 6: Diagram of RTC module.

F. Arduino

Arduino is an open-source electronics platform based on easy-to-use hardware and software. It is an open-source project that created microcontroller-based kits for building digital devices and interactive objects that can sense and control physical devices. Arduino has been in thousands of different projects and applications. It is able to read inputs such as light on a sensor, a finger on a button, or a Twitter message and then turn it into an output. Arduino has been chosen as the controller because of compact size, inexpensive, simple and clear programming environment [9]. In this system, arduino used as microcontroller to operate the program and execute the process associated with the proposed design.

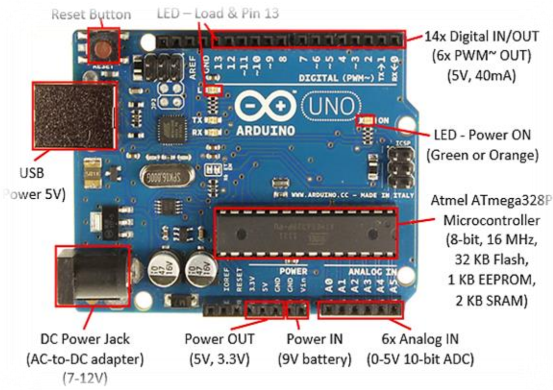

Fig. 7: Diagram of Arduino.

G.

LCD (Liquid Crystal Display) screen is an electronic display module and find a wide range of applications. A 16x2 LCD display is a very basic module and is very commonly used in various devices and circuits. These modules are preferred over seven segments and other multi segment LEDs. The reasons being: LCDs are economical; easily programmable; have no limitation of displaying special & even custom characters (unlike in seven segments), animations and so on [10]. In this project, the LCD display will use to display the total power usage.

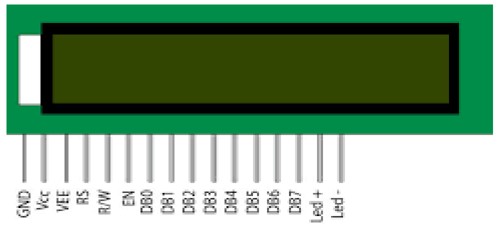

Fig. 8: Pin diagram of 16x2 LCD display.

Software Development

Almost 60% of the project consists of software part. The microcontroller required a program to operate and execute the process associated with the proposed design. Arduino software has been used as the interface between software and hardware for this project. The complete flowchart which indicates the whole operation of the system is as shown in Figure 9. To make it more specific, this project focusses on the specific place which is at highway and the target users is road users.

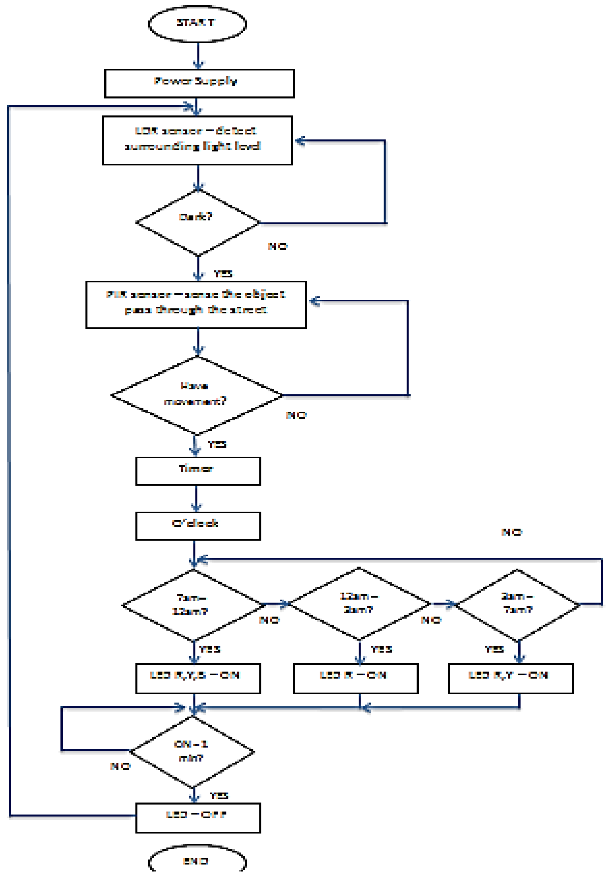

Fig. 9: Flowchart of the system.

Figure 4 : Diagram of Arduino Uno.

This project designs the street lighting functioning completely 24 hours because will consider the condition for a rainy day or when the light intensity is low. Actually, the total lamp for this project is 12 poles of lamps where one PIR sensor that responsible to send the signal to turn ON three lamp poles. The PIR sensor was located before that 3 lamp pole. So, the lamps will ON before the car arrives at this lamp.

The source for street lights is from a power supply that responsible to turn ON and OFF the street lights. The intelligent street light system flow is based on two conditions where the street lamps ON when in the dark day and when there is a vehicle that pass through the street. LDR used in this system to detect the surrounding light level. After the surrounding is dark, the light sensor will activate the system to be ready to detect any object and vehicle by using PIR sensor.

When PIR1 sense a movement, LED line 1 which is R1, Y1 and B1 will ON. When PIR2 sense a movement, LED R2, Y2 and B2 will ON and then R1, Y1 and B1 will turn OFF. The system then will continuously until PIR4 and then the system will loop to the initial condition. The period of the lamps ON based on the speed of a vehicle that passes through three lamps. The street lamps was programmed to light up based on the mode where normal mode is from 7.01am until12.00am, mode 1 for 12.01am until 3.00am and mode 2 for 3.01 until 7.00am based on the traffic flow. The number of lamps ON by using 3 phase concept where LED red, yellow and blue line will ON in a normal mode, LED red line only will ON in mode 1 and LED red and yellow line will ON in mode 2. The power usage also will be displayed on the LCD screen.

Other than that, this project also considers about pole damage detection. GSM module used to communicate between the street lamps and the main server. Whenever lamp will not glow, the LDR sensor will send a signal to microprocessor and then microprocessor will command GSM module to send a message about the location of the damaged lamps to the maintenance department (GSM module uses AT command to send message). Hence, it can be used to identify the faulty lamps.

III. RESULTS AND DISCUSSIONS

A prototype of the intelligent street lighting system is developed and the whole prototype design is as shown in Figure 10. The design of the project was done with 12 LEDs, 4 PIR sensors and 13 LDR sensors. For indicator part have 1 LCD screen, 4 LED for PIR sensors, 12 switches for disconnected the lamps to show the damage lamp for demonstration. All the wiring and connection are connected to the Arduino board. This project works properly and success presented low cost and better efficient solution for intelligent street light system.

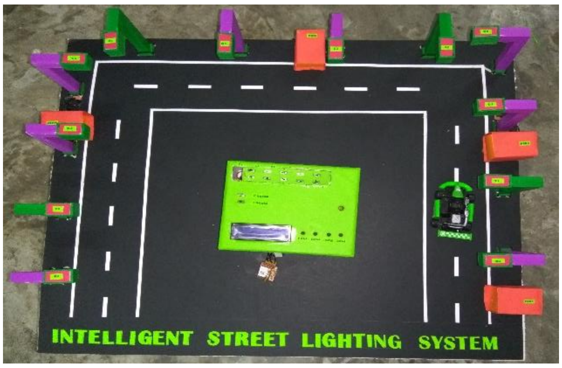

Fig. 10: Prototype of proposed design project.

A. *Energy Utilization*

For energy efficiency of intelligent street lighting system project, the usage of energy was analyzed by using the method of calculation. The power usage for this project was less than the normal power usage of street lights that existing today that will be shown based on the calculation below by using equation (1), (2) and (3) [11]. This is because the power consumption based on the number of lamps ON by using 3 phase concept and mode. Plus, this system using LED as the light module which is better in saving energy compared with other lamps.

Assuming that the street lighting functioning completely 12 hours within 7.00 p.m. until 7.00 a.m. The total power consumed by 1 HPS is 400W and 1 LED is 200W. Besides, 12 nodes are used to be working power consumed and the lists of formulae used for the calculation of energy utilization are given as below:

$$D = A \ X \ B \ X \ C \tag{1}$$

$$E = D \ X \ 30 \tag{2}$$

$$P = (E1 - E2) / E1 \ X \ 100 \tag{3}$$

Where, A = Total power consumed

B = Number of nodes

C = Number of working hours per day

D = Power consumed per day

E = Power consumed per month

P = Energy saved per month

a) Using High Pressure Sodium (HPS)

Total power consumed by 1 HPS, A = 400W

Number of nodes, B = 12

Number of working hours per day, C = 12

D = 12 x 12 x 400

= 57.6 kWh/day

E = 57.6 x 30

= 1728 kWh/month

b) Using LED

Total power consumed by 1 LED, A = 200W

Number of nodes, B = 12

Number of working hours per day, C = 12

D = 12 x 12 x 200

= 28.8 kWh/day

E = 28.8 x 30

= 864 kWh/month

c) Using LED (for intelligent street light system)

Total power consumed by 1 LED, A = 200W

Number of nodes, B = B1 + B2 + B3

Where,

B1 = 12 (fully light ON from 7pm – 12 am)

B2 = 4 (light ON when PIR sensor detect movement from 12am – 3am)

B3 = 8 (light ON when PIR sensor detect movement from 3am – 7am)

Number of working hours per day, C = C1 + C2 + C3

Assume,

C1 = 5 hours (fully light ON from 7pm – 12 am / traffic heavy)

C2 = 1 hour (light ON when PIR sensor detect movement from 12am – 3am)

C3 =3 hours (light ON when PIR sensor detect movement from 3am – 7am)

Therefore, C =9 hours

D = [(5 x 12) + (1 x 4) + (3 x 8)] x 200

= 17.6 kWh/day

E = 17.6 x 30

= 528 kWh/month

From the calculation above, comparison of the energy saved between HPS lamps and LED lamp is obtained. Based on this calculation, Table 1 shown the percentage of energy saved per month between High Pressure Sodium (HPS) lamps, Light Emitting Diode (LED) for public street lighting and LED for automation system.

Table 1: Comparison of energy saving between LED and HPS

Type of lamps used	**Percentage of energy saving**
LED for intelligent street lighting system vs HPS for public street lighting	69.44%
LED for intelligent street lighting system vs LED for public street lighting	38.89%

About 38.89 % energy can be saved when compared LED for intelligent street lighting automation system with LED used for public street lighting. However, replacing HPS lamps with LED as street lighting automation system offers around 69.44% of power saving. The difference value between usages of HPS lamps quite high compared than the usage of LED. Consequently, usage of LED gives more energy saving compared than High Pressure Sodium (HPS) lamps.

B. Calculation for Estimated Power Saving

The estimated power saving was calculated by using equation (4), (5) and (6) [11]. The calculation is based on Malaysian street lighting tariff that shows the calculation of energy saving for intelligent street lighting automation system and simple payback period (SPP) [12]. The lists of formulae used for the calculation for estimated power saving are given as below:

$$G = (E\ (\text{LED not installing PIR sensor}) - E\ (\text{LED installing PIR sensor})) \times T \quad (1)$$

$$H = D\ (\text{LED installing PIR sensor}) \times C \times 30\ \text{days} \times T \times K \quad (2)$$

$$SPP = F / J \quad (3)$$

Where, C = Number of working hours per day

D = Power consumed per day

E = Power consumed per month

F = Total initial investment

G = Saving per month (RM)

H = Operation cost per month (RM)

J = Saving per year (RM)

K = Number of PIR sensor

T = Malaysian street lighting tariff = 0.192 sen

SPP = Simple Payback Period

Where, Total cost for LED = RM 0.10 x 12 = RM 1.20

Total cost for PIR sensor = RM 4.00 x 4 = RM 16.00

Total cost for LDR sensor = RM 0.70 x 13 = RM 9.10

Cost of controller = RM 40.00

Cost of RTC module = RM 3.00

Cost of GSM module = RM 25.00

Total initial investment, F = RM 94.30

G = (864 – 528) x 0.192 sen

= RM 64.51

H = 0.0176 x 9 x 30 x 0.192 x 4

= RM 3.65

J = (G – H) X 12 months

= (64.51 – 3.65) X 12

= RM 730.32

SPP = 94.30 / 730.32

= 0.129 years

= 1.5 months

From the calculation above, approximately 1.5 months are required to recover the initial investment through project savings. This project focuses for small area about 12 numbers of street lamps. Therefore, the simple payback period of automation system will reduce for installation in the large area compared to the small area.

IV. CONCLUSIONS

This paper elaborates the design and construction of intelligent street lighting system circuit. By referring all the results, it can be concluded that both hardware and software development of this project meet the objective of design. PIR and LDR sensor are two the main conditions in working the circuit that have been satisfied the circuit will do the desired work according to the specific program. In addition, this project also considers about the damaged lamp that can send location to the maintenance department by using low power consumption of GSM module. Based on the calculation of energy utilization, about 38.89 % energy can be saved when compared LED for intelligent street lighting automation system with LED used for public street lighting. However, replacing High Pressure Sodium (HPS) lamps with LED as street lighting automation system offers around 69.44% of power saving. The difference value between usages of HPS lamps quite high compared than the usage of LED. Consequently, usage of LED gives more energy saving compared than High Pressure Sodium (HPS) lamps. The payback period also can be minimized which is approximately 1.5 months are required to recover the initial investment through project savings by using this system. So, this project success presented low cost and better efficient solution for intelligent street light system. The methods for this project will bring a revolution in the field of automation of street lights.

V. REFERENCES

[1] Deepanshu Khandelwal, Bijo M Thomas, Kritika Mehndiratta and Nitin Kumar. (2015). “Sensor-based automatic street lighting system”. Vol.2, No. 2, pp 24-27.

[2] www.jpj.gov.my/portalrasmijabatanpengangkutanjalanMalaysia, retrieved on 20 October 2016

[3] Nitish Kumar Jha and Anustup Biswal. (2016). “Advanced street lights”. Vol.5 No.1, pp 704-707.

[4] Shubham Singhmar, Mohit Kumar and Ishika Goyal. (2016). “Automatic street light control system using relays and LDR”. Vol.3, No. 1, pp 20-22.

[5] Swarnava Majumdar and Kuntal Roy. (2013). “A power saving passive infrared sensor module”. Vol.4, No. 6, pp 1654- 1660.

[6] Pilar Elejoste, Ignacio Angulo, Asier Perallos, Aitor Chertudi and Asier Moreno. (2013). “An easy to deplot street light control system based on wireless communication and LED technology”. Vol. 1, No.13, pp 6492-6523.

[7] M. Shariz Ansari, Tanmay Srivastava, Rishabh Saxena and Saurabh Singh. (2015). “GSM based street light automation”, Vol.4, No.5, pp 4415-4418.

[8] Archana. G, Aishwarya. N, Anitha. J and Vijay Kumar. (2015). “Intelligent street light system”. Vol. 3, No. 4, pp 16-18.

[9] Mustafa Saad, Abdalhalim Farij, Ahamed Salah and Abdalroof Abdaljalil. (2014). “Automatic street light control system using microcontroller”. Pp 92-96.

[10] Parkash, Prabu V and Dandu Rajendra. (2016). “Internet of things based intelligent street lighting system for smart city”. Vol. 5, No. 5, pp 7684-7691.

[11] N.L. Ramli, N. Mohd Yamin, S. Ab Ghani, N. Md Saad and S. A. Md Sharif. (2015). “Implement of passive infrared sensor in street lighting automation system”. Vol.10, No. 22, pp 17120-17126.

[12] https://www.tnb.com.my/residential/apply-for-streetlights

Non-Conventional Multilevel Inverter for Photovoltaic Applications

Noor Syaza Nadhira Mohamad Subri
Faculty of Electrical Engineering
Universiti Teknologi Malaysia (UTM)
Johor, Malaysia
noorsyazanadhira@gmail.com

Naziha Ahmad Azli
Faculty of Electrical Engineering
Universiti Teknologi Malaysia (UTM)
Johor, Malaysia
naziha@fke.utm.my

***Abstract*—Conventional multilevel inverters for photovoltaic (PV) application have been widely used in recent years. However, main problem of conventional multilevel inverter is higher number of power switches needed in order to obtain high quality of output waveform which eventually lead to high power losses. This paper presents non-conventional multilevel inverter (NcMI) for PV application with reduced number of power switches. The performance of nine level NcMI single phase with respect to number of switches and total harmonic distortion (THD) with PV as its input source is simulated by using MATLAB/Simulink and discussed**

Keywords—– PV array; MPPT; Multilevel inverter; Power switches; structure; PWM

I. INTRODUCTION

Multilevel inverter is widely used nowadays especially in renewable energy application. This is a result from the power demands combined with the interest in green technology especially in photovoltaic (PV) system [1].

Multilevel inverter itself refer to an enhancement of 2-level inverter which can provide desired alternating output voltage from several levels of dc voltage at input. There are three type of common used multilevel inverter which are cascaded h-bridge multilevel inverter, diode clamped multilevel inverter and flying capacitor multilevel inverter. Diode clamped multilevel inverter and flying capacitor multilevel inverter require higher number of power switches compared to cascaded H- bridge multilevel inverter [6].

For PV application, the most promising type of multilevel inverter is cascaded H-bridge which has separated dc voltage that is suitable for integration of renewable energy resources [2] . However, CHMI is still being considered to have large number of power switches [6]. Thus, a lot of new topologies have been proposed in order to minimise the power switching losses hence will produce better quality of output waveform.

In this paper, a non-conventional topology proposed in [3] has been analysed and fed with PV as the input sources. In this structure, a nine level symmetry NcMI is connected with PV array. Conventional Boost converter is also used in this system in order to increase the value of output voltage according to desired voltage. Boost converter is controlled by using maximum power point tracking (MPPT) algorithm. MPPT is used to track the maximum power and maximised the generated energy [7].

This topology has the capability to produce output voltage with reduced number of power switches which will reduce the circuit complexity and suitable for PV system. A comparison between CHMI structure with NcMI proposed in [3] is carried out and an analysis of NcMI with PV sources in term of system structure and THD has been made.

.

II. LITERATURE REVIEW

A. Photovoltaic array module

Photovoltaic (PV) system is a system that converts sunlight directly into electricity. Each photovoltaic array contains groups of PV cells. PV cell is basically a semiconductor diode which is being exposed to light [7]

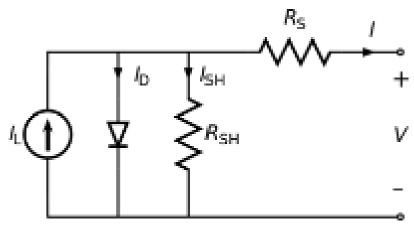

Fig. 1. Equivalent circuit of PV module

Equivalent circuit is shown in Fig. 1. The current source, I_L is parallel to the diode while R_{SH} and R_S represent parallel and series resistance respectively. Equations of current and voltage used in PV array are as follows

$$I = I_L - I_D \tag{1}$$

$$I = I_L - \left[\exp\left(V + \frac{R_S I}{V_t a}\right) - 1\right] - \frac{V + R_S I}{R_{SH}} \tag{2}$$

Where

$I_D = I_O \, exp(qV/akT)$
$I_O = leakage\ current\ of\ the\ diode$

$q = electron\ charge$
$k = Boltzmann\ constant$
$T = temperature\ of\ pn\ junction$
$a = diode\ ideality\ constant$
$V_t = N_s kT/q$, N_s is number of cells connected in series.

Higher number of Cells connected in series will provide higher output voltage while higher number of cells connected in parallel will increase the current [7]. Next, Maximum power point (MPP) is being expressed as

$$P_{max} = V_{max} \times I_{max} = \gamma V_{OC} I_{SC} \qquad (3)$$

γ is the cell fill factor that determine the quality of the cell. By using MATLAB/Simulink, the parameter of Kyocera Solar SU53BU is chosen as shown in table below

TABLE I: *SPECIFICATIONS OF PV ARRAY MODULE IN MATLAB/SIMULINK*

Parameter	Values
Maximum power (P_{max})	53.1
Voltage at P_{max} (V_{mp})	7.78
Current at P_{max} (I_{mp})	6.82
Short circuit current (I_{SC})	7.4
Open- circuit voltage (V_{OC})	9.6
No of cells in series (N_s)	16
No of cells in parallel (N_p)	1

B. Maximum Power Point Tracking (MPPT)

MPPT is refer to a control system which will allow the module to produce maximum power depends on the variation of irradiance and temperature [8]. Many methods of finding MPPT have been developed but perturb and observe (P&O) is the most commonly used as it is simple and cost less.

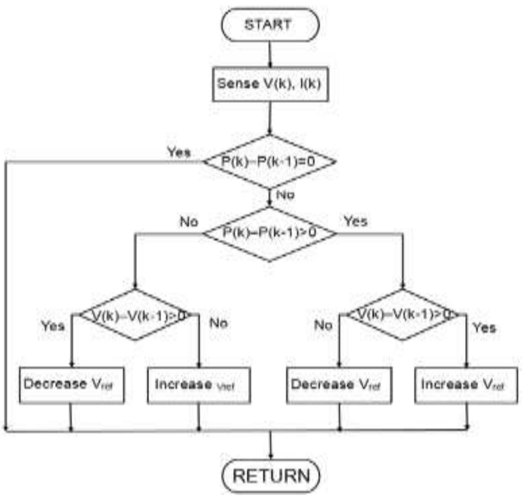

Fig.2. Flowchart of perturb and observe (P&O) process

C. Conventional cascaded H-bridge Multilevel inverter (CHMI)

This topology consists of series m-level cascaded inverter and has separated dc sources for each single phase full bridge inverter or H-bridge as shown in Figure 2.1. Each cells capable to generate three different output voltages: *+Vdc, 0,* and *–Vdc*. The ac output voltages, V_o is the sum of inverter outputs which is represented as below:

$$N = 2n + 1 \qquad (4)$$

Where *N* is number of levels, *s* is the number of dc sources [3]. Fig. 3 shows the configuration of CHMI circuit

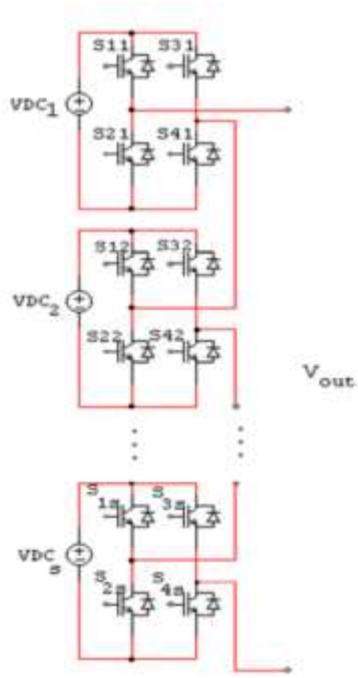

Fig.3. conventional cascaded H-bridge multilevel inverter

Cascaded H-bridge inverter is said to have some advantages over the other two methods which will be discussed later. One of the advantages is, it is requires less number of power switches compared to diode clamped and flying capacitor inverters. Therefore the switching losses will be lower hence will improve the output waveform [4].

Cascaded H-bridge also requires cheaper manufacturing process as it is easily to be modularized. The disadvantages of cascaded H-bridge is limitation of application as it requires separate dc voltages [3]

D. Non-conventional multilevel inverter (NcMI)

As stated in [5], the proposed multilevel inverter consists of *n* dc sources and *n-1* bidirectional power switches. S_1, S_2,… S_{n-1},. Those bidirectional power switches cannot be turned on simultaneously in order to avoid short circuit. Zero output voltages are obtained by adding unidirectional switches S_a,S_b, S_c, and S_d.

S_d, and S_c, need to be turned on in order to provide negative and positive output. Both switches also only requires fundamental frequency to work which is one of the advantages of this topology. The overall of arrangement of this topology is shown in Fig. 4

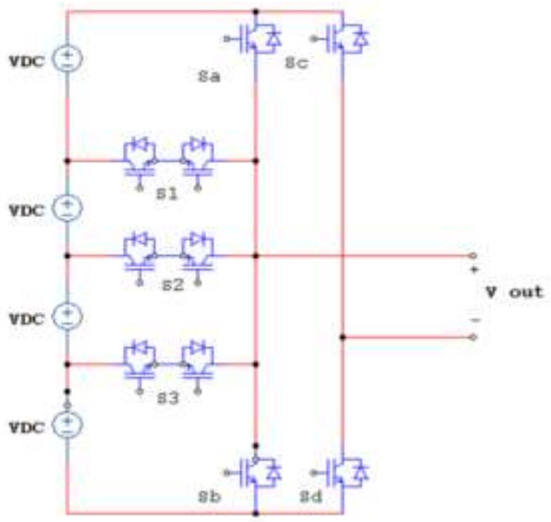

Fig. 4. Non-conventional multilevel inverter proposed in [3]

TABLE 1: *SWITCHING STATES OF PROPOSED TOPOLOGY IN [3]*

Switches states											Output levels
S_1	S_2	S_3	...	S_{n-3}	S_{n-2}	S_{n-1}	S_a	S_b	S_c	S_d	
0	0	0	...	0	0	1	0	0	0	1	VDC
0	0	0	...	0	1	0	0	0	0	1	2VDC
0	0	0	...	1	0	0	0	0	0	1	3VDC
.	.	.	...	.	.	.	.	.	.	.	.
.	.	.	...	.	.	.	.	.	.	.	.
.	.	.	...	.	.	.	.	.	.	.	.
0	0	1	...	0	0	1	0	0	0	1	(n-3)VDC
0	1	0	...	0	0	1	0	0	0	1	(n-2)VDC
1	0	0	...	0	0	1	0	0	0	1	(n-1)VDC
0	0	0	...	0	0	0	1	0	0	1	nVDC
–	–	–	...	–	–	–	0	1	0	1	0
–	–	–	...	–	–	–	1	0	1	0	
1	0	0	...	0	0	0	0	0	1	0	-VDC
0	1	0	...	0	0	0	0	0	1	0	-2VDC
0	0	1	...	0	0	0	0	0	1	0	-3VDC
.	.	.	...	.	.	.	.	.	.	.	.
.	.	.	...	.	.	.	.	.	.	.	.
.	.	.	...	.	.	.	.	.	.	.	.
0	1	0	...	1	0	0	0	0	1	0	-(n-3)VDC
0	0	0	...	0	1	0	0	0	1	0	-(n-2)VDC
0	0	0	...	0	0	1	0	0	1	0	-(n-1)VDC
0	0	0	...	0	0	0	0	1	1	0	-nVDC

Useful equations that need to be considered;

$$N_{level} = 2n + 1 \quad (5)$$
$$N_s = n + 3 \quad (6)$$
$$N_{drive} = N_s = n + 3 \quad (7)$$
$$N_{IGBT} = 2n + 2 \quad (8)$$

Where;

n = number of DC sources
N_{level} = number of level
N_s = number of switches
N_{drive} = number of gate drivers
N_{IGBT} = number of IGBTs

As stated in [5], the proposed multilevel inverter consists of *n* dc sources and *n-1* bidirectional power switches. S_1, S_2,... S_{n-1},. Those bidirectional power switches cannot be turned on simultaneously in order to avoid short circuit. Zero output voltages are obtained by adding unidirectional switches S_a,S_b, S_c, and S_d.

S_d, and S_c, need to be turned on in order to provide negative and positive output. Both switches also only requires fundamental frequency to work which is one of the advantages of this topology. The overall of arrangement of this topology is shown in Figure 4

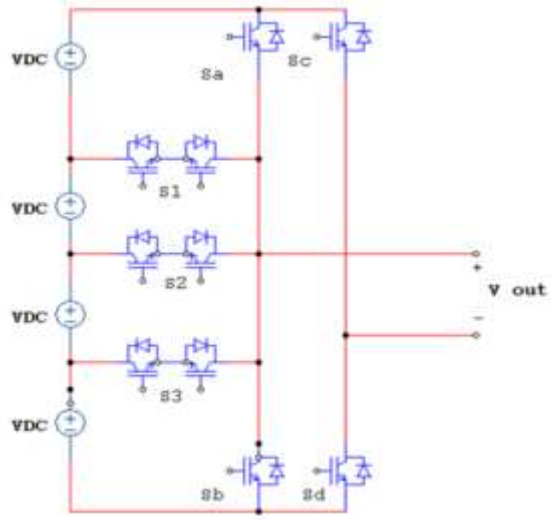

Figure 4: *Non-conventional multilevel inverter proposed in [3]*

Table 2: *Switching states of proposed topology in [3]*

Switches states											Output levels
S_1	S_2	S_3	...	S_{n-3}	S_{n-2}	S_{n-1}	S_a	S_b	S_c	S_d	
0	0	0	...	0	0	1	0	0	0	1	VDC
0	0	0	...	0	1	0	0	0	0	1	2VDC
0	0	0	...	1	0	0	0	0	0	1	3VDC
.	.	.	...	.	.	.	.	.	.	.	.
.	.	.	...	.	.	.	.	.	.	.	.
.	.	.	...	.	.	.	.	.	.	.	.
0	0	1	...	0	0	1	0	0	0	1	(n-3)VDC
0	1	0	...	0	0	1	0	0	0	1	(n-2)VDC
1	0	0	...	0	0	1	0	0	0	1	(n-1)VDC
0	0	0	...	0	0	0	1	0	0	1	nVDC
–	–	–	...	–	–	–	0	1	0	1	0
–	–	–	...	–	–	–	1	0	1	0	
1	0	0	...	0	0	0	0	0	1	0	-VDC
0	1	0	...	0	0	0	0	0	1	0	-2VDC
0	0	1	...	0	0	0	0	0	1	0	-3VDC
.	.	.	...	.	.	.	.	.	.	.	.
.	.	.	...	.	.	.	.	.	.	.	.
.	.	.	...	.	.	.	.	.	.	.	.
0	1	0	...	1	0	0	0	0	1	0	-(n-3)VDC
0	0	0	...	0	1	0	0	0	1	0	-(n-2)VDC
0	0	0	...	0	0	1	0	0	1	0	-(n-1)VDC
0	0	0	...	0	0	0	0	1	1	0	-nVDC

Useful equations that need to be considered;

$$N_{level} = 2n + 1 \quad (5)$$
$$N_s = n + 3 \quad (6)$$
$$N_{drive} = N_s = n + 3 \quad (7)$$
$$N_{IGBT} = 2n + 2 \quad (8)$$

Where;
n = number of DC sources
Nlevel = number of level
Ns = number of switches
Ndrive = number of gate drivers
NIGBT = number of IGBTS

III. SIMULATION STUDY

The components involve in implementation of PV as the input sources is conventional boost converter which it's duty cycle will be controlled by MPPT, non-conventional multilevel inverter proposed in [3] and also LC filter. The overall system is clearly illustrated as Fig. 5 below

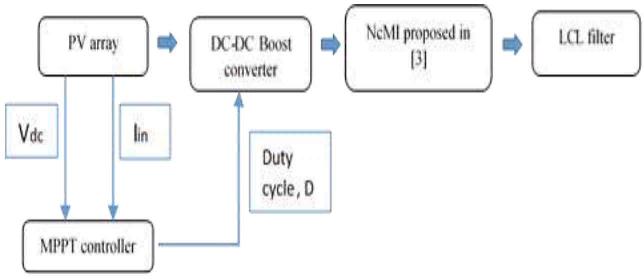

Fig. 5. Overall system for PV implementation

A. Simulation of P&O algorithm and boost converter

The modelling of P&O algorithm and conventional boost converter are done based on [8]. The P&O algorithm plays an important role in controlling the duty cycle of boost converter. P&O method will sense the input voltage and modify the voltage of the dc link between PV and converter. Detailed subsystem modeling of MPPT and boost converter are shown in Fig. 6 and Fig. 7 respectively

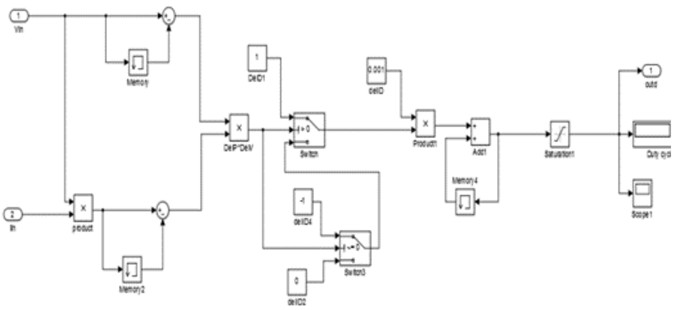

Fig. 6. SIMULINK model of P&O method

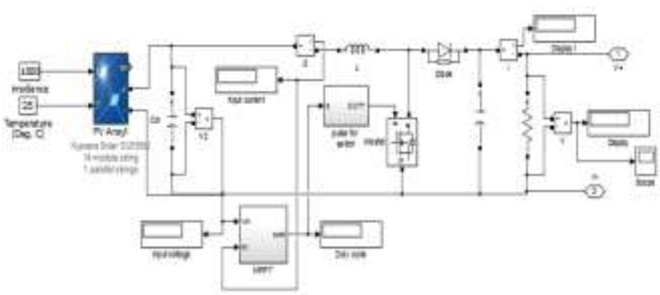

Fig. 7. SIMULINK model for MPPT and boost converter

B. Simulation of NcMI as proposed in [3]

Before PV array were fed to NcMI, A nine level NcMI is simulated in MATLAB/Simulink with dc sources are assumed to be 100 V each. The output voltage waveform and THD value are obtained as below

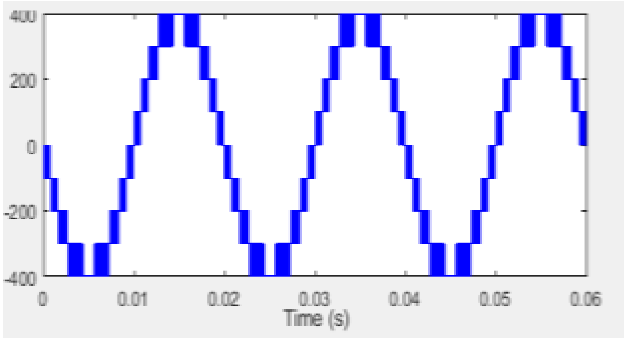

Fig. 8. Output voltage waveform for 100 V dc each

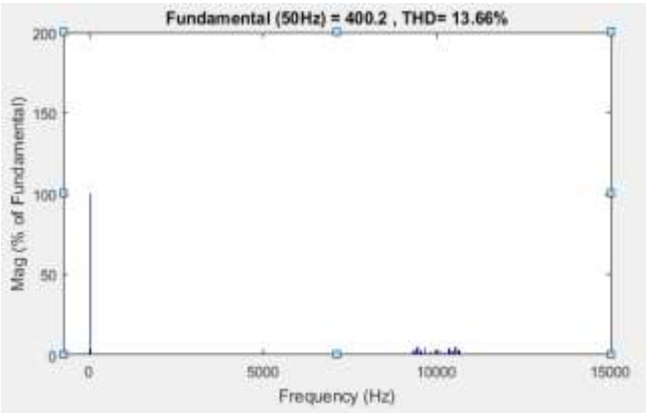

Fig. 9. THD for nine level NcMI

C. Simulation of NcMI with PV as input sources

Kyocera Solar SU53BU PV module is chosen in MATLAB/Simulink block set. Each PV array is connected to dc link which is located between PV array and boost converter. Full model of NcMI with PV sources is simulated and shown as in Fig. 10

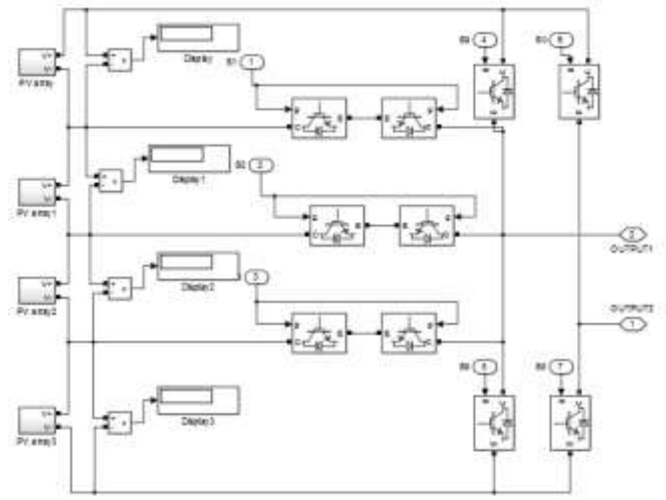

Fig. 10. Nine level NcMI with PV as input sources

IV. RESULT AND DISCUSSION

The simulation of nine level NcMI with PV implementation is done in MATLAB/Simulink. The PV array is set according to the specification of Kyocera Solar SU53BU with 14 series module string and 1 parallel module. The irradiance and temperature of the solar PV is set to be $1000\, W/m^2$ and 25℃ respectively. The multilevel waveform is generated using modified single-carrier pulse width modulation (MSPWM) [3].

The comparison between numbers of switches in CHMI with NcMI is shown in Fig. 11. NcMI requires less number of switches compared to CHMI. Less number of power switches will have less switching losses hence will lead to less complexity in circuit and also better output waveform.

Fig. 12. Shows the output of nine level inverter voltage waveform before LC filter is connected. The PV voltage applied is approximately 82 V but the output voltage is boost up by boost converter. Boost converter will increase the voltage to approximately 164 V at $1000\, W/m^2$. Output voltage is varies according to irradiance and temperature. The higher the irradiance at a certain places, the higher the output voltage. Higher ripple voltage is eliminated by using LC filter with specifications of L= 10 mH, C= 2μF and R = 145 Ω as shown in Fig. 13

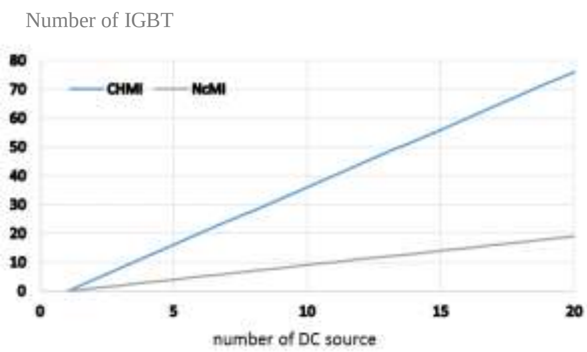

Fig. 1. Comparison on number of IGBTs and DC sources for CHMI and NcMI

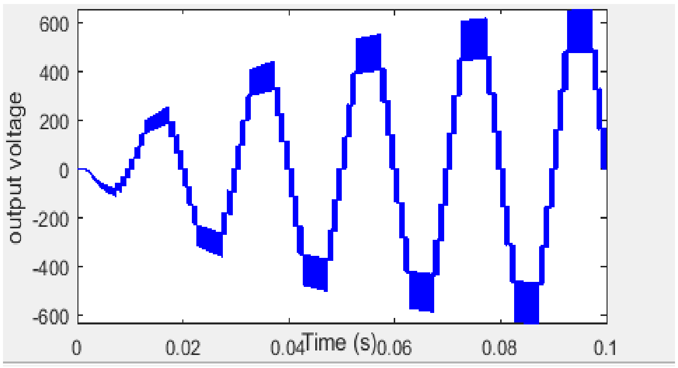

Fig. 12. Output voltage waveform nine level NcMI with PV at 1000 W/m²

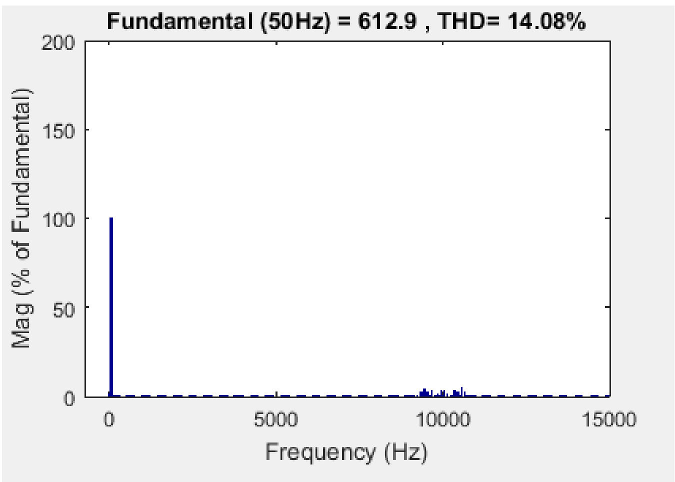

Fig. 13. THD value for nine level NcMI with PV

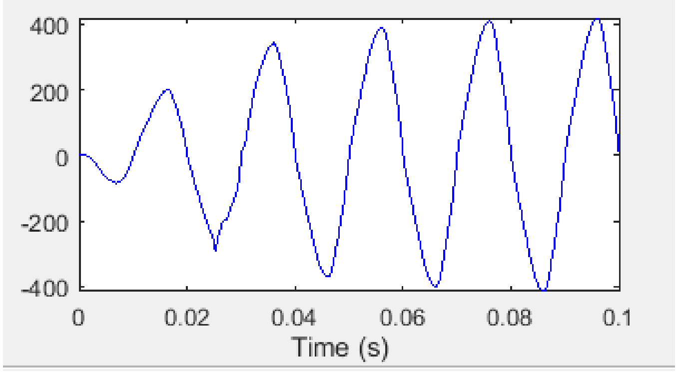

Fig. 13. Filtered output waveform

V. CONCLUSION

In this paper, a comparison of number of power switches has been made between CHMI and NcMI configuration. It is shown that NcMI topology proposed in [3] has more advantages compared with conventional one. This topology also has been fed with PV sources and can be applied in high power applications. NcMI is shown to be a good candidate for PV system application. By using NcMI instead of CHMI for PV application, the reduction of power losses can be achieved hence will increase the efficiency of the system.

REFERENCES

[1] M. Kaliamoorthy, V. Rajasekaran, and G. PraveenRaj, "A novel single phase cascaded multilevel inverter for hybrid renewable energy sources," in *2015 International Conference on Advanced Computing and Communication Systems*, 2015, pp. 1-10.

[2] D. Sankar and C. A. Babu, "Cascaded H bridge multilevel inverter topologies for PV application: A comparison," in *2016 International Conference on Circuit, Power and Computing Technologies (ICCPCT)*, 2016, pp. 1-5.

[3] S. K. a. L. M. Tolbert, "Multilevel Power Converters," ed The University of Tennessee: The University of Tennessee.

[4] T. Agarwal. (2015, 15). *Multilevel inverter - Types and Advantages*. Available: https://www.elprocus.com/multilevel-inverter-types-advantages/

[5] L. Mohammadalibeigy and N. A. Azli, "A new symmetric multilevel inverter structure with less number of power switches," in *2014 IEEE Conference on Energy Conversion (CENCON)*, 2014, pp. 321-324.

[6] M. M. Biswas, S. Podder and M. Z. R. Khan, "Modified H-bridge multilevel inverter for Photovoltaic micro-grid systems," *2016 9th International Conference on Electrical and Computer Engineering (ICECE)*, Dhaka, 2016, pp. 377-380

[7] M. Chithra and S. G. B. Dasan, "Analysis of cascaded H bridge multilevel inverters with photovoltaic arrays," *2011 International Conference on Emerging Trends in Electrical and Computer Technology*, Tamil Nadu, 2011, pp. 442-447

[8] S. Sumathi, L. Ashok Kumar, and P. Surekha, "Application of MATLAB/SIMULINK in Solar PV Systems," pp. 59-143, 2015.

Improvement of Available Transfer Capability Using Static Var Compensator

Mohamad 'Afifi bin Mohamad Razak
Faculty of Electrical Engineering
Universiti Teknologi Malaysia
Johor Bahru, Malaysia.
afifirazak.1994@gmail.com

Mohd Hafiz bin Habibuddin
Department of Electrical Power Engineering
Faculty of Electrical Engineering
Universiti Teknologi Malaysia
Johor Bahru, Malaysia.
mhafiz@fke.utm.my

Abstract— **in this paper the purpose of this project is to improve Available Transfer Capability (ATC) by a utilization of Flexible AC Transmission System (FACTS) device into the transmission system. In this project, a type of FACTS device, Static Variable Compensator (SVC) which is used to control the power flow and stability of the power system was placed into 5 bus test system in order to increase the ATC value in the system. A Repetitive Power Flow (RPF) method is used to evaluate the feasible ATC value within voltage limit. Newton-Raphson power analysis with incorporated SVC into MATLAB programming is used for load flow analysis in this project. From the study, it is observed that SVC can be used on the transmission line in order to improve ATC which can be determined the increasing of power transfer capability in the systems.**

Keywords—Available Transfer Capability, Flexible AC Transmission System, Static Variable Compensator, Repetitive Power Flow, Newton-Raphson.

I. INTRODUCTION

In a term of deregulated power system structure, a common transmission network will be shared by the power procedures and customers for wheeling power from the purpose of era to the point of utilization. In this open get to environment, all gatherings may attempt to create the vitality from the less expensive hotspot for higher margin benefit, which may prompt to over-burdening and blockage of transmission network in certain passages. This may cause the line flow, voltage and stability limits to be violated and in a meantime undermine the system security. Therefore, these utilities need to determine their "Available Transfer Capability" adequately in order to maintain the system reliability while serving a large range of bilateral and multilateral transactions. According to the definition of Available Transfer Capability (ATC), is a measurement of the transfer capability which is. Staying in the physical transmission organize for further business action far beyond officially dedicated utilizations [1]. In calculating ATC, it can be determined as a function of increasing the power transfer between two areas through prescribed interfaces.
Therefore, the utilization of Flexible AC Transmission System or FACTS devices which is the power electronic based framework that controls at least one air conditioning transmission framework parameters to enhance ability and to build control exchange capability [2] is expected to upgrade ATC of the transmission framework also. A Static Var Compensator (SVC) device is an arrangement of electrical gadgets for giving quick acting responsive power on high-voltage power transmission devices [4][5]. SVCs are a piece of the Flexible AC transmission framework device family, managing voltage, power factors, harmonics and settling the system [6] [7].

II. LITERATURE REVIEW

A. Static Var Compensator (SVC)

Static Var Compensator (SVC) is a shunt connected FACTS controller which its main function is to control the voltage at a given bus by controlling its identical reactance [17]. Essentially it comprises of a thyristor controlled reactor (TCR) and fixed capacitor (FC) [17].Basically, there are several type of the SVC, and as appeared in figure underneath 2(a) and 2(b) [17].

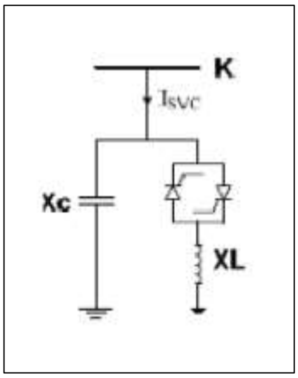

(a)

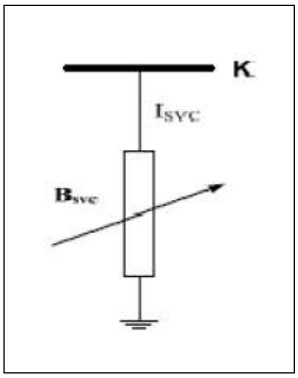

(b)

Fig. 1. (a) SVC firing angle mod (b) SVC total susceptance model.

SVC firing angle was the first model. For this model the comparable reactance X_{svc}, act as a function of a change in firing angle α, is build up by a fixed capacitive reactance and the parallel combination of a thyristor controlled reactor (TCR) equivalent admittance as shown in Fig.2 (a). To achieve a given level of compensation, the model gives an information about SVC firing angle required. Total susceptance model was the second model. The fundamental frequency equivalent susceptance of all shunt modules in this model represents change in susceptance B_{svc} making up the SVC as shown in Fig.2 (b).

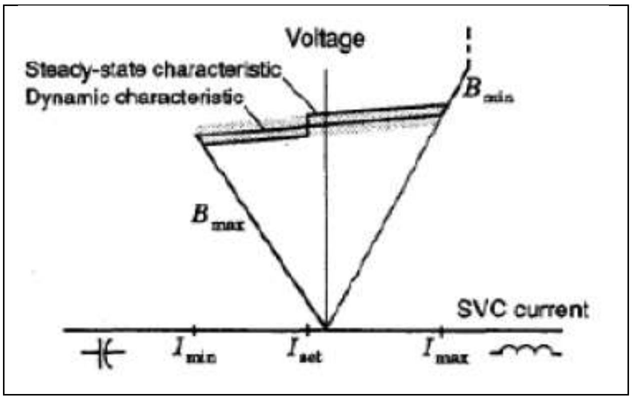

Fig. 2. Steady state and dynamic voltage or current characteristics of the SVC.

Fig.3 demonstrates the enduring state and element voltage-current qualities of the SVC. In the dynamic control range, current or susceptance and responsive power is fluctuated to direct voltage as indicated by a slope (droop) trademark. The incline esteem relies on upon the craved voltage direction, the coveted sharing of receptive power creation between different sources and different needs of the framework. The slant is regularly (1% until 5%). At as far as possible, the SVC turns into a shunt capacitor. At as far as possible, the SVC turns into a shunt reactor (the present or receptive power may likewise be restricted. SVC terminating edge model is executed in this paper. Therefore this model was able to produce as for sinusoidal voltage. SVC parameters must be resolved by pay necessities. For the capacitive limit, a shunt capacitor will produce the SVC. While, the SVC becomes a shunt reactor during the inductive limit, (reactive power or the current may also be limited). In this paper, SVC firing angle model was implemented. Hence, with respect to sinusoidal voltage, the model can be developed. According to the compensation requirements, SVC parameters have to be determined. With the bus voltage (voltage at the bus where SVC is to be connected) V_{bus} and Q_{svc}as the capacity of the SVC, the value of the capacitance and TCR inductance are;

$$X_C = \frac{V^2bus}{Q_{svc}} \text{ and } X_L = \frac{X_c}{2} \quad (1)$$

As a frequency (f) Hz,

$$c = \frac{1}{2\pi f X_c{}'} \text{ and } = \frac{X_L}{2\pi f'} \quad (2)$$

In this wake of estimating the capacitance and inductance, it is important to decide the underlying working state of the SVC. At that point select the underlying terminating edge α in manner which under this working requirement the SVC did not trade any power for the AC system. When the effective reactance's X_C and X_L cancel each other out, this firing angle will correspond to the case. Under this operative condition, there is no current leaving or entering the SVC and the SVC effective reactance X_{SVC} is infinite which indicates the AC system and the power exchange between the SVC is zero. Referring to the capacitive and inductive reactance's, each SVC has their own firing angle – reactive power characteristics, Q_{SVC} (∝) which is a function of the capacitive and inductive reactance's. Using a graph similar to the Fig.3, the firing angle initial condition can be determined. To determine this plot, the following steps may be used. First and foremost, it is essential gaining the quality reactance X_{SVC} as a function of the firing angle ∝, using the fundamental frequency TCR equivalent reactance,

$$X_{TCR}.X_{TCR} = \frac{\pi X_L}{\sigma - \sin\sigma} \text{ and } \sigma = 2(\pi - \alpha) \quad (3)$$

where X_L is the reactance of the linear inductor, σ and α are the thyristor conduction and firing angles, respectively. The TCR conducts fully at α = 90 and the X_L will produce equivalent reactance, X_{TCR}. The TCR is blocked at α = 180, and its equivalent reactance becomes very large such as infinite. By the parallel combination of both these components, the total effective reactance of the SVC, including the TCR and capacitive reactance was determined.

$$X_{SVC} = \frac{X_C X_{TCR}}{X_C + X_{TCR}} = \frac{\pi X_C X_L}{X_C - (\sigma - \sin\sigma) + \pi X_L} \quad (4)$$

Where X_{SVC} is a function of the conduction, σ. Quality reactance of the SVC is a function of the firing angle. The reactive power Q_{SVC} (α) is given by

$$Q_{SVC} = V_{bus}^2 \frac{X_{C\,[2\,(\pi-\alpha)+\sin 2\alpha]-\pi X_L}}{\pi X_C X_L} \quad (5)$$

As stated by the equation above, Q_{SVC} will become zero when the effective reactance X_{SVC} is extremely large. When the following relationship approaches zero, this condition is satisfied.

$$X_C[2(\pi - \alpha) + \sin 2\alpha] - \pi X_L = 0 \quad (6)$$

As initial condition in the open loop control of the SVC, the value of the firing angle α that satisfies the equation above is used.

B. Available Transfer Capability

In a term of a deregulated power system structure, a common transmission network will be shared by the power producers and customers for wheeling power from the purpose of era to the point of utilization [1]. In this open get to environment, all parties may attempt to create the vitality from a cheaper source for higher margin profit, which lead to overloading and congestion of transmission network in certain corridors [1]. This may cause the line flow, voltage and stability limits to be violated and in a meantime undermine the system security [1]. Therefore, these utilities need to determine their "Available Transfer Capability" adequately in order to maintain the framework unwavering quality while serving a huge scope of two-sided and multilateral exchanges [1]. The electric transmission utilities in the United States are required to post the data of ATC of their transmission organize through the open access same time information system (OASIS) for day-ahead and ongoing dependable operation [1].

Power transaction between a specific seller bus or area can be committed only if available sufficient ATC through prescribed interfaces [1]. Thus, the exchange ability for holding transmission administrations, planning firm and non-firm exchanges and for masterminding crisis exchanges between vender transport or areas or buyer bus or area of an interconnected power system network can be used [1]. A continuously compute, updated and posted to OASIS requires the ATC among areas of an interconnected power system network and also for critical transmission paths between area following to any change in the system conditions [1].

C. ATC Definition

North American Electric Reliability Council (NERC) characterizes Available Transfer Capability (ATC) is a measure of the move capacity staying in the physical transmission arrange for further business action far beyond officially dedicated employments [1]. Numerically, ATC is characterized as the Total Transfer Capability (TTC) less the Transmission Reliability Margin (TRM), less the whole of existing transmission duties (which incorporates retail client administrations) and the Capacity Benefit Margin (CBM), appeared in Figure 3[1]. Add up to Total Transfer Capability (TTC) is characterized as the measure of electric power that can be exchanged over the interconnected transmission organize in a dependable way while meeting the greater part of a predefined set of characterized pre-possibility and post-possibility framework conditions[1].

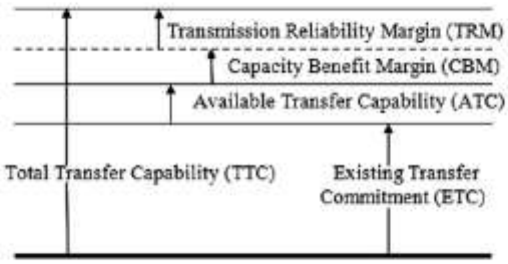

Fig. 3. Basic definition of ATC.

Which the Transmission Reliability Margin (TRM) is characterized as that measure of transmission exchange ability important to guarantee that the interconnected transmission system is secure under a sensible scope of vulnerabilities in framework conditions and Capacity Benefit Margin (CBM) is characterized as that measure of transmission exchange capacity held by load serving elements to guarantee access to era from interconnected frameworks to meet era unwavering quality necessities [1]. Mathematically, ATC is defined as:

$$ATC = TTC - TRM - \{ETC + CBM\} \tag{7}$$

D. Repetitive Power Flow (RPF) Method

This method is done by increasing the real power transfer at load bus of sink area repeatedly until the limits are violated [1]. The limit that is considered in this project is the voltage limits. The procedure in using this method to compute the ATC will be explained later in the Chapter 3 [1]. This method is clearly simple, easy to understand and suitable with the MATLAB programming in the determination of the ATC rather than other method [1]. However, in using this method, we must consider safety, be careful, and monitor any violation of the limitation [9].

E. Optimal Location of SVC

Nowadays, with increasing of load demand, the power transmission network must be expanded to fulfill the demand, but the issue of environment, right-of-away and the problem of the cost had limit the transmission network expansion [14]. Therefore to overcome the problem of fulfilling the increasing of load demand without construct the new transmission line, the use of FACTS devices are the only answer for that problem of the cost had limited the transmission [14]. Due to the price of FACTS devices that categories as expensive therefore FACTS devices must be placed at an optimal location to achieved the great performance of the device [14].

For determining the optimal location of SVC placement in power system network, several objectives must be considering [15], that is:

a) Reduction in the real power loss of the particular line
b) Reduction in the total losses system real power loss
c) Reduction in the total system reactive power loss
d) Maximum relief of congestion in the system

However, in this project, the other objective in determining the optimal location to install SVC is considering the value of the ATC can be improved [14]. Thus, this objective can be achieved by placing SVC in the line that obtained the highest value of ATC.

III. METHODOLOGY

In this project, the simulation of the selected 5 bus test system is done using MATLAB coding which involved power flow solution by Newton Raphson method instead of Gauss Seidel method as for the load flow analysis. The utilization of SVC into the into the test system also been used in MATLAB coding by modified admittance bus matrix in power flow. The violation of the voltage limits is included in determining the ATC for the test system using Repetitive Power Flow (RPF) method.

The project will be started with a less number of bus and lines of the test system first and followed by more number of bus and lines of the test system. After selecting the test system, the power flow simulation by Newton Raphson method will be run in MATLAB programming which involves power flow solution of the test system. Next, the RPF method were applied by increasing the real power transfer at load bus of sink area the run the simulation again and check whether there is violation occurs to any limitation. If no limits violated occur, the step in increasing the real power transfer at load bus of sink area is repeated until the limits is violated. After that, ATC will be computed by getting the difference of the real power transfer at load bus of sink area is repeated until the limits are violated with the real power transfer at load bus of sink area of test system.

The utilization of SVC into the test system has also been used in MATLAB coding by modifying admittance matrix in MATLAB coding. In placing the SVC, the suitable parameter setting of the SVC must be ensured, which will be discussed in the next chapter. Next, run the simulation again to get the result of ATC after utilize SVC into the test system with the applying of RPF method. The result of ATC of the test system with and without utilization of SVC will be compared.

IV. RESULT AND DISCUSSION

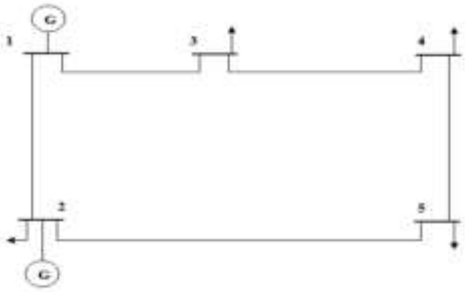

Fig. 4. 5 bus test system.

The Figure 4 shows the selected 5 bus test system to be used in this project. It is consists of slack bus (Bus 1), generator bus (Bus 2) and three load buses (Bus 3, Bus 4 and Bus 5). The position of slack bus was change depend on cases. For case 1, Bus 1 which is a slack bus is chosen as source area where as Bus 2 which is a load bus is chosen as a sink area for the power transfer that will be used in calculating the ATC. In Case 2, Bus 1 act as a slack bus where it is functioning as source area, while role for sink area, Bus 3 were chose as load bus. For the next case which is Case 3, it is almost the same with the previous case but the selected bus for that role is the only things differ. In this case, Bus 3 plays the role as a slack bus and it is responsible to be a source area. While the bus that responsible for power transfer is Bus 4 where it is act as load bus and performed as sink area and may execute the calculation for ATC. Next case is case 4 where Bus 2 act as slack bus and it is known as source area. Besides slack bus, it is also known as swing bus and role for load bus, Bus 5 were chose to do ATC calculation for power transfer and act as sink area. For the final case, Bus 4 were chose as slack bus and it is performs same task as Bus 2 in the previous case where it is act as source area. In this case, bus that is responsible to execute ATC calculation based from the power transfer is Bus 5 where it act as sink bus and sink area. The power flow solution is done for the case 1 until case 5 that was use the original selected 5 bus test system without any increasing of real power of load bus at sink area with no applying of SVC into the system. The Figure 5 shows the results of the ATC from the power transfer that was done for the 5 cases.

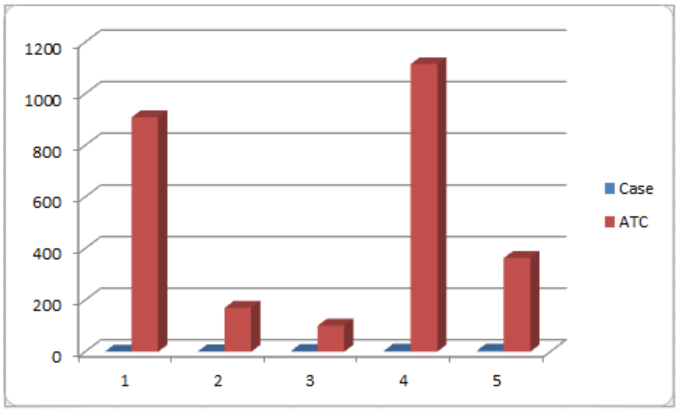

Fig. 5. Shows the statistic of ATC against cases

The Table 1 shows the simulation result obtained of the 5 bus test system for all the cases.

TABLE I. POWER FLOW SOLUTION OF 5 BUS TEST SYSTEM FOR 5 CASES

Case	Original (First iteration)		New Value (After iteration)		Available Transfer Capability (ATC)
	MW	MVAR	MW	MVAR	
1	22.700	89.096	931.700	1234.222	909
2	3.400	89.090	173.400	273.387	170
3	8.600	90.733	109.600	201.961	101
4	95.200	88.562	1210.200	1442.702	1115
5	95.200	89.524	459.200	554.182	363

From the table 1, the value of ATC for all cases was recorded. The value of ATC for case 4 which is the line between Bus 2 and Bus 5 was record the highest value. So, the line between Bus 2 and Bus 5 will selected to be analyze .The power flow solution for ATC is done by using RPF method in which the real power of load Bus 5 at sink area is increased by 1 MW on each iteration with considering of voltage limit. It is done before and after incorporating SVC into the selected 5 bus test system. The load Bus 5 is chosen to be sink area that will be increased because it can transfer more real power load with the highest value of ATC obtained rather than other buses by using trial and error method. The Table 2 shows the simulation result that was obtained after incorporating SVC.

Without incorporating SVC, only RPF method was applied with considering the voltage limit. But, in applying the SVC parallel to the line between Bus 2 and Bus 5, the reactance of transmission line need to be varied in the range of -0.7 p.u. to 0.2 p.u. of the original reactance of the line until the optimal value is achieved [19]. Therefore, it was found the optimum value for SVC is X_L= 0.1134 p.u. and X_C = 0.2267 p.u. of the original reactance of the line due to its highest values of ATC obtained among all the others line number. Furthermore, the placement of SVC is located parallel to the line Bus 2 and 5 due to its highest value of ATC obtained compared to other lines. The voltage limit and the parameter of SVC is compensating reactance (X_c) are shown as below. The limitations of the test system are as follow:
Voltage limit = 0.95 < [V] < 1.05 p.u.

Thus, the parameter of SVC need to add at the diagonal matric of Ybus system as shown below:

$$Ybus(n,m) = Ybus(n,m) + 0.3401j \quad (8)$$

Where,
n = number of row in the matrices
m = number of column in the matrices

TABLE II. IMPROVEMENT OF ATC IN EVERY YBUS SYSTEM

Ybus	Original (First iteration)		New Value (After iteration)		Available Transfer Capability (ATC)	Improvement (%)
	MW	MVAR	MW	MVAR		
Ybus(1,1)	95.200	100.252	1363.200	1649.430	1268	13.72%
Ybus(2,2)	95.200	100.252	1362.200	1648.126	1267	13.63%
Ybus(3,3)	95.200	100.787	-	-	-	-
Ybus(4,4)	95.200	100.652	-	-	-	-
Ybus(5,5)	95.200	100.114	1362.200	1648.126	1267	13.63%
Ybus(6,6)	95.200	100.247	-	-	-	-

V. CONCLUSION

This paper proposed the improvement of ATC by using SVC. The following simulation results have been obtained. First, the power flow solution is done for the original selected 5 bus test system without any increasing of real power of load bus at sink area with no applying of SVC into the system. Second, without incorporating SVC, only RPF method was applied with considering the voltage limit and the limitations of the test system is between 0.95V to 1.05V. Third, in applying the SVC parallel to line, the reactance of transmission line need to be varied in the certain range of the original reactance of the line until the optimal value is achieved. The value of ATC was successfully improved in 5 bus test system by utilization of SVC into the system.

VI. REFERENCES

[1] T. Nireekshana, G. Kesava Rao and S. Siva Naga Raju, Enhancement of ATC with FACTS devices using Real-code Genetic Algorithm, Electrical Power and Energy System 43 (2012) 1276-1284.

[2] Harinder Sawhney and B. Jeyasurya, Application of Unified Power Flow Controller for Available Transfer Capability Enhancement, Electric Power Systems Research 69 (2004) 155-160.

[3] N. A. E. R. C. (NCER), “Available Transfer Capability – Definitions and Determination,” June 1996.

[4] Jin Han Teng (2003). Stability Constrained Available Transfer Capability. Bachelor of Engineering Thesis. The University of Queensland, Australia.

[5] M. Y. Hassan (2010). Power System Control. (3^{rd} ed.). Faculty of Electrical Engineering Universiti Teknologi Malaysia, Skudai.

[6] Islam Youcef Djilani Kobibi, Samir Hadjeri and Mohammed Abdeldjalil Djehaf, Study of UPFC Optimal Location Considering Loss Reduction and Improvement of Voltage Stability and Power Flow, Leonardo Journal of Sciences, Issue 24, p. 85-100, January-June 2014.

[7] Gastaldello, D.S., A.N. Souza, C.C.O. Ramos, P. da Costa Junior and M.G. Zago, 2012. “Fault location in underground systems using artificial neural networks and PSCAD/EMTDC” INES 2012 IEEE 16th International Conference on Intelligent Engineering Systems, Lisbon, Portugal.

[8] H. B. Nagesh and P. S. Puttaswamy, Power Flow Model of Static Var Compensator and Enhancement of Voltage Stability, Vol. 3, Issue 2, pp. 499-507.

[9] M. J. Ali Arzani, Y. Alinejad-Beromi, “Available Transfer Capability Enhancement Using Series FACTS Devices in a Designed Multi-Machine Power System.”

[10] Mohd Hizham Bin Abu Samah (2010). Voltage Stability Enhancement Via Voltage Control By Using Thyristor Controlled Series Compensator (TCSC). Bachelor of Engineering (Electrical) Thesis. Universiti Teknologi Malaysia, Skudai.

[11] Rao, K. N., Amamath, J. and Kumar, K. A. (2007), Voltage Constrained Available Transfer Capability Enhancement with FACTS Devices. ARPN Journal of Engineering and Applied Sciences. Vol. 2, No.6.

[12] Selvantheran A/L Gunasegaran (2012). Voltage Profile Improvement in Transmission Line using FACTS Devices. Bachelor of Engineering (Electrical) Thesis. Universiti Teknologi Malaysia, Skudai.

Solar Powered-Smart Jacket

Amiruddin Bin Mohd Johan
Faculty of Electrical Engineering,
University Technology Malaysia
Johor Bahru, Malaysia
Amiruddinjohan1@gmail.com

Dalila Binti Md.Said
Faculty of Electrical Engineering,
University Technology Malaysia
Johor Bahru, Malaysia
dalila@utm.my

***Abstract*—Solar Powered-Smart Jacket is jackets that are design specifically for the use of motorcyclist. Usually motorcyclist wear jacket to overcome coldness. But some jacket in the market doesn't provide enough to the user. Smart Jacket is design equipped with heating element that is build inside the jacket to warm up the wearer during the cold weather, for example during rainy day and at night. By implementing this system, the jacket will provide enough heat for the users. Meanwhile, the source to power up this jacket is by using solar powerbank. Solar energy is used in this system in order to conserve energy and to maximize the use of renewable energy in our daily life.**

Smart jacket is the innovation of regular jacket into a jacket that can be control by using android platform. Android platform is used due to its ability to synchronize with arduino. The connections between them are done by using Bluetooth module (HC-05). The on or off of this heating element can be control whether by using smart phone that are equipped with android operating system or by switch. In addition, users can also monitor the current temperature condition through smartphone. This will help the users to determine whether the heating element should be used or not.

Keywords*—*heating element,solar powerbank,bluettoth module

I. INTRODUCTION

In the rising era of globalization, fabrics and clothing industry are on demand right now. People are eager to try a new fashion outlook that is stylish, elegant and comfortable to use. The examples of clothing that are used are such as jacket. Jacket is cloth that people wear usually during cold day, winter and people in low temperature country. Fabrics of the jacket are usually made of textile that can insulate heat and giving comfortable feeling even during cold day. But, is the normal jacket gives enough heat to the wearer.

This is why we need heating element inside of our jacket. The heating element will provide enough heat to the wearer even it is freezing outside. Solar Powered –Smart Jacket is a smart jacket that generated by solar energy. The system of the jacket is fully generated by the solar energy. The jacket provide heating element inside the jacket itself. The heating element inside the jacket is operating automatically by using special sensor that are attach to it. If the temperature of surrounding reaching below the setting value, the system will trigger it and switching it on. To make it useable to the customer, heating

element inside the jacket can also be control by using smartphone. Solar source also can be used as a charger for phone or gps.

The market of this product is for bikers, hikers, and people that live in cold temperature country. For bikers, probably they will need this when they are riding at night. Hikers will need this jacket along the time as they are climbing up the mountain, the temperature will be decreased and they need to be heated. People that are lived in low temperature country will need this jacket every time they go outside. Smart jacket will heat them up. But in Malaysia, our target market is for bikers due to geographical factor of Malaysia which is not a cold and high lander country.

II. LITERATURE REVIEW

A. What is heating suit?

Heating suit is a garment that allow user to control the temperature by using electrical devices that are attach or embedded inside the jacket. The benefits and practicality of this suit is the reason for the project to be done. This is the suit or jacket that allow users to wear it easily, comfortable and in the same time allowing the users to utilize it according to the temperature of the surrounding. If the suit is featured in the market and being introduce to general public and with such function ,it can prevent the unexpected condition that are caused by extreme temperature towards the human body [5].

Nowadays, there are many technological solutions that made people under comfortable condition by keeping surrounding thermal in the right condition. But most of it is used I the car, houses and non-mobility places. What would happen if a person need to go outside facing extreme weather?. The current solution nowadays is by adding layers of coats or jackets but sometimes if the weather is too serious, layers of jacket does not solve the solution. This is the reason why heating jacket is introduced. The suit will allow the users to control the internal temperature inside the jacket according to the user's comfortability [5].

B. Bad effect of cold weather to human

Cooling of body parts may result in various cold injuries - nonfreezing injuries, freezing injuries - and hypothermia which is the most serious. Nonfreezing cold injuries include chilblain, immersion foot and trench foot. Frostnip and frostbite are freezing injuries [6].

Toes, fingers, ears and nose are at greatest risk because these areas do not have major muscles to produce heat. In addition, the body will preserve heat by favoring the internal organs and thus reducing the flow of blood to the extremities under cold conditions. Hands and feet tend to get cold more quickly than the torso because:

1. They lose heat more rapidly since they have a higher surface area-to-volume ratio, and

2. They are more likely to be in contact with colder surfaces than other parts of the body.

Hypothermia is the most dangerous cold injury that occur due to excessive lost of heat in the body. Hyperthermia can cause death to the patient.

Chilblains is the effect of too much exposure to air temperature that are range from 0°C to 16°C.It will cause the skin to be redness, tingling, pain and swelling.

Immersion foot can occurs due to individuals that has wet feet. Usually this effect occurs at the range temperature of 10°C (50°F) and below. The nerve and muscle tissue are always the most primary injury. There are many symptoms such as numbness and tingling, pain, itching, leg, feet or hands will be swelling or there blister develop. At first, the skin will be reddish and turn to blue or purple in color when the injury continuous. In serious cases, gangrene may occur.

Trenchfoot is the cause of too long exposure in wet places from freezing point to about 10°c.The effect is depend on how long we are exposed to the surrounding. The range is from several hours to many days. And it is all depend on the temperature. There are different between trenchfoot and immersion foot. Immersion foot may occur at a higher temperature ant its around 10°c and above. But temperature for Trenchfoot is more likely to happen at 10°c and lower. The same problem will occur if a person wears wet gloves for a long time in a cold condition. The symptom is more likely like immersion foot.

One thing that we should know is the sense of pain will be lost if we are expose for too long in a cold condition. Feeling of cold and also pain will start to loss due to decreasing of temperature and in other word, the loss of numbness. There will be serious injury if no pain to be felt by a person.

Next, a person will confront with muscular weakness and drowsiness. This is what we call hypothermia and it will occur if the temperature of the body drop below 33°C . Shivering, dilated of pupils and loss of consciousness are another symptom of it. When temperatures of the body reach 27°C, coma sets in. The heart beat will stop at 20°C, and at 17°C the brain will stop functioning.

In regular cold environments, body's temperature usually does not fall too much. It is around 1°C to 2°C below normal. This is the human ability that can adapt to a certain temperature. But, in a serious temperature, the body cannot adapt anymore and the heat loss cannot be control. This will cause body temperature to drop too much .The excessive loss of temperature will cause hypothermia [6].

C. Heat Balance equation for human body

Human body temperature is around 37^0c and within this temperature heat balance within body and surrounding are normal. On average, heat that is generated within the body must be balanced to heat moving out of the body. For a normal body, there will be dynamic balance of the temperature.

If the heat generated is greater than the heat release, the body temperature will eventually rise and vice versa. There is an equation to calculated heat transfer of the body. When there is no net gain or loss of heat, this means that the body is in balance temperature condition. Thermal audit is the name for the process to determine heat transfer between the body and environments.

There are many forms to represent the heat balance equation. However the basic are just the same. Metabolic rate of the body (M), mechanical work (w) and the remainder is released as the heat. Heat transfer for conduction (K), convection (c), radiation (r) and evaporation (e).Heat storage (s) and heat storage must be 0 to be balanced. If the heat storage is positive that's means the temperature rise and when heat storage is negative, that's means there is net heat loss of the body [7].

D. Product that is available in the market

TABLE I. PRODUCT THAT IS AVAILABLE IN THE MARKET

PRODUCT		ADVANTAGES	DISADVANTAGES
	**Warmgear Next Gen 2-in-1 Power Bank Heated Puffy Jacket [8]**	Using macro-heating technology and high tech rechargeable battery	Cost are too expensive
	**Heater body suit [9]**	1.300 Grams 3M Thinsulate Ultra Insulation 2.Treated with Durable Water Repellent (Water Resistant)	1.Cost are too expensive 2.The suit is to thick, not suitable to move around
	Exoglo heated vest [10]	1.Heated up by heating element that generate by battery 2.Windproof 3.Water resistant	1.The battery can't last up for a long time 2. Battery is sold separately, which means increase in cost.

E. Heating Element

This is a literature review on temperature control flexible heating panel. This is the invention of flexible panel heating system equip with sensor and controlled temperature. The panel of the heating element is thin and flexible characteristically. But the old design is lack of sensitivity. This is due to heat emitting surface are evenly placed with numbers of thermostat [10].The invention is focusing on the sensing and controlling of the temperature of the system.

This new invention has solved the problem. The new product provides a controllable temperature, flexible, thin and has a safe surface heating-emitting system. The system is done by inserting the temperature sensing between the two heat-emitting carbon surfaces. All of them are made into a piece of sheet [10].

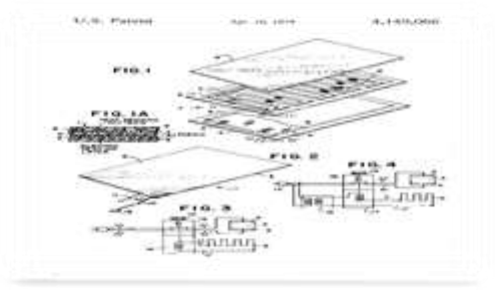

Fig. 1. Heating element

III. METHODOLOGY

This section will be explaining the work flow how the Solar Powered-Smart Jacket can be build. The process involved the component and hardware used to solve this project.

A. Flowchart

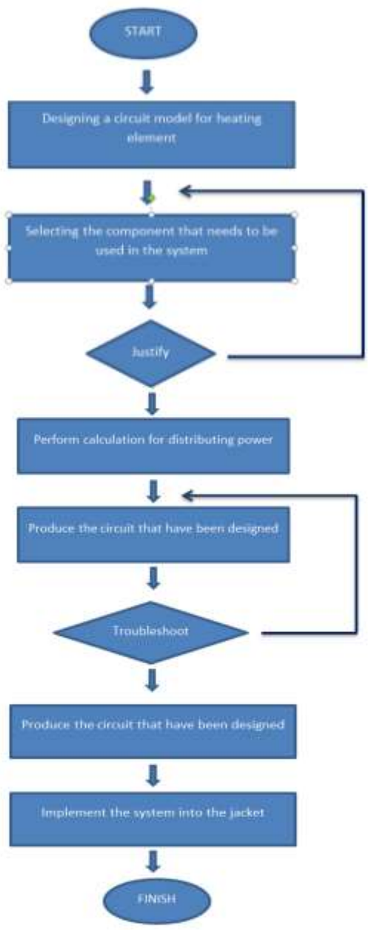

Fig. 2. Flowchart for the project

The project is started by designing a circuit model for heating element. After that, the component that needs to be used in the system is selected. Following by that, a justification need to be consider to weather the component choose is suitable or not. The action continuous by performing calculation on distributing power of the system. This action need to be done because with the calculation, we know how many heating element that should we use according to our limited source. Next, the production of the circuit is done by doing testing. Troubleshoot will be done during the testing session if there is error to the system. After struggling with the testing, the circuit real circuit can be build and finally it can be implemented into the jacket.

B. Design

This is the design of the jacket that will be used to build this project. Given below is the image of front and back view of the jacket.

Fig. 3. Front view of the jacket

The Smart Jacket are equip with portable solar power bank and also a pouch bag to keep phone or gps safely inside it. Both of them are connected to jacket by using strapping and can be pulled off anytime.

Fig. 4. Front view of the jacket

As we see in the picture, there were two heating element that are attaching on the back side of the jacket. It will be connected to the source. The heating element will provide heat to the customer.It was placed behind the back so that the temperature can distribute nicely throughout the jacket.

To connect both of the heating element, 5v-relay is used to trigger the signal from the arduino. As the signal received by the relay, the heating element will turn on and the temperature will rise slowly until the max temperature achieved.

C. Circuit Connection

Fig. 5. Circuit connection for the system

As we can see in figure 5,the source of the arduino is a solar energy based.It provide 5v voltage to start up the arduino.Connected to the arduino also is a temperature sensor that used to detect the surrounding temperature.Hc-05 or bluettooth module are also being used in this system.The function of the bluettooth module is as a transmitter or receiver from the arduino to smartphone and vice versa.Heating element is one of the important component of the system.Without it,the system cannot be function.LCD is used to display the temperature value of the surrounding.

D. Arduino

Fig. 6. Layout of the Arduino Uno

Each of the 14 digital pins on the Uno can be used as an input or output, using pinMode(), digitalWrite(), and digitalRead() functions. They operate at 5 volts. Each pin can provide or receive a maximum of 40 mA and has an internal pull-up resistor (disconnected by default) of 20-50 k Ohms. In addition, some pins have specialized functions [1]:

- **Serial: 0 (RX) and 1 (TX).** Used to receive (RX) and transmit (TX) TTL serial data. These pins are connected to the corresponding pins of the ATmega8U2 USB-to-TTL Serial chip.
- **External Interrupts: 2 and 3.** These pins can be configured to trigger an interrupt on a low value, a rising or falling edge, or a change in value. See the attachInterrupt() function for details.
- **PWM: 3, 5, 6, 9, 10, and 11.** Provide 8-bit PWM output with the analogWrite() function.
- **SPI: 10 (SS), 11 (MOSI), 12 (MISO), 13 (SCK).** These pins support SPI communication, which, although provided by the underlying hardware, is not currently included in the Arduino language.
- **LED: 13.** LED are built in features. When there is HIGH ,Led will turn on and vice versa.

There are some pins on the board:

- **AREF.** Reference voltage for the analog inputs.
- **Reset.** Bring this line LOW to reset the microcontroller.

The power pins are as follows:

- **VIN.** The input voltage to the Arduino board when it's using an external power source (as opposed to 5 volts from the USB connection or other regulated power source). You can supply voltage through this pin, or if supplying voltage via the power jack, access it through this pin.
- **5V.** The regulated power supply used to power the microcontroller and other components on the board. This can come either from VIN via an on-board regulator, or be supplied by USB or another regulated 5V supply.
- **3V3.** A 3.3 volt supply generated by the on-board regulator.
- **GND.** Ground pins.

E. Bluetooth module HC-05

Bluetooth is a high range wireless communication technology that is designed for short range distance [15]. A Bluetooth module is usually a hardware component that provides a wireless product to work with the computer or in some cases, the Bluetooth may be an accessory or peripheral, or a wireless headphone [17]. In this project Bluetooth module is used as hardware to connect from phone to Arduino Uno to control the heating element on/off. Below is the connection diagram of Bluetooth module that is connected to Arduino Uno.

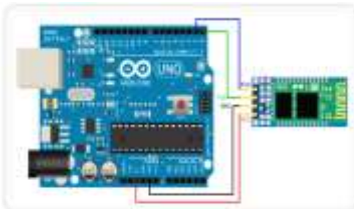

Fig. 7. Bluetooth module(HC-05) connected to arduino

As we can see in the diagram, RX pin from Bluetooth module is connected to slot 1 in Arduino. The TX pin will be connected to slot 0 in arduino. Both of this pin will transmit and receive data for the system. If this connection is default, there will be nothing happen to the system. The Vcc pin is connected to 5V voltage. This will be the input voltage for the Bluetooth Module. GND pin will be connected to the GND slot of Arduino [16]. This will discharge the voltage.

This is the specifications of the Bluetooth module that will be used in the system [19]:

- Dimensions: 4.4 cm x 1.6 cm x 0.7 cm (1.73 in x 0.63 in x 0.28 in)
- Weight: 7g (0.25 oz)
- Range: ~10 m (~33 ft)
- Supply voltage: 3.6-6V
- BT-Name: linvor

F. *Temperature sensor(LM35)*

Fig. 8. Temperature sensor (LM35)

The LM35 series are precision integrated-circuit temperature devices with an output voltage linearly-proportional to the Centigrade temperature. The LM35 device has an advantage over linear temperature sensors calibrated in Kelvin, as the user is not required to subtract a large constant voltage from the output to obtain convenient Centigrade scaling. LM 35 detects a range of temperature between -55^{0}c-150^{0}c. The low-output impedance, linear output , and precise inherent calibration of the LM35 device makes interfacing to readout or control circuitry especially easy. The device is used with single power supplies, or with plus and minus supplies.

As the LM35 device draws only 60 µA from the supply, it has very low self-heating of less than 0.1°C in still air. The LM35 device is rated to operate over a −55°C to 150°C temperature range, while the LM35C device is rated for a −40°C to 110°C range (−10° with improved accuracy [21].

G. *Heating Element*

Heating element is the most important part in this system. It is used to heat up the wearer so that users are comfortable with the cold condition. It needs to be apply 5-12 VDC and it will be heated up and creating a little heating pad. On one side, it's just a gigantic resistor. On the other hand, it's flexible, light, and can be wrapped around a project. Originally designed for portable wearable heating pads. It will be connected to the relay and when the relay trigger the signal, it will be switch on.

The specification is as below [4]:

- Dimensions: 110.65mm / 4.35" x 70.45mm / 2.77" x 1.54mm / 0.06"
- Wire Length: 35.8mm / 1.4"
- Weight: 2.53g
- Insulation: Polyimide film ('Kapton')
- Fabric made of Polyester filament and micro stainless steel fiber
- Power requirements: 5V DC up to 1A

Fig. 9. Heating Element/Heating Pad

IV. Result

The result below is the calculation for the power distribution for the system. A good distribution power is required to ensure that the system work perfectly.

Output for the source:

1) output 1: DC 5V (1A)

> P=VI

=5*1

=5W

2) output 2 : DC 5V (2.1A)

> P=VI

=5*2.1

=10.5W

Design references:

Testing conditions

(1)The width of the Heating Textile is 5 cm

(2)The diameter of metal conductive yarn is about 0.27 mm

(3)The pitch of the conductive yarn in the Fabric is about 4 mm

(4)The input voltage to the Textile is 5, 7.4, 9, 12 Voltage, respectively.

Table 1 (INPUT, VOLTAGE: 5V)

Length of the Textile	4cm	4.8cm	5.2cm	6.0cm	6.8cm	7.6cm	8.4cm	9.2cm	10.4cm
Current, A	1.5	1.3	1.2	1.05	0.95	0.9	0.86	0.80	0.74
Temperature, ℃	130	95	88	80	68	60	52	46	40

Fig. 10. Heating Element/Heating Pad

Power use for heating pad:

According to table 1, for the length of 10.4cm current is 0.74A and voltage is 5V.

P=VI

=5*0.74

=3.7W

Thus, we are using 2 heating pad for our system.

P=3.7*2

=7.4W

From the calculation above we can see that the source voltage can only providing enough power for 2 heating pad only. If we want to add more heating pad, we need to increase our source voltage so that it has enough power to generate the heating element.

V. Conclusion

As for conclusion, this project would be very benefit to the people due to its practicality. The heating element system that embedded in the suit or jacket will provide comfort ability to the users during cold day. Although it is cold outside, there no reason for us to go out there. The application of the system can also be apply in any suit as long as it has enough sources to generate it. The innovation to use solar to generate the system is very useful because there is not always be a plug for us to charge. But solar energy can be used anywhere no matter where you go. The system of heating element also display the usefulness of Arduino to do any task that ease human life. By using smart jacket, people are curbing from being exposed to extreme weather. Extreme weather can cause a lot of bad effects to us. Hypothermia for example, it will cause fatal if no serious action to be taken.

For the recommendation, I hope this project would be improving more according to the users demand. There a lot of room for improvements to be done. Maybe if we improve it by applying both cooling and heating, it would be interesting. As far as we know, Malaysia is a hot country. So it’s a good idea

Acknowledgment

In the name of Allah S.W.T, the most gracious and merciful. Allhamdullilah, all praise to Allah for his blessing in my life. Peace be upon to the prophet Muhammad S.A.W.

First off all, I want to thank my supervisor Dr. Dalila Binti MD Said that willing to assist me, sharing advice and motivation during the project was done.Not to forget my father and my mother Mohd Johan mahfar and Kamsiah Supandi that always supporting me to solve this project.

A big thanks also for fellow friends that willing to give help and moral support during the project was done.Thank you very much.

References

[1] Arduino Home, https://www.arduino.cc/, retrieved on March 6, 2016.

[2] Wook-Sung Yoo and Sameer Ahamed Shaik,(2016), Development of Home Management System Using Arduino and AppInventor, Fairfiel University Fairfield, CT, USA

[3] Datasheet for relay module,www.cyctron.com, retrieved on 18 December 2016

[4] Electric Heating Pad, https://www.adafruit.com/product/1481 , retrieved on 18 December 2016

[5] Gregory Paul and Edward Gim,David Westerfeld, (2014),Battery powered heating and cooling suit, University of New York, Stony Brook

[6] Cold Environments - Health Effects and First Aid, https://www.ccohs.ca/oshanswers/phys_agents/cold_health.html, retrieved on 18 December 2016

[7] Ken Parson,(2014),Human Thermal Environment, United States

[8] heating suit, http://cozywinters.com/battery-heated-clothing.html, retrieved on 18 December 2016

[9] heater body suit, http://heaterbodysuit.com/ , retrieved on 18 December 2016

[10] AkitoshI Nibe,(1975),Temperature control flexible electric heating panel

[11] Dilip Raja, Arduino LCD, http://circuitdigest.com/microcontroller-projects/arduino-lcd-interfacing-tutorial, Retrieved on 21 Dec 2016

[12]http://batteryuniversity.com/learn/archive/is_lithium_ion_the_ideal_battery

[13] Soteris A.Kologirou, (2014),Solar Energy enginnering, Process and System, Boulevard , Lengfordlane, Kingdolton, Uk

[14] http://www.conserve-energy-future.com/Advantages_SolarEnergy.php

[15] Mayoogh Girish, (2016), Arduino Bluetooth Interfacing-Simplest tutorial on Bluetooth basic,Retrieved from https://diyhacking.com/arduino-bluetooth-basics

[16] Mohannad Rawasdesd, Arduino AND Bluetooth HC-05 Connecting easily, retrieved from http://www.instructables.com/id/Arduino-AND-Bluetooth-HC-05-Connecting-easily/step3/Arduino-

[17] Wijetunge S.P,(2008),Design and Implementation of a Bluetooth based General Purpose Controlling Module,Sri Lanka.

[18] solar powerbank, http://www.lazada.com.my/solar-power-bank-20000-mah , retrieved on 20 Dec 2016

[19] Arduino - JY-MCU, retrieved from ~ Bluetooth http://robotosh.blogspot.my/2012/07/arduino-jy-mcu-bluetooth.html

[20] Julyan Illet, (1997), How to use intelligent L.C.D,

[21] Datasheet,(1999),LM35 Precision Centigrade Temperature Sensors,Texas Instruments

Smart Traffic Light using Fuzzy Logic Controller

Mohd Faiz Bin Mohd Rifin
Faculty of Electrical Engineering
Universiti Teknologi Malaysia
Johor Bahru, Malaysia.
Mohd.faiz.rifin@gmail.com

Azhar Bin Khairuddin
Department of Electrical Power Engineering
Faculty of Electrical Engineering
Universiti Teknologi Malaysia
Johor Bahru, Malaysia.
azharkhairuddin@utm.my

***Abstract*— Nowadays, the high traffic density on Malaysian roads due to rapid increase of the number of vehicles has become a serious issue for road traffic planner. There is a need for a good traffic flow control to ease the traffic congestion. This paper introduces a smart traffic light system by using fuzzy logic that controls the timing of the system to minimize waiting time with reduced cycle length and delay time while increasing the number of vehicles through the junction with improved capacity per lane. A MATLAB simulation and hardware development of traffic light system using fuzzy logic controller are presented. The fuzzy logic controller has been developed based on density of vehicle at green and red phases and arrival rate at current green phase. The output from the traffic light system using fuzzy controller is the duration time of green phase, junction candidate for the next green phase and the decision on whether to extend or terminate the green phase. The traffic light system is compared with pre-timed controller system. The results show that traffic light using fuzzy logic controller has better performance than pre-timed system in terms of minimum waiting time and contributed to smooth traffic flows for all junctions.**

Keywords—Smart Traffic Light System, Fuzzy Logic Controller, Isolated Road Intersection, Pre-timed system

I. INTRODUCTION

The rapid development in the urban areas will generate economic activity that will attract more people, leading to problems such as slums, traffic jams and so on. Based on the report of the Kuala Lumpur Structure Plan 2020 [1], only 20 percent of the population of Kuala Lumpur utilises public transport. This situation has contributed to the increase in the number of cars on the road and causing traffic jams and pollution.

According to the data from Malaysia Automotive Info[1] the number of new passenger and commercial vehicles registered in for the year 1980 to September 2016 are increasing day by day. If the number of road user is automatically increasing the congestion in our country will also increase. Therefore, to avoid this situation happen government have to consider the best solution, which is government need to improve the traffic light system in our country.

In Malaysia, the types of traffic light controller commonly used are pre-timed and semi-actuated modes. For pre-timed mode, the green and red phase durations are set at a constant value for each phase. So, this controller mode is not suitable to manage traffic flow at intersections, especially during peak hours. Furthermore, most of the existing traffic light timing system are not influenced with the volume of traffic flow. The main objective of the proposed traffic controller using a fuzzy logic controller is that the traffic light system can adapt to the changing conditions of traffic volumes. A fuzzy logic based traffic light controller is developed that is able to operate like human thinking in giving decisions to traffic lights related to traffic flow for a four-junction road intersection.

II. FUZZY LOGIC CONTROL SYSTEM DESIGN

In this paper, fuzzy logic system is developed based on Mamdani-Type Fuzzy Inference System in MATLAB Toolbox. Fuzzy logic controller traffic light system is divided into three modules which are Next Phase Module, Green Phase Module and Extension Green Phase Module. Figure 1 presents the proposed design of fuzzy logic system for traffic light.

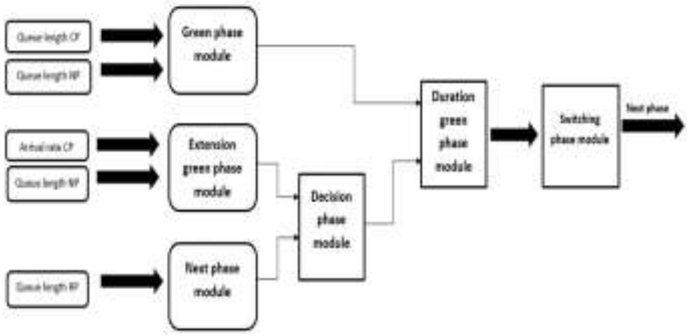

Fig. 1. Block diagram for the system

The procedure of the signal control system is as follows.

Step 1 : System gets the necessary data from the detectors at every junction.
Step 2 : The controller specifies which of the current red phases should be switched to green light in the next phase.
Step 3 : The controller specifies the duration time for green phase.
Step 4 : Green light will be ON, and at the last 5 seconds arrival rate sensor will be ON .

Step 5 : After 5 seconds , the controller specifies whether current green phase should be extended or terminated.
Step 5.1 : If the current green phase should be terminated, then the controller terminates the current green phase and switches the selected red phase in step 2 to green and the procedure goes back to step 1.
Step 5.2 : If current green phase should be extended, then the procedure goes to step 4.

A. *Next Phase Module*

This module will determine the next candidate for green phase depending on traffic condition at all red phase lanes. Figure 2 shows the phases of the simulated junction for intersection. This intersection is designed based on the traffic model from traffic light at Sri Pulai Perdana junction. This module controls the phase sequence based on the density of vehicles at all red phases.

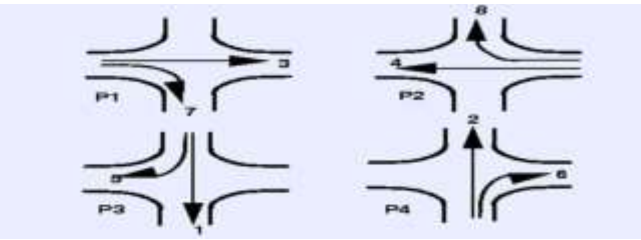

Fig. 2. Four phase junction

Fuzzy logic makes decisions based on weight W (Pi) of each phase, where Pi = A, B, C,D, which refers to the four lanes considered at the junction. In this project, the weight is defined by the density of vehicle in each red phase. The density of vehicles is measured using the vehicle detector that is installed in every lane. The fuzzy logic system will give priority to the phase with highest demand for green phase.

Densities of the vehicle at all red phase lanes are used as the three-input variable and the output are the candidate for next green phase for the fuzzy logic inference system in this project. The structure of the fuzzy logic system controller consists of input membership function, output membership and fuzzy rule set function as shown in Figure 3.

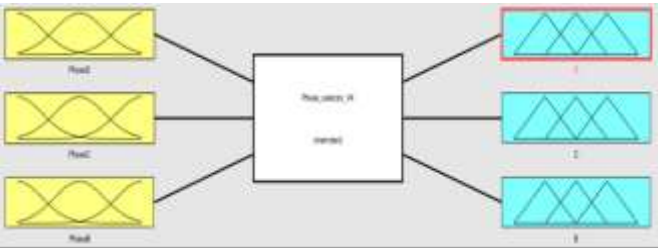

Fig. 3. Structure of Fuzzy Logic For Next Phase Module

The density of vehicle is assumed to be ranged from 0 - 100 vehicles. The input membership function of vehicle density is divided into four ranges which is Very Short (VS) = -25 to 25, Short (S) = 0 to 50, Long (L) = 25 to 75, and Very Long (VL) = 50 to 100. The fuzzy logic rule is designed based on “IF-THEN” conditions. All of the fuzzy rules for controlling system are established by using the “IF-AND-THEN” statement.

For example:

IF density of vehicle on lane D is very long AND

density of vehicle on lane C is long AND

density of vehicle on lane B is very long

THEN next green phase is lane D

B. *Green Phase Module*

This module contains fuzzy logic that will determine the duration time for green light. There are 25 rules in this fuzzy rule. The input of the membership function is density of vehicle at current green phase (CP) and density of vehicle at next green phase (NP). Fuzzy logic will make decisions based on these two inputs. Figure 4 shows the structure of a fuzzy logic design for the green phase duration.

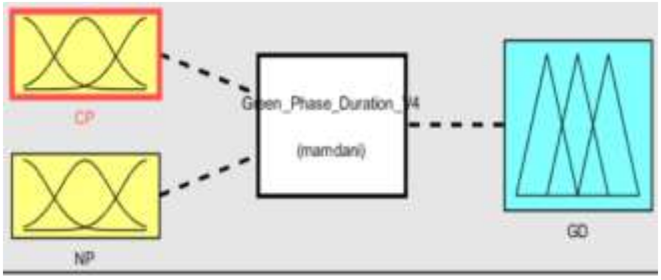

Fig. 4. Structure Of Fuzzy Logic For Green Phase Module

The density of vehicle at a current green phase and at the next green phase is assumed to be range from 0 to 100 vehicles. The input membership function of vehicle density is divided into four ranges which is Very Short (VS) = -25 to 25, Short (S) = 0 to 50, Long (L) = 25 to 75, and Very Long (VL) = 50 to 100. For the output variable, duration time for green light (GD) is assumed to be ranged from 0 to 30 second and subdivided into four ranges which are Very Short (VS) = -7.5 to 7.5, Short (S) = 0 to 15, Long (L) = 7.5 to 22.5 and Very Long (VL) = 15 to 30.

C. *Extension Green Phase Module.*

The purpose of this module is to extend or terminate the current green phase based on set of fuzzy rules. The fuzzy rule decides whether to extend or terminate the current green phase by comparing the traffic condition at the current green phase and traffic condition at the next green phase, which are the arrival rate at the current green phase and the density of vehicle at the next green phase candidate. An arrival rate is measured based on the vehicles that pass through the set point in an interval of time. Figure 5 shows the input and output of fuzzy logic system for extension of green phase module.

This module will run at the last 5 seconds of the duration green time at green phase. For example, assume that phase A is a current green phase, duration time for phase A is 50 seconds and the next phase module is already selected as the next candidate for green phase. Green light will be ON at phase A for 45 seconds, that is after 5 second extension that the phase module gets the date of arrival rate at current green phase from vehicle detector. In this paper, we measure the arrival rate of vehicle at the current green phase by considering the number of vehicles passing through the detector in 5 seconds. If the arrival rate is high and the density of vehicle at the next green phase is low, then the current green phase will be extended. If the arrival rate is low and the density of vehicle is very high, then the current green phase will be terminated and the next green phase will be ON.

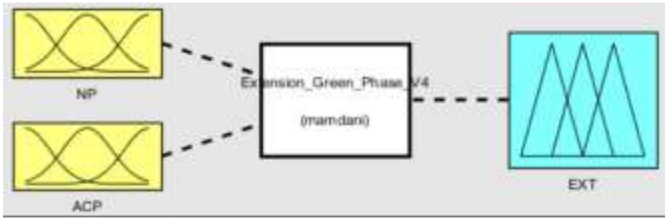

Fig. 5. Structure Of Fuzzy Logic For Extension Module

There are two inputs of membership function of this fuzzy system which is arrival rate and density of vehicle at next green phase. The density of vehicle input is the same as for the other module, which is Very Short (VS) = -25 to 25, Short (S) = 0 to 50, Long (L) = 25 to 75, and Very Long (VL) = 50 to 100. For arrival rate, we assume the input from 0 to 20 and divided into four ranges which are Few = -5 to 5, Small = 0 to 10, Medium = 5 to 15 and Many = 10 to 20. While for the output of this fuzzy logic we assume the range from 0 to 20 seconds, which is Zero = -5 to 5, short = 0 to 10, medium = 5 to 15 and long = 10 to 20.

III. Hardware

Figure 6 shows the hardware setup for traffic light system using fuzzy logic controller. In this project, Arduino Mega 2560 are used for the controller and LCD (Liquid Crystal Display) screen are used to display the data or information from controller. Next, red, yellow and green LEDs are used for traffic light indicator and infrared sensors are used for arrival rate sensors. These sensor will count the number of vehicles that are coming on each lane. Slide switches are used to represent PIR sensors that are supposed to measure the density of vehicles waiting at red phase junctions.

A. Working and concept of controller

Initially the sensor senses the density of vehicle that are waiting at red phase and transfers the data to microcontroller. Every junction has its own sensor to detect the density of vehicles. The microcontroller analyzes the data to determine which junction has high traffic density. Then it compares the traffic density and arranges the sequence of junction and the timer for the green phase based on fuzzy logic system that has been set in the controller. After that, the microcontroller sends the signal to the light indication system for the traffic light signaling. If one of the junction is on green light, the sensor will sense the density of vehicles at other red junctions and send the data to microcontroller to be analyzed for the next junction as candidate for green phase. At the same time, on green phase junction, the last 5 seconds for the green phase arrival sensor will be activated to count for the vehicles that are coming into the lane. The microcontroller compares the data from arrival sensor and next green phase sensor. Then, it will decide whether to terminate the current green phase and change to the next green phase or to extend the timer for the current green phase based on fuzzy logic system.

Fig. 6. Traffic light prototype

IV. Result and Analysis

To test the performance of the traffic light system, the developed fuzzy logic controller has been compared with pre-timed controller system. The parameters considered in this comparison are waiting time, delay time and capacity per lane. The better controller will be selected based on the lowest waiting time and delay time and high capacity per lane.

In this work, delay time is calculated by using

$$D = \frac{Co}{2}\frac{\left(1-\frac{gi}{Co}\right)^2}{(1-\frac{qi}{S})} \tag{1}$$

Equation (2) is used to calculate the capacity per lane:

$$Ci = Si(\frac{gi}{Co}) \tag{2}$$

Table 1 shows the data for traffic light based on pre-timed controller. The data have been obtained from on-site observation at traffic light junction of Sri Pulai Perdana.

TABLE I. PRE-TIMED SYSTEM.

Junction	**Maximum green light time (sec)**	**Sequence Number**	**Cycle length (sec)**
Junction 1	90	1	276
Junction 2	106	2	
Junction 3	60	3	
Junction 4	20	4	

There are three different traffic conditions considered in the testing of the methods, namely low, medium and high traffic volumes.

At low traffic volume, the flow rate of vehicle at the intersection is set between 0 to 900 vehicles per hour. The flow rate for medium traffic volume is between 900 to 2700 vehicles per hour and for the high traffic volume, the flow rate is greater than 2700 vehicles per hour. The testing has been done for eight cycle, where there are various vehicle densities and arrival rate for each cycle.

A. Results

The results of the testing of the traffic light system using fuzzy logic controller and pre-timed controller are illustrated in Figures 7 to 9 and Table II. The result consists of the green phase duration time, extension time for green phase, cycle length, average capacity per lane and average delay time for each cycle.

B. Discussion

The aspects considered for performance comparison between traffic light system using fuzzy logic controller and that using pre-timed controller are cycle length, delay time and capacity per lane. Referring to Figure 7 and Table 2, results show that fuzzy logic controller performs better than pre-timed controller at low traffic condition. Fuzzy logic controller provides shortest cycle length than pre-timed with an average of about 25.82% reduction in cycle length compared to the pre-timed system. Next, fuzzy logic controller also performs better than pre-timed controller in term of delay time, for which it reduces the average delay time for about 26.53% as compared to pre-timed system. In capacity per lane aspect, the fuzzy logic controller also performs better than pre-timed controller, for which it improves to 47.76% in capacity per lane compared to pre-timed controller.

In the second testing, the traffic volume is medium. The results in Figure 8 and Table 2 shows that fuzzy logic controller performs better than pre-timed controller in all three aspects. The fuzzy logic controller shows shortest cycle and also reduces delay time although the traffic volume is increased, which are 14.95% reduction in cycle length and 25.83% reduction in delay time compared to pre-timed system. The fuzzy logic controller also performs better than pre-timed controller in term of capacity per lane for which it improves 17.65% capacity per lane in medium traffic condition compared to pre-timed system.

Fig. 7. Result for low traffic volume

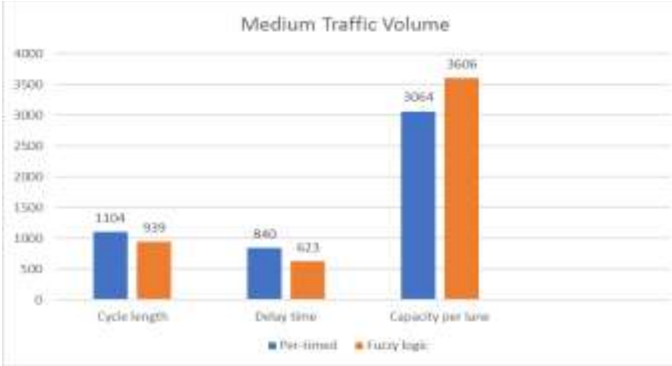

Fig. 8. Result for medium traffic volume

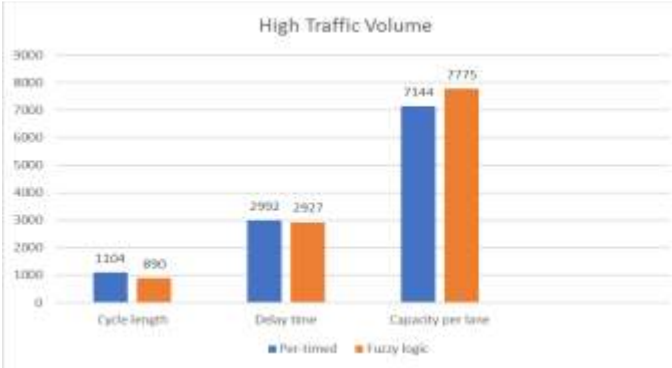

Fig. 9. Result for high traffic volume

TABLE II. Result

Traffic volume	Cycle length	Capacity per lane	Delay time
Low traffic volume	Reduce 25.82 %	Increase 47.76 %	Reduce 26.53 %
Medium traffic volume	Reduce 14.95 %	Increase 17.65 %	Reduce 25.83 %
High traffic volume	Reduce 19.38 %	Increase 8.83 %	Reduce 2.17 %

Results for the third test, for which the traffic volume is high, are shown in Figure 10 and Table 2. The traffic light with fuzzy logic controller shows 19.38% and 2.17% reduction in cycle length and delay time, respectively as compared to pre-timed system. For capacity per lane, the fuzzy logic controller shows 8.83% improvement compared to pre-timed system.

V. Conclusion

The traffic light system with fuzzy logic controller in general performs better than the traditional method which is pre-timed system or fixed timer system based on the flexibility of the system. The system is able to adapt to real time traffic conditions and can change timing for traffic signal based on traffic conditions and extend or terminate the green time slot based on whatever traffic condition at the junction.

A simulation and hardware implementation for traffic light system using fuzzy logic controller has been carried out to compare the performance of the system with pre-timed system. The testing and simulation have been done in different traffic conditions. From the results for the testing and simulation it can be observed that the fuzzy logic controller has better performance in terms of cycle length, delay time and capacity per lane. The system with fuzzy logic controller can minimize waiting time and delay time while increasing the capacity of vehicle pass through the intersection. The developed system can benefit local municipalities in providing traffic light system that can ensure smooth and efficient traffic flow at road intersections in Johor.

REFERENCES

[1] Malaysia Automotive Info. Summary Of New Passenger & Commercial Vehicles Registered In Malaysia For The Year 1980 To March 2017. 2008 . http://www.maa.org.my/info_summary.htm

[2] Klein, L. A. Sensor technologies and data requirements for ITS. Boston: Artech House, 2001.

[3] Lilly, J. H. Fuzzy control and identification. Hoboken, NJ: Wiley, 2010.

[4] Passino, K. M., and Yurkovich, S. Fuzzy control. Menlo Park, CA: Addison-Wesley, 1998.

[5] Mannering, F. L., and Kilareski, W. P. Principles of highway engineering and traffic analysis. New York: Wiley, 1990..

[6] Othman Che Puan, Che Ros Ismail and Nordiana Mashros, "Kejuruteraan Lalu Lintas", Desktop Publication, First Edition. 2014.

[7] Guberinić, S., Šenborn, G., and Lazić, B. Optimal traffic control: urban intersections. Boca Raton, FL: CRC Press. 2008.

[8] Hamed Homaei, S. R. Hejazi and Seyed Ali Mohamad Dehghan. A New Traffic Light Controller Using Fuzzy Logic for a Full Single Junction Involving Emergency Vehicle Pre-emption. Journal of Uncertain Systems : Vol.9, No.1, pp.49-61, 2015.

[9] Azura Che Soh, Lai Guan Rhung and Haslina Md. Sarkan. MATLAB Simulation of Fuzzy Traffic Controller for Multilane Isolated Intersection. (IJCSE) International Journal on Computer Science and Engineering Vol. 02, No. 04, 2010,924-933.

[10] A.R. Zade and D.R. Dandekar. Simulation of Adaptive Traffic Signal Controller in MATLAB Simulink Based On Fuzzy Inference System. National Conference on Innovative Paradigms in Engineering and Technology. 2012.

[11] Nuratiqa Kamarudi. Kempas Flyover Traffic Light System Comparative Study. Bachelor Degree thesis, Faculty of Electrical Engineering Universiti Teknologi Malaysia, Skudai. 2015.

[12] Iskandar Bin Aminudin (2014). Preemption Sequence Of A Traffic Light For Emergency Vehicles (Degree's thesis, Universiti Teknologi Malaysia). Skudai: Faculty of Electrical Engineering.

[13] Mohammad Hossein Fazel Zarandi, Shabnam Rezapour. A Fuzzy Signal Controller for Isolated Intersections. Journal of Uncertain Systems Vol.3, No.3,pp.174-182,2009. http://www.worldacademicunion.com/journal/jus/jusVol03No3paper02.pdf (Accessed 2016-9-29)

[14] Tan Kok Khiang, Marzuki Khalid, Rubiyah Yusof. Intelligent Traffic Light Control System (N.D.). Center for Artificial Intelligence and Robotics. Malaysian Journal of Computer Science, Vol. 9 No. 2, December 1996, pp. 29-35

[15] Syed Ali Abbas, Syed Muhammad Sheraz, Dr. Humera Noor. Fuzzy Rule Based Traffic Signal Control System for Oversaturated Intersections (N.D.). Department of Computer and Information Systems Engineering NED University of Engineering and Technology, Karachi Pakistan.

[16] I.N.Askerzade (Askerbeyli), Mustafa Mahmood. Control The Extension Time Of Traffic Light In Single Junction By Using Fuzzy Logic. International Journal of Electrical and Computer Sciences IJECS-IJENS Vol:10 No:02. http://ijens.org/104702-6969%20IJECS-IJENS.pdf (Accessed 2016-9-30)

24V SLA Battery Charger and its Performance in Term of Charging and Discharging

Farah Athirah Bt Abu Kasim
Department of Electrical Power Engineering
Faculty of Electrical Engineering
Universiti Teknologi Malaysia
farah_athirah321@yahoo.com

Azhar Bin Khairuddin
Department of Electrical Power Engineering
Faculty of Electrical Engineering
Universiti Teknologi Malaysia
azharkhairuddin@utm.my

***Abstract*— Battery has played a major in many applications such as electric vehicle and uninterruptable power supply (UPS). Battery becomes a must choice because it can provide immediate power when needed. Among the battery family, sealed lead-acid battery become a popular choice because it came in variety of output voltage and rechargeable. Although the sealed lead-acid is rechargeable, problems still occur when recharging the battery. The battery tend to undergo overcharge if there is no cut-off situation to stop the charging process. This paper represents the performance of lead acid battery in terms of overcharging, charging and discharging process. The method used in this paper is constant voltage method using voltage regulator to fix the output voltage of a preset magnitude that remains constant regardless of changes to its input voltage or load conditions. The output of this project would be displaying the voltage-time graph as well as the charging and discharging state of the lead-acid battery.**

Keywords—sealed lead acid battery; overcharging; charging and discharging; voltage regulator

I. Introduction

A battery cell consists of two lead plates a positive plate covered with a paste of lead dioxide and a negative made of sponge lead, with an insulating material (separator) in between. The plates are enclosed in a plastic battery case and then submersed in an electrolyte consisting of water and sulfuric acid. Each cell is capable of storing 2.1 volts[1]. In order for lead acid cell to produce a voltage, it must first receive a (forming) charge voltage of at least 2.1-volts/cell from a charger. Sealed lead acid batteries do not generate voltage on their own; they only store a charge from another source[1]. This is the reason sealed lead acid batteries are called storage batteries, because they only store a charge. The storage battery or secondary battery is such battery where electrical energy can be stored as chemical energy and this chemical energy is then converted to electrical energy as when required. The conversion of electrical energy into chemical energy by applying external electrical source is known as charging of battery[2]. Whereas conversion of chemical energy into electrical energy for supplying the external load is known as discharging of secondary battery.

II. Literature Review

A. *Type of Batteries*

There are two different types of batteries, one is primary batteries and other one is secondary batteries[2]. The main uses of batteries are in industrial and household areas.

- Primary Battery

A primary battery is one that cannot easily be recharged after one use, and are discarded following discharge. Most primary cells utilize electrolytes that are contained within absorbent material or a separator, and are thus termed dry cells. Primary battery cost less and are commonly found in devices that have low current drain such as wristwatches, remote controls, alarm clocks and children's toys. Apart from being inexpensive, primary batteries have more advantages – they are widely available, posses high energy density, long storage life and are environmentally friendly[3]. These batteries can produce current immediately after assembly.

- Secondary battery

Secondary batteries are the batteries in which these must be charged before using it. These batteries are assembled with active materials that are in discharged state. These are generally called as rechargeable batteries. The chemical reactions that take place in rechargeable batteries are reversible reactions. That is the main reason it is called as rechargeable. In these batteries liquid is present in a container which is unsealed. They are unsealed because the hydrogen gas that is produced by these secondary batteries should be ventilated to ensure the safe dispersal[3]. The common type of rechargeable batteries is lead-acid battery. These batteries can supply very high electrical energy. Their initial cost is higher but they can be reused many times.

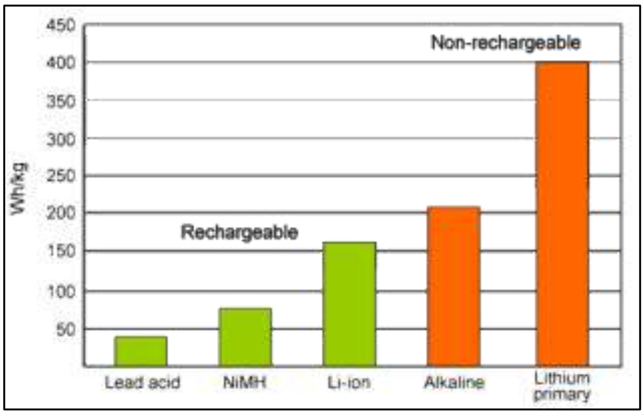

Fig. 1. Comparison of battery with respective watt hour.

A sealed lead acid battery (SLA) or gel cell is a lead acid battery that has the sulfuric acid electrolyte coagulated (thickened) so it cannot spill out. They are partially sealed, but have vents in case gases are accidentally released for example by overcharging. SLA can be used for smaller applications where they are turned upside down. They are more expensive than normal lead acid batteries, but they are also safer. SLA use different chemicals than dry cells, so they are rechargeable. In SLA battery, electric power is stored as chemical energy of the battery cell plates. The number and size of the plates determine the capacity of the battery. The capacity is measured in ampere hours (Ah). 60 ampere hours are one of the widespread sizes; and this means that a fully charged new battery can provide 12 ampere power during 5 hours[4].

Nowadays, batteries mostly belong either to the sealed type, where the electrolyte is absorbed in a porous mat or ossified to get a gel-like mass; or the conventional ”flooded” batteries. The sealed batteries are, without exception, provided with some kind of safety valve that will open if the battery is put to incorrect use[5]. The sealed batteries are also called valve-regulated or maintenance-free batteries; under normal circumstances they require no maintenance.

i. SLA Voltage and Specifications

Table I roughly shows the different voltages of SLA with their respective characteristics. The highlighted column is used in this paper which is 24v of SLA battery.

TABLE I. SLA VOLTAGE AND SPECIFICATIONS [6]

Battery Pack Volt	**Charging Current**	**Input Voltage**	**Capacity range to charge**
6v SLA	1.2A	110-240V	1.2 - 20Ah
6V&12V SLA	3.0A	110-240V	6V (3-20Ah) 12V (3-20Ah)
12V SLA	0.8A	110-240V	0.8 - 20Ah
	1.0A	110-240V	1.0 - 10Ah
	3.0A	110-240V	3.0 - 25Ah
	10.0A	110-240V	10 -110Ah
24V SLA	1.5A	110-240V	7 - 12Ah
	3.0A	110-240V	3- 40Ah
	6.0A	110-240V	7.5- 60Ah
	15A	96-260V	40A-200Ah
36V SLA	1.8A	110-240V	2 - 25Ah
	2.5A	100V - 240V	2.5 - 60Ah
	6.0A	110V	6 - 60Ah
48V SLA	3.0A	110-240V	3 - 30Ah
	6.0A	110V	6 - 60Ah
72V SLA	20A	110	20-120Ah

ii. Factors Affecting Lead Acid Battery Life

- Temperature Effects

Predicted battery existence is particular by using batteries' manufacturer established in an environment at or close to the suggested temperature of 25°C (77°F).[3] From the suggested temperature, the age of battery is decreased.[3] The aging scenario can cause positive plates become corrosive, grid shape, and strap, which will increase exponentially as a function of temperature.[3]

- Discharge Cycles

The lead acid battery failure, as defined by means of a decrease in capacity and the oxidization of positive plates, raise with the quantity of discharge cycles and the intensity of discharge.[3] SLA batteries have lead calcium grid systems are in particular vulnerable to getting older because of repeated cycling.[3] Any discharge over eight percent of the rated ability is defined as a deep discharge.[3] Most of the manufacture supply guarantee primarily based on the quantity of discharge cycles.[3]

- Overcharging

Itermittent charging at high voltages, including equal charge, can advantage the battery through get rid sulfation of the plate and clean the plates.[3] However, overcharging routine damages the plates. [3] Overcharging is extra charge after the SLA battery is completely charged.[7] Battery life will shorten due to continuous overcharging.[7]

- Undercharging

Batteries lose ability due to self-discharge if the battery are constantly undercharged.[3] The undercharge situation is shown by the way of a small particular gravity, small voltage cell, or brighter shade at the battery plates.[3] The undercharged battery won't be at complete capacity and will end up completely damaged from sulfation.[3] Persistent undercharging outcomes in a dangerous building up of lead sulfate on the plates, called sulfation.[3]

- Over discharge

Hydration takes place in the battery that is over discharged and not right away recharged, or battery which stays in a discharged situation for a prolonged time (together with would possibly occur at some point of lengthy-term garage).[8] Hydration effects while the lead and lead compounds of the plates dilute in the water of a discharged cell. Then it form lead hydrate, that's deposited at the separators.[8] More than one internal quick circuits arise between the positive and negative plates when the cell is recharged. The cell is completely broken as soon as hydration is obvious.[3]

B. *Charging and Discharging*

The internal resistance of the battery itself makes it hard to manipulate the charging and discharging procedure because the capacity of the battery is anticipated by way of the capacity distinction among the two electrodes of the battery, named external voltage.[9] While the efficiency of the battery is improved by its inner resistance of the deterioration, the outside voltage is just too high to prevent charging despite the fact that the battery has no longer stored enough amount of energy.[4]

Potential energy is restored when undergo charging process. Thus, making it once more available for electrical current to be supplied for the next discharge.[5] The reversible electrochemical technique is shown as below.[5]

$$\underset{\substack{\text{(Lead dioxide)}\\ \text{Positive}\\ \text{Active}\\ \text{Material}}}{PbO_2} + \underset{\substack{\text{(Sulphuric acid)}\\ \text{Electrolyte}}}{2H_2SO_4} + \underset{\substack{\text{(Spongy lead)}\\ \text{Negative}\\ \text{Active}\\ \text{Material}}}{Pb} \underset{\text{Charge}}{\overset{\text{Discharge}}{\rightleftharpoons}} \underset{\substack{\text{(Lead sulphate)}\\ \text{Positive}\\ \text{Active}\\ \text{Material}}}{PbSO_4} + \underset{\substack{\text{(Water)}\\ \text{Electrolyte}}}{2H_2O} + \underset{\substack{\text{(Lead sulphate)}\\ \text{Negative}\\ \text{Active}\\ \text{Material}}}{PbSO_4} \quad (1)$$

Voltage increases when charging starts while when discharging starts, voltage will decreases.[4] Furthermore, discharge time becomes shorter with each cycle due to variety of cycles increase.[4] The battery deteriorates and it takes place despite the constant discharge current as a result of the growth in internal resistance.[4] Hence, battery voltage hastily depletes in proportion to the importance of the inner resistance, subsequently discharging to 10.5 v turns into faster.[10]

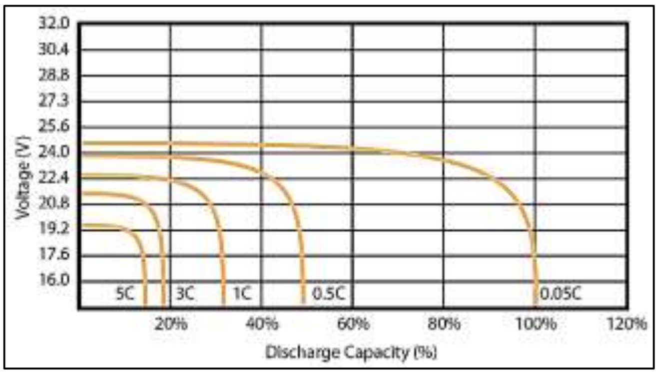

Fig. 2. Discharge capacity of SLA battery[11]

C. *SLA Features*

- Sealed/Maintenance-Free

The valve regulated, spill-proof construction of the SLA battery allows trouble-free, safe operation in any position. There is no need to add electrolyte, as gases generated during over-charge are recombined in a unique “oxygen cycle”[12]

- Long Shelf Life

A low self-discharge rate permits storage of fully charged batteries for up to a year at room temperature before charging is required. Lower storage temperatures enhance shelf life characteristics even further[12].

- Design Flexibility

Batteries may be used in series and/or parallel to obtain choice of voltage and capacity. Due to recent design breakthroughs, the same battery may be used in either cyclic or standby applications. Over 50 models are available to choose from[12].

- Deep Discharge Recovery

Special separators, advanced plate composition, and a carefully balanced electrolyte system have greatly improved the ability of recovering from excessively deep discharge[12].

- Economical

The high watt-hour per dollar value is made possible by the materials used in a sealed lead-acid battery: they are readily available and low in cost[12].

- Easy Handling

No special handling precautions or shipping containers — surface or air — are required due to the leak-proof construction. Classified as non-hazardous commodity[12].

- Wide Operating Temperature Range

SLA batteries may be discharged over a temperature range of -40°C to +60°C (-40°F to +140°F) and charged at temperatures ranging from -20°C to +50°C (4°F to +122°F)[12].

- Rugged Construction

The high impact resistant battery case is made either of non-conductive ABS plastic or styrene. Large capacity batteries frequently have polypropylene cases. All of these case materials impart great resistance to shock, vibration, chemicals and heat[12].

- Long Service Life

Under normal operating conditions, four or five years of dependable service life can be expected in stand-by applications, or between 200-1000 charge/discharge cycles depending on average depth of discharge[12].

D. *SLA Application*

Battery systems using 24 volts are found in mobility applications. They usually involve a pair of twelve volt batteries hooked in series, or four 6 volt batteries in series[12].

▪ Cycle Use

Portable VTR/TV, tape recorders, radios, and etc. Power tools, lawn mowers and vacuum cleaners, Cameras and Photographic equipment, Portable personal computers, word processors, portable terminals and etc. Portable measuring equipment, Portable telephone sets, various power toys and recreational equipment, Lighting equipment[12].

▪ Standby Use

Communications and electric equipment, Emergency lighting equipment, Fire alarms and security systems, Various telemeter equipment, Office computers, processors and other office automation equipment Robots, control equipment and other factory automation equipment, UPS power supplies, Emergency power supplies in power generation plants and substations Telecommunications[12].

- Solar Cell Power Generation

Street lighting, Water pumping stations, Portable handheld power supplies, Small town power systems[12].

III. Methodology

A. Constant Voltage Charging Method

A constant voltage charger is basically a DC power supply which in its simplest form may consist of a step down transformer from the mains with a rectifier to provide the DC voltage to charge the battery. The SLA cells used for cars and backup power systems typically use constant voltage chargers. Constant-voltage (often called constant-potential) chargers maintain nearly the same voltage input to the battery throughout the charging process, regardless of the battery's state of charge. Constant-voltage chargers provide a high initial current to the battery because of the greater potential difference between the battery and charger. A constant-voltage charger may return as much as 70% of the previous discharge in the first 30 minutes[13]. As the battery charges its voltage increases quickly. This reduces the potential that has been driving the current, with a corresponding rapid decrease in charge current. As a result, even though the battery reaches partial charge quickly, obtaining a full charge requires prolonged charging. Given this behavior, constant-voltage chargers are frequently found in applications that normally allow extended charging periods to attain full charge. Constant-voltage chargers should not be used where there is frequent cycling of the battery. Repeated discharges without returning the cell to its full charge will eventually decrease the battery capacity and may damage individual cells[13]. The figure below show the illustration of using constant voltage method:

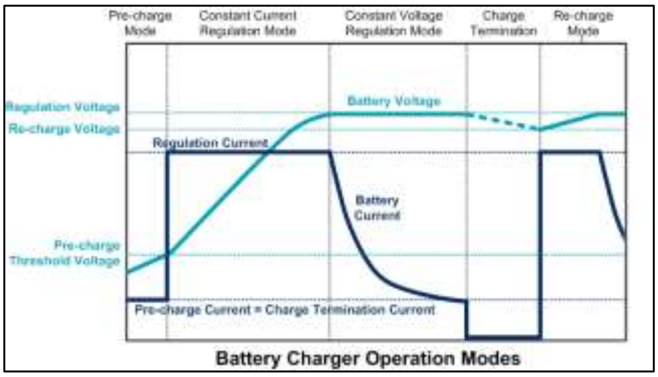

Fig. 3. Illustration of using constant voltage method[14]

B. Circuit Implementation

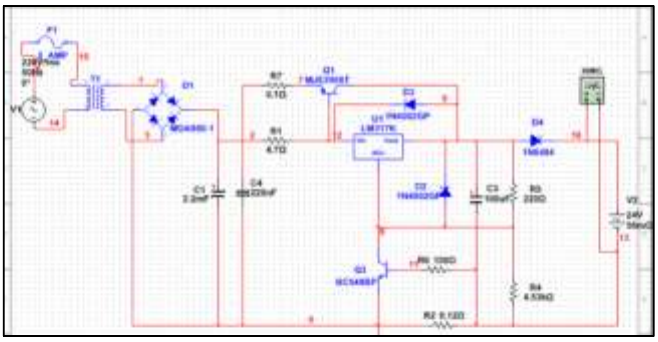

Fig. 4. 24V SLA battery charger circuit.

The stimulation is developed using Multisim software to obtain the output voltage of the circuit by using constant voltage concept. Theoretically, the output voltage should be at a fixed value. Hence, the method is called constant voltage method. The lead acid used in this project is SLA lead acid battery. Flooded lead acid battery is commonly used in Uninterruptible Power Supply (UPS) system[15].

C. Circuit Division

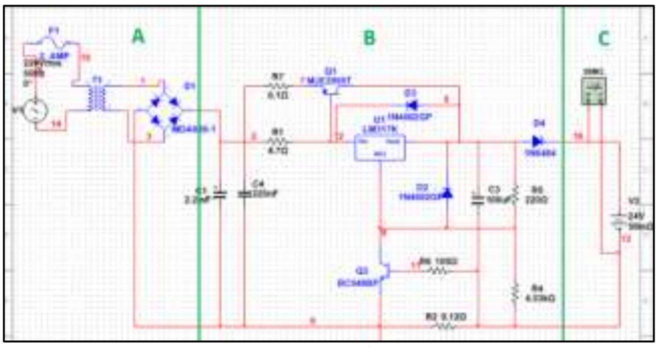

Fig. 5. Division of the circuit

As shown in Fig.5 , the circuit is divided into three part which are A, B and C. For part A, the first stage of the circuit is a transformer which is a step-down type that changes the amplitude of the input voltage. In this circuit, 220/30V transformer is used to step-down the AC mains 220V to 30V AC supply. Then the rectification process takes place to allow the current flows in one direction. Part B is the charging circuit that consists of voltage regulator, transistor, diodes and resistor. At this part, the voltage regulator to maintain a constant voltage level. For part C, the output voltage is measured using multimeter and also in form of transient analysis to confirm the required output voltage of 24V.

IV. Result And Discussion

A. Charging Response

As for the results, the transient response of the circuit is formed using Multisim software. This transient response explained the pattern of charging SLA battery in a fast way.

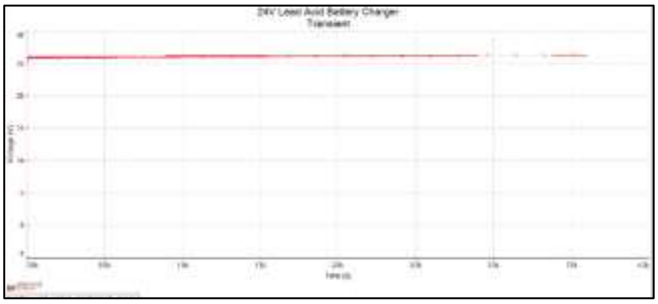

Fig. 6. The transient response in one hour

The transient response in Fig 6 shows the process of charging SLA battery in one hours which is 3600 in seconds with 0.1 maximum step[16]. With the starting point of 0V, it does take some time before the steady state part which is at 24V. By using transient response, performance of any system can be easily analyzed compared to non standard input signals.

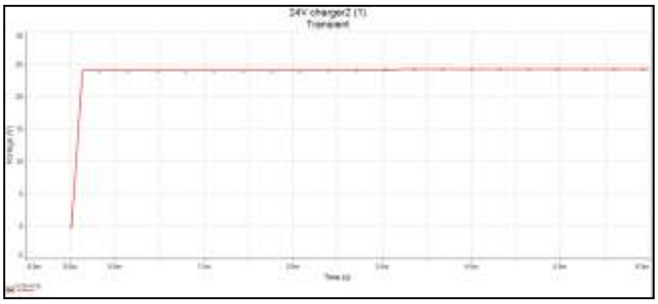

Fig. 7. The detailed view of the response

In Fig 7, the pattern for charging SLA battery is clearly plotted. The charging process slightly increase from 0 to 24V. In real life, the charging process takes around 7-8 hours to be in a fully charged state. The time taken can be measured using Eqn 2.

$$T = Ah / A \qquad (2)$$

From Equation (2), T is the time taken to fully charge the SLA battery, A is the current of the charger and Ah is the measurement of battery capacity. Since charging current should be 10% of the Ah rating of battery[17], the time taken for a battery to fully charged can be obtained. The table below shows the several of Ah value with 24V battery.

TABLE II. TIME TAKEN FOR THE BATTERY TO RECHARGE ACCORDING TO ITS CAPACITY (AH) AND RECHARGING CURRENT (A)

SLA Battery Voltage (V)	Battery Capacity, Ah (amp hr)	Battery Capacity, Ah (amp hr) $+40\%$ *losses* (Ah)	Charging Current, A (A)	Charging Current, A $\pm$ *losses* (A)	Charging Time of Battery, T (hr)
24	12	16.8	1.2	1.3	12
	26	36.4	2.6	2.7	13.48
	51	71.4	5.1	5.2	13.73
	74	103.6	7.4	7.5	13.81
	86	120.4	8.6	8.7	13.84
	92	128.8	9.2	9.3	13.85
	100	140	10	10.1	13.86

B. 24V SLA Battery Model

The circuit is implemented in Multisim because Matlab software component is not enough to perform the circuit stimulation in it. However, the model of lead acid battery battery is only can be obtained in Matlab. Thus, the circuit implementation that was stimulated by Multisim need an equivalent model of SLA battery to ensure that the circuit functioning well in term of charging and discharging. From the research, to represent the block model of SLA battery, a connection of resistor and capacitor is needed as shown in Fig 8

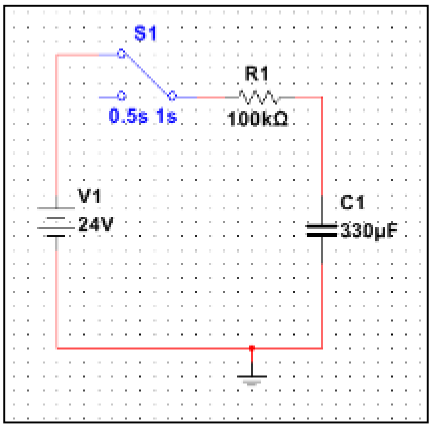

Fig. 8. The capacitor charging when switch is at A while discharging when switch is at B .

By using the Equation (3),

$$\tau = R \times C \qquad (3)$$

τ is time constant, while R and C is resistor and capacitor value used in the circuit respectively. Time constant is the amount of time it takes for the capacitor voltage to increase approximately 63.2% from its present value to its final value which is the voltage of the battery[18]. The graph of voltage against time is plotted.

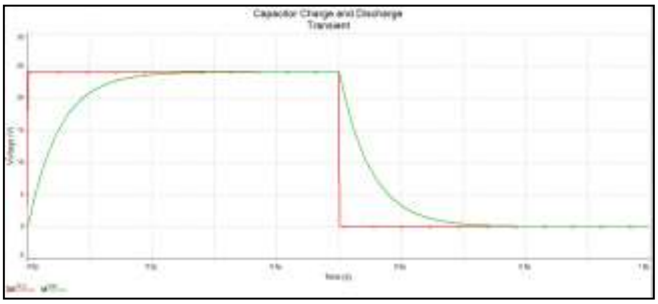

Fig. 9. Graph voltage capacitor charging and discharging against time

The graph from Fig. 9.shows that the sample of charging and charging of a battery through a model of battery that is made from resistor and capacitor. The first phase shows the charging part while the second phase shows the discharging part of a resistor and capacitor. Form Fig. 9., 24V of output was obtained to show that the battery is fully charged. The charging battery circuit is experimentally proved and can be used to implement in the real life application.

V. CONCLUSION

As for the conclusion, by using the constant voltage method, the output voltage will not exceed 24V due to voltage regulator that function as to fix the output voltage. So that, the SLA battery will not go through overcharging process. This type of charging method can both charge at a reasonable rate and maintain the battery at full charge without damage. In addition, the charging time of battery is based on the battery capacity and it's charging current. The transient response and charging discharging graph of the battery shows that the circuit implemented is successful.

REFERENCES

[1]D. Linden and T. B. Reddy, *HANDBOOK OF BATTERIES*. .

[2]V. L. Battery, "CHARGING METHODS - CONTINUED," no. August, 2005.

[3]T. Paper, "TECHNICAL PAPER LEAD ACID BATTERY working – LIFETIME STUDY Valve Regulated Lead Acid (VRLA) Batteries Factors affecting battery life :," pp. 1–13.

[4]S. J. Hou, Y. Onishi, S. Minami, and H. Ikeda, "Charging and Discharging Method of Lead Acid Batteries Based on Internal Voltage Control," pp. 1–5.

[5]T. Bulletin, "Charging Valve Regulated Lead Acid Batteries."

[6]C. Information, F. Lead, and A. Batteries, "BU - 403 : Charging Lead Acid," pp. 1–77, 2016.

[7]B. Chargers, C. Methods, B. Chargers, C. Methods, and E. Pages, "Battery Chargers and Charging Methods," pp. 1–6, 2016.

[9]J. Alzieu and H. Smimite, "Development of an on-board charge and discharge management system for electric-vehicle batteries," vol. 53, pp. 327–333, 1995.

[10]D. M. Jochim, "Fast charging of lead-acid batteries," vol. 4, pp. 33–38, 1994.

[12]A. Datta, "Design of a Lead Acid Battery Charger System," *Thesis*, 2009.

[13]C. Login, "Mayhem also on Facebook!," pp. 1–3, 2016.

[14]T. Morgan, C. Sealed, and L. Acid, "Guide to charging Sealed Lead Acid batteries Guide to charging Sealed Lead Acid batteries."

[15]N. P. Ramesh, K. M. Dnyaneshwar, and B. S. Vishwas, "Lead Acid Battery Charger Literature Review : Methodology :," vol. 100, pp. 408–411.

[16]I. I. T. O. Vrla, "Gelled Electrolyte (Gel) and Absorbed Glass Mat (AGM) Batteries EAST PENN Expertise and American Workmanship I : How it Works ABOUT VRLA BATTERIES."

[17]J. W. Stevens and G. P. Corey, "A Study of Lead-Acid Battery Efficiency Near Top-of-Charge and the Impact on PV System Design."

[18]K. R. Bullock and A. J. Salkind, "17 . VALVE REGULATED LEAD - ACID BATTERIES."

High-voltage Switch for Pulse Electric Field Application using Series Connected MOSFET

Produce fast switching performance and voltage balancing using series-connected MOSFET

Muhammad Ashraff bin Mohd Yamen
Department of Electrical Power Engineering
Faculty of Electrical Engineering, Universiti Teknologi Malaysia
Johor Bharu, Malysia
muhammadashraff04@yahoo.com

Mohamed Afendi bin Mohamed Piah
Institute of High Voltage and High Current
Faculty of Electrical Engineering, Universiti Teknologi Malaysia
Johor Bharu, Malysia
fendi@fke.utm.my

***Abstract*— The most common method of producing high voltage switch is by using pulse generator which is complicated because of the bigger size and the cost is high. The proposed using power semiconductor as switching device realizes that it will overcome the weaknesses of pulse generator. So, this paper will present the ability and capability of metal-oxide field effect transistor (MOSFET) as switching device. The main idea of this paper is to connect the MOSFETs in series where five MOSFETs were used for simulation test. The paper will show switching performance through the waveforms produced for each of the MOSFET where voltage balancing and fast switching are the main problem associated in this project. It is a must for switching system to reach fast turn ON/OFF and voltage balancing is needed as the devices are connecting in series to avoid damage on the MOSFETs. For simulation , the aim of the test was to switch 2.5 kV of supply voltage and reach voltage balancing with 500 V for each device with consideration of voltage limit of the MOSFET which is 1000 V. This paper also will describe more on application of pulse electric field (PEF)**

Keywords*— *series connection; MOSFET; voltage balancing; fast switching, PEF

INTRODUCTION

Power semiconductor device technology has widely developed further in order to ensure the device functions well to be applied in many industrial applications involving high voltage and current ratings. As result, today we have been introduced to various power semiconductor devices such as insulated gate bipolar transistor (IGBT), integrated gate commutated thyristor (IGCT) and metal-oxide field effect transistor (MOSFET). In this present day, few researches has been done involving series operation of power semiconductor devices in high voltage application to withstand the high voltage with limited voltage rating devices. This is due to increasing demand for the systems or applications like high voltage switch, high voltage dc transmission system (HVDC) and flexible ac transmission [1].

Generally, in case of turn ON and turn OFF, MOSFET gives an advantage over any other power semiconductor devices because it is relatively simple compare to others [3]. As the market increase in power semiconductor technology, MOSFET are widely used to replace IGBT. This is because MOSFET can produce low ON stage voltage drop, low switching losses, nearly zero recovery losses and high switching frequency limits [4].

As series connection of power semiconductor device is required, approaching voltage balancing among the devices is a must in the circuit. When applying series connection of the devices, several problems might occur such as complexity of the circuit, low reliability, and limited number of devices that can be used. So, obtaining voltage balancing is the solution for the problems [1]. For example, if we are using five MOSFETs connected in series with 5 kV source, the voltage drop for each device should be balanced and equal which is 1 kV for each MOSFET. This result can be seen through the output graph during circuit testing which is the waveforms produced represent each MOSFET in the circuit.

A. Problem Statement

The idea of using MOSFET in this project instead of other power semiconductor devices in switching application is because of the characteristics of the device itself to act as a very good switching component. The main reason is the MOSFET can create a switching signal faster than other power semiconductor devices. As series connection of MOSFETs will be applied in this project, the voltage balancing is needed. In order to obtain the voltage balancing, few things need to be considered such as the selection of MOSFET model, the circuit design, and the value of other electronic components used in the circuit. It is very important to gain the voltage balancing for each MOSFET to avoid any damage of the power semiconductor device.

B. Objectives

The objectives of this project are :

1) To create a very fast high voltage switching system with fast turn ON and turn OFF using series connected MOSFET.

2) To obtain and reach voltage balancing in the circuit for each MOSFET.

3) To obtain a perfect square wave for each MOSFET that represents fast turn ON and turn OFF.

LITERATURE REVIEW

A. MOSFET as Switching Device

Basically, years ago the technology of high voltage switch was in huge scale using pulse generator that cause the increasing in cost of installation. Then, as the technology nowadays are getting higher and better, power semiconductor has been applied as the switching device for a better performance.

MOSFET has a very huge potential and advantages to act as switch for high speed high voltage application such as pulsed power commonly. In order to improve the switching speed, it is best to use package that are specially designed to minimize the parasitic inductance in the circuit. By applying radio frequency (RF) MOSFET model, we can obtain average low parasitic inductance nearly to 1 nH [5].

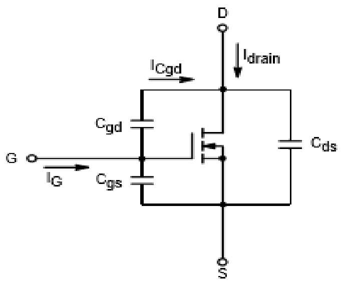

Figure 2. Simplified equivalent circuit of MOSFET

In addition, MOSFET can be defined as charge controlled device. Figure 2 is the simplified equivalent circuit that represent MOSFET. There are few parameters in MOSFET which are equivalent input capacitance (Ciss), reverse transfer capacitance (Crss) and equivalent output capacitance (Coss). So, the fast turn ON and OFF of the depends on how fast the capacitance is charged and discharged [6].

B. Pulse Electric Field Application

Pulse electric filed (PEF) is the basic principle in electroporation. The term of electroporation was widely known as non-thermal energy efficient alternative for heat pasteurization techniques. In food industrial technology, PEF was used to destroy cell membranes of the unwanted cells. This application can be done by applying source of high voltage with short duration pulse across the food [8].

The main advantage of this technique is the ability of the technology to maintain the quality of the food and dairy products as all the bacteria were killed. High voltage pulsed electric field that had been exposed to the cells may cause a dielectric breakdown to happen on the cell membrane. This breakdown can happen in two ways which are reversible breakdown and irreversible. The reversible breakdown are widely used in science, medicine and biotechnology while irreversible breakdown used in application that related to microorganism such as bacteria, yeasts and viruses [9]. Figure 3 shows the effect of PEF on cell membrane. Electric field that produced from the pulse will destroy the membrane and kill the bacteria inside [10]

Figure 3. Effect of PEF on cell membrane

The main purpose of food processing is food preservation. It is a must to ensure the high quality of food and the food will not be affected during the process [12]. Heat pasteurization and PEF method both share the similar function in food industries which is to kill microorganisms inside the food. But PEF application is much better on maintaining the food taste and quality compared to heat pasteurization. This is because heat pasteurization uses heat to reduce the level of bacteria, spores and other agents that will spoil the quality of the food. Compare to PEF, foods will stay cool because there are no heat applied [13]. Figure 3 shows the basic units of the PEF food processing system that proves no heat applied.

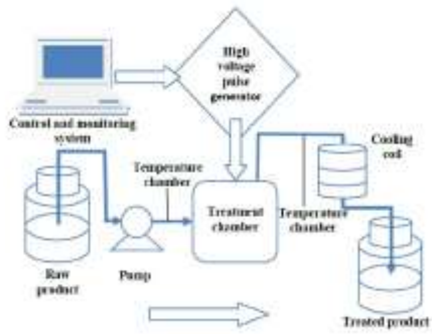

Figure 3. Flowchart of PEF food processing system

The pump will flow the food or substances into the treatment chamber from raw product tank. The electrodes that were placed inside the treatment chamber will received the generated high voltage electrical pulse. Then, the electrodes will conduct and transmit the high intensity electrical pulse to the food inside the chamber. The cooling coil were used to control the temperature of the food during treatment. The treated product will accumulate in a tank for next process of food production [14].

C. Series Connection of MOSFET

Power semiconductor devices connected in series are easily applicable for both low and high side switches [15]. In this case, fast MOSFET was used as switch and the MOSFET should be able to switch within a short rise time. The use of semiconductor switch can produce low vibration of switching moments. Compare to pulse generator, the use of semiconductor device as switching element can produce less noise or vibration of switching moments [16].

Series connection is needed so that each MOSFET can withstand the high voltage with limited voltage rating devices. In other words, voltage balancing among the MOSFET is the main issue when applying series connected MOSFET to the circuit. Since this applications able to reach it's voltage ratings until several tens of kilo volts, the power processing cannot be accomplished with any single device. So, several devices should be connected in series and operated simultaneously [1].

D. Voltage Balance

Obtaining voltage balance among the MOSFET during series connection is very crucial to avoid any damage from occur on the MOSFET. In order to obtain the voltage balancing, there are few methods can be applied on the circuit such as adding snubber, additional circuitry, resistor parallel with MOSFET and series stack.

Applying balancing resistors in parallel with each device is one of the way to reach balance voltage drop for each MOSFET. Placing resistor across the MOSFET is to avoid biasing on the gate side. In addition, zener diode can be placed between gate and source pin to protect from overvoltage [19].

For applications that related to pulse power generation, power semiconductor devices like MOSFET, IGBT and thyristor has shown their potential to be applied in the circuit. But, power semiconductor has it's disadvantage which is the low capability of the power device. To overcome this disadvantage, power semiconductor device were connected in stack with series connection. Nowadays, stacked MOSFET has become a common thing in switching circuit [22].

Stacking MOSFET can increase the capability of the switching performance. But, several things need to be considered when stacking the MOSFET. For instance equal voltage distribution, fast and synchronise switching and avoiding excess voltage stress in the circuit [16]. Besides that, stacked MOSFET also used in circuit to overcome the problem that related to limited breakdown voltage of MOSFET [23].

RESEARCH METHODOLOGY

A. Project Workflow

The first stage of the workflow is to do researches based on the title of the project. The designed of the circuit had been studied in order to obtain the exact design of the circuit. Mathematical modelling also needed to calculate the parameters of the circuit. Besides that, literature review on operation of high voltage switch and the application of the system to industry had been done.

After researches done and obtained the information needed, the project proceed with the circuit design. The circuit was designed using Multisim software and run the simulation to get the result. If the result is not satisfying which mean did not achieve the objectives, the modification need to be done on the circuit design. This step were repeated until the objectives reached before move to next stage.

B. Basic Circuit Design

Basic circuit design is very important as a reference to obtain the equation of the circuit. As the main objective of the project is to achieve voltage balancing, this basic circuit design use two MOSFET that stacked in series . The circuit design is shown in Figure4 . The idea for this basic circuit was to give 2 kV power supply to the circuit and the voltage from drain to source among the MOSFET will reach until 1 kV which is balance to each other. This idea was derived in Equation (8).

Figure 4. Basic circuit of series connected MOSFET

The circuit used the method of applying resistor, R1 and R2 that were parallel to each power semiconductor device and zener diode, D2 and D1 at gate and source terminal of the MOSFET.

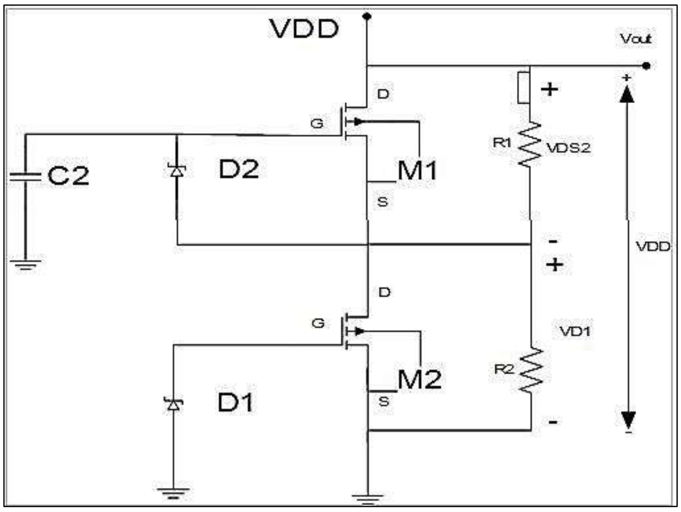

The purpose of the zener diodes were to avoid overvoltage in the circuit while the presence of resistors were to avoid biasing on the gate side.

C. Mathematical Modelling

The main objective of the basic circuit is to obtain the equation of the circuit. Mathematical modelling works were done base on the circuit and the equation on capacitor, C2 was obtained. The C2 allows simultaneous and synchronous switching of MOSFETs configurations with a single trigger signal.

As the circuit in Figure 4 was in stack series, the voltage gain,A_{V2} of MOSFETs, M1 and M2 can be calculated from

$$A_{V2} = \frac{\Delta V_{D1}}{\Delta V_{GS2}} \quad (1)$$

where $\Delta V_{GS2}$is the voltage from pulse circuit. $V_{D1}$is the voltage across the MOSFET. As the voltage across the MOSFET will be the same, so the value of V_{D1}equal to V_{D2}. Eq. (2) can be used to find the effective gate source capacitance,C'_{gs2} .

$$C'_{gs2} = C_{gs2} + C_{zener} + A_{V2}(C_{gd2}) \tag{2}$$

where the capacitance of the zener, C_{zener} can be obtained from datasheet of zener diode used. The value of gate to source capacitance, C_{gs2} is equal to the input capacitance, C_{iss} as shown in Eq. (3) while gate to drain capacitance, C_{gd2} is equal to reversible capacitance, C_{rss} of the MOSFET as shown in Eq. (4). Multiplication of A_{V2} with C_{gd2} will produce miller capacitance.

$$C_{iss} = C_{gs2} \tag{3}$$

$$C_{rss} = C_{gd2} \tag{4}$$

Both Ciss and Crss can be obtained from the datasheet of the MOSFET used. The change in gate to source voltage, ΔV_{GS2} is given by

$$\Delta V_{GS2} = \frac{\Delta V_{D1} C_2}{C_2 + C'_{gs2}} \tag{5}$$

Expressing capacitor, C_2:

$$\Delta V_{GS2}(C_2 + C'_{gs2}) = \Delta V_{D1} C_2$$

$$\Delta V_{GS2} C_2 + \Delta V_{GS2} C'_{gs2} = \Delta V_{D1} C_2$$

$$\Delta V_{GS2} C_2 - \Delta V_{D1} C_2 = -\Delta V_{GS2} C'_{gs2}$$

$$(C_2[\Delta V_{GS2} - \Delta V_{D1}]) = (-V_{GS2} C'_{gs2}) \times -1$$

$$C_2[\Delta V_{D1} - \Delta V_{GS2}] = V_{GS2} C'_{gs2}$$

$$C_2 = \frac{\Delta V_{GS2} C'_{gs2}}{\Delta V_{D1} - \Delta V_{GS2}} \tag{6}$$

This mathematical modelling is the same method for voltage relationship such as third array capacitor. So, the gain for the third array A_{V3} is given by

$$A_{V3} = \frac{\Delta V_{D2}}{\Delta V_{GS3}} \tag{7}$$

If applied voltage V_{DD} is equally divided to each arrays in series, then

$$\Delta V_{D2} = 2\Delta V_{D1} \tag{8}$$

where V_{D2} is the total voltage drop across the two MOSFETs that connected in series. Therefore, when adding the 3rd array, the value of coupling capacitance, C_3 is

$$C_3 \simeq \frac{1}{2} C_2$$

In general,

$$C_n \simeq \frac{1}{n-1} C_2 \tag{9}$$

In conclusion, the derivation of the circuit from Figure 4 has come out with final equation which is in Eq. (9) where *n* is the number of series MOSFETs on the circuit. This equation can be applied to any number of connected series of MOSFETs.

D. Testing in Software

Before proceed with circuit design in Multisim software, few calculations need to be done by using the equation obtained from mathematical modeling. For MOSFET selection, its is a must to study the specification of the MOSFET before using it. Table 1 shows the specifications of the selected MOSFET and zener model. As the high-voltage that will be supplied to the circuit is 2 kV and five MOSFETs connecting in series, the expected voltage drop for each MOSFET is 500 V.

TABLE 1 : SPECIFICATIONS OF MOSFET AND ZENER

	Parameters	Typ.	Units
V_{DSS}	drain-to-source breakdown voltage	1000	V
C_{iss}	input capacitance	1600	pF
C_{rss}	reverse transfer capacitance	56	pF
t_r	rise time	33	ns
t_f	fall time	30	ns
C_z	zener capacitance	60	pF

For capacitor that connected to each MOSFET, calculations on the value of the capacitor had been done based on the Eq. (1) until Eq. (9). The circuit was designed based on the basic circuit from Figure 4. As the main idea is to use five MOSFETs that connected in series, Figure 5 shows the circuit diagram on the series MOSFETs that will be run in Multisim software.

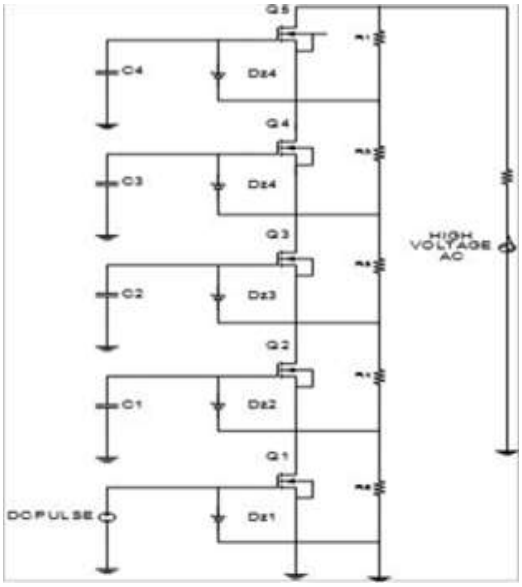

Figure 5. Five series-connected MOSFETs

RESULT AND DISCUSSIONS

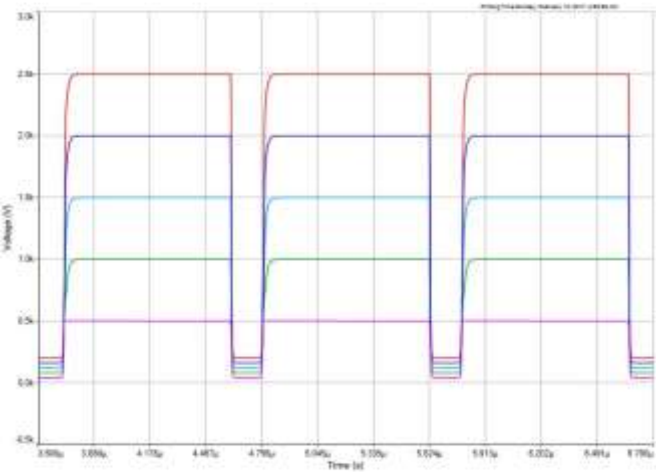

Fig. 6 Output waveform

The waveform shown in Fig. 6 is the complete circuit result for all MOSFETs using Multisim software. Each colour of the waveforms represent the MOSFETs in the circuit. As five MOSFETs were used, so five colours appear in the waveform.

The waveforms formed a very well five square waves which means the switching system reached a very fast turn ON and OFF. From the observation, the switching performance during turn ON produce nearly complete square wave while during turn OFF, the voltage dropped very fast and formed a shape close to complete square wave. It is best to apply in PEF application because strong PEF needs a very fast switching performance.

The difference between each MOSFET is 500 V which means the value of voltage drop for each of it, that switched the power supply of 2.5 kV. From Figure 6, the peak voltage reached for the whole circuit was equal to the value of power supply represented by the red colour of waveform. So, no over voltage occur in the circuit as the function of zener diode that connected to each MOSFET was to protect the MOSFET and avoid overvoltage. If one of the MOSFET reach more than 1000 V, the MOSFET will damage

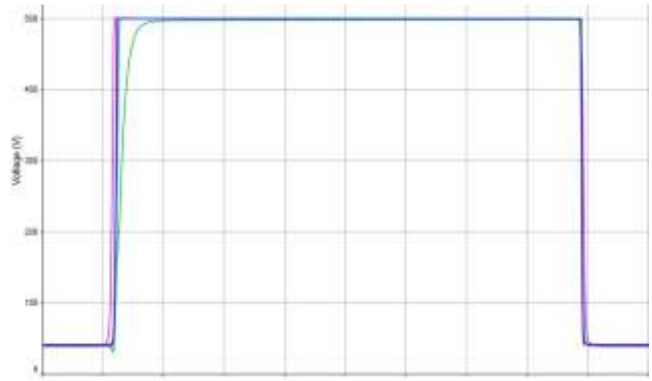

Figure 7. V_{ds} at each MOSFET

Figure 7 showsV_{ds} at each MOSFET. The MOSFETs share the same value of peak voltage 500 V. This is due to the characteristic of drain to source blocking voltage, V_{DSS} of the MOSFET is 1000 V and voltage balancing for each MOSFET is 500 V. Voltage balancing is important to avoid any MOSFET in the circuit reach voltage drop reach more than it's Vdss. The diagram clearly shows all the peak voltage accumulated at one level of voltage. Therefore, the supply power of 2.5 kV were equally shared by all the MOSFETs in the circuit :

$$500V = \frac{2.5kV}{4}$$

CONCLUSION

Series connected MOSFETs switching unit has been succesfully tested and operated by the voltage supply of 2.5 kV, delivering peak voltage of 500 V each. The objectives achieved as the simulation result shows voltage balance amongst the MOSFET and very fast turn ON and OFF. The MOSFETs were safe from any over voltage because voltage balancing is the main priority when connected the power device in series. This paper had shown that power semiconductor can act as a switching device as it can reduce cost, simple and extendibility. This method can be used in the application of PEF because the faster the switching the stronger the PEF produced.

REFERENCES

[1] Ju Won Baek, Dong-Wook Yoo and Heung-Geun Kim, "High-voltage switch using series-connected IGBTs with simple auxiliary circuit," in IEEE Transactions on Industry Applications, vol. 37, no. 6, pp. 1832-1839, Nov/Dec 2001

[2] C. Ma, K. Yoshida and K. Honda, "Si-IGBT versus SiC-MOSFET — Anisolated bidirectional resonant LLC DC-DC converter for distributed

power systems,"*2015 54th Annual Conference of the Society of Instrument* and Control Engineers of Japan (SICE), Hangzhou, 2015, pp. 894-899

[3] K. Vechalapu, S. Bhattacharya and E. Aleoiza, "Performance evaluation of series connected 1700V SiC MOSFET devices," *2015 IEEE 3rd Workshop on Wide Bandgap Power Devices and Applications (WiPDA)*, Blacksburg, VA, 2015, pp. 184-191

[4] T. Tang and C. Burkhart, "Hybrid MOSFET/Driver for Ultra-Fast Switching," *2008 IEEE International Power Modulators and High Voltage Conference*, LasVegas, NE, 2008, pp.128-130

[5] C. S. Mitter. *Active Inrush Current Limiting Uisng MOSFETS.* Application Nite # AN1542. Motorola

[6] Irek Klonowski, Volker Heinz, Stefan Toepfl, Guojon Gunnarson, Guojon Porkelson, "Applications of Pulsed Eelectric Field Technology For the Food Insudtry" *Icelandic Fisheries Laboratories Report Summary,* April 2006, Iceland, pp 1-10

[7] V. Gowrisree, K. Udayakumar and P. Gautam, "Application of High Voltage Pulses in the Preservation of Orange Juice," *2005 Annual IEEE India Conference - Indicon*, 2005, pp. 502-504

[8] I. Benavente and M. Miguez, "A HV pulse generator for PEF applications," *2013 7th Argentine School of Micro-Nanoelectronics, Technolog and Applications*, Buenos Aires, 2013, pp. 44-48

[9] V. Gowrisree, K. Udayakumar and P. Gautam, "Application of High Voltage Pulses in the Preservation of Orange Juice," *2005 Annual IEEE India Conference - Indicon*, 2005, pp. 502-504

[10] M. P. J. Gaudreau, T. Hawkey, J. Petry and M. A. Kempkes, "A solid state pulsed power system for food processing," *PPPS-2001 Pulsed Power Plasma Science 2001. 28th IEEE International Conference on Plasma Science and 13th IEEE International Pulsed Power Conference.* Las Vegas, NV, USA, 2001, pp. 1174-1177 vol.2

[11] Ayman Amer Eissa. *Structure and Function of Food Engineering.*

InTech. 2012

[12] F. V. Robinson and V. Hamidi, "Series connecting devices for high-voltage power conversion," *2007 42nd International Universities Power Engineering Conference*, Brighton, 2007, pp. 1134-1139

[13] M. Sack, S. Keipert, M. Hochberg, M. Greule and G. Mueller, "Design Considerations for a Fast Stacked-MOSFET Switch," in *IEEE Transactions on Plasma Science*, vol. 41, no. 10, pp. 2630-2636, Oct. 2013

[14] R. J. Beaker, B. P. Johnson, "Series connection of power MOSFETs for high-speed, high-voltage switching application" *Rev. Sci. Instrum. 64 (6),* Reno, Nevada, pp. 1655-1656

[15] W. Jiang, T. Matsuda, K. Yatsui and A. Tokuchi, "MHz pulsed power generator using MOSFET," *Conference Record of the Twenty-Fifth International Power Modulator Symposium, 2002 and 2002 High-Voltage Workshop.*, 2002, pp. 599-601

[16] D. Okula, "Series Stacked Switches for Radar Transmitters,"*Conference Record of the 2006 Twenty-Seventh International Power Modulator* Symposium, Arlington, VA, 2006, pp.

Slow Stream Hydropower for Small Dam Application

Muhammad Nur Qusyairi bin Amdan
Faculty of Electrical Engineering
Universiti Teknologi Malaysia
Johor Bahru, Malaysia
qusyairiamdan178@gmail.com

Mohammad Yusri Hassan
Centre of Electrical Energy System (CEES)
Universiti Teknologi Malaysia
Johor Bahru, Malaysia

yusrih@utm.my

***Abstract*— Electrical energy is important in our daily lives to operate the electrical appliances around us. Electrical energy can be harnessed by converting potential energy. Potential energy can be get by flowing or falling water and can convert to electrical energy by turning of water wheel into useful mechanical power. In this journal, the main objective is to develop the slow stream hydropower for a small dam application so that from the development users can use useless water at small dam to generate electricity. The flow of water will be studied and the analysis will be conducted. After getting the data, the water wheel or turbine will be designed based on the flow of water. The suitable generator will be chosen and their drives system between generator and turbine. As expected outcome, the recreation area around the dam can be lighten up with a stand-alone system. Overall, this project will help users to reduce electricity usage by developing sustainability.**

Keywords—component; formatting; style; styling; insert (key words)

I. Introduction

Access to energy is a fundamental element for human development especially electrical energy that need to supply for computers, light and others important instrument. Basically, electrical power can be generated using a renewable and non-renewable source. Renewable source that can be used to generate electricity are using wind, solar, hydro and other. Non-renewable source that is used to provide electrical power are from burning charcoal, gas and nuclear [1]. Today, most of energy needed daily consumption is produce by burning fossil fuels – coal, oil and natural gas. But this fossil fuels are supposed to be about exhausted in 30-50 years [2]. So that, in this millennium era, electrical energy that produce by renewable energy is important in term of environment, society and moral awareness.

II. Literature Review

A. Sustainable Development and Renewable Energy

Sustainable development is defined as development that meets the needs of the present without compromising the ability of future generations to meet their own needs. It must be legally sound, politically advantageous, socially accepted, environmentally sustainable, economically viable and technical feasible [3]. That mean the sustainable development must take care the environment and surrounding condition in present and future generation. As we know, renewable energy is one of many ways to develop sustainable and this renewable energy has been used by man since the oldest times. Wind mills and water mills employed natural resources during many decades, as earliest source of energy production for agriculture and small-scale industrial processes in Denmark [2]. For many decades, the renewable energy has been applied. Why not in this present and future? Much more technologies must be applied to reach the maximum level of sustainability.

B. Small Hydropower.

Hydropower can be obtained where a flow of water from a higher place to a lower place such as waterfall. By run of river hydropower facilities also can generate electricity by placing a small turbine into a waterway and does not need the construction of large dam. Some hydropower technologies do not need dams to operate, if the water flow is strong enough to turn the turbine. This condition will affect the economics of developing hydropower project. Most of high and medium hydropower are fairly mature. But for low head water flow, there is a need to look at this smaller hydropower applications and some of the newer hydropower technologies must be done [4]. Hydropower can be classified according to available head at a side or by power output rating. A typical classification of this system is illustrated in Table I [4].

TABLE I. Hydropower classifications by power output rating

Classification	***Description***
Small Hydro	1 – 15 MW; usually feeding into a grid
Mini-hydro	Above 100Kw, below 1 MW; either stand-alone or feeding into the grid
Micro-hydro	From 5 kW, up to 100 Kw; usually proving power for a small community in remote areas away from the grid

The smallest project, which is micro hydropower are designed to use the water resources available at specific site. Micro hydropower installation is usually use run of water system which do not require a large dam, and only channels the water via pipe or conduit down to the turbine [4]. This micro hydropower also can only use the flow of existing dam as their pressure to turn the turbine.

The calculation on hydropower energy can be calculated from knowing the basic parameter of energy. Then the energy calculation as shown by equation.

$$Energy\ released\ =\ mgH \tag{1}$$

Where,
m = mass,
g = gravity,
H = gross head of vertical distance.

The mass of water can be defined as density time volume of it.

$$Energy\ released\ =\ VpgH \tag{2}$$

The rate of flow, Q can be taken using current meter and can be expressed in terms of power. The S.I. unit for power is Watt.

$$Gross\ power\ =\ pQgH \tag{3}$$

However, the production of power by turbine is impossible to be same as power input. This is due to efficiency issue including frictional loss and copper loss at alternator. For the final output power can derived as show below.

$$Net\ power\ = npqgH \tag{4}$$

Where,

n = efficiency.

C. Hydropower Component

Figure 1 shown the typical slow stream hydropower using water wheel turbine.

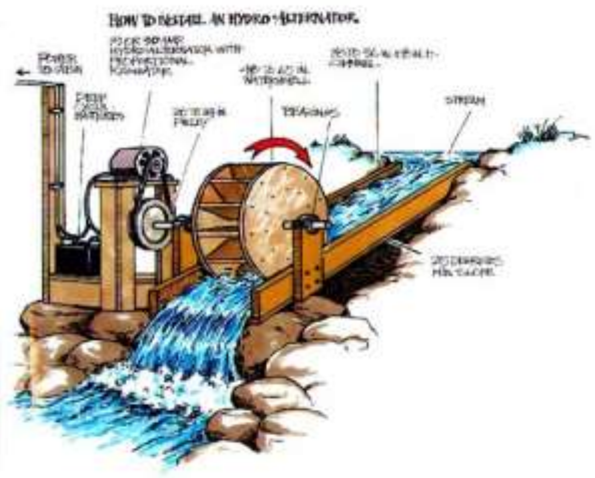

Fig. 1. *Component of slow stream hydropower*

The main component of the slow stream hydropower are rate of water flow, turbine or water wheel, drive systems, generator and output terminal

D. Turbines

Waterwheel are one of traditional turbine. This turbine reacts as a prime mover of a hydro scheme and this type of turbine is relevant nowadays for a very small-scale power generation [5]. There are many types of waterwheel such as undershot paddle wheels, overshot wheels and breastshot wheels. The different between these wheels' is the water flow in their tip. The figure below shown the differences.

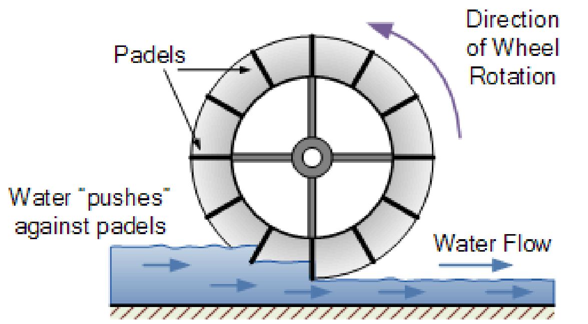

Fig. 2. *Undershot Paddle Wheels*

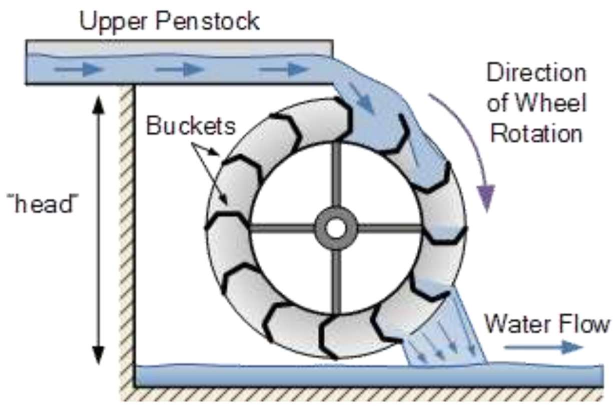

Fig. 3. *Ovwershot Wheels*

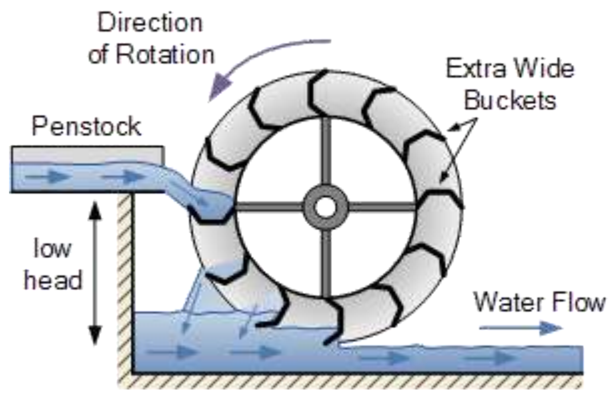

Fig. 4. *Breastshot Wheels*

For a many year, wheel was built with strong shaft and robust spokes. In generally, this wheel was made in wooden and changed gradually to a better material such as iron and steel. The changing of material makes wheel turbine more efficient [5]. Historic wheel is a relevant equipment in this present world, but it should be noted that the wheel will operate in 24 hours per day. This operation time will degrade the turbine by time, so it need to remember that ongoing maintenance and repair will be necessary.

Choice of turbine is important and the type must be choose based on economical, places and others measurement. The turbine also can be choose based on their efficiency. Figure 5 shown the graph of efficiency of several turbine characteristics [5].

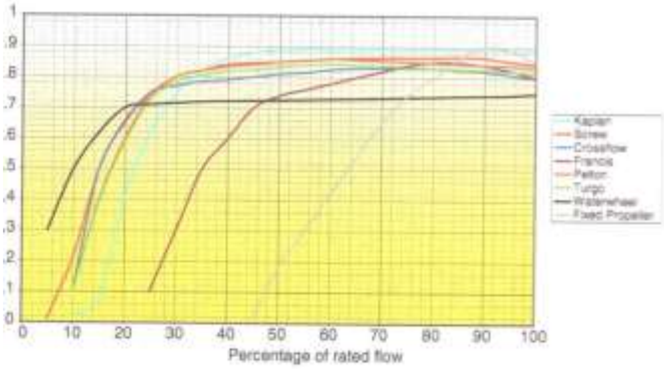

Fig. 5. *Graph percentage of rated flow against efficiency*

It hard to use historic wheels on a professional basic, since cost of install and maintenance hard to estimate. But, a mechanically adept mill owner can successfully complete the process, and end up with a system which is satisfy with efficient and historically [5].

E. Generators

The template is used to format your paper and style the text. All margins, column widths

The purpose of generator is to convert the rotary mechanical power of turbine or prime mover into electrical power [5]. Until recently, hydropower installation always used synchronous generators to produce electricity [7]. The reason for choosing synchronous generators is about their availability and low cost. In addition, not even generators can generate electricity. Induction motor also have been installed as generators for hydropower [7]. But, this part of chapter 2 will focused more on synchronous generators, or more specific is automotive alternator.

Basically, alternator is a three-phase generator with a built-in rectifier circuit that consisting 6 diodes. The alternator will generate Alternating Current supply by the turn of rotor and interact with the magnetic field that produce by stator. The diodes are use as voltage converter that change from Alternating Current supply to Direct Current supply. Therefore, the output of the alternator will be a Direct Current to charge battery as shown in Figure 6.

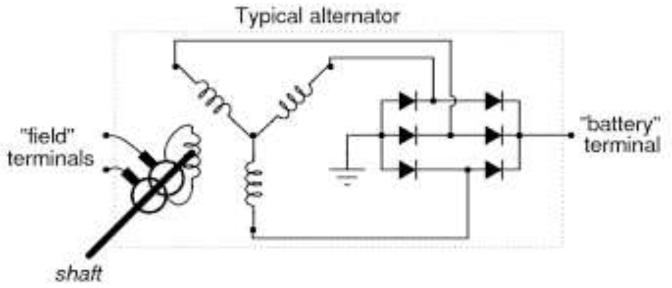

Fig. 6. *Alternator circuit*

This automotive alternator is manufactured in large numbers, and readily available in market and inexpensive [6]. This alternator has reasonable second-hand value and their small size will make them move easily.

Figure 7 show the performance curve that provide by the alternator from DENSO Auto Parts company.

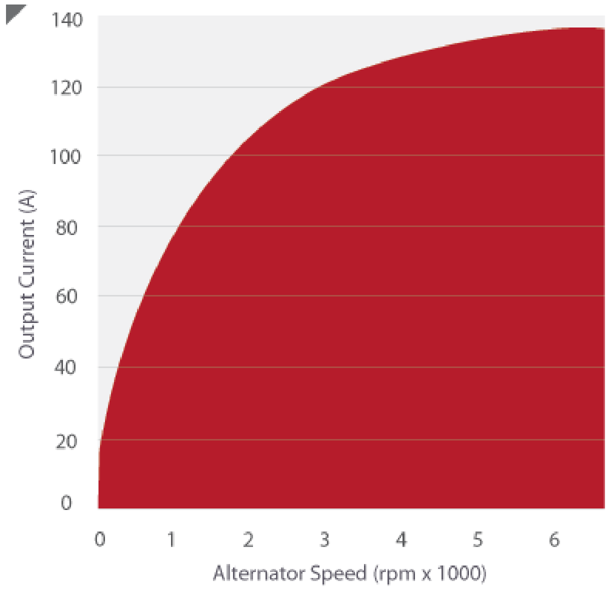

Fig. 7. *Alternator performance curve from DENSO.*

F. Drive Systems

The purpose of drive system is to transmit power from turbine to the generator. The drive is comprised the generator shaft, turbine shaft, bearing to support shaft, pulleys, belts or others component. Figure 7 shows the example of belt drive system.

Fig. 7. *Pulley and belt*

The ratio of drive that determine the torque transfer to the generator can be calculated using this formula.

$$Ratio\ of\ drive\ = \frac{(circumference\ of\ turbine\ pulley)}{(circumference\ of\ generator\ pulley)} \quad (5)$$

III. METHODOLOGY

This chapter will briefly explain about the method that will be conducted in this project. Generally, it will be the guideline in completing this project. At first this project will begin with a preliminary study. It's important to have a good understanding of hydropower system including their components. It would help to understand about what to be accomplished with this project. After a preliminary study, the rate of flow must be taken at the chosen places. After completing collecting data, the relationship between rate of flow and turbine must be estimated. Then, the choosing of generator and designing a turbine must be done. Lastly, all part need to be integrated and testing must be taken place. Figure 8 shows the flow of methodology by flowchart.

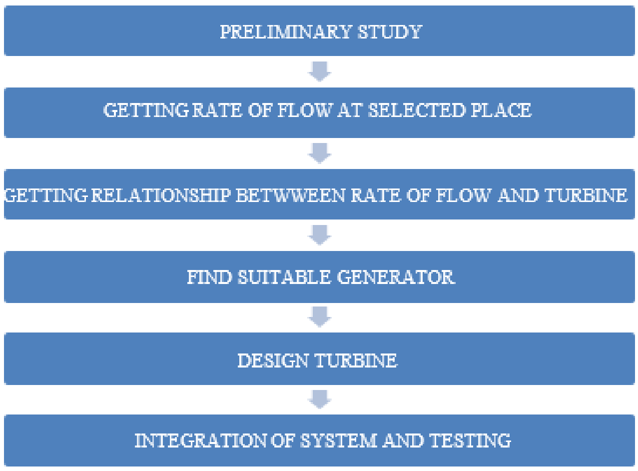

Fig. 8. *Flow of methodology*

A. *Preliminary study*

For preliminary study part, it will be more on focusing to find out the best work of this field. To complete this part a proper research must be conducted. As a result, this part has been explaining about the term and the knowledge that similar for this project. It is explained about sustainable development and renewable energy; small hydropower; hydropower components, turbines, generators and drive system.

B. *Getting Rate of Flow at Selected Places*

. The rate of flow will be taken at the case study places, that is at Tasik Ilmu as shown in Figure 9.

Fig. 9. *The case study dam*

The finding of rate of flow is using the measurement items naming as current meter. The meter will take the velocity of water and the level of water. Then the value of rate of flow can be estimated. Figure 10 shows the picture of current meter.

Fig. 10. *Current meter.*

C. *Getting Relationship between Rate of Flow and Turbine.*

After getting the data of rate of flow. Then, the relationship between rate of flow and turbine was estimated. How fast the rotational of turbine that have been design when get the pressure that showing by rate of flow. For a preliminary result, the value of rate of flow can estimated the total power that can be produced by one software. The software name as Hydropower by Casimir. This software came from India and can find it in their website.

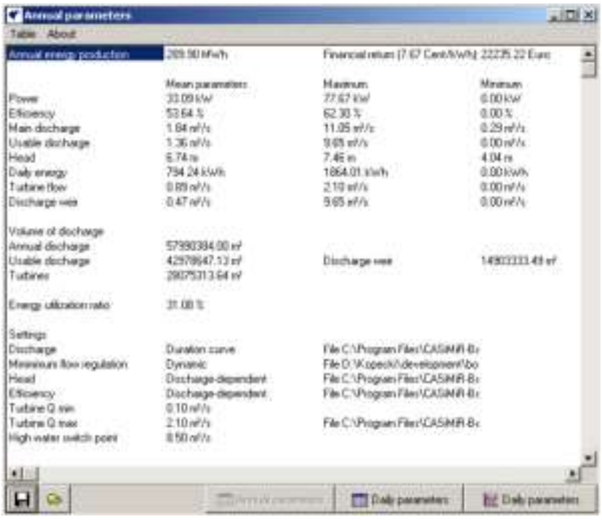

Fig. 11. The Estimation of output power.

D. Find Suitable Generator and Designing Turbine

This process has been done in preliminary study. But, in this part the generator used that is alternator are more specific in terms of size, capacity and others. Figure 12 show the example of alternator used.

Fig. 12. Example of alternator

Figure 13 shows the type of waterwheel that will build to get an electricity.

Fig. 13. Example of waterwheel turbine.

E. Integratin of System and Testing.

After all part of slow stream hydropower complete, the integration of all part need to be done. The integration makes a fully system of hydropower and can be testing on their output voltage and others.

IV. Result and Discussion

There are three part of result that will be in this part. First, the design and arrangement of slow stream hydropower. Second, the characteristic of rate of flow at Tasik Ilmu and estimated gross power. Third, the slow stream hydropower can generate electricity that can cover the capacity of lighting in Tasik Ilmu.

A. Designing Turbine

Figure 14 shows the final design of the waterwheel with an alternator that will generated electricity. This design consists of turbine itself, shaft, bearing block, belt and pulleys. All measurement has been considered before design it.

The design of turbine will always depend on type of water that flow in the location that wanted to be install. There is some flexibility to change the design to another better design to get more efficiency in generating electricity.

B. Characteristic of rate of flow and estimated gross power

In this part, the result shows about the calculation that have been made using the speed of water. The speed of water in Tasik Ilmu was taken by the measurement that mention in literature review. The calculation also followed the equation that mention in literature review.

Fig. 14. *Waterwheel turbine have been design.*

TABLE II. GROSS POWER

10 Second	At Water fall		
	Speed m/s	***Rate of flow, m^3/s***	***Gross power, W***
1	0.758	0.015	0.22
2	0.717	0.014	0.21
3	0.745	0.015	0.22
4	0.684	0.013	0.19
5	0.841	0.017	0.25
		Average	0.218

For addition information, the width of the turbine is 0.5*m* and the height of water flow is 0.04*m*. So that, the sectional area that involved in calculation is $0.02m^2$. For the water density and gravitational constant, the value are 1 kg/m^3 and $9.81\ m/s^2$ respectively. For the height of the dam, from highest level of water to turbine, the length is 1.5*m*. Table II show the calculation that have been made.

B. Generating electricity from altenator

From the literature review, we confirm that the alternator generates with constant voltage. So that the generating will be 13.5V constantly. Besides, the power will depend on the rotational that be given by the turbine. The graph of current versus rotational as shown in literature review.

V. CONCLUSION

In conclusion, the slow stream hydropower can give so many benefit. This journal only focusing on concept of slow stream hydropower. To get better result, the study of all part in hydropower system must be more specific. In overall, this hydropower will help users to reduce electricity cost by developing sustainable energy.

REFERENCES

[1] M. Maria and T. Mannhart, "Analysis of the Power System of Malaysia," no. 03635605, Technische Universitat Munchen.

[2] Ion Bostan (2013). "*Resilient Energy Systems, Renewable: Wind, Solar, Hydro"*, 2013G.

[3] Charles Ken Adu Boahen (2013). *"Prefeasibility Studies For Mini Hydro Power Generation On Kintampo Falls*", Kwame Nkrumah University of Science and Technology, June 2013

[4] Richard J. Campbell (2011). "Hydropower from Small and Low-Head Hydro Technologies and prospects". Nova Science Publishers, 2011

[5] Chris Elliott (2014). "Planning and Installing Micro-Hydro Systems : A Guide for Designers, Installers and Engineers", Routledge from Taylor and Francis Group.

[6] Adam Harvey (1993) "*Micro-Hydro Design Manual A guide to small-scale water power schemes"*. Practical Action Publishing, United Kingdom, 1993.

[7] Nigel Smith (1994). *"Motors as Generators for Micro-hydro Power"*. Practical Action Publishing, United Kingdom, 1994, 2008

[8] Natural Resources Canada (2004). *"Micro-Hydropower System : A Buyer's Guide"*. Her Majesty the Queen in Right of Canada, 2004

UTM
UNIVERSITI TEKNOLOGI MALAYSIA
Faculty of Electrical Engineering

ISBN 978-967-0194-96-7
9 789670 194967